Organic Petrology, Maturity, Hydrocarbon Potential and Thermal History of the Upper Devonian and Carboniferous in the Liard Basin, northern Canada.

by

Judith Potter

A thesis
presented to
The University of Newcastle upon Tyne
in fulfillment of the requirement of the degree of
Doctor of Philosophy
in
Fossil Fuels and Environmental Geochemistry

Newcastle upon Tyne
September 1998

DECLARATION

I hereby certify that the work described herein is my own, except where otherwise acknowledged, and that it has not been submitted previously for a degree at this or any other university.

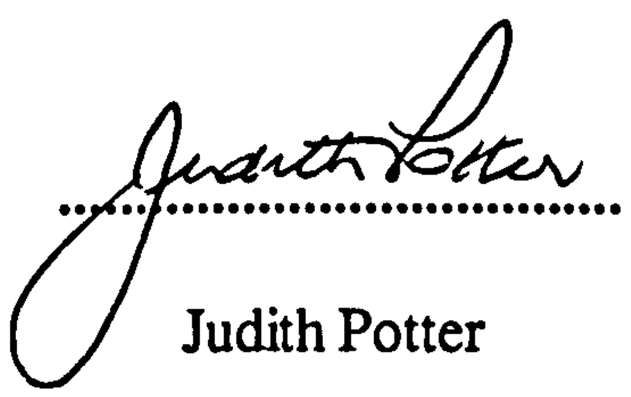

Judith Potter

ABSTRACT

Organic petrology and RockEval-TOC pyrolysis studies were carried out on over 600 samples of shales, siltstones, marls and coals from forty three sections in the Upper Devonian and Carboniferous strata of the northern part of the Liard Basin and adjacent areas of northern Canada between latitudes 59° 30' N and 60° 30' N and longitudes 121° 30' W and 125° W, to determine the hydrocarbon source potential, thermal maturity and thermal history. The focus of the study is on the optical characteristics and genesis of bitumens and their viability as indicators of thermal maturity.

Total organic carbon (TOC) contents indicate that potential oil and gas source rocks occur in the Muskwa, Kotcho, Besa River, Exshaw, Lower Banff, Yohin, Clausen, Golata and Mattson formations; the latter includes thin algal laminites and sapropelic coals. Hydrogen versus oxygen indices indicate that the organic matter comprises Type II kerogen, except for the Golata and Mattson formations which contain mixed Type II and Type III kerogen. Petrographic analysis indicates that the organic components consist of primary and secondary liptinites of marine origin and indigenous microscopic bitumens. In addition, shales in the Golata and Mattson contain structured liptinite macerals, predominantly sporinite derived from Carboniferous mega- and microspores.

A genetic classification of microscopic bitumens is established using optical properties and "morphological associations" with primary organic constituents. It is proposed that indigenous bitumens are intermediate products or by-products of hydrocarbon generation from primary macerals. Six types are recognised. The weakly fluorescing, low reflecting types 1, 2 and 3 are associated with, and presumably originate from, alginite, sporinite and bituminite, respectively. Type 4 bitumen is a matrix pore-filling solid showing intermediate reflectance and no fluorescence; it is interpreted as a by-product of thermal maturation of matrix bituminite. Type 5 and 6 are highly reflecting with well-defined margins and are probably polycondensation products of hydrocarbons generated during diagenesis.

The type 1 and 2 bitumens occur over a maturity range of 0.55% - 0.6% VR_o up to 1.3%, and 1.5%, respectively. Type 3 and type 4 bitumens span broader maturity ranges (0.4% to 2.5% VR_o; and 4.0% VR_o, respectively) and show strong positive correlations between R_o and depth (Type 3: R^2 = 0.61 to 0.99; and Type 4: R^2= 0.8 to 0.96) and Tmax, suggesting that thermal maturity in this region is closely related to the burial history. Vitrinite reflectance equivalent data suggest that the source rocks in the deepest part of the basin are gas-prone while the oil-generating potential increases from west to east and in the younger strata. Correlations between type 4 bitumen reflectance and measured vitrinite reflectance follows closely the relationship demonstrated by Jacob (1985): VR_o= ($B4R_o$ x 0.618) + 0.4. Type 3 bitumen R_o is closely related to that of type 4 ($B3R_o$ = 0.73 x $B4R_o$) and vitrinite [VR_o = (0.817 x $B3R_o$) + 0.41]. Minor "discontinuities" in the bitumen R_o - depth plots are attributed to suppression of the Type 3 and 4 bitumen R_o in TOC-rich, black shales of the Muskwa, Besa River, Upper Kotcho, Exshaw and Lower Banff, which may be associated with sulphur-rich kerogen. High maturity (reflectance) gradients for the Upper Devonian (0.15 to 0.47 log%R_o/km) indicate that significantly higher geothermal gradients prevailed, relative to the Carboniferous (0.09 to 0.26 log%R_o /km); these gradients were highest in the western part of the study area throughout the Upper Palaeozoic. Basin modeling using VR_o equivalent data to constrain the thermal history also suggests that significantly higher regional heat flows prevailed during the Upper Devonian, particularly in the region of the Kotaneelee and Beaver River gasfields.

Bitumen reflectance anomalies and bitumen cokes observed near the Bovie Fault suggest it was an additional source of thermal conductivity/convection during the Upper Devonian. Similar trends and anomalously high Ro gradients in the northwestern part of the Liard Basin, suggest an additional thermal event, e.g. hydrothermal activity, may have occurred during the Upper Devonian-Lower Carboniferous, promoting early (?Late Carboniferous) or even syndepositional petroleum generation and may be related to Middle and Upper Devonian SEDEX mineralization.

Table of Contents

ACKNOWLEDGEMENTS

There are many individuals and companies to whom I should like to express my greatest appreciation for financial, data-gathering and technical assistance in this project. The following companies provided financial assistance and facilitated data collection:

Wascana Energy (formerly SaskOil)
Canadian Hunter Exploration Ltd.
Shell Canada

In addition, I am indebted to the Geological Survey of Canada-Calgary for financial support, the use of geochemical and petrological laboratory facilities, library and computer and office resources, technical services; and to D. Marchioni, PetroLogic Services and W.J. McDougall & Associates for unlimited use of their microscope facilities.

Those individuals at GSC Calgary to whom I am deeply and especially grateful for thought-provoking discussions, technical assistance and critical reviews are: Drs. Lavern Stasiuk, Fari Goodarzi, Barry C. Richards and Mark Obermajer. In particular, I would like to thank Dr. David Morrow, for his continual support for this project and providing unlimited time and technical assistance, interminable patience for my "cyber-ineptitudes", for his enthusiasm and encouragement. Thanks also to Bill McDougall, Brian Rutley, Glen Edwards, Claudia Thompson, Lloyd Snowdon, Martin Fowler and Kirk Osadetz for their many contributions. I feel privileged to have worked with, and learned much, from these enthusiastic, tireless and committed scientists and have benefitted greatly by the excellent research environment provided by the GSC - Calgary.

I am particulary grateful to Dr. Fari Goodarzi for facilitating my studies, initiating and supervising the work and for the many hours of technical advise and helpful discussion; and to Dr. Richard Tyson for his support and constructive comments throughout the project and for critically reviewing the thesis. Thank you Richard for your patience and continued support. I would also like to thank Dr. Steve Larter, Yvonne and Ann Thwaites of the Newcastle Research Group in Fossil Fuels and Environmental Geochemistry for facilitating the completion of this work from such a distance.

Finally, I am thankful for the love, patience and encouragement of my family: husband Dean, daughter Kate, and sons, Drew and Jamie. I will always be indebted to you all for allowing me to do what I set out to do, knowing that I would miss many valuable moments of our time together. I dedicate this work to you and hope that your dreams and goals in life are one and the same.

PUBLICATIONS RELEVANT TO THIS THESIS

The following publications result from the research documented in this thesis. All of the data pertaining to the petrography and geochemistry of the Upper Devonian and Lower Carboniferous in the Liard Basin is included in the thesis and whenever it is relevant to do so, some of the discussion may be included. No attempt is made to incorporate the full extent of the publications into this document; the reader is referred to reprints of the original publications which are enclosed in the pocket inside the back cover of the thesis.

Cameron, A.R., Potter, J. and Goodarzi, F., 1994. Coal and oil shale of Early Carboniferous age in northern Canada: significance for palaeoenvironmental and palaeoclimatic interpretations. *Palaeogeography, Palaeoclimatology and Palaeoecology*, **106**, 135-155.

Morrow, D.W., Potter, J. Richards, B.C. and Goodarzi, F., 1993. Paleozoic burial and organic maturation in the Liard Basin Region, northern Canada. *Bulletin of Canadian Petroleum Geology*, **41**, 17-31.

Potter, J. , Richards, B.C. and Cameron, A.R., 1993a. The petrology and origin of coals from the Lower Carboniferous Mattson Formation, southwestern District of Mackenzie, Canada. *International Journal of Coal Geology*, **24**, 113-140.

Potter, J., Richards, B.C., Morrow, D.W. and Goodarzi, F., 1993b. The organic petrology and thermal maturity of Lower Carboniferous and Upper Devonian source rocks in the Liard Basin at Jackfish Gap-Yohin Ridge and North Beaver River, Northern Canada: implications for hydrocarbon exploration. *Energy Sources*, **15**, 289-314.

Morrow, D. W. and Potter , J., 1998. Internal stratigraphy, petrography and porosity development of the Manetoe Dolomite in the region of the Pointed Mountain and Kotaneelee Gas Fields. *In: Hogg, J.R. (ed.) Oil and Gas Pools of the Western Canada Sedimentary Basin,* Canadian Society Petroleum Geologists Special Publication S-51, pp. 137-161.

LIST OF FIGURES

LIST OF TABLES

LIST of PLATES

1.0 INTRODUCTION

The Liard Basin (Fig. 1) is considered a frontier exploration basin (Leckie *et al.*, 1991) with only eighteen wells having been drilled, mostly in the southern portion of the Liard Basin, during the late 1950's and early 1960's. This resulted in development of Canada's most northerly gas fields at Beaver River, Pointed Mountain and Kotaneelee (located east and west of longitude 124° W and between 60° N and 60° 27'N) (Morrow *et al.*, 1993). Since 1992, there has been a flurry of drilling activity following renewed economic interest in the region, especially in the areas north and east of Fort Liard, and in northeastern British Columbia. Despite this, there is limited information available regarding the source rock potential and thermal maturity of the region.

Estimation of hydrocarbon source potential by characterization of the dispersed organic matter or kerogen using geochemical and organic petrological techniques has become an integral part of hydrocarbon exploration in frontier basins (Brooks, 1981; Tissot & Welte, 1984). This involves identifying the potential source rocks, measuring the total amount of organic matter present, the type or quality of the organic matter and the level of thermal maturity attained (Hood *et al.*, 1975; Dow, 1977). In addition, reconstructing the burial and thermal histories of a sedimentary basin are facets of basin modeling that help determine the timing of hydrocarbon generation and ultimately, the hydrocarbon potential of the basin (Waples, 1980; Tissot & Welte, 1984; Tissot et al., 1987).

Conventional parameters used to evaluate thermal maturity and constrain the thermal histories of hydrocarbon source rocks, such as vitrinite reflectance (VR_o; Durand *et al.*, 1986), cannot always be applied to Palaeozoic rocks of marine origin. Vitrinite is the predominant group of macerals found in humic coals and its reflectance is related to the level of coalification (Stach, 1982; Teichmüller, 1982). It may also be found dispersed in sedimentary rocks deposited in terrestrial (e.g. lacustrine, fluvial) and marginal marine environments (e.g. deltaic, lagoonal, nearshore shelf). However, vitrinite is a product of the coalification or thermal maturation of humic substances derived from the cellulose and lignin of terrestrial plants (Teichmüller, 1982) and therefore it is rare to absent in marine rocks (e.g. basinal shales) and in rocks of pre-Upper Devonian age. Durand *et al.* (1986) indicate that vitrinite-like macerals derived from algal remains occur in marine and lacustrine rocks, but they are chemically distinct from terrestrial vitrinites, although

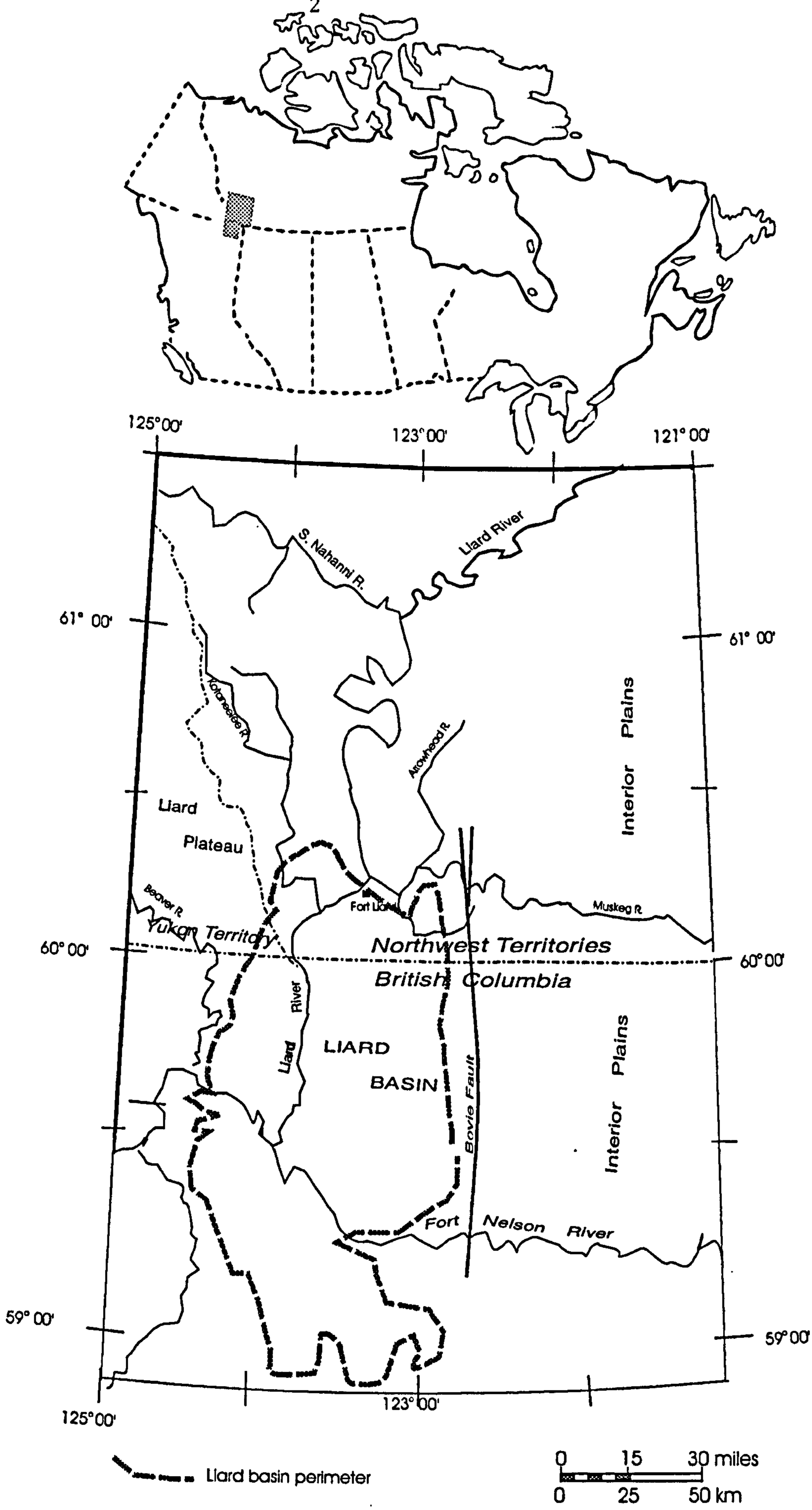

Figure 1. Index map of Canada showing the location of the Liard Basin (from Leckie *et al.* 1991, modified).

corpohuminite-like bodies derived from algal akinetes with similar optical properties and maturation tracks to vitrinites have been identified in the Lower Palaeozoic of Saskatchewan by Stasiuk *et al.*, 1994.

The use of vitrinite reflectance in the Liard Basin is extremely limited. The Upper Devonian strata are exclusively marine in origin and potential hydrocarbon source rocks are predominantly shales and marls which accumulated in a basinal setting. Carboniferous strata in this region are also predominantly of marine origin, except for the Upper Viséan-Serpukhovian Mattson Formation which comprises sandstone-dominated delta plain deposits and includes thin coals and carbonaceous shales. The coals are localized to the region around the Tlogotsho Plateau (Fig. 1) and dispersed vitrinite in found in only three surface sections in this area. The viability of bitumen reflectance as an alternative maturation parameter is therefore examined in terms of : 1) qualification of the indigenous nature of the bitumens (i.e. their origins, organic affinities and modes of genesis); 2) optical trends with increasing depth and maturity, and their relationship to the tectonic history of the region; and 3) basin modeling applications.

1.1 ORGANIC PETROLOGY AND HYDROCARBON POTENTIAL

Petroleum and gaseous hydrocarbons are generated biogenically and during thermal maturation of organic matter (kerogen) dispersed in sedimentary rocks (Evans & Staplin, 1970; Dow, 1977; Hunt, 1979; Tissot & Welte, 1984). The type of hydrocarbons generated (e.g crude oil, condensate, wet gas, dry gas), depends upon the nature of the organic matter or kerogen in the source rock and its diagenetic state (Tissot *et al.*, 1974; Leythaeuser *et al.*, 1980), the latter being controlled by the composition of the biological source and redox conditions at the time of deposition (Demaison & Moore, 1980; Huc, 1988, 1990). Most petroleum source rocks were formed in dysaerobic to anoxic, marine environments (Demaison & Moore, 1980; Tyson, 1987), predominantly on the continental shelf and upper slope, in regions associated with moderate to high organic productivity (Demaison & Moore, 1980).

Kerogen types

The term "kerogen" refers to the fossil organic matter in sedimentary rocks that is

insoluble in common organic solvents (Durand, 1980) and in aqueous alkaline solutions (Tissot & Welte, 1984). Kerogen may include "geochemical fossils", i.e. organic compounds that are chemically and biochemically resistant to the processes involved in transportation, sedimentation, burial and diagenesis (Eglinton, 1968; Tissot & Welte, 1984, p. 97), as well as the complex organic polymers produced by reconstitution and diagenesis of biologically degraded sedimentary organic matter. The geochemical fossils include saturated hydrocarbons, vegetable waxes, resins, sporopollenin and chitin (Durand, 1980). Palynological and petrographic examination of kerogen is commonly done after separating the organic matter from the rock matrix using HF and HCl. Visual examination using transmitted or reflected light microscopy indicates that kerogen is composed of amorphous and structured liptinitic components; phytoclasts (vitrinite and inertinite fragments; *sensu* Tyson, 1995), zooclasts and microfossils may be minor components (Combaz, 1975). The structured liptinites are similar to the those found in oil shales and coals (especially sapropelic coals) which are predominantly derived from higher plants and algae (Robert, 1981; Alpern, 1981; Hutton & Cook, 1981). Amorphous kerogen is usually present in significantly greater proportions in dispersed organic matter than in coals.

Kerogens assemblages are geochemically classified according to elemental H/C: O/C ratios, into four types, I, II, III, (Tissot *et al.*, 1974) and IV (Harwood, 1977; Brooks, 1981; Peters, 1986; Fig. 2). The elemental compositions of these different types of kerogen have been shown to be analogous to those of coal macerals belonging to the liptinite (Types I & II), vitrinite (Type III) and inertinite (Type IV) groups (van Krevelen, 1961; Durand, 1975; Harwood, 1977; Peters, 1986) and they follow similar evolutionary trends on thermal maturation. Kerogens with the greatest hydrocarbon-generating potential are lipid-rich, typically having high H/C (> 1) and low O/C ratios (<0.12; Types I and II). Type I kerogen is typically hydrogen-rich, commonly derived from alginite and is most abundant in oil shales (Alpern, 1981) and boghead coals (Durand, 1975). Type II kerogen is derived from lipid-rich algae, bacteria, zoo- and phytoplankton, and lipid-rich components of terrestrial plants, such as spores, cuticles, resins. Type I and II kerogens are oil-prone (Tissot, 1973; Durand, 1975), i.e. they generate liquid hydrocarbons when thermally mature (Fig. 2b), and are found in source rocks deposited in variety of non-marine and marine environments, where organic matter is preserved due to anoxic

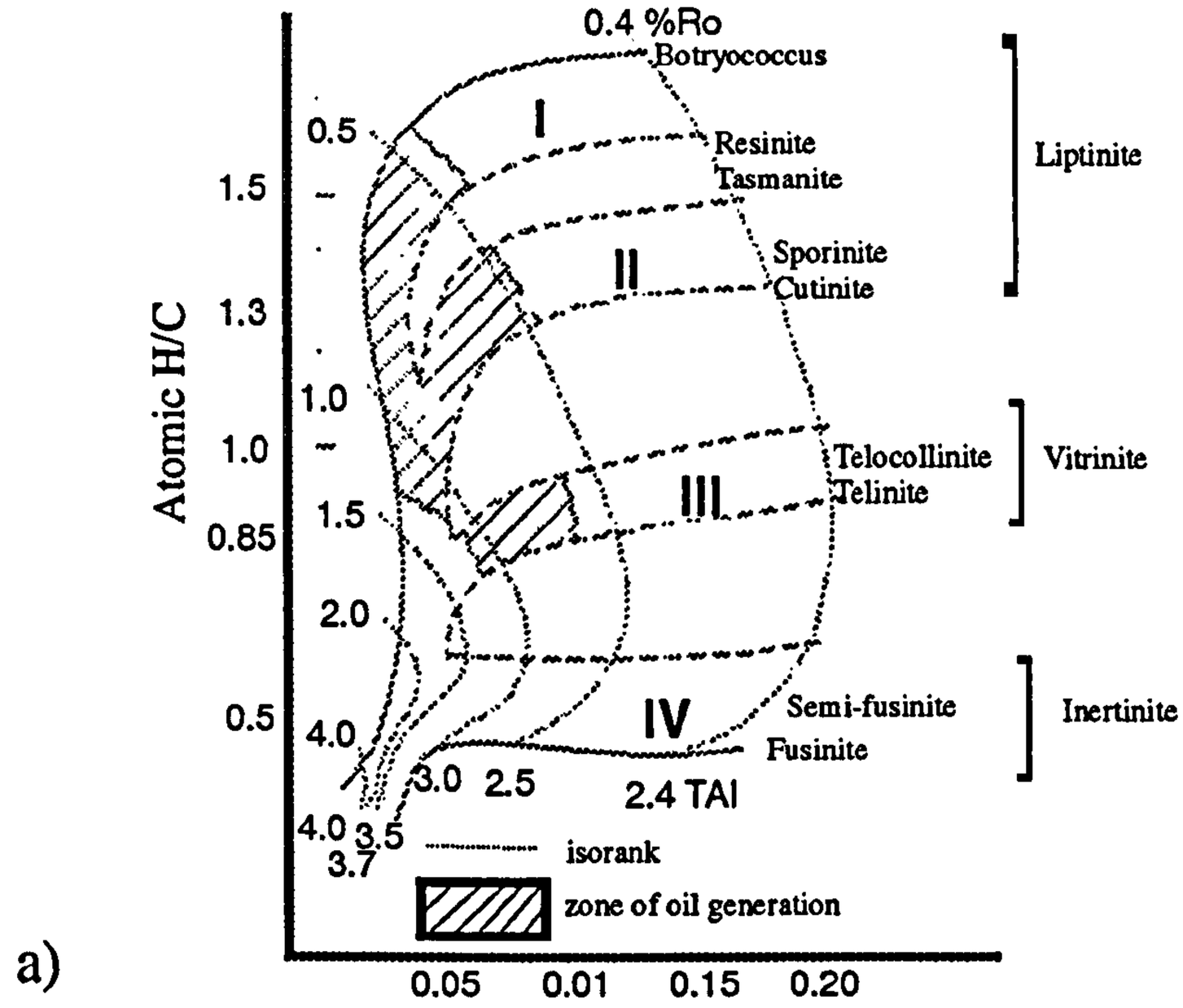

a)

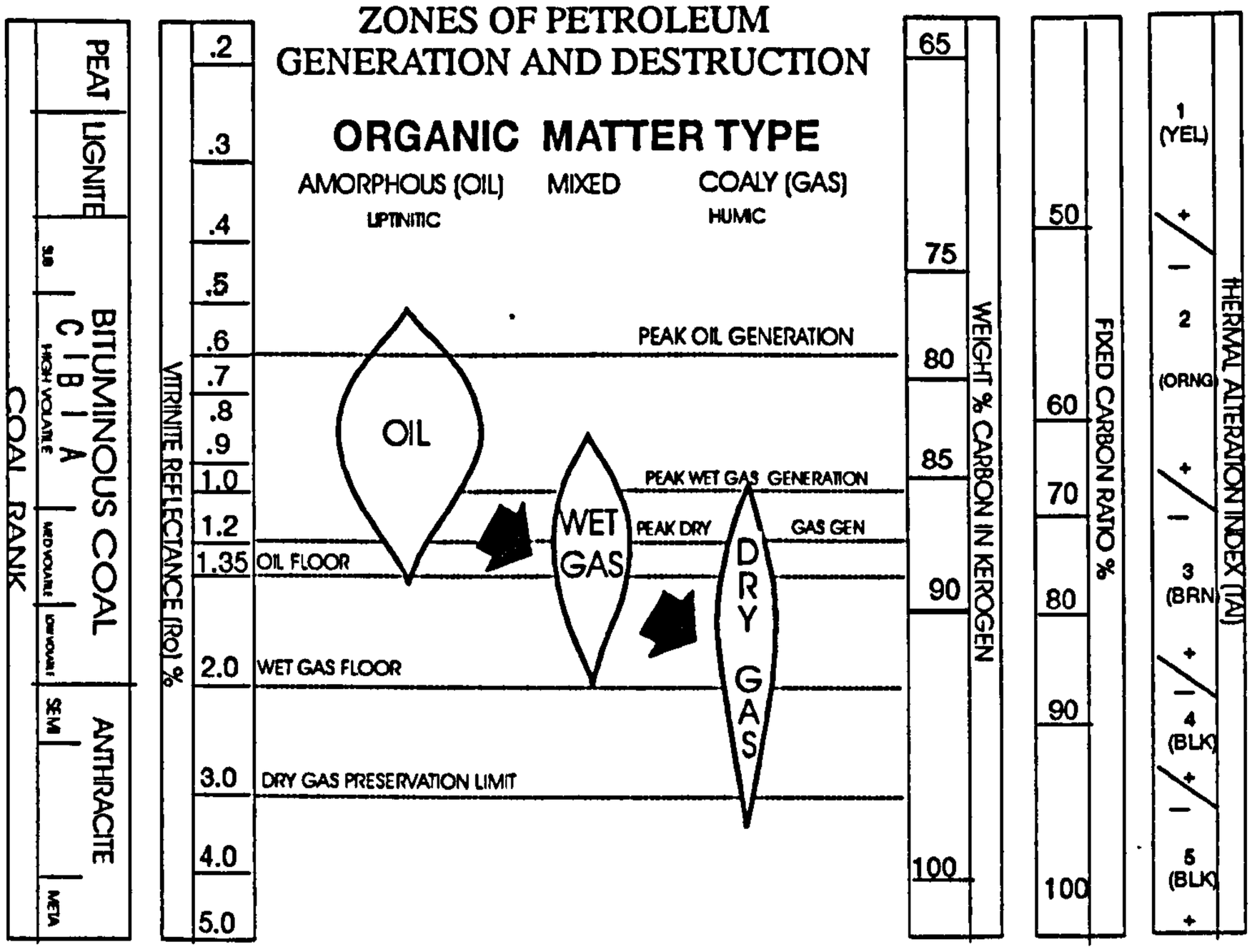

b)

Figure 2. a) Van Krevelen diagram showing kerogen type, thermal evolution and products (after Brooks, 1981, modified see Stasiuk *et al.*, 1990); b) Kerogen types, maturation pathways and oil generation (Dow, 1977).

conditions (Demaison & Moore, 1980). Type III kerogen is oxygen-rich due to an abundance of oxygen-bearing functional groups typically found in "humic" matter (Tyson, 1992, p.13); the vitrinite macerals are produced by coalification of cellulosic and lignified tissues of terrestrial plants but Type III kerogen may also reflect "humic" degradation products of marine organic matter. Type III kerogen is typically hydrogen-poor and therefore wet gas-prone (Tissot & Welte, 1984; Harwood, 1986), i.e. it produces predominantly gas (and condensate) when thermally mature. Type IV kerogen is oxygen-rich and hydrogen-poor, and often corresponds to inertinite macerals produced by bacterial oxidation or combustion of organic matter; the hydrocarbon potential is typically poor; it can generate only small amounts of gas upon maturation (Snowdon & Fowler, 1986). Powell and Snowdon (1982) have developed a hydrocarbon generation model that relates the type of hydrocarbon products to the type of source rock kerogen for northern and western Canadian hydrocarbon-producing regions (Fig. 3).

Although vitrinite is not an important source of liquid hydrocarbons, its reflectance is the industry standard for determining the level of thermal maturation; precise recognition of vitrinite is thus very important. Mukhopadhyay (1994) reviews some of the problems associated with identification of vitrinites. True vitrinites are the remains of cellulosic and lignified tissues of ancient plants which have been biochemically and geochemically altered to varying degrees; there are many types of vitrinite (i.e. vitrinite macerals), just as there are many different groups of plants, types of plant tissues, and variations in the depositional and diagenetic environment (Stach, 1982). Typically, vitrinite is the dominant group of maceral constituents in humic coals (Stach, 1982); it is also found in organic matter accumulated in non-marine and marginal marine facies. Furthermore, vitrinite occurs only in rocks of Devonian age and younger, reflecting the evolution of terrestrial plants (Teichmüller & Teichmüller, 1982).

Vitrinite-like organic matter of uncertain origin has been identified microscopically in marine and lacustrine sedimentary rocks of early Palaeozoic age; it possesses optical properties similar to true vitrinite but lacks morphological definition and it also differs chemically (Nissenbaum & Kaplan, 1972; Larter & Sentfle, 1985). Durand *et al.* (1986) also point out visual similarities between dispersed vitrinites in shales and true vitrinites of coals, but note that not only are they chemically different, but their maturation patterns also

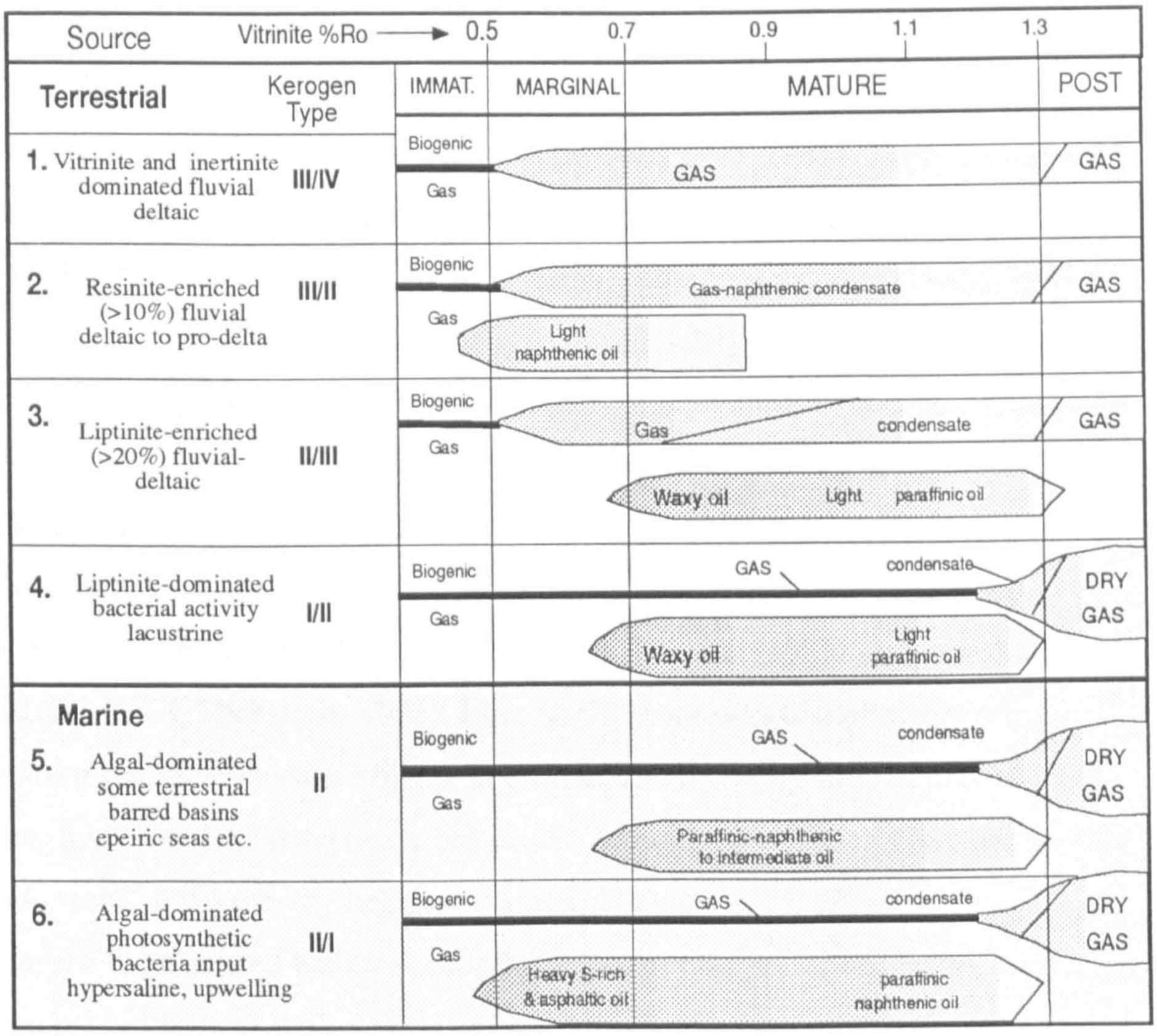

Figure 3. Hydrocarbon generation model illustrating the relationship between kerogen type, source rock palaeoenvironment and type of generated hydrocarbons (from Stasiuk, 1991; based on Powell & Snowdon, 1983).

differ. Early recognition of differences between the reflectance of vitrinites in coals and other sedimentary rocks was, in part, attributed to the host lithology (Bostick & Forster, 1975).

Solid Bitumens

Dispersed solid polycondensed hydrocarbons, or "bitumens", are also relatively common in hydrocarbon source rocks. They are amorphous solids which occupy pore spaces, intergranular spaces, fractures and veins (Robert, 1973, 1981). They assume the shape of the occupied cavities and can only be distinguished from primary macerals such as liptodetrinite and vitrodetrinite, when observed in whole rock samples (Jacob, 1989). Jacob, (*ibid.*) considers all dispersed bitumens to be secondary in origin. His classification recognizes three groups: naphthenic, asphaltic bitumens, and impsonites (Fig. 4); further subdivision is based purely on physical and optical properties including reflectance, fluorescence, microsolubility in CS_2 and micro-flow point (Abraham, 1960; Jacob, 1989; Fig. 5). Geochemical analysis of some of the bitumens have shown that the genetic relationships inferred by Jacob (1983) and Jacob and Hiltmann (1985) are unsubstantiated (Khavari-Khorasani & Michelson, 1993). Hunt (1978) considers that bitumens are generated from plankton which are higher in protein, and therefore sulphur and nitrogen, than organic matter derived from terrestrial plants. Although the origin of bitumens is still poorly understood, it is generally held that dispersed bitumens (i.e. except for the "migrabitumens" associated with metamorphic zones of mineralization, Jacob, 1989), may be residual products of the cracking of petroleum liquids (pyrobitumens) or hydrocarbon fractionation during secondary migration; they may also be products of biodegradation during diagenesis (Klubov, 1993) or may form during early catagenesis, as a result of the early generation of a heteroatomic organic phase (Reidiger, 1993) from sulphur-rich kerogen (Powell *et al.*, 1975; Powell & Snowdon, 1993). Machel *et al.* (1995) consider bitumens as possibly arising from the polymerization of the products of either bacterial sulphate-reduction or thermo-sulphate reduction of high or low molecular weight hydrocarbons (alkanes, alkenes and methane) or carbohydrates, in the presence of SO_4^{2-} ions. Lewan (1990) found that slow vaporization and removal of pyrolysates during hydrous pyrolysis experiments promotes conversion of soluble bitumen to solid bitumens

Maceral Group	Maceral subgroup	Maceral
Migrabitumen		ozocerite
	asphaltite	asphalt
		gilsonite
		glance pitch
		grahamite
	impsonite	wurtzilite
		albertite
		epi-impsonite
		meso-impsonite
		cata-impsonite

a)

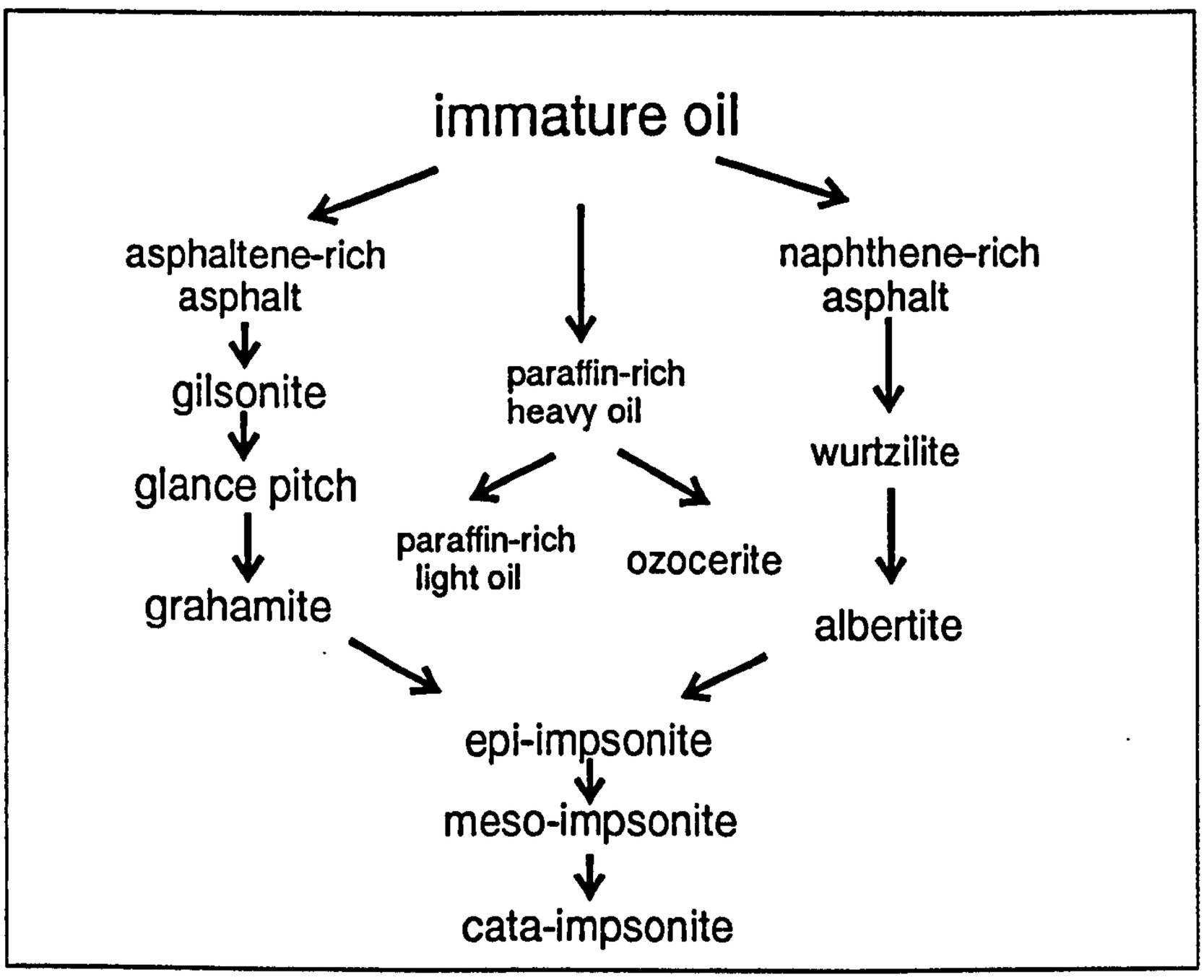

b)

Figure 4. a) Classification and b) genesis of solid " migrabitumens" (after Jacob, 1989).

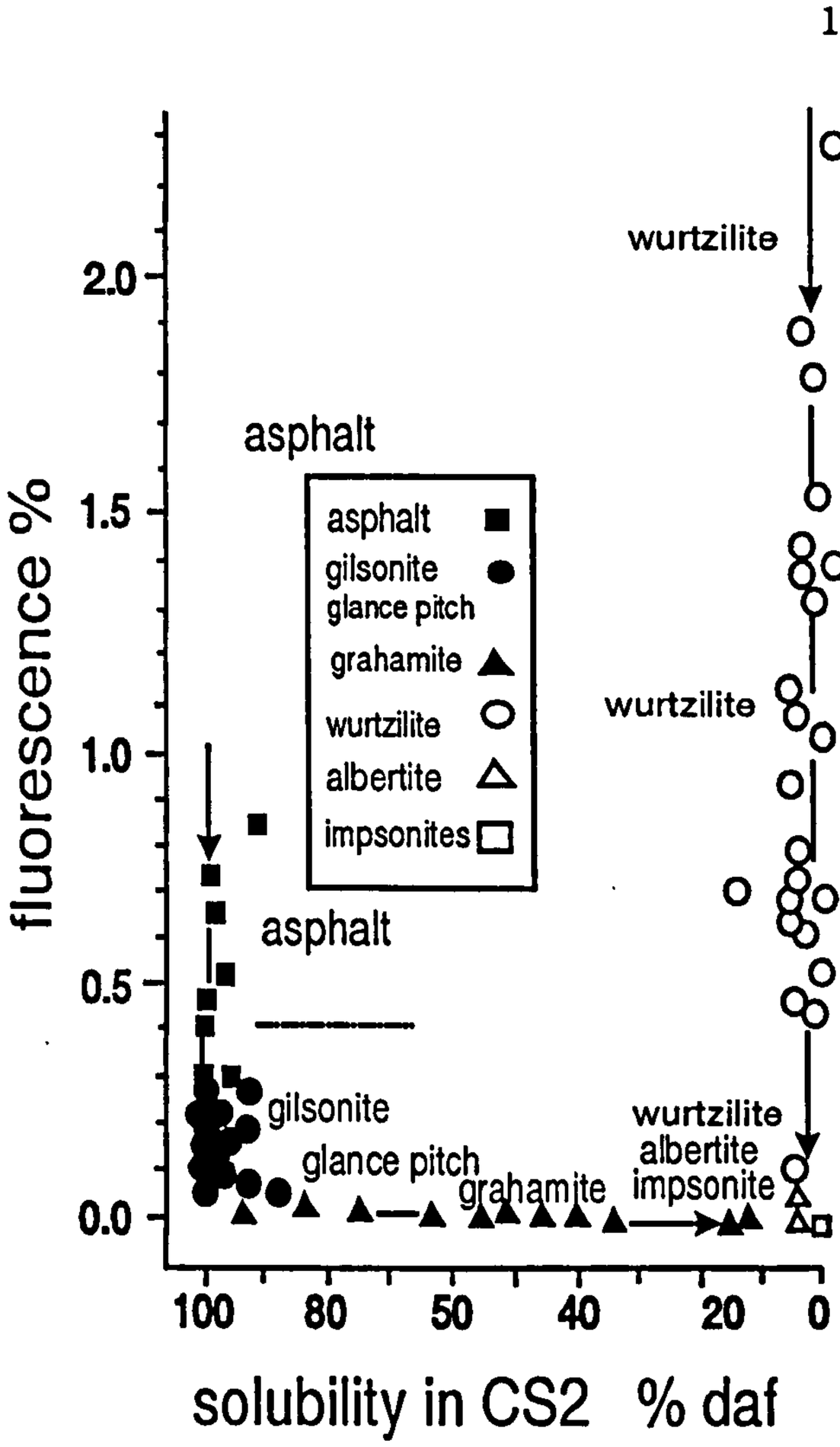

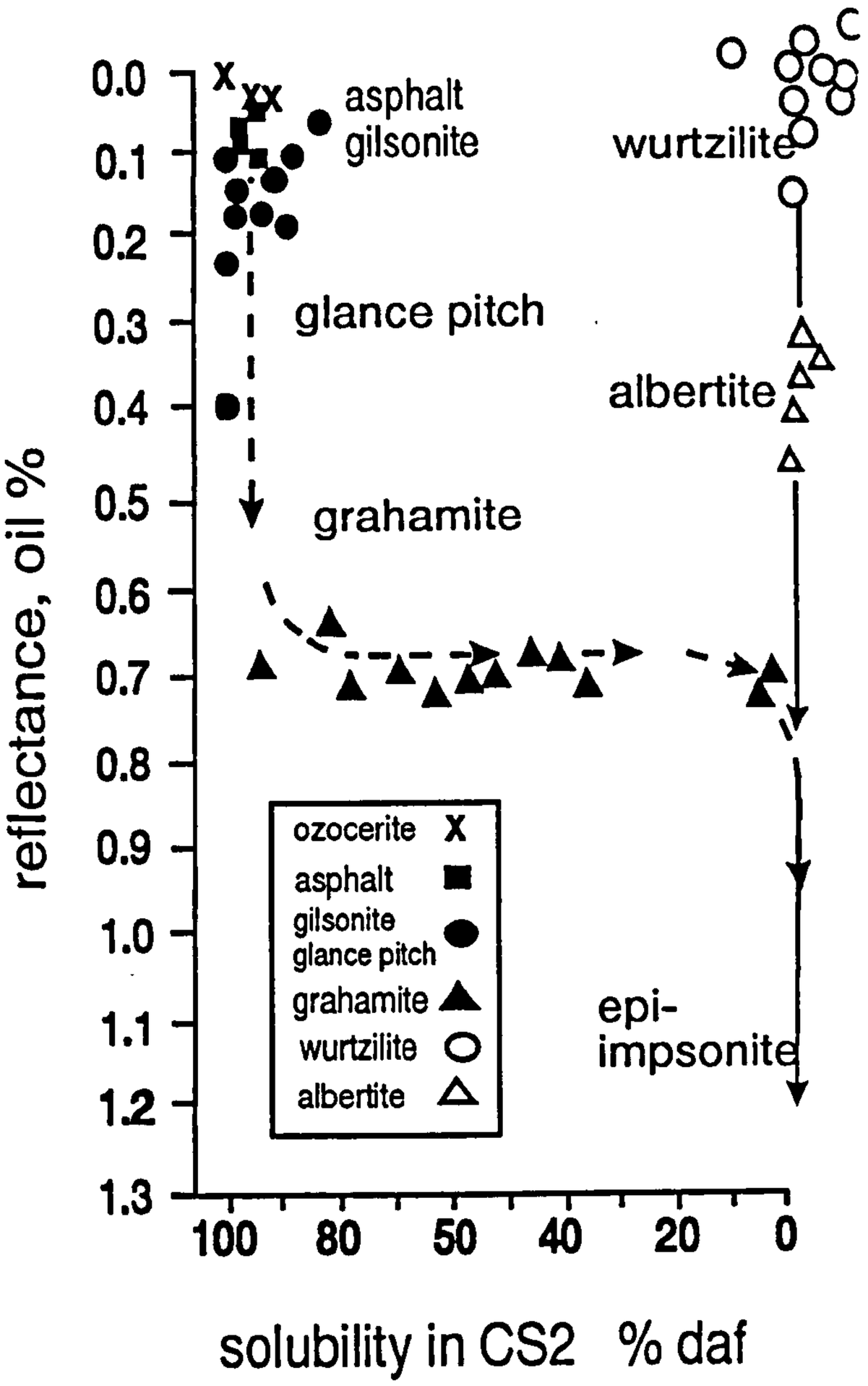

Reflectance, fluorescence intensity, microsolubility and micro-flowpoint of bitumens

	Random reflectance in oil (%)	Fluorescence (special masked uranyl glass standard = 1%)	Microsolubility in immersion oil and petroleum ether	Microflow-point (oC)
Ozocerite	<0.01 - ca. 0.02	ca. 9.0 - >50	soluble	ca. 30 - ca.90
Wurtzilite	<0.01 - ca.0.1	ca. 0.1 - >2.0	insoluble	does not flow
Albertite	ca. 0.1 - ca. 0.7	<0.1	insoluble	does not flow
Asphalt	ca. 0.02 - ca. 0.07	ca. 0.4 - > 4.0	soluble	< 104
Gilsonite	ca. 0.07 - ca.0.11	ca. 0.05 - ca. 0.4	soluble	ca. 104-ca. 164
Glance pitch	ca. 0.11 - ca. 0.3	ca. 0.05- ca. 0.2	soluble	ca. 104-ca. 164
Grahamite	ca. 0.3 - ca. 0.7	<0.05	slightly soluble or insoluble	> 164 - ca. 287
Epi-impsonite	ca. 0.7 - 2.0	<0.02	insoluble	does not flow
Meso-impsonite	2.0 - 3.5	<0.01	insoluble	does not flow
Cata-impsonite	3.5 - ca. 10	<0.01	insoluble	does not flow

Figure 5. Physicochemical properties of migrabitumens, according to Jacob (1989).

by recombination of free radical fragments which form carbon-carbon bonds and cross-linkages.

Curiale (1986) investigated solid bitumens geochemically from a genetic standpoint, and viewed dispersed bitumens simply as "organic matter that has migrated from its source". On the basis of aromaticity and H/C ratios, he related them to the source and classified them, according to thermal maturity, into pre- and post-oil bitumens; pre-oil bitumens being "produced in, or close to, the source rock" (Fig. 6). Gentzis (1991) recognized the presence of bitumens generated *in situ* due to thermal maturation of primary organic matter in Palaeozoic and Mesozoic strata of the Canadian Arctic. In this study, and in work by Landis and Castaño (1995), the genesis of dispersed bitumens is also viewed as a consequence of the thermal maturation of primary organic matter, occurring within the source rock at various stages of maturity and according to kerogen type. While Landis and Castaño (*ibid.*) recognize morphologically similar (granular and homogeneous) indigenous bitumens to some of those described in section 2.3, they make no reference to their kerogen precursors. A genetic classification of indigenous bitumens is used in this study and is discussed in detail in Section 2.3 and Chapter 3.

Thermal maturation

It is generally accepted that, following diagenesis, thermal maturation or "catagenesis" is the predominant process by which economic quantities of hydrocarbons are produced from the kerogen in source rocks (Vassoyevich *et al.*, 1969; Tissot *et al.*, 1971); this occurs subject to burial of the kerogen to depths at which temperatures are in the 60°C to 150°C range (Tissot & Espitalié, 1975). Generation of petroleum and gaseous hydrocarbons results from thermal rupturing of C-heteroatom, C-H and C-C bonds which requires activation energies of between 38 and 74 kcal/mole (Sweeney *et al.*, 1987; Sweeney & Burnham, 1990). The burial temperatures required to effect these reactions range from 100°C to 150°C for hydrocarbon generation (Quigley *et al.*, 1987); oil to gas cracking which involves cleavage of C-C bonds (catagenic gas generation) requires significantly higher temperatures, between 150°C and 220°C (*ibid.*). These values all depend upon kerogen type and the depths at which these reactions take place is a function of the local geothermal conditions (Tissot & Espitalié, 1975; Demaison, 1975).

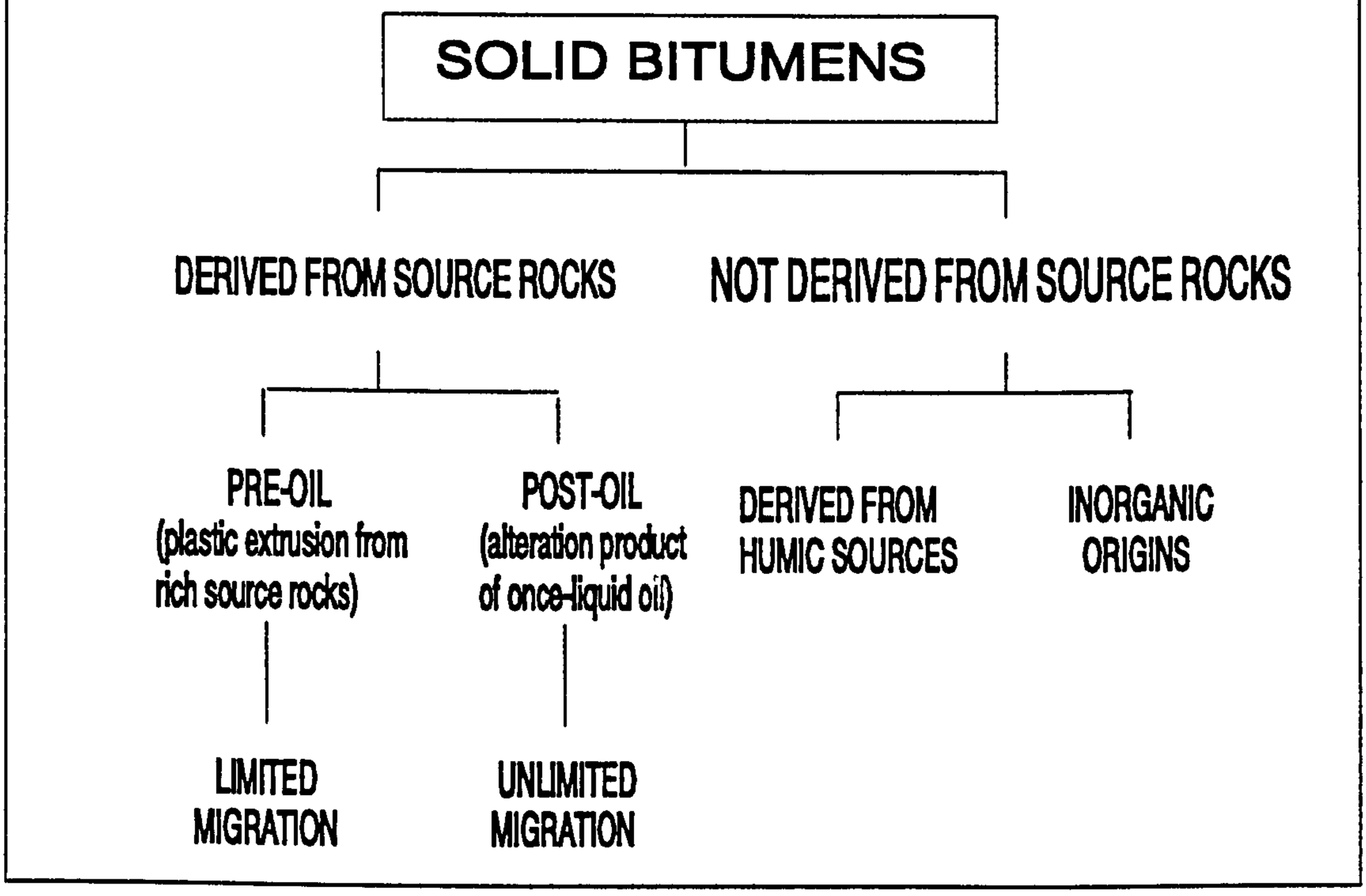

a)

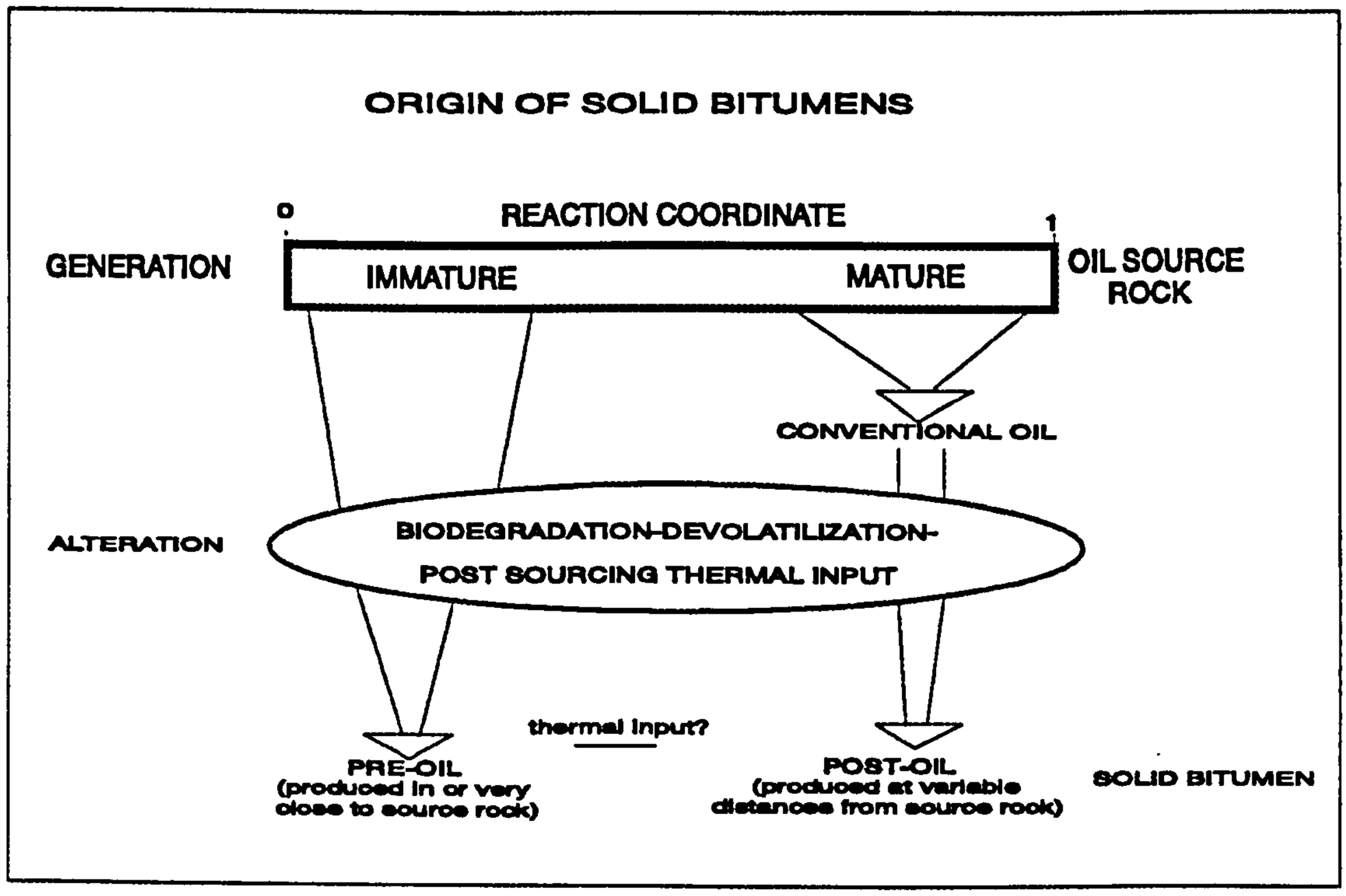

b)

Figure 6. a) Genetic classification of solid bitumens, after Curiale (1986) modified.
b) Mechanism for production of solid bitumen (pre- and post-oil), from Curiale (1986).

In addition to elemental analysis, the thermal evolution of kerogen can be evaluated chemically by using oxidation, hydrogenolysis, or pyrolysis to simulate thermal degradation. Many methods have been used to do this, including liquid chromatography, gas chromatography (Radke *et al.*, 1984; Leyhaeuser *et al.*, 1980), gas chromatography-mass spectrometry (Cornford *et al.*, 1979), high-pressure liquid-gas chromatography (Radke & Welte, 1981), infra-red spectroscopy (Ganz & Kalkreuth, 1987; Christy *et al.*, 1989), pyrolysis-gas chromatography (Tissot & Welte, 1984; Horsefield *et al.*, 1989) hydrous pyrolysis (Lewan, 1985, 1990, 1992; Lewan & Williams, 1987; Lewan *et al.*, 1979; Winters *et al.*, 1983). While effectively yielding chemical parameters for kerogen type and maturation, these methods are highly specialized, time-consuming and require isolation of the kerogen from the mineral matrix of the source rock. Espitalié *et al.* (1977) developed a rapid, inexpensive method of kerogen characterization and source rock analysis using pulverized drill cuttings or whole rock samples. The Rock-Eval Pyrolysis method is carried out in conjunction with TOC analysis and provides information regarding the kerogen type and thermal maturity; it is widely used in source rock evaluation but the results require careful consideration (Larter, 1984; Peters, 1986). The Tmax parameter is considered a very reliable indicator of thermal maturity of Type II and Type III kerogens, but not for Type I (Espitalié, 1986). A more detailed account of Rock-Eval Pyrolysis is given in section 2.4.

The chemical changes that occur within the kerogen are reflected in the changing optical properties of the microscopically recognizable constituents (Hood & Castaño, 1974; Hood *et al.*, 1975; Dow, 1977). Changes in the reflectance of vitrinite-like components express the increasing aromatization of the kerogen and decreasing H/C as hydrocarbons are released due thermal rupturing of C-C and C-heteroatom bonds, in much the same way as vitrinite reflectance changes with increasing coalification (Teichmüller & Teichmüller, 1966, 1982; Teichmüller, 1971; McCartney & Teichmüller, 1972). Fluoresence characteristics of liptinite macerals, such as an increase in the ratio of the intensity of the red (650 nm) to green (500) fluorescence (Q) and a red-shift in the wavelength at which maximum fluorescence occurs (λ max) were also found to change with increasing maturation and coalification (Ottenjahn *et al.*, 1975; Teichmüller & Wolf, 1977; Teichmüller & Durand, 1983).Teichmüller and Durand (1983) compared the

fluorescence characteristics of liptinite and vitrinite macerals in coals to the results of Rock-Eval pyrolysis and concluded that Tmax could be used as a maturity parameter in coals. Espitalié (1986) demonstrated good correlations between the Tmax parameter derived by Rock-Eval Pyrolysis and vitrinite reflectance for organic matter of Type II and III, up to a VR_o of 1.5% (after this the S2 peak disappears and Tmax cannot be determined). Dow (1977) related the level of thermal maturation of different types of kerogen with zones of petroleum formation and destruction, defining the "oil window" in terms of the vitrinite reflectance (VR_o): 0.5% and 1.3% VR_o representing the respective "birth and "death" lines for oil generation. Heroux *et al.* (1979) and Mukhopadhyay (1994) have published reviews of the major petrographic and geochemical maturity parameters and their relationship to hydrocarbon generation.

Hydrocarbon source potential

Momper (1978) reviewed the essential requirements for commercial oil/gas accumulations, the first of which is an effective source system with a minimum of 0.5% organic carbon and 30% clay minerals in argillaceous rocks, kerogen composed exclusively or partly of a combination of lipid-rich, amorphous, sapropelic and structured liptinites with a relatively high hydrogen content (H/C ratio is > 1.0), a favourable thermal history such that the kerogen has past peak oil generation (>83-84% C), and oil generation and over-pressuring sufficient to expel hydrocarbons. Zielinski and McIver (1982) and Dembicki and Pirkle (1985) have devised source potential rating indices for individual source units, based upon the organic richness (TOC), formation thickness and maturity, in order to permit regional mapping of hydrocarbon potential. Dembicki and Pirkle (*ibid.*) devised separate oil and gas maturity factors based on vitrinite reflectance data, although other maturity parameters such Time Temperature Index (TTI; Lopatin, 1971; Waples, 1980) or Thermal Alteration Index (TAI; Staplin, 1969) can also be used; eight separate stages of oil or gas generation are each represented by maturity factors, ranging from 0.0 to 1.0, with 1.0 representing peak oil/gas generation (Fig. 7).

BASIN MODELING

Basin modeling is the integration of geophysical, stratigraphic and geochemical

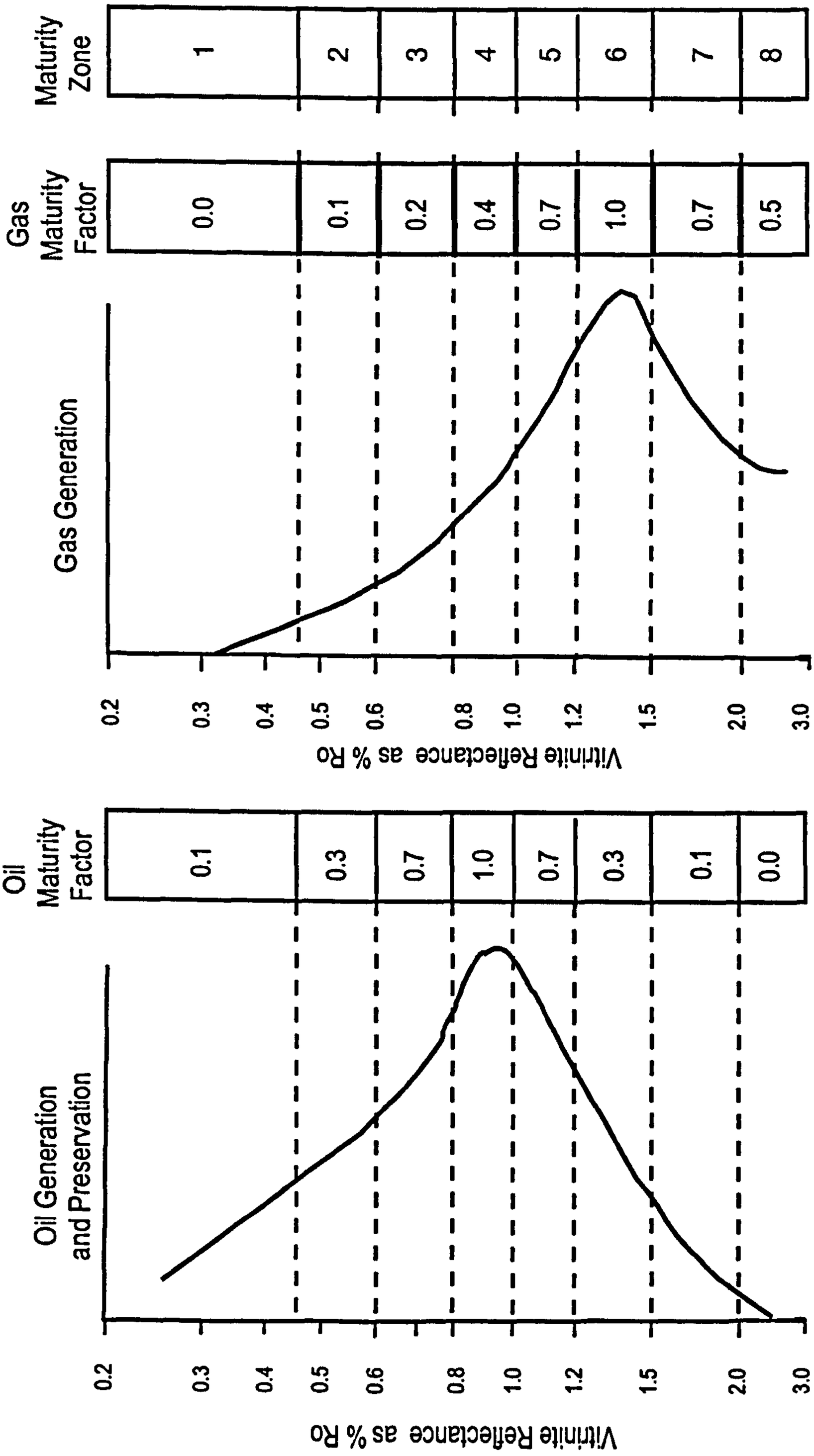

Figure 7. Oil and gas generation curves plotted vs. vitrinite reflectance (% Ro) and subdivided into maturity zones. Maturity scaling factors for oil and gas generation are given for each zone (from Dembicki & Pirkle, 1985, Figure 1).

data from a sedimentary basin to generate a model whereby the hydrocarbon potential of source rock can be determined at any time in its history (Tissot & Welte, 1984). With the development of sophisticated modeling programs and recent advancements in the capabilities of personal computers, basin-modeling has become an integral part of hydrocarbon exploration in frontier and offshore basins. The products of most modeling programs are burial and thermal history curves which relate the stratigraphic, burial and maturation histories of a given area to the timing of hydrocarbon generation.

Catagenesis involves the thermal evolution of sedimentary organic matter and simultaneous generation of the hydrocarbon products. During catagenesis, the chemical and physical properties of the kerogen, like coal, change as a result of thermally-induced chemical reactions over time (Karweil, 1956). Because these reactions are irreversible, the maximum temperature to which the kerogen was subjected during burial, governs the thermal maturity of the kerogen. Reconstructing the palaeotemperature history (thermal modeling) is therefore a critical aspect of the assessment of the hydrocarbon potential of a sedimentary basin (Welte & Yukler, 1980; Tissot & Welte, 1984). Kerogen maturation and hydrocarbon potential are thus ultimately governed by the geological history, i.e. geothermal regime (palaeotemperatures, regional and local geothermal gradients, thermal conductivity of host rocks), burial history (rates, depth and length of burial) and tectonic history (Welte &Yukler, 1980). Hydrocarbon generation and expulsion potential is greatest in young, rapidly buried source rocks (Dow, 1977).

Many thermal history modeling methods involve initial reconstruction of the burial and tectonic history of the region (basin modeling) followed by application of the time-temperature index (TTI) concept of Lopatin (1971) to determine organic maturation; this step links vitrinite maturation directly to burial time as a function of sediment temperature (Waples, 1980) and thereby relates the timing of hydrocarbon generation to the burial history. This approach to basin modeling is based on the assumption that kerogen maturation proceeds by a series of first order reactions, at a rate that doubles with every 10°C increase in burial temperature, according to the Arrhenius equation ($k = A.e^{-Ea/RT}$ where k = Arrhenius rate constant; A = frequency factor; Ea = activation energy; R= universal gas constant; T= temperature). This basic approach is still used by Barker (1989) and Lerche *et al.* (1984). The first of the kinetic models was proposed by Tissot (1969) and Tissot and Welte (1984) who viewed kerogen degradation as a series of first order

reactions triggered at a single, low activation energy. As depth and temperature increase, the kerogen is irreversibly broken down as the C-heteroatom, C-O, C-H and C-C bonds are sequentially thermally ruptured, producing heavy heteroatomic compounds, carbon dioxide and water, and finally hydrocarbons (Tissot & Welte, 1984). More recently, Burnham and Braun (1985) and Burnham and Sweeney (1989) recognized that there are a range of chemical reactions involved in kerogen degradation that must be accommodated in any kinetics-based, thermal model. In their attempts to determine organic maturation (vitrinite reflectance), Burnham and Sweeney (*ibid.*), use a single Arrhenius reaction rate factor in the application of first order reaction kinetics to vitrinite degradation and a distribution of activation energies ranging from 38 to 76 kcal per mole, for four reactions that involve the elimination of water, carbon dioxide, methane and higher hydrocarbons. The resulting maturation is predicted in terms of vitrinite reflectance and has the advantage of application over a wide maturity range (0.5% to 4.0% VR_o). Furthermore, their results suggest that the relationship between vitrinite reflectance and oil generation is independent of heating rate. Larter (1989) also used a kinetic approach to thermal modeling using pyrolysis data (phenol yields) to predict the vitrinite reflectance but the application range is limited to the oil window (0.5 to 1.4% VR_o).

While a number of conceptual models have been reported in the literature, many petroleum companies have developed modeling programs for their own use. Many are based on modeling programs that are commercially available such as *Basinmod* (1992) and *Matoil* (1990). The basic requirements and products are similar. Input data requires accurate information regarding the stratigraphy, ages of rocks layers and layer thickness, as well as lithological information. In young and constantly subsiding basins, this information can be determined fairly accurately and directly by careful interpretation of geophysical logs and lithologic studies of core and drill-hole cuttings and measurements of bottomhole temperatures. In regions with more complex geological and subsidence histories, ages and durations of unconformities and estimates of age and thickness of the eroded intervals and variations in the geothermal gradient determined based on available geological information; this introduces a significant level of subjectivity into the process of basin modeling. Successful models are therefore built upon a comprehensive knowledge of the regional geology and geological history of an area.

In unmetamorphosed sequences, the maturation of sedimentary organic matter is a

product primarily of heating due to burial; the chemical composition evolves in a manner similar to coalification trends in coal-bearing sequences (Dow, 1977; Fig. 2b). The level of thermal maturation attained by the organic constituents is an irreversible expression of the maximum temperatures encountered on burial (Barker *et al.*, 1986; Barker, 1989) and therefore geochemical or petrographic parameters can be used to constrain the burial temperatures (Dow, 1977; Barker, 1983; Durand *et al.*, 1986; Barker & Pawlewitz, 1989). Geochemical maturity parameters which are relatively simple to determine routinely, such as Tmax, the temperature at which maximum hydrocarbon yield is obtained through laboratory pyrolysis of kerogen (Espitalié, 1986), or petrologic characteristics that reflect directly the chemical changes in the kerogen resulting from thermal alteration, such as vitrinite reflectance measurement (Teichmüller, 1982), are the most widely used. Vitrinite reflectance (VR_o) remains the preferred choice of maturation parameters used for modeling because it is relatively easy to obtain. Further discussion on the applicability and limitations on the use of vitrinite reflectance is given in the section on "Reflectance data in basin modeling". Most programs also incorporate the thermal conductivity of the rocks and compaction history of the rock layers into the model.

The modeling output files are commonly represented graphically by burial history curves and the oil window is superimposed showing the timing and history of hydrocarbon generation (Fig. 8).

Reflectance data in basin modeling

(i) Vitrinite

Most reflectance data can be obtained relatively easily from borehole core samples or drill cuttings; the samples require minimal pretreatment and measurements can be taken from samples with relatively low organic contents (<1%). The use of reflectance measurements is not limited to organic-rich, fine-grained rocks, but it can also be applied to organically lean sediments. Although the level of sophistication of basin modeling techniques has grown significantly in recent years (Larter, 1989), most programs continue to use vitrinite reflectance data (VR_o) to constrain the temperature because, despite limitations (Barker, 1985; Barker & Pawlewicz, 1985) and variability (Buiskool Toxopeus, 1983), it is probably the most definitive parameter (Price & Barker, 1985; Durand *et al.*, 1986). It is used to establish maximum burial temperatures and to define the

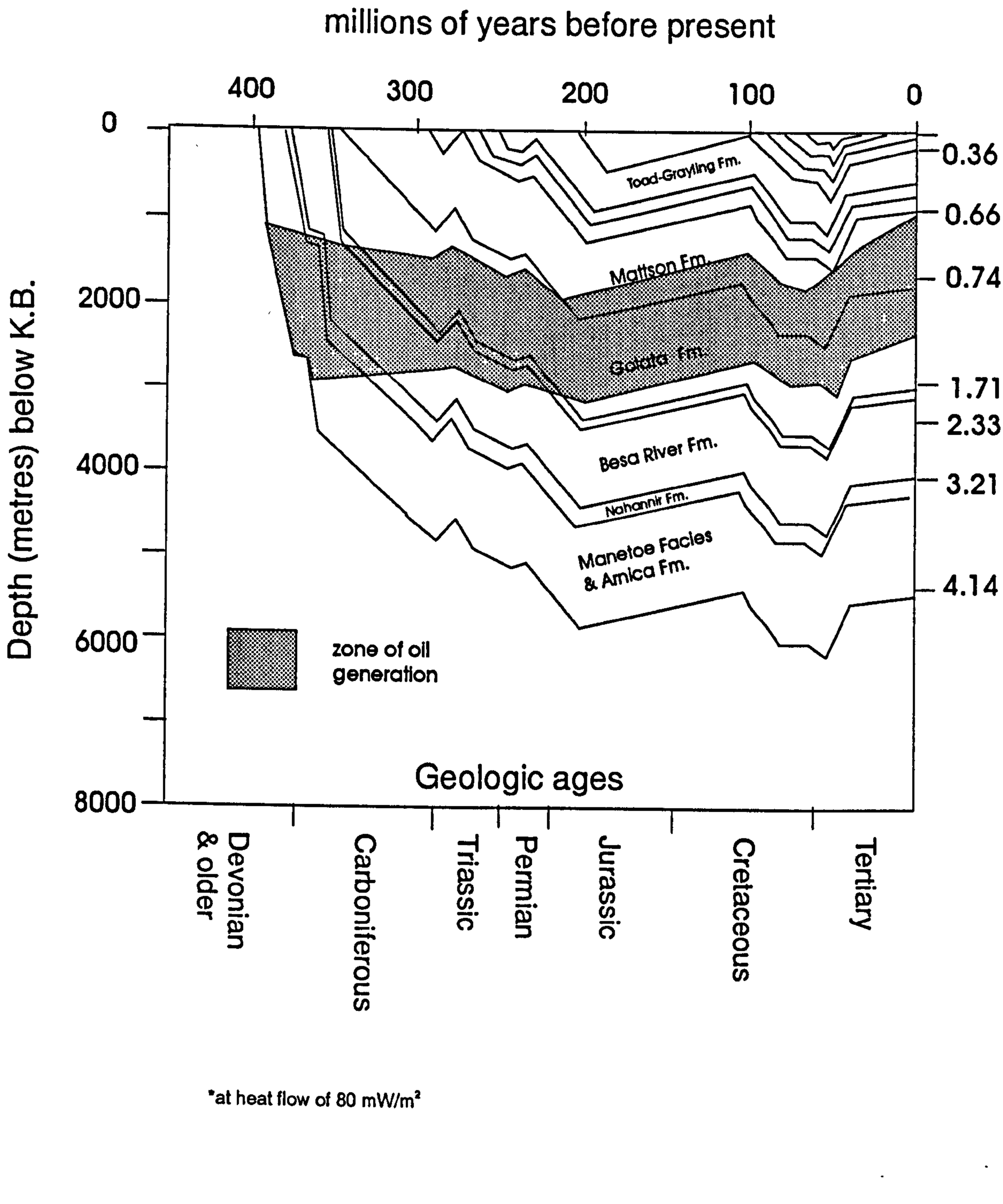

*at heat flow of 80 mW/m²

Figure 8. Hydrocarbon generation and burial history for the Pan Am Beaver River G-01 well (from Morrow *et al.*, 1993).

boundaries of the oil window (Dow, 1977; Fig. 2). However, Durand *et al.* (1986) caution that vitrinite reflectance should not be used to constrain the burial temperatures in basin modeling once the reflectance exceeds 2% VR_o because the kinetics are no longer the same.

The potential problems associated with the use of vitrinite reflectance are relatively well-known (Barker, 1983; Price & Barker,1985; Barker & Pawlewitz, 1985b; Durand *et al.*, 1987). In addition to the subjectivity of particle selection and the accuracy of measurement, it is clear that "vitrinite" in marine and lacustrine sediments has a different composition and maturation track to the vitrinite of coals derived from terrestrial plant remains (cf. Larter & Sentfle, 1985; Durand *et al.*, 1986). It has also been recognized that reflectance can be suppressed in liptinite-rich coals (e.g. Hutton & Cook, 1980; Kalkreuth, 1982). Price and Barker (1985) observed similar anomalies in source rocks rich in amorphous Type II kerogen, which they attributed to absorption of early-generated, hydrogen-rich hydrocarbons (vitrinite being still porous at low maturity). Apart from underestimation of source rock maturity, the effects of vitrinite suppression can result in significant overestimation of the amount of section eroded by extrapolation of the log Ro-depth profiles (Price & Barker, 1985).

(ii) Bitumen

Samples containing vitrinite are rare in the sample suite used in this study, due to both facies and stratigraphic controls on vitrinite occurrence; however, limited vitrinite reflectance data was obtained from surface sections in the northern part of the study area around the Tlogotsho Plateau. Most of the reflectance data are derived from indigenous bitumens and bitumen-like intermediate products or by-products of thermal maturation of liptinites; these may be analogous to the "prebitumens" of Jacob (1984) and "pre-oil" and "post-oil" bitumens of Curiale (1986). Although any organic components not originally deposited within the sediment are considered secondary according to the maceral concept (Teichmüller, 1982c), in this study they are considered as primary bitumens if they are indigenous to the source rock, i.e. generated *in situ*.

The use of bitumen reflectance as an indication of thermal maturation is well established. Jacob and Hiltmann (1985) related the reflectance of solid bitumens to that of vitrinite reflectance in coal-bearing sections in northwest Germany. Reidiger (1991)

correlated the reflectance of solid bitumens in the Triassic source rocks of the Western Canada Sedimentary Basin to Tmax, and Gentzis (1991) used Jacob's relationship (BRo = 0.618 × VR_o + 0.4; Fig. 9) to determine the thermal maturation in Palaeozoic and Mesozoic sediments in the Canadian Arctic. More recently, Landis and Castaño (1995) demonstrated strong correlations between "homogeneous" bitumen and vitrinite reflectance and bulk chemical properties of hydrocarbon source rocks. Therefore, while there is sufficient evidence in the literature to warrant the use of bitumen reflectance as an indicator of thermal maturation, it is apparent from the organic maturation studies conducted by Reidiger *et al.* (1989), Reidiger (1991) and Gentzis (1991) that several populations of bitumens may be present in organic-rich sediments but the selection of which bitumen population to use is subjective and thus somewhat arbitrary, being based on the middle reflectance range. This can result in significant errors in the estimation of organic maturation if bitumen reflectance data alone is used and not supported or substantiated by geochemical or additional petrographic data. In addition to the problems of relating bitumen reflectance to oil generation and thermal maturity, bitumen reflectance anomalies (R_o suppression) have been observed in sulphur-enriched source rocks (Fowler *et al.*, 1994). Koch (1997) has indicated that the upper limits for vitrinite and bituminite reflectance are 6% and 4% R_o random, respectively; similar limits may be applicable to bitumens.

In this study, the use of bitumen reflectance as a maturation parameter is investigated with respect to bitumen genesis and hydrocarbon generation models with a view to establishing criteria for obtaining the most reliable maturity data. For modeling purposes, all data are converted to VR_o equivalents using Jacob's relationship (Jacob, 1984) and whenever possible, are supplemented by Rock-Eval parameters (Tmax), palynological information (e.g. thermal alteration index, TAI, *sensu* Staplin, 1969) or conodont alteration indices (CAI *sensu* Epstein *et al.*, 1977). To this end, many different populations of bitumen have been examined within a variety of organic-rich and organic-lean rocks ranging in age from middle Devonian to Cretaceous, and spanning a broad range of thermal maturity (0.4%-4.5% VR_o).

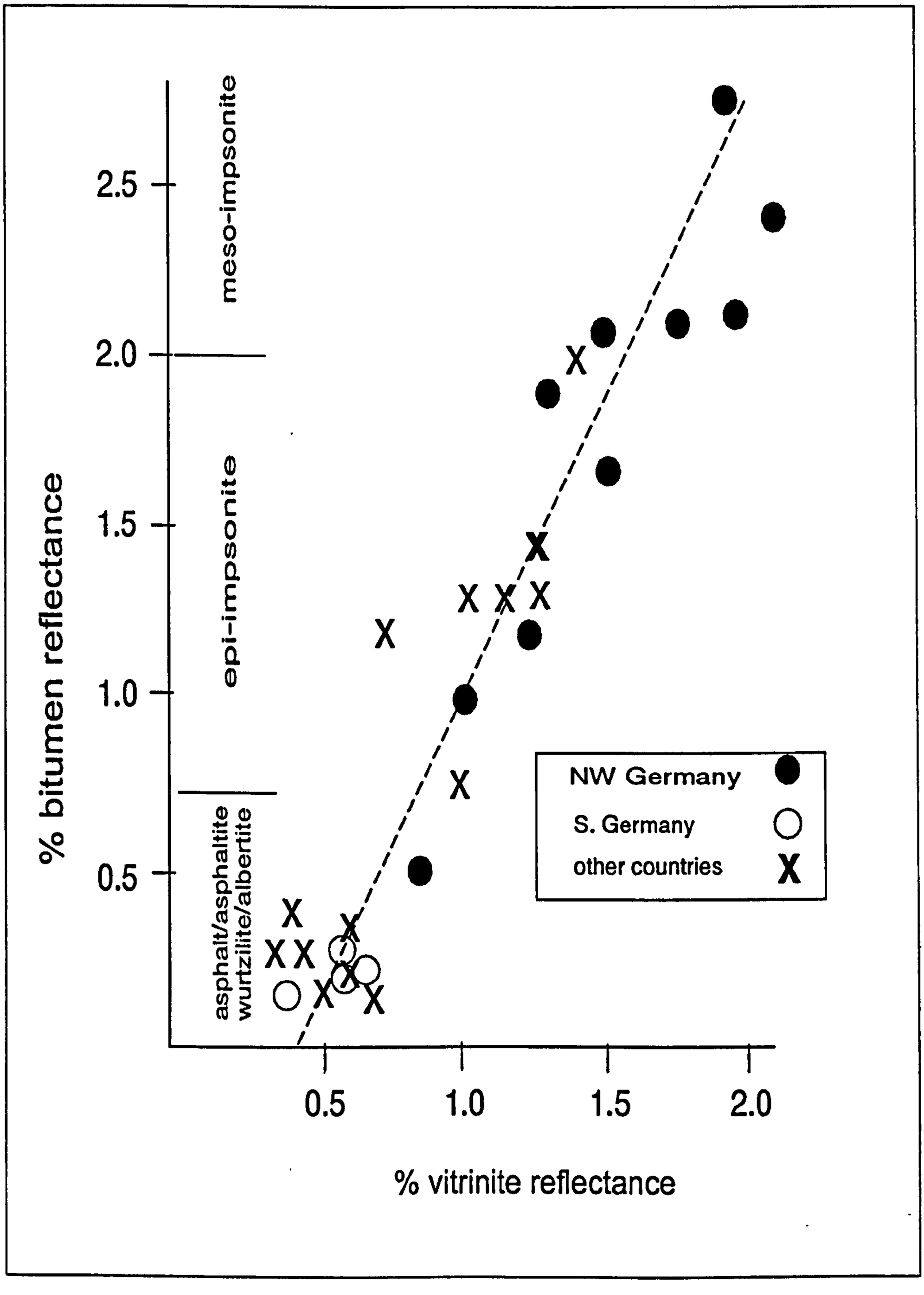

Figure 9. Jacob's relationship between vitrinite and migrabitumen reflectance (Jacob, 1985).

1.3 THE STUDY AREA

The study area is located on the western margin of the Interior Plains of Northern Canada between latitudes 59° 30' N and 61° 30' N and longitudes 121° 30' W and 125° 00' W and encompasses an area of approximately 40,000 km^2 (15,445 square miles). Geographically, this is the region drained by the Liard River and its tributaries, the Nahanni, LaBiche, Beaver, Jackfish, Muskeg and Petitot Rivers which span the southeastern Yukon Territory, the southwestern corner of the Northwest Territories (District of Mackenzie) and Northeastern British Columbia. It is a region of broad variations in physiography and geology. The western portion consists of the Liard Plateau, a mountainous region over 1500m above sea level (Torrie, 1973), the Kotaneelee Range and the Liard Range; the northern region comprises the southern tip of the Mackenzie Mountains (Douglas *et al.*, 1970) and the Nahanni Range; and to the east lies the Great Slave Plain (Fig. 10).

Geology and Stratigraphy

Most of the study area is shown on the Southern Mackenzie Mountains Map 1141A, Scale 1:506880) and includes the northern part of the Liard Basin (i.e. north of 59° 30'N) which is predominantly located in northeastern British Columbia. Geologically, the term "Liard Basin" refers to a major tectono-stratigraphic element, bound to the west by the Rocky Mountain Foothills and to the east by the Bovie Fault Zone (Fig. 10). Leckie *et al.* (1991) define "the Liard Basin" as the basinal structure located to the west of the Bovie Fault Zone (Fig. 1). Although it is recognized as a Tertiary Foreland Basin (Wright *et al.*, 1994), it is characterized by an anomalously thick wedge of Upper Palaeozoic carbonates and siliciclastic rocks (Gabrielse, 1967) and a forerunner of the Liard Basin, as it is known today, has therefore been in existence since Middle to Upper Devonian times (Peltzer, 1966).

To facilitate presentation and discussion of the results, the study area is broken down into two major components: the Liard Basin located to the west of the Bovie Fault Zone; and the Interior Plains/Platform, located to the east of the Bovie Fault Zone (Fig. 10). According to Richards (1989), the Upper Devonian and Lower Carboniferous basin-fill in the study area consists of "a thick, shallowing-upwards succession of continental

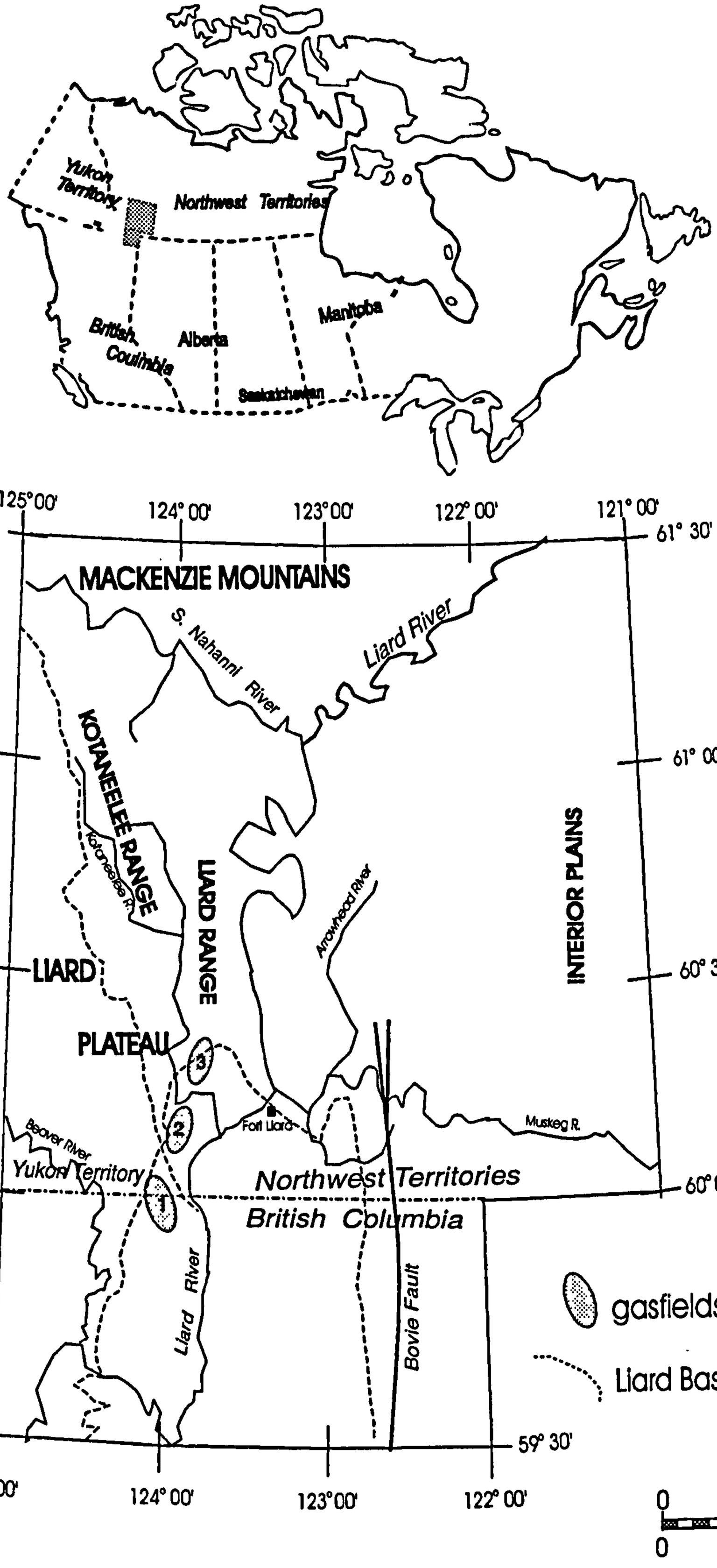

Figure 10. The study area showing geomorphic divisions (from Scott & Klassen, 1993) and gasfields (1 Beaver River; 2 Kotaneelee; and 3 Pointed Mountain; from Morrow *et al.*, 1993).

terrace deposits, which accumulated on the western margin of the downwarped North American Plate". Extensive surface exposure of the Upper Devonian and Carboniferous occurs within a series of north-south trending anticlines and synclines (Fig. 11) to the west which are capped by Cretaceous strata that thins to the south and east approaching the exposed Precambrian basement (Fig. 12).

The geology of the region is described by Douglas, (1959; 1976), Douglas *et al.* (1963), Douglas and Norris, (1960; 1976a; 1976b); and Harker (1961; 1963). The stratigraphy of the Upper Devonian of the Northwest Territories was described in detail by Peltzer (1966), Torrie (1973), de Wit *et al.* (1973) and Meir-Drees (1989); and in Northeast British Columbia, by Peltzer (1966) and Halbertsma (1959). The Carboniferous Mattson Formation was first described by Patton (1958). The Upper Devonian and Carboniferous stratigraphy and sedimentology in the region north of latitude 60° have subsequently been described in detail by Richards, (1983, 1989). The stratigraphic nomenclature used in this report follows that of Peltzer (1966), Torrie (1973), de Wit *et al.* (1973) and Richards (1989) and is summarized in Fig. 13.

While much of the study area formed part of an emergent land mass during the Lower Palaeozoic, shallow water sediments dominated by carbonates were deposited on a broad continental shelf (Mackenzie Shelf) over much of this area during the middle Devonian (Morrow & Geldsetzer, 1988). During Upper Devonian times, the Mackenzie Basin was established giving rise to a thick accumulation of basinal shales and siltstones of the Besa River Formation in the Liard Basin. During the same period, inner shelf deposits comprising shales and siltstones of the Fort Simpson Formation were deposited marginal to the cratonic platform in the Interior Plains to the east (Figs. 12 & 13). The Fort Simpson Formation is the basal unit of the Woodbend Group and is overlain by shallow water carbonates and siliciclastics (the Winterburn Group) that include the Redknife, Trout River, Tetcho and Kotcho formations. The Woodbend and Winterburn Groups were deposited within the platform (Morrow & Geldsetzer, 1988) following a brief period of deep water accumulation of siliciclastics that gave rise to black shales of the Muskwa Formation. The lower part of the Besa River contains two organic-rich, highly radioactive, black shale intervals which may be stratigraphically equivalent to the exceedingly organic-rich shales of either the Muskwa (Late Devonian) or Exshaw (Late Devonian-Early Carboniferous) formations (Figs. 13 & 14).

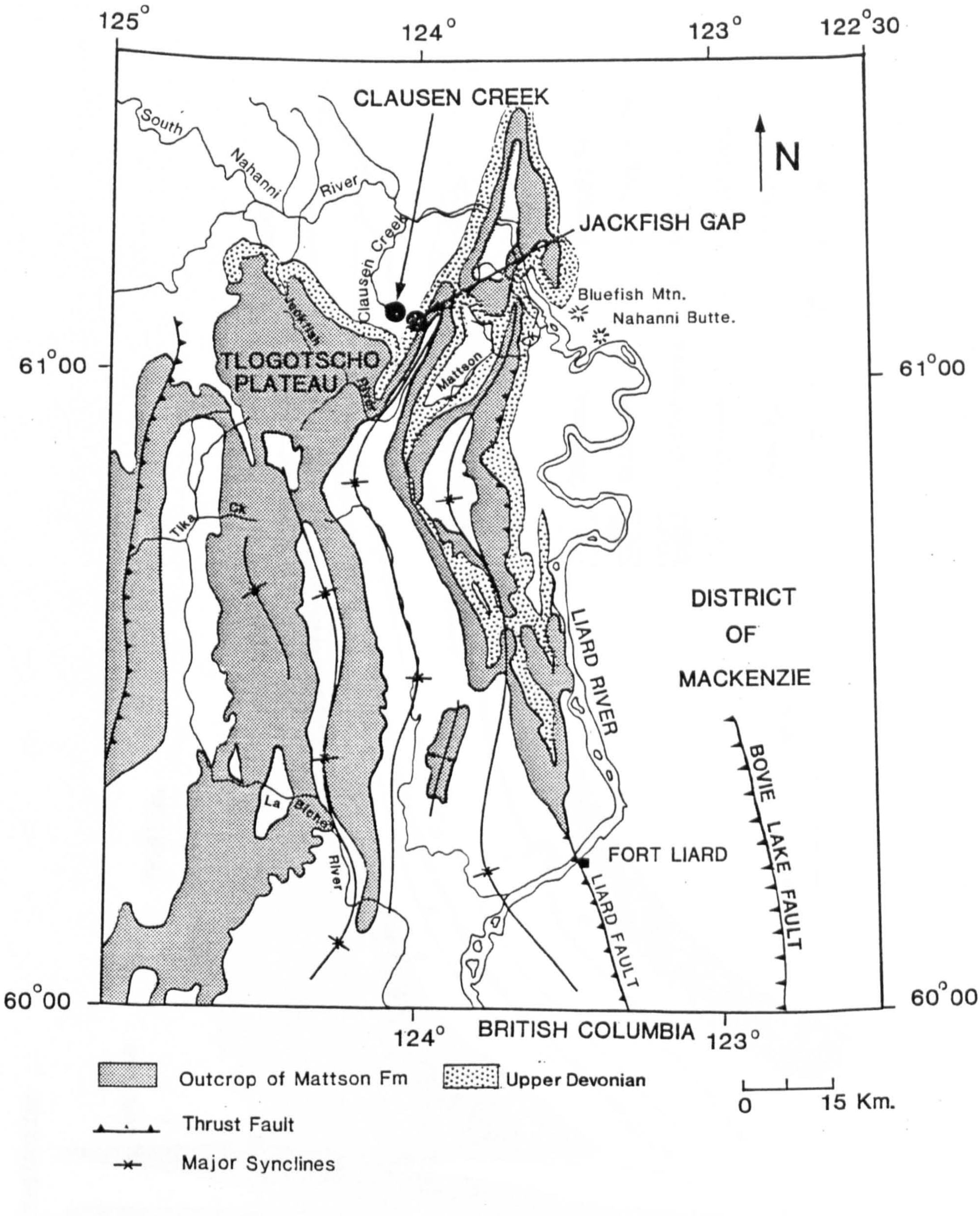

Figure 11. Surface geology of the Liard Basin in the Yukon and Northwest Territories (from Richards, 1989, modified).

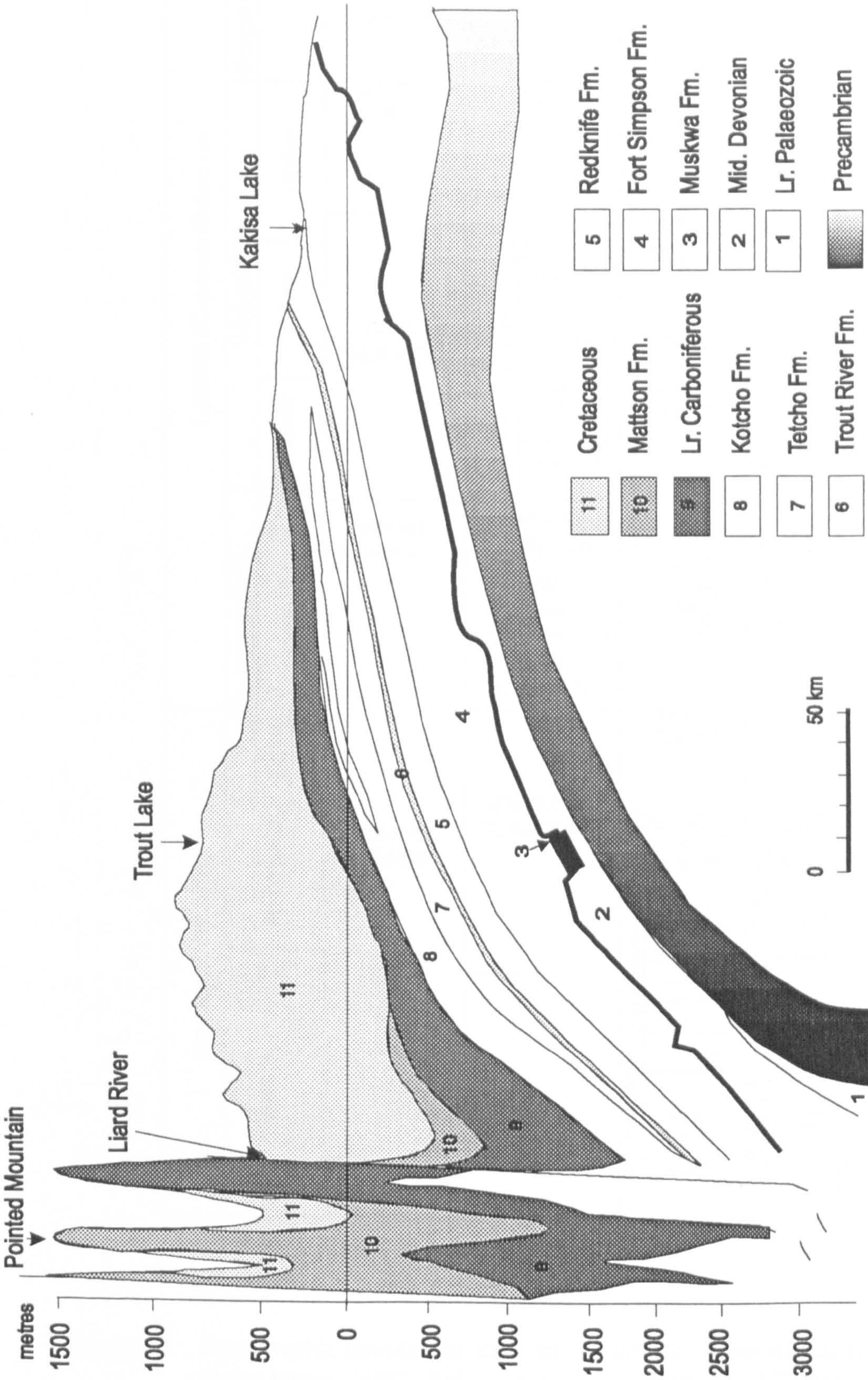

Figure 12. Cross section along latitude 60° 30' (from de Wit *et al.*, 1973, modified).

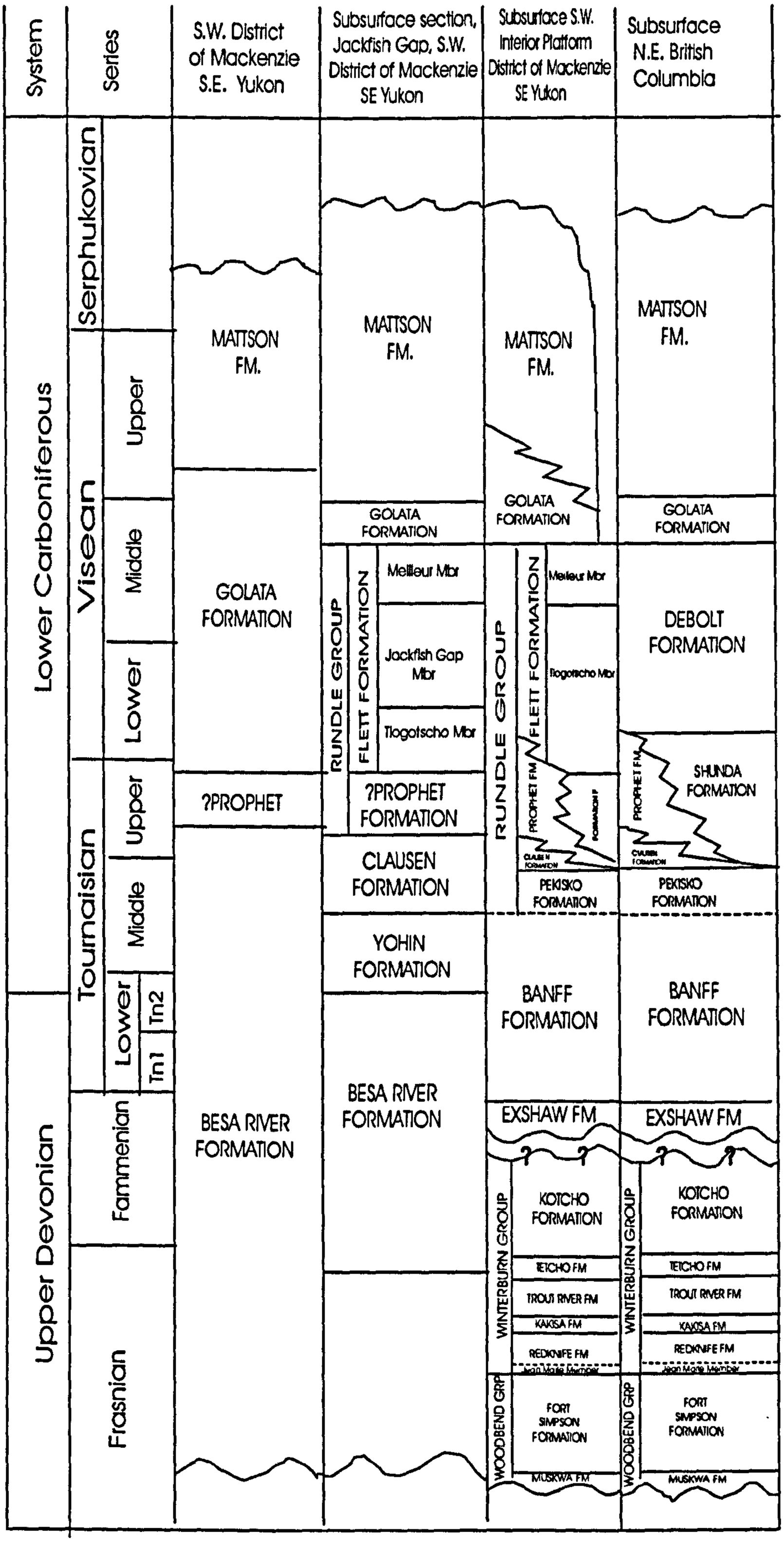

Figure 13. Stratigraphic column for study area; compiled from Richards (1989), Meier-Drees (1989), Belyea & Maclaren (1961) and Torrie (1974).

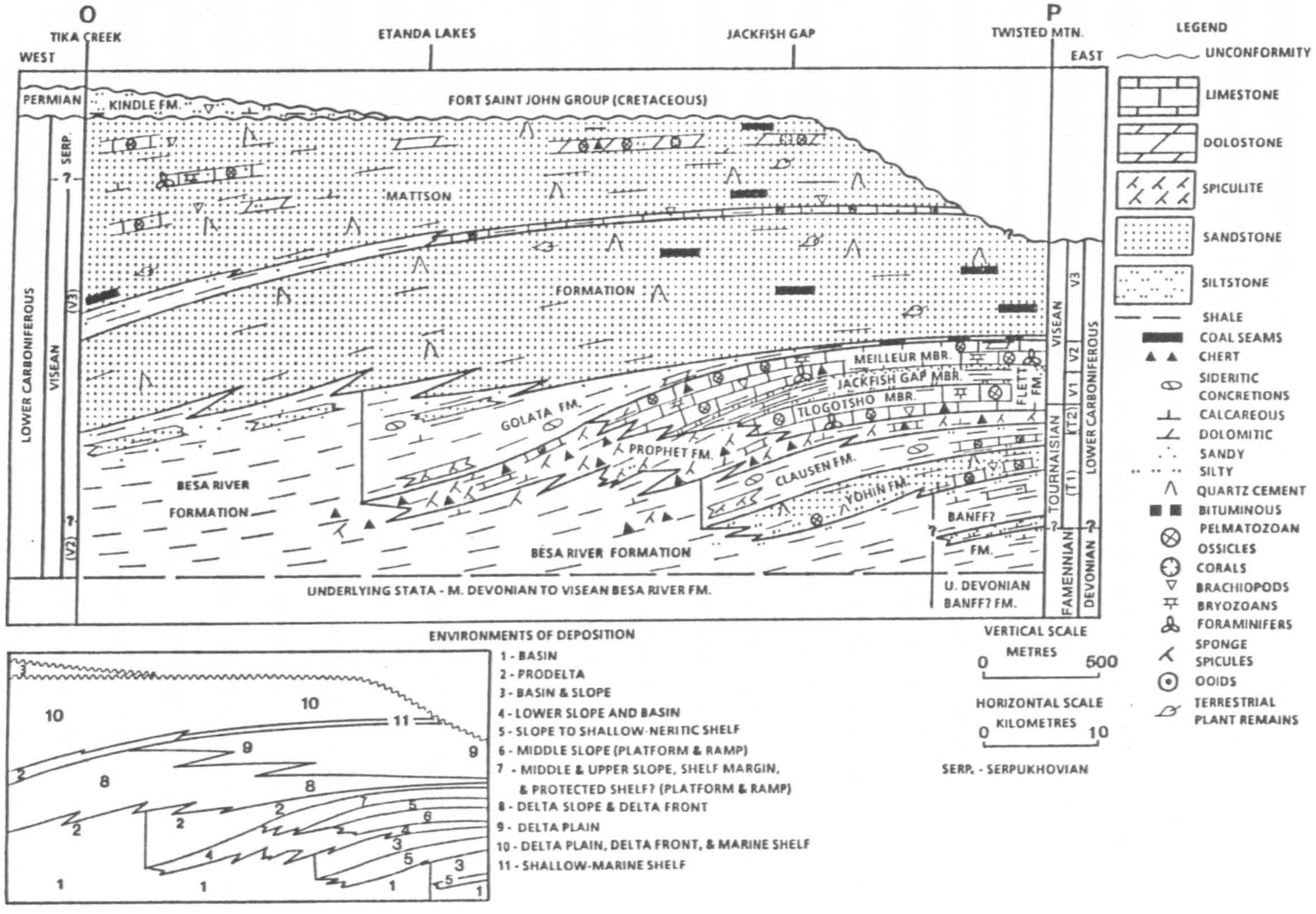

Figure 14. Schematic cross-section of the Lower Carboniferous in the Liard Basin, southwestern District of Mackenzie (Richards, 1989, Figure 7).

During Carboniferous times, a Carboniferous foreland basin, the Prophet Trough, developed on the western margin of the ancestral North American Plate marginal to the cratonic platform (Richards *et al.*, 1993) and occupied the western part of the study area. (The central section was formerly designated the Liard Trough by Douglas (1970) but subdivision of the trough has subsequently been abandoned.) Active subsidence within the trough during the Lower Carboniferous, resulted in an extremely thick accumulation of siliciclastics (Besa River) in the axis of the trough which intertongue north and eastwards with basin and shelf deposits of the Exshaw, Banff, Yohin, Clausen, Prophet and Golata formations; and with carbonate platform and ramp deposits of the Prophet Formation and the Rundle Group which formed marginal to the interior craton (Fig. 12).

The Lower Exshaw Formation (Fig. 15) is a thin (2-10 m), but laterally persistent, radioactive brown to black shale that was deposited in relatively deep waters of a dysoxic-anoxic basin (Richards, 1993) throughout most of the eastern part of the study area during late Fammenian to middle ?Tournaisian time. It is a prominent source rock found throughout the Alberta Basin to the south. In the study area, it is conformably overlain by basinal, calcareous shales of the Banff and Clausen formations, sandstone-dominated shelf deposits of the Yohin Formation and the prodelta shales of the Golata Formation.

An overall marine regression during Viséan times, culminated in the deposition of a thick sequence of deltaic deposits. The Mattson Formation (and its equivalent, the Kiskatinaw Formation in northeastern British Columbia), is a sandstone-dominated sequence of delta plain, delta front and shallow marine shelf deposits which includes shales, siltstones, thin limestones, delta top lacustrine/lagoonal shales and sapropelic coals (Potter *et al.*, 1993). This was followed by a significant period of emergence that led to the erosion or non-deposition of Upper Carboniferous strata throughout the region. Details of the stratigraphy, sedimentology and geologic and tectonic settings of the Lower Carboniferous are given in Richards (1983; 1989) and Richards *et al.* (1993).

The potential source rocks in the Upper Devonian-Lower Carboniferous succession in the study area are the basinal shales of the Muskwa, Besa River (Devonian-Carboniferous), Fort Simpson, Kotcho (Devonian), Exshaw (Devonian-Carboniferous), and Banff formations, plus the basinal, slope and pro-delta shales of the Clausen, Golata and Yohin formations and the delta-top shales and thin coals of the middle and upper Mattson Formation. Typically, these intervals give anomalously high gamma ray and low

IMPERIAL SUN ARROWHEAD I-46

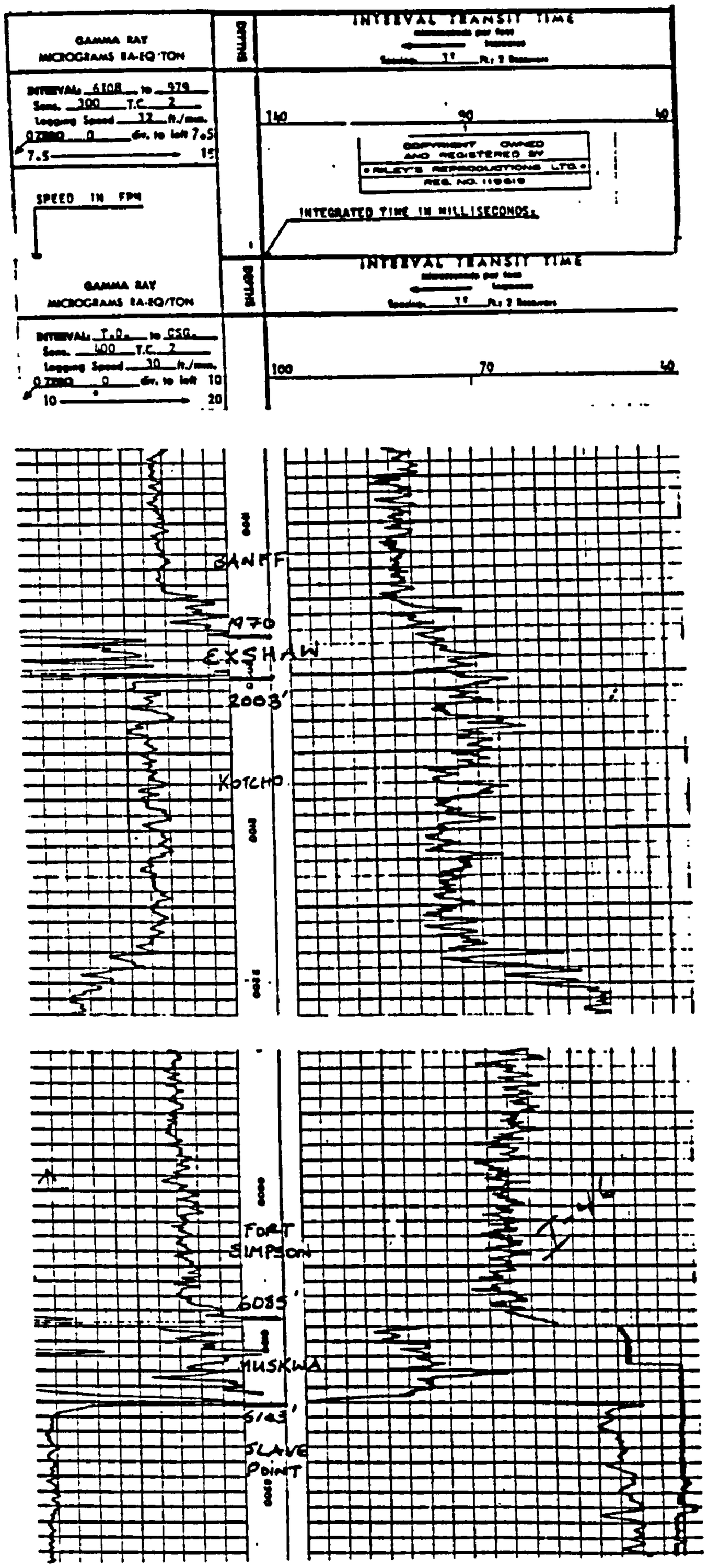

Figure 15. Gamma ray-sonic geophysical log signatures for the Exshaw and Muskwa formations in the Imperial Sun Arrowhead I-46 section.

sonic log signatures on geophysical well logs (Fig. 15).

Previous work

Palynological studies of the Golata and Mattson formations have been carried out by Staplin (1960), Braman and Hills (1977), Utting (1981) and Bamber *et al.* (1984); Hacquebard and Barss (1957) have also reported on the palynology of coals from the Mattson Formation south of the Nahanni River. Preliminary studies of the petrology of the coals were carried out by Cameron and Pratt (1982) but these were limited to reflectance and maceral group analysis of only two samples from the Jackfish Gap area. During the course of the present study, Potter *et al.* (1993) conducted a study of the reflectance and maceral composition of coals outcropping in the Jackfish Gap-Clausen Creek region, concluding that they were sapropelic coals of lacustrine origin that formed within the delta plain. Cameron *et al.* (1994) compared them to Lower Carboniferous coals found in the Hoiydahl Dome (northern Yukon) and Sverdrup Basin (Canadian Arctic).

Feinstein *et al.* (1988) conducted thermal maturity studies in the Mackenzie Corridor, Northwest and Yukon Territories which included Rock-Eval pyrolysis and reflectance data. Preliminary data on the organic petrology and maturity of potential source rocks in the Beaver River and Jackfish Gap areas of the Liard Basin were published by Potter *et al.* (1993). A broad regional study of the thermal history and organic maturation trends in Cambrian to Tertiary strata was carried out by Link and Bustin (1989) in the northern Yukon and northern District of Mackenzie between latitudes 65° and 69° N and longitudes 120° to 140° W. Source rock maturity was found to vary with structural complexity and the Lower Palaeozoic was overmature throughout the area. Basin modeling using vitrinite reflectance data from the Beaver River, Kotaneelee and Island River districts was interpreted by Morrow *et al.* (1993) to indicate high Palaeozoic heat flows and late Palaeozoic to early Mesozoic maturation and migration of oil and gas. More recently, Morrow and Gallagher (in press) have reinterpreted some of this data using inverse modeling procedures.

2.0 ANALYTICAL METHODS

2.1 SAMPLING PROCEDURES

Upper Devonian and Lower Carboniferous shale, marl and siltstone samples were collected from outcrop localities in the north and west, and from 40 subsurface borehole sections throughout the study area (Fig. 16). The outcrop samples were collected primarily from thick exposures of the Besa River and Mattson formations at Jackfish Gap (type section of the Mattson Formation), Yohin Ridge, Clausen Creek and Tika Creek by Dr. B.C. Richards of the Geological Survey of Canada during the course of several field mapping projects in the southeastern Yukon and southwest District of Mackenzie. The subsurface samples were collected by the author, predominantly from drill cuttings obtained from exploration wells drilled between 1958 and 1993. Samples were also obtained from cored intervals in the Lower Carboniferous (Mattson Formation) in a limited number of wells. In the subsurface sections, Cretaceous and Permian samples were collected in addition to samples from the Upper Devonian and Lower Carboniferous in order that vertical reflectance profiles could be constructed for the whole section and relatively complete reflectance data sets could be obtained for basin modeling. Figure 16 shows the sampling locations; the UTM coordinates of all sample locations numbers of samples collected at each are listed in Table 1 and stratigraphic intervals sampled at each locality are shown in Table 2.

Samples were selected on the basis of organic richness. Gamma ray and sonic geophysical logs (Fig. 15) were used to infer intervals with TOC contents >0.5%. Shales, marls, siltstones and coals were preferentially selected to reduce the potential for reworked organic matter. When plentiful drill cuttings were available, the samples were washed and air dried and approximately 50g were collected for petrographic analysis, Rock-Eval pyrolysis and TOC analysis. Sample sizes were restricted to 5-10g of cuttings in sections where small, washed sample sets were available, due to provincial (B.C.) and Canadian Federal government regulations governing sampling. In such cases, only petrographic analyses were carried out. All samples were hand-picked and representative splits were used for petrographic analysis and Rock-Eval-TOC determinations.

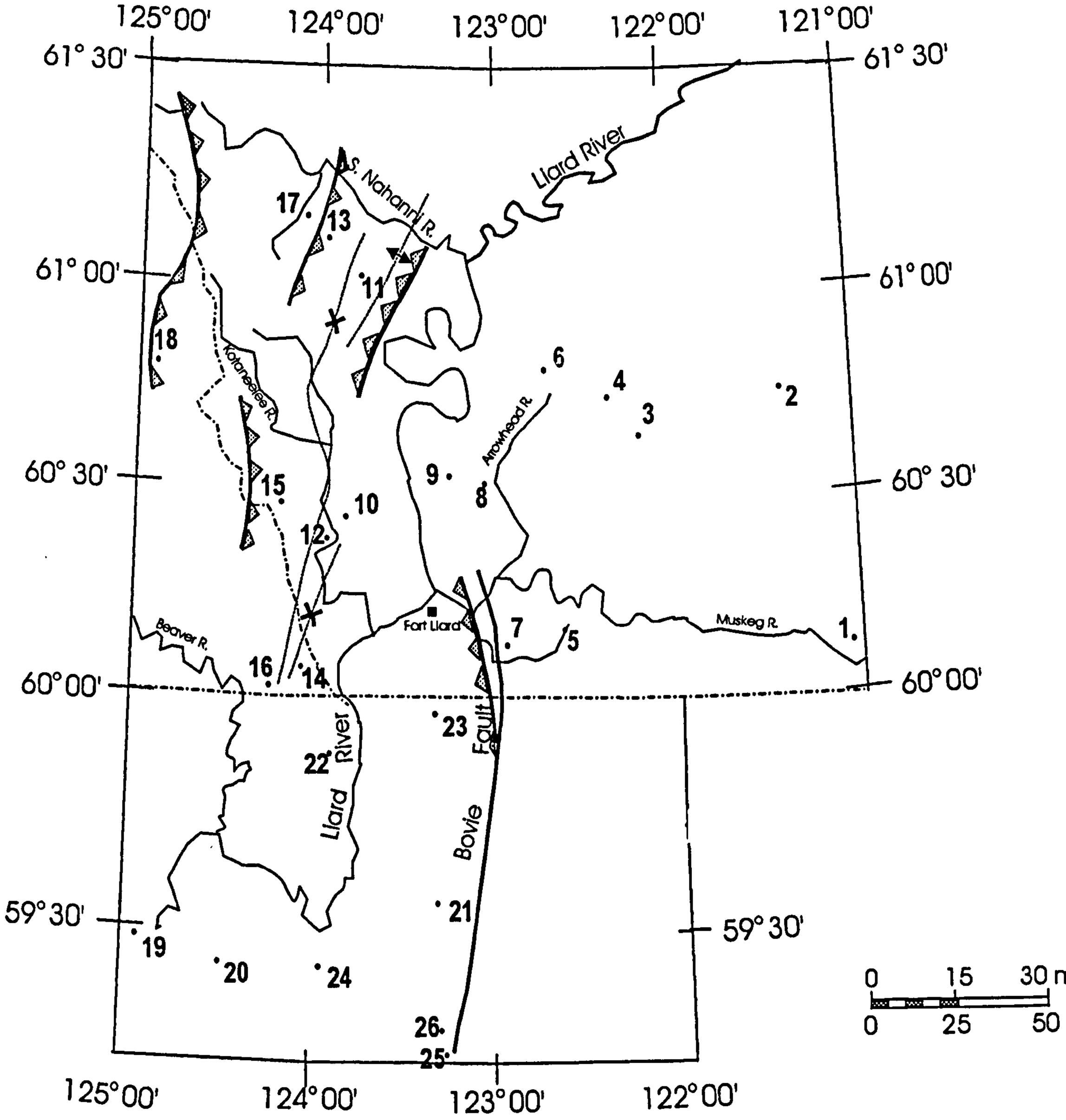

Figure 16. Sample location map.

Sec	Well name	Location	Number of Samples [2]		GSC #	Type of Analysis carried out			
#[1]		latitude longitude	Cuttings[2]	Cores[2]		PQ [3]	VRo	REv	TOC
1	Imperial Island River No.1	N60° 09' 19" W121° 08' 16"	15 (13)	51 (32) + 41[3]	C186751	65 (?)	65	36	36
2	Dome *et al.* Trout Lake H-45	N60° 44' 20" W121° 22' 44"	15 (14)		C186768	15	15	10	10
3	Murphy *et al.* Muskeg River No.1	N60° 43' 38" W122° 03' 45"	18 (16)		C186767	18	18	18	18
4	Imperial Sun Arrowhead I-46	N60° 45' 37" W122° 22' 47"	13 (10)	10 (8) + 9[3]	C186757	23	23	0	0
5	Pan Am Home Signal Celibeta No. 7	N60° 09' 24" W122° 37' 44"	27 (25)		C186765	27	27	16	16
6	Imperial Sun Netla C-07 (F-7)	N60° 46' 15" W122° 46' 15"	21 (17)		C186764	21	21	12	12
8	Texaco NFA Bovie Lake J-72	N60° 11' 39" W122° 58' 44"	33 (31)	2	C186762	33	33	33	33
8	Texaco Arrowhead N-2	N60° 31' 46" W123° 01' 18"	26 (23)		C186758	24	24	18	18
9	Amoco East Flett H-13	N60° 32' 28" W123° 17' 15"	8 (6)		C186759	8	8	6	6
10	Amoco Pointed Mountain P-24	N60° 48' 54" W123° 48' 57"	11 (8)		C186760	11	11	8	8
11	Pan Am Mattson Creek A-1	N60° 02' 01" W123°48' 03"	12		C1867--	12	12	1	1
12	Pan Am Pointed Mountain P-53	N60° 22' 46" W123° 54' 34"	30 (29)		C186766	30	30	29	29
13	Jackfish Gap-Yohin Ridge	N61° 06' W123° 59'		40 (39)		39	39		
14	Canada Southern *et al.* N. Beaver R. I-27	N60° 07' W124° 04'	34 (30)		C186754	34	34	34	34
15	Pan Am Kotaneelee	N60° 26' 51" W124° 11' 56"	16 (14)		C186755	16	16	16	
16	Pan Am Beaver G-01	N60° 00' 25 W124° 15' 48"	36 (28)	15 (4)	C186752	33	33	24	24
17	Clausen Creek	N61° 08' 01" W124° 02' 01"		11 (11)		11	11	11	11
18	Tika Creek	N60° 43' 47" W124° 53' 29"		27 (27)		27	27	15	15

Table 1 Sampling locations, sample numbers and analyses.

	Aquitaine *et al.* Tatoo	a-2-H NTS 94-O-11		6 (6)	C186775	6 (5)	6	6	6
23	Arco Maxhamish [5]	b-21-K NTS 94-O-14	15 (1)		C186776	15	15		
	Amin-Aquitaine Windflower	d-87-A NTS 94-O-11		5 (5)	C186773	5 (7)	5		
21	IOE Pan Am Viscount	a-77-d NTS 94-O-11	21 (6)	30 (14)	C186771	16 (8)	16	16	16
	GDP Noel Poplar [5]	d-35-G NTS 94-O-4	11 (2)		C186778	11	11		
22	Imperial Pan Am LaBiche	b-55-E NTS 94-O-13	24 (7)	14 (4)	C186772	38	38	18	18
	Amoco *et al.* LaBiche [5]	a-67-D NTS 94-O-13	14 (1)		C186777	14	14		
20	Imperial IOE Dunedin	a-75-E NTS 94-N-8	21		C186770	21	21	16	16
19	Central Leduc Toad River No.1	c-10-E NTS 94-N-7		13 (10)	C186774	13	13		
	Total		421	224		610	610	343	343

[1] section numbers used in Fig. 15
[2] number in column 3 is the total number of samples collected and analyzed for VRo and Rock-Eval-TOC; number in parentheses indicates the number of Upper Devonian and Lower Carboniferous samples analysed
[3] P-Q = qualitative organic petrology; number in parentheses indicates samples for palynology
[4] indicates samples collected for CAI analysis
[5] RockEval -TOC data made available by Canadian Hunter Exploration Ltd.

Table 1 (continued).

		[2] M. Dev	Upper Devonian[2]								Lower Carboniferous[2]								Per	Lr K
#[1]	**Well name**		M	FS	RK	TR	Te	UD	Ko	BR	Ex	Bf	Yo	Cl	Pr	Fl/ F	Go	Ma	K/F	FSJ
1	Imperial Island River No.1		X	X	X	X	X		X		X	X								X
2	Dome *et al.* Trout Lake H-45		X	X	X				X		X	X								X
3	Murphy *et al.* Muskeg River No.1		X	X	X	X	X	X	X		X	X								X
4	Imperial Sun Arrowhead I-46	X	X	X	X	X		X			X	X								
5	Pan Am Home Signal Celibeta No. 7	X	X	X	X	X	X	X	X		X	X		X	X	X			X	X
6	Imperial Sun Netla C-07 (F-7)	X	X	X	X	X		X	X		X	X								
7	Texaco NFA Bovie Lake J-72		X	X		X	X	X	X		X	X		X	X	X		X	X	
8	Texaco Arrowhead N-2			X	X	X		X	X		X	X		X	X	X		X		X
9	Amoco East Flett H-13													X	X	X				
10	Amoco Pointed Mountain P-24																	X	X	X
11	Pan Am Mattson Creek A-1	X		X				X				X								
12	Pan Am Pointed Mountain P-53	X								X					X	X	X	X		X
13	Jackfish Gap-Yohin Ridge												X	X	X	X	X	X		
14	Canada Southern *et al.* N. Beaver R. I-27									X					X		X	X	X	
15	Pan Am Kotaneelee									X					X		X			X
16	Pan Am Beaver G-01	X								X					X		X		X	X
17	Clausen Creek									X					X			X		
18	Tika Creek									X								X		

Table 2 Upper Devonian and Carboniferous stratigraphic intervals sampled Liard Basin, north of latitude 59° 30' N.

	Stratigraphy	[2] M. Dev.	Upper Dev.[2]	Lower Carboniferous[2]							Perm[2]		Trias[2]	Cretaceous[2]	
														Lr.	Up.
#[1]	Well Name		BR	Bf	Pe	Cl	Pr	De	Go	Kis	TF	Be	T-G	FSJ	D/W/K
	Aquitaine *et al.* Tatoo a-2-D									X					
23	Arco Maxhamish b-21-K									X	X	X	X	X	
	Amin-Aquitaine Windflower d-87-A									X					
21	IOE Pan Am Viscount a-77-D			X		X		X	X	X	X	X	X	X	X
	GDP Noel Poplar d-35-G								X	X		X	X	X	X
22	Imperial Pan Am LaBiche b-55-E									X	X	X	X	X	
	Amoco *et al.* LaBiche a-67-D									X		X	X	X	X
20	Imperial IOE Dunedin a-75-E									X	X	X	X	X	
19	Central Leduc Toad River No.1	X	X							X					

[1] section number used in Fig. 15;
[2] M. Dev = Mid. Devonian; M=Muskwa Fm.; FS = Fort Simpson Fm.; RK = Redknife Fm.;TR = Trout River Fm.; Te = Tetcho Fm.;UD = Undifferentiated Upper Devonian shales; Ko = Kotcho Fm.; BR = Besa River Ex = Exshaw Fm.; Bf = Banff Fm.; Pe = Pekisko Fm.; Yo = Yohin Fm.; Cl = Clausen Fm.; Pr = Prophet Fm.; De = Debolt Fm.; Fl = Flett Fm. or Formation F.; Go = Golata Fm.; Ma = Mattson Fm.; Kis = Kiskatinaw Per = Permian (Kindle, Fantasque);TF = Taylor Flat Fm.; Be = Belloy Fm; T-G = Toad -Grayling fms.; LrK = Lr. Cretaceous (Fort St. John Gp); UpK = Upper Cretaceous; .D = Dunvegan-Fort Nelson Fms.; W = Wapiti Fm.,K = Kotaneelee Fm.

Table 2 (continued).

2.2 SAMPLE PREPARATION

Sample splits were prepared for Rock-Eval by crushing whole rock cuttings to a fine powder with a mortar and pestle. For petrographic analysis, no size reduction of the cuttings was employed except for core and outcrop samples. In this case, oriented blocks or particulate samples were prepared by crushing to -20 mesh size (= 840μm).

For petrography, particulate and oriented block samples were made into epoxy pellets by placing the sample into one inch diameter Metaserv molds and impregnating with Beuhler epoxide resin. The surface of the cured pellets was ground off automatically on a Beuhler Automet wheel using 240, followed by 600 grade carborundum grits and distilled water as the lubricant, under approximately 35lbs pressure. The pellets were then polished for 3-4 minutes using a similar procedure and increasingly finer grades of alumina powders: 0.3 μm alumina (with distilled water on Texmet paper) followed by 0.05μm alumina (with distilled water on silk). The samples were thoroughly washed with water between each of the polishing and grinding stages (*cf.* Pratt, 1986), the final washing being done in an ultrasonic bath. Finally, the samples were air-dried.

2.3 ORGANIC PETROLOGY

Qualitative organic petrology of polished core and whole rock cuttings samples were carried out using a Zeiss Universal (UMSP) incident light microscope equipped with white light (12V 50W halogen) and fluorescent light sources (HBO 100W) using a x40 epiplan- neofluor oil immersion objective. Samples were alternatively observed in plane-polarized white light and then blue light, the latter using a 400-440nm excitation filter (with 460nm beam splitter and 470nm barrier filter) and non-fluorescing immersion oils (n = 1.812 at 25°C). The principal lithology of the rock matrix was assessed microscopically and coded according to the scheme in Table 3.

Numeric code	1	2	3	4	5	6	7	8	9
Rock type	carbonate	calc.[a] shale	marl	carb.[b] shale	shale	cherty shale	carb.[b] siltstone	siltstone (lean)	coal

[a]calc. = calcareous [b]carb. = carbonaceous

Table 3 Numeric codes for rock matrix lithology (see Appendix A, Tables 1-13).

Optical identification of the various macerals in coals and source rocks is based on internationally- recognized definitions described in ICCP handbooks (1963, 1971, 1975, 1995) and Stach *et al.* (1982); brief descriptions are given in Table 4. Because organic richness is measured using a significantly more accurate method (section 2.3), no attempt is made to determine the abundance of the various maceral species using petrographic methods except to indicate the dominant and subordinate kerogen types. This follows the findings of Powell *et al.* (1982), who indicated that the abundance of amorphous organic matter in kerogen concentrates is commonly overestimated by petrographic methods, and that of Cole (1993) who demonstrated that there was no correlation between TOC and visually-determined estimates of kerogen abundance in whole rock samples. Many samples contained only bitumens (no primary macerals) and the TOC values were less than 1%, so only the ranked relative abundances of organic components were assessed visually. These appear in the samples descriptions given in Appendix C.

Reflectance measurements were carried out on selected alginite, sporinite, vitrinite and bituminite macerals together with all identified bitumen populations. Random reflectance (R_om) measurements were carried out using a Zeiss Universal microscope-photometer system and polarized, monochromatic light (546nm). Schott precision glass and diamond standards were used to calibrate the instruments before, after and mid-way through each analysis, in accordance with standard procedures (Mackowsky, 1983; ICCP, 1975, Bustin *et al.*, 1983). For coals, the mean random reflectance values quoted are based on a minimum of one hundred measurements on each maceral type. For dispersed organic matter, mean random reflectance is determined from between 5 and 50 measured values (Appendix D). The reflectance data were collected and processed using an HP personal computer and Zeiss "Coflex" software. In samples of elevated maturity, apparent R_{max} and R_{min} were determined on high grade bitumens to establish individual bitumen populations displaying significant optical anisotropy (bireflectance); however, true R_{max} and R_{min} can only be determined on samples oriented parallel to bedding (Davis, 1978).

Classification of indigenous solid bitumens

Petrographic identification of solid bitumens can only be accomplished using whole rock samples and is based on relative differences in the optical properties, i.e. reflectance and fluorescence and the morphology by virtue of association with the primary organic

Reflected light	Transmitted light	Multimode illumination
huminite/vitrinite collotelinite* detrovitrinite*	woody	vitrinite
inertinite fusinite semifusinite funginite** macrinite micrinite inertodetrinite	coaly	inertinite
liptinite sporinite cutinite suberinite resinite chlorophyllinite liptodetrinite	herbaceous	liptinite
alginite	algal	
bituminite exsudatinite	amorphous	amorphinite
faunal relicts		faunal relicts
mineral-bituminous groundmass (matrix bituminite)***	amorphous	bituminous mineral groundmass bitumen
Teichmüller & Ottenjann (1977); * ICCP (1995); ** ICCP, 1998; *** Creaney (1980)	Burgess (1974)	van Gijzel (1979); Sentfle *et al.* (1987), modified

Table 4 Classification of coal and source rock macerals (from Sentfle *et al.*, 1996; modified).

components and the rock matrix. All solid bitumens are amorphous in nature and the shape of the bitumen mass assumes the shape of the space or pore that it occupies; the size can therefore vary from fractions of a micrometre to fractions of a metre depending on the mode of origin or emplacement. Two classes of bitumens are recognized in this study: indigenous (or primary) bitumens and migrated (or secondary) bitumens. The migrated bitumens are pore, microfracture- or vein-filling solids whose geochemical and optical properties are completely independent of the organic components of the rock in which they are found. It is the indigenous bitumens which are important from the aspect of hydrocarbon generation and thermal maturity.

The indigenous bitumens are those which are generated within the source rock as a consequence of organic maturation of primary or secondary macerals (Table 5). A variety of different forms are illustrated in Plates I to V and their unique properties are described below. The various populations of indigenous bitumens observed in Devonian to Upper Cretaceous strata in the study area can be distinguished on the basis of reflectance and fluorescence differences. Low, medium and high reflectance populations are recognized. Further subdivision into bitumen types is based on morphological, optical and genetic characteristics, i.e. differences in morphology, reflectance, fluorescence properties and affiliation with other organic components.

The low reflectance bitumens (types 1, 2 & 3) are found in relatively lean (less than 0.5% TOC) shales and siltstones as well as rocks with higher TOC values. Types 1 and 2 are related to primary liptinite macerals (alginite, sporinite); they are typically massive or homogeneous in nature. They show weak fluorescence when observed in blue light and are directly spatially associated with the precursor macerals, usually occupying microporosity in the matrix marginal to the primary maceral, or internal porosity which is interpreted to have been created by shrinkage of the original kerogen as hydrocarbons and bitumen were generated through thermal maturation. In the case of alginites, the bitumen commonly forms a thin rind or film on the surface. With thin stringers of lamalginite, the bitumen lies within the plane of the bedding, on the surface of the alginite itself (Plates II and III). Bitumens associated with sporinite, occur as a coating on the surface or enclosed within the spore lumina (Plate III). The reflectance and fluorescence of the bitumen is used to distinguish types 1 and 2. Type 1 typically shows low reflectance, rarely more than 0.04 $\%R_o$ greater than the R_o of the primary maceral, and exhibits weak yellow-brown fluorescence with

Relative reflectance*	Reflectance increasing----------▸					
	low Ro			medium Ro	high	very high
Bitumen type	1	2	3	4	5	6
Maceral affiliation	alginite sporinite	liptinite-bituminite transition	bituminites I & II**	mineral-bituminous matrix***	early hydrocarbons	pyrobitumens

* Gentzis, 1991; ** Teichmüller & Ottenjann, 1977; *cf.* amorphinite (van Gijzel, 1959; Sentfle *et al.*, 1987); *** Robert (1981); cf. matrix bituminite (Creaney , 1980).

Table 5 Petrographic and genetic classification of solid bitumens.

slight positive alteration. The reflectance of the type 2 bitumen is typically an order of magnitude greater than type 1, between 0.1 and 0.25% greater than the primary maceral, and shows weak brown fluorescence but no alteration. Stasiuk (1991) and Stasiuk and Osadetz (1993) and Stasiuk and Fowler (1994) have observed similar materials in source rocks in the Ordovician of the Williston Basin and the Devonian of the Canadian Arctic, considering them to be alginite-bitumen transitional macerals.

Low reflectance bitumen (type 3) is related to the secondary macerals termed bituminites I and II by Teichmüller (1978); the bitumen associated with bituminite I is commonly homogeneous while that associated with bituminite II is commonly granular or microporous in nature and has poorly defined margins that diffuse into the associated bituminite (Plate IV). Neither of the type 3 bitumens show fluorescence under blue light. These bitumens are found in close proximity to, or directly in contact with, the precursor macerals and occupy porosity created by geochemical alteration of the kerogen structure as hydrocarbon and bitumens are generated through thermal degradation.

Medium reflectance (type 4) bitumen is observed only in shales and siltstones with TOC values greater than 0.5% and is associated with the amorphous mineral-bituminous groundmass (Robert, 1981; *cf.* matrix bituminite, Creaney, 1980). It is typically homogeneous in nature and occurs in small pods (rarely greater than 50 µm in diameter) within the mineral-bituminous matrix of shale interstices or laminae (Plate V). The margins are well defined and these bitumens commonly occupy pore space in which euhedral to subhedral dolomite crystals are also present. The reflectance is in the order of 0.3% R_o greater than the type 3 bitumen for a rock whose vitrinite reflectance equivalent falls in the peak of the oil window (ca. 0.85% R_o). No fluorescence is observed in either blue or UV light.

The high reflectance bitumens (types 5 & 6) are homogeneous with well defined margins and occur within the organic-mineral matrix of shales and within the shaley interstices of silty shales and within the intercrystalline porosity of siltstones. They are related by reflectance to the other indigenous bitumens but have a reflectance an order of magnitude greater than them (Plate V) and do not show fluorescence. They are interpreted to be either by-products of early generation formed through polycondensation reactions in hydrocarbons generated during late diagenesis or early catagenesis. These highly reflective bitumens are referred to in this study as pyrobitumens (Table 5). The organic affiliations and

modes of genesis of the indigenous bitumens will be discussed in more detail in Chapter 3.

Vitrinite and vitrinite reflectance equivalent values derived from the indigenous bitumens are used to determine thermal maturity of the kerogen in potential Upper Devonian and Lower Carboniferous source rocks in terms of the oil and gas windows defined by Dow (1977)(Fig. 2b).

2.4 ROCK-EVAL

Selected cuttings, core and outcrop samples were analyzed, in-house, at GSC Canada-Calgary[1], with a Delsi Rock-Eval II pyrolysis unit equipped with a Total Organic Carbon (TOC) analysis module; consequently, "Rock-Eval" analyses herein refer to TOC as well as the conventional pyrolysis parameters. Weighed (100mg) samples of powered rock were inserted into the sample carriage and then transferred into the pyrolysis oven where pyrolysis and subsequently, oxidation, take place. Duplicate runs were carried out on each sample using procedures described by Espitalié *et al.* (1977) and Espitalié (1986). The instruments were calibrated using 100mg IFP standards at the beginning, and after every fifteen runs.

Rock-Eval programmed pyrolysis takes place in an inert atmosphere (helium) at a preselected rate of heating, and occurs in three stages: 1) volatilization of the free gaseous and liquid hydrocarbons, at 300° C - detected by a flame-ionization detector and recorded as the S1 peak; 2) thermal cracking of the heavy hydrocarbons and insoluble kerogen between 300° and 600° C, yielding lighter hydrocarbons which are also detected by the flame ionization detector, and recorded as the S2 peak; and 3) desorption of CO_2 adsorbed on to the molecular sieve which is detected by a thermal conductivity detector, yielding the S3 peak. Figure 17 shows a hypothetical pyrogram illustrating the relative distributions of the S1, S2 and S3 peaks.

Oxidation occurs in two stages: 1) combustion of the rock produces CO_2 which is adsorbed on to a molecular sieve in the TOC module at 70° C ; 2) desorption of CO_2 on the molecular sieve by reheating at 250° C and passing it to a conductivity detector within the TOC module, yielding an S4 peak. The S4 peak is not normally cited separately in the

---

[1]Geological Survey of Canada-Calgary, formerly the Institute of Sedimentary and Petroleum Geology (ISPG)

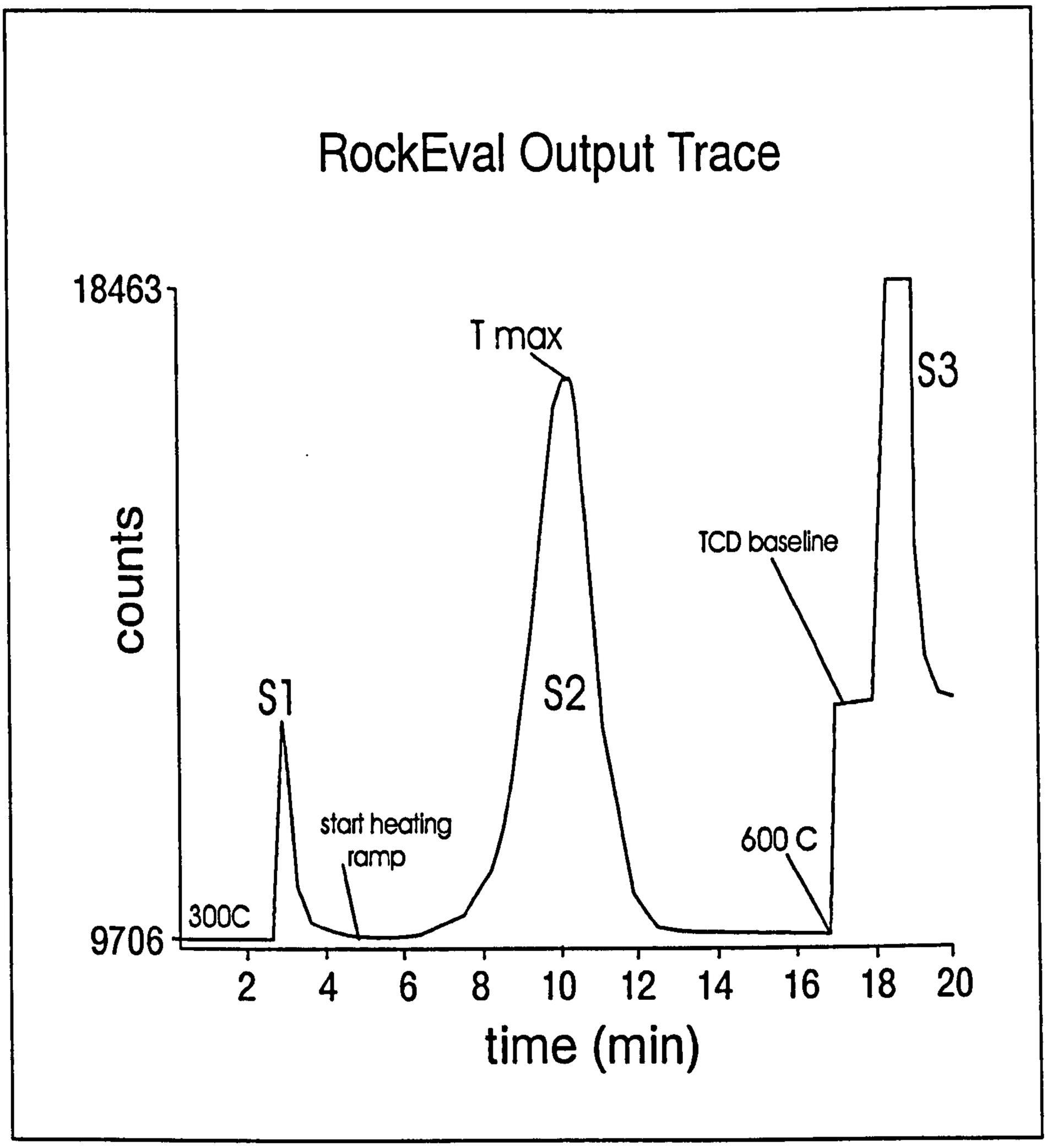

Figure 17. Pyrogram produced by RockEval pyrolysis showing S1, S2 and S3 peaks and Tmax determination (from Snowdon & Fowler, 1986).

results, but it is used to determine the amount of organic matter (TOC) in the rock according to the following formula:

$$\% \text{ TOC} = k\,(S1 + S2) / 10 + S4/10.$$

The S1 peak is an indication of the light indigenous hydrocarbons present within a source rock and correlates to extractable hydrocarbons. The S2 peak is a measure of the quantity of hydrocarbons produced by thermal conversion (pyrolysis) of the kerogen and CS_2-soluble bitumen in the sample and is therefore indicative of the genetic potential; the temperature at which

maximum hydrocarbon generation occurs (which corresponds to the temperature of the S2 peak) is the Tmax value, which is used as an indication of the thermal maturity for Type II and Type III kerogen (Espitalié, 1986). An S2 peak of greater than 0.2mg HC/g rock is used as the threshold for reliability of Tmax data (Peters, 1986; Peters & Cassa, 1994). The S1 + S2 value is measure of the overall genetic potential of the source rock. The S2:S3 ratio is an indication of kerogen type, and so also are the hydrogen index (S2/TOC × 100) and the oxygen index (S3/TOC×100). The Production index (PI) is determined by S1/ S1+S2 and is an indication of the oil-generating potential; and the decrease in the hydrogen index (i.e. between depth 0m and Xm) ÷ the initial hydrogen index (at depth 0m) is the Transformation Ratio, which is also a good indication of thermal maturity for Type III kerogen. The general guidelines used for the evaluation of hydrocarbon-generating potential, kerogen type and maturity using Rock-Eval pyrolysis data are summarized in Table 6. The units used for S1, S2 and S3 values are mg HC/g rock.

In addition, the empirical data obtained by rapid pyrolysis can be used to determine the kerogen type and level of maturity by analogy with elemental analysis (H/C, O/C) of coals and kerogens (Espitalié *et al.*, 1977; Fig. 2). Espitalié *et al.* (1977) demonstrate correlations between the H/C ratio of kerogens and the hydrogen index (S2/TOC × 100) and also the O/C ratio and oxygen index (S3/TOC×100). These pyrolysis parameters can also be plotted on a modified van Krevelen diagram to indicate the kerogen type and maturation (Fig. 18).

Other maturation parameters

In addition to or, in the absence of, reflectance and Tmax data, visual or qualitative

a

SOURCE POTENTIAL						
ROCK-EVAL PARAMETER	V. POOR	POOR	FAIR	GOOD	V.GOOD	EXCEL
S1 value*	0.0-0.25	0.25-0.50	0.5-1.0	1.0-2.0	2.0-4.0	> 4.0
S2 value*		<2.0	2.0-5.0	5.0-10.0	10-20	>20
TOC carbonate		0.0-0.12	0.12-0.25	0.25-0.5	0.5-1.0	1.0-2.0
TOC shale		0.0-0.5	0.5-1.0	1.0-2.0	2.0-4.0	4.0-8.0

*mg/g rock

b

ROCK-EVAL PARAMETER	KEROGEN TYPE TYPE I	TYPE II	TYPE III
S1: S2	10-5	5.0-2.5	0 - 5
Pyrolized carbon (PC)	0.8 (TOC)	0.5 (TOC)	0.1-0.3 (TOC)
Hydrogen Index (HI)	900-600	600-300	<300
Oxygen Index (OI)	0-15	15-75	>75
S2:S3	>15	10-15	1-10

c

ROCK-EVAL PARAMETER	MATURITY (PRODUCTS) Immature (gas)	Mature (oil)	Postmature (gas)
T max °C	<435	435-465	>465
S2:S3	>5.0	5.0-2.5	2.5-0.0
S1:S2	<2.0	2-6	>6.0

d

ROCK-EVAL PARAMETER	OIL GENERATION Immature (gas)	Mature (oil)	Postmature (gas)
S1/ S1+ S2**	<0.1	0.1-0.4	>0.5

** Production Index (PI)

Table 6 Interpretation of Rock-Eval pyrolysis results with respect to a) source rating; b) kerogen type; c) maturity (oil, gas); and d) oil generation (from Peters & Cassa, 1994, modified).

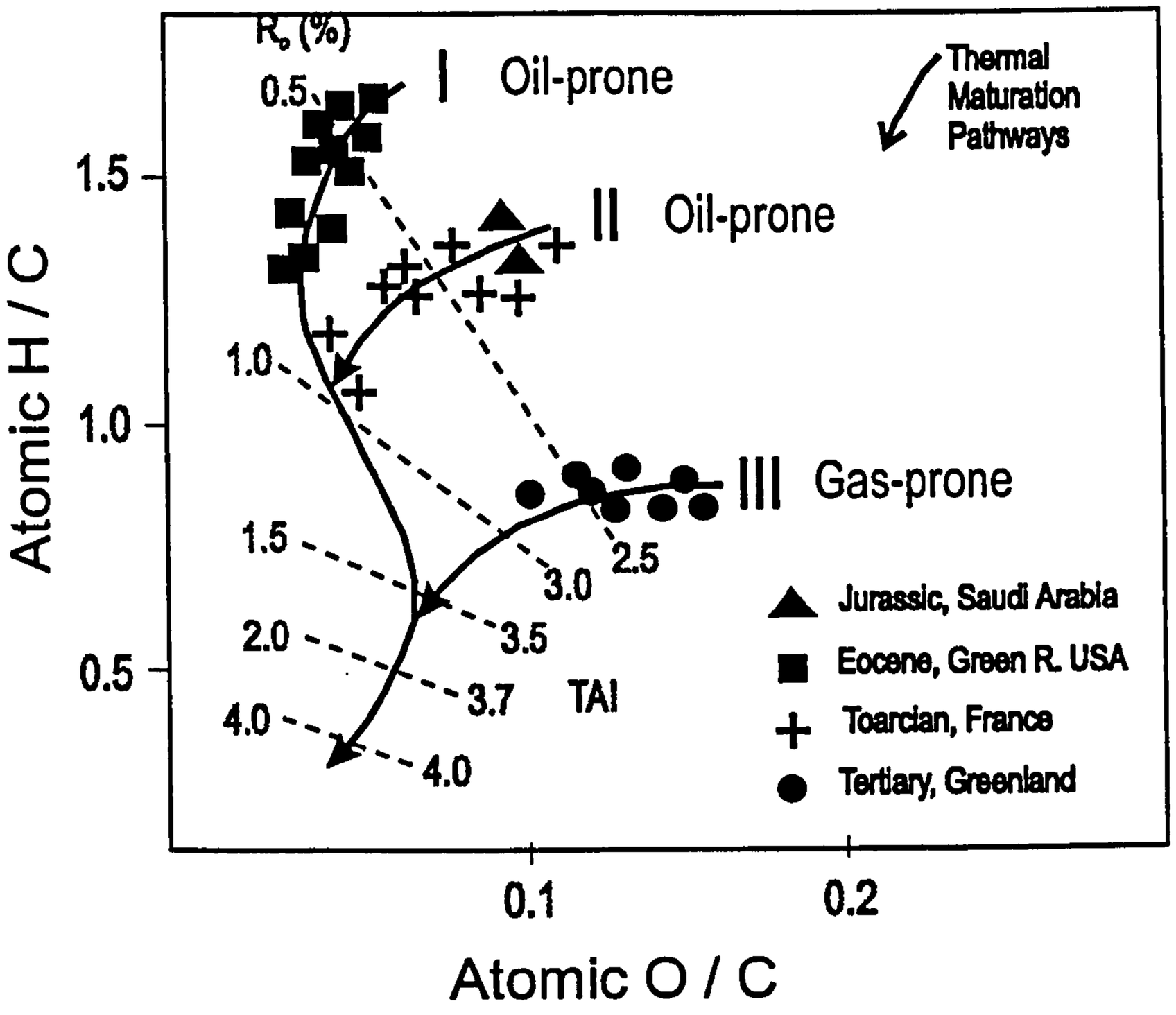

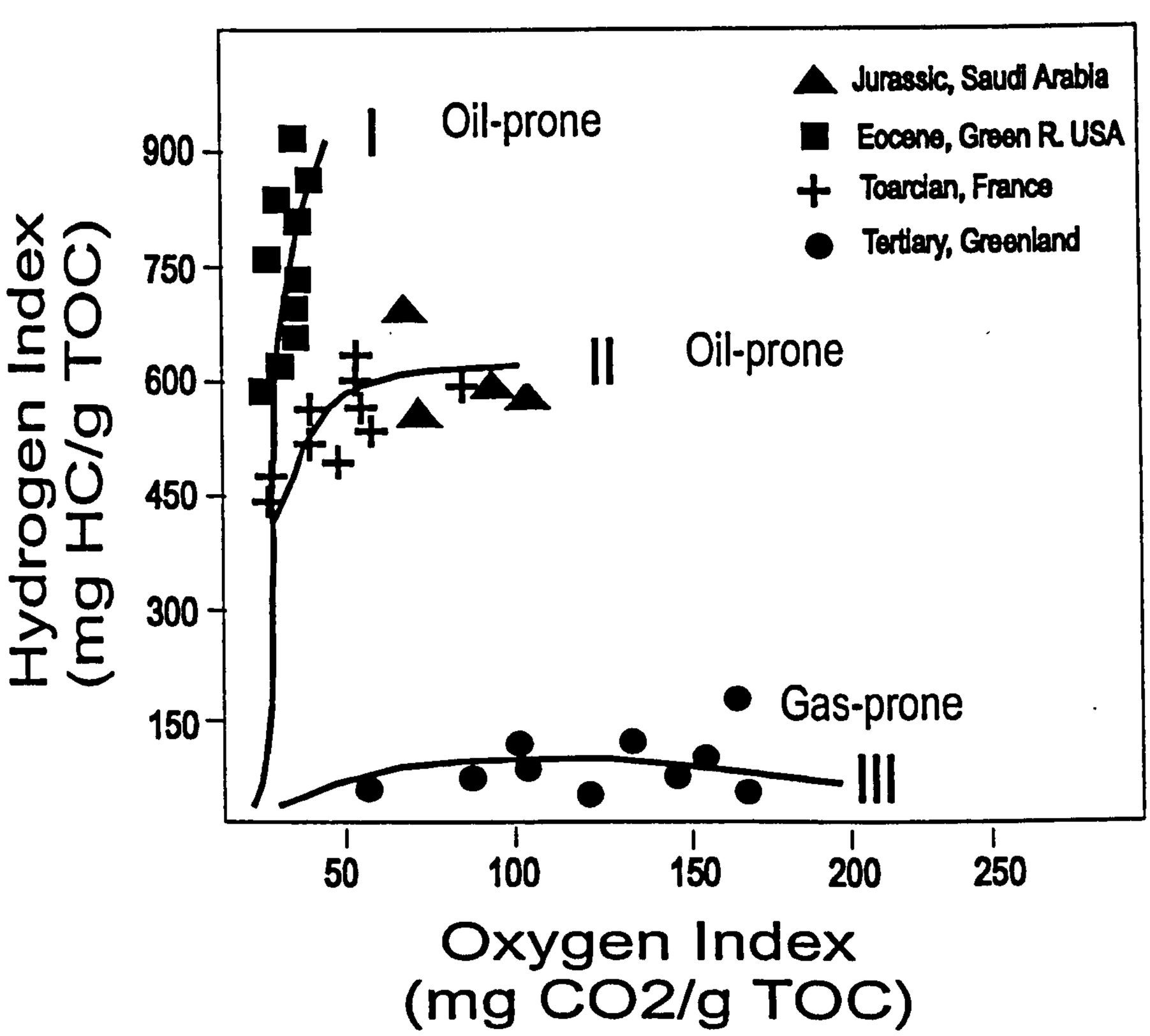

Figure 18. Correlation between Atomic H/C and O/C ratios and Hydrogen and Oxygen Indices determined byRock-Eval pyrolysis (Espitalié *et al.* 1977).

spectral analysis, quantitative spectral fluorescence were carried out and conodont alteration (CAI) and thermal alteration indices (TAI) were used when available. The qualitative spectral analyses were carried out on fluorescing liptinite macerals such as alginite and sporinite macerals. The fluorescence colour, as observed under blue light illumination, was graded numerically to reflect colour shifts associated with increasing maturation. The fluorescence index used is shown in Table 7.

Fluoresence index	1	2	3	4 4d*	5	6	7	8	9	10
colour	green	light yellow	med yellow	butter yellow	yellow-orange	orange	light brown	med brown	dark brown	black

* 4d = dull yellow

Table 7 Liptinite fluorescence index

Spectral fluorescence was carried out on selected macerals (sporinite and *Tasmanites* alginite) from coals and shales of the Mattson Formation. The spectral scan procedure consisted of illuminating the sample with incident UV light (365nm) and measuring the intensity of the fluorescence emitted, at 10 nm intervals, throughout the spectral range from 400 to 750nm. The spectral curves are corrected by a "black body" scan to standardize the instrument and remove the effects of spectral variations in the incident light beam, optical system and photomultiplier response. The spectrum obtained is characterized by the shape of the curve which is described by two parameters (Fig. 19):

1) Lambda max (λ max) the wavelength at which the maximum intensity occurs;
2) Red\Green quotient (Q): R\G = Intensity at 650 nm ÷ Intensity at 500nm.

The Conodont Alteration Index (CAI) was determined for 15 samples (Table 1) by J. Docherty at the Geological Survey of Canada, according to Epstein *et al.* (1977). Thermal Alteration Index (TAI) was determined on 10 samples by J. Utting based on the approach of Staplin (1969). Table 8 shows the relationships between vitrinite reflectance, bitumen reflectance, CAI and TAI.

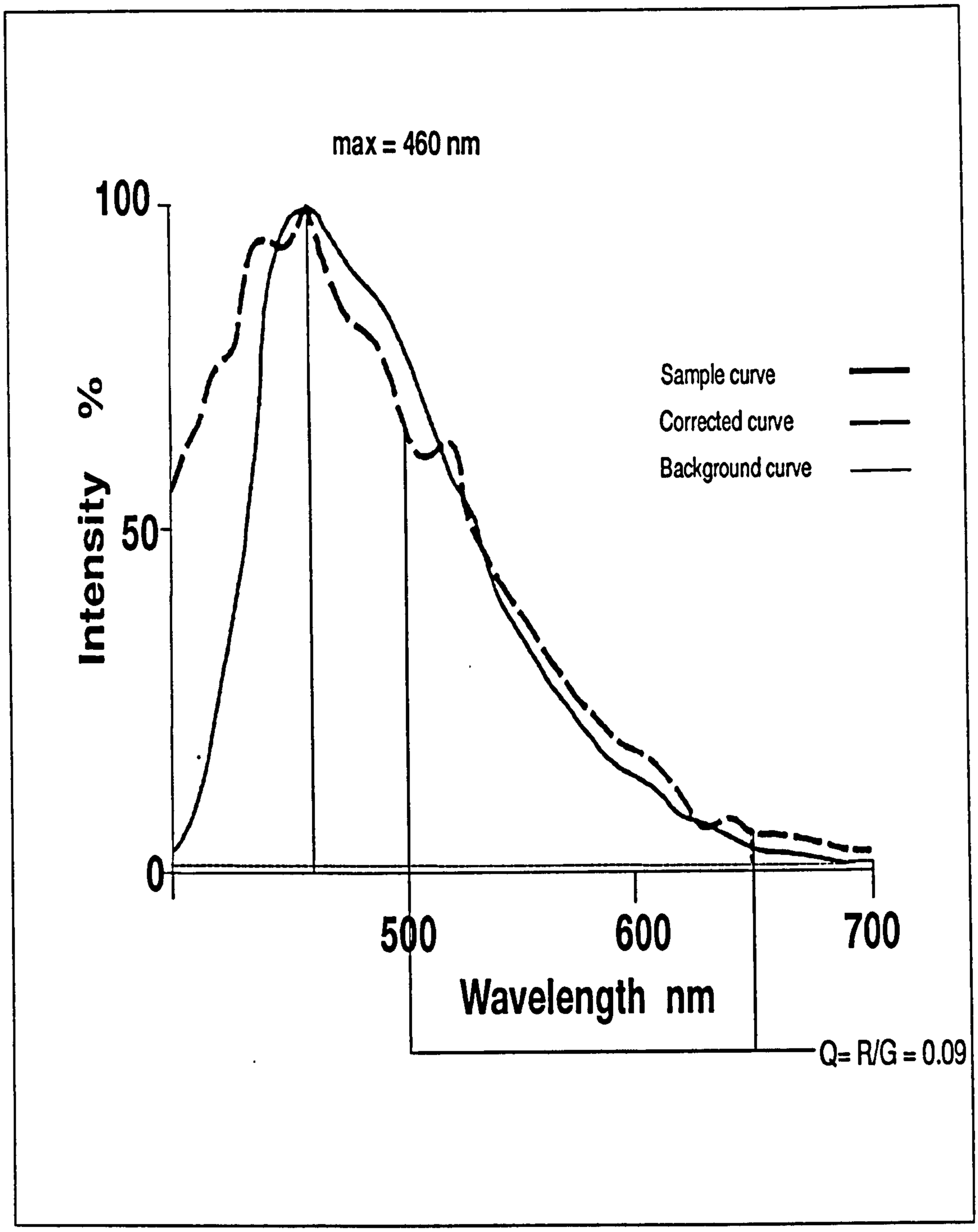

Figure 19. Fluorescence characteristics of resinite from Hat Creek coal, from Bustin *et al.* (1983).

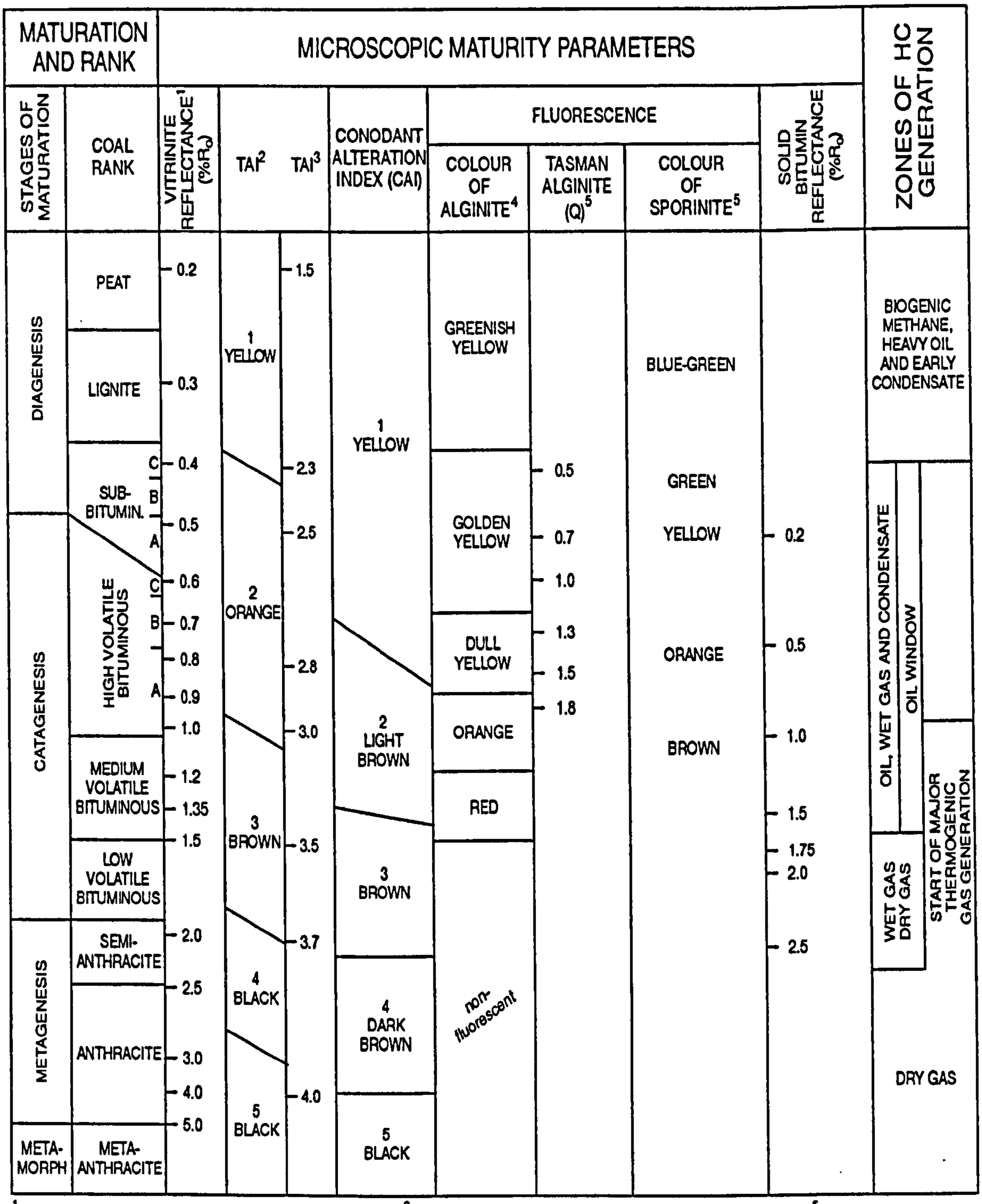

[1]from Teichmüller and Teichmüller, 1982
[2]from Staplin, 1969
[3]from Jones and Edison, 1978
[4]from Mukhopadhyay and Rullkötter, 1986
[5]from van Gijzel, 1981

Table 8. Correlations between optical maturity parameters (from Mukhopadhyay, 1994).

2.5 HYDROCARBON SOURCE POTENTIAL

The unit thickness, %TOC and maturity values based on measured or VR_o equivalent values derived from bitumen reflectance data or other maturity parameters, are applied to determine source rock potential of individual stratigraphic intervals using to the method of Dembicki and Pirkle (1985) illustrated in Figure 7.

2.6 BASIN MODELING

Vitrinite reflectance measurements and VR_o equivalent values determined on medium R_o bitumen (type 4; according to Jacob & Hiltmann, 1985) were used in this study to constrain the maximum burial temperatures in basin modeling using the *Burial 3a* program. *Burial 3a* is a two-part *Fortran* program that creates a stratigraphic and heat flow model and calculates burial history curves for a stratigraphic section which can include eroded layers; the program also makes provision for erosion through several layers. For each layer at each age, the following are calculated: thermal conductivity, temperature, R_o max. It accounts for compaction due to burial of the various lithologic units in the section. The program is modified from the "Burial" program developed by Osadetz and Mottershead (1994), which takes an empirical approach to modeling based on the time-temperature relations (i.e. the Time Temperature Index, TTI of Waples, 1980), by incorporating a subroutine that uses the Easy Ro algorithm of Sweeney and Burnham (1990) instead of TTI (Morrow and Issler, unpublished work). In addition, the *Burial* programme was modified to include a subroutine that performs a statistical comparison between the measured and calculated Ro data (*Burial 3b*; Morrow and Issler, unpublished work). It is suitable for analysis of the Liard Basin because of the complex geologic history associated with the Upper Devonian, Lower Carboniferous and overlying Mesozoic and Cenozoic strata. A schematic flow diagram of the program logic is given in Figure 20.

"Burial" recognizes the deposition and removal due to erosion of individual stratigraphic unit as separate events, and in doing so, acknowledges stratigraphic unconformities. The first stage in the modeling process (*Burial 3a*) is to compile a detailed reconstruction of the chronostratigraphic history of the named stratigraphic sequence. An example compiled for the Imperial Island River No.1 section is given in Table 9. Each event is assigned a geological age, in sequential order of occurrence, beginning with the

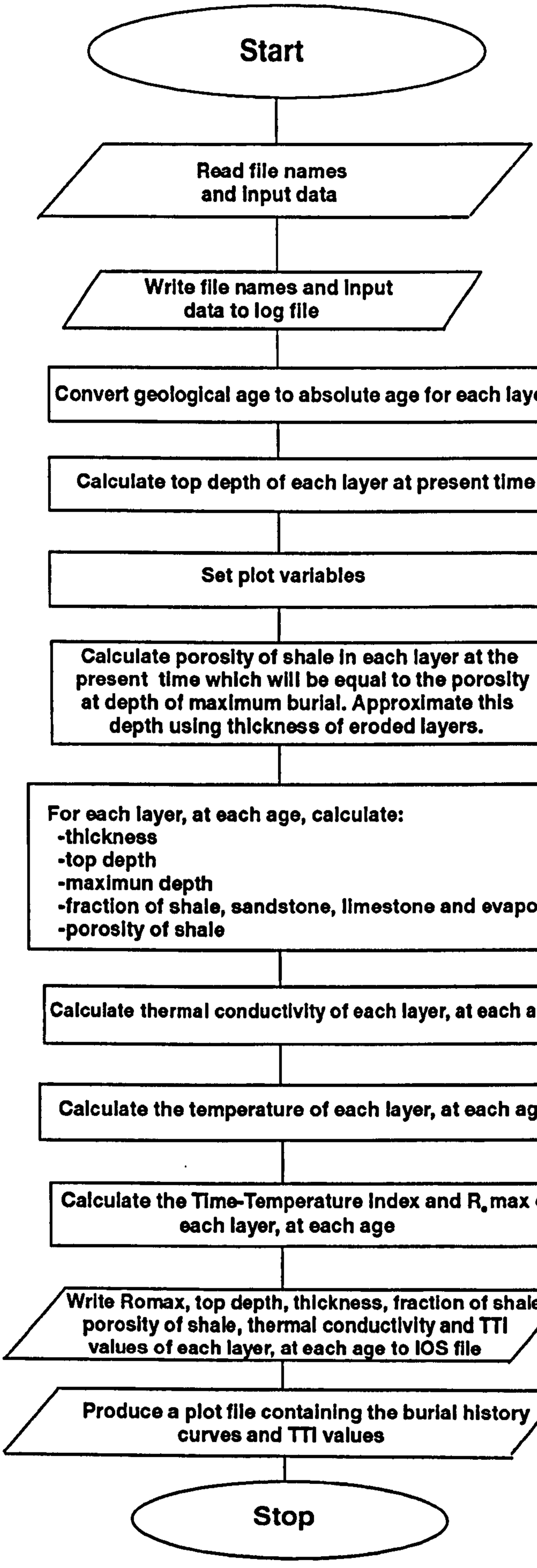

Figure 20. Schematic flow chart illustrating the logic of "Burial" model of Osadetz and Mottershead (1982), modified.

Event no.	Age no.	Contact Format	Age (m yrs)	Desciption of Event	T/F	Thickness (m)	Age
1	Age 1	38	415	Base of sequence	T	000.00	
2	Age 2	38	401	Granite wash (regolith) deposition	T	025.00	
3	Age 3	38	392	Chinchaga	T	078.00	Eifelian
4	Age 4	38	386	Keg River +Evie Mbr	T	090.5	Eifelian-Givetian
5	Age 5	38	380	Mid Devonian Sh/Lmst (?Sulphur Point)	T	106.00	late Givetian
6	Age 6	38	377	Slave Point	T	117.00	late Givetian
7	Age 7	38	373	Muskwa +Fort Simpson	T	530.00	Frasnian
8	Age 8	38	370	Jean Marie	T	15.20	late Frasnian
9	Age 9	38	369	Redknife	T	142.80	
10	Age 10	38	367	Kakisa + Trout River	T	672.00	Fammenian
11	Age 11	38	365	Tetcho	T	076.00	Fammenian
12	Age 12	38	363	Kotcho	T	212.5	Fammenian
13	Age 13	38	353	Exshaw + Banff	T	370.00	late Fammenian-T1
14	Age 14	38	350	Rundle-part remaining (Pekisko)	T	003.00	Tournaisian -T2
15	Age 15	26	347	Rundle	F	310.00	Tournaisian -T3
				-part eroded at Sub-Cretaceous Unconformity			
16	Age 16	19	346	Rundle deposition Tournasian	F	025.00	Tournaisian-T3
				-part eroded at Sub-Permian Unconformity			
17	Age 17	18	330	Mattson	F	150.00	Serphukovian
18	Age 18	38	295	Sub-Permian Unconformity (Mattson erosion)	T	000.00	
19	Age 19	38	290	Sub-Permian Unconformity (Rundle erosion)	F	000.00	
20	Age 20	25	280	Kindle	F	020.00	Ass-Sak-Art
21	Age 21	22	262	Fantasque	F	025.00	Guad (Road-War)
22	Age 22	38	250	Sub-Triassic Unconformity (Fantasque erosion)	T	000.00	
23	Age 23	24	230	Toad-Grayling	F	140.00	Scythian-Norian
24	Age 24	38	205	Sub-Cretaceous unconformity (Toad-Grayling erosion)	T	000.00	
25	Age 25	38	190	Sub-Cretaceous unconformity (Kindle erosion)	T	000.00	
26	Age 26	38	185	Sub-Cretaceous unconformity (Rundle erosion)	T	000.00	
27	Age 27	38	112	Buckinghorse	T	197.5	Early-mid Albian
28	Age 28	38	108	Sikanni	T	085.00	M. Albian
29	Age 29	38	102	Sully	T	177.00	Late Albian
30	Age 30	38	96	Dunvegan deposition -part remainimg	T	166.00	M-Late Cenomanian
31	Age 31	36	95	Dunvegan deposition -part eroded At Sub-Cretaceous Unconformity	F	084.00	
32	Age 32	35	15	Kotaneelee	F	200.00	Santonian-Campanian
33	Age 33	34	71	Wapiti	F	200.00	Maastrichtian
34	Age 34	38	65	Sub-Tertiary unconformity (Wapiti erosion)	T	000.00	
35	Age 35	38	60	Sub-Tertiary unconformity (Kotaneelee erosion)	T	000.00	
36	Age 36	38	40	Sub-Tertiary Unconformity (Dunvegan erosion)	T	000.00	
37	Age 37	38	02	Quaternary deposition	T	020.00	

Table 9 Stratigraphic classification and data from Imperial Island River No.1.

oldest. Unconformities are considered true layers by virtue of the erosional events they represent but are assigned zero (0.00m) thickness. Using this information together with heat flow, lithological information and maturity data, three input files are compiled:

1) Dat file: Name.dat; 2) Age file: Name.age; 3) R_o file: Name.ro.

Table 10a summarizes the information contained in the input data file "Name.dat". The data file (Name.dat) requires detailed stratigraphic information regarding the relative age and thickness of each stratigraphic unit numbered in accordance with the age of the event in which it was formed. It is laid out in twelve columns and the number of rows corresponds to the number of events leading to the formation of the named stratigraphic sequence. Column 1 is thickness of the unit (in feet or metres); column 2 is a declaration of the units existence, as either a true or false layer (T or F[2]); column 3 is the contact format - if the unit described in column 2 is a true layer, then the number in column 3 is the total number of layers recorded +1; if it is a false layer, then the number in column 3 is the number of the event during which the unit was eroded + 1; columns 4 to 10 record the lithology of the unit: column 4 = % shale; column 5 = % sandstone; column 6 = % lst; column 7 = % dolomite; column 8 = %siltstone; column 9 = % evaporite; column 10 = % chert. In column 11, a heat flow (mW m^{-2} sec^{-1}) is assigned to each unit, the values based on calculated heat flows in the northern Yukon reported by Majorowitz *et al.* (1988). In column 12, the present surface temperature (°C) is recorded.

The "Name.Age" file (Table 10 b) contains additional chronostratigraphic information on the age and duration of each geologic event (Table 9). Data is entered in two columns and the number of rows corresponds to the number of events leading to the formation of the named stratigraphic sequence: column 1 gives the age of the event/unit by assigned number; and in column 2, the corresponding age in millions of years of the unit/event is recorded. Geological ages are assigned using palynological information, when available, and by reference to the Geological Time Chart (Okulitch *et al.*, 1995). Actual numbers in millions of years represent the estimated time that deposition or erosion began

---

[2] T = true layer, if present; F= false layer , if eroded; unconformities are recognized as true layers.

Column no	1	2	3	4	5	6	7	8	9	10	11	12
Input data	layer thickness (m)	unit is "true" or "false" layer	contact format: N rec + 1 or N ero + 1	% shale	% sandstone	% limestone	% dolomite	% siltstone	% evaporite	% chert	heat flow mW m^{-2} sec^{-1}	present day surface temperature (° C)

a) Information required for input file "name.dat" .

Column no.	1	2
input data	Age no.	Age, millions yrs

b) Information required for input file " name.age"

Column no.	1	2
input data	Vitrinite Ro equivalent	sample depth (m)

c) Information required for input file "name.ro"

Table 10 Data required for compilation of input files for *Burial 3* modeling program of Osadetz and Mottershead (1994), modified.

i.e. the base of a stratigraphic interval.

The "Name.Ro" file (Table 10 c) contains maturation data. The data is compiled in two columns and the number of rows corresponds to the number of events involved in the formation of the named stratigraphic sequence. The first column records the age of the stratigraphic event during which a particular unit was deposited, and the second column contains the maturation level in vitrinite reflectance equivalent (% R_o). Examples of the input files compiled for the following well sections are given in Appendix E: Imperial Island River No. 1, Canada Southern *et al.* North Beaver River YT 1-27 and Pan Am Beaver G-01.

The program then computes the thermal conductivities of individual lithologies based on thermal conductivity data from Majorowitz *et al.* (1989) and lithological compaction due to burial. The output files present the following data:

1. Layer thickness changes with time (thick.age)
2. History of the Ro values for each layer (Ro.age)
3. Temperature history for each layer (temp.age)
4. Ro values for the top of each layer
5. Age of the sampled horizons (smage.age)
6. Temperature of the sampled horizons (stemp.age)

The latter two files, 5 (smage.age) and 6 (Stemp.age), serve as input files for the second part of the program (*Burial 3b*) which computes the Ro values (Scalc.Ro) for the sampled horizons and compares them with the measured Ro values using the Kolmogorov-Smirnov Test for the non-parametric comparison of two sets of unbinned data (Press *et al.*, 1992). The output is a probability index for the proposed burial history model based on the fit of the measured and calculated Ro data.

3.0 BITUMEN GENESIS AND REFLECTANCE IN RELATION TO HYDROCARBON GENERATION

The petrography of the indigenous bitumens in potential source rocks is examined from a genetic standpoint and a bitumen generation model is proposed (Fig. 21) that links the occurrence and genesis of the different bitumen populations observed to hydrocarbon generation. A genetic link between bitumen and primary dispersed organic matter is important because it proves the indigenous nature of the microscopic bitumens. Furthermore, if the "microbitumens" are formed as a natural consequence of thermal alteration of primary organic matter (coincident with hydrocarbon generation) and the optical and chemical properties of those bitumens change progressively with subsequent thermal alteration or transformation, then this further justifies their use and enhances their credibility as indicators of thermal maturity.

3.1 GENESIS OF INDIGENOUS BITUMENS

Four populations of indigenous solid bitumens are recognized in the Upper Palaeozoic of the study area (Fig. 21a). The relationships observed between the bitumens and macerals of the Liptinite group strongly suggest that the microscopic bitumens are formed directly from the individual liptinites as a consequence of thermal maturation (Plates I to V, X). The most compelling evidence comes from samples which are currently within the oil window, i.e. with VR_o equivalent values (VR_o eq.) between 0.45 and 1.3%.

Low-reflecting, type I bitumen (**type 1**) is directly associated with the liptinite macerals sporinite and alginite (subtypes s and a, respectively). When observed under incident white light, the type 1 bitumen is a weakly reflecting, dark grey mass, commonly less than 30µm diameter, occurring within transparent brown-orange (sporinite) or red (alginite) liptinitic bodies (Plates I & II) or forming a thin rind on their surface. The reflectance is between 0.09% to 0.4%R_o and is commonly ca. 0.20%R_o in the middle of the oil window (i.e. 0.85% VR_o). The generation of type 1 bitumen from structured liptinite macerals occurs only in samples with VR_o eq. values of at least 0.7%.

Low-reflecting, type 2 bitumen (**type 2**) occurs external to the structured liptinite maceral but commonly remains within the same pore, either as a surface coating on the

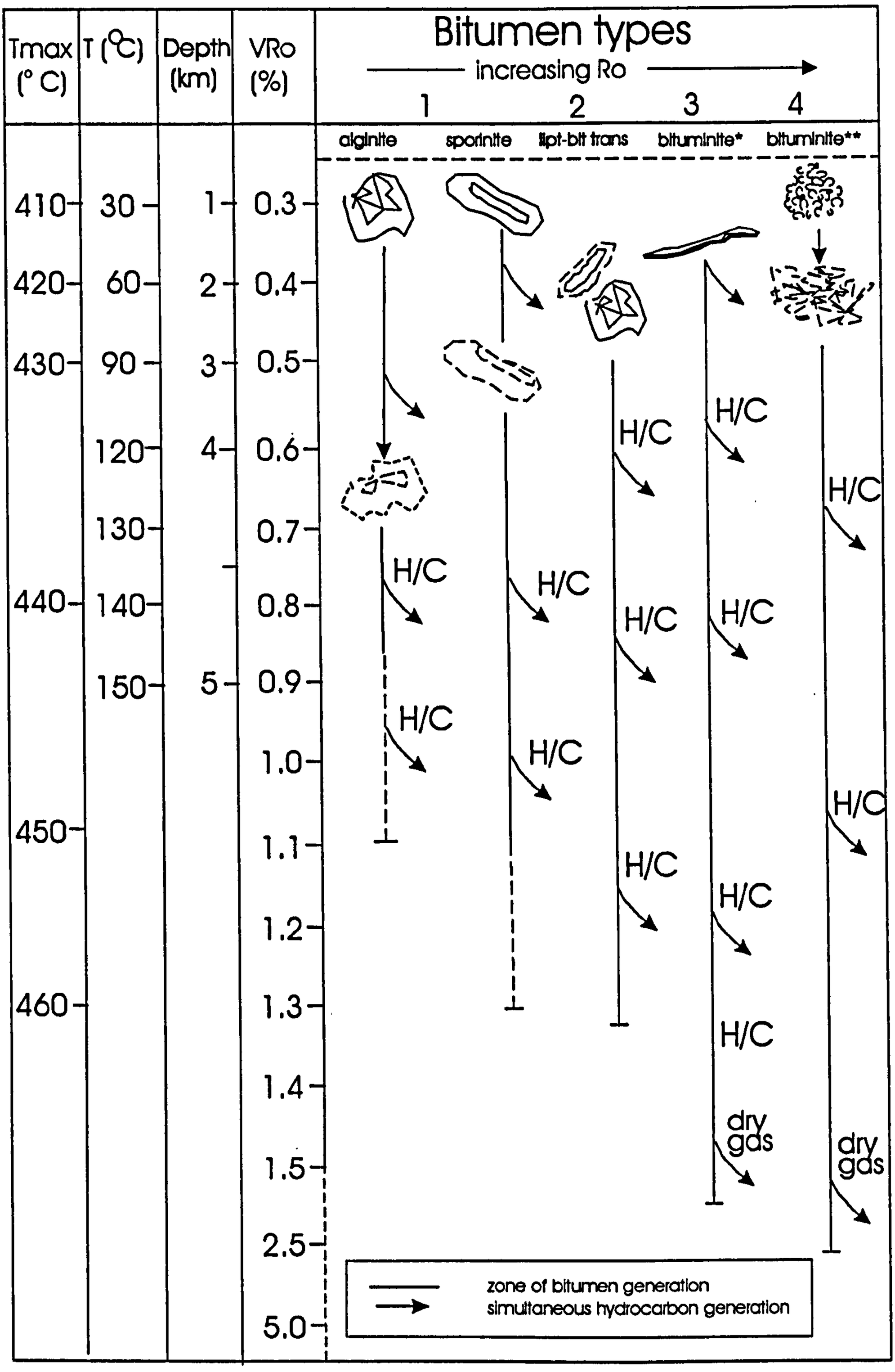

Figure 21. A model for the genesis of indigenous, microscopic bitumens from liptinitic kerogen.

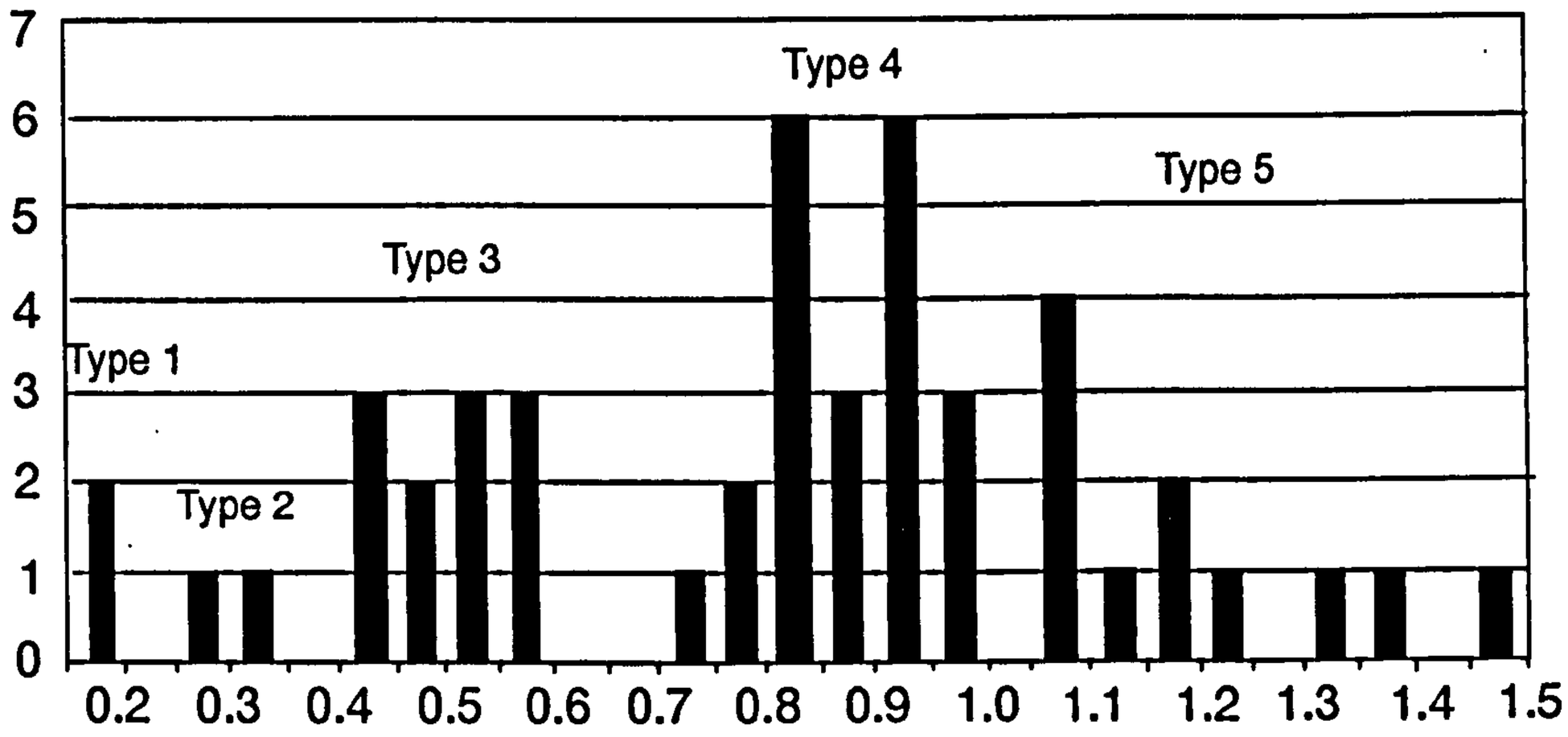

a

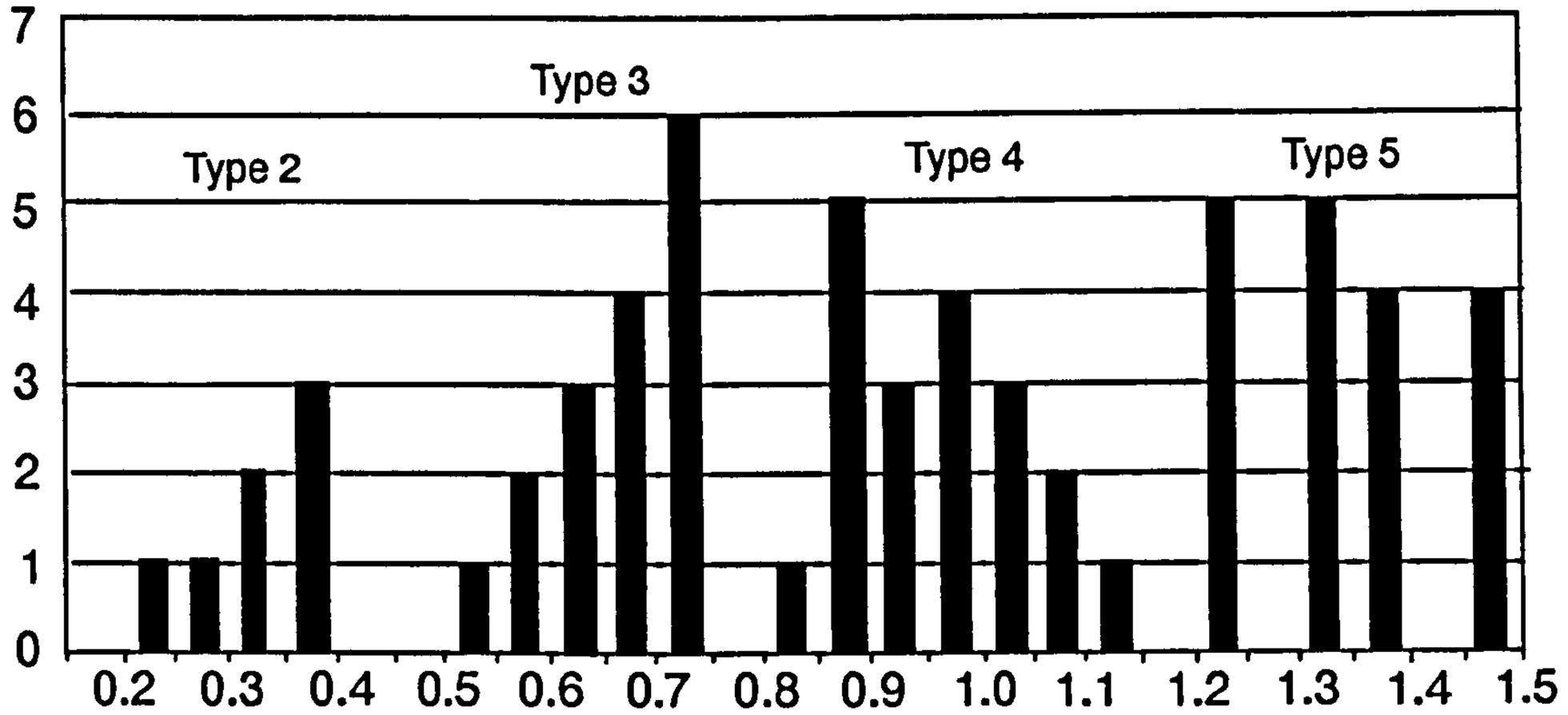

b

Figure 21a. Reflectance histograms for the indigenous bitumen in samples from the Amoco LaBiche a-67-D section at: a) 1220m, and b) 1561 m, illustrating 5 and 4 distinctive populations, respectively.

PLATE I
TYPE 1 MICROBITUMENS

a) White light image of type 1 bitumen generated from *Tasmanites* alginite in the Exshaw Formation at Imperial Island River No.1. Typically the bitumen does not have well-defined margins and many micropores. Superficial scratches are indicative of the softness of the bitumen.

b) Fluorescent light image of a). Type 1 bitumen shows weak fluorescence, similar or slightly stronger than the primary liptinite, and positive alteration. Note the fluorescent halo surrounding the bitumen caused by the diffusion of hydrocarbons from the thermally altered alginite into the bituminous matrix.

c) White light image showing early generation of very weakly reflecting type 1 bitumen (arrow) from reddish brown liptinite (?alginite) embedded in a marl from the Flett Formation, Pan Am Pointed Mountain, P-53.

d) Fluorescent light image of c). The colour and intensity of the fluorescence from the bitumen and and the liptinite are similar during the early stages of bitumen generation.

Magnification: scale bar shown on a) applies to all photomicrographs.

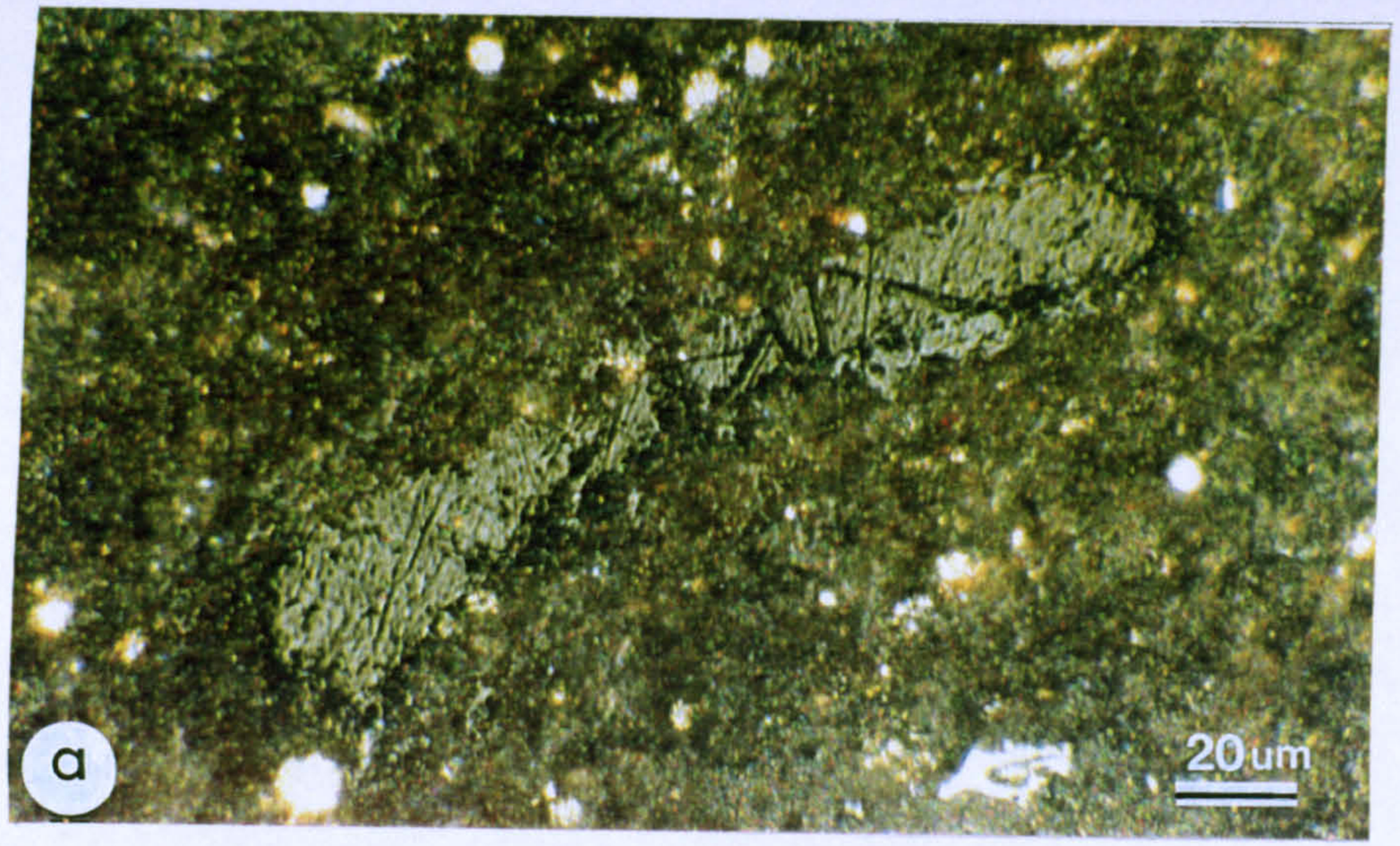

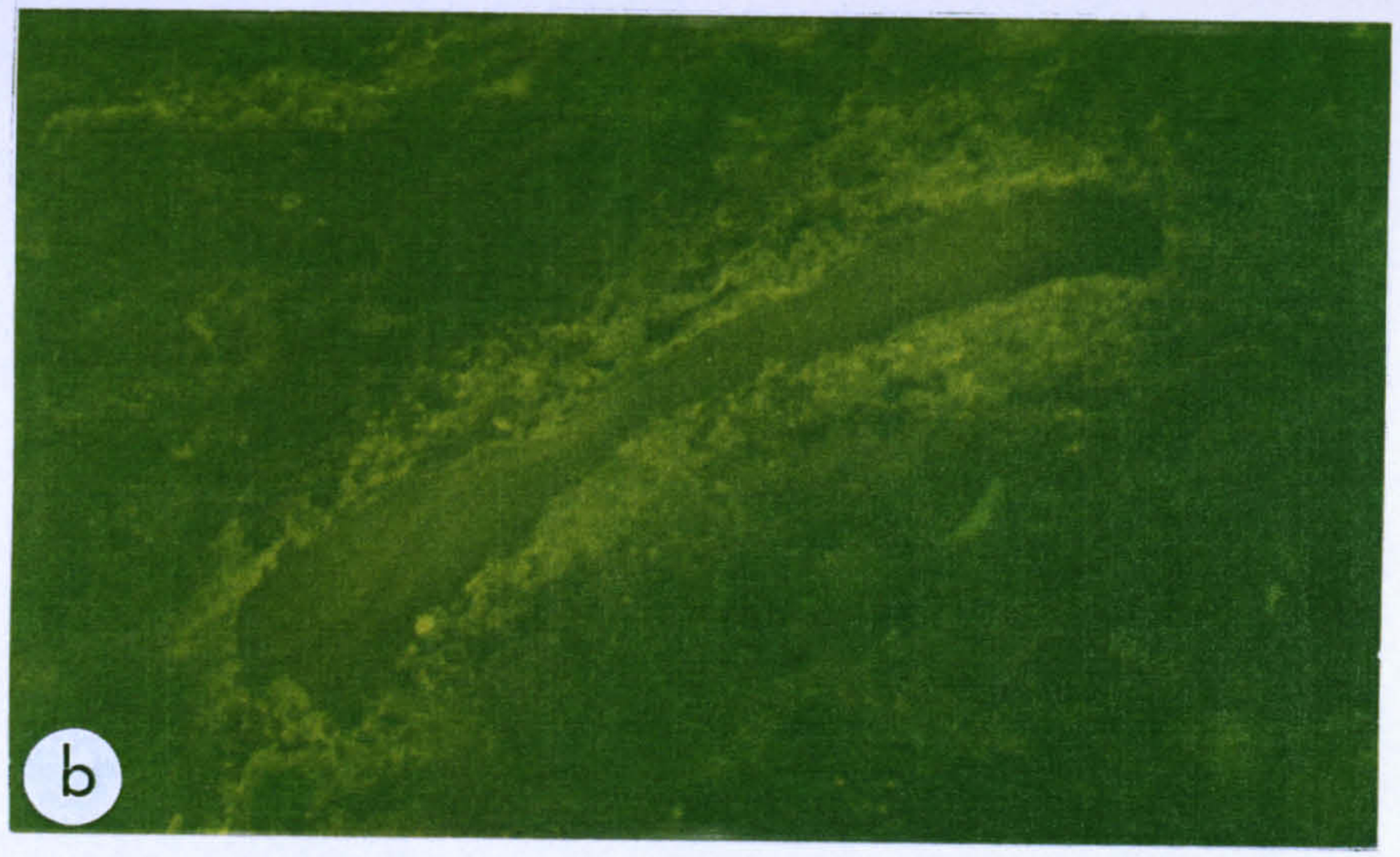

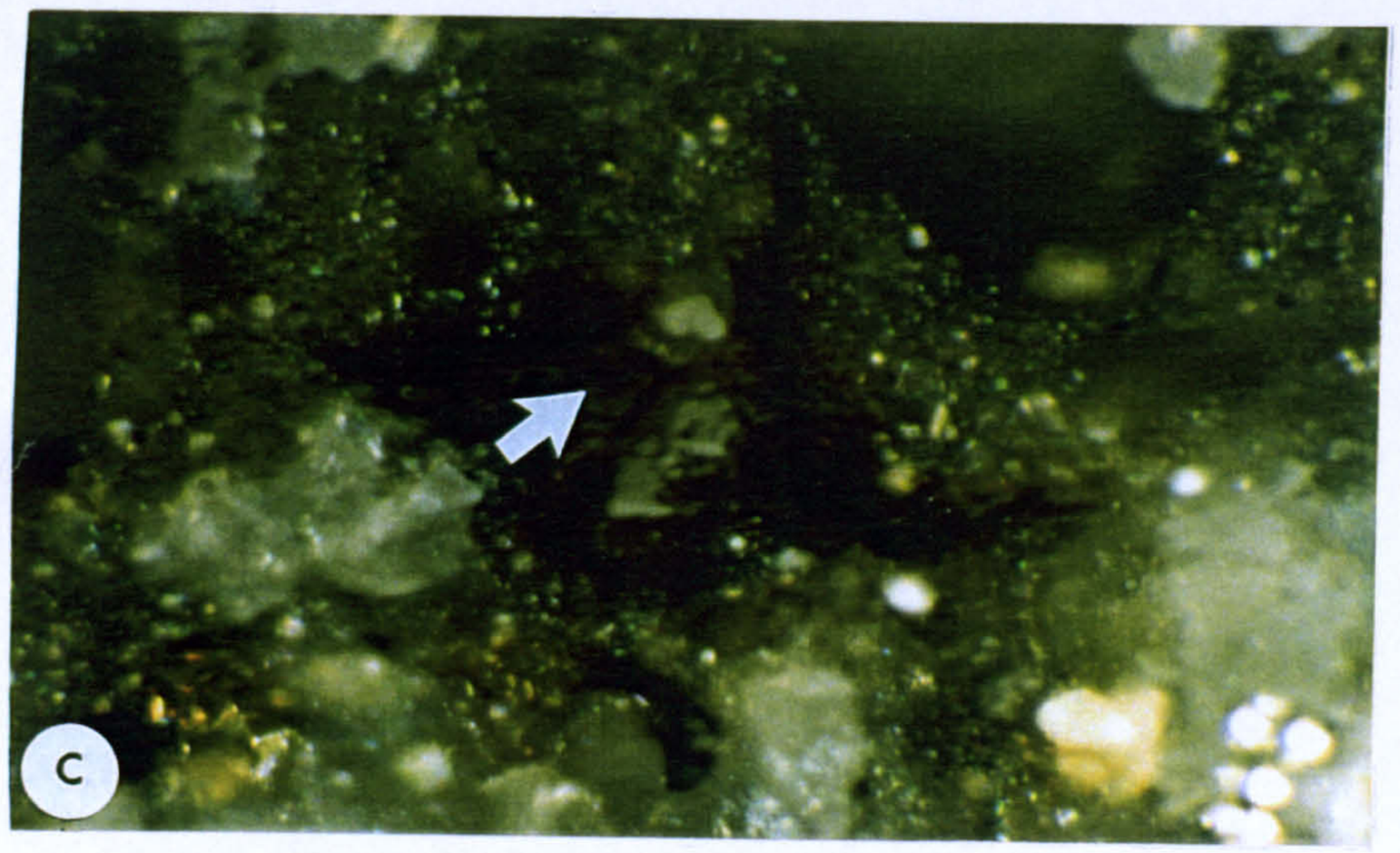

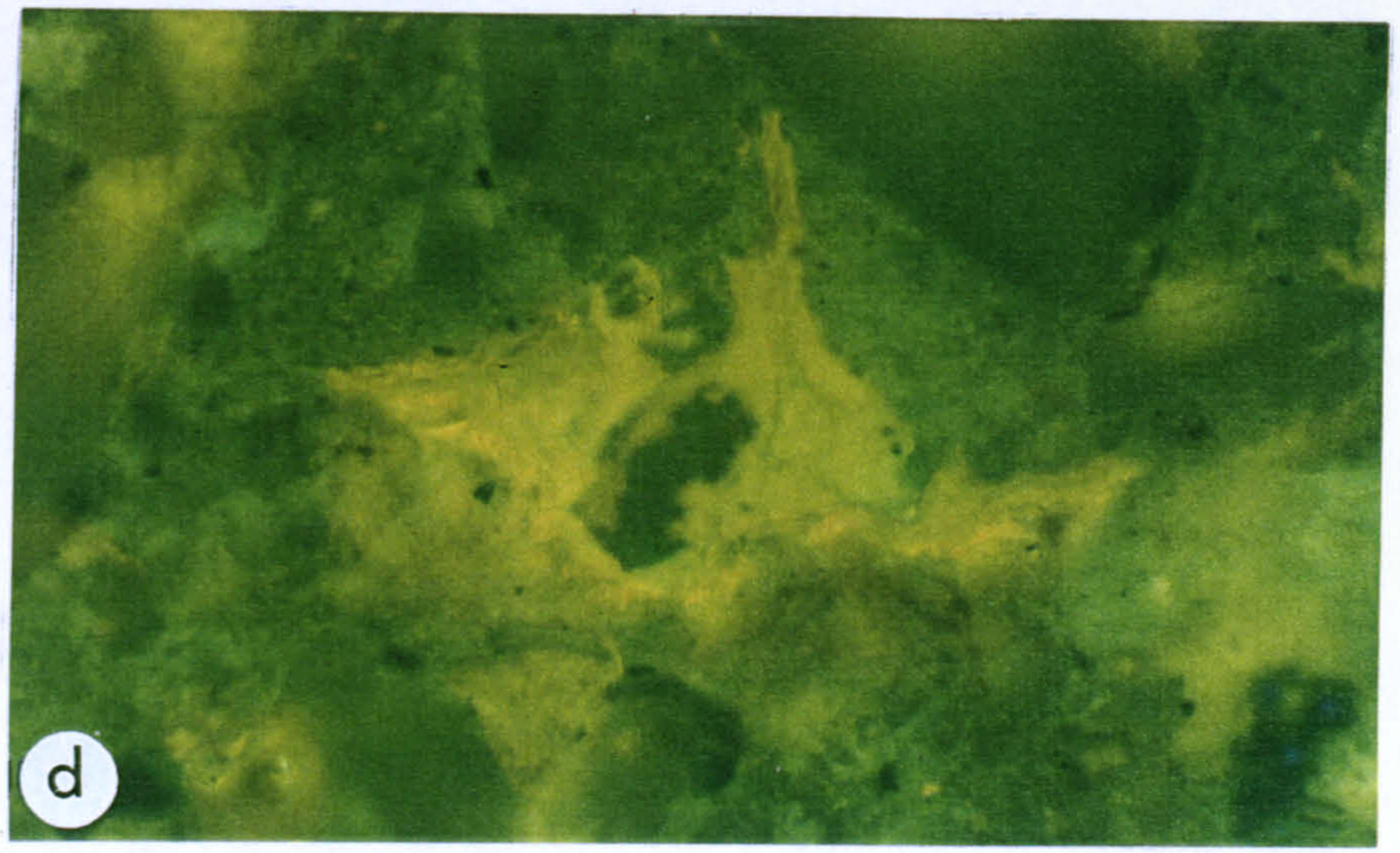

61a.

PLATE II
TYPE 1 MICROBITUMENS

a) Type 1 bitumen in the Banff Formation at Imperial Sun Netla C-07. The bitumen typically exhibits weak reflectance, a microporous appearance, sometimes referred to as "granular", and occupies the pore created by the shrinking liptinite precursor.

b) Fluorescent light image of a). Note the fluorescent halo in the bituminous matrix caused by adsorption of hydrocarbons generated from the primary liptinite.

c) In sections perpendicular to the microlamination, weakly reflecting sinuous strings of type 1 bitumen are found parallel to bedding and internal microfractures. Exshaw Formation, Imperial Island River No.1.

d) Fluorescent light image of c). At peak oil generation stage, type 1 bitumens show strong fluorescence intensity and positive alteration.

e) Reddish brown litpinite (?alginite) showing early type 1 bitumen generation; the bitumen is typically located along the margins of the liptinite or lining the pore walls; Mattson Formation, Pan Am Pointed Mountain P-24.

f) Fluorescent light image of e).

g) White light image showing early type 1 bitumen generation (centre) from sporinite (*Densosporites*) in the Mattson Formation, Amoco Bovie Lake, M-05.

h) Fluorescent light image of g).

i) Type 1 bitumen (0.32% R_o) generated from sporinite (*Murospora)* in the Mattson Formation at Clausen Creek.

j) Weakly reflecting lenses of bitumen embedded in, and generated from within a phosphatic ?pellet in Formation F, Pan Am *et al.* Celibeta No. 7.

k) Weakly reflecting type 1 bitumen encasing and exuding from within a ?faecal pellet in the Exshaw Formation at Imperial Island River No.1.

Magnification: scale bar shown on a) applies also to b); scale bar shown on c) applies also to d)-h), j) & k).

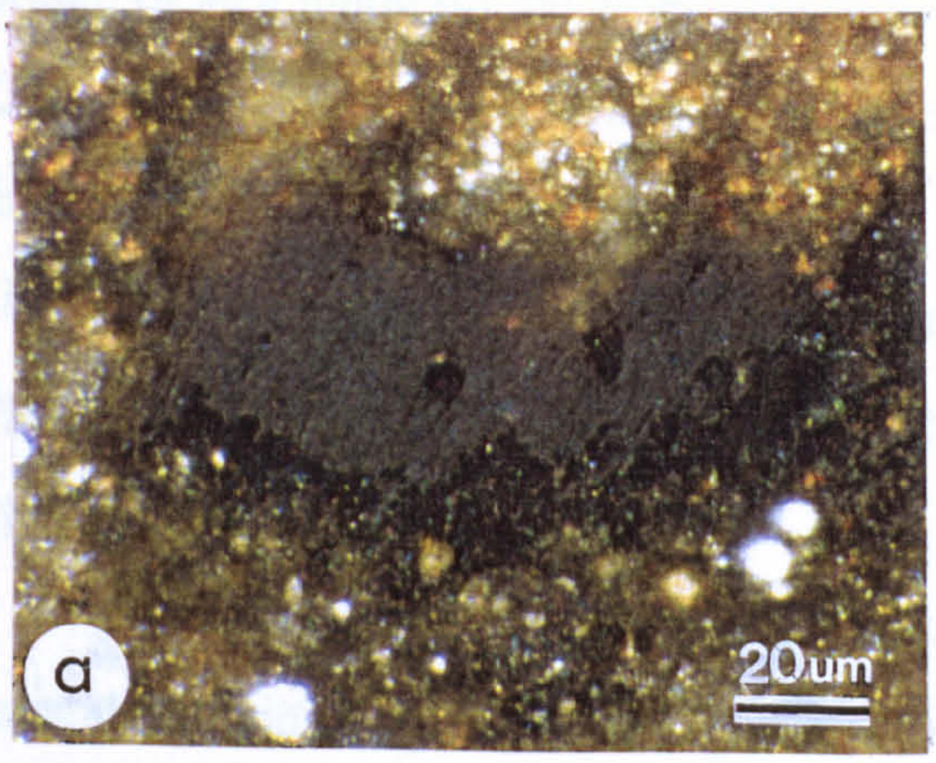
a
20um

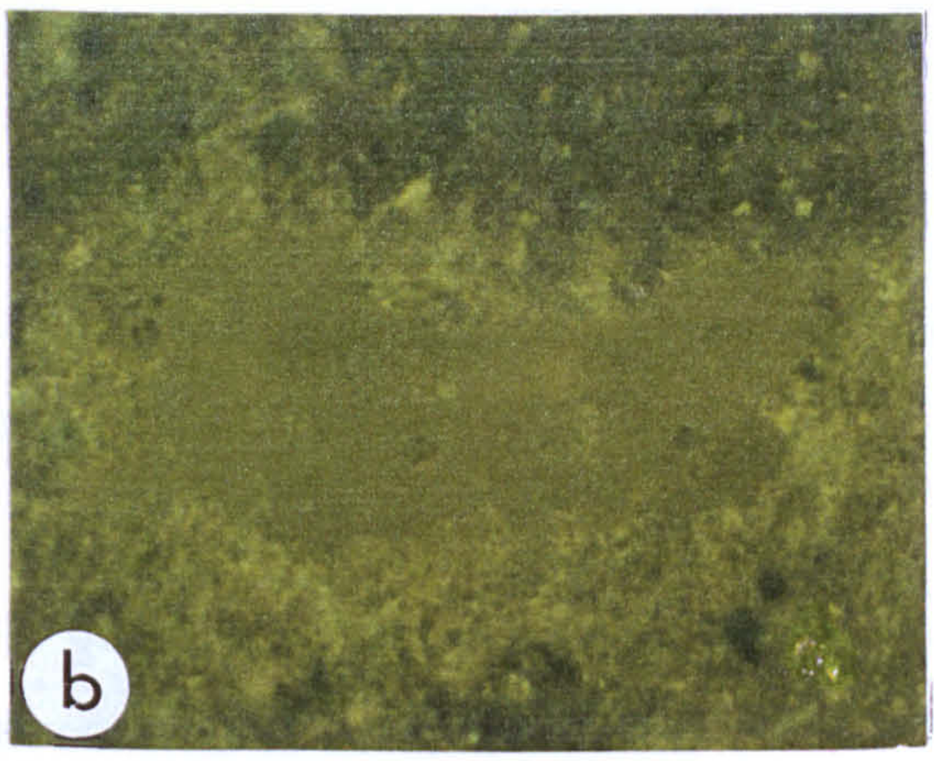
b

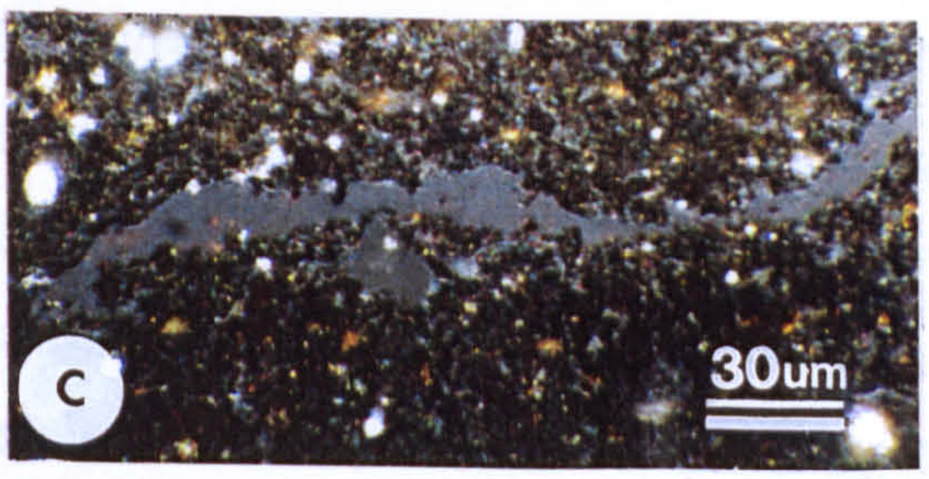
c
30um


d

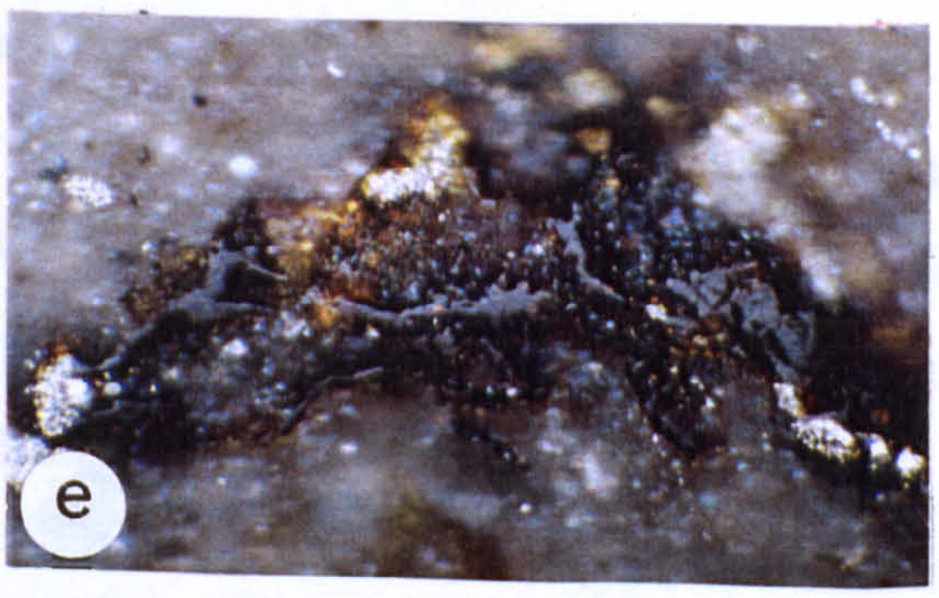
e

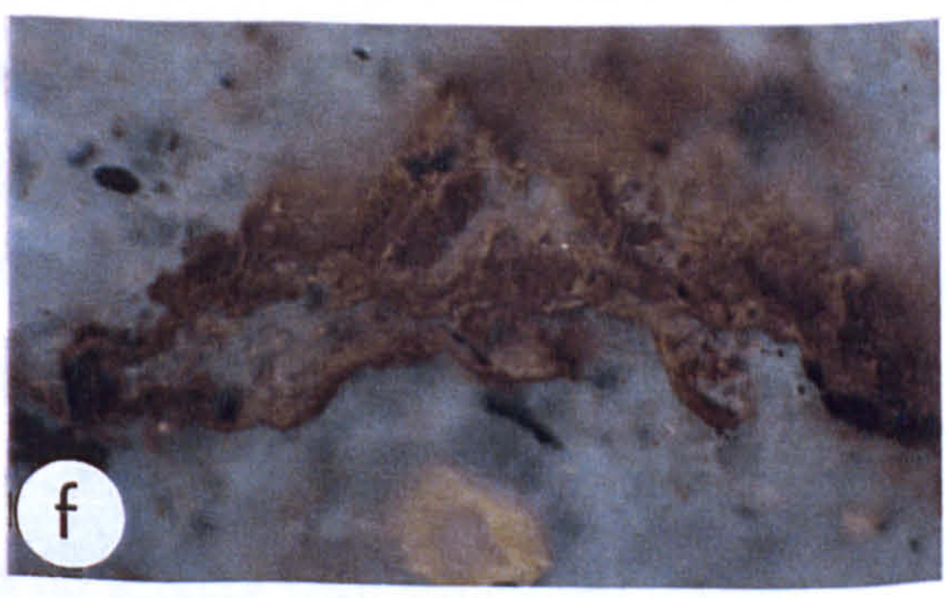
f


g


h


i
15 um

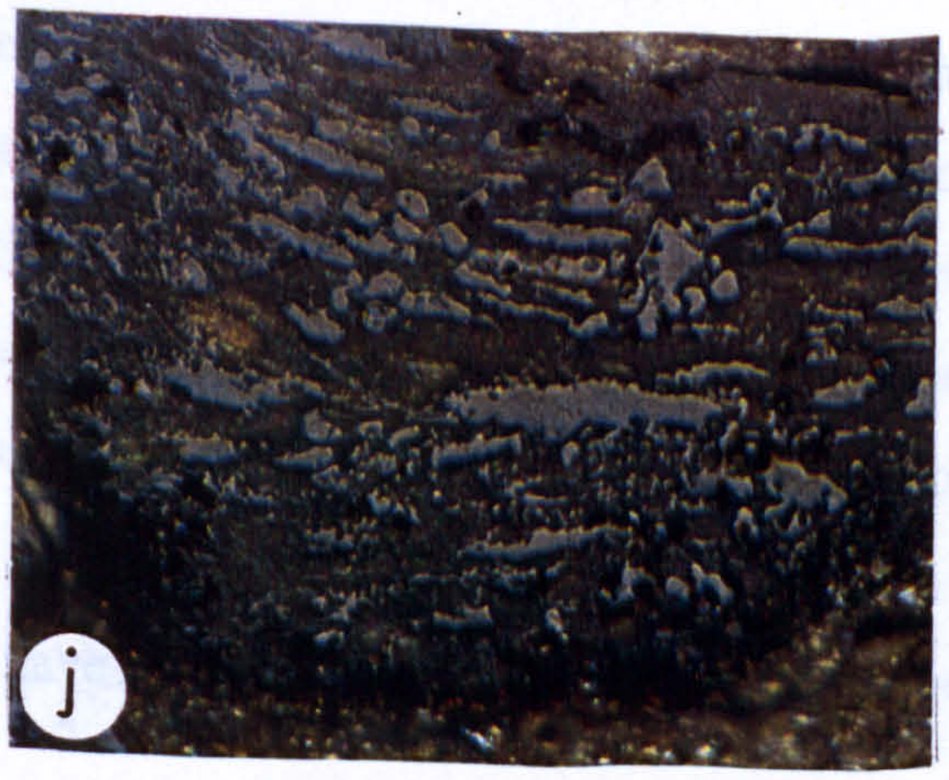
j

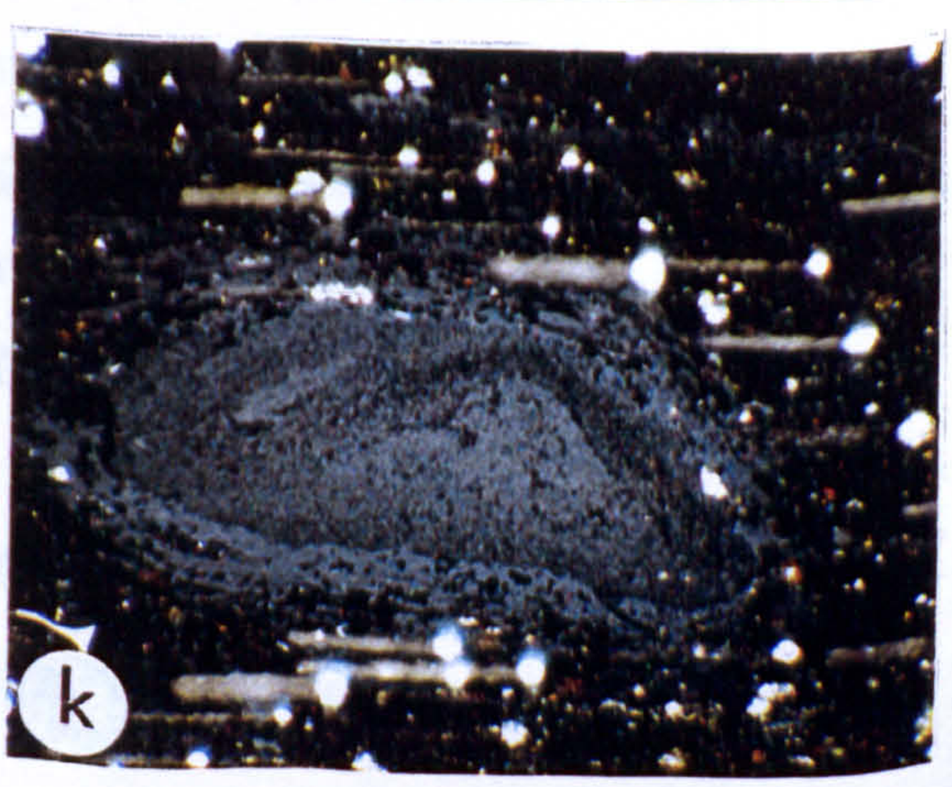
k

liptinite or as a lining on the inner wall of the pore (Plate III); the reflectance is between 0.22% to 0.75%R_o and is commonly between 0.4% and 0.55%R_o in the middle of the oil window. This is interpreted as early-formed bitumen that has exuded from the liptinite and is in the earliest stage of migration out of the liptinite-bearing pore. It may have a granular appearance, especially when derived from sporinite (Plate IIIa, f & g), otherwise it appears homogeneous in nature.

Low-reflecting, type 3 (**type 3**) bitumen is directly associated with the liptinite maceral bituminite, which is usually the dominant constituent of marine source rocks (Teichmüller, 1977). When viewed in sections perpendicular to the bedding planes of the rock, bituminite commonly occurs as bedding-parallel lenses or elongate "stringers". Type 3 bitumen commonly forms a complimentary, thin elongate film on the surface of the bituminite or coats the inner wall of the pore enclosing the bituminite (Plate IV). Surface scratches are a common feature, indicating the softness of the bitumen. The reflectance is relatively low but higher than that of types 1 and 2 (0.15%R_o higher than that of type 2 in the middle of the oil window) and it is commonly equivalent to 75% to 80% of the reflectance of the type 4 bitumen. Type 3 is found in most source rocks, regardless of their richness and is observed in rocks with maturation levels as low as 0.4% VR_o eq. and as high as 2.5% VR_o eq.

Medium reflectance (**type 4**) bitumen has no affinity with structured liptinite macerals but is present as a homogeneous mass in micropores within the bituminous matrix, lining microfractures or in voids associated with the growth of dolomite crystals. The shape is dictated by the void it occupies (Plate V) but, unlike the pyrobitumens (e.g. type 5 below), the margins of the type 4 bitumen are rounded and often ill-defined, sometimes having a corroded appearance which grades into the bituminous matrix. The observed interfingering with the bituminous groundmass of shales and mudstones, and their occurrence in argillites lacking structured liptinites, suggest that these type 4 bitumen originate from the matrix bituminite. The reflectance is intermediate between those associated with liptinites and the pyrobitumens. Type 4 bitumen occurs over an extensive maturity range, from 0.4% to over 4% VR_o eq.

High reflectance (type 5) bitumens (**pyrobitumen**) are amorphous, homogeneous and have well-defined and commonly linear margins. They occupy vuggy pores and

PLATE III
TYPE 2 MICROBITUMENS

a) Type 2 bitumen (0.35% R_o) derived from sporinite in the Mattson Formation, Aquitaine *et al.* Tatoo a-2-D.

b) Type 2 bitumen adhering to the walls of a pore in marl from the Prophet Formation, Pan Am *et al.* Celibeta C-07.

c) Type 2 bitumen almost fills the porosity created by thermal destruction of the primary liptinite in shale from the Flett Formation, Texaco Arrowhead N-2.

d) Type 2 bitumen (0.32% R_o) derived from sporinite in the Mattson Formation, Aquitaine *et al.* Tatoo a-2-D.

e) Type 2 bitumen (0.31% R_o) derived from reddish brown sporinite in shale from the Mattson Formation at Clausen Creek.

f) Type 2 bitumen derived from sporinite in the Mattson Formation, Aquitaine *et al.* Tatoo a-2-D; note the accumulation of the bitumen along the pore wall.

g) Two generations of bitumen (types 1 & 2) generated from sporinite in the Mattson Formation at Clausen Creek; Type 1 (weakly reflecting, 0.25% R_o) is currently in the process of being generated from the primary sporinite while type 2 bitumen (0.45% R_o) adheres to the surface.

h) Type 2 bitumen generated from ?alginite in the Banff Formation at Imperial Sun Netla C-07 occupies the pore created by shrinkage of primary liptinite.

Magnification: scale bar shown on b) applies also to c) - h).

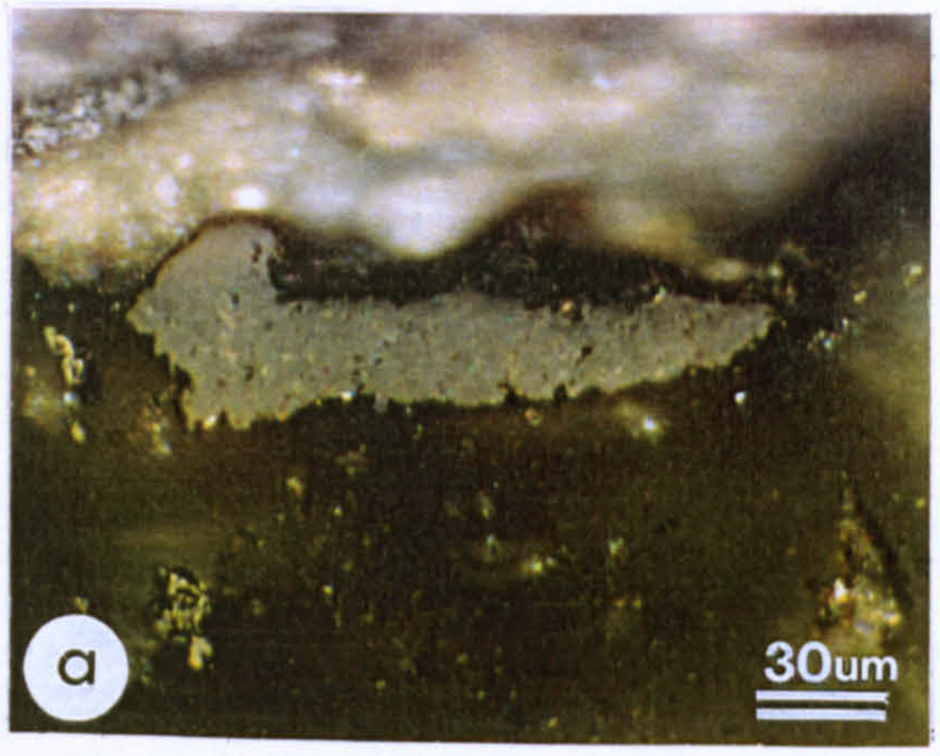
a
30um

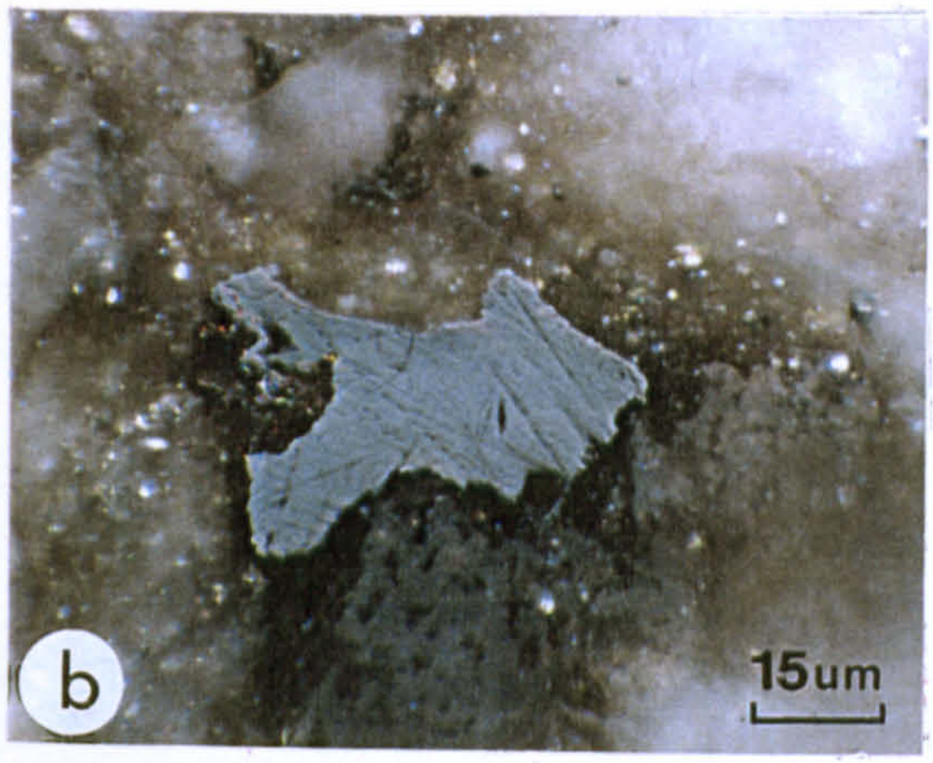
b
15um

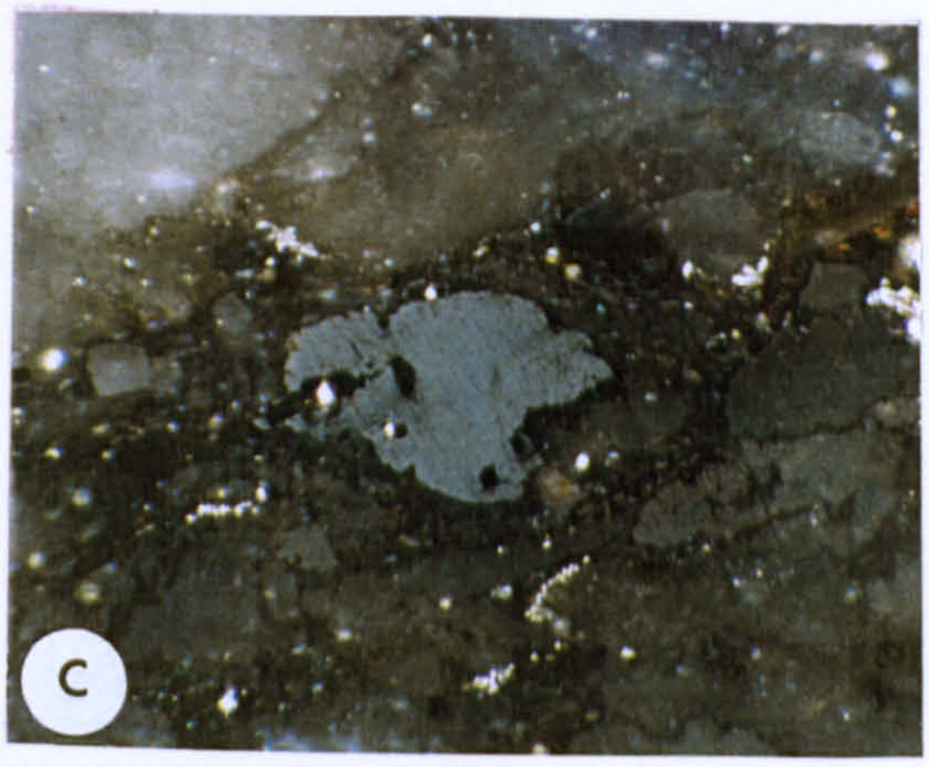
c

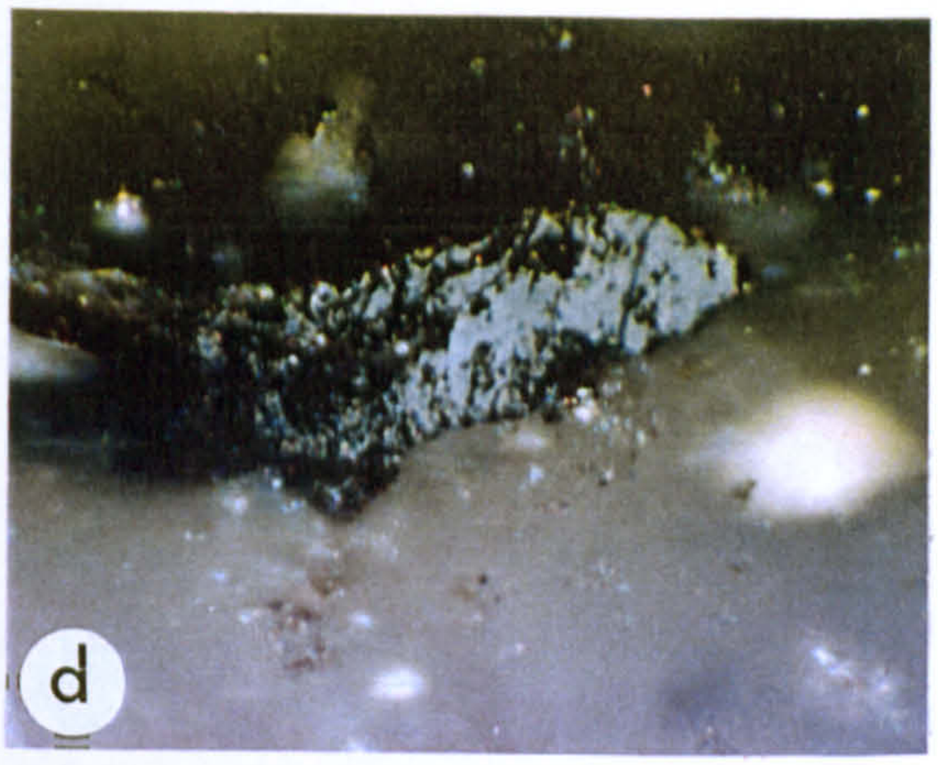
d

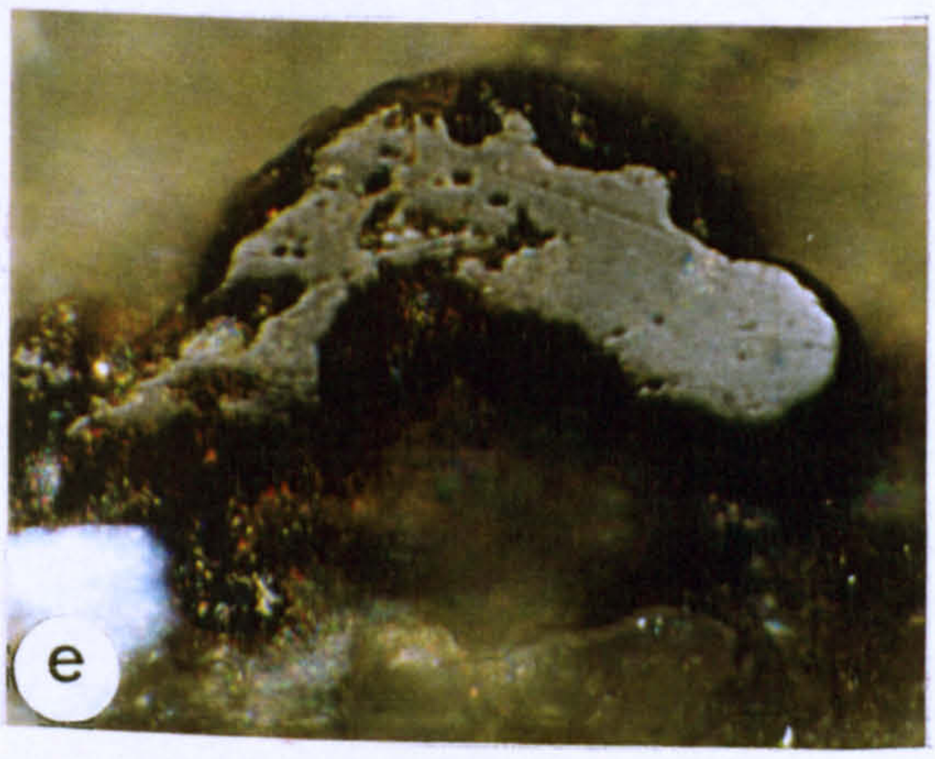
e

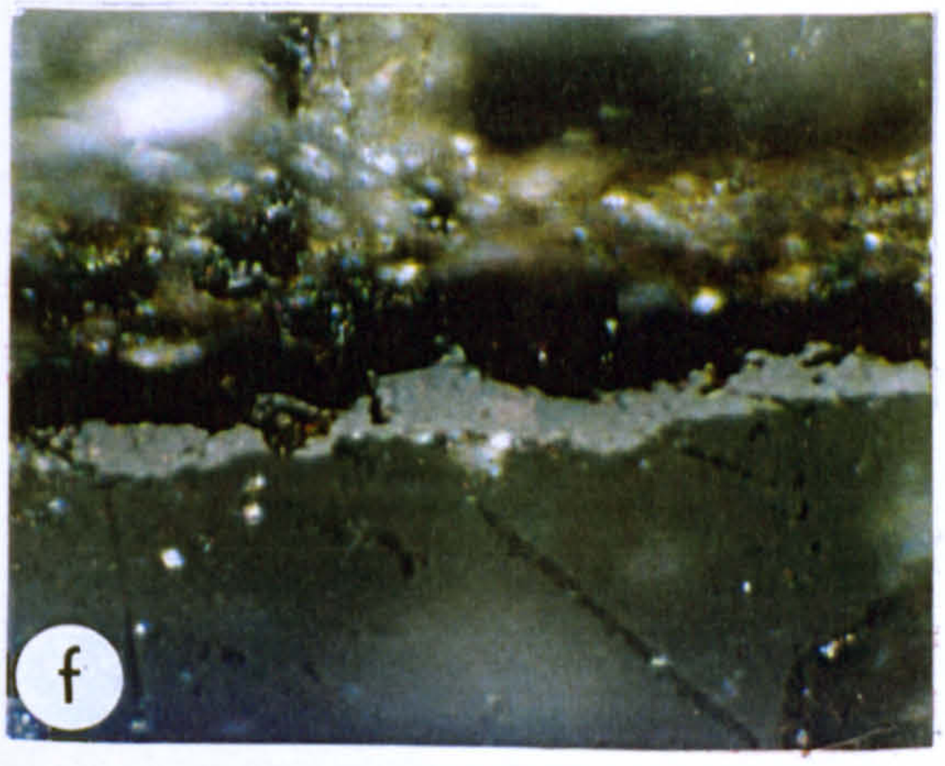
f

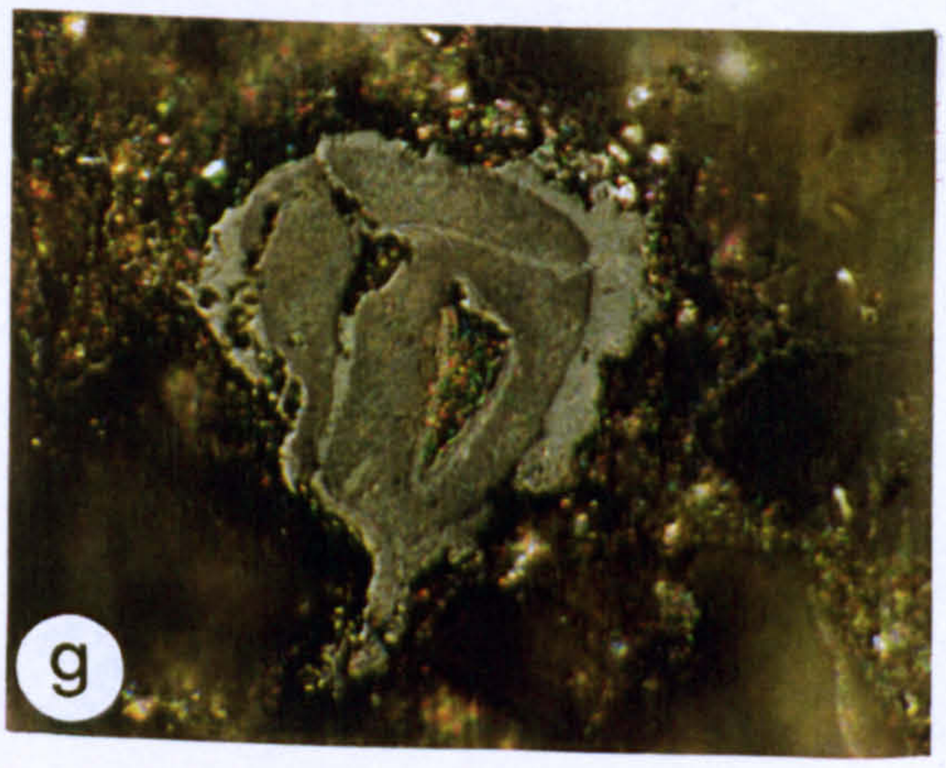
g

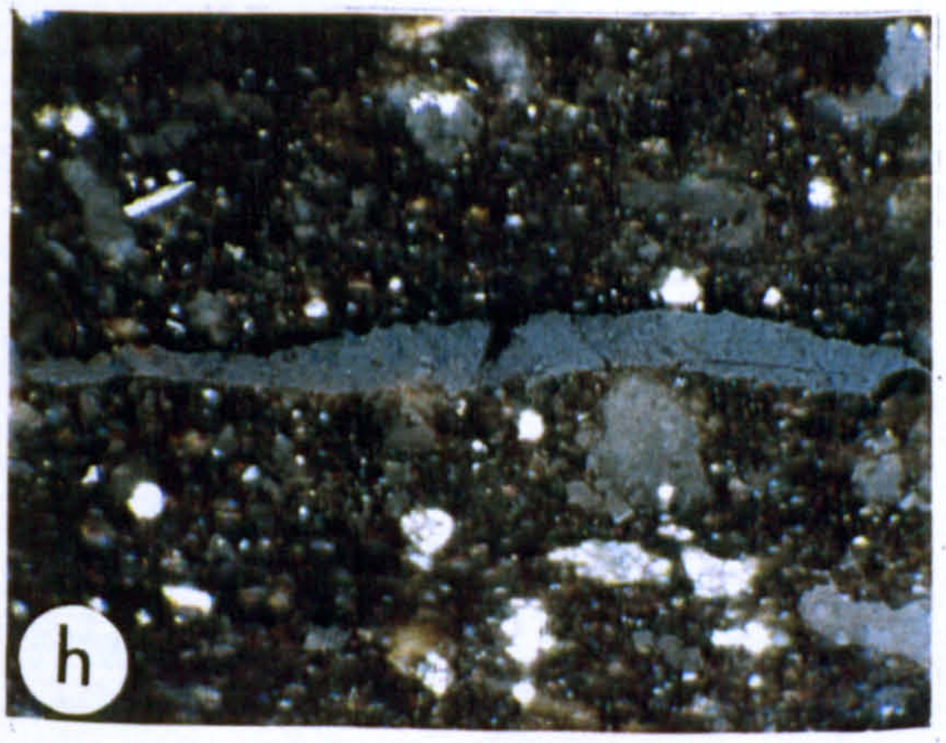
h

PLATE IV
TYPE 3 MICROBITUMENS

a) Type 3 bitumen (0.52% R_o) derived from bituminite I in the Mattson Formation at Clausen Creek is typically "granular" or microporous.

b) Slightly more massive Type 3 bitumen derived from bituminite in the Mattson Formation at Aquitaine *et al.*Tatoo a-2-D.

c) Type 3 bitumen (1.0% R_o) derived from bituminite in the Lower Banff Formation at B.A. Texaco Arrowhead N-2.

d) Type 3 bitumen derived from bituminite in the Mattson Formation at Pan Am Pointed Mountain P-24.

e) Chain-like arrangement of Type 3 bitumen inclusions in bituminite lense in the Lower Banff Formation at B.A.Texaco Arrowhead N-2.

f) Irregular amorphous mass of Type 3 bitumen (0.61% R_o) derived from bituminite in the Golata Formation at Pan Am Kotaneelee; arrow shows typical small, isolated inclusion of bitumen 3 trapped against the wall of a small pore.

g) Large accumulation of type 3 bitumen from the Mattson Formation at Pan Am Pointed Mountain P-53.

h) Type 3 bitumen (0.76% R_o) derived from bituminite in the Mattson Formation at Clausen Creek.

i) High grade type 3 bitumen (1.3 % R_o) derived from bituminite in the Besa River Formation at Pan Am Beaver G-01. (? metaexudatinite of Teichmüller & Ottenjann, 1977).

Magnification: scale bar shown on a) applies also to d), e), f), and h); scale bar shown on b) applies also to c), g) & i).

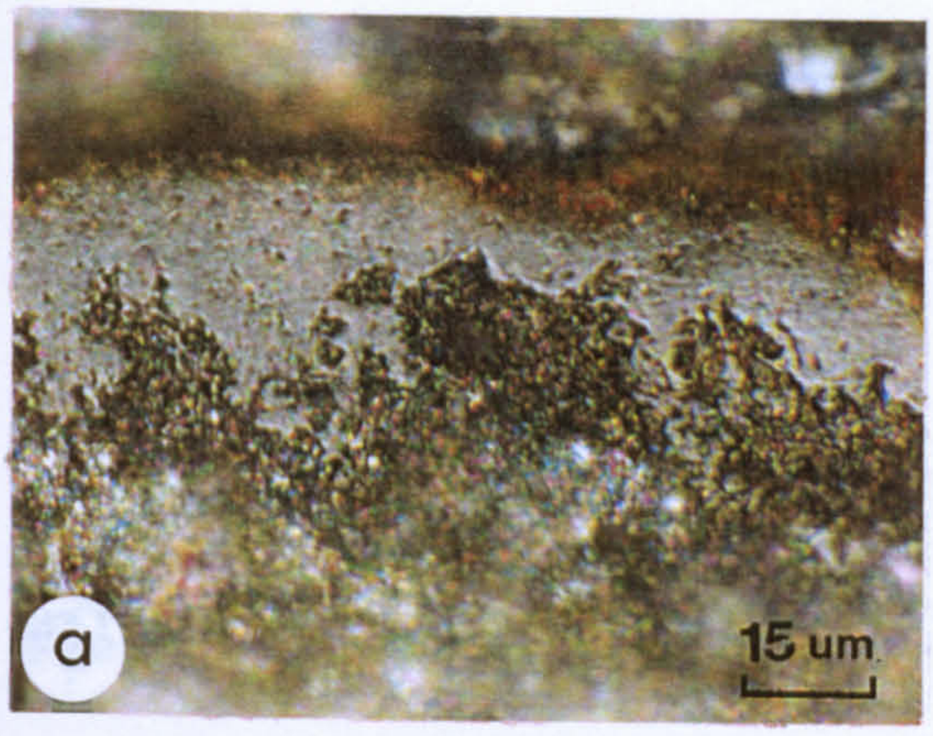
a
15 um

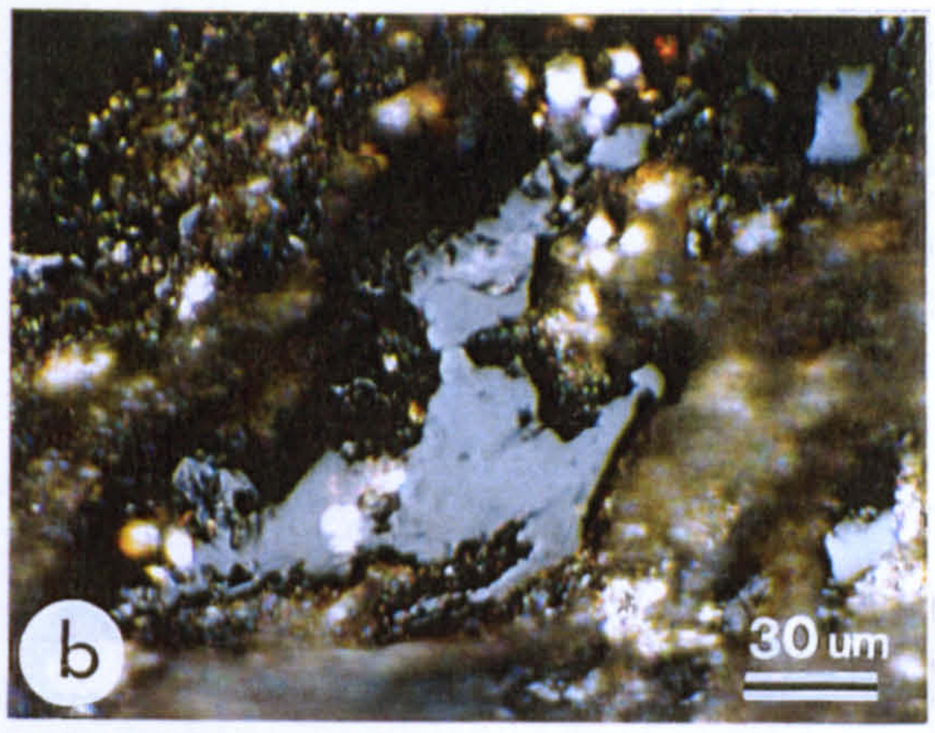
b
30 um

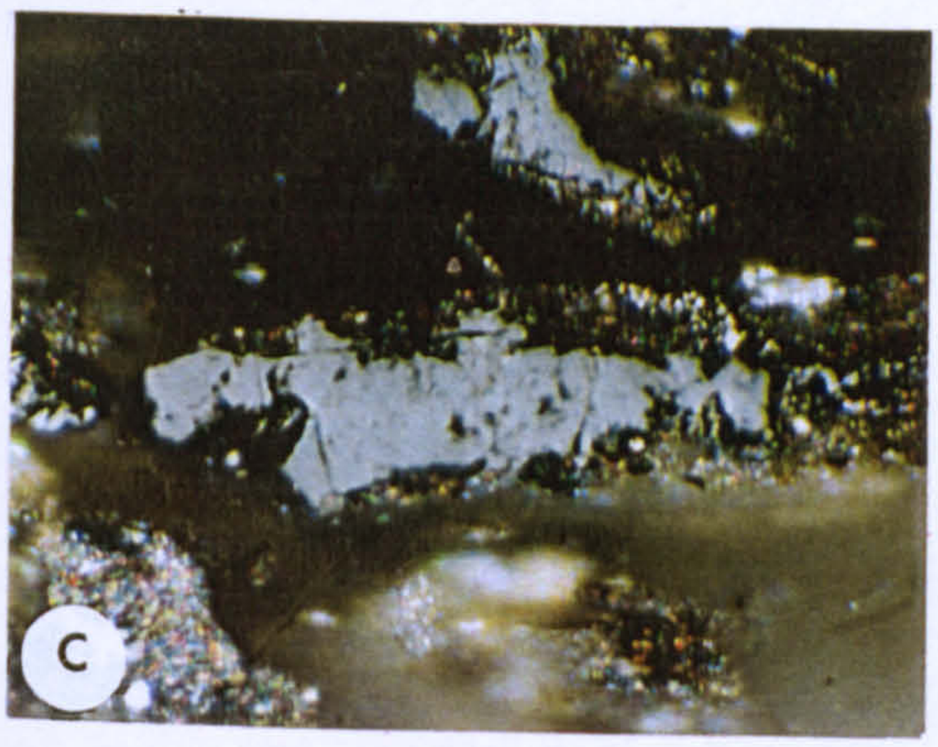
c


d

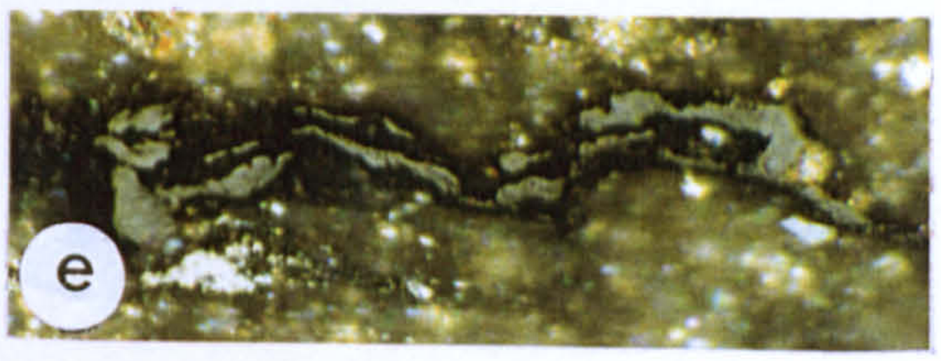
e


f

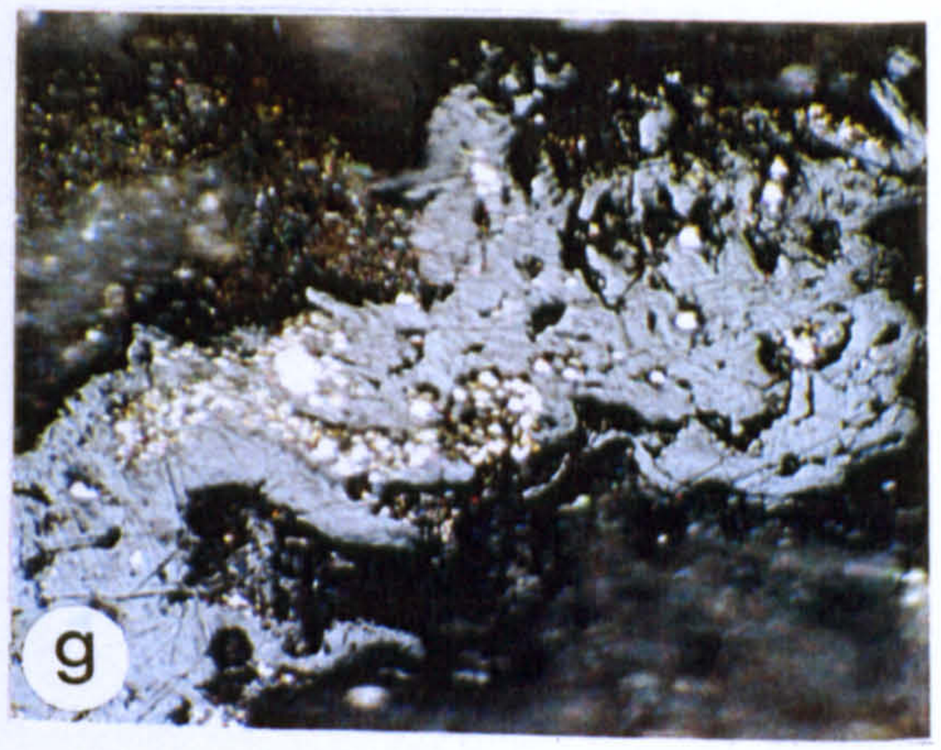
g

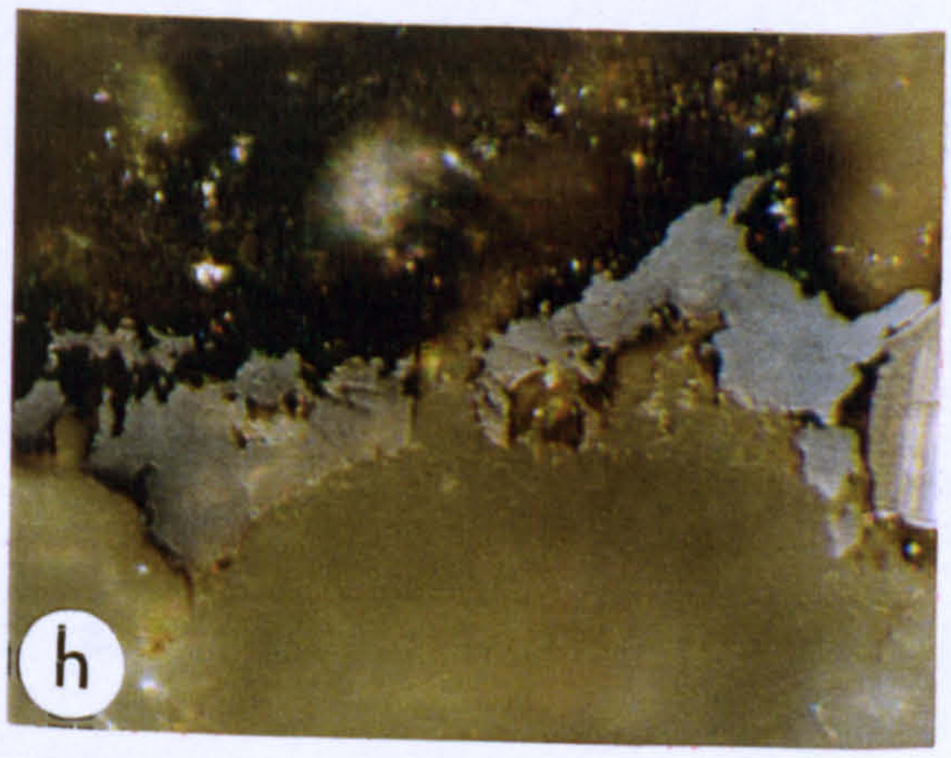
h

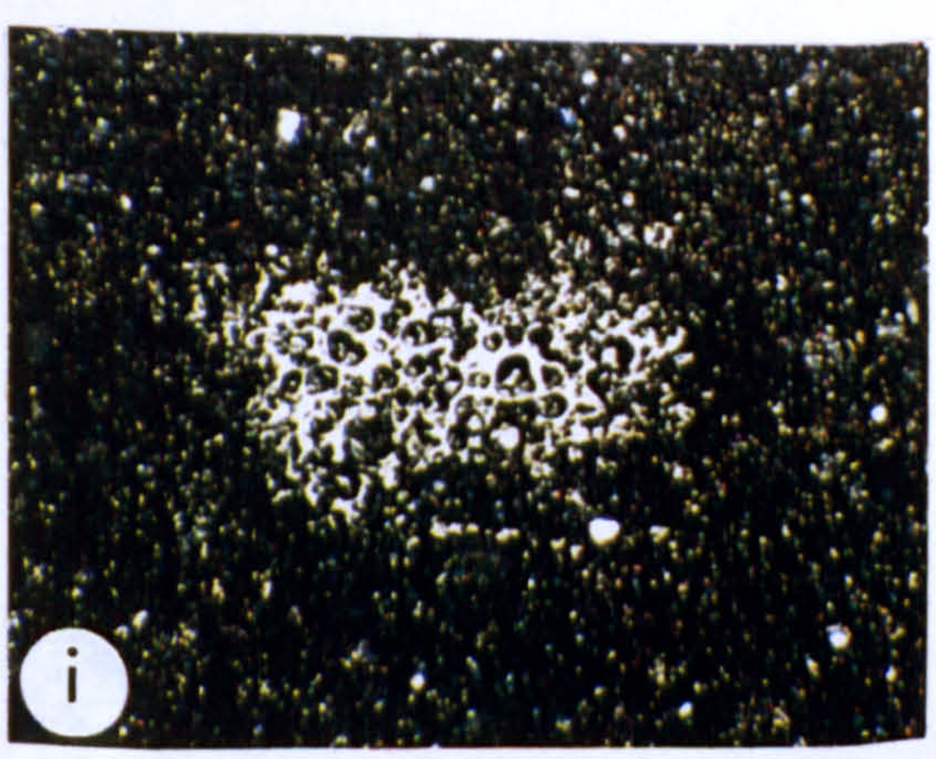
i

PLATE V
TYPE 4 & 5 MICROBITUMENS

a) Type 4 bitumen (0.79% R_o) impregnating aggregate of ?pellets; Mattson Formation at Tatoo a-2-D.

b) Amorphous massive type 4 bitumen (0.74% R_o) in shale matrix in the Mattson Formation at Tatoo a-2-D.

c) Highly reflecting amorphous bitumen possibly derived from the bituminous matrix in shale from the Besa River Formation, Canada Southern *et al.* North Beaver River.

d) Type 4 bitumen partially filling porosity formed by thermal degradation of organic consituents commonly associated with the growth of dolomite crystals in the Prophet Formation. Pan Am Pointed Mountain P-53.

e) & f) Massive accumulation of type 4 bitumen associated with pores and dolomite crystal growth in the Besa River Formation, Pan Am Kotaneellee. Under plane polarized light (e) the bitumen appears highly reflective, but under crossed polars (f) anisotropy with first order interference colours indicates intense heating of the bitumen to produce a bitumen coke.

g) Globular mass of type 4 bitumen (0.75% Ro) with diffuse margins in bituminous matrix of shale from the Exshaw Formation, B.A. Texaco Arrowhead N-2.

h) Highly reflective type 4 bitumen infilling pores in shale from the Mattson Formation at Canada Southern *et al.* North Beaver.

i) Highly reflective type 5 bitumen infilling fractures in a carbonate shell fragment in the shale from the Prophet Formation, Canada Southern *et al.* North Beaver; the High Ro (pyro)bitumens typically have sharp well-defined margins, internal fractures and polygonal outlines.

Magnification: scale bar shown on a) applies also to d), e), f), and h); scale bar shown on b) applies also to c) g) & i).

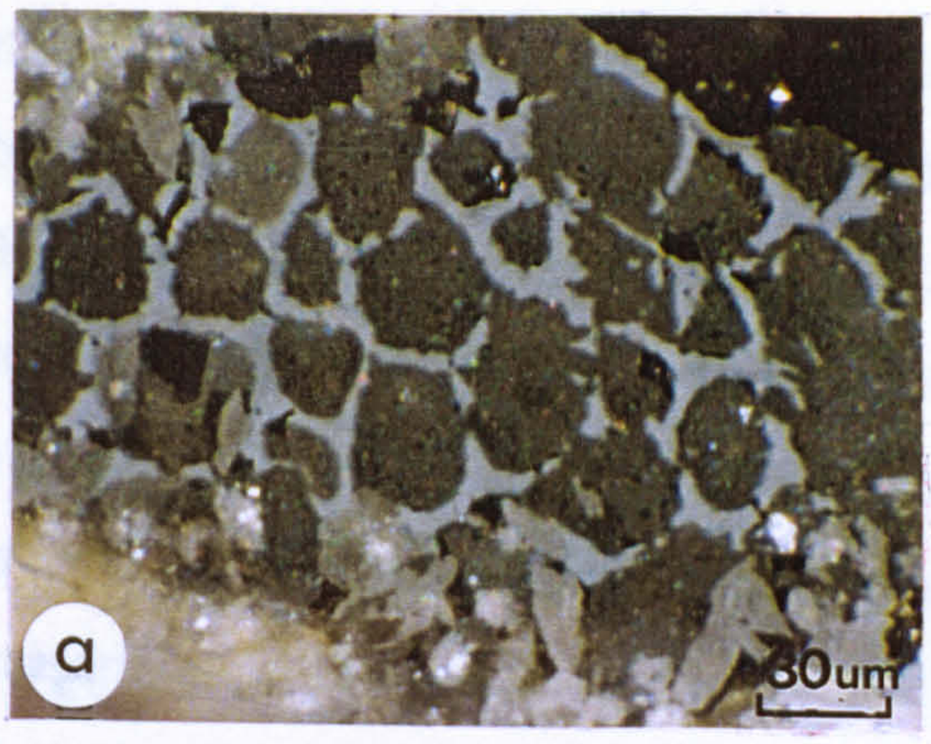
a
30um

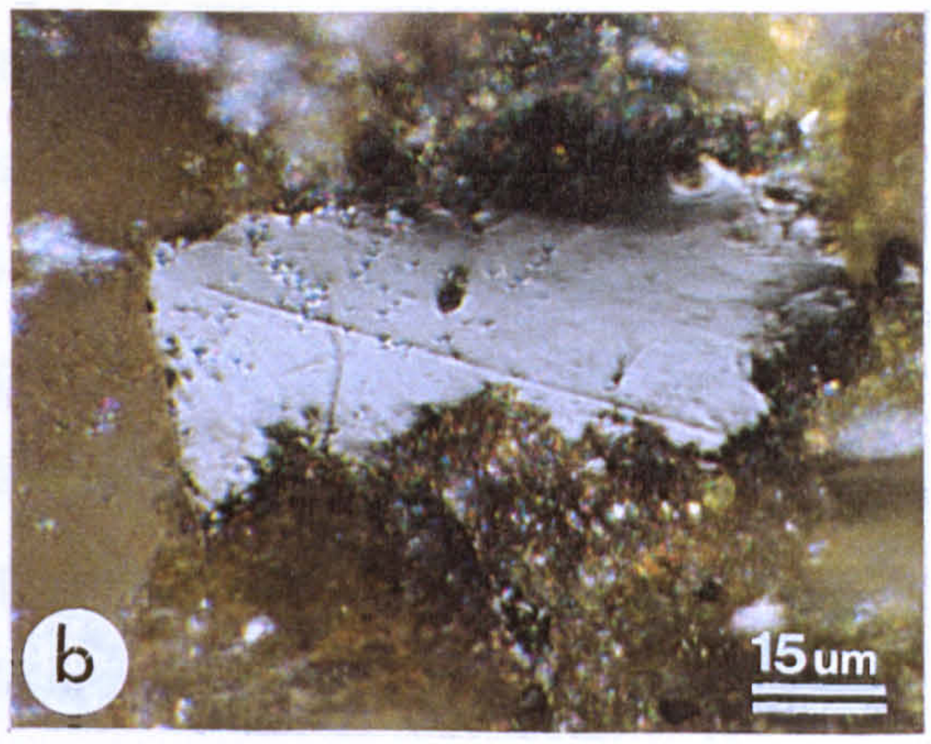
b
15 um

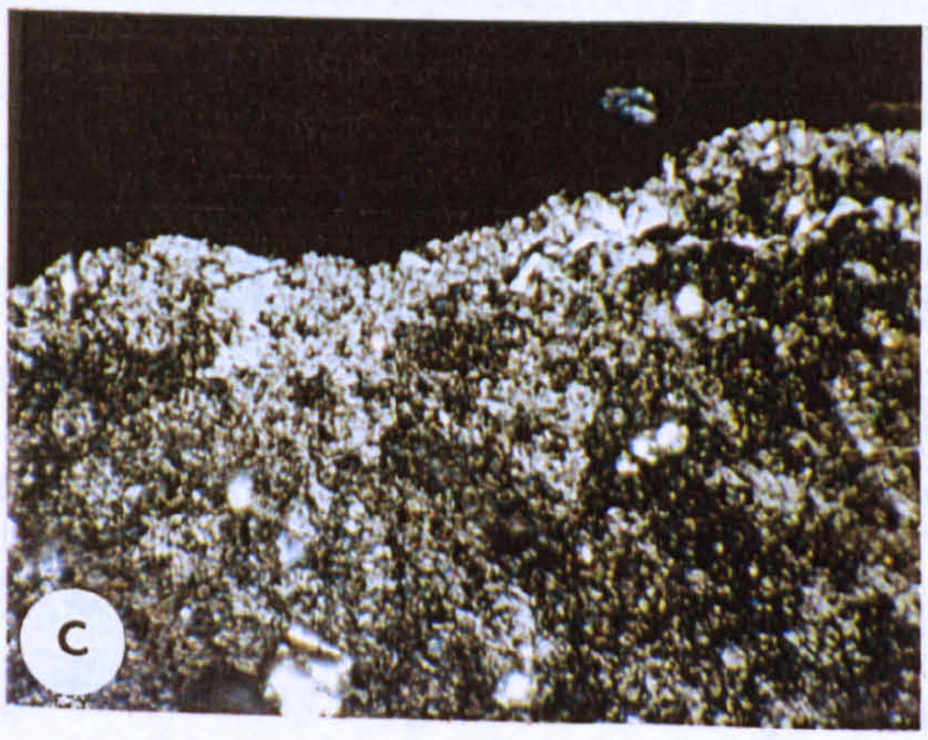
c

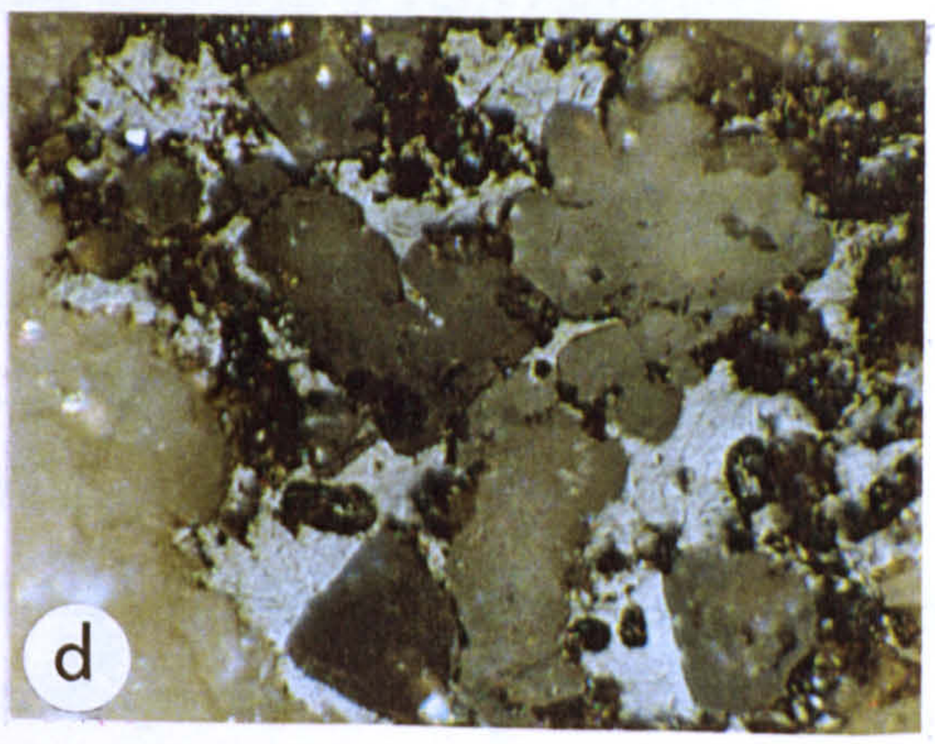
d


e

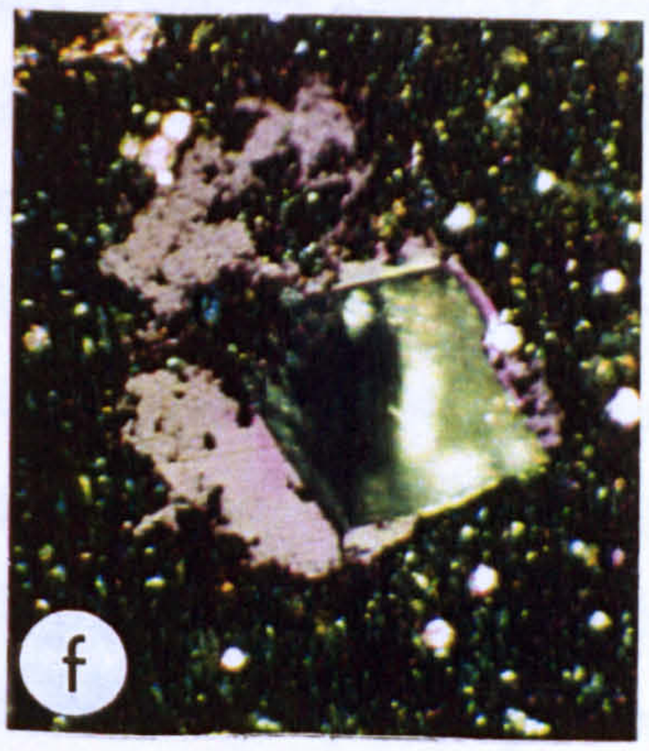
f

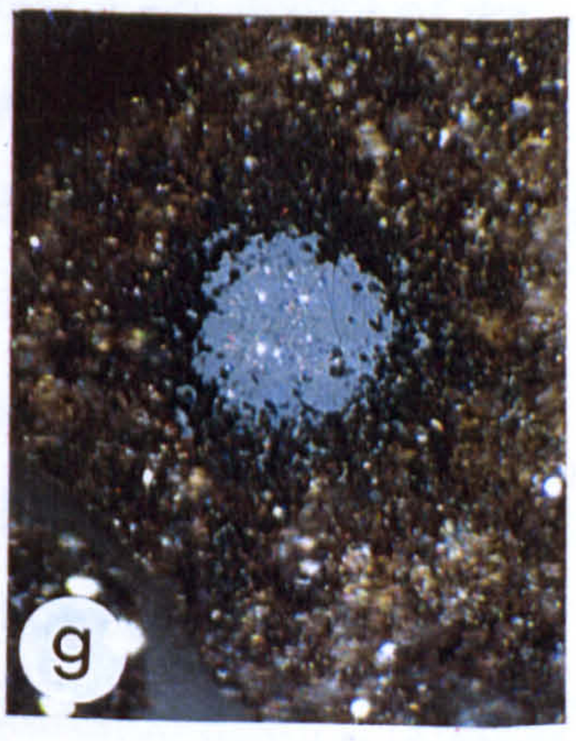
g

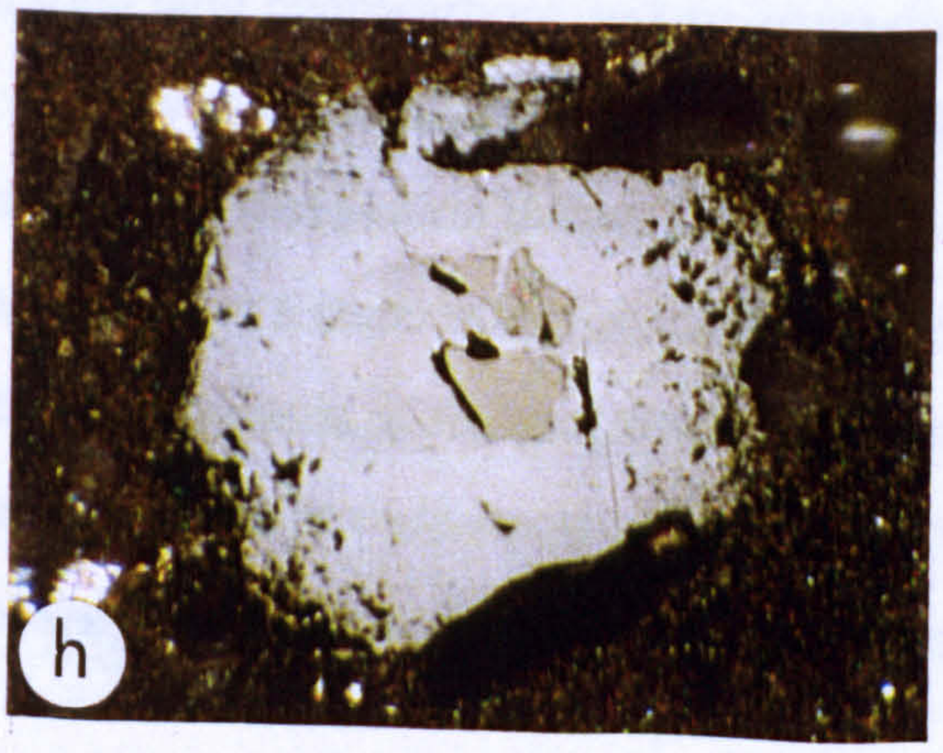
h


i

fractures in the rock matrix and occur in both organic-rich and -lean source rocks and carbonates, having no association with primary macerals. Division into subtypes 5a and 5b is based entirely on reflectance: type 5a has a lower reflectance than type 5b; the reflectance of type 5a may be in the range 1.0% to 3.5% and type 5b reflectance is commonly 1.5% to 5.5% VR_o equivalent, and appears to be unrelated to the maturity of the host rock. Type 5b bitumen is found in rocks at all levels of maturity and is interpreted as a residue from migrated oil (having migrated prior to compaction) which is not necessarily sourced from the rock in which it is found. Type 5a may be a product of polycondensation of hydrocarbons generated during diagenesis or early catagenesis, equivalent to the "post-oil bitumens" of Curiale (1986).

The bitumen generation model proposed herein (Fig. 21) relates the genesis of the low Ro (types 1, 2 & 3), medium Ro (type 4; and possibly type 5a pyrobitumens) to thermal maturation of indigenous organic matter. These microscopic bitumens are generated *in situ*, in contrast to the type 5b pyrobitumens which may be externally sourced. The occurrence of the microscopic bitumens corresponds to the late diagenetic to catagenic maturity range over which hydrocarbons are generated. The greatest abundance and diversity of bitumen types occurs in samples which are presently in the middle of the oil window (ca. 0.8% to 1.0%VR_o) because at this maturity, all types of liptinite actively generate hydrocarbons. The bitumens are thus probably generated as by-products of liquid hydrocarbon generation from the thermal degradation of primary liptinite macerals. The stages at which the bitumens appear in the source rock coincide with (i) the evolution of hydrocarbons during early catagenesis (ca. 0.4% VR_o; types 2, 3 & 4) and (ii) prior to peak hydrocarbon generation (ca. 0.85% VR_o; type 1). Once generated, both they and the primary kerogen increase in reflectance during any subsequent maturation history, possibly generating light hydrocarbons and an increasingly condensed, polyaromatic residue.

Khavari-Khorasani and Michelson (1993) showed that bitumens such as albertite undergo thermal evolution during hydrous pyrolysis that involves polycondensation and aromatization in a manner similar to kerogen and, with increasing aromatization, the reflectance increases. If the progressive increase in reflectance of the microscopic bitumens is related to other maturity parameters such as vitrinite reflectance or Tmax, then it should be possible to use bitumen reflectance to evaluate the thermal evolution (Jacob, 1989;

Bertrand, 1993; Reidiger, 1993).

It is significant that the type 3 and type 4 bitumens first appear early in the thermal evolution of the liptinites, at a reflectance of ca. 0.4% to 0.5% VR_o eq. They are present throughout the oil window and beyond, to a reflectance of 2.5% (type 3) and up to 4.5% (type 4). Teichmüller and Ottenjann (1977) noted that "petroleum source rocks contain microscopically invisible lipoid substances adsorbed on to the clay minerals of the rock matrix" which is released as tar by organic solvents, or by heating to 500°C; and they are the principal source of hydrocarbons. They (*ibid.*) noted that a major change in the fluorescence characteristics of the bituminous matrix (*cf.* "matrix bituminite" *sensu* Creaney (1980); "amorphinite" *sensu* Sentfle *et al.*, 1987) occurs between 0.35% and 0.55% VR_o, which corresponds to a pronounced increase in the release of hydrocarbons. Similarly, Jacob (1989) noted that solid "migrabitumens" develop in source rocks between 0.35% and 0.60% VR_o and suggested that algae were a possible source.

It is interesting to note that Powell and Snowdon (1983) found that wet gas and liquid hydrocarbons were generated from Type II source rocks in the Western Canada Sedimentary Basin at ca. 0.45% VR_o , the same level of maturity at which the type 3 and 4 bitumens observed in this study appear. Khavari-Khorasani and Michelson (1993) suggest that hydrocarbon generation during early catagenesis may be related to the breakdown of oxygen and sulphur-bearing bridges in bitumen, at lower activation energies. This is also consistent with the early generation of sulphur-rich and asphaltic oils from sulphur-rich kerogen in the Western Canada Sedimentary Basin observed by Powell and Snowdon (1983). Powell (1975) indicates that insoluble hydrogen-rich pyrobitumens are probably generated by polymerization of NSO- and asphaltene-rich oils. It is therefore suggested that the amorphous liptinites, i.e. the bituminous matrix and the bituminites, in the shales from the Liard Basin may be richer in NSO compounds and asphaltenes than the structured liptinites (sporinite, cutinite and alginite) causing them to generate bitumens and liquid hydrocarbons at the lower activation energies normally associated with early catagenesis. Asphaltenes and asphaltic bitumens are stable at high temperatures and maturities (Jacob, 1983) which may be the reason why the type 3 and type 4 bitumens in this study are present in source rocks with maturities elevated well beyond the oil window (2.5% and 4.5%, respectively). Jacob (1989) also considers carbon disulphide-insoluble bitumens such

as albertites and wurtzilites to be residues from source material capable of generating hydrocarbons.

The low Ro types 1 and 2 bitumens first appear in source rocks of the study area at approximately 0.6% to 0.7%VR_o (Appendix D) and they are present throughout the oil window but do not occur beyond the upper limit of the oil window (1.3% VR_o for type 1), or just beyond (ca. 1.5% for type 2). Khavari-Khorasani and Murchison (1988) noted that the generation of petroleum hydrocarbons from liptinites occurs in specific order of thermal maturity and the fluorescence characteristics of liptinite macerals follow a similar pattern. Cutinite and sporinite (which are abundant in the shales of the Golata and Mattson formations) generate hydrocarbons at a VR_o eq. of 0.55% to 0.60%; this is approximately related to the "first coalification jump of the liptinites" described by Teichmüller (1982). Alginites do not generate hydrocarbons prior to a maturity of 0.7% VR_o (Khavari-Khorasani & Murchison, 1988). In this study, type 1 and 2 bitumens associated with structured liptinites such as sporinite, cutinite and alginite, first appear at higher maturity levels than the type 3 and type 4 bitumens (ca. 0.6% to 0.75% R_o) which is consistent with the observations of Khavari-Khorasani and Murchison (1988). The disappearance of types 1 and 2 bitumens at approximately the upper limits of the oil window, suggests that they thermally degrade to volatile and liquid hydrocarbons. It must be assumed therefore that the composition of these bitumens includes a high proportion of aliphatic and non-condensed aromatic hydrocarbons. Jacob (1985) refers to solids that are transitional between the organic source material and the solid bitumens as "pre-bitumens"despite that fact that he adhered to the non-genetic, generic classification of bitumens based on physical and chemical properties. He also acknowledged that micro-organisms such as alginites are a possible source material (*ibid.*).

The proposed genetic model for the formation of microscopic indigenous bitumens agrees with more recent classifications of bitumens which emphasize the genetic origins of large accumulations of solid bitumens and acknowledge the progressive generation of lower molecular weight hydrocarbons from bitumen progenitors. Curiale (1986) used the aromaticity, H/C ratios and biomarkers of a variety of commonly-occurring solid bitumen to establish that the occurrence of solid bitumens is related genetically to hydrocarbon generation from source rocks. His genetic classification of solid bitumens acknowledges

pre-oil, syn-oil and post-oil bitumen generation (*ibid.*). Klubov's (1993) bitumen classification recognizes that successive generations of liquid and asphaltic bitumens are produced from catagenesis Type II kerogen by a process of "progressive naphthide formation".

In summary, according to the bitumen genesis model proposed herein, indigenous microscopic bitumens are natural by-products of petroleum generation from liptinite in source rocks. Furthermore, the maturation range over which each type of bitumen is observed is specific and reflects: (i) the thermal threshold required to initiate hydrocarbon and bitumen generation from primary (or secondary) organic material; and (ii) the physicochemical nature of the bitumen by-product. Establishing *in situ* generation of microscopic bitumens within the source rock is an essential prerequisite to the use of bitumen reflectance as a maturation index; furthermore it permits petrographers to discriminate different bitumen populations and thereby produce more consistent and reliable equivalent vitrinite reflectance values.

3.2 REFLECTANCE OF INDIGENOUS BITUMENS

Reflectance data were obtained from dispersed organic matter identified as indigenous microscopic bitumen in over 600 samples from the Upper Devonian and Lower Carboniferous strata. The data set is used to study the applicability of bitumen reflectance as a maturation parameter for use in marine successions where vitrinite is absent or rare (typically the case for distal source rock facies). The samples represent broad ranges of age, burial depths, thermal maturity, lithofacies and depositional environments. While most of the samples range in age from late Devonian (Frasnian) to early Carboniferous (Serphukovian), reflectance measurements were also made on bitumens in shales from the middle Devonian (Givetian), Permian and Cretaceous (Albian to Maastrichtian) strata in the same sections of the Northwest Territories and southeastern Yukon in order to determine the R_o gradients and constrain the thermal history. Bitumen reflectance was also measured on shales of Triassic, Jurassic, Cretaceous and Tertiary ages from sections in northeastern British Columbia. The reflectance data set therefore spans middle Devonian to Tertiary (approximately 300 million years). The measured bitumen reflectance values obtained, over a well depth range of 0 to 13,500 ft. (4,115 m), range from 0.15% to 5.50%. The

depositional environments range from deep marine, basinal deposits, continental slope and shelf to carbonate platform, and marginal marine (-subtidal to -peritidal) to deltaic (including supratidal and terrestrial) environments.

For each sample, the reflectance of between 2 and 4 populations of bitumens was measured. Individual results are documented in Appendix C. Table 11 shows the correlations, derived by linear regression analysis, between the reflectance of the various populations of indigenous, microscopic bitumens. The correlation between reflectance of the type 3 and type 4 bitumens is very strong ($R^2 = 0.9$) and the standard deviation of *y* is reasonably small (0.05) while that between the type 3 and 4 and type 2 bitumen is less ($R^2 = 0.6$) and the standard deviation somewhat larger (0.1). This supports the interpretation of the visual observations that they are generated by a common process (thermal degradation of dispersed macerals) which invokes progressive changes in the physicochemical nature of the bitumens. These changes are manifested in optical properties, such as the reflectance, which increases in a manner similar to that observed in vitrinite. Landis and Castaño (1995) demonstrated decreasing H/C ratios and increasing aromaticity with increasing reflectance of indigenous, microscopic solid hydrocarbons (i.e. bitumens).

3.3 BITUMEN REFLECTANCE AS A MATURATION INDEX.

Jacob (1995), Jacob and Hiltmann (1985) were the first to demonstrate the use of bitumen reflectance (BR_o) as a maturation parameter from which vitrinite reflectance (VR_o) equivalent values could be determined by a simple calculation:

$$VR_o = (0.618 \times BR_o) + 0.4.$$

Since then, studies have been published in which bitumen reflectance has been used to determine maturation trends in marine successions in Canada (e.g. Gentzis, 1991; Reidiger, 1991, 1993). Few regional studies, except that of Potter *et al.* (1993b) and Landis and Castaño (1995), include reflectance on both vitrinite and bitumens in the same stratigraphic intervals from the same locations and this is only study in which dispersed vitrinites and bitumens are compared (Table 12), other studies having used vitrinite data from coals in adjacent stratigraphic sections.

Gentzis (1991) showed that numerous populations of microscopic solid bitumens exist in the Devonian shales of the Canadian Arctic but his selection of the bitumen

x y	Low Ro type 2 bitumen equation	 R^2 *S.D. *y*	Low Ro type 3 bitumen equation	 R^2 *S.D. *y*	Medium Ro type 4 bitumen equation	 R^2 *S.D. *y*	Vitrinite equation	 R^2 *S.D. *y*
Low Ro bitumen type 2	-	- -	$y = 0.71x - 0.03$	0.60 0.09	$y = 0.55x - 0.05$	0.61 0.08	$y = 0.92x - 0.433$	0.64 0.09
Low Ro bitumen type 3	$y = 0.853x + 0.23$	0.60 0.10	-	- -	$y = 0.73x$	0.90 0.05	$y = 1.15x - 0.44$	0.82 0.06
Medium Ro (amorphous) bitumen	$y = 1.095x + 0.33$	0.61 0.21	$y = 1.23x + 0.06$	0.90 0.06	-	- -	$y = 1.4x - 0.50$	0.88 0.07
Vitrinite	$y = 0.695x + 0.6$	0.64 0.08	$y = 0.817x + 0.41$	0.81	$y = 0.61x + 0.41$	0.88 0.05	-	- -

* S.D. = standard deviation from the mean

Table 11 Correlations between bitumen reflectance and measured vitrinite.

population with the lowest reflectance as a maturation parameter appears to be subjective. Reidiger (1993) also acknowledges numerous populations of microscopic solid bitumens in shales from the Triassic Nordegg Member of the Western Canada Sedimentary Basin and concluded that they were generated at the same time; however, she measured only the reflectance of bitumen found in moldic porosity and found that Jacob's relationship did not hold beyond 0.72% (VR_o eq.). More recently, Landis and Castaño (1995) presented strong correlations between solid hydrocarbon (bitumen) reflectance ("SHR_o") and vitrinite reflectance (VR_o); however, they (*ibid.*) cited the reflectance of only the "homogeneous" bitumen (e.g. non-granular and non-anisotropic forms) as the definitive index for maturation. The relationship they found between VR_o and BR_o (*ibid.*) does not agree with that of Jacob (1985).

Samples in which indigenous, microscopic bitumens and dispersed true vitrinite coexist are located in the Golata and Mattson formations at Jackfish Gap, Clausen Creek, Tika Creek, Pointed Mountain (10, 12), Bovie Lake (7) and Tatoo (25; Table 12). It is interesting to note that the relationship that Landis and Castaño (1995) found between their homogeneous bitumen and vitrinite ($y = 1.09x - 0.41$) is similar to that obtained for type 3 bitumen during this study ($y = 1.15x - 0.44$). The type 3 bitumen (this study) is therefore probably equivalent to the homogeneous bitumens of Landis and Castaño (*ibid.*). It is also significant that the relationship between the measured medium Ro (type 4) bitumen and vitrinite in this study ($y = 0.61x + 0.41$) is almost identical to that determined by Jacob and Hiltmann (1985). This appears to confirm that the type 4 bitumen is a bitumen and not a bituminite. Reidiger (1993) indicates that bitumens in the Nordegg Formation do not follow Jacob's relationship above a VR_o equivalent (VR_o eq.) of 0.72%; however, if a genetic approach to bitumen generation is followed, it is apparent that Reidiger's bitumen reflectance data (*ibid.*; Fig. 8) comprises data from two different populations of indigenous bitumens, which may account for the anomalous Tmax distributions obtained (*ibid.*; Fig. 5). Extrapolation of Reidiger's two different bitumen R_o trends indicates that one population is generated at 0.4%, and the other at 0.6%, VR_o eq. This would suggest differing sources and that these bitumens may correspond to the type 4 medium R_o and low R_o bitumens of this study. The data plotted on the line ($VR_o = 0.618BR_o + 0.4$) probably corresponds to type 4 bitumen (which, according to this study, begins maturing ca. 0.4% VR_o) and the

second line (VR_o = 0.277BRo + 0.57) to low Ro bitumen of structured liptinitic origin.

The correlation between the measured vitrinite reflectance (Table 12) and the data calculated from the type 4 bitumen (VR_o eq.) using Jacob's formula, is illustrated in Figure 22. Statistically, the correlation coefficient is not high (R^2 = 0.57) and there is a fairly broad scatter in the calculated vitrinite data. There are a number of possible reasons for this:

(i) ideally, vitrinite reflectance should be measured on collotelinite (ICCP, 1994; formerly telocollinite, ICCP, 1975), but the vitrinites measured in this study are predominantly collodetrinite (ICCP, 1994; formerly desmocollinite *sensu* ICCP, 1975) i.e. a vitrinite maceral which commonly forms a groundmass for other macerals such as as sporinites and inertinites. At this level of maturation (0.8% to 0.9% VR_o), the difference in reflectance between collotelinite (ICCP, 1994) and collodetrinite could be expected to be up to 0.4% lower than the measured R_o maximum of the vitrinite (Mukhopadhyay, 1994);

(ii) the vitrinite reflectance in the source rocks of the Mattson Formation may be suppressed as it is in the coals (Potter *et al.*, 1993a); and

(iii) variations in the lithology of the enclosing rocks can cause the reflectance gradient to increase or decrease due to differences in the thermal conductivities of the rocks (Bostick & Foster, 1985; Jones *et al.*, 1982; Stasiuk, 1988).

A number of studies have reported observations of vitrinite reflectance suppression (i.e. the R_o values being lower than expected) in shales within the oil window (Hutton & Cook, 1980; Kalkreuth, 1982; Price & Barker, 1985; Goodarzi *et al.*, 1987; Mukhopadhyay, 1994). Some have inferred that it may be due the formation of perhydrous vitrinite by the incorporation of lipids into the biopolymers formed from cellulose, lignin and tannins (Zang *et al.*, 1994), or to adsorption of migrated bitumen or hydrocarbons (Suarez-Ruiz *et al.*, 1994). The points that fall below the main trend in Figure 23 are from shales in the outcrops sections of the Mattson Formation at Jackfish Gap. Here there are vitrinites in the overlying coals which show weak fluorescence (typical of perhydrous vitrinite) and resulting in a difference of 0.5% R_o random between the collodetrinite and the perhydrous vitrinite (Potter *et al.*, 1993a). In the same samples, the measured vitrinite was collodetrinite which displays weak fluoresce and contains an abundance of mature sporinite. Collodetrinite (the lowest reflecting vitrinite) was selectively chosen because of

SAMPLE LOCATION	Sample No.		REFLECTANCE vitrinite[1]			$VR_{o\,eq.}$[3]	
	GSC #	I.D.	mean	S.D.[2]	n	B 3	B 4
Texaco NFA Bovie Lake J-72	C186762	-1260	0.79	0.00	2	0.75	-
Pan Am Pointed Mountain P-53	C186766	-1950	0.73	0.00	1	0.75	0.73
Pan Am Pointed Mountain P-53	C186766	-2160	0.80	0.03	2	0.81	0.79
Pan Am Pointed Mountain P-53	C186766	-2780	0.83	0.06	6	0.78	0.81
Pan Am Pointed Mountain P-53	C186766	-3195	0.82	0.04	4	-	0.81
Pan Am Pointed Mountain P-53	C186766	-3870	0.85	0.02	7	0.81	0.84
Pan Am Pointed Mountain P-53	C186766	-4310	0.96	0.03	3	0.89	0.91
Amoco Pointed Mountain P-24	C186760	-3380	0.80	0.03	4	0.82	0.78
Amoco Pointed Mountain P-24	C186760	-4500	0.80	0.03	13	0.80	0.80
Amoco Pointed Mountain P-24	C186760	-4890	0.85	0.05	17	0.81	0.78
Amoco Pointed Mountain P-24	C186760	-5140	0.89	0.05	5	0.82	0.80
Amoco Pointed Mountain P-24	C186760	-5340	0.91	0.04	5	-	0.83
Jackfish Gap-Yohin Ridge	C58709	3894	0.80	0.02	2	0.77	0.84
Jackfish Gap-Yohin Ridge	C58711	3986	0.83	0.03	3	0.86	0.84
Jackfish Gap-Yohin Ridge	C58713	4096	0.80	0.00	1	0.84	0.85
Jackfish Gap-Yohin Ridge	C58719	4413	0.90	0.03	5	0.94	0.89
Jackfish Gap-Yohin Ridge	C58726	4633	0.81	0	4	0.86	0.85
Jackfish Gap-Yohin Ridge	C58730	4754	0.74	0.04	8	-	-
Jackfish Gap-Yohin Ridge	C58736	4859	0.79	0.03	8	0.85	0.84
Jackfish Gap-Yohin Ridge	C58737	4862	0.78	0.02	10	-	-
Jackfish Gap-Yohin Ridge	C58759	5535	0.74	0.00	1	-	0.76
Jackfish Gap-Yohin Ridge	C58764	5640	0.74	0.02	9	-	0.71
Jackfish Gap-Yohin Ridge	C58765	5640	0.74	0.04	19	0.71	0.75
Jackfish Gap-Yohin Ridge	C58793	6385	0.72	0.01	3	-	0.70
Jackfish Gap-Yohin Ridge	C58804	6724	0.68	0.03	25	-	-
Jackfish Gap-Yohin Ridge	C58806	6754	0.66	0.03	38	-	-
Jackfish Gap-Yohin Ridge	C58838	7246	0.65	0.04	25	-	-
Clausen Creek	C74277	3414	0.76	0.01	2	0.78	0.76
Clausen Creek	C74276	3414	0.74	0.02	6	-	0.78
Clausen Creek	C74309	4283	0.75	0.01	11	-	
Aquitaine *et al.* Tatoo a-2-D	C186775	-1617.5	0.81	0.03	11	0.81	
Aquitaine *et al.* Tatoo a-2-D	C186775	-1625.5	0.79	0.02	9	0.83	
Aquitaine *et al.* Tatoo a-2-D	C186775	-1631	0.79	0.02	9	0.82	
Aquitaine *et al.* Tatoo a-2-D	C186775	-1655	0.80	0.00	1	0.80	

[1] measured vitrinite reflectance; [2] S.D. = standard deviation from the mean;
[3] VR_o eq. = calculated from measured reflectance of type 3 (B3) and type 4 (B4) bitumens.

Table 12 Measured and calculated vitrinite reflectance data from the Mattson Formation.

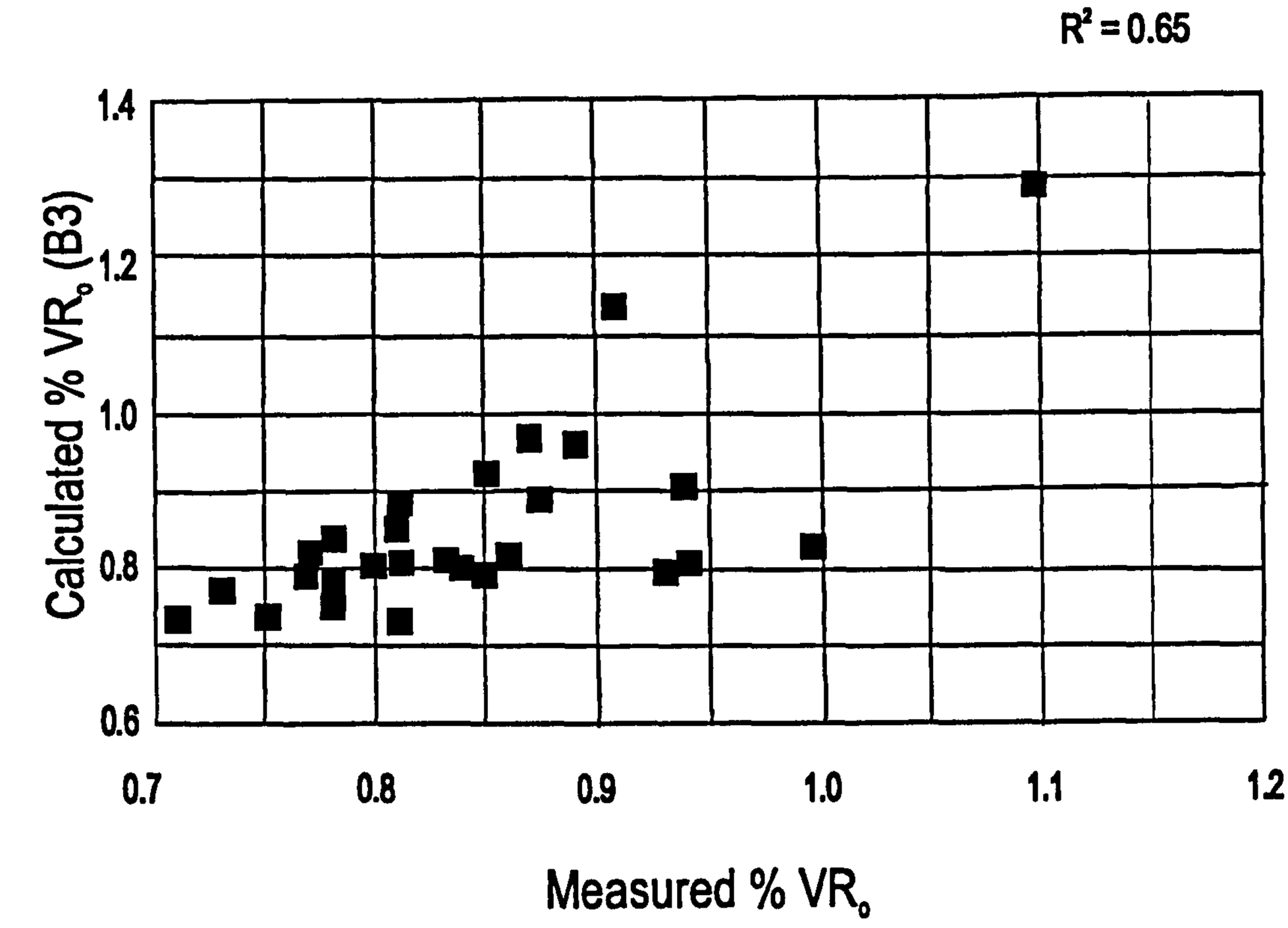

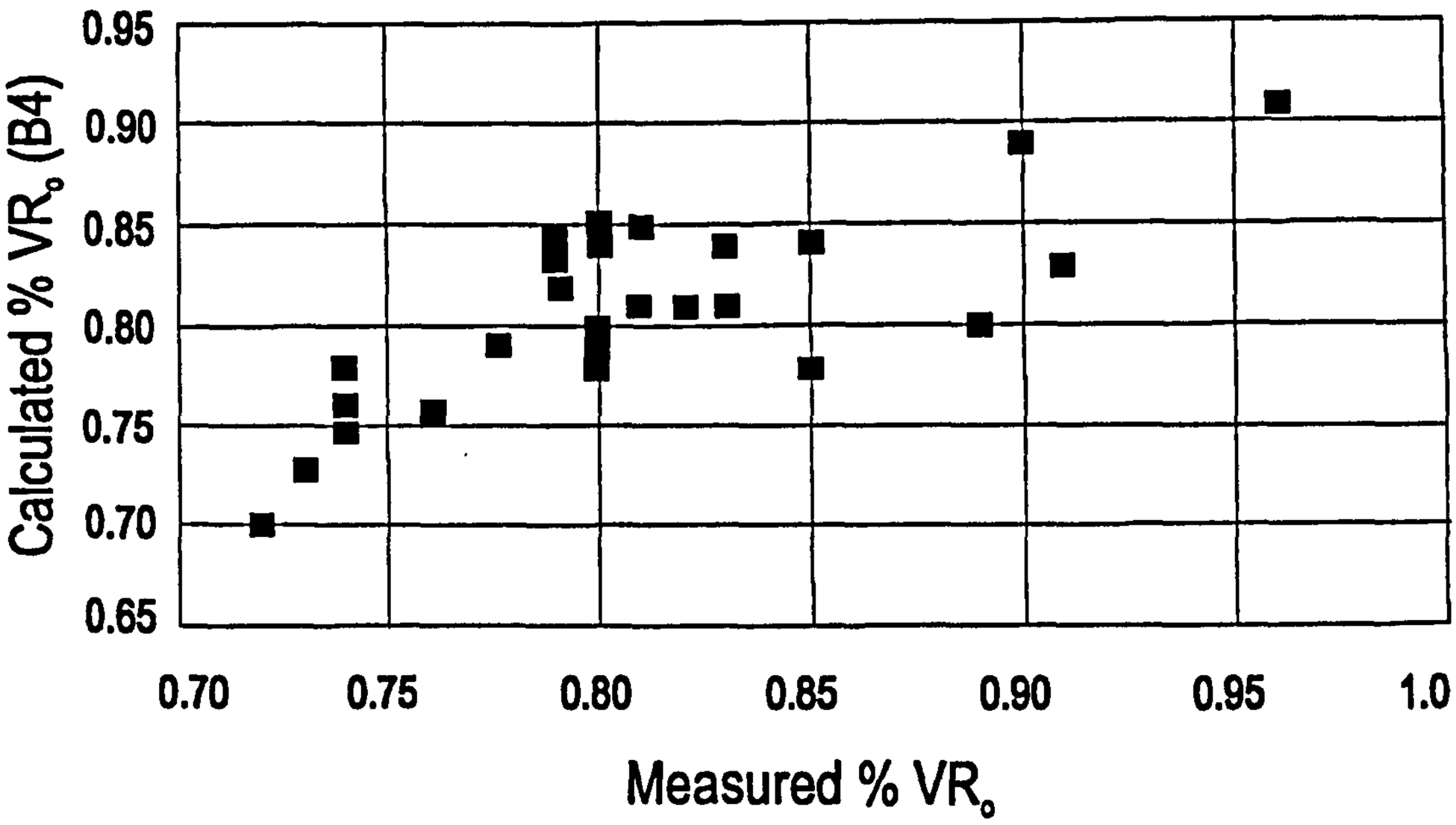

Figure 22. Correlation between measured VR_o based on: a) type 3 bitumen R_o , and b) type 4 bitumen R_o.

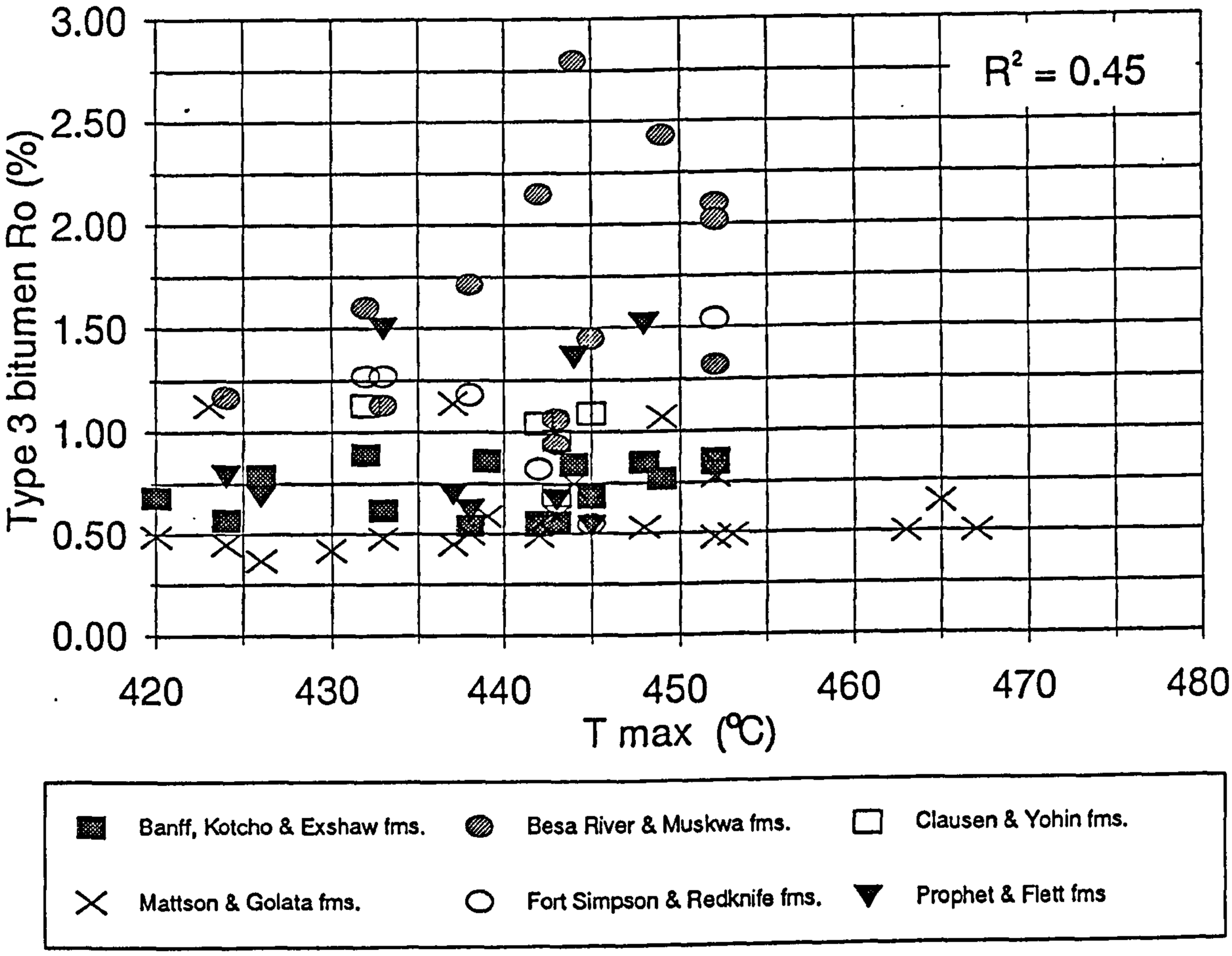

Figure 23. Correlations between Tmax and: a) type 3 bitumen Ro, and b) vitrinite Ro equivalent derived from type 3 bitumen.

its association with other coal macerals of the liptinite or inertinite groups which provided certainty of its identity because at maturation levels between 0.8 and 1.1% R_o, it is very difficult to distinguish optically between vitrinite and coexisting type 4 bitumen in the same sample. Reflectance data from the Mattson Formation at Pointed Mountain (12) were also included in Figure 22 and these points tend to plot above the main trend (i.e. the reflectance of the measured vitrinite are higher than that of those calculated from medium Ro (type 4) bitumen). These samples are extensively dolomitized and the vitrinites are non-fluorescing and therefore the reflectance may have been elevated by hot dolomitizing fluids. Morrow *et al.* (1993) attributed pre-Cretaceous dolomitization of the middle Devonian reservoir rocks in the Beaver River area to hydrothermal activity (Morrow *et al.*, 1986).

The relationships between Tmax and type 3 bitumen R_o and its VR_o equivalents, and type 4 bitumen R_o and its VR_o equivalents, are shown in Figures 23 and 24, respectively. The correlations are relatively poor. Marginally better correlations are observed between Tmax and the measured data than the calculated VR_o eq. values; and the correlation between Tmax and type 3 bitumen R_o is better that for Tmax and type 4 bitumen. The observed distributions do not appear to be related to either the lithology or the TOC content of the host rocks, but maturity and organic facies may play a role. When the data are plotted according to the formation of origin, the postmature samples (as determined by R_o values, i.e. those from the Besa River and Muskwa formations) have Tmax values which fall well expected values. For mature samples, more consistent trends are shown by samples from individual formations which suggests that the organic facies influences the Tmax. Overall, the Tmax values are lower that expected and this may be attributable to the lack of primary organic matter contributing to the S2 peak, i.e. the S2 peak from which the Tmax is calculated, is derived from pyrolysis of the bitumens as well as primary macerals.

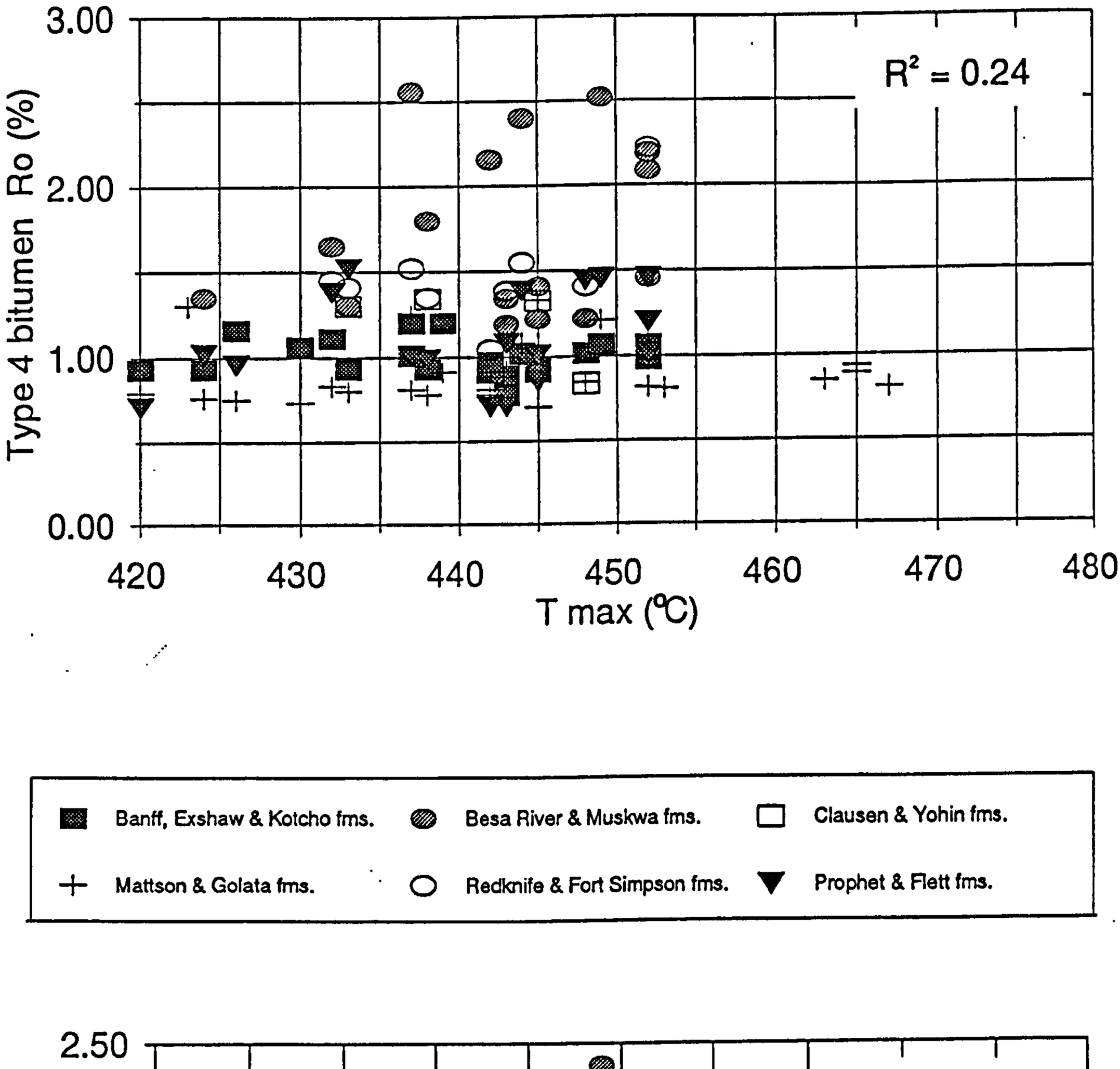

Figure 24. Correlations between Tmax and : a) type 4 bitumen Ro, and b) vitrinite Ro equivalent derived from type 4 bitumen.

4.0 KEROGEN TYPE, PETROGRAPHIC COMPOSITION, THERMAL MATURITY AND HYDROCARBON POTENTIAL

The TOC content, petrographic composition, maturity and hydrocarbon potential of all organic-rich units from the Upper Devonian Muskwa Formation to the Lower Carboniferous Mattson Formation were examined but only those with TOC values > 0.5% and having potential to generate oil or gas are discussed in detail. Sampling locations and sections are shown in Table 1 and Figure 16 and are referred to by the section numbers shown in Figure 16. Petrographic descriptions are tabulated in Appendix A, Rock-Eval results are listed in Appendix B, and the measured reflectance and fluorescence data are presented in Appendix C.

4.1 MUSKWA FORMATION

The Muskwa Formation is a thin, extremely radioactive, fondoform shale unit developed at the base of the Upper Devonian (Moore, 1993) in the Eastern Plains. It is stratigraphically equivalent to the Horn River Formation in the Mattson Creek area (Fig. 16). The Muskwa Formation occurs at greatest depth, and is thickest (70.1m), near the Bovie Fault zone (section 8), and thins significantly to the north and to the east, dwindling to less than 8m in the northeastern part of the study area.

Organic richness

Total Organic Carbon values for the Muskwa Formation range from 0.88% to 4.28% (Appendix B1), indicating the Muskwa Formation is, or has been, a good to excellent hydrocarbon source rock. The TOC values are lowest where the Muskwa is marly and moderately well-dolomitized near the Bovie Fault. The low TOC samples have extensive microfracture networks developed parallel and perpendicular to bedding. The highest TOC values are recorded from the more northerly and central locations (4.28% and 4.5% at Arrowhead and Mattson Creek, respectively) and are characterized by minor amounts of dolomite; these locations are more or less coincident with the axis of the Liard Basin (Leckie *et al.*, 1991). Typically, the dolomites are euhedral to subhedral crystals and occupy micropores within the shale matrix. The inverse relationship observed between

dolomite and TOC content suggests that dolomitization occurred synchronously with thermal maturation of the bituminous matrix. It is suggested that the dolomite growth occurred in pores created by a reduction in the volume of the organic matter as hydrocarbons were generated from it, resulting in a decrease in the TOC values with organic maturation.

Organic petrology

The Muskwa samples are black shales and mudstones that are characteristically well-laminated on a microscopic scale. The principal organic constituent is dark brown to black, bituminite matrix associated with a high proportion of pervasive micrinite (Appendix A1). The dark colour of the matrix bituminite (cf. Creaney, 1977) is evidence of its elevated thermal maturity (Peters *et al.*,1982). Micrinite is a common constituent of Carboniferous bituminous coals (Teichmüller, 1968, 1984) although Shiboaka (1978) and others have observed micrinite in low rank coals. Teichmüller (1974) considered bituminite to be a precursor of micrinite. Teichmüller and Ottenjahn (1977) observed micrinite in black shales from the Posidonia Formation of western Germany and attributed its occurrence to the diagenesis of bituminites, linking its formation to the generation of hydrocarbons; transmission electron microscope studies of shales by Taylor and Lui (1989) drew similar conclusions. Stasiuk (1988) observed a bituminite-micrinite association in Lower Cretaceous shales in Saskatchewan which he considered to be a source of biogenic gas. Subsequently, he observed pods, lenses and irregular patches of micrinite which resembled clusters of coccoidal bacteria associated with bituminite in immature to marginally mature, Devonian shales of the Williston Basin (Stasiuk, 1993). He concluded that micrinite is a residual product of microbial breakdown of unicellular alginite, which may even be derived from the bacteria themselves, rather than a product of thermal maturation (*ibid.*) as previously suggested by Teichmüller (1968, 1982) and Teichmüller and Wolf (1977). Potter *et al.* (1993a) discuss the association of bituminite and micrinite in terms of the origin of micrinite in Lower Carboniferous sapropelic coals, suggesting that it forms during diagenesis from the anaerobic bacterial remains that are associated with the degradation of primary organic matter. While the high reflectance of micrinite distinguishes it readily from the dark bituminous matrix, unlike most of the highly reflective macerals belonging to the inertinite group, micrinite is not chemically inert; it is

suggested that this might be because it is derived from bacterial lipids and nucleic acids (*ibid.*). Alternatively, Faraj and Mackinnon (1993) have indicated that the micrinite in some Australian coals should be redined as kaolinite, on the basis of SED-EDS studies.

The subordinate macerals are microscopic bitumens showing distinctive habits and affiliations and exhibiting a marked range in reflectance (Appendix C1). Two types of bitumen are common in the Muskwa Formation. The first type exhibits the lowest reflectivity and typically occurs as elongate wisps and stringers arranged parallel to bedding in a similar fashion to thin-walled alginites of the Leiosphaeridiales-type (cf. Stasiuk, 1988). Typically, it is relatively isotropic and the reflectance is generally greater than 1.2% R_o and as high as 2.0%. Within section 3, these bitumens show reflectivities between 1.5% and 2.0% R_o and the bireflectance[1] ranges from 0.1% to 0.3%, over that range. Despite the high reflectance values, these bitumens are classified as low R_o, type 3, the term low Ro being used in a relative fashion to classify the bitumen population having the lowest reflectance. The low Ro, type 3 bitumen is interpreted as having been derived by thermal disintegration of bituminites of algal origin because of the observed similarities in habit and distribution of these two macerals. Bitumens having a lower reflectance (1.2% R_o) than these are rare but, when present, occur as pods ca. 50-70mm long, often having a "hatched" surface relief (Plate 1).

The second common type of bitumen is the isotropic medium R_o (type 4) bitumen which typically occurs in pods or in pores in the matrix (Plate V). It has no affiliation with primary structures other than the bituminous shale matrix.

Within sections 4 and 7, significant anisotropy is exhibited in both low reflectance (type 3) and medium R_o (type 4) bitumens. Within section 4, the anisotropy is manifested in the form of a high, apparent bireflectance[2] (0.2%-0.4%R_o in the reflectance range 1.8-2.4%R_o), but in section 7, it takes the form of a very fine-grained, optical mosaic (Plate VI). Mosaic textures are typical of semicokes formed by thermal alteration of bitumens or vitrinite during laboratory hydrogenation, usually under hydrogen-deficient conditions (Marsh *et al.*, 1973; Potter *et al.*, 1986); they can also form naturally by direct thermal alteration of sedimentary organic matter in contact metamorphic aureoles (Creaney, 1977).

The lack of structured liptinites in the Muskwa may be related to elevated thermal

---

[1]The bireflectance values (R_o max-R_o min) are apparent values only since true Rmax and Rmin values can only be determined on samples oriented perpendicular to bedding.

PLATE VI
PETROGRAPHIC COMPONENTS OF THE MUSKWA FORMATION

a) High grade, granular type 3 microbitumen in dark brown to black bituminous matrix containing pervasive micrinite and pyrite, viewed in plane parallel to bedding; Imperial Sun Arrowhead I-46 section.

b) As a), viewed perpendicular to bedding; Imperial Sun Arrowhead I-46 section.

c) Medium Ro, type 4 bitumen in intercrystalline porosity of annealed microfracture emplaced at about, or just after, peak oil generation; Texaco Bovie Lake J-72.

d), e) Anisotropic, granular, type 3 bitumen in plane polarized light (d) and under crossed polars with wavelength plate insert (e); the granular appearance is the result of the development of a fine anisotropic mosaic texture; the first order interference colours are indicative of cokes formed by intense heating. Texaco Bovie Lake J-72.

f) One section of the dolomitized remains of a filamentous alga, or cyanobacterial trichome, impregnated with low Ro bitumen (0.17% Ro); whole filament ca. 800µm in length. Texaco Bovie Lake J-72.

g), h) Highly reflective, carbonate-filled cenospheres derived from bitumen. Mineral-filled central vacuoles are formed by rapid devolatilization of the organic matter due to combustion or pyrolysis. Texaco Bovie Lake J-72.

Magnification: scale bar shown on a) applies also to d), e) & f); scale bar shown on b) applies also to c), g) & h).

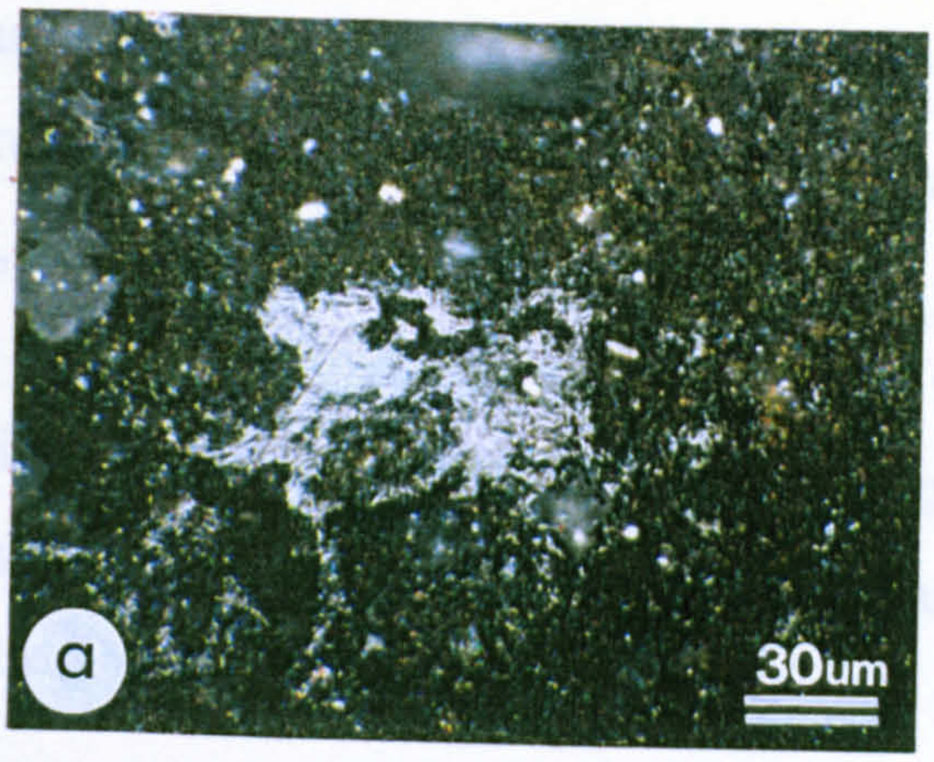
a
30um

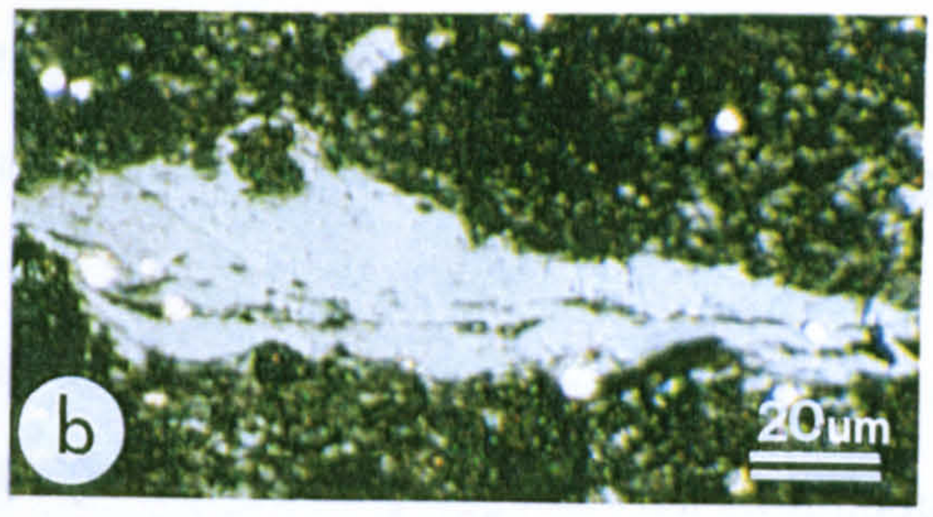
b
20um

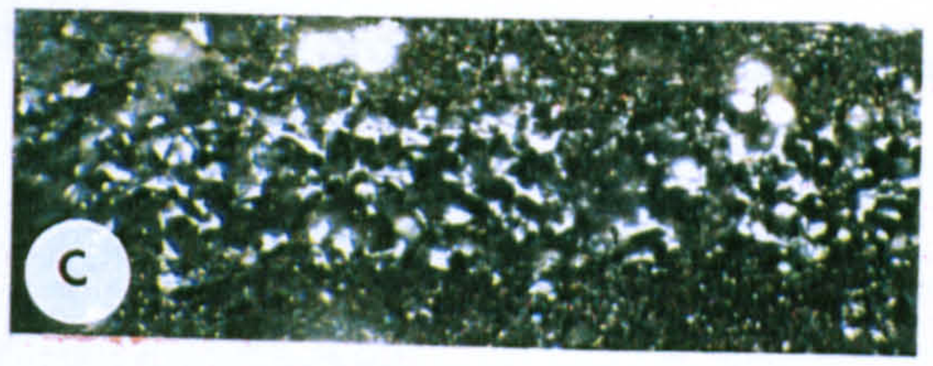
c

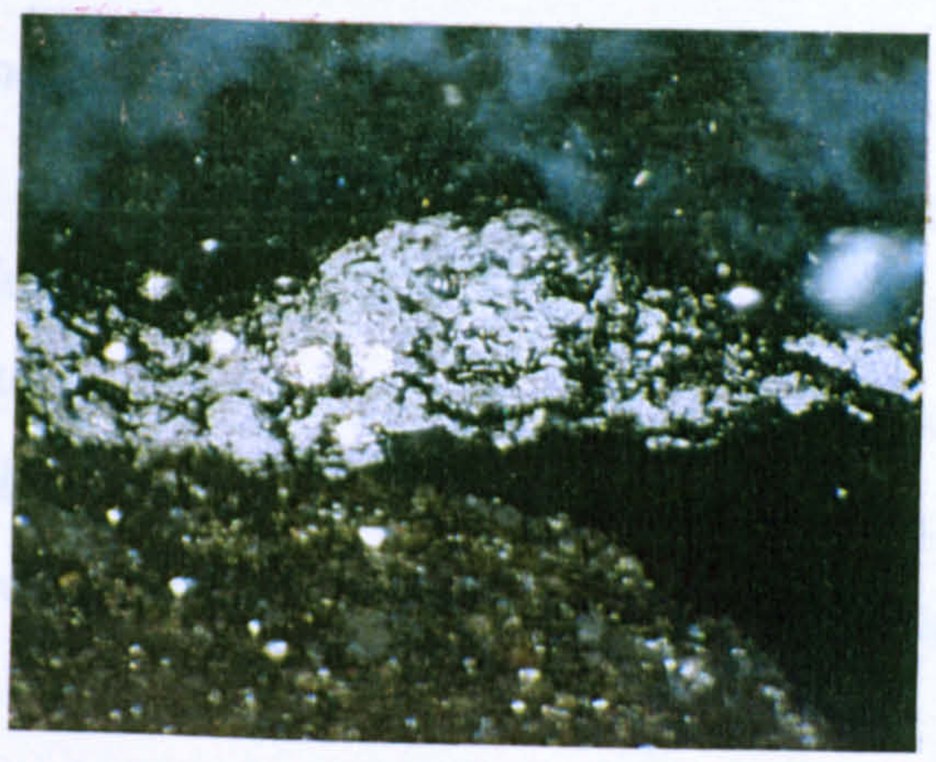
d

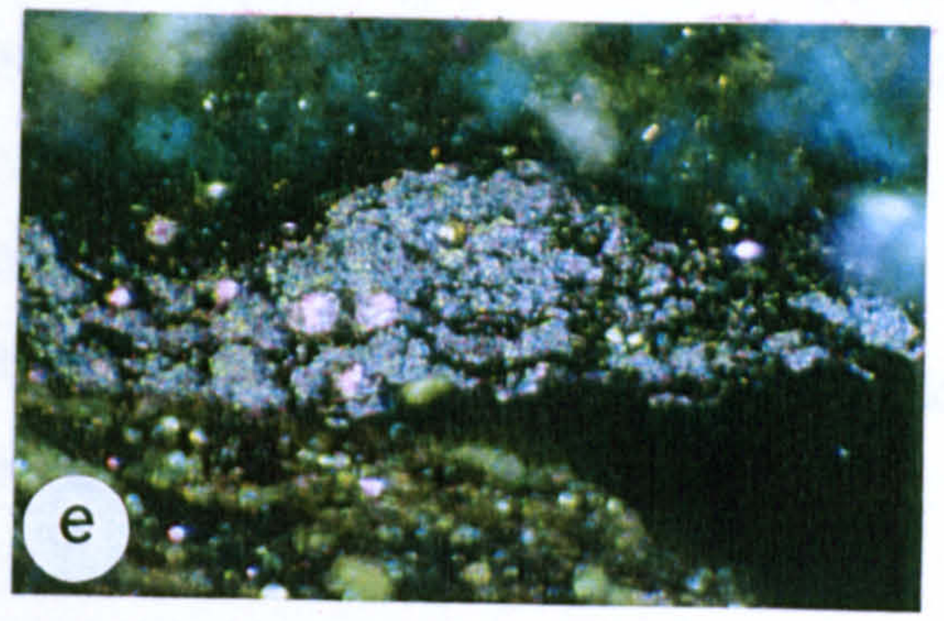
e


f

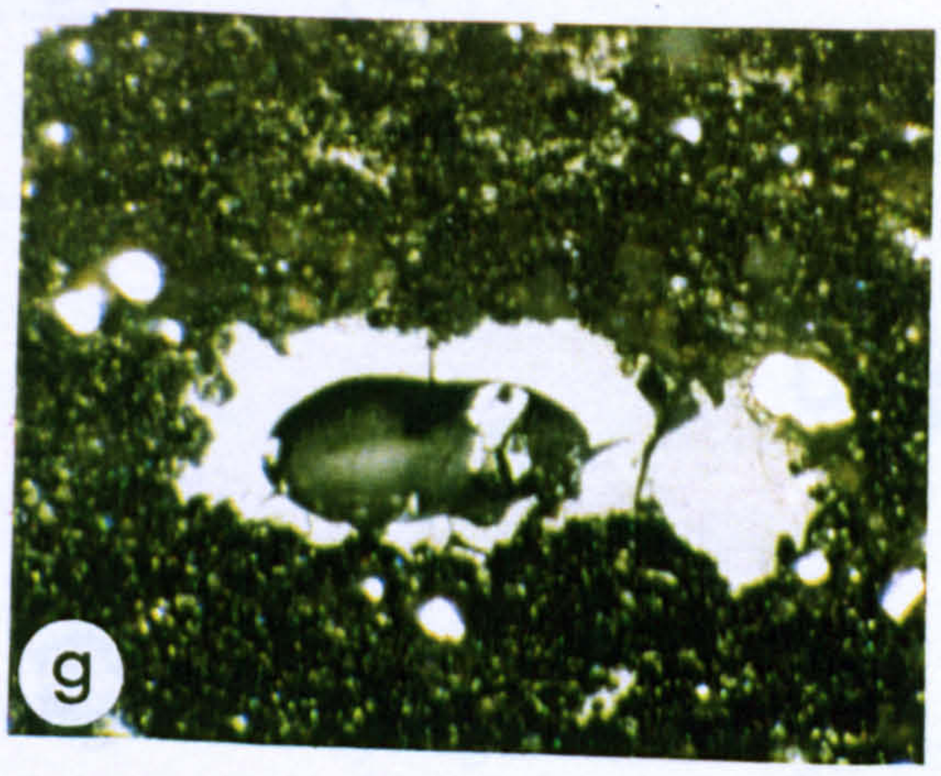
g


h

maturity (cf. Peters *et al.*, 1982) but the former presence of alginite is suggested by the preservation of dolomitized algal filaments associated with low Ro type 1 bitumen (0.17% R_o) in a sample from Bovie Lake (7).

The petrographic characteristics of the Muskwa Formation suggest that it originally contained a typical marine kerogen composed of a very organic-rich bituminous matrix with bedding-parallel alginite and bituminite stringers producing a finely laminated rock fabric.

Rock-Eval pyrolysis

Except for one sample (#9531 in section 7; Appendix B1), the S1, S2 and S3 values recorded for the Muskwa Formation are all less than 1.0, indicating poor source potential. The samples plot close to the end of the kerogen evolution pathway on the hydrogen index versus oxygen plot (Fig. 25), which suggests that elevated maturity would account for the poor potential in such rich source rocks.

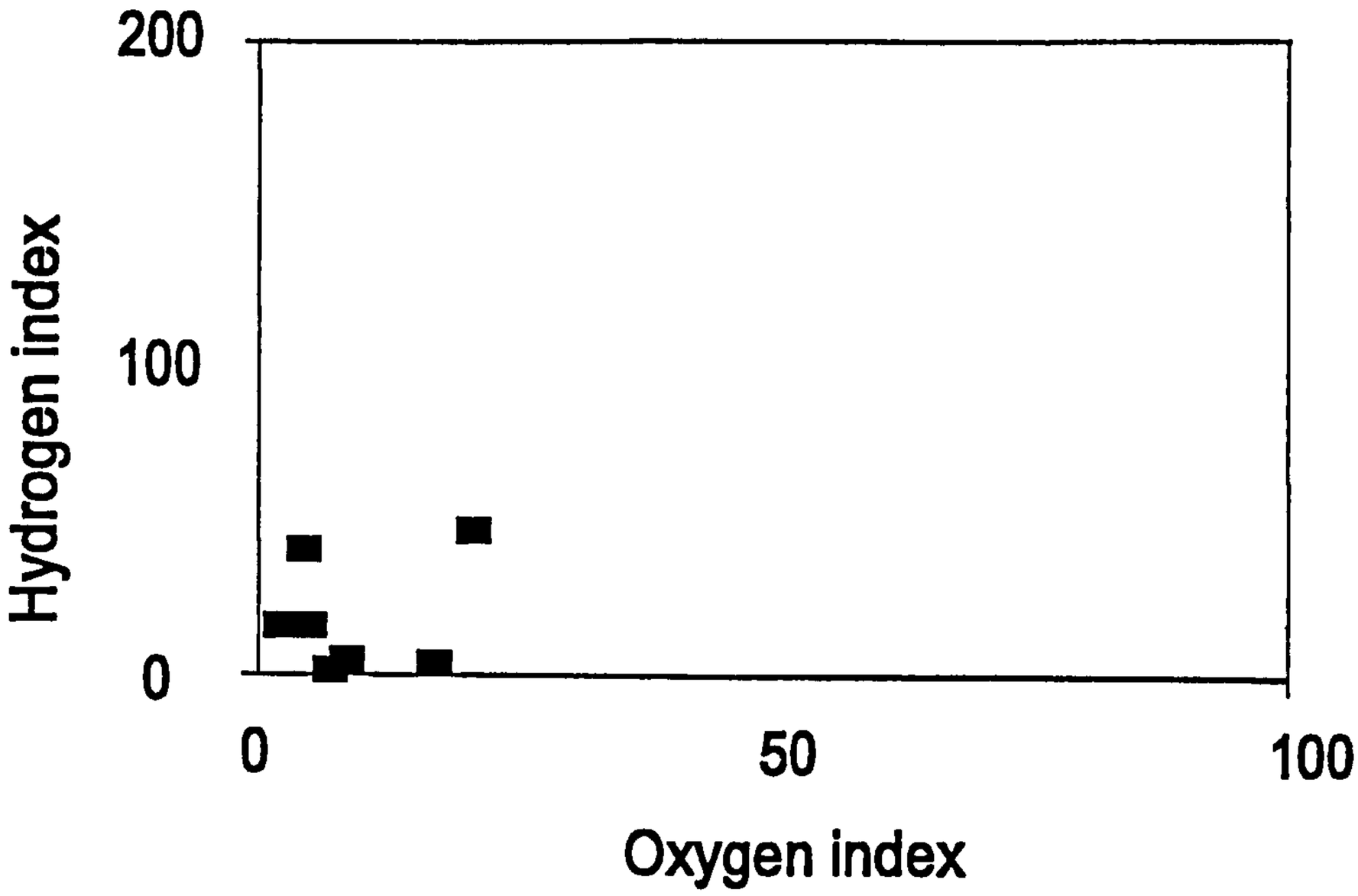

Figure 25. Hydrogen versus oxygen indices for the Muskwa Formation.

The values for the hydrogen and oxygen indices are too low to give any indication of kerogen type but the S2:S3 ratios for samples with R_o values ca. 1.4-1.6% (<2.0%) are between 2 and 10 which suggests that the kerogen type is Type II to Type III. The high S1 and S2 values obtained for the Bovie Lake sample # 9531 (6.6 and 1.46, respectively) are anomalous in that they are typical of an active source rock with excellent hydrocarbon potential; and yet, optical anisotropy was observed in the bitumens, suggesting that the kerogen was exposed to significantly higher temperatures than the 80°C to 140°C required for petroleum generation (cf. Tissot & Espitalié, 1975). Petrographic analysis of this sample indicates an extensive internal microfracture network lined with calcite which suggests that hydrocarbons trapped within the microfracture system could account for the anomalously high S1 value.

Maturation

Measured bitumen reflectance and VR_o eq. vitrinite values are shown in Appendix C1. The calculated vitrinite reflectance varies from 1.4 % R_o to 2.3% R_o, confirming that the Muskwa has reached elevated maturity throughout the area. According to Dow (1977), such values exceed the upper limits of the oil generation window as defined by vitrinite reflectance (1.3%), indicating that the potential for the generation of liquid hydrocarbons from the Muskwa has expired. However, nine of the samples analysed fall within the "gas window" (1.3-2.5% R_o) and therefore the Muskwa may still have the potential to generate gas.

The log values of the vitrinite reflectance equivalents (VR_o eq.) are plotted against depth in Figure 26. In general, the R_o increases significantly with depth, as observed by Teichmüller and Teichmüller (1966). There is good agreement between the bitumen and VR_o eq. values from samples ca. 6-7000 ft (ca. 1828m - 2133m) depth range; they both fall between 1.39% and 1.46%. The regional reflectance patterns for the Muskwa Formation, shown in Figure 27, indicate an increase in thermal maturity from the northeast to southwest, which is consistent with the structural contour trends for Cretaceous strata on the margins of the Liard Basin shown by Leckie *et al.* (1991, Fig. 2). Anomalously high R_o values, in excess of 2.0%, were obtained from the Muskwa Formation at Celibeta (5) and Bovie Lake (7). Although these are also the deepest samples (at 2146m and 2885 m,

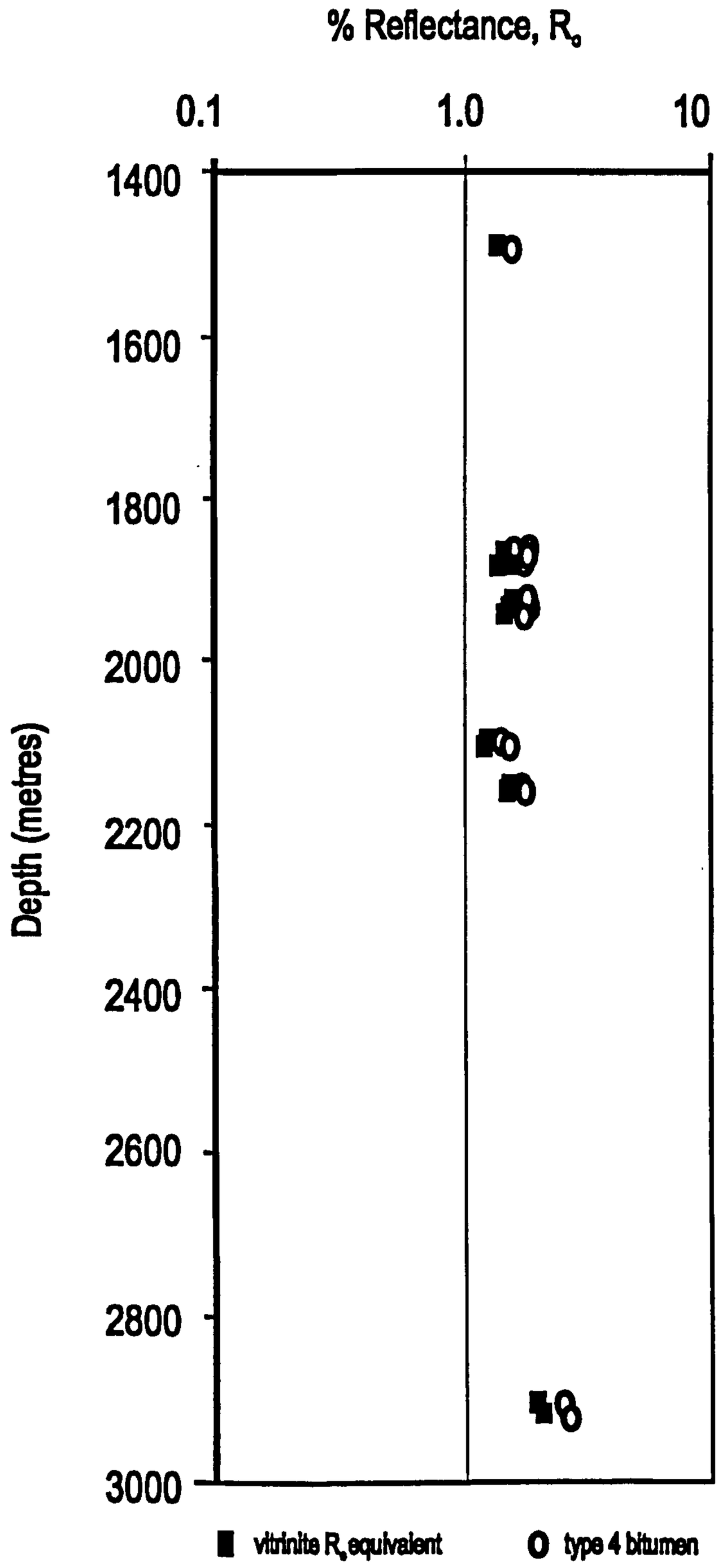

Figure 26. Percent Ro bitumen type 4 and vitrinite equivalent data (calculated from type 4 bitumen)versus depth , Muskwa Formation.

respectively), anisotropy was observed in the bitumens at both locations. Furthermore, there is only 33m difference in depth between the Muskwa in sections (5) and (1) and yet the difference in VR_o eq. values recorded is significant (0.6% R_o) and no anisotropic bitumens are observed at section 1, suggesting that factors other than basinal subsidence have influenced the thermal maturity. As the Celibeta (5) and Bovie Lake (7) sections are located near the Bovie Fault Zone (Fig. 16), it is possible that this has been the source of significant additional heat flow.

Anomalously high VR_o eq. values (mean: 2.4% R_o) are found in the Horn River Formation (Muskwa equivalent) at a shallow depth (500m) at Mattson Creek (11). This section is located in an upthrust block of Upper Devonian-Lower Carboniferous strata near the Mattson Anticline. It is therefore likely that the maturation patterns in this area will fit with those of the Liard Basin rather than the Eastern Plains region.

The Tmax values range from 376 to 551 (560, including data from Feinstein *et al.*, 1988). Contrary to Tmax–vitrinite R_o trends reported by Espitalié *et al.* (1988), the highest R_o values correspond to the lowest Tmax values (which are attributed to low S1 and negligible S2 values); for samples with R_o values less than 2%, the correlation between Tmax and VR_o eq. fits the expected trends observed by Espitalié *et al.* (1988).

Hydrocarbon potential

The hydrocarbon potential ratings for the Muskwa Formation are shown in Table 13. While organic richness is greatest at Bovie Lake (7), elevated reflectivity values indicate it is well past peak gas generating potential. The gas source potential is better to the northeast (Fig. 27).

4.2 FORT SIMPSON FORMATION

The Fort Simpson Formation is a thick basinal, dark grey to greenish grey, calcareous shale to siltstone unit which rests conformably upon the Muskwa Formation in the Eastern Plains. It is thickest (746.5m) in the southwestern part of the plains, to the east of the Bovie Fault Zone at the Bovie Lake section (7) and, like the underlying Muskwa Formation, it thins to the north and east, thinning to 493m in the Muskeg River section (3) and 199m at Trout Lake (2). The results of petrographic, geochemical analysis and

Section no.*	Thickness (m) (A)	% TOC (B)	Organic richness (A x B = C)	Maturity % VRo	Oil maturity factor (E)	Gas maturity factor (F)	Oil source potential (C x E)	Gas source potential (C x F)
1	6.95	2.24	15.57	1.40	0.30	1.00	4.67	15.57
4	9.95	3.50	34.83	1.43	0.30	1.00	49.80	34.83
7	16.31	2.50	40.78	2.24	0.00	0.50	0.00	20.39
5	25.67	0.88	22.59	2.00	0.05	0.60	1.13	13.55
6	3.93	2.63	10.34	1.45	0.30	1.00	3.10	10.34
2	7.25	1.67	12.11	1.44	0.30	1.00	3.63	12.11
3	8.46	2.60	22.00	1.46	0.30	1.00	6.60	22.00

*numbers refer to sections in Fig. 16: 1 = Imperial Island River No. 1; 4 = Imperial Sun Arrowhead I-46; 7 = Texaco N.F.A. Bovie Lake J-72; 5 = Pan Am *et al.* Celibeta No. 7; 6 = Imperial Sun Netla C-07; 2 = Dome *et al.* Trout Lake H-45; 3 = Murphy *et al.* Muskeg River No. 1;

Table 13 Hydrocarbon potential of the Muskwa Formation: gas source potential rating (based on the method of Dembicki & Pirkle, 1985).

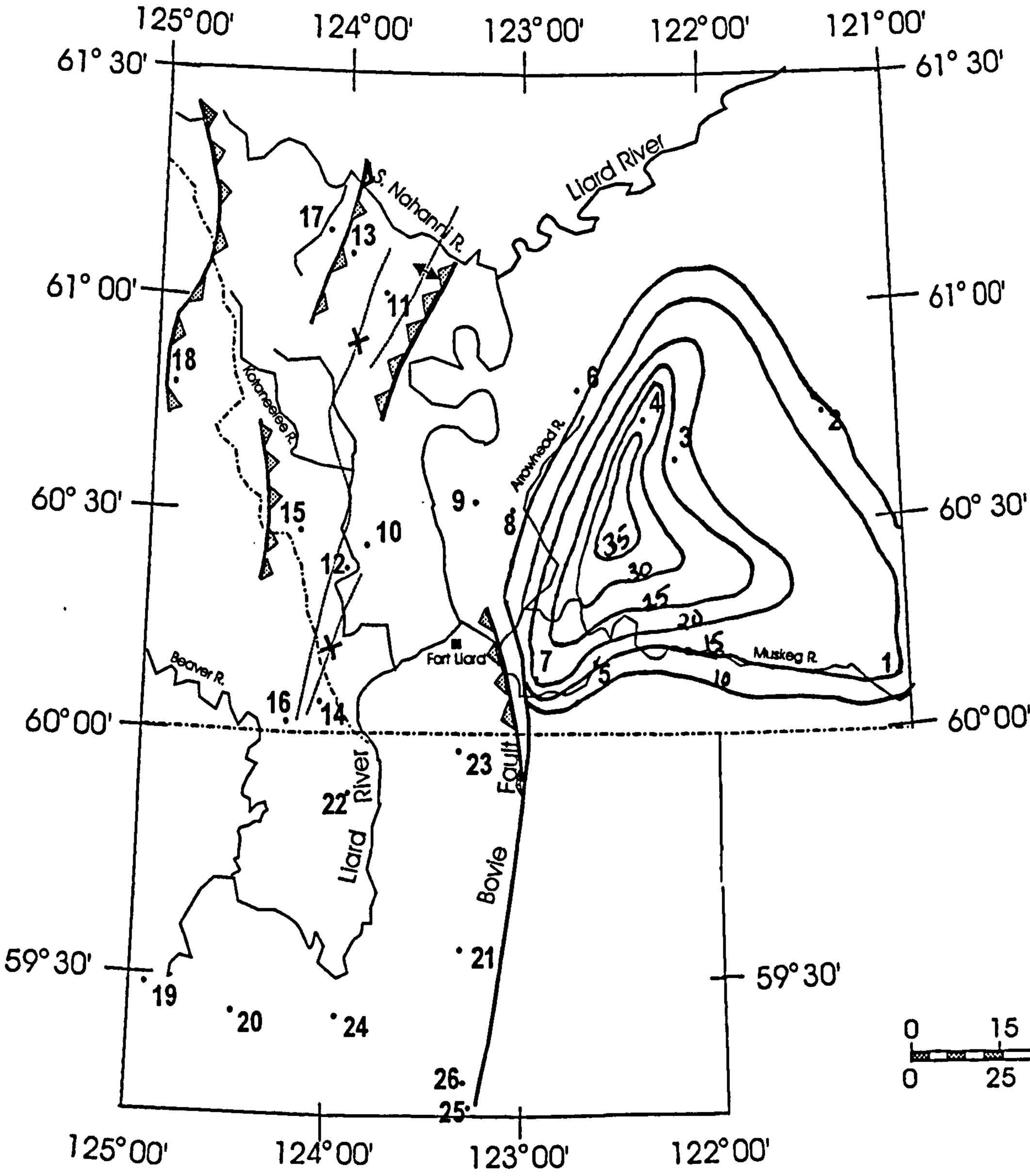

1. Imperial Island River No.1
2. Dome *et al.* Trout Lake H-45
3. Murphy *et al.* Muskeg River No.1
4. Imperial Sun Arrowhead I-46
5. Pan Am Home Signal Celibeta No.7
6. Imperial *et al.* Sun Netla C-07
7. Texaco N.F.A. Bovie Lake J-72
8. B.A. Texaco Arrowhead N-2
9. Amoco East Flett H-13
10. Amoco Pointed Mountain P-24
11. Pan Am Mattson Creek A-1
12. Pan Am Pointed Mountain P-53
13. Jackfish Gap-Yohin Ridge
14. Canada Southern *et al.* North Beaver River I-27
15. Pan Am Kotanellee 0-67
16. Pan Am Beaver River G-01
17. Clausen Creek
18. Tika Creek
19. Central Leduc Toad River No.1
20. IOE Dunedin a-75-E
21. Amoco LaBiche a-67-D
22. Imperial Pan Am LaBiche b-55-E
23. Arco Maxhamish b-21-K
24. IOE Pan Am Viscount a-77-D
25. Aquitaine *et al.* Tatoo a-2-D
26. Amin-Aquitaine Windflower d-87-A

Figure 27. Regional variation in hydrocarbon potential: gas source ratings for the Muskwa Formation (based on Dembicki & Pirkle, 1985); contours are drawn by eye based on data shown in Table 13.

bitumen reflectance measurements of some 38 samples from this stratigraphic unit are shown in Appendices A2, B2 and C2, respectively. Total organic carbon contents for the Fort Simpson Formation samples are consistently low (<1.0%) and organic petrology reveals moderately well-dolomitized, organic-poor shales devoid of an organic bituminous matrix but having finely-dispersed liptinite and indigenous bitumens. None of the samples show any significant S1, S2 or S3 peaks upon Rock-Eval pyrolysis. The hydrocarbon potential of this unit is very poor and is therefore not discussed further. Equivalent vitrinite reflectance (VR_o eq.) values vary between 1.2% and 1.76% indicating the kerogen is postmature; the highest values are recorded near the Bovie Fault and in the basinal depocentre. Log R_o versus depth plots (Fig. 28) show a reasonably good trend of R_o increasing with depth and there is no correlation between the reflectance data and Tmax values.

4.3 REDKNIFE FORMATION

In the Eastern Plains region, the Redknife Formation rests conformably on the Fort Simpson Formation. The lower part, the Jean Marie Member, is a thin, bioclastic, shallow shelf limestone and is an important reservoir rock in the Alberta Basin and in northeastern British Columbia. The upper units comprise dark grey-green mudstone-shale with reddish-brown silty interbeds and bitumen-filled fractures. The red colouration of the siltstone may be attributable to the formation of ferroan dolomite during early diagenesis; ferroan dolomite formation in calcareous shales has been shown to accompany methanogenesis and the fermentation of organic matter in the absence of sulphate ions (Scoffin, 1987). The shale unit varies in thickness from 100m to 200m and is thickest in the north and eastern part of the Eastern Plains around Arrowhead, Muskeg River and Trout Lake (sections 2, 3 and 4). The results of petrographic geochemical and reflectance analyses of 15 samples from the "shale member" of the Redknife Formation are shown in Appendices A3, B3 and C3.

The TOC content is less than 1% at all locations. The organic components of the Redknife Formation are dominated by dispersed, reddish-brown bituminite strings and flecks (<5 µm) distributed throughout a relatively barren, dolomitised rock matrix containing abundant fresh pyrite grains and tetrahedra. Low R_o (types 2 and 3), medium R_o and high R_o bitumens are also present and are occasionally the dominant components. The low R_o bitumens are typically associated with the bituminites and tend to be granular in nature. The

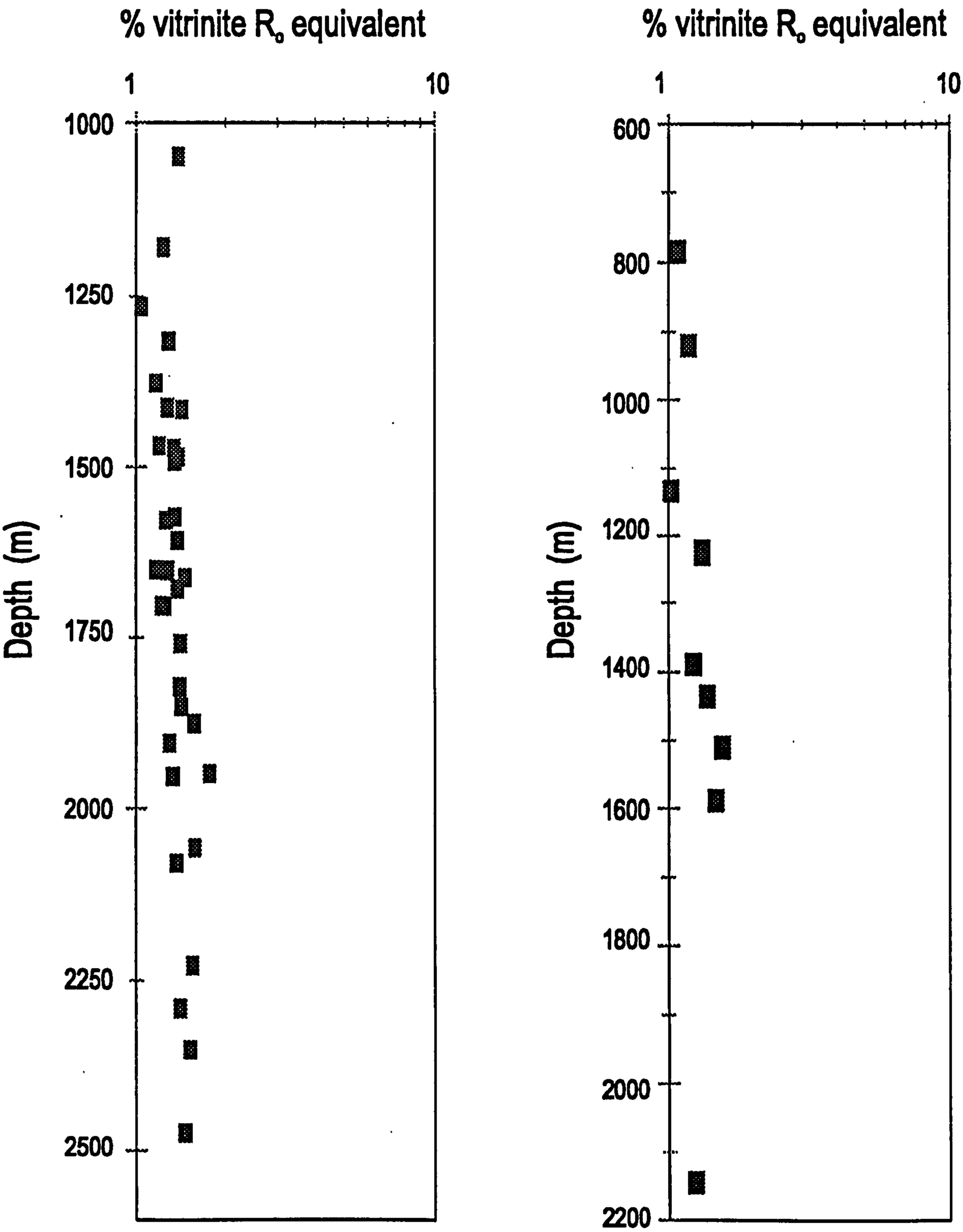

a) Fort Simpson Fm.

b) Redknife Fm.

Figure 28. Vitrinite reflectance equivalent versus depth for a) the Fort Simpson Formation; and b) the Redknife Formation.

medium R_o bitumens are amorphous and pore-filling. Primary macerals are absent except for rare traces of straw-yellow to reddish-orange Tasmanales-type alginite (phycomata ca. 50-80 µm in diameter) and straw-yellow algal bodies , <5µm in diameter. The predominance of secondary macerals and indigenous bitumens suggests that the kerogen was originally dominated by dispersed thin-walled, marine alginites of the Leiosphaeridiales variety. Liptodetrinite shows strong yellow-orange fluorescence at Island River (1) and Netla (6). Rock-Eval pyrolysis yields S1, S2 and S3 values that are significantly less than 0.2 mg/g rock indicating an absence of hydrocarbon potential.

Three population of bitumens are present: in addition to the high reflectance pyrobitumens, there are the low R_o bitumens (types 2 and 3) and type 4 bitumen of medium reflectance. The presence of two populations of low R_o bitumens is consistent with the products of thermal maturation of the primary organic matter derived from a typical Type II kerogen consisting of algal matter and bituminite. Measured bitumen reflectance and VR_o eq. data, derived from the medium R_o bitumens are given in Appendix C3. The calculated vitrinite reflectance varies from 1.14% at Trout Lake (2) to 1.48% at Celibeta (5), suggesting that the maturation level of the kerogen in the Redknife, although variable, is marginally within the oil window (upper limit 1.3 %VR_o, according to Dow, 1977). The regional VR_o pattern shows that the most northern and easterly sections sampled are mature and those to the west and south are postmature. This compliments the regional maturation patterns observed in the underlying formations.

The log of the reflectance (% VR_o eq.) recorded in the Redknife Formation plotted against depth shows a consistent downhole increase (Fig. 28) and the regional reflectance patterns increase in R_o from the northeast to southwest in much the same way as the structural and depositional contours for the Redknife Formation, suggesting that maturation and depositional trends are related to the underlying tectonic structures. The reflectance patterns mirror those of the Fort Simpson and Muskwa formations but the thermal effect of the Bovie Fault on regional maturation patterns appears to be less pronounced than in the underlying strata. The Tmax data do not show any correlation with the measured or calculated reflectance data, nor with the fluorescence characteristics of the samples.

4.4 KOTCHO FORMATION and UPPER DEVONIAN SHALES

The top of the Upper Devonian succession in the Eastern Plains region consists of

limestones and dark grey to grey-green shales of the Kotcho Formation. These may or may not be underlain by undifferentiated Upper Devonian shales. The shales are all somewhat calcareous and variously fissile, grey to black and bituminous in nature. In the study area, the Kotcho-Upper Devonian shale succession is thickest at the southwestern portion of the Eastern Plains region at Bovie Lake (7) and thins to about 278 m towards the north and east at Netla (6) and Trout Lake (2); between these locations there is a tongue or belt which is over 312 m thick. The top of the succession dips significantly from 407.8m at the Trout Lake section (2) to 1703.1m at Bovie Lake (7), in the southwestern portion of the Eastern Plains, near the Bovie Fault Zone.

Organic carbon contents of the Upper Devonian shales are low (TOC< 0.5%) but those in the Kotcho Formation are over 1% at several locations (Appendix B4): Island River (1); Netla (6); Muskeg River (3); and Bovie Lake (7). The petrographic characteristics are documented in Appendix A4. The rock matrix is typically calcareous to marly and variously bitumen-stained (orange-brown) with bituminous micro-laminations in samples with >1% TOC. The kerogen is generally black, dark or light brown, pervasive and tends to be finely dispersed and intimately associated with pyrite tetrahedra, framboids and clusters, especially the alginite. Primary and secondary macerals are present as well as indigenous bitumens; matrix bituminite is generally lacking, particularly in low TOC samples.

Primary macerals such as alginite are more abundant in these shales than in the formations previously discussed; they are predominantly thin-walled Leiosphaeridiales-type alginite draped along the bedding planes and displaying strong, mid-yellow to dull-yellow fluorescence when observed under blue light. Prasinophyte phycomata (*Tasmanites*-type) alginite (ca. 50-80µm) and rare coccoidal algae are present also. Straw-coloured alginites (<5µm) are also common components. Zooclasts (Plate VIIa, b) and acritarchs are rare, as are inertinitic fragments. Dark brown, non-fluorescing bituminites presumed to be derived by reworking or diagenesis of algal remains are present and are often the dominant constituents. Bedding-parallel stringers of orange-brown, non-fluorescing, bituminite and some having wispy forms ca. <5µm diameter, pervade the matrix. The bituminites are frequently associated with fine granular, highly-reflective micrinite. This assemblage of primary and secondary macerals is fairly representative of a typical marine, Type II kerogen. The presence of, and fluorescence of, the primary macerals (Appendix C4) would suggest that the shales of the Kotcho Formation and undifferentiated Upper Devonian are significantly

PLATE VII
ORGANIC FOSSILS OF THE KOTCHO AND EXSHAW FORMATIONS

a), b) Cross section through a weakly reflecting and fluorescing, ?chitinous fish bone impregnated with weakly reflecting, brown bitumen; a) in white light; b) in fluorescent light (400-440nm excitation); Kotcho Formation, Texaco Bovie Lake J-72.

c), d) Longitudinal cross section through weakly reflecting, mildly fluorescing chitinous ?fish bone. Porosity in the bone itself is filled with moderately strong, yellow-fluorescing bitumen; c) in white light; d) in fluoresecent light (400-440nm excitation); Exshaw Formation, Imperial Sun Netla I-46.

e), f) Prasinophyte alginite (?Leiosphaeridiales) in the Banff (e) and Exshaw (f) formations.

Magnification: scale bar shown on a) applies to all photomicrographs.

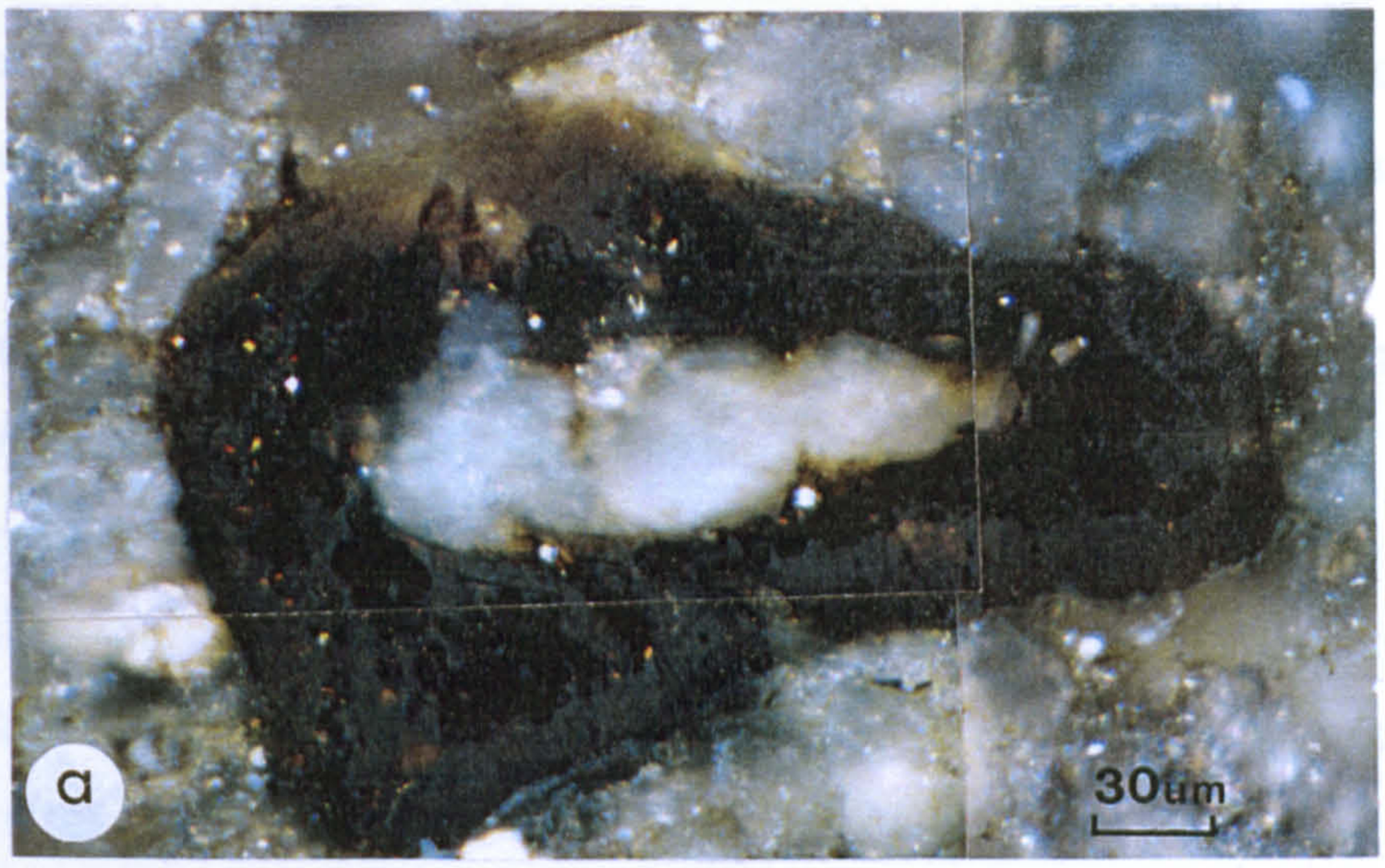
a
30um

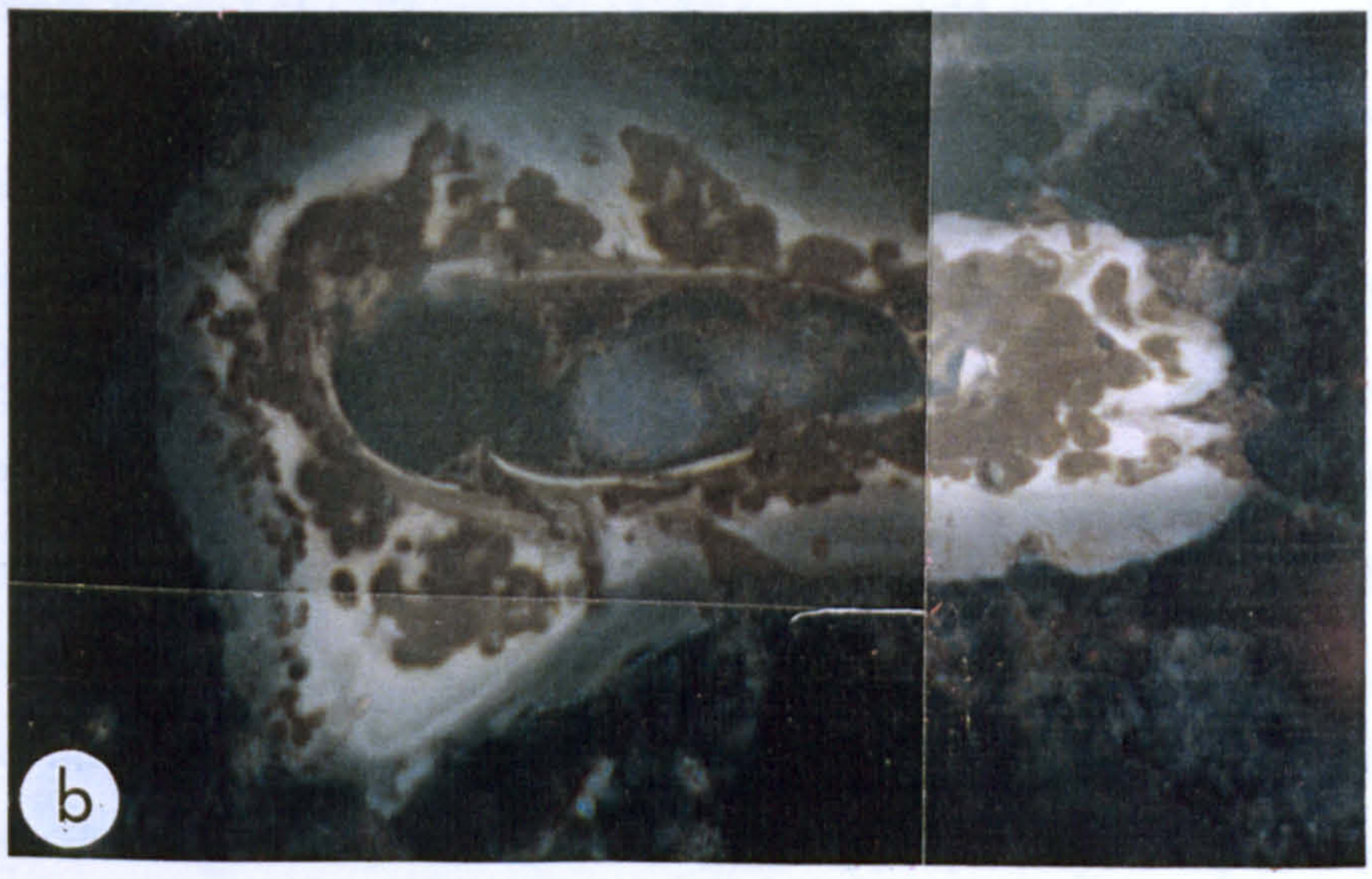
b

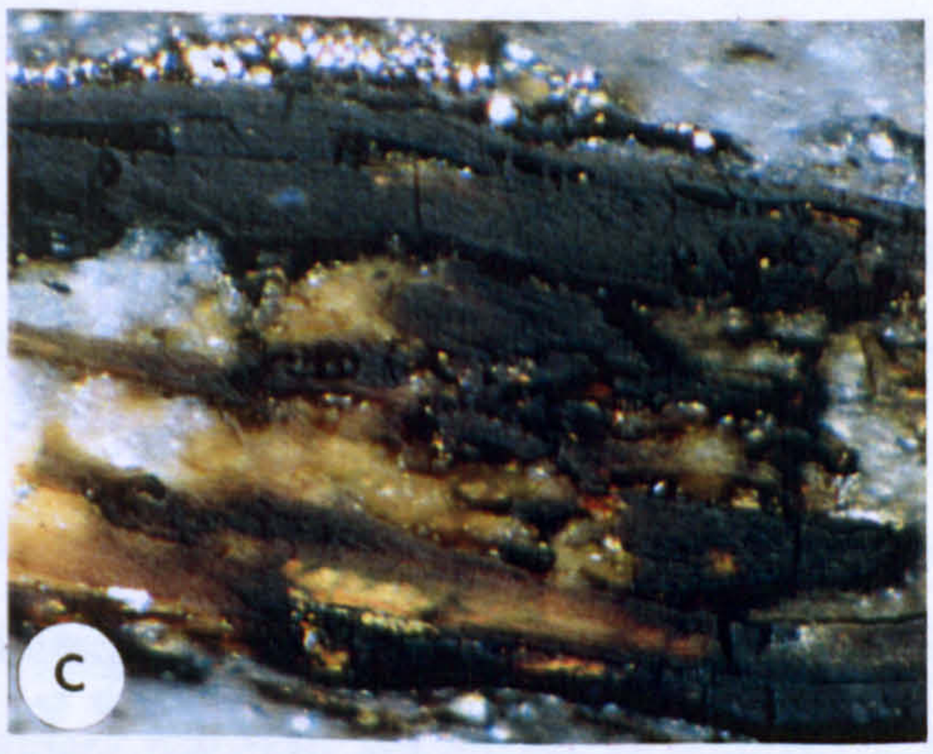
c


d


e


f

lower in maturity than in the underlying formations; however, the fluorescence is principally observed in the micro-alginite (<5um) and it has been observed by the present author and by L.D. Stasiuk (pers. comm.) that the fluorescence of micro-alginite (< 5µm) extends beyond the upper limits of the oil window.

Indigenous bitumens are also present in these shales, including low, medium and high-reflecting types. The low reflecting bitumens are the most abundant; type 1 is associated with primary algal material; type 2 (the liptinite-bitumen transitional bitumen) is also found directly associated with the alginite and differs only in having a higher reflectivity than the type 1; low Ro type 3 bitumens are the most abundant and they are associated directly with the algal bituminite.

Samples from Bovie Lake (7) were the only ones to yield significant S1 peaks (8.2 and 6.6, respectively) upon Rock-Eval pyrolysis, indicating good hydrocarbon potential but the mean production index in these samples is 0.86, suggesting that the samples are mature and most of the hydrocarbon has been expelled. The moderate S2 value (2.53) and low production index (0.18) obtained from Island River (1) samples indicates that hydrocarbon potential still exists although the S3 peak may be indicative of a slightly more gas-prone kerogen which appears to be supported by the relatively high S2:S3 ratio (4.5). Hydrogen and oxygen indices (Fig. 29) plot at the lower left hand side of the HI-OI diagram and the trend stretches out along the left axis indicating a tendency towards hydrogen enrichment that typifies a Type II kerogen which has reached an elevated maturity. Samples from the Island River section (1) show slight oxygen enrichment and there is evidence of extensive reworking of the organic components as well as oxygen-rich, organic components such as inertinite and ?vitrinite. The latter suggests that the Island River section was closer to the upper Devonian shoreline than any of the other sections.

The presence of all three varieties (types 1, 2 and 3) of low Ro indigenous bitumens in the Kotcho-Upper Devonian shales is an indirect and qualitative indication that the kerogen is within the productive zone of the oil window (Chapter 3). The fact that primary and secondary macerals are dominant over the indigenous bitumens also indicates that the kerogen is in a mature state of hydrocarbon generation. For sections east of Bovie Lake, the

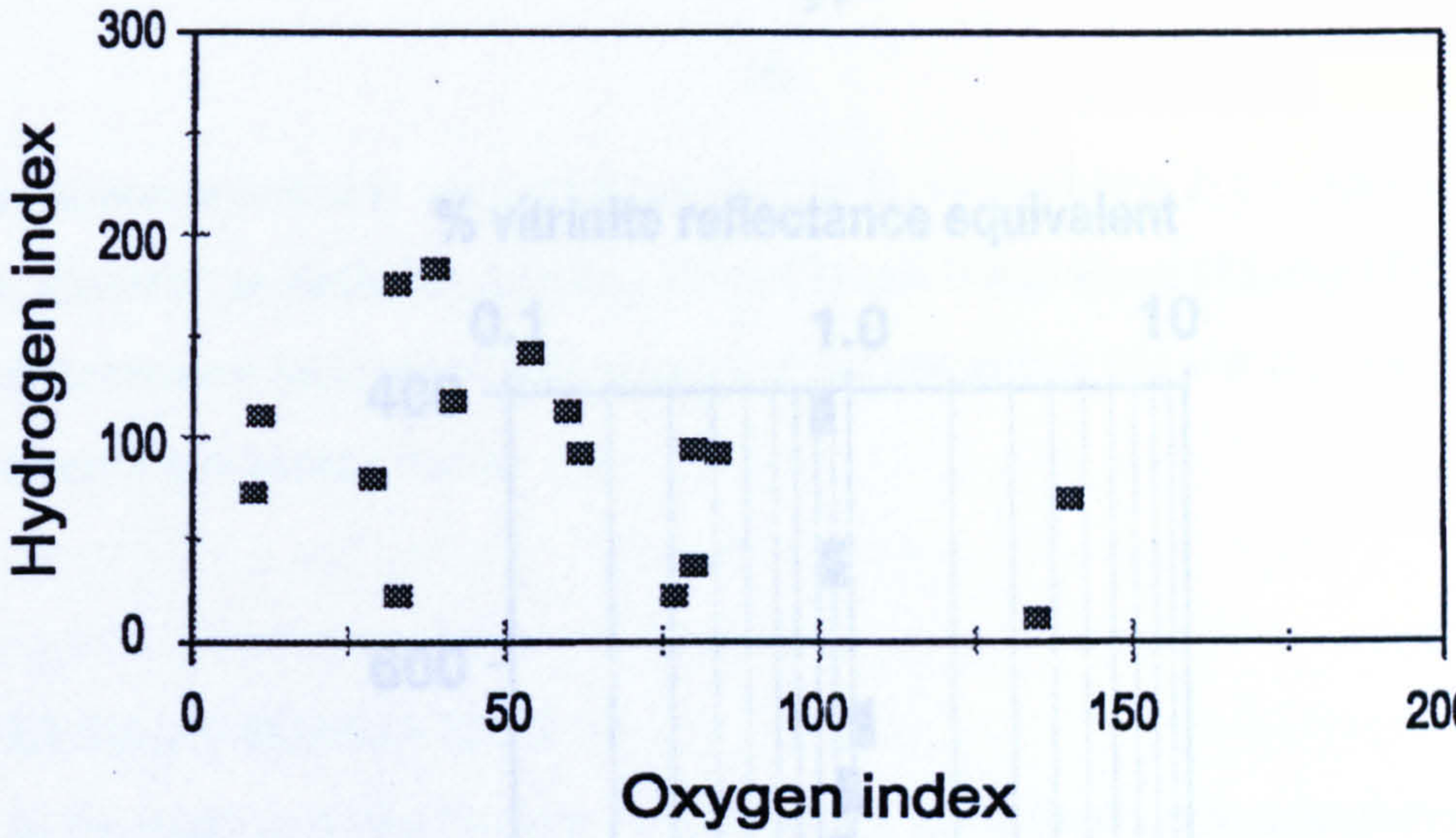

Figure 29. Hydrogen versus oxygen index for the Kotcho and Upper Devonian shales.

data (Tmax: ca. 440°) indicate maturation levels in the peak of the oil window. Several samples yielded a Tmax of <400 which may in part be due to low TOC values, but such numbers are typical of shales in the older underlying formations which are postmature or spent; production indices of >0.5 support an overmature state. Furthermore, the relationship between Tmax and depth shows a positive correlation except at greatest depth (where postmaturity is to be expected) where the values fall below 400.

Bitumen and VRo eq. data generally agree with the Tmax data. Kerogen in shales from Bovie Lake (7) has an average VR_o eq. of 1.33% R_o which indicates that the Upper Devonian-Kotcho unit is postmature for oil but at the lower end of the gas window at this location. Sections to the north and east fall marginally within the upper limits of the oil window (1.19 to 1.27% VR_o eq.) and at Netla (6) and Island River (1), VR_o eq. values between 0.9 and 1.08% R_o indicate the Kotcho-Upper Devonian shales are mature for oil generation. The correlation between vitrinite reflectance eq. and depth (Fig. 30) is positive, although not strong ($R^2 = 0.57$), and the relationship between Tmax and VR_o eq. is poor.

In summary, the Kotcho-Upper Devonian shales close to the Bovie Fault (section 7) are postmature for oil generation but, according to Powell and Snowdon (1983) and Dembicki and Pirkle (1985), a TOC of >1%, together with a Type II marine kerogen composition and a vitrinite reflectance eq. of ca. 1.3% still suggests the potential to generate data (Tmax: ca. 440°) indicate maturation levels in the peak of the oil window. Several dry gas or paraffinic condensate. To the east and northeast, TOC values less than 1% suggest

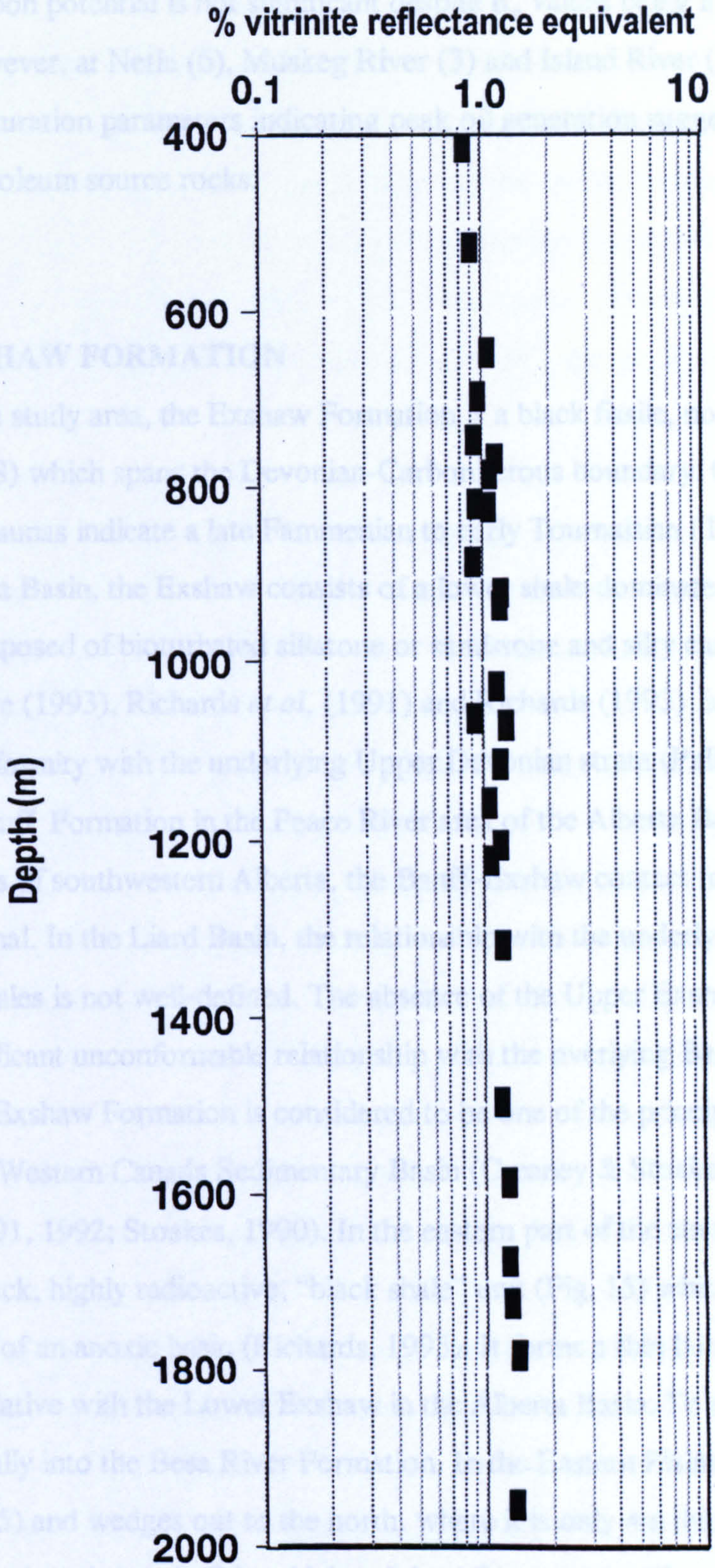

Figure 30. Vitrinite reflectance equivalent data, derived from type 4 bitumen Ro, versus depth for the Kotcho Formation and Upper Devonian shales.

the hydrocarbon potential is not significant despite R_o values being in the peak of the oil window; however, at Netla (6), Muskeg River (3) and Island River (1), the TOC values of >1% and maturation parameters indicating peak oil generation suggest that they should be effective petroleum source rocks.

4.5 EXSHAW FORMATION

In the study area, the Exshaw Formation is a black fissile, non-calcareous shale unit (Patton, 1958) which spans the Devonian-Carboniferous boundary. Conodont and brachiopod faunas indicate a late Fammenian to early Tournaisian (T2) age (Moore, 1993). In the Alberta Basin, the Exshaw consists of a lower shale-dominated member and an upper member composed of bioturbated siltstone or sandstone and silty carbonates (Richards *et al.* 1991). Moore (1993), Richards *et al.* (1991) and Richards (1993) indicate that there may be some disconformity with the underlying Upper Devonian strata (Palliser-Wabamun) and the overlying Banff Formation in the Peace River area of the Alberta Basin, although in the Front Ranges of southwestern Alberta, the Banff–Exshaw contact may be disconformable but gradational. In the Liard Basin, the relationship with the underlying Kotcho and Upper Devonian shales is not well-defined. The absence of the Upper Exshaw in this area suggests a more significant unconformable relationship with the overlying Banff Formation.

The Exshaw Formation is considered to be one of the principal hydrocarbon source rocks in the Western Canada Sedimentary Basin (Creaney & Stoakes, 1987; Allan & Creaney, 1991, 1992; Stoakes, 1990). In the eastern part of the study area, it consists of a brown to black, highly radioactive, "black shale" unit (Fig. 15) which formed in moderately deep waters of an anoxic basin (Richards, 1993). It forms a thin but laterally persistent unit that is correlative with the Lower Exshaw in the Alberta Basin. To the south and west, it grades laterally into the Besa River Formation. In the Eastern Plains, it is thickest (25.9 m) at Celibeta (5) and wedges out to the north, where it is only 4m thick at Netla (6), and eastwards – where it is only 7.3m thick at Island River (1) and Trout Lake (2). It occurs at greatest depth (5396 ft; 1544.7m) near the Bovie Fault, at Bovie Lake (7). At Trout Lake (2); it occurs at relatively shallow depth (390.5m).

Organic richness

With TOC values ranging from 1.6 to 15.7%, the Exshaw Formation has very good to excellent source potential throughout the region (Appendix B5). Exceptionally high values (mean 14.8%) are found at Island River (1) but at Arrowhead (4), the mean value for the interval is 3.2% – still indicating very good potential. Elsewhere values are between 1.6% and 2% indicating that it has good source potential. The high TOC values are consistent with the accumulation of organic matter in a starved dysoxic-anoxic basin.

Organic Petrology

Samples from the Exshaw Formation are typically dark brown to black, highly bituminous, laminated, pyritic and slightly dolomitic mudstones; samples with lower TOC values have silty laminae. The petrographic characteristics of the Exshaw Formation are detailed in Appendix A5. Pyrite is common and typically framboidal; dolomite is usually in the form of discrete rhombs which are distributed throughout the organic-rich matrix. Well-developed microfracture networks occur in all samples. These comprise subvertical microfractures that connect with en-echelon microfractures running parallel to the internal lamination which feather out at the margins in a chevron-fashion. Such microtextures are commonly well-developed in mature source rocks and reflect the internal migration of hydrocarbons (Belin, 1992). [Thermal drying of cuttings samples enhances the microfracture network visually. When viewed in fluorescent light the matrix marginal to the fractures commonly fluoresces while the fluorescence of the matrix is extinguished by heating].

The dominant organic component is a dense dark brown to black bituminous matrix ("matrix bituminite" *sensu* Creaney, 1981; "groundmass" of lacustrine kerogen *sensu* Robert, 1977). Typically, it shows very weak reflectance and weak brown fluorescence with positive alteration (Plate VIIIa, b). It has a variable micrinite content (cf. bituminite III *sensu* Teichmüller, 1977) and incorporates pervasive weakly-reflective bituminous ?pellet-like organoclasts, ca. 100-300µm in diameter, which may be phosphatic (cf. Reidiger, 1991). The pellet margins are poorly defined and have a 'corroded' appearance as they disseminate into the matrix. The pellet matrix is typically dark grey and granular (Plate VIIIc) with pervasive inclusions of low-reflecting bitumen; the reflectance (0.11%) does not vary with thermal maturation levels. This may due to the mineralized (apatite-rich) nature of the

organic matrix. The micro-laminations and concentrations of faecal pellets can be taken as an indication of a lack of benthic fauna which suggests anoxia in the depositional environment. In the Exshaw samples at Island River (1), the bituminous matrix surrounding pellets and low Ro bitumens inclusions typically show strong yellow fluorescence with positive alteration relative to the matrix (Plate VIIId). As the inclusions are composed of low Ro bitumens which are generated from pellets or liptinites by thermal maturation, the high intensity fluorescence probably results from hydrocarbons generated by the liptinite being simultaneously adsorbed onto the surrounding matrix bituminite. The enhanced fluorescence of the matrix at the pellet-matrix contact is therefore an indication of an active source rock in the early stages of hydrocarbon generation. In the same samples, the bituminous matrix shows varying degrees of fluorescence intensity and colouration; the highly fluorescing zones are interpreted as hydrocarbon-rich areas formed by early generation of oils from unidentified (< 5µm diameter) algal detritus dispersed throughout the matrix, i.e. liptodetrinite (the "micro-algal" matter in Appendix A, Table A5).

Primary macerals such as alginite are present but not abundant. Algal bodies with affinities to thick-walled, *Tasmanites*-type phycomata (Plate VIIIe, f) and thin-walled *Leiosphaeridiales*-type prasinophyte alginite (Plate VIIe, f) are identified indicating a marine origin for the kerogen. Secondary macerals such as bituminites of ?algal origin are very common. Also present as minor components are ?chitinous remains, possibly fish scales and fish bones (Plates VIIc, d; VIIIg, h) which have low-reflecting and highly fluorescing bitumen inclusions (?exsudatinites) in their microfractures and internal pores (Plates VIIc, d; and VIIIg, h); this is another indication of mature kerogen having generated hydrocarbons and *in situ* bitumens. Mineralized remains of ?calcareous nannofossils are present in the samples with lower TOC values. Rare inertinite components having the reflectance of fusinite are probably faunal in origin.

Low reflecting bitumens, predominantly types 2 and 3, are present in variable abundance but are always subordinate to the bituminous matrix. They commonly occupy the porosity created by thermal destruction of primary liptinite macerals and bituminite. The distribution of the bitumen is predominantly parallel to the internal microlaminations and microfractures enhancing the laminated appearance. Pore-filling interstitial medium Ro (type 4) bitumens are also present; they are generally subordinate to the low Ro bitumens and are

PLATE VIII
PETROGRAPHIC COMPONENTS OF THE EXSHAW FORMATION

a) Dark reddish-brown mineral-bituminous matrix impregnated with weakly reflecting (medium grey) amorphous bitumen shown in white light; Imperial Island River No.1.

b) Fluorescent light image of a) using 440-440nm excitation. The mineral bituminous groundmass shows very weak autofluorescence while the bitumen fluorescence is stronger and yellow.

c) Weakly reflecting faecal pellet (0.18% R_o) with weakly reflecting type 1 bitumen exuding from it or adhereing to the surface. Imperial Island River No. 1.

d) Fluorescent light image of c) at higher magnification; note the relatively strong yellow fluorescence of the bitumen on the surface of the pellet but also the weak greenish-yellow fluorescence halo created by hydrocarbons adsorbed on to the mineral bituminous matrix indicating that the bitumen and the hyrocarbons are generated at the same time; the less labile bitumen is deposited nearest to the source.

e) White light image of weakly reflecting (0.08% R_o) alginite derived from large prasinophyte (*Tasmanites*) algal phycoma. Imperial Island River No. 1.

f) Fluorescent light (400-440nm excitation) image of e); note the strong fluorescence of the alginite (λmax = 580nm).

g) White light image of weakly reflecting, chitinous fish bone. Imperial Island River No. 1.

h) Fluorescent light image of g) showing the weakly fluorescing chitin and internal porosity filled by strongly fluorescent exsudatinite (400-440nm excitation).

Magnification: scale bar shown on a applies also to b), d), e) & f); scale bar shown on g) applies also to h).

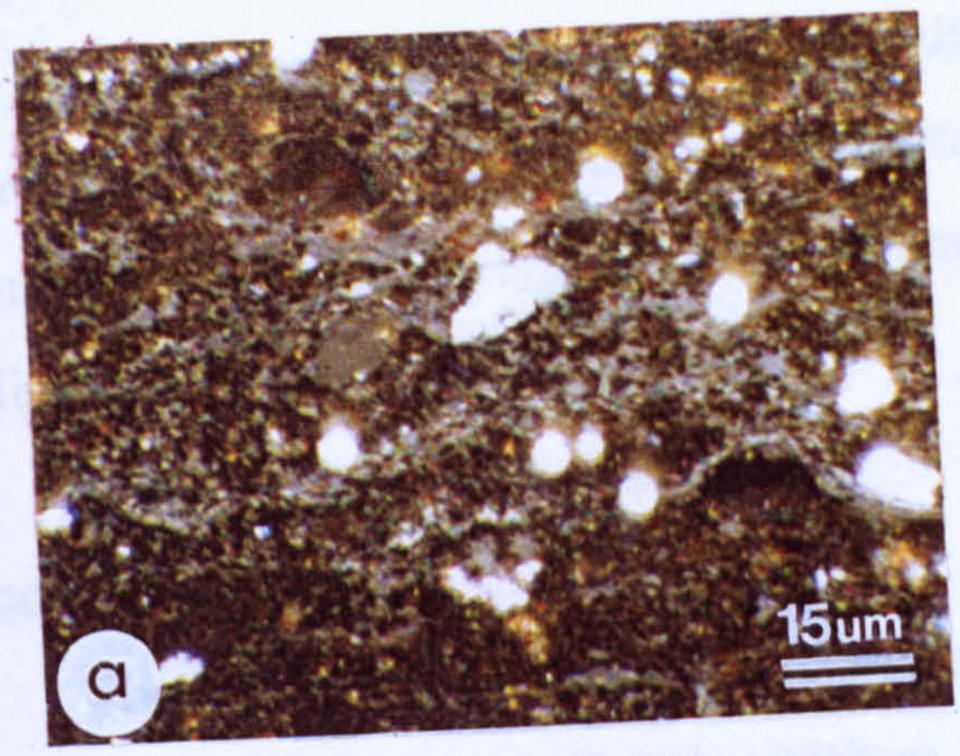
15um
a

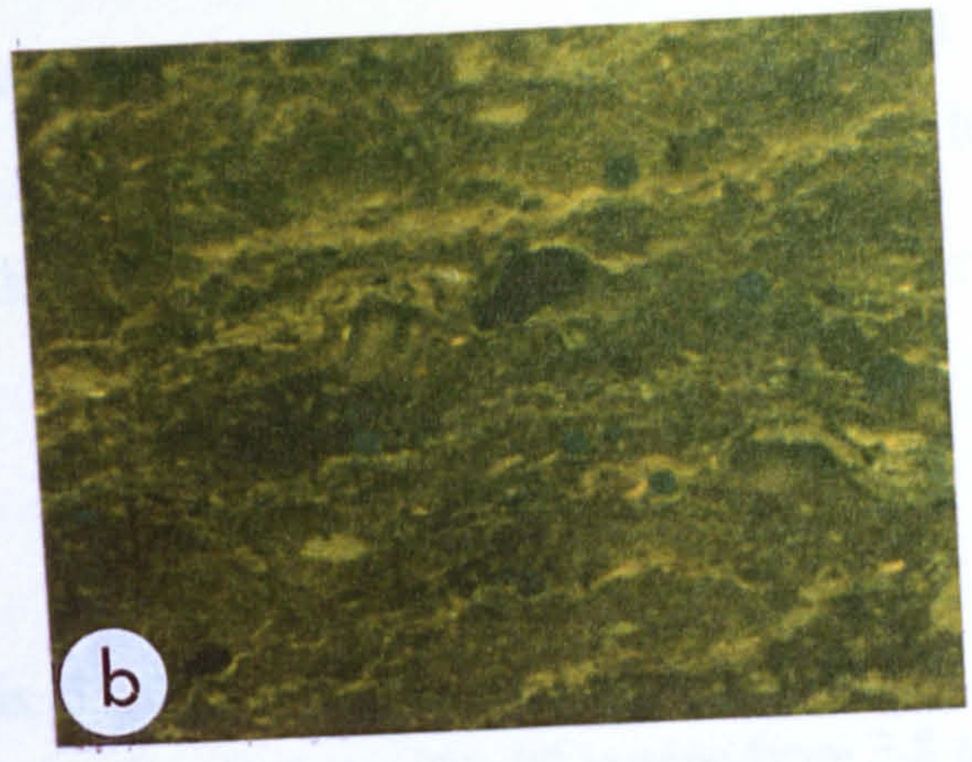
b

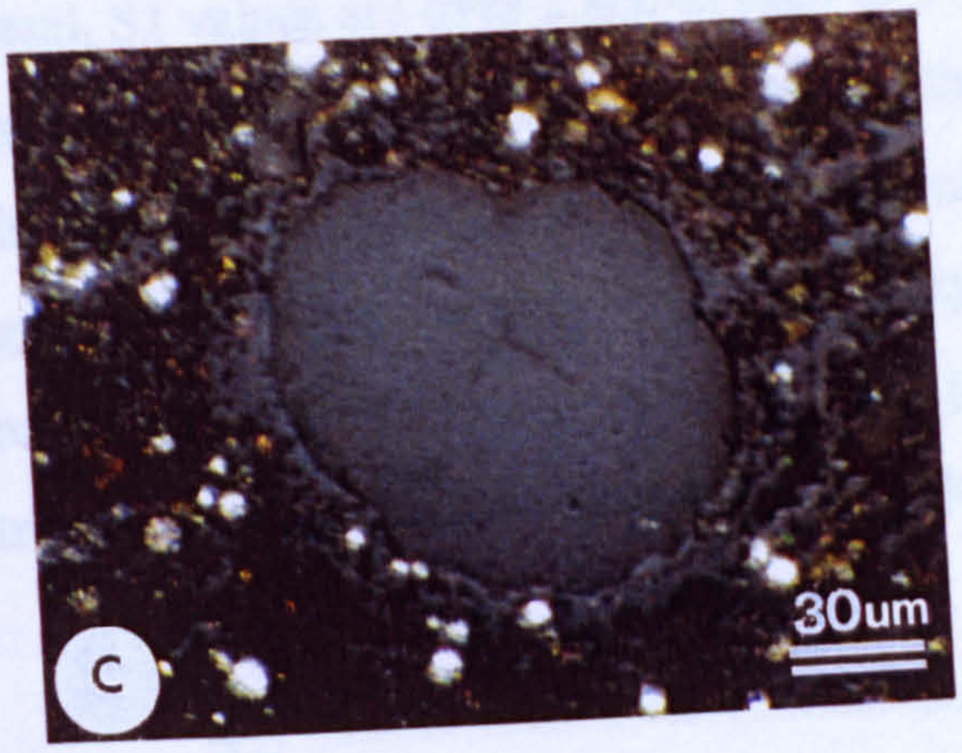
30um
c


d

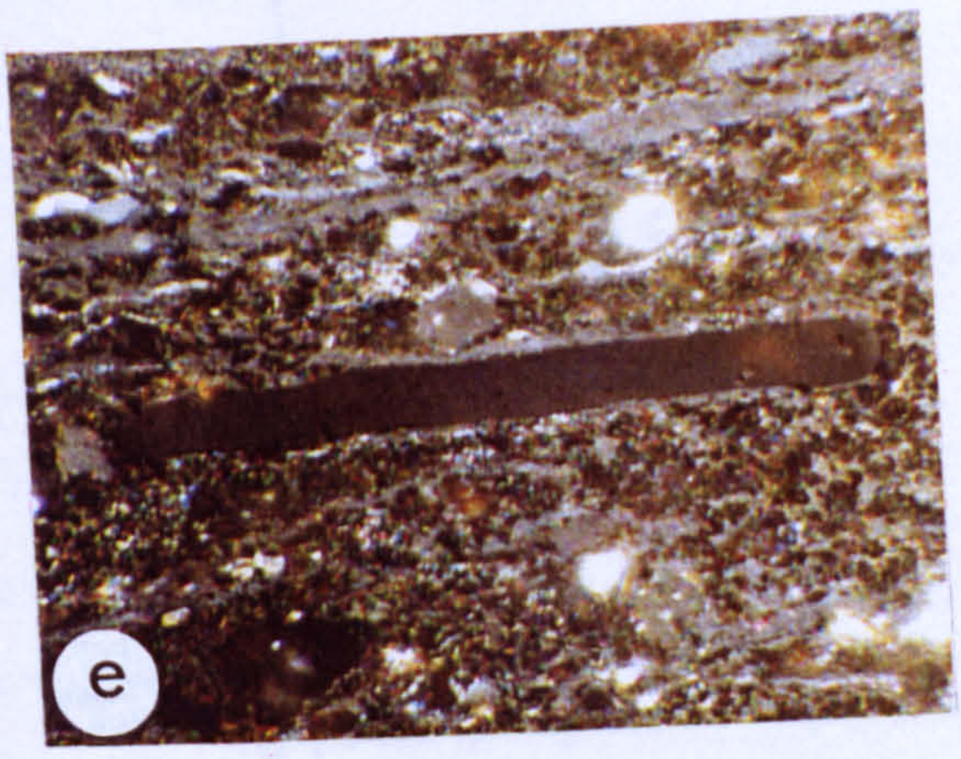
e


f

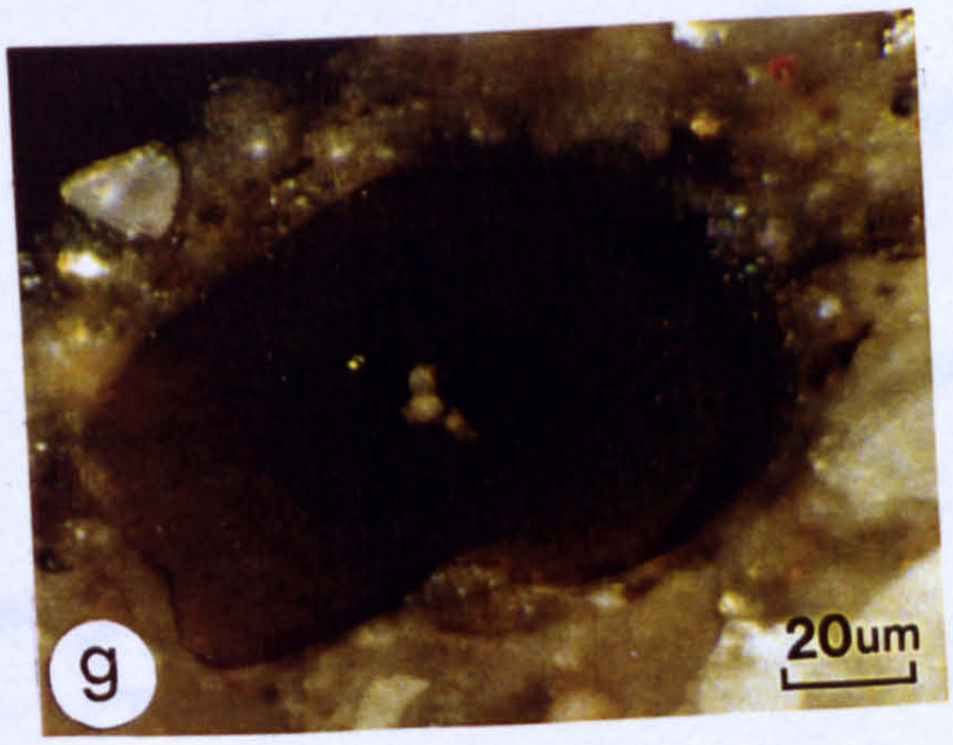
20um
g

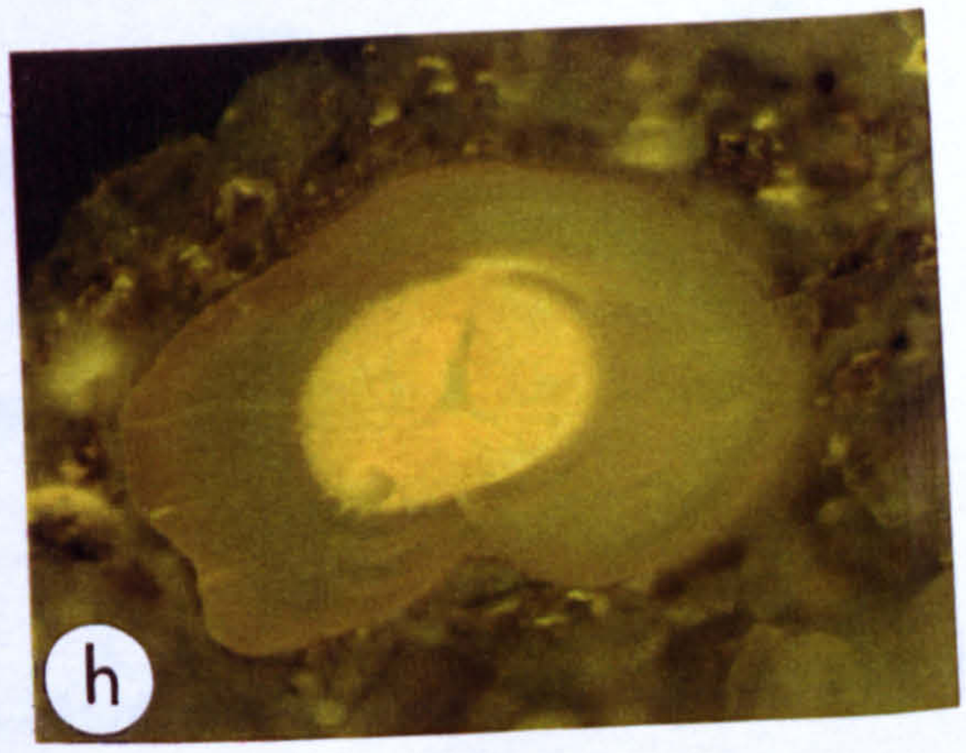
h

associated with dolomite.

In summary, petrographic analysis indicates that the Exshaw has good to excellent source rock potential and is actively generating hydrocarbons. The kerogen is dominated by bituminite but includes a typical marine assemblage of primary liptinite macerals and indigenous bitumens.

Rock-Eval pyrolysis

The S1 and S2 values shown in Appendix B5 are significant for all but one sample; in general, S1 values are over 2 and as high as 14.7 at Bovie Lake (7); S2 ranges from 3.8 to 60 at Island River (1). These values suggest that the Exshaw is in an active state of hydrocarbon generation throughout the Eastern Plains. The modified van Krevelen diagram (Fig. 31) shows that the samples have low oxygen indices, which is typical of hydrogen-rich kerogen. They also fall along the maturation pathway for Type I and II kerogens. The petrographic characteristics of the Exshaw indicate a Type II kerogen.

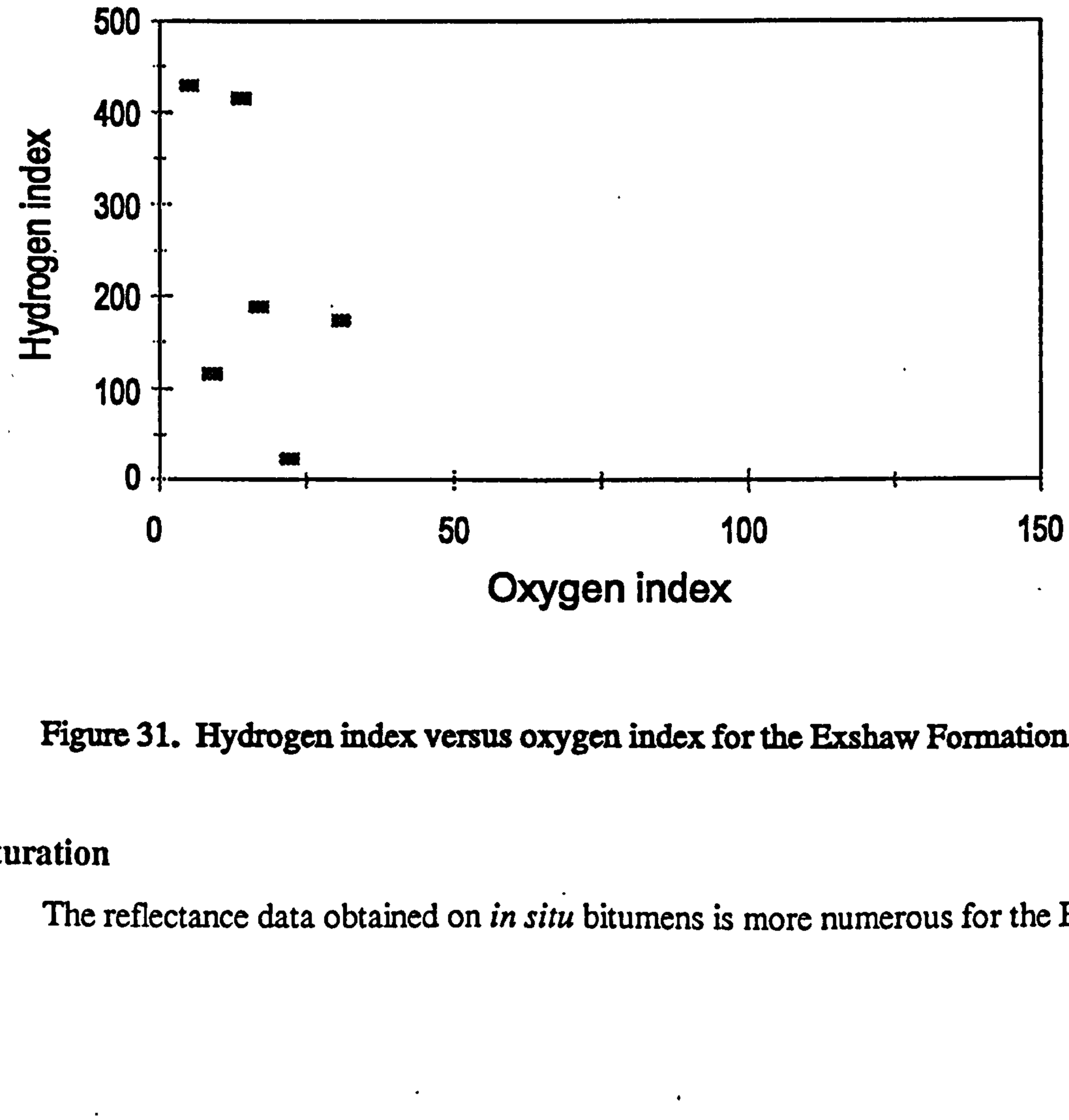

Figure 31. Hydrogen index versus oxygen index for the Exshaw Formation.

Maturation

The reflectance data obtained on *in situ* bitumens is more numerous for the Exshaw

Formation than for the formations previously reported. More reflectance populations are evident which probably reflects: 1) the significantly higher proportion of organic matter, and 2) the more complex organic facies related to a greater variety of macerals capable of generating hydrocarbons in the oil window. For example, different reflectance populations of indigenous bitumen are recognized for different varieties of alginite. Under these conditions, the genetic approach to classification of the bitumens, which forms the basis of this study, is critical to their subsequent use as maturation indices.

Measured bitumen reflectance (type 4 bitumen) and bitumen-derived VR_o eq. values data are shown in Appendix C5. Vitrinite reflectance equivalent values range from 0.91% to 1.07%. All reflectance values fall within the oil window (0.50%-1.30% R_o) for kerogen formed in anoxic environments (Powell & Snowdon, 1983) around the peak oil generation zone (0.85-1.10%), suggesting that the Exshaw Formation to the east of the Bovie Fault is currently capable of generating hydrocarbons.

The vitrinite reflectance equivalent values are positively correlated with depth, conforming to Hilt's Law (Hilt, 1873; Teichmüller & Teichmüller, 1968), suggesting the maturation is related to the present day depth of burial. The data from the Arrowhead section (4) does not fit this trend; the vitrinite Ro, and therefore the measured bitumen Ro, are higher than expected for the depth and regional trends suggesting that the data from this section should be re-examined. The maturation pattern defined by vitrinite reflectance equivalent data fits reasonably well with the maturation patterns observed in underlying strata. The difference in maturation between the westerly sections in the Eastern Plains, i.e. marginal to the Bovie Fault, and those in the east (at Island River and Trout Lake) is significantly lower in the Exshaw Formation, suggesting that the influence of the Bovie Fault decreased through time.

The Tmax values (Appendix B, Table B5) fall between 424°C and 452°C; the latter is the value obtained at Arrowhead (8) and indicates the upper end of the oil generation window. All other values fall within the oil window, which agrees with the petrographic data and observations.

The means of six fluorescence spectral scans on *Tasmanites*-type alginite in the Imperial Island River sample yielded a Q value (Red/Green quotient) of 1.4 ; λmax is 604 nm, also based on the average of six spectral scans. These values correspond to vitrinite

reflectance values of ca. 0.8% R_o (cf. Mukhopadhyay, 1981) which is similar to the 0.82%R_o measured on the type 4 bitumen.

Conodont alteration indices obtained for the Exshaw Formation in the Imperial Island River No. 1 (1) are ca. 1.0 to 1.5. This would indicate a lower maturity than those indicated by the reflectance, fluorescence and Tmax data.

Hydrocarbon potential

The hydrocarbon potential ratings for the Exshaw Formation are shown in Table 14. Organic richness is greatest in the Island River area. This is also the area of lowest maturity and the best petroleum (Fig. 32) and gas potential (Fig. 33).

4.6 BANFF FORMATION

In the study area, the Banff Formation is dominated by a dark blue-grey shales with mudstones, and locally, minor siltstones and skeletal limestones (Richards, 1989). It rests conformably on the Exshaw Formation and the contact is gradational; in the western part of the study area it grades laterally into the Besa River Formation (Richards, 1993). It is conformably overlain by Rundle Group in the west (Liard Plateau) and unconformably by Cretaceous strata (Fort St. John Group) in the western part of the Eastern Plains, where it thins rapidly to the east, pinching out against the Precambrian basement (Fig. 13). The Banff is thinnest in the northern part of the Eastern Plains study portion of the area at Trout Lake (section 2; 102 m) and Arrowhead (section 4; 101.5 m) but thickens rapidly to the west, reaching a thickness of 566m in the Bovie Lake (7). At Viscount (21), the only Banff section sampled in Northeast British Columbia, the total thickness is unknown.

Banff samples show a significant range in TOC values, from 0.1 to 2.5%, (Appendix B6) and most sections, except Viscount (24; TOC = 0.2%), have intervals with "fair to good" source potential. Samples from the basal Banff at Mattson Creek (11) are reasonably enriched (1.6 to 3.9%) as are those from Bovie Lake (section 7: 1-2%). The regional range of TOC values is also similar to that recorded stratigraphically in each section; the richest zone, which shows relatively high TOC values (1.5%, 2.5% TOC), occurs in the Lower Banff,

Section no.*	Thickness (m)	% TOC B	Organic richness (A x B = C)	Maturity % VRo	Oil maturity factor (E)	Gas Maturity factor (F)	Oil source potential (C x E)	Gas source potential (C x F)
1	7	14.8	103.6	0.91	1	0.4	103.6	41.4
4	11	1.61	17.71	1.07	0.7	0.7	12.4	12.4
7	16.5	1.8	29.7	1.06	0.7	0.7	20.8	20.8
3	8.5	1.44	12.24	0.93	1	0.7	12.24	8.6
8	21.3	21.3	68.16	1.05	0.7	0.4	47.7	27.3

*numbers refer to sections in Fig. 16: 1 = Imperial Island River No. 1; 4 = Imperial Sun Arrowhead I-46; 7 = Texaco N.F.A. Bovie Lake J-72; 3 = Murphy *et al.* Muskeg River No. 1; 8 = B.A. Texaco Arrowhead N-2;

Table 14 Hydrocarbon potential of the Exshaw Formation (based on the method of Dembicki & Pirkle, 1985).

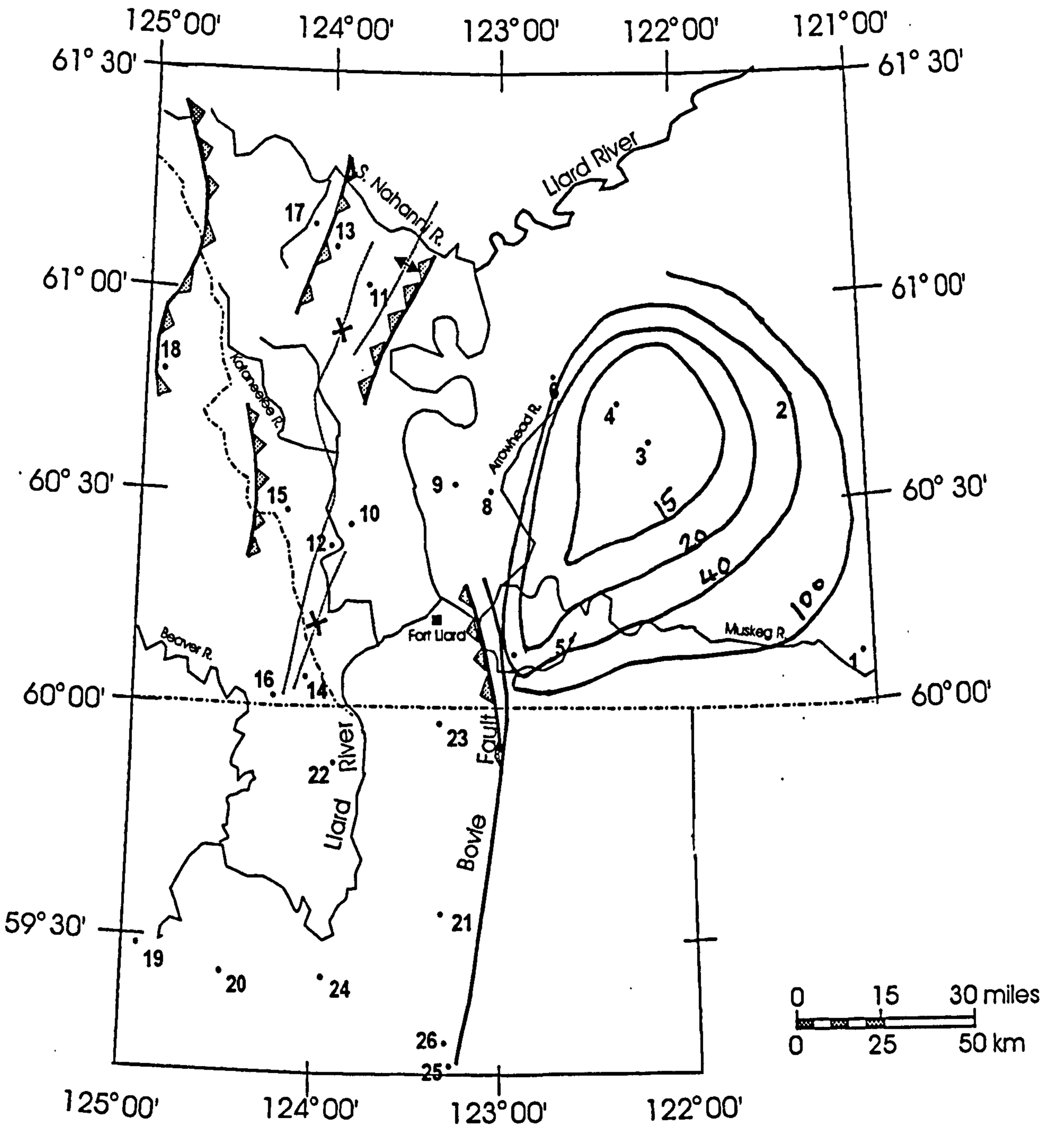

3 **location as shown in Figure 16**

Figure 32. Regional variation in oil source potential for the Exshaw Formation (based on Dembicki & Pirkle, 1985); contours are drawn by eye based on data shown in Table 14.

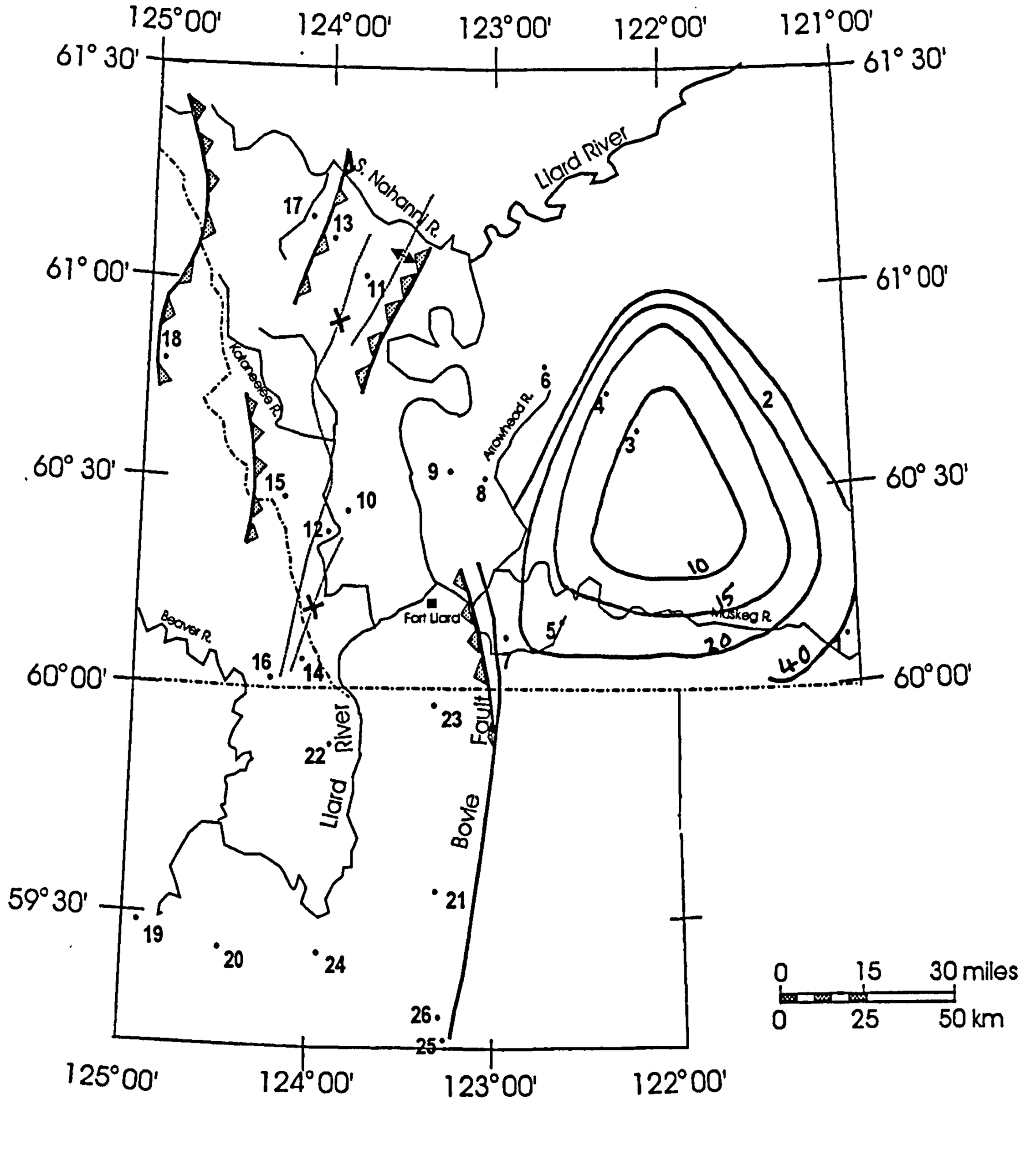

3 **location as shown in Figure 16**

Figure 33. Regional variation in gas source potential for the Exshaw Formation (based on Dembicki & Pirkle, 1985); contours are drawn by eye based on data shown in Table 14.

just above the basal contact with the Exshaw Formation. In the Island River section (1), another rich zone occurs at 698 ft. (212.8m) above the base of the Banff.

The kerogen is liptinitic and predominantly marine in origin (Appendix A6); the dominant component in the samples with TOC values greater than 1% is dense amorphous matrix bituminite. The bituminite shows variable levels of fluorescence but exhibits a weak intensity and green-brown colour in the Imperial Island River section (1). At Mattson Creek (11), the bituminite is directly associated with pervasive, fine-grained micrinite (bituminite III). Other primary liptinite macerals are typically dispersed throughout the matrix; these are dominated by alginite (telalginite), particularly thin-walled Leiosphaeridales-type prasinophytes and thick-walled *Tasmanites* prasinophytes. They exhibit moderately intense fluorescence in the yellow range (fluorescence index 3-4), indicating the kerogen is in the mature (oil window) stage of thermal maturation. In the Island River (1) samples, the *Tasmanites* alginite shows strong yellow fluorescence, indicating it is in the peak of the oil window (ca. 0.85% VR_o eq.). Fluorescing liptodetrinite, by definition too small to be identified by the petrographic microscope (< 5µm), pervades the matrix. In the Island River section (1), sporinite is present also, represented by trilete triangulate spores ca. 60-80µm diameter with morphologic affinity to *Murospora* – a typical lower Carboniferous genus. Utting (in Richards, 1989) also found a variety of Carboniferous microspores in the Banff, at Island River (1).

Secondary macerals such as bituminite stringers, presumed to be derived by biochemical alteration of alginite, are very commonly found draped along laminae. In most samples some acritarchs are present; fish scales are present, but rare. Vitrinite-like macerals as well as inertinites, semifusinite and fusinites are present, but only at Island River (1) and Muskeg River (3). While they may be cavings from the overlying Cretaceous strata (Fort St. John Group) which typically contains deltaic sediments and thin coals, they may be indigenous to the Banff in the Eastern Plains region as Carboniferous spores from terrestrial plants are also present.

The primary and secondary maceral assemblages for most of the samples examined is fairly typical of Type II marine kerogen, with contributions from terrestrial organic matter. This is consistent with the interpretations of Richards (1989), who concluded that the Banff Formation was deposited during one of the many NW to SE marine transgressions over the

Late Devonian-early Carboniferous continental shelf; and that the lower Banff in this region was deposited in a more basinal setting during a regional transgression, while the Upper Banff shows lithofacies characteristic a shallow neritic shelf, suggesting a progressive shallowing and finally regression related to local sea level fluctuations. Subsequently, Richards (pers. comm.) has noted that, to the north of the study area, the Upper Banff includes very shallow water and even supratidal clastics and therefore the northeastern part of the study area may have been close to the shoreline during Banff times. Morrow and Geldsetzer (1988) also imply that the southern part shelf was not completely inundated during late Devonian-early Carboniferous transgressions. The maceral assemblages in the Banff at Island River (1) and Muskeg River (3) may therefore indicate the proximity of the continental margin in early Carboniferous times.

Low and medium reflectance bitumens are common subordinate components, especially type 4 bitumens and low reflectance type 3 bitumens associated with liptinite macerals. These suggest that the liptinite macerals and the amorphous matrix are actively undergoing thermal maturation generating indigenous bitumens as by-products of hydrocarbon generation. However, numerous samples, particularly those from Island River (1) and Muskeg River (3), possess minor quantities of macerals such as sporinites, inertinites and vitrinite-like components, typically found in terrestrial kerogen. The presence of *Tasmanites* and *Leiosphaeridia*, confirms a marine origin for the kerogen but the contributions from terrestrial environments suggests a nearshore marine setting for the Banff in the eastern part of the study area.

The petrographic characteristics of the Banff Formation at Mattson Creek (11) and Viscount (24) are significantly different from those in the Eastern Plains region. The predominance of secondary macerals such as micrinite-bituminite and indigenous low and medium Ro bitumens and lack of primary macerals indicate kerogen of elevated maturity.

Rock-Eval pyrolysis yields S1 and S2 yields vary significantly both vertically and laterally within the Banff: the S1 values range from less than 0.1 to 9 and S2 from 0.1 to 4.7 (Appendix B6). Samples from the Bovie Lake section (7) all have high S1 (7.0-9.35) and S2 (1.0-4.7) values, suggesting that the Lower Banff at this location has good potential and is actively generating hydrocarbons. Significant S1 and S2 values were obtained also from Arrowhead (8) and Mattson Creek (11). Production indices (S1/S1+S2) of greater than 0.5

suggest that the hydrocarbon production is in advanced stages and therefore the kerogen is very mature at Bovie Lake (7) and Mattson Creek (11). At Viscount (24), both S1 and S2 are low and the production index is high suggesting that the poor source potential is due to post maturity.

Hydrogen indices (HI) in the Banff Formation are generally low (50–200) and oxygen indices vary from low (0) to high (230). The hydrogen index versus oxygen index plot (Fig. 34) indicates that the Banff, in general, is a mature type II kerogen. Samples from Bovie Lake (7) (which are also those with the highest TOC values) exhibit higher hydrogen indices (270) but the data suggest some oxygen enrichment of the kerogen in samples from the northeastern part of the study area (e.g. at Arrowhead, section 8) which is compatible with the occurrence of oxygen-rich macerals such as inertinites and vitrinite.

Reflectance measurements of three populations of indigenous low R_o bitumens, medium R_o and high Ro pyrobitumens in the Banff are given in Appendix C (Table C6), together with the VR_o eq. values. The presence of three populations of low Ro bitumens is taken as an indication of a thermal maturity range of 0.7 to 1.1% VR_o because at higher maturity the types 1 and 2 bitumens are not present; this is consistent with the maturation range of the structured liptinite macerals (0.75% to 1.1%VR_o). Measured vitrinite data were also obtained from numerous samples at Island River (1) and one sample from each of the Muskeg River (3) and Arrowhead N-2 (4). These agree quite well with the type 4 bitumen reflectance which translates into 0.9% to 1.4% VR_o eq. All reflectance values from sections in the Eastern Plains region fall within the oil window which, together with qualitative petrographic analysis, indicates the Banff is mature east of the Bovie Fault. The highest VR_o eq. values occur to the west (1.14 % at Celibeta (5);1.07% VR_o at Bovie Lake (7) while the lowest values (0.91%-0.93% VR_o eq.) are found furthest east. This follows the trends observed in the underlying Exshaw and Upper Devonian. Although high reflectance values (1.8%-1.9% VR_o eq.) at Mattson Creek (11) indicate it is postmature for oil at this location, high TOC values (1.5 -3.8%) suggest it remains a potential source of thermogenic gas.

The relationship between VR_o and depth is shown in Figure 35. The log Ro vitrinite equivalent values of samples from sections in the Eastern Plains increase with depth which suggests all samples experienced the same thermal regime. The higher than expected R_o values observed at Celibeta (5) are attributed to oxidation (cf. Mackowsky, 1982).

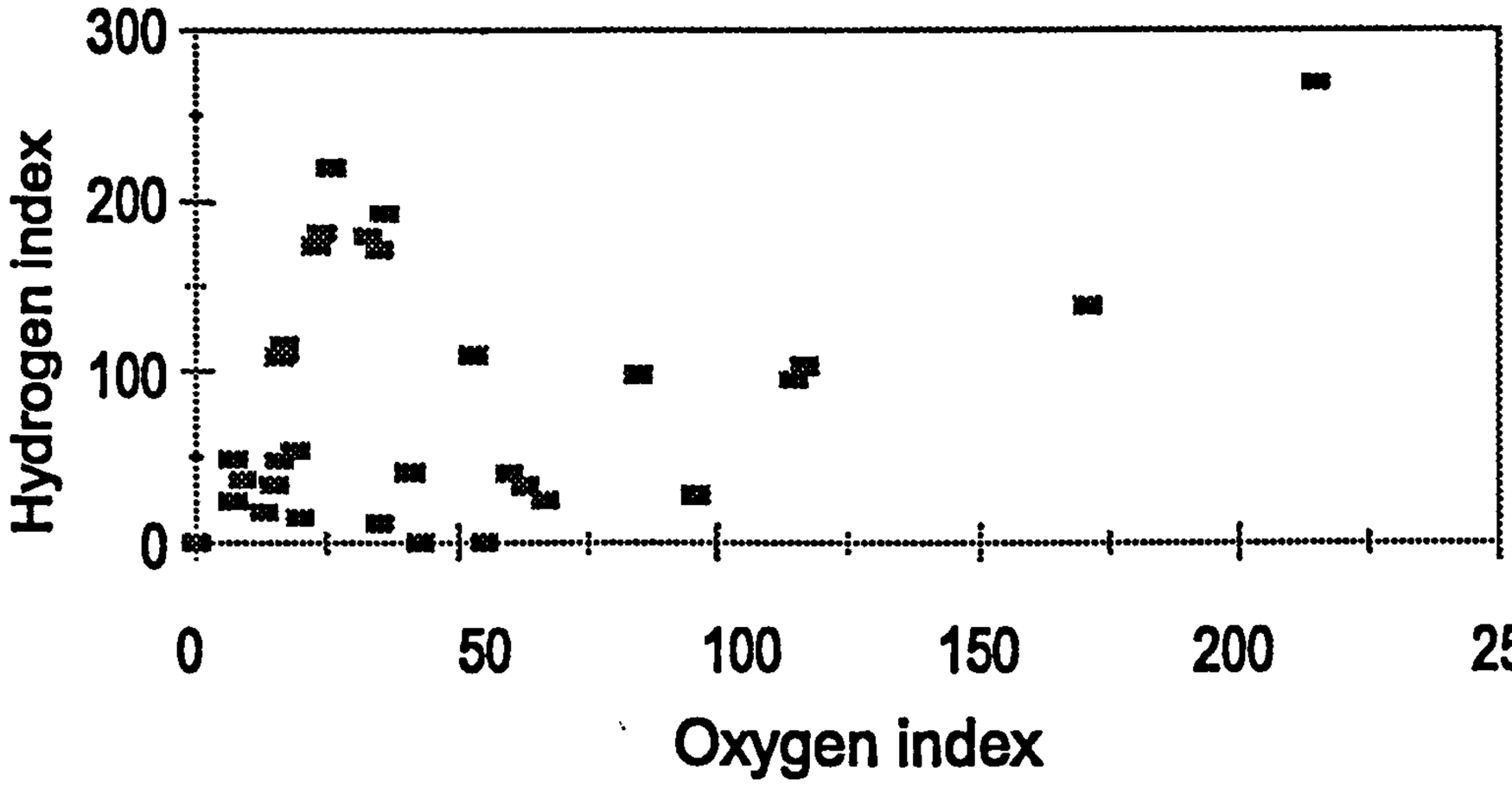

Figure 34 Hydrogen versus oxygen index, Banff Formation

Reflectance data from Arrowhead (4) are also higher than expected. The samples from Mattson Creek and Viscount (24) have significantly higher mean reflectance (1.87% and 1.56% VR_o equivalents, respectively) but these are positively correlated with depth. This suggests that these samples experienced a different thermal regime or burial history.

The Tmax data (Appendix B6) for most of the samples (440° to 445°C) plot in the middle of the oil window, which would correspond to VR_o of 0.75-0.8% for Type II kerogen (MATOIL, 1990). Sections to the west and north (e.g. Arrowhead, section 8) are slightly higher values (444°C to 452°C) which indicate the upper end of the oil window, ca. 1.1% VR_o (MATOIL, 1990) and sections to the east slightly lower (438°C-440°C) which fits with the general regional reflectance patterns observed. Values of 440°C at Bovie Lake (7) indicate peak oil generation which is somewhat lower maturity than suggested by the VRo eq. values and production indices suggests (0.70 to 0.90). Although Tmax shows a reasonably strong increase with depth (Fig. 35), the correlation between Tmax and VR_o eq. data is poor. Perhaps the most significant disagreement between the Tmax and reflectance data occurs at Muskeg River (3), where reflectance data suggests the Banff is in the peak of the oil window while Tmax data suggests it is immature.

Interestingly, the Tmax data for the Arrowhead section (8) (448 °C, 452°C) are

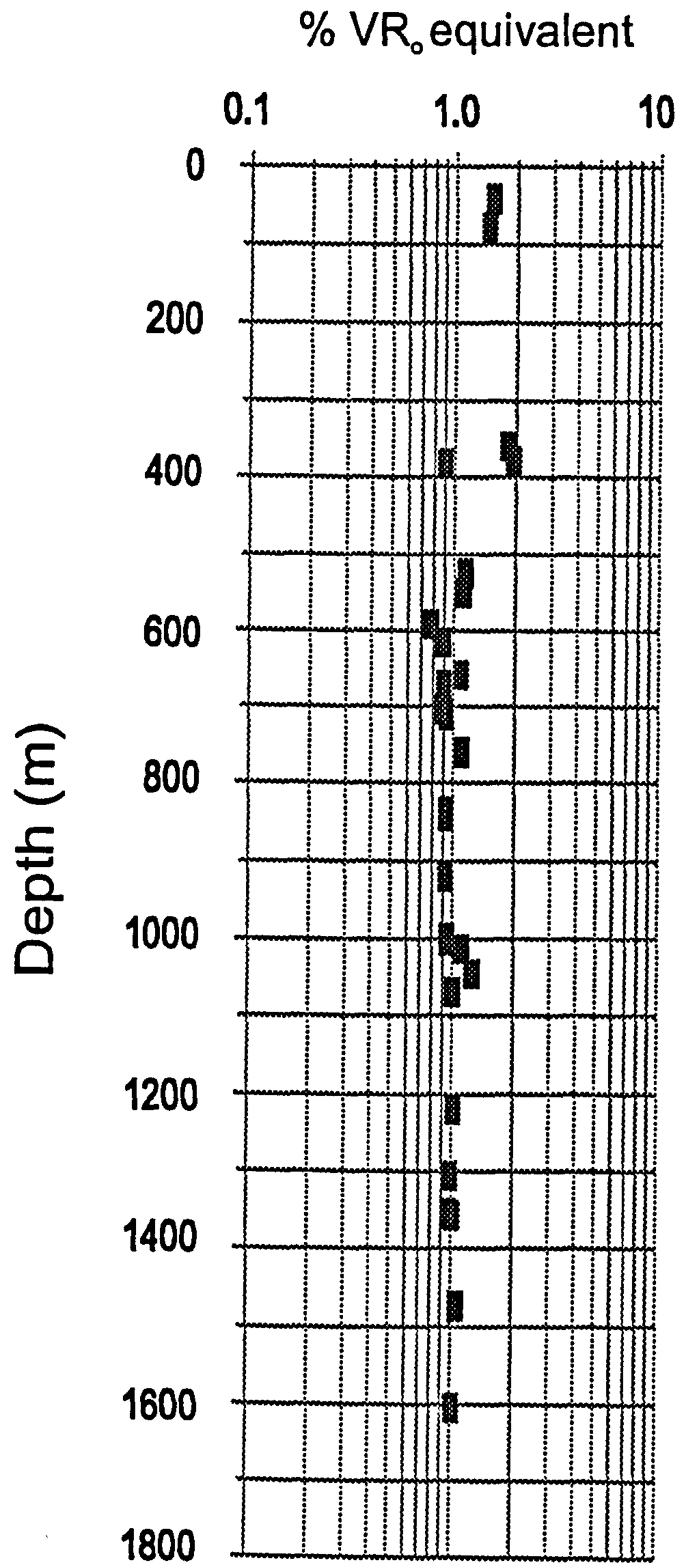

Figure 35. Vitrinite reflectance equivalent values derived from type 4 bitumen Ro data, versus depth in the Banff Formation.

relatively high and would correspond to about 1.1% VR_o, according to the Matoil correlations for Type II kerogen (MATOIL, 1990), i.e. the upper end of the oil window. Although no Rock-Eval data were obtained for the other Arrowhead section (4) due to sample size restrictions, the reflectance data are similar to samples from section (8) so the reflectance anomalies noted previously for the Arrowhead samples may indeed be real.

The mean Tmax for value for Mattson Creek (11: 486°C) indicates overmaturity but the TOC values are significant (1.5-3.8%) and the Banff probably has generated, and is probably still actively generating, thermogenic gas. By contrast, the Tmax for overmature Banff samples from Viscount is anomalously low, which probably reflects the low TOC.

The CAI values from the Banff are in the 1.0-1.5 range which is also lower than expected, relative to the reflectance data and Tmax data.

Hydrocarbon potential

The hydrocarbon potential ratings for the Banff Formation are shown in Table 15. Organic richness is greatest in the Bovie Lake (7) and Island River (1) areas and these are the areas of greatest oil source potential (Fig. 36); Bovie Lake has the highest gas potential also (Fig. 37).

4.7 BESA RIVER FORMATION

The Besa River Formation is a thick basinal shales sequence of Upper Devonian - Lower Carboniferous age which occurs in the Liard Basin and is ca. 1000m thick at the type section (Kidd, 1964; Peltzer, 1966) and Beaver River (16). It grades eastwards into the Exshaw and Banff formations at Mattson Creek (11) and in the Interior Plains (sections 1-9). It is predominantly a fine-grained, moderately radioactive "black shale", slightly dolomitic in places, which commonly has one or two highly radioactive, uraniferous zones (the "1st and 2nd black shale" members) which have been equated stratigraphically with the Muskwa and Exshaw formations (Peltzer, 1966; Richards, 1993).

The thickness of the Besa River varies significantly due to folding, faults and multiple thrust planes. Of the sections sampled, it is thickest on the flanks of the Pointed Mountain Anticline, (at section 12; 1658m), and within the Kotaneelee Syncline, (at section 15; 1280m ; Figure 11). The thinnest section occurs on the western flanks of the Liard Basin

Section no.*	Thickness (m) (A)	% TOC (B)	Organic richness (A x B = C)	Maturity % VRo	Oil maturity factor (E)	Gas maturity factor (F)	Oil source potential (C x E)	Gas source potential (C x F)
1	401.08	1.04	417.12	0.93	1.00	0.40	417	167
7	566.08	1.63	922.71	1.07	0.70	0.70	646	646
5	388.88	0.60	233.33	1.11	0.70	0.70	163	163
6	21.35	1.22	26.05	1.10	0.70	0.70	18	18
3	173.85	1.45	252.08	0.91	1.0	0.40	252	101
8	515.76	1.02	526.08	1.01	0.70	0.70	368	368

*numbers refer to sections in Figure 16: 1 = Imperial Island River No. 1; 7 = Texaco N.F.A. Bovie Lake J-72; 5 = Pan Am *et al.* Celibeta No. 7; 6 = Imperial Sun Netla C-07; 3 = Murphy *et al.* Muskeg River No. 1; 8 = B.A. Texaco Arrowhead N-2.

Table 15 Hydrocarbon potential of the Banff Formation (based on the method of Dembicki & Pirkle, 1985).

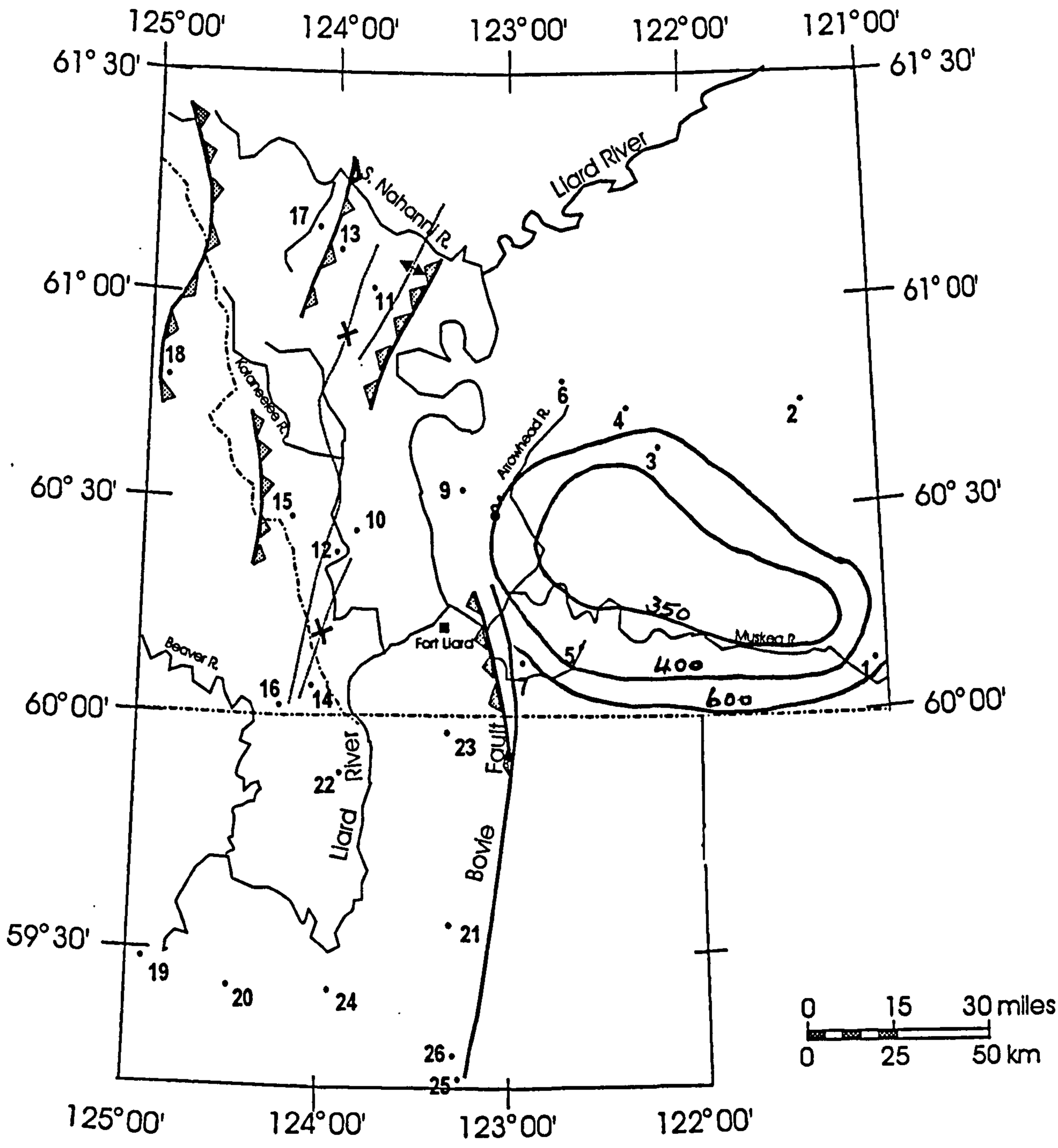

3 **location as shown in Figure 16**

Figure 36. Regional variation in oil source potential for the Banff Formation (based on Dembicki & Pirkle, 1985); contours are drawn by eye based on data shown in Table 15.

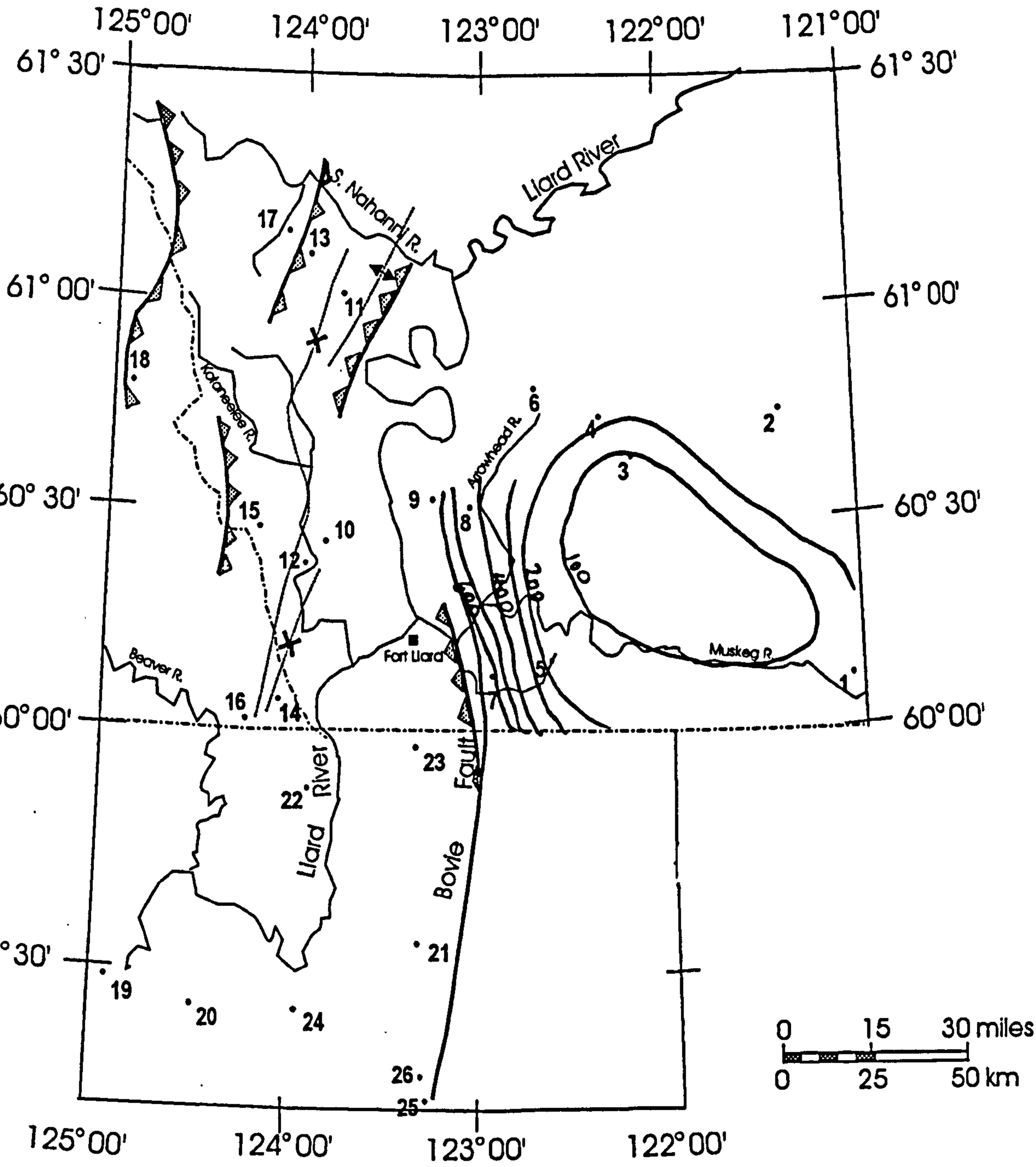

3 **location as shown in Figure 16**

Figure 37. Regional variation in gas source potential for the Banff Formation (based on Dembicki & Pirkle, 1985); contours are drawn by eye based on data shown in Table 15.

at Viscount (section 24: 533.4m) where it is at its shallowest depth (1072.9m). It occurs at greatest depth (3706.4m) at North Beaver River (14), but at the Beaver River section (16) and Kotaneelee (15) it occurs at a depth of 3130m. At Clausen Creek (17), thrusting has brought the Besa River to the surface and the top occurs at +320m above sea level; the base is not exposed but the thickness must be assumed to be considerably greater than the 320m of section exposed.

The great thickness of the Besa River Formation at the more westerly locations indicates the presence of a rapidly-subsiding, starved marine basin (the Liard Basin) in northeastern British Columbia (Peltzer, 1966; Figures 1 & 13). Peltzer (*ibid.*) suggests that a stratified water column was responsible for the accumulation of the black shale members.

Organic Richness

The TOC content of the Besa River Formation varies considerably from 0.4 to 6.0% (Appendix B7) and therefore mean values do not adequately reflect the richness shown by some intervals. Approximately half of the sampled intervals have TOC values over 1% which suggests fair to good source potential, and the lower part of the Besa River contains intervals which are extremely rich in organic matter at all locations. For example, in the N. Beaver River section (14) the "1st Black Shale" (at a depth of 3258-3315.9m) has 6% TOC and the "2nd Black Shale" (at 3331.5-3337.3m) has a TOC of 4.2%. Similar intervals at Beaver River (16) and Pointed Mountain (12) contain 3.4 % and 3.5% TOC respectively. These intervals may have excellent source potential.

Organic petrography

The petrographic characteristics of the Besa River are summarized in Appendix A7. The Besa River is, at all locations, a very pyritic, moderately to well-dolomitized, laminated, variably organic-rich shale. Internal microfractures link up with the internal laminations to create extensive organic networks which form the principal pathways through which hydrocarbon migration and expulsion probably took place (cf. Belin, 1992). The organic constituents are predominantly amorphous liptinites and associated secondary macerals, primary bitumens and pyrobitumens. The dominant constituent in most of the samples is a dense, dark brown to black, matrix bituminite which is typically the dominant component of

marine source rocks of Upper Devonian age containing Type II kerogen in the Western Canada Sedimentary Basin (Powell & Snowdon, 1983). It is intimately mixed with fine granular, highly reflective, white micrinite which, unlike other inertinites, has a higher hydrogen content and is reactive. Theories on the origins of micrinite have been discussed earlier in this chapter (Section 4.1, Organic petrology of the Muskwa Formation) and in Potter *et al.*, 1993 (copy located in the back pocket). In this study, micrinite is observed in mature and postmature source rocks but it can also occur in low rank coals (Shiboaka, 1983; Potter *et al.*, 1993), and immature (Stasiuk, 1993) source rocks and therefore it is suggested that factors other than maturation affect the formation of micrinite. In light of the reactivity of micrinite, it is suggested that, while the relatively high reflectivity may be thermally induced, the reflectance may develop at relatively low temperatures (40-50°C), i.e. during early diagenesis. Factors such as pH and Eh may also be important in the formation of micrinite.

Primary structured liptinite is relatively rare in the Besa River samples; however, highly reflective, "meta-alginite" derived from *Tasmanites* and *Leiosphaeridia* is present at Kotaneelee (5) and Beaver River (16). There is also ample evidence to suggest that alginite was the dominant contributor to the bituminite and bitumen present. Firstly, most of the samples contain low R_o type 3 bitumen, which is derived from bituminite, an amorphous maceral that may be formed by biochemical or oxidative reworking of alginite (Teichmüller, 1985; Teichmuller & Ottenjahn, 1977). Secondly, in samples from Clausen Creek (17) and N. Beaver River (14), dolomitized remains of filamentous alginite, ?phycomata or acritarchs and other organic fossils are preserved. The permineralized trichomes (Plate IX a,b.) are approximately 30 µm wide, elongate (ca. 400+ µm) and exhibit chain-like cell structure, resembling modern forms of filamentous S-bacteria (cf. Peniguel, *et al.*, 1989). Morphologically, they bear a strong resemblance to trichomes from cyanobacteria found in stratiform carbonates in the Proterozoic of the Yukon Territory (Awramik, 1984) and Western Australia (Walker *et al.*, 1983) and also to the filaments observed in the Muskwa Formation (Plate VIf). The ?phycomata/acritarchs are approximately 30-40µm in diameter and have an irregular or modified slit-like aperture suggesting they may be akinetes but there is insufficient detail to identify them (Plate IXa, f, g). The organic fossils are aggregates of cells (Plate IXc, d, e) that resemble ancient coccoid cyanobacteria from the

PLATE IX
PETROGRAPHIC COMPONENTS OF THE BESA RIVER FORMATION

a), b) Fluorescent light image (400-440nm excitation) of dolomitized ?cyanobacterial trichomes or filaments found in the First Black Shale Member at Clausen Creek.

c) White light image of dolomitized ?bacterial remains shown in d).

d), e) Fluorescent light (400-440nm excitation) images of primitive ?diacromorphic cyanobacterial remains or other prokaryotic organisms.

f), g) Fluorescent light images of dolomitized ?prasinophyte phycomata or ?acritarchs, both f) and g) have small, irregular apertures (shaded areas indicated by arrows) which suggest that they may have been cyst-like structures of a primitive prokarote with a life cycle of alternating vegetative and resting stages. First Black Shale Member, Clausen Creek.

h) High reflecting type 3 bitumen in the Besa River at Pan Am Beaver G-01.

i) High reflecting type 4 bitumen in the Besa River at Canada Southern *et al.* North Beaver River.

Magnification: scale bar shown on a) applies also to b - g) ; scale bar shown on h) applies also to i).

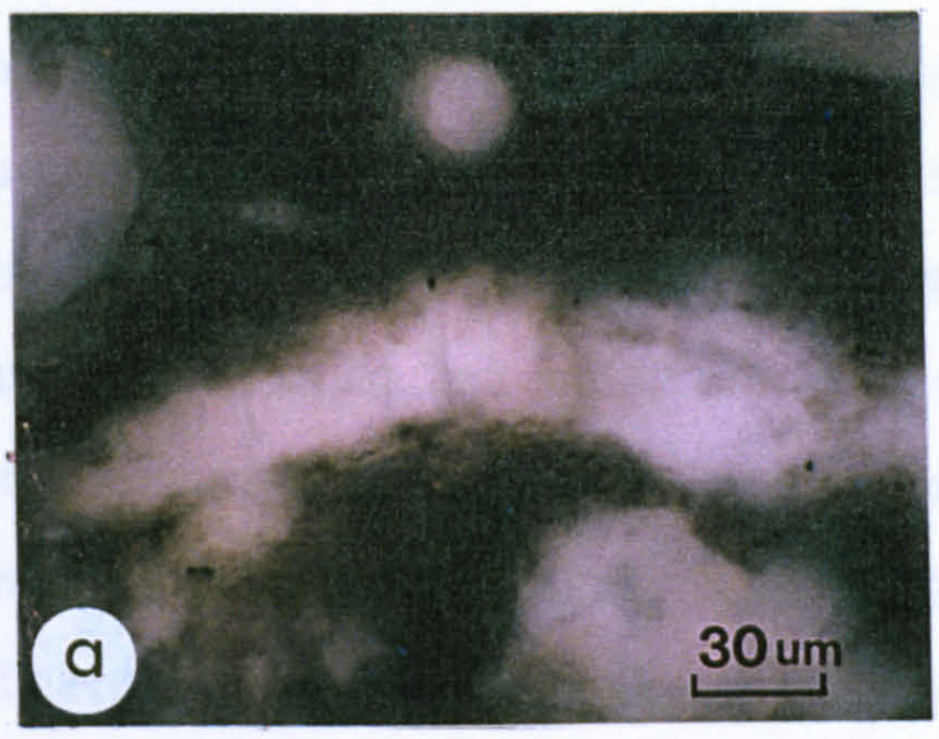
a
30 um

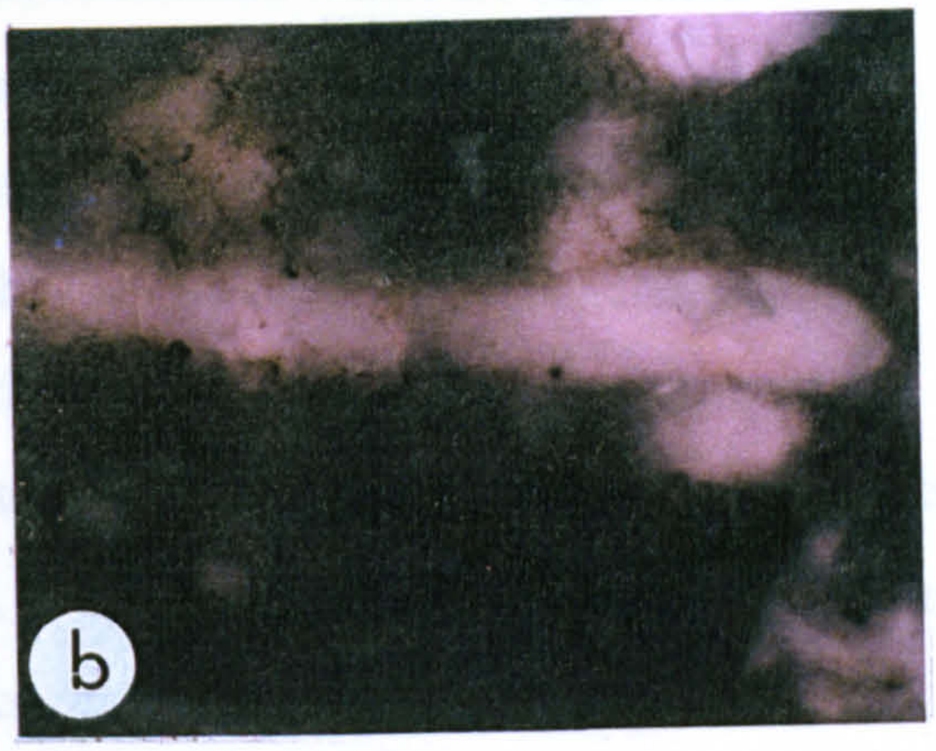
b

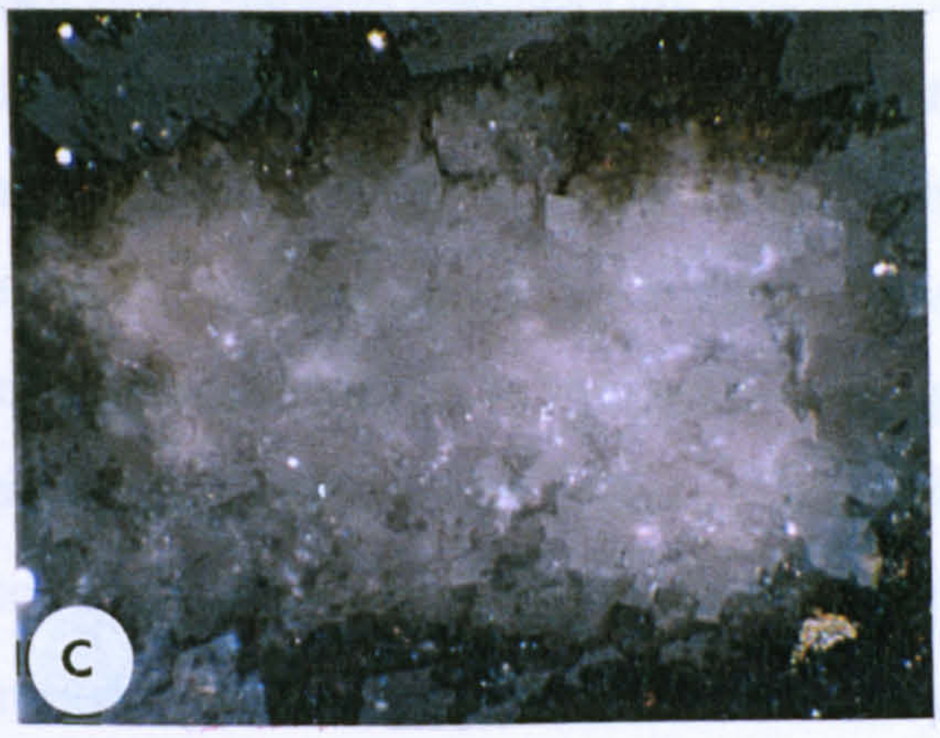
c

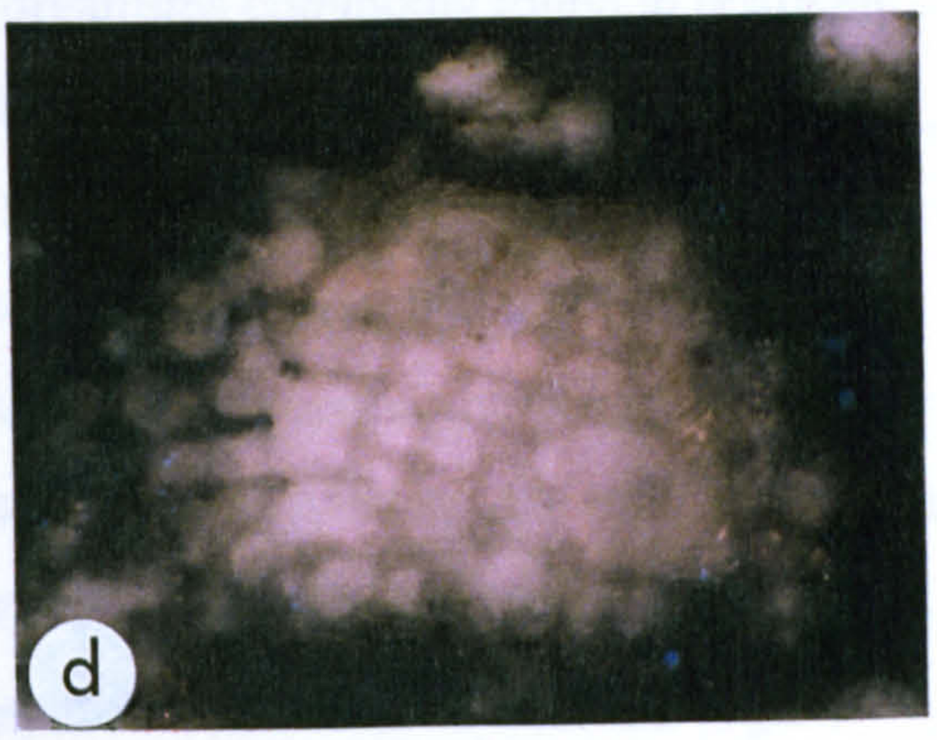
d


e


f

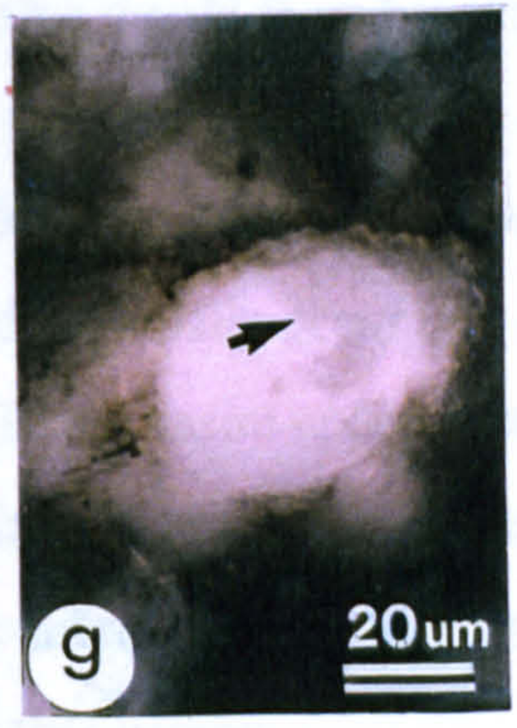
g
20 um

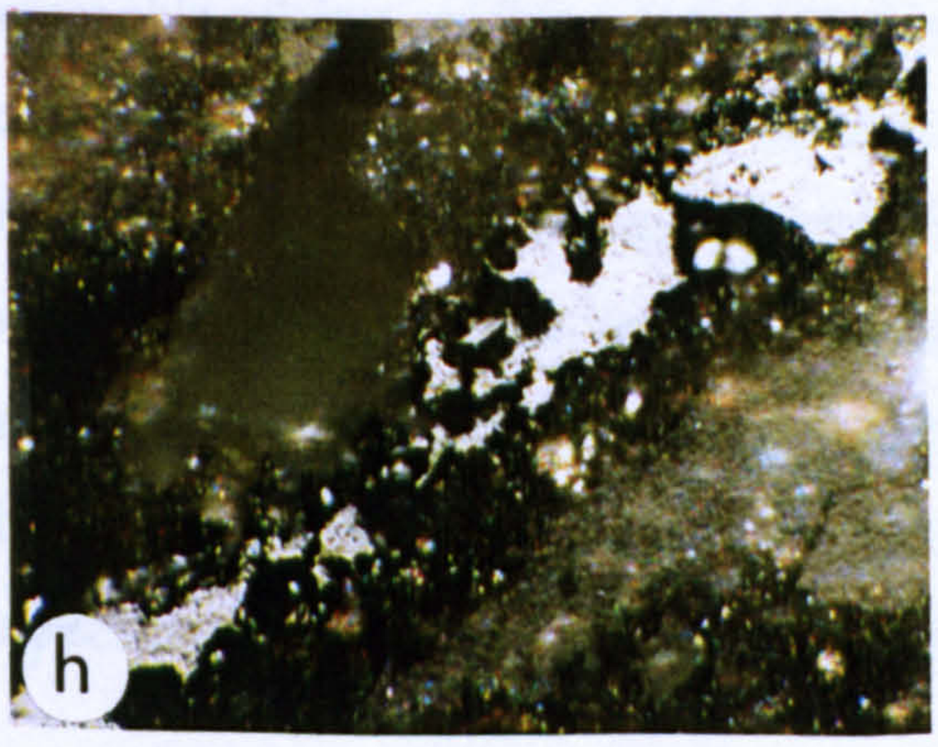
h

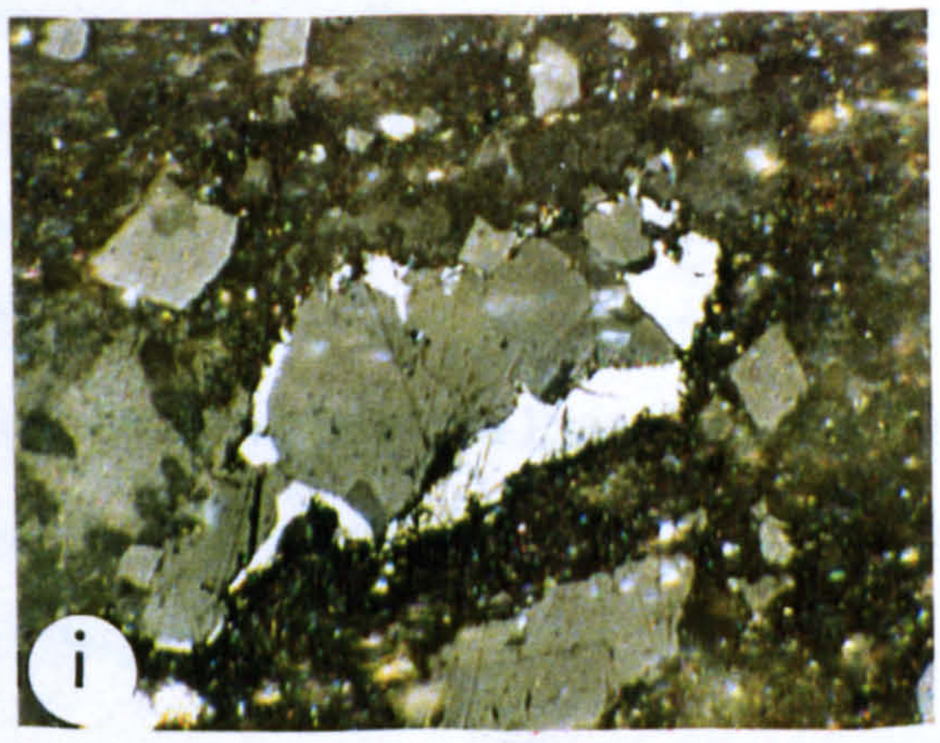
i

Precambrian Paradise Creek Formation of Western Australia which are attributed to the genus ?Eucapsis (Licari *et al.*, 1969, in Walker *et al.*,1983). The trichomes, ?phycomata/acritarchs and cyanobacteria-like remains are visible only under fluorescent light (blue or UV). Peniguel *et al.* (1989) describe various types of Recent and fossil cyanobacteria noting their importance in hot springs, hypersaline and very quiet water marine environments (mostly shallow sub- and intertidal) and in hydrocarbon source rocks. Similar ancient examples (Schopf & Barghoorn, 1967) are stromatolite-forming organisms and have been described from Precambrian rocks all over the world (Schopf & Walter, 1982). Most modern examples are mat-forming organisms commonly found in relatively shallow water but are typically associated with sulphate- or sulphide-rich environments (Cohen, 1984). The Besa River Formation does not show any other evidence of shallow intertidal or subtidal facies that might be linked with ancient microbial mat (stromatolite) formation or evaporites. In reviewing the origins of the high concentrations of uranium found in these black shales, Peltzer (1966) offers a unique hypothesis. He (*ibid.*) considers either a volcanic source for the uranium, or the influx of dense sulphate-rich brines in a stratified water column during the marine transgression that occurred over this region during Banff times. He (*ibid.*) suggests that a highly concentrated brine would form beneath the normal marine waters as they transgressed northwards over the salt pans of the Upper Devonian Potlatch anhydrites of southern Alberta, creating a stratified water column. Slow mixing of the sulphate-rich bottom and normal marine waters would eventually occur leading to a high nutrient supply within the seas advancing into the Liard Basin; under these conditions, planktonic life would fluorish resulting in rapid accumulations of organic matter which would be preserved in the reducing and acidic conditions prevailing in the fondoform shales of the Besa River Formation. Tyson (1995, p. 255) indicates that benthic, chemotrophic sulphur-oxidizing bacteria are commonly found in the oxygen-minimum layer at depths of between 150 and 500m in modern environments, and that a large number of geological studies suggest analogous occurrences of thiobacterial mats occur in dysoxic-suboxic laminated black shale facies. Hoffman (1976), on the other hand, indicates that ancient stromatolites are found in a wide variety of environments in the Precambrian of the northwestern Canadian shield and described columnar stromatolites formed in a deep basinal marine setting in greywacke marls of the middle Precambrian McLean Formation.

Primitive life forms, including large bacteria resembling these mineralized trichomes and metal-encrusted bacteria, have also been described from mats and hydrothermal "chimneys" or "black-smokers" on the floors of the deep ocean (ca. 2700m depth) far below the photic zone (Lilley *et al.*, 1987). Among the complex microbial communities are sulphur-oxidizing bacteria and anaerobic sulphate-reducing bacteria (Lilley *et al.*, 1987). Mat-forming, methane-oxidizing bacteria are also found in the vicinity of modern vents, in the vent waters and in the trophosomes of the tube worms that colonise the vents (Jannasch, 1987). Metallic sulphides are abundant in the Besa River samples (although pyrite is the only mineral positively identified) and sedimentary exhalative (SEDEX) minerals are common in the Devonian of northeastern British Columbia and the southeastern Yukon (Carne & Cathro, 1982; Mako & Shanks, 1984). Carne and Cathro (1982) describe stratabound, black shale-hosted ore deposits within the Besa River Formation and its equivalents in the Selwyn Basin (Black Clastic Group) which was a major tectono-stratigraphic feature during middle and upper Devonian times.

In relation to hydrothermal activity along faults, it is worth noting that Simoneit (1984, 1985) has shown that hydrothermal activity in the deep sea sediments in the Guaymas Basin off the coast of California (along the East Pacific Rise–San Andreas rift-transcurrent fault system) causes almost instantaneous (geologically speaking) hydrocarbon generation from sedimentary organic matter, which is predominantly phytoplankton and microbial detritus. The products include condensates and naphthenic to waxy hydrocarbons, asphaltenes; and polyaromatic hydrocarbons (PAH's); the former group are produced thermogenically from immature organic matter; the latter are a product of high temperature resynthesis and aromatization of hydrocarbons in the vents.

Although subordinate to the matrix bituminite, indigenous bitumens are also abundant in the Besa River, particularly in the "black shale" members (Plate IXh, i). They are dominated by Low R_o type 3 bitumens (which are associated with bituminite), medium R_o (type 4) and high R_o bitumens. The medium and high R_o (pyrobitumens) are the most abundant. Typically, they are pore-filling solids dispersed throughout the matrix and are not associated with structured liptinite macerals. Together, the paucity of primary macerals and low R_o type 2 and 3 bitumens derived from them, and the assemblage of amorphous liptinite-secondary macerals and indigenous bitumens (derived from primary liptinite

macerals) is characteristic of kerogen which has matured through the oil window and is now of elevated maturity.

The observed elevated maturity may not be entirely burial-induced. At Kotaneelee (15), North Beaver River (14) and Toad River (19), the bitumens display fine granular, mosaic textures and domain anisotropy (Plate IX). Such textures are typically found in semi-cokes formed by laboratory carbonization of vitrinites (Patrick *et al.*, 1963; Murchison, 1978) and petroleum and coal-tar pitches (Grint & Marsh, 1979; Grint, 1979; Marsh *et al.*, 1974) and in hydrogenation residues from coals and pitch-like substances (Mitchell *et al.*, 1977; Mackay *et al.*, 1984). In a natural geological setting, similar optical properties are observed in dispersed sedimentary organic matter associated with igneous intrusions (Jones & Creaney, 1977; Johnson, 1977). The fine-grained, optically anisotropic mosaics are typically formed by thermal alteration of non-graphitizing carbons such as bitumens (Khavari-Khorasani & Murchison, 1978) and low rank coals (Potter *et al.*, 1986), sulphur-rich pyrobitumens and NSO-rich, asphaltic reservoir bitumens from the Upper Devonian reefs of Western Alberta (Stasiuk, 1997). However, thermal alteration of bitumen in the hydrogen-rich, anoxic environment of a black shale is probably resembles hydrogenation conditions more than carbonization; under hydrogenation conditions, semi-cokes form by excessive thermal alteration, when hydrogen becomes depleted, at temperature between 500° and 600°C. The presence of fine-grained, anisotropic mosaics in the pyrobitumens in the Besa River together with the lack of metamorphic minerals in the host rock, suggests that the bitumens were heated to temperatures in excess of 450°C for a brief period of time.

In addition to the optically anisotropic mosaic textures, the pyrobitumens contain small vesicles which may or may not be filled with carbonate minerals. Vesiculation typically results from rapid devolatilization of the more reactive organic components of coals and bitumens (Goodarzi & Murchison, 1977) is seen in the products of laboratory carbonization (Goodarzi & Murchison, 1977), pyrolysis (Potter *et al.*, 1984) and hydrogenation (Potter *et al.*, 1986), all processes which involve subjecting carbonaceous materials to high temperatures (ca. 400-800°C). This suggests the bitumens were affected by a dynamic heat source rather that gradual heating associated with regionally high heat flow.

It is apparent that the bitumens in the Besa River at Kotaneelee (15) have been associated with elevated temperatures that are consistent with a thermal event that occurred

early in the diagenetic history of the source rocks, not long after the microscopic bitumens were formed, probably during the hydrocarbon generation stage of maturity. The temperatures suggested by the optical properties of the pyrobitumens are consistent with those to be found within a metamorphic aureole of an igneous intrusion (300°-1100°C) or induced by hydrothermal fluids (450°-650°C). Igneous activity has been recorded in the Earn Group (Besa River equivalent) during Fammenian times (Morrow & Geldstetzer, 1988) and syenite intrusions occur approximately 65 miles (100 km) to the northwest of Kotaneelee (15) which have been dated as Cretaceous in age (Douglas *et al.*, 1976). Also, the occurrence of hydrothermal deposits in the Besa River in northeastern British Columbia (Galata) and southeastern Yukon (Macmillan Pass) suggests that hydrothermal activity may be responsible for the anomalous thermal alteration of the organic matter.

Rock-Eval Pyrolysis.

The results of Rock-Eval pyrolysis are shown Appendix B7. The mean S1 values for the Beaver River (14, 16) and Pointed Mountain (12, 14) sections are between 1.0 to 1.46 but significantly higher (1.72-2.5) for the black shale members which have also high TOC values (3.0 to 3.5%, respectively). Mean S2 values (<0.6) and high production indices (0.70- 0.86), indicate that they are postmature. As these are gas wells, it must be assumed that the low temperature pyrolysis products are comprised of catagenic gas; however, despite moderately high TOC values in the same interval at Kotaneelee, the black shale samples show low S1 (<0.4) and S2 (0.2) values. Petrographic analysis of these samples indicates that most of the remaining bitumen or organic matter is in the form vesicular, anisotropic semi-cokes. As previously discussed, these are (graphitic) solid products of intense thermal alteration of the organic constituents and so it can be concluded that most of the volatiles and any liquid hydrocarbons were driven off at the time of the thermal event. At Clausen Creek, the basal outcrop sample also has a high TOC value (2.6%), but modest S1 and S2 values (1.18 and 2.0, respectively) and a relatively low production index (0.38), indicating it is a mature source rock.

Hydrogen and oxygen indices are low for all samples; most samples have hydrogen indices less than 100 mgHC/g rock and oxygen indices less than 80 mgHC/g rock. As a result, the data are clustered in the bottom, left-hand corner of the modified van Krevelen

diagram (Fig. 38). This is indicative of a highly carbonaceous residual organic matter of an elevated maturation level for any type of kerogen (Tissot *et al.*,1974); one must therefore rely upon petrographic analysis to determine the original type of kerogen present.

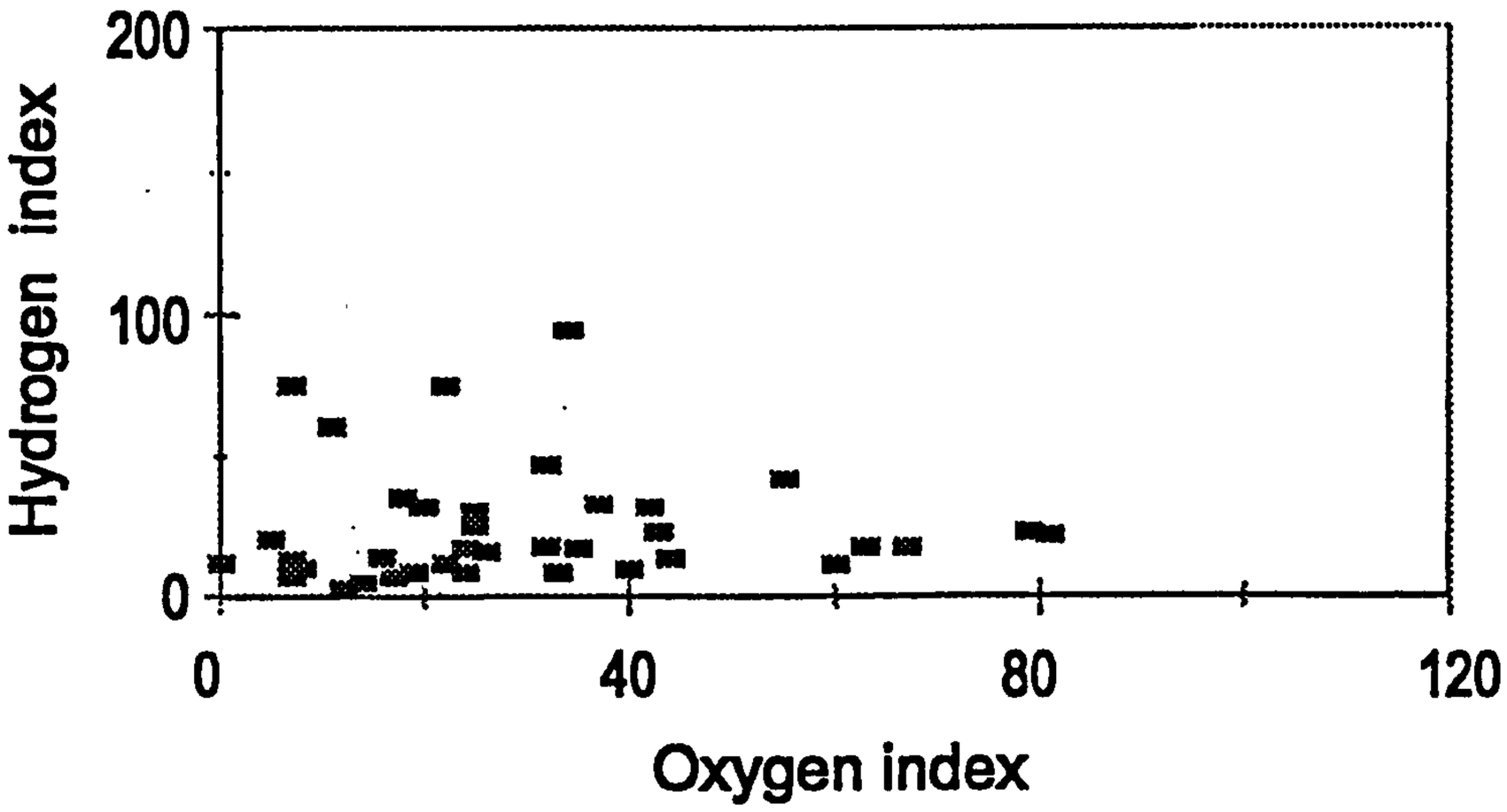

Figure 38 . Hydrogen index versus oxygen index for the Besa River Formation.

Maturity

The Tmax data shown in Appendix B7 indicate that samples from Clausen Creek (17) and Pointed Mountain (12) are the only ones with Tmax values that plot within the oil window. At Clausen Creek, values range from 453°C at the top of the Besa River to 465°C at base of the exposed section (which is probably well above the base of the formation) which indicates a thermal maturity in the early catagenic gas zone (Tissot *et* al., 1974). At Pointed Mountain, the Tmax values of samples from the upper part of the Besa River (440° - 448 °C) fall within the peak oil generation zone. The Tmax values for all other sections fall well below the lower limits for the oil window defined by Tissot *et al.*(1974) (i.e. less than 432 °C) and many are anomalously low, i.e. in the 300-400 °C range. Some of the latter values are derived from samples with appreciably high TOC values, e.g. sample# 10875 at N. Beaver River, which has a TOC of 6.0%. In this sample, the S1 value is over 1 but the S2 value is low (0.3), indicating that upon pyrolysis, peak hydrocarbon generation starts at low temperatures suggesting that the sample is in the

catagenic gas generation stage. The low hydrogen and oxygen indices (Fig. 38) would support this observation (cf. Tissot *et al.*, 1974). This pattern also appears to be true for most of the samples with Tmax values below 400°C. Furthermore, no correlation exists between Tmax and depth (Appendix B8), except in the outcrop section at Clausen Creek (17).

The measured bitumen and corresponding vitrinite reflectance equivalent data, calculated using Jacob's formula (Appendix C7), confirm that the Besa River kerogen falls within the upper limits of the oil window at Clausen Creek (17) (VR_o = 1.19 to 1.36%) and Pointed Mountain (12) (VR_o = 1.28 to 1.6%). At all localities, the VR_o values are between 1.7 and 2.7% R_o, which indicates that the kerogen is in the catagenic gas stage of thermal maturity. A VR_o eq. value of 2.5% recorded at Toad River (19) suggests that the maturity exceeds the gas generation window and therefore the hydrocarbon potential of the Besa River is exhausted at this location. Samples with high reflectance data that do not fit the observed trends display significant quantities of anisotropic semicokes and vesicular bitumen residues. The reflectance and bireflectance of these thermally altered semi-cokes is typically significantly higher than the non-anisotropic samples from the same well sections (Goodarzi & Murchison, 1977; Potter *et al.*,1986). The pyrobitumens also display a high bireflectance (Rmax: 4.6, Rmin 4.3%; bireflectance = 1.2%) which is typical of laboratory carbonized bitumens (Khavari-Khorasani *et al.*,1978; Murchison, 1978) and naturally-occurring semi-cokes (Johnson, 1977).

The positive correlations observed between reflectance (VR_o equivalent) and depth (Fig. 39) and the similar R_o gradients in the super- and subsurface samples, suggest that the geothermal regime was imposed prior to thrusting and elevation of the strata at Clausen Creek (which occurred during the Laramide orogeny).

The regional patterns of reflectance indicate that the highest R_o values occur in the most westerly subsurface, i.e. at Beaver River (16), Kotaneelee (15) and Toad River (19). It is in these locations that the Besa River kerogen contains thermally-induced semicokes. Although the Besa River at Pointed Mountain (12) occurs at comparable depths to the Kotaneelee section, the maturity is significantly lower than in the other subsurface sections. This suggests that either the two sections experienced significantly different tectonic histories, or the more westerly section at Kotaneelee was affected by a thermal event in addition to the geothermal maturation that accompanied burial. The petrographic

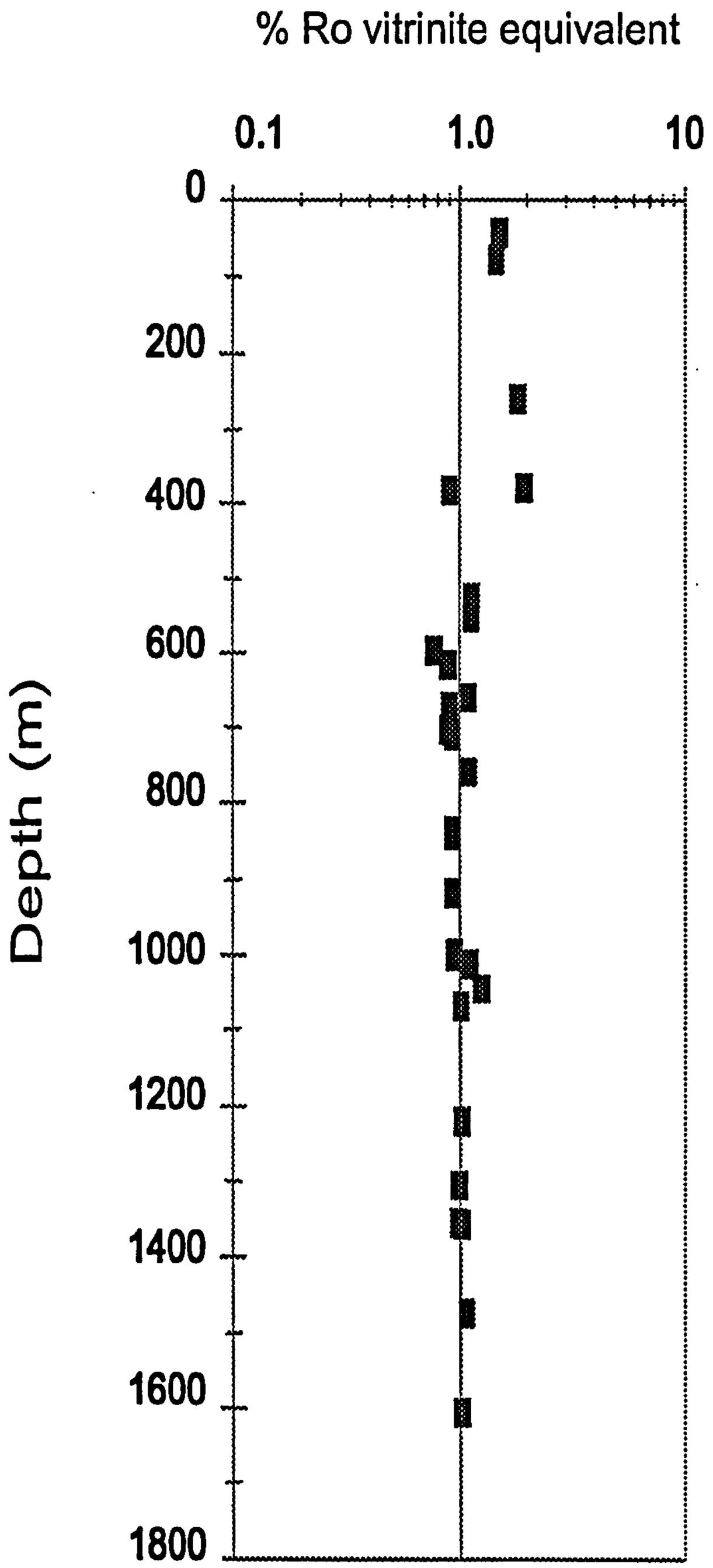

Figure 39. Vitrinite reflectance equivalent derived from type 4 bitumen Ro data versus depth in the Besa River Formation.

evidence relating to the formation of semi-cokes suggest the latter.

Hydrocarbon generation potential

The Besa River Formation in the study area has TOC values that indicate good to excellent source potential, particularly in the black shale members which are very rich in organic matter. It has little or no remaining oil generating potential (Table 16) at any of the locations sampled but the catagenic gas potential is excellent at Beaver River and Pointed Mountain (12). The black shale members are effective sources at North Beaver River (14) and Kotaneelee (15); and at Toad River No. 1 (19), the gas potential has been exhausted (despite high TOC values) due to elevated maturity. The latter may be due to additional thermal event that has led to the formation of relatively inert semicokes and significantly reduced the gas-generating potential.

4.8 YOHIN AND CLAUSEN FORMATIONS.

In the western Mackenzie Mountain region, the Besa River is overlain by the dark basinal shales of middle to upper Tournaisian age (TN2-TN3) which have been designated as the Yohin and Clausen formations by Richards (1989). The Yohin may be considered stratigraphically equivalent to the Upper Banff in the Interior Plains Region. In the Liard Basin, both formations are shale-dominated basinal deposits but eastwards they become interbedded with sandstones and siltstones which have been interpreted as basin-slope deposits (Richards, 1989; his Figure 14). The Yohin Formation was sampled at one locality only (Jackfish Gap-Yohin Ridge) where it has a thickness of 48.8m.

The total organic carbon contents (TOC) of four samples from the Yohin and nine samples from the Clausen Formation are shown in Appendix B8. The TOC values for the Yohin are 1.0% and 1.8% respectively, which indicates good source rock potential. For the Clausen Formation, they range from 0.50 to 2.1%, which suggests that there may be some source rock potential.

At Jackfish Gap-Yohin Ridge (13), the Yohin and Clausen Formations are cherty finely-laminated paper shales (with silty shale laminae), containing abundant organic matter and pyrite. Their petrographic characteristics are included in Appendix A8. The bituminous matrix is dark, weakly fluorescing and slightly micrinitic. Semifusinite and sclerotinite (funginite) are rare to moderately common, as is fluorescing liptodetrinite. The primary maceral assemblage is consistent with the shelf margin-slope to basinal setting

Section no.*	Thickness (m) (A)	% TOC (B)	Organic richness (A x B = C)	Maturity % VRo	Oil maturity factor (E)	Gas maturity factor (F)	Oil source potential (C x E)	Gas source potential (C x F)
12	1659.20	0.90	1493.28	1.47	0.30	1.00	447.98	1493.28
14	93.30	3.13	2911.90	2.00	0.10	0.60	291.19	1747.14
15								
16	982.70	1.40	1375.78	2.25	0.00	0.50	0.50	687.89

(A)

Section no.*	Thickness (m) (A)	% TOC (B)	Organic richness (A x B = C)	Maturity % VRo	Oil maturity factor (E)	Gas maturity factor (F)	Oil source potential (C x E)	Gas source potential (C x F)
12	138.00	2.50	345	1.54	0.20	0.80	69.00	276
14	38.10	5.10	194.31	2.48	0.00	0.50	0.00	97.16
15								
16	320.25	1.89	605.27	2.60	0.00	0.50	0.00	302.64

*numbers refer to sections in Fig. 16: 12 = Pan Am Pointed Mountain P-53; 14 = Canada Southern *et al.*, N. Beaver River I-27; 15 = Pan Am Kotanneelee O-67; 16 = Pan Am Beaver River G-01.

(B)

Table 16 Hydrocarbon generating potential of (A) the Besa River Formation; and (B) the "first and second black shales".

envisioned by Richards (1989). Low R_o bitumens associated with algal bituminites and medium R_o (type 4) bitumens are the dominant macerals, suggesting that the Yohin Fm. kerogen has already passed through the mature stage of thermal alteration (catagenesis). At Viscount (21), the Clausen Formation is much leaner in organic matter (particularly the shale matrix) but the dispersed kerogen and bitumens are similar in type and maturity to those observed at Jackfish Gap-Yohin Ridge (13).

In the subsurface sections in the Interior Plains, the Clausen Formation is much siltier and cherty or dolomitic. Liptodetrinite is commonly dispersed throughout the shale matrix together with thin-walled alginites. Relicts of Tasmanitid relicts and sporinite are present but rare. Orange-brown bituminite stringers are common, as are medium and low R_o bitumens. Pore-filling type 4 bitumens are associated with the thin-walled Leiosphaeridiales alginite which lie parallel to the bedding and show a weak, dull orange fluorescence. The fluorescence characteristics of the low R_o bitumens are similar to those of the alginite. At Arrowhead (8), dolomitized filamentous and coccoid alginite, similar to those observed in the Besa River at Clausen Creek, are present.

The S1 values for the Yohin Formation are negligible (<0.2) and S2 values are low (0.2 to 0.36) as is the production index (Appendix B8), suggesting that the hydrocarbon potential is limited. By contrast, S1 for the Clausen varies from 0.1 to 6.6; and S2 values range from 0.21. This suggests that shales in the Clausen Formation have significant hydrocarbon potential and may be active source rocks, particularly in the southwestern part of the Interior Plains at Bovie Lake (7).

The modified van Krevelen diagram (Fig. 40) indicates that the kerogen is of advanced maturity in the Yohin Formation at Jackfish Gap-Yohin Ridge. As all points plot near the origin, the Rock-Eval data do not indicate kerogen type although petrographic analysis suggests the organic components are compatible with an original typical marine Type II kerogen. A broader scatter is evident in the hydrogen and oxygen indices for the Clausen Formation; however, most of these plot in the Type II kerogen maturation pathway (Tissot *et al.*, 1974) but two samples appear to fit the maturation trend for Type III kerogen. The Rock-Eval results agree with the petrographic composition of the Yohin and Clausen formations at Jackfish Gap-Yohin Ridge, which shows abundant vitrinite (Type III) and inertinite (fusinite and funginite), suggesting that at the northern margin of

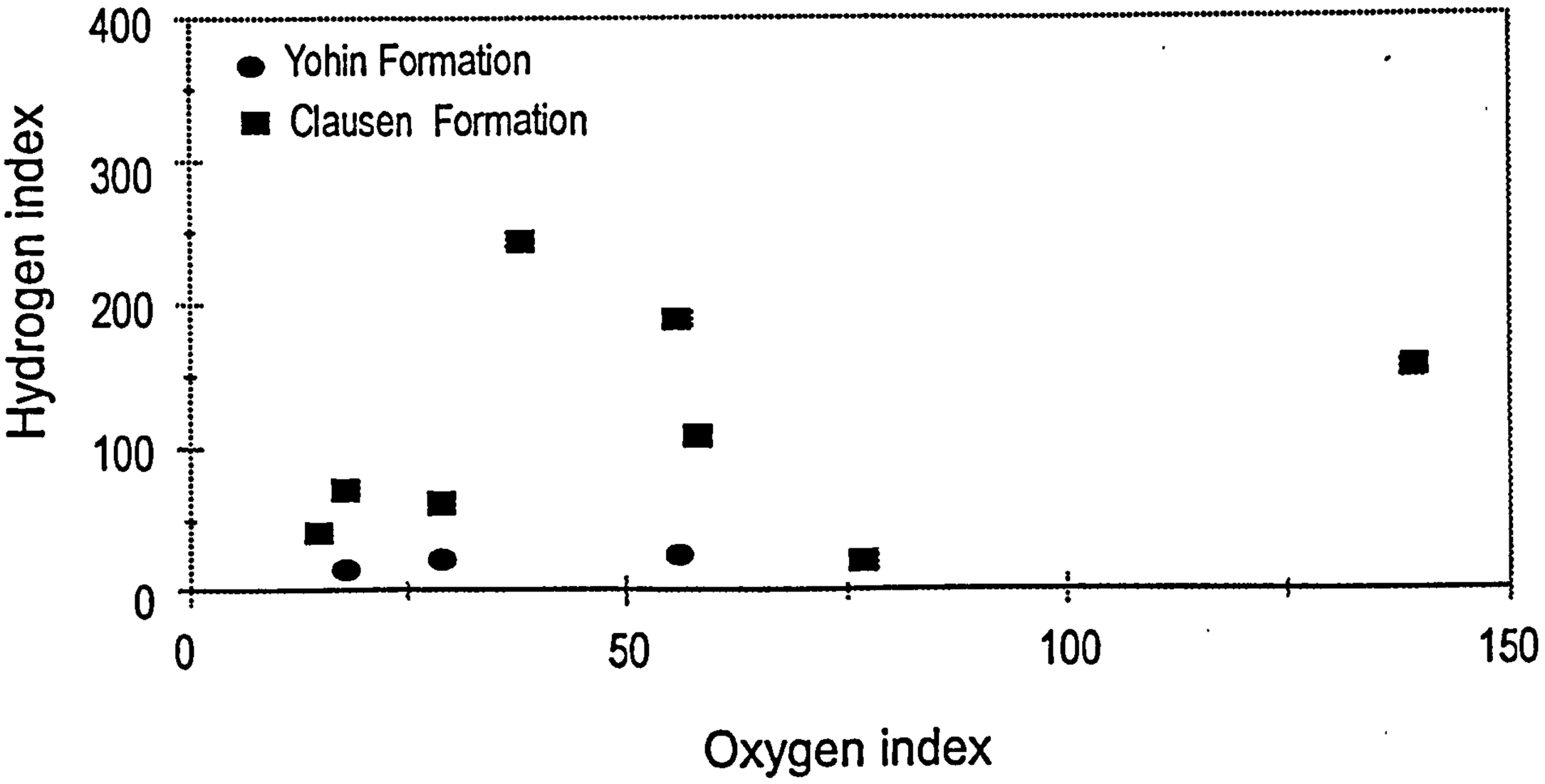

Figure 40. Hydrogen index versus oxygen index for the Yohin and Clausen formations.

the Liard Basin, the kerogen composition was influenced by the Lower Carboniferous shoreline.

Measured bitumen reflectance data and fluorescence indices were obtained on all samples (Appendix C8). Vitrinite reflectance equivalent values, calculated from the type 4 bitumen (medium R_o) indicate that the maturity of the Yohin and Clausen samples is between 0.78 and 1.34% VR_o. The Clausen samples fall within the oil window at all localities. At East Flett (9), they are of lowest maturity and in the early stages of oil generation (0.78% to 0.84%VR_o eq.). The Tmax values at this locality range from 428° to 430°C, which also suggests early catagenesis. At all other subsurface locations, the vitrinite R_o equivalences indicate the shales in the Clausen Formation are in the peak oil generation stage (0.88% to 0.94% VR_o equivalent) and median T max values (Appendix B8) of 440° and 442° C at Bovie Lake (7) and Celibeta (5) would support these observations. The VR_o values from the outcrop sections at Jackfish Gap-Yohin Ridge fall in the upper range of the oil window (1.1-1.7%, VR_o) as also indicated by the Tmax (458 °C). The fluorescence indices (Appendix C8) and maceral-bitumen assemblages compliment the increasing VR_o eq. values.

At Jackfish Gap-Yohin Ridge, samples from the Yohin show slightly higher VR_o

eq. values (1.11%-1.34%; Appendix C8) which indicate that it is at the upper limit of the oil window. The Tmax (474° - 483 °C) also suggests that maturity corresponds to the catagenic gas stage of hydrocarbon generation (Appendix B8). The lack of fluorescence in all primary macerals except for the microscopic alginite (?liptodetrinite) and the dominance of indigenous bitumens supports these observations also. At Jackfish Gap-Yohin Ridge, the medium R_o bitumens in both the Yohin and Clausen formations show pronounced anisotropy in the form of bireflectance (ca. 0.2%), which is typical of bitumens in postmature source rocks (Khavari-Khorasani & Murchison, 1978).

In general, the correlation between vitrinite reflectance eq. data calculated from the type 4 bitumen and the Tmax temperature is reasonably good (Fig. 41). Anomalously high Ro values in the Clausen Formation at Celibeta (5) are attributed to oxidation as values corresponding to a Tmax of 439°C should be only about 0.8% (cf. Mattoil, 1990); this is borne out by petrographic observations which indicate oxidation of the pyrite and oxidation rims with elevated reflectance around the liptinitic macerals. Oxidation, coupled with heating, has been shown to result in elevated vitrinite reflectance (Benedict & Berry, 1964; Nandi *et al.*, 1977; Bustin *et al.*, 1985) as opposed to natural oxidation related to weathering, during which is characterized by particle rims having a reducted reflectance (Alperne & Maume, 1969; Crelling *et al.*, 1979). The reflectance of unoxidized samples

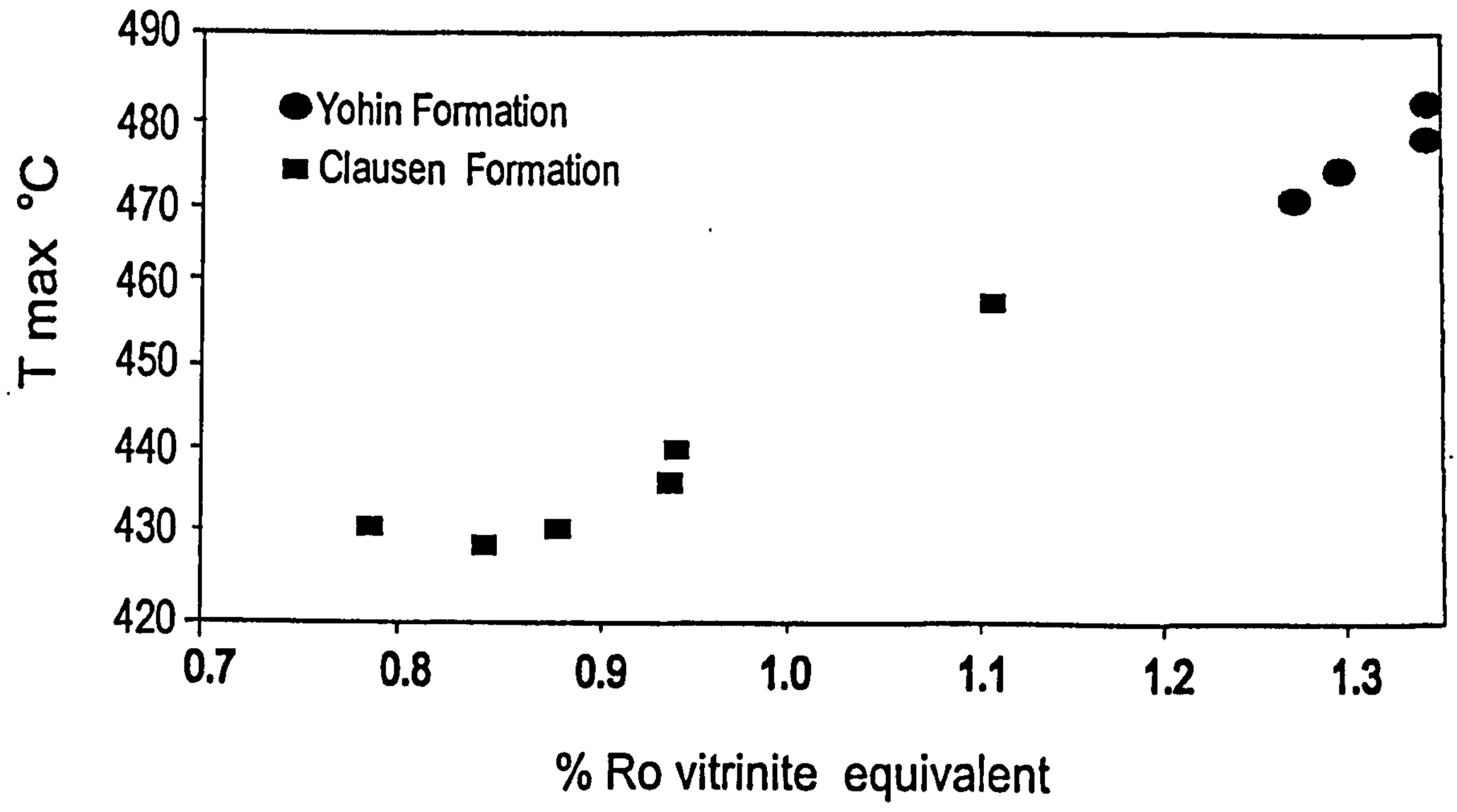

Figure 41. Tmax versus reflectance for the Yohin and Clausen formations.

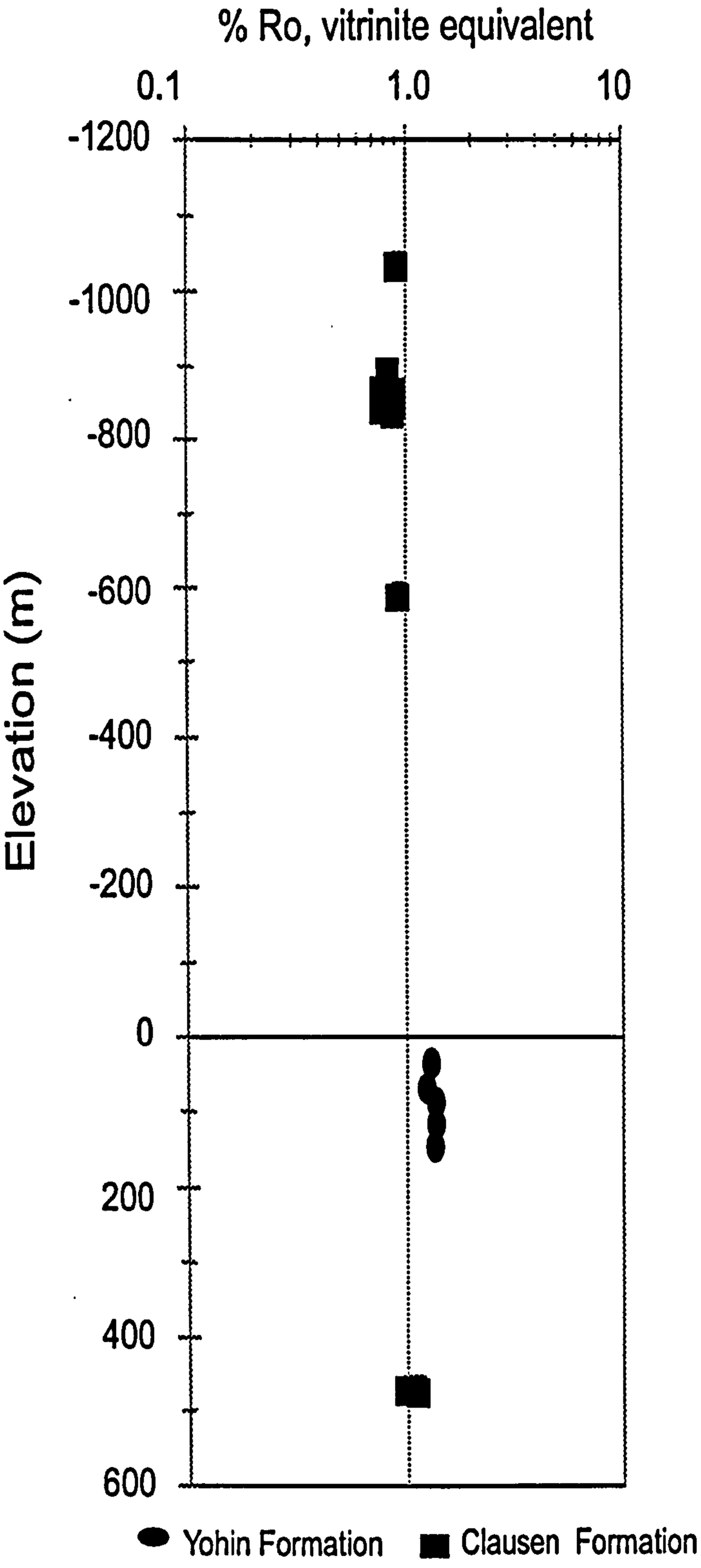

Figure 42. Vitrinite reflectance equivalent derived from type 4 bitumen Ro data versus depth for the Yohin and Clausen formations.

show a positive relationship with depth (Fig. 42) and the regional bitumen and VR_o eq. values decrease progressively northwards from the Bovie Lake-Celibeta areas. However, in the outcrop sections at Jackfish Gap-Yohin Ridge, reflectance data for the Yohin Formation are greater than those of the overlying Clausen Formation and the overall maturity is greater than that observed in the subsurface samples in the Interior Plains. This suggests that the outcrop belt was located in a deeper part of the basin (to the west) during the Lower Carboniferous as well as Upper Devonian times. The higher R_o values reflect pre-Permian or pre-Laramide burial depths (section 5.0); the present day thermal maturation pattern was therefore imposed prior to uplift during the Laramide orogeny (Late Cretaceous-Tertiary). The reasonably good correlation between Tmax and depth would support this view.

The oil generating potential of the Yohin Formation is modest due to its limited thickness but the Bovie Lake area has the best potential (oil maturity factor: 143) and is currently at peak maturity. Gas potential is greatest in the Clausen Formation of the outcrop belt (gas maturity factor: 266;).

3.9 RUNDLE GROUP

The Rundle Group is a carbonate-dominated sequence of upper Tournaisian (TN3) to middle (V2) age comprising the Pekisko, Prophet, "F" and Flett formations (Richards, 1989), which sit conformably above the Banff Formation in the Interior Plains region and ?on the Besa River in the Liard Basin. The stratigraphic relationships are somewhat complex (Fig. 12). Dark grey to black shales and mudstones occur within each of the formations but they are dominated by spiculitic lime packstones and siltstones (Prophet, Formation F) and lime grainstones and packstones (Pekisko, Flett). They have been interpreted as slope-shelf margin and neritic shelf deposits which include platform and ramp facies (Richards, *ibid.*; Figure 7). Together they range in thickness from 160m in the Interior Plains to 750m in the centre of the basin. They are discussed collectively here because of their stratigraphic relationships (Richards, 1989) and the small number of samples from some individual formations (e.g. Flett, Formation F and Pekisko).

The TOC values for shales in the Prophet Formation and Formation F range from 0.2 to 6.2% (Appendix B9). Good to excellent source potential occurs in the richest shales

from the centre of the basin, at North Beaver River (14) where TOC values range from 1.0-6.2% (mean: 4.3%) and at Beaver River (range: 1.0-3.2%; mean: 2.2%). Elsewhere the TOC values of these formations are between 1 and 2%. Total organic carbon contents for shales from the Meilleur Member of the Flett Formation (Appendix B9) are relatively low (>0.5% to 1.3%) but also show modest source potential.

Shales of the Prophet Formation vary from pyritic, laminated, black shales to silty fossiliferous shales containing crinoids, bryozoans and calcareous microfossils to highly dolomitized shales. Petrographic analysis shows that the TOC-rich samples from the Canada Southern well (14) contain significant amounts of lignitic coal which are interpretated as contaminants or drilling mud additives. The true TOC values of the drill cuttings are therefore obscured because the contaminating coal particles alone could account for the TOC values of 2-6%. The non-coaly kerogen is dominated by indigenous bitumens of the low R_o, medium R_o (type 4) and high R_o (pyrobitumen) types which were generated *in situ* from primary liptinitic macerals, indicating that indigenous dispersed organic matter was also present. As a result, the TOC values from the uppermost samples (1 to 1.5%) could be considered as being representative of the least-contaminated samples.

In the Prophet samples from the Interior Plains at East Flett (9), Celibeta (5), Bovie Lake (7) and Arrowhead (8), the kerogen is dominated by thin-walled *Leiosphaeridia* alginite and bituminite stringers. Low R_o type 2 and 3 bitumen, as well as pore-filling type 4 bitumen; these are subordinate to the liptinite macerals, which implies thermally mature kerogen in the hydrocarbon generation stage (section 2.3). Rare marine indicators such as Tasmanales alginite, acritarchs and ?scolecodonts are present. By contrast, indigenous bitumens are dominant over primary macerals in samples from the Liard Basin (i.e. at N. Beaver River, (14), Beaver River (16), Kotaneelee (15), Pointed Mountain (12) and Viscount (24), indicating elevated maturity. Partially pore-filling medium R_o bitumens are commonly associated with these highly dolomitized samples. In the TOC-rich Viscount section (24), clusters of dolomite rhombs are commonly found pervading the matrix in a similar manner to those observed in the Besa River at Clausen Creek, i.e. where putative cyanobacterial remains are preserved. Examination of the dolomite clusters in fluorescent light did not reveal any organic pseudomorphs; however, dolomitized filamentous and coccoid cyanobacterial remains were observed in the Prophet Formation at Pointed Mountain (section 12; Appendix A9). At Clausen Creek and Jackfish Gap-Yohin Ridge

(17, 13), indigenous bitumens of the medium R_o and low R_o types are subordinate to liptinitic kerogen. These samples are therefore similar in composition and maturity to those in the Eastern Plains.

Shales from the Meilleur Member of the Flett Formation at East Flett (9), Pointed Mountain (15) and Jackfish Gap-Yohin Ridge (13) sections are marly and pyritic with crinoid fragments. The organic matter is dominated by bituminite stringers and thin-walled alginites; and small amounts of primarily Low Ro type 3 indigenous bitumen. Organic networks occur in the bituminous matrix in the Prophet at Viscount (24) and in the Flett-Meilleur Member at East Flett (9). The network of internal microfractures is interpreted as forming due to maturation and shrinkage of the organic matrix which provides a 3-dimensional network of conduits for transmission of fluids, including hydrocarbons.

Rock-Eval pyrolysis data are summarized in Appendix B9. The S1 and S2 values are generally low (>0.2) for the Prophet and Flett formations, except at Bovie Lake and Beaver River where S1 and S2 values exceed 0.5 mg/g rock. High S2 and S3 values in the Prophet samples from North Beaver River (14) are attributed to the low rank coal contaminants in the cuttings samples. The S1 values at Bovie Lake range from 1.39 to 3.15 and the S2 from 1.21 to 1.63, suggesting that the Prophet may have good source potential at this location. These samples, together with those at Celibeta (5), have production indices 0.55 to 0.66 indicating late stage oil generation. Production indices of 0.2 to 0.4 at Arrowhead (8) and East Flett (9) suggest that the more easterly locations sections, are in the peak oil generation stage.

The relatively low S1 and S2 values in the Prophet in the Liard Basin (e.g. at Beaver River (16) and Kotanelee (15), suggest elevated maturity and this is supported by high production indices (0.7 to 1.0). The S1 values for the Prophet at Pointed Mountain (14) and Viscount (24) are lower (< 0.6) but the production indices indicate that it may still be in the oil window. The marly shales within the Flett Formation have low S1 and S2 values and low production indices (0.2 and 0.4, respectively) suggesting they are in the peak of oil generation.

The modified van Krevelen diagram (Fig. 43) shows that the Prophet and Flett samples plot at the mature (lower left) of the kerogen maturation pathway (see Fig. 2a), apart from those from Bovie Lake (7) which plot on the Type II maturation path. Along with the other petrographic and stratigraphic data from the Rundle Group, suggests a

marine and liptinitic (Type II) kerogen. Samples from the Flett at Jackfish Gap-Yohin Ridge and the Prophet at Clausen Creek show an anomalous oxygen enrichment and also exhibits a higher content of oxygen-rich inertinite macerals (semifusinite) or signs of oxidation (limonite) respectively.

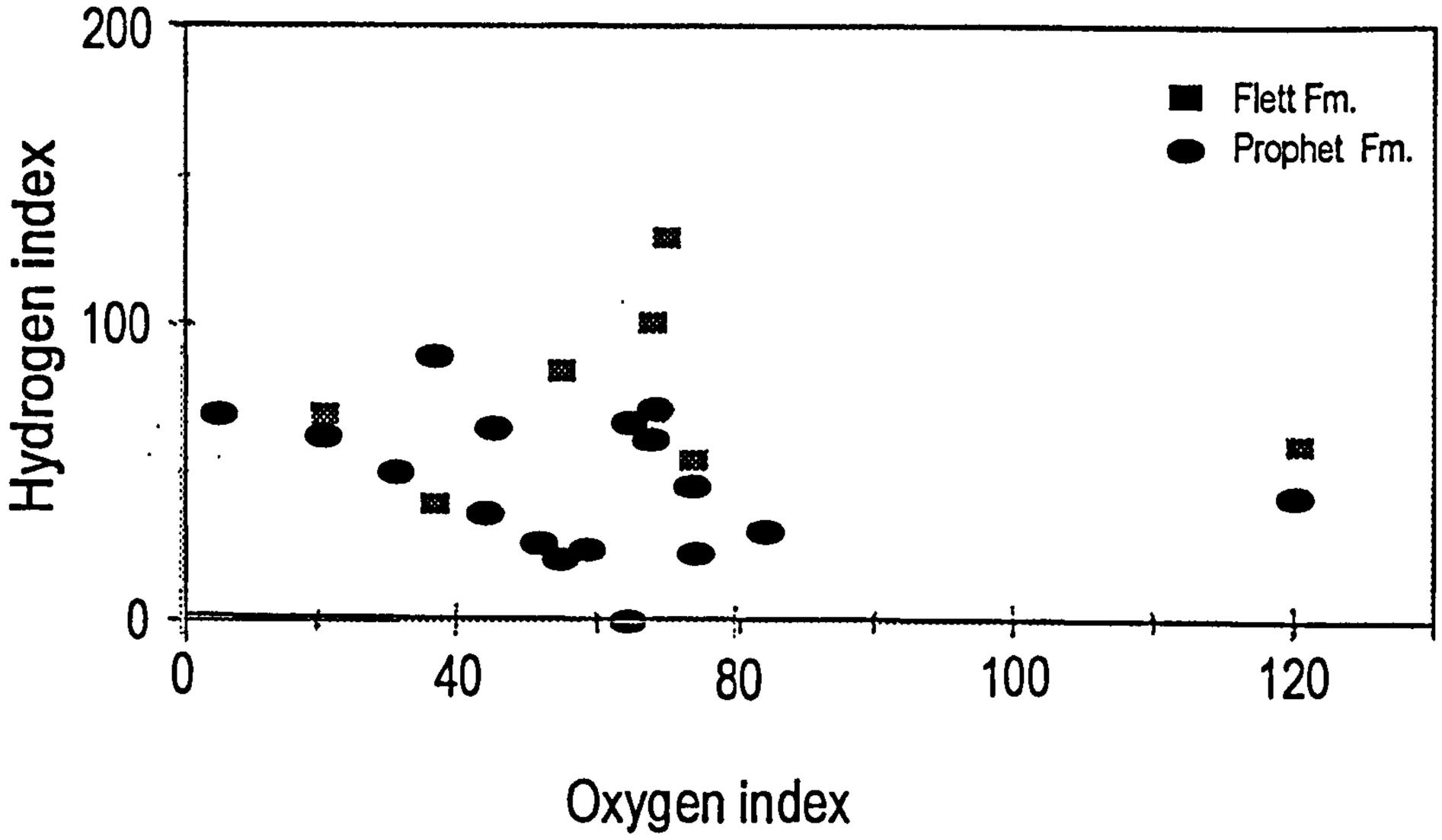

Figure 43. Hydrogen index versus oxygen index for the Rundle Group samples.

Although vitrinite reflectance data was not obtained for the Rundle samples, numerous populations of bitumens are present making it possible to calculate the vitrinite reflectance equivalent (Appendix C9). The range of VR_o eq. values falls between 0.68 and 1.60%, spanning the oil and gas windows. Shales from the Prophet Formation in the Eastern Plains region have VR_o values in the middle of the oil window, ranging from 0.71% at East Flett (9) and increasing southwards to 0.86% at Arrowhead (8) and 0.88% at Celibeta (5). An extrapolated VR_o value (using low Ro type 2 bitumen reflectance and the formula in Table 11) for the Prophet in Bovie Lake (7) is 0.90% VR_o eq., which would indicate peak oil generation for Type II kerogen. In the outcrop sections at Jackfish Gap (13) and Clausen Creek (17), VR_o eq. Values from 1.05% to 1.10%, indicate the Prophet is at the upper end of the oil window and more mature than in the Plains Region. At Pointed Mountain (12) and Viscount (24) belt, the VR_o values are in a similar range (ca. 1%) indicating late oil generation. To the west and south of the Pointed Mountain Anticline, the Prophet

Formation has significantly higher Ro values, in the 1.46% to 1.52% range, at Kotaneelee (15), Beaver River 16) and North Beaver River (14); these indicate that the Prophet is at the peak stage of catagenic gas generation.

The Tmax values for the Rundle Group do not show much variation with depth or reflectance ($R^2 = 0.13$); however, reflectance versus depth plots show that the surface outcrop samples plot in a separate field from the subsurface samples due to differences in present elevation; the correlation for the former is strong ($R^2 = 0.83$) but less so for the latter subsurface samples (0.45). Furthermore, the gradients for the two trends samples are similar, suggesting that both regions experienced similar thermal histories prior to uplift of the outcrop sections. The thermal maturity therefore appears not only to be related to the depth of burial but also to have been imposed before the Laramide orogeny (i.e. pre-Late Cretaceous).

3.10 GOLATA FORMATION

The Golata Formation is of Viséan age (V3) and is dominated by dark grey to olive-black shales and mudstones with minor sandstones and siltstones. It directly underlies the Mattson Formation and overlies either the Prophet or Flett Formations of the Rundle Group (Richards, 1989) in the Liard Basin. It is more than 1254m thick at Beaver River (16) where it occurs at a depth of 1787.4m but it thins significantly to the north, east and especially to the south where it is only 26.2m thick at Viscount (24; depth to top:2563.4m). Richards (*ibid.*) interprets the Golata as prodelta deposits that are transitional between the carbonate platform-ramp deposits of the Rundle Group and the deltaic deposits of the overlying Mattson Formation. It was deposited on slopes marginal to the carbonate buildups, at depths ranging from shallow subtidal to well below wave base and include turbidites at depths sufficient for turbidite deposition (Fig. 14).

Organic richness

Most of the samples from the Golata Formation yield TOC values greater than 1% (Appendix B10). Samples from Beaver River (16) have values ranging from 1.20% to 4.89%; and the 1850-2300m interval is particularly rich (TOC: 2.2% to 4.7%).

Organic Petrography

The shales of the Golata Formation are sometimes fine-grained to silty with interbedded siltstones; they contain siliceous microfossils (?radiolaria) are variably dolomitized. They are distinct from the Upper Devonian and Lower Carboniferous intervals by virtue of their containing primary and secondary macerals of the liptinite group, a variety of bitumens, and also macerals of the vitrinite and inertinite groups (Plates XI-XV) . The petrographic characteristics are shown in Appendix A10.

Matrix bituminite is the dominant maceral and forms the organic matrix; it is intimately associated with pervasive micrinite, whose precence may indicate elevated maturity (cf. Teichmüller, 1982). Indigenous low and medium R_o bitumens are also abundant, particularly in the samples from Kotaneelee (15) and N. Beaver River (12). Low R_o type 3 bitumen is commonly associated with elongate stringers of dark brown to black bituminite. The dimensions and habit of the bitumen are similar to those of thin-walled Leiosphaeridia alginite, suggesting there is a precursor-product relationship. Amorphous, pore-filling type 4 bitumen inclusions are commonly found throughout the matrix.

The primary liptinites are dominated by elongate, thin-walled alginite (*Leiosphaeridia*) and sporinite. At Beaver River (16), meta-alginite with high reflectance (>1% R_o) is present suggesting the liptinite has been subjected to high temperatures. The sporinite includes triangulate microspore taxa such as *Densosporites* (Plate XI), a typical Lower Carboniferous genus (Hacquebard & Barss, 1957; Braman & Hills, 1977; Utting, in Richards, 1989), and also megaspores (Plate XII). Many of them exhibit a dull orange fluorescence. The microspores at Kotaneelee are mature, because they are currently generating low R_o bitumen of the type 2 variety (Plate X).

Vitrinite grains (of the order of 250 µm in length) are moderately common throughout the western region (section 15, 14 & 12). They often show some vestige of cell structure (Plate XVI) and may contain thin bands of inertinite (Plate XVI). They are associated with clusters of pyrite framboids. Cellular inertinite particles, predominantly fusinite, are present also. The frequency of vitrinite, inertinite and pteridophyte spores suggests proximity to (or redeposition from) an active source of terrestrial organic matter, which is compatible with Richards' interpretation that the Golata represents slope deposits associated with the carbonate platforms of the Prophet Formation (Richards, 1989).

Highly reflective, amorphous pyrobitumen in the Beaver River section (16) is

vesicular and has anisotropic mosaic textures indicative of severe thermal alteration of bitumens (temperatures exceeding 400 °C; refer to section 4.7 organic petrology of the Besa River).

Rock-Eval pyrolysis

Rock-Eval pyrolysis data for the Golata Formation are shown in Appendix B10. The S1 values are between 0.80-2.5 and the S2 values are between 0.2 and 1.2, except for the 2279.90-2587.75 m interval at Beaver River (16) which yields S1 values of 4.9, an S2 value of 1.98 and an S3 value of 13.78 mgHC/g rock. The S2:S3 (26.30) is typical of a Type I kerogen (as implied by the maturation pathway on Fig. 44). Other intervals exhibit lower pyrolysis yields but S1 and S2 values from samples in the uppermost Golata at Beaver River (16) have S1 and S2 values > 1; S1 and S2 values in the lower part are >0.5 indicating minor hydrocarbon potential, although production indices of 0.4 and 0.5 suggest the maturation is already advanced. Production indices from Pointed Mountain (12 and Viscount (21) suggest that the samples are mature. All other samples plot at the bottom left of the modified van Krevelen diagram, indicating elevated maturity and providing little indication of kerogen type except for a sample with high oxygen:hydrogen ratio in the basal Golata at North Beaver River (14).

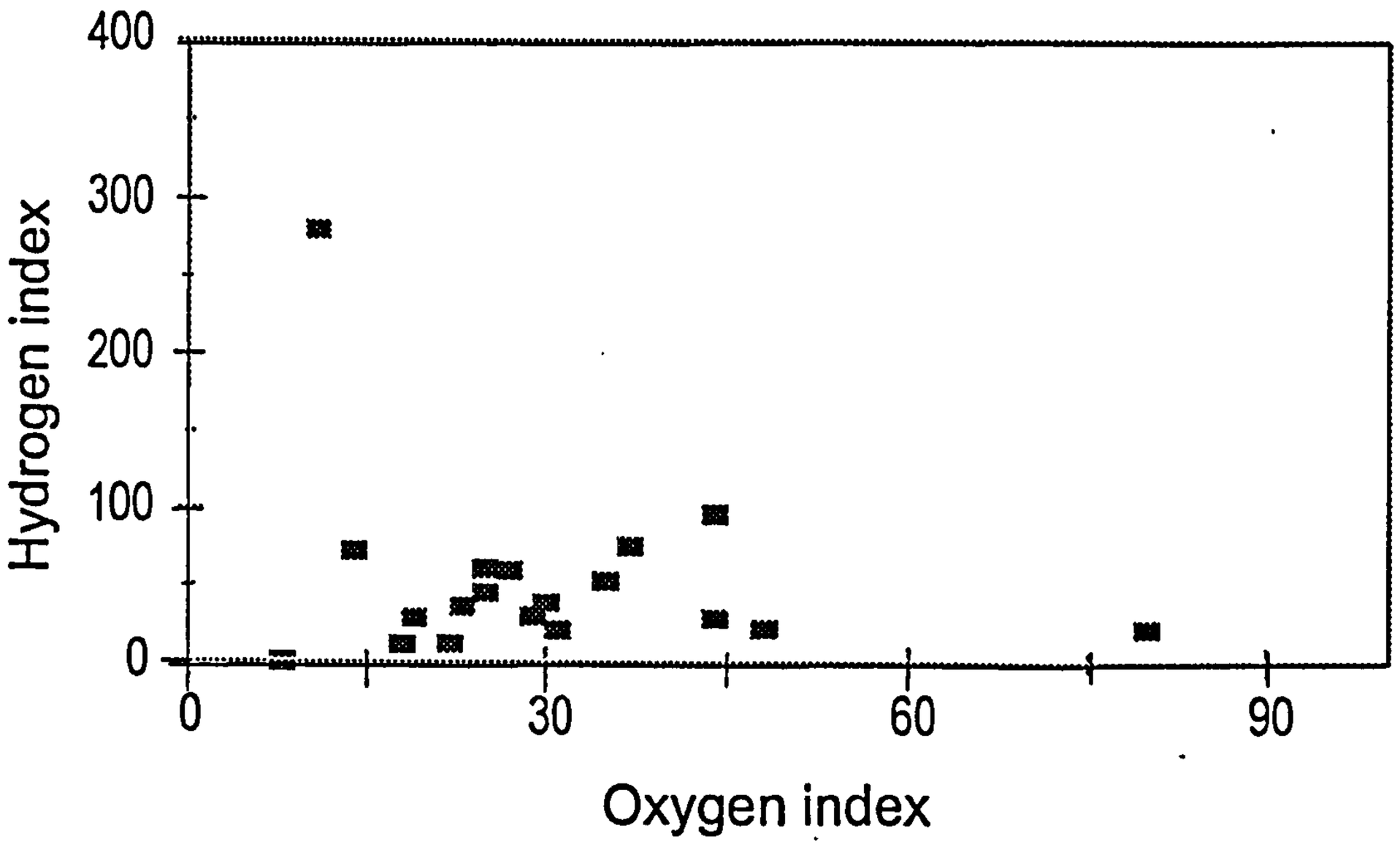

Figure 44. Hydrogen versus oxygen index for the Golata Formation.

Maturity

Bitumen, vitrinite and vitrinite reflectance data for the Golata Formation were obtained for the Golata Formation (Appendix C10). Measured and calculated vitrinite reflectance data are available for only two samples (from sections 12 and 16). These differ by 0.5% R_o. The petrographic characteristics suggest this discrepancy may reflect the presence of reworked vitrinite.

The calculated VR_o eq. values range from 0.93% at Pointed Mountain (12) to 1.46% in the basal Golata at Beaver River (16), indicating the upper end of the oil generation window where oil generation from Type II kerogen declines at the expense of catagenic gas formation (Powell & Snowdon, 1984). However, a VR_o eq. of 0.93 %, supported by fluorescence indices of 6-7 (Appendix C10) for the low R_o bitumen and 5 for sporinite, indicates that the Pointed Mountain samples are still in the peak oil generation phase. At both Beaver River sections, VR_o eq. values of 1.2% to 1.46% R_o, indicate that the Golata Formation has surpassed peak oil generation. The lack of fluorescence supports an elevated maturation state.

The Tmax data are very inconsistent for this suite of samples. Values of 450-460°C tend to be found in shales with TOC values >1.0% and indicate mature samples at or beyond the upper limits of the oil generation window; samples with <1% TOC have Tmax values either below 400°C (well below the oil window) or approaching 500°C. The high Tmax (498°C) recorded at Viscount (21) is obviously anomalous because this sample has a low production index and the VR_o data indicate it is marginally mature with regard to oil generation.

While the relationship between vitrinite reflectance and present day burial depth appears to be reasonably good (Fig. 45), the VRo values at Kotaneelee (1.16% Ro) are higher than at Pointed Mountain (0.93% R_o) despite the Golata Formation at Kotaneelee occuring at a significantly higher elevation. This suggest that maturation of the kerogen in the Golata Formation is related to the pre-thrusting (pre-Laramide) burial history. Furthermore, the Golata is very thick and the Ro values at Kotaneelee are lower in the lowermost samples. This suggests that there may have been some structural thickening of the Golata in the Kotaneelee area.

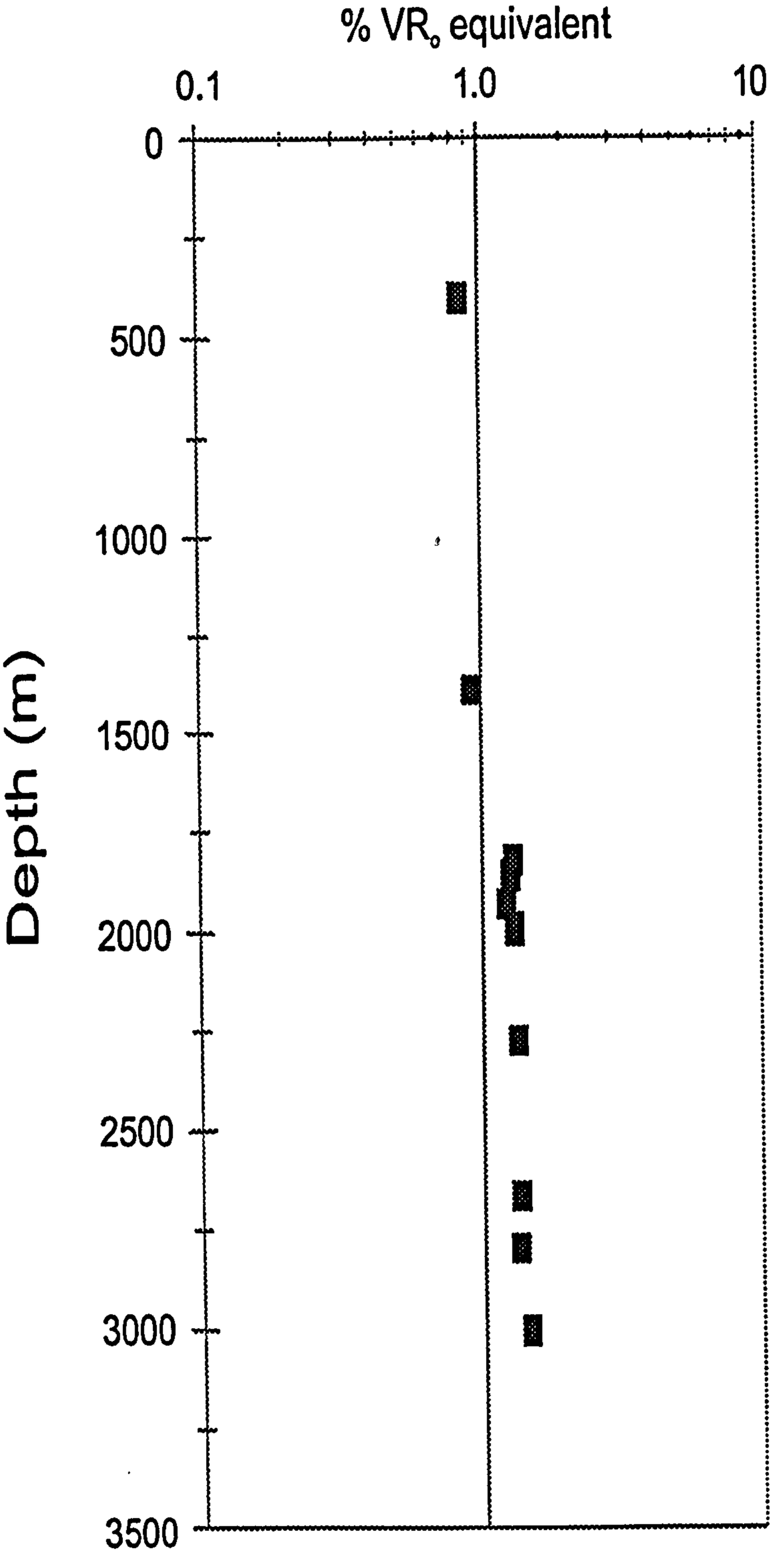

Figure 45. Vitrinite reflectance equivalent derived from type 4 bitumen Ro data versus depth, Golata Formation.

Hydrocarbon potential

Oil and gas source potential ratings for the Golata Formation are best at Beaver River (Table 17; Fig. 46). The combination of thickness, high TOC values (4.6%) and maturity 1.34-1.40% R_o suggest it is an excellent source of catagenic gas.

3.11 MATTSON FORMATION

The Mattson Formation (Patton, 1958), and its stratigraphic equivalents in northeastern British Columbia (the Kiskatinaw and lower Taylor Flat formations), are the youngest of the Lower Carboniferous strata to exist beneath the sub-Permian unconformity in the Liard Basin. It is overlain by the Permain Kindle and Fantasque Formations and conformably overlies the Flett, Golata and Besa River Formations (Richards, pers. comm.). The northern sections are estimated to be of Late Viséan (V3) to Early Namurian age but the base of the Mattson becomes younger to the southwest (Fig. 12). Consisting largely of sandstones, siltstones, shales and minor coals and limestones (Harker, 1961), the Mattson Formation has been interpreted by Richards (1989) as being deposited in a prograding delta system during several delta cycles. The deltas are interpreted as fluvially-dominated, wave- and tide- influenced deltas of lobate form. Thick Platte-type braided stream sediments were common within the delta plain during middle and upper Mattson times. Coal, shales and sandstones occur within coarsening-upwards sequences of braided stream, overbank and delta front deposits. From north to south, the delta plain grades laterally into delta front and slope deposits and eventually intercalates with the prodelta shales of the Golata and Besa River formations (Fig. 12; Potter *et al.*,1993a, back pocket). Richards (1989) concludes that the siliciclastics of the Lower Mattson, Golata and Besa River all have a northern provenance.

The type section of the Mattson Formation is at Jackfish Gap where it is 1008.7m thick. It is thickest in the outcrop belt at Tika Creek (18) where it attains a thickness of 1412 m. It thins to the south, where it occurs in the subsurface at LaBiche (21, 22) and at Viscount (24), it is only 233.2 m thick. In the Interior Plains (east of the Bovie Fault), the Mattson Formation thins rapidly south- and eastwards and is less than 20 to 40m thick east of the Bovie Fault. The erosional edge of the Mattson Formation occurs to the east of Bovie Lake (7) and west of East Flett (9) and Arrowhead (8) (Fig. 12).

Palynological studies of the Mattson Formation have been conducted by numerous

Location (section no.)*	Thickness (m) A	% TOC (B)	Organic richness (A x B = C)	Maturity VRo eq	Oil maturity Factor (E)	Gas maturity factor (F)	Oil source potential (C x E)	Gas source potential (C x F)
12	135.03	1.56	210.65	0.92	1.00	0.40	210.65	84.26
14	274.30	1.75	480.03	1.27	0.30	1.00	144.01	480.03
15	680.00	0.92	625.60	1.18	0.70	0.90	437.92	563.04
16	1254.00	2	2508.00	1.36	0.30	1.00	752.40	2508.00
24	26.20	0.9	23.58	1.18	0.70	0.90	16.51	21.22

Table 17 Regional hydrocarbon potential of the Golata Formation.

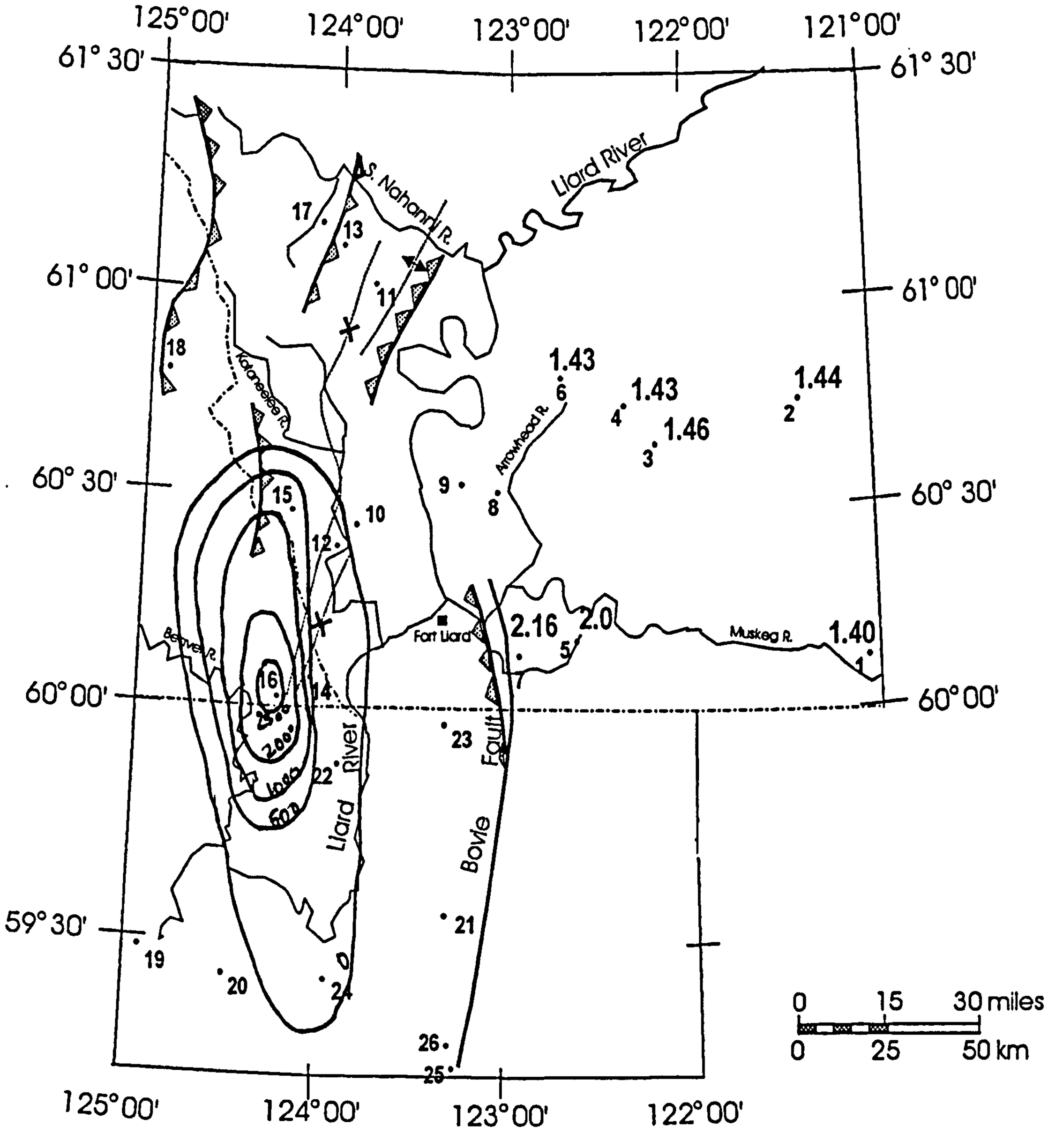

3 location as shown in Figure 16

Figure 46. Regional variation in gas source potential for the Golata Formation (based on Dembicki & Pirkle, 1985); contours are drawn by eye based on data shown in Table 27.

workers (Hacquebard & Barss 1957; Sullivan, 1965; Barss, 1967; Braman, 1976; Braman & Hills, 1977; and Utting, 1989). Braman and Hills (*ibid.*) concluded that the type Mattson (13) is of middle to late Viséan age.

Organic richness

The Mattson Formation TOC data are shown in Appendix B11. In the sections north of latitude 60°, the TOC values vary from 1.0% - 18.4% suggesting that the Mattson Formation has very good to excellent potential for generating hydrocarbons. Some of the highest values occur in the Beaver River area and in the outcrop belt north of 60° 30'. South of 60° (northeastern British Columbia), TOC values range from 0 to 5% although Mattson-Kiskatinaw shales from Dunedin (20) and Windflower (26) contain very little organic matter.

Coals of the Mattson Formation

Coals ranging in thickness from 0.3m to 1.5m occur in the lower, middle and upper Mattson sections at Clausen Creek and Jackfish Gap (Potter *et al.*, 1993). Typically they are black, massive or non-banded and without lustre. Discontinuous coaly clasts of a similar nature characterize the 1719m interval (samples C58764, C58765) at Jackfish Gap. These samples show up as very organic-rich intervals with TOC values between 45% and 75% TOC. Elemental analyses of the coals and coaly clasts are shown in Table 18. The high ash content of sample C58838 indicates that it is a carbargillite (*sensu* Stach, 1982) and the elemental carbon and volatile matter contents correspond to a high volatile bituminous coal rank (Teichmüller & Teichmüller, 1982).

Sample no.	Moisture*	Ash	Fixed carbon*	Volatile matter*	Total sulphur	C %	H %	O %	N %	S %
C58730	3.4	2.4	65.5	34.5	1.25	78.4	2.98	14.88	1.03	1.25
C58838	7.8	43.9	54.9	45.1	0.35	72.5	2.98	23.42	0.72	0.35
C74309	2.54	4.32	67.5	32.5	1.64	79.6	4.53	13.1	1.11	1.64

*** dry, ash-free basis**

Table 18 Proximate and ultimate analysis of coal samples from the Mattson Formation.

Petrographic characteristics of the shales

The shales of the Mattson Formation are unique in the Upper Devonian and Lower Carboniferous succession in the Liard Basin because of the dominance of terrestrial organic matter (Appendix A11-13). Like most organic-rich shales, they are commonly laminated and matrix bituminite, and associated micrinite, is usually an important component of the organic-rich laminae. The structured liptinite includes thick-walled microspores, ranging in size from 25µm to 100µm diameter, whose morphological characteristics are sufficiently well preserved to permit identification under blue light fluorescence (Plate XI). Typical lower Carboniferous genera such as *Reticulatisporites, Densosporites, Murospora, Labiadensites and ?Convolutispora* have been recorded by Hacquebard and Barss (1957), Braman and Hills (1977) and Utting (1983). *Murospora* (Plate XI), which Utting (*ibid.*) considers to be a Namurian genus, was identified in the upper Mattson. Compressed reticulate and muronate spores, similar to those observed in the Carboniferous coals (Baldur Seam) of the Ruhr coalfield (named *Baculexinus* and *Stratexinus* by Stach, 1968) have morphological affinities with *Reticulatisporites* and *?Convolutispora. Murospora* and *Reticulatisporites* are considered to be derived from lycopods and pteridosperms. Habib *et al.* (1966) consider the presence of *Densosporites* to indicate a marginal marine environment similar to the Everglades in southern Florida. Thin-walled microspores are common, as well as thin- and thick-walled, highly ornate megaspores (Plate XII) which range from 800µm to >1000µm in diameter. The thick-walled megaspores are granular in appearance and show dull yellow fluorescence in blue light. Typically, they have extensive baculate processes in the equatorial plane, which are up to 100µm in length and appear resinous under fluorescence. Similar, heavily ornamented megaspores are common in the Upper Devonian coals of the Canadian Arctic Islands (Goodarzi & Gentzis, 1991). The dimensions and ornamentation suggest that they may belong to the genus *Setosisporites* or *Radiatisporites* which have been described from the Upper Viséan and Westphalian strata in the Lublin Coal Basin, Poland (Dybova-Jachowicz *et al.*, 1987). Microspore sporangia have also been observed. Fluorescing, thin walled cutinite (Plates XIII & XIV) is also present in samples from the outcrop belt and Bovie Lake (27).

Other prominent structured liptinites include common telalginite of the *Pila*

variety, analogous to those produced by the extant freshwater colonial chlorophyte alga *Botryococcus* (Plate XIII). *Pila*-type *Botryococcus* is the principal component of boghead coals such as the Scottish torbanites and the Permian coals of Autun, France (Teichmüller, 1975). Minor amounts of probable marine Leiosphaerid prasinophyte alginite are also present (Plate XIII). The occurrence of alginites of both marine and freshwater origin suggest that the shales of the Mattson were formed in a marginal marine setting in which there was a mixing of fresh and marine waters. The *Pila* alginite is most common in the northern part of the Liard Basin (Jackfish Gap, Pointed Mountain), in the Eastern Plains (Arrowhead and Bovie Lake) and the most easterly sections in northeast British Columbia (Maxhamish, Tatoo and Windflower). This suggests that the freshwater influx was from the northeast and it penetrated as far south and west as Pointed Mountain (Fig. 12) in the Northwest Territories and just beyond the trace of the Bovie Fault in British Columbia. The presence of acritarchs including "hystrichosphaerids", with leiosphaerid alginite in the Beaver River area (sections 14 and16) confirms a more basinward organic facies (Chow *et al.*, 1995).

Lenses and stringers of dark brown to black bituminite is very common, particularly in the western sections of the outcrop belt (e.g. at Tika Creek) and Liard Basin (e.g. Beaver River, Dunedin, Viscount and LaBiche) (Appendix C12). The habit, size and distribution relative to the bedding planes suggests that the bituminite formed *in situ* by oxidative reworking of alginite derived from prasinophyte algae, and therefore the liptinites in the Mattson Formation in the southwestern parts of the Liard Basin were probably dominantly marine. Exsudatinite- an amorphous, highly fluorescing liptinite maceral considered to be generated during the expulsion of hydrocarbons from liptinites (Teichmüller, 1982) is also present. Liptodetrinite - unidentified fluorescing liptinite particles <5µm in diameter - are finely dispersed throughout most samples; they are considered to be the remains of planktonic organisms.

Dispersed vitrinite is present in many of the Mattson Formation (Plate XV), particularly in the more northern sections, where *Pila* is found (Tika Creek, Jackfish Gap. Clausen Creek, Pointed Mountain, Tatoo, Arrowhead and Bovie Lake*)*. Typically, the vitrinites are relatively large fragments (100-200µm) with definite particle margins (unlike the indigenous bitumens whose margins are often poorly-defined and appear "corroded"). The vitrinite commonly consists of granular collotelinite showing some cell structure or

collodetrinite with inclusions of inertinite macerals (Plate XV), i.e. they occur as a bimacerite microlithotype.

Inertinite macerals, mostly formed by oxidation (i.e. reworking, combustion or pyrolysis) of terrestrial higher plant materials, are also common in the Mattson shales. Typically, they are fusinites and semifusinites showing clear cell structures (Plate XV). In addition, funginites (formerly sclerotinite *sensu* ICCP, 1972) derived from fungal spores, is present in the outcrop sections (Tika Creek, Clausen Creek and Jackfish Gap-Yohin Ridge) confirming the input from terrestrial sources. At Tika Creek, cenospheres are also present. These are vesicular bodies derived by rapid and intense heating of primary organic matter and bitumens; they are common components of the residues forming during coal/bitumen hydrogenation (Mitchell *et al.*, 1977), combustion (Vleeskens *et al.*, 1987) or pyrolysis (Potter *et al.*, 1985).

Indigenous bitumens, predominantly the medium R_o type 4 and Low R_o type 2 and 3 (i.e those directly associated with bituminites and liptinites) are present in most samples; however, there is a regional pattern to the occurrence, type and amount of bitumen present. In the northern outcrop belt and sections in the Eastern Plains of the Northwest Territories and northeastern British Columbia (near the Bovie Fault), the bitumens, are dominantly of the low Ro types 2 and 3 and type 4 and they are subordinate to the primary macerals (liptinites, matrix bituminite and bituminite). In the west (i.e. Beaver River, North Beaver River, Dunedin, Viscount and LaBiche areas), the bitumens are similar in type but they are among the dominant components. As the bitumens are by-products of maturation, this suggests that the organic components in the samples from the southwestern portion of the study area are more mature that those to the north and east. The indigenous bitumens of the Mattson Formation in the Tatoo section (25) are extensively permineralized by pyrite and other unidentified metallic minerals.

Petrographic characteristics of the coals

The coal beds of the Mattson Formation are no more than 1.5m thick and occur exclusively in the outcrop belt at Clausen Creek, Jackfish Gap and Tika Creek. They are found in the middle and upper Mattson together with coaly clasts in shale and dark brown to black, finely-laminated shales. As indicated above, the proximate and elemental analysis of the coals indicate that they are in the high volatile bituminous rank range. The

composition of the coals is somewhat different from the Carboniferous coals from Great Britain, Europe (Potter *et al.*, 1993a) and the Appalachian region of the United States but there are some similarities with Lower Carboniferous coals from Nova Scotia and New Brunswick and strong similarities with coals from the northern Yukon (Cameron *et al.*, 1994). Details of the unique petrographic composition of the Mattson coals are presented and discussed in Potter *et al.* (1993a; back pocket). Only aspects relevant to the interpretation of the depositional setting, burial and thermal history of the Mattson Formation are reiterated below.

Unlike most Carboniferous coals found in the northern hemisphere, which are bright, banded humic coals dominated by the lithotypes vitrain and clarain, the coals in the Mattson Formation are not vitrinite-rich (Table 19). The microscopic composition is dominated by inertinite (57%-67%) with subordinate liptinite (17-27%); and only (<15 %) vitrinite. Mineral matter is a minor component (2% or less).

Maceral Group	Vitrinite				Liptinite					Inertinite								M
%Maceral Sample #	Ct	Cd	Ge	Vt	Sp	Cu	Ld	Al	Lp	Fu	Sf	Ma	Sm	Mi	Id	Sc	In	
Jackfish Gap-																		
C58730	3	12	<1	15	23	2	2	-	27	1	17	3	15	17	1	2	57	<1
C58737	3	10	-	13	18	2	+	+	20	2	28	8	7	94	1	1	67	<1
C58738	18	24	5	47	5	-	-	29	34	5	1		2	-	1	-	9	18*
C58764	4	18	1	23	12	3	2	+	17	1	27	5	6	26	2	1	67	2
Clausen Ck																		
C74309	7	7	1	15	12	3	2	+	17	1	27	5	6	26	2	1	67	2

Ct = collotelinite; Cd = collodetrinite; Ge = gelinite; Sp = sporinite; Cu = cutinite; Ld = liptodetrinite; Al = alginite; Fu = fusinite; Sf = semifusinite; Ma = macrinite; Sm = semimacrinite' Mi = micrinite; Id = inertodetrinite; Sc = sclerotinite; M = mineral matter; Vt = total vitrinite; Lp = total liptinite; In = total inertinite.
* includes 7% mineral matter and 11% matrix bituminite in shale

Table 19 Maceral composition of coals from the Mattson Formation.

Unlike the bright banded humic coals, in which the inertinite is usually dominated by fusinite and semifusinite, the dominant inertinite macerals in the Mattson coals are

unstructured micrinite and semimacrinite (20-36 vol.%; Potter *et al.*, 1990). The micrinite is typically concentrated into lenses and bands >100µm thick and forms the bulk of the coal matrix in which most of the other inertinite macerals are embedded (Plate XVI). When present, the semifusinite, which characteristically shows well-preserved cell structure, rarely shows open cell lumina. The cell walls have a highly gelified appearance making it transitional to semimacrinite and macrinite and suggesting prolonged gelification in a sub-aquatic environment. The other inertinitic components have been grouped with the macrinite and semimacrinite macerals and these occur in lenses and clusters and in durite and inertite bands (Plate XVI). A variety of macrinite and semimacrinites bodies occurs. Some are solid and these are referred to as herein as "clastic inertinites" because they appear like clusters of inertinitic bodies concentrated by sedimentary processes. They resemble the phlobaphinitic bodies commonly observed in brown coals and lignites and may be derived from tannins formed by condensation of the humic substances from aquatic plants (Teichmüller, 1982). Taylor *et al.* (1989) described similar inertinites in durite from Permian coals in Australia. Some have internal vacuoles and pores and resemble sclerotinites and resino-inertinites reported from Gondwana coals (Misra *et al.*, 1990). Others resemble sections of the resin rodlets derived from the seed fern *Medullosa* (Lyons *et al.*, 1982). Teichmüller (1982) notes high concentrations of macrinites in brown coals accumulated sub-aquatically.

The liptinite is dominated by sporinite (12-23 vol.%) and, while this is typical of many Carboniferous coals, humic coals rarely have such an abundance of sporinite; coals high in sporinite are typically sapropelic (non-banded) coals, commonly referred to as "cannels" (Teichmüller, 1982). Vitrinite is represented by 7-18 vol.% of collodetrinite which forms a matrix for inertinite and liptinite maceral. Telovitrinite is rare but comprises two varieties of collotelinite: one with a reflectance some 0.4% lower than the collotelinite in humic bands and exhibiting weak fluorescence (typical of perhydrous vitrinites; Goodarzi *et al.*, 1987; Robert, 1988), the other with higher reflectance and lacking fluorescence. Both types are associated with micrinite bands (Plate XVI).

The laminated, dull black shale/coal (?carbargillite) near the top of the Mattson succession consists of coaly laminae dominated by vitrinite (collotelinite with collodetrinite and gelinite) and associated with liptinites (dominantly sporinite) and inertinite (fusinite and semifusinite). Shaley laminae having high concentrations of alginite (29 vol.%: dominantly

lamalginite) and matrix bituminite (latter 11 vol.%).

The Mattson coals bear many of the characteristics of sapropelic coals which support a subaquatic origin::

a) lack of seatearth or underclay (i.e. an associated palaeosol)

b) the dull, non-banded appearance typical of coals/peats derived from woody plants

c) the microscopic composition, viz. à viz. the clusters of clastic inertinite formed by sedimentation from water; a high proportion of liptinite macerals (sporinite and alginite) which suggest concentration by surface water currents; and intermixing of micrinite, bituminite and perhydrous vitrinite suggests deposition from a subaquatic organic-rich mud or gyttae.

Sedimentological and petrological studies by Richards (1989) indicate that most of the Mattson Formation accumulated in a deltaic depositional setting therefore, it is suggested that the coals were deposited in ponds and lakes on the delta plain. The coal beds in the upper Mattson at Jackfish Gap sit atop a series of shallow neritic and shoreline carbonates and sandstones; they are interbedded with algal laminites having mixed freshwater and marine affinities. This suggests the sapropelic coals may have been of lagoonal origin; cannel coals of a similar nature, such as the Santo Thomas cannel coal in Texas, are reported to have formed in a lagoonal setting in wave-dominated deltas associated with fluvial systems (Evans, 1975).

Organic facies

The regional distribution of individual macerals, submacerals and maceral varieties of the liptinite group and the distribution of inertinite and vitrinite can be used to establish two distinctive organic facies within the Mattson Formation (Fig. 47): Facies A - marginal marine; and Facies B: marine-neritic shelf. The liptinites of Facies A is dominated by sporinite, with variable amounts of *Pila* alginite, and vitrinite and inertinite are relatively abundant.There are two subfacies: subfacies A1 includes thin sapropelic coals (cannels) and algal laminites and reflects the combination of organic elements found in a deltaic setting; subfacies A2 does not contain coal but there is a significant contribution of probably marine Leiosphaeridiales alginite and this represents neritic environments with mixed terrestrial and marine organic matter. Facies B is dominated by bituminite of algal origin, marine alginite (Leiosphaeridiales and *Tasmanites*) and sporinites which have dull ochrous yellow fluorescence suggesting they have been extensively transported and reworked. The organic facies distribution represented in

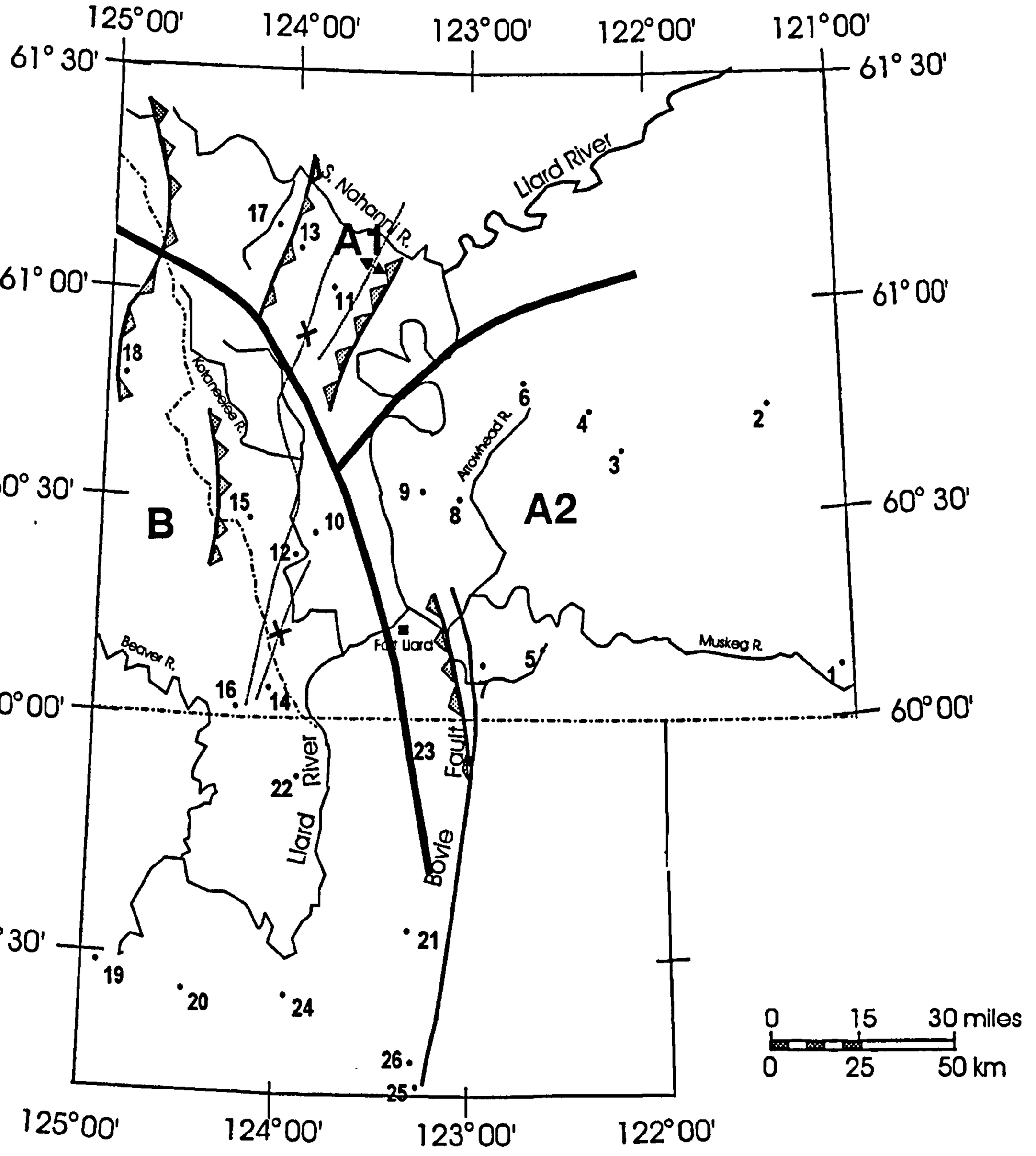

3 location as shown in Fig. 16

Organic Facies:
- A - marginal marine
  - A1 - deltaic
  - A2 - neritic
- B - shallow marine shelf

Figure 47. Organic facies map of the Mattson Formation. Organic facies A & B are arbitrary letter codes used only in this work.

Fig. 47 suggests that shales in the southwest are shallow marine while to the north, the terrestrial influence is dominant and marginal marine, deltaic facies prevail in the northern Liard Basin at Clausen Creek-Jackfish Gap and give way eastwards and southeastwards to a less deltaic, coastal facies. This is consistent with Richards' (1989) interpretation of a lobate delta system prograding southwards (into the Lower Carboniferous ?Selwyn Basin) from a northerly source. The middle and upper Mattson are characterized by delta top sediments including fluvial (braided stream) and distributary channels, overbank deposits and lake sediments. Richards (pers. comm.) interprets the sandstones at the top of the upper Mattson at Jackfish Gap to be aeolian in origin and therefore the delta top yields to prograding terrestrial sediments - possibly coastal dunes. Similarly, the petrographic composition of the upper Mattson suggests that the terrestrial influence appears to increase into the uppermost Mattson even in the more westerly basinward sections in the mountain belt (e.g. at Tika Creek and Beaver River) which supports Richards' view of a southward-prograding delta established during Mattson times.

Rock-Eval pyrolysis

The results of Rock-Eval analysis are shown in Appendix B11. The S1, S2 and S3 are >0.5 for virtually all samples from the Mattson Formation and its stratigraphic equivalents. In the sections north of latitude 60° N, high TOC, S1 (>2) and S2 (>4) occur in the Bovie Lake, Beaver River and Pointed Mountain areas and in the outcrop belt (Appendix B11b) suggesting good to excellent hydrocarbon generating potential. In northeastern British Columbia (Appendix B11c), high TOC values complimented by moderately high S1 values are found only in the Taylor Flat interval at Viscount (24) and in the middle and Upper Mattson/Kiskatinaw at Tatoo (25). Exceptionally low S1, S2 and TOC values were recorded at Dunedin and at Windflower (Appendix B11c). These results suggest that the Mattson Formation has significant hydrocarbon potential in selected intervals throughout the Liard Basin except in the extreme west and along the Bovie Fault in the Windflower area.

The modified van Krevelen diagram (Fig. 48) shows that all the Mattson samples cluster around the origin of the diagram, suggesting elevated maturity. However, those with hydrogen indices >100 and oxygen ca. 50 probably reflect a higher liptinite (paticularly sporinite) content. Samples with low hydrogen indices and oxygen indices greater than >50, reflect the presence of oxygen-rich macerals such as vitrinite and inertinite.

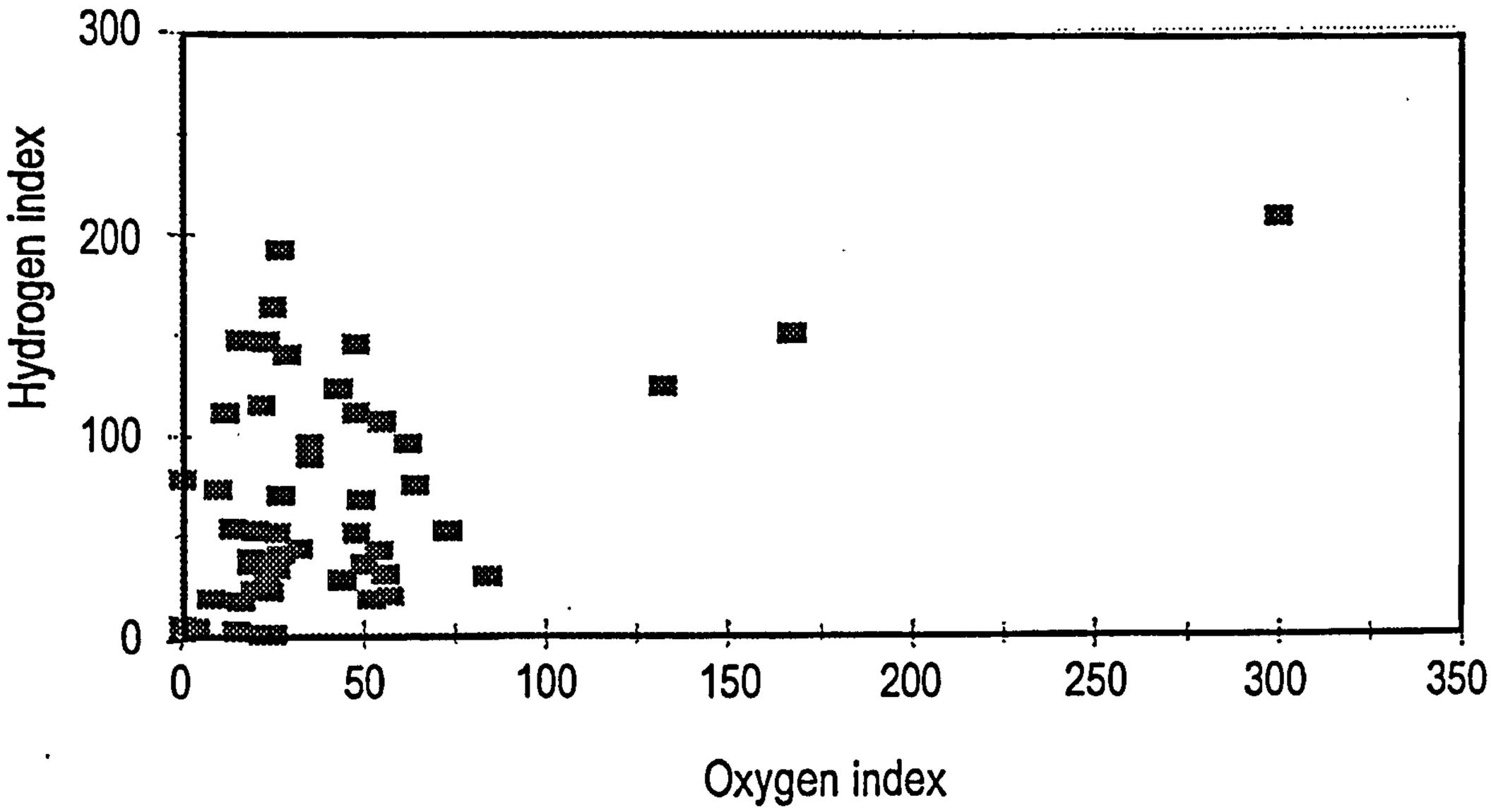

Figure 48. Hydrogen index versus oxygen index for the Mattson Formation.

Maturity

The optical thermal maturity data are given in Appendix C11 and the Tmax data in Appendix A11. There are significant variations in maturity in the Mattson Formation that tend to reflect regional differences. In the Interior Plains, the calculated and measured vitrinite reflectance data fall between 0.77% and 1.24% VR_o indicating that the shales of the Mattson Formation are currently mature and at the peak of the oil generation. Shales showing the highest maturity occur in the southeastern Yukon at Beaver River (16) and North Beaver River (14); these yield reflectance data in the 0.97% to 1.24% R_o range, representing late stage catagenesis. Production indices ca. 0.4 (Appendix C11a) appear to confirm that most of the liquid hydrocarbons have already been generated. Using measured and extrapolated vitrinite reflectance data, the areas of lowest maturity are in the Eastern Plains at Bovie Lake (8, 27), the most easterly occurrences of the Mattson Formation sampled; the VR_o values here are in the order of 0.6% and 0.8% R_o, respectively. It has been inferred (section 4.6) that the effects of heating on organic matter associated with the Bovie Fault were significantly reduced by Lower Banff times and this appears to be confirmed by the low maturity observed in the Mattson Formation. Furthermore, the increasing thickness of the Mattson Formation, from ca. 30m at Arrowhead (8) to 1400 m at Tika Creek, suggests the observed westerly increase in R_o

can probably be attributed to active subsidence and increasingly deeper burial during Mattson times.

Figure 49 illustrates the reasonably good correlation between the equivalent vitrinite reflectance data and the present elevation. The outcrop samples (between 0 and 1000m elevation) show vitrinite reflectance between 0.7 and 0.99%, which is in the same range as the subsurface samples from the Interior Plains and Pointed Mountain (points between 0 and -5200 ft.) suggesting that the current maturation patterns and maximum burial depths in the Mattson Formation were established by Upper Cretaceous time.

The higher Ro values are found in the sections in which the Mattson occurs at greatest depth (Fig. 49), which follows Hilts' Law (Hilt, 1873); the rather smooth curve suggests that thermal maturity was associated with deep burial rather than additional heat sources. There are three exceptions to this pattern: the Mattson at Tika Creek (0 to 200m), Dunedin (-3170 to -3658m), and Windflower (-503m). Two of these are the most westerly sample location in the study area (Tika Creek and Dunedin); here the reflectance data are orders of magnitude greater than in the rest of the Mattson Formation. Furthermore, the bitumens from which the vitrinite R_o data were derived show significant degrees of optical anisotropy. This anisotropy is manifested in significantly increased bireflectance[2] so that the standard deviations from the mean measured R_o values (Appendix C11) are abnormally high (ca. 0.2% for bitumen with mean R_o values of 2.5%, versus 0.02% for bitumen with R_o values in the 0.2-0.8% range). This is typical of organic matter subjected to extreme heat and/or pressure and this occurrence at sections located at the western edge of the basin reflects similar maturation patterns observed in the Upper Devonian-Lower Carboniferous Besa River Formation. Bitumens in the samples from the Windflower section (27) have abnormally high reflectivity which, when converted to vitrinite reflectance equivalents, would indicate a VR_o of 11.4% (graphite has an R_o of 12%). Koch (1997) indicates that 6% is the upper limit for application of vitrinite reflectance as a maturation index. This range of values also exceeds that in the dataset used by Jacob (1984). Consequently, the 11 % R_o indicates only that some major alteration of the organic matter has occurred in the Mattson Formation at Windflower. It is significant that this section is located along the Bovie Fault zone. The Windflower samples are also highly mineralized (pyrite and ?other sulphides).

---

[2] Bireflectance = Rmax - Rmin

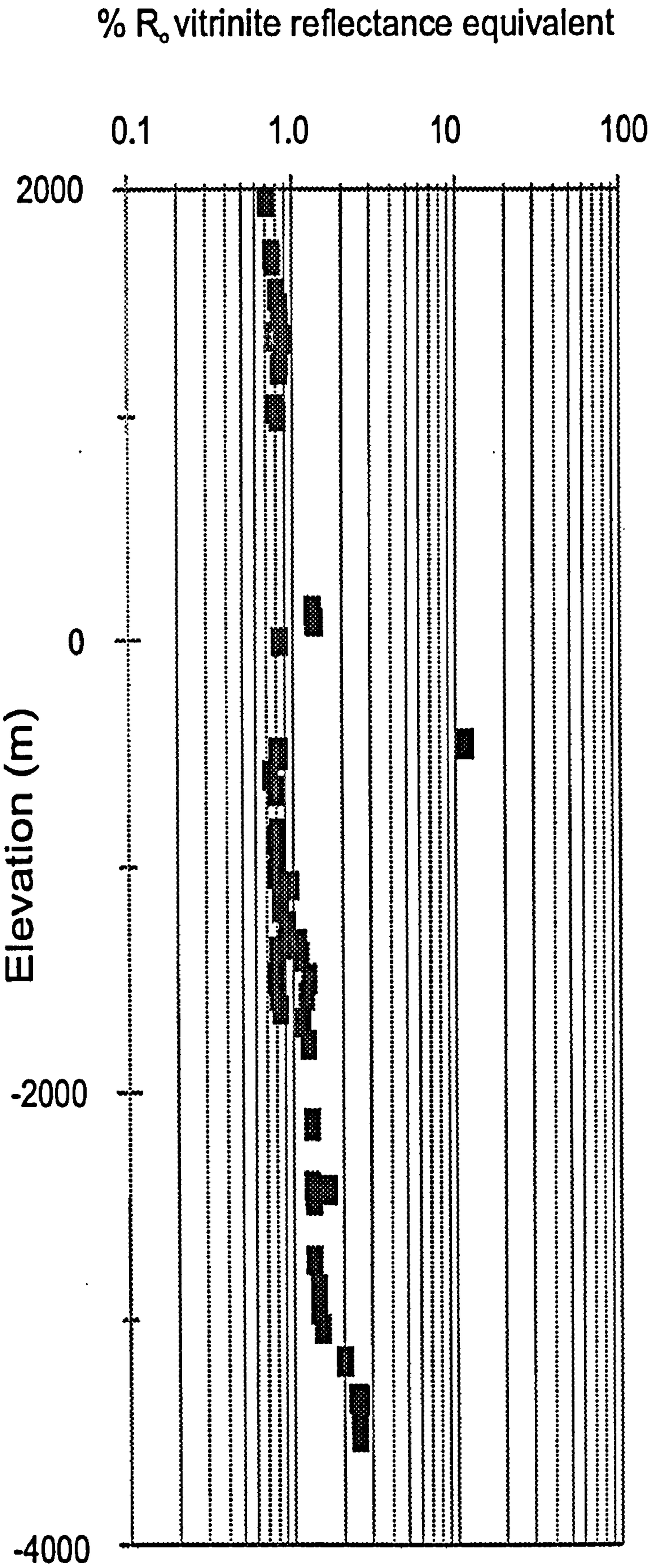

Figure 49. Vitrinite reflectance equivalent derived from type 4 bitumen Ro data versus elevation in the Mattson Formation.

The Tmax distribution reflects both the variations in TOC and the regional maturation patterns. The Tmax values from samples in the outcrop belt at Jackfish Gap and Clausen Creek are clustered within the oil window (430-452°C) which correlates with the petrographic data, except for the high values observed at low elevations at Tika Creek (Fig. 50). In the subsurface samples, between 500m and 3050m depth, there is a positive correlation with depth (except for samples with negligible TOC values). Similarly, the deep samples from Dunedin (> 3000m depth) have exceptionally low TOC and Tmax values below 400, and so also do the samples from the Windflower section; the reflectance data suggests that both are due to elevated maturation levels (e.g. VR_o values of 2.0-2.5%). The correlation between Tmax and VR_o equivalent data is reasonable within the 0.6-1.0% reflectance range (Fig. 51); above the 1.3% VR_o, the Tmax data is usually well under 400, which probably reflects low TOC values at advanced maturation level - which can be typical of spent source rocks or high grade, organic-lean shales.

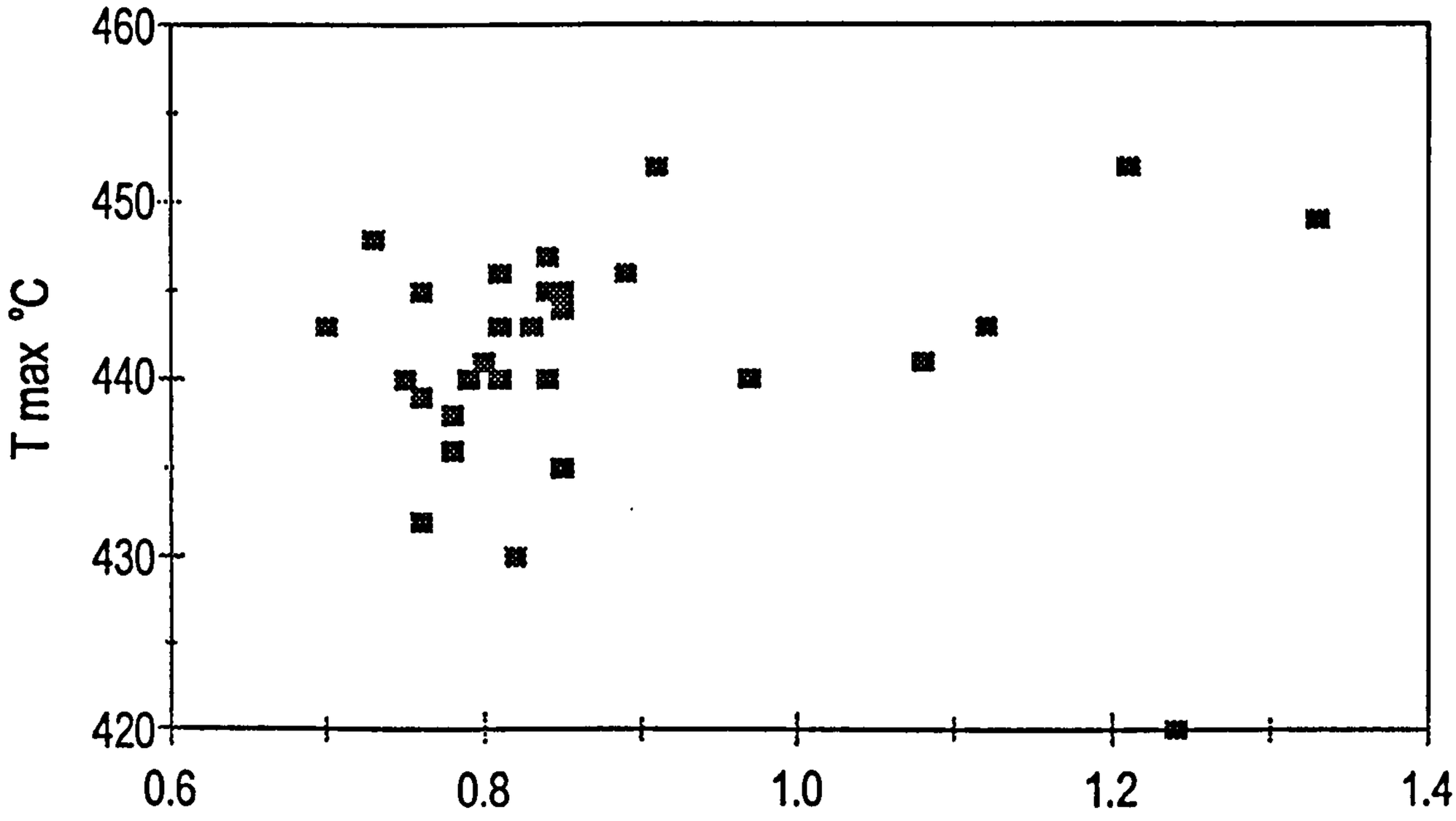

Figure 51. Correlation between Tmax and reflectance.

Qualitative fluorescence indices were obtained for samples with maturition levels that fall within the range of the oil window (Table 7; Appendix C11). The sporinite has a broader

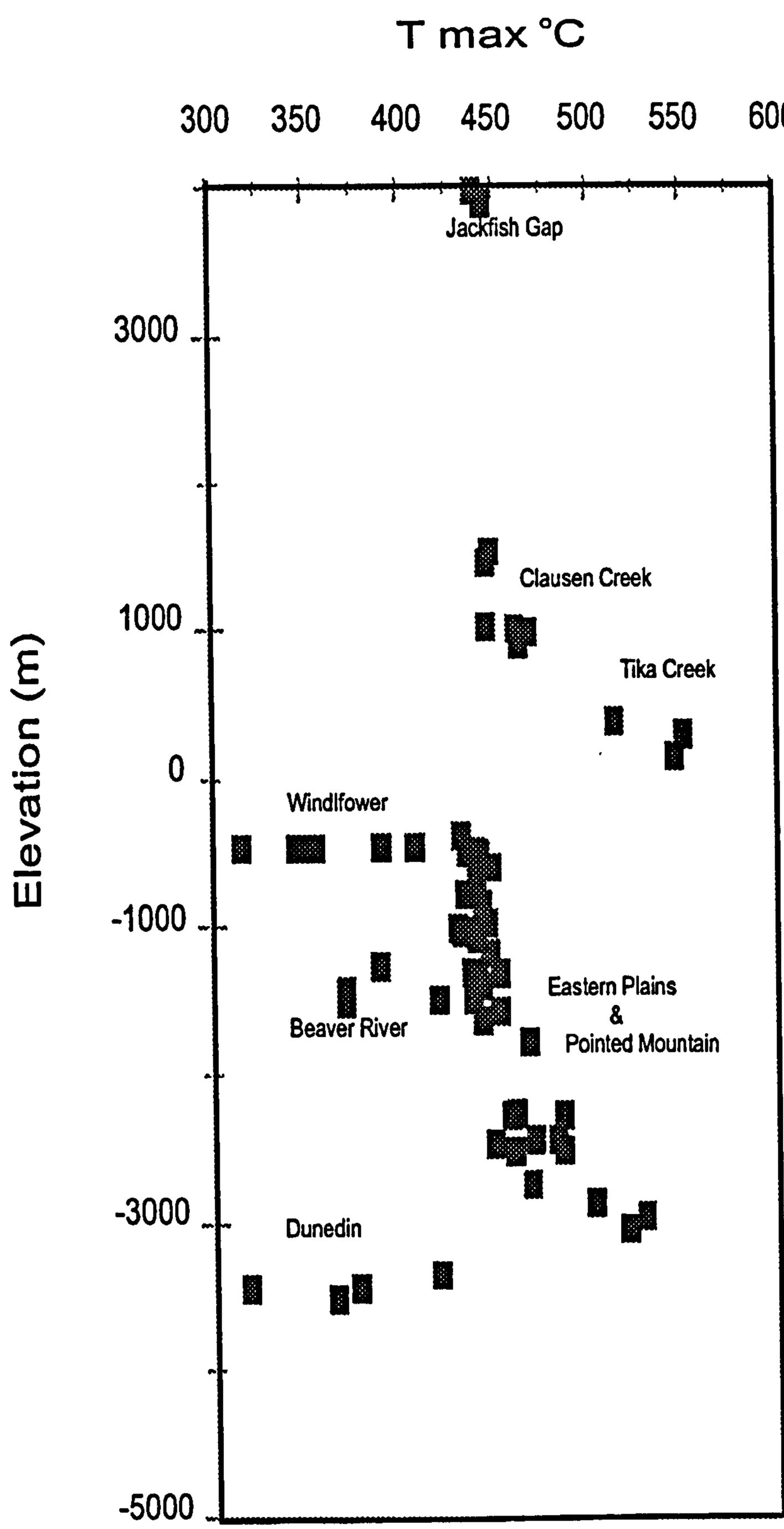

Figure 50. Tmax versus elevation in the Mattson Formation; anomalously low values are related to elevated maturity and lack of primary organic matter.

colour range than the alginite and the colours are one or two increments higher. Oxidized sporinite exhibits a distinctive dull, ochre-yellow (Appendix A11). Furthermore, the elevated fluorescence indices for sporinite correspond to elevated VR_o equivalent values, proving the utility of the sporinite and alginite fluorescence. Lambda max (λ max) and red/green quotients (Q) were also measured on the sporinite. Measured Q values for sporinites are between 1.2 and 1.7 (0.65-0.85 % VR_o eq. range) and their λ max falls between 590 and 700nm; alginites (*Tasmanites* and *Leiosphaeridia*) yield Q values of between 1.2 and 1.5 and a λ max between 510 and 700 for the same range of VR_o values (Appendix C11).The spectral values for the Mattson are within the expected range for liptinitic components in the oil window (Teichmüller & Ottenjahn, 1977).

Hydrocarbon potential of the Mattson Formation

The present-day hydrocarbon potential of shales in the Mattson Formation is extremely good too excellent. Rock-Eval and petrographic analysis of shales and coaly intervals in the outcrop belt indicate there are numerous intervals which are extremely rich in sporinite-dominated Type II kerogen; algal laminites are also present, commonly in association with sapropelic coals in the middle and upper Mattson. Detailed petrographic and sedimentological studies of the Mattson Formation by Richards (1989) demonstrate sandstone-siltstone lithofacies of shallow shelf, deltaic and aeolian origin (B.C. Richards, pers. comm.) and therefore the Mattson Formation may have numerous intervals with promising reservoir properties as well as potential source rock potential.

Table 20 indicates the regional variations in hydrocarbon source potential. As the lithology of the Mattson is dominated by sandstones and siltstones, the thickness of potential source rock represents one tenth of the total thickness of the Mattson at each location. The most organic-rich shales and sapropelic coals occur in the outcrop belt at Clausen Creek and Jackfish Gap and they are currently at peak oil generation; clearly they have the greatest hydrocarbon potential. On average, subsurface samples of Mattson shales tend to be less TOC-rich although many locations have TOC-rich intervals with values ranging from 3-19% and maturation parameters indicate they are currently in the oil window. While they would be considered active source rocks with good to excellent hydrocarbon potential, the total thickness of shale is not great. According to Table 20, the Pointed Mountain area has the best overall source potential. Some of the thickest shales occur in the westerly sections, at Tika

Section no.*	Thickness (m) A	% TOC B	Organic richness (A x B = C)	Maturity % VRo	Oil maturity Factor (E)	Gas maturity Factor (F)	Oil source potential (C x E)	Gas source potential (C x F)
7	2.3	1.62	3.73	0.90	1.0	0.4	3.73	1.49
8	2.1	3.84	8.06	0.90	1.0	0.4	8.06	3.23
10	96	1.84	197.6	0.80	1.0	0.4	176.6	70.7
12	134	1.98	265.3	0.82	1.0	0.4	265.3	106.1
13	30.45	8.74	266.6	0.82	1.0	0.4	266.6	106.6
14	67	4.61	308.9	1.12	0.7	0.7	216.2	216.2
16	95	1.49	141.6	0.90	1.0	0.4	141.6	56.6
17	274	25.28	6926.7	0.78	0.7	0.2	4848.7	1385.3
18	44	1.67	73.5	1.34	0.3	1.0	22.0	73.5
20	53	0.87	45.9	2.45	0.0	0.5	0.0	22.9
22	78	1.13	88.1	1.41	0.3	1.0	26.4	88.1
24	23	0.95	21.9	1.31	0.3	1.0	6.6	21.9
25	1.8	2.4	4.3	0.82	1.0	0.4	4.3	1.7
26	305	0.09	12.2	11.49	0.0	0.0	0.0	0.0
27	26	5.2	135.2	0.82	1.0	0.4	135.2	54.1

*7 = Texaco N.F.A. Bovie Lake J-72; 8 = B.A. Texaco Arrowhead N-2; 10 = Amoco Pointed Mountain P-24; 12 = Pan Am Pointed Mountain P-53; 13 = Jackfish Gap-Yohin Ridge; 14 = Canada Southern *et al.*, N. Beaver River I-27; 16 = Pan Am Beaver River G-01; 17 = Clausen Creek; 18 = Tika Creek; 20 = IOE Dunedin 94-N-8; 22 = Imperial Pan Am LaBiche b-55-E; 24 = IOE Pan Am Viscounta-77-D; 25 = Aquitain *et al.*, Tatoo a-2-D; 26 = Amin-Aquitqaine Windflower d-87-A; 27 =

Table 20 Hydrocarbon source potential ratings for the Mattson Formation (using the method of Dembicki & Pirkle, 1985).

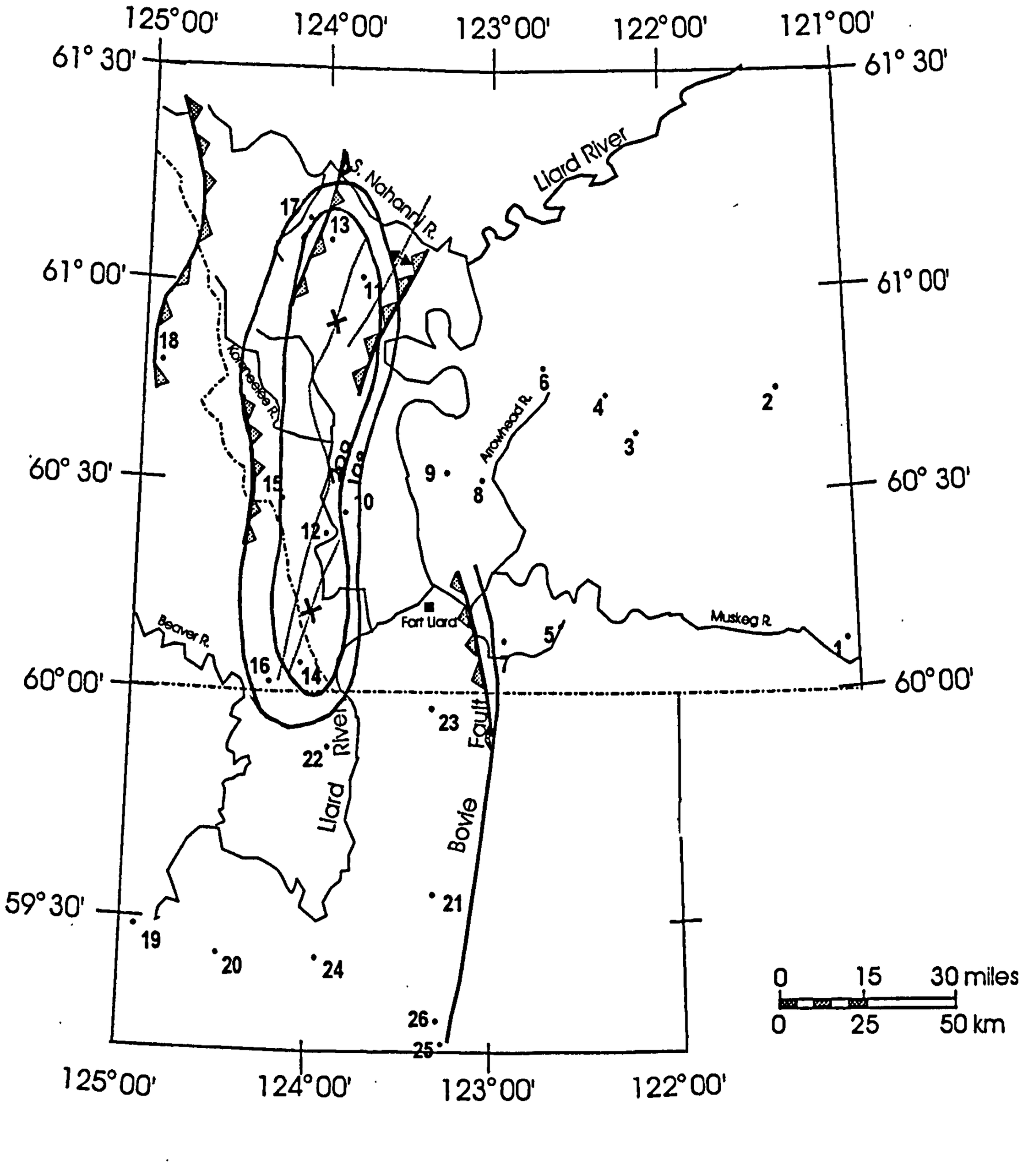

3 location as shown in Figure 16

Figure 52. Regional variation in hydrocarbon source potential for the Mattson Formation (based on Dembicki & Pirkle, 1985); contours are drawn by eye based on data shown in Table 20.

Creek (18) and Dunedin (20) and, on average, they have slightly lower TOC values which can be attributed to the elevated maturity levels. Reflectance values indicate that the kerogen is currently in the gas generation of thermal degradation or well beyond (e.g. at Dunedin); however, petrographic and geochemical characteristics of the Mattson Formation in the western part of the study area suggest that prior to uplift in the Upper Cretaceous, significant amounts of hydrocarbons were probably generated from these source rocks.

PLATE X
INDIGENOUS BITUMENS OF THE GOLATA AND MATTSON FORMATIONS

a) Light grey, granular type 2 (0.43 $\%R_o$) bitumen (b2) derived from megaspore(s) at an early stage of thermal alteration; the megaspore is currently in the process of generating weakly reflecting type 1 bitumen (b1); note the slightly higher reflectance and "granular", dense nature of the type 1 bitumen relative to the homogeneous sporinite with red internal reflections.

b) Dark grey sporinite (centre) with coatings, pore and fracture linings of type 1 bitumen (0.26$\%R_o$).

c) Sporinite or type 1 bitumen (dark grey) with an external film and infill of type 2 bitumen (light grey).

d), e) Granular type 2 bitumen (0.30$\%R_o$) derived from dark red-brown sporinite.

f) Type 2 bitumen (b1) with 0.36$\%R_o$ reflectance, coating red-brown alginite (a) which has a high concentration of euhedral pyrite crystals (p) embedded in it.

g) Type 3 bitumen (0.76% R_o) associated with dark brown-black bituminite.

h) Homogenous type 4 bitumen (0.79$\%R_o$) filling the interstitial porosity in a cluster of weakly reflecting faecal pellets (0.26$\%R_o$) in marly shale.

Magnification: scale bar shown on a) applies also to b), d), e), g) and h); scale bar shown on c) applies also to f).

163a

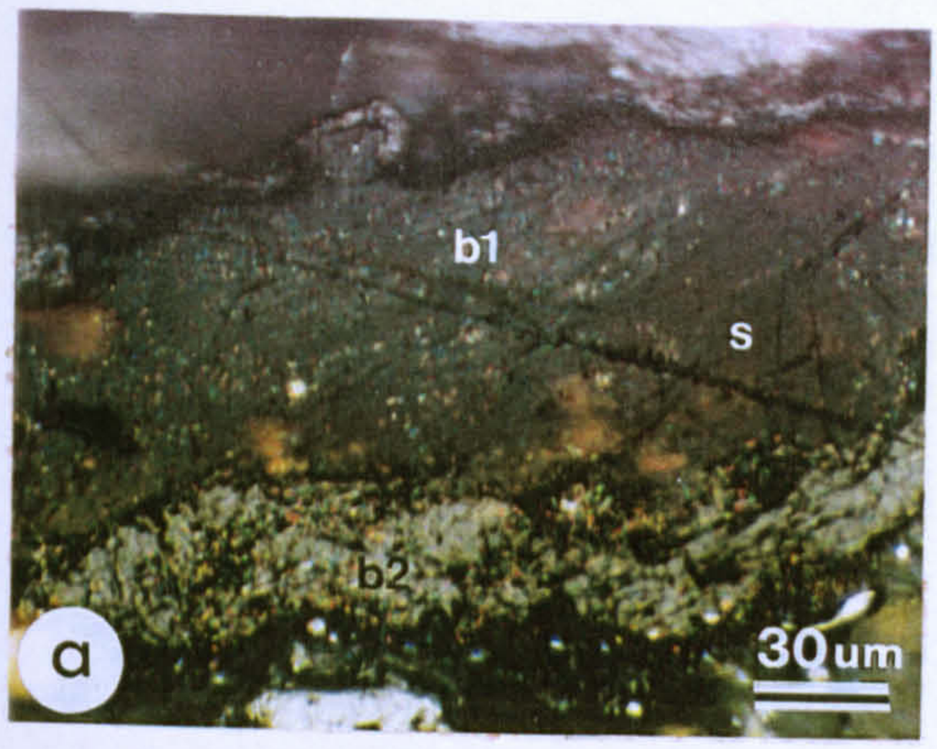

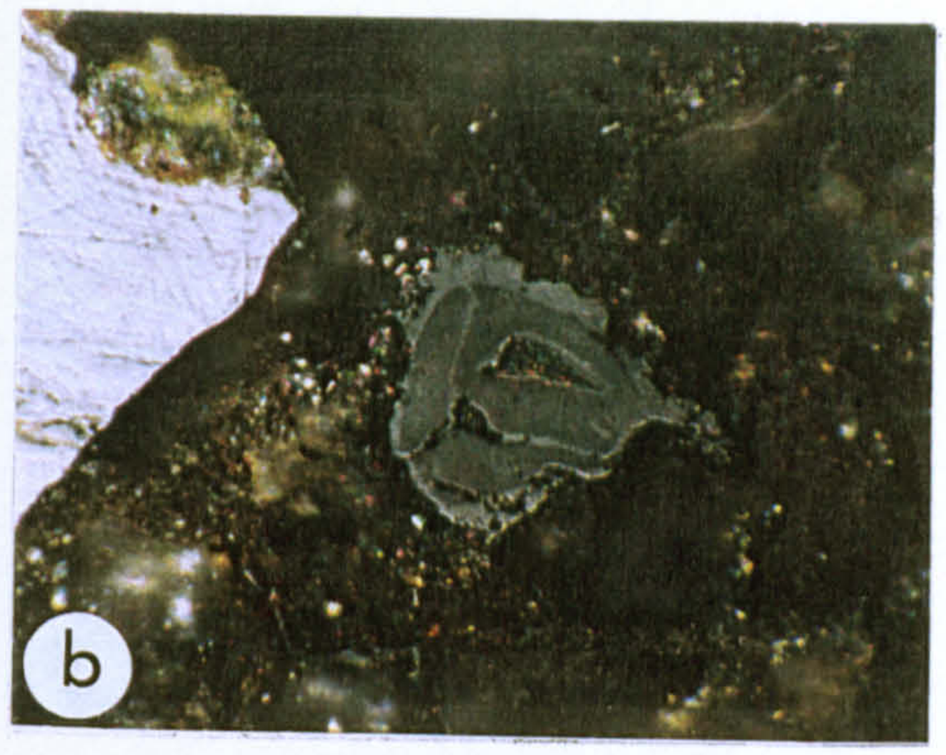

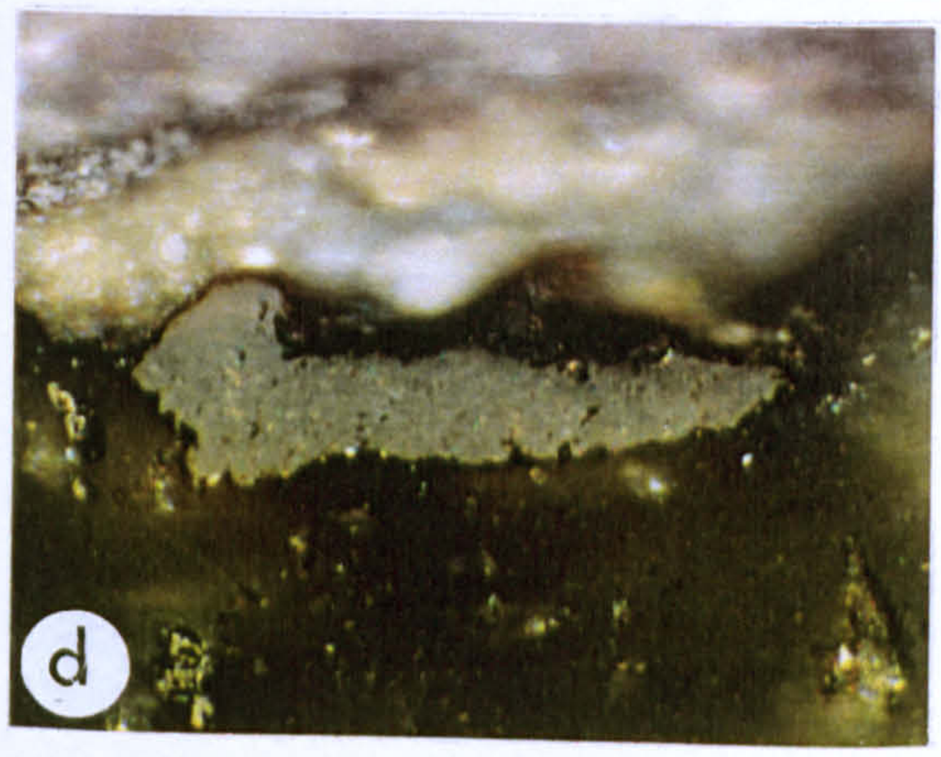

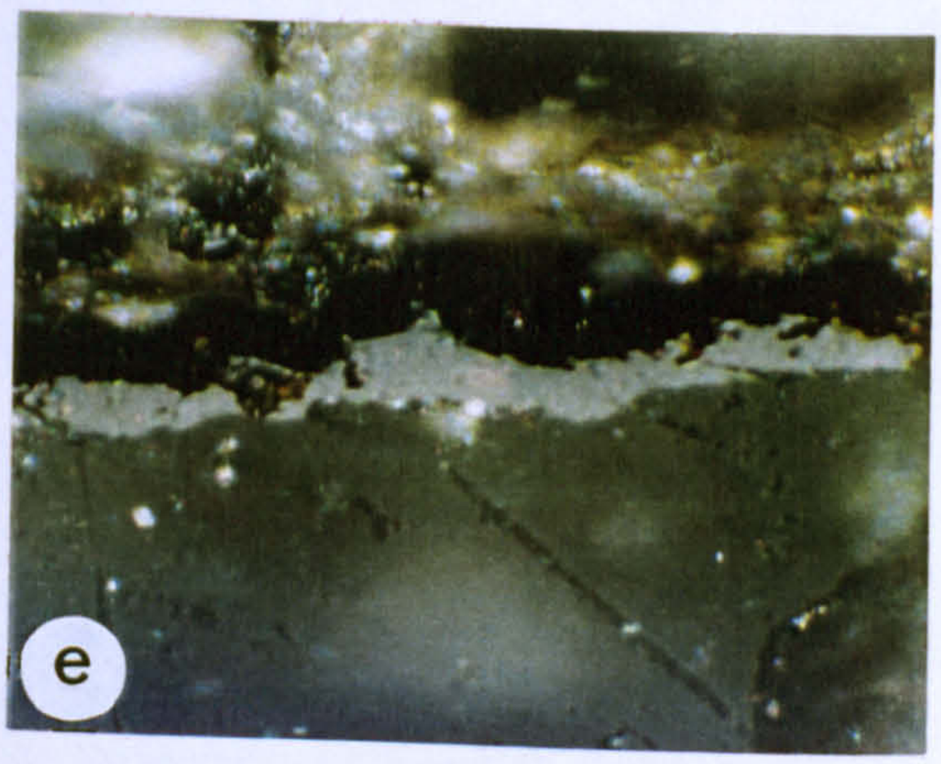

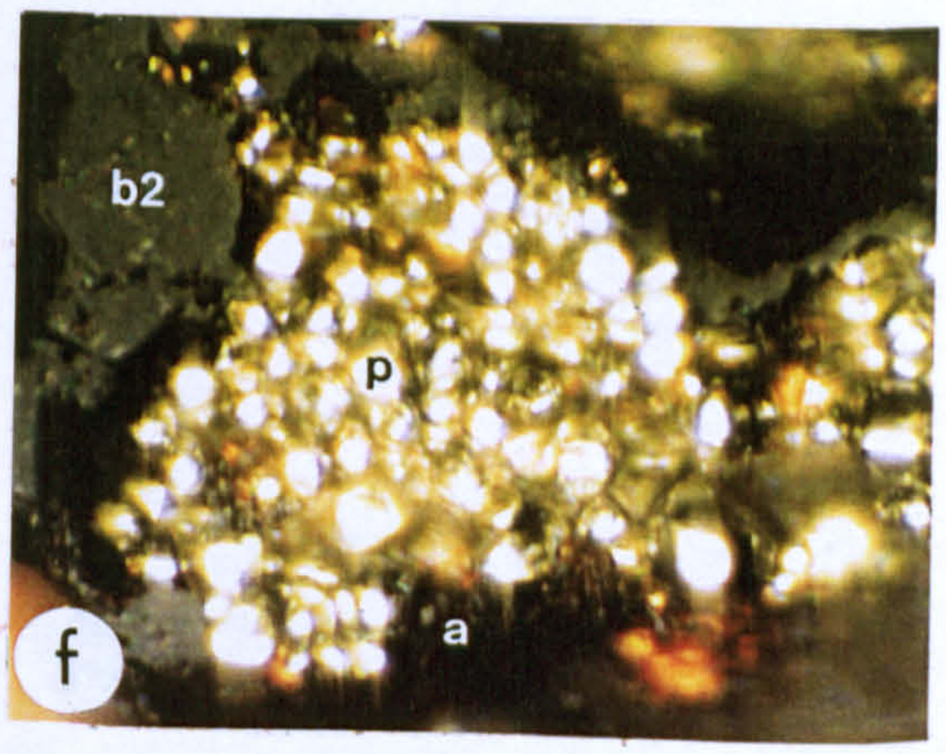

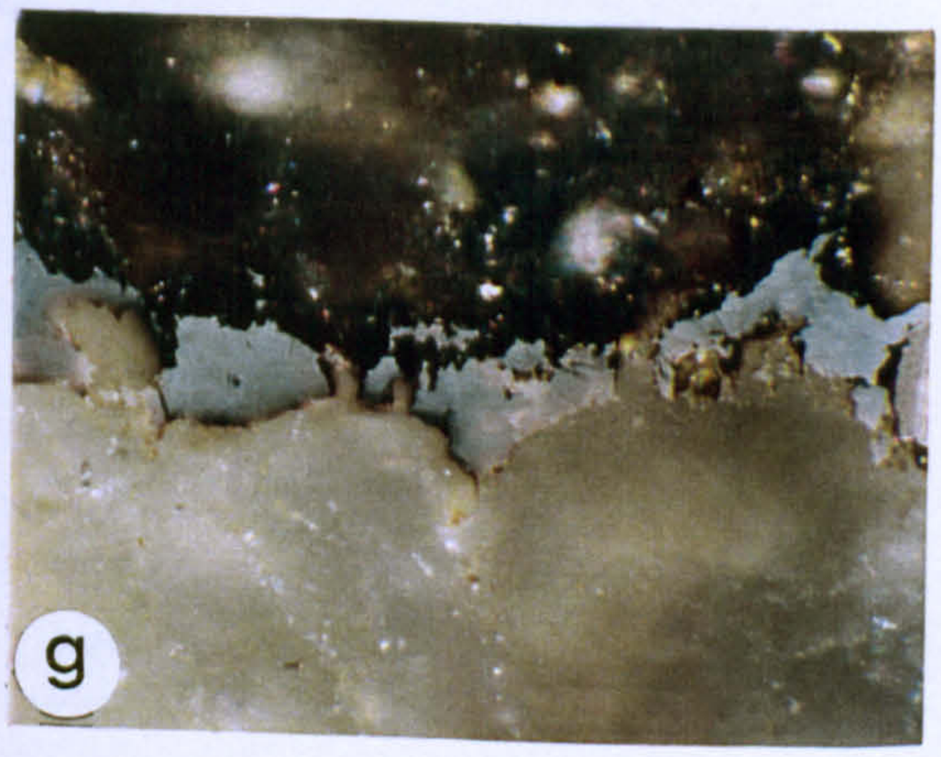

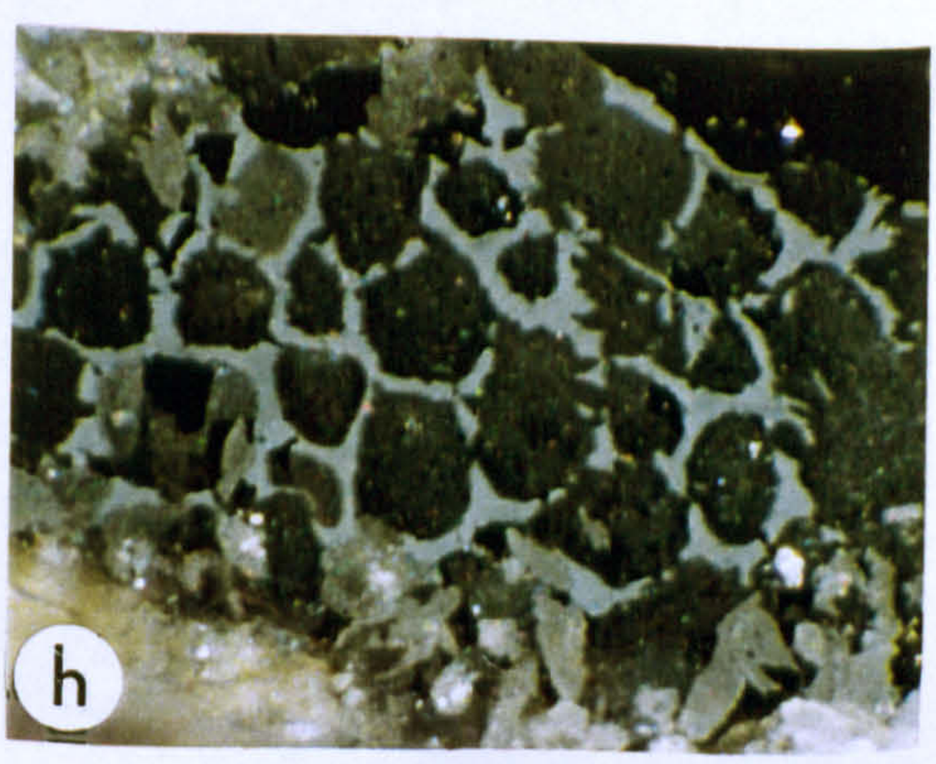

PLATE XI
SPORINITE (MICROSPORES) OF THE GOLATA AND MATTSON FORMATIONS

a) ?*Reticulatisporites* in the Golata Formation at Jackfish Gap.

b) ?*Murospora aurita* in the Mattson Formation at Clausen Creek.

c) ?*Pteridiospora* and acritarchs in Mattson Formation at IOE *et al.* Bovie Lake M-05; inset is from the Mattson at Pan Am Pointed Mountain P-24.

d), e) & f) *Murospora* - described by Stach, (1968) as the "dumb-bell spore" showing well-preserved trilete mark; the intine is thin and shows significantly higher intensity fluoresence with shorter wavelength than the much thicker exine; this is evident on b) also.

g) Thick walled crassispore showing moderately high intensity fluorescence (λ max: 650-680); the Carboniferous genera are very similar to those described from the Lower Carboniferous of the Ruhr region by Stach (1968), many of which have since been reassigned to other genera.

h), i) *Densosporites* in fluorescent (h) and white light (i) views.

j) Thick walled crassispore (?*Denexinus* of Stach, 1968) showing showing reflectance variations between the intine and exine.

k) Thick walled crassispore may be similar to ?*Theissenexinus* of Stach (1968).

l) Thin-walled tenuispore (?*Verexinus* of Stach, 1968) in shales of the Golata Formation.

m), n) White (m) and fluorescent light (n) images of highly ornamented Carboniferous crassispore (?*Baculexinus* of Stach, 1968)

All photomicrographs were taken from polished blocks using fluorescent incident light except for i), j) & m), which were obtained using white light.

Magnification: scale bar shown on a) applies also to b), h) & i); scale bar shown on c) also applies to f), g), j), k) , l), m) & n).

16th.

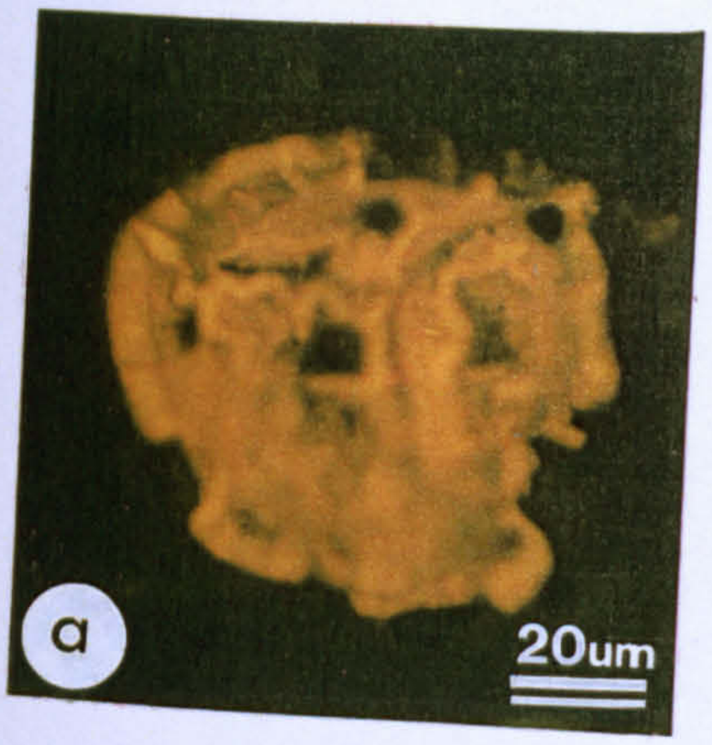

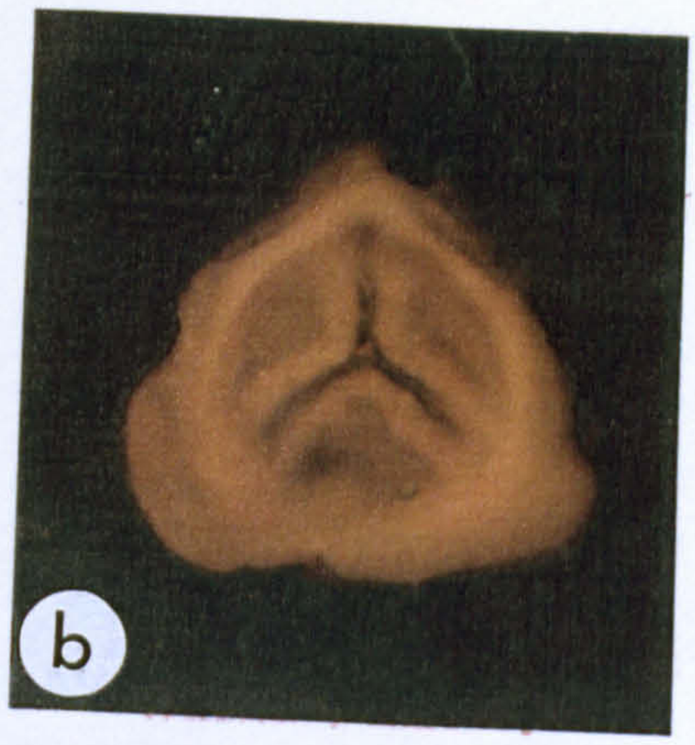

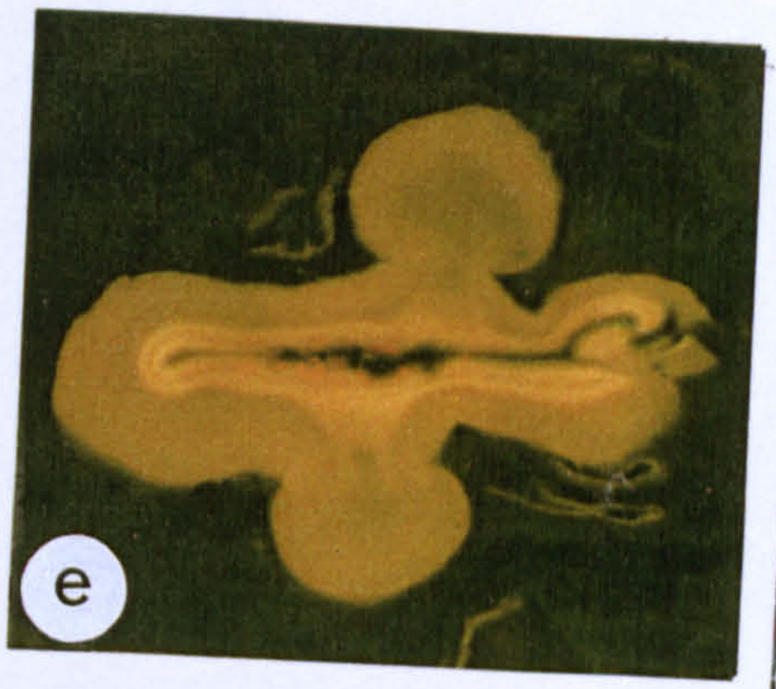

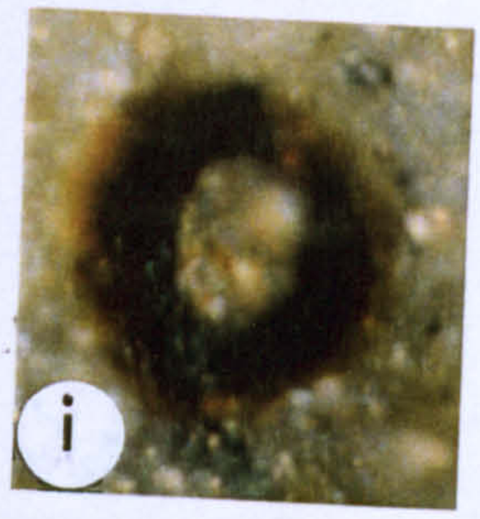

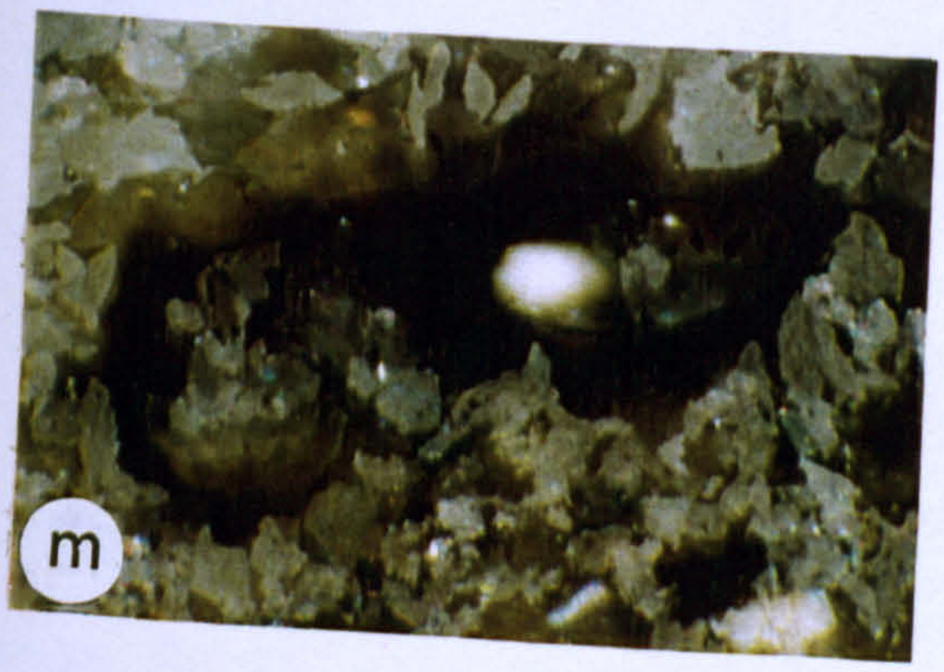

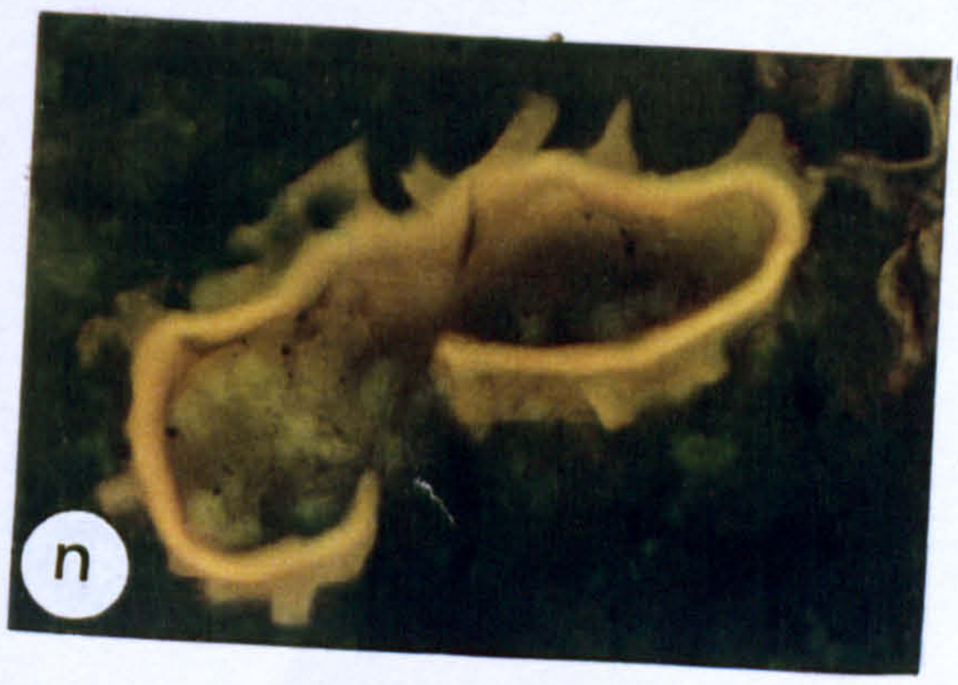

PLATE XII

SPORINITE (MEGASPORES) OF THE MATTSON FORMATION

a) thick-walled, highly ornamented ?*Setosisporites* from the Mattson Formation at Jackfish Gap; note the very granular nature of the exine.

b) thick-walled, highly ornamented megaspore from the Mattson Formation showing abundant surface processes.

All photomicrographs are composites from polished sections viewed in fluorescent light (400-440 nm excitation) under oil immersion.

PLATE XIII
CUTINITE AND SPORINITE OF THE GOLATA AND MATTSON FORMATIONS

a) High concentrations of thick-walled (crassi-) cutinite in the Mattson Formation at Jackfish Gap.

b) Cutinite (centre) has higher intensity fluoresence than the associated sporinite debris and has typical serrated margins. Mattson Formation at Clausen Creek.

c), d) Plan view (parallel to bedding) of cutinite in fluorescent blue (c) and white (d) light.

e) Thin-walled prasinophyte alginite (? Leiosphaeridiales) from the Mattson Formation.

f), g), h), i) Alginite comprising typical Carboniferous coccoid alga (?*Pila*) which is synonymous with the freshwater species *Botryococcus*.

j) ?*Pila* alginite showing details of coccoid form.

Magnification: Scale bar shown in a) applies also to c), d), e), f), & h); scale bar shown on b) applies also to g), i) & j).

166a

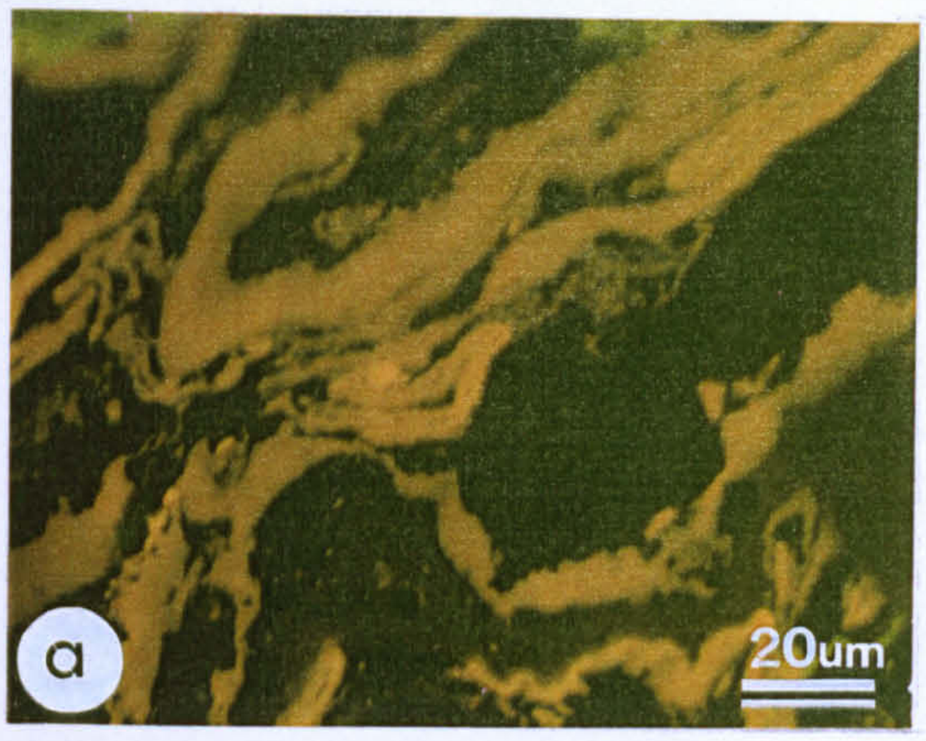

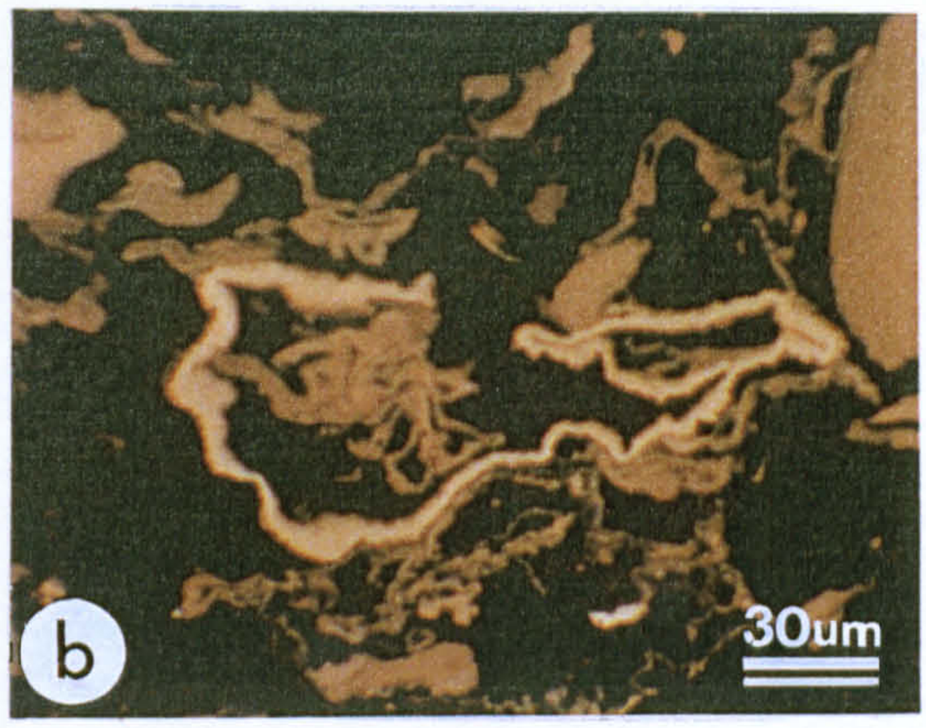

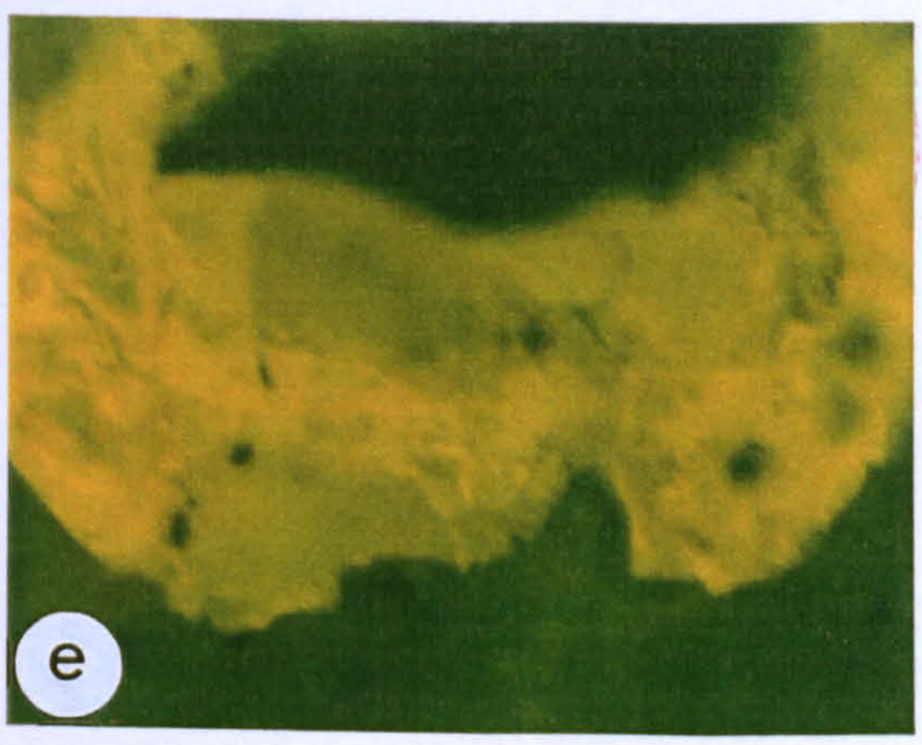

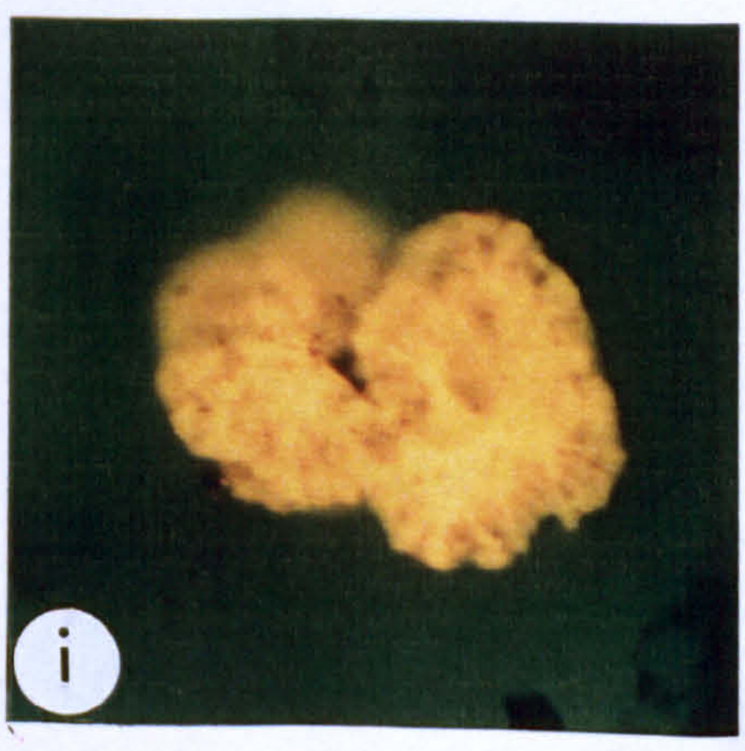

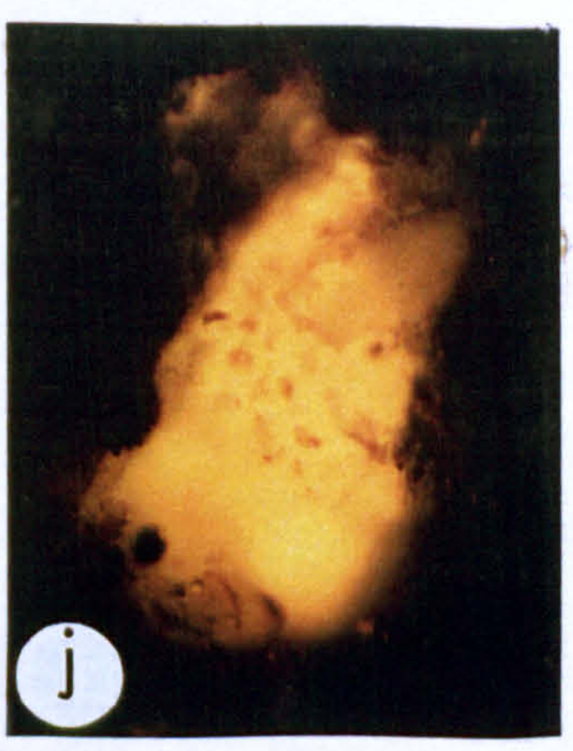

PLATE XIII
CUTINITE AND SPORINITE OF THE GOLATA AND MATTSON FORMATIONS

a) High concentrations of thick-walled (crassi-) cutinite in the Mattson Formation at Jackfish Gap.

b) Cutinite (centre) has higher intensity fluoresence than the associated sporinite debris and has typical serrated margins. Mattson Formation at Clausen Creek.

c), d) Plan view (parallel to bedding) of cutinite in fluorescent blue (c) and white (d) light.

e) Thin-walled prasinophyte alginite (? Leiosphaeridiales) from the Mattson Formation.

f), g), h), i) Alginite comprising typical Carboniferous coccoid alga (?*Pila*) which is synonymous with the freshwater species *Botryococcus*.

j) ?*Pila* alginite showing details of coccoid form.

Magnification: Scale bar shown in a) applies also to c), d), e), f), & h); scale bar shown on b) applies also to g), i) & j).

PLATE XIV

CUTINITE FROM THE MATTSON FORMATION

a) Composite photomicrograph of cutinite enclosing and encased by weakly reflecting perhydrous vitrinite (?mesophyll tissue of a leaf or pinule); white incident light.

b) Fluorescent incident light view of a); note the weak fluorescence of the perhydrous vitrinite.

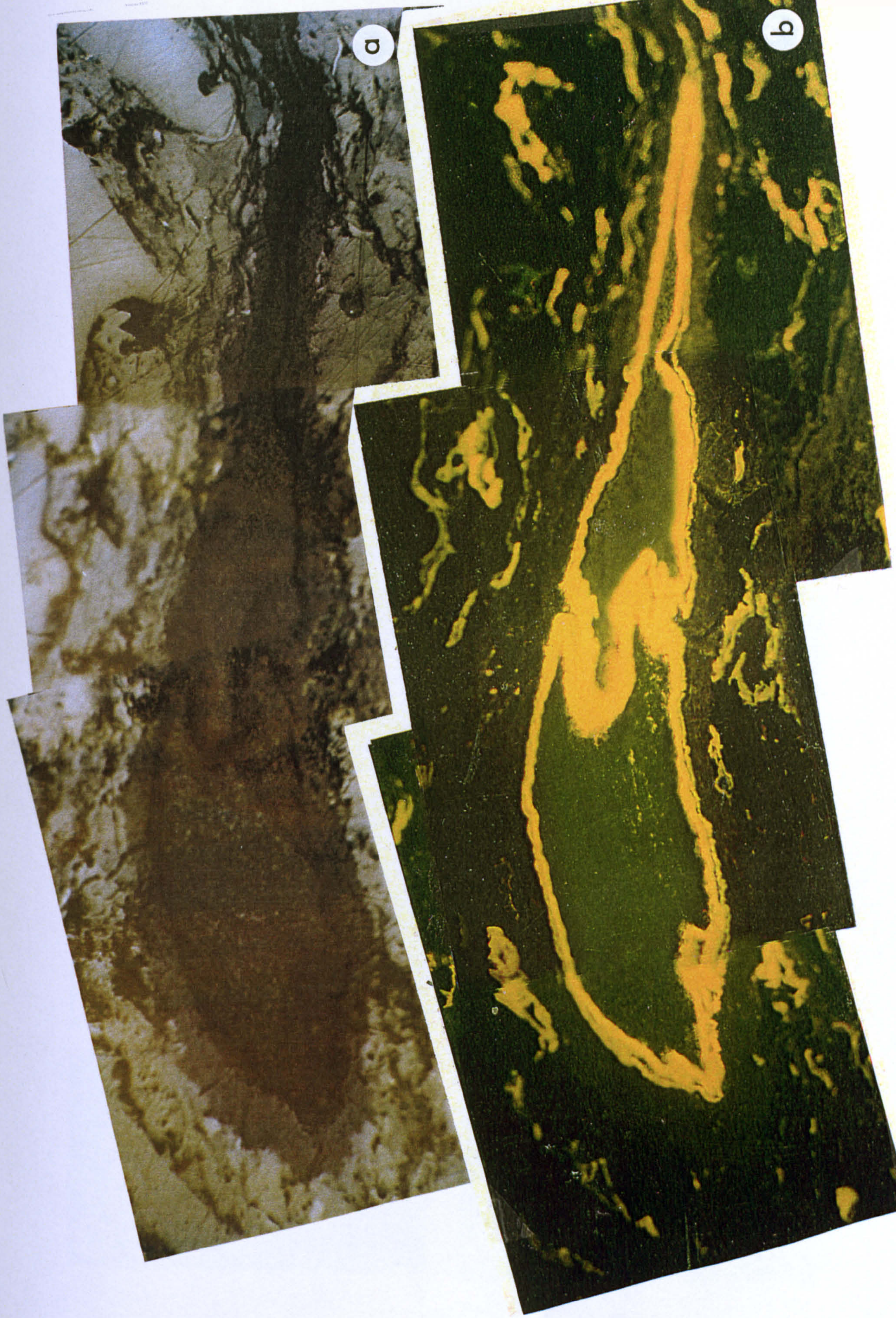
a
b

PLATE XV
VITRINITE AND INERTINITE IN THE GOLATA AND MATTSON FORMATIONS

a) Dispersed vitrinite (0.61% R_o) with inclusions of framboidal pyrite; Golata Formation at Pan Am Kotaneellee.

b) Gelovitrinite in the Mattson Formation at Pan Am Pointed Mountain P-24.

c) Dispersed vitrinite in the Mattson Formation at Clausen Creek.

d) Oxidized vitrinite showing characteristic elevated reflectance and polygonal fractures. Mattson Formation, Aquitaine *et al.* Tatoo a-2-D.

e) Dispersed vitrinite in the Mattson Formation at Clausen Creek.

f) Vitrinite with inclusions of inertinite in the Mattson Formation at Clausen Creek.

g) Fusinite with well-preserved cell struacture in the Mattson Formation at Aquitaine *et al.* Tatoo a-2-D.

h) Fragmented fusinite in the Mattson Formation at Aquitaine *et al.* Tatoo a-2-D.

i) Funginite (?or cenospheres) in the Mattson at Clausen Creek.

j) Semifusinite in shales of the Mattson Formation at Clausen Creek.

Magnification: scale bar a) applies to all photomicrographs.

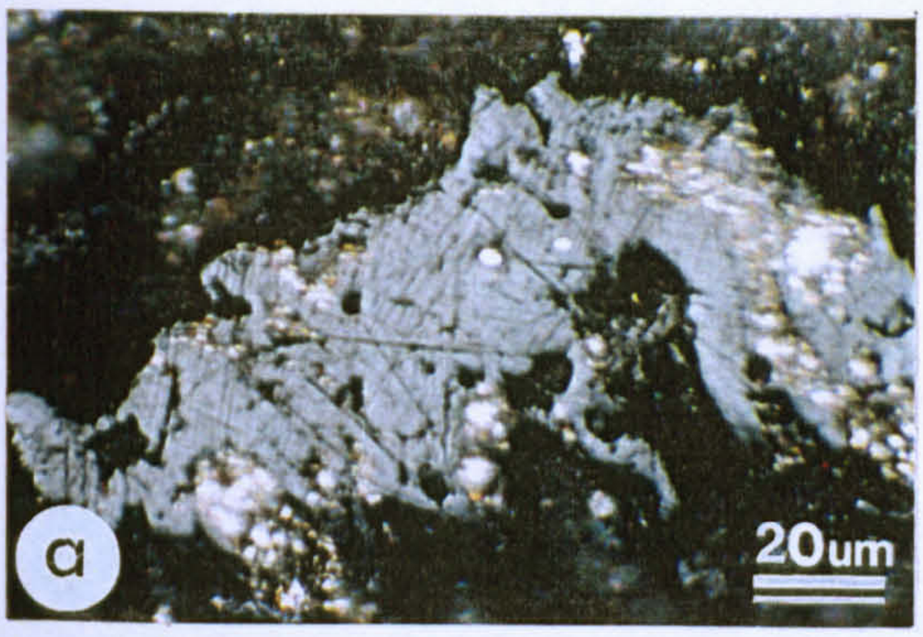
a
20um

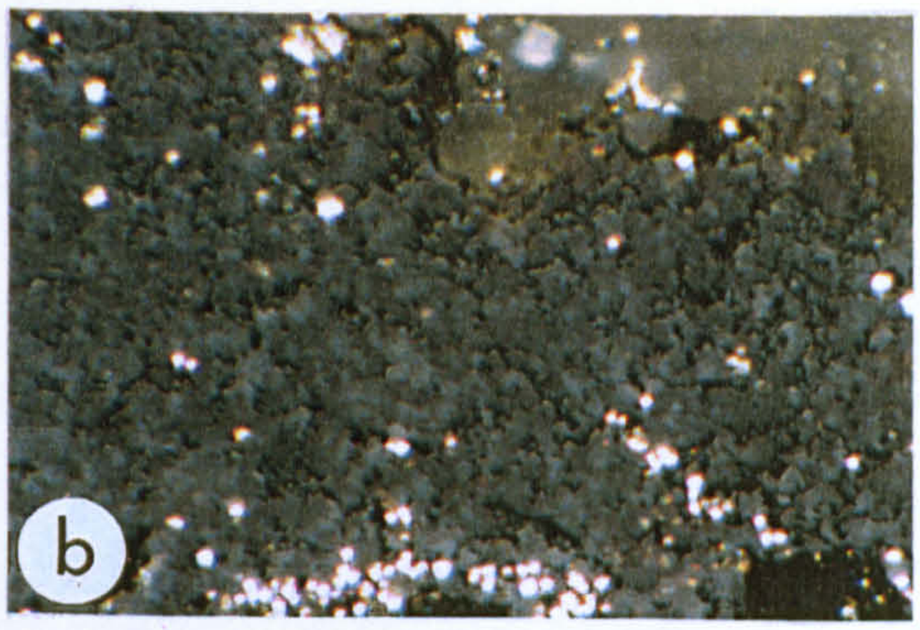
b


c

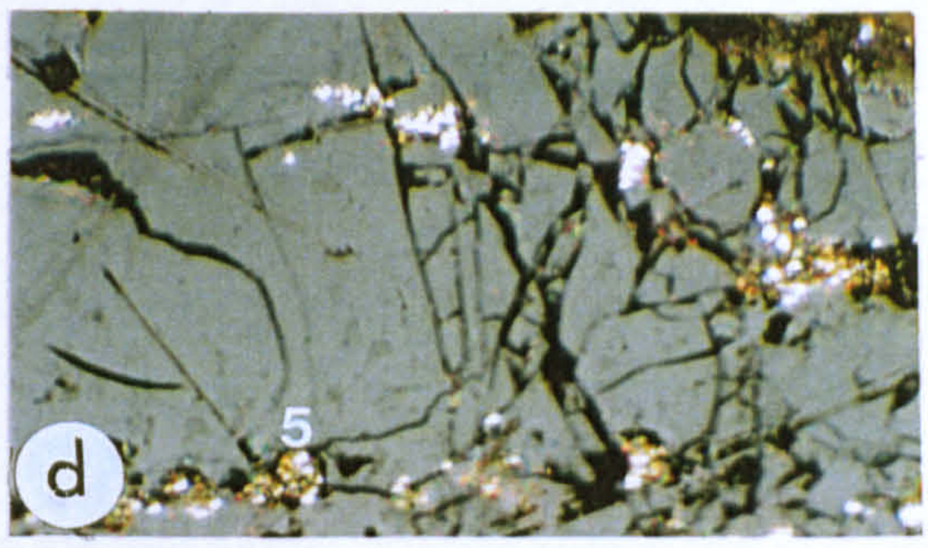
d
5


e


f

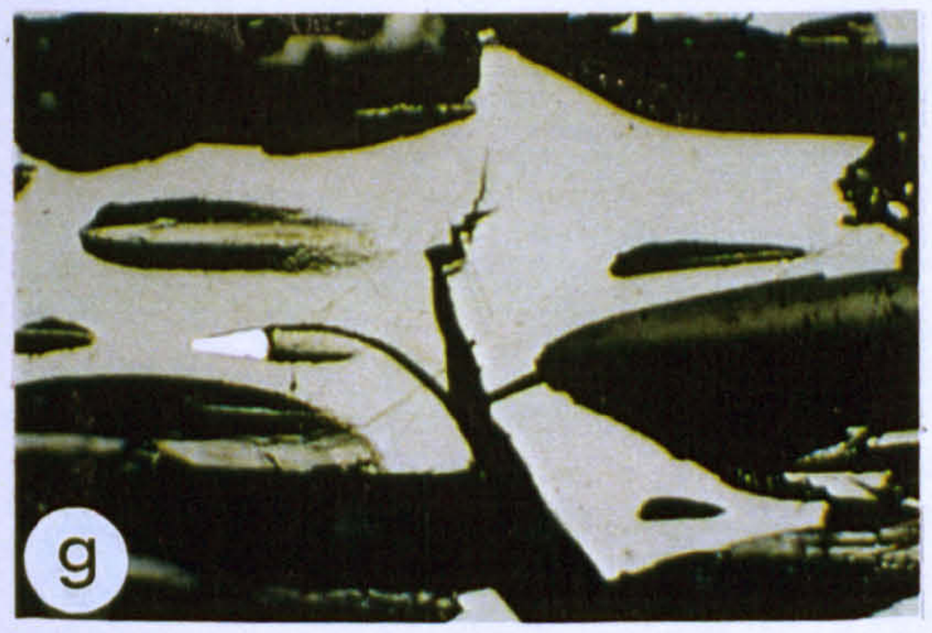
g

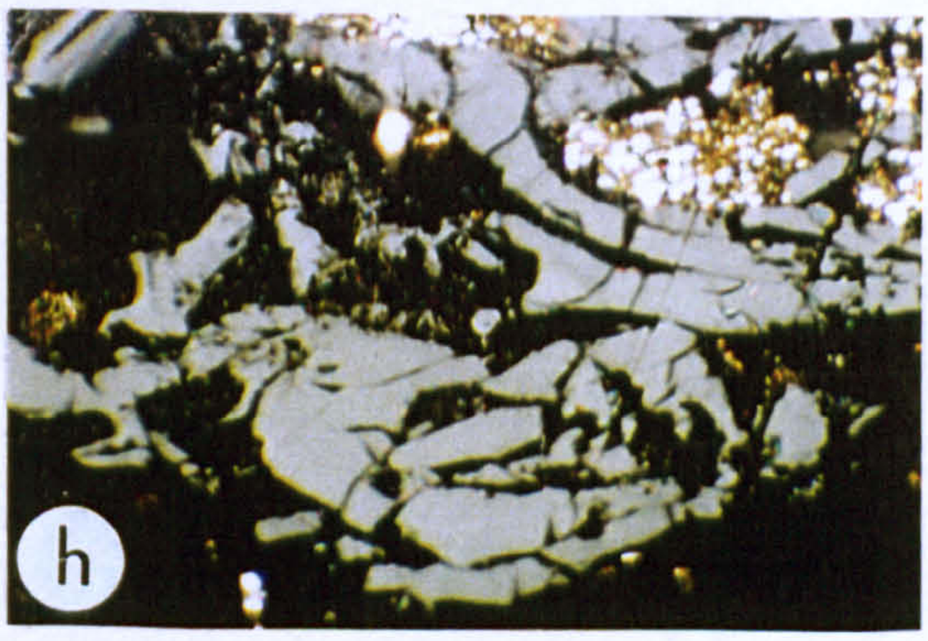
h

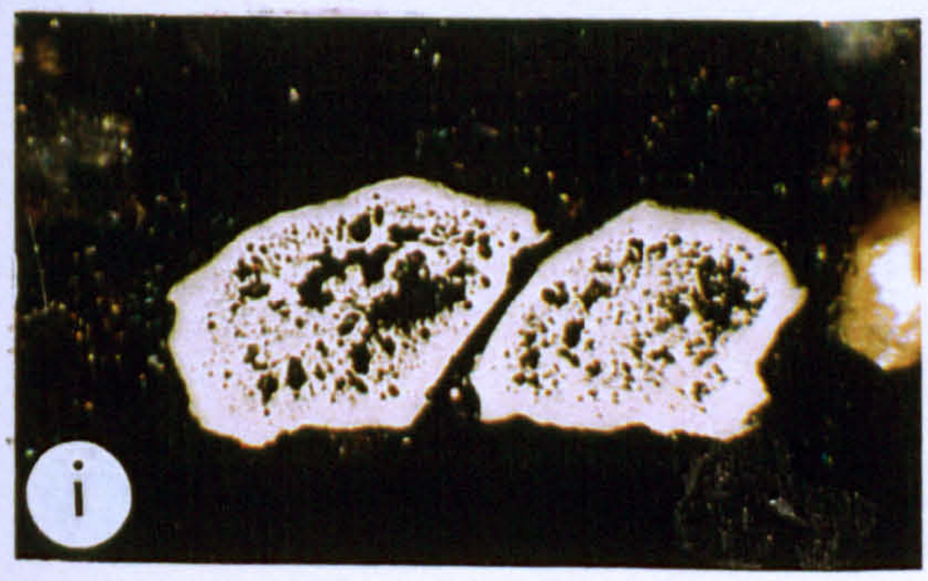
i

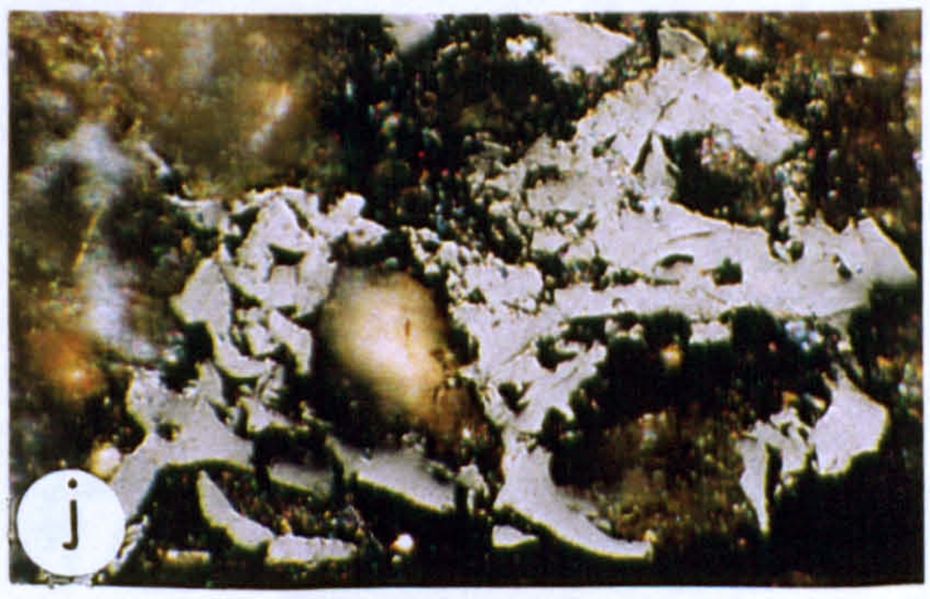
j

PLATE XVI
PETROGRAPHIC FEATURES OF THE COALS IN THE MATTSON FORMATION

a) Vitrinite band (centre; 0.74%R_o) with lenses of granular micrinite (white) threaded throughout; sporinite (microspores) and inertinites dominate the band below.

b) Granular, white micrinite (centre, right) interwoven with dark, weakly reflecting perhydrous vitrinite (0.58%R_o) embedded in inertinite-rich coal. Perhydrous vitrinite or bituminite is commonly found in association with micrinite in sapropelic coals.

c) Micrinite (m) concentrated into an inertite layer with mega-, microspores and inertinite; high concentrations of micrinite suggest the coals are sapropelic in nature.

d) Dark, weakly-reflecting, highly-ornamented Carboniferous megaspore(s).

e) Gelovitrinite or semimacrinite? (g) amid semifusinite (sf) and spore-rich (sp) bands. Highly gelified plant tissues are commonly found in coals which accumulated in a subaquatic setting.

f) Perhydrous vitrinite (v) invading a mass of clastic inertinite - Stach (1968) would have called the inertinitic material "massive micrinite". Large accumulations of unstructured inertinite are typical of coals derived from aquatic plants (Teichmüller, 1982, p. 281).

g) A cluster of highly reflective "resino-inertinites" encased in cutinite (cu) from a seed-fern (*Medullosa*).

h) Mass of clastic inertinites which is typical of a coal formed subaquatically.

Magnification: scale bar shown in a applies to all photomicrographs


30um
a


b

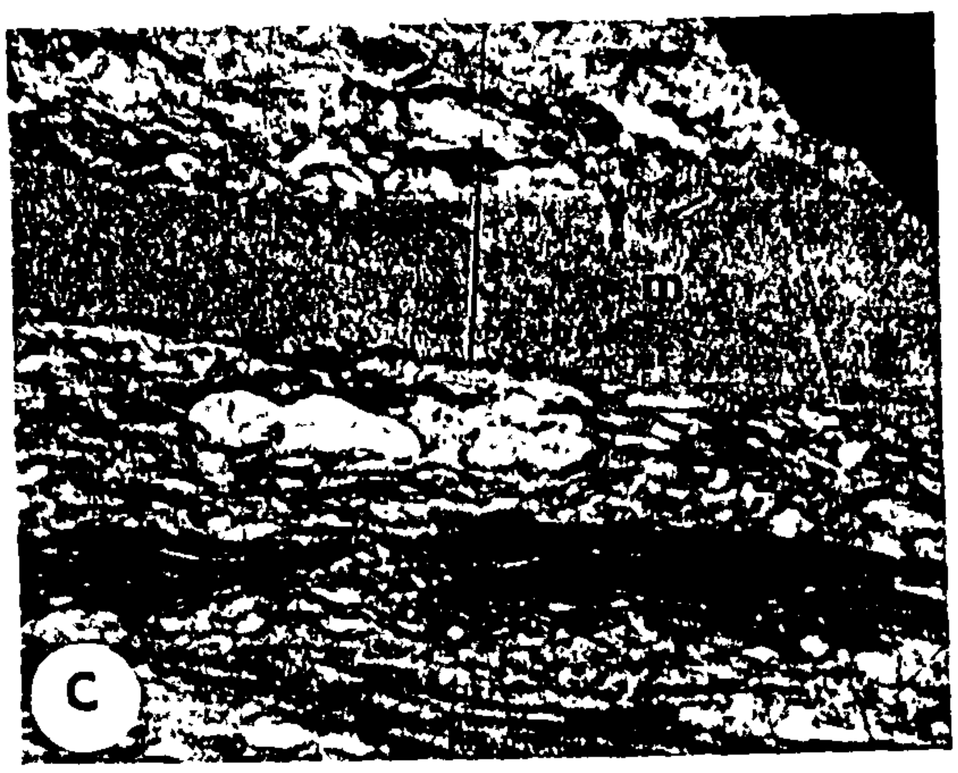
c


S
d


Si
S
e


V
f

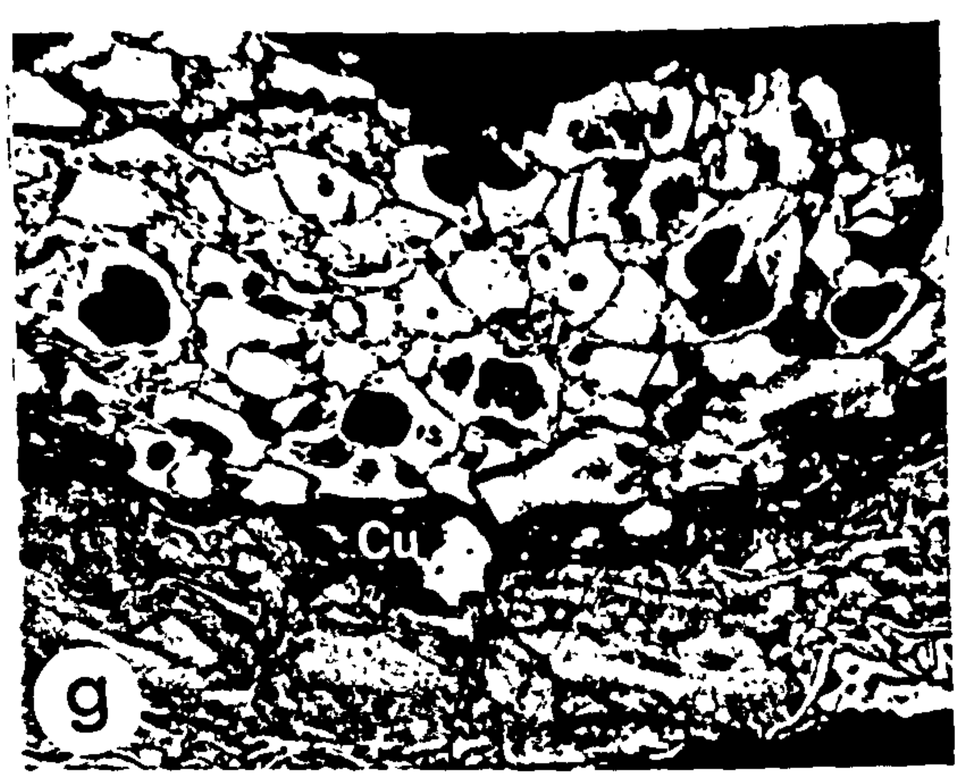
Cu
g


h

5.0 THERMAL HISTORY OF THE LIARD BASIN

A general overview of the thermal history of the Liard Basin has been compiled by examination of the changes in reflectance of the indigenous bitumens with depth. Reflectance-depth profiles are constructed for all vertical sections but only one section is illustrated in Fig. 53. Vertical Ro-depth profiles for the other sections are shown in Appendix D.

5.1 VERTICAL REFLECTANCE PROFILES

According to Dow (1977), kerogen maturation and petroleum generation follows first-order reactions which are time- and temperature- dependent. The resulting maturation therefore varies exponentially with temperature and linearly with time. As burial depth and temperature are related by the geothermal gradient in any given area, vertical reflectance profiles are an indication of the burial history. This is the basic premise of most basin modeling programs.

The results of linear regression analysis of depth and reflectance relationships for Upper Devonian to Cretaceous (or Tertiary) (most commonly utilizing data from medium Ro type 4 and low Ro type 3 bitumen) for the Upper Devonian and Lower Carboniferous are shown in Table 21. The correlation coefficients (R^2) vary from 0.78 to 0.96 for the medium Ro bitumens, and 0.61 to 0.99 for the low Ro (type 3) bitumens. A lineal and a semi-log plot of the R_o of several bitumen populations versus depth from the Island River section (1) are illustrated in Fig. 53.

Overall, the strong Ro-depth correlations shown in all sections indicate that the present day maturation patterns observed in the Liard Basin are closely related to the burial history. The samples which are most deeply buried today generally accumulated in the deepest parts of the basin and show the highest R_o values, with the exception of the sections located in the Pointed Mountain Anticline (the two Pointed Mountain sections) and the Kotaneelee Anticline (Mattson Creek) and the surface samples which were elevated by folding, faulting or thrusting during the Laramide Orogeny. According to Dow (1977), the trend of the log R_o values versus depth follows a straight line if there has been continual subsidence in a basin with a time-invariant geothermal gradient. The lineal trends

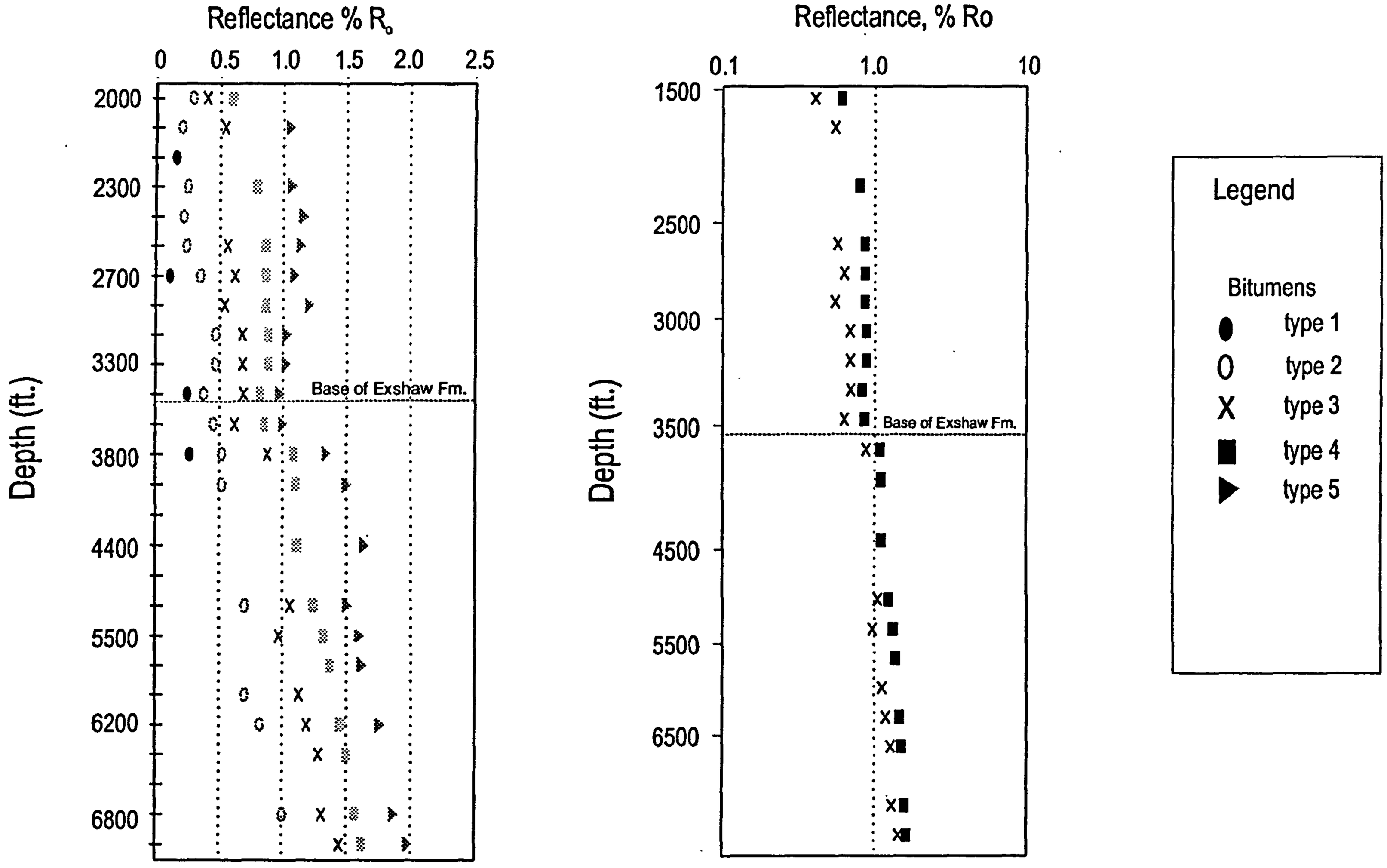

Figure 53 Bitumen reflectance versus depth plots from the Imperial Island River No.1 section: a) linear plot, bitumen types 1, 2, 3, 4 and 5; b) semilog plot, low Ro type 3 and medium Ro type bitumens.

shown in Appendix D suggest that there was relatively continued subsidence throughout the Liard Basin during the Upper Devonian-Lower Carboniferous. A significant displacement of the R_o profile occurs at the stratigraphic level of the Cretaceous-Permian unconformity in all sections that have available Cretaceous data; this represents a major period of tectonic activity in the Western Canada Sedimentary Basin consistent with numerous phases of uplift and erosion of Jurassic, Triassic and Late Carboniferous strata during the Laramide orogeny.

5.2 REFLECTANCE (Ro) GRADIENTS

The variation in R_o between the top and bottom of a vertical section represents the maturity or R_o gradient (measured in $\%R_o$ per km) and is a reflection of the heating capacity of the rocks and the geothermal gradient in effect over a given time interval Bustin (1991). The relationship between % Ro and depth in the Western Canada sedimentary basin is logarithmic (England & Bustin (1986); Stasiuk *et al.*, 1993) and this is also evident in the study area from the data shown in section 5.1 and Appendix D.

The correlation coefficients (R^2 values) for R_o and depth (Table 21) change if the data are split into Upper Devonian and Carboniferous data sets (Tables 22 & 23)which suggests that the Ro gradients (and therefore the geothermal gradients) changed over time. For most sections, the R^2 values improve slightly for the Devonian (Table 22) and generally, also for the Carboniferous (Table 23). The correlations between reflectance and depth are better for the medium Ro type 4 bitumen (R^2 = 0.6 to 1.0; see Tables 21 to 23) than for the low Ro bitumen (type 3); Carboniferous correlation coefficients observed in the Muskeg River (3) and Arrowhead (4) sections are poor (R^2 = 0.37). The effect of dividing the data set appears to follow a regional pattern. For the sections in the western part of the study area, i.e. the Liard Basin (Kotaneelee, Beaver River and North Beaver River), the R^2 values are improved by this procedure, particularly the Carboniferous data. This may be due to the elevated maturation levels found in the western region (basinal regime) relative to the Interior Platform to the east. Elevated maturation levels effectively homogenize the dispersed organic matter and reduce the variety of indigenous bitumens and the number of bitumen populations.

Reflectance, % Ro	Medium Ro bitumen					Low Ro bitumen 3				
Location	K	std err Y	R^2	n	deg fr*	K	std err Y	R^2	n	deg fr*
Imperial Island River No. 1	0.30	0.06	0.96	18	16	0.07	0.07	0.95	16	14
Murphy *et al.* Muskeg River No.1	0.48	0.12	0.89	14	12	0.19	0.07	0.95	14	12
Imperial Sun Arrowead I-46	0.94	0.14	0.78	19	17	0.31	0.17	0.88	20	18
Imperial Sun Netla C-07	0.27	0.08	0.95	16	14	0.19	0.10	0.82	14	12
B.A. Texaco Arrowhead N-2	0.22	0.1	0.88	19	17	0.16	0.19	0.61	10	8
Amoco East Flett H-13										
Pan Am Home S. Celibeta No.7	0.46	0.02	0.92	20	18	0.41	0.06	0.95	20	18
Texaco NFA Bovie Lake J-72	-0.73	0.21	0.92	15	13	0.13	0.19	0.86	13	11
Amoco Pointed Mountain P-53	0.09	0.14	0.91	23	21	0.01	0.10	0.94	20	18
Pan Am Mattson Creek A-1	1.51	0.19	0.94	9	7	1.36	0.05	0.99	3	1
Pan Am Kotaneellee 0-67	0.21	0.12	0.99	4	2	0.21	0.21	0.94	4	2
Canada Southern *et al.* N Beaver R.	-0.34	0.35	0.84	21	19	-0.21	0.26	0.88	12	10
Pan Am Beaver River G-01	-0.45	0.35	0.88	24	22	-0.21	0.16	0.96	17	15

* degrees of freedom

Table 21 Correlations between measured Ro values and depth for Carboniferous and Devonian data based on linear regression analysis.

Reflectance, % Ro	Medium Ro bitumen					Low Ro bitumen 3				
Location	K	std err Y	R^2	n	deg fr*	K	std err Y	R^2	n	deg fr*
Imperial Island River No. 1	0.28	0.06	0.95	11	9	0.01	0.08	0.90	9	7
Murphy *et al.* Muskeg River No.1	0.61	0.11	0.86	11	9	0.28	0.06	0.95	11	9
Imperial Sun Arrowead I-46	1.24	0.06	0.74	11	9	0.02	0.17	0.86	16	14
Imperial Sun Netla C-07	0.23	0.08	0.94	13	11	0.06	0.09	0.86	12	10
B.A. Texaco Arrowhead N-2	-0.1	0.05	0.97	8	6	-0.75	0.12	0.92	4	2
Pan Am Home S. Celibeta No.7	0.47	0.13	0.82	13	11	0.63	0.08	0.69	9	7
Texaco NFA Bovie Lake J-72	-1.17	0.19	0.92	10	8	-0.39	0.21	0.77	6	4
Amoco Pointed Mountain P-53	-0.74	0.12	0.92	10	8	-0.25	0.10	0.88	7	5
Pan Am Mattson Creek A-1	1.54	0.03	0.96	3	1	0.79	0.0	1	2	0
Pan Am Kotaneellee 0-67	-7.83	0.0	1	2	0	-1.38	0	1	2	0
Canada Southern *et al.* N Beaver R	-3.72	0.25	0.91	7	5	-1.85	0.48	0.73	3	1
Pan Am Beaver River G-01	-3.97	0.14	0.95	10	8	-2.01	0.19	0.79	6	4

* degrees of freedom

Table 22 Correlations between measured bitumen Ro and depth for Upper Devonian based on linear regression analysis.

Reflectance, % Ro	Medium Ro bitumen					Low Ro bitumen 3				
Location	K	std err Y	R^2	n	deg fr*	K	std err Y	R^2	n	deg fr*
Imperial Island River No. 1	0.62	0.02	0.83	6	4	0.26	0.05	0.63	7	5
Murphy *et al.* Muskeg River No.1	0.09	0.01	0.96	3	1	1.06	0.03	0.37	3	1
Imperial Sun Arrowead I-46	1.73	0.01	0.96	3	1	0.8	0.02	0.1	4	2
Imperial Sun Netla C-07	-4.44	0.02	0.98	3	1	-1.26	0.0	1	2	0
B.A. Texaco Arrowhead N-2	0.64	0.04	0.63	10	8	0.67	0.4	0.58	6	4
Amoco East Flett H-13	0.26	0.06	0.72	6	4					
Pan Am Home S. Celibeta No.7	0.52	0.09	0.82	8	6	0.39	0.04	0.92	11	9
Texaco NFA Bovie Lake J-72	0.26	0.17	0.52	5	3	0.59	0.03	0.86	5	3
Pan Am Pointed Mountain P-24	0.23	0.02	0.57	5	3	0.43	0.02	0.78	5	3
Amoco Pointed Mountain P-53	0.33	0.06	0.92	13	11	0.18	0.07	0.87	13	11
Pan Am Mattson Creek A-1	1.63	0.09	0.95	5	3					
Pan Am Kotaneellee 0-67	0.53	0.2	0.94	3	1	0.5	0.07	0.65	4	2
Canada Southern *et al.* N Beaver R	0.48	0.08	0.93	13	11	0.26	0.09	0.91	9	7
Pan Am Beaver River G-01	0.25	0.13	0.91	14	12	0.04	0.04	0.99	12	10
Clausen Creek	1.53	0.09	0.92	7	5	1.11	0.1	0.82	5	3
Jackfish Gap	1.44	0.08	0.94	26	24	1.09	0.07	0.89	28	26

* degrees of freedom

Table 23 Correlations between measured Ro and depth for Carboniferous strata based on linear regression analysis.

Improved R^2 values are not readily apparent in the Carboniferous in the Eastern Plains/Platform Region. Here the regional maturity has been shown to be significantly lower than in the western part of the Liard Basin and, as a result, a greater number of bitumen populations/bitumen types are present in any one sample (Fig. 53). In addition, greater variation in the organic facies has been demonstrated in the Mattson Formation lithofacies to the east implying more variable liptinite precursors for the indigenous bitumens. Consequently, the dependability of the bitumen data varies somewhat with maturation levels and organic facies which suggests that care must be exercised in determining the genetic links between the micro-bitumens. This may be the reason for the poor correlations between depth and bitumen reflectance in the Carboniferous of the Arrowhead and Muskeg River sections. The relationships between indigenous bitumens from different types of liptinite should therefore be investigated further.

The observed improvements in the R^2 values observed when the data are split into Devonian and Carboniferous subsets are attributed to differences in the R_o gradients during the Upper Devonian and Lower Carboniferous. In addition to this stratigraphic differentiation, the R_o gradients follow first order variations, i.e. they vary geographically within the basin (notably from west to east), and third order variations (i.e local; Bustin, 1991).

For the Upper Devonian, reflectance gradients are low to moderate (0.15 - 0.21 log%R_o/km) and have a fairly uniform distribution in the sections from the Interior Plains (Table 24). There is an east to west increase from 0.11 log%R_o/km at Trout Lake (2) to 0.18 log%R_o/km at Celibeta (5) but the R_o gradient at Bovie Lake (7) is significantly higher (0.21 log%R_o/km) than those recorded for the other sections in the Eastern Plains Region and may represent a local (third order) anomaly. Petrographic evidence (sections 4.1 to 4.7) indicates that organic matter in all Upper Devonian strata in the latter section show elevated maturation characteristics which are attributed to additional thermal effects probably associated with thermal conductivity along the Bovie Fault system immediately to the west.

Reflectance gradients for the Upper Devonian in sections west of the Bovie Fault are significantly higher than those in the Eastern Plains, ranging from 0.25 log%R_o/km at

Location	Depth (m)		Type 4 bitumen Ro (%)		Vitrinite Ro equivalent (%)		m	b	VRo gradient, log % R_o per km
	base	top	max	min	max	min			
Imperial Island River No. 1	2105.9	1062.5	1.63	0.85	1.41	0.92	6562.5	1127.8	0.15
Murphy *et al.* Muskeg River No.1	1923.6	743.7	1.71	0.85	1.46	0.93	6242.7	712.8	0.16
Imperial Sun Arrowhead I-46	2084.5	765.0	2.61	1.47	2.0	1.30	8685.0	297.9	0.12
Imperial Sun Netla C-07	1924.8	693.4	1.67	0.92	1.43	0.97	2071.2	-1040.6	0.15
B.A. Texaco Arrowhead N-2	2470.4	1495.0	1.72	1.25	1.17	1.17	6166.8	1437.1	0.15
Dome *et al.* Trout Lake H-45	1490.5	414.5	1.54	0.96	1.35	0.99	9019.9	304.8	0.11
Pan Am Home S. Celibeta No.7	2151.9	1205.5	2.0	1.30	1.64	1.20	5596.9	711.0	0.18
Texaco NFA Bovie Lake J-72	2929.4	1722.4	3.08	1.46	2.3	1.30	4632.6	1325.6	0.21
Amoco Pointed Mountain P-53	3294.9	2270.8	1.85	1.31	1.54	1.22	3368.5	2662.3	0.30
Pan Am Mattson Creek A-1	591.3	438.9	3.55	2.92	2.38	2.20	2113.8	-280.9	0.47
Pan Am Kotaneellee 0-67	2379.0	2316.5	3.2	2.91	2.38	2.20	1837.0	1688.0	0.54
Canada Southern *et al.* N Beaver R	3815.8	2779.8	3.50	2.10	2.56	1.72	6380.5	829.7	0.16
Pan Am Beaver River G-01	3223.3	4129.7	3.80	2.02	2.75	1.65	4083.0	2301.6	0.25

Table 24 Ro gradients for the Devonian of the Yukon and Northwest Territories, derived by linear regression analysis relating depth and maturity by the equation: y = mx +b (y = depth; m = x variable; x = VRo; b = intercept of y).

North Beaver River (14) to 0.54 log%R_o/km at Kotaneelee (section 15; Table 24). It is interesting to note that organic matter in the Besa River at Kotaneelee also showed evidence of an additional strong thermal event in the Upper Devonian (section 4.7).

Reflectance gradients for the Carboniferous (Table 25) follow a similar regional (first order) pattern. Most of the sections in the Eastern Plains Region, have low to moderate gradients of 0.09-0.21 log%R_o/km and similar values are found in the Pointed Mountain P-53 section (12; 0.12 log%R_o/km); the discrepancy between the R_o gradients at P-53 and P-24 (0.12 vs 0.07 log%R_o/km) at this location may reflect repetition of the Carboniferous section due to thrusting in the Amoco Pointed Mountain P-24 section (10) which produces an anomalously thick section of the Mattson Formation; in the latter section the R_o gradient is anomalously low (0.07%R_o/km). The R_o gradient at Bovie Lake (7) is relatively low, but in the same range as the other sections east of the Bovie Fault, suggesting that thermal activity along the fault, which was evident during the Upper Devonian, had subsided during the Lower Carboniferous. Higher values at the Muskeg River (3) and East Flett sections (9) may represent local (third order) anomalies.

The Carboniferous R_o gradients for sections west of the Bovie Fault (excluding Pointed Mountain) follow similar trends to those observed in the Eastern Plains; R_o gradients in the Beaver River area (0.13 to 0.14 log%R_o/km) are comparable but increase markedly westwards to 0.26 log%R_o/km at Kotaneelee (15), and 0.25 log%R_o/km at Mattson Creek (11). Once again, there is a suggestion that a significant additional thermal influence prevailed along the western margin of the Liard Basin. Dow (1977) demonstrated that younger stratigraphic sections with lower geothermal gradients yield steep maturation (R_o) profiles while older stratigraphic sections and higher geothermal gradients yield shallower profiles. The shallow R_o gradients observed in the Upper Devonian (Appendix D) would therefore suggest that higher geothermal gradients prevailed in the Upper Devonian, while the steep R_o gradients typical of the post-Devonian in the Liard Basin indicate that a lower geothermal gradient was established during the Lower Carboniferous.

The regional trends in the Upper Devonian and Lower Carboniferous R_o gradients are similar: high R_o gradients in the western part of the study area diminishing towards the east. The highest regional gradients occur in the Beaver River area which suggests that the

Location	Depth (m)		Type 4 bitumen		Vitrinite Ro		m	b	VRo gradient, log % R_o per km
	base	top	max	min	max	min			
Imperial Island River No. 1	1056.1	704.1	0.85	0.79	0.93	0.87	6256.51	1120.3	0.12
Murphy *et al.* Muskeg River No.1	722.4	672.1	0.86	0.81	0.93	0.9	3070.6	812.2	0.20
Imperial Sun Arrowhead I-46	606.55	391.7	1.1	1.18	1.13	1.07	-3811.1	735.2	0.12
Imperial Sun Netla C-07	621.8	595.9	0.81	0.6	0.9	0.77	187.4	451.7	0.12
B.A. Texaco Arrowhead N-2	1415.8	713.2	1.05	0.76	1.02	0.87	10808.0	1567.1	0.10
Amoco East Flett H-13	885.4	199.6	1.01	0.71	0.83	0.60	4854.0	1309.1	0.21
Pan Am Home S. Celibeta No.7	1057.7	527.3	1.25	0.82	1.17	0.91	4517.8	691.0	0.09
Texaco NFA Bovie Lake J-72	165.0	1033.3	1.35	0.88	1.23	0.94	9366.0	1339.8	0.10
Pan Am Pointed Mountain P-24	2185.7	594.4	1.29	0.54	1.2	0.73	14260.1	2807.8	0.07
Amoco Pointed Mountain P-53	3310.1	594.36	2.58	0.54	1.99	0.73	8177.9	1690.7	0.12
Pan Am Mattson Creek A-1	378.0	36.6	2.48	1.7	1.91	1.45	2886.6	-420.15	0.25
Pan Am Kotaneellee 0-67	1281.0	402.3	1.71	0.73	1.46	0.85	3763.6	666.1	0.26
Canada Southern *et al.* N Beaver R	3333.9	1002.5	3.5	0.79	2.56	0.89	7742.6	1082.7	0.13
Pan Am Beaver River G-01	4018.8	877.8	3.43	0.60	2.52	0.77	7024.9	1554.9	0.14
Clausen Creek	1004.0	469.7	1.23	0.58	1.16	0.75	4683.9	623.1	0.21
Tika Creek	+6.55	+44.5	1.57	1.50	1.37	1.33	-3678.1	562.3	0.27
Jackfish Gap	194.6	16.9	1.52	0.48	1.34	0.69	6738.7	830.9	0.15

Table 25 Ro gradients for the Carboniferous of the Yukon and Northwest Territories, derived by linear regression analysis relating depth and maturity by the equation: y = mx +b (y = depth; m = x variable; x = Vro; b = intercept of y).

effects of the sediment thickness/burial depth are reflected in the R_o gradients at these locations which are nearer to the basin axis (cf.. Leckie *et al.*, 1991) in Northeast British Columbia. To the north of N60° 00', the basin axis is hard to define because of the faulting and thrusting that took place during the Laramide orogeny (Richards, 1993). The highest R_o gradients in the Carboniferous are found in the northern outcrop sections at Clausen Creek (0.21 log%R_o/km) and Tika Creek (0.27 log%R_o/km) where the present-day thickness of the Mattson Formation is greatest; and in the western subsurface sections at Kotanneelee (0.26 log%R_o/km) and Mattson Creek (0.25 log%R_o/km). The observed relationships between R_o and burial depth are supported by the correlations shown in Tables 21 to 23. These data may reflect the buildup of a very thick sequence of deltaic sediments during Mattson times (cf. Richards, 1989).

Significant R_o gradient anomalies unrelated to sediment thickness are observed in the Upper Devonian and Lower Carboniferous at Kotaneelee (15: Devonian: 0.54 log%R_o/km; Carboniferous: 0.26 log%R_o/km) and at Mattson Creek (11: Devonian: 0.47 log%R_o/km; Carboniferous: 0.25 log% R_o/km.). These sections are located to the west of the axis of the Liard Basin and therefore sediment thickness and burial history therefore cannot account for the high gradients observed. Furthermore, the Carboniferous R_o gradient found at Clausen Creek (0.21 log% R_o/km) is significantly higher than that found at Jackfish Gap (0.15 log%R_o/km) which is only ca. 30km to the east. This suggests that an additional thermal source may have existed on the western and northwestern margins of the study area which caused high heat flow in the western part of the basin during the Upper Devonian and Carboniferous. Declining R_o gradients suggest that this additional thermal influence gradually diminished southwards, towards the centre and also eastwards to the eastern parts of the basin and was strongest during the Upper Devonian.

5.3 REFLECTANCE (Ro) DISCONTINUITIES

Changes in maturation profiles within a vertical stratigraphic section which are manifested in displacements in the R_o trend and changes in the R_o gradient with depth, can indicate major unconformities (Dow, 1977). The demonstrated differences in R_o gradients between the Carboniferous and Upper Devonian suggest that there may be marked R_o discontinuities or unconformities at some point in the Upper Devonian-Carboniferous section within the study area. Furthermore, Macqueen and Sandberg (1970) suggest that

the Exshaw Formation (Fammenian-Tournaisian) sits disconformably on the Upper Fammenian in the Alberta Basin, but the contact (Exshaw-Kotcho) may be conformable on the Northern Interior Plains. Richards (1993) indicates that the Banff-Exshaw contact may also be disconformable south of the Peace River Embayment, but to the north, is it probably conformable. With the exception of two sections (Island River and Pointed Mountain-12), the vertical R_o profiles shown Appendix D do not show any significant displacement with depth at the Exshaw-Kotcho boundary, or within the Exshaw Formation. Moore (1993) argues against a major pre-Exshaw unconformity in the stratigraphic record of the Alberta Basin and northeastern British Columbia and the reflectance profiles presented here would appear to support this.

Despite the evidence to suggest that no major R_o disconformity exists, the data in most of the sections in the Eastern Plains suggest that an R_o discontinuity occurs in the Exshaw Formation which appears to be related to lower than expected R_o values for the amorphous, medium Ro bitumens. This phenomenon is also observed in the upper part of the Kotcho Formation, the upper Mattson; and also in the Black shale facies of the Besa River (Appendix D).

Lower than expected (suppressed) vitrinite R_o values were noted by Hutton and Cook (1980) and Kalkreuth (1982); Price and Barker (1985), and Gentzis and Goodarzi, (1993) recognised similar anomalies in petroleum source rocks rich in amorphous liptinite macerals and attributed this effect to adsorption of hydrogen-rich hydrocarbons. This phenomenon has not been documented in relation to bitumen reflectance studies. Most of the Lower Banff, Exshaw and Upper Kotcho samples in which the R_o suppression is noted in the Liard Basin are within the oil window, either currently at peak oil generation stage or just beyond, which is compatible with the view that suppression is linked to hydrocarbon adsorption. However, samples in the Besa River at the more westerly locations (e.g. Beaver River, Mattson Creek) also exhibit R_o suppression and these are beyond the oil window in terms of thermal maturation. It has been noted that R_o suppression occurs in Devonian source rocks in Western Canada (L. Stasiuk, pers. comm.) and may be related to the more sulphur-rich kerogens that are typical of the anoxic, basinal organofacies associated with Type II marine kerogens (Powell & Snowdon, 1983). Powell and Snowdon (*ibid.*) also note that under extremely euxinic

conditions, Type II kerogens generate asphaltene-rich, immature oils which chemically resemble low molecular weight kerogen (?bitumens) and are capable of migrating at low levels of maturity. It is significant that all samples in the Liard Basin exhibiting R_o suppression are those which exhibit the highest TOC values for that given stratigraphic interval. High organic carbon contents are typical of highly anoxic conditions associated with bottoms waters in deep basins (Demaison & Moore, 1980; Chow *et al.*, 1995). Fowler *et al.* (1994) have linked the occurrence of bitumens at Pine Point in the Northwest Territories to the process of dolomitization and thermochemical sulphate reduction. All of the black shales with suppressed R_o values in the Liard Basin exhibit varying degrees of dolomitization and the bitumens are often spatially associated with dolomite, which either occupies the same pore space or coats the surface of euhedral to anhedral dolomite crystals (ca. 50 to >1000 µm in length).

It would appear, based on the preceding discussion, that the apparent "discontinuities" in the R_o profiles observed in the Liard Basin reflect Ro suppression in source rocks facies rather than stratigraphic discontiniuties or disconformities. Consequently, the R_o profiles do not support the existence of major unconformities in the Upper Devonian-Lower Carboniferous in the Liard Basin; this has important implications for the application of basin modeling programs.

5.4 BASIN MODELING

The burial and thermal histories of the Imperial Island River No.1(1); Pan Am Beaver River G-01 (16); and Canada Southern et al. North Beaver River (14) sections were reconstructed using the two part computer program *Burial 3a and 3b* (Chapter 2). These sections are considered to be representative stratigraphic sections from the Eastern Plains/Interior Platform and the Western Mountain Belt/Liard Basin. The R_o values and R_o gradients from these two regions, located east and west of the Bovie Fault, indicate that the geothermal histories were somewhat different. Higher heat flows and geothermal gradients prevailed in the western part of the basin relative to the east. Sections with maturation gradients considered to be affected by additional heat sources (e.g. Kotaneelee (15), Bovie Lake (7) and Celibeta (5) were excluded from this excercise because the program incorporates elements from the Easy %Ro model of Sweeney and Burnham (1990) which applies only to continuously subsiding basins.

Imperial Island River

The stratigraphic and lithological information required to compile IIR.dat input file is shown in Table 27. These data are derived from gamma ray-sonic geophysical logs, stratigraphic logs and visual examination of cores and drill cuttings. The stratigraphy and reconstructed burial history model, which is required to generate the IIR.dat and IIR.age input files, is summarized in Table 28. The .dat file also includes information about the thermal history in terms of heat flow and surface temperatures at each age. Heat flow data are based on pre-Cretaceous geothermal gradients of 65°C/km (135 mW/m^2) and Cenozoic gradients of 35°C/km (80 mW/m^2) (from Morrow *et al.*, 1993; Feinstein *et al.*,1996) ; heat flow values are derived from Middleton's (1982) equation for calculating geothermal gradients from log Ro /depth curves:

(i) R_o gradient, G = 194.8 m, where m is the slope of the line.

(ii) the heat flow = G x sediment thermal conductivity.

The actual input files (iir.dat; iir.age and iir.ro) are included in Appendix E. Using these files the burial program computes a stratigraphic (depth) profile for each layer at each age, taking sediment compaction into account and creating a burial history model in file called "thick.age" which can be used to construct a burial plot for the basin. The maximum temperature for each layer at each age is also calculated based on the heat flow information supplied in the .dat file and this is used to calculate the maximum burial temperature. These data then serve as input files for the second part of the Burial program *(Burial 3b)* and theoretical Ro profile for the model presented. The measured R_o values and projected R_o values are compared using the Kolmogorov-Smirnov Test for the non-parametric comparison of two sets of unbinned data (i.e. "K-S Statistic") in the output file "Scalc.Ro".

The Burial history model was run using using nine different heat flow scenarios which are summarized in Table 30. The details of each of the .dat input files are shown in Appendix E. The resulting "K-S Statistic" and probabilities for these models are also shown in Table 30, together with the correlations between measured and predicted Ro values (results of Burial 3b : Scalc.Ro = output file); the measured Ro values and the R_o values predicted by each of the models are shown in Table 31. The "measured" vitrinite values predicted by each of the models are shown in Table 31. The "measured" vitrinite

Formation	Fm top	present thickness	original thickness	Lithology					
	ft	m	m	shale	sst	lst	dol	siltst	evap	chert
Quaternary		20	20		0.5			0.5		
Wapiti		0.0	350		0.5			0.5		
Kotaneelee		0.0	400	0.70	0.15			0.15		
Sub-Tertiary Unconformity										
Dunvegan		166	250		1.0					
Sully	610	177	177	0.5	0.2		0.3			
Sikanni	1190	85	85		1.0					
Buckinghorse	1470	197.5	197.5	0.8				0.2		
Sub-Cretaceous Unconformity										
Toad-Grayling		0.0	140							
Sub-Triassic Unconformity										
Fantasque		0.0	25							
Kindle		0.0	20							
Sub-Permian Unconformity										
Mattson		0.0	150							
Rundle	2118	3	338	0.15		0.85		0.2		
Banff-Exshaw	2222	372	372	0.6		0.3		0.1		
Kotcho	3468	212.5	212.5	0.65		0.35				
Tetcho	4165	76.2	76.2			0.85	0.15			
Trout River-Kakisa	4415	71.6	71.6	0.1	0.6	0.1		0.2		
Redknife	4650	143.3	143.3	0.7			0.05	0.2		
Jean Marie Mbr	5120	15.2	15.2			0.65	0.35			
Fort Simpson-Muskwa	5170	530	530	0.7	0.05		0.1	0.15		
Slave Point	6908	117.35	117.35							
Middle Devonian	7293	106	106			0.1	0.9			
Keg River-Evie Mbr	7640	90.5	90.5							
Chinchaga	7936	78	78							
Sub-Devonian Unconformity										
Granite wash	8167	25	25							
PC basement	8192									

Table 27 Stratigraphic and lithologic information required to generate the IIR.dat file.

Event no.	Age no.	Contact Format	Age (m yrs)	Description of Event	T/F	Thickness (m)	Age
1	Age 1	38	415	Base of sequence	T	000.00	
2	Age 2	38	401	Granite wash (regolith) deposition	T	025.00	
3	Age 3	38	392	Chinchaga	T	078.00	Eifelian
4	Age 4	38	386	Keg River + Evie Mbr	T	090.5	Eifelian-Givetian
5	Age 5	38	380	Mid Devonian Sh/Lmst (?Sulphur Point)	T	106.00	Late Givetian
6	Age 6	38	377	Slave Point	T	117.00	Late Givetian
7	Age 7	38	373	Muskwa + Fort Simpson	T	530.00	Frasnian
8	Age 8	38	370	Jean Marie	T	15.20	Late Frasnian
9	Age 9	38	369	Redknife	T	142.80	
10	Age 10	38	367	Kakisa + Trout River	T	672.00	Fammenian
11	Age 11	38	365	Tetchó	T	076.00	Fammenian
12	Age 12	38	363	Kotcho	T	212.5	Fammenian
13	Age 13	38	353	Exshaw + Banff	T	370.00	late Fammenian-T1
14	Age 14	38	350	Rundle-part remaining (Pekisko)	T	003.00	Tournaisian -
T2 15	Age 15	26	347	Rundle	F	310.00	Tournaisian -
T3				(part eroded at Sub-Cretaceous Unconformity)			
16	Age 16	19	346	Rundle deposition Tournasian	F	025.00	Tournaisian-
T3				(part eroded at Sub-Permian Unconformity)			
17	Age 17	18	330	Mattson	F	150.00	Serphukovian
18	Age 18	38	295	Sub-Permian Unconformity (Mattson erosion)	T	000.00	
19	Age 19	38	290	Sub-Permian Unconformity (Rundle erosion)	F	000.00	
20	Age 20	25	280	Kindle	F	020.00	Ass-Sak-Art
21	Age 21	22	262	Fantasque	F	025.00	Guad (Road-War)
22	Age 22	38	250	Sub-Triassic Unconformity (Fantasque erosion)	T	000.00	
23	Age 23	24	230	Toad-Grayling	F	140.00	Scythian-Norian
24	Age 24	38	205	Sub-Cretaceous unconformity (Toad-Grayling erosion)	T	000.00	
25	Age 25	38	190	Sub-Cretaceous unconformity (Kindle erosion)	T	000.00	
26	Age 26	38	185	Sub-Cretaceous unconformity (Rundle erosion)	T	000.00	
27	Age 27	38	112	Buckinghorse	T	197.5	Early-mid Albian
28	Age 28	38	108	Sikanni	T	085.00	M. Albian
29	Age 29	38	102	Sully	T	177.00	Late Albian
30	Age 30	38	96	Dunvegan deposition -part remainimg	T	166.00	M-Late Cenomanian
31	Age 31	36	95	Dunvegan deposition -part eroded at Sub-Cretaceous Unconformity	F	084.00	
32	Age 32	35	85	Kotaneelee	F	200.00	Santon-Campanian
33	Age 33	34	71	Wapiti	F	200.00	Maastrichtian
34	Age 34	38	65	Sub-Tertiary unconformity (Wapiti erosion)	T	000.00	
35	Age 35	38	60	Sub-Tertiary unconformity (Kotaneelee erosion)	T	000.00	
36	Age 36	38	40	Sub-Tertiary Unconformity (Dunvegan erosion)	T	000.00	
37	Age 37	38	02	Quaternary deposition	T	020.00	

Table 28 Stratigraphy and reconstructed burial history of the Imperial Island River No.1 section.

Imperial Island River No.1 G-50

Column # 1 Thickness (m)	2 T/F	3 Event #	4 Sh	5 Sst	6 Lst	7 Dol	8 Silt	9 Evap	10 Chert	11 Heat flow*	12 T°C**	13 AGE
0000.0	T	38	0.000	0.000	0.000	0.000	0.000	0.000	0.000	080.0	025.0	AGE1
0025.0	T	38	0.600	0.020	0.000	0.000	0.200	0.000	0.000	080.0	025.0	AGE2
0078.0	T	38	0.100	0.000	0.000	0.250	0.450	0.200	0.000	080.0	025.0	AGE3
0090.5	T	38	0.000	0.000	0.100	0.800	0.100	0.000	0.000	080.0	025.0	AGE4
0106.0	T	38	0.000	0.000	0.100	0.900	0.000	0.000	0.000	080.0	025.0	AGE5
0117.0	T	38	0.000	0.000	0.200	0.800	0.000	0.000	0.000	150.0	025.0	AGE6
0530.0	T	38	0.700	0.050	0.000	0.100	0.150	0.000	0.000	150.0	025.0	AGE7
0015.2	T	38	0.000	0.000	0.650	0.350	0.000	0.000	0.000	150.0	025.0	AGE8
0140.2	T	38	0.700	0.000	0.000	0.050	0.200	0.000	0.000	150.0	025.0	AGE9
0672.0	T	38	0.100	0.600	0.100	0.000	0.200	0.000	0.000	150.0	025.0	AGE10
0076.0	T	38	0.000	0.000	0.850	0.150	0.000	0.000	0.000	150.0	025.0	AGE11
0212.5	T	38	0.650	0.000	0.350	0.000	0.000	0.000	0.000	150.0	025.0	AGE12
0370.0	T	38	0.600	0.000	0.300	0.000	0.100	0.000	0.000	140.0	025.0	AGE13
0003.0	T	38	0.150	0.000	0.850	0.000	0.000	0.000	0.000	140.0	025.0	AGE14
0310.0	F	26	0.000	0.000	0.400	0.000	0.000	0.000	0.600	140.0	025.0	AGE15
0025.0	F	19	0.500	0.000	0.400	0.000	0.000	0.000	0.100	120.0	025.0	AGE16
0150.0	F	18	0.150	0.600	0.050	0.000	0.200	0.000	0.000	120.0	025.0	AGE17
0000.0	T	38	0.000	0.000	0.000	0.000	0.000	0.000	0.000	120.0	025.0	AGE18
0000.0	T	38	0.000	0.000	0.000	0.000	0.000	0.000	0.000	100.0	025.0	AGE19
0020.0	F	25	0.250	0.500	0.000	0.000	0.250	0.000	0.000	100.0	025.0	AGE20
0025.0	F	22	0.500	0.000	0.000	0.000	0.000	0.000	0.500	100.0	025.0	AGE21
0000.0	T	38	0.000	0.000	0.000	0.000	0.000	0.000	0.000	080.0	025.0	AGE22
0140.0	F	24	0.200	0.000	0.000	0.100	0.700	0.000	0.000	080.0	025.0	AGE23
0000.0	T	38	0.000	0.000	0.000	0.000	0.000	0.000	0.000	080.0	025.0	AGE24
0000.0	T	38	0.000	0.000	0.000	0.000	0.000	0.000	0.000	080.0	025.0	AGE25
0000.0	T	38	0.000	0.000	0.000	0.000	0.000	0.000	0.000	080.0	025.0	AGE26
0197.5	T	38	0.800	0.000	0.000	0.000	0.200	0.000	0.000	080.0	025.0	AGE27
0085.0	T	38	0.000	1.000	0.000	0.000	0.000	0.000	0.000	080.0	015.0	AGE28
0177.0	T	38	0.500	0.200	0.000	0.000	0.300	0.000	0.000	060.0	015.0	AGE29
0166.0	T	38	0.000	1.000	0.000	0.000	0.000	0.000	0.000	060.0	015.0	AGE30
0084.0	F	36	0.000	1.000	0.000	0.000	0.000	0.000	0.000	060.0	015.0	AGE31
0400.0	F	35	0.700	0.150	0.000	0.000	0.150	0.000	0.000	060.0	015.0	AGE32
0350.0	F	34	0.000	0.500	0.000	0.000	0.500	0.000	0.000	060.0	015.0	AGE33
0000.0	T	38	0.000	0.000	0.000	0.000	0.000	0.000	0.000	060.0	015.0	AGE34
0000.0	T	38	0.000	0.000	0.000	0.000	0.000	0.000	0.000	080.0	010.0	AGE35
0000.0	T	38	0.000	0.000	0.000	0.000	0.000	0.000	0.000	080.0	010.0	AGE36
0020.0	T	38	0.000	0.500	0.000	0.000	0.500	0.000	0.000	080.0	010.0	AGE37

* m W/m^{-1} sec^{-1} ** average surface temperature for given age: Devonian-Carboniferous: 25°C; Jurassic-Cretaceous: 25°C; Tertiary: 15°C; present day: 10°C

Table 29 Input .dat file for Burial 3a thermal history modeling of Imperial Island River No. 1.

Model #	Thermal characteristics	K-S Statistic	Probability	Predicted Ro and measured Ro data (ScalcRo)
1	as per Table 29; high heat flow (150 mW/m/sec) in the Middle & Upper Devonian gradually decreasing to present day (85 mW/m/sec)	9.47E-01	1.34E-08	$R^2 = 0.95$
2	high heat flow throughout the Palaeozoic with abrubt decrease in post Permian times	6.96E-01	8.42E-01	$R^2 = 0.94$
3	consistently high Palaeozoic heat flow to Permian gradually decreasing to present day	8.42E-01	6.97E-07	$R^2 = 0.94$
4	elevated heat flow (100 mW/m/sec) during the Laramide (Cretaceous-Tertiary)	8.42E-01	6.77E-07	$R^2 = 0.91$
5	higher Devonian heat flow (200 mW/m/sec)	8.42E-01	6.97E-07	$R^2 = 0.92$
6	higher heat flow (200 mW/m/sec) extended into the Cretaceous ; relatively low Tertiary heat flow (100mW/m/sec)	5.88E-01	1.77E-03	$R^2 = 0.94$
7	high Devonian heat flow (200 mW/m/sec) extended into Cretaceous; higher Tertiary heat flow (150 mW/m/sec)	5.26E-01	6.00E-03	$R^2 = 0.94$
8	consistent heat flow (150 mW/m/sec) to present day	5.26E-01	6.40E-03	$R^2 = 0.96$
9	consistent heat flow (150mW/m/sec) except for periods of uplift during Permian to Cretaceous	5.26E-01	6.005E-03	$R^2 = 0.96$

Table 30 Results of thermal modeling of Ro data from the Imperial Island River No.1.

Meas Ro	Predicted Ro (from Scalc Ro file) for Model # 1							
Vro*	1	2	3	4	5	6	7	8/9
0.77	0.30	0.30	0.30	0.35	0.34	0.35	0.50	0.85
0.89	0.30	0.30	0.30	0.42	0.41	0.42	0.62	0.94
0.93	0.34	0.35	0.34	0.42	0.42	0.42	0.63	1.07
0.93	0.34	0.35	0.35	0.42	0.42	0.42	0.63	1.07
0.93	0.35	0.35	0.35	0.42	0.42	0.50	0.73	1.16
0.94	0.35	0.42	0.42	0.50	0.50	0.50	0.73	1.26
0.94	0.35	0.42	0.42	0.50	0.50	0.50	0.73	1.26
0.91	0.35	0.42	0.42	0.50	0.50	0.62	0.74	1.33
0.93	0.41	0.42	0.42	0.50	0.50	0.62	0.74	1.35
1.07	0.42	0.50	0.50	0.50	0.51	0.73	0.85	1.48
1.08	0.42	0.50	0.50	0.62	0.62	0 .73	0.86	1.59
1.09	0.50	0.62	0.62	0.62	0.62	0.85	1.10	1.76
1.17	0.62	0.73	0.73	0.73	0.73	1.37	1.37	2.24
1.22	0.62	0.73	0.73	0.73	0.74	1.37	1.38	2.33
1.25	0.62	0.73	0.73	0.73	0.74	1.37	1.38	2.34
1.30	0.73	0.85	0.85	0.86	0.86	1.71	1.72	2.74
1.33	0.73	0.86	0.86	0.86	0.86	1.71	1.72	2.84
1.37	0.74	1.10	1.10	1.10	1.10	2.12	2.12	3.20
1.41	0.85	1.10	1.10	1.10	1.10	2.12	2.13	3.29
R2 =	0.95	0.94	0.94	0.91	0.92	0.94	0.94	0.96

* vitrinite reflectance equivalent, calculated from amorphous (type 4) bitumen Ro

Table 31 Measured and predicted Ro values from the Imperial Island River No. 1.

reflectance (VR_o) values are calculated from the amorphous (type 4) bitumen reflectance(R_om) values.

Model #1 produces the best K-S Statistic (i.e. value closest to 1.0; 9.47E-01) while model # 2 shows the highest probability (8.42E -01); both models suggest that high heat flow prevailed during the Upper Devonian and significantly low values during the Mesozoic and Cenozoic. The principal difference between the two models is the rate of declining heat flow over time. In model #1, the heat flow decline is gradual and in model #2 it occurs abruptly in post-Permian times. Direct comparisons between the measured and predicted R_o values (from Burial 3b output file "Scalc.Ro"; Table 31) would suggest that the fit of the predicted Ro values to the measured Ro is not very good for any of the models; however, strong relationships between measured and predicted Ro values are confirmed by linear regression analysis (R^2 values in column 5, Table 30). While high heat flows in the Upper Devonian followed by lower Mesozoic and Cenozoic values satisfies the burial history model, the predicted Ro values for the Upper Devonian fall significantly short of the measured Ro values. Increasing the heat flows in the Carboniferous (models 7- 9) produces a better match for the predicted and measured Ro values but pushes the predicted upper Devonian data far beyond the actual values. The model is therefore only sensitive to major and long-lasting changes in heat flow and does not readily respond to minor adjustments.

Canada Southern *et al.*, North Beaver River I-46

The stratigraphic and lithological information required to compile the CSNBR.dat input file is shown in Table 32 The stratigraphy and reconstructed burial history, also required to generate the CSNBR.dat and CSNBR.age input files are shown in Table 33. The CSNBR.dat file for the first model run with the Burial 3a program is shown in Table 34.

Five heat flow models were used in this exercise. The input files are included in Appendix E12 to E18.The heat flow scenario for CSNBR model #1 is the same as that of Model #1 for the Imperial Island River section, the other four have different heat flow combinations which are summarized in Table 35. The results of the second part of the Burial 3b program (Scalc.Ro files), which compares the measured and predicted Ro

Formation	Fm top	present thickness	original thickness	Lithology						
	ft	m	m	shale	sst	lst	dol	siltst	evap	chert
Quaternary		0.0	15		0.5			0.5		
Wapiti		0.0	150		0.5			0.5		
Kotaneelee		0.0	50	0.70	0.15			0.15		
Sub-Tertiary Unconformity										
Dunvegan		0.0	50		1.0					
Sully		0.0	150	0.5	0.2		0.3			
Sikanni		0.0	30		1.0					
Lepine		0.0	170	0.8	0.1			0.1		
Scatter	1470	57.9	70		0.5			0.5		
Garbutt		225	225	0.25	0.5			0.25		
Sub-Cretaceous Unconformity										
Toad-Grayling		348.4	800	0.8	0.1			0.1		
Sub-Triassic Unconformity										
Fantasque		175	190	0.5					0.5	
Kindle		158	158	0.25	0.5			0.25		
Sub-Permian Unconformity										
Mattson	3559	695	1020	0.15	0.65			0.2		
Golata	5690	274	274	0.75	0.1			0.15		
Prophet	6590	765	765	0.25		0.5			0.25	
Besa River -up	9100	594	594	0.85				0.1	0.05	
Besa River -lr	11049	338.3	338.3	0.95					0.05	
Nahanni	12160	213.7	213.70				0.95		0.05	
Headless	12861	197.1	197.07	0.05			0.95			
Sub-Headless (Devonian Carbonates)	13508	176.8	176.80		0.05		0.95			
Base of sequence	14080									

Table 32 Stratigraphic and lithological information required to generate the CSNBR.dat file.

Event no.	Age no.	Contact Format	Age (m yrs)	Description of Event	T/F	Thickness (m)	Age
1	Age 1	37	410	Base of sequence	T	000.00	Seginin-Eifellian
2	Age 2	37	400	Sub-Headless (carbonates) deposition	T	177.00	Eifelian
3	Age 3	37	385	Headless deposition	T	197.00	Eifelian
4	Age 4	37	380	Nahanni deposition	T	214.00	Eifelian-Givetian
5	Age 5	37	370	Besa River-lower deposition	T	338.00	Givetian-Frasnian
6	Age 6	37	360	Besa River -upper deposition	T	594.00	Fras'n-Fammenian
7	Age 7	37	346	Prophet deposition	T	765.00	Tournaisian (T3)
8	Age 8	37	334	Golata deposition	T	274.00	Viséan (V2-V3)
9	Age 9	37	330	Mattson - Lr , deposition remaining part	T	695.00	Viséan (V3)
10	Age 10	11	324	Mattson - Upper, deposition (eroded at sub-Permian Unconformity)	F	325.00	V3-Serphukhovian
11	Age 11	36	285	Sub-Permian Unconformity	T	000.00	
12	Age 12	36	274	Kindle deposition	T	158.00	Artinskian
13	Age 13	36	260	Fantasque deposition, part remaining	T	175.00	Kazanian-Tatarian
14	Age 14	36	255	Fantasque deposition (eroded at sub-Triassic Unconformity)	T	015.00	Tatarian
15	Age 15	36	250	Sub-Triassic Unconformity	T	000.00	
16	Age 16	36	240	Toad-Grayling deposition (remaining part	T	348.4	Anisian
17	Age 17	18	220	Toad-Grayling deposition (eroded at sub-Permian Unconformity)	F	452.00	
18	Age 18	36	160	Sub-Cretaceous Unconformity	T	000.00	
19	Age 19	36	112	Garbutt deposition	T	225.00	Albian
20	Age 20	36	108	Scatter deposition	T	057.90	Albian
21	Age 21	34	107	Scatter deposition (part remaining) (eroded at sub-Tertiary Unconformity)	F	012.00	L-M. Albian
22	Age 22	33	105	Lepine deposition	F	170.0	M. Albian
23	Age 23	32	103	Sikanni deposition	F	030.00	Up. Albian
24	Age 24	31	100	Sully deposition (Toad-Grayling erosion)	F	150.00	Up. Albian
25	Age 25	30	96	Dunvegan deposition	F	050.00	Cenomanian
26	Age 26	29	85	Kotaneellee deposition	F	050.00	Santonian
27	Age 27	28	77	Wapiti	F	150.00	Campanian
28	Age 28	36	60	Sub-Tertiary Unconformity	T	000.00	
29	Age 29	36	55	Sub-TU - Kotaneelee erosion	T	000.00	
30	Age 30	36	53	Sub-TU - Dunvegan erosion	T	000.00	
31	Age 31	36	49	Sub-TU- Sully erosion	T	000.0	
32	Age 32	36	47	Sub-TU - Sikanni erosion	T	000.00	
33	Age 33	34	45	Sub-TU - Lepine erosion	T	000.00	
34	Age 34	36	44	Sub-TU - Scatter erosion	T	000.00	
35	Age 35	36	0.5	Quaternary deposition			

Table 33 Stratigraphy and reconstructed burial history from Canada Southern *et al.* North Beaver River YT I-27.

Canada Southern *et al.* N. Beaver R YT I-27

Column # 1 Thickness (m)	2 T/F	3 Event #	4 Sh	5 Sst	6 Lst	7 Dol	8 Silt	9 Evap	10 Chrt	11 Heat flow*	12 T°C**	13 AGE
0000.0	T	36	0.000	0.000	0.000	0.000	0.000	0.000	0.000	080.0	025.0	AGE1
0176.8	T	36	0.000	0.050	0.000	0.950	0.000	0.000	0.000	080.0	025.0	AGE2
0197.1	T	36	0.050	0.000	0.000	0.950	0.000	0.000	0.000	080.0	025.0	AGE3
0213.7	T	36	0.000	0.000	0.000	0.950	0.000	0.000	0.050	080.0	025.0	AGE4
0338.3	T	36	0.950	0.000	0.000	0.000	0.000	0.000	0.050	080.0	025.0	AGE5
0594.0	T	36	0.850	0.000	0.000	0.000	0.100	0.000	0.050	150.0	025.0	AGE7
0274.0	T	36	0.750	0.100	0.000	0.000	0.150	0.000	0.000	150.0	025.0	AGE8
0695.0	T	36	0.150	0.650	0.000	0.000	0.200	0.000	0.000	150.0	025.0	AGE9
0325.0	F	11	0.150	0.650	0.000	0.000	0.200	0.000	0.000	150.0	025.0	AGE10
0000.0	T	36	0.000	0.000	0.000	0.000	0.000	0.000	0.000	150.0	025.0	AGE11
0158.0	T	36	0.250	0.500	0.000	0.000	0.250	0.000	0.000	150.0	025.0	AGE12
0175.0	T	36	0.500	0.000	0.000	0.000	0.000	0.000	0.500	140.0	025.0	AGE13
0015.0	F	15	0.500	0.000	0.000	0.000	0.000	0.000	0.500	140.0	025.0	AGE14
0000.0	T	36	0.000	0.000	0.000	0.000	0.000	0.000	0.000	140.0	025.0	AGE15
0348.4	T	36	0.800	0.100	0.000	0.000	0.100	0.000	0.000	120.0	025.0	AGE16
0452.0	F	18	0.800	0.100	0.000	0.000	0.100	0.000	0.000	120.0	025.0	AGE17
0000.0	T	36	0.000	0.000	0.000	0.000	0.000	0.000	0.000	120.0	025.0	AGE18
0225.0	T	36	0.250	0.500	0.000	0.000	0.250	0.000	0.000	100.0	025.0	AGE19
0057.9	T	36	0.000	0.500	0.000	0.000	0.500	0.000	0.000	100.0	025.0	AGE20
0012.0	F	34	0.000	0.500	0.000	0.000	0 500	0.000	0.000	080.0	025.8	AGE21
0170.0	F	33	0.800	0.100	0.000	0.000	0.100	0.000	0.000	080.0	025.0	AGE22
0030.0	F	32	0.000	1.000	0.000	0.000	0.000	0.000	0.000	080.0	025.0	AGE23
0150.0	F	31	0.500	0.200	0.000	0.000	0.300	0.000	0.000	080.0	025.0	AGE24
0050.0	F	30	0.000	1.000	0.000	0.000	0.000	0.000	0.000	080.0	025.0	AGE25
0050.0	F	29	0.700	0.150	0.000	0.000	0.150	0.000	0.000	080.0	025.0	AGE26
0150.0	F	28	0.000	0.500	0.000	0.000	0.500	0.000	0.000	080.0	025.0	AGE27
0000.0	T	36	0.000	0.000	0.000	0.000	0.000	0.000	0.000	080.0	015.0	AGE28
0000.0	T	36	0.000	0.000	0.000	0.000	0.000	0.000	0.000	060.0	015.0	AGE29
0000.0	T	36	0.000	0.000	0.000	0.000	0.000	0.000	0.000	060.0	015.0	AGE31
0000.0	T	36	0.000	0.000	0.000	0.000	0.000	0.000	0.000	060.0	015.0	AGE32
0000.0	T	36	0.000	0.000	0.000	0.000	0.000	0.000	0.000	060.0	015.0	AGE33
0000.0	T	36	0.000	0.000	0.000	0.000	0.000	0.000	0.000	060.0	015.0	AGE34
0000.0	T	36	0.000	0.000	0.000	0.000	0.000	0.000	0.000	080.0	010.0	AGE35
0015.0	T	37	0.000	0.500	0.000	0.000	0.500	0.000	0.000	080.0	010.0	AGE36

* mW/m^{-1} sec^{-1}

** average surface temperature for given age: Devonian-Carboniferous: 25°C; Jurassic-Cretaceous: 25°C; Tertiary: 15°C; present day: 10°C

Table 34 Input.dat file for Burial 3a thermal history modeling of Canada Southern *et al.* North Beaver River YT I-27.

values, are shown in Table 36. Model #3, which advocates high heat flow throughout the Upper Palaeozoic and Mesozoic (ca. 100mW/m/sec), gives the highest K-S Statistic and probability and good correlations ($R^2 = 0.96$) between measured and predicted Ro values. However, Model #1 has similar probability and correlation coefficient to model #3 (Table 35) and model #1 produced the best fit for the Imperial Island River section. Comparisons between the measured and predicted VR_o values from each of the models are shown in Table 36. In all cases, except model #3, the predicted Ro values exceed the measured Ro values for the Devonian significantly. Conversely, predicted Ro values from models #3 and #4 are a better match for the measured values from the top of the Carboniferous section (Table 36). While the apparent fit of the Ro values does appear to be strong, linear regression analysis shows that there are good correlations between measured and predicted VR_o values from models 1, 2 and 3 ($R^2 = 0.96$, 0.94 and 0.96 respectively; see Table 35). Although models #4 and #5, which advocate low Devonian heat flows, show significantly lower correlation coefficients and probabilities (Table 35) and yet the predicted Ro values are a better match for the vitrinite reflectance equivalent data (derived from the type 4 bitumen reflectance). Predicted Ro values from model #1 show the best match for the Upper Devonian measured Ro values (see Ro values located at the bottom of columns VRo and #1, Table 36).

Pan Am Beaver River G-01

The stratigraphic and lithologic information required to compile the .dat input file for the Burial 3a program to model the Pan Am Beaver River G-01 section was derived from geophysical log data and examination of drill cuttings samples (see Table 37). The chronostratigraphic data also required for the .dat input file is shown in Table 38; this file was compiled by analysis of the regional stratigraphy and dates according to the Geologic Time chart published by Okulich *et al.* (1995).

Five thermal history models were run with the Pan Am Beaver Ro data; the input files for these are included in Appendix E 19-25. The .dat files for the the first model is show in Table 39; the heat flow scenario used is similar to that of Morrow *et al.* (1993) which is similar to the model #1 of the Imperial Island River and Canada Southern *et al.* I-27 sections. Details of the .dat input files for the other four models are given in

Model #	Thermal characteristics	K-S Statistic	Probability	Predicted Ro and measured Ro data (ScalcRo)
1	as per Table 34; high heat flow (150 mW/m/sec) begins in Upper Devonian-Carboniferous gradually decreasing to present day (85 W/m/sec)	3.809E-01	7.05E-02	$R^2 = 0.96$
2	increased heat flow in middle Devonian and throughout the upper Palaeozoic with gradual decrease to present day	3.809E-01	7.05E-02	$R^2 = 0.94$
3	consistently high Palaeozoic heat flow (100 mW/m/sec) to Cretaceous gradually decreasing to present day	6.66E-01	7.13E-05	$R^2 = 0.96$
4	elevated heat flow (200 mW/m/sec) in Upper Devonian to Cretaceous	6.19E-01	2.92E-04	$R^2 = 0.64$
5	low Devonian heat flow (60 mW/m/sec) with abrupt increase (150 mW/m/sec) at the Devonian - Carboniferous boundary and increasing to 200 mW/m/sec during Late Palaeozoic - Triassic time	6.19E-01	2.92E-04	$R^2 = 0.67$

Table 35 Results of thermal modeling of Ro data from the Canada Southern *et al.* North Beaver River YT I-27.

Meas Ro*	Predicted Ro (from Scalc.Ro file) for Model #				
VRo	1	2	3	4	5
0.89	0.50	0.50	0.42	0.85	0.85
0.97	0.50	0.50	0.42	0.86	0.86
1.08	0.62	0.62	0.50	1.11	1.11
1.12	0.62	0.62	0.50	1.37	1.37
1.24	0.63	0.63	0.50	1.38	1.38
1.21	0.73	0.73	0.62	1.71	1.71
1.30	0.85	0.85	0.63	2.12	2.12
1.23	0.86	0.86	0.73	2.54	2.54
1.38	1.10	1.10	0.74	3.04	3.04
1.39	1.11	1.11	0.85	3.50	3.50
1.46	1.11	1.37	0.85	3.90	3.51
1.52	1.37	1.38	0.86	3.91	3.91
1.56	1.38	1.70	1.10	3.91	3.91
1.45	1.38	1.71	1.10	4.20	3.91
1.70	1.38	1.71	1.10	4.20	4.20
1.76	1.71	2.12	1.11	4.50	4.20
1.80	1.72	2.13	1.11	4.68	4.50
1.86	2.12	2.55	1.37	4.70	4.70
2.40	2.54	3.90	1.70	4.70	4.70
2.56	2.54	3.04	1.71	4.70	4.70
2.9	3.51	4.20	2.13	4.70	4.70
R2	0.96	0.94	0.96	0.64	0.66

* vitrinite reflectance equivalent, calculated from amorphous (type 4) bitumen Ro

Table 36 Measured and predicted Ro values from the Canada Southern *et al.* North Beaver River YT I-27 section.

Formation	Fm top	present thickness	original thickness	Lithology					
	ft	m	m	shale	sst	lst	dol	siltst	evap	chert
Quaternary		15.0	15		0.5			0.5		
Wapiti		0.0	140		0.5			0.5		
Kotaneelee		0.0	45	0.70	0.15			0.15		
Sub-Tertiary Unconformity										
Dunvegan		0.0	45		1.0					
Sully		0.0	140	0.5	0.2		0.3			
Sikanni		0.0	25		1.0					
Lepine		0.0	163	0.8	0.1				0.1	
Scatter	1207	0.0	70		0.5				0.5	
Garbutt		122.0	152	0.25	0.5				0.25	
Sub-Cretaceous Unconformity										
Toad-Grayling		297.0	800	0.8	0.1				0.1	
Sub-Triassic Unconformity										
Fantasque	1424	189.0	200	0.5						0.5
Kindle	2090	220.0	220	0.25	0.5			0.25		
Sub-Permian Unconformity										
Mattson	2765	9450.0	1200	0.15	0.65			0.2		
Golata	5860	1254.0	1254	0.75	0.1			0.15		
Prophet	9978	89.0	89	0.25		0.5				0.25
Besa River -up	10270	411.0	411	0.85				0.1		0.05
Besa River -lr	12143	571.0	571	0.95						0.05
Nahanni	13492	247.0	247				0.95			0.05
Headless	12861	30.0	30	0.05			0.95			
Sub-Headless (Devonian Carbonates)	13508	1200.0	1200		0.05		0.95			
Base of sequence	14080									

Table 37 Stratigraphic and lithological information required to generate the Pan Am Beaver River G-01.dat file.

Event no.	Age no.	Contact Format	Age (m yrs)	Description of Event	T/F	Thickness (m)	Age
1	Age 1	37	396	Base of sequence	T	000.00	Up Silurian
2	Age 2	37	384	Sub-Headless (carboniates) deposition	T	1200.00	Pridolian-Emsian
3	Age 3	37	383	Headless deposition	T	30.00	Eifelian
4	Age 4	37	376	Nahanni deposition	T	247.00	Eifelian
5	Age 5	37	360	Besa River-lower deposition	T	571.00	Frasnian
6	Age 6	37	354	Besa River -upper deposition	T	411.00	Tournaisian
7	Age 7	37	344	Prophet deposition	T	89.00	Tournaisian -Viséan
8	Age 8	37	337	Golata deposition	T	1254.00	Viséan (V2-V3)
9	Age 9	37	289	Mattson - Lr , deposition remaining part	T	945.00	Viséan (V3)
10	Age 10	11	276	Mattson - Upper, deposition	F	225.00	V3-Serphukhovian
				(eroded at sub-Permian Unconformity)			
11	Age 11	36	286	Sub-Permian Unconformity	T	000.00	
12	Age 12	36	258	Kindle deposition	T	220.00	Artinskian
13	Age 13	36	246	Fantasque deposition, part remaining	T	189.00	Perm (Kaz-Tar)
14	Age 14	36	245	Fantasque deposition	T	011.00	Kazanian-Tartarian
				(eroded at sub-Triassic Unconformity)			
15	Age 15	36	240	Sub-Triassic Unconformity	T	000.00	
16	Age 16	36	240	Toad-Grayling deposition (remaining pt)	T	297.0	Triassic
17	Age 17	18	208	Toad-Grayling deposition	F	503.00	
				(eroded at sub-Permian Unconformity)			
18	Age 18	36	113	Sub-Cretaceous Unconformity	T	000.00	
19	Age 19	36	111	Garbutt deposition (part remaining)	T	122.00	Albian
20	Age 20	36	109	Garbutt deposition	T	30.00	Albian
				(eroded at sub-Tertiary Unconformity)	F		
21	Age 21	34	106	Scatter deposition	F	070.00	Albian
				(eroded at sub-Tertiary Unconformity)			
22	Age 22	33	102	Lepine deposition	F	163.00	Albian
				(eroded at sub-Tertiary Unconformity)			
23	Age 23	32	101	Sikanni deposition	F	025.00	Albian
				(eroded at sub-Tertiary Unconformity)			
24	Age 24	31	98	Sully deposition	F	140.00	Albian-Cenomanian
				(eroded at sub-Tertiary Unconformity)			
25	Age 25	30	87.5	Dunvegan deposition	F	045.00	Cenomanian
				(eroded at sub-Tertiary Unconformity)			
26	Age 26	29	74.5	Kotaneellee deposition	F	050.00	Santonian-Campanian
				(eroded at sub-Tertiary Unconformity)			
27	Age 27	28	67	Wapiti	F	150.00	Maastrichtian
				(eroded at sub-Tertiary Unconformity)			
28	Age 28	36	62	Sub-Tertiary Unconformity	T	000.00	
29	Age 29	36	60.5	Sub-TU - Kotaneelee erosion	T	000.00	
30	Age 30	36	59	Sub-TU - Dunvegan erosion	T	000.00	
31	Age 31	36	54	Sub-TU- Sully erosion	T	000.0	
32	Age 32	36	53	Sub-TU - Sikanni erosion	T	000.00	
33	Age 33	34	48	Sub-TU - Lepine erosion	T	000.00	
34	Age 34	36	46	Sub-TU - Scatter erosion	T	000.00	
35	Age 35	36	45	Sub-TU- Garbutt erosion	T	000.00	
36	Age 36	37	0.5	Quaternary deposition	T	015.00	Pleistocene

Table 38 Stratigraphy and reconstructed burial history from Pan Am Beaver River G-01.

Pan Am Beaver River YT G-01

Column # 1 Thickness (M)	2 T/F	3 Event	4 Sh	5 Sst	6 Lst	7 Dol	8 Silt	9 Evap	10 Chrt	11 Heat	12 T°C	13 AGE
0000.0	T	37	0.000	0.000	0.000	0.000	0.000	0.000	0.000	080.0	025.0	AGE1
1200.0	T	37	0.000	0.050	0.000	0.950	0.000	0.000	0.000	080.0	025.0	AGE2
0030.0	T	37	0.050	0.000	0.000	0.950	0.000	0.000	0.000	080.0	025.0	AGE3
0247.0	T	37	0.000	0.000	0.000	0.950	0.000	0.000	0.050	080.0	025.0	AGE4
0571.0	T	37	0.950	0.000	0.000	0.000	0.000	0.000	0.050	080.0	025.0	AGE5
0411.0	T	37	0.850	0.000	0.000	0.000	0.100	0.000	0.050	150.0	025.0	AGE6
0089.0	T	37	0.250	0.000	0.500	0.000	0.000	0.000	0.250	150.0	025.0	AGE7
1254.0	T	37	0.750	0.100	0.000	0.000	0.150	0.000	0.000	150.0	025.0	AGE8
0945.0	T	37	0.150	0.650	0.000	0.000	0.200	0.000	0.000	150.0	025.0	AGE9
0255.0	F	11	0.150	0.650	0.000	0.000	0.200	0.000	0.000	150.0	025.0	AGE10
0000.0	T	37	0.000	0.000	0.000	0.000	0.000	0.000	0.000	150.0	025.0	AGE11
0220.0	T	37	0.250	0.500	0.000	0.000	0.250	0.000	0.000	150.0	025.0	AGE12
0189.0	T	37	0.500	0.000	0.000	0.000	0.000	0.000	0.500	140.0	025.0	AGE13
0011.0	F	15	0.500	0.000	0.000	0.000	0.000	0.000	0.500	140.0	025.0	AGE14
0000.0	T	37	0.000	0.000	0.000	0.000	0.000	0.000	0.000	140.0	025.0	AGE15
0297.0	T	37	0.800	0.100	0.000	0.000	0.100	0.000	0.000	120.0	025.0	AGE16
0503.0	F	18	0.800	0.100	0.000	0.000	0.100	0.000	0.000	120.0	025.0	AGE17
0000.0	T	37	0.000	0.000	0.000	0.000	0.000	0.000	0.000	120.0	025.0	AGE18
0122.0	T	37	0.250	0.500	0.000	0.000	0.250	0.000	0.000	100.0	025.0	AGE19
0030.0	F	35	0.250	0.500	0.000	0.000	0.250	0.000	0.000	100.0	025.0	AGE20
0070.0	F	34	0.000	0.500	0.000	0.000	0.500	0.000	0.000	100.0	025.0	AGE21
0170.0	F	33	0.800	0.100	0.000	0.000	0.100	0.000	0.000	080.0	025.0	AGE22
0030.0	F	32	0.000	1.000	0.000	0.000	0.000	0.000	0.000	080.0	025.0	AGE23
0150.0	F	31	0.500	0.200	0.000	0.000	0.300	0.000	0.000	080.0	025.0	AGE24
0050.0	F	30	0.000	1.000	0.000	0.000	0.000	0.000	0.000	080.0	025.0	AGE25
0050.0	F	29	0.700	0.150	0.000	0.000	0.150	0.000	0.000	080.0	025.0	AGE26
0150.0	F	28	0.000	0.500	0.000	0.000	0.500	0.000	0.000	080.0	025.0	AGE27
0000.0	T	37	0.000	0.000	0.000	0.000	0.000	0.000	0.000	080.0	015.0	AGE28
0000.0	T	37	0.000	0.000	0.000	0.000	0.000	0.000	0.000	060.0	015.0	AGE29
0000.0	T	37	0.000	0.000	0.000	0.000	0.000	0.000	0.000	060.0	015.0	AGE30
0000.0	T	37	0.000	0.000	0.000	0.000	0.000	0.000	0.000	060.0	015.0	AGE31
0000.0	T	37	0.000	0.000	0.000	0.000	0.000	0.000	0.000	060.0	015.0	AGE32
0000.0	T	37	0.000	0.000	0.000	0.000	0.000	0.000	0.000	060.0	015.0	AGE33
0000.0	T	37	0.000	0.000	0.000	0.000	0.000	0.000	0.000	060.0	015.0	AGE34
0000.0	T	37	0.000	0.000	0.000	0.000	0.000	0.000	0.000	080.0	010.0	AGE35
0015.0	T	37	0.000	0.500	0.000	0.000	0.500	0.000	0.000	080.0	010.0	AGE36

* mW/m/sec

Table 39 Input .dat file for thermal history modeling of Pan Am Beaver River G-01.

Appendices E22-25; the differences between the models relate mainly to heat flow with time and are summarized in Table 40, together with the statistical results of the *Burial* program. The results indicate that the heat flow scenario of model #1 appears to have the best fit for the Ro data and stratigraphic model provided (Table 40). This implies high regional heat flows during the Upper Devonian-Carboniferous which decrease gradually to the present day. Although the relationship between the measured Ro data (input file: Pan Am Beaver G-01.Ro) and the Ro data predicted by model #1 (output file from *Burial* 3b: Scalc.Ro) appears to be good (R^2 = 0.96), the apparent fit shown in Table 41 is certainly not good. The predicted values at the base of the section (4.2% Ro) far exceed the measured values (2.72% Ro). The other four models represent a variety of heat flow Correlations between the measured and predicted Ro values are reasonably good for the Pan Am Beaver River sections from models #1, #2 and #3 (R^2 = 0.96, 0.94, 0.96 respectively; Table 40). Models #1 and #3 advocate high (150 mW/m/sec) and moderately high (100 W/m/sec) heat flows in the Upper Palaeozoic, declining gradually throughout the Mesozoic and Tertiary to present day values (80 mW/m/sec; Majorowitz *et al.*, 1989). The probability of either of these models being representative of the true burial and thermal history of the Beaver River area is reasonably good (Table 40) but best for model #1 (probability 9.99E-01). Conversely, models #3 and #4, which advocate high heat flows during the Laramide orogeny and Mesozoic times, yield only moderate K-S statistical fits and significantly lower probabilities (see Table 40). Furthermore, the correlations between the measured and predicted Ro values for these two models are relatively poor (av. R^2 = 0.65).

5.5 THERMAL HISTORY OF THE LIARD BASIN

It would appear from the results of modeling that significantly higher heat flows (of the order 150 mW/m/sec) prevailed throughout the study area during the Upper Devonian and Lower Carboniferous relative to today. Furthermore, the most favoured thermal history model suggests that heat flows have been gradually declining to present day values (80 mW/m/sec). However, the Ro values predicted using such a thermal history model do not adequately satisfy the Ro values observed and any adjustments in the model to produce a better fit to the measured and predicted Ro data requires significant changes

Model #	Thermal characteristics	K-S Statistic	Probability	Predicted Ro and measured Ro data (ScalcRo)
1	as per Table 39; high heat flow (150 mW/m/sec) begins in Upper Devonian-Carboniferous gradually decreasing to present day (85 mW/m/sec)	9.52E-02	9.99E-01	$R^2 = 0.96$
2	low Upper Devonian-Carboniferous heat flow (60 mW/m/sec) followed by high Laramide heat flow (150 mW/m/sec) declining to present day	6.25E-01	7.33E-04	$R^2 = 0.94$
3	mod high Visean -Cretaceous heat flow (100 mW/m/sec) to Cretaceous gradually decreasing to present day	3.33E-01	1.09E-01	$R^2 = 0.96$
4	consistent, elevated heat flow (120m W/m/sec) Visean to Cretaceous	4.16E-01	2.13E-02	$R^2 = 0.64$
5	low Devonian heat flow (80 mW/m/sec) with abrupt increase (180 mW/m/sec) in Visean to Triassic time gradual decline to present day	5.41E-01	9.32E-04	$R^2 = 0.67$

Table 40 Results of thermal modeling of Ro data from the Pan Am Beaver River G-01 section.

200

Meas Ro*	Predicted Ro (from Scalc.Ro file) for Model #				
VRo	1	2	3	4	5
0.77	0.50	0.63	0.42	0.50	0.50
0.81	0.50	0.73	0.50	0.50	0.62
0.84	0.62	0.74	0.51	0.62	0.62
0.92	0.63	0.85	0.63	0.63	0.63
1.14	0.74	1.10	0.73	0.85	0.86
1.27	0.86	1.38	0.73	0.86	1.10
1.31	1.10	1.71	0.74	1.10	1.11
1.31	1.10	2.12	0.86	1.10	1.11
1.34	1.37	3.04	1.37	1.38	1.71
1.36	1.72	3.51	1.38	1.72	2.54
1.35	2.12	3.51	1.71	2.12	2.55
1.46	2.54	3.91	1.71	2.54	3.51
1.49	2.55	3.91	1.72	2.54	3.51
1.56	2.55	3.91	1.72	2.54	3.51
1.65	2.55	4.20	1.72	2.55	3.91
1.89	3.04	4.52	2.12	3.04	3.91
2.09	3.51	4.52	2.13	3.50	4.20
2.16	3.51	4.69	2.54	3.51	4.52
2.19	3.91	4.69	2.55	3.51	4.69
2.50	3.91	4.69	2.55	3.91	4.69
2.56	4.20	4.69	3.04	3.91	4.69
2.69	4.20	4.69	3.04	3.91	4.69
2.52	4.20	4.69	3.04	4.20	4.69
2.72	4.20	4.69	3.04	4.20	4.69
R^2	0.93	0.76	0.94	0.93	0.84

* vitrinite reflectance equivalent, calculated from amorphous (type 4) bitumen Ro

Table 41 Measured and predicted Ro values generated by the Burial 3 program using Pan Am Beaver River G-01 models.

to the burial model. There are a number of factors to consider with regard to the unconvincing relationships between the Ro values:

(i) bitumen R_o data from which the VRo data are derived, may not be a good indicators of thermal maturation;

(ii) the *Burial* modeling program is not sensitive enough to minor adjustments in the thermal history;

(iii) the thermal maturation patterns observed within the Liard Basin and associated regions may not simply be a function of burial.

In Chapters 3 and 4 of this document, sufficient evidence has been presented to conclude that bitumen reflectance, measured on a genetically-specified population of indigenous bitumens and converted to a vitrinite reflectance equivalent, either using Jacob's equation or one of those shown in Table 11, is an acceptable if not preferred indication of organic maturation in marine sedimentary rocks.

Modeling programs such as Burial are based on the fairly simple assumption the thermal maturation is a function of time and temperature (Lopatin, 1971; Waples, 1980). Mukhopahyay *et al.* (1994b) used a kinetic model (*Basinmod*[1]) in thermal modelling of the Mesozoic and Tertiary of the Scotian Shelf and achieved a reasonably good fit between the measured and predicted Ro values but pointed out that the observed discrepancies could be attributed to abnormal heat transfer associated with changes in the thermal conductivities of the rocks. While the *Burial* program accounts for compaction due to burial as well as variations in the thermal conductivities of the rocks, the level of sophistication is low with respect to the kinetics of the thermochemical evolution of organic matter. Thermal models such as TTI-based programs are based on very simple kinetics which assumes that the rate of chemical reaction (viz a viz maturation) doubles with every 10°C increase in temperature and assumes a single low activation energy for the reaction (20 kcal/mole). The thermal evolution of organic matter, to which the

---

[1] Registered trademark

reflectance is directly related, is known to involve a number of different chemical reactions which represent the breaking of C-C bonds, C-O bonds and C-H bonds, which are manifested in the loss of -CH_4 methane, CO_2 H_2, H_2O and eventually hydrocarbons chains. All of these reactions require significantly higher activation energies than are assumed in the Lopatin model, i.e. between 38 and 75 kcal/mole (Burnham & Sweeney, 1989). Larter (1989) also agrees that an average of 50 kcal/mole is a more realistic activation energy for the thermal evolution (maturation) of vitrinite. Kinetic models should therefore be able to achieve a more realistic prediction of the resulting maturation.

Issler (1984) demonstrated that TTI-based modeling programs are not applicable to certain basins, specifically those in which erosion has been significant and cannot be determined accurately. The Liard Basin and its associated regions have experienced several tectonic cycles involving uplift and erosion resulting in major unconformities (sub Permian, sub-Triassic, sub-Cretaceous, sub-Tertiary) during which vast amounts of section may have been eroded. This may significantly affect the heating due to burial (TTI) calculated by the program if the burial history is not representative; however, Morrow *et al.* (1993) estimate that the low levels of maturity at the top of the Palaeozoic indicate that there was little post-Palaeozoic burial in this region. Issler (*ibid.*) indicates that errors can also occur in the dating of the sedimentary layers and, ultimately these result in erroneous predictions for maturation levels.

Regardless of the level of sophistication of the modeling program used, all are based on a large number of variables which can lead to a high degree of subjectivity; the results are therefore only as good as the input data (Barker, 1985). The fact that the heat flow models fit the Ro data sets from the Devonian and post-Carboniferous and post-Carboniferous separately suggest that the thermal history may have been more complicated than a simple burial model. The other alternative is that there existed additional heat source(s) which contributed significantly to the maturation patterns and measured Ro values observed in the Liard Basin area.

In *Burial 3* changes made to the heat flow in the .dat input files must be significant and long-lasting in order to produce a significant change in the predicted Ro data. Adjusting the heat flow to fit the Devonian data results in Ro values that do not fit the Carboniferous and younger data points. Conversely, increasing post Palaeozoic heat flow in an attempt to improve the fit of the measured and predicted Ro values in the

Scalc.Ro subroutine, results in significant overestimation of the Devonian Ro values. The Burial model is therefore insensitive to short-lived changes in heat flow and will therefore not respond to the effects of additional heat source(s) such as igneous or hydrothermal activity.

As no major unconformities between the Upper Devonian and Carboniferous have been demonstrated in the Liard Basin, it is suggested that the regional heat flow patterns and a simple burial model were not entirely responsible for the thermal maturation patterns observed in the Liard Basin. In order to fit the measured Ro and the Ro values predicted by the Burial program , it is necessary to invoke additional heating (?from an external source) which would elevate the Upper Devonian Ro values to the Ro levels observed without increasing the Lower Carboniferous and post-Carboniferous values. It is suggested that such heating occurred in the form of short-lived pulses rather than regional changes in the geothermal gradient. The higher Ro values recorded and the maturation trends observed in the western part of the basin, together with some of the observed petrographic characteristics, strongly suggest there were additional heat source(s) in the western part of the basin. This is discussed further in the final chapter.

6.0 SUMMARY AND DISCUSSION

This study was initiated to examine the source potential and maturation levels of the Upper Devonian and Carboniferous in the Liard Basin and adjacent areas to the east with regard to the future hydrocarbon potential. The reluctance of oil and gas companies to explore this frontier region until recently is partly due to the lack of available geochemical and petrological data on which to base source rock evaluations, maturity trends and reconstruct thermal history models. This is in sharp contrast to the amount of data available in the more extensively explored and productive sub-basins of the Western Canada Sedimentary, such as the Alberta Basin and the Williston Basin. The small number and low density of drillholes and wells available for sampling, the paucity and poor condition of drill cuttings and core samples, the remoteness of the basin and the high costs of exploration drilling have also contributed to this and to some degree, so has the lack of confidence in using less conventional maturity parameters, such as bitumen reflectance.

Maturity parameters

The results of this study suggest that there are numerous units in the Upper Devonian and Lower Carboniferous of the Liard Basin and the adjacent Eastern Plains of the Northwest Territories which have hydrocarbon source potential but the maturity varies significantly throughout the basin. The large variations in maturity are partly responsible for the strong tendency to rely on petrological analysis to evaluate the hydrocarbon potential because the reliablity of the Rock-Eval data is uncertain at elevated maturity. Furthermore, in the absence of vitrinite for reflectance measurement and inadequate TOC levels to give reliable Tmax data, the study focuses on understanding the mode of origin and changing optical properties of the microscopic bitumens (which are commonly abundant and often dominant in mature and postmature source rocks) that might justify their credibity as dependable maturation indices. This is particularly important in marine basins in which vitrinite is lacking, for mapping maturation trends in frontier basins like the Liard Basin where maturity is extremely variable and often quite high, and in basin modeling so that vertical maturity profiles based on reflectance can be determined in organic lean rocks and provide data from Lower Palaeozoic strata where vitrinite is

absent.

It has been demonstrated that a genetic approach to the classification of microscopic bitumens provides a sound basis for bitumen reflectance determination. This approach was adopted based on preliminary observations of a relationships between the primary organic constituents and the microscopic (solid) bitumens. Spatial relationship and mutual associations (which shall be termed "morphologically-distinct" populations) of bitumens with different organic macerals suggested that the bitumens are indigenous to the source rocks and are produced as products of thermal evolution of the maceral components of the kerogen. The microscopic bitumens are therefore indigenous to the source rocks.

The classification of bitumens into types according to the optical characteristics and the relationship to the source (liptinite macerals) is essential in order to subsequently calculate an equivalent vitrinite reflectance maturity. Furthermore the relative proportions of various types of microbitumens permits visual estimation of the maturity, in a more general sense, e.g. immature, mature and postmature. As with other maturity parameters, the reliability of the bitumen reflectance data improves when as many correlative parameters as possible are used.

There is good agreement between the reflectance of the Type 3 and 4 bitumens and depth, and with other maturation parameters such as Tmax, alginite and sporinite fluorescence, condont alteration index (CAI) and thermal alteration index (TAI); alone, these parameters all have very limited applications in this region and they can only be used in immature and mature source rocks. For rocks within that maturity range, the relationship that is demonstrated between Tmax and bitumen Ro is particularly good. The relationship between the reflectance of the Type 4 bitumen and the measured vitrinite values from the Mattson Formation at the outcrop sections in the Tlogotscho Plateau area, is also good and falls very close to that of Jacob's relationship between "migrabitumen" and vitrinite (VRo = BRo × 0.618 +0.4). In the Liard Basin, this bitumen (type 4) is present over a broad maturity range (0.4% to ca. 4.0 eq.). Furthermore, the lower threshold of type 4 bitumen occurrence is lower than the generally-accepted limits of 0.5%VRo for the oil window (*sensu* Dow, 1977), which implies that it may be associated with early hydrocarbon generation from sulphur-rich kerogens (Powell & Snowdon,

1983). Powell (1984) suggests that bitumens are formed by polymerization of NSO/asphaltenes in the kerogen and Machel *et al.* (1995) indicate that bitumens are formed as by-products of thermochemical sulphate reduction associated with thermal maturation of crude oil, by polymerization of the oxidized products. A second population of bitumens (type 3) is almost as common in the Liard Basin source rocks as the type 4 but it has a lower application range. Type 3 bitumen is present in rocks from 0.45% to ca. 2% VRo equivalent and therefore it can still be used over a broad maturity range. The reflectance of type 3 bitumen bears a strong relationship to that of the type 4 bitumen (%Ro type 3 bitumen = 0.73 × %Ro type 4 bitumen) and also to vitrinite (VRo = 0.817 * %Ro type 3 bitumen + 0.41). Similar correlations for amorphous bitumen and VRo were obtained by Landis and Castaņo (1995) which suggests that the type 3 bitumen Ro is the index they use for maturation but their studies are based only on distinct reflectance populations without any genetic implications which makes it more difficult for other workers to apply.

In this study, bitumen reflectance has been successfully determined on samples with very low (0.2%) as well as very high TOC values (12%, 60%); facies ranging from terrestrial to basinal marine and over a maturation range of 0.4% to 4.5% VRo equivalents; and in rocks of Devonian to Tertiary age. Therefore, as a maturation parameter. This testifies to its wide applicability. However, it is suspected that (like vitrinite) bitumen reflectance succumbs to reflectance suppression in hydrogen-saturated conditions such a those that occur in a very organic-rich active source rock or a sapropelic coal with perhydrous vitrinite (Price & Barker, 1985).

Source potential

Organic petrological studies of the source rocks in the Upper Devonian and Lower Carboniferous in the Liard Basin indicate that bitumens are abundant in all of the source rocks and vitrinite is scarce to absent. Use of alternative parameters is therefore essential in order to study the maturation trends in this area. In most of the source rocks examined, four distinct morphological/reflectance populations are present (types 1,2,3 and 4). Bitumen reflectance, TOC data and the proportions of the various bitumen types suggest that although the Muskwa Formation is now postmature for oil generation, it was an

excellent source rock at some point in its history. The high TOC values suggest that it retains excellent potential for gas generation in the Interior Plains east of the Bovie Fault. No hydrocarbon potential exists in the Fort Simpson or the Redknife Formations but, throughout the Plains region, most of the Upper Devonian and Lower Carboniferous units (i.e. the Lower Banff, Besa River, Yohin, Clausen, Prophet, Golata and Mattson formations) contain shales which show moderate to good hydrocarbon potential and maturity variations ranging from peak oil generation in the more easterly sections of the Eastern Plains to increasingly higher maturity (good for condensate and gas potential) westwards towards the Bovie Fault Zone. The more noteworthy source rocks include the lower Exshaw, which is a prominent source rock in the Alberta Basin (Richards *et al.*, 1991), the Lower Banff, the Besa River and the Mattson formations. The Lower Exshaw is thin but laterally persistent and has excellent hydrocarbon potential in the eastern Plains. The TOC values are anomalously high (12%) and the Type II kerogen is currently at peak oil generation stage of maturity in the Island River area. The lower Banff has petrographic characteristics similar to those of the Exshaw in the Island River area, and although associated with significantly lower TOC values, it would classify as a good source rock. The Besa River Formation also contains excellent gas source rocks in the 1st and 2nd Black shale members. The organic petrological characteristics of these intervals are very similar to those of the Muskwa and postmature Lower Exshaw of the Alberta Basin and their abundant indigenous bitumens were likely derived from a typical Type II marine kerogen. Bitumen reflectance data indicate that these intervals are at the lower boundary of the gas window (1.2% VR_o eq.) in the Pointed Mountain region, elsewhere, the black shale intervals are of elevated maturity (ca. 2.5% VR_o in the Beaver River) which increases even more westwards; however, high TOC values suggest that the "Black shales" may still have good gas potential.

Shales in the middle and upper Mattson Formation in the outcrop belt (Jackfish Gap, Clausen Creek) contains numerous thin, sporinite-rich cannel coals (Potter *et al.*, 1993) which have excellent potential for generating hydrocarbons and contain a high proportion of sporinite and fluorescing vitrinite. Horsefield *et al.* (1988) have shown geochemically that resinite and fluorescing vitrinite are responsible for significantly elevating the petroleum-producing ability of Tertiary coals from northwest Java which are

considered to be a prime source of the high molecular weight paraffinic oils typically found in the Ardjuna Basin. These same coals contain a high proportion of matrix bituminite which is considered to be the principal source of the paraffinic oils (ibid.). The cannel coals of the Mattson Formation contain a high proportion of micrinite (which is derived by thermal alteration of matrix bituminite) and the vitrinite is perhydrous (Potter *et al.*,1993) which suggests that these coals may have been a source of paraffinic oil during the Carboniferous if, as Morrow *et al.* (1993) suggest that, the Carboniferous of the Liard Basin has encounted very little post-Paleozoic burial, then the present rank of maturity (high volatile bituminous; 0.8% VR_o) must have been attained by the end of the Carboniferous. Currently, such coals have only been detected in outcrop sections.

At the outcrop sections at Jackfish Gap and Clausen Creek, the cannel coals in the upper Mattson are interbedded with black, organic-rich, algal laminites interpreted to have been deposited in a lagoonal setting. In northeastern British Columbia, coals are absent in the Mattson Formation and the terrestrial influence, depicted by the abundance of sporinite decreases southwards and westwards. While shales of the Golata and Mattson formations are in the peak oil generation level of maturation (0.9% VRo equivalent) in the Pointed Mountain area and east of the Bovie Fault Zone, the maturation is significantly higher, i.e. the upper end of the oil window (1.1-1.3% VR_o eq.) in the centre of the Basin at Viscount (B.C.) and Beaver River (N.W.T). This suggests that while the Golata and Mattson formations maintain oil-generating potential at Pointed Mountain (and to the south at Maxhamish and Tatoo), gas-generation from these intervals is favored in the Beaver River (N.W.T.) and LaBiche (B.C.) areas and further to the southwest at Dunedin, where the Mattson occurs at depths in excess of 10,000 ft. (> 3000 m), the maturation is extremely high (2.4% VRo equivalent) and exceeds even the limits of the gas window.

Anomalously high Ro values are found for bitumens in the Mattson section at Windflower (26) and all samples have exceptionally high sulphide mineral contents. This section is located close to the Bovie Fault and has evidently been affected by hot mineralizing fluids.

Maturation trends

The broad trends in reflectance determined for the Upper Devonian and

Carboniferous generally follow the structure contours and present-day burial depths. Whether the data set is examined on a formation basis or as vertical sections through the Mesozoic and Upper Paleozoic sequence, there is a consistent increase in maturity from east to west and from north to south towards the basin axis (cf. Leckie *et al.*, 1991) indicating that the regional maturation is clearly linked to basin subsidence. To the east of the Bovie fault, numerous units are in the peak oil generation stage while to the west, the Upper Devonian is postmature and the Lower Carboniferous is mature for gas. The VRo values obtained in the Pointed Mountain area are similar to those in the Eastern Plains and in the outcrop belt to the north so that folding and thrusting of the Upper Paleozoic at Pointed Mountain has therefore created something of a thermal low in an area of rather elevated maturity that is generally more conducive to gas generation.

The Ro-depth gradients are distinctly different for the Upper Devonian and Lower Carboniferous strata in this area: the Devonian gradients are much steeper than those observed in the Carboniferous suggesting that high geothermal gradients prevailed during the Upper Devonian. Basin modeling results also imply that very high heat flows prevailed in the Upper Devonian. These observations are consistent with those of Morrow *et al.* (1993) who favour a Late Devonian heating event as being responsible for the high maturity observed in the Beaver River and Kotaneelee regions.

The Ro values predicted by the burial and thermal models do not overlap the measured values for the whole Upper Palaeozoic and this appears to be due to insensitivity of the modeling program to short duration changes in heat flow. Most TTI-based modeling programs are only applicable to basins which have experienced continual subsidence and those in which the maturation patterns reflect only heating due to burial. It is suggested that the best fit of the data would be accomplished if it was possible to accommodate short-duration, episodic heating into the model. Consequently, it must be concluded that the maturation patterns observed in the Liard are related basin subsidence and deep burial but that additional Upper Devonian heating event affected the sediments along the western margin of the Liard Basin and along the Bovie Fault.

Thermal history

Significant (positive) thermal anomalies are indicated by maturity parameters and

distinctive petrographic characteristics of the organic matter around the Bovie Fault Zone (Windflower, Bovie Lake and Celibeta) and all along the western margin of the basin (Dunedin, Kotaneelee, Tika Creek, Clausen Creek). Petrographic characteristics of the bitumens in the Muskwa and Fort Simpson Formations bear the mark of intense thermal alteration. Under laboratory-simulated carbonization conditions, a nisotropic semicokes such as those observed in the Muskwa, can form from bitumens at elevated temperatures in excess of 600 °C. In a hydrogen-saturated environment, which would be more representative of a maturing source rock, and where pores and internal microfractures would be filled mixtures of water, hydrocarbon fluids or gas, such textures can form from bitumens at temperatures ca. 380 °C to 450°C (Potter et al., 1984). The observed reflectance anomalies, which signify elevated maturation relative to the regional maturation pattern, are less pronounced in the Carboniferous strata suggesting that the Bovie Fault was a source of deep conductive heat during the Upper Devonian. Optically anisotropic bitumens in the Fort Simpson Formation, have high bireflectance, which is typical of isotropic cokes formed under mild carbonization conditions (Grint & Marsh, 1984) or under intense heat and pressure, (Goodarzi & Murchison, 1979). In the Mattson Formation at Windflower in northeast British Columbia, anomalously high Ro values (>10% Ro) for bitumens and a high degree of sulphide mineralization in the shales suggests that the fault may also have been a source of hydrothermal fluids.

As in the Muskwa Formation at Bovie Lake, highly anisotropic cokes are present in the Besa River along the west side of the basin (Kotaneelee), together with cenospheres similar to those that from high temperature flash pyrolysis of low grade organic matter (Energy Research Unit, 1983) or oxidative combustion. The characteristic mosaic anisotropy which develops results from the ordering and growth of polyaromatic nuclei as peripheral functional groups and hydrocarbons chains are lost due to C-C bond rupturing. This results in condensation of the aromatic nucleic and planar directional growth of aromatic layers (Katz & Hirsch, 1964). The cenospheres also suggest rapid thermal devolatilisation of organic components more consistent with pulses of intense heating in proximity to the source rocks. Burial history modeling for the Pan Am Beaver and Kotaneelee sections by Morrow *et al.* (1993) indicated that given a burial history similar to that discussed in Chapter 5, and heat flows of 150 mW/m/sec, the Besa River Formation

entered the oil window ca. 340 million years ago and oil generation was complete by ca. 280 million years B.P., i.e. in the pre-Permian. Considering the petrographic evidence for intense thermal heating, it is suggested that hydrocarbon generation from the Besa may even have occurred quite early in the history of the Besa River, relatively soon after deposition. Modern environments where this is currently occurring include the Guayamas Basin- part of the system of spreading ridges and tranform faults that define the northern tip of the east Pacific Rise System. Simoneit (1985) describes instantaneous petroleum genesis at temperatures in excess of 315°C which he refers to as "hydrothermal petroleum". Geochemically, the products are similar to those associated with "thermocracking" of organic matter which generates polyaromatic condensation products that accumulate within the sediment and whose pyrolysis products show complete expulsion of the pyrolysate. According to Simoneit (1983), ancient sites of hydrothermal petroleum generation such as the Guyamas Basin are associated with large amounts of thermogenic gas. The Beaver River and Kotaneelee gasfields represent thermogenic gas accumulations. According to Barker and Pawlewitz (1985), temperatures of 342 °C would be required to bring about the a reflectance equivalent to that observed in the Devonian at the base of the Kotaneelee section (4.4 % VRo equivalent) under hydrothermal conditions. Simoneit (1985) has observed "discharge of hydrothermal fluids up to 1km above sea floor vents in the Guaymas Basin. which, coupled with large amounts of accessible petroleum, represents a major carbon source for the generation of microbial biomass at the vent sites".

Morrow (1986) suggests a hydrothermal heat source was responsible for recirculating evaporatic brines from the Elk Point Basin into the Liard Basin and associated areas, giving rise to the middle Devonian Manetoe Facies Dolomite, a widespread diagenetic dolomite facies which is the reservoir for the Beaver River, Kotaneelee and Pointed Mountain Gasfields. Morrow (*ibid.*) also indicates that ^{86}Sr isotope data implies an early, pre-Mesozoic origin for the dolomite cements. A hydrothermal regime is compatible with the temperatures required for semicoke formation and the regional Ro distributions in this area. Furthermore, the Besa River Formation contains a very high proportion of pyrite which is mostly massive and tetrahedral in nature. Machel *et al.* (1995) indicate that cubic (tetrahedral) pyrite is indication of thermochemical sulphate reduction rather than pyrite of bacterial origin.

Hydrothermal lead-zinc-pyrite deposits are known from the middle Devonian of the southeastern Yukon and southwestern Northwest Territories and northeastern British Columbia. Furthermore, Carne and Cathro (1982) describe stratabound, shale-hosted sedimentary exhalative sulphide (SEDEX) mineral deposits from the Besa River in the Selwyn Basin just to the northwest of the study area; the model they propose for the lead-zinc-pyrite deposits at Macmillan Pass in the southern Yukon is that of hydrothermal mounds located along the strike of major NNW-SSE trending graben-faults that define the edge of the Selwyn Basin. Davies (1996) suggests there is close spatial and temporal relationship between the hydrothermal dolomite-hosted lead-zinc deposits in northeastern British Columbia and the stratabound SEDEX and hydrothermal dolomite hydrocarbon reservoirs. This lends further support to the suggestion that hydrothermal activity on the western margin of the Liard Basin may have been responsible for early maturation of the organic matter in Upper Devonian source rocks.

A study of the early Palaeozoic tectonic framework and palaeogeography of the Canadian Cordillera by Cecile *et al.* (1997) indicates that the Canadian Cordilleran "miogeocline" (which includes the study area) was formed in Late Proterozoic as a result of rifting. The Atlantic-type margin continued to have distinct periods of rifting and extension throughout its history. Cecile *et al.* (1997), identified the Liard "Depression" as a significant depocentre that existed well into the Devonian and suggests that a prominent Paleozoic structure, the NE-SW trending "Liard Line" zone, defined by erosional and depositional pinch-outs of the Ordovician to Lower Devonian, may have been an ancient transfer fault. The rifted eastern upper plate margin inherits numerous deep graben-types faults along which hydrothermal fluids can be transmitted. Additional heat sources along the inferred western margin of the Liard Basin may be related to hydrothermal activity that persisted throughout the Upper Devonian and early Carboniferous and contributed to the high maturation levels observed in the Besa River.

7.0 CONCLUSIONS

1. Gas source rocks are numerous in the Upper Devonian in the Liard Basin west of the Bovie Fault Zone.

2. Oil and gas source rocks occur in the Upper Devonian and Carboniferous of the Eastern Plains, east of the Bovie Fault Zone ; the Carboniferous ones are currently in the peak oil generation stage of maturity.

3. Indigenous solid microbitumens are commonly the most abundant type of organic matter in the source rocks and can be reliable maturity parameters provided they are classified into morphologically-distinct types and identified with the precursor macerals.

4. Regional maturation patterns are closely related to basin subsidence, except along the Bovie Fault Zone and the western and southwestern margins of the study area.

5. A thermal anomaly is strongly manifested along the western margin of the basin and the effects decrease northeast and eastwards. Vertical Ro-depth profiles, Ro gradients, petrographic characteristics of the organic matter and the results of basin modeling point to a Late Devonian heating event in the Liard Basin. Hydrothermal activity related to the emplacement of base metal deposits and hydrothermal dolomites may have been responsible.

6. The Bovie Fault was also a source of convective heating during the Upper Devonian resulting in local thermal anomalies and maturation patterns.

REFERENCES

ABRAHAM, H. 1960. *Asphalts and Allied Substances. 1. Historical Review and Natural Raw Materials*. Princeton University Press, Princeton, NJ, 370pp.

AITKEN, J.D. 1993. Tectonic framework. *In*: STOTT, D.F. & AITKEN, J.D. (eds) *Sedimentary Cover of the The Craton in Canada*, Geological Survey of Canada, pp. 45-54 (also Geological Society of America, *The Geology of North America*, D-1).

ALPERN, B. 1981. Les schistes bitumineux: constitution, reserves, valorisation. *In*: *Geology of Coal, Oil Shales and Kerogens. Bulletin Centre Recherche Exploration-Production, Elf Aquitaine*, 5, 319-352.

ALPERN, B. & MAUME, F. 1969. Etude pétrographique de l'oxidation naturelle et artificielle des houilles. Review Industrial Minéralogie, **51**, 979-997.

AWRAMIK, S.A. 1984. Ancient stromatolites and microbial mats. *In*: COHEN, Y, CASTENHOLZ, R.W. & HALVORSON, H.O. (eds) *Microbial Mats: Stromatolites*, Alan R. Liss Inc., New York, pp. 1-22.

BAMBER, E.W., MACQUEEN, R.W. & RICHARDS, B.C. 1984. Facies relationships at the Mississippian carbonate platform margin, western Canada. *In*: BELT, E.S. & MACQUEEN, R.W. (eds) *Sedimentology and Geochemistry*, Neuvième Congrès International de Stratigraphie et de Géologie du Carbonifère, 1979, *Compte Rendu*, **3**, 461-470.

BARKER, C.E. 1983a. The influence of time on metamorphism of sedimentary organic matter in selected geothermal systems, western North America. *Geology*, **11**, 384-388.

BARKER, C.E. 1989b. Temperature and Time in the thermal maturation of sedimentary organic matter. *In*: NAESER, N.D. & M^{C}CULLOCH, T.H. (eds.) *Thermal History of Sedimentary Basins-methods and case histories*, Springer, New York, pp. 75-98.

BARKER, C.E. & PAWLEWICZ, M. J. 1985a. The Correlation of vitrinite reflectance with maximum temperature in humic organic matter. *In*: BUNTEBARTH, G. & STEGENA, L. (eds) *Paleogeothermics* **5**, Springer, Berlin, pp. 79-83.

BARKER, C.E. & PAWLEWICZ, M. J. 1985b. Calculation of vitrinite reflectance from thermal histories and peak temperatures. *In*: MUKHOPADHYAY, P.K. & DOW, W.G. (eds) *Vitrinite Reflectance as a Maturity Parameter: Application and Limitations*. ACS Symposium Series **570**, American Chemical Society, Washington D.C., pp. 216-229.

BARKER, C.E., CRYSDALE, B.L. & PAWLEWITZ, M.J. 1986. The relationship between vitrinite reflectance, metamorphic grade and temperature in the Cerro Prieto, Salton Sea and East Mesa geothermal systems. Salton Trough, United States and Mexico. *In*: MUMPTON, F.A. (ed.) *Studies in Diagenesis*, United States Geological Survey Bulletin, **1578**, 83-95.

BARSS, M.S. 1967. Carboniferous and Permian Spores of Canada. *Geological Survey of Canada*, Paper 67-**11**, 94pp.

BASINMOD™ 1992. *A Modular Basin Modeling System*. Platte River Associates, Denver Colorado.

BELIN, S. 1992. Application of back-scattered electron imaging to the study of source rock microtextures. *Organic Geochemistry*, **18**, 333-346.

BELYEA, H.R. & MCLAREN, D.J. 1961. Upper Devonian formations southern part of Northwest Territories, northeastern British Columbia, and Northwestern Alberta. *Geological Survey of Canada*, Paper 61-**29**, 74pp.

BENEDICT , L.G. & BERRY, W.F. 1964. Recognition and measurement of coal oxidation, *Geological Society of America, Bituminous Coal Research Report*, Monroeville, Pa., 41pp.

BERTRAND, R. 1990. Correlations among the Reflectances of vitrinite, chitinozoans, graptolites and scolecodonts. *Organic Geochemistry*, **15**, 565-574.

BERTRAND, R. 1993. Standardization of solid bitumen reflectance to vitrinite in some Paleozoic sequences of Canada. *Energy Sources*, **15**, 269-287.

BLACKBURN, K.B. & TEMPERLY, B.N. 1936. *Botryococcus* and the algal coals. *Transactions Royal Society Edinburgh*, **58**, 841-868.

BOSTICK, N. & FOSTER, J.N. 1972. Comparison of vitrinite reflectance in coal seams and in kerogens of sandstones, shales, and limestones in the same part of a sedimentary succession. *In*: B. ALPERN (ed.) *Pétrographie organique et potentiel pétrolier*. Éditions du Centre Nationale de la Recherche Scientifique, Paris, pp. 13-25.

BRAMAN, D.R. 1976. Palynology and Paleoecology of the Mattson Formation, northwest Canada. *Bulletin of Canadian Petroleum Geology*, **25**, 582-630.

BRAMAN, D.R. & HILLS. L. V. 1977. Palynology and paleontology of the Mattson Formation, Northwest Canada. *Bulletin Canadian Petroleum Geology*, **25**, 582-630.

BUISKOOL TOXOPEUS, J.M.A. 1983. Selection criteria for the use of vitrinite reflectance as a maturity tool. *In*: BROOKS, J. (ed.) *Petroleum Geochemistry and Exploration of Europe*, Blackwell Scientific, pp. 295-307.

BUSTIN, R.M.B (1991). Organic maturity in the western Canada sedimentary basin. International Journal of Coal Geology, **19**, 319-358.

BROOKS, J. 1981. Organic maturation of sedimentary organic matter and petroleum exploration: a review. *In*: BROOKS, J. (ed.) *Organic Maturation studies and Fossil Fuels Exploration*, Academic Press, London, pp. 1-38.

BURNHAM, A.K. & BRAUN, R.L. 1985. General kinetic model of Oil Shale Pyrolysis. *In Situ*, **9**, 1-23.

BURNHAM, A.K. & SWEENEY, J.J. 1989. A chemical model of vitrinite maturation and reflectance. *Geochemica Cosmochemica Acta*, **53**, 2649-2657.

BUSTIN, R.M., CAMERON, A.R., GRIEVE, D.A. & KALKREUTH, W.D. 1983. *Coal Petrology, its Principles, Methods and Applications*. (2nd edition), Geological Association of Canada, Short Course Notes **3**, 230pp.

CAMERON, A.R. & PRATT, K. 1982. Report on rank and maceral composition of coals in the Mattson Formation, Mackenzie District, N.W.T. *Geological Survey of Canada*, unpublished internal report, 2pp.

CAMERON, A.R., POTTER, J. & GOODARZI, 1994. Coal and oil shale of Early Carboniferous age in northern Canada: significance for paleoenvironmental and paleoclimatic interpretations. *Palaeogeography, Palaeoclimatology and Palaeoecology*, **106**, 135-155.

CARNE, R.C. & CATHRO, R.J. 1982. Sedimentary exhalative (SEDEX) zinc-lead-silver deposits, northern Canadian Cordillera. *Canadian Mining and Metallurgical Bulletin*,**75**, 66-75.

CECILE, M., MORROW, D.W. & WILLIAMS, G.K. 1997. Early Paleozoic (Cambrian to Early Devonian) tectonic framework, Canadian Cordillera, *Bulletin of Canadian Petroleum Geology*, **45**, 64-74.

CHOW, N., WENDTE, J & STASIUK, L.D. 1995. Productivity versus preservation controls on two organic-rich carbonate facies in the Devonian of Alberta: sedimentological and organic petrological evidence. *Bulletin of Canadian Petroleum Geology*, **43**, 433-460.

COHEN, Y.1984. The Solar Lake cyanobacterial mats: strategies of photosynthetic life under sulphide. *In*: COHEN, Y, CASTENHOLZ, R.W. & HALVORSON, H.O. (eds) *Microbial Mats: Stromatolites*, Alan R. Liss Inc., New York, pp. 133-148.

COLE. K. 1993. *The regional geology, organic petrology and geochemistry of the Middle Jurassic Gravelbourg Formation in southern Saskatchewan.* Unpublished M.Sc. Thesis, University of Regina, 147pp.

COMBAZ, A. 1975. Essai de classification des rôches carbonées et des constituants organiques des rôches sédimentaires. *In*: ALPERN, B. (ed) *Pétrographie de la matière organique des sédiments, relations avec la paléotempérature et le potential pétrolier*. Éditions du Centre Nationale de la Recherche Scientifique, Paris, pp. 93-101.

CORNFORD, C., RULLKÖTTER, J. & WELTE, D. 1979. Organic geochemistry of DSDP Leg 47A, Site 397 Eastern North Atlantic: organic petrography and extractable hydrocarbons. *In*: VON RAD, U. & RYAN, W.B.F. *Initial Reports of the Deep Sea Drilling Project*, 67 (1), Washington, U.S.A., pp. 511-522.

CREANEY, S. (1980). The organic petrology of the Upper Cretaceous Boundary Creek Formation, Beaufort-Mackenzie Basin. *Bulletin of Canadian Petroleum Geology*, **28**, 112-123.

CREANEY, S. & ALLEN, J.A. 1991. Oil families in the Western Canada Basin. *Bulletin of Canadian Petroleum Geology*, **39**, 107-122.

CREANEY, S. & ALLEN, J.A. 1992. Petroleum systems in the Foreland Basin of Western Canada. *In*: MACQUEEN, R.W. & LECKIE, D.A. (eds) *Foreland Basins and Fold Belts*, American Association of Petroleum Geologists Memoir, **55**, Tulsa, pp. 295-308.

CRELLING, J.C., SCHRDER, R.H. & BENEDCIT, L.G. 1979. Effects of weathered coal on the coking properties and coke quality. *Fuel*, **58**, 524-546.

CURIALE, J. 1985. Origin of solid bitumens, with emphasis on biological markers. *Organic Geochemistry, Advances* **10**, 559-580.

DAVIES, G. (1966). *Hydrothermal Dolomite (HTD) Reservoir Facies: Global Perspectives on Tectonic-Structural and Temporal Linkages between MVT and SEDEX Pb-Zn Ore Bodies, and Subsurface HTD Reservoir Facies*. Pools '96. Canadian Society of Petroleum Geologists Short course notes, 167pp.

DAVIS, A. 1978. The reflectance of coal. *In*: KARR. C. (ed.) *Analytical Methods for Coal and Coal Products*. Academic, New York, pp. 27-81.

DEMAISON, G.J. 1975. Relationship of coal rank to paleotemperatures in sedimentary rocks. *In*: ALPERN , B. (ed.) *Pétrographie de la Matière Organique des Sédiments, relations avec la Paléotempérature et le Potential Pétrolier*. Éditions du Centre National de la Recherche Scientifique, Paris, pp. 217-224.

DEMAISON, G.J. & MOORE, G.T. 1980. Anoxic environments and oil source bed genesis. *American Association of Petroleum Geologists Bulletin*, **64**, 1170-1209.

DEMBICKI, H. & PIRKLE, F.L. 1985. Regional source rock mapping using a source potential rating index. *American Association of Petroleum Geologists Bulletin*, **69**, 567-581.

de WIT, R., GRONBERG, E.C., RICHARDS, W.B. & RICHMOND, W.O. 1973. Tathlina District. *In*: MCCROSSAN, R.G. (ed.) *Future Petroleum Provinces of Canada*, Canadian Society of Petroleum Geologists Memoir, **1**, pp. 187-212.

DOUGLAS, R.J.W. 1970 (ed.) *Geology and Economic Minerals of Canada*. Geological Survey of Canada Economic Minerals Report No.1, 838pp.

DOUGLAS, R.J.W 1976. *Geology -La Biche River, District of Mackenzie*. Geological Survey of Canada, Map 1380A, 1:250,000.

DOUGLAS, R.J.W. & NORRIS, D.K. 1959. Fort Liard and La Biche map-areas, Northwest Territories and Yukon, *Geological Survey of Canada*, Paper 59-6, 23pp.

DOUGLAS, R.J.W. & NORRIS, D.K. 1976a. *Geology Fort Liard, District of Mackenzie*. Geological Survey of Canada, Map 1379A, 1:250,000.

DOUGLAS, R.J.W. & NORRIS, D.K. 1976b. *Geology - Sibbeston Lake, District of Mackenzie*. Geological Survey of Canada, Map 1377A, 1:250,000.

DOUGLAS, R.J. W., HARKER, P. & NORRIS, D.K. 1963. *Geology Southern Mackenzie Mountains area, Yukon Territory and District of Mackenzie*. Geological Survey of Canada, Map 1141A, 1:506,880.

DOUGLAS, R.J.W., BRADY, W.B., HARKER, P., STOTT, D.F. & HAGE, C.O. 1976. *Geology of La Biche River, District of Mackenzie*. Geological Survey of Canada, Map 1380A, 1:250,000.

DOW, W. G. 1977. Kerogen studies and geological interpretations. *Journal of Geochemical Exploration*, **7**, 79-99.

DURAND, B. 1975. Indices optiques, potentiel pétrolier et histoire des sédiments. *In*: Alpern, B. (ed.) *Pétrographie de la matière organique des sédiments, relations avec la paléotempérature et le potential pétrolier*. Éditions du Centre Nationale de la Recherche Scientifique, Paris, pp. 205-216.

DURAND, B. 1980. Sedimentary organic matter and kerogen. Definition and quantitative importance. *In*: B. DURAND, B. (ed.) *Kerogen: Insoluble Organic Matter From Sedimentary Rocks*, Éditions Technip, Paris, pp. 13-34.

DURAND, B., PARATTE, M. & BERTRAND, P. 1983. Le potential en huile de charbons: Une approache géochemique. *Revue de l'Institut Français Pétrole*, **38**, 709-721.

DURAND, B., ALPERN, B., PITTION & PRADIER, B.1986. Reflectance of vitrinite as a control of thermal history of sediments. *In*: BURRUS, J. (ed.) *Thermal Modeling in Sedimentary Basins*, Insitut Français Pétrole Research Conferences on Exploration, Carcan, France, June 3-7, 1985. Éditions Technip, Paris, pp. 441-473.

DYBOVA-JACHOWICZ, S., JACHOWICZ, A., KARCZEWSKA, J., LAHKAR, G., LOBOZIAK, S., PIERART, P., TURNAU & ZOLDANI, Z. 1987. *Revision of Carboniferous Megaspores with Gula. Part III*. Prace Instytutu Geologicznego CXXXI, Wydawnictwa Geologiczne, Warsaw, 49pp.

EGLINTON, G. 1968. Hydrocarbons and fatty acids in living organisms and recent and ancient sediments. *In*: SCHENK, P. & HAVENAAR, I. (eds) *Organic Geochemistry, Advances*, Pergammon Press, London, pp. 1-24.

ENERGY RESEARCH UNIT, 1983. *Characterization of solid residues from coal liquefaction processes*, Report to CANMET, EMR Canada under DSS Contract # OST-00067.

ENGLAND, T.D.J. & BUSTIN, R.M.B. 1986. Thermal maturation of the Western Canada Sedimentary Basin south of the Red Deer River: 1) Alberta Plains. *Bulletin of Canadian Petroleum Geology*, **34**, 71-90.

EPSTEIN, A.G., EPSTEIN, J.B. & HARRIS, L.D. 1977. *Conodont Color Alteration - an Index to Organic Metamorphism.*United States Geological Survey Professional Paper 995, Washington, 27pp.

ESPITALIÉ, J. 1986. Use of Tmax as a maturation index for different types of organic matter. Comparison with vitrinite reflectance. *In*: BURRUS. J. (ed.) *Thermal Modeling in Sedimentary Basins*, Proceedings l'Institut Français Pétrole Research Conferences on Exploration, Carcans, France, June 3-7, 1985. Éditions Technip, Paris, pp. 475-496.

ESPITALIÉ, J.F., MADEC, M., TISSOT, B., MENNIG, J.J. & LEPLAT. P. 1977. Source rock characterization method for petroleum exploration, Ninth Offshore Technology Conference, Houston, pp. 439-442.

ESPITALIÉ, J.F., DEROO, G. & MARQUIS, F. 1985. La pyrolyse Rock-Eval et ses applications (deuxieme partis): *Revue de l'Institut Français du Pétrole*, **40**, 775-784.

EVANS, T.J. 1975. Cannel coal and stratigraphic setting. *In*: *Uranium, Coal and Gas*, Triple Energy Field Trip Guidebook, Duval, Webb, and Zapata Counties, Texas. *Corpus Christi Geological Society*, p. 15.

EVANS, C.R. & STAPLIN, F.L. 1970. Regional facies of Organic Metamorphism. *In: Geochemical Prospecting for Oil and Gas.* International Geochemical Exploration Symposium, Toronto, 1970, (3rd Edition), Canadian Institute of Mining and Metallurgy Special Volume **11**, 517-520.

FARAJ, B.S.M. & MACKINNON, I.D.R. 1993. Micrinite in southerm hemisphere sub-bituminous and bituminous coals: redefined as fine-grained kaolinite. *Organic Geochemistry*, **6**, 823-842.

FEINSTEIN, S., BROOKS, P.W., GENTZIS, T., GOODARZI, F., SNOWDON, L.R. & WILLIAMS, G.K. (1988). Thermal Maturity in the Mackenzie Corridor, Northwest and Yukon Territories, Canada. *Geological Survey of Canada Open File Report* **1944**.

FEINSTEIN, S., ISSLER, D., SNOWDON, L.R. & WILLIAMS, G.K. 1996. Characterization of major unconformities by paleothermometric and paleobarometric methods: application to the Mackenzie Plain, Northwest Territories, Canada. *Bulletin Canadian Petroleum Geology*, **44**, 55-71.

GABRIELSE, H. 1967. Tectonic Evolution of the northern Canadian Cordillera. *Canadian Journal of Earth Sciences*, **4**, 271-298.

GANZ, W. & KALKREUTH, W.D. 1987. Application of infrared spectroscopy to the classification of kerogen types and the evaluation of source rock and oil shale potential. *Fuel*, **66**, 708-711.

GENTZIS, T.,1991. *Regional Maturity and Source-rock Potential of Palaeozoic and Mesozoic Strata*. Melville Island, Arctic Canada. Unpublished Ph.D. Thesis, University of Newcastle-upon-Tyne, 238 pp.

GENTZIS, T. & GOODARZI, F. 1989. Organic petrology of a self-burning wastepile from Coleman Alberta, Canada. *International of Journal Coal Petrology*, **11**, 257-271.

GOODARZI, F. 1975. *Some Factors Affecting the Carbonization Behaviour of Coal Macerals*. Unpublished Ph.D. Thesis, University of Newcastle-upon Tyne, 347pp.

GOODARZI, F. & MURCHISON, D.G.M. 1977. Effect of prolonged heating on the optical properties of vitrinite. *Fuel*, **56**, 90-96.

GOODARZI, F. & GENTZIS, T. 1991. Petrology, depositional environment and utilization potential of Devonian cannel coals from Melville Island, Arctic Canada. *Bulletin Societié Géologique Français*, **162**, 239-253.

GOODARZI, F., NASSICHUK, W.W., SNOWDON, L.R. & DAVIES. G.R. 1987. Organic petrology and RockEval analyses of the Carboniferous Emma Fjord Formation in the Sverdrup Basin, Canadian Arctic Island Archipelago. *Marine and Petroleum Geology*, **4**, 132-145.

GORDEY, S.P, ABBOTT, J.G., TEMPELMANN-KLUIT, D.J. & GABRIELSE, H. 1987. "Antler" clastics in the Canadian Cordillera. *Geology*, **15**, 103-107.

GRINT, A. & MARSH, H. 1981. Carbonisation of coal blends: mespohase formation and coke properties. *Fuel*, **60**, 1115-1120.

GRINT, A., SWEITLIK, U. & MARSH, H. 1979. Carbonization and liquid crystal development. 9. Co-carbonization of vitrains with Ashland A200 Petroleum Pitch. *Fuel*, **58**, 642-650.

HABIB, D., RIEGEL, W. & SPACKMAN, W. 1966. Relationship of spore and pollen assemblages in the Lower Kittanning Coal to overlying faunal facies. *Journal of Palaeonotology*, **40**, 756-759.

HACQUEBARD, P.A. & BARSS, M.S. 1957. A carboniferous spore assemblage in coal from the South Nahanni River area, Northwest Territories. *Geological Survey of Canada Bulletin*, **40**, 1-63.

HARKER, P. 1961. Summary account of Carboniferous and Permian formations, southwestern District of Mackenzie. *Geological Survey of Canada*, Paper 61-**1**, 9pp.

HARKER, P. 1963. Carboniferous and Permian formations, southwestern District of Mackenzie. *Geological Survey of Canada*, Bulletin **95**, 91pp.

HARWOOD, J. 1977. Oil and Gas generation by laboratory pyrolysis of kerogen. *American Association of Petroleum Geologists Bulletin*, **61**, 2082-2102.

HEROUX, Y., CHAGNON, A. & BERTRAND, R. 1979. Compilation and correlation of major thermal maturation indicators. *American Association of Petroleum Geologists Bulletin*, **63**, 2128-2144.

HILT, C. 1873. Die Beziehungen zwischen der Zusammensetzung und den technischen Eigenschaften der Steinkohle. Sitzber. *Aachener Bezirksvereinigung* **1**, 4.

HIRSCH, B. 1958. Conclusions from X-ray scattering on vitrain coals. Conference on the Scientific use of Coals. Sheffield, A29- A33.

HOFFMAN, P. 1976. Environmental diversity of Middle Precambrian stromatolites. *In*: WALKER, M.R. (ed.) *Stromatolites*, Developments in Sedimentology, 20. Elsevier, Amsterdam, pp. 599-612.

HOOD, A. & CASTAÑO, J. 1974. Organic metamorphism. Its relationship to petroleum generation and application to studies of authigenic minerals. *Coordinating Committee Offshore Prospecting Technology Bulletin*, **8**, 85-118.

HOOD, A., GUTJAHR, C.C.M. & HEACOCK, R.L. 1975. Organic metamorphism and the generation of petroleum. *American Association of Petroleum Geologists Bulletin*, **59**, 986-996.

HORSEFIELD, B., YORDY, K.L. & CRELLING, J.C 1988. Determining the Petroleum-generating Potential of Coal using Organic Geochemistry and Organic Petrology. *Organic Geochemistry*, **13**, 121-129.

HUC, A.Y. 1988. Sedimentology of organic matter. *In*: FRIMMEL, F.H. & CHRISTMAN, R.F. (eds) *Humic Substances and Their Role in the Environment*, Dahlem Konferenzen, John Wiley, pp. 215-243.

HUC, A.Y. 1990. Understanding organic facies: A key to improved quantitative petroleum evaluation of sedimentary basins. *In*: HUC, A.Y. (ed.) *Deposition of Organic Facies*,AAPG Studies in Geology **30**, pp. 1-12.

HUNT, J.M. 1978. Characterization of bitumens and coals. *American Association of Petroleum Geologists Bulletin*, **62**, 301-303.

HUNT, J.M. 1979. *Petroleum Geology and Geochemistry*. (1st Edition) Freeman, San Francisco, 617pp.

HUTTON, A. C. & COOK, A.C. 1980. Influence of alginite on reflectance of vitrinite from Joadja, NSW, and some other coals and oil shales containing alginite. *Fuel*, **59**, 711- 714.

HUTTON, A.C. & COOK, A.C. 1981. Classification of oil shales. *Bulletin Centre Recherche Exploration-Production, Elf Aquitaine*, **5**, 319-352.

HUTTON, A.C., KANTSLER, A.J. & COOK, A.C. 1980. Organic matter in oil shales. *Australian Petroleum Exploration Association Journal*, **20**, 44-68.

INTERNATIONAL COMMITTEE FOR COAL PETROLOGY 1963. *Handbook of Coal Petrology*. (1st Edition), Centre Nationale de la Recherche Scientifique, Paris.

INTERNATIONAL COMMITTEE FOR COAL PETROLOGY 1971. *Handbook of Coal Petrology*. (1st supplement to 2nd Edition), Centre Nationale de la Recherche Scientifique, Paris.

INTERNATIONAL COMMITTEE FOR COAL PETROLOGY 1975. *Handbook of Coal Petrology*. (2nd supplement to 2nd Edition), Centre Nationale de la Recherche Scientifique, Paris.

INTERNATIONAL COMMITTEE FOR COAL PETROLOGY 1995. *Vitrinite classification, ICCP System 1994*. Aachen, Germany, 24pp.

INTERNATIONAL COMMITTEE FOR COAL PETROLOGY 1998. *Inertinite classification*, Draft document of Commission I, 49th ICCP Auckland, New Zealand pp. 9-12.

ISSLER, D.R. 1984. Calculation of organic maturation levels for offshore eastern Canada - implications for general application of Lopatin's method. *Canadian Journal of Earth Science*, **21**, 477- 488.

JACOB, H. 1983. Mikroscopische Analyse fester bis halbfester Erdölbitumina. *Microscopica Acta*, **87**, 277-291.

JACOB, H. 1985. Migration and Maturity in Prospecting for Oil and Gas; A Model Study in NW Germany. *Erdöl und Kohle-Erdgas-Petrochemie. Brennstoff-Chemie*, **38**, 365.

JACOB, H. 1989. Classification, structure, genesis and practical importance of natural solid oil bitumen ("migrabitumen"). *International Journal of Coal Geology*, **11**, 65-79.

JACOB, H.& HILTMANN, W. 1985. Disperse bitumen solids as an indicator for migration and maturity within the scope of prospecting for petroleum and natural gas - A model for NW Germany. Final report on DGMK Project 267, Deutsche Geslllschaft fur Mineralolwissenschaft und Köhlechemie E.V., Hamburg 1985, 54pp.

JANNISCH, H.W. 1987. Microbial processes at deep sea hydrothermal Vents. *In*: RONA, P.A., BOSTROM, K., LAUBIER L. & SMITH Jr., K.L. (eds) *Hydrothermal Processes at Seafloor Spreading Centres*, NATO Conferences Series **12**, Plenum Press, New York, 677-709.

JOHNSON, J. 1977. *A Geothermal Study of the Lower Carboniferous along the Howick Shore, Northeast Northumberland*, (U.K.). Unpublished M.Sc. Dissertation, University of Newcastle-upon-Tyne, 47pp.

JONES, J.M. & CREANEY, S. 1977. Optical character of thermally metamorphosed coals of northern England. *Journal of Microscopy*, **109**, 105-118.

JONES, J.M., MURCHISON, D.G.M., & SALEH, S.A. 1972. Variation in vitrinite reflectivity in relation to lithology. *In*: WEHNER & H.R. VON GAERTNER H. (eds.) *Advances* in *Organic Geochemistry 1971*, Pergammon, pp. 601-612.

KALKREUTH, W. D. 1982. Rank and petrographic composition of selected Jurassic-Cretaceous coals of British Columbia, Canada. *Bulletin of Canadian Petroleum Geology*, **30**, 112-139.

KARWEIL, J. 1956. Due metamorphose der Kohlen vom Standpunkt der physicalischen Chemie. *Deutsch Geologishes Gestampt*, **107**, 132-138.

KHAVARI-KHORASANI, G. & MURCHISON, D.G.M. 1978. Thermally metamorphosed bitumen from Windy Knoll, Derbyshire, England. *Chemical Geology*, **22**, 91-105.

KHAVARI-KHORASANI, G. & MURCHISON, D.G.M. 1988. Order of generation of petroleum hydrocarbons from liptinitic macerals with increasing thermal maturity. *Fuel*, **67**, 1160-1162.

KIDD, F.A. 1964. The Besa River Formation. *Bulletin of Canadian Petroleum Geology*, **11**, 369-372.

KLUBOV, B.A. 1993. A new scheme for the formation and classification of bitumens. *Journal of Petroleum Geology*, **16**, 335-344.

KOCH, J. 1997. Upper limits for vitrinite and bituminite reflectance as coalification parameters. *International Journal of Coal Geology*, **33**, 169-173.

LANDIS, C.R. & CASTAŇO, J.R. 1995. Maturation and bulk chemical properties of a suite of solid hydrocarbons. *Organic Geochemistry*, **22**, 137-149.

LARTER, S. R. 1984. Application of analytical pyrolysis techniques to kerogen characterization and fossil fuel exploration/exploitation. *In*: VOORHEES, K. (ed.) *Analytical Pyrolysis: Methods and Application*, Butterworth, London, pp. 212-275.

LARTER, S. R. 1989. Chemical models of vitrinite reflectance evolution. *Geologische Rundschau*, **78**, 349-359.

LARTER, S.R. & SENTFLE, J. T. 1985. Improved kerogen typing for petroleum source rock analysis. *Nature*, **318**, 277-280.

LECKIE, D.A., POTOCKI, D.J. & VISSER, K. 1991. The Lower Cretaceous Chinkeh Formation: A Frontier Type Play in the Liard Basin of Western Canada. *American Association of Petroleum Geologists Bulletin*, **75**, 1324-1352.

LERCHE, I, YARZAB, R.F. & KENDALL, C.G.ST C. 1984. Determination of paleoheat flux from vitrinite reflectance data. *American Association of Petroleum Geologists Bulletin*, **68**, 1704-1717.

LEWAN, M.D. 1985. Evaluation of petroleum generation by hydrous pyrolysis experimentation. *Transactions Royal Society London*, Series A, **315**, 123-134.

LEWAN, M.D. 1990. Laboratory simulation of petroleum formation. *In*: ENGEL, M.H. & MACKO, S.A. (eds), *Organic Geochemistry*, Plenum, New York, pp. 419-442.

LEWAN, M.D. 1992. Assessing natural oil expulsion by source rocks by laboratory pyrolysis. *In*: MAGOON, L.B. & DOW, W.G. (eds), *The Petroleum System - from Source to Trap*. American Association of Petroleum Geologists, Memoir, **60**, 201-210.

LEWAN, M.D. & WILLIAMS, J. A. 1987. Evaluation of petroleum generation from resinites by hydrous pyrolysis. *American Association Petroleum Geologists Bulletin*, **71**, 207-214.

LEWAN, M.D., WINTERS, J.C. & MACDONALD, J.H. 1979. Generation of oil-like pyrolysates from organic-rich shales. *Science*, **23**, 879-899.

LEYTHAEUSER, K.F.A., HAGEMANN, H.W., HOLLERBACH, R.W.T.H. & SCHAEFER, K.F.A. 1980. Hydrocarbon generation in source beds as a function of type and maturation of their organic matter: as mass balance approach. *In*: *Origin, Migration and Accumulation of Hydrocarbons*. Proceedings 10th World Petroleum Congress, **2**, pp. 31-41, Heyden, London.

LILLEY, M.D., BAROSS, J.A. & GORDON, L.L. 1987. Reduced gases and bacteria in hydrothermal fluids: the Galapagos Spreading Center and 21°N East Pacific Rise. *In*: RONA, P.A., BOSTROM, K., LAUBIER L. & SMITH Jr. K.L (eds) *Hydrothermal Processes at Seafloor Spreading Centres*, NATO Conferences Series **12**, Plenum, New York, pp. 411-450.

LINK, C. M. & BUSTIN, R.M. 1989. Organic maturation and thermal history of Phanerozoic strata in northern Yukon and northwestern District of Mackenzie. *Bulletin of Canadian Petroleum Geology*, **37**, 266-292.

LISTER, G.S., ETHERIDGE, M.A. & SYMONDS, P.A. 1986. Detachment faulting and the evolution of passive continental margins. *Geology*, **14**, 246-250.

LOPATIN, N.V. 1971. Temperature and geologic time as a factor in coalification. *Akademiya Nauk SSSR Izvestiya, Seriya Geologicheskaya*, **3**, 95-106.

LYONS, P.C., FINKELMAN, R.B., THOMPSON, C.L., BROWN, F.W. & HATCHER, P.G. 1982. Properties, origin and nomenclature of rodlets of the inertinite maceral group in coals of the Central Appalachian Basin, U.S.A. *Internal Journal of Coal Geology*, **1**, 313-346.

MACHEL, H.G., KROUSE, H.R. & SASSEN., R. 1995. Products and distinguishing criteria of bacterial and thermochemical sulphate reduction. *Applied Geochemistry*, **10**, 373-389.

MACKAY, G., NG, N. & RUSSELL, N.J. 1984. Information sheets on hydrogenation residues.- nomenclature. Draft proposal to Commission III, International Committee for Coal Petrology, Calgary, 1984.

MACQUEEN, R.W. & SANDBERG, C.A. 1970. Stratigraphy, age and inter-regional correlation of the Exshaw Formation, Alberta Rocky Mountains and Foothills. *Bulletin of Canadian Petroleum Geology*, **18**, 32-66.

MACKOWSKY, M.-Th. 1982. Methods and Tools of Examination. *In*: STACH, E., MACKOWSKY, M.-TH., TEICHMÜLLER, M., TAYLOR, G.H., CHANDRA & TEICHMÜLLER, R., *Stach's Textbook of Coal Petrology*. (3rd Edition), Gebrüder Borntraeger, New York , pp. 295-371.

MAJOROWITZ, J.A, JONES F.W. & JESSOP, A.M. 1989. Preliminary geothermics of the sedimentary basins in the Yukon and Northwest Territories (60°N - 70°N) - estimates from petroleum bottom-hole temperature Data. *Bulletin of Canadian Petroleum Geology*, **36**, 39-51.

MAKO, D.A. & SHANKS, W.C. 1984. Stratiform sulphide and barite-fluorite mineralization of the Vulcan Prospect, Northwest Territories: exhalation of basinal brines along a fault continental margin. *Canadian Journal of Earth Sciences*, **21**, 78-91.

MARSH, H., DACHILLE, F., ILEY, M., WALKER, P.L. & WHANG, P.W. 1973. Carbonization and liquid crystal (mesophase) development. 4. Carbonization of coal-tar pitches and coals of increasing rank. *Fuel*, **52**, 253-261.

MATOIL™ (1990). *A Quantitative Model of Hydrocarbon Generation for the Personal Computer*. Bureau d'Etudes Industrielles et de Cooperation de l'Institute Français du Petrole. Reuil-Malmaison, France.

McCARTNEY, J.T & TEICHMULLER, M. 1972. Classification of coals according to the degree of coalification by reflectance of the vitrinite component. *Fuel*, **51**, 64-68.

MEIR-DREES, N. C. 1989. Sedimentology and facies analysis of Devonian rocks, southern District of Mackenzie, Northwest Territories, Canada.. *Geologica Ultraiectina*, **63**, 202pp.

MICHELSON, J.K. & KHAVARI-KHORASANI, G. 1990. Monitoring chemical alterations of individual oil-prone macerals by means of microscopical fluorescence spectroscopy combined with multivariate data analysis. *Organic Geochemistry*, **15**, 172-192.

MISRA, B.K., SINGH, B.D. & NAVALE, G.K.B. 1990. Resino-inertinites of Indian Permian coals-their origin, genesis and classification. *International Journal of Coal Geology*, **14**, 277-293.

MIDDLETON, M.F. 1982. Tectonic history from vitrinite reflectance. *Geophysical Journal of the Royal Astronomical Society*, **68**, 121-132.

MITCHELL, G.D., DAVIS, A. & SPACKMAN, W. 1977. A petrographic classification of solid residues from the hydrogenation of bituminous coals. *In*: ELLINGTON, R.T. (ed.) *Liquid Fuels from Coal*, Academic Press Inc., New York, pp. 255-271.

MOMPER, J.A. 1978. Oil migration limitations suggested by geological considerations. *In*: *Physical and Chemical Constraints on Petroleum Migration*, AAPG Short Course Notes, **1**, AAPG National Meeting, Oklahoma City, American Association of Petroleum Geologists, 60pp.

MOORE, P.F. 1993. Devonian. *In*: STOTT, D.F. & AITKEN, J.D. (eds) *Sedimentary Cover of The Craton in Canada*, Geological Survey of Canada, **5**, pp. 151-200 (<u>also</u> Geological Society of America, *The Geology of North America*, D-1).

MORROW, D.W & GALLAGHER, K. (in press). A novel approach for constraining heat flow histories in sedimentary basins. *In*: DUPPENBECKER, S.J. & ILIFFE, J.E. (eds) *Basin Modelling: Practice and Progress*, Geological Society of London, Special Publication, **141**, 223-239.

MORROW, D.W., CUMMING, G.L. & KOEPNICK, R.B. 1986. Manetoe Facies - a gas-bearing, megacrystalline, Devonian dolomite, Yukon and Northwest Territories, Canada. *American Association of Petroleum Geologists Bulletin*, **70**, 702-720.

MORROW, D.W. & ISSLER, D. R. 1993. Calculation of vitrinite reflectance from thermal histories: a comparison of some models. *American Association of Petroleum Geologists*, **77**, 610-624.

MORROW, D.W. & GELDSETZER, H.H.J. 1998. Devonian of the Eastern Canadian Cordillera. Canadian Society of Petroleum Geologists Memoir, **14**, 85-121.

MORROW, D.W. & POTTER, J. 1998. Internal stratigraphy, petrography and porosity development of the Manetoe Dolomite in the region of the Pointed Mountain and Kotaneelee gas fields. *In: HOGG, J.R. (ed.) Oil and Gas Pools of the Western Canada Sedimentary Basin*, Canadian Society Petroleum Geologists Special Publication **51**, 137-161.

MORROW, D.W., POTTER, J. RICHARDS, B.C. & GOODARZI, F. 1993. Paleozoic burial and organic maturation in the Liard Basin region, northern Canada. *Bulletin of Canadian Petroleum Geology*, **41**, 17-31.

MUKHOPADHYAY, P. 1994. Vitrinite reflectance as a maturity parameter: petrographic and molecular characterization and its applications to basin modeling. *In:* MUKHOPADHYAY, P. & DOW, W.G. (eds) *Vitrinite Reflectance as a Maturity Parameter: Applications and Limitations*, ACS Symposium Series **570**, American Chemical Society, Washington D.C., pp. 1-25.

MUKHOPADHYAY, P., WADE, J.A. & WILLIAMSON, M.A. 1994b. Measured versus predicted vitrinite reflectance from Scotian Basin wells. *In*: MUKHOPADHYAY, P. & DOW, W.G. (eds) *Vitrinite Reflectance as a Maturity Parameter: Applications and Limitations*, ACS Symposium Series **570**, American Chemical Society, Washington D.C., pp. 231-246.

MURCHISON, D.G.M. 1978. Optical Properties of Carbonized vitrinites. *In*: KARR, K.C. (ed.) *Analytical Methods for Coal and Coal Products*, **2**, Academic, NewYork, pp. 416-464.

NANDI, B.N., CIAVAGLIA, L.A. & MONTGOMERY, D.S. 1977. The variation of the microhardness and reflectance of coal under conditions of oxidation simulating weathering. *Journal of Microscopy*, **109**, 93-103.

NISSENBAUM, A. & KAPLAN, J.R. 1972. Chemical and isotopic evidence for the in situ origin of marine humic substances. *Limnology and Oceanography*, 17 , 570-582.

OKULITCH, A.V. (coordinator), 1995. *Geologic Time Scale 1995*. Geological Survey of Canada Geological Atlas, Open File 3040.

OSADETZ, K. & MOTTERSHEAD, K. 1992. Burial: A program that calculates and draws the burial history curves and thermal maturity history for a stratigraphic section. *Geological Survey of Canada*, Paper **19-91**, 44pp.

OTTENJANN, K., TEICHMÜLLER, M. & WOLF, M. 1975. Spectral fluorescence measurements of sporinites in reflected light and their applicability for coalification studies. *Journal of Microscopy*, **109**, 1-28.

PATRICK, J.W., REYNOLDS, M.J. & SHAW, F.H. 1973. Development of optical anisotropy in vitrains during carbonization. *Fuel*, **52**, 198-204.

PATTON, W.J.H. 1958. Mississippian Succession in South Nahanni River Area, Northwest Territories. *In*: GOODMAN, A.J. (ed.), *Jurassic and Carboniferous of Western Canada*, John Andrew Allan Memorial Volume American Association of Petroleum Geologists, pp. 309-326.

PELTZER, E.E. 1966. Mineralogy, geochemistry and stratigraphy of the Besa River Shale, British Columbia. *Bulletin of Canadian Petroleum Geology*, **14**, 273-321.

PENIGUEL, G., COUDERC, R. & SEYVE, C. 1989. Les microalgues actuelles et fossiles - interests stratigraphique et pètrolier. *Bulletin Centre Recherche Exploration-Production, Elf-Aquitaine*, **13**, 455-482.

PETERS, K.E. 1986. Guidelines for evaluating petroleum source rock using programmed pyrolysis. *American Association of Petroleum Geologists Bulletin*, **70**, 318-329.

PETERS, K.E. & CASSA, M.R. 1994. Applied source rock geochemistry. *In*: MAGOON, L.B. & DOW, W.G. (eds) *The Petroleum System - from Source to Trap*. American Association Petroleum Geologists, Memoir, **60**, 93-120.

PETERS, K.E., ISHIWATARI, R. & KAPLAN, I.R. 1982. Color of Kerogen as Index of Organic Maturity. *In*: CLUFF, R.M. & BARROWS, M.H. (compilers) Hydrocarbon Source Rock and Generation Evaluation (Origin of Petroleum III). American Association of Petroleum Geologists Reprint Series No.24, pp.70-77.

POTTER, J., DAWSON, W.H., RAHIMI, P. & McDOUGALL, W.J. 1986. Characterization of coprocessing residues. *In*: MOULJIN, J.A., CHERMIN, K.A. & NATER, H.A.G. (eds) *1987 International Conference on Coal Science and Technology*, Maastricht, Netherlands, 1985, Elsevier, pp. 391-394.

POTTER, J., RICHARDS, B.C., MORROW, D.W. & GOODARZI, F. 1993. The Organic petrology and thermal maturity of Lower Carboniferous and Upper Devonian source rocks in the Liard Basin at Jackfish Gap -Yohin Ridge and North Beaver River, Northern Canada: implications for hydrocarbon exploration. *Energy Sources*, **15**, 289-314.

POWELL, T.G. 1984. Some Aspects of the hydrocarbon geochemistry of a Devonian barrier reef complex Western Canada. *In*: PALACAS, J.G.(ed.) *Petroleum Geochemistry and Source Rock Potential of Carbonate Rocks*. American Association of Petroleum Geologists Studies in Geology Series, **18**, pp. 45-61.

POWELL, T.G. & SNOWDON, L.R. 1983. A composite hydrocarbon generation model: implications for evaluation of basins for oil and gas. *Erdöl und Köhle, Erdgas, Petrochemie*, **63**, 163-169.

POWELL, T.G., CREANEY, S. & SNOWDON, L.R. 1982. Limitations of use of organic petrographic techniques for identification of petroleum source rocks. American Association of Petroleum Geologists Bulletin, **66**, 430-435.

PRATT, K.C., 1986. *Summary of preparation techniques for organic petrography*. Institute Sedimentary and Petroleum Geology Internal report, Geological Survey of Canada, 12pp.

PRESS, W.H., TEUKOLSKY, S.A., VETTERLING, W.T. & FLANNERY, B.P. 1992. Are two distributions different? K-S test for unbinned distributions. *In*: *Numerical Recipes in Fortran and the art of Statistical Compilation*. University of Cambridge Press, pp. 617-620.

SCHOPF, J.M. & WALTER, M.R. 1982. Origin and early evolution of cyanobacteria: the Geological evidence. *In*: CARR, N.G. & WHITTON, B.A. (eds) *The Biology of Cyanobacteria*. University of California Press, Berkeley, pp. 543-564.

SCOFFIN, T., 1987. Diagenesis of Impure Limestones. In: *An Introduction to Carbonate Sediments and Rocks*, (p.139). Blackie, Glasgow & London.

SENTFLE, J., BROWN, J.H. & LARTER, S.R. 1987. Refinement of organic petrographic methods for kerogen characterization. *International Journal of Coal Petrology*, **7**, 105-117.

SENTFLE, J.T., LANDIS, C.R. & M'LAUGHLIN, R. 1996. Organic petrographic approach to kerogen characterization. *In*: ENGEL, M.H. & MACKO, S.A. (eds) *Organic Geochemistry: Principles and Applications*. Plenum Press, New York, pp. 355-396.

SHERWOOD, N.R. & COOK, A.C. 1986. Organic matter in the Tooloebuc Formation. *In*: GRAVESTOCK, D.I., MOORE, P.S.& PITT, G.M. (eds.) *Contributions to the Geology of and Hydrocarbon Potential of the Eromanga Basin*, Geological Society of Australia, Special Publication, **12**, pp. 255-65.

SHIBOAKA, M. 1983. Genesis of micrinite in some Australian coals. *Fuel*, **62**, 639-644.

SIMONEIT, B.R., 1983. Effects of hydrothermal activity on sedimentary organic matter: Guaymas Basin, Gulf of California - Petroleum genesis and proto-kerogen degradation. *In*: RONA, P.A., BOSTROM, K., LAUBIER, L. & SMITH, K.L. Jr. (eds) *Hydrothermal Processes at Sea floor Spreading Centres*. Plenum Press, New York, pp. 451-471.

SIMONEIT, B.R. 1984. Hydrothermal effects on organic matter-high vs low temperature components. *Organic Geochemistry*, **6**, 857-864.

SIMONEIT, B.R. 1985. Hydrothermal petroleum: genesis, migration, and deposition in Guaymas Basin, Gulf of California. *Canadian Journal of Earth Sciences*, **22**, 919-929.

SNOWDON, L.R. & FOWLER, M.R. 1986. The interpretation of geochemical data. Unpublished Short Course Notes, *Geological Survey of Canada*.

STACH , E. 1968. Basic Principles of Coal Petrology: macerals, microlithotypes and some effects of coalification. *In*: MURCHISON ,G.G. & WESTOLL, T.S. (eds) *Coal and Coal-bearing Strata*, Oliver and Boyd, Edinburgh, pp. 3-17.

STACH, E. 1982. The microscopically recognizable constituents of coal. *In*: STACH, E., MACKOWSKY, M.-TH., TEICHMÜLLER, M., TAYLOR, G.H., CHANDRA & TEICHMÜLLER, R. *Stach's Textbook of Coal Petrology*. *(2nd* Edition) Gebrüder Borntraeger, New York, pp. 87-139.

STAPLIN, F. L. 1969. Sedimentary organic matter, organic metamorphism and oil and gas occurrence. *Bulletin of Canadian Petroleum Geology*, **17**, 44-66.

STAPLIN, F. L., 1960. Upper Mississippian plant spores from the Golata Formation, Alberta, Canada. *Palaeontographica*, **107**, 1-40.

STASIUK, L.D. 1988. *Thermal maturation and Organic Petrology of Mesozoic Strata of Southern Saskatchewan*. Unpublished M.Sc. thesis, University of Regina, 178pp.

STASIUK, L.D. 1991. Organic petrology and petroleum formation in Paleozoic rocks of Northern Williston Basin, Canada. Unpublished Ph.D. thesis, University of Regina, 312pp.

STASIUK, L.D. 1993. Algal bloom episodes and the formation of bituminite and micrinite in hydrocarbon source rocks: evidence from the Devonian and Mississippian, northern Williston Basin, Canada. *International Journal of Coal Geology*, **24**, 195-210.

STASIUK, L.D. 1994. Fluorescence properties of Paleozoic oil-prone alginite in relation to hydrocarbon generation, Williston Basin, Saskatchewan, Canada. *Marine and Petroleum Geology*, **11**, 219-231.

STASIUK, L.D. (1998). The origin of pyrobitumens in Upper Devonian Leduc Formation gas reservoirs, Alberta, Canada: an optical and EDS study of oil and gas transformation. *Marine and Petroleum Geology*, **14**, 915-929.

STASIUK. L.D. & FOWLER, M.G. 1994. Paleozoic hydrocarbon source rocks, Truro Island, Arctic Canada: organic petrology, organic geochemistry and thermal maturity. *Bulletin of Canadian Petroleum Geology*, **42**, 419-431

STASIUK, L.D. & OSADETZ, K.G. 1993. Thermal maturity, alginite-bitumen transformation, and hydrocarbon generation in Upper Ordovician source rocks, Saskatchewan, Canada. *Energy Sources*, **15**, 205-237.

STASIUK, L.D. , OSADETZ, K. G. & POTTER, J. 1990. Fluorescence spectral analysis and hydrocarbon exploration; examples from potential Paleozoic source rocks, Saskatchewan. *In*: BECK, L.S. & HARPER, C.T. (eds) *Modern Exploration Techniques*. Saskatchewan Geological Society Special Publication, **10**, pp. 242-251.

STASIUK, L.D, GOODARZI, F. & POTTER, J. 1993. Thermal maturity of Mesozoic strata of southern Saskatchewan. *Bulletin of Canadian Petroleum Geology*, **41**, 218-231.

STASIUK, L.D, GOODARZI, F. & FOWLER, M.G. 1994. Corpohuminite from Canadian Paleozoic source rocks: petrology and reflectance. *In:* MUKHOPADHYAY, P. & DOW, W.G. (eds) *Vitrinite Reflectance as a Maturity Parameter: Applications and Limitations*, ACS Symposium Series **570**, American Chemical Society, Washington D.C., pp. 52-63.

STOAKES, F. 1990. Hydrocarbon source rocks of the Exshaw Formation in Alberta. *In*: Hydrocarbon Source Rocks of the Exshaw Duvernay Formations, Alberta. Stoakes Campbell Geoconsulting Ltd.

STOTT, D.F. & KLASSEN, R.W. 1993. Geomorphic Divisions. *In*: STOTT, D.F. & AITKEN, J.D. (eds.) *Sedimentary Cover of the The Craton in Canada*, Geological Survey of Canada, pp. 31-44. (also Geological Society of America, *The Geology of North America*, D-1).

SULLIVAN, H. 1965. Palynological evidence concerning the regional differentiation of Upper Mississippian floras. *Pollen and Spores*, **7**, 539-563.

SWEENEY, J. & BURNHAM, A.K. 1990. Evaluation of a Simple model of vitrinite reflectance based on chemical kinetics. *American Association of Petroleum Geologists Bulletin*, **74**, 1559-1570.

TAYLOR, G. & LIU, S. 1989. Micrinite - its nature, origin and significance. *International Journal of Coal Geology*, **14**, 29-46.

TEICHMÜLLER, M. 1974. Uber neue Macerale der Liptinite-Gruppe und die Entstehung des micrinites. *Fortschritte der Geologishe Rheinland-Westfalen*, **243**, 37-64.

TEICHMÜLLER, M. 1982a. Origin of the petrographic constituents of coal. *In*: STACH, E., MACKOWSKY, M.-Th., TEICHMÜLLER, M. , TAYLOR, G.H., CHANDRA, D. & TEICHMÜLLER, R., *Stach's Textbook of Coal Petrology*. (2nd Edition) Gebrüder Borntraeger, New York, pp. 219-294.

TEICHMÜLLER, M. 1982b. The importance of coal petrology in prospecting for oil and gas. *In*: STACH , E., MACKOWSKY, M.-Th., TEICHMULLER, M. , TAYLOR, G.H., CHANDRA, D & TEICHMÜLLER, R., *Stach's Textbook of Coal Petrology*. (2nd Edition), Gebrüder Borntraeger, New York, 381- 413.

TEICHMÜLLER, M. 1982c. The origin of sapropelic coals. *In*: STACH , E., MACKOWSKY, M.-Th., TEICHMÜLLER, M. , TAYLOR, G.H., CHANDRA, D. & TEICHMÜLLER, R., *Stach's Textbook of Coal Petrology*. (2nd Edition) Gebrüder Borntraeger, New York, pp. 291-293.

TEICHMÜLLER, M. 1982d . Fluorescence-microscopical changes of liptinites and vitrinites during coalification and their relationship to bitumen generation and coking behaviour. *Geologisches Landesamt NordRhein-Westfalen*, Krefeld, 1982.

TEICHMÜLLER, M. 1985. Bituminite in rocks other than coal. Draft document of the International Committee for Coal Petrology Nomenclature Subcommission.

TEICHMÜLLER, M. & DURAND, B. 1983. Fluorescence microscopical rank studies on liptinites and vitrinites in peats and coals and comparison with results of Rock-Eval pyrolysis. *International Journal of Coal Geology*, **2**, 197-230.

TEICHMÜLLER, M. & OTTENJANN, K. 1977. Liptinites and Lipoid substances in a petroleum source rock. *Erdol und Kohle, Erdgas, Petrochemie. Brenstoff Chemie*, **30**, 387- 398.

TEICHMÜLLER, M. & TEICHMÜLLER R. 1966. *Geological Causes of Coalification - Coal Science*. Advances in Chemistry Series **55**. Washington, D.C., pp. 135-155.

TEICHMÜLLER, M. & TEICHMÜLLER R. 1966. Geological aspects of coal metamorphism. In: MURCHISON D.G. & WESTOLL, T.S. (eds) *Coal and Coal-Bearing Strata*, Oliver and Boyd, London, pp. 233-267.

TEICHMÜLLER, M. & TEICHMÜLLER R. 1982. The geological basis for coal formation. In: STACH , E., MACKOWSKY, M.-Th., TEICHMÜLLER, M. , TAYLOR, G.H., CHANDRA, D & TEICHMÜLLER, R., *Stach's Textbook of Coal Petrology*. (2nd Edition), Gebrüder Borntraeger, New York, pp. 5-82.

TISSOT, B., CALIFET-DEBYSER, Y., DEROO, G. & OUDIN, J.L. 1981. Origin and evolution of hydrocarbons in early Toarcian shales, Paris Basin, France. *American Association of Petroleum Geologists Bulletin*, **55**, 2173-2193.

TISSOT, B., DURAND, B., ESPITALIÉ, J. & COMBAZ, A. 1974. Influence of Nature and diagenesis of organic matter in petroleum generation. *American Association of Petroleum Geologists Bulletin*, **58**, 499-506.

TISSOT, B. & ESPITALIÉ, J. 1975. L'evolution thermique de la matière organique des sediments: application d'une simulation mathematique. *Revue de l' Institut Français Pètrole*, **30**, 743-777.

TISSOT, B.P. & WELTE, D.H. 1984. *Petroleum Formation and Occurrence*. (2ndEdition) Springer, New York, 699pp.

TISSOT, B.P., PELET, R. & UNGERER, P. 1987. Thermal History of sedimentary basins, maturation indices, and kinetics of oil and gas generation. *American Association of Petroleum Geologists Bulletin*, **71**, 1445-1466.

TORRIE, J.E. 1973. North eastern British Columbia. *In*: McCROSSAN, R.G. (ed.) *Future Petroleum Provinces of Canada*, Canadian Society Petroleum Geologists Memoir, **1**, pp. 151-186.

TYSON, R.V. 1987. The genesis and palynofacies characteristics of marine petroleum source rocks. *In*: BROOKS , J. & FLEET, A.J. (eds) *Marine Petroleum Source Rocks*, Geological Society of London Special Publication **26**, pp. 47-67.

TYSON, RV. & PEARSON, T.H. 1991. Modern and ancient continental shelf anoxia: an overview. *In*: TYSON, R.V.& PEARSON, T.H. (eds) *Modern and Ancient Continental Shelf Anoxia*. Geological Society of London Special Publication **58**, pp. 1-24.

TYSON, R. V. 1995. *Sedimentary Organic Matter: Organic Facies and Palynofacies*. Chapman and Hall, London, 615pp.

UTTING, J. 1987. Palynology of the Lower Carboniferous Winsor Group and Winsor-Canso Boundary Beds of Nova Scotia, New Brunswick and Newfoundland. Geological Survey of Canada Bulletin **374**, 92pp.

UTTING, J. 1981. Palynology of samples from the Mattson Formation (Mississippian) of the Jackfish Gap , southwest District of Mackenzie, NTS 95 64. *Geological Survey of Canada* Internal report **1-1981-JU.**

UTTING, J. 1989. Palynomorphs and TAI data. In: RICHARDS, B.C. *Uppermost Devonian and Lower Carboniferous Stratigraphy, Sedimentation, and Diagenesis, southwestern District of Mackenzie and southeastern Yukon Territory. Geological Survey of Canada Bulletin* **390**, Appendix E, 13pp.

VASSOYEVICH, N.B., YU, I., KORCHAGINA, N.V., LOPATIN, N.V. & CHERNYSHEV, V.V. 1969. Principal phase of oil formation. International Geology Reviews 1970, **12**, 1276-1296.

van GIJZEL, P. 1979. Manual of the Techniques and some Geological Applications of Fluorescence Microscopy; American Association of Stratigraphic Palynologists-Core Laboratories Workshop, Dallas Texas.

van KREVELEN. D.W., 1981. *Coal Typology-Chemistry-Physics-Constitution.* (2nd Edition). Elsevier, Amsterdam, 314pp.

VLEESKENS, J.M., VAN HAASTEREN, A.W.M.B., ROOS, C.M. & GERRITS, B.J., 1987. Effect of coke formation on combustion efficiency during recycling of FBC fly ash. *In*: MOULJIN, J.A., CHERMIN, K.A. & NATER, H.A.G. (eds) *1985 International Conference on Coal Science and Technology*, Maastricht, Netherlands, 1985. Elsevier Science, Amsterdam, pp. 881-884.

WALKER, J.C.G., KLEIN, C., SCHIDLOWSKI, M., SCHOPF, J.W., STEVENSON, D.J & WALTER, M. 1983. Environmental evolution of the Archean-Early Proterozoic Earth. *In*: SCHOPF, J.W. (ed.) *Earth's Earliest Biosphere: its origin and evolution.* Princeton University Press, Princeton, pp. 260-320.

WAPLES, D. 1980. Time and temperature in petroleum formation: application of lopatin's method to petroleum exploration. *American Association of Petroleum Geologists Bulletin* **64**, 916-926.

WELTE, D.H. & YUKLER, A. 1980. Evolution of sedimentary basins from the standpoint of petroleum origin and accumulation - an approach for a quantitative basin study. *Organic Geochemistry*, **2**, 1-8.

WINTERS, J.C., WILLIAMS, J.A. & LEWAN, M.D. 1983. A laboratory study of petroleum generation by hydrous pyrolysis. *In:* M. BJORÖY *et al.* (eds) *Gas chromatography-mass spectrometry*. Advances in Organic geochemistry 1981, Wiley, Chichester, pp. 524-533.

WRIGHT, G.W., McMECHAN, M.E. & POTTER, D.E.G. 1994. Structure and architecture of the Western Canada Sedimentary Basin. *In:* MOSSOP, G.& SHETSEN, I. (compilers) *Geologic Atlas of the Western Canada Sedimentary Basin*, Canadian Society Petroleum Geologists-Alberta Research Council, Calgary, pp. 25-40.

ZIELINSKI, R.E. & M^cIVER, R.D. 1982. Synthesis of organic geochemical data from the eastern gas shales. *SPE/DOE Unconventional Gas Recovery Symposium*, Preprint 10793, pp. 39-50.

APPENDIX A
ORGANIC PETROLOGY
(by formation)

Appendix A

Sample I.D. numbers refer to subsurface depths in feet; + value indicates outcrop section elevations in feet;
Abbreviations: assoc. = associated; ext. = extensive; dev. developed; abt. = abundant; blk.= black; frac. = fracture; m'frac. = microfracture; w. =- with; ind. = indigenous; Ct. = calcite; //l = parallel; lamin. = laminated; vert. = vertical; horiz. = horizontal; org.-rich = organic-rich; dol. = dolomitic/dolomitized; brn = brown; stn = staining; bitum. = bituminous; interbed.= interbedded; th.wall = thick walled; tw = thin-walled; birefl.= bireflectance; mod. = moderate/moderately; alg. = algal; med. Ro = medium reflectance; strgs = strings/stringers; framb. = framboidal; crass. = crassispores; Leiosph. = Leiospheridiales;

Well location	Samp No. GSC C#	I.D.	Rock type	Notes	Dominant macerals	Subordinate macerals
Imperial Island R.	186751	6906	3-4d	pyritic, laminated org rich shale, anisotropic bitumen	bituminite-micrinite matrix, med & high Ro bitumens	bituminite-alginite
Dome *et al* Trout L	186768	4890	4-5d	organofacies differs from above; ext-dev. microfracture network	blk matrix bituminite-micrinite, indigenous bitumens	
Murphy Muskeg R	186767	6311	4	indig. microporous bitumens; ext-dev. microfracture network	blk matrix bituminite-micrinite;	
Imp Sun Arrowhead	186764	6110	4	blk shele, ext. vert. and horiz. microfracture network	blk matrix bituminite-micrinite	med & high Ro bitumens
Imp Sun Arrowhead	186764	6116	4	laminated shale; abt carbonate, abt pyrite ?algal laminite	blk bituminte-micrinite matrix	Type 3 bitumen, type 4 bitumen
Imp Sun Arrowhead	186764	6122	4	blk shale, abt pyrite, rare dolomite, frac network	blk bituminite-micrinite matrix	anisotropic type 4 & 5 bitumen
Imp Sun Arrowhead	186764	6134	4	lamin blk shale,toothlike microfossil; abt, dolomite,pyrite	blk bituminite-micrite matrix	Type 3 bitumen> type 4 bitumen
P.A. Home Celibeta	186765	7060	4	marly shale w. microfractures; ext-dev organic network	blk matrix bituminite, low Ro 3 bitumen	
Texaco Bovie L	186762	9535	4	v. organic rich shale w. Ct-lined microfractures	bituminous matrix-micrinite, bituminite III,	Type 3, 4 & 5 bitumens
Texaco Bovie L	186762	9598	4	bitumens assoc. pores/dolomite w. anisotropic mosaics	blk bituminite-micrinite matrix, bituminite III,	high grade typ 3 & 4 bitumens
Texaco Bovie L	186762	9613.5	4	bitumens w. mosaic textures (thermal alteration)	bituminous matrix-micrinite, bituminite III,	high grade type 3 & 4 bitumens
Texaco Bovie L	186762	9611	4	type 3 bitumens //l bedding, well laminated	blk micritic ,bituminous matrix,	high grade type 3 & 4 bitumens
Imperial Netla	186764	6285	4-d	blk-marly pyritic shale, dolomitic, microfracture network	blk matrix bituminite-micrinite (95%)	high grade type 4 & 5 bitumens
Imperial Netla	186764	6315	4	type 4 bitumens assoc. dolomite-fill pore/microfracture network	blk matrix bituminite-micrinite	Type 4 bitumens in micropores
Pan Am Mattson Ck	1867–	1600	4-d	laminated, dolomitic, blk bituminous shale , abt pyrite	blk matrix bituminite-micrinite	Type 3 (algal) & 4 bitumen
Pan Am Mattson Ck	1867–	1640	4-d	pyritic shale , abt. euhedral dolomite, pervasive pyrite	blk matrix bituminite-micrinite	med Ro and high R bitumens

org -rich = organic-rich; blk = black; indig. = indigenous; assoc. = associated with; w. = with; //l = parallel to; Ct = calcite; ext = extensively; dev. = developed; ; abt=abundant

Table A1 Petrographic characteristics of the Muskwa Formation.

Well location	Sample No GSC C#	I.D.	Rock type	Notes	Dominant macerals	subordinate macerals	Interpetation of orinigal kerogen
B-A Texaco Arrowhead N-2	C186752	7005	6-7	pervasivebituminite suggests formerly liptodetrinite	indigenous bitumens	microbituminite abt	II
B-A Texaco Arrowhead N-2	C186758	7505	6-7	former h/c source rock	bituminite //l bdg,	ind bitumens	II
B-A Texaco Arrowhead N-2	C186758	8105	6-7	residual/indigenous bitumens	bituminite		
Imperial Sun Arrowhead I-46	C186757	4640	2	Ro variations due to oxidation	indigenous bitumens	bituminite	
Imperial Sun Arrowhead I-46	C186757	5160	5-8	some oxidation/heating			
Imperial Sun Arrowhead I-46	C186757	5510	5-d				
Texaco NFA Bovie Lake J-72	C186762	7305	5		indigenous bitumens	bituminite III (micrinite)	II
Texaco NFA Bovie Lake J-72	C186762	7705	4	bitumin spore has same Ro as med,Ro bit (1.86)	indig. bitumens		II
Texaco NFA Bovie Lake J-72	C186762	8855	5		dispersed bitumens		
Texaco NFA Bovie Lake J-72	C186762	9470	4	high Ro bit show high birefl and basic anisotropy		dispersed bitumens	II
Imperial Sun Netla C07	C186764	4145	7/8-d	dol. marl interbed brn shale (?Fe dolomite)	Low & med Ro bitumens	alginite (Leiosph-type)	II
Imperial Sun Netla C07	C186764	4515	3/4	dol. marl interbed brn shale (?Fe dolomite)	low , med Ro bitumens	dolomitized alginite, alg bituminite	II
Imperial Sun Netla C07	C186764	4815	3/2-d	type 3 bitumen assoc Tasmanites	algal bituminites	low & med Robitumens	II
Imperial Sun Netla C07	C186764	5175	5		med, high Ro bitumens	algal bituminite	II
Imperial Sun Netla C07	C186764	5420	5		med & high Ro bitumens	algal bituminite, low Ro bitumens	II
Imperial Sun Netla C07	C186764	5971	5	interbed brn(algal bituminite) and grey (barren) shales	med & high Ro bitumens	low Ro bitumens , alg bituminite	II
Murphy *et al.* Muskeg River No.1	C186767	4870	2	no low Ro bitumens (?converted to H/C)	bituminite fr litpodetrinite	med & high Ro bitumens only	
Murphy *et al.* Muskeg River No.1	C186767	5275	2-d	extensive oxidation	med and high Ro bitumens	bituminite (liptodetrinite)	
Murphy *et al.* Muskeg River No.1	C186767	5765	2	fresh pyrite- little oxidation	med Ro pore-fill bitumens	bituminite (liptodetrininite)	
Murphy *et al.* Muskeg River No.1	C186767	6065	2	dk stain matrix; high std dev Ro bitumens-anisotropy	dk brn-blk bituminite fr. liptodetrinite	med and low Ro bitumens	
Pan Am Home Signal Celibeta #7	C186765	5455	2-d	dol shale fresh pyrite abt	ind. bitumens and bituminite assoc pyrite		
Pan Am Home Signal Celibeta #7	C186765	5775	2-d	dol shale; ?oxidation	med and high Ro bitumens		
Pan Am Home Signal Celibeta #7	C186765	6145	2-d	lean shale	med and high Ro bitumens	pervasive bituminite (microalginite)	II
Pan Am Home Signal Celibeta #7	C186765	6385	2-d	lean shale	med and high Ro bitumens	(algal) bituminite	II
Pan Am Home Signal Celibeta #7	C186765	6740	2-d	lean shale	(alg) bituminite //l bdg, liptodetrinite	low & med Ro bitumens	II
Dome *et al.* Trout Lake H-45	C186768	3440	2-d	high bireflectance in bitumens	dk brn-blk bituminite specs, strings, micrinite	pore-filling bitumens	II
Dome *et al.* Trout Lake H-45	C186768	3870	2-d	bituminite "ghosts" of *Tasmanites*, m'alginite	pervasive dk brn bituminite specks	pore-filling bitumens, bitumen ass bituminite	
Dome *et al.* Trout Lake H-45	C186768	4311	2-d	bitumen\ite assoc. Tasmanitid residue :1.1% Ro	dk brn bituminite flecks & stringers (Leiosp)	pore-filling and granular ,low Ro bit3	II
Dome *et al.* Trout Lake H-45	C186768	4630	2-d	significant bireflectance in med Ro bitumen	dk brn flecks & strings of alg bituminite	microalgal bituminite, *Leioshaeridia*	II
Dome *et al.* Trout Lake H-45	C186768	4830	2-d		pore-fill bitumen (med Ro)	dk brn bituminite* low Ro bits	II
Dome *et al.* Trout Lake H-45	C186768	4890	4-5d	organofacies diff. from above; m'frac network well dev	blk matrix bituminite-micrinite,	indenous bitumens	
Imperial Island River No.1	C186751	5418	2-d/4	calc nannofossils; bitumens assoc. bituminites (assoc. liptodetrinite)	disp bitumen, brn bituminite specks &strings	liptodetrinite ; algin	
Imperial Island River No.1	C186751	5590.3	8	amorphous med Ro bitumen inclusions	bituminites		
Imperial Island River No.1	C186751	5899	8	?calcareous nannofossils	bitumens and bituminite	bituminite assoc alginite	II
Imperial Island River No.1	C186751	6240	5		med Ro bitumens		
Imperial Island River No.1	C186751-	6619	2-d	calcareus nannofossils	med Ro bitumens		
Imperial Island River No.1	C186751-	6814	4	pyritic shale, laminated;organic network	blk bituminite stringers assoc alginite		II
Pan Am Mattson Creek A-1	C1967--	1440	5	cenospheres suggests severe thermal alteration	bituminite-micrinite, liptodetrinite	anisotropic cenospheres	

* (microalginite and liptinite.-derived)

Table A2 Petrographic characteristics of the Fort Simpson Formation.

Well location	Sample No. GSC #	I.D.	Rock type	Notes	Dominant macerals	subordinate macerals	Inferred original kerogen type
B-A Texaco Arrowhead N-2	C-186758	5835	5	no low Ro bitumens assoc liptinites	bituminites , indigenous bitumens		II
B-A Texaco Arrowhead N-2	C-186758	6245	5	sl. Brn staining of natrix formerly abt liptodetrinite	bituminites, indigenous bitumens		II
Imperial Sun Arrowhead I-46	C186757	4010	5-d		residuaNindigenous bitumens	bituminite	II
Texaco NFA Bovie Lake J-72	C186762	6725	1/3	?Exshaw cavings	bituminites in carbonate		
Texaco NFA Bovie Lake J-72	C186762	6950	5/1		bituminite-micrinite matrix	bituminite III	
Imperial Sun Netla C07	C186764	3715	3-d	pyritic, mod dolomitization	alg bituminite, matrix bituminite, th.wall. & cocc .alginite	low Ro bitumens ass bituminite	II
Murphy *et al.* Muskeg River #1	C186767	4030	2		rare bituminite (micro) flecks	rare bitumens	II
Murphy *et al.* Muskeg River #1	C186767	4430	2	high Ro dev reflect sample poor sample quality	rare bituminite flecks	rare bitumens	II
Pan Am Home Signal Celibeta 7	C186765	4675	5-7	red shale-siltstone- ?oxidation or ferroan dolomite	bituminite (alg cysts)	med & granular low Ro bitumens	II
Pan Am Home Signal Celibeta 7	C186765	4935	5-7	red-brn dolomitic shale-siltstone	bituminite (algal cysts) assoc low Ro bitumen	med and high Ro bitumens	II
Pan Am Home Signal Celibeta 7	C186765	5210	5	fresh pyrite	bituminite-liptodetrinite, high Ro bitumens	rare low Ro bitumens	II
Dome *et al.* Trout Lake H-45	C186768	2570	2-d	abt pyrite terahedra; *Tasmanites*, *Leiosphaeridia* ?*Nostocopsis*-type alginite	brn bituminite wisps & specks	Tasmanales & *Nostocopsis* alginite rare bitumens	II
Dome *et al.* Trout Lake H-45	C186768	2800	2-d	No Ro data	brn bituminite flecks, & stringers, granular bitumen		II
Dome *et al.* Trout Lake H-45	C186768	3020	2-d	high Ro faunal remains 2.62% Ro	abt brn bituminite stringers (alg), med & low Ro bitumens		II
Imperial Island River No.1	C186751	4818	8	bitumen-filled ?coccolith/calc nannofossils	dispersed and void-fill bitumens	liptodetrinite	II

Table A3 Petrographic characteristics of the Redknife Formation.

Well location	Sample No. GSC #	I.D.	Rock type	Notes	Dominant maceral	subordinate maceral	Inferred original kerogen type
B-A Texaco Arrowhead N-2	C186758	4905	5/6/3	no low Ro ind bitumen\ites ass liptinites	bituminites, ind bitumens	bituminite, ind bitumen	II
B-A Texaco Arrowhead N-2	C186758	5205	5-d	no low Ro ind bitumen\ites ass liptinites	bituminites, ind bitumens		
B-A Texaco Arrowhead N-2	C186758	5495	5	no low Ro ind bitumen\ites ass liptinites	bituminites , ind bitumens		II
Imperial Sun Arrowhead I-46	C186757	2510	5-d	pyrite framboids oxidized			II
Imperial Sun Arrowhead I-46	C186757	3010	4/7	oxidation apparent	bituminite; resid bitumens		II
Imperial Sun Arrowhead I-46	C186757	3510	5				II
Texaco NFA Bovie Lake J-72	C186762	5651	2-d/3	? Exshaw cavings	bituminite III-micrinite		
Texaco NFA Bovie Lake J-72	C186762	5845	5-d		bituminite III-micrinite	ind bitumen rare	II
Texaco NFA Bovie Lake J-72	C186762	5885	3	formerly algal encrustation of carbonate	bituminite III-micrinite	rare bitumens	II
Texaco NFA Bovie Lake J-72	C186762	6405	5	brn staining evident	ind bitumens in pores	bitumnite III (lenses and wisps)	II
Imperial Sun Netla C07	C186764	2275	3	low matrix bituminite v. pyritic	dispersed (alg) bituminite	low & med Ro bitumens	II
Imperial Sun Netla C07	C186764	2680	3/5	?cavings from Banff?	algal bituminite, Leiosph.-type and micro alginite	low and med Ro bitumens	II
Imperial Sun Netla C07	C186764	2895	3/4	ferroan dolomite common, pyritic	algal bituminite, Leios-type alg	low, med and high Ro bitumens	II
Imperial Sun Netla C07	C186764	3190	3	low Ro bitumens ass alginites,faunal inert	Leiosph. and coccoid alginite, alg bituminite	?bones, low Ro bitumens liptodet, Tasmanites, chitin,	II
Murphy *et al.* Muskeg River #1	C186767	2440	2/3	microfracs //l bdg; pyritic shale;dolomitized	brn bituminite strings, alginite,	ind bitumens	II
Murphy *et al.* Muskeg River #1	C186767	2690	2/3	reflectance variable - oxidation	dk brn(alg) bituminite & Leios algin //l bdg	low and med Ro bitumens	II
Murphy *et al.* Muskeg River #1	C186767	3060	2-d	? marly cavings; calc shale , pyritic	liptodetrinite-algal cysts, tw algin	low and med Ro bitumens	II
Murphy *et al.* Muskeg River No.1	C186767	3365	2	alg bituminite //l bdg; low Ro bitumens assoc. algal bituminite	dk brn alg bituminite strgs // bdg	low and med Ro bitumens	II
Pan Am Home Signal Celibeta #7	C186765	3655	5/4	mod dolomit'n; bitum. lamin ?Exshaw caving	red/brn alg bituminite	low Ro bitumens assoc bituminite	II
Pan Am Home Signal Celibeta #7	C186765	3955	5	lean shale; fresh pyrite framboids	low, med and high Ro bitumens	?chitin	II
Pan Am Home Signal Celibeta #7	C186765	4325	5	lean shale, bitum intercalations,pyritic	bitumininites, ind bitumens	low and med Ro bitumens	II
Dome *et al.* Trout Lake H-45	C186768	1360	3/4	organofacies resembles Exshaw	matrix bituminite,alg bituminite , Stringers, alginite	low & med Ro bitumens , ?pellet bitumen	II
Dome *et al.* Trout Lake H-45	C186768	1730	2-4d	add. bitumen pop in carbonate (Ro=2%); mod. dolomitization	bituminite-micrinite, bituminite, alginite	alginite (Leios, acritarchs) litpodetrinite, bitumens	II
Dome *et al.* Trout Lake H-45	C186768	2115	4	abt. fresh pyrite tetrahedra	bituminite stringers,(alg & m'alg) liptodetrinite , alginite,	acritarchs; rare ind bitumens	II
Dome *et al.* Trout Lake H-45	C186768	2570	2-d	abt. pyrite terahedra	brn bituminite wisps &specks	Tasmanales & ?Nostocopsis alg, rare bitumens	II
Imperial Island River No.1	C186751	3486	2-d	abt. framb. pyrite-some alteration-limonite	bituminite stringers, liptodetrinite alginite,?faunal inertinite,	low & med Ro bitumens	II
Imperial Island River No.1	C186751	3797	2	bituminite, med & low Ro bitumens	liptodetrinite, alginite,	faunal inertinite	II
Imperial Island River No.1	C186751	4010	5			faunal inertinite	
Imperial Island River No.1	C186751	4102	1	abt. pyrite assoc brn bituminites	bituminite(alg). low & med Ro bitumens	faunal inertinite	II

Table A4 Petrographic characteristics of the Kotcho Formation & Upper Devonian shales.

Well location	Sample No. GSC C#	I.D.	Rock type	Notes	Dominant macerals	subordinate macerals	inferred original kerogen type
B-A Texaco Arrowhead N2	C-186758-	4635	4	?med Ro bit suppressed; excel organic networks	matrix bit>bituminite-micrinite,	alginite ind bitumen, alg detrinites	II
B-A Texaco Arrowhead N2	C-186758-	4645	4	?med Ro bit suppressed; excel organic networks	matrix bituminite-micrinite	faunal inert, ind bitumens	II
Imperial Sun Arrowhead I46	C186757-	1990	4-lam	v. pyritic, sl dolomitic, organic networks //l bdg	matrix bituminite, alginites	low Ro bitumens; micro alginites Tasm, Leios,	II
Texaco NFA Bovie Lake J72	C186762-	5415	3/4-d	pervasive dolomite	matrix bituminite-micrinite	ind bitumens; fish bones/chitin	II
Imperial Sun Netla C07	C186764-	2040	3	much biodegr alginite, low Ro bitumen as alginite	algal? bituminite, col and microalginite, ?pellets	low Ro bitumens (indig), chitin,bones/spines	II
Murphy Muskeg River No.1	C186767-	2370		thermal drying causes oxidation along m'fracture network	dk brn matrix bituminite-micrinite	microalginite, Tasmanites, low & med Ro bitumens	II
Pan Am HS Celibeta No. 7	C186765-	3470	4	bitumens assoc organic /m'frac network; fresh pyrite ; rare dolomite	dk brn matrix bituminite,	low Ro bitumen; faunal inert med & high Ro bitumen; Tasmanales alginite	II
Dome *et al.* Trout Lake H-45	C186768-	1295	3/4	extensive bitumen/m'frac network	low Ro bitumens; micrinite	alg bituminite,alginites (Tasman. Leiosp) liptodetrinite	II
Imperial Island River No.1	C186751	3465	4	laminated shale, rich sce rock;organic network	matrix bituminite, alginite, low and med Ro bitumens	faunal inertinite,pellets, micro'alginite (acritarchs)	II
Imperial Island River No.1	C186751	3470	4	organic-rich shale, abt pyrite framboids pervasive dolomite	matrix bituminite	low and med Ro bitumens liptodetrinite (m'alginite) bituminite stringers	II

Table A5 Petrographic characteristics of the Exshaw Formation.

Well location	Sample No. GSC C#	I.D.	Rock type	Notes	Dominant maceral	subordinate macerals	Inferred OM Type
B-A Texaco Arrowhead N-2	C186758	3245	5-7-d	dolomitized litpodetrinite + corals ?Pekisko cavngs	bituminite strgs, liptodetrinite (algal)	indigenous bitumen, pyrobitumen	II
B-A Texaco Arrowhead N-2	C186758	3505	2	Tasmanales alg - Fluor index=6	bituminite strgs, alginites	indigenous bitumens	II
B-A Texaco Arrowhead N-2	C186758	4005	5-7		dispersed microalginites (liptodetrinite)	indigenous bitumens	II
B-A Texaco Arrowhead N-2	C186758	4285	2	oxidized sample-limonite; rare Tasmanales	dispersed bituminites, alginites	Tasmanales, indig. bitumens	II
B-A Texaco Arrowhead N-2	C186758	4445	4		matrix bituminite,micrinite, liptodetrinite	faunal inerts,ind bitumens	II
B-A Texaco Arrowhead N-2	C186758	4455	4	laminated organic rich shale; excel organic networks	matrix bit, bituminite, micrinite	faunal inerts, fish scale	II
Imperial Sun Arrowhead I-46	C186757	1725	8-d	only microalginites fluoresce	bitumininite stringers	indigenious bitumens	II
Imperial Sun Arrowhead I-46	C186757	1810	7	fluorescence only when dolomitized			
Imperial Sun Arrowhead I-46	C186757	1910	8		bituminite-liptinite	indigenous bitumens	II
Texaco NFA Bovie Lake J-72	C186762	3645	5		bituminite strgs assoc alginite, low Ro bitumen	liptodetrinite, microsporinite	II
Texaco NFA Bovie Lake J-72	C186762	3935	5	brn staining of matrix, dolomitization of alginite	bituminite, alginite, algal detrinite	low and med Ro bitumens	II
Texaco NFA Bovie Lake J-72	C186762	4335	5	brn staining of matrix; alginite assoc carbonate	matrix bituminite, bituminite strgs, alginite	indigenous bitumens	II
Texaco NFA Bovie Lake J-72	C186762	4835	5		bituminite-micrinite association	indig. bitumens	II
Texaco NFA Bovie Lake J-72	C186762	5265	3/4		matrix bituminite, bituminite strgs	liptodetrinite, indig bitumens	II
Imperial Sun Netla C07	C186764	1955	2-d/8	Tasmanites present	liptodetrinite (plkt), alginite	bitumen incl (dolomite), and med Ro bitumen	II
Imperial Sun Netla C07	C186764	2020	2/4	low Ro bitumens assoc alginite	bituminite, alginite (Leiosph,Tasman, Nostocop)	bitumens, chitin, spines	II
Murphy *et al.* Muskeg River #1	C186767	1915	2/3	laminated shale,pyritic; budding coccoid microalginite	matrix bituminite-micrinite, algal bituminite //l bdg	microalgin. thin-wall alginite col onial alginite and sporinite	II
Murphy *et al.* Muskeg River No.1	C186767	2205	7/4		bituminite strings; alginite (tw Tasm, microalg)	alginite (tw Tasm, microalg)	II
Murphy *et al.* Muskeg River No.1	C186767	2335		select dolom. alginites; oxidized pyrite;annealed microfracture; oxidation -no fluorescence	bituminite strings- alginite //l bdg; microalginite		II
Pan Am Home Signal Celibeta 7	C186765	2165	4	oxidized pyrite	(algal) bituminite, liptodetrinite , bitumens	low Ro & high Ro bitumens	II
Pan Am Home Signal Celibeta 7	C186765	2491	4/5	no evident oxidation; pervasive microfractures	matrix bituminite, bituminite stringers,alginite disp liptinite, bitumens	thin-walled w algnite (Leiosph.)	II
Pan Am Home Signal Celibeta 7	C186765	2920	2	bituminite-microalginite, Leiosh alginite	bituminite-liptodetrinite, tw (Leio) alginite	low , med and high Ro bitumens	II
Pan Am Home Signal Celibeta 7	C186765	3325	4	oxidation evident -lge Ro range; mod dolomitization	liptodetrinite (alg bodies), algal bituminite	med Ro bitumen	II
Pan Am Home Signal Celibeta 7	C186765	3430	4	no fluorescence- ?oxidation	(alg) bituminite //l bdg; liptodetrinite, twalginite	low, med & high Ro bitumens	II

Table A6 Petrographic characteristics of the Banff Formation.

Well location	Sample No. GSC C#	I.D.	Rock type		Dominant maceral	subordinate macerals	Original OM type
Dome *et al.* Trout Lake H-45	C186768	1250	4	dolomotized colonial alginites	alginite (Tasm, Leiosh), liptodetrinite, bituminite	low and med Ro bitumens, rare conodont	II
Imperial Island River No.1	C186751	2134	5	oxidation of pyrite	alginite-bituminite	vitrinite-like, m'alginite, ?trilete spore	II
Imperial Island River No.1	C186751	2140	5				
Imperial Island River No.1	C186751	2310	5	bituminite-alginite	med Ro bitumen		II
Imperial Island River No.1	C186751	2456	5	oxidised/reworked OM	bituminites, liptodetrinite sporinite,(rew)		
Imperial Island River No.1	C186751	2747	3/4	nearshore marine o'facies:vitrinite , Tasmanites, sporinites	bituminite, sporinite (crass) inertinite	vitrinite (bimacerite), liptodetrinite, bitumen	II
Imperial Island River No.1	C186751	2760	2	marginal marine o'facies	bituminite strings, liptodetrinite, sporinite (fresh & reworked)	vitrinite & inertinite inclusions, fish sc. calcareous nannofossils	II
Imperial Island River No.1	C186751	3012	5	sporinite common (?Murospora)-nearshore marine	liptodetrinite, bituminite stringers, sporinite	m'alginite, vitrinite (rew)	II
Imperial Island River No.1	C186751	3275	5	bitumen-stained matrix; *Tasmanites*, *Leiosphaeridia*	matrix bituminite, bituminite str., alginite, liptodetrinite	faunal inertinite, med Ro bitumens	II
Imperial Island River No.1	C186751	3288	3/4		matrix bituminite. liptodetrinite, alginite	med Ro bitumen, faunal inertinite	II
Pan Am Mattson Creek A-1	C196779	260	5-d		blk bituminite-micrinite, alg bituminite	high Ro bitumens	
Pan Am Mattson Creek A-1	C196779	680	5/7	abt pyrite	algal bituminite-micrinite	high Ro bitumens	
Pan Am Mattson Creek A-1	C196779	860	7/5	abt pyrite	bituminite-micrinite, algal bituminite		
Pan Am Mattson Creek A-1	C196779	1000	7/5				
Pan Am Mattson Creek A-1	C196779	1180	7/5				
Pan Am Mattson Creek A-1	C196779	1240	5	bitumens have large bireflectance due to anisotropy	bituminite-micrinite, bituminite assoc microalg & lamalginite		
IOE Pan Am Viscount a-77-D	C186771	9975	5/7	bituminous shale w. Silty laminae	matrix bituminite and low Ro bitumens	bituminites (m'alg & *Tasmanites*)	
IOE Pan Am Viscount a-77-D	C186771	10375	5/7	lean shale w. Dispersedbituminites	blk algal bituminite strgs & lenses	tw bitumiites (w alginites); amor bitumens	
IOE Pan Am Viscount a-77-D	C186771	10440	5/7	lean shale w. Dispersedbituminites	blk algal bituminite strgs & lenses	tw bitumiites (w alginites); amor bitumens	

Table A6, continued.

Well location	Sample No. C number	I.D.	Rock type	Notes	Dominant maceral	subordinate maceral
Canada Southern N. Beaver R 1-27	C186754-	9120	4	pyritic, v. dolimitic shale +?gypsum/magnesite	amorphous bitumens with Ro anisotropy	pyrobitumens
Canada Southern N. Beaver R 1-27	C186754-	9389	5-d	well-dolomitized		
Canada Southern N. Beaver R 1-27	C186754-	9659	5-d	well-dolomitized,		
Canada Southern N. Beaver R 1-27	C186754-	10319	3-4-d	well-dolomitized (xenotopic dolomite)		
Canada Southern N. Beaver R 1-27	C186754-	10665	4-d	pyrite assoc dolomite;	abt bituminite-micrite groundmass	high Ro bitumens
Canada Southern N. Beaver R 1-27	C186754-	10875	3/4	former source rock- algal laminite	abt blk bituminite-micrite; bitumens show ing mosaic anisotropy	bitumens with anisotropic mosaics
Canada Southern N. Beaver R 1-27	C186754-	10939	3/4	rich source rock, pyritic ;	abt blk-brn bituminite-micrinite matrix	vesicular indigeous bitumens
Pan Am Pointed Mountain P-53	C186766-	7450		lean shale; laminated , could be Prophet caving	med & high Ro (amorphous bitumens);	blk bituminite IV-micrinite (algal origin)o low Ro bitumen rare
Pan Am Pointed Mountain P-53	C186766-	7610	3-d	sample similar to Prophet shale	med Ro bitumen (pores-fill),	high Ro bitumen-fracture-fill
Pan Am Pointed Mountain P-53	C186766-	7810	4-d	bituminous laminae assoc en eschelon m'fracs	med & high Ro bitumens (amorph)	blk bituminite strings //l bdg; matrix bituminite-micrinite
Pan Am Pointed Mountain P-53	C186766-	8115	5-d	no low Ro bitumen; en eschelon m'fracs-stained	med Ro & high Ro bitumens	blk bituminite stgs, ; dk bituminite-micrinite strgs
Pan Am Pointed Mountain P-53	C186766-	8410	5	lean shale	rare med & high Ro bitumens	blk bituminite strgs assoc thin veneer bitumen\ite
Pan Am Pointed Mountain P-53	C186766-	8535	3/4	previously OM rich shale; anisotropic bitumens	med & high Ro bitumens	blk bituminite strgs assoc. micrinite
Pan Am Pointed Mountain P-53	C186766-	8930	3/4	laminated bit shale; no Ro data		
Pan Am Pointed Mountain P-53	C186766-	9200	4	formerly OM-rich, fine-gr. shale source-rock	matrix bituminite-micrinite,	low Ro bitumens med & high Ro bitumens
Pan Am Pointed Mountain P-53	C186766-	9630	3/4			
Pan Am Pointed Mountain P-53	C186766-	10105	3/4	no med Ro bitumens; high Ro bitumens ass dolomite	high Ro bitumens;bituminite-micrinite matrix	low Ro bitumen
Pan Am Pointed Mountain P-53	C186766-	10410	4	v.v. OM-rich shale, minor dolom;abt pyrite	blk bituminite-micrinite matrix,	med & high Ro pf bitumens
Pan Am Pointed Mountain P-53	C186766-	10810	4	v blk bit lam shale, fracture network, pyritic	blk bituminite-micrinite high Ro bitumens	low Ro bitumens rare
Pan Am Pointed Mountain P-53	C186766-	10860	4	bituminous laminae = fracture networks	blk matrix bituminite-micrinite	rare bitumens
Pan Am Beaver G-01, YT	C186752-	10575	4	sl. dolomitized; am bitumens assoc. carbonate	bituminite-alginite, micrinite, high Ro biitumens	liptodetrinite, micrinitized alginite //l bedding
Pan Am Beaver G-01, YT	C186752-	10865	4			
Pan Am Beaver G-01, YT	C186752-	11635	4		blk matrix bituminie-micrinite, high Ro bitumens	algal bituminites & ass bitumens
Pan Am Beaver G-01, YT	C186752-	12015	4			
Pan Am Beaver G-01, YT	C186752-	12265	4	laminated shale	blk matrix bituminie-micrinie, am bitumens	bitumens assoc. bituminite, carbonate
Pan Am Beaver G-01, YT	C186752-	12665	4		blk matrix bituminite-micrinite, bitumens	algal bituminite-micrinite

Table A7 Petrographic characteristics of the Besa River Formation.

Well location	Sample No. C number	I.D.	Rock type	Notes	Dominant maceral	subordinate maceral
Pan Am Beaver G-01, YT	C186752-	12915	4	very bituminous shale	blk matrix bituminite-micrinite, high Ro bitumens	bitumens associated w. bituminite, meta alginite
Pan Am Beaver G-01, YT	C186752-	12975	4	v. rich bituminous shale	blk matrix bituminite-micrinite, high Ro bitumens	meta alginite associated w. bitumens
Pan Am Beaver G-01, YT	C186752-	13185	4			
Pan Am Kotaneelee YT 0-67	C186755-	5040	7-d		bituminite-micrinite	high Ro bitumens
Pan Am Kotaneelee YT 0-67	C186755-	6000	5		bituminite-micrinite	highly reflecting bitumens
Pan Am Kotaneelee YT 0-67	C186755-	7000	4	bitumens are vesicular and show,?mosaics domain anisotropy	micrinite-bituminite, high Ro bitumens	med Ro bitumens
Pan Am Kotaneelee YT 0-67	C186755-	7595	4	sub-micron bitumen groundmass, bitumen-aniso domains	low bitumen granular, microporous	
Pan Am Kotaneelee YT 0-67	C186755-	7615	4	high Ro bitumens show domain anisotropy	sub-micron bitumen groundmass, vesicular bitumens	bitumens associated w. carbonate
Pan Am Kotaneelee YT 0-67	C186755-	7800	4	bitumens have high bireflectance (0.4%), vesicular, an d domain anisotropy	abt micrinite-bituminite, high, med Ro bitumens	vesicular bitumens with domain anisotropy
Pan Am Kotaneelee YT 0-67	C186755-	7900	4	fine bitumen stringers w.mosaic anisotropy, cenospheres	micrinite-bituminite groundmass	stringers of granular bitumen
Pan Am Kotaneelee YT 0-67	C186755-	7920	4		bituminite-micrinite groundmass	stringers of granular bitumens
Clausen Creek	C74201	+16.4	2-4	dolomitized cyanobacteria	matrix bituminite, liptodetrinite (alg)	acritarchs, med & high Ro bitumens
Clausen Creek	C74202	+44.3	4	abt dolomite pseudomorh cyanobacteria	matrix bituminite, liptodetrinite dolomitized cyanobacteria	med & low Ro bitumens
Clausen Creek	C74207	+377.3	2-d	abt framboidal pyrite	med & high Ro bitumens	liptodetrinite, acritarchs
Clausen Creek	C74212	?	5	highly oxidized sample	low & med Ro bitumens	med & Low Ro bitumens
Clausen Creek	C74213	+1045.3	3-4-blk,	abt dolom filamentous cyanobateria	low, med & high Ro bitumens, dolom cyanobacteria	matrix bituminite
Central Leduc Toad R. No.1	C186774	4057	4	laminates org-rich sh, massive lensoid & framboidal pyrite abt	blk bituminite-micrinite	bituminite, high gr bitumens
Central Leduc Toad R. No.1	C186774	4371	4	abt framboidal pyrite lenses & framboids	blk bitum. Matrix-micrinite	anisotropic semicokes & high bitumens
Central Leduc Toad R. No.1	C186774	4452	4	high pyrite concentrations	blk bituminite-micrinite matrix	rare bitumens
Central Leduc Toad R. No.1	C186774	5176	4		blk bituminite-micrinite	abt ind high grade bitumens
Central Leduc Toad R. No.1	C186774	5354	4		blk bituminite-micrinite	abt ind high grade bitumens

Table A7, continued.

Sample location	Sample No. GSC C#	I.D.	Rock unit	Rock type	Notes	Dominant maceral	subordinate maceral	Inferred OM Type
Amoco East Flett H-13	C186759	-2780	Clausen	6/3		alginites, alg detrinites	indigenous bitumens	II
Amoco East Flett H-13	C186759	-2905	Clausen	1/5	oxidized pyrite	bituminites	indigenous bitumens	II
B-A Texaco Arrowhead N-2	C-186758	-2645	Clausen	5-d	dolomitized cocc and filam cyano bacteria abt	liptodet+alginite	indigenous bitumens and spores	I-II
B-A Texaco Arrowhead N-2	C-186758	-2745	Clausen		highly dolomitized	bituminite>alginite	indigenous bitumens	II
B-A Texaco Arrowhead N-2	C-186758	-2805	Clausen	5-d	dolomitized ?algal liptodetrintie	bituminite, liptodetrinites (algal)	indigenous bitumens	II
Texaco NFA Bovie Lake J-72	C186762	-3290	Clausen	3/4/5	fluor. low Ro bitumen ass liptinite			II
Texaco NFA Bovie Lake J-72	C186762	-3390	Clausen	4	brown staining of matrix	alginite-bituminite, low Ro bitumens	liptodetrinite	II
P A H S Celibeta No. 7	C186765	-1931	Clausen	2	spicules, pyritic; m'frac network in dk brn bitum laminae	matrix & algal bituminite, low Ro bitumen	faunal inertinite, high Ro bitumens	II
P A H S Celibeta No. 7	C186765-	-1991	Clausen	5	oxidation rims on cuttings; no fluorescence	brn bituminite stringers, high Ro bitumen	alg liptodetrinite; medium and low Ro bitumens	II
Jackfish Gap-Yohin Ridge	C52180	C52180	Clausen	4	type 4 (med Ro) bitumen shows bireflectance	matrix bituminite, amorph bitumens liptodetrinite	rare vitrinite, fusinite	II/III
Jackfish Gap-Yohin Ridge	C52181	C52181	Clausen	4		matrix bituminite	vitrinite, fusinite	II/III
Pan Am Viscount a-77-D	C186771	-9675	Clausen	5	prophet cavings laminated sh	matrix bituminite ; algal bituminites	amorph (med) and low Ro bitumens	II
Jackfish Gap-Yohin Ridge	C58505	C58505	Yohin	4		amorph bitumens, bituminite	high Ro bitumens	
Jackfish Gap-Yohin Ridge	C52163	C52163	Yohin	4/8	bireflecting amorp bitumens 1.28%Ro min, 1.5 %Ro max	amorph bitumens, low Ro bitumens bituminite III	rare semifusinite Low Ro bitumens ass alg bituminite	II
Jackfish Gap-Yohin Ridge	C52166	C52166	Yohin	4		amorph bitumens bituminite	?vitrinite, semifusinite	II
Jackfish Gap-Yohin Ridge	C58503	C58503	Yohin	2	abt OM; little shale matrix	amorphous bitumens 100-300 µm,	bituminite III	II
Jackfish Gap-Yohin Ridge	C51174	C51174	Yohin	7				
Jackfish Gap-Yohin Ridge	C58502	C58502	Yohin	4	Type 4 bitumen shows bireflectance	Type 4 bitumen	algal bituminite assoc. low Ro bitumens	II

Table A8 Petrographic characteristics of the Yohin and Clausen formations.

Sample location	Sample No. C number	I.D.	Rock fm.	Notes	Dominant maceral	Subordinate
Amoco East Flett H-13	C186759-	-1440	Flett-Meill	bitumen migrating through organic network ca. 0.7-0.8% VRo	alginites, bituminites	indigenous bitumens
Amoco East Flett H-13	C186759-	-1620	Flett-Meill	bitumen rare; sammple highly dolomitized	bituminites	indigenous bitumens rare
Amoco East Flett H-13	C186759-	-1860	Flett-Meill	reworked algal	alginites	liptodetrinite, ind bitumens
Pan Am Pointed Mountain P-53	C186766-	-5050	Flett	shale consists of?Golata cavings		
Pan Am Pointed Mountain P-53	C186766-	-5100	Flett	sporinite-rich shale ?Mattson caving		
Jackfish Gap-Yohin Ridge	C52106	3187.33	Flett	fluorescence alginite & bitumens same	liptinite-bitumenites colonial alginites	
Jackfish Gap-Yohin Ridge	C52115	3405.18	Flett	mildly oxidized (pyrite-limonite)	alginite-bituminite bitumens ass alginites,	amorph bitumen
Jackfish Gap-Yohin Ridge	C58522	3534.77	Flett	highly altered pyrite, abt disp OM	lipt-bituminites, amorphous bitumens	rew OM, liptodetrinite
Jackfish Gap-Yohin Ridge	C58523	3534.77	Flett			
Jackfish Gap-Yohin Ridge	C74336	3628.81	Flett		alginite-bituminites,	low Ro bitumens, lamalginite
Jackfish Gap-Yohin Ridge	C74338	3684.05	Flett	all pyrite is oxidized	alginites-bituminite, ind bitumens liptodetrinite, colonial alginite	
Jackfish Gap-Yohin Ridge	C52152	3793.64	Flett	abt liptinite-bituminite	amorphous bitumens, alginites	
Jackfish Gap-Yohin Ridge	C52157	3852.69	Flett	fossilif. sh, fresh pyrite minor oxidation	bituminites ass. liptinite, am bitumens	reworked OM incl semifusinite
Amoco East Flett H-13	C186759-	-2445	Prophet		alginites, bituminites	low, med Ro indenous bitumens
B-A Texaco Arrowhead N-2	C-186758	-2485	Prophet	highly dolomitized suggest permeability assoc early oil	bituminites>alginites	Low & med Ro indigenous bitumens
Texaco NFA Bovie Lake J-72	C186762-	-2665	Prophet	?Mattson cavings	Bituminite, alginite,	
Texaco NFA Bovie Lake J-72	C186762-	-2935	Prophet		low Ro bit assoc alginite; lge colon algin,	Leiosphaeridiales, bituminite, alginite
Pan Am *et al.* Celibeta No. 7	C186765-	-1730	Prophet	rare Tasmanales alginite;	high Ro bitumens, alg.liptinite-bituminite	low Ro bitumens Leiosph alginite common
Pan Am *et al.* Celibeta No. 7	C186765-	-1850	Prophet	microfracture network; dolomitized liptodetrinite; spicules	(algal) bituminite in lenses matrix bituminite;	low & med Ro bitumens
Canada South *et al.* N. Beaver R.	C186754-	-7139	Prophet	pyritic	amorp bitumens assoc pores & dolomite	low Ro bitumens assoc alg bituminite
Canada South *et al.* N. Beaver R.	C186754-	-7540	Prophet	pyrite lenses composed of framboids; coal caving	alg bituminite //l bdg-micrinite, ind bitumens	coal contaminant
Canada South *et al.* N. Beaver R.	C186754-	-7860	Prophet	poor in organic matter	ind. amorph bitumens, (low , med, high Ro)	pyrobitumen
Canada South *et al.* N. Beaver R.	C186754-	-8585	Prophet	lignitic coal contaminant	amorph bitumens (low , med & high Ro)	pyrobitumens
Canada South *et al.* N. Beaver R.	C186754-	-8815	Prophet	abt pyrite;humic coal contaminants	huminites,densinite, liptinies	
Canada South *et al.* N. Beaver R.	C186754-	-8860	Prophet	abt frambiodal pyrite	amorph ous, indigenous , pore-fill bitumens	

Table A9 Petrographic characteristics of the Rundle Group.

Sample location	Sample No. C number	I.D.	Rock	Notes	Dominant maceral	Subordinate maceral
Pan Am Pointed Mountain P-53	C186766-	-5230	Prophet	fossiliferous shale (crinoids, bryozoans),	blk bituminite, liptinitic debris, am\pf bitumens	dol cyanobacteria
Pan Am Pointed Mountain P-53	C186766-	-5565	Prophet	low bit2 ass spor;low bit 3 assoc bit stgs	bituminite strgs, sporinite, bitumens (am pf, low)	sporinite (Murospora),
Pan Am Pointed Mountain P-53	C186766-	-5900	Prophet	matur. limit of fluorescence in liptinite	am (med Ro) & low Ro bitumens, liptinite	
Pan Am Pointed Mountain P-53	C186766-	-6270	Prophet	low bit 2 assoc. spor, med is pore-fill no fluorescence	low Ro bitumen & med Ro pf bitumens,	bituminite (blk) ctringers, bitumen assoc. spores
Pan Am Pointed Mountain P-53	C186766-	-6810	Prophet	high Ro bitumen shows Ro anisotropy	med (amorph) bitumen, blk bituminite strgs	low Ro bitumens //lbdg
Pan Am Pointed Mountain P-53	C186766-	-7171	Prophet	TOC low due to elevated maturity	med & high Ro bitumens (amorph)	low Ro bitumens
Pan Am Beaver G-01, YT	C186752-	-10129	Prophet		amorph, med and low Ro bitumen stringers	pyrobitumens
Pan Am Beaver G-01, YT	C186752-	-10183	Prophet		amorph, med and low Ro bitumen stringers	pyrobitumens
Pan Am Kotaneelee YT 0-67	C186755-	-4200	Prophet	microgran amorp bitumen, high Ro bitumens	?cenosphere algal structures	
Jackfish Gap-Yohin Ridge	C52064	2610.56	Prophet	calc sh w. colon calc microfossils, v pyritic	low Ro bitumens assoc. liptinite	
Jackfish Gap-Yohin Ridge	C52067	2692.58	Prophet	rare om		
Jackfish Gap-Yohin Ridge	C58517	2730.64	Prophet	platy blk shale, abt pyrite, undolomitized	bitumens assoc alginites, bituminite	vitrinite, fusinite, sporinite
Clausen Creek	C74220	1541.99	Prophet	masses of framboidal pyrite, abt Fe oxides	low, med & high Ro bitumens	liptodetrinite
Clausen Creek	C74234	2224.41	Prophet	limonite-rich shale	med & low Ro bitumens asso liptinite	acritarchs, ?scolecodonts
Pan Am Viscout a-77-D	C186771	-9625	Prophet	pyritic , laminated blk shale, microfract netw	dense k brn -blk matrix bituminite	low and med Ro bitumens
Pan Am Viscout a-77-D	C186771	-9675	Prophet	highly dolomotized shale(like cyanobacteria)	dense dk brn -blk matrix bituminite	med and low Ro bitumens
B-A Texaco Arrowhead N-2	C186758	-2340	Form'n F	dolomitized filamentous cyanobacteria,	bituminite>alginites	indigenous bitumens col alginites; rare *Tasmanites*
Pan Am *et al.* Celibeta No. 7	C186765	-1045	Form'n F	pellet bitumen ca. 2% Ro; fish scales	liptinite-bituminite	med & low Ro bitumens faunal inertinite;
Pan Am *et al.* Signal Celibeta # 7	C186765	-1496	Form'n F	?liptodetrinite incl?Nostocopsis	liptinite(inc Leiosph)-bituminite, liptodetrinite	med & low Ro bitumens
Pan Am *et al.* Signal Celibeta # 7	C186765	-2045	Pekisko	oxidation evident (no fluorescence)	(algal) bituminite,	low & med Ro bitumens

Table A9, continued.

Sample location	Sample No. C number	I.D.	Rock	Notes	Dominant maceral	Subordinate maceral
Canada Southern *et al.* N. Beaver River YT 1-27	C187854	-5989	4/7-d	shale i/b siltstone mod. well-dolomitized; terrestr. om inc inert bitumens w. aniso mosaic	bituminite-micrinite; ind bitumens	fusinite , pyrobitumens- vesicular, mosaic
Canada Southern *et al.* N. Beaver River YT 1-27	C187854	-6349	4-d		bituminite-micrinite strgs, ind bitumens	
Canada Southern *et al.* N. Beaver River YT 1-27	C187854	-6640	8		bituminite-micrinite assoc? mature alginite	
Pan Am Pointed Mountain P-53	C186766	-4570	4	low Ro bitumen (0.42% Ro) from sporinite	reworked coaly, brn bituminite, rew sporinite	low &med Ro bitumens, vitrinite
Pan Am Pointed Mountain P-53	C186766	-4805	4	little/ no rew Type III	rew sporinite (microsp) abt, bituminite, liptodetrinite	low & med Ro bitumens, megaspores
Pan Am Beaver G-01, YT	C186752	-6120	4		alg bitumintie-micrinite, amorp bitumens	
Pan Am Beaver G-01, YT	C186752	-6540				
Pan Am Beaver G-01, YT	C186752	-6565	4		bitumens assoc. alg bituminte-micrinite //l bdg	
Pan Am Beaver G-01, YT	C186752	-7140	4/1			
Pan Am Beaver G-01, YT	C186752	-7480	5	pyrite & cherty shale, siliceous microfossils	amorphous bitumens (med and High Ro)	low Ro bitumens assoc bituminite, micrinite
Pan Am Beaver G-01, YT	C186752	-7840	5		bitumens assoc (?algal) bituminite	low Ro bitumens assoc bituminite II, micrinite
Pan Am Beaver G-01, YT	C186752	-8766	5/4			
Pan Am Beaver G-01, YT	C186752	-8800	5/1			
Pan Am Beaver G-01, YT	C186752	-9210	5			
Pan Am Beaver G-01, YT	C186752	-9505	5/1			
Pan Am Beaver G-01, YT	C186752	-9880	5/1			
Pan Am Kotaneelee YT 0-67	C186755	-1320	5		reworked vitrinite, bitumen assoc bituminite	?vitrinite, inertinites
Pan Am Kotaneelee YT 0-67	C186755	-1620	7		dispersed bitumens, inertinites	matured sporinites (Densosporites)
Pan Am Kotaneelee YT 0-67	C186755	-1980	5-7			indigenous bitumens
Pan Am Kotaneelee YT 0-67	C186755	-2600	7			low and high Ro bitumens
Pan Am Kotaneelee YT 0-67	C186755	-3500	5			low and high Ro bitmens
IOE Pan Am Viscount a-77-D	C186774	-8420	5	highly dolomitized, platy sg	matrix bituminite-micrinite	low Ro type 3, med & high Ro bitumens

Table A10 Petrographic characteristics of the Golata Formation.

Sample location	Sample No GSC C#	I.D.*	Rock type	Notes	Dominant macerals	subordinate macerals	
B-A Texaco Arrowhead N-2	C186758-	-2180	2	TOC data available for 2080 ft. interval only	liptinites-alginite , m'spor, assoc low Ro bitumens	rew vitrinite, semifusinite	
Texaco NFA Bovie Lake J-72	C186762-	-1260	4	abt trilete spores , reworked spores, ?*Reticulatisporites*	bituminous matrix and sporinite	ind. bitumens;alginite, vitrinite	
IOE Bovie Lake M-05	C186753-	-1606	4	fresh water- lagoonal/lacustrine/delta top	reworked sporinite, fr. sporinite,bitum-micrite	*Pila (Botryococcus* -type) alginite	
IOE Bovie Lake M-05	C186753-	-1606.7	4	no vitrinite; typical L. Carb. spore assemblage	matrix bituminite-micrinite, sporinite,	alginite, micoralginite, inertinite	
Canada S. *et al.* N. Beaver R 1-27	C186754-	-3549	4-d	high TOC /low T max due to coal contaminant	massive interstit amorph bitumen, 4 populations		
Canada S. *et al.* N. Beaver River 1-27	C186754-	-4389	4/7	v. pyritic shale minor coal contaminant	alg bituminite-micrinite, bitumens	amorph (med Ro)bitumen assoc carbonate	
Canada S. *et al.* N. Beaver River 1-27	C186754-	-4578	4/7	v. pyritic, minor Kindle cavings, H/C source	alg bituminite assoc low Ro and amorp med Ro bitumen	pyrobitumens	
Canada S. *et al.* N. Beaver River 1-27	C186754-	-4885	5	high TOC /low T max due to coal contaminant	alg bituminite, med & low Ro bitumens	micrinite, liptodetrinite	
Canada S. *et al.* N. Beaver River 1-27	C186754-	-5139	5-d	minor Kindle (Permian) cavings	alg-bituminite-micrinite lenses //l bdg assoc ind bitumens	amorph. bitumen (med Ro) assoc pores & dolomite, pyrobitumen	
Pan Am Pointed Mountain P-53	C186766-	-2160	4	abt coaly OM, pyrite	ind amorp & lip-assoc bitumens, rework om	alginite (*Leiosp, ?Pila*) sporinite,faunal inert	
Pan Am Pointed Mountain P-53	C186766-	-2780	3/4	sporinite incl *Densosporites*; alginite incl *Pila*	low & med Ro ind. bitumens;sporinite	rew terr om>bitumens>alginite; vitrinite, inert	
Pan Am Pointed Mountain P-53	C186766-	-3195	3/4	low bit2 from sporinite (0.15% Ro); no algal bituminite	inertodetrinite, sporinite (*Murospora*), matrix bituminite	semifusinite, vitrinite, alginite, tw microspores	
Pan Am Pointed Mountain P-53	C186766-	-3870	5	sporinite (0.19% Ro) incl m'spores & *Murospora*	rew vitrinite, inertodetrinite, sporinite , amorp bitumen	low &med Robitumens, alginite, liptodetrinite	
Pan Am Pointed Mountain P-53	C186766-	-4310	3/4	abt carbonate inclusions	reworked coaly , brn bituminite strgs, sporinite	bituminite, med & low Ro bitumens, vitriniite	
Amoco Pointed Mountain P-24	C186760-	-2570	5		biodegraded sporinite, alginite ass bituminite strgs	low & med Ro bitumens	
Amoco Pointed Mountain P-24	C186760-	-2855	5				
Amoco Pointed Mountain P-24	C186760-	-3380	5-d	trilete spores present	alginite/tw sporinite assoc bituminite strgs, liptodetrinite	low Ro bitumens ass alginite,lipt-bituminite ;	
Amoco Pointed Mountain P-24	C186760-	-3995	9				
Amoco Pointed Mountain P-24	C186760-	-4500	4/9	coal + shale:VRo coal (telovitrinite-ctel): 0.80% Vro shale (detrovitrinite- cd): 0.77%	coal (collotel+gelinite), sporinite; shale: collodetrinite, alginite	semifusinite,*Pila (Botyrococcus-type*)alginite	
Amoco Pointed Mountain P-24	C186760-	-4890	1/4	vitrinite in CO3 (gelinite) & shale	low Ro bitumen, vitrinite (gelinite), sporinite	alginite (*Leiosph & Pila*) semifusinite, fusinite	
Amoco Pointed Mountain P-24	C186760-	-5140	4		low & med Ro bitumens abt vitrinite (shale) sporinite,	alginite/bituminite	
Amoco Pointed Mountain P-24	C186760-	-5340	5/1	low Ro bitumens & sporinite>>type III and med Ro bit	low Ro bitumens, sporinites	vitrinite, semifusinite,alginite, med Robitumen	
Pan Am Beaver G-01, YT	C186752-	-2880	4	pyritic shale,dispersed OM abt	amorphous bituminite assoc matrix, alg bituminite	faunal inertinite, Leiosph-type alginite //l bdg	II
Pan Am Beaver G-01, YT	C186752-	-3250	5	pyritic shale	amorph (med Ro) bitumens;low Ro bitumens	algal liptinite strgs //l bdg	
Pan Am Beaver G-01, YT	C186752-	-3475	4		algal bituminite ass low Ro bitumens, matrix bituminite	lamalginite, microalginite, Tasmanales alginite	II
Pan Am Beaver G-01, YT	C186752-	-3700	5-7	oxidized silty shale	reworked om, bituminite	tw alginite, liptodetrinite	II
Pan Am Beaver G-01, YT	C186752-	-3795	5-7	ferrugenous(hematite,limonite) \oxidized silty shale	reworked OM and bituminites	?rework OM incl ?faunal inertinite	II
Pan Am Beaver G-01, YT	C186752-	-4135	5-7		?algal bituminite stringers		II
Pan Am Beaver G-01, YT	C186752-	-4690	3/5	pyritic shale, marly , silty	algal bituminite stgs, bituminite-micrinite	liptodetrinite	II
Pan Am Beaver G-01, YT	C186752-	-4965	3-4		algal bituminite		II
Pan Am Beaver G-01, YT	C186752-	-5520	4	pyritic shale	bitumens assoc (alg?) bituminite-micrinite //l bdg	liptodetrinite	
Pan Am Beaver G-01, YT	C186752-	-5835	4	marly , v. pyritic shale	liptodetrinite, alg bituminite-micrinite, amorp bitumens		

* depths (ft) below K.B.

Table A11 Petrographic characteristics of the Mattson Formation shales, southeastern Yukon.

Sample location	Sample No GSC C#	I.D.*	Rock type	Notes	Dominant macerals	subordinate macerals	Type
Tika Creek	C58558	103	5-d	lam shale/siltstone	interstitial med and high Ro bitumens in shale	bitumens in siltstone laminae	
Tika Creek	C58562	147	4	matrix bituminite-micrinite, liptodetrinite,	algal bituminite	sporinite (trilete)	II
Tika Creek	C58565	163	4	dolomitized siltstone w. shaley laminae	interstitial bitumens, brn stain	pyrobitumens	II
Tika Creek	C58572	218	9/4	dolomitic siltstone om-rich	blk bituminous matrix		
Tika Creek	C58703	262	7	dolomitic siltstone om-rich	high Ro bitumens		
Tika Creek	C58704	282	7	silty shale	med and high Ro bitumens	vitrinite w. cell structure 1.2-1.6% Ro	II/III
Tika Creek	C58705	292	4	dk fine gr shale; basic aniso cenospheres	bituminite-micrinite matrix and strgs	fusiinite, sclerotinite,sporinite, bitumen low Ro 1.6%	II/III
Tika Creek	C58581	382	4	Limonitic silty shale om-poor	bituminite-micrinite	granular low Ro bitumen	II
Tika Creek	C58591	460	4	dk bitum shale w. silt lamina	matrix bituminite-micrinite,bituminite strgs	?chitin	II
Tika Creek	C58601	609	4/5	silty shale abt limonite	matrix bituminite-micrinite, bituminite strgs, lamalginite	cenosperes/alg cysts, inertinite; liptodetrinite	II
Tika Creek	C58604	674	4	limonitic shale; pyrite lenses framboids	bituminite-micrinite matrix & strgs //l bdg	alginite, (*Leiosphaeridia ?Tasmanites*)	II
Tika Creek	C58606	703	4	laminated pyritic shale (oxidized)	liptodetrinite conc. In bituminous laminae	alg bituminite-micrinite; metasporinite	II
Tika Creek	C58608	716	4	limonitic shale (?oxod pyrite)	bituminite-micrinite strgs	sporinites and alginite //l bdg rew vitrinite	II
Tika Creek	C58611	749	4	laminated.,limonitic shale-formerly pyrite	bituminite-micrinite ; algal bitumininite strgs	rew vitrinite, fusinite , lipto (algal) detrinite,	
Tika Creek	C58614	754	4/5	dolomitic shale	bituminite-micriniite, intercrystalline	indigenous bitumen inclusions	
Tika Creek	C58625	902	4	laminated.,limonitic shale-formerly pyrite	bituminite-micrinite ; algal bitumininite strgs	rew vitrinite, fusinite , lipto (algal) detrinite	II/III
Tika Creek	C58631	984	5	shale with high conc massive pyrite (oxid)	bituminite-micrinite strgs (algal)	bituminite from liptodetrinite	II
Tika Creek	C58638	1008	5	silty shale	bituminite-micrinite clasts and strgs (liptinite origin)	bituminite from ?spores/alginite	
Tika Creek	C58634	1019	5	silty shale w. abt pyrite ▲ & framboids	dk bituminous matrix and strgs //l bdg		
Tika Creek	C58640	1052	4/1	dolostone w. pervasive pyrite framboids	brn strgs bituminite	?bituminitized sporinite	
Tika Creek	C58681	1467	4	lean shale w. bituminite specks	bituminite from liptodetrininte (microalginite)	fluorescing acritarchs 7-10 µm	
Tika Creek	C58690	1543	4/5	bituminous siltstone w. dolomite & pyrite	blk bituminous matrix-micrinite	indigenous low Ro bitumens ca. 0.53% Ro	
Jackfish Gap-Yohin Ridge	C58709	3894	8	rel barren siltstone	matrix and lipt-bituminites, liptodetrinite sporinite	alginite , rew OM	II
Jackfish Gap-Yohin Ridge	C58711	3986	7	well-laminated shale, nearshore marine	matrix bituminite, alginite strgs sporinite, liptodetrinite	*Tasman ites* alginite, fusinite,vitrinite (f+rew)	II
Jackfish Gap-Yohin Ridge	C58713	4096	4	marginal marine; no coaly kerogen	abt sporinite & bituminite derivatives, alginite	alginite-*Pila,Tasmanites*, rare inertinite, cutinite	II
Jackfish Gap-Yohin Ridge	C58719	4413	4	highly oxidized-pyrite completely oxidized	bituminite-micrinite-liptinite, sporinite	alginites incl *Tasmanites* (rew)	II
Jackfish Gap-Yohin Ridge	C58723	4562	4	no vitrinite	bitumens assoc liptinite-bituminite ,sporinite	alginite *(Tasmanales,Leiosphaeridicales)*	II
Jackfish Gap-Yohin Ridge	C58726	4633	7	Shale>>coal laminae	vitrinite in shale & coal (collotelinite)		
Jackfish Gap-Yohin Ridge	C58730	4754	9	Ro low due to sapropelic nature of coal	inertinite (macrinite, semifusinite, detrital) sporinite	detrovitrinite>>telovitrinite>gelovitrinite	II/IV
Jackfish Gap-Yohin Ridge	C58736	4859	7	lean silty shale w . om in interstices	bitumens assoc bituminite III	sporinite	II/III
Jackfish Gap-Yohin Ridge	C58737	4862	9	sapropelic coal, minor vitrinite	semimacrinite/semifusinite., sporinite	vitrinite:detrovit>telovitrinite>gelovitrinite;sclerotinite	II/IV
Jackfish Gap-Yohin Ridge	C58749	5043	7	sandstone with plant remains			III
Jackfish Gap-Yohin Ridge	C58750	5052	4	mixed rew terrestrial om -marginal marine	bitumen ass bituminite strgs, sporinite (mega +crassispores)		II/III
Jackfish Gap-Yohin Ridge	C58753	5081	4	marginal marine	amorphous bitumen, liptinite-bituminite,		II/III
Jackfish Gap-Yohin Ridge	C58759	5535	4	mixed marine and rew terrestrial OM	rew OM liptinite-bituminite, bitumens ass sporinite, alginite		II/III
Jackfish Gap-Yohin Ridge	C58764	5640	9/7	sapropelic coal :inert>>vitrinite>liptinite	semifusinite, semimacrinite, micrinite, gelo & collodetrintte		II/III
Jackfish Gap-Yohin Ridge	C58765	5640	5	mixed marine/terrestrial kerogen-pyritic	vitrinite, fusinite sporinite		III
Jackfish Gap-Yohin Ridge	C58793	6385	5	oxidized sample;	rew vitrinite, fusinite	freshwater & marine alginites	II/III
Jackfish Gap-Yohin Ridge	C58804	6724	4	vitrinite in microlayers; lacustrine origin	vitrinite(gelinite, collodetrinite) sporinites		III
Jackfish Gap-Yohin Ridge	C58806	6754	4/9	laminated shale/sapropelic coal	vitrinite (gelo-, telo- & collodetrinite) fusinite, sporinite,	amorphinite	II/III
Jackfish Gap-Yohin Ridge	C58838	7246	9/4	sapropelic coal-laminite-lagoonal/lacustrine laminated shale	inertinite (semimacinite, semifusinite, detroinert), sporinite lamalginite, amorphinite bituminite II, *Pila* alginite	alginite	II/III
						resinite/exsudatinite,reworked sporinite	I/II/III/IV
Clausen Creek	C74273	3297	4-blk	typical L. Carbonif. spore assemblage	liptinite (sporinite)low & med Ro bitumens	*Tasmanites*, megspores, faunal inertinite	II
Clausen Creek	C74277	3414	4	mixed terrestrial/marine kerogen (?deltaic)	low Ro bitumens, liptinite (sporinites)	*alginites:Tasmanites, Pila, Leiosph;* Sfus,Vitrinite	II/III
Clausen Creek	C74276	3414	4	coaly (terrrstrial) kerogen	low Ro bitumens, sporinites, liptodetr., matrix bituminite	semifus,vitrinite,gelinite-micrinite,*Tasmanites*alginit	II/III
Clausen Creek	C74309	4283	9	sapropelic coal-durite	liptinites (sporinite),inertinites (semifusinite, micrinite)	vitrinite, *Tasmanites & Pils* alginite	II/III/IV
Clausen Creek	C74316	4457	4-brn	highly oxidized; mixed terr/marine om	liptinite (sporinite) vitrinite, rew vitrinite, bitumens	liptodetrinite, bimacerite (vittinite + micrinite)	II/III

* ft above base of section

Table A12. Petrographic characteristics of the Mattson Formation shales in the outcrop belt, southwestern District of Mackenzie.

Sample location	Sample No GSC C#	I.D.*	Rock type	Notes	Dominant macerals	subordinate macerals	Inferred OM
IOE Dunedin a-75-E	C186770	-10450	4		matrix bituminite		
IOE Dunedin a-75-E	C186770	-10977	4/7	bitum sh w. silty laminae	algal bituminite strings//l bdg ass low Ro bitumen 3	amorphous (med Ro) bitumens; ?sporinite	
IOE Dunedin a-75-E	C186770	-10983	5	dolomitzed fine gr blk shale	low Ro bitumens assoc alg bituminite	med Ro bitumens; sporinite (Murospora)	
IOE Dunedin a-75-E	C186770	-10998	4	bitumen-stained matrix	low Ro bitumen assoc blk bituminites	bituminite clasts <100 um	
IOE Dunedin a-75-E	C186770	-11254	4/7	intergranular amorph bitumen -silt	low Ro bitumen assoc bituminite (shale)	lipt debris sphaeromorphs	
IOE Dunedin a-75-E	C186770	-11264		bitumen-stained matrix	wispy bituminite //l bdg assoc low ro bitumens	spores + liptinite debris	
IOE Dunedin a-75-E	C186770	-11286					
IOE Dunedin a-75-E	C186770	-11522	4	v. bituminous shale	blk bituminite-micrinite	fusinite; bitumen assoc sporinite, dispersed liptodetrinite	
IOE Dunedin a-75-E	C186770	-11531	4/7	shaley laminae in siltstone	brn-blk matrix bituminite in shale		
IOE Dunedin a-75-E	C186770	-12130					
IOE Pan Am Viscount a-77-D	C186771	-7425					
IOE Pan Am Viscount a-77-D	C186771	-7475					
IOE Pan Am Viscount a-77-D	C186771	-7477					
IOE Pan Am Viscount a-77-D	C186771	-7895	4	laminated OM-rich minor siltst;dolom	matrix bituminite; algal bituminite abt	low Ro 3 med & high Ro bitumens	II
IOE Pan Am Viscount a-77-D	C186771	-8005					
IOE Pan Am Viscount a-77-D	C186771	-8006					
IOE Pan Am Viscount a-77-D	C186771	-8011					
IOE Pan Am Viscount a-77-D	C186771	-8095	5	calc-dolomitized shale; fram. pyrite	disp blk bituminite strgs brn-stained matrix	bitumens assoc bit stgs	
IOE Pan Am Viscount a-77-D	C186771	-8245					
Imperial P. A. LaBiche b-55-E	C186772	-8265					
Imperial P. A. LaBiche b-55-E	C186772	-8970		highly dolomized blk shale	amorp & low Ro type 3 bitumens	*bitumen from sporinite; inertinite	
Imperial P. A. LaBiche b-55-E	C186772	-9385		shale matrix lean, dispersed om rich	blk bituminite assoc. low Ro bitumen	amorph bitumen; pyrobitumen	
Imperial P. A. LaBiche b-55-E	C186772	-9675		blk org rich shale; pyritic	blk matrix bituminite, bituminites (lipt)	bitumens assoc. bituminite and sporinite pyrobitumen	
Imperial P. A. LaBiche b-55-E	C186772	-9960		dk shale w abt dispersed OM	amorph med Ro bitumen; bitumen ass bituminite str	liptinite-bitumen transitional macerals	
Amoco LaBiche a-67-D	C186777	-7950			amorphous med Ro bitumen	low Ro type 3 bitumen (lipt) and lipt-bit transition	
Arco Maxhamish b-21-K	C186776	-5855		lt brn stained matrix	bitumens assoc. bituminite and liptinite	liptinite (sporinite and alginite)	
Arco Maxhamish b-21-K	C186776	-7005		laminated shale; weak fluor spores & matrix	bitumens assoc. lipt & matrix bituminite	inertinites, sporinite	
Arco Maxhamish b-21-K	C186776	-7025		laminated shale; weak fluor spores & matrix	bitumens assoc. lipt & matrix bituminite	inertinites, sporinite	
Aquitaine *et al.* Tatoo a-2-D	C186775	-1617.5	4	laminated, canneloid shale, vitrinite presetn	amorph bitumen sporinite vitrinite (collotel)	inertinite, *Pila*-alginite	
Aquitaine *et al.* Tatoo a-2-D	C186775	-1625.5	4	siltstone w. sporinite & org inclusions	ox vitrinite inertinite sporinite w. bitumen inclusions	liptinite-bitumen transitions , microsporinite. *Pila*	
Aquitaine *et al.* Tatoo a-2-D	C186775	-1631	4	shale w. silty i/bs & abt dispersed OM	bituminite (lip), sporinite, gelinite	rew *Pila* alginite, inertinite, trans bitumens tw microspores	
Aquitaine *et al.* Tatoo a-2-D	C186775	-1647C		shale w. silst lam;alginite-encrusted pyrite frds	liptinite (sporinites), rew alginite (*Pila*)	tw *Leiosphaeridia* alginte (rew), *Murospora*, vitrinite, pyrofusinit	
Aquitaine *et al.* Tatoo a-2-D	C186775	-1655	4	laminated shale	matrix bituminite, sporodetrinite, lipt bituminite	tw *Leiosphaeridia & Pila* alginites	
Aquitaine *et al.* Tatoo a-2-D	C186775	-1661.5		laminated shale; freshwater alginites	sporinite-gran trilete rew sporinite	tw *Leiosphaeridia & Pila* type alginites, bitumens	
Aquitaine Windflower d-87-A	C186773	-1496		grey siltstone & finely dispersed OM	graphitized & pyritized om; pyrobitumens	acritarchs & bituminites, microspores	
Aquitaine Windflower d-87-A	C186773	-1503		grey siltstone & finely dispersed OM	graphitized & pyritized relict om; pyrobitumens	vesicular pyrobitumens	
Aquitaine Windflower d-87-A	C186773	-1515		siltstone with highest OM contents	graphitized & pyritized relict om; pyrobitumens		
Aquitaine Windflower d-87-A	C186773	-1519		grey siltstone & fineltydispersed OM	graphitized & pyritized relict om; pyrobitumens		
Aquitaine Windflower d-87-A	C186773	-1528		grey siltstone & finely dispersed OM	graphitized & pyritized relict om; pyrobitumens		

* depths (ft) below K.B.

Table A13 Petrographic characteristics of the Mattson Formation shales, northeastern British Columbia.

APPENDIX B
Results of RockEval\TOC pyrolysis (by formation)

Well location	Sample No.		Depth		Unit	Tmax	TOC	S1	S2	S3	S2/S3	PI	HI	OI
	C no.	I.D	ft	m		°C	%	mg[3]	mg[3]	mg[3]				
Imperial Island River	186751	6906	6902-6908C[1]	2103.73-2105.55	Muskwa	421	2.24	0.52	0.37	0.12	3.18	0.58	16	5
Dome *et al.* Trout Lake	186768	4890	4881-4900	1487.73-1493.52	Muskwa	477	1.67	0.41	0.67	0.07	10.00	0.37	41	4
Murphy Muskeg River	186767	6311	6301-2	1920.54-1926.34	Muskwa	551	2.60	0.16	0.46	0.07	7.24	0.26	18	2
Imp Sun Arrowhead	186767	6110	6100-6120	1859.28-1865.38	Muskwa	[2]561	4.28	0.04	0.62	0.10		0.06	14	2
Imp Sun Arrowhead	186767	6116.4	6116.4C[1]	1864.28	Muskwa	[2]546	2.57	0.02	0.65	0.06		0.03	25	2
Imp Sun Arrowhead	186767	6122.4	6122.4C[1]	1866.06	Muskwa	[2]560	3.27	0.04	0.69	0.14		0.06	21	4
Imp Sun Arrowhead	186767	6134	6134C[1]	1869.64	Muskwa	[2]565	3.95	0.04	0.81	0.18		0.01	20	4
Pan Am Home Celibeta	186765	7060	7041-8	2146.09-2158	Muskwa	420	0.88	0.07	0.03	0.15	0.20	0.70	3	17
Texaco Bovie Lake	186762	9535	9531-40	2905.05-2907.79	Muskwa	413	3.06	6.60	1.46	0.66	2.22	0.82	47	21
Texaco Bovie Lake	186762	9613.5	9597-9630C[1]	2925.16-2935.22	Muskwa									
Texaco Bovie Lake	186762	9598	9598C[1]	2925.5	Muskwa	376	2.00	0.10	0.15	0.18	0.30	0.43	6	9
Texaco Bovie Lake	186762	9611	9611C[1]	2929.4	Muskwa									
Imperial Sun Netla	186764	6285	6271-6300	1911.40-1920.24	Muskwa	464	2.63	0.25	0.05	0.19	0.26	0.83	1	7
Pan Am Mattson Creek	1867---	1600	1600-1610	487.68-490.73	Horn River	394	3.45	3.07	1.1	0.42	2.61	0.74	31	12
Pan Am Mattson Creek	1867---	1640	1640-1650	499.89-502.92	Horn River	393	4.50	3.93	1.27	0.18	6.38	0.75	26	3

[1] C = core samples [2] Data from Feinstein *et al.* (1988) [3] per g rock

Table B1 Rock-Eval data for the Muskwa Formation and stratigraphic equivalents.

Well location	Sample no. C no.	I.D.	Depth ft	m	Tmax °C	TOC %	S1 mg[3]	S2 mg[3]	S3 mg[3]	S2\S3	PI	HI	O
BA-Texaco Arrowhead N-2	C186758	7005	7000-10	2133.6-2136.65	347	0.23	0.32	0.17	0.18	0.88	0.66	70	81
B-A Texaco Arrowhead N-2	C186758	7505	7500-10	2286-2289.05	350	0.24	0.30	0.18	0.26	0.71	0.63	75	108
B-A Texaco Arrowhead N-2	C186758	8105	8100-10	2468.88-2471.93	348	0.20	0.15	0.10	0.13	0.75	0.63	47	63
Texaco NFA Bovie Lake J-72	C186762	7305	7291-7330	2222.29-2234.18	377	0.92	6.68	1.44	0.56	2.57	0.83	157	60
Texaco NFA Bovie Lake J-72	C186762	7705	7681-7710	2341.17-2350	380	0.90	6.56	1.58	0.61	2.58	0.61	168	65
Texaco NFA Bovie Lake J-72	C186762	8855	8841-70	2694.73-2703.57		1.00	6.67	1.90	0.55	3.63	0.77	193	53
Texaco NFA Bovie Lake J-72	C186762	9470	9460-80	2883.48-2889.5	413	1.76	6.60	1.46	0.59	4.77	0.76	164	34
Imperial Sun Netla C07	C186764	4145	4111-40	1253.03-1261.87	433	0.77	0.05	0.46	0.15	3.06	0.10	59	19
Imperial Sun Netla C07	C186764	4515	4501-30	1371.90-1380.75	440	0.33	0.03	0.07	0.02	3.50	0.30	21	6
Imperial Sun Netla C07	C186764	4815	4801-30	1463.35-1472.18	xxx	0.28	0.02	0.00	0.00	xxx	1.00	0	0
Imperial Sun Netla C07	C186764	5175	5161-90	1573.07-1581.91	358	0.32	0.01	0.04	0.00	xxx	0.25	12	0
Imperial Sun Netla C07	C186764	5971	5951-80	1813.86-1822.70	358	0.35	0.01	0.00	0.00	xx	0.00	0	0
Murphy *et al.* Muskeg R. No.1	C186767	5275	5270-80	1606.29-1609.34	392	0.22	0.00	0.00	0.05	0.40	0.00	9	21
Murphy *et al.* Muskeg R. No.1	C186767	6065	6051-80	1844.34-1853.18	412	0.22	0.00	0.00	0.01	1.00	0.01	0	4
Pan Am H. S.Celibeta No. 7	C186765	5455	5441-70	1658.41-1667.26	449	0.26	0.03	0.15	0.12	1.25	0.17	57	46
Pan Am H. S.Celibeta No. 7	C186765	5775	5761-90	1755.95-1765	458	0.26	0.08	0.22	0.19	1.15	0.27	50	43
Pan Am H. S.Celibeta No. 7	C186765	6145	6121-70	1865.68-1880.62	xxx	0.18	0.00	0.00	0.05	0.00	0.00	0	27
Pan Am H. S.Celibeta No. 7	C186765	6385	6371-6400	1941.88-1950.72	xxx	0.13	0.00	0.00	0.05	0.00	0.00	0	38
Pan Am H. S.Celibeta No. 7	C186765	6740	6721-6-	2048.56-2060.45	319	0.88	0.00	0.02	0.07	0.28	0.00	11	41
Dome *et al.* Trout Lake H-45	C186768	3440	3431-50	1045.77-1051.56	380	0.21	0.05	0.06	0.07	1.00	0.50	32	32
Dome *et al.* Trout Lake H-45	C186768	3870	3861-80	1176.83-1182.62	355	0.12	0.03	0.02	0.13	0.16	0.75	15	100
Dome *et al.* Trout Lake H-45	C186768	4311	4301-20	1310.95-1316.74	308	0.11	0.05	0.02	0.27	0.05	0.84	13	240
Dome *et al.* Trout Lake H-45	C186768	4630	4621-40	1408.48-1414.27	405	0.13	0.06	0.01	0.10	0.60	0.55	44	76
Dome *et al.* Trout Lake H-45	C186768	4830	4821-40	1469.44-1475.23	380	0.11	0.03	0.02	0.20	0.19	0.50	32	177
Imperial Island River No.1	C186751	5418	5409-27C[1]	1648.66-1654.14	407	0.30	0.00	0.00	0.01	0.00	0.00	3	6
Imperial Island River No.1	C186751	5587.3	5587.3C[1]	1703.07	337	0.31	0.18	0.05	0.10	0.42	0.80	16	34
Imperial Island River No.1	C186751	5899	5899C[1]	1790.01	340	0.14	0.02	0.03	0.08	0.52	0.42	29	57
Imperial Island River No.1	C186751	6619	6614-24C[1]	2017.47-2019	339	0.13	0.04	0.06	0.15	0.38	0.50	42	111
Imperial Island River No.1	C186751	6814	6814C[1]	2076.91	386	0.46	0.01	0.03	0.00	0.00	0.25	6	2
Pan Am Mattson Creek A-1	C1967–	1440	1440	438.91	376	3.27	3.18	0.90	0.32	2.81	0.78	27	9

[1] C = core samples [2] Data from Feinstein *et al.* (1988) [3] per g rock

Table B2 Rock-Eval data for the Fort Simpson Formation.

Well Location	Sample No. C no.	. I.D	Depth ft	m	Tmax °C	TOC %	S1 mg[3]	S2 mg[3]	S3 mg[3]	S2\S3	PI	HI	OI
B-A Texaco Arrowhead N-2	C-186758	5835	5830-40	1776.98-1780.0	375	0.43	0.28	0.18	0.13	1.41	0.62	43	30
B-A Texaco Arrowhead N-2	C-186758	6242	6240-5	1901.95-1905	346	0.22	0.71	0.38	0.29	1.28	0.67	148	116
Texaco NFA Bovie Lake J-72	C186762	6950	6941-6	2115.62-2121.41	375	1.05	8.42	1.69	0.61	2.73	0.83	155	57
Murphy et al. Muskeg River No.1	C186767	4430	4421-4440	1347.52-4440	509	0.22	0.0	0.04	0.03	2.66	0.12	36	11
Pan Am Home Signal Celibeta	C186765	4675	4661-4700	1420.67-1432.56	444	0.32	0.03	0.24	0.20	1.20	0.12	0	62
Pan Am Home Signal Celibeta	C186765	4935	4921-90	1499.92-1520.95	xxx	0.15	0.00	0.00	0.07	0.00	0.00	0	0
Pan Am Home Signal Celibeta	C186765	5210	5191-5230	1581.91-1594.1	448	0.29	0.03	0.24	0.09	2.66	0.12	82	31
Dome *et al.* Trout Lake H-45	C186768	2570	2561-80	783.34-786.38	430	0.14	0.07	0.10	0.10	0.96	0.44	66	75
Dome *et al.* Trout Lake H-45	C186768	2800	2791-2810	850.69-856.49	428	0.24	0.02	0.15	0.10	1.91	0.23	72	39
Dome *et al.* Trout Lake H-45	C186768	3020	3011-30	917.75-923.54	457	0.20	0.06	0.09	0.06	1.50	0.43	45	30
Imperial Island River No.1	C186751	4818	4818C[1]	1468.53	xx	0.30	0.01	0.01	0.04	0.25	0.75	3	9

[1] C = core samples [2] Data from Feinstein *et al.* (1988) [3] per g rock

Table B3 Rock-Eval data for the Redknife Formation.

Well location	Sample No.		Depth		Rock	Tmax	TOC	S1	S2	S3	S2\S3	PI	HI	OI
	C no.	I.D.	ft	m	Unit	°C	%	mg[3]	mg[3]	mg[3]				
B-A Texaco Arrowhead N-2	C186758	4905	4900-10	1493.52-1496.57	Kotcho-UDev	389	0.15	0.14	0.10	0.21	0.51	0.58	70	140
B-A Texaco Arrowhead N-2	C186758	5205	5200-10	1584.96-1588.0	Kot-UDev	***	0.12	0.05	0.02	0.07	0.26	0.79	22	77
B-A Texaco Arrowhead N-2	C186758	5495	5490-5000	1673.35-1524	Kot-UDev	***	0.15	0.09	0.06	0.12	0.46	0.64	37	80
Imperial Sun Arrowhead I-46	C186757	2510	2500-2520	762-768.1	Up. Dev	441	0.44	0.02	0.04	0.36	0.11	0.33	9	51
Imperial Sun Arrowhead I-46	C186757	3010	3000-3020	9144-920.5	Up. Dev									
Imperial SunArrowhead I-46	C186757	3510	3500-3520	1066.8-1072.89	Up Dev	431	0.45	0.05	0.23	0.43	0.50	0.18	51	95
Texaco Bovie Lake J-72	C186762	5651	5611-90	1710.23-1734.31	Kotcho	369	1.07	8.23	1.52	0.58	2.60	0.85	142	54
Texaco Bovie Lake J-72	C186762	5885	5881-91	792.53-1795.27	Up Dev									
Texaco Bovie Lake J-72	C186762	6405	6391-6420	1947.98-1956.82	Up Dev	367	0.91	6.68	1.05	0.55	1.93	0.87	113	60
Imperial Sun Netla C07	C186764	2275	2261-90	289.15-697.99	Kotcho	442	1.30	0.08	1.45	0.15	9.66	0.05	111	11
Imperial Sun Netla C07	C186764	2680	2671-90	814.12-819.91	Kotcho									
Imperial Sun Netla C07	C186764	2895	2881-2910	878.12-886.97	Kotcho	442	1.30	0.04	0.94	0.14	6.71	0.04	73	10
Imperial Sun Netla C07	C186764	3190	3161-3200	963.47-975.36	Kotcho									
Murphy *et al.* Muskeg River.1	C186767	2440	2421-60	737.92-749.81	Kotcho	420	1.00	0.04	0.22	0.33	0.65	0.16	22	33
Murphy *et al.* Muskeg River.1	C186767	2690	2681-2700	817.69-822.96	Kotcho									
Murphy *et al.* Muskeg River.1	C186767	3060	3051-70	929.94-935.73	Kotcho									
Murphy *et al.* Muskeg River 1	C186767	3365	3351-80	1024.43-1030.22	Kotcho	426	0.44	0.03	0.35	0.13	2.72	0.07	80	29
Pan Am Signal Celibeta #7	C186765	3655	3651-90	1112.82-1124.71	Kotcho	439	0.36	0.04	0.34	0.29	1.17	0.11	94	80
Pan Am Signal Celibeta #7	C186765	3955	3941-70	1201-21-1210.56	Kotcho	437	0.70	0.08	0.65	0.44	1.47	0.11	92	62
Pan Am Signal Celibeta #7	C186765	4325	4310-40	1313.68-1322.83	Up. Dev	440	0.25	0.03	0.23	0.21	1.09	0.12	92	84
Dome *et al.* Trout Lake H-45	C186768	1360	1340-80	408.43-420.62	Kotcho									
Dome *et al.* Trout Lake H-45	C186768	1730	1720-40	525.25-530.35	Kotcho									
Dome *et al.* Trout Lake H-45	C186768	2115	2101-20	640.38-646.17	Kotcho	430	0.33	0.14	0.58	0.11	5.40	0.20	176	33
Imperial Island River No.1	C186751	3486	3486C[1]	1057.65	Kotcho	379	0.35	0.05	0.04	0.47	0.09	0.60	11	135
Imperial Island River No.1	C186751	3797	3797-3806C[1]	1157.32-1160.07	Kotcho									
Imperial Island River No.1	C186751	4010	4098-4118C[1]	1249.07-1255.17	Kotcho									
Imperial Island River No.1	C186751	4102	4101-03C[1]	1249.98-1250.59	Kotcho	451	1.32	0.57	2.53	0.63	4.50	0.18	183	39

[1] C = core samples [2] Data from Feinstein *et al.* (1988) [3] per g rock

Table B4 Rock-Eval data for the Kotcho and Upper Devonian shales.

Well location	Sample No. GSC C#	I.D.	Depth ft	m	Tmax °C	TOC %	S1 mg[3]	S2 mg[3]	S3 mg[3]	S2\S3	PI	HI	OI
B-A Texaco Arrowhead N-2	C186758-	4635	4545-50	1385.32-1386.84	452	2.19	2.18	3.8	0.68	5.61	0.35	174	31
B-A Texaco Arrowhead N-2	C186758-	4645	4640-50	1414.27-1417.32	452	4.22	3.42	8.0	0.73	11.07	0.30	189	17
Imperial Sun Arrowhead I-46	C186757-	1990	1980-2000	298.7-609.6	434	1.61	0.02	1.12	0.92	1.22	0.02	69	57
Texaco NFA Bovie Lake J-72	C186762-	5415	5401-30	1646.22-1655.06	449	1.80	14.70	6.95	0.55	12.63	0.68	117	9
Imperial Sun Netla C-07	C186764-	2040	2031-50	619.05-624.84									
Murphy *et al.* Muskeg River No.1	C186767-	2370	2361-80	719.63-725.42	424	1.44	0.09	0.36	0.32	1.10	0.19	24	22
Pan Am Home Signal Celibeta #7	C186765-	3470*	3451-90	1051.86-1063.75									
Dome *et al.* Trout Lake H-45	C186768-	1295*	1290-1300	393.19-396.24									
Imperial Island River No.1	C186751-	3465	3465C[1]	1056.13	445	15.72	8.80	65.00	1.80	31.50	0.12	416	14
Imperial Island River No.1	C186751-	3470	3470C[1]	1057.66	445	13.90	6.90	60.00	0.80	74.50	0.10	430	5

[1] C = core samples [2] Data from Feinstein *et al.* (1988) [3] per g rock * not enough sample for Rock-Eval analysis in addition to petrography

Table B5 Rock-Eval data for the Exshaw Formation.

Well location	Sample No		Depth		Tmax	TOC	S1	S2	S3	S2\S3	PI	HI	OI
	GSC C#	I.D.	ft	m		°C	%	mg	mg	mg			
B-A Texaco Arrowhead N-2	C-186758-	3245	3240-50	987.55-990.6	395	0.20	0.19	0.19	0.24	0.82	0.52	95	115
B-A Texaco Arrowhead N-2	C-186758-	3505	3500-10	1066.8-1069.85	437	0.21	0.20	0.29	0.33	0.81	0.42	139	171
B-A Texaco Arrowhead N-2	C-186758-	4005	4000-10	1220.73-1222.25	444	0.17	0.19	0.18	0.20	0.87	0.53	103	117
B-A Texaco Arrowhead N-2	C-186758-	4285	4280-90	1304.5 -1395.98	350	0.53	1.56	1.45	1.14	1.25	0.53	269	215
B-A Texaco Arrowhead N-2	C-186758-	4445	4440-50	1353.31-1356.36	452	1.50	1.01	2.58	0.54	4.77	0.28	172	35
B-A Texaco Arrowhead N-2	C-186758-	4455	4450-60	1356.36-1359.41	448	2.50	1.80	4.44	0.59	7.35	0.30	175	23
Imperial Sun Arrowhead I-46	C186757-	1725	1710-40	521-530.52									
Imperial Sun Arrowhead I-46	C186757-	1810	1800-20	548.64 -554.74									
Imperial Sun Arrowhead I-46	C186757-	1910	1900-1910	579.12-585.21									
Texaco NFA Bovie Lake J-72	C186762-	3645	3631-60	1106.73-1115.57	440	1.70	7.60	3.50	0.63	5.30	0.70	193	36
Texaco NFA Bovie Lake J-72	C186762-	3935	3921-50	1195.12-1203.96	440	2.02	9.35	3.72	0.69	5.30	0.72	180	33
Texaco NFA Bovie Lake J-72	C186762-	4335	4321-50	1317.04-1325.88	442	2.13	9.00	4.70	0.58	8.12	0.66	220	26
Texaco NFA Bovie Lake J-72	C186762-	4835	4821-50	1469.44-1478.28	366	1.00	8.46	1.00	0.87	1.13	0.90	98	85
Texaco NFA Bovie Lake J-72	C186762-	5265	5251-80	1600.50-1609.34	394	1.30	7.60	1.47	0.70	2.19	0.84	110	53
Imperial Sun Netla C07	C186764-	1955	1941-70	591.62-600.45	443	1.14	0.06	1.33	0.20	6.65	0.04	116	17
Imperial Sun Netla C07	C186764-	2020	2001-40	609.90-621.79	443	1.42	0.10	1.56	0.23	6.78	0.06	109	16
Murphy *et al.* Muskeg River No.1	C186767-	1915	1901-30	579.42-588.26	431	2.12	0.10	2.32	0.37	5.35	0.04	111	17
Murphy *et al.* Muskeg River No.1	C186767-	2205	2191-2220	667.82-676.66	418	0.82	0.00	0.10	0.29	0.32	0.10	11	35
Murphy *et al.* Muskeg River No.1	C186767-	2335	2321-50	707.44-716.28	xxx	0.44	0.01	0.00	0.19	0.00	0.00	0	43
Pan Am Home Signal Celibeta # 7	C186765-	2165	2151-80	665.62-664.46									
Pan Am Home Signal Celibeta # 7	C186765-	2491	2471-2510	753.16-2510									

Table B6 Rock-Eval data for the Banff Formation.

Well location	Sample No		Depth		Tmax	TOC	S1	S2	S3	S2\S3	PI	HI	OI
	GSC C#	I.D.	ft	m	°C	%	mg[3]	mg[3]	mg[3]				
Pan Am Home Signal Celibeta # 7	C186765-	2920	2911-30	886.97-893.06	432	0.25	0.00	0.07	0.24	0.29	0.00	28	96
Pan Am Home Signal Celibeta # 7	C186765-	3325	3311-40	1013.46-1018.03	432	0.95	0.04	0.38	0.57	0.66	0.10	40	60
Pan Am Home Signal Celibeta #7	C186765-	3430	3311-40	1009.19-1018.03									
Dome *et al.* Trout Lake H-45	C186768-	1250	1240-60	377.95-3840.48									
Imperial Island River No.1	C186751-	2134	2134C[1]	650.44	437	1.32	0.13	0.45	0.20	2.89	0.22	34	15
Imperial Island River No.1	C186751-	2140	2140C[1]	652.27									
Imperial Island River No.1	C186751-	2310	2310C[1]	704.08	366	0.21	0.00	0.00	0.01	1.00	0.00	0	0
Imperial Island River No.1	C186751-	2456	2456C[1]	748.59	378	0.12	0.00	0.03	0.08	0.41	0.00	25	67
Imperial Island River No.1	C186751-	2747	2747C[1]	837.28	442	1.52	0.20	0.84	0.29	2.82	0.19	54	19
Imperial Island River No.1	C186751-	2760	2760C[1]	841.24	433	0.63	0.10	0.23	0.40	0.42	0.38	33	63
Imperial Island River No.1	C186751-	3012	3012C[1]	918.06	438	0.52	0.07	0.26	0.05	6.50	0.22	49	7
Imperial Island River No.1	C186751-	3275	3275C[1]	998.22									
Imperial Island River No.1	C186751-	3288	3288C[1]	1002.18	445	0.99	0.28	1.80	0.24	8.95	0.14	182	24
Pan Am Mattson Creek A-1	C196779	140	140	42.67	xx	0.70	0.23	0.00	0.39	0.0	1.0	0	55
Pan Am Mattson Creek A-1	C196779	260	260	79.25	300	0.69	0.11	0.14	0.80	0.78	0.80	15	20
Pan Am Mattson Creek A-1	C196779	680	680	207.26	486	0.62	0.30	0.23	0.06	3.83	0.58	37	9
Pan Am Mattson Creek A-1	C196779	860	680	262.13	414	0.49	0.30	0.24	0.08	3.00	0.56	48	16
Pan Am Mattson Creek A-1	C196779	1000	1000	304.8	486	0.77	0.32	0.32	0.11	2.90	0.50	41	41
Pan Am Mattson Creek A-1	C196779	1180	1180	359.66	369	1.58	0.99	0.30	0.22	1.36	0.77	18	13
Pan Am Mattson Creek A-1	C196779	1240	1240	377.95	375	3.86	4.13	0.97	0.28	3.46	0.83	25	7
IOE PA Viscount a-77-D	C186771	9975	9950-9980	3040.4-41.9	xx	0.21	0.13	0.15	0.16	1.38	0.49	68	75
IOE PA Viscount a-77-D	C186771	10375	10361-10390	3158.0-66.9									
IOE PA Viscount a-77-D	C186771	10440	10421-10460	3176.3-3188.2	323	0.22	0.10	0.10	0.14	0.63	0.58	34	59

[1] C = core samples [2] Data from Feinstein *et al.* (1988) [3] per g rock

Table B6 (continued).

Well location	Sample No.		Depth		Tmax	TOC	S1	S2	S3	S2\S3	PI	HI	OI
	C number	I.D.	ft	m	°C	%	mg[3]	mg[3]	mg[3]				
Canada Southern N. Beaver R. 1-	27C186754-	9120	9120	2779.77	420	1.82	0.60	0.17	0.45	0.37	0.79	9	24
Canada Southern N. Beaver R. 1-	27C186754-	9389	9370-9399	2855.97-2864.82	423	1.95	0.41	0.47	1.57	0.30	0.44	23	79
Canada Southern N. Beaver R 1-27	C186754-	9659	9650-9669	41.32-2947.11	384	1.34	0.54	0.25	0.33	0.75	0.68	17	24
Canada Southern N. Beaver R 1-27	C186754-	10319	10310-10329	3142.49-3148.28	3.25	0.56	1.04	1.41	0.74	0.35	xxx	32	42
Canada Southern N. Beaver R 1-27	C186754-	10665	10660-10679	3249.17-3254.96	465	3.32	0.63	0.52	0.87	0.60	0.55	16	26
Canada Southern N. Beaver R 1-27	C186754-	10875	10869-10879	3258.00-3315.92*	380	6.02	1.06	0.30	0.28	1.04	0.79	7	7
Canada Southern N. Beaver R 1-27	C186754-	10939	10930-10949	3331.46-3337.25**	418	4.17	1.46	0.61	0.70	0.87	0.71	14	16
Pan Am Pointed Mountain P-53	C186766-	7450	7441-60	268.02-2273.80	448	0.72	0.23	0.17	0.40	0.41	0.78	22	55
Pan Am Pointed Mountain P-53	C186766-	7610	7601-20	2316.78-2322.58	356	0.54	0.20	0.06	0.32	0.20	0.78	12	60
Pan Am Pointed Mountain P-53	C186766-	7810	7801-20	2377.75-2383.54	422	0.71	0.20	0.13	0.47	0.27	0.62	18	67
Pan Am Pointed Mountain P-53	C186766-	8115	8110-20	2471.93-2474.98	441	0.66	0.18	0.11	0.23	0.48	0.6	17	35
Pan Am Pointed Mountain P-53	C186766-	8410	8401-20	2560.62-2566.42	440	0.63	0.14	0.09	0.16	0.56	0.64	14	25
Pan Am Pointed Mountain P-53	C186766-	8535	8531-40	2600.25-2602.99	448	0.80	0.20	0.16	0.50	0.30	0.57	20	63
Pan Am Pointed Mountain P-53	C186766-	8930	8920-40	2718.82-2724.91	333	0.67	0.15	0.08	0.31	0.32	0.62	14	44
Pan Am Pointed Mountain P-53	C186766-	9200	9191-9210	2801.42-2807.21	345	0.35	0.08	0.08	0.15	0.53	0.50	23	43
Pan Am Pointed Mountain P-53	C186766-	9630	9621-40	2932.48-2938.27	393	0.50	0.07	0.05	0.18	0.27	0.58	9	33
Pan Am Pointed Mountain P-53	C186766-	10105	10091-10120	3075.74-3084.58	318	0.50	0.14	0.05	0.21	0.20	0.74	10	40
Pan Am Pointed Mountain P-53	C186766-	10410	10401-20	3170.22-3176.02*	340	3.50	1.02	0.15	0.52	0.37	0.86	5	14
Pan Am Pointed Mountain P-53	C186766-	10810	10801-20	3292.14-3297.94	350	0.74	0.17	0.10	0.17	0.57	0.67	12	22
Pan Am Pointed Mountain P-53	C186766-	10860	10851-10870	3307.38-3313.17**	396	1.40	0.24	0.20	0.44	0.57	0.57	23	37
Pan Am Beaver G-01, YT	C186752-	10575	10550-580C	3215.64-3224.78	95	0.90	0.37	0.22	0.23	0.97	0.62	25	25
Pan Am Beaver G-01, YT	C186752-	10865	10850-880C	'3311.65-3316.22									

* 1st Black Shale ** 2nd Black Shale [1] C = core samples [2] Data from Feinstein *et al.* (1988) [3] per g rock

Table B7 Rock-Eval data for the Besa River Formation.

Well location	Sample No.		Depth		Tmax	TOC	S1	S2	S3	S2\S3	PI	HI	OI
	C number	I.D.	ft	m	°C	%	mg[3]	mg[3]	mg[3]				
Pan Am Beaver G-01, YT	C186752-	11635	11620-650C[1]	3541.77-3550.92*	362	3.35	1.72	0.42	0.27	1.66	0.80	13	7
Pan Am Beaver G-01, YT	C186752-	12015	12000-030C[1]	3657.60-3666.74*	362	3.04	2.52	0.60	0.16	3.90	0.81	20	5
Pan Am Beaver G-01, YT	C186752-	12265	12250-280C[1]	3733.80-3742.94	363	0.72	0.40	0.10	0.05	2.00	0.81	13	7
Pan Am Beaver G-01, YT	C186752-	12665	12660-670C[1]	3858.77-3862.81	347	0.41	0.19	0.01	0.05	0.18	0.95	2	12
Pan Am Beaver G-01, YT	C186752-	12915	12900-930C[1]	3931.92-3941.06**	399	0.83	0.23	0.03	0.11	0.27	0.93	3	12
Pan Am Beaver G-01, YT	C186752-	12975	12960-990C[1]	3954.78-3959.35**	362	1.20	1.04	0.43	0.21	2.00	0.72	35	18
Pan Am Beaver G-01, YT	C186752-	13185	13170-200C[1]	4014.224023.36**	372	0.95	0.69	0.31	0.19	1.55	0.70	32	20
Pan Am Kotaneelee YT 0-67	C186755-	5040	5040	1536.19	374	1.22	0.33	0.12	0.24	0.50	0.75	9	19
Pan Am Kotaneelee YT 0-67	C186755-	6000	6000	1828.8	369	0.72	0.34	0.16	0.59	0.27	0.68	22	81
Pan Am Kotaneelee YT 0-67	C186755-	7000	7000	2133.6*	364	1.43	0.60	0.27	0.46	0.59	0.80	18	32
Pan Am Kotaneelee YT 0-67	C186755-	7595	7590-7600	2314.95-2316.48*	336	1.39	0.28	0.10	0.23	0.43	0.74	7	17
Pan Am Kotaneelee YT 0-67	C186755-	7615	7600-7630	2316.48-2325.62	336								
Pan Am Kotaneelee YT 0-67	C186755-	7800	7800	2377.44	362	1.26	0.39	0.16	0.01	16.0	0.72	12	0
Pan Am Kotaneelee YT 0-67	C186755-	7900	7890-7910	2404.87-2325.62**	372	2.10	0.37	0.21	0.18	1.16	0.64	10	8
Pan Am Kotaneelee YT 0-67	C186755-	7920	7910-7930	2414.01-2417.06	372								
Clausen Creek	C74201	+16.44[4]	+16.44	+5.0	465	2.26	0.72	1.38	0.26	5.41	0.34	60	11
Clausen Creek	C74202	+44.3[4]	+13.5	+13.5	465	2.62	1.18	2.00	0.19	10.95	0.38	75	7
Clausen Creek	C74207	+377.29[4]	+377.29	+115.0	463	0.60	0.56	0.58	0.20	2.81	0.50	95	34
Clausen Creek	C74212				467	0.52	0.09	0.25	0.17	1.47	0.28	47	32
Clausen Creek	C74213	+1043.3[4]	+1043.3	+318.0	453	0.70	0.38	0.52	0.16	3.28	0.44	75	22

[1] C = core samples [2] Data from Feinstein *et al.* (1988) [3] per g rock [4] elevations above base of section * 1st Black Shale ** 2nd Black Shale

Table B7 (continued).

Location	Sample No. GSC C#	I.D.	Depth ft	Depth m	Rock unit	Tmax °C	TOC %	S1 mg[3]	S2 mg[3]	S3 mg[3]	S2\S3	PI	HI	OI
Amoco East Flett H-13	C186759-	2780	2770-90	844.30-850.34	Clausen	430	0.49	0.10	0.38	0.09	4.10	0.21	72	18
Amoco East Flett H-13	C186759-	2905	2900-10	883.92-886.97	Clausen	428	0.45	0.11	0.29	0.13	2.21	0.29	63	29
B-A Texaco Arrowhead N-2	C186758-	2645	2640-50	804.67-807.72	Clausen									
B-A Texaco Arrowhead N-2	C186758-	2745	2740-50	530.35-838.20	Clausen									
B-A Texaco Arrowhead N-2	C186758-	2805	2800-2810	853.44-856.49	Clausen	430	0.18	0.31	0.28	0.25	1.10	0.53	155	139
Texaco NFA Bovie Lake J-72	C186762-	3290	3281-3300	1000-1005.84`	Clausen	435	1.02	5.76	2.02	0.57	3.59	0.74	190	56
Texaco NFA Bovie Lake J-72	C186762-	3390	3381-3900	1030.52-1188.72	Clausen	440	1.60	6.58	4.32	0.50	8.84	0.61	244	38
Pan Am Home Signal Celibeta # 7	C186765-	1931	1911-50	582.47-594.36	Clausen	436	2.08	0.10	2.28	1.21	1.88	0.04	109	58
Pan Am Home Signal Celibeta # 7	C186765-	1991	1971-2010	600.76-612.65	Clausen	442	0.93	0.03	0.21	0.72	0.29	0.12	22	77
Jackfish Gap-Yohin Ridge	C52180-	1546	1545.6[4]	471.1	Clausen	458	1.52	0.20	0.63	0.24	2.79	0.23	41	15
Jackfish Gap-Yohin Ridge	C52181-	1551	1550.52[4]	472.6	Clausen									
Pan Am Viscount a-77-D	C186771-	9775	-9761-9	-2975.15-2984	Clausen									
Jackfish Gap-Yohin Ridge	C58505-	55	55.44[4]	16.9	Yohin	483	1.50	0.07	0.25	0.32	0.75	0.23	16	21
Jackfish Gap-Yohin Ridge	C52163-	133	132.56[4]	40.4	Yohin	476	1.12	0.12	0.26	0.26	1.02	0.32	23	22
Jackfish Gap-Yohin Ridge	C52166-	166	166.01[4]	50.6	Yohin									
Jackfish Gap-Yohin Ridge	C58503-	344	343.5[4]	104.7	Yohin	476	1.80	0.03	0.36	0.29	1.22	0.08	19	16
Jackfish Gap-Yohin Ridge	C51174-	420	419.6[4]	127.9	Yohin									
Jackfish Gap-Yohin Ridge	C58502-	520	519.68[4]	158.4	Yohin	474	1.00	0.06	0.25	0.21	1.21	0.20	26	22

[1] C = core samples [2] Data from Feinstein *et al.* (1988) [3] per g rock [4] elevation above base of section

Table B8 Rock-Eval pyrolysis data for the Yohin and Clausen formations.

Sample location	Sample no. GSC C#	I.D.	ft	Depth m	Rock unit	Tmax °C	TOC %	S1 mg[3]	S2 mg[3]	S3 mg[3]	S2\S3	PI	HI	OI
Amoco East Flett H-13	C186759-	-1440	-1430-50	-435.86-441.96	Flett-Meil									
Amoco East Flett H-13	C186759-	-1620	-1610-30	-490.72-496.82	Flett-Meil									
Amoco East Flett H-13	C186759-	-1860	-1850-70	-563.88-569.98	Flett-Meil	431	0.49	0.06	0.20	0.18	1.11	0.24	40	37
Pan Am Pointed Mountain P53	C186766-	-5050	-5041-60	-1536.49-1542.29	Flett	451	1.32	0.25	0.90	0.28	3.29	0.22	70	21
Pan Am Pointed Mountain P53	C186766-	-5100	-5091-5110	-1551.73-1557.53	Flett									
Jackfish Gap-Yohin Ridge	C52106-3187.33C[1]		3187.33	3187.33- 971.5	Flett									
Jackfish Gap-Yohin Ridge	C52115-3405.18C		3405.18	1037.9	Flett	437	0.27	0.27	0.36	0.19	1.89	0.43	130	70
Jackfish Gap-Yohin Ridge	C58522-3534.77C[1]		3534.77	1077.4	Flett									
Jackfish Gap-Yohin Ridge	C58523-3534.77C[1]		3534.77	1077.4	Flett									
Jackfish Gap-Yohin Ridge	C74336-3628.81C[1]		3628.81	1105.9	Flett	440	0.66	0.13	0.57	0.37	1.53	0.19	85	55
Jackfish Gap-Yohin Ridge	C74338-3684.05C[1]		3684.05	1122.9	Flett	438	0.48	0.06	0.26	0.36	0.74	0.20	55	74
Jackfish Gap-Yohin Ridge	C52152-3793.64C[1]		3793.64	1156.3	Flett	440	0.46	0.15	0.46	0.32	1.50	0.25	101	68
Jackfish Gap-Yohin Ridge	C52157-3852.69C[1]		3852.69	1174.3	Flett	434	0.28	0.13	0.18	0.46	0.48	0.45	60	161
Amoco East Flett H-13	C186759-	-2445	-2440-60	-743.71-249.81	Prophet	432	0.50	0.07	0.50	0.13	4.45	0.13	90	21
B-A Texaco Arrowhead N-2	C-186758-	-2485	-2480-90	-755.90-758.95	Prophet									
Texaco NFA Bovie Lake J-72	C186762-	-2665	-2651-80	-808.02-816.64	Prophet	433	0.55	1.39	1.21	0.40	3.06	0.54	212	69
Texaco NFA Bovie Lake J-72	C186762-	-2935	-2921-50	-890.32-899.16	Prophet	439	0.88	3.15	1.63	0.56	2.91	0.66	185	65
Pan Am *et al.* Celibeta No. 7	C186765-	-1730	-1721-40	-524.56-530.35	Prophet									
Pan Am *et al.* Celibeta No. 7	C186765-	-1850	-1841-70	-560.83-569.97	Prophet									
Can. S. *et al.* N. Beaver R. 1-27	C186754-	-7139	-7130-7150	-2173.22-2179.32	Prophet	503	1.06	0.19	0.18	0.33	0.53	0.56	16	31
Can. S. *et al.* N. Beaver R. 1-27	C186754-	-7540	-7530-7550	-2295.14-2301.24	Prophet	395	1.50	0.50	0.33				22	
Can. S. *et al.* N. Beaver R. 1-27	C186754-	-7860	-7850-7860	-2392.68-2395.73	Prophet	427	3.25	0.43	1.49	2.14	0.73	0.26	47	6

[1] C = core samples [2] Data from Feinstein *et al.* (1988) [3] per g rock

Table B9 Rock-Eval pyrolysis data for the Rundle Group.

Sample location	Sample no.		Depth		Rock	Tmax	TOC	S1	S2	S3	S2\S3	PI	HI	OI
	GSC C#	I.D.	ft	m	unit	°C	%	mg[3]	mg[3]	mg[3]				
Can. S. *et al.* N. Beaver R. 1-27	C186754-	-8585	-8570-8599	-2612.14-2620.97	Prophet	428	5.15	0.59	3.13	3.07	1.04	0.16	63	59
Can. S. *et al.* N. Beaver R. 1-27	C186754-	-8815	-8810-8819	-2685.28-2688.03	Prophet	425	6.20	0.66	2.72	3.17	0.87	0.20	43	50
Can. S. *et al.* N. Beaver R. 1-27	C186754-	-8860	-8859-8870	-2700.22-2703.57	Prophet	438	2.60	0.50	1.68				63	
Pan Am Pointed Mountain P-53	C186766-	-5230	-5221-40	-1591.36-1597.15	Prophet	450	0.55	0.16	0.29	0.20	1.49	0.37	54	36
Pan Am Pointed Mountain P-53	C186766-	-5565	-5551-80	-1691.94-1700.78	Prophet	450	0.94	0.25	0.66	0.45	1.50	0.28	71	46
Pan Am Pointed Mountain P-53	C186766-	-5900	-5891-5910	-1795.58-1801.36	Prophet	453	0.85	0.24	0.58	0.38	1.53	0.30	68	44
Pan Am Pointed Mountain P-53	C186766-	-6270	-6261-80	-1911.40-1914.14	Prophet	456	0.65	0.27	0.37	0.35	1.07	0.42	56	52
Pan Am Pointed Mountain P-53	C186766-	-6810	-6201-20	-1890.06-1895.86	Prophet	391	0.77	0.59	0.58	0.65	0.90	0.50	75	84
Pan Am Pointed Mountain P-53	C186766-	-7171	-7161-80	-2182.67-2188.46	Prophet	406	0.50	0.25	0.27	0.30	0.88	0.49	51	59
Pan Am Beaver G-01, YT	C186752-	-10129	-10125-13	-3086.1-3088.54	Prophet	325	3.08	1.00	0.20	0.16	1.26	0.82	7	5
Pan Am Beaver G-01, YT	C186752-	-10183	-10181-184.5C[1]	-3103.17-3104.23	Prophet	xxx	1.32	0.18	0.00	0.11	0.00	1.00	0	8
Pan Am Kotaneelee YT 0-67	C186755-	-4200	-4200	-1280.16	Prophet	366	1.06	0.59	0.26	0.06	4.33	0.70	24	5
Jackfish Gap-Yohin Ridge	C52064-	2610.56	2610.56	795.7	Prophet									
Jackfish Gap-Yohin Ridge	C52067-	2692.58	2692.58	820.7	Prophet	434	0.50	0.06	0.24	0.45	0.49	0.25	43	87
Jackfish Gap-Yohin Ridge	C58517-	2730.64	2730.64	832.3	Prophet									
Clausen Creek	C74220-	1541.99	1541.99	470	Prophet	453	0.22	0.07	0.15	0.49	0.29	0.31	66	223
Clausen Creek	C74234-	2224.41	2224.41	678	Prophet	449	1.14	0.09	0.42	0.45	0.97	0.18	37	38
Pan Am Viscount a-77-D	C186771-	-9625	-9611-40		Prophet	382	1.03	0.45	0.28	0.24	1.14	0.24	27	23
Pan Am Viscount a-77-D	C186771-	-9675	-9661-90		Prophet	447	1.13	0.47	0.35	0.23	1.52	0.23	31	20
B-A Texaco Arrowhead N-2	C186758-	-2340	-2330-50	-710.18-716.28	Form'n F									
Pan Am *et al.* Celibeta No. 7	C186765-	-1045	-1031-50	-314.25-323.09	Form'n F	432	1.72	0.07	1.21	0.87	1.39	0.05	70	50
Pan Am *et al.* Celibeta No. 7	C186765-	-1496	-1495-97	-455.67-1497	Form'n F									
Pan Am *et al.* Celibeta No. 7	C186765-	-2045	-2021-50	-616.00-624.84	Pekisko									

[1] C = core samples [2] Data from Feinstein *et al.* (1988) [3] per g rock

Table B9, continued.

Sample location	Sample No.		Depth		Tmax	TOC	S1	S2	S3	S2\S3	PI	HI	OI
	GSC C#	I.D.	ft	m °C	%	mg[3]	mg[3]	mg					
Canada Southern *et al.* N. Beaver R. YT 1-27	C187854-	5989	5970-6019	1819.66-1834.59	457	2.27	0.58	1.15	0.79	1.46	0.34	53	35
Canada Southern *et al.* N. Beaver R. YT 1-27	C187854-	6349	6330-6369	1929.38-1941.27	486	1.58	0.25	0.47	0.71	0.65	0.35	29	44
Canada Southern *et al.* N. Beaver R. YT 1-27	C187854-	6640	6630-6659	2020.82-2029.66	493	1.40	0.19	0.38	1.11	0.49	0.34	22	80
Pan Am Pointed Mountain P-53	C186766-	4570	4561-80	1390.19-1395.98	452	1.17	0.20	0.70	0.32	2.22	0.22	60	27
Pan Am Pointed Mountain P-53	C186766-	4805	4801-10	1463.34-466.09	461	1.95	0.35	1.48	0.73	2.50	0.21	75	37
Pan Am Beaver G-01, YT	C186752-	6120	6110-30	1862.33-16868.42	465	2.33	1.51	1.69	0 33	5.26	0.48	72	14
Pan Am Beaver G-01, YT	C186752-	6540	6530-50	1990.34-1996.44									
Pan Am Beaver G-01, YT	C186752-	6565	6850-80	2087.88-2097.02	476	2.12	1.05	1.32	0.54	2.46	0.45	61	25
Pan Am Beaver G-01, YT	C186752-	7140	7130-50	2173.22-2179.32	493	2.51	0.79	1.11	0.65	1.70	0.41	45	25
Pan Am Beaver G-01, YT	C186752-	7480	7470-90	2279.90-2587.75	428	4.89	1.98	13.78	0.54	26.29	0.13	280	11
Pan Am Beaver G-01, YT	C186752-	7840	7830-60	2386.58-2395.73	487	1.95	0.56	0.77	0.59	1.30	0.43	39	30
Pan Am Beaver G-01, YT	C186752-	8766	8765-67C[1]	2671.57-2672.18									
Pan Am Beaver G-01, YT	C186752-	8800	8795-8805C[1]	2680.71-2683.76	xxx	1.06	0.10	0.00	0.09	0.00	1.00	0	8
Pan Am Beaver G-01, YT	C186752-	9210	9200-20	2804.16-2801.26	402	1.23	0.36	0.36	0.24	1.53	0.50	29	19
Pan Am Beaver G-01, YT	C186752-	9505	9490-9520	2892.55-2901.69	430	1.20	0.28	0.25	0.37	0.68	0.53	21	31
Pan Am Beaver G-01, YT	C186752-	9880	9870-90	3008.37-3014.47	425	1.15	0.35	0.37	0.33	1.24	0.49	30	29
Pan Am Kotaneelee YT 0-67	C186755-	1320	1320	402.34	450	0.81	0.41	0.78	0.36	2.16	0.35	96	44
Pan Am Kotaneelee YT 0-67	C186755-	1620	1620	493.77	462	1.26	0.16	0.46	0.30	1.53	0.26	36	23
Pan Am Kotaneelee YT 0-67	C186755-	1980	1980	603.50	435	0.95	0.22	0.21	0.46	0.45	0.52	22	48
Pan Am Kotaneelee YT 0-67	C186755-	2600	2600	792.48	331	0.39	0.09	0.09	0.15	0.60	0.50	11	18
Pan Am Kotaneelee YT 0-67	C186755-	3500	3500	1066.8	348	1.19	0.27	0.15	0.27	0.55	0.64	12	22
OIE Pan Am Viscount a-77-D	C186774-	8420	8401-40	2560.6-2572.51	498	0.90	0.13	0.35	0.62	0.57	0.28	39	68

[1] C = core samples [2] Data from Feinstein *et al.* (1988) [3] per g rock

Table B10 Rock-Eval data for the Golata Formation.

Sample location	Samp No.		Depth		Rock	Tmax	TOC	S1	S2	S3	S2\S3	PI	HI	OI
	GSC C#	I.D.	ft	m	fm	°C	%	mg[3]	mg[3]	mg[3]				
B-A Texaco Arrowhead N-2	C-186758-	-2180	2170-90		Mattson		3.84*							
Texaco NFA Bovie Lake J-72	C186762-	-1260	1251-70	381.3-387.1	Mattson	432	1.62	6.69	1.76	0.67	2.62	0.79	108	40
IOE Bovie Lake M-05	C186753-	-1606	1603-09C[1]	488.59-490.42	Mattson	435	5.22	1.70	4.17	3.66	1.36	0.27	97	70
IOE Bovie Lake M-05	C186753-	-1606.7	1606.7C[1]	489.72	Mattson	439	5.23	1.68	6.52	1.59	4.19	0.20	124	30
Canada South. *et al.* N. Beaver R.1-27	C186754-	-3549	3540-3559	1078.99-1084.78	Mattson	440	4.80	3.00	4.68	1.08	3.27	0.39	97	23
Canada South. *et al.* N. Beaver R.1-27	C186754-	-4389	4370-4419	1331.97-1346.91	Mattson	441	2.12	0.88	1.15	0.98	1.16	0.43	53	46
Canada South. *et al.* N. Beaver R.1-27	C186754-	-4578	4570-4589	1392.94-1398.73	Mattson	443	1.07	0.43	0.56	0.59	0.94	0.44	52	55
Canada South. *et al.* N. Beaver R.1-27	C186754-	-4885	4880-4889	1487.42-1490.17	Mattson	420	18.40	2.77	16.93	11.36	1.48	0.15	90	62
Canada South. *et al.* N. Beaver R.1-27	C186754-	-5139	5130-5149	1563.62-1569.42	Mattson	452	1.25	0.27	0.52	0.55	0.95	0.34	41	43
Pan Am Pointed Mountain P-53	C186766-	-1950	1941-60	591.17-597.41	Mattson	448	1.99	0.65	1.38	0.71	1.94	0.32	69	35
Pan Am Pointed Mountain P-53	C186766-	-2160	2151-70	655.62-661.42	Mattson	440	2.20	0.52	2.45	0.46	5.47	0.18	112	20
Pan Am Pointed Mountain P-53	C186766-	-2780	2761-90	841.55-850.39	Mattson	443	2.93	0.51	2.72	0.76	3.55	0.16	94	26
Pan Am Pointed Mountain P-53	C186766-	-3195	3181-3210	969.57-978.41	Mattson	446	1.84	0.63	1.40	0.65	2.15	0.31	76	35
Pan Am Pointed Mountain P-53	C186766-	-3870	3161-80	1176.83-1182.62	Mattson	447	1.74	0.38	0.10	0.43	2.25	0.29	64	27
Pan Am Pointed Mountain P-53	C186766-	-4310	4301-20	1310.94-1316.73	Mattson	452	1.18	0.18	0.60	0.54	1.11	0.24	54	49
Amoco Pointed Mountain P-24	C186760-	-2570	2560-80	780.29-786.38	Mattson	434	1.18	0.19	1.60	0.57	2.83	0.11	146	48
Amoco Pointed Mountain P-24	C186760-	-2855	2850-60	868.68-871.73	Mattson									
Amoco Pointed Mountain P-24	C186760-	-3380	3370-90	1027.17-1033.27	Mattson	436	0.84	0.19	1.10	0.56	1.96	0.15	125	64
Amoco Pointed Mountain P-24	C186760-	-3995	3990-4000	1033.27-1219.20	Mattson									
Amoco Pointed Mountain P-24	C186760-	-4500	4590-4610	1371.6-1405.13	Mattson	441	4.70	0.95	11.40	0.70	16.69	1.03	241	14
Amoco Pointed Mountain P-24	C186760-	-4890	4871-4910	1484.68-1496.68	Mattson	438	1.54	0.46	2.00	0.73	2.71	0.19	129	48
Amoco Pointed Mountain P-24	C186760-	-5140	5130-50	1563.62-1569.72	Mattson									
Amoco Pointed Mountain P-24	C186760-	-5340	5330-50	1624.6-1630.68	Mattson	443	0.95	0.15	0.90	1.27	0.70	0.14	100	132
Pan Am Beaver G-01, YT	C186752-	-2880	2860-2900	2671.57-2672.18	Mattson		rich							
Pan Am Beaver G-01, YT	C186752-	-3250	3220-60	981.46-993.65	Mattson									
Pan Am Beaver G-01, YT	C186752-	-3475	3470-80	1057.66-1060.70	Mattson									
Pan Am Beaver G-01, YT	C186752-	-3700	3690-3710	1124.71-1130.81	Mattson									
Pan Am Beaver G-01, YT	C186752-	-3795	3790-3800	115.19-1158.24	Mattson									
Pan Am Beaver G-01, YT	C186752-	-4135	4120-4150	1255.77-1264.92	Mattson	389	1.26	1.66	1.29	0.47	2.70	0.56	102	37
Pan Am Beaver G-01, YT	C186752-	-4690	4680-4700	1426.46-1432.56	Mattson	371	1.12	2.50	1.58	0.38	4.21	0.62	147	33
Pan Am Beaver G-01, YT	C186752-	-4965	4950-80	1508.76-1517.90	Mattson	371	1.60	4.17	2.39	0.40	5.88	0.64	149	25
Pan Am Beaver G-01, YT	C186752-	-5520	5510-30	1679.45-1685.54	Mattson									
Pan Am Beaver G-01, YT	C186752-	-5835	5820-50	1773.94-1783.08	Mattson	467	1.76	1.80	1.89	0.35	5.38	0.49	108	20

*TOC data available from Shell Canada for 2080 ft (634m) interval [1] C = core samples [2] Data from Feinstein *et al.* (1988) [3] per g rock

Table B11 Rock-Eval pyrolysis data for the Mattson Formation.

Sample location	Samp No		Elevation*		Rock	Tmax	TOC	S1	S2	S3	S2\S3	PI	HI	OI
	GSC C#	I.D.	ft	m	fm	°C	%	mg[3]	mg[3]	mg[3]				
Tika Creek	C58558	103.5	103.5	31.55	Mattson									
Tika Creek	C58562	147	147	44.81	Mattson	546	3.77	0.07	0.68	0.86	0.80	0.08	18	23
Tika Creek	C58705	370	367-382	111.87-116.44	Mattson	551	4.30	0.05	0.95	0.33	2.93	0.05	22	8
Tika Creek	C58581	382	382	121	Mattson	514	1.29	0.04	0.23	0.59	0.38	0.16	17	47
Tika Creek	C58591	459	457-461	139.3-140.5	Mattson	513	1.81	0.10	0.57	0.41	1.32	0.16	30	23
Tika Creek	C58601	609	607-611	185-186.24	Mattson	504	1.66	0.04	0.42	0.27	1.52	0.10	27	18
Tika Creek	C58604	674	673-674	205.14-205.44	Mattson	496	1.34	0.05	0.42	0.29	1.44	0.11	31	22
Tika Creek	C58606	703	702-704	213.98-214.58	Mattson	524	1.23	0.04	0.27	0.30	0.96	0.13	23	24
Tika Creek	C58608	716	715-716	217.94-218.2	Mattson	482	1.73	0.06	0.64	0.29	2.32	0.09	36	16
Tika Creek	C58611	749	748-749	228-228.3	Mattson	490	1.60	0.07	0.49	0.37	1.43	0.12	34	23
Tika Creek	C58625	902	901.5-902.5	274.78-275.09	Mattson	463	1.50	0.16	0.79	0.85	0.92	0.17	52	56
Tika Creek	C58631	984	983.2-985.2	299.68-300.29	Mattson	468	0.94	0.02	0.28	0.18	1.54	0.07	30	20
Tika Creek	C58638	1008	1008-1008.8	307.24-307.5	Mattson	461	0.84	0.05	0.30	0.16	1.94	0.14	36	19
Tika Creek	C58634	1019	1018.5-1020.3	310.44-310.9	Mattson	446	1.58	0.36	0.68	0.42	1.62	0.35	43	26
Tika Creek	C58681	1467	1467.52	447.3	Mattson	446	0.74	0.03	0.33	0.36	0.90	0.07	44	48
Tika Creek	C58690	1542	1541.5-1543.6	469.9-470.48	Mattson	448	1.00	0.36	1.48	0.85	1.76	0.20	148	84
Jackfish Gap-Yohin Ridge	C58709	3894	3894.35	1187	Mattson	445	0.46	0.08	0.19	0.18	10.5	0.22	39	50
Jackfish Gap-Yohin Ridge	C58711	3986	3986.22	1215	Mattson	440	1.43	0.07	0.63	0.63	1.01	0.15	44	54
Jackfish Gap-Yohin Ridge	C58713	4096	4096.13	1248.5	Mattson	435	5.03	0.17	6.90	0.82	7.60	0.03	138	23
Jackfish Gap-Yohin Ridge	C58719	4413	4412.72	1345	Mattson	446	2.60	0.08	1.44	0.63	1.98	0.08	55	32
Jackfish Gap-Yohin Ridge	C58723	4562	4562	1390.5	Mattson	444	7.39	0.45	8.50	0.93	9.21	0.05	154	16
Jackfish Gap-Yohin Ridge	C58726	4633	4632.55	1412	Mattson	445	3.31	0.14	2.63	0.55	5.93	0.07	112	19
Jackfish Gap-Yohin Ridge	C58750	5052	5052.49	1540	Mattson	443	2.66	0.18	4.18	0.33	12.5	0.04	160	12
Jackfish Gap-Yohin Ridge	C58753	5081	5081.03	1548.7	Mattson	440	2.45	0.08	0.50	0.93	0.56	0.15	20	37
Jackfish Gap-Yohin Ridge	C58759	5535	5534.77	1687	Mattson	445	2.20	0.11	1.87	0.23	8.03	0.06	85	11
Jackfish Gap-Yohin Ridge	C58765	5640	5639.76	1719	Mattson	440	4.89	0.37	8.40	0.38	11.3	0.05	192	12
Jackfish Gap-Yohin Ridge	C58793	6385	6384.5	1946	Mattson	443	1.83	0.13	2.13	0.88	2.52	0.08	116	57
Jackfish Gap-Yohin Ridge	C58806	6754	6753.61	2058.5	Mattson	447	34.65	1.03	17.40	11.65	1.50	0.06	50	33
Jackfish Gap-Yohin Ridge	C58838	7246	7245.74	2228.5	Mattson	452	45.18	0.00	0.90	12.43	0.07	0.00	2	27
Clausen Creek	C74273	3297	3296.59	1004.8	Mattson	430	12.08	0.07	25.10	0.88	28.7	0.03	206	22
Clausen Creek	C74277	3414	3414.04	1040.6	Mattson	432	10.15	0.50	14.4	1.25	11.5	0.03	141	12
Clausen Creek	C74309	4283	4283.13	1305.5	Mattson	437	74.84	6.71	105.3	11.63	9.08	0.06	140	15
Clausen Creek	C74316	4457	4457.35	1358.6	Mattson	439	4.04	0.05	0.73	1.69	0.43	0.06	18	42

[1] C = core samples [2] Data from Feinstein *et al.* (1988) [3] per g rock [4] elevation above base of section

Table B11 Rock-Eval pyrolysis data for the Mattson Formation in the outcrop belt.

Sample location	Samp No		Depth		Rock	Tmax	TOC	S1	S2	S3	S2\S3	PI	HI	OI
	GSC C#	I.D.	ft	m	fm	°C	%	mg[3]	mg[3]	mg[3]				
IOE Dunedin a-75-E	C186770	-10450	10431-470	3179.37-91.26	Kiskatinaw									
IOE Dunedin a-75-E	C186770	-10977	10977C[1]	3345.79	Kiskatinaw	420	0.45	0.01	0.02	0.07	0.14	0.50	4	29
IOE Dunedin a-75-E	C186770	-10983	10983C[1]	3347.62	Kiskatinaw									
IOE Dunedin a-75-E	C186770	-10998	10998C[1]	3352.19	Kiskatinaw									
IOE Dunedin a-75-E	C186770	-11254	11254C[1]	3430.22	Kiskatinaw									
IOE Dunedin a-75-E	C186770	-11264	11264C[1]	3433.27	Kiskatinaw	377	0.35	0.00	0.01	0.12	0.05		2	0
IOE Dunedin a-75-E	C186770	-11286	11286C[1]	3439.97	Kiskatinaw	319	0.33	0.00	0.02	0.00			3	0
IOE Dunedin a-75-E	C186770	-11522	11522C[1]	3511.9	Kiskatinaw	365	0.80	0.08	0.11	0.00		0.42	13	0
IOE Dunedin a-75-E	C186770	-11531	11531C[1]	3514.65	Kiskatinaw									
IOE Dunedin a-75-E	C186770	-12130	12100-60	3688.1-3706.4	Kiskatinaw	367	2.38	0.28	0.26	0.16	1.58	0.52	10	6
IOE Pan Am Viscount a-77-D	C186771	-7425	7425	2263.14	K-TF*	460	1.90	0.36	1.68	0.00		0.18	87	0
IOE Pan Am Viscount a-77-D	C186771	-7475	7461-90	2274.11-82.95	K-TF*	457	3.15	1.55	2.49	0.12	22.00	0.38	79	4
IOE Pan Am Viscount a-77-D	C186771	-7477	7477C	2278.98	Kiskatinaw	485	0.20	0.10	0.17	0.00		0.37	87	0
IOE Pan Am Viscount a-77-D	C186771	-7895	7881-8110	2402.12-71.93	Kiskatinaw									
IOE Pan Am Viscount a-77-D	C186771	-8005	8000-10C[1]	2438.441.45	Kiskatinaw									
IOE Pan Am Viscount a-77-D	C186771	-8006	8006C[1]	2440.22	Kiskatinaw	470	0.50	0.06	0.24	0.00	0.00	0.20	50	0
IOE Pan Am Viscount a-77-D	C186771	-8011	8011C[1]	2441.75	Kiskatinaw	482	0.47	0.07	0.25	0.00		0.22	53	0
IOE Pan Am Viscount a-77-D	C186771	8095	8081-8110	2463.09-71.93	Kiskatinaw	449	1.36	0.22	0.98	0.35	2.80	0.19	71	25
IOE Pan Am Viscount a-77-D	C186771	-8245	8245C[1]	2513.07	Kiskatinaw	485	0.96	0.08	0.27	0.00		0.22	28	0
Imperial Pan Am LaBiche b-55-E	C186772	-8265	8240-90	2511.55-26.79	Kiskatinaw	459	2.24	0.36	1.06	0.20	5.36	0.26	47	9
Imperial Pan Am LaBiche b-55-E	C186772	-8970	8961-80	2731.31-37.10	Kiskatinaw	468	0.64	0.08	0.26	0.15	1.78	0.24	41	22
Imperial Pan Am LaBiche b-55-E	C186772	-9385	9381-90	2859.33-62.07	Kiskatinaw	502	0.67	0.06	0.18	0.49	0.36	0.25	26	73
Imperial Pan Am LaBiche b-55-E	C186772	-9675	9661-9700	2944.67-56.56	Kiskatinaw	529	1.14	0.06	0.26	0.31	0.85	0.18	22	27
Imperial Pan Am LaBiche b-55-E	C186772	-9960	9921-10000	3023.92-48.00	Kiskatinaw	520	1.00	0.07	0.25	0.44	0.57	0.22	24	44
Aquitaine *et al.* Tatoo a-2-D	C186775	-1617.5	1617.5C[1]	492.4	Kiskatinaw	437	5.00	0.74	12.60	0.90	14.03	0.06	249	18
Aquitaine *et al.* Tatoo a-2-D	C186775	-1625.5	1625.5C[1]	495.3	Kiskatinaw	436	0.54	0.18	0.41	1.67	0.24	0.31	74	305
Aquitaine *et al.* Tatoo a-2-D	C186775	-1631	1631C[1]	497.13	Kiskatinaw	440	2.18	0.54	3.06	0.39	7.64	0.16	136	18
Aquitaine *et al.* Tatoo a-2-D	C186775	1647C	1647C[1]	502	Kiskatinaw	438	2.50	0.71	3.89	0.66	5.93	0.16	151	26
Aquitaine *et al.* Tatoo a-2-D	C186775	-1655	1655C[1]	504.44	Kiskatinaw	440	2.39	0.49	4.80	1.03	4.65	0.09	208	45
Aquitaine *et al.* Tatoo a-2-D	C186775	-1661.5	1661.5C[1]	506.43	Kiskatinaw	442	1.80	0.25	2.95	0.94	3.13	0.26	164	52
Aquitaine Windflower d-87-A	C186773	-1496	1496C[1]	455.68	Kiskatinaw	408	0.05	0.01	0.12	0.00	15.00	0.09	280	10
Aquitaine Windflower d-87-A	C186773	-1503	1503C[1]	458.11	Kiskatinaw	390	0.03	0.01	0.05	0.33	0.11	0.06	136	1000
Aquitaine Windflower d-87-A	C186773	-1515	1515C[1]	461.77	Kiskatinaw	316	0.03	0.02	0.04	0.05	0.93	0.33	149	167
Aquitaine Windflower d-87-A	C186773	-1519	1519C[1]	462.99	Kiskatinaw	345	0.03	0.01	0.05	0.07	0.66	0.25	150	300
Aquitaine Windflower d-87-A	C186773	-1528	1528C[1]	465.73	Kiskatinaw	355	0.04	0.02	0.07	0.01	3.50	0.25	175	25

[1] C – core samples [2] Data from Feinstein *et al.* (1988) [3] per g rock

Table B11 Rock-Eval pyrolysis data for the Mattson-Kiskatinaw Formation in northeastern British Columbia.

APPENDIX C

Bitumen, reflectance, vitrinite reflectance and fluorescence data (by formation).

SAMPLE LOCATION	SAMPLE No		BITUMENS															VRo
			LOW Ro						MED Ro				HIGH Ro					
			Type 1			Type 2			Type 3			Type 4			Type 5			Type 6	Calculated
	C no.	I.D.	%R_o			%R_o			%R_o			%R_o			%R_o			% Ro	(Jacob, 1985)
			mean	s.d.	n	mean	s.d.	n	mean	s.d.	n	mean	s.d.	n	mean	s.d.	n	mean	
Imperial Island River	186751	6906							1.45	0.03	7	1.63	0.09	11	1.98	0.18	24	2.15	1.40
Dome *et al.*Trout Lake	186768	4890							1.17	0.10	28	1.54	0.10	24	1.89	0.05	6		1.44
Murphy Muskeg River	186767	6311				1.08	0.08	7	1.32	0.07	10	1.71	0.08	11	2.20	0.16	6	3.29	1.46
Imp Sun Arrowhead	186764	6110										1.67	0.14	14	2.20	0.00	1		1.43
Imp Sun Arrowhead	186764	6116										1.60	0.16	29	2.10	0.12	25		1.39
Imp Sun Arrowhead	186764	6122							1.25	0.07	4	1.67	0.16	31	2.10	0.13	51		1.43
Imp Sun Arrowhead	186764	6135							1.40	0.00	1	1.70	0.13	4	2.10	0.13	13		1.45
P.A. HomeCelibeta	186765	7060				1.26	0.07	2	2.00	0.25	26	2.60	0.37	2					2.00
Texaco Bovie Lake	186762	9535							2.00	0.14	23	2.90	0.14	46	4.40	0.23	5		2.19
Texaco Bovie Lake	186762	9598																	
Texaco Bovie Lake	186762	9613.5							2.02	0.15	14	3.08	0.28	50					2.30
Texaco Bovie Lake	186762	9611																	
Imperial Sun Netla	186764	6285							1.16	0.07	7	1.69	0.03	2	2.00	0.00	1	2.00	1.44
Imperial Sun Netla	186764	6315							1.23	0.15	38	1.67	0.10	15	2.10	0.17	3	2.27	1.46
P.A. Mattson Creek	1867–	1600							2.30	0.00	1	3.20	0.20	2	4.10	0.03	2	4.30	2.37
P. A. Mattson Creek	1867–	1640							2.80	0.00	1	3.55	0.05	2	4.10	0.30	6	4.70	2.59

rew. Vitr = reworked vitrinite; Sfus = semifusinite Vro = vitrinite reflectance

Table C1 Bitumen reflectance data from the Muskwa Formation and its stratigraphic equivalents.

SAMPLE LOCATION	SAMPLE No.		BITUMENS																FLUOR INDEX	VRo (Jacob 1985)
			LOW Ro						MED Ro				HIGH Ro							
			Type 1			Type2			Type 3			Type 4			Type 5			Type 6		
			% R_o			% R_o			% R_o			% R_o			% R_o			% R_o		
	GSC C#	I.D.	mean	s.d	n	mean	s.d .	n	mean	s.d.	n	mean	s.d.	n	mean	s.d.	n	mean	Alginite	
B-A Texaco Arrowhead	186758	7005							1.27	0.05	2	1.63	0.15	16	2.09	0.12	3	2.20		1.45
B-A Texaco Arrowhead	186758	7505				1.0	0.04	3	1.27	0.07	4	1.70	0.12	4	1.97	0.12	9	2.30		1.41
B-A Texaco Arrowhead	186758	8105							1.36	0.08	4	1.72	0.11	8	2.10	0.16	10	2.27		1.46
Imperial Sun Arrowhead	186757	4640							1.17	0.08	9	1.65	0.15	49	2.10	0.13	12			1.42
Imperial Sun Arrowhead	186757	5160							1.37	0.00	1	1.53	0.00	1	2.10	0. 00	1			1.35
Imperial Sun Arrowhead	186757	5510										1.58	0.14	15	2.10	0.15	17			1.38
Texaco NFA Bovie Lake	186762	7305				0.98	0.04	2				1.86	0.05	4	2.20	0.18	19			1.55
Texaco NFA Bovie Lake	186762	7705				1.10	0.10	2				1.82	0.12	16	2.25	0.08	12			1.52
Texaco NFA Bovie Lake	186762	8855							1.50	0.16	7				2.40	0.23	26	3.30		
Texaco NFA Bovie Lake	186762	9470							1.54	0.16	3				2.95	0.31	17	4.10		
Imperial Sun Netla	186764	4145	0.27	0.07	2	0.45	0.08	11	0.82	0.03	2	1.04	0.11	14	1.50	0.09	2	1.90	3	1.04
Imperial Sun Netla	186764	4515				0.58	0.06	3	0.82	0.04	2	1.25	0.08	16	1.48	0.06	8	1.92	4d	1.17
Imperial Sun Netla	186764	4815				0.67	0.00	1	0.86	0.04	4	1.30	0.09	12	1.58	0.07	2	1.86		1.20
Imperial Sun Netla	186764	5175				0.67	0.02	2	0.88	0.00	1	1.39	0.08	5	1.61	0.03	2	2.20		1.26
Imperial Sun Netla	186764	5420				0.61	0.00	1				1.42	0.11	15	1.62	0.04	5	2.10		1.28
Imperial Sun Netla	186764	5971							1.00	0.18	2	1.62	0.12	18	1.89	0.04	8	2.20		1.40
Murphy *et al.* Muskeg R	186767	4870							1.15	0.12	19	1.61	0.10	19	1.96	0.16	19			1.39
Murphy *et al.* Muskeg R	186767	5275							1.23	0.08	6	1.58	0.08	13	1.90	0.11	10	2.46		1.38
Murphy *et al.* Muskeg R	186767	5765							1.26	0.09	16	1.63	0.10	34	2.10	0.07	4			1.41
Murphy *et al.* Muskeg R	186767	6065				1.08	0.05	3	1.32	0.08	12	1.65	0.13	17	2.05	0.06	3	2.43		1.42
Pan Am Home Celibeta	186765	5455							1.20	0.12	2	1.71	0.08	3	2.06	0.12	11	3.20		1.46
Pan Am Home Celibeta	186765	5775							1.16	0.00	1				2.76	0.12	4	3.60		
Pan Am Home Celibeta	186765	6145							1.25	0.16	2	1.90	0.02	19	2.60	0.18	10	3.25		1.57
Pan Am Home Celibeta	186765	6385							1.24	0.08	2	2.20	0.11	4	2.65	0.15	2	3.25		1.76
Pan Am Home Celibeta	186765	6740							1.29	0.17	2	1.91	0.15	15	2.52	0.19	14	3.27		1.58
Dome *et al.* Trout Lake	186768	3	0.16	0.00	1				1.29	0.06	6	1.60	0.22	13	2.15	0.14	4	3.25		1.39
Dome *et al.* Trout Lake	186768	3870							1.11	0.00	1	1.37	0.08	6	1.90	0.11	7			1.24
Dome *et al.* Trout Lake	186768	4311							1.08	0.07	6	1.45	0.10	9	2.03	0.19	16			1.29
Dome *et al.* Trout Lake	186768	4630							1.08	0.12	4	1.43	0.11	23	2.12	0.30	17			1.28
Dome *et al.* Trout Lake	186768	4830							1.13	0.09	4	1.53	0.11	24	1.96	0.20	17	2.71		1.34
Dome *et al.* Trout Lake	186768	4890							1.17	0.10	28	1.54	0.10	24	1.89	0.05	6			1.35
Imperial Island River	186751	541				0.70	0.29	7	1.06	0.03	9	1.24	0.05	7	1.51	0.06	3			1.17
Imperial Island River	186751	5587.3							0.97	0.01	1	1.32	0.04	6	1.60	0.00	1	1.82		1.22
Imperial Island River	186751	5590.3										1.37	0.10	6	1.62	0.11	3	2.14		1.25
Imperial Island River	186751	5899				0.70	0.10	8	1.13	0.13	15									
Imperial Island River	186751	6240				0.82	0.09	5	1.19	0.13	6	1.46	0.05	4	1.76	0.08	2			1.30
Imperial Island River	186751	6400							1.28	0.03	4	1.50	0.00	1						1.33
Imperial Island River	186751	6814				1.00	0.00	1	1.31	0.07	4	1.57	0.02	2	1.87	0.00	1			1.37
Pan Am Mattson Creek	1967-	1440										1.94	0.24	10	2.92	0.20	9	3.51		1.60

Table C2 Bitumen reflectance and fluorescence data from the Fort Simpson Formation.

SAMPLE LOCATION	SAMPLE No.		BITUMENS															FLUORESCENCE INDEX			VRo calculated (Jacob, 1985
			LOW Ro Type 1 % R_o			Type 2 % R_o			Type 3 % R_o			MEDIUM Ro Type 4 % R_o			HIGH Ro Type 5 % R_o			Type 6 % R_o			
	C no.	I.D.	mean	s.d.	n	mean	s.d.	n	mean	s.d.	n	mean	s.d.	n	mean	s.d.	n	mean	m'alg	Leio	spor	
B-A Texaco Arrowhead N-2	186758	5835				0.78	0.08	2	1.21	0.00	1	1.53	0.00	1	1.74	0.12	3					1.34
B-A Texaco Arrowhead	186758	6245										1.63	0.13	16	2.01	0.13	16	2.27				1.40
Imperial Sun Arrowhead I-46	186757	4010							0.84	0.00	1	1.49	0.04	8	1.75	0.04	5		6-7			1.32
Texaco NFA Bovie Lake J-72	186762	6725				0.96	0.07	9	1.16	0.05	4	1.63	0.17	5					6-7			1.40
Texaco NFA Bovie Lake J-72	186762	6950				0.98	0.04	2				1.61	0.07	11				2.00				1.39
Imperial Sun Netla C07	186764	3715	0.22	0.00	1	0.42	0.07	7	0.96	0.12	7	1.20	0.00	1	1.53	0.05	2			5,5-d		1.02
Murphy *et al.* Muskeg River 1	186767	4030				0.57	0.02	2	0.85	0.00	2				1.49	0.00	1					
Murphy *et al.* Muskeg River	186767	4430				0.58	0.00	2	1.09	0.07	9	1.35	0.08	12	1.78	0.10	7	2.10				1.23
Pan Am Home Signal Celibeta	186765	4675				0.75	0.13	3				1.58	0.11	8	1.99	0.10	6					1.37
Pan Am Home Signal Celibeta	186765	4935				0.72	0.00	1							1.88	0.08	4					
Pan Am Home Signal Celibeta	186765	5210							1.22	0.00	1	1.75	0.01	5	2.10	0.00	1					1.48
Dome *et al.* Trout Lake H-45	186768	2570										1.10	0.07	10	1.45	0.08	10	1.63				1.08
Dome *et al.* Trout Lake H-45	186768	2800																				
Dome *et al.* Trout Lake H-45	186768	3020										1.27	0.05	6	1.53	0.09	6	1.85				1.18
Imperial Island River No.1	186751	4818																	5-6			

Table C3 Bitumen reflectance and fluorescence data for the Redknife Formation.

SAMPLE LOCATION	SAMPLE No		BITUMENS															FLUORESCENCE			VRo
			LOW Ro						MEDIUM Ro				HIGH Ro					INDEX			calculated
			Type 1			Type 2			Type 3			Type 4			Type 5			Type 6				(Jacob, 1985)
			% R_o			% R_o			% R_o			% R_o			% R_o			% R_o				
	C no.	I.D.	mean	s.d.	n	mean	s.d.	n	mean	s.d.	n	mean	s.d.	n	mean	s.d.	n	mean	m'alg	Leio	spor	
B-A Texaco Arrowhead N-2	186758	4905							1.03	0.04	5	1.28	0.05	3	1.54	0.08	3					1.19
B-A Texaco Arrowhead N-2	186758	5205	0.52	0.00	1	0.82	0.00	1	1.13	0.05	4	1.42	0.07	4	1.67	0.15	5					1.27
B-A Texaco Arrowhead N-2	186758	5495				0.76	0.08	2	1.13	0.00	1	1.43	0.05	5	1.70	0.18	7					1.28
Imperial Sun Arrowhead I-46	186757	2510							1.04	0.06	2	1.21	0.00	1	1.57	0.08	2	2.00				1.29
Imperial Sun Arrowhead I-46	186757	3010	0.38	0.01	2	0.59	0.09	5	0.85	0.06	6	1.32	0.04	3	1.50	0.00	1			6	6-7	1.22
Imperial Sun Arrowhead I-46	186757	351	0.38	0.02	2	0.59	0.03	5	0.82	0.08	12	1.42	0.12	5				1.99				1.27
Texaco NFA Bovie Lake J-72	186762	5651	0.57	0.02	2	0.77	0.00	1	1.08	0.19	6	1.46	0.02	2								1.30
Texaco NFA Bovie Lake J-72	186762	584				0.82	0.00	1	1.06	0.00	1	1.63	0.14	2								
Texaco NFA Bovie Lake J-72	186762	5885				0.80	0.00	1							1.70	0.00	1					
Texaco NFA Bovie Lake J-72	186762	6405				0.85	0.09	4	1.15	0.00	1	1.55	0.12	8	1.93					9		1.36
Imperial Sun Netla C07	186764	227	0.13	0.01	2	0.37	0.09	3				0.92	0.03	3	1.20	0.03	2					0.97
Imperial Sun Netla C07	186764	2680	0.28	0.03	1	0.35	0.06	6	0.67	0.05	14	0.86	0.02	3	1.10					4		0.93
Imperial Sun Netla C07	186764	2895	0.22[1]	0.00	1	0.37	0.02	4	0.54	0.07	12	0.83	0.06	3	1.20	0.09	6			4-5d		0.91
Imperial Sun Netla C07	186764	3190	0.18[1]	0.12	2	0.46	0.07	5												4-5		
Murphy *et al.* Muskeg River #1	186767	2440	0.22	0.04	5	0.46	0.05	11	0.68	0.03	5	0.85	0.00	1	1.29	0.02	3	1.72	4-d	6	4-d	0.93
Murphy *et al.* Muskeg River #1	186767	2690	0.23	0.03	16	0.44	0.05	13	0.81	0.05	7	1.09	0.01	2				1.72	4-d	4-d		1.07
Murphy *et al.* Muskeg River #.1	186767	3060	0.23	0.02	10	0.54	0.06	6	0.82	0.04	4	1.14	0.00	1	1.31	0.04	3	1.74	4			1.10
Murphy *et al.* Muskeg River #1	186767	3365	0.31	0.06	15	0.58	0.02	7	0.79	0.00	1				1.24	0.00			4	7		1.17
Pan Am Home Celibeta #7	186765	3655	0.34	0.03	3	0.56	0.00	1	0.86	0.04	6	1.30	0.10	5	1.60	0.05	5	1.87	6			1.20
Pan Am Home Celibeta # 7	186765	3955	0.45	0.05	2	0.62	0.00	1				1.30	0.04	2				2.02				1.20
Pan Am Home Celibeta #7	186765	4325	0.48	0.07	2	0.58	0.00	1				1.32	0.05	3	1.62	0.01	2					1.22
Dome *et al.* Trout Lake H-45	186768	1360				0.39	0.00	1	0.48	0.04	2	0.71	0.04	2	0.95	0.05	1	2.53	4	4	7	0.84
Dome *et al.* Trout Lake H-45	186768	1730				0.34	0.00	1				0.80	0.00	1	1.19	0.02	2	1.57	4	5-6	7	0.89
Dome *et al.* Trout Lake H-45	186768	2115										1.07	0.00	1	1.39	0.00	1	1.61				1.06
Dome *et al.* Trout Lake H-45	186768	2570										1.10	0.07	10	1.45	0.08	10	1.63				1.08
Imperial Island River #1	186751	3486				0.45	0.03	2	0.85	0.05	6	1.00	0.00	1					5			1.06
Imperial Island River #1	186751	3797	0.27	0.00	1	0.52	0.03	3	0.88	0.02	4	1.09	0.03	5	1.34	0.05	2	1.87	6			1.07
Imperial Island River #1	186751	4010				0.52	0.09	3				1.10	0.03	3	1.50	0.00	1					1.08
Imperial Island River #1	186751	4102																		9		

[1] Chitin

Table C4 Bitumen reflectance and fluorescence data for the Kotcho Formation -Upper Devonian shales.

SAMPLE LOCATION	SAMPLE No.	BITUMENS																FLUORESCENCE				VRo
		LOW Ro									MEDIUM Ro			HIGH Ro				INDEX				calculated (Jacob, 1985)
		Type 1			Type 2			Type 3			Type 4			T ype 5			Type 6				Type 1	
		% R_o			% R_o			% R_o			% R_o			% R_o			% R_o				bitumen	
	C no. I.D.	mean	s.d.	n	mean	s.d.	n	mean	s.d.	n	mean	s.d.	n	mean	s.d.	n	mean	m'alg	Leio	spor		
B-A Texaco Arrowhead N-2	C-186758- 4635	0.37	0 .00	1	0.50	0.04	10	0.85	0.13	19	1.07	0.09	14					5-6	6-7	9		1.06
B-A Texaco Arrowhead N-2	C-186758- 4645				0.58	0.07	16	0.86	0.02	19	1.05	0.08	5	1.80	0.08	5		6	6-7	9		1.05
Imperial Sun Arrowhead I-46	C186757- 1990	0..31	0.02	12	0.50	0.06	13	0.84	0.05	16	1.10	0.01	2	1.50				4	5-6	7-8		1.07
Texaco NFA Bovie Lake J-72	C186762- 5415				0.59	0.08	8	0.77	0.03	4	1.08	0.08	8	1.52	0.04	3	1.80	6			7	1.06
Imperial Sun Netla C07	C186764- 2040	0.13	0.03	4	0.42	0.05	10	0.65	0.00	1	0.81	0.07	7									0.90
Murphy *et al.* Muskeg River #1	C186767- 2370	0.23	0.04	3				0.57	0.05	7	0.86	0.06	2	1.53				3	4			0.93
Pan Am Home Signal Celibeta#7	C186765- 3470				0.36	0.04	3	0.58	0.08	15	0.88	0.07	4	1.25	0.14	17	1.60					0.94
Dome *et al.* Trout Lake H-45	C186768- 1295	0.18	0.01	7	0.24	0.03	48	0.46	0.01	4				1.53	0.00	1	2.40	4	Tas-4			
Imperial Island River No.1	C186751- 3465	0.25	0.03	14	0.38	0.05	7	0.69	0.08	2	0.82	0.02	2	0.97	0.05	8	2.78	4d				0.91
Imperial Island River No.1	C186751 3470																	4d				

Table C5 Bitumen reflectance and fluorescence data from the Exshaw Formation.

SAMPLE LOCATION	SAMPLE No.		PHYTOCLASTS				BITUMENS																FLUORESCENCE INDEX					VRo calculated (Jacob, 1985)
			Vitrinite			Rew Vit.	LOW Ro Type 1			Type 2			Type 3			MED Ro Type 4			HIGH Ro Type 5			Type 6	Iginites		bitum.	low Ro		
	GSC C#	I.D.	% R_o mean	s.d.	n	% R_o mean	% R_o mean	s.d.	n	% R_o mean	s.d.	n	% R_o mean	s.d.	n	% R_o mean	s.d.	n	% R_o mean	s.d.	n	% R_o mean	m'alg	Leio	matrix	bitumen	spor	
B-A Texaco Arrowhead N-2	C-186758-	3245																					5					
B-A Texaco Arrowhead N-2	C-186758-	3505					0.19	0.05	8	0.32	0.07	2				0.99	0.06	4	1.28	0.00	1			5				1.01
B-A Texaco Arrowhead N-2	C-186758-	4005								0.37	0.11	5	0.84	0.00	1	1.00	0.07	3						6-7				1.02
B-A Texaco Arrowhead N-2	C-186758-	4285								0.37	0.11	5	0.96	0.05	4	1.20	0.00	1					7					0.99
B-A Texaco Arrowhead N-2	C-186758-	4445								0.52	0.09	3	0.84	0.04	2	0.94	0.06	8					5-6		9			0.98
B-A Texaco Arrowhead N-2	C-186758-	4455								0.58	0.03	2	0.85	0.03	2	1.00	0.08	21	1.76	0.20	10	2.08	5-6		9	9		1.02
Imperial Sun Arrowhead I-46	C186757-	1725					0.21	0.11	8				0.82	0.05	3	1.18	0.00	1				2.10	4-5					1.13
Imperial Sun Arrowhead I-46	C186757-	1810	1.28			1.40							0.85	0.05	2	1.17	0.00	1	1.40				6	6-7		6-7		1.12
Imperial Sun Arrowhead I-46	C186757-	1910								0.40	0.08	1	0.81	0.02	5				1.56	0.11	3		5-6	5-6				
Texaco Bovie Lake J-72	C186762-	3645					0.35	0.05	20	0.56	0.05	7							1.10	0.00	1			4-7	7		5-6	
Texaco Bovie Lake J-72	C186762-	3935					0.41	0.03	4	0.61	0.04	4	0.74	0.01	3								4	4				
Texaco Bovie Lake J-72	C186762-	4335					0.33	0.02	5	0.66	0.00	1	0.78	0.00	1				1.30				4	4	7			
Texaco Bovie Lake J-72	C186762-	4835								0.70	0.08	3				1.09	0.16	2	1.35	0.00	1		6/7	6/7				1.07
Texaco Bovie Lake J-72	C186762-	5265														1.01	0.06	6	1.31	0.03	2		6	6				1.02
Imperial Sun Netla C07	C186764-	1955					0.17	0.00	1	0.26	0.04	3	0.60	0.06	9								1	2-3				0.77
Imperial Sun Netla C07	C186764-	2020					0.13	0.00	1	0.38	0.09	14	0.52	0.05	4	0.79	0.05	2	1.20	0.00	1		2	3-4				0.89
Murphy Muskeg River No.1	C186767-	1915	0.80	0.00	1		0.25	0.04	27	0.42	0.05	12											2-3	3			4-5	
Murphy Muskeg River No.1	C186767-	2205					0.26	0.02	8				0.59	0.07	14	0.81	0.01	3	1.07	0.08	6		2	4		4 0.90		
Murphy Muskeg River No.1	C186767-	2335											0.53	0.04	3	0.86	0.05	9	1.06	0.07	3	2.00						0.93
Pan Am HS Celibeta No. 7	C186765-	2165								0.48	0.00	1	0.65	0.03	3	1.12	0.11	6	1.46	0.03	4	1.70	2	3				1.09
Pan Am HS Celibeta No. 7	C186765-	2491											0.74	0.06	6	1.13	0.04	2	1.47	0.07	6	1.97						1.10
Pan Am HS Celibeta No.7	C186765-	2920					0.37	0.00	1				0.76	0.10	6				1.50	0.08	4			3-4				
Pan Am HS Celibeta No.7	C186765-	3325					0.29	0.00	1				0.89	0.00	1							1.97		4-5				1.11
Pan Am HS Celibeta No.7	C186765-	3430								0.68	0.00	1	0.88	0.03	12	1.37	0.38	5	1.55	0.10	5	2.11	6					1.25
Dome *et al.* Trout Lake H-45	C186768-	1250																										

Table C6 Bitumen reflectance, vitrinite reflectance and fluorescence data for the Banff Formation.

SAMPLE LOCATION	SAMPLE No.		PHYTOCLASTS					BITUMENS														FLUORESCENCE INDEX				VRo
			Vitrinite			Rew Vit.	Sfus	LOW Ro						MED Ro			HIGH Ro									Calculated (Jacob, 1985)
								Type 1			Type 2			Type 3			Type 4			Type 5			Type 6			
			% R_o			% R_o	% R_o	% R_o			% R_o			% R_o			% R_o			% R_o			% R_o	Alginites		bitum	low Ro	
	GSC C#	I.D.	mean	s.d.	n	mean	spot	mean	s.d.	n	mean	s.d.	n	mean	s.d.	n	mean	s.d.	n	mean	s.d.	n	mean	m'alg	Leio	matrix	bitumen	spor	
Dome *et al.*Trout Lake H-45	C186768	1290																										
Pan Am HS Celibeta No. 7	C186765-	2920						0.37	0.00	1				0.76	0.10	6				1.50	0.08	4			3-4				
Pan Am HS Celibeta No. 7	C186765-	3325						0.29	0.00	1				0.89	0.00	1	1.15	0.08	6				1.97		4-5				1.11
Pan Am HS Celibeta No. 7	C186765-	3430									0.68	0.00	1	0.88	0.00	2	1.37	0.38	10	1.55	0.10	5	2.11	6					1.25
Dome *et al.*Trout Lake H-45	C186768	1250									0.32	0.02	4				0.81	0.05	11	1.44	0.03	6	1.89	4	4	Tas-4d			0.90
Imperial Island River #1	C186751-	2134	0.80	0.05	16	0.98					0.20	0.10	2	0.54	0.03	3				1.05	0.04	13	1.52						
Imperial Island River #1	C186751-	2140	0.82	0.01	4	1.16		0.16	0.00	2													1.57						
Imperial Island River #1	C186751-	2310				1.17					0.25	0.00	1				0.79	0.01	3	1.07	0.10	2			3	7			0.89
Imperial Island River #1	C186751-	2456									0.22	0.00	1							1.16	0.05	5	1.66			7			
Imperial Island River #1	C186751-	2747	0.96	0.04	2		1.62				0.24	0.01	2	0.56	0.03	6	0.86	0.08	6	1.14	0.04	3		1-2	-3			4	0.93
Imperial Island River #1	C186751-	2760						0.11	0.01	2	0.35	0.01	2	0.62	0.00	1	0.86	0.05	10	1.09	0.07	6		1-2				4	0.93
Imperial Island River #1	C186751-	3012	0.91	0.00	1	1.02								0.54	0.00	1	0.86	0.04	3	1.21	0.12	3	1.7						0.93
Imperial Island River #1	C186751-	3275									0.47	0.02	2	0.68	0.00	2	0.88	0.02	2	1.03	0.01	2			3		0.94		
Imperial Island River #1	C186751-	3288									0.47	0.04	2	0.68	0.00	2	0.88	0.02	2	1.02	0.02	2			3	7			0.94
Pan Am Mattson Creek A1	C196779-	140															1.80	0.00	1	2.20	0.00	1							1.51
Pan Am Mattson Creek A1	C196779-	260												1.48	0.00	1	1.70	0.00	1	2.51	0.09	4	3.43						1.45
Pan Am Mattson Creek A1	C196779-	680																					3.50						
Pan Am Mattson Creek A1	C196779	860																		2.60	0.08	2	3.70						
Pan Am Mattson Creek A1	C196779-	1000																		3.00	0.00	1	4.50						
Pan Am Mattson Creek A1	C196779-	1180															2.29	0.30	10	3.25	0.25	9	4.80						1.82
Pan Am Mattson Creek A1	C196779-	1240															2.48	0.09	4	3.36	0.50	14	4.50						1.93
IOE P A Viscount a-77-D	C186771-	9975									1.26	0.05	2	1.50	0.04	5	1.78	0.02	2	1.97	0.11	2	2.63						1.50
IOE P A Viscount a-77-D	C186771-	10375									1.25	0.03	2	1.48	0.05	3	1.86	0.00	1				2.74						1.55
IOE P A Viscount a-77-D	C186771-	10440									1.27	0.00	3	1.47	0.05	3	1.80	0.03	3	2.32	0.30	6	5.06						1.51

Table C6, continued.

SAMPLE LOCATION	SAMPLE No.	BITUMENS															FLUORESCENCE INDEX				VRo calculated (Jacob, 1985)
		LOW Ro						MEDIUM Ro				HIGH Ro									
		Type 1			Type 2			Type 3			Type 4			Type 5			Type 6				
		% R_o			% R_o			% R_o			% R_o			% R_o			% R_o				
	C no. I.D.	mean	s.d.	n	mean	s.d.	n	mean	s.d.	n	mean	s.d..	n	mean	s.d.	n	mean	m'alg	Leio	spor	bitumen	
Canada Southern *et al.* N. Beaver R. 1-27	C186754- 9120										2.10	0.21	9				4.70					1.70
Canada Southern *et al.* N. Beaver R. 1-27	C186754- 9389										2.20	0.00	1	3.50	0.25	3	4.60					1.76
Canada Southern *et al.* N. Beaver R. 1-27	C186754- 9659							1.71	0.00	1	2.20	0.24	17	2.97	0.03	3	4.60					1.80
Canada Southern et al. N. Beaver R. 1-27	C186754-10319										2.36	0.18	9	3.20	0.31	5						1.86
Canada Southern *et al.* N. Beaver R. 1-27	C186754-10665													3.61	0.13	4	4.90					
Canada Southern *et al.* N. Beaver R. 1-27	C186754-10875							2.80	0.00	1	3.23	0.22	11	4.20								2.40
Canada Southern *et al.* N. Beaver R.1-27	C186754-10939										3.50	0.13	7	4.40	0.29	6	5.13					2.56
Pan Am Pointed Mountain P-53	C186766- 7450							1.00	0.00	1	1.31	0.10	6	1.53	0.00	1						1.21
Pan Am Pointed Mountain P-53	C186766- 7610							1.04	0.06	4	1.31	0.03	5	1.70	0.06	6						1.21
Pan Am Pointed Mountain P-53	C186766- 7810							1.04	0.04	8	1.26	0.11	12	1.58	0.11	11	1.80					1.18
Pan Am Pointed Mountain P-53	C186766- 8115							1.15	0.00	1	1.36	0.08	5	1.79	0.11	4	1.90+					1.24
Pan Am Pointed Mountain P-53	C186766- 8410										1.33	0.00	1	1.70	0.10	2						1.22
Pan Am Pointed Mountain P-53	C186766- 8535										1.48	0.00	1	1.97	0.17	9	2.82					1.31
Pan Am Pointed Mountain P-53	C186766- 8930																					
Pan Am Pointed Mountain P-53	C186766- 9200										1.58	0.11	8	2.05	0.31	24	3.22					1.38
Pan Am Pointed Mountain P-53	C186766- 9630							1.46	0.00	1	1.72	0.00	1	2.32	0.12	6	2.99					1.46
Pan Am Pointed Mountain P-53	C186766-10105							1.47	0.06	2				2.41	0.28	16	3.49					
Pan Am Pointed Mountain P-53	C186766-10410																					
Pan Am Pointed Mountain P-53	C186766-10810										1.85	0.20	4	2.40	0.31	5	3.20					1.54
Pan Am Pointed Mountain P-53	C186766-10860							1.48	0.16	2							3.90					
Pan Am Beaver G-01, YT	C186752-10575	1.26	0.00	1				1.60	0.12	3	2.02	0.18	10	3.40			4.50					1.65
Pan Am Beaver G-01, YT	C186752- 10865										2.41	0.32	2	3.50	0.25	3						1.89
Pan Am Beaver G-01, YT	C186752- 11635							2.10	0.00	1	2.74	0.22	10									2.09
Pan Am Beaver G-01, YT	C186752- 12015							2.15	0.00	1	2.85	0.04	2	3.76								2.16
Pan Am Beaver G-01, YT	C186752- 12265							2.60	0.00	1	2.90	0.00	1	3.70	0.00	1	4.15					2.19
Pan Am Beaver G-01, YT	C186752- 12665													3.40	0.00	1	4.30					2.50
Pan Am Beaver G-01, YT	C186752- 12915							2.53	0.00	1	3.50			3.80	0.22	7						2.56
Pan Am Beaver G-01, YT	C186752- 12975										3.70			4.00			4.70					2.69
Pan Am Beaver G-01, YT	C186752- 13185							2.43	0.12	3	3.43	0.30	7	4.10	4.90							2.52

Table C7 Bitumen reflectance data for the Besa River Formation.

SAMPLE LOCATION	SAMPLE No.		PHYTOCLASTS	BITUMENS															FLUORESCENCE	VRo
			Sfus	LOW Ro						MED Ro			HIGH Ro						INDEX	Calculated
				Type 1			Type 2			Type 3			Type 4			Type 5			Type 6		(Jacob, 1985)
			% R_o	% R_o			% R_o			% R_o			% R_o			% R_o			% R_o		
	GSC C#	I.D.	spot	mean	s.d.	n	mean	s.d.	n	mean	s.d.	n	mean	s.d.	n	mean	s.d.	n	mean	m'alg	
Pan Am Kotaneelee YT 0-67	C186755-	5040														2.60	0.00	1	3.10		
Pan Am Kotaneelee YT 0-67	C186755-	6000								1.37	0.00	1	2.80	0.00	1	3.60					2.18
Pan Am Kotaneelee YT 0-67	C186755-	7000											3.20	0.26	15	4.10	0.40	3			2.38
Pan Am Kotaneelee YT 0-67	C186755-	7595								2.10	0.00	1	2.91	0.15	10	3.73	0.09	8	5.17		2.20
Pan Am Kotaneelee YT 0-67	C186755-	7615																			
Pan Am Kotaneelee YT 0-67	C186755-	7800											3.20	0.18	12	4.29	0.27	7			2.38
Pan Am Kotaneelee YT 0-67	C186755-	7900																			
Pan Am Kotaneelee YT 0-67	C186755-	7920																			
Clausen Creek	C74202	+13.5					0.59	0.07	3	1.13	0.07	5	1.45	0.02	2	2.20	0.05	2	3.70		1.30
Clausen Creek	C74201	+16.44											1.32	0.07	4	2.09	0.00	1	3.99	5	1.22
Clausen Creek	C74207	+377.29					0.56	0.01	7	1.06	0.02	3	1.52	0.01	2	2.00	0.02	2	3.8		1.34
Clausen Creek	C74212						0.62	0.00	1	1.09	0.04	4	1.56	0.00	1	2.06	0.06	2			1.36
Clausen Creek	C74213	+1043.3		0.39	0.00	1	0.60	0.05	5	0.94	0.08	7	1.28	0.08	7	1.64	0.08	4		5	1.19
Central Leduc Toad R. No.1	C186774	4057											3.40	0.81	20	4.62	0.23	29	5.56		2.50
Central Leduc Toad R. No.1	C186774	4371	4.75										3.40	0.22	4	4.28	0.38	19	4.87		
Central Leduc Toad R. No. 1	C186774	4452											3.66	0.07	3	4.42	0.20	6	5.05		2.63
Central Leduc Toad R. No. 1	C186774	5176					2.20	0.12	4	3.07	0.26	10	3.94	0.28	38	4.65	0.13	17	5.21		3.27
Central Leduc Toad R. No. 1	C186774	5354								3.42	0.14	4	3.98	0.11	9	4.53	0.20	14	5.39		3.19

Table C7 continued.

SAMPLE LOCATION	SAMPLE No.		PHYTOCLASTS				BITUMENS																FLUORESCENCE INDEX				VRo
			Vitrinite				Low Ro Type 1			Type 2			Type 3			Med Ro Type 4			High Ro Type 5			Type 6					Calculated (Jacob, 1985)
			% R_o				% R_o			% R_o			% R_o			% R_o			% R_o			% R_o	Alginite		Bitum.	Low Ro		
	CGS #	I.D.	mean	s.d.	n		mean	s.d.	n	mean	s.d.	n	mean	s.d.	n	mean	s.d.	n	mean	s.d.	n	mean	m'alg	Leio	matrix	bitumen	spor	
Amoco East Flett H-13	C186759	-2780								0.25	0.06	5				0.61	0.09	3	0.86	0.02	2		1-2	3-4				0.78
Amoco East Flett H-13	C186759	-2905								0.26	0.01	3				0.71	0.00	1	0.89	0.07	4							0.84
B-A Texaco Arrowhead N-2	C186758	-2645											0.60	0.00	1				1.23	0.00	1		3	3				
B-A Texaco Arrowhead N-2	C186758	-2745								0.44	0.10	5				0.77	0.02	2	1.20	0.00	1							0.88
B-A Texaco Arrowhead N-2	C186758	-2805					0.25	0.01	2	0.35	0.01	2				0.77	0.07	4							6-7	6-7		0.88
Texaco NFA Bovie Lake J-72	C186762	-3290								0.38	0.04	10	0.56	0.04	6				1.20	0.00	1					7	5	
Texaco NFA Bovie Lake J-72	C186762	-3390					0.34	0.07	6	0.57			0.69			0.88	0.00	1									5	0.94
Pan Am H S Celibeta#7	C186765	-1931											0.64	0.06	5	0.88	0.06	2	1.30	0.00	1	1.80	4	4-5	8-9			0.94
Pan Am H S Celibeta#7	C186765	-1991											0.68	0.05	2	0.88+												
Jackfish Gap-Yohin Ridge	C52180	1545.2								0.68	0.06	2	0.96	0.05	6	1.15	0.09	17	1.52	0.12	15	2.00						1.11
Jackfish Gap-Yohin Ridge	C52181	1548.5								0.51	0.08	12	1.02	0.04	3	1.25	0.03	7										1.17
Jackfish Gap-Yohin Ridge	C58505	55.44											1.05	0.07	9	1.52	0.15	12	1.83	0.02	2	2.29						1.34
Jackfish Gap-Yohin Ridge	C52163	132.54								0.95	0.03	2	1.13	0.02	5	1.50	0.10	6	1.82	0.05	3	2.31						1.33
Jackfish Gap-Yohin Ridge	C52166	166.0	1.30	0.04	4		0.58	0.00	1	0.89	0.00	1	1.15	0.09	8	1.49	0.11	15	1.93	0.07	4		6					1.32
Jackfish Gap-Yohin Ridge	C58503	343.5											1.04	0.06	15	1.46	0.13	26	1.94	0.16	5		5/6					1.30
Jackfish Gap-Yohin Ridge	C51174	419.6																										
Jackfish Gap-Yohin Ridge	C58502	519.68								0.71	0.00	1	1.09	0.06	10	1.34	0.09	23	1.70	0.11	10							1.23

Table C8. Bitumen and vitrinite reflectance data for the Yohin and Clausen formations.

SAMPLE LOCATION	SAMPLE No.	ROCK	PHYTOCLASTS			BITUMENS																FLUORESCENCE INDEX				VRo calculated
			Vitrinite			LOW Ro						MED Ro			HIGH Ro											
						Type 1			Type 2			Type 3			Type 4			Type 5			Type 6					
			% R_o			% R_o			% R_o			% R_o			% R_o			% R_o			% R_o	Alginite	Bitum	Low Ro	(Jacob, 1985)
			mean	s.d.	n	mean	s.d.	n	mean	s.d.	n	mean	s.d.	n	mean	s.d.	n	mean	s.d.	n	mean	m'alg	Leio	matrix	bitumen	spor	
Amoco East Flett H-13	C186759-	-1440	Flett-Meill						0.27	0.04	51				0.46	0.06	42	0.89	0.00	1	1.31	2		3	7		0.68
Amoco East Flett H-13	C186759-	-1620	Flett-Meill						0.27	0.05	6				0.50	0.11	6	1.06	0.11	7							0.71
Amoco East Flett H-13	C186759-	-1860	Flett-Meill						0.27	0.03	5				0.50	0.12	3	0.93	0.08	4		3-4			6-7		0.71
Jackfish Gap-Yohin Ridge	C52106	3187.33	Flett			0.24	0.05	4	0.39	0.01	4	0.69	0.03	3								4-5					
Jackfish Gap-Yohin Ridge	C52115	3405.18	Flett			0.28	0.01	2	0.44	0.06	9	0.69	0.02	3	0.90	0.02	3	1.30	0.00	1			5		5		0.96
Jackfish Gap-Yohin Ridge	C58522	3534.77	Flett			0.27	0.03	3	0.39	0.01	2	0.59	0.02	2	0.78	0.06	2	1.23	0.03	3							0.88
Jackfish Gap-Yohin Ridge	C58523	3534.77	Flett						0.37	0.05	5	0.68	0.02	4				1.22									
Jackfish Gap-Yohin Ridge	C74336	3628.81	Flett						0.37	0.06	8	0.59	0.06	4													
Jackfish Gap-Yohin Ridge	C74338	3684.05	Flett			0.18	0.00	1	0.41	0.06	7	0.54	0.06	6									3				
Jackfish Gap-Yohin Ridge	C52152	3793.64	Flett			0.20	0.00	1	0.37	0.05	9	0.54	0.06	26	0.75	0.03	3										0.86
Jackfish Gap-Yohin Ridge	C52157	3852.69	Flett	1.18		0.29	0.02	3	0.47			0.68	0.00	1				1.92									0.82
Amoco East Flett H-13	C186759-	-2445	Prophet			0.28	0.06	8				0.50	0.03	2				1.09	0.16	4		2	3-4		7		0.71
B-A Texaco Arrowhead N-2	C-186758-	-2485	Prophet			0.25	0.03	8	0.39	0.05	5	0.60	0.03	5	0.75	0.02	2	1.02	0.16	2		3			7		0.86
Texaco NFA Bovie Lake J-72	C186762-	-2665	Prophet																			3				4/5	
Texaco NFA Bovie Lake J-72	C186762-	-2935	Prophet						0.35	0.07	7							1.00	0.00	1		2/3					
Pan Am *et al.* Celibeta No. 7	C186765-	-1730	Prophet			0.25	0.00	1				0.66	0.04	6	0.82	0.04	2	1.10	0.00	1			4		7-8		0.91
Pan Am *et al.* Celibeta No. 7	C186765-	-1850	Prophet									0.57	0.00	1				1.20	0.00	1		3-4					
Can South *et al.* N. Beaver R1-27	C186754-	-7139	Prophet												1.58	0.06	7	1.92	0.14	16		2.6					1.38
Can South *et al.* N. Beaver R1-27	C186754-	-7540	Prophet									1.36	0.05	6	1.60	0.05	9	1.98	0.07	7	2.85						1.39
Can South *et al.* N. Beaver R1-27	C186754-	-7860	Prophet												1.72	0.05	4	2.14	0.20	18							1.46
Can South *et al.* N. Beaver R1-27	C186754-	-8585	Prophet									1.50	0.00	1	1.82	0.16	22				3.00						1.50
Can South *et al.* N. Beaver R1-27	C186754-	-8815	Prophet												1.87	0.00	1				4.50						1.56
Can South *et al.* N. Beaver R1-27	C186754-	-8860	Prophet									1.52	0.001		1.70	0.1	8	2.90	0.00	1	5.50						1.45

Table C9 Bitumen reflectance and fluorescence data for the Rundle Group.

SAMPLE LOCATION	SAMPLE No.		ROCK UNIT	BITUMENS																FLUORESCENCE INDEX			VRo calculated (Jacob, 1985)
				LOW Ro								MEDIUM Ro			HIGH Ro								
				Type 1			Type 2			Type 3			Type 4			T ype 5			Type 6				
				% R_o			% R_o			% R_o			% R_o			% R_o			% R_o				
	C no.	I.D.		mean	s.d.	n	mean	s.d.	n	mean	s.d.	n	mean	s.d.	n	mean	s.d.	n	mean	m'alg	Leio	Low Ro bitumen	
Pan Am Pointed Mountain P-53	C186766-	-5230	Prophet				0.44	0.04	3	0.67	0.08	8	0.99	0.08	13	1.65	0.1	5					1.01
Pan Am Pointed Mountain P-53	C186766-	-5565	Prophet	0.25	0.02	2	0.54			0.62	0.07	21	0.96	0.14	13	1.62	0.12	3				6/7	0.99
Pan Am Pointed Mountain P-53	C186766-	-5900	Prophet				0.48	0.01	2	0.8	0.04	6	1.01	0.1	24	1.61	0.14	5					1.02
Pan Am Pointed Mountain P-53	C186766-	-6810	Prophet				0.41	0.03	2	0.79	0.05	7	1.01	0.13	1	1.6	0.0	1					
Pan Am Pointed Mountain P-53	C186766-	-7171	Prophet										1.29	0.0	1	1.68ca.		1					1.20
Pan Am Beaver G-01, YT	C186752-	-10129	Prophet										1.76	0.06	2	2.15							1.49
Pan Am Beaver G-01, YT	C186752-	-10183	Prophet										1.87	0.02	2	2.65			3.00				1.56
Pan Am Kotaneelee YT 0-67	C186755-	-4200	Prophet										1.71	0.0	1	2.19	0.17	18	2.90				1.46
Jackfish Gap-Yohin Ridge	C52064	2610.56	Prophet	0.30	0.06	3	0.42	0.00	1	0.66	0.05	2	1.00	0.00	1	1.68	0.00	1					1.02
Jackfish Gap-Yohin Ridge	C52067	2692.58	Prophet	0.27	0.00	1	0.49	0.00	1	0.67	0.00	1	1.10	0.00	1	1.58	0.00	1					1.08
Jackfish Gap-Yohin Ridge	C58517	2730.64	Prophet	0.26	0.04	5	0.47	0.05	7	0.66	0.02	3	0.87	0.00	1	1.45	0.00	1					0.94
Clausen Creek	C74220	1541.99	Prophet				0.44	0.03	4				0.91	0.01	2	1.23	0.08	2	1.64				1.16
Clausen Creek	C74234	2224.41	Prophet	0.18	0.0	1	0.58	0.06	3	0.76	0.05	6	0.99	0.05	10	1.15	0.03	4	1.40				1.01
Pan Am Viscout a-77-D	C186771	-9625	Prophet																				
Pan Am Viscout a-77-D	C186771	-9675	Prophet																				
B-A Texaco Arrowhead N-2	C-186758	-2340	Form'n	0.26	0.04	8	0.33	0.01	6	0.54	0.02	3	0.76	0.01	6	1.10	0.16	3		2	2-3	7	0.87
Pan Am *et al.* Celibeta No. 7	C186765-	-1045	Form'n F	0.25	0.02	3				0.55	0.10	3								2	4		
Pan Am *et al.* Celibeta No. 7	C186765-	-1496	Form'n F				0.42	0.08	2	0.64	0.01	3	0.78	0.00	1	1.00	0.10	3			4	7-8	0.88
Pan Am *et al.* Celibeta No. 7	C186765-	-2045	Pekisko							0.55	0.00	1											

Table C9, continued.

SAMPLE LOCATION	SAMPLE No.	PHYTOCLASTS				BITUMENS														FLUORESCENCE INDEX				VRo calculated (Jacob, 1985)
		Vitrinite				Low Ro						Med Ro			High Ro									
						Type 1			Type 2			Type 3			Type 4			Type 5			Type 6			
		% Ro				% Ro			% Ro			% Ro			% Ro			% Ro			% Ro			
	CGS # I.D.	mean	s.d.	n		mean	s.d.	n	mean	s.d.	n	mean	s.d.	n	mean	s.d.	n	mean	s.d.	n	mean				
Canada South. *et al.* N. Beaver R. 1-27	C187854- 5989											1.13	0.1	4	1.45	0.00	6	1.64	0.12	10	2.20				1.30
Canada South. *et al.* N. Beaver R. 1-27	C187854- 6349														1.35	0.06	3	1.80	0.09	15	2.27				1.23
Canada South. *et al.* N. Beaver R. 1-27	C187854- 6640																								
Pan Am Pointed Mountain P-53	C186766- 4570	0.89	0.00	1		0.30	0.08	5	0.42	0.07	20	0.85	0.04	4	1.20			1.37					9		5	0.93
Pan Am Pointed Mountain P-53	C186766- 4805					0.27	0.07	4	0.58	0.07	17							1.67	0.06	2				6/7		
Pan Am Beaver G-01, YT	C186752- 6120														1.40	0.00	1								1.27
Pan Am Beaver G-01, YT	C186752- 6540	0.78	0.00	1								1.01	0.03	3	1.41	0.10	6								1.31
Pan Am Beaver G-01, YT	C186752- 6565											0.94	0.02	2	1.47	0.00	1	1.68	0.00	1			9			1.31
Pan Am Beaver G-01, YT	C186752- 7140																								
Pan Am Beaver G-01, YT	C186752- 7480											1.12	0.08	3	1.52	0.06	7				1.90				1.34
Pan Am Beaver G-01, YT	C186752- 7840	1.40	0.00	1																					
Pan Am Beaver G-01, YT	C186752- 8766														1.55	0.05	4	1.74	0.08	8	1.85				1.36
Pan Am Beaver G-01, YT	C186752- 8800																				2.07				
Pan Am Beaver G-01, YT	C186752- 9210														1.53	0.00	1				2.00				1.35
Pan Am Beaver G-01, YT	C186752- 9505											1.45	0.00	1							2.10				
Pan Am Beaver G-01, YT	C186752- 9880														1.72	0.00	1						1.46		
Pan Am Kotaneelee YT 0-67	C186755- 1320	0.82	0.00	1					0.63	0.03	5	0.73	0.01	2	1.30	0.00	1								1.20
Pan Am Kotaneelee YT 0-67	C186755- 1620																								
Pan Am Kotaneelee YT 0-67	C186755- 1980																								
Pan Am Kotaneelee YT 0-67	C186755- 2600								0.71	0.06	3				1.18	0.03	2								1.13
Pan Am Kotaneelee YT 0-67	C186755- 3500																								
IOE Pan Am Viscount a-77-D	C186774- 8420											1.11	0.06	11	1.27	0.02	4	1.78	0.05	11	2.08				1.18

Table C10 Bitumen and vitrinite reflectance data for the Golata Formation.

SAMPLE LOCATION	SAMPLE No.		PHYTOCLASTS						BITUMENS																		FLUORESCENCE INDEX					VRo calculated (Jacob, 1985)	TAI
			Vitrinite			Rew Vitr	SFus	Low Ro Type 1			Type 2			Type 3			Med Ro Type 4			High Ro Type 5			Type 6									
			% Ro			% Ro	% Ro	% Ro			% Ro			% Ro			% Ro			% Ro			% Ro									
	CGS #	I.D.	mean	s.d.	n	mean	spot	mean	s.d.	n	mean	s.d.	n	mean	s.d.	n	mean	s.d.	n	mean	s.d.	n	mean			m'alg	Leio	Bitum. matrix	Low Ro bitumen	spor		
B-A Texaco Arrowhead N-2	C186758	-2180																							1-2	3					
Texaco NFA Bovie Lake J-72	C186762	-1260	0.79	0.00	2			0.33	0.06	7	0.42	0.00	1	0.64	0.07	2										2/3		4/5				2+
IOE Bovie Lake M-05	C186753	-1606	0.60 (est)																						3	1/2		2/3				2
IOE Bovie Lake M-05	C186753	-1606.7	0.60 (est)																													2
Canada S. *et al.* N. Beaver R.1-27	C186754	-3549												0.78	0.04	8	0.93	0.04	11	1.56	0.15	2	2.32							0.97		
Canada S. *et al.* N. Beaver R. 1-27	C186754	-4389												0.75	0.04	3	1.10	0.10	5	1.48	0.06	3	2.38							1.08		
Canada S. *et al.* N. Beaver R. 1-27	C186754	-4578												0.85	0.04	3	1.17	0.06	4	1.52	0.00	1	2.49							1.12		
Canada S. *et al.* N. Beaver R. 1-27	C186754	-4885												1.14	0.02	2	1.36	0.04	2				2.30							1.24		
Canada S. *et al.* N. Beaver R. 1-27	C186754	-5139									0.83	0.02	2	1.07	0.05	7	1.31	0.02	2	1.58	0.03	2	2.13							1.21		
Pan Am Pointed Mountain P-53	C186766	-1950	0.73											0.42	0.02	3	0.54	0.05	5	0.90	0.07	8				2/3			4/5	0.73		
Pan Am Pointed Mountain P-53	C186766	-2160	0.80	0.03	2			0.22	0.07	13	0.36	0.07	14	0.49	0.07	41	0.63	0.06	26	1.10	0.00	1			2/3	3	9		4	0.79		
Pan Am Pointed Mountain P-53	C186766	-2780	0.83	0.06	6		1.2	0.22	0.05	21	0.30	0.02	2	0.45	0.08	10	0.66	0.05	25	1.10	0.00	1				3		7	4	0.81		
Pan Am Pointed Mountain P-53	C186766	-3195	0.82	0.04	4		0.91	0.21	0.05	9	0.37	0.09	11				0.67	0.05	20	1.20	0.22	12				3/4			4	0.81		
Pan Am Pointed Mountain P-53	C186766	-3870	0.85	0.02	7			0.28	0.05	8	0.42	0.08	12	0.49	0.00	1	0.72	0.07	17	1.20	0.07	2							4	0.84		
Pan Am Pointed Mountain P-53	C186766	-4310	0.96	0.03	3			0.26	0.03	4	0.43	0.08	29	0.59	0.00	1	0.83	0.10	5	1.02	0.00	1					9		5	0.91		
Amoco Pointed Mountain P-24	C186760	-2570									0.33	0.04	9	0.45	0.00	1									2	2/3						
Amoco Pointed Mountain P-24	C186760	-2855																													0.78		
Amoco Pointed Mountain P-24	C186760	-3995																															
Amoco Pointed Mountain P-24	C186760	-4500	0.80	0.03	13	0.84	spor-	0.19	0.02	11	0.33	0.02	6	0.48	0.02	2	0.64	0.05	21							4	9		4/5	0.80		
Amoco Pointed Mountain P-24	C186760	-4890	0.85	0.05	17		spor-	0.20	0.02	11	0.34	0.05	10	0.49	0.01	2	0.62	0.05	7	1.15	0.09	8	1.28			3/4			4	0.78		
Amoco Pointed Mountain P-24	C186760	-5140	0.89	0.05	5						0.46	0.09	8	0.50	0.05	15	0.65	0.05	25	1.10	0.04	2							4	0.80		
Amoco Pointed Mountain P-24	C186760	-5340	0.91	0.04	5						0.42	0.06	24				0.70	0.04	5	1.10	0.09	5				4			4/5	0.83		
Pan Am Beaver G-01, YT	C186752	-2880									0.30	0.02	19	0.55	0.03	19																
Pan Am Beaver G-01, YT	C186752	-3250									0.38	0.00	1	0.58	0.06	12	0.77	0.00	1												0.88		
Pan Am Beaver G-01, YT	C186752	-3475									0.28	0.03	6	0.39	0.03	4	0.56	0.00	1														
Pan Am Beaver G-01, YT	C186752	-3700												0.78	0.05	2									3/4	4/5	7/8	7					
Pan Am Beaver G-01, YT	C186752	-3795									0.59	0.04	5	0.91	0.00	11	1.20																
Pan Am Beaver G-01, YT	C186752	-4135									0.59	0.04	5	0.94	0.08	5	1.20								3/4		7-8	7		1.14		
Pan Am Beaver G-01, YT	C186752	-4690																							5		8					
Pan Am Beaver G-01, YT	C186752	-4965												0.82	0.00	1										6/7						
Pan Am Beaver G-01, YT	C186752	-5520															1.20	0.00	1												1.14		
Pan Am Beaver G-01, YT	C186752	-5835									0.76	0.00	1	0.97	0.03	5																

Table C11a Bitumen and vitrinite reflectance data for the Mattson Formation.

SAMPLE LOCATION	SAMPLE No.		PHYTOCLASTS						BITUMENS																FLUORESCENCE INDEX				VRo calculated (Jacob, 1985)	TAI
			Vitrinite			Rew Vitr	SFus		Low Ro Type 1			Type 2			Type 3			Med Ro Type 4			High Ro Type 5			Type 6							
			% Ro			% Ro	% Ro		% Ro			% Ro			% Ro			% Ro			% Ro			% Ro							
	CGS #	I.D.	mean	s.d.	n	mean	spot		mean	s.d.	n	mean	s.d.	n	mean	s.d.	n	mean	s.d.	n	mean	s.d.	n	mean				Bitum. m'alg	Low Ro Leio matrix	bitumen	spor		
Tika Creek	C58558	103													1.19	0.0	1														
Tika Creek	C58562	147													1.1												3					
Tika Creek	C58565	163																														
Tika Creek	C58572	218																														
Tika Creek	C58703	262																														
Tika Creek	C58704	282													1.21	0.03	3	1.57	0.07	3	1.87	0.10	2	2.50						1.37	
Tika Creek	C58705	292													1.18	0.00	1	1.52	0.12	3	2.00	0.10	2							1.34	
Tika Creek	C58581	382																			1.84	0.15	3								
Tika Creek	C58591	460																1.50	0.00	1	1.84	0.00	1							1.33	
Tika Creek	C58601	609																1.77	0.03	4										1.49	
Jackfish Gap-Yohin Ridge	C58709	3894	0.80	0.02	2										0.44	0.03	2	0.72	0.00	1	1.02	0.00	1	1.49			3		4	0.84	
Jackfish Gap-Yohin Ridge	C58711	3986	0.83	0.03	3				0.11	0.01	3	0.23	0.00	1	0.55	0.01	3	0.72	0.01	3	1.08	0.00	2	1.45						0.84	
Jackfish Gap-Yohin Ridge	C58713	4096	0.80	0.00	1			1.24	0.12	0.02	5	0.25	0.03	18	0.53	0.05	22	0.73	0.03	4	1.04	0.03	4	1.67			2-3		9	0.85	
Jackfish Gap-Yohin Ridge	C58719	4413	0.90	0.03	5				0.13	0.00	1	0.30	0.02	2	0.65	0.07	10	0.79	0.04	10	1.08	0.04	5	1.35					4d	0.89	
Jackfish Gap-Yohin Ridge	C58723	4562							0.16	0.02	6	0.25	0.02	14	0.50	0.07	10	0.73	0.03	13	1.09	0.07	7	1.36					4d	0.85	
Jackfish Gap-Yohin Ridge	C58726	4633	0.81	0.00	4Cd *				0.18	0.01	3	0.34	0.00	1	0.55	0.06	9	0.73	0.02	2											0.85	
Jackfish Gap-Yohin Ridge	C58730	4754	0.74	0.04	8			1.38	0.18	0.00	4	0.24	0.01	30															3-4			
Jackfish Gap-Yohin Ridge	C58736	4859	0.79	0.03	8				0.17	0.00	1	0.22	0.01	2	0.54	0.07	15	0.71	0.01	2	1.18	0.09	9	1.29					6-7	0.84	
Jackfish Gap-Yohin Ridge	C58737	4862	0.78	0.02	10			1.37	0.19	0.00	1	0.25	0.05	15										1.35							
Jackfish Gap-Yohin Ridge	C58749	5043													0.51	0.00	0 1				1.29							4			
Jackfish Gap-Yohin Ridge	C58750	5052							0.17	0.02	3	0.33	0.01	2	0.50	0.04	27	0.67	0.02	8	1.10	0.03	7			2			3	0.81	
Jackfish Gap-Yohin Ridge	C58753	5081				0.9			0.14	0.00	1	0.29	0.00	1	0.49	0.05	8	0.66	0.04	18									3	0.81	
Jackfish Gap-Yohin Ridge	C58759	5535	0.74	0.00	1	1.01			0.13	0.01	2	0.25	0.02	4	0.49	0.03	4	0.59	0.04	9	0.98	0.10	9	1.43			2			4d	0.76	
Jackfish Gap-Yohin Ridge	C58764	5640	0.74	0.02	9	1.65																					2					
Jackfish Gap-Yohin Ridge	C58765	5640	0.74	0.04	19							0.32	0.03	3	0.37	0.01	4	0.56	0.03	6	1.18										0.75	
Jackfish Gap-Yohin Ridge	C58785	6224																														
Jackfish Gap-Yohin Ridge	C58793	6385	0.72	0.01	3													0.48	0.06	5	1.01	0.05	5							0.70	
Jackfish Gap-Yohin Ridge	C58804	6724	0.68	0.03	25							0.29	0.03	2													4d		6-7			
Jackfish Gap-Yohin Ridge	C58806	6754	0.66	0.03	38							0.28	0.02	3													2					
Jackfish Gap-Yohin Ridge	C58838	7246	0.65	0.04	25							0.27	0.04	6															7	6		
Clausen Creek	C74273	3297							0.18	0.01	7	0.36	0.01	2	0.48	0.06	13	0.68	0.05	5	0.99	0.02	3	1.40					4d	3/4	0.82	
Clausen Creek	C74277	3414	0.76	0.01	2				0.18	0.02	4	0.28	0.01	3	0.45	0.00	1	0.59	0.05	17	0.87	0.08	5	1.25							0.76	
Clausen Creek	C74276	3414	0.74	0.02	6	1.11	1.40		0.16	0.01	2	0.20	0.00	1	0.62	0.06	8							1.60						3	0.78	
Clausen Creek	C74309	4283	0.75	0.01	11																						1/2	1/2		2/3		
Clausen Creek	C74316	4457							0.15	0.00	1				0.48	0.01	2	0.58	0.01	2	0.82	0.00	1	1.07			1-2			2-3	0.76	

Table C11b Bitumen and vitrinite reflectance data from the Mattson Formation.

SAMPLE LOCATION	SAMPLE No.		PHYTOCLASTS					BITUMENS															FLUORESCENCE					VRo	TAI
			Vitrinite			Rew Vitr	SFus	Low Ro Type 1			Type 2			Type 3			Med Ro Type 4			High Ro Type 5			Type 6	INDEX					calculated (Jacob, 1985)	
			% Ro			% Ro	% Ro	% Ro			% Ro			% Ro			% Ro			% Ro			% Ro	Bitum.	Low Ro					
	CGS #	I.D.	mean	s.d.	n	mean	spot	mean	s.d.	n	mean	s.d.	n	mean	s.d.	n	mean	s.d.	n	mean	s.d.	n	mean	m'alg	Leio	matrix	bitumen	spor		
IOE Dunedin a-75-E	C186770	-10450												2.15	0.12	13	2.62	0.09	4	3.19	0.32	20							2.02	
IOE Dunedin a-75-E	C186770	-10977												2.57	0.25	40	3.21	0.23	21	4.38	0.50	12							2.38	
IOE Dunedin a-75-E	C186770	-10983												2.62	0.26	19	3.40	0.30	9	4.50	0.50	2	6.18						2.50	
IOE Dunedin a-75-E	C186770	-10998												2.52	0.20	5	3.44	0.30	4	4.05	0.00	1							2.53	
IOE Dunedin a-75-E	C186770	-11254												2.62	0.10	8	3.37	0.22	35	4.50	0.48	5	6.22						2.48	
IOE Dunedin a-75-E	C186770	-11264															3.30	0.00	1										2.44	
IOE Dunedin a-75-E	C186770	-11286												2.59	0.18	22	3.30	0.31	38	4.61	0.33	6							2.44	
IOE Dunedin a-75-E	C186770	-11522					3.59							2.77	0.17	2	3.35	0.15	11										2.47	
IOE Dunedin a-75-E	C186770	-11531																												
IOE Dunedin a-75-E	C186770	-12130																												
IOE Pan Am Viscount a-77-D	C186771	-7425																												
IOE Pan Am Viscount a-77-D	C186771	-7475																												3-3.5
IOE Pan Am Viscount a-77-D	C186771	-7477																												3
IOE Pan Am Viscount a-77-D	C186771	-7895									0.85	0.03	9	1.18	0.03	14	1.44	0.08	23	2.09	0.23	12	3.20						1.29	
IOE Pan Am Viscount a-77-D	C186771	-8005												1.19	0.04	10	1.47	0.02	3	2.04	0.15	2	3.01						1.31	
IOE Pan Am Viscount a-77-D	C186771	-8006																												
IOE Pan Am Viscount a-77-D	C186771	-8011																												3
IOE Pan Am Viscount a-77-D	C186771	-8095									0.93	0.05	21	1.15	0.07	24	1.51	0.08	22	1.93	0.08	4							1.33	
IOE Pan Am Viscount a-77-D	C186771	-8245																												
Imperial Pan Am LaBiche b-55-E	C186772	-8265																												
Imperial Pan Am LaBiche b-55-E	C186772	-8970					2.89	1.04	0.11	13	0.54	0.00	1				1.51	0.09	11	1.89	0.17	3							1.33	
Imperial Pan Am LaBiche b-55-E	C186772	-9385												1.25	0.08	20	1.63	0.08	20	2.07	0.21	4	3.76						1.41	
Imperial Pan Am LaBiche b-55-E	C186772	-9675					1.33*							0.91	0.09	12	1.64	0.07	10	2.19	0.24	7							1.41	
Imperial Pan Am LaBiche b-55-E	C186772	-9960					1.47*							1.24	0.07	7	1.75	0.08	20	2.32	0.16	11							1.48	
Amoco LaBiche a-67-D	C186777	-7950												1.14	0.00	1	1.55	0.11	6	1.97	0.15	20	2.53						1.36	
Arco Maxhamish b-21-K	C186776	-5855						0.20	0.02	2	0.58	0.03	10	0.92	0.10	9	1.35	0.06	12						5				1.23	
Arco Maxhamish b-21-K	C186776	-7005					1.96	0.32	0.05	3	0.57	0.04	5	1.02	0.09	8	1.44	0.08	20					4d		9	7-8		1.29	
Arco Maxhamish b-21-K	C186776	-7025					1.96	0.32	0.05	3	0.57	0.04	6	1.02	0.09	8	1.44	0.08	20					4d		9	7-8		1.29	
Aquitaine *et al.* Tatoo a-2-D	C186775	-1617.5	0.81	0.03	11		1.31	0.15	0.02	7	0.31	0.05	6				0.66	0.04	31						3	7	5		0.81	
Aquitaine *et al.* Tatoo a-2-D	C186775	-1625.5	0.79	0.02	9	1.33	1.58	0.19	0.02	2							0.69	0.06	25	1.49	0.02	2							0.83	
Aquitaine *et al.* Tatoo a-2-D	C186775	-1631	0.79	0.02	9	1.01	1.60	0.10	0.01	2	0.24	0.04	9				0.68	0.06	7	1.38	0.05	2							0.82	
Aquitaine *et al.* Tatoo a-2-D	C186775	-1647C																									4-5			
Aquitaine *et al.* Tatoo a-2-D	C186775	-1655	0.80	0.00	1	0.91		0.16	0.02	5	0.25	0.03	8	0.46	0.03	8	0.64	0.00	1							5	4-5		0.80	
Aquitaine *et al.* Tatoo a-2-D	C186775	-1661.5						0.18	0.03	7	0.29	0.05	3	0.49	0.05	3	0.70	0.01	5	0.89	0.00	2							0.83	
Aquitaine Windflower d-87-A	C186773	-1496												10.46	2.0	6	17.87	2.3	3	>20									11.44	2.5

*collodetrinite

Table C11c. Bitumen and vitrinite reflectance data for the Mattson Formation (British Columbia).

APPENDIX D
Bitumen reflectance-depth profiles

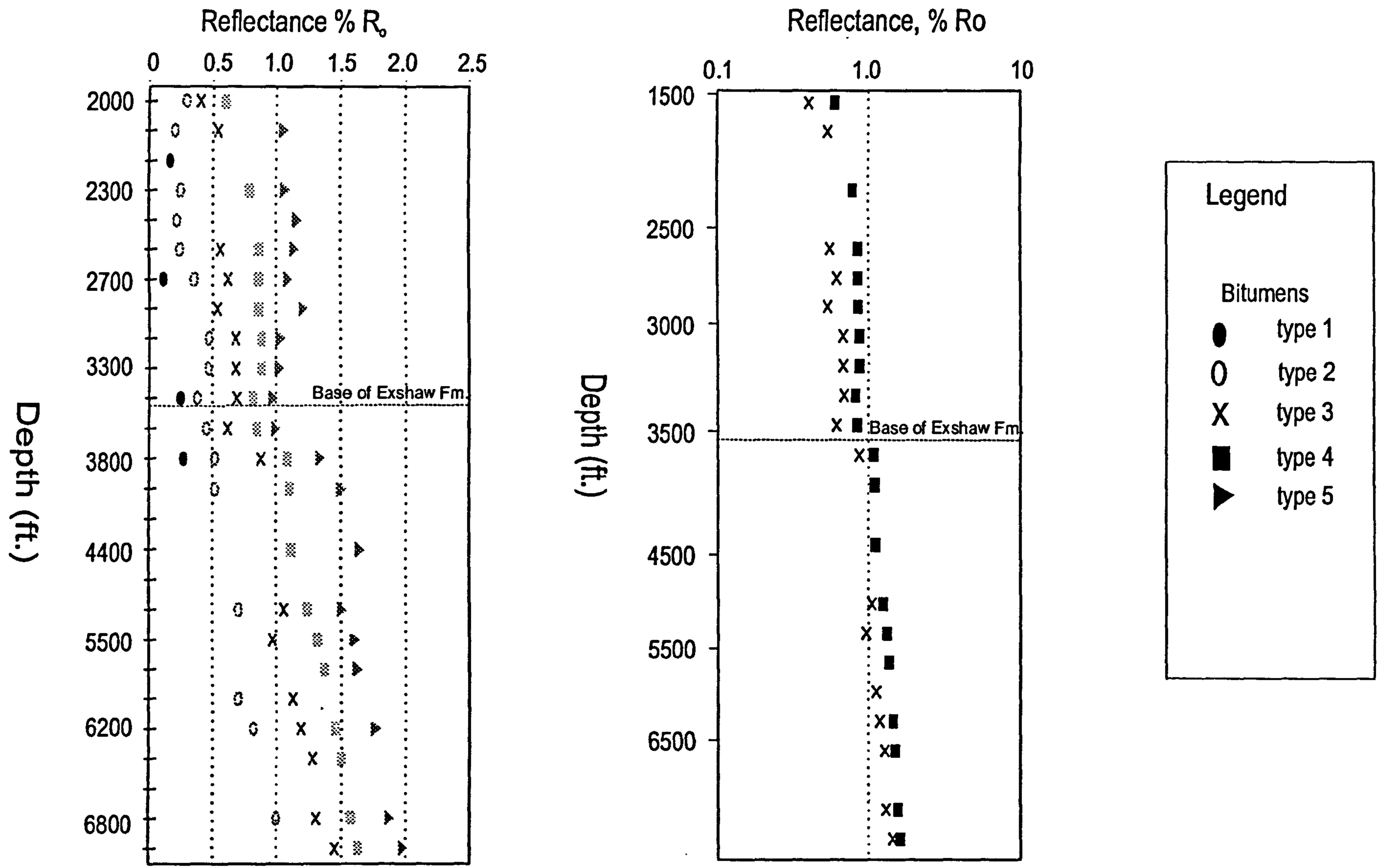

Figure D1 Bitumen reflectance - depth profiles for the Imperial Island River No.1 section: a) linear plot; b) semilog plot.

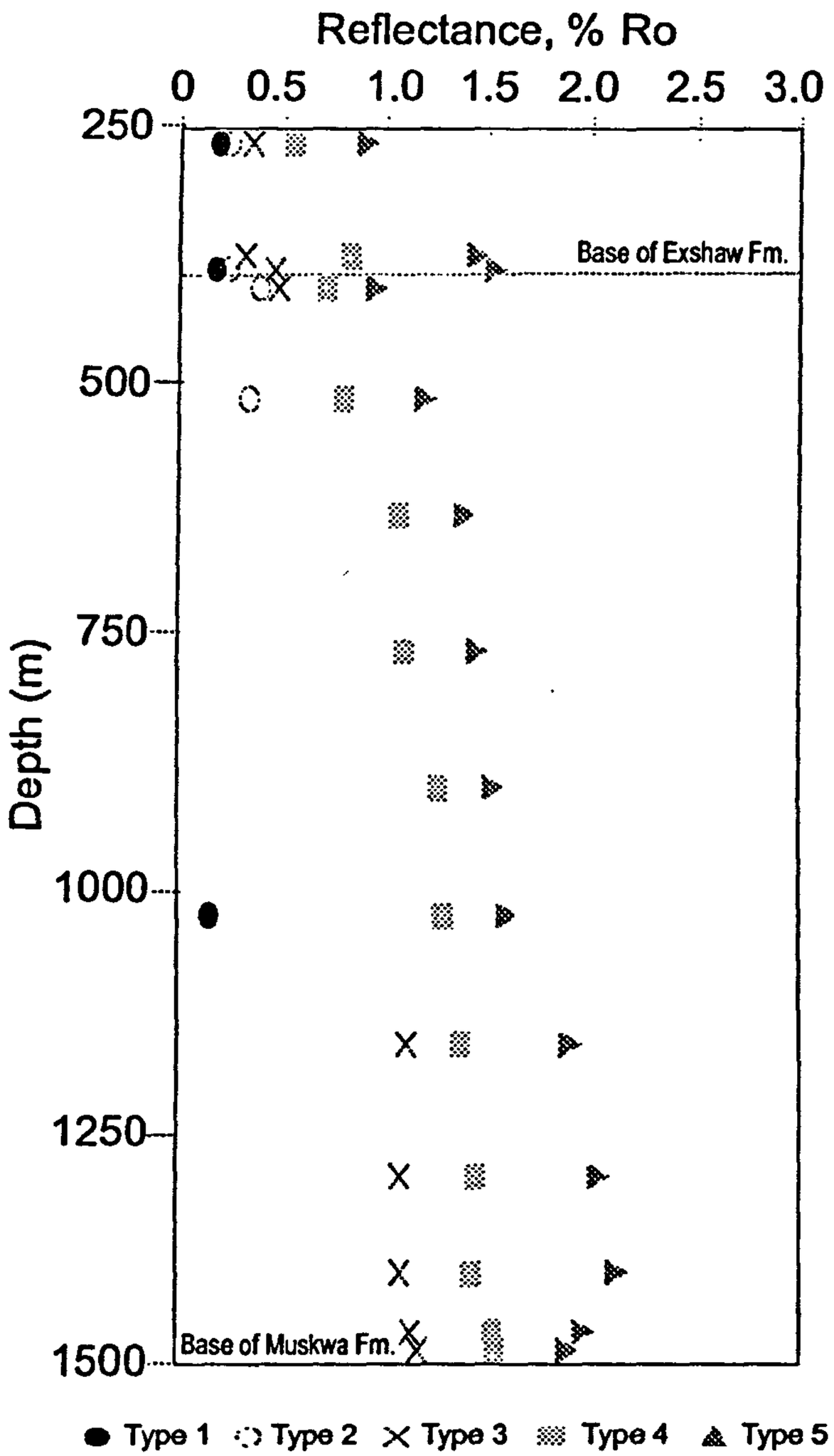

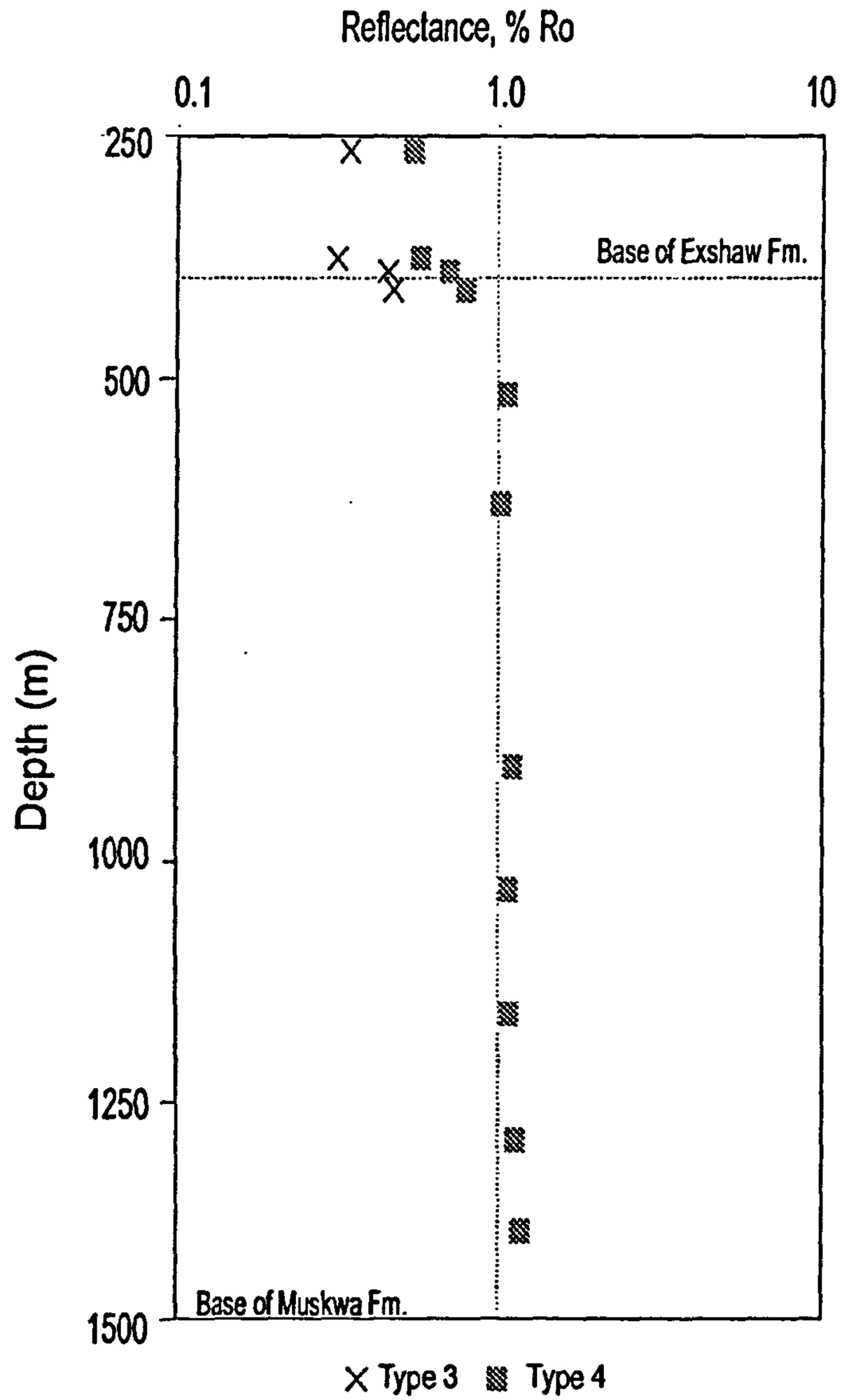

Figure D2 Bitumen reflectance - depth profiles for the Dome *et al.* Trout Lake H-45 section: a) linear plot; b) semilog plot.

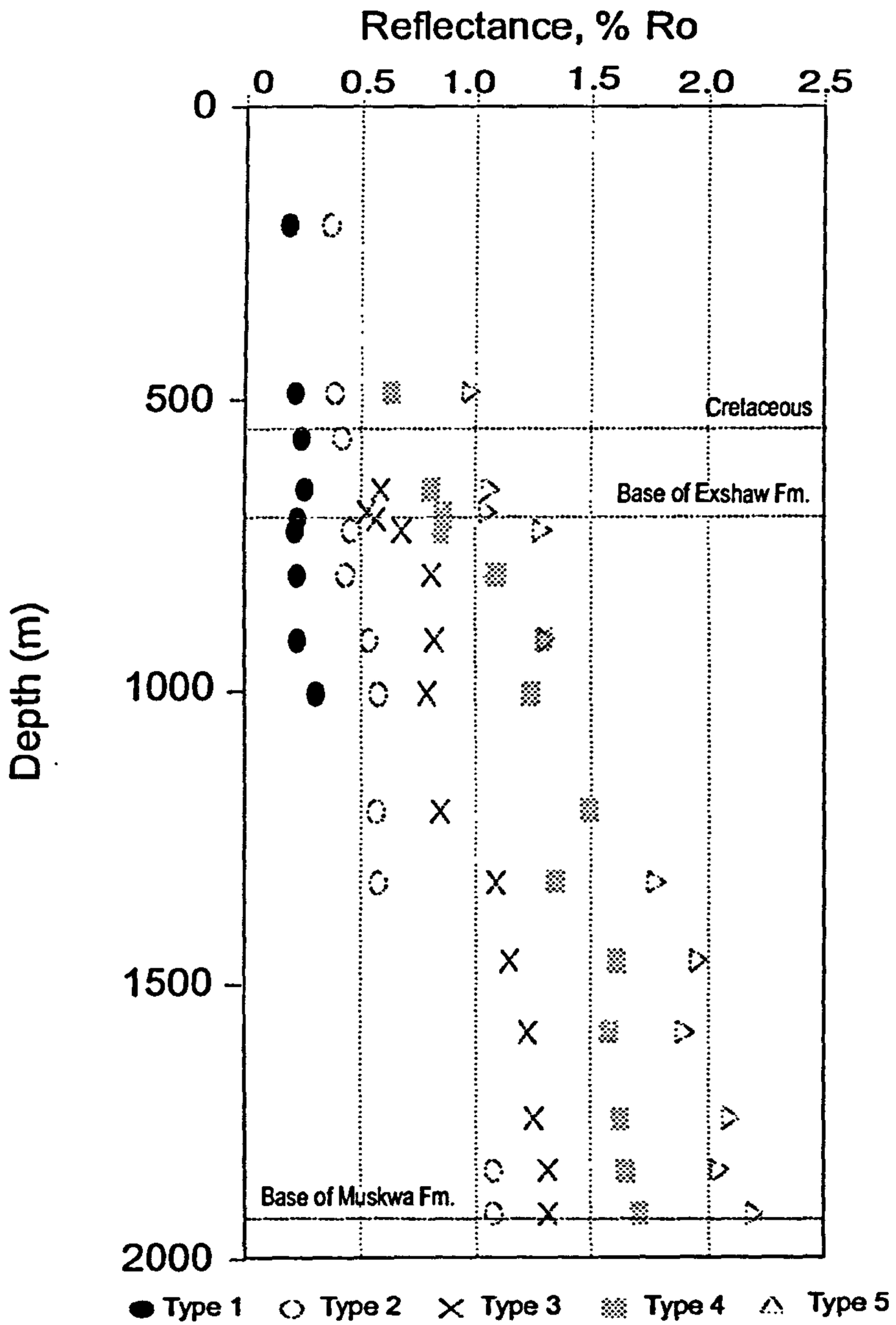

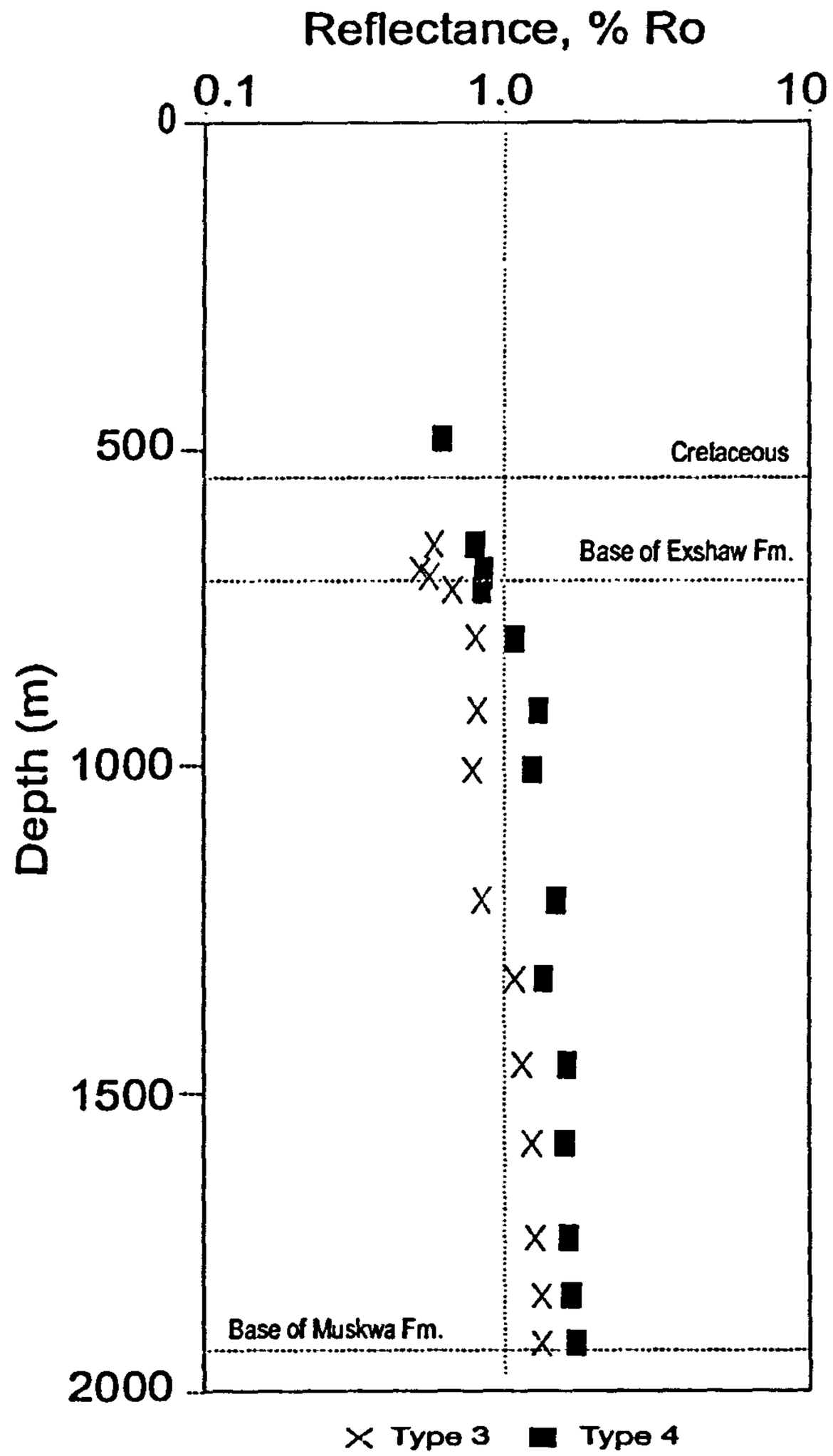

Figure D3 Bitumen Ro- depth profiles for the Murphy *et al.* Muskeg River No.1 section; a) linear plot; b) semilog plot.

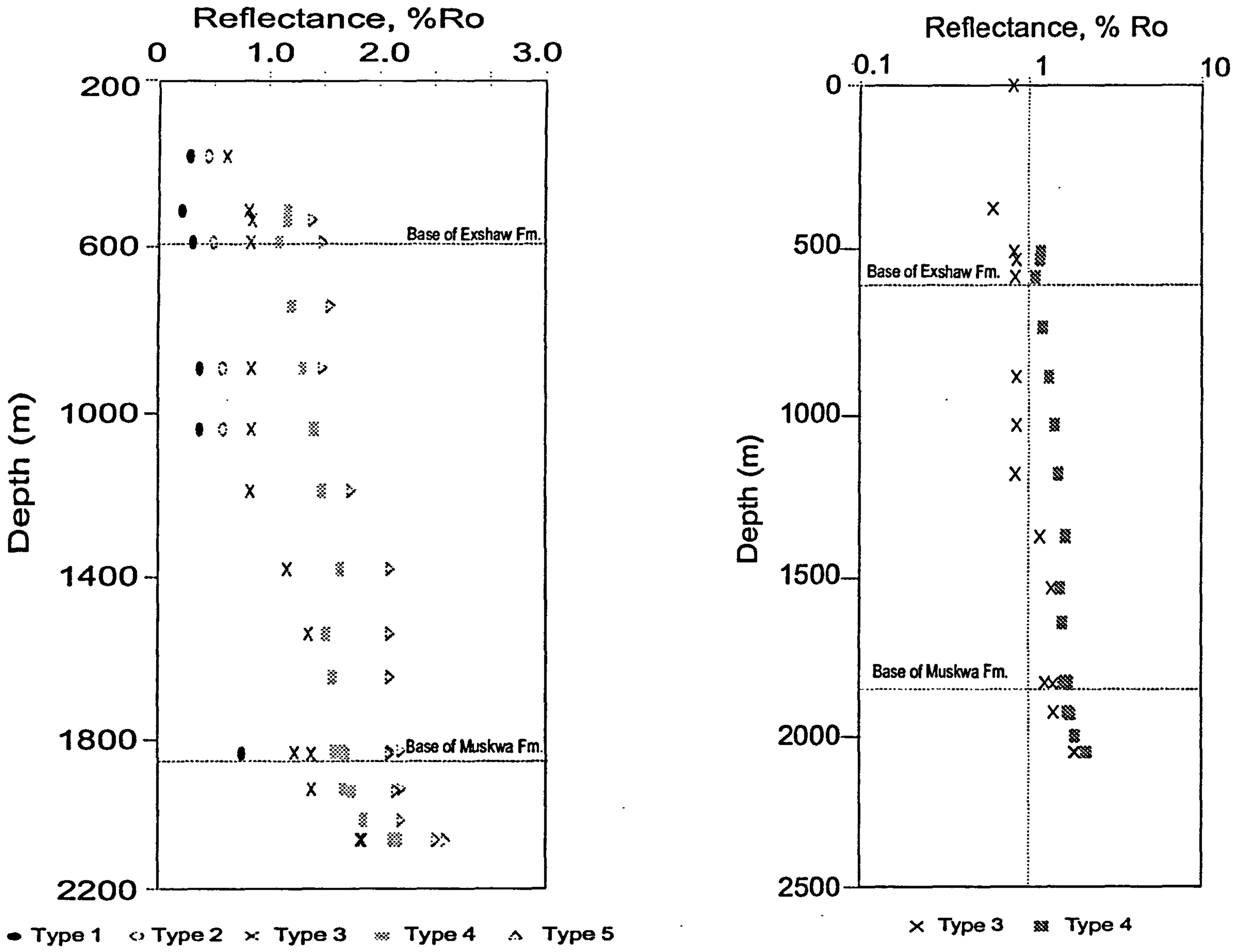

Figure D4 Bitumen reflectance - depth plots for the Imperial Sun Arrowhead I-46 section; a) linear plot; b) semilog plot.

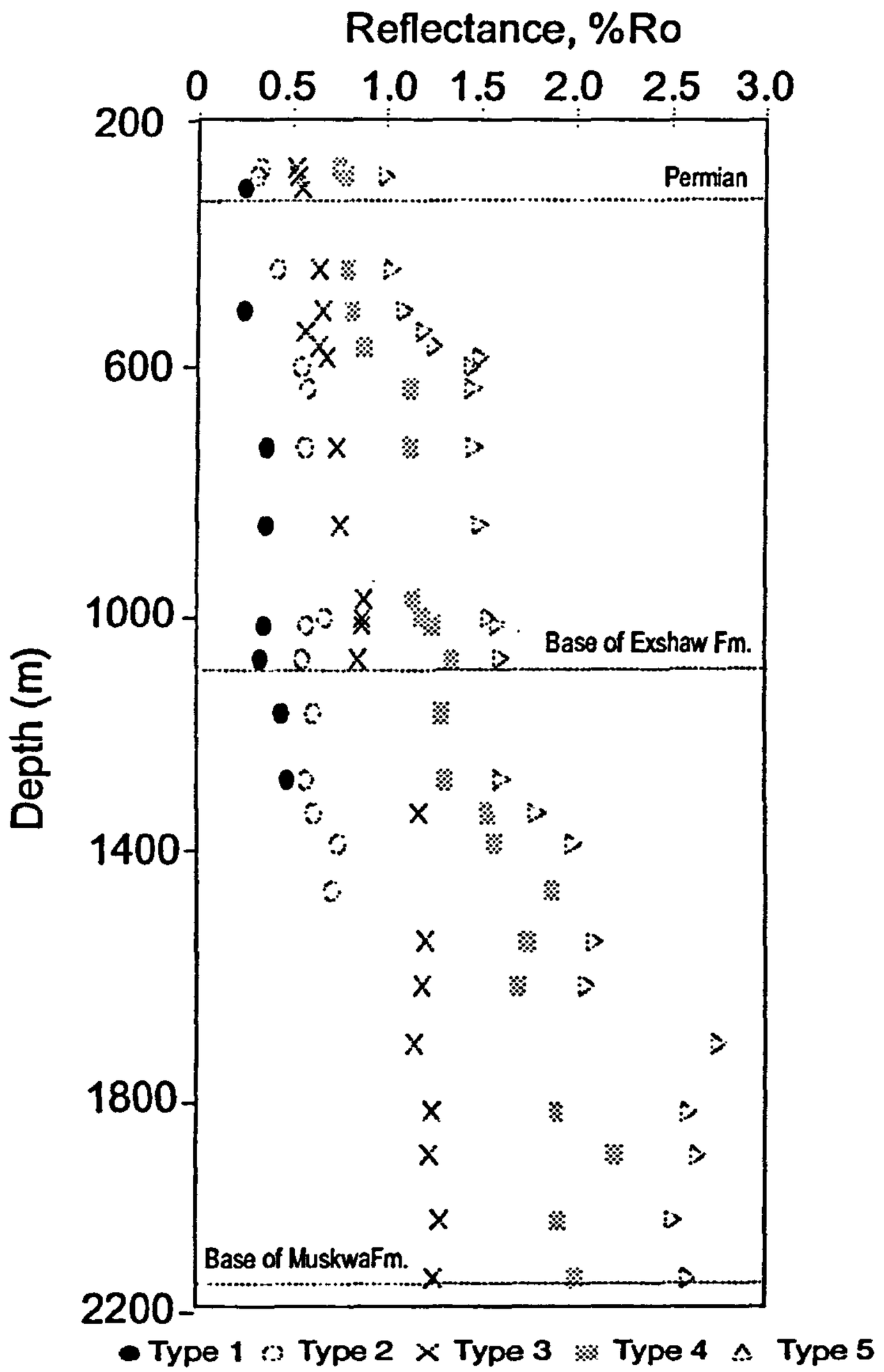

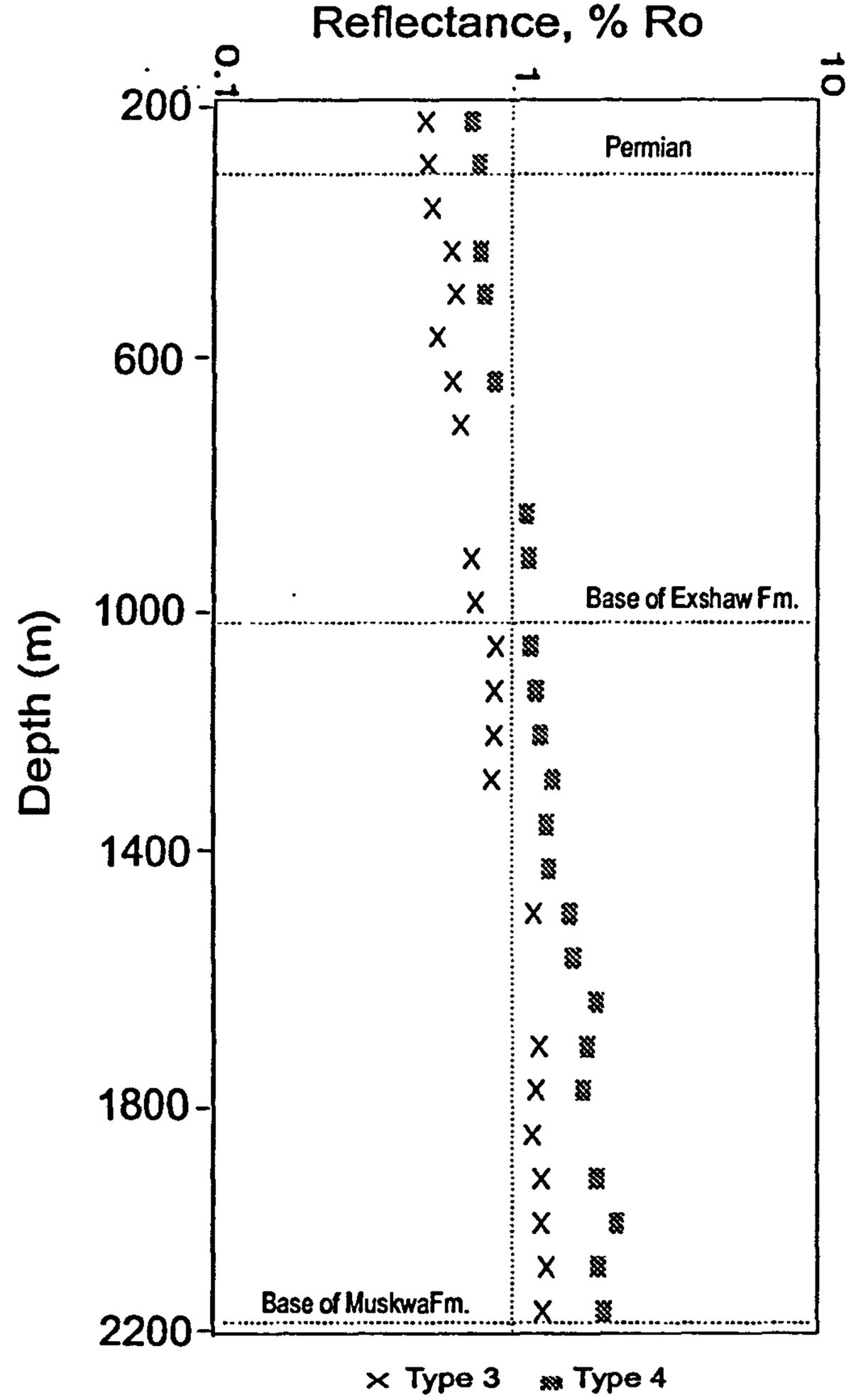

Figure D5 Bitumen Reflectance - depth plotss for the Pan Am *et al.* Celibeta No. 7; a) linear; b) semilog.

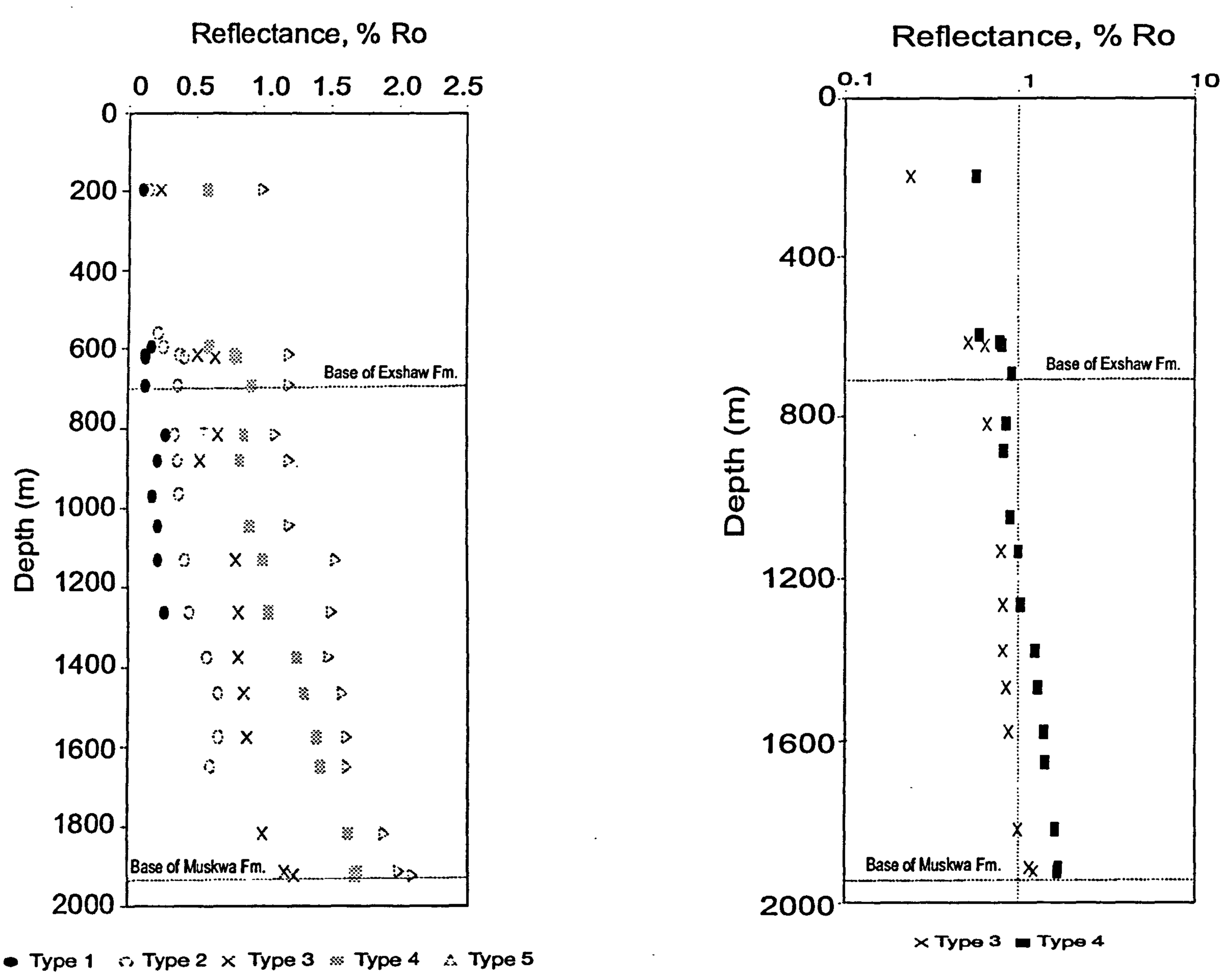

Figure D6 Bitumen Ro - depth plots for the Imperial Sun Netla C-07 section; a) linear; b) semilog.

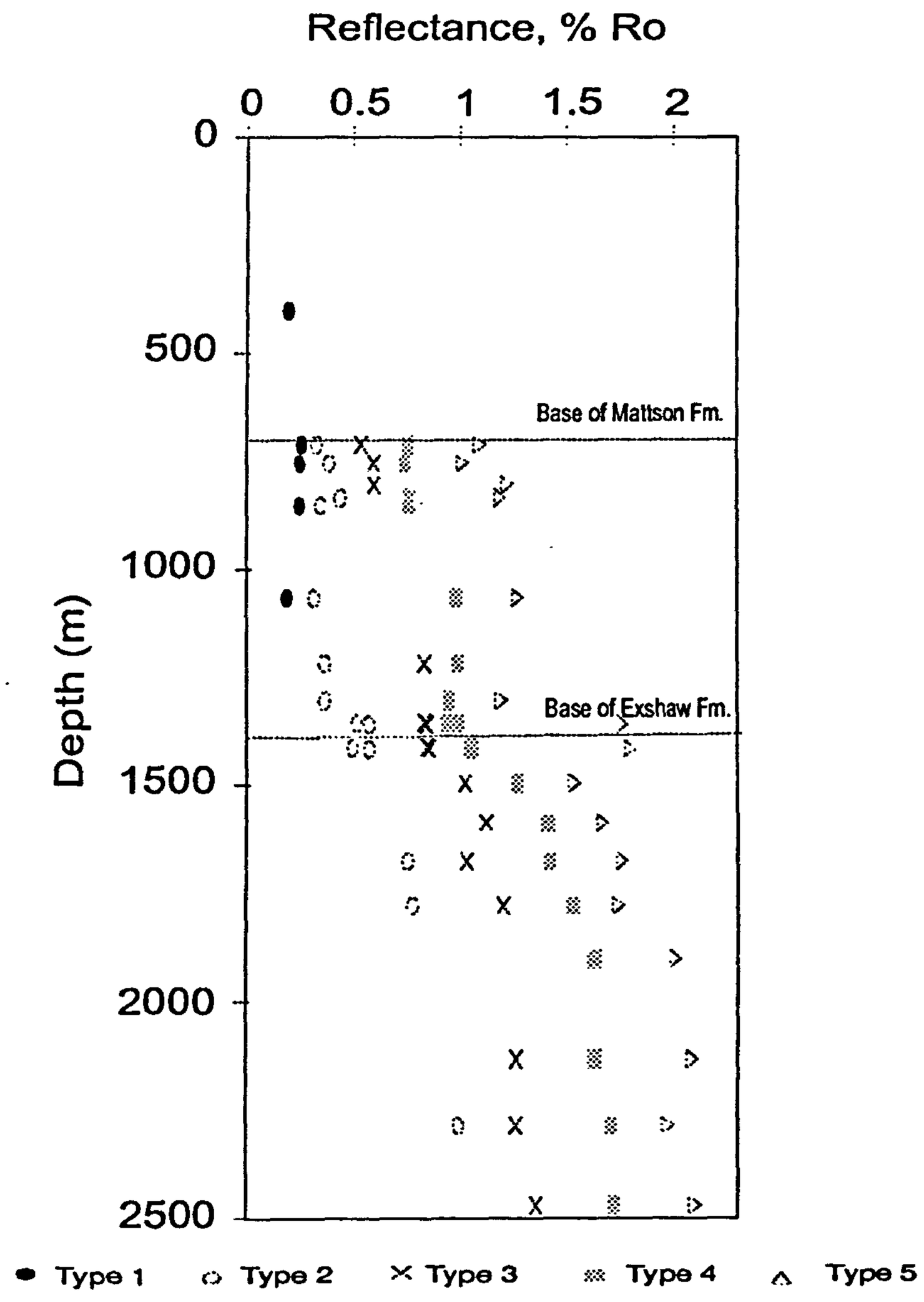

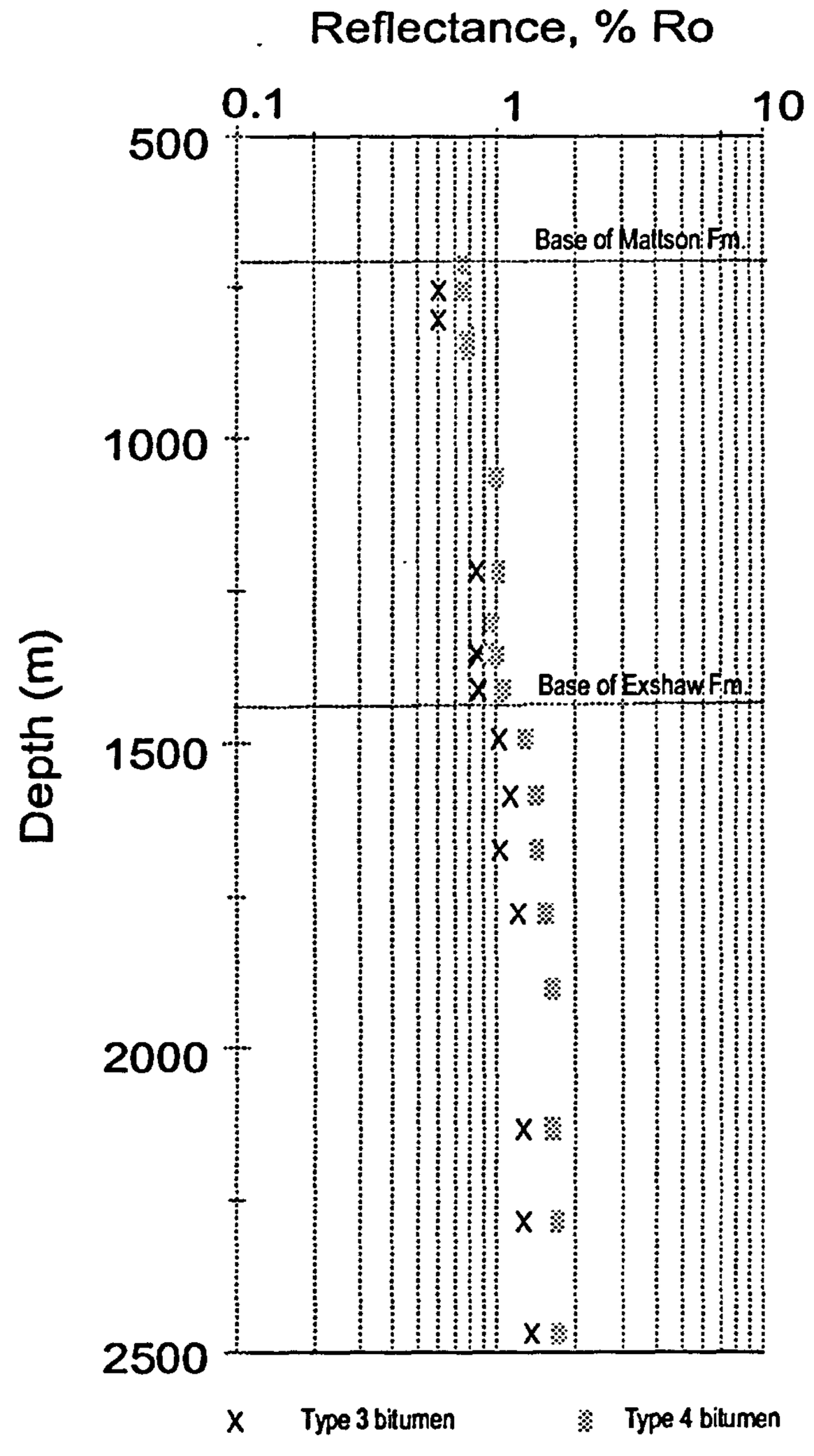

Figure D7 Bitumen reflectance - depth plots for the B.A. Texaco Arrowhead N-2 section; a) linear; b)semilog.

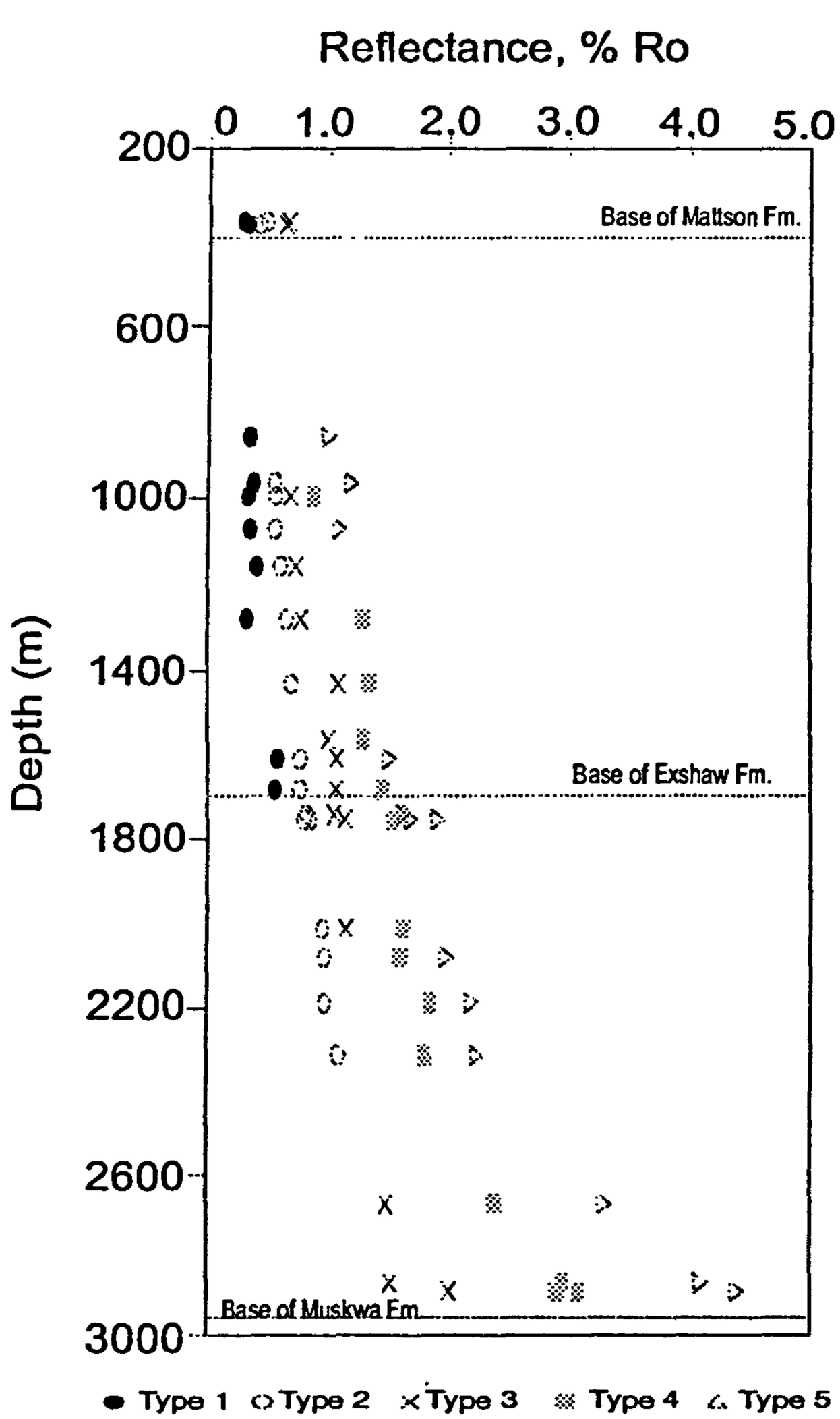

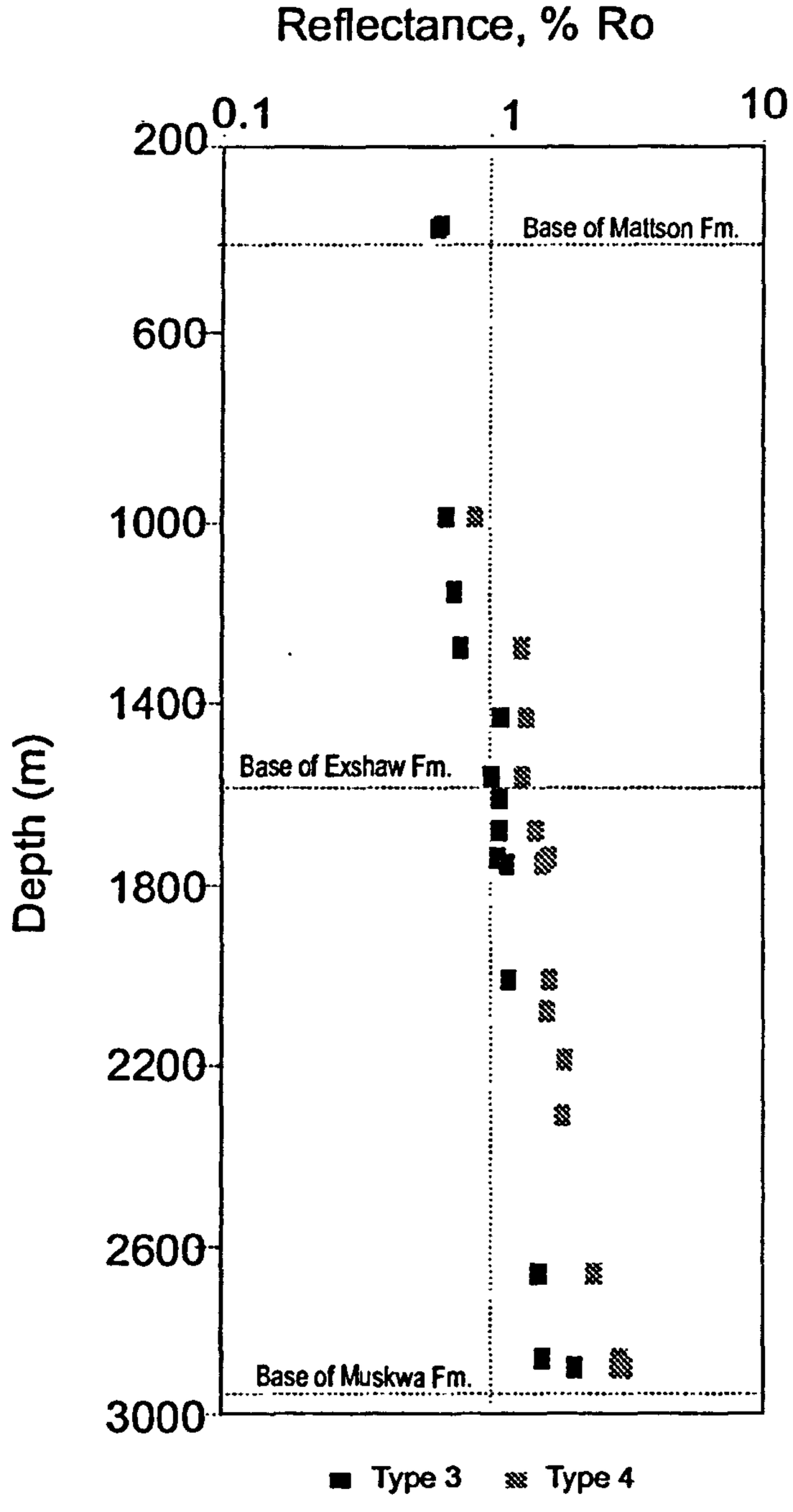

Figure D8 Bitumen reflectance - depth plots of the Texaco Bovie Lake J-72 section: a) linear; b) semilog.

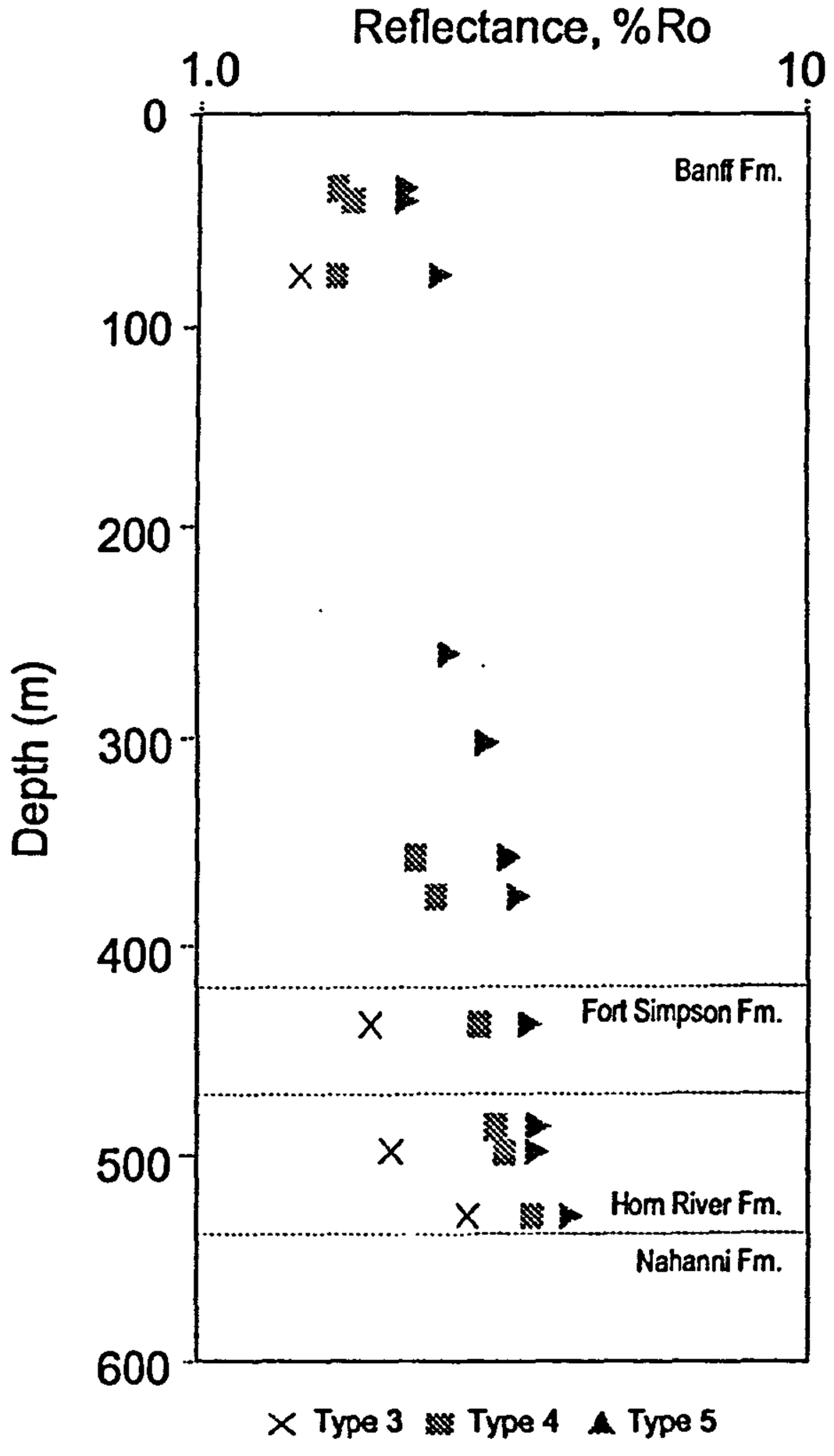

Pan Am Mattson Creek A-1

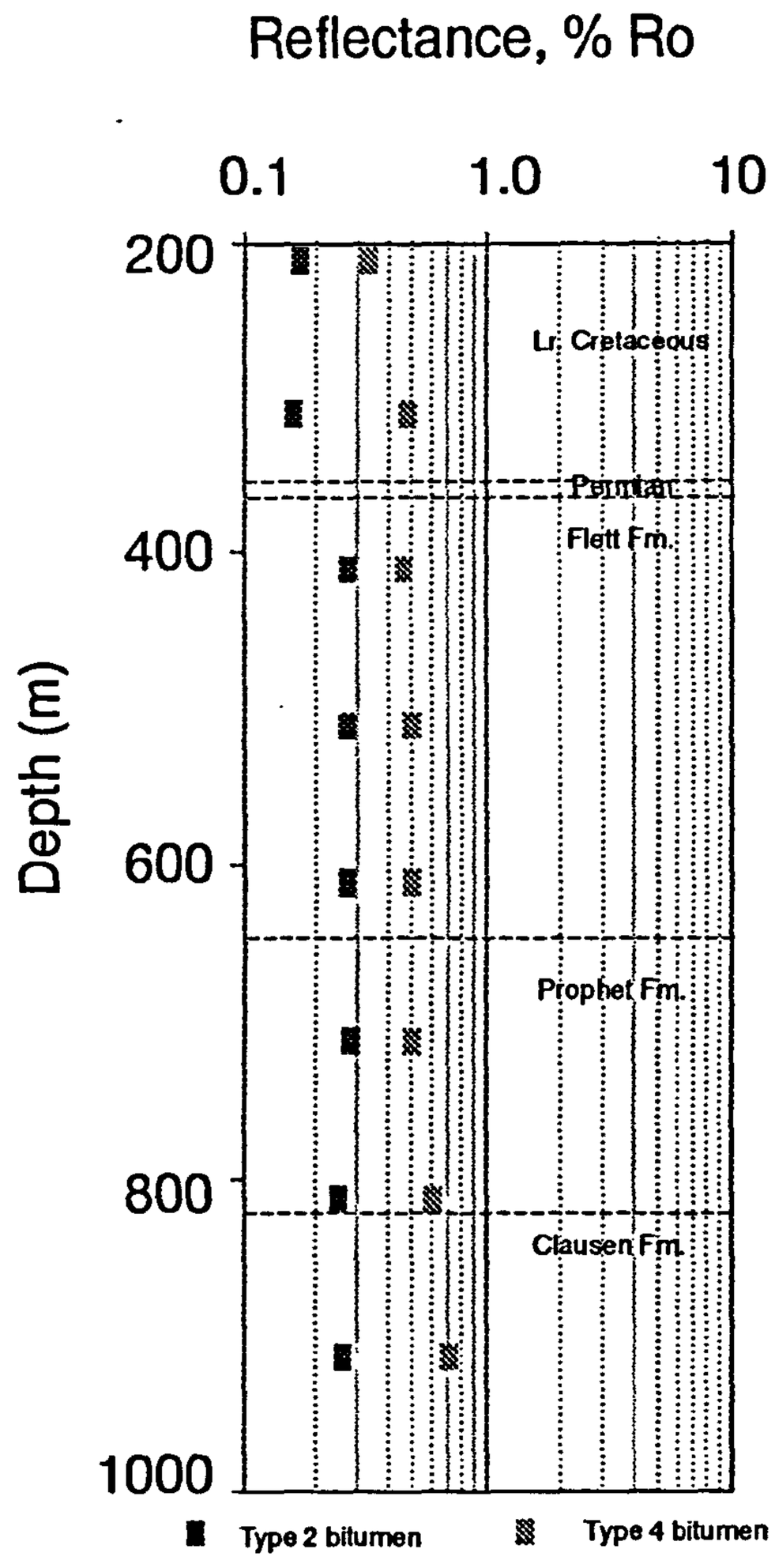

Amoco East Flett

Figure D 9 Bitumen reflectance - depth semilog plots for the a) Pan Am Mattson Creek A-1 and b) Amoco East Flett sections..

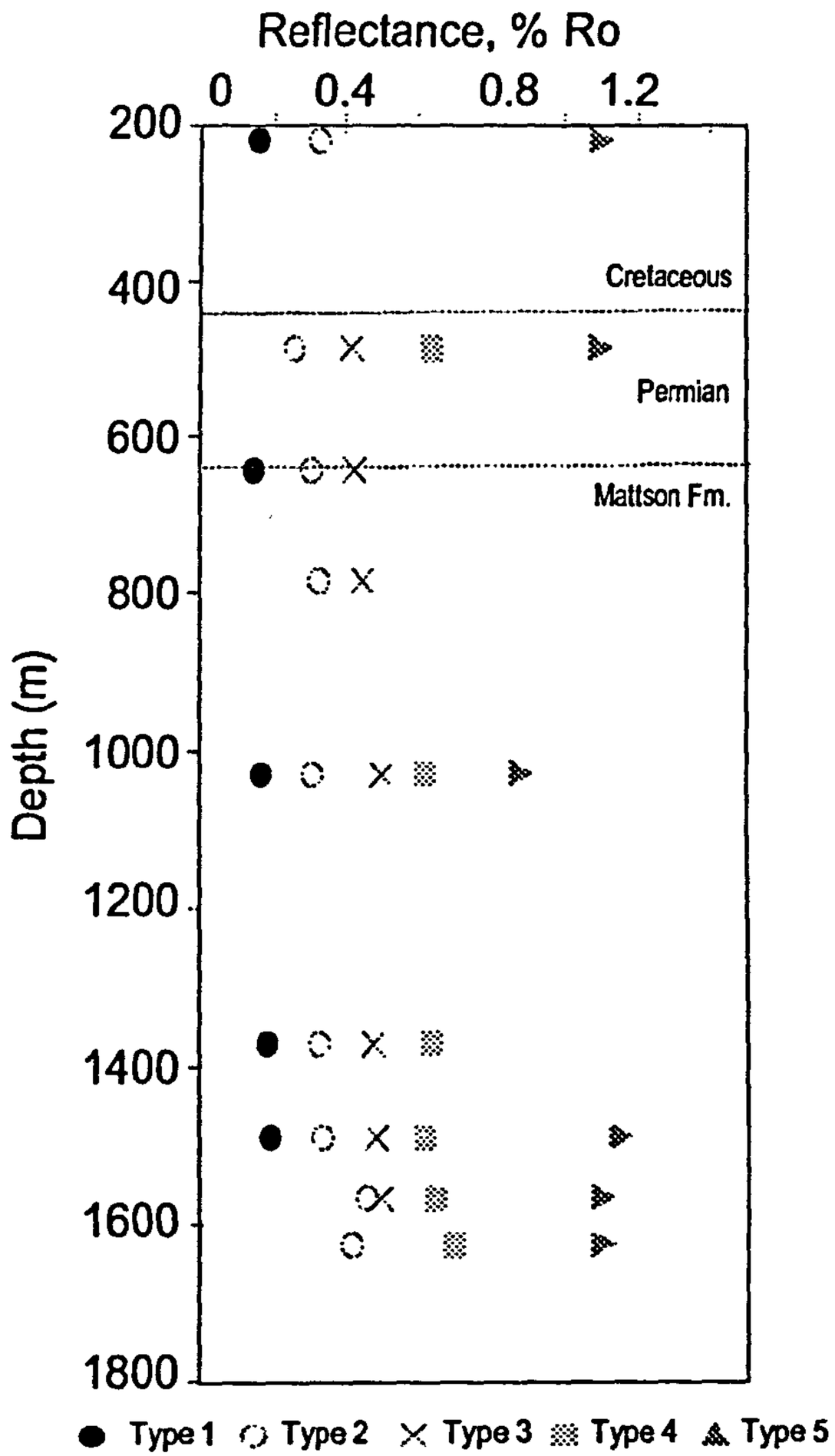

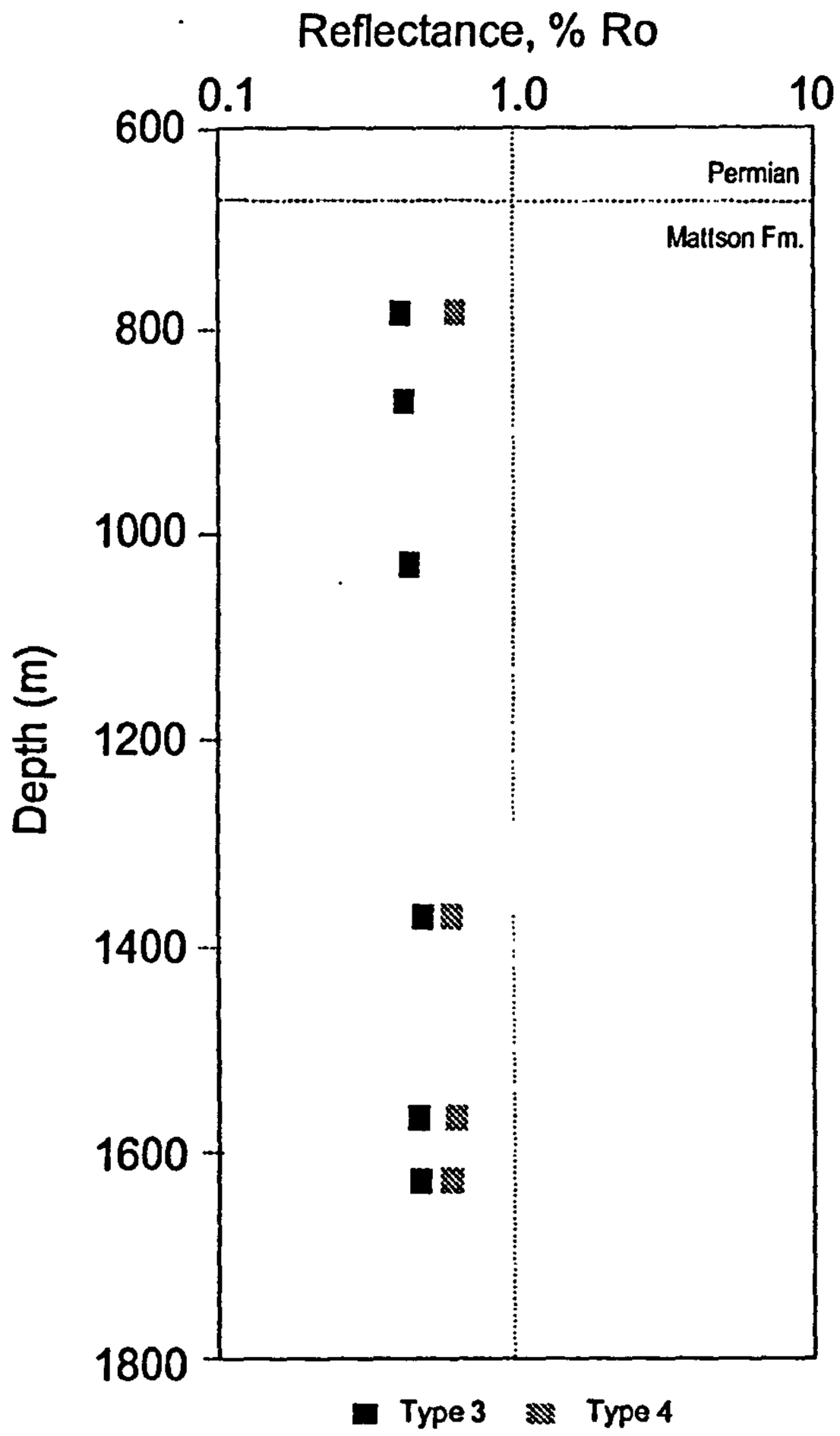

Figure D10 Bitumen reflectance - depth profiles for the Pan Am Pointed Mountain P-24 section; a) linear; b) semilog.

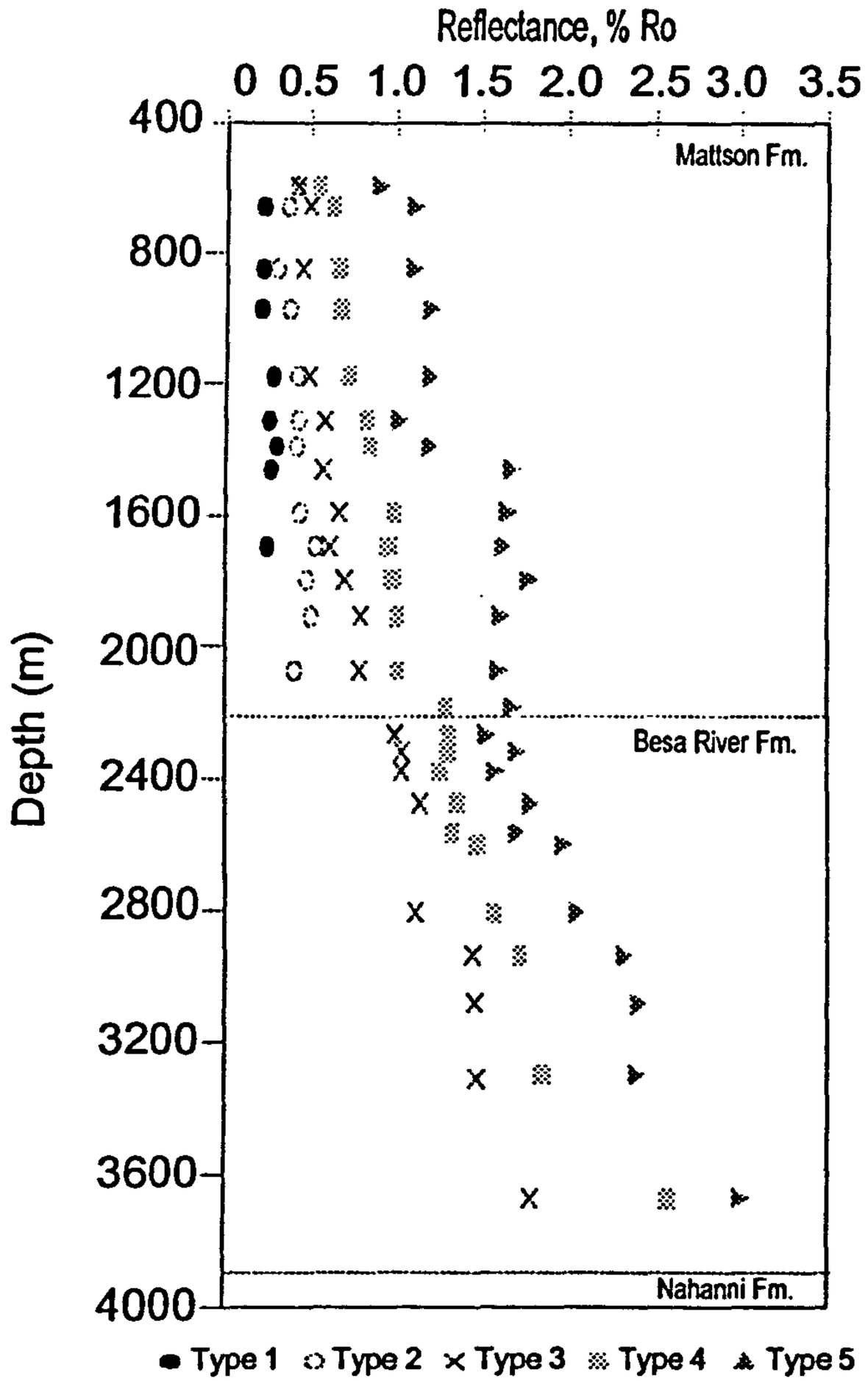

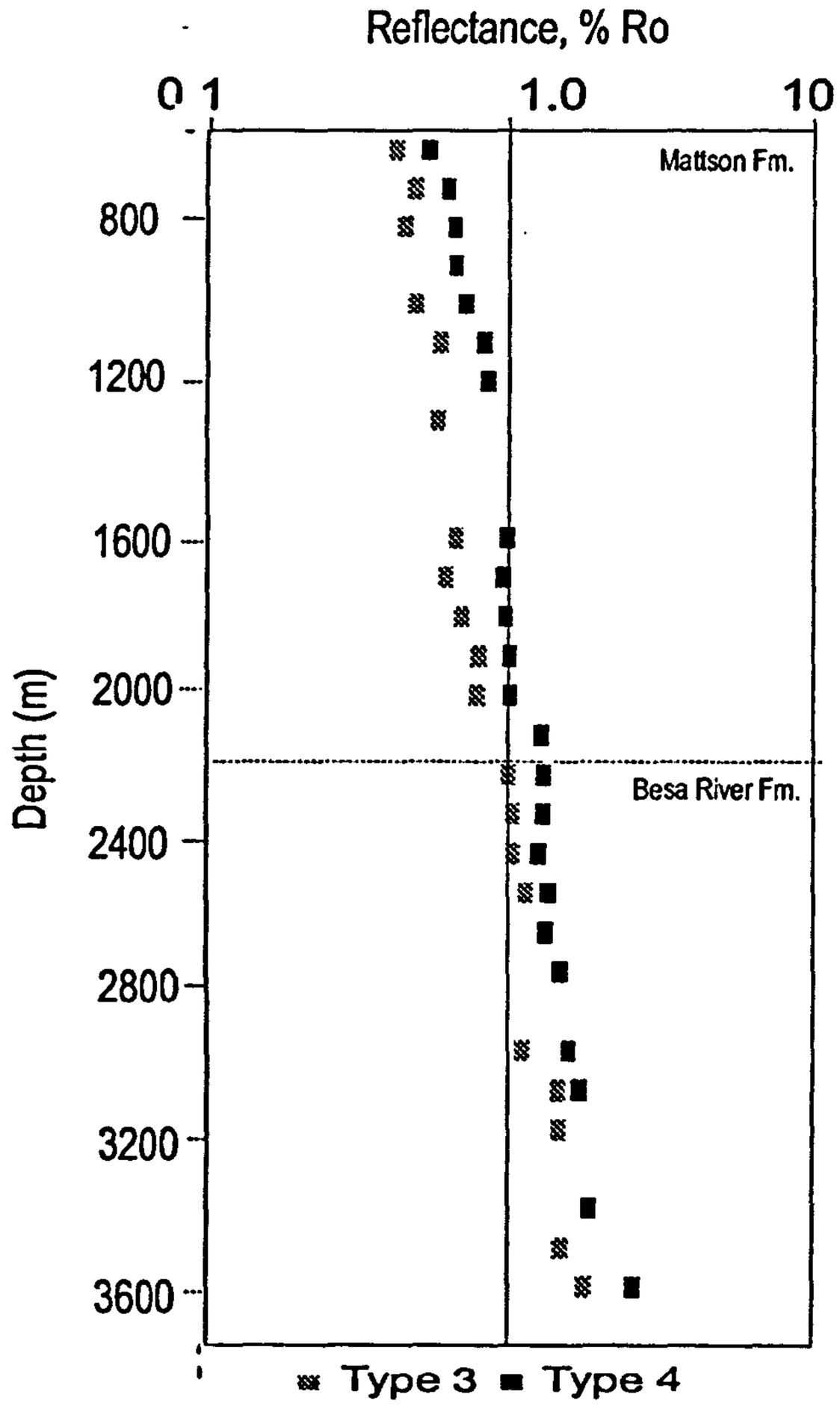

Figure D12 Bitumen reflectance - depth plots for the Amoco Pointed Mountain P-53 section; a) linear; b) semilog.

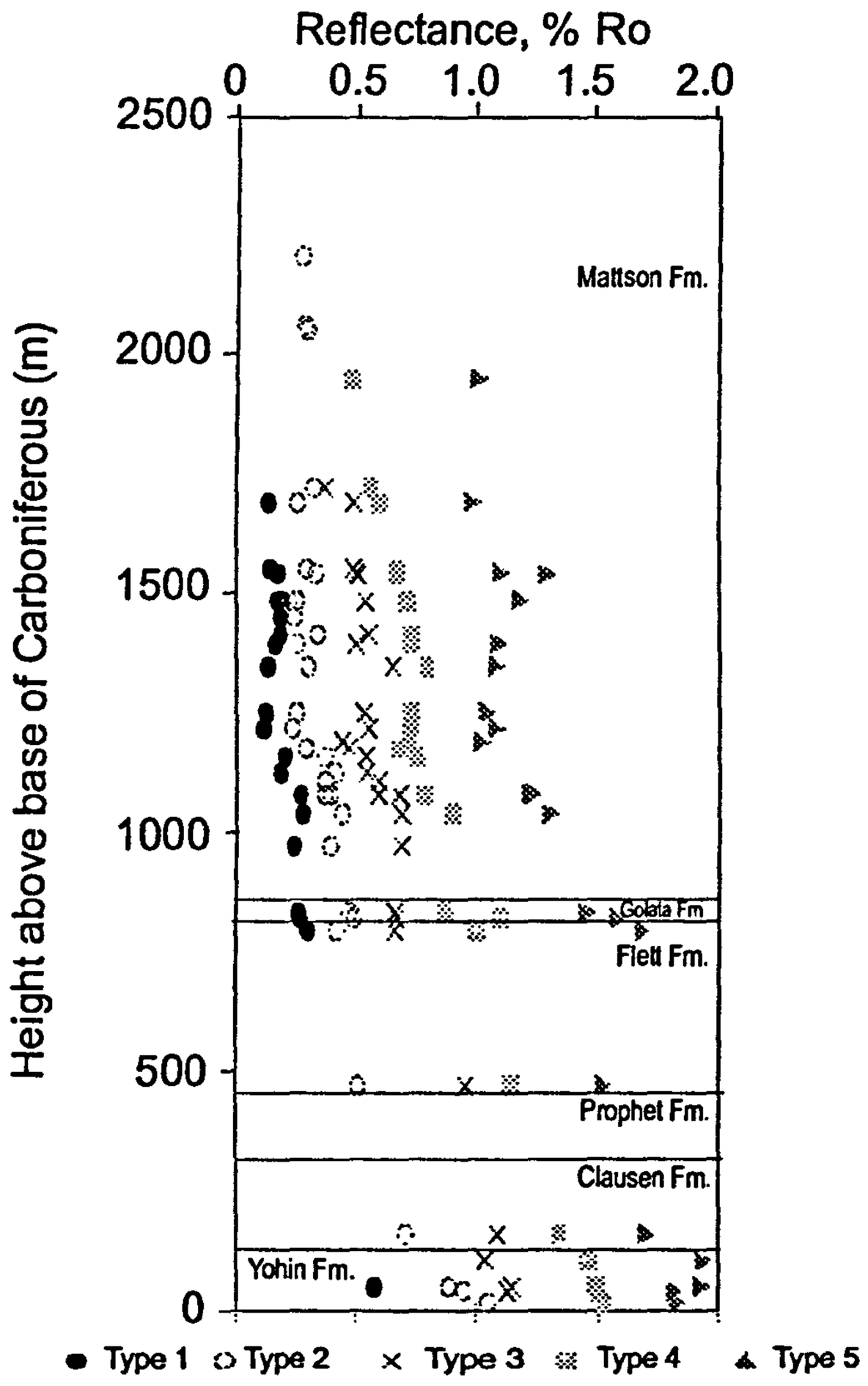

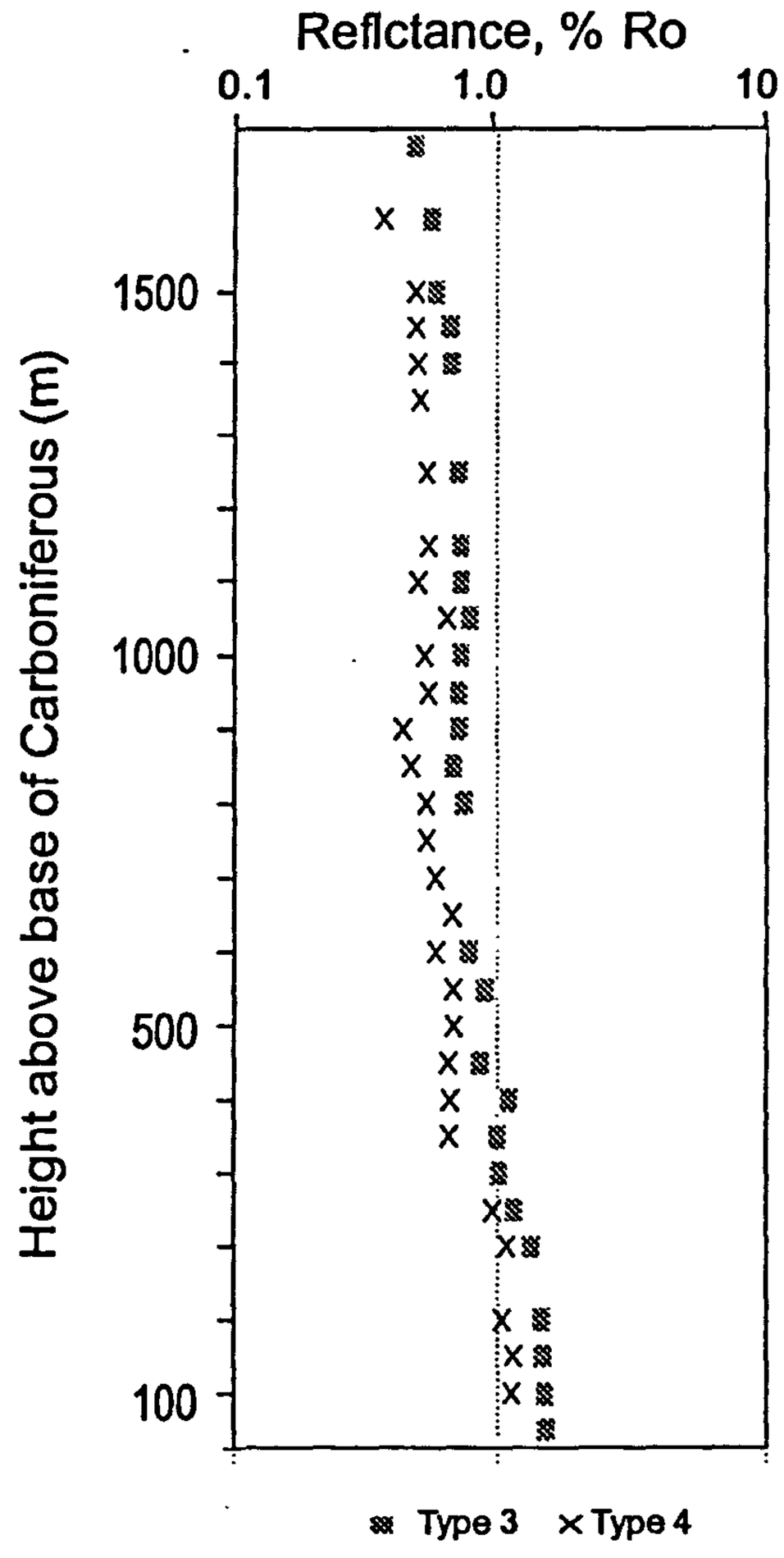

Figure D13 Bitumen reflectance - depth profiles for the Jackfish Gap - Yohin Ridge sections; a) linear; b) semilog.

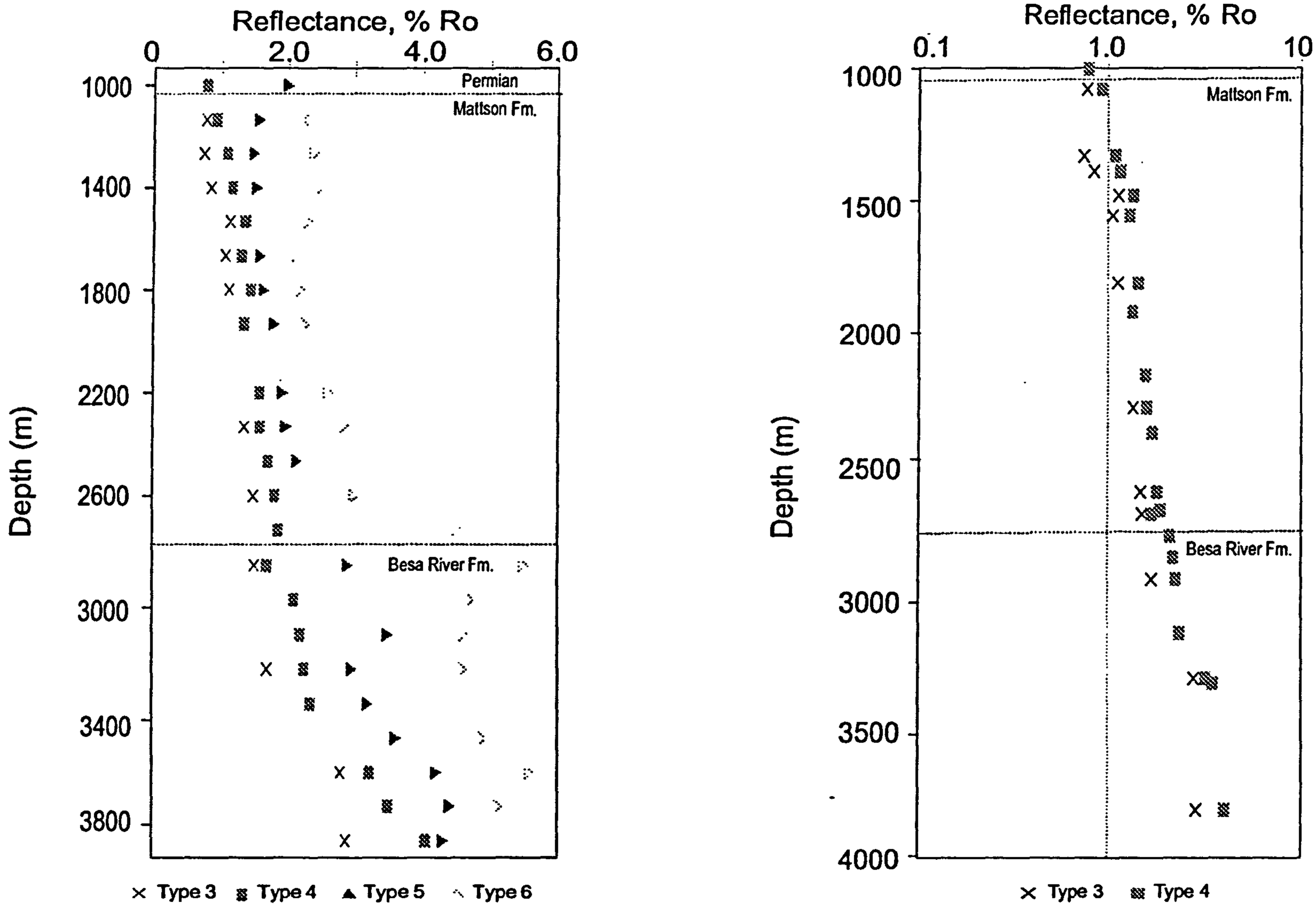

Figure D14 Bitumen reflectance - depth profiles for the Canada Southern *et al.* N. Beaver River I-27 section; a) linear; b) semilog.

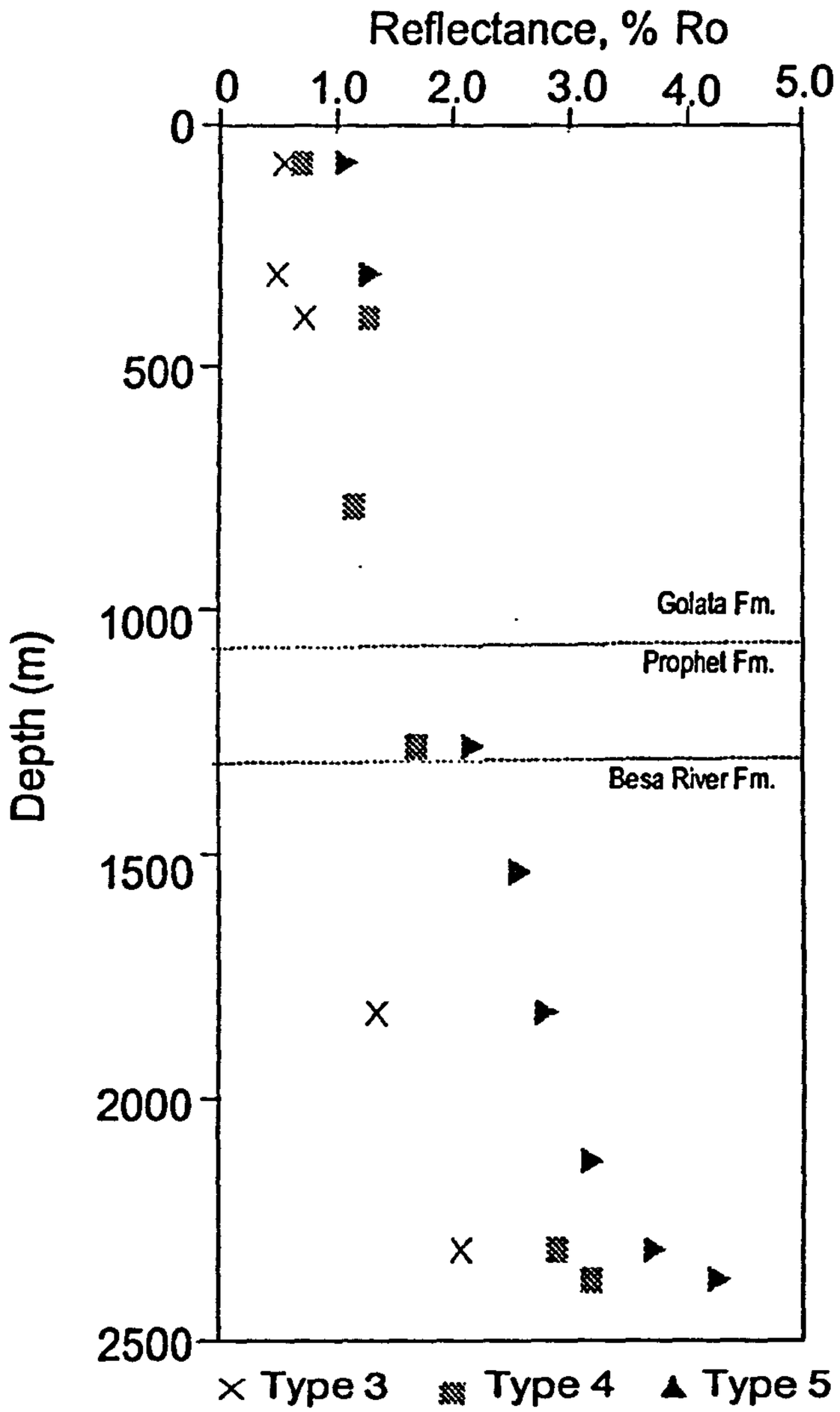

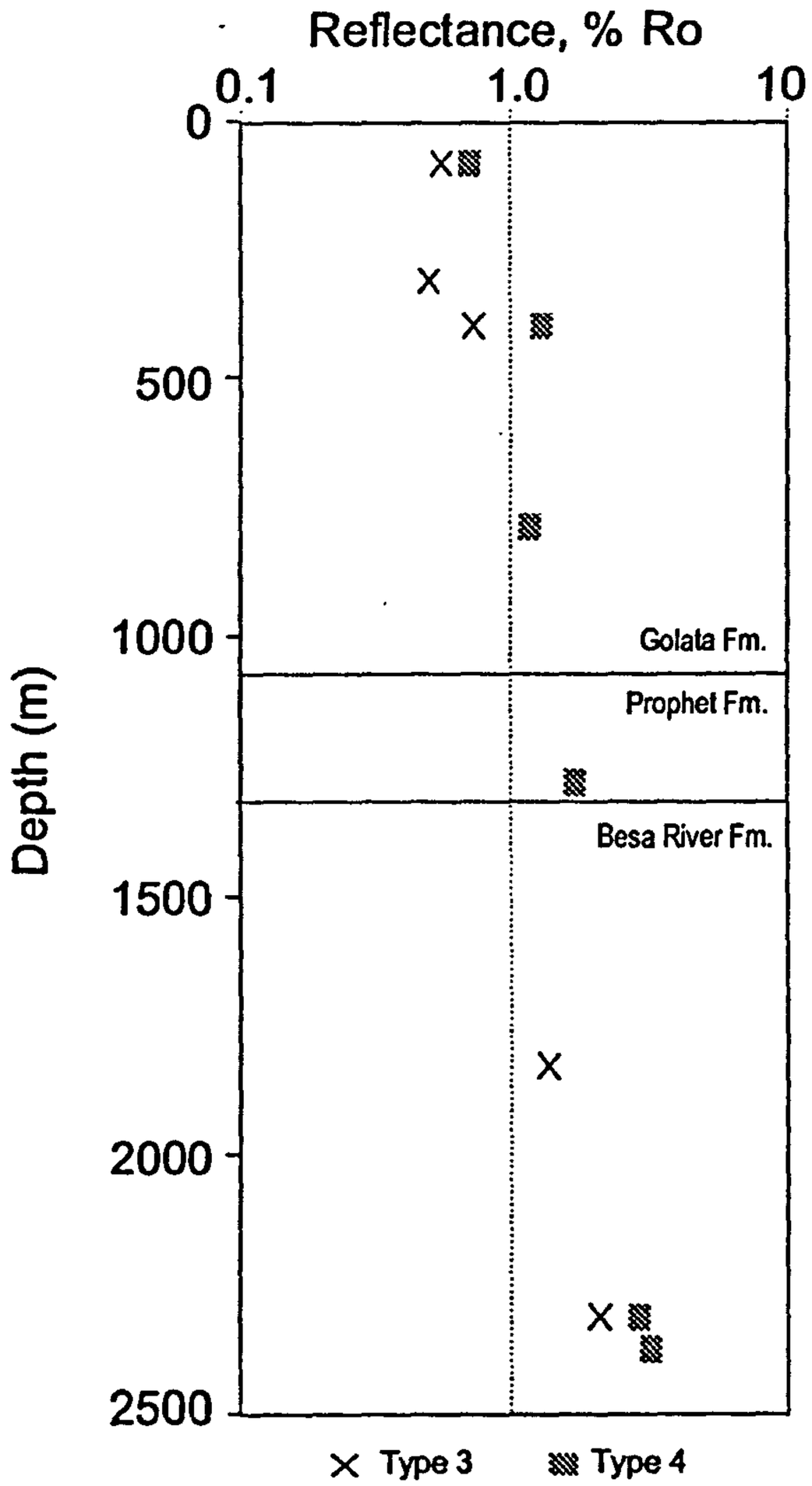

Figure D15 Bitumen reflectance - depth profiles for the Pan Am Kotanneelee 0-67 section; a) linear; b) semilog.

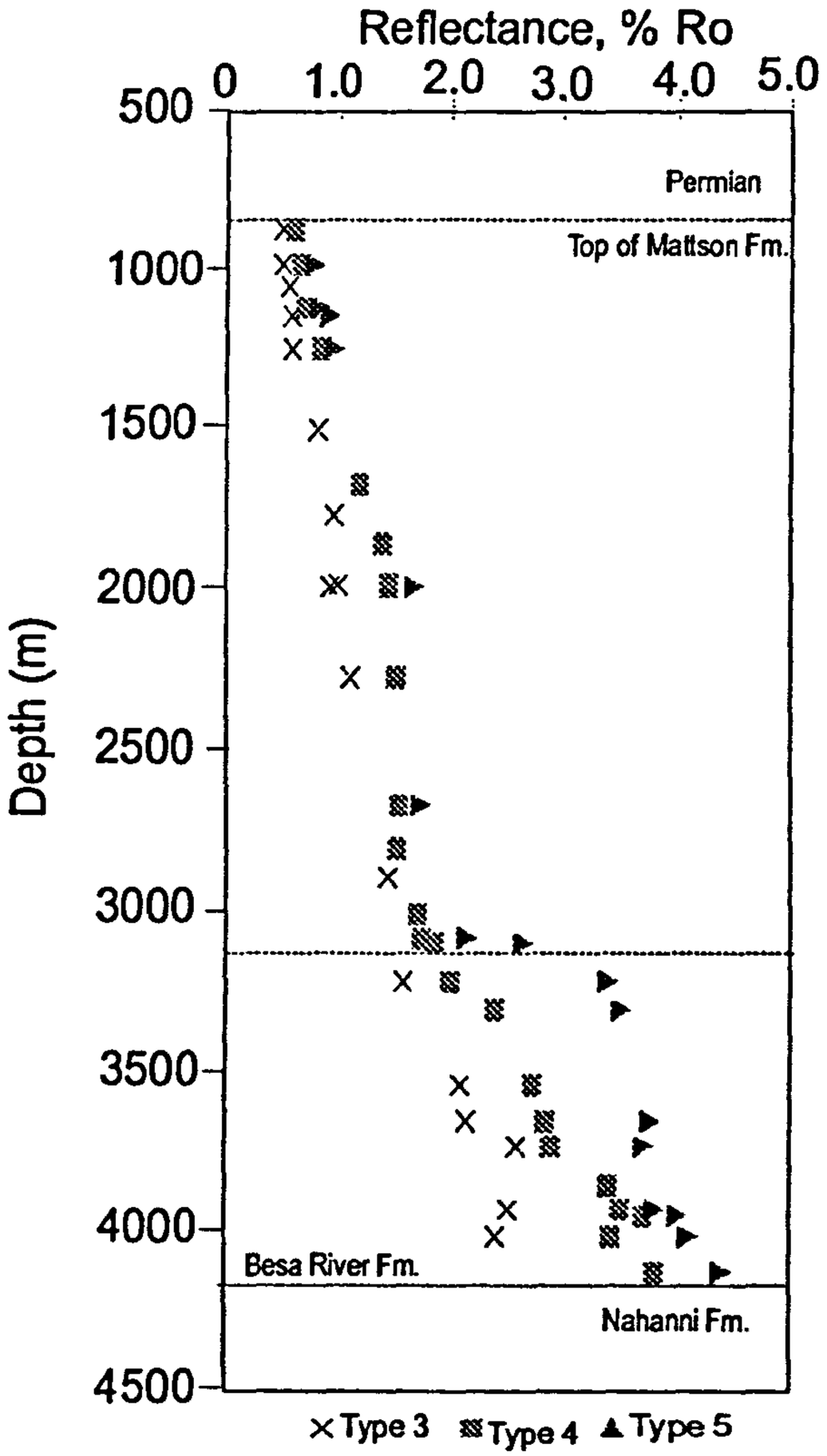

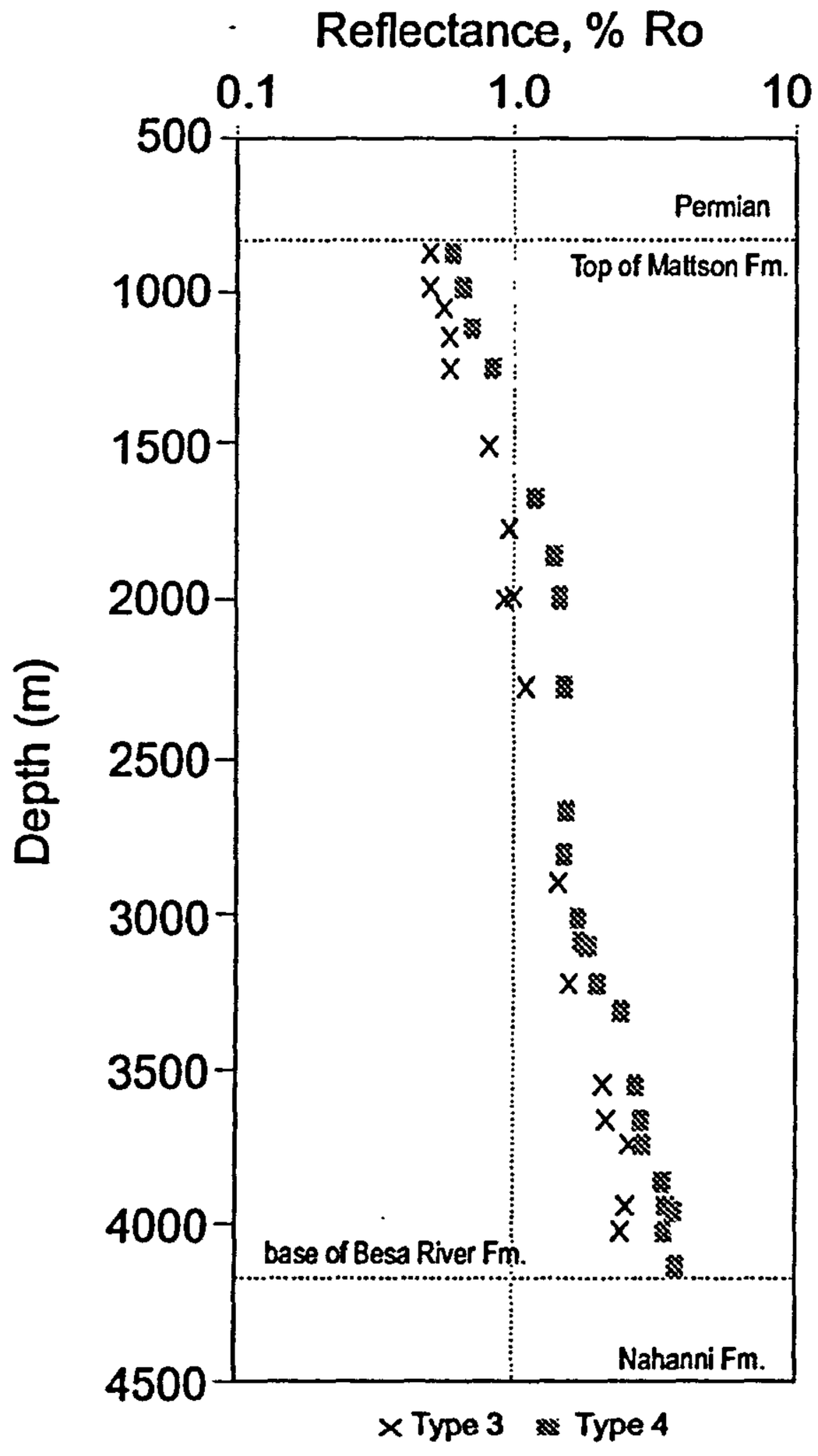

Figure D16 Bitumen reflectance - depth profiles for the Pan Am Beaver River G-01 section; a) linear; b) semilog.

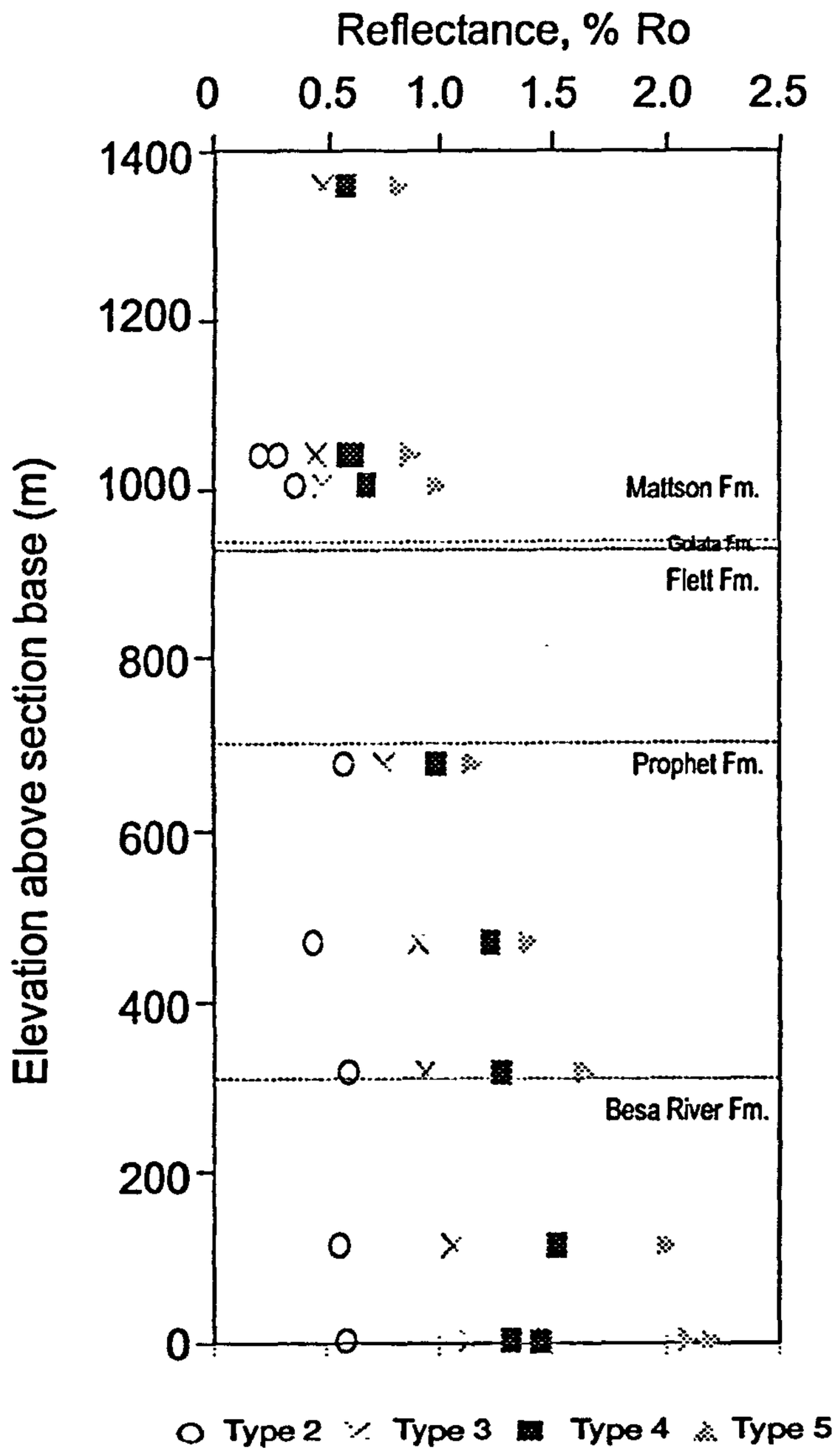

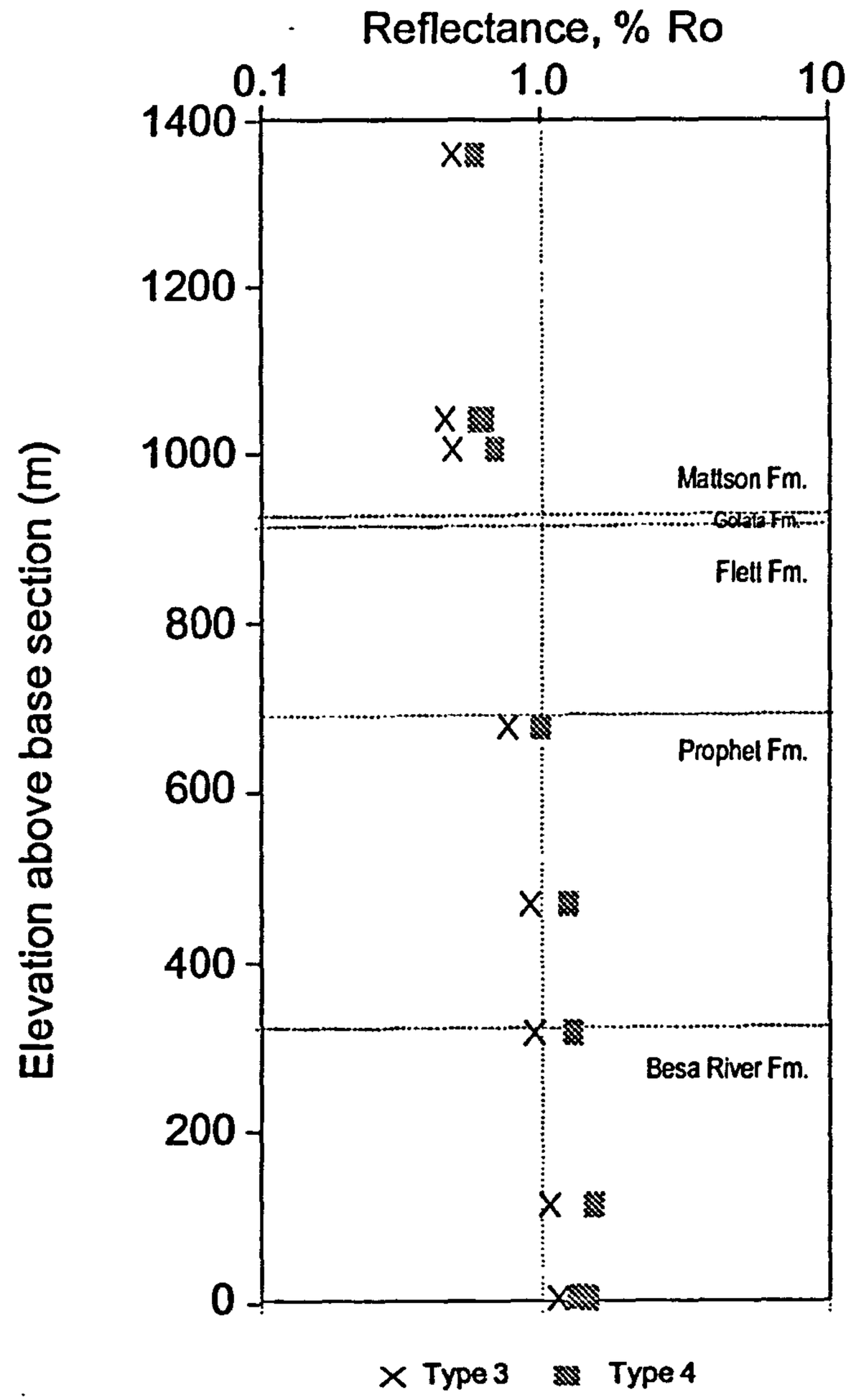

Figure D17 Bitumen reflectance - depth plots for the Clausen Creek section; a) linear; b) semilog.

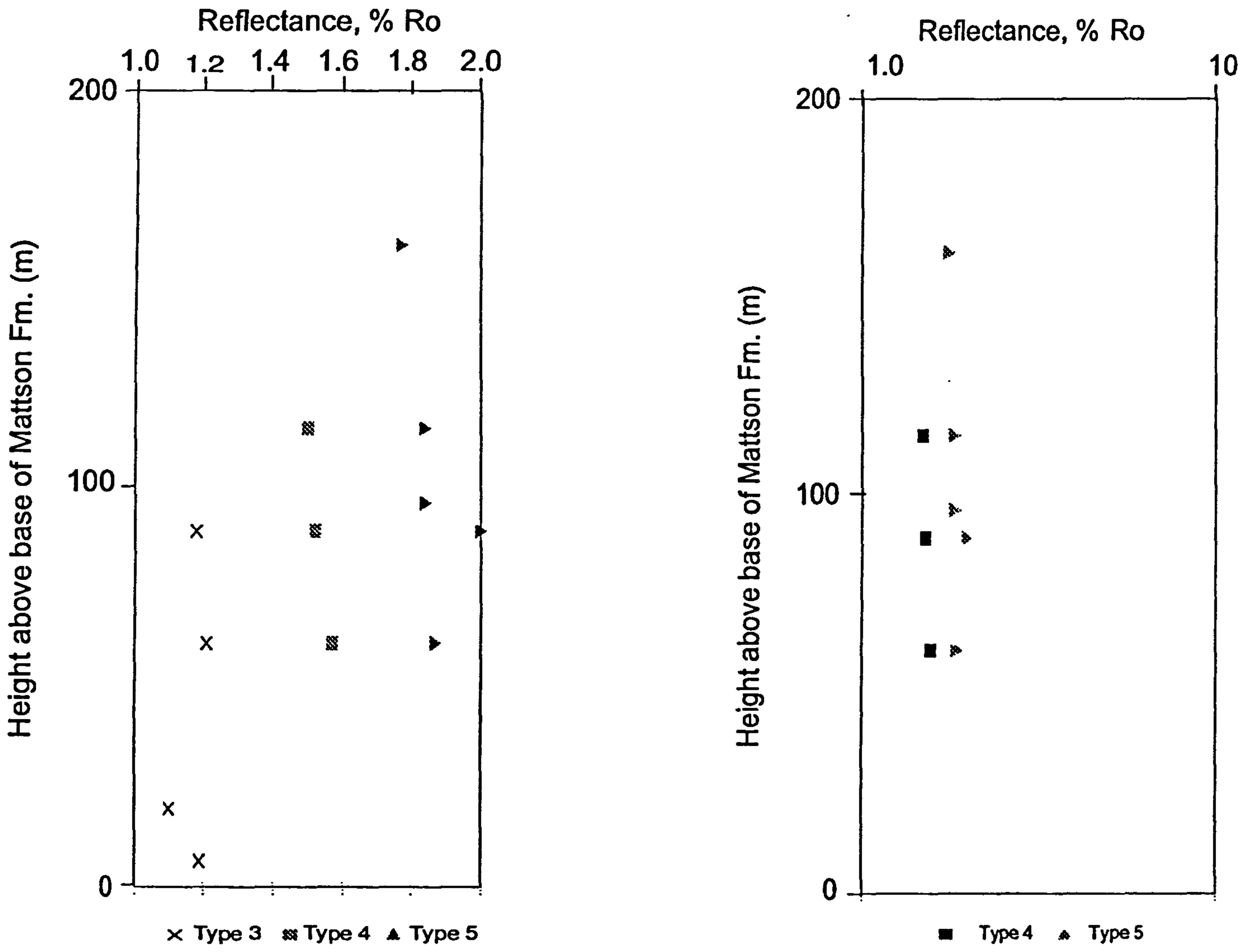

Figure D18 Bitumen reflectance - depth plots for the Tika Creek section; a) linear; b) semilog.

APPENDIX E
Basin modeling files

Input files for "*Burial*" modeling program

BURIAL 3a Input file: Imperial Island River.age
(input data shown in bold type)

Age 1	**415**	Base of sequence	
Age 2	**401**	Granite wash (regolith) deposition	
Age 3	**392**	Chinchaga	Eifelian
Age 4	**386**	Keg River	Eifelian-Givetian
		Evie Mbr	
Age 5	**380**	Mid Devonian Sh/Lms(?Sulphur Point)	late Givetian
Age 6	**377**	Slave Point	Late Givetian
Age 7	**373**	Muskwa	
		Fort Simpson	Frasnian
Age 8	**370**	Jean Marie	Late Frasnian
Age 9	**369**	Redknife	
Age 10	**367**	Kakisa	Fammenian
		Trout River	
Age 11	**365**	Tetcho	Fammenian
Age 12	**363**	Kotcho	Fammenian
Age 13	**353**	Exshaw	late Fammenian
		Banff	-T1
Age 14	**350**	Rundle-part remainig (Pekisko)	Tournasian -T2
Age 15	**347**	Rundle-part eroded	
		(at Sub Cret Unconformity)	Tournasian -T3
Age 16	**346**	Rundle deposition-part eroded	
		(At Sub-permian Unconformity)	Tournasian-T3
Age 17	**330**	Mattson	Serphukovian
Age 18	**295**	Sub-Permian Unconformity	
		-Mattson erosion	
Age 19	**290**	Sub-Permian Unconformity	
		-Rundle erosion	
Age 20	**280**	Kindle	Ass-Sak-Art
Age 21	**262**	Fantasque	Guad (Road-War)
Age 22	**250**	Sub-Triassic Unconformity	
		-Fantasque erosion	
Age 23	**230**	Toad-Grayling	Scythian-Norian
Age 24	**205**	Sub-Cretaceous unconformity	
		Toad-Grayling ersosion	
Age 25	**190**	Sub-Cretaceous unconformity	
		Kindle erosion	
Age 26	**185**	Sub-Cretaceous unconformity	
		Rundle erosion	
Age 27	**112**	Buckinghorse	Early-mid Albian
Age 28	**108**	Sikanni	M. Albian
Age 29	**102**	Sully	Late Albian
Age 30	**96**	Dunvegan deposition-part remainimg	M-Late Cenomanian
Age 31	**95**	Dunvegan deposition-part eroded	
Age 32	**15**	Kotaneelee	Santon-Campaignian
Age 33	**71**	Wapiti	Maastrichtian
Age 34	**65**	Sub-Tertiary unconformity	
		-Wapiti erosion	
Age 35	**60**	Sub-Tertiary unconformity	
		-Kotaneelee erosion	
Age 36	**40**	Sub-Tertiary Unconformity	
		-Dunvegan erosion	
Age 37	**2**	Quaternary deposition	

BURIAL 3a Input File : Imperial Island River No. 1.

AGE #	Event	T/F	Thickness (m)		Seq #
37	Quaternary deposition	T	020.0	38	age 37
36	Sub Tertiary unconformity - Dunvegan erosion	T	00.00	38	age 36
35	Sub-Tertiary Unconformity -Kotaneelee erosion	T	00.00	38	age 35
34	Sub-Tertiary Unconformity -Wapiti erosion	T	00.00	38	age 34
33	Wapiti deposition	F	200.00	34	age 33
32	Kotaneelee deposition	F	200.00	35	age 32
31	Dunvegan deposit.-part eroded at Sub-Tertiary Unconform	F	084.00	36	age 31
30	Dunvegan deposit.-part remain	T	166.00	38	age 30
29	Sully deposition	T	177.00	38	age 29
28	Sikanni deposition	T	085.00	38	age 28
27	Buckinghorse deposition	T	197.5	38	age 27
26	Sub-Cretaceous Unconformity -Rundle erosion	T	000.00	38	age 26
25	Sub-Cretaceous Unconformity -Kindle erosion	T	000.00	38	age 25
24	Sub-Cretaceous Unconformity -Toad-Grayling erosion	T	000.00	38	age 24
23	Toad-Grayling deposition	F	140.00	24	age 23
22	Sub-Triassic unconformity -Fantasque erosion	T	000.00	38	age 22
21	Fantasque deposition (eroded STriUnconf)	F	025.00	22	age 21
20	Kindle deposition (Eroded at STerUncon)	F	020.00	25	age 20
19	Sub-Permian Unconformity -Rundle erosion	T	000.00	38	age 19
18	Sub-Permian Unconformity -Mattson erosion	T	000.00	38	age 18
17	Mattson deposition (eroded at SPerm unconf)	F	150.00	18	age 17
16	Rundle deposition-part eroded (at Sub-Permian Unconformity)	F	025.00	19	age 16
15	Rundle Gp deposition-part eroded (at Sub-Cretaceous Unconformity)	F	310.00	26	age 15
14	Rundle Gp deposition-part remaining	T	003.00	38	Age 14
13	Banff+Exshaw deposition	T	370.00	38	age 13
12	Kotcho deposition	T	212.5	38	age 12
11	Tetcho depisition	T	076.00	38	age 11
10	Trout River +Kakisa deposition	T	672.00	38	age 10
9	Redkife deposition	T	140.20	38	age 9
8	Jean Marie deposition	T	15.20	38	age 8
7	Fort Simpson + Muskwa deposition	T	530.00	38	age 7
6	Slave Point deposition	T	117.00	38	age 6
5	Mid Devonian Sh/Lsts	T	106.00	38	age 5
4	EvieMbr + Keg River deposition	T	090.5	38	age 4
3	Chinchaga deposition	T	078.00	38	age 3
2	Granite wash deposition	T	025.00	38	age 2
1	Base of Sequence	T	000.00	38	age 1

BURIAL 3a Input File: Imperial Island River.Ro
(input data shown in bold type)

Imperial Island River No.1
N60 09' 29" W121 08' 16"

Samp No.	Depth		Rock	Stratigraphy Med Ro-amorphous			VRo	Depth
C186751-	ft	m	fm	mean	st dev	n	calc*	m
1994	1994C*	607.77	Cretac	0.60	0.05	11	**0.77**	**607.77**
2134	2134C	650.44	Banff					**650.44**
2140	2140C	652.27	Banff					**652.27**
2310	2310C	704.08	Banff	0.79	0.01	3	**0.89**	**704.09**
2456	2456C	748.59	Banff					**748.59**
2747	2747C	837.28	Banff	0.86	0.08	6	**0.93**	**837.29**
2760	2760C	841.24	Banff	0.86	0.05	10	**0.93**	**841.25**
3012	3012C	918.06	Banff	0.86	0.04	3	**0.93**	**918.06**
3275	3275C	998.22	Banff	0.88	0.02	2	**0.94**	**998.22**
3288	3288C	1002.18	Banff	0.88	0.02	2	**0.94**	**1002.18**
3465	3465C	1056.13	Exshaw	0.82	0.02	2	**0.91**	**1056.13**
3486	3486C	1057.65	Kotcho	0.85	0.05	6	**0.93**	**1062.53**
3797	3797-3806C	1157.32-1160.07	Kotcho	1.09	0.03	5	**1.07**	**1157.33**
4010	4098-4118C	1249.07-1255.17	Kotcho	1.10	0.03	3	**1.08**	**1222.25**
4102	4101-03C	1249.98-1250.59	Kotcho					**1250.29**
4426	4426C	1349.04	Trout River	1.11			**1.09**	**1349.04**
4818	4818C	1468.53	Redknife					**1468.53**
5418	5409-27C	1648.66-1654.14	FtSimpson	1.24	0.05	7	**1.17**	**1651.41**
5587.3	5587.3C	1703.07	FtSimpson	1.32	0.04	6	**1.22**	**1703.01**
5590.3	5590.3C	1703.92	FtSimpson	1.37	0.10	6	**1.25**	**1703.92**
5899	5899C	1790.01	FtSimpson					**1798.02**
6240	6240C	1901.95	FtSimpson	1.46	0.05	4	**1.30**	**1901.95**
6400	6400C	1950.72	FtSimpson	1.50	0.00	1	**1.33**	**1950.72**
6619	6614-24C	2017.47-2019	FtSimpson					**2017.47**
6814	6814C	2076.91	FtSimpson	1.57	0.02	2	**1.37**	**2076.91**
6906	6902-6908C	2103.73-2105.55	Muskwa	1.63	0.09	11	**1.41**	**2104.95**

*after Jacob, 1985 : Vro=(BRo*0.618)+0.4

BURIAL 3A Input file: Imperial Island River.dat - Model 1

```
Imperial Island River No.1 G-50
M
0000.0 T 38 0.000 0.000 0.000 0.000 0.000 0.000 0.000 080.0 025.0  AGE1
0025.0 T 38 0.600 0.020 0.000 0.000 0.200 0.000 0.000 080.0 025.0  AGE2
0078.0 T 38 0.100 0.000 0.000 0.250 0.450 0.200 0.000 080.0 025.0  AGE3
0090.5 T 38 0.000 0.000 0.100 0.800 0.100 0.000 0.000 080.0 025.0  AGE4
0106.0 T 38 0.000 0.000 0.100 0.900 0.000 0.000 0.000 080.0 025.0  AGE5
0117.0 T 38 0.000 0.000 0.200 0.800 0.000 0.000 0.000 150.0 025.0  AGE6
0530.0 T 38 0.700 0.050 0.000 0.100 0.150 0.000 0.000 150.0 025.0  AGE7
0015.2 T 38 0.000 0.000 0.650 0.350 0.000 0.000 0.000 150.0 025.0  AGE8
0140.2 T 38 0.700 0.000 0.000 0.050 0.200 0.000 0.000 150.0 025.0  AGE9
0672.0 T 38 0.100 0.600 0.100 0.000 0.200 0.000 0.000 150.0 025.0  AGE10
0076.0 T 38 0.000 0.000 0.850 0.150 0.000 0.000 0.000 150.0 025.0  AGE11
0212.5 T 38 0.650 0.000 0.350 0.000 0.000 0.000 0.000 150.0 025.0  AGE12
0370.0 T 38 0.600 0.000 0.300 0.000 0.100 0.000 0.000 140.0 025.0  AGE13
0003.0 T 38 0.150 0.000 0.850 0.000 0.000 0.000 0.000 140.0 025.0  AGE14
0310.0 F 26 0.000 0.000 0.400 0.000 0.000 0.000 0.600 140.0 025.0  AGE15
0025.0 F 19 0.500 0.000 0.400 0.000 0.000 0.000 0.100 120.0 025.0  AGE16
0150.0 F 18 0.150 0.600 0.050 0.000 0.200 0.000 0.000 120.0 025.0  AGE17
0000.0 T 38 0.000 0.000 0.000 0.000 0.000 0.000 0.000 120.0 025.0  AGE18
0000.0 T 38 0.000 0.000 0.000 0.000 0.000 0.000 0.000 100.0 025.0  AGE19
0020.0 F 25 0.250 0.500 0.000 0.000 0.250 0.000 0.000 100.0 025.0  AGE20
0025.0 F 22 0.500 0.000 0.000 0.000 0.000 0.000 0.500 100.0 025.0  AGE21
0000.0 T 38 0.000 0.000 0.000 0.000 0.000 0.000 0.000 080.0 025.0  AGE22
0140.0 F 24 0.200 0.000 0.000 0.100 0.700 0.000 0.000 080.0 025.0  AGE23
0000.0 T 38 0.000 0.000 0.000 0.000 0.000 0.000 0.000 080.0 025.0  AGE24
0000.0 T 38 0.000 0.000 0.000 0.000 0.000 0.000 0.000 080.0 025.0  AGE25
0000.0 T 38 0.000 0.000 0.000 0.000 0.000 0.000 0.000 080.0 025.0  AGE26
0197.5 T 38 0.800 0.000 0.000 0.000 0.200 0.000 0.000 080.0 025.0  AGE27
0085.0 T 38 0.000 1.000 0.000 0.000 0.000 0.000 0.000 080.0 015.0  AGE28
0177.0 T 38 0.500 0.200 0.000 0.000 0.300 0.000 0.000 060.0 015.0  AGE29
0166.0 T 38 0.000 1.000 0.000 0.000 0.000 0.000 0.000 060.0 015.0  AGE30
0084.0 F 36 0.000 1.000 0.000 0.000 0.000 0.000 0.000 060.0 015.0  AGE31
0400.0 F 35 0.700 0.150 0.000 0.000 0.150 0.000 0.000 060.0 015.0  AGE32
0350.0 F 34 0.000 0.500 0.000 0.000 0.500 0.000 0.000 060.0 015.0  AGE33
0000.0 T 38 0.000 0.000 0.000 0.000 0.000 0.000 0.000 060.0 015.0  AGE34
0000.0 T 38 0.000 0.000 0.000 0.000 0.000 0.000 0.000 080.0 010.0  AGE35
0000.0 T 38 0.000 0.000 0.000 0.000 0.000 0.000 0.000 080.0 010.0  AGE36
0020.0 T 38 0.000 0.500 0.000 0.000 0.500 0.000 0.000 080.0 010.0  AGE37
```

Burial 3a Input file: Imperial Island River No.1 G-50.dat - Model 2

M
0000.0 T 38 0.000 0.000 0.000 0.000 0.000 0.000 0.000 150.0 025.0 AGE1
0025.0 T 38 0.600 0.020 0.000 0.000 0.200 0.000 0.000 150.0 025.0 AGE2
0078.0 T 38 0.100 0.000 0.000 0.250 0.450 0.200 0.000 150.0 025.0 AGE3
0090.5 T 38 0.000 0.000 0.100 0.800 0.100 0.000 0.000 150.0 025.0 AGE4
0106.0 T 38 0.000 0.000 0.100 0.900 0.000 0.000 0.000 150.0 025.0 AGE5
0117.0 T 38 0.000 0.000 0.200 0.800 0.000 0.000 0.000 150.0 025.0 AGE6
0530.0 T 38 0.700 0.050 0.000 0.100 0.150 0.000 0.000 150.0 025.0 AGE7
0015.2 T 38 0.000 0.000 0.650 0.350 0.000 0.000 0.000 150.0 025.0 AGE8
0140.2 T 38 0.700 0.000 0.000 0.050 0.200 0.000 0.000 150.0 025.0 AGE9
0672.0 T 38 0.100 0.600 0.100 0.000 0.200 0.000 0.000 150.0 025.0 AGE10
0076.0 T 38 0.000 0.000 0.850 0.150 0.000 0.000 0.000 150.0 025.0 AGE11
0212.5 T 38 0.650 0.000 0.350 0.000 0.000 0.000 0.000 150.0 025.0 AGE12
0370.0 T 38 0.600 0.000 0.300 0.000 0.100 0.000 0.000 150.0 025.0 AGE13
0003.0 T 38 0.150 0.000 0.850 0.000 0.000 0.000 0.000 150.0 025.0 AGE14
0310.0 F 26 0.000 0.000 0.400 0.000 0.000 0.000 0.600 150.0 025.0 AGE15
0025.0 F 19 0.500 0.000 0.400 0.000 0.000 0.000 0.100 150.0 025.0 AGE16
0150.0 F 18 0.150 0.600 0.050 0.000 0.200 0.000 0.000 150.0 025.0 AGE17
0000.0 T 38 0.000 0.000 0.000 0.000 0.000 0.000 0.000 150.0 025.0 AGE18
0000.0 T 38 0.000 0.000 0.000 0.000 0.000 0.000 0.000 150.0 025.0 AGE19
0020.0 F 25 0.250 0.500 0.000 0.000 0.250 0.000 0.000 150.0 025.0 AGE20
0025.0 F 22 0.500 0.000 0.000 0.000 0.000 0.000 0.500 100.0 025.0 AGE21
0000.0 T 38 0.000 0.000 0.000 0.000 0.000 0.000 0.000 080.0 025.0 AGE22
0140.0 F 24 0.200 0.000 0.000 0.100 0.700 0.000 0.000 080.0 025.0 AGE23
0000.0 T 38 0.000 0.000 0.000 0.000 0.000 0.000 0.000 080.0 025.0 AGE24
0000.0 T 38 0.000 0.000 0.000 0.000 0.000 0.000 0.000 080.0 025.0 AGE25
0000.0 T 38 0.000 0.000 0.000 0.000 0.000 0.000 0.000 080.0 025.0 AGE26
0197.5 T 38 0.800 0.000 0.000 0.000 0.200 0.000 0.000 080.0 025.0 AGE27
0085.0 T 38 0.000 1.000 0.000 0.000 0.000 0.000 0.000 080.0 015.0 AGE28
0177.0 T 38 0.500 0.200 0.000 0.000 0.300 0.000 0.000 060.0 015.0 AGE29
0166.0 T 38 0.000 1.000 0.000 0.000 0.000 0.000 0.000 060.0 015.0 AGE30
0084.0 F 36 0.000 1.000 0.000 0.000 0.000 0.000 0.000 060.0 015.0 AGE31
0400.0 F 35 0.700 0.150 0.000 0.000 0.150 0.000 0.000 060.0 015.0 AGE32
0350.0 F 34 0.000 0.500 0.000 0.000 0.500 0.000 0.000 060.0 015.0 AGE33
0000.0 T 38 0.000 0.000 0.000 0.000 0.000 0.000 0.000 060.0 015.0 AGE34
0000.0 T 38 0.000 0.000 0.000 0.000 0.000 0.000 0.000 080.0 010.0 AGE35
0000.0 T 38 0.000 0.000 0.000 0.000 0.000 0.000 0.000 080.0 010.0 AGE36
0020.0 T 38 0.000 0.500 0.000 0.000 0.500 0.000 0.000 080.0 010.0 AGE37

Burial 3a: Input file - Imperial Island River No.1 G-50.dat - Model 3

M
0000.0 T 38 0.000 0.000 0.000 0.000 0.000 0.000 0.000 150.0 025.0 AGE1
0025.0 T 38 0.600 0.020 0.000 0.000 0.200 0.000 0.000 150.0 025.0 AGE2
0078.0 T 38 0.100 0.000 0.000 0.250 0.450 0.200 0.000 150.0 025.0 AGE3
0090.5 T 38 0.000 0.000 0.100 0.800 0.100 0.000 0.000 150.0 025.0 AGE4
0106.0 T 38 0.000 0.000 0.100 0.900 0.000 0.000 0.000 150.0 025.0 AGE5
0117.0 T 38 0.000 0.000 0.200 0.800 0.000 0.000 0.000 150.0 025.0 AGE6
0530.0 T 38 0.700 0.050 0.000 0.100 0.150 0.000 0.000 150.0 025.0 AGE7
0015.2 T 38 0.000 0.000 0.650 0.350 0.000 0.000 0.000 150.0 025.0 AGE8
0140.2 T 38 0.700 0.000 0.000 0.050 0.200 0.000 0.000 150.0 025.0 AGE9
0672.0 T 38 0.100 0.600 0.100 0.000 0.200 0.000 0.000 150.0 025.0 AGE10
0076.0 T 38 0.000 0.000 0.850 0.150 0.000 0.000 0.000 150.0 025.0 AGE11
0212.5 T 38 0.650 0.000 0.350 0.000 0.000 0.000 0.000 150.0 025.0 AGE12
0370.0 T 38 0.600 0.000 0.300 0.000 0.100 0.000 0.000 150.0 025.0 AGE13
0003.0 T 38 0.150 0.000 0.850 0.000 0.000 0.000 0.000 150.0 025.0 AGE14
0310.0 F 26 0.000 0.000 0.400 0.000 0.000 0.000 0.600 150.0 025.0 AGE15
0025.0 F 19 0.500 0.000 0.400 0.000 0.000 0.000 0.100 150.0 025.0 AGE16
0150.0 F 18 0.150 0.600 0.050 0.000 0.200 0.000 0.000 150.0 025.0 AGE17
0000.0 T 38 0.000 0.000 0.000 0.000 0.000 0.000 0.000 150.0 025.0 AGE18
0000.0 T 38 0.000 0.000 0.000 0.000 0.000 0.000 0.000 150.0 025.0 AGE19
0020.0 F 25 0.250 0.500 0.000 0.000 0.250 0.000 0.000 150.0 025.0 AGE20
0025.0 F 22 0.500 0.000 0.000 0.000 0.000 0.000 0.500 120.0 025.0 AGE21
0000.0 T 38 0.000 0.000 0.000 0.000 0.000 0.000 0.000 120.0 025.0 AGE22
0140.0 F 24 0.200 0.000 0.000 0.100 0.700 0.000 0.000 120.0 025.0 AGE23
0000.0 T 38 0.000 0.000 0.000 0.000 0.000 0.000 0.000 120.0 025.0 AGE24
0000.0 T 38 0.000 0.000 0.000 0.000 0.000 0.000 0.000 120.0 025.0 AGE25
0000.0 T 38 0.000 0.000 0.000 0.000 0.000 0.000 0.000 120.0 025.0 AGE26
0197.5 T 38 0.800 0.000 0.000 0.000 0.200 0.000 0.000 080.0 025.0 AGE27
0085.0 T 38 0.000 1.000 0.000 0.000 0.000 0.000 0.000 080.0 015.0 AGE28
0177.0 T 38 0.500 0.200 0.000 0.000 0.300 0.000 0.000 060.0 015.0 AGE29
0166.0 T 38 0.000 1.000 0.000 0.000 0.000 0.000 0.000 060.0 015.0 AGE30
0084.0 F 36 0.000 1.000 0.000 0.000 0.000 0.000 0.000 060.0 015.0 AGE31
0400.0 F 35 0.700 0.150 0.000 0.000 0.150 0.000 0.000 060.0 015.0 AGE32
0350.0 F 34 0.000 0.500 0.000 0.000 0.500 0.000 0.000 060.0 015.0 AGE33
0000.0 T 38 0.000 0.000 0.000 0.000 0.000 0.000 0.000 060.0 015.0 AGE34
0000.0 T 38 0.000 0.000 0.000 0.000 0.000 0.000 0.000 080.0 010.0 AGE35
0000.0 T 38 0.000 0.000 0.000 0.000 0.000 0.000 0.000 080.0 010.0 AGE36
0020.0 T 38 0.000 0.500 0.000 0.000 0.500 0.000 0.000 080.0 010.0 AGE37

Burial 3a Input file: Imperial Island River No.1 G-50.dat Model 4
M

0000.0 T 38 0.000 0.000 0.000 0.000 0.000 0.000 0.000 150.0 025.0 AGE1
0025.0 T 38 0.600 0.020 0.000 0.000 0.200 0.000 0.000 150.0 025.0 AGE2
0078.0 T 38 0.100 0.000 0.000 0.250 0.450 0.200 0.000 150.0 025.0 AGE3
0090.5 T 38 0.000 0.000 0.100 0.800 0.100 0.000 0.000 150.0 025.0 AGE4
0106.0 T 38 0.000 0.000 0.100 0.900 0.000 0.000 0.000 150.0 025.0 AGE5
0117.0 T 38 0.000 0.000 0.200 0.800 0.000 0.000 0.000 150.0 025.0 AGE6
0530.0 T 38 0.700 0.050 0.000 0.100 0.150 0.000 0.000 150.0 025.0 AGE7
0015.2 T 38 0.000 0.000 0.650 0.350 0.000 0.000 0.000 150.0 025.0 AGE8
0140.2 T 38 0.700 0.000 0.000 0.050 0.200 0.000 0.000 150.0 025.0 AGE9
0672.0 T 38 0.100 0.600 0.100 0.000 0.200 0.000 0.000 150.0 025.0 AGE10
0076.0 T 38 0.000 0.000 0.850 0.150 0.000 0.000 0.000 150.0 025.0 AGE11
0212.5 T 38 0.650 0.000 0.350 0.000 0.000 0.000 0.000 150.0 025.0 AGE12
0370.0 T 38 0.600 0.000 0.300 0.000 0.100 0.000 0.000 150.0 025.0 AGE13
0003.0 T 38 0.150 0.000 0.850 0.000 0.000 0.000 0.000 150.0 025.0 AGE14
0310.0 F 26 0.000 0.000 0.400 0.000 0.000 0.000 0.600 150.0 025.0 AGE15
0025.0 F 19 0.500 0.000 0.400 0.000 0.000 0.000 0.100 150.0 025.0 AGE16
0150.0 F 18 0.150 0.600 0.050 0.000 0.200 0.000 0.000 150.0 025.0 AGE17
0000.0 T 38 0.000 0.000 0.000 0.000 0.000 0.000 0.000 150.0 025.0 AGE18
0000.0 T 38 0.000 0.000 0.000 0.000 0.000 0.000 0.000 150.0 025.0 AGE19
0020.0 F 25 0.250 0.500 0.000 0.000 0.250 0.000 0.000 150.0 025.0 AGE20
0025.0 F 22 0.500 0.000 0.000 0.000 0.000 0.000 0.500 120.0 025.0 AGE21
0000.0 T 38 0.000 0.000 0.000 0.000 0.000 0.000 0.000 120.0 025.0 AGE22
0140.0 F 24 0.200 0.000 0.000 0.100 0.700 0.000 0.000 120.0 025.0 AGE23
0000.0 T 38 0.000 0.000 0.000 0.000 0.000 0.000 0.000 120.0 025.0 AGE24
0000.0 T 38 0.000 0.000 0.000 0.000 0.000 0.000 0.000 120.0 025.0 AGE25
0000.0 T 38 0.000 0.000 0.000 0.000 0.000 0.000 0.000 120.0 025.0 AGE26
0197.5 T 38 0.800 0.000 0.000 0.000 0.200 0.000 0.000 100.0 025.0 AGE27
0085.0 T 38 0.000 1.000 0.000 0.000 0.000 0.000 0.000 100.0 015.0 AGE28
0177.0 T 38 0.500 0.200 0.000 0.000 0.300 0.000 0.000 100.0 015.0 AGE29
0166.0 T 38 0.000 1.000 0.000 0.000 0.000 0.000 0.000 100.0 015.0 AGE30
0084.0 F 36 0.000 1.000 0.000 0.000 0.000 0.000 0.000 100.0 015.0 AGE31
0400.0 F 35 0.700 0.150 0.000 0.000 0.150 0.000 0.000 100.0 015.0 AGE32
0350.0 F 34 0.000 0.500 0.000 0.000 0.500 0.000 0.000 100.0 015.0 AGE33
0000.0 T 38 0.000 0.000 0.000 0.000 0.000 0.000 0.000 100.0 015.0 AGE34
0000.0 T 38 0.000 0.000 0.000 0.000 0.000 0.000 0.000 100.0 010.0 AGE35
0000.0 T 38 0.000 0.000 0.000 0.000 0.000 0.000 0.000 100.0 010.0 AGE36
0020.0 T 38 0.000 0.500 0.000 0.000 0.500 0.000 0.000 085.0 010.0 AGE37

Burial 3a Input file: Imperial Island River No.1 G-50.dat Model 5

M
0000.0 T 38 0.000 0.000 0.000 0.000 0.000 0.000 0.000 200.0 025.0 AGE1
0025.0 T 38 0.600 0.020 0.000 0.000 0.200 0.000 0.000 200.0 025.0 AGE2
0078.0 T 38 0.100 0.000 0.000 0.250 0.450 0.200 0.000 200.0 025.0 AGE3
0090.5 T 38 0.000 0.000 0.100 0.800 0.100 0.000 0.000 200.0 025.0 AGE4
0106.0 T 38 0.000 0.000 0.100 0.900 0.000 0.000 0.000 200.0 025.0 AGE5
0117.0 T 38 0.000 0.000 0.200 0.800 0.000 0.000 0.000 200.0 025.0 AGE6
0530.0 T 38 0.700 0.050 0.000 0.100 0.150 0.000 0.000 200.0 025.0 AGE7
0015.2 T 38 0.000 0.000 0.650 0.350 0.000 0.000 0.000 200.0 025.0 AGE8
0140.2 T 38 0.700 0.000 0.000 0.050 0.200 0.000 0.000 200.0 025.0 AGE9
0672.0 T 38 0.100 0.600 0.100 0.000 0.200 0.000 0.000 200.0 025.0 AGE10
0076.0 T 38 0.000 0.000 0.850 0.150 0.000 0.000 0.000 200.0 025.0 AGE11
0212.5 T 38 0.650 0.000 0.350 0.000 0.000 0.000 0.000 200.0 025.0 AGE12
0370.0 T 38 0.600 0.000 0.300 0.000 0.100 0.000 0.000 150.0 025.0 AGE13
0003.0 T 38 0.150 0.000 0.850 0.000 0.000 0.000 0.000 150.0 025.0 AGE14
0310.0 F 26 0.000 0.000 0.400 0.000 0.000 0.000 0.600 150.0 025.0 AGE15
0025.0 F 19 0.500 0.000 0.400 0.000 0.000 0.000 0.100 150.0 025.0 AGE16
0150.0 F 18 0.150 0.600 0.050 0.000 0.200 0.000 0.000 150.0 025.0 AGE17
0000.0 T 38 0.000 0.000 0.000 0.000 0.000 0.000 0.000 150.0 025.0 AGE18
0000.0 T 38 0.000 0.000 0.000 0.000 0.000 0.000 0.000 150.0 025.0 AGE19
0020.0 F 25 0.250 0.500 0.000 0.000 0.250 0.000 0.000 150.0 025.0 AGE20
0025.0 F 22 0.500 0.000 0.000 0.000 0.000 0.000 0.500 120.0 025.0 AGE21
0000.0 T 38 0.000 0.000 0.000 0.000 0.000 0.000 0.000 120.0 025.0 AGE22
0140.0 F 24 0.200 0.000 0.000 0.100 0.700 0.000 0.000 120.0 025.0 AGE23
0000.0 T 38 0.000 0.000 0.000 0.000 0.000 0.000 0.000 120.0 025.0 AGE24
0000.0 T 38 0.000 0.000 0.000 0.000 0.000 0.000 0.000 120.0 025.0 AGE25
0000.0 T 38 0.000 0.000 0.000 0.000 0.000 0.000 0.000 120.0 025.0 AGE26
0197.5 T 38 0.800 0.000 0.000 0.000 0.200 0.000 0.000 100.0 025.0 AGE27
0085.0 T 38 0.000 1.000 0.000 0.000 0.000 0.000 0.000 100.0 015.0 AGE28
0177.0 T 38 0.500 0.200 0.000 0.000 0.300 0.000 0.000 100.0 015.0 AGE29
0166.0 T 38 0.000 1.000 0.000 0.000 0.000 0.000 0.000 100.0 015.0 AGE30
0084.0 F 36 0.000 1.000 0.000 0.000 0.000 0.000 0.000 100.0 015.0 AGE31
0400.0 F 35 0.700 0.150 0.000 0.000 0.150 0.000 0.000 100.0 015.0 AGE32
0350.0 F 34 0.000 0.500 0.000 0.000 0.500 0.000 0.000 100.0 015.0 AGE33
0000.0 T 38 0.000 0.000 0.000 0.000 0.000 0.000 0.000 100.0 015.0 AGE34
0000.0 T 38 0.000 0.000 0.000 0.000 0.000 0.000 0.000 100.0 010.0 AGE35
0000.0 T 38 0.000 0.000 0.000 0.000 0.000 0.000 0.000 100.0 010.0 AGE36
0020.0 T 38 0.000 0.500 0.000 0.000 0.500 0.000 0.000 085.0 010.0 AGE37

Burial 3a Input file: Imperial Island River No.1 G-50.dat Model 6

M

0000.0 T 38 0.000 0.000 0.000 0.000 0.000 0.000 0.000 200.0 025.0 AGE1
0025.0 T 38 0.600 0.020 0.000 0.000 0.200 0.000 0.000 200.0 025.0 AGE2
0078.0 T 38 0.100 0.000 0.000 0.250 0.450 0.200 0.000 200.0 025.0 AGE3
0090.5 T 38 0.000 0.000 0.100 0.800 0.100 0.000 0.000 200.0 025.0 AGE4
0106.0 T 38 0.000 0.000 0.100 0.900 0.000 0.000 0.000 200.0 025.0 AGE5
0117.0 T 38 0.000 0.000 0.200 0.800 0.000 0.000 0.000 200.0 025.0 AGE6
0530.0 T 38 0.700 0.050 0.000 0.100 0.150 0.000 0.000 200.0 025.0 AGE7
0015.2 T 38 0.000 0.000 0.650 0.350 0.000 0.000 0.000 200.0 025.0 AGE8
0140.2 T 38 0.700 0.000 0.000 0.050 0.200 0.000 0.000 200.0 025.0 AGE9
0672.0 T 38 0.100 0.600 0.100 0.000 0.200 0.000 0.000 200.0 025.0 AGE10
0076.0 T 38 0.000 0.000 0.850 0.150 0.000 0.000 0.000 200.0 025.0 AGE11
0212.5 T 38 0.650 0.000 0.350 0.000 0.000 0.000 0.000 200.0 025.0 AGE12
0370.0 T 38 0.600 0.000 0.300 0.000 0.100 0.000 0.000 200.0 025.0 AGE13
0003.0 T 38 0.150 0.000 0.850 0.000 0.000 0.000 0.000 200.0 025.0 AGE14
0310.0 F 26 0.000 0.000 0.400 0.000 0.000 0.000 0.600 200.0 025.0 AGE15
0025.0 F 19 0.500 0.000 0.400 0.000 0.000 0.000 0.100 200.0 025.0 AGE16
0150.0 F 18 0.150 0.600 0.050 0.000 0.200 0.000 0.000 200.0 025.0 AGE17
0000.0 T 38 0.000 0.000 0.000 0.000 0.000 0.000 0.000 200.0 025.0 AGE18
0000.0 T 38 0.000 0.000 0.000 0.000 0.000 0.000 0.000 200.0 025.0 AGE19
0020.0 F 25 0.250 0.500 0.000 0.000 0.250 0.000 0.000 200.0 025.0 AGE20
0025.0 F 22 0.500 0.000 0.000 0.000 0.000 0.000 0.500 200.0 025.0 AGE21
0000.0 T 38 0.000 0.000 0.000 0.000 0.000 0.000 0.000 200.0 025.0 AGE22
0140.0 F 24 0.200 0.000 0.000 0.100 0.700 0.000 0.000 200.0 025.0 AGE23
0000.0 T 38 0.000 0.000 0.000 0.000 0.000 0.000 0.000 200.0 025.0 AGE24
0000.0 T 38 0.000 0.000 0.000 0.000 0.000 0.000 0.000 200.0 025.0 AGE25
0000.0 T 38 0.000 0.000 0.000 0.000 0.000 0.000 0.000 200.0 025.0 AGE26
0197.5 T 38 0.800 0.000 0.000 0.000 0.200 0.000 0.000 200.0 025.0 AGE27
0085.0 T 38 0.000 1.000 0.000 0.000 0.000 0.000 0.000 100.0 015.0 AGE28
0177.0 T 38 0.500 0.200 0.000 0.000 0.300 0.000 0.000 100.0 015.0 AGE29
0166.0 T 38 0.000 1.000 0.000 0.000 0.000 0.000 0.000 100.0 015.0 AGE30
0084.0 F 36 0.000 1.000 0.000 0.000 0.000 0.000 0.000 100.0 015.0 AGE31
0400.0 F 35 0.700 0.150 0.000 0.000 0.150 0.000 0.000 100.0 015.0 AGE32
0350.0 F 34 0.000 0.500 0.000 0.000 0.500 0.000 0.000 100.0 015.0 AGE33
0000.0 T 38 0.000 0.000 0.000 0.000 0.000 0.000 0.000 100.0 015.0 AGE34
0000.0 T 38 0.000 0.000 0.000 0.000 0.000 0.000 0.000 100.0 010.0 AGE35
0000.0 T 38 0.000 0.000 0.000 0.000 0.000 0.000 0.000 100.0 010.0 AGE36
0020.0 T 38 0.000 0.500 0.000 0.000 0.500 0.000 0.000 085.0 010.0 AGE37

Burial 3a Inout file: Imperial Island River No.1 G-50.dat Model 7
M

0000.0 T 38 0.000 0.000 0.000 0.000 0.000 0.000 0.000 200.0 025.0 AGE1
0025.0 T 38 0.600 0.020 0.000 0.000 0.200 0.000 0.000 200.0 025.0 AGE2
0078.0 T 38 0.100 0.000 0.000 0.250 0.450 0.200 0.000 200.0 025.0 AGE3
0090.5 T 38 0.000 0.000 0.100 0.800 0.100 0.000 0.000 200.0 025.0 AGE4
0106.0 T 38 0.000 0.000 0.100 0.900 0.000 0.000 0.000 200.0 025.0 AGE5
0117.0 T 38 0.000 0.000 0.200 0.800 0.000 0.000 0.000 200.0 025.0 AGE6
0530.0 T 38 0.700 0.050 0.000 0.100 0.150 0.000 0.000 200.0 025.0 AGE7
0015.2 T 38 0.000 0.000 0.650 0.350 0.000 0.000 0.000 200.0 025.0 AGE8
0140.2 T 38 0.700 0.000 0.000 0.050 0.200 0.000 0.000 200.0 025.0 AGE9
0672.0 T 38 0.100 0.600 0.100 0.000 0.200 0.000 0.000 200.0 025.0 AGE10
0076.0 T 38 0.000 0.000 0.850 0.150 0.000 0.000 0.000 200.0 025.0 AGE11
0212.5 T 38 0.650 0.000 0.350 0.000 0.000 0.000 0.000 200.0 025.0 AGE12
0370.0 T 38 0.600 0.000 0.300 0.000 0.100 0.000 0.000 200.0 025.0 AGE13
0003.0 T 38 0.150 0.000 0.850 0.000 0.000 0.000 0.000 200.0 025.0 AGE14
0310.0 F 26 0.000 0.000 0.400 0.000 0.000 0.000 0.600 200.0 025.0 AGE15
0025.0 F 19 0.500 0.000 0.400 0.000 0.000 0.000 0.100 200.0 025.0 AGE16
0150.0 F 18 0.150 0.600 0.050 0.000 0.200 0.000 0.000 200.0 025.0 AGE17
0000.0 T 38 0.000 0.000 0.000 0.000 0.000 0.000 0.000 200.0 025.0 AGE18
0000.0 T 38 0.000 0.000 0.000 0.000 0.000 0.000 0.000 200.0 025.0 AGE19
0020.0 F 25 0.250 0.500 0.000 0.000 0.250 0.000 0.000 200.0 025.0 AGE20
0025.0 F 22 0.500 0.000 0.000 0.000 0.000 0.000 0.500 200.0 025.0 AGE21
0000.0 T 38 0.000 0.000 0.000 0.000 0.000 0.000 0.000 200.0 025.0 AGE22
0140.0 F 24 0.200 0.000 0.000 0.100 0.700 0.000 0.000 200.0 025.0 AGE23
0000.0 T 38 0.000 0.000 0.000 0.000 0.000 0.000 0.000 200.0 025.0 AGE24
0000.0 T 38 0.000 0.000 0.000 0.000 0.000 0.000 0.000 200.0 025.0 AGE25
0000.0 T 38 0.000 0.000 0.000 0.000 0.000 0.000 0.000 200.0 025.0 AGE26
0197.5 T 38 0.800 0.000 0.000 0.000 0.200 0.000 0.000 200.0 025.0 AGE27
0085.0 T 38 0.000 1.000 0.000 0.000 0.000 0.000 0.000 150.0 015.0 AGE28
0177.0 T 38 0.500 0.200 0.000 0.000 0.300 0.000 0.000 150.0 015.0 AGE29
0166.0 T 38 0.000 1.000 0.000 0.000 0.000 0.000 0.000 150.0 015.0 AGE30
0084.0 F 36 0.000 1.000 0.000 0.000 0.000 0.000 0.000 150.0 015.0 AGE31
0400.0 F 35 0.700 0.150 0.000 0.000 0.150 0.000 0.000 150.0 015.0 AGE32
0350.0 F 34 0.000 0.500 0.000 0.000 0.500 0.000 0.000 150.0 015.0 AGE33
0000.0 T 38 0.000 0.000 0.000 0.000 0.000 0.000 0.000 150.0 015.0 AGE34
0000.0 T 38 0.000 0.000 0.000 0.000 0.000 0.000 0.000 150.0 010.0 AGE35
0000.0 T 38 0.000 0.000 0.000 0.000 0.000 0.000 0.000 150.0 010.0 AGE36
0020.0 T 38 0.000 0.500 0.000 0.000 0.500 0.000 0.000 085.0 010.0 AGE37

Burial 3a Input file: Imperial Island River No.1 G-50.dat Model 8

M

0000.0 T 38 0.000 0.000 0.000 0.000 0.000 0.000 0.000 150.0 025.0 AGE1
0025.0 T 38 0.600 0.020 0.000 0.000 0.200 0.000 0.000 150.0 025.0 AGE2
0078.0 T 38 0.100 0.000 0.000 0.250 0.450 0.200 0.000 150.0 025.0 AGE3
0090.5 T 38 0.000 0.000 0.100 0.800 0.100 0.000 0.000 150.0 025.0 AGE4
0106.0 T 38 0.000 0.000 0.100 0.900 0.000 0.000 0.000 150.0 025.0 AGE5
0117.0 T 38 0.000 0.000 0.200 0.800 0.000 0.000 0.000 150.0 025.0 AGE6
0530.0 T 38 0.700 0.050 0.000 0.100 0.150 0.000 0.000 150.0 025.0 AGE7
0015.2 T 38 0.000 0.000 0.650 0.350 0.000 0.000 0.000 150.0 025.0 AGE8
0140.2 T 38 0.700 0.000 0.000 0.050 0.200 0.000 0.000 150.0 025.0 AGE9
0672.0 T 38 0.100 0.600 0.100 0.000 0.200 0.000 0.000 150.0 025.0 AGE10
0076.0 T 38 0.000 0.000 0.850 0.150 0.000 0.000 0.000 150.0 025.0 AGE11
0212.5 T 38 0.650 0.000 0.350 0.000 0.000 0.000 0.000 150.0 025.0 AGE12
0370.0 T 38 0.600 0.000 0.300 0.000 0.100 0.000 0.000 150.0 025.0 AGE13
0003.0 T 38 0.150 0.000 0.850 0.000 0.000 0.000 0.000 150.0 025.0 AGE14
0310.0 F 26 0.000 0.000 0.400 0.000 0.000 0.000 0.600 150.0 025.0 AGE15
0025.0 F 19 0.500 0.000 0.400 0.000 0.000 0.000 0.100 150.0 025.0 AGE16
0150.0 F 18 0.150 0.600 0.050 0.000 0.200 0.000 0.000 150.0 025.0 AGE17
0000.0 T 38 0.000 0.000 0.000 0.000 0.000 0.000 0.000 150.0 025.0 AGE18
0000.0 T 38 0.000 0.000 0.000 0.000 0.000 0.000 0.000 150.0 025.0 AGE19
0020.0 F 25 0.250 0.500 0.000 0.000 0.250 0.000 0.000 150.0 025.0 AGE20
0025.0 F 22 0.500 0.000 0.000 0.000 0.000 0.000 0.500 150.0 025.0 AGE21
0000.0 T 38 0.000 0.000 0.000 0.000 0.000 0.000 0.000 150.0 025.0 AGE22
0140.0 F 24 0.200 0.000 0.000 0.100 0.700 0.000 0.000 150.0 025.0 AGE23
0000.0 T 38 0.000 0.000 0.000 0.000 0.000 0.000 0.000 150.0 025.0 AGE24
0000.0 T 38 0.000 0.000 0.000 0.000 0.000 0.000 0.000 150.0 025.0 AGE25
0000.0 T 38 0.000 0.000 0.000 0.000 0.000 0.000 0.000 150.0 025.0 AGE26
0197.5 T 38 0.800 0.000 0.000 0.000 0.200 0.000 0.000 150.0 025.0 AGE27
0085.0 T 38 0.000 1.000 0.000 0.000 0.000 0.000 0.000 150.0 015.0 AGE28
0177.0 T 38 0.500 0.200 0.000 0.000 0.300 0.000 0.000 150.0 015.0 AGE29
0166.0 T 38 0.000 1.000 0.000 0.000 0.000 0.000 0.000 150.0 015.0 AGE30
0084.0 F 36 0.000 1.000 0.000 0.000 0.000 0.000 0.000 150.0 015.0 AGE31
0400.0 F 35 0.700 0.150 0.000 0.000 0.150 0.000 0.000 150.0 015.0 AGE32
0350.0 F 34 0.000 0.500 0.000 0.000 0.500 0.000 0.000 150.0 015.0 AGE33
0000.0 T 38 0.000 0.000 0.000 0.000 0.000 0.000 0.000 150.0 015.0 AGE34
0000.0 T 38 0.000 0.000 0.000 0.000 0.000 0.000 0.000 150.0 010.0 AGE35
0000.0 T 38 0.000 0.000 0.000 0.000 0.000 0.000 0.000 150.0 010.0 AGE36
0020.0 T 38 0.000 0.500 0.000 0.000 0.500 0.000 0.000 080.0 010.0 AGE37

Burial 3a Input file: Imperial Island River No.1 G-50.dat Model 9

M
0000.0 T 38 0.000 0.000 0.000 0.000 0.000 0.000 0.000 150.0 025.0 AGE1
0025.0 T 38 0.600 0.020 0.000 0.000 0.200 0.000 0.000 150.0 025.0 AGE2
0078.0 T 38 0.100 0.000 0.000 0.250 0.450 0.200 0.000 150.0 025.0 AGE3
0090.5 T 38 0.000 0.000 0.100 0.800 0.100 0.000 0.000 150.0 025.0 AGE4
0106.0 T 38 0.000 0.000 0.100 0.900 0.000 0.000 0.000 150.0 025.0 AGE5
0117.0 T 38 0.000 0.000 0.200 0.800 0.000 0.000 0.000 150.0 025.0 AGE6
0530.0 T 38 0.700 0.050 0.000 0.100 0.150 0.000 0.000 150.0 025.0 AGE7
0015.2 T 38 0.000 0.000 0.650 0.350 0.000 0.000 0.000 150.0 025.0 AGE8
0140.2 T 38 0.700 0.000 0.000 0.050 0.200 0.000 0.000 150.0 025.0 AGE9
0672.0 T 38 0.100 0.600 0.100 0.000 0.200 0.000 0.000 150.0 025.0 AGE10
0076.0 T 38 0.000 0.000 0.850 0.150 0.000 0.000 0.000 150.0 025.0 AGE11
0212.5 T 38 0.650 0.000 0.350 0.000 0.000 0.000 0.000 150.0 025.0 AGE12
0370.0 T 38 0.600 0.000 0.300 0.000 0.100 0.000 0.000 150.0 025.0 AGE13
0003.0 T 38 0.150 0.000 0.850 0.000 0.000 0.000 0.000 150.0 025.0 AGE14
0310.0 F 26 0.000 0.000 0.400 0.000 0.000 0.000 0.600 150.0 025.0 AGE15
0025.0 F 19 0.500 0.000 0.400 0.000 0.000 0.000 0.100 150.0 025.0 AGE16
0150.0 F 18 0.150 0.600 0.050 0.000 0.200 0.000 0.000 150.0 025.0 AGE17
0000.0 T 38 0.000 0.000 0.000 0.000 0.000 0.000 0.000 100.0 025.0 AGE18
0000.0 T 38 0.000 0.000 0.000 0.000 0.000 0.000 0.000 100.0 025.0 AGE19
0020.0 F 25 0.250 0.500 0.000 0.000 0.250 0.000 0.000 100.0 025.0 AGE20
0025.0 F 22 0.500 0.000 0.000 0.000 0.000 0.000 0.500 100.0 025.0 AGE21
0000.0 T 38 0.000 0.000 0.000 0.000 0.000 0.000 0.000 100.0 025.0 AGE22
0140.0 F 24 0.200 0.000 0.000 0.100 0.700 0.000 0.000 100.0 025.0 AGE23
0000.0 T 38 0.000 0.000 0.000 0.000 0.000 0.000 0.000 100.0 025.0 AGE24
0000.0 T 38 0.000 0.000 0.000 0.000 0.000 0.000 0.000 100.0 025.0 AGE25
0000.0 T 38 0.000 0.000 0.000 0.000 0.000 0.000 0.000 100.0 025.0 AGE26
0197.5 T 38 0.800 0.000 0.000 0.000 0.200 0.000 0.000 150.0 025.0 AGE27
0085.0 T 38 0.000 1.000 0.000 0.000 0.000 0.000 0.000 150.0 015.0 AGE28
0177.0 T 38 0.500 0.200 0.000 0.000 0.300 0.000 0.000 150.0 015.0 AGE29
0166.0 T 38 0.000 1.000 0.000 0.000 0.000 0.000 0.000 150.0 015.0 AGE30
0084.0 F 36 0.000 1.000 0.000 0.000 0.000 0.000 0.000 150.0 015.0 AGE31
0400.0 F 35 0.700 0.150 0.000 0.000 0.150 0.000 0.000 150.0 015.0 AGE32
0350.0 F 34 0.000 0.500 0.000 0.000 0.500 0.000 0.000 150.0 015.0 AGE33
0000.0 T 38 0.000 0.000 0.000 0.000 0.000 0.000 0.000 150.0 015.0 AGE34
0000.0 T 38 0.000 0.000 0.000 0.000 0.000 0.000 0.000 150.0 010.0 AGE35
0000.0 T 38 0.000 0.000 0.000 0.000 0.000 0.000 0.000 150.0 010.0 AGE36
0020.0 T 38 0.000 0.500 0.000 0.000 0.500 0.000 0.000 080.0 010.0 AGE37

BURIAL 3A Input file: Canada Southern et al. N. Beaver R. YT I-46 .age
(input data shown in bold type)

Age 1	**410**	Base of sequence	Seginin-Eifellian
Age 2	**400**	Sub-Headless (carboniates) deposition	Eifelian
Age 3	**385**	Headless deposition	Eifelian
Age 4	**380**	Nahanni deposition	Eifelian-Giv etian
Age 5	**370**	Besa River-lower deposition	Givetian-Frasnian
Age 6	**360**	Besa River -upper deposition	Frasn-Fammenian
Age 7	**346**	Prophet deposition	Tournasian (T3)
Age 8	**334**	Golata deposition	Visean (V2-V3)
Age 9	**330**	Mattson - Lr , deposition remaining part	Visean 9V3)
Age 10	**324**	Mattson - Upper, deposition (eroded at sub-Permian unconformity)	V3-Serphukhovian
Age 11	**285**	Sub-Permian unconformity	
Age 12	**274**	Kindle deposition	Artinskian
Age 13	**260**	Fantasque deposition, part remaining	Kazanian-Tatarian
Age 14	**255**	Fantasque deposition (eroded at sub-Triassic unconformity)	Tatanian
Age 15	**250**	Sub-Triassic Unconformity	
Age 16	**240**	Toad-Grayling deposition (remaining part)	Anisian
Age 17	**220**	Toad-Grayling deposition (eroded at sub-Permian unconformity)	
Age 18	**160**	Sub-Cretaceous Unconformity	
Age 19	**112**	Garbutt deposition	Albian
Age 20	**108**	Scatter deposition	Albian
Age 21	**107**	Scatter deposition (part remaining) (eroded at sub-Tertiary unconformity)	L-M. Albian
Age 22	**105**	Lepine deposition	M. Albian
Age 23	**103**	Sikanni deposition	Up. Albian
Age 24	**100**	Sully deposition (Toad-Grayling erosion)	Up. Albian
Age 25	**96**	Dunvegan deposition	Cenomanian
Age 26	**85**	Kotaneellee deposition	Santonian
Age 27	**77**	Wapiti	Campaignian
Age 28	**60**	Sub-Tertiary Unconformity	
Age 29	**55**	Sub-TU - Kotaneelee erosion	
Age 30	**53**	Sub-TU - Dunvegan erosion	
Age 31	**49**	Sub-TU- Sully erosion	
Age 32	**47**	Sub-TU - Sikanni erosion	
Age 33	**45**	Sub-TU - Lepine erosion	
Age 34	**44**	Sub-TU - Scatter erosion	
Age 35	**0.5**	Quaternary deposition	

Burial 3a Input file: Canada Southern et al. North Beaver River .Ro
(input data shown in bold type)

Canada Southern et al. N. Beaver River YT 1-27
N60 07' W124 04'

Samp No. C186754-	Depth ft	Depth m	Stratigraphy Rock fm	Reflectance Med Ro-amorphous mean	st dev	n	VRo calc*	Depth m
3289	3280-3299	999.74. -1005.54	Kindle	0.79	0.02	2	**0.89**	**1002.49**
3549	3540-3559	1078.99-1084.78	Mattson	0.93	0.04	11	**0.97**	**1081.74**
4389	4370-4419	1331.97-1346.91	Mattson	1.1	0.1	5	**1.08**	**1337.77**
4578	4570-4589	1392.94-1398.73	Mattson	1.17	0.06	4	**1.12**	**1395.37**
4885	4880-4889	1487.42-1490.17	Mattson	1.36	0.04	2	**1.24**	**1488.95**
5139	5130-5149	1563.62-1569.42	Mattson	1.31	0.02	2	**1.21**	**1566.37**
5989	5970-6019	1819.66-1834.59	Golata	1.45	0	6	**1.30**	**1825.45**
6349	6330-6369	1929.38-1941.27	Golata	1.35	0.06	3	**1.23**	**1935.18**
6640	6630-6659	2020.82-2029.66	Golata					2023.87
7139	7130-7150	2173.22-2179.32	Prophet	1.58	0.06	7	**1.38**	**2175.97**
7540	7530-7550	2295.14-2301.24	Prophet	1.6	0.05	9	**1.39**	**2298.19**
7860	7850-7860	2392.68-2395.73	Prophet	1.72	0.05	4	**1.46**	**2395.73**
8585	8570-8599	2612.14-2620.97	Prophet	1.82	0.16	22	**1.52**	**2616.71**
8815	8810-8819	2685.28-2688.03	Prophet	1.87	0	1	**1.56**	**2686.82**
8860	8859-8870	2700.22-2703.57	Prophet	1.7	0.1	8	**1.45**	**2700.53**
9120	9120	2779.77	Besa River	2.1	0.21	9	**1.70**	**2779.78**
9389	9370-9399	2855.97-2864.82	Besa River	2.2	0	1	**1.76**	**2861.77**
9659	9650-9669	2941.32-2947.11	Besa River	2.26	0.24	17	**1.80**	**2944.06**
10319	10310-10329	3142.49-3148.28	Besa River	2.36	0.18	9	**1.86**	**3145.23**
10665	10660-10679	3249.17-3254.96	Besa River					3250.69
10875	10869-10879	3258.00-3315.92	Besa River*	3.23	0.22	11	**2.40**	**3314.7**
10939	10930-10949	3331.46-3337.25	Besa River**	3.5	0.13	7	**2.56**	**3334.21**
12519	12510-12529	3813.05-3818.84	Nahanni	4.05	0.35	22	**2.90**	**3815.79**

* black sh
** ?Muskwa

Burial 3a Input file: Canada Southern et al. N. Beaver R YT I-27.dat - Model 1

M

0000.0	T	36	0.000	0.000	0.000	0.000	0.000	0.000	0.000	080.0	025.0	AGE1
0176.8	T	36	0.000	0.050	0.000	0.950	0.000	0.000	0.000	080.0	025.0	AGE2
0197.1	T	36	0.050	0.000	0.000	0.950	0.000	0.000	0.000	080.0	025.0	AGE3
0213.7	T	36	0.000	0.000	0.000	0.950	0.000	0.000	0.050	080.0	025.0	AGE4
0338.3	T	36	0.950	0.000	0.000	0.000	0.000	0.000	0.050	080.0	025.0	AGE5
0594.0	T	36	0.850	0.000	0.000	0.000	0.100	0.000	0.050	150.0	025.0	AGE7
0274.0	T	36	0.750	0.100	0.000	0.000	0.150	0.000	0.000	150.0	025.0	AGE8
0695.0	T	36	0.150	0.650	0.000	0.000	0.200	0.000	0.000	150.0	025.0	AGE9
0325.0	F	11	0.150	0.650	0.000	0.000	0.200	0.000	0.000	150.0	025.0	AGE10
0000.0	T	36	0.000	0.000	0.000	0.000	0.000	0.000	0.000	150.0	025.0	AGE11
0158.0	T	36	0.250	0.500	0.000	0.000	0.250	0.000	0.000	150.0	025.0	AGE12
0175.0	T	36	0.500	0.000	0.000	0.000	0.000	0.000	0.500	140.0	025.0	AGE13
0015.0	F	15	0.500	0.000	0.000	0.000	0.000	0.000	0.500	140.0	025.0	AGE14
0000.0	T	36	0.000	0.000	0.000	0.000	0.000	0.000	0.000	140.0	025.0	AGE15
0348.4	T	36	0.800	0.100	0.000	0.000	0.100	0.000	0.000	120.0	025.0	AGE16
0452.0	F	18	0.800	0.100	0.000	0.000	0.100	0.000	0.000	120.0	025.0	AGE17
0000.0	T	36	0.000	0.000	0.000	0.000	0.000	0.000	0.000	120.0	025.0	AGE18
0225.0	T	36	0.250	0.500	0.000	0.000	0.250	0.000	0.000	100.0	025.0	AGE19
0057.9	T	36	0.000	0.500	0.000	0.000	0.500	0.000	0.000	100.0	025.0	AGE20
0012.0	F	34	0.000	0.500	0.000	0.000	0 500	0.000	0.000	080.0	025.8	AGE21
0170.0	F	33	0.800	0.100	0.000	0.000	0.100	0.000	0.000	080.0	025.0	AGE22
0030.0	F	32	0.000	1.000	0.000	0.000	0.000	0.000	0.000	080.0	025.0	AGE23
0150.0	F	31	0.500	0.200	0.000	0.000	0.300	0.000	0.000	080.0	025.0	AGE24
0050.0	F	30	0.000	1.000	0.000	0.000	0.000	0.000	0.000	080.0	025.0	AGE25
0050.0	F	29	0.700	0.150	0.000	0.000	0.150	0.000	0.000	080.0	025.0	AGE26
0150.0	F	28	0.000	0.500	0.000	0.000	0.500	0.000	0.000	080.0	025.0	AGE27
0000.0	T	36	0.000	0.000	0.000	0.000	0.000	0.000	0.000	080.0	015.0	AGE28
0000.0	T	36	0.000	0.000	0.000	0.000	0.000	0.000	0.000	060.0	015.0	AGE29
0000.0	T	36	0.000	0.000	0.000	0.000	0.000	0.000	0.000	060.0	015.0	AGE31
0000.0	T	36	0.000	0.000	0.000	0.000	0.000	0.000	0.000	060.0	015.0	AGE32
0000.0	T	36	0.000	0.000	0.000	0.000	0.000	0.000	0.000	060.0	015.0	AGE33
0000.0	T	36	0.000	0.000	0.000	0.000	0.000	0.000	0.000	060.0	015.0	AGE34
0000.0	T	36	0.000	0.000	0.000	0.000	0.000	0.000	0.000	080.0	010.0	AGE35
0015.0	T	37	0.000	0.500	0.000	0.000	0.500	0.000	0.000	080.0	010.0	AGE36

Burial 3a Input file: Canada Southern et al. N. Beaver R YT I-27.dat - Model 2

M												
0000.0	T	36	0.000	0.000	0.000	0.000	0.000	0.000	0.000	100.0	025.0	AGE1
0176.8	T	36	0.000	0.050	0.000	0.950	0.000	0.000	0.000	100.0	025.0	AGE2
0197.1	T	36	0.050	0.000	0.000	0.950	0.000	0.000	0.000	080.0	025.0	AGE3
0213.7	T	36	0.000	0.000	0.000	0.950	0.000	0.000	0.050	080.0	025.0	AGE4
0338.3	T	36	0.950	0.000	0.000	0.000	0.000	0.000	0.050	080.0	025.0	AGE5
0594.0	T	36	0.850	0.000	0.000	0.000	0.100	0.000	0.050	180.0	025.0	AGE7
0274.0	T	36	0.750	0.100	0.000	0.000	0.150	0.000	0.000	180.0	025.0	AGE8
0695.0	T	36	0.150	0.650	0.000	0.000	0.200	0.000	0.000	180.0	025.0	AGE9
0325.0	F	11	0.150	0.650	0.000	0.000	0.200	0.000	0.000	180.0	025.0	AGE10
0000.0	T	36	0.000	0.000	0.000	0.000	0.000	0.000	0.000	180.0	025.0	AGE11
0158.0	T	36	0.250	0.500	0.000	0.000	0.250	0.000	0.000	180.0	025.0	AGE12
0175.0	T	36	0.500	0.000	0.000	0.000	0.000	0.000	0.500	150.0	025.0	AGE13
0015.0	F	15	0.500	0.000	0.000	0.000	0.000	0.000	0.500	150.0	025.0	AGE14
0000.0	T	36	0.000	0.000	0.000	0.000	0.000	0.000	0.000	150.0	025.0	AGE15
0348.4	T	36	0.800	0.100	0.000	0.000	0.100	0.000	0.000	130.0	025.0	AGE16
0452.0	F	18	0.800	0.100	0.000	0.000	0.100	0.000	0.000	120.0	025.0	AGE17
0000.0	T	36	0.000	0.000	0.000	0.000	0.000	0.000	0.000	120.0	025.0	AGE18
0225.0	T	36	0.250	0.500	0.000	0.000	0.250	0.000	0.000	100.0	025.0	AGE19
0057.9	T	36	0.000	0.500	0.000	0.000	0.500	0.000	0.000	100.0	025.0	AGE20
0012.0	F	34	0.000	0.500	0.000	0.000	0 500	0.000	0.000	080.0	025.8	AGE21
0170.0	F	33	0.800	0.100	0.000	0.000	0.100	0.000	0.000	080.0	025.0	AGE22
0030.0	F	32	0.000	1.000	0.000	0.000	0.000	0.000	0.000	080.0	025.0	AGE23
0150.0	F	31	0.500	0.200	0.000	0.000	0.300	0.000	0.000	080.0	025.0	AGE24
0050.0	F	30	0.000	1.000	0.000	0.000	0.000	0.000	0.000	080.0	025.0	AGE25
0050.0	F	29	0.700	0.150	0.000	0.000	0.150	0.000	0.000	080.0	025.0	AGE26
0150.0	F	28	0.000	0.500	0.000	0.000	0.500	0.000	0.000	080.0	025.0	AGE27
0000.0	T	36	0.000	0.000	0.000	0.000	0.000	0.000	0.000	080.0	015.0	AGE28
0000.0	T	36	0.000	0.000	0.000	0.000	0.000	0.000	0.000	060.0	015.0	AGE29
0000.0	T	36	0.000	0.000	0.000	0.000	0.000	0.000	0.000	060.0	015.0	AGE31
0000.0	T	36	0.000	0.000	0.000	0.000	0.000	0.000	0.000	060.0	015.0	AGE32
0000.0	T	36	0.000	0.000	0.000	0.000	0.000	0.000	0.000	060.0	015.0	AGE33
0000.0	T	36	0.000	0.000	0.000	0.000	0.000	0.000	0.000	060.0	015.0	AGE34
0000.0	T	36	0.000	0.000	0.000	0.000	0.000	0.000	0.000	080.0	010.0	AGE35
0015.0	T	37	0.000	0.500	0.000	0.000	0.500	0.000	0.000	080.0	010.0	AGE36

Burial 3a Input file: Canada Southern et al. N. Beaver R YT I-27.dat - Model 3

M

0000.0	T	36	0.000	0.000	0.000	0.000	0.000	0.000	0.000	100.0	025.0	AGE1
0176.8	T	36	0.000	0.050	0.000	0.950	0.000	0.000	0.000	100.0	025.0	AGE2
0197.1	T	36	0.050	0.000	0.000	0.950	0.000	0.000	0.000	100.0	025.0	AGE3
0213.7	T	36	0.000	0.000	0.000	0.950	0.000	0.000	0.050	100.0	025.0	AGE4
0338.3	T	36	0.950	0.000	0.000	0.000	0.000	0.000	0.050	100.0	025.0	AGE5
0594.0	T	36	0.850	0.000	0.000	0.000	0.100	0.000	0.050	100.0	025.0	AGE7
0274.0	T	36	0.750	0.100	0.000	0.000	0.150	0.000	0.000	100.0	025.0	AGE8
0695.0	T	36	0.150	0.650	0.000	0.000	0.200	0.000	0.000	100.0	025.0	AGE9
0325.0	F	11	0.150	0.650	0.000	0.000	0.200	0.000	0.000	100.0	025.0	AGE10
0000.0	T	36	0.000	0.000	0.000	0.000	0.000	0.000	0.000	100.0	025.0	AGE11
0158.0	T	36	0.250	0.500	0.000	0.000	0.250	0.000	0.000	100.0	025.0	AGE12
0175.0	T	36	0.500	0.000	0.000	0.000	0.000	0.000	0.500	100.0	025.0	AGE13
0015.0	F	15	0.500	0.000	0.000	0.000.	0.000	0.000	0.500	100.0	025.0	AGE14
0000.0	T	36	0.000	0.000	0.000	0.000	0.000	0.000	0.000	100.0	025.0	AGE15
0348.4	T	36	0.800	0.100	0.000	0.000	0.100	0.000	0.000	100.0	025.0	AGE16
0452.0	F	18	0.800	0.100	0.000	0.000	0.100	0.000	0.000	100.0	025.0	AGE17
0000.0	T	36	0.000	0.000	0.000	0.000	0.000	0.000	0.000	100.0	025.0	AGE18
0225.0	T	36	0.250	0.500	0.000	0.000	0.250	0.000	0.000	100.0	025.0	AGE19
0057.9	T	36	0.000	0.500	0.000	0.000	0.500	0.000	0.000	100.0	025.0	AGE20
0012.0	F	34	0.000	0.500	0.000	0.000	0 500	0.000	0.000	080.0	025.8	AGE21
0170.0	F	33	0.800	0.100	0.000	0.000	0.100	0.000	0.000	080.0	025.0	AGE22
0030.0	F	32	0.000	1.000	0.000	0.000	0.000	0.000	0.000	080.0	025.0	AGE23
0150.0	F	31	0.500	0.200	0.000	0.000	0.300	0.000	0.000	080.0	025.0	AGE24
0050.0	F	30	0.000	1.000	0.000	0.000	0.000	0.000	0.000	080.0	025.0	AGE25
0050.0	F	29	0.700	0.150	0.000	0.000	0.150	0.000	0.000	080.0	025.0	AGE26
0150.0	F	28	0.000	0.500	0.000	0.000	0.500	0.000	0.000	080.0	025.0	AGE27
0000.0	T	36	0.000	0.000	0.000	0.000	0.000	0.000	0.000	080.0	015.0	AGE28
0000.0	T	36	0.000	0.000	0.000	0.000	0.000	0.000	0.000	060.0	015.0	AGE29
0000.0	T	36	0.000	0.000	0.000	0.000	0.000	0.000	0.000	060.0	015.0	AGE31
0000.0	T	36	0.000	0.000	0.000	0.000	0.000	0.000	0.000	060.0	015.0	AGE32
0000.0	T	36	0.000	0.000	0.000	0.000	0.000	0.000	0.000	060.0	015.0	AGE33
0000.0	T	36	0.000	0.000	0.000	0.000	0.000	0.000	0.000	060.0	015.0	AGE34
0000.0	T	36	0.000	0.000	0.000	0.000	0.000	0.000	0.000	080.0	010.0	AGE35
0015.0	T	37	0.000	0.500	0.000	0.000	0.500	0.000	0.000	080.0	010.0	AGE36

Burial 3a Input file: Canada Southern et al. N. Beaver R YT I-27.dat - Model 4

M

0000.0	T	36	0.000	0.000	0.000	0.000	0.000	0.000	0.000	100.0	025.0	AGE1
0176.8	T	36	0.000	0.050	0.000	0.950	0.000	0.000	0.000	100.0	025.0	AGE2
0197.1	T	36	0.050	0.000	0.000	0.950	0.000	0.000	0.000	100.0	025.0	AGE3
0213.7	T	36	0.000	0.000	0.000	0.950	0.000	0.000	0.050	100.0	025.0	AGE4
0338.3	T	36	0.950	0.000	0.000	0.000	0.000	0.000	0.050	100.0	025.0	AGE5
0594.0	T	36	0.850	0.000	0.000	0.000	0.100	0.000	0.050	200.0	025.0	AGE7
0274.0	T	36	0.750	0.100	0.000	0.000	0.150	0.000	0.000	200.0	025.0	AGE8
0695.0	T	36	0.150	0.650	0.000	0.000	0.200	0.000	0.000	200.0	025.0	AGE9
0325.0	F	11	0.150	0.650	0.000	0.000	0.200	0.000	0.000	200.0	025.0	AGE10
0000.0	T	36	0.000	0.000	0.000	0.000	0.000	0.000	0.000	200.0	025.0	AGE11
0158.0	T	36	0.250	0.500	0.000	0.000	0.250	0.000	0.000	200.0	025.0	AGE12
0175.0	T	36	0.500	0.000	0.000	0.000	0.000	0.000	0.500	200.0	025.0	AGE13
0015.0	F	15	0.500	0.000	0.000	0.000	0.000	0.000	0.500	200.0	025.0	AGE14
0000.0	T	36	0.000	0.000	0.000	0.000	0.000	0.000	0.000	200.0	025.0	AGE15
0348.4	T	36	0.800	0.100	0.000	0.000	0.100	0.000	0.000	200.0	025.0	AGE16
0452.0	F	18	0.800	0.100	0.000	0.000	0.100	0.000	0.000	200.0	025.0	AGE17
0000.0	T	36	0.000	0.000	0.000	0.000	0.000	0.000	0.000	200.0	025.0	AGE18
0225.0	T	36	0.250	0.500	0.000	0.000	0.250	0.000	0.000	100.0	025.0	AGE19
0057.9	T	36	0.000	0.500	0.000	0.000	0.500	0.000	0.000	100.0	025.0	AGE20
0012.0	F	34	0.000	0.500	0.000	0.000	0 500	0.000	0.000	080.0	025.8	AGE21
0170.0	F	33	0.800	0.100	0.000	0.000	0.100	0.000	0.000	080.0	025.0	AGE22
0030.0	F	32	0.000	1.000	0.000	0.000	0.000	0.000	0.000	080.0	025.0	AGE23
0150.0	F	31	0.500	0.200	0.000	0.000	0.300	0.000	0.000	080.0	025.0	AGE24
0050.0	F	30	0.000	1.000	0.000	0.000	0.000	0.000	0.000	080.0	025.0	AGE25
0050.0	F	29	0.700	0.150	0.000	0.000	0.150	0.000	0.000	080.0	025.0	AGE26
0150.0	F	28	0.000	0.500	0.000	0.000	0.500	0.000	0.000	080.0	025.0	AGE27
0000.0	T	36	0.000	0.000	0.000	0.000	0.000	0.000	0.000	080.0	015.0	AGE28
0000.0	T	36	0.000	0.000	0.000	0.000	0.000	0.000	0.000	060.0	015.0	AGE29
0000.0	T	36	0.000	0.000	0.000	0.000	0.000	0.000	0.000	060.0	015.0	AGE31
0000.0	T	36	0.000	0.000	0.000	0.000	0.000	0.000	0.000	060.0	015.0	AGE32
0000.0	T	36	0.000	0.000	0.000	0.000	0.000	0.000	0.000	060.0	015.0	AGE33
0000.0	T	36	0.000	0.000	0.000	0.000	0.000	0.000	0.000	060.0	015.0	AGE34
0000.0	T	36	0.000	0.000	0.000	0.000	0.000	0.000	0.000	080.0	010.0	AGE35
0015.0	T	37	0.000	0.500	0.000	0.000	0.500	0.000	0.000	080.0	010.0	AGE36

Burial 3a: Input file Canada Southern et al. N. Beaver R YT I-27.dat Model 5

M

0000.0 T 36 0.000 0.000 0.000 0.000 0.000 0.000 0.000 060.0 025.0 AGE1
0176.8 T 36 0.000 0.050 0.000 0.950 0.000 0.000 0.000 060.0 025.0 AGE2
0197.1 T 36 0.050 0.000 0.000 0.950 0.000 0.000 0.000 060.0 025.0 AGE3
0213.7 T 36 0.000 0.000 0.000 0.950 0.000 0.000 0.050 060.0 025.0 AGE4
0338.3 T 36 0.950 0.000 0.000 0.000 0.000 0.000 0.050 060.0 025.0 AGE5
0594.0 T 36 0.850 0.000 0.000 0.000 0.100 0.000 0.050 150.0 025.0 AGE6
0765.0 T 36 0.250 0.000 0.500 0.000 0.000 0.000 0.250 150.0 025.0 AGE7
0274.0 T 36 0.750 0.100 0.000 0.000 0.150 0.000 0.000 150.0 025.0 AGE8
0695.0 T 36 0.150 0.650 0.000 0.000 0.200 0.000 0.000 200.0 025.0 AGE9
0325.0 F 11 0.150 0.650 0.000 0.000 0.200 0.000 0.000 200.0 025.0 AGE10
0000.0 T 36 0.000 0.000 0.000 0.000 0.000 0.000 0.000 200.0 025.0 AGE11
0158.0 T 36 0.250 0.500 0.000 0.000 0.250 0.000 0.000 200.0 025.0 AGE12
0175.0 T 36 0.500 0.000 0.000 0.000 0.000 0.000 0.500 200.0 025.0 AGE13
0015.0 F 15 0.500 0.000 0.000 0.000 0.000 0.000 0.500 200.0 025.0 AGE14
0000.0 T 36 0.000 0.000 0.000 0.000 0.000 0.000 0.000 200.0 025.0 AGE15
0348.4 T 36 0.800 0.100 0.000 0.000 0.100 0.000 0.000 200.0 025.0 AGE16
0452.0 F 18 0.800 0.100 0.000 0.000 0.100 0.000 0.000 200.0 025.0 AGE17
0000.0 T 36 0.000 0.000 0.000 0.000 0.000 0.000 0.000 200.0 025.0 AGE18
0225.0 T 36 0.250 0.500 0.000 0.000 0.250 0.000 0.000 100.0 025.0 AGE19
0057.9 T 36 0.000 0.500 0.000 0.000 0.500 0.000 0.000 100.0 025.0 AGE20
0012.0 F 34 0.000 0.500 0.000 0.000 0 500 0.000 0.000 080.0 025.8 AGE21
0170.0 F 33 0.800 0.100 0.000 0.000 0.100 0.000 0.000 080.0 025.0 AGE22
0030.0 F 32 0.000 1.000 0.000 0.000 0.000 0.000 0.000 080.0 025.0 AGE23
0150.0 F 31 0.500 0.200 0.000 0.000 0.300 0.000 0.000 080.0 025.0 AGE24
0050.0 F 30 0.000 1.000 0.000 0.000 0.000 0.000 0.000 080.0 025.0 AGE25
0050.0 F 29 0.700 0.150 0.000 0.000 0.150 0.000 0.000 080.0 025.0 AGE26
0150.0 F 28 0.000 0.500 0.000 0.000 0.500 0.000 0.000 080.0 025.0 AGE27
0000.0 T 36 0.000 0.000 0.000 0.000 0.000 0.000 0.000 080.0 015.0 AGE28
0000.0 T 36 0.000 0.000 0.000 0.000 0.000 0.000 0.000 060.0 015.0 AGE29
0000.0 T 36 0.000 0.000 0.000 0.000 0.000 0.000 0.000 060.0 015.0 AGE30
0000.0 T 36 0.000 0.000 0.000 0.000 0.000 0.000 0.000 060.0 015.0 AGE31
0000.0 T 36 0.000 0.000 0.000 0.000 0.000 0.000 0.000 060.0 015.0 AGE32
0000.0 T 36 0.000 0.000 0.000 0.000 0.000 0.000 0.000 060.0 015.0 AGE33
0000.0 T 36 0.000 0.000 0.000 0.000 0.000 0.000 0.000 060.0 015.0 AGE34
0000.0 T 36 0.000 0.000 0.000 0.000 0.000 0.000 0.000 080.0 010.0 AGE35
0015.0 T 37 0.000 0.500 0.000 0.000 0.500 0.000 0.000 080.0 010.0 AGE36

Burial 3a Input file: Canada Southern et al. N. Beaver R YT I-27.dat - Model 5

M

0000.0	T	36	0.000	0.000	0.000	0.000	0.000	0.000	0.000	080.0	025.0	AGE1
0176.8	T	36	0.000	0.050	0.000	0.950	0.000	0.000	0.000	080.0	025.0	AGE2
0197.1	T	36	0.050	0.000	0.000	0.950	0.000	0.000	0.000	080.0	025.0	AGE3
0213.7	T	36	0.000	0.000	0.000	0.950	0.000	0.000	0.050	080.0	025.0	AGE4
0338.3	T	36	0.950	0.000	0.000	0.000	0.000	0.000	0.050	080.0	025.0	AGE5
0594.0	T	36	0.850	0.000	0.000	0.000	0.100	0.000	0.050	150.0	025.0	AGE7
0274.0	T	36	0.750	0.100	0.000	0.000	0.150	0.000	0.000	150.0	025.0	AGE8
0695.0	T	36	0.150	0.650	0.000	0.000	0.200	0.000	0.000	150.0	025.0	AGE9
0325.0	F	11	0.150	0.650	0.000	0.000	0.200	0.000	0.000	150.0	025.0	AGE10
0000.0	T	36	0.000	0.000	0.000	0.000	0.000	0.000	0.000	150.0	025.0	AGE11
0158.0	T	36	0.250	0.500	0.000	0.000	0.250	0.000	0.000	150.0	025.0	AGE12
0175.0	T	36	0.500	0.000	0.000	0.000	0.000	0.000	0.500	140.0	025.0	AGE13
0015.0	F	15	0.500	0.000	0.000	0.000	0.000	0.000	0.500	140.0	025.0	AGE14
0000.0	T	36	0.000	0.000	0.000	0.000	0.000	0.000	0.000	140.0	025.0	AGE15
0348.4	T	36	0.800	0.100	0.000	0.000	0.100	0.000	0.000	120.0	025.0	AGE16
0452.0	F	18	0.800	0.100	0.000	0.000	0.100	0.000	0.000	120.0	025.0	AGE17
0000.0	T	36	0.000	0.000	0.000	0.000	0.000	0.000	0.000	120.0	025.0	AGE18
0225.0	T	36	0.250	0.500	0.000	0.000	0.250	0.000	0.000	100.0	025.0	AGE19
0057.9	T	36	0.000	0.500	0.000	0.000	0.500	0.000	0.000	100.0	025.0	AGE20
0012.0	F	34	0.000	0.500	0.000	0.000	0 500	0.000	0.000	080.0	025.8	AGE21
0170.0	F	33	0.800	0.100	0.000	0.000	0.100	0.000	0.000	080.0	025.0	AGE22
0030.0	F	32	0.000	1.000	0.000	0.000	0.000	0.000	0.000	080.0	025.0	AGE23
0150.0	F	31	0.500	0.200	0.000	0.000	0.300	0.000	0.000	080.0	025.0	AGE24
0050.0	F	30	0.000	1.000	0.000	0.000	0.000	0.000	0.000	080.0	025.0	AGE25
0050.0	F	29	0.700	0.150	0.000	0.000	0.150	0.000	0.000	080.0	025.0	AGE26
0150.0	F	28	0.000	0.500	0.000	0.000	0.500	0.000	0.000	080.0	025.0	AGE27
0000.0	T	36	0.000	0.000	0.000	0.000	0.000	0.000	0.000	080.0	015.0	AGE28
0000.0	T	36	0.000	0.000	0.000	0.000	0.000	0.000	0.000	060.0	015.0	AGE29
0000.0	T	36	0.000	0.000	0.000	0.000	0.000	0.000	0.000	060.0	015.0	AGE31
0000.0	T	36	0.000	0.000	0.000	0.000	0.000	0.000	0.000	060.0	015.0	AGE32
0000.0	T	36	0.000	0.000	0.000	0.000	0.000	0.000	0.000	060.0	015.0	AGE33
0000.0	T	36	0.000	0.000	0.000	0.000	0.000	0.000	0.000	060.0	015.0	AGE34
0000.0	T	36	0.000	0.000	0.000	0.000	0.000	0.000	0.000	080.0	010.0	AGE35
0015.0	T	37	0.000	0.500	0.000	0.000	0.500	0.000	0.000	080.0	010.0	AGE36

BURIAL 3a Input file: Pan Am Beaver G-01.age
(Input data shown in bold type)

Age 1	**396**	Base of sequence	Up Silurian
Age 2	**384**	Sub-Headless (carboniates) deposition	Pridolian-Emsian
Age 3	**383**	Headless deposition	Eifelian
Age 4	**376**	Nahanni deposition	Eifelian
Age 5	**360**	Besa River-lower deposition	Frasnian
Age 6	**354**	Besa River -upper deposition	Tournasian
Age 7	**344**	Prophet deposition	Tournasian -Visean
Age 8	**337**	Golata deposition	Visean (V2-V3)
Age 9	**289**	Mattson - Lr , deposition remaining part	Visean (V3)
Age 10	**276**	Mattson - Upper, deposition	V3-Serphukhovian
		(eroded at sub-Permian unconformity)	
Age 11	**286**	Sub-Permian unconformity	
Age 12	**258**	Kindle deposition	Artinskian
Age 13	**246**	Fantasque deposition, part remaining	Perm(Kaz-Tar)
Age 14	**245**	Fantasque deposition	Kazanian-Tartarian
		(eroded at sub-Triassic unconformity)	
Age 15	**240**	Sub-Triassic Unconformity	
Age 16	**240**	Toad-Grayling deposition (remaining part)	Trias
Age 17	**208**	Toad-Grayling deposition	
		(eroded at sub-Permian unconformity)	
Age 18	**113**	Sub-Cretaceous Unconformity	
Age 19	**111**	Garbutt deposition (part remaining)	Albian
Age 20	**109**	Garbutt deposition	Albian
		(eroded at sub-Tertiary unconformity)	
Age 21	**106**	Scatter deposition	Albian
		(eroded at sub-Tertiary unconformity)	
Age 22	**102**	Lepine deposition	Albian
		(eroded at sub-Tertiary unconformity)	
Age 23	**101**	Sikanni deposition	Albian
		(eroded at sub-Tertiary unconformity)	
Age 24	**98**	Sully deposition	Albian-Cenomaian
		(eroded at sub-Tertiary unconformity)	
Age 25	**87.5**	Dunvegan deposition	Cenomanian
		(eroded at sub-Tertiary unconformity)	
Age 26	**74.5**	Kotaneellee deposition	Santonian-Campaignian
		eroded at sub-Tertiary unconformity)	
Age 27	67	Wapiti	Maastrictian
		(eroded at sub-Tertiary unconformity)	
Age 28	**62**	Sub-Tertiary Unconformity	
Age 29	**60.5**	Sub-TU - Kotaneelee erosion	
Age 30	**59**	Sub-TU - Dunvegan erosion	
Age 31	**54**	Sub-TU- Sully erosion	
Age 32	**53**	Sub-TU - Sikanni erosion	
Age 33	**48**	Sub-TU - Lepine erosion	
Age 34	**46**	Sub-TU - Scatter erosion	
Age 35	**45**	Sub-TU- Garbutt erosion	
Age 36	**0.5**	Quaternary deposition	Pleistocene

BURIAL 3a Input file Pan Am Beaver River G-01.Ro
(Input data shown in bold type)

Pan Am Beaver G-01, YT
N60 00' 25" W124 15' 48"

Samp No.	Depth		Stratigraphy Rock	Reflectance Med Ro-amorphous			V Ro	Depth
C186752-	ft	m	fm	mean	st dev	n	Calc*	m
2880	2860-2900	2671.57-2672.18	Mattson	0.60	0.03	11	**0.77**	**877.82**
3250	3220-60	981.46-993.65	Mattson	0.66	0.02	6	**0.81**	**990.60**
3475	3470-80	1057.66-1060.70	Mattson					
3700	3690-3710	1124.71-1130.81	Mattson	0.71	0.00	1	**0.84**	**1127.76**
3795	3790-3800	115.19-1158.24	Mattson					
4135	4120-4150	1255.77-1264.92	Mattson	0.84	0.00	1	**0.92**	**1260.35**
4690	4680-4700	1426.46-1432.56	Mattson					
4965	4950-80	1508.76-1517.90	Mattson					
5520	5510-30	1679.45-1685.54	Mattson	1.20	0.00	1	**1.14**	**1682.50**
5835	5820-50	1773.94-1783.08	Mattson					
6120	6110-30	1862.33-16868.42	Golata	1.40	0.00	1	**1.27**	**1865.38**
6540	6530-50	1990.34-1996.44	Golata	1.47	0.10	6	**1.31**	**1993.39**
6565	6850-80	2087.88-2097.02	Golata	1.47	0.00	1	**1.31**	**2001.01**
7140	7130-50	2173.22-2179.32	Golata					
7480	7470-90	2279.90-2587.75	Golata	1.52	0.06	7	**1.34**	**2279.90**
7840	7830-60	2386.58-2395.73	Golata					
8766	8765-8767C	2671.57-2672.18	Golata	1.55	0.05	4	**1.36**	**2671.88**
8800	8795-8805C	2680.71-2683.76	Golata	0.03				
9210	9200-20	2804.16-2801.26	Golata	1.53	0.00	1	**1.35**	**2807.21**
9505	9490-9520	2892.55-2901.69	Golata					
9880	9870-90	3008.37-3014.47	Golata	1.72			**1.46**	**3011.42**
10129	10125-133C	3086.1-3088.54	Prophet	1.76	0.06	2	**1.49**	**3087.32**
10183	10181-184.45C	3103.17-3104.23	Prophet	1.87	0.02	2	**1.56**	**3103.78**
10575	10550-580C	3215.64-3224.78	Besa River	2.02	0.18	10	**1.65**	**3223.26**
10865	10850-880C	'3311.65-3316.22	Besa River	2.41	0.32	2	**1.89**	**3311.65**
11635	11620-650C	3541.77-3550.92	Besa River*	2.74	0.22	10	**2.09**	**3546.35**
12015	12000-030C	3657.60-3666.74	Besa River*	2.85	0.04	2	**2.16**	**3662.17**
12265	12250-280C	3733.80-3742.94	Besa River	2.90	0.00	1	**2.19**	**3738.37**
12665	12660-670C	3858.77-3862.81	Besa River	3.40	0.00	1	**2.50**	**3860.29**
12915	12900-930C	'3931.92-3941.06	Besa River**	3.50			**2.56**	**3936.49**
12975	12960-990C	3954.78-3959.35	Besa River**	3.70			**2.69**	**3954.78**
13185	13170-200C	4014.224023.36	Besa River**	3.43	0.30	7	**2.52**	**4018.79**
13549	13530-368C	4123.94-4074.57	Nahanni	3.8			**2.75**	**4129.74**

BURIAL 3A PanAm Beaver River G-01.dat Model #1

Pan Am Beaver River YT G-01
M
0000.0 T 37 0.000 0.000 0.000 0.000 0.000 0.000 0.000 080.0 025.0 AGE1
1200.0 T 37 0.000 0.050 0.000 0.950 0.000 0.000 0.000 080.0 025.0 AGE2
0030.0 T 37 0.050 0.000 0.000 0.950 0.000 0.000 0.000 080.0 025.0 AGE3
0247.0 T 37 0.000 0.000 0.000 0.950 0.000 0.000 0.050 080.0 025.0 AGE4
0571.0 T 37 0.950 0.000 0.000 0.000 0.000 0.000 0.050 080.0 025.0 AGE5
0411.0 T 37 0.850 0.000 0.000 0.000 0.100 0.000 0.050 150.0 025.0 AGE6
0089.0 T 37 0.250 0.000 0.500 0.000 0.000 0.000 0.250 150.0 025.0 AGE7
1254.0 T 37 0.750 0.100 0.000 0.000 0.150 0.000 0.000 150.0 025.0 AGE8
0945.0 T 37 0.150 0.650 0.000 0.000 0.200 0.000 0.000 150.0 025.0 AGE9
0255.0 F 11 0.150 0.650 0.000 0.000 0.200 0.000 0.000 150.0 025.0 AGE10
0000.0 T 37 0.000 0.000 0.000 0.000 0.000 0.000 0.000 150.0 025.0 AGE11
0220.0 T 37 0.250 0.500 0.000 0.000 0.250 0.000 0.000 150.0 025.0 AGE12
0189.0 T 37 0.500 0.000 0.000 0.000 0.000 0.000 0.500 140.0 025.0 AGE13
0011.0 F 15 0.500 0.000 0.000 0.000 0.000 0.000 0.500 140.0 025.0 AGE14
0000.0 T 37 0.000 0.000 0.000 0.000 0.000 0.000 0.000 140.0 025.0 AGE15
0297.0 T 37 0.800 0.100 0.000 0.000 0.100 0.000 0.000 120.0 025.0 AGE16
0503.0 F 18 0.800 0.100 0.000 0.000 0.100 0.000 0.000 120.0 025.0 AGE17
0000.0 T 37 0.000 0.000 0.000 0.000 0.000 0.000 0.000 120.0 025.0 AGE18
0122.0 T 37 0.250 0.500 0.000 0.000 0.250 0.000 0.000 100.0 025.0 AGE19
0030.0 F 35 0.250 0.500 0.000 0.000 0.250 0.000 0.000 100.0 025.0 AGE20
0070.0 F 34 0.000 0.500 0.000 0.000 0.500 0.000 0.000 100.0 025.0 AGE21
0170.0 F 33 0.800 0.100 0.000 0.000 0.100 0.000 0.000 080.0 025.0 AGE22
0030.0 F 32 0.000 1.000 0.000 0.000 0.000 0.000 0.000 080.0 025.0 AGE23
0150.0 F 31 0.500 0.200 0.000 0.000 0.300 0.000 0.000 080.0 025.0 AGE24
0050.0 F 30 0.000 1.000 0.000 0.000 0.000 0.000 0.000 080.0 025.0 AGE25
0050.0 F 29 0.700 0.150 0.000 0.000 0.150 0.000 0.000 080.0 025.0 AGE26
0150.0 F 28 0.000 0.500 0.000 0.000 0.500 0.000 0.000 080.0 025.0 AGE27
0000.0 T 37 0.000 0.000 0.000 0.000 0.000 0.000 0.000 080.0 015.0 AGE28
0000.0 T 37 0.000 0.000 0.000 0.000 0.000 0.000 0.000 060.0 015.0 AGE29
0000.0 T 37 0.000 0.000 0.000 0.000 0.000 0.000 0.000 060.0 015.0 AGE30
0000.0 T 37 0.000 0.000 0.000 0.000 0.000 0.000 0.000 060.0 015.0 AGE31
0000.0 T 37 0.000 0.000 0.000 0.000 0.000 0.000 0.000 060.0 015.0 AGE32
0000.0 T 37 0.000 0.000 0.000 0.000 0.000 0.000 0.000 060.0 015.0 AGE33
0000.0 T 37 0.000 0.000 0.000 0.000 0.000 0.000 0.000 060.0 015.0 AGE34
0000.0 T 37 0.000 0.000 0.000 0.000 0.000 0.000 0.000 080.0 010.0 AGE35
0015.0 T 37 0.000 0.500 0.000 0.000 0.500 0.000 0.000 080.0 010.0 AGE36

Pan Am Beaver River YT G-01 Model 2
M
0000.0 T 37 0.000 0.000 0.000 0.000 0.000 0.000 0.000 060.0 025.0 AGE1
1200.0 T 37 0.000 0.050 0.000 0.950 0.000 0.000 0.000 060.0 025.0 AGE2
0030.0 T 37 0.050 0.000 0.000 0.950 0.000 0.000 0.000 060.0 025.0 AGE3
0247.0 T 37 0.000 0.000 0.000 0.950 0.000 0.000 0.050 060.0 025.0 AGE4
0571.0 T 37 0.950 0.000 0.000 0.000 0.000 0.000 0.050 060.0 025.0 AGE5
0411.0 T 37 0.850 0.000 0.000 0.000 0.100 0.000 0.050 060.0 025.0 AGE6
0089.0 T 37 0.250 0.000 0.500 0.000 0.000 0.000 0.250 060.0 025.0 AGE7
1254.0 T 37 0.750 0.100 0.000 0.000 0.150 0.000 0.000 060.0 025.0 AGE8
0945.0 T 37 0.150 0.650 0.000 0.000 0.200 0.000 0.000 060.0 025.0 AGE9
0255.0 F 11 0.150 0.650 0.000 0.000 0.200 0.000 0.000 060.0 025.0 AGE10
0000.0 T 37 0.000 0.000 0.000 0.000 0.000 0.000 0.000 060.0 025.0 AGE11
0220.0 T 37 0.250 0.500 0.000 0.000 0.250 0.000 0.000 060.0 025.0 AGE12
0189.0 T 37 0.500 0.000 0.000 0.000 0.000 0.000 0.500 060.0 025.0 AGE13
0011.0 F 15 0.500 0.000 0.000 0.000 0.000 0.000 0.500 060.0 025.0 AGE14
0000.0 T 37 0.000 0.000 0.000 0.000 0.000 0.000 0.000 060.0 025.0 AGE15
0297.0 T 37 0.800 0.100 0.000 0.000 0.100 0.000 0.000 060.0 025.0 AGE16
0503.0 F 18 0.800 0.100 0.000 0.000 0.100 0.000 0.000 060.0 025.0 AGE17
0000.0 T 37 0.000 0.000 0.000 0.000 0.000 0.000 0.000 150.0 025.0 AGE18
0122.0 T 37 0.250 0.500 0.000 0.000 0.250 0.000 0.000 150.0 025.0 AGE19
0030.0 F 35 0.250 0.500 0.000 0.000 0.250 0.000 0.000 150.0 025.0 AGE20
0070.0 F 34 0.000 0.500 0.000 0.000 0.500 0.000 0.000 150.0 025.0 AGE21
0170.0 F 33 0.800 0.100 0.000 0.000 0.100 0.000 0.000 150.0 025.0 AGE22
0030.0 F 32 0.000 1.000 0.000 0.000 0.000 0.000 0.000 150.0 025.0 AGE23
0150.0 F 31 0.500 0.200 0.000 0.000 0.300 0.000 0.000 150.0 025.0 AGE24
0050.0 F 30 0.000 1.000 0.000 0.000 0.000 0.000 0.000 150.0 025.0 AGE25
0050.0 F 29 0.700 0.150 0.000 0.000 0.150 0.000 0.000 150.0 025.0 AGE26
0150.0 F 28 0.000 0.500 0.000 0.000 0.500 0.000 0.000 150.0 025.0 AGE27
0000.0 T 37 0.000 0.000 0.000 0.000 0.000 0.000 0.000 150.0 015.0 AGE28
0000.0 T 37 0.000 0.000 0.000 0.000 0.000 0.000 0.000 140.0 015.0 AGE29
0000.0 T 37 0.000 0.000 0.000 0.000 0.000 0.000 0.000 130.0 015.0 AGE30
0000.0 T 37 0.000 0.000 0.000 0.000 0.000 0.000 0.000 110.0 015.0 AGE31
0000.0 T 37 0.000 0.000 0.000 0.000 0.000 0.000 0.000 100.0 015.0 AGE32
0000.0 T 37 0.000 0.000 0.000 0.000 0.000 0.000 0.000 080.0 015.0 AGE33
0000.0 T 37 0.000 0.000 0.000 0.000 0.000 0.000 0.000 080.0 015.0 AGE34
0000.0 T 37 0.000 0.000 0.000 0.000 0.000 0.000 0.000 080.0 010.0 AGE35
0015.0 T 37 0.000 0.500 0.000 0.000 0.500 0.000 0.000 080.0 010.0 AGE36

Pan Am Beaver River YT G-01 Model 3
M
0000.0 T 37 0.000 0.000 0.000 0.000 0.000 0.000 0.000 080.0 025.0 AGE1
1200.0 T 37 0.000 0.050 0.000 0.950 0.000 0.000 0.000 080.0 025.0 AGE2
0030.0 T 37 0.050 0.000 0.000 0.950 0.000 0.000 0.000 080.0 025.0 AGE3
0247.0 T 37 0.000 0.000 0.000 0.950 0.000 0.000 0.050 080.0 025.0 AGE4
0571.0 T 37 0.950 0.000 0.000 0.000 0.000 0.000 0.050 080.0 025.0 AGE5
0411.0 T 37 0.850 0.000 0.000 0.000 0.100 0.000 0.050 100.0 025.0 AGE6
0089.0 T 37 0.250 0.000 0.500 0.000 0.000 0.000 0.250 100.0 025.0 AGE7
1254.0 T 37 0.750 0.100 0.000 0.000 0.150 0.000 0.000 100.0 025.0 AGE8
0945.0 T 37 0.150 0.650 0.000 0.000 0.200 0.000 0.000 100.0 025.0 AGE9
0255.0 F 11 0.150 0.650 0.000 0.000 0.200 0.000 0.000 100.0 025.0 AGE10
0000.0 T 37 0.000 0.000 0.000 0.000 0.000 0.000 0.000 100.0 025.0 AGE11
0220.0 T 37 0.250 0.500 0.000 0.000 0.250 0.000 0.000 100.0 025.0 AGE12
0189.0 T 37 0.500 0.000 0.000 0.000 0.000 0.000 0.500 100.0 025.0 AGE13
0011.0 F 15 0.500 0.000 0.000 0.000 0.000 0.000 0.500 100.0 025.0 AGE14
0000.0 T 37 0.000 0.000 0.000 0.000 0.000 0.000 0.000 100.0 025,0 AGE15
0297.0 T 37 0.800 0.100 0.000 0.000 0.100 0.000 0.000 100.0 025.0 AGE16
0503.0 F 18 0.800 0.100 0.000 0.000 0.100 0.000 0.000 100.0 025.0 AGE17
0000.0 T 37 0.000 0.000 0.000 0.000 0.000 0.000 0.000 100.0 025.0 AGE18
0122.0 T 37 0.250 0.500 0.000 0.000 0.250 0.000 0.000 100.0 025.0 AGE19
0030.0 F 35 0.250 0.500 0.000 0.000 0.250 0.000 0.000 100.0 025.0 AGE20
0070.0 F 34 0.000 0.500 0.000 0.000 0.500 0.000 0.000 100.0 025.0 AGE21
0170.0 F 33 0.800 0.100 0.000 0.000 0.100 0.000 0.000 080.0 025.0 AGE22
0030.0 F 32 0.000 1.000 0.000 0.000 0.000 0.000 0.000 080.0 025.0 AGE23
0150.0 F 31 0.500 0.200 0.000 0.000 0.300 0.000 0.000 080.0 025.0 AGE24
0050.0 F 30 0.000 1.000 0.000 0.000 0.000 0.000 0.000 080.0 025.0 AGE25
0050.0 F 29 0.700 0.150 0.000 0.000 0.150 0.000 0.000 080.0 025.0 AGE26
0150.0 F 28 0.000 0.500 0.000 0.000 0.500 0.000 0.000 080.0 025.0 AGE27
0000.0 T 37 0.000 0.000 0.000 0.000 0.000 0.000 0.000 080.0 015.0 AGE28
0000.0 T 37 0.000 0.000 0.000 0.000 0.000 0.000 0.000 060.0 015.0 AGE29
0000.0 T 37 0.000 0.000 0.000 0.000 0.000 0.000 0.000 060.0 015.0 AGE30
0000.0 T 37 0.000 0.000 0.000 0.000 0.000 0.000 0.000 060.0 015.0 AGE31
0000.0 T 37 0.000 0.000 0.000 0.000 0.000 0.000 0.000 060.0 015.0 AGE32
0000.0 T 37 0.000 0.000 0.000 0.000 0.000 0.000 0.000 060.0 015.0 AGE33
0000.0 T 37 0.000 0.000 0.000 0.000 0.000 0.000 0.000 060.0 015.0 AGE34
0000.0 T 37 0.000 0.000 0.000 0.000 0.000 0.000 0.000 080.0 010.0 AGE35
0015.0 T 37 0.000 0.500 0.000 0.000 0.500 0.000 0.000 080.0 010.0 AGE36

Pan Am Beaver River YT G-01 Model 4
M
0000.0 T 37 0.000 0.000 0.000 0.000 0.000 0.000 0.000 075.0 025.0 AGE1
1200.0 T 37 0.000 0.050 0.000 0.950 0.000 0.000 0.000 075.0 025.0 AGE2
0030.0 T 37 0.050 0.000 0.000 0.950 0.000 0.000 0.000 075.0 025.0 AGE3
0247.0 T 37 0.000 0.000 0.000 0.950 0.000 0.000 0.050 080.0 025.0 AGE4
0571.0 T 37 0.950 0.000 0.000 0.000 0.000 0.000 0.050 080.0 025.0 AGE5
0411.0 T 37 0.850 0.000 0.000 0.000 0.100 0.000 0.050 100.0 025.0 AGE6
0089.0 T 37 0.250 0.000 0.500 0.000 0.000 0.000 0.250 100.0 025.0 AGE7
1254.0 T 37 0.750 0.100 0.000 0.000 0.150 0.000 0.000 080.0 025.0 AGE8
0945.0 T 37 0.150 0.650 0.000 0.000 0.200 0.000 0.000 120.0 025.0 AGE9
0255.0 F 11 0.150 0.650 0.000 0.000 0.200 0.000 0.000 120.0 025.0 AGE10
0000.0 T 37 0.000 0.000 0.000 0.000 0.000 0.000 0.000 120.0 025.0 AGE11
0220.0 T 37 0.250 0.500 0.000 0.000 0.250 0.000 0.000 120.0 025.0 AGE12
0189.0 T 37 0.500 0.000 0.000 0.000 0.000 0.000 0.500 120.0 025.0 AGE13
0011.0 F 15 0.500 0.000 0.000 0.000 0.000 0.000 0.500 120.0 025.0 AGE14
0000.0 T 37 0.000 0.000 0.000 0.000 0.000 0.000 0.000 120.0 025.0 AGE15
0297.0 T 37 0.800 0.100 0.000 0.000 0.100 0.000 0.000 120.0 025.0 AGE16
0503.0 F 18 0.800 0.100 0.000 0.000 0.100 0.000 0.000 120.0 025.0 AGE17
0000.0 T 37 0.000 0.000 0.000 0.000 0.000 0.000 0.000 120.0 025.0 AGE18
0122.0 T 37 0.250 0.500 0.000 0.000 0.250 0.000 0.000 120.0 025.0 AGE19
0030.0 F 35 0.250 0.500 0.000 0.000 0.250 0.000 0.000 120.0 025.0 AGE20
0070.0 F 34 0.000 0.500 0.000 0.000 0.500 0.000 0.000 120.0 025.0 AGE21
0170.0 F 33 0.800 0.100 0.000 0.000 0.100 0.000 0.000 120.0 025.0 AGE22
0030.0 F 32 0.000 1.000 0.000 0.000 0.000 0.000 0.000 120.0 025.0 AGE23
0150.0 F 31 0.500 0.200 0.000 0.000 0.300 0.000 0.000 120.0 025.0 AGE24
0050.0 F 30 0.000 1.000 0.000 0.000 0.000 0.000 0.000 120.0 025.0 AGE25
0050.0 F 29 0.700 0.150 0.000 0.000 0.150 0.000 0.000 100.0 025.0 AGE26
0150.0 F 28 0.000 0.500 0.000 0.000 0.500 0.000 0.000 100.0 025.0 AGE27
0000.0 T 37 0.000 0.000 0.000 0.000 0.000 0.000 0.000 100.0 015.0 AGE28
0000.0 T 37 0.000 0.000 0.000 0.000 0.000 0.000 0.000 100.0 015.0 AGE29
0000.0 T 37 0.000 0.000 0.000 0.000 0.000 0.000 0.000 100.0 015.0 AGE30
0000.0 T 37 0.000 0.000 0.000 0.000 0.000 0.000 0.000 100.0 015.0 AGE31
0000.0 T 37 0.000 0.000 0.000 0.000 0.000 0.000 0.000 100.0 015.0 AGE32
0000.0 T 37 0.000 0.000 0.000 0.000 0.000 0.000 0.000 100.0 015.0 AGE33
0000.0 T 37 0.000 0.000 0.000 0.000 0.000 0.000 0.000 100.0 015.0 AGE34
0000.0 T 37 0.000 0.000 0.000 0.000 0.000 0.000 0.000 080.0 010.0 AGE35
0015.0 T 37 0.000 0.500 0.000 0.000 0.500 0.000 0.000 080.0 010.0 AGE36

Pan Am Beaver River YT G-01 Model 5
M
0000.0 T 37 0.000 0.000 0.000 0.000 0.000 0.000 0.000 080.0 025.0 AGE1
1200.0 T 37 0.000 0.050 0.000 0.950 0.000 0.000 0.000 080.0 025.0 AGE2
0030.0 T 37 0.050 0.000 0.000 0.950 0.000 0.000 0.000 080.0 025.0 AGE3
0247.0 T 37 0.000 0.000 0.000 0.950 0.000 0.000 0.050 080.0 025.0 AGE4
0571.0 T 37 0.950 0.000 0.000 0.000 0.000 0.000 0.050 080.0 025.0 AGE5
0411.0 T 37 0.850 0.000 0.000 0.000 0.100 0.000 0.050 100.0 025.0 AGE6
0089.0 T 37 0.250 0.000 0.500 0.000 0.000 0.000 0.250 100.0 025.0 AGE7
1254.0 T 37 0.750 0.100 0.000 0.000 0.150 0.000 0.000 180.0 025.0 AGE8
0945.0 T 37 0.150 0.650 0.000 0.000 0.200 0.000 0.000 180.0 025.0 AGE9
0255.0 F 11 0.150 0.650 0.000 0.000 0.200 0.000 0.000 180.0 025.0 AGE10
0000.0 T 37 0.000 0.000 0.000 0.000 0.000 0.000 0.000 180.0 025.0 AGE11
0220.0 T 37 0.250 0.500 0.000 0.000 0.250 0.000 0.000 180.0 025.0 AGE12
0189.0 T 37 0.500 0.000 0.000 0.000 0.000 0.000 0.500 180.0 025.0 AGE13
0011.0 F 15 0.500 0.000 0.000 0.000 0.000 0.000 0.500 180.0 025.0 AGE14
0000.0 T 37 0.000 0.000 0.000 0.000 0.000 0.000 0.000 150.0 025.0 AGE15
0297.0 T 37 0.800 0.100 0.000 0.000 0.100 0.000 0.000 140.0 025.0 AGE16
0503.0 F 18 0.800 0.100 0.000 0.000 0.100 0.000 0.000 130.0 025.0 AGE17
0000.0 T 37 0.000 0.000 0.000 0.000 0.000 0.000 0.000 120.0 025.0 AGE18
0122.0 T 37 0.250 0.500 0.000 0.000 0.250 0.000 0.000 100.0 025.0 AGE19
0030.0 F 35 0.250 0.500 0.000 0.000 0.250 0.000 0.000 100.0 025.0 AGE20
0070.0 F 34 0.000 0.500 0.000 0.000 0.500 0.000 0.000 100.0 025.0 AGE21
0170.0 F 33 0.800 0.100 0.000 0.000 0.100 0.000 0.000 080.0 025.0 AGE22
0030.0 F 32 0.000 1.000 0.000 0.000 0.000 0.000 0.000 080.0 025.0 AGE23
0150.0 F 31 0.500 0.200 0.000 0.000 0.300 0.000 0.000 080.0 025.0 AGE24
0050.0 F 30 0.000 1.000 0.000 0.000 0.000 0.000 0.000 080.0 025.0 AGE25
0050.0 F 29 0.700 0.150 0.000 0.000 0.150 0.000 0.000 080.0 025.0 AGE26
0150.0 F 28 0.000 0.500 0.000 0.000 0.500 0.000 0.000 080.0 025.0 AGE27
0000.0 T 37 0.000 0.000 0.000 0.000 0.000 0.000 0.000 080.0 015.0 AGE28
0000.0 T 37 0.000 0.000 0.000 0.000 0.000 0.000 0.000 060.0 015.0 AGE29
0000.0 T 37 0.000 0.000 0.000 0.000 0.000 0.000 0.000 060.0 015.0 AGE30
0000.0 T 37 0.000 0.000 0.000 0.000 0.000 0.000 0.000 060.0 015.0 AGE31
0000.0 T 37 0.000 0.000 0.000 0.000 0.000 0.000 0.000 060.0 015.0 AGE32
0000.0 T 37 0.000 0.000 0.000 0.000 0.000 0.000 0.000 060.0 015.0 AGE33
0000.0 T 37 0.000 0.000 0.000 0.000 0.000 0.000 0.000 060.0 015.0 AGE34
0000.0 T 37 0.000 0.000 0.000 0.000 0.000 0.000 0.000 080.0 010.0 AGE35
0015.0 T 37 0.000 0.500 0.000 0.000 0.500 0.000 0.000 080.0 010.0 AGE36

Internal Stratigraphy, Petrography and Porosity Development of the Manetoe Dolomite in the Region of the Pointed Mountain and Kotaneelee Gas Fields

David W. Morrow and Judith Potter
Geological Survey of Canada, Calgary
3303 33rd St. N.W.
Calgary, Alberta
T2L 2A7

Abstract

Cores of the thick peritidal argillaceous dololaminite shoreface sequence of Headless equivalent strata within the subsurface Manetoe Dolomite in Liard Basin display lithologies similar to the thick peritidal dolomitic wackestone facies of the lower part of the Dunedin Formation of northeast British Columbia. This supports the concept that the Nahanni and Headless formations in the subsurface of Liard Basin formed a transgressive sedimentary package similar to the Dunedin before dolomitization, unlike the Nahanni-Headless sequence of the Mackenzie Mountains farther north.

Manetoe Dolomite in cores from gas fields in Liard Basin display evidence of at least one, and possibly several, solution excavation events. Cavern-fill deposits postdate, and possibly formed contemporaneously with, emplacement of the Manetoe Dolomite. Movement of hydrocarbons into Manetoe Dolomite reservoirs postdated the episode(s) of cavern excavation. Gas and bitumen in the La Biche Field indicates that cavern-fillings are in contact with source rock. Reservoir bitumens that completely occlude prebitumen porosity of the Manetoe Dolomite may represent deasphalted oil. Bitumens in overlying strata display a consistent downward increase in reflectivity that parallels the downward increase in vitrinite reflectance and in Tmax.

The present day porosities of the Manetoe Dolomite and Nahanni limestone in cores from the gas fields are consistent with depth-dependent burial porosity loss accompanied by occlusion of porosity by mineral cements and bitumen. Additional porosity loss may have occurred from more time-dependent processes such as stylotization. Permeability, particularly vertical permeability, has been enhanced by dolomitization, except possibly in cases where pre-dolomitization porosity and permeability was high. Late stage fracture porosity is not pervasive, and, in most cores, is not present.

Introduction

The Manetoe Dolomite and its associated gas fields lie in the subsurface of the Liard Basin (Gabrielse, 1967) west of the Liard River across the border of the Yukon and Northwest Territories (Fig. 1). Large masses of fractured white sparry dolomite form the reservoir rock at depths ranging from 2600 metres to 3400 metres subsea in the Pointed Mountain and Kotaneelee gas fields (Figs. 2 and 3). Other nonproducing fields, such as the Liard and La Biche fields (Price, 1994), developed within the Manetoe Dolomite of this region and occur at shallower depths. The Manetoe Dolomite itself extends north to nearly 63° N latitude. It is present across an area of more than 30,000 km^2 in the south-central Mackenzie Mountains (Morrow *et al.*, 1990). The Manetoe Dolomite is mainly stratiform, or stratabound, and is confined to a thin stratigraphic interval, commonly 10 to 40 metres thick, within the Landry and uppermost Arnica formations and immediately underneath the shaly limestones of the Headless Formation (Fig. 4). However, in some areas, such as at the gas fields, the Manetoe Dolomite extends vertically several hundred metres upwards through the Headless Formation and into the overlying Nahanni Formation (Fig. 4). It is in these areas where dolomitization extends vertically upwards into the Nahanni that the Manetoe is prospective for hydrocarbons.

The Beaver River, Kotaneelee and Pointed Mountain gas fields have an initial combined estimated gas reserve of about 15.5 x 10^9m^3, and have had a cumulative gas production of about 10.0 x 10^9m^3 (Morrell *et al.*, 1995). Gas in these fields is almost entirely contained within intercrystalline pore space of the matrix dolomite (Snowdon, 1977) and is almost entirely methane (Ward, 1994). Other gases present include CO_2 (<15%) and N_2 (<10%). H_2S constitutes less than a few per cent and He (0.05%) is present in trace amounts (Ward, 1994).

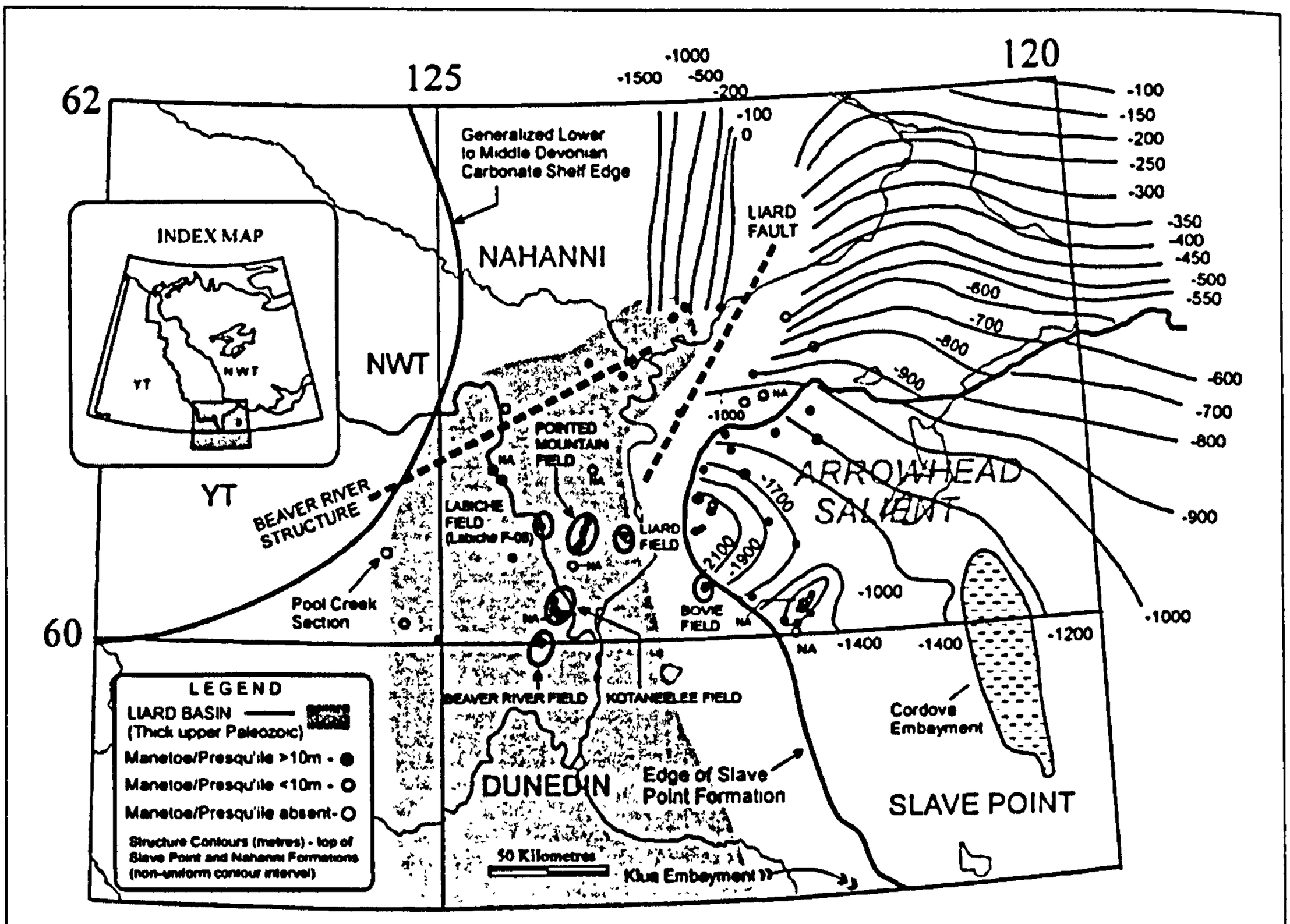

Fig. 1. Index map showing locations of gas fields, Liard Basin, Arrowhead Salient of the Presqu'ile Barrier and trends of major basement structures (Liard Fault and Beaver River Structure).

Gas columns in these fields are in excess of 600 metres and production is aided by an active water drive in addition to gas expansion (Ward, 1994; Meding, 1994). This water drive is provided by a regional aquifer which flows through lower Paleozoic carbonate strata west to east from the Mackenzie and Franklin Mountains and discharges rather saline water into the Liard and Mackenzie Rivers (Ward, 1994). The basal black shales of the Besa River Formation, or Horn River equivalent shales (Fig. 4), act as an upward confining layer to this regional aquifer. These black shales also act as a seal against the upward migration of gas which is entrapped in dolomitized sections of Arnica to Nahanni strata (Fig. 4) in areas of structural closure such as at the Pointed Mountain and Kotaneelee fields (Figs. 2 and 3). These organic-rich shales with up to 5% TOC (total organic carbon) probably also were the main source beds for hydrocarbon in these fields (Fig. 5; Morrow *et al.*, 1993).

Liquid hydrocarbons were generated from Besa River source beds in late Paleozoic time and initial migration of oil probably occurred before the end of Paleozoic time (Morrow *et al.*, 1993). This was primarily the consequence of rapid and deep Carboniferous burial in Liard Basin (Fig. 1) under conditions of high heat flow (Morrow *et al.*, 1993). The northern edge of this upper Paleozoic depocentre is close and parallel to the northeast contination of the Beaver River Fault in the La Biche River map area (Douglas, 1976). The Beaver River Fault and its northeast continuation are named here as the "Beaver River Structure" (Fig. 1). The prominent east-west bend in the Nahanni Thrust Fault at Nahanni Butte at the junction of the South Nahanni and Liard rivers, as mapped on the Sibbeston Lake map area (Douglas and Norris, 1976), marks the eastern traceable limit of this hypothesized Beaver River Structure.

There is a profound difference in structural style north and south of the Beaver River Structure. Thrust faults north of the structure are almost all eastward-verging, with the normal eastward-directed movement on Laramide thrusts. South of the structure, thrust faults are dominantly west-verging. West-verging thrust faults,

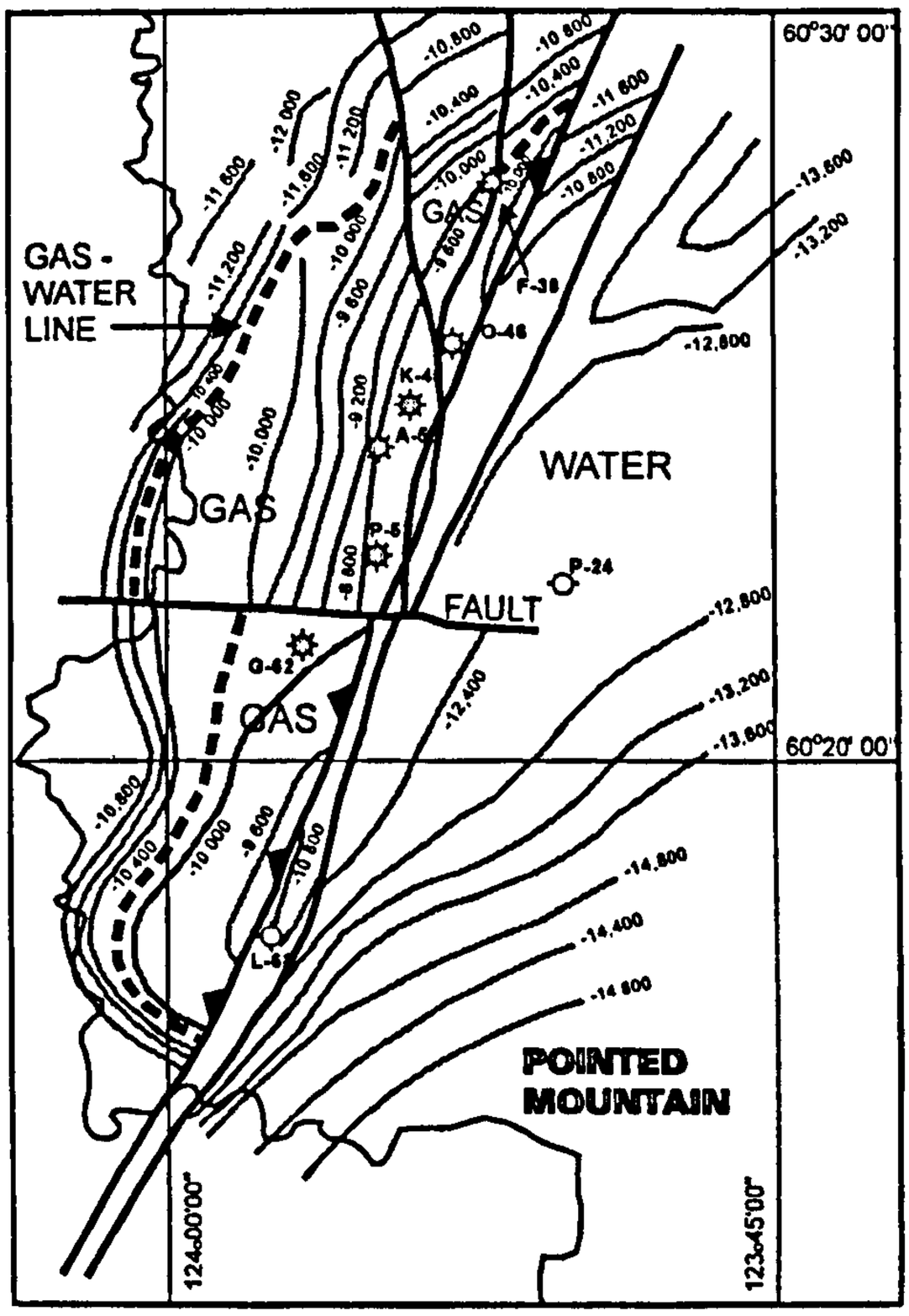

Fig. 2. Seismic depth map of the top of the Manetoe Dolomite (Nahanni equivalent) at the Pointed Mountain gas field, Northwest Territories (Amoco Canada Petroleum Company Ltd., 1964).

such as the Beaver River Thrust, the Larsen Thrust, the La Biche Fault, the Dendale Thrust, and the Kotaneelee Fault (Douglas and Norris, 1976 and Fig. 3), are the norm, rather than the exception south of the Beaver River Structure. The more "normal" eastward dominant sense of Laramide thrust fault movement reasserts itself only south of the border with British Columbia.

It seems possible that this profound change in structural style is a manifestation of a deep Precambrian crustal fault that was periodically reactivated during times of tectonism, such as the Laramide Orogeny. The Beaver River Structure also may have played an earlier role in forming the northern margin of Liard Basin in late Paleozoic time. Other, similar ancient NE-SW oriented Precambrian crustal faults are known to have segmented the miogeocline of western Canada in Paleozoic time (Cecile *et al.*,1997).

In addition to the hypothesized Beaver River Structure, the Liard Fault is another ancient fault that may have been active in late Paleozoic time within the region of the gas fields. The Liard Fault is a NNE-SSW trending structure that has offset the top of the Devonian carbonates (Williams, 1981; Fig. 1). Morrow *et al.* (1990) suggested that the Pointed Mountain, Kotaneelee and Beaver River fields fall along the southward continuation of this fault. They suggested that post-Devonian movement along this fault may have provided vertical permeability that localized, or focussed the upward flow of brines responsible for Manetoe dolomitization.

This study is an attempt to define more precisely stratigraphic correlations within the intensely dolomitized Manetoe Dolomite of the gas fields, and to document episodes of mineral cementation (*e.g.* dolomite, calcite, quartz) and of bitumen emplacement, or the bitumen-like residual hydrocarbons that are commonly referred to as "reservoir bitumen" (Lomando, 1992). Petrographic relationships between these phases are used to define the sequence of events during burial diagenesis and fluid movements within Liard Basin. The inferred time of oil generation and migration is a key factor in determining the age of the Manetoe dolomitization event (Morrow and Aulstead, 1995). Another objective is to identify and characterize episodes of pore space creation and porosity destruction. The data and interpretations contained here are derived from a core display given at a core conference (Morrow, 1996) which accompanied the 1996 annual meeting of the Canadian Society of Petroleum Geologists (Pools '96).

Stratigraphy of Manetoe Reservoirs - Pointed Mountain, Kotaneelee and La Biche Fields

Stratigraphic cross-sections across the Pointed Mountain and Kotaneelee fields are shown in Figure 6 in addition to the "one well field" at La Biche F-08. In all wells of the Pointed Mountain and Kotaneelee fields the lower Devonian carbonates beneath the top of the Nahanni Formation and beneath the Middle to Upper Devonian Besa River shale are completely dolomitized and overprinted by the Manetoe Dolomite. However, the correlative sequence in the CPOG *et al.* La Biche F-08 well is incompletely dolomitized and contains numerous intervals of undolomitized Nahanni fossiliferous lime wackestone. Across most of the southern Mackenzie Mountains and in the subsurface of the Interior Plains east of the Mackenzie Mountains the Manetoe Dolomite is more stratiform and is confined stratigraphically to a zone of variable thickness commonly less than 30 metres thick and is dominantly, or entirely, developed within the Landry Formation (Morrow *et al.*, 1990).

In spite of the total dolomitization of the Arnica to

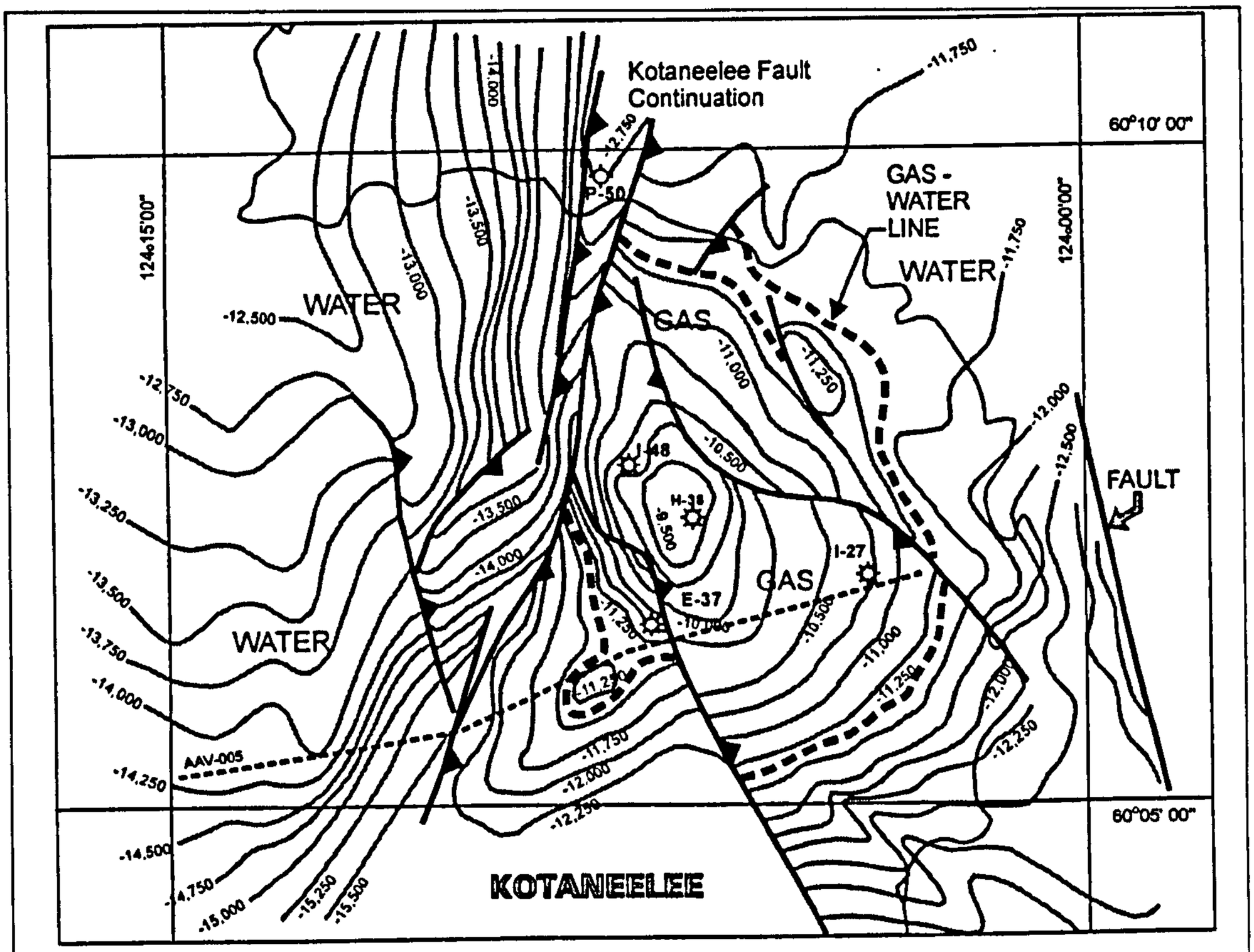

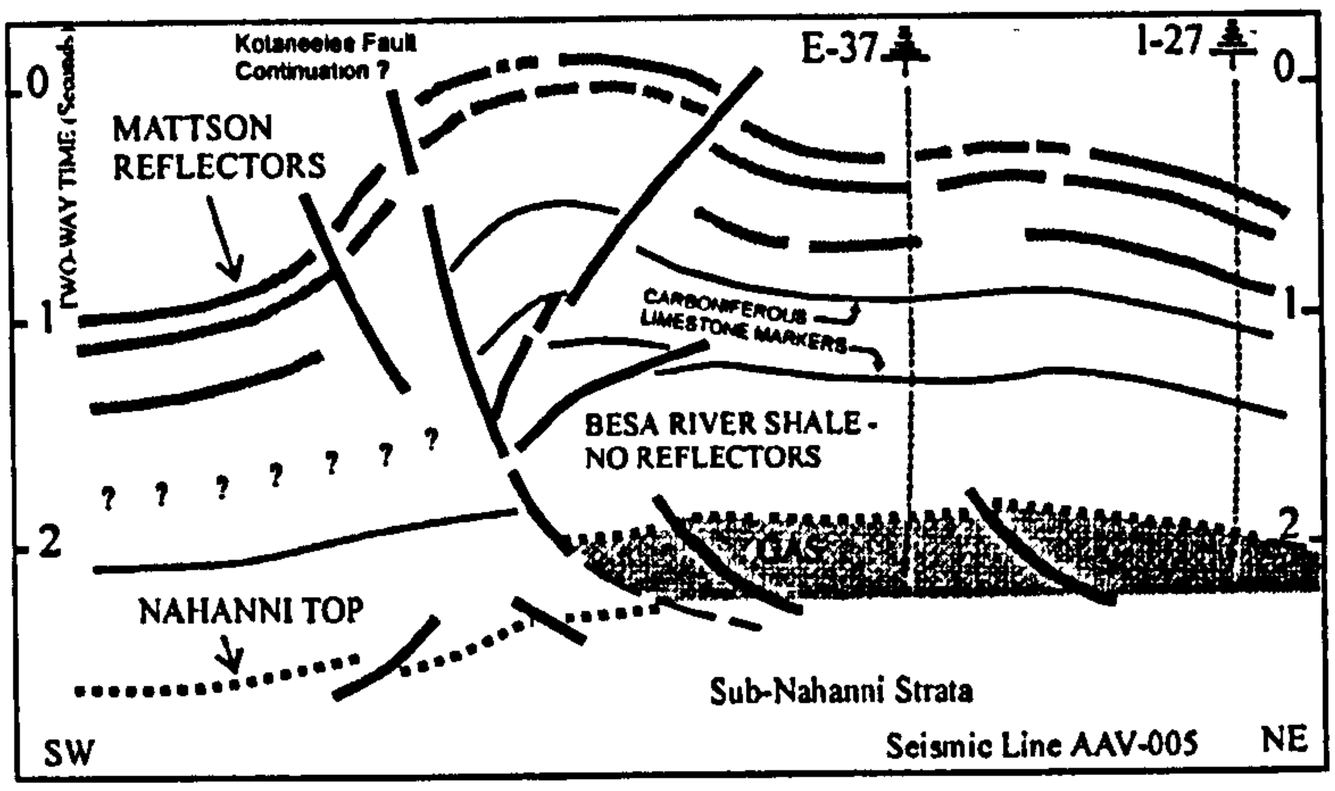

Fig. 3. Seismic depth map of the top of the Manetoe Dolomite (Nahanni equivalent) at the Kotaneelee gas field, Yukon Territory (Columbia Gas Development of Canada Ltd., 1979). Also shown is seismic reflection line AAV-005 across the southern part of the Kotaneelee field.

Nahanni interval in the gas field wells, predolomitization rock textures and faunal content, and the distinctive log characteristics (*e.g.* gamma-ray log) of argillaceous intervals, such as Headless Formation strata, remain discernible. Previously, a thin argillaceous interval, or marker horizon, within the completely dolomitized Nahanni sequence of the Pointed Mountain Field was mapped as Headless Formation (Morrow and Aulstead, 1995). More detailed lithostratigraphic correlations indicate that, within the lower Devonian of the gas fields, this marker interval occurs within the Nahanni Formation itself, rather than beneath the Nahanni, and is about 100 metres above the top of Headless equivalent strata (Fig. 6).

The top of the Nahanni Formation in the region of the gas fields is strongly diachronous and is progressively

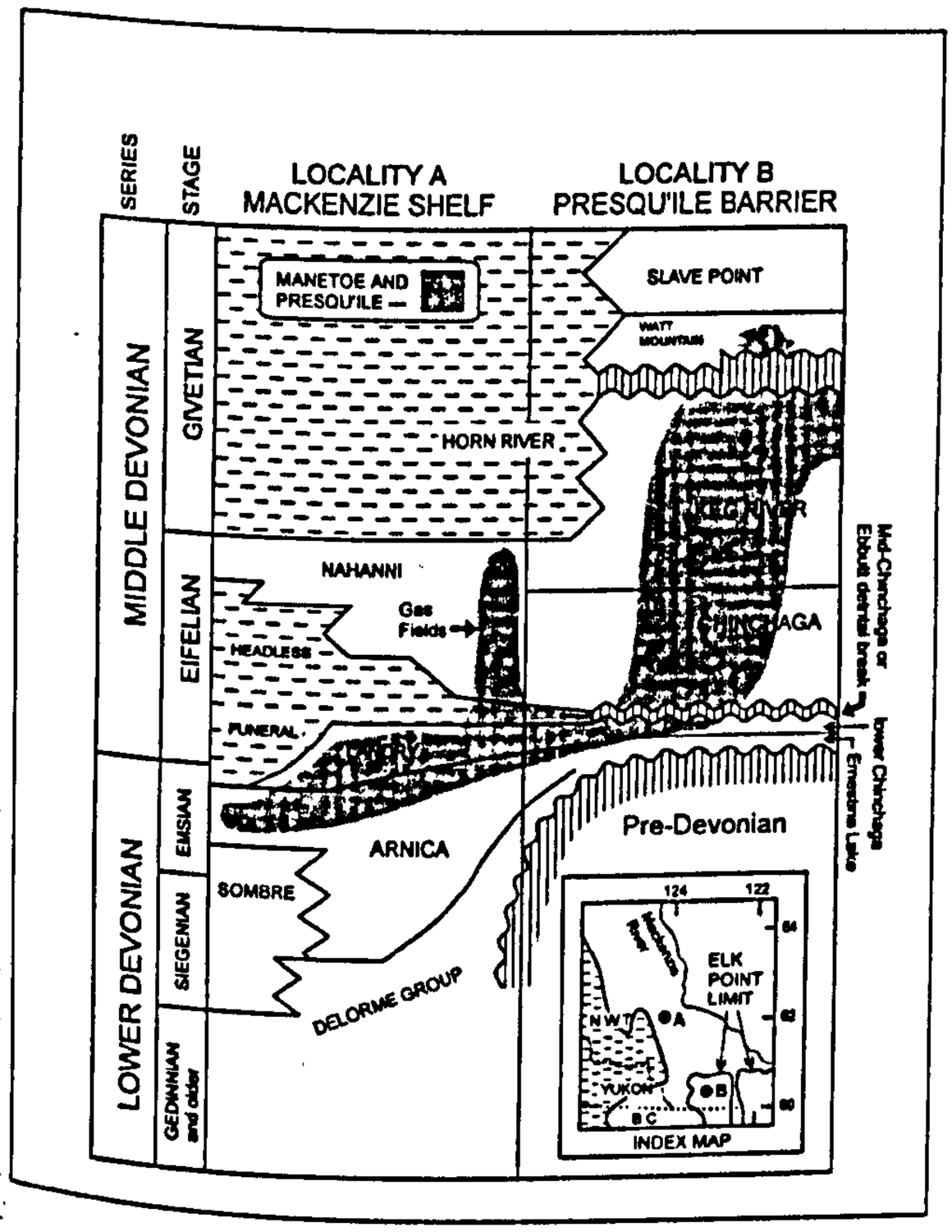

Fig. 4. Schematic stratigraphic chart illustrating the distribution of the Presqu'ile and Manetoe dolomites from the Arrowhead Salient of the Presqu'ile Barrier northwestwards to the Mackenzie Shelf sequence beneath Liard Basin and the southern Mackenzie Mountains.

younger eastward towards the Arrowhead Salient (Morrow and Aulstead, 1995). Conodonts collected from the uppermost beds of the Nahanni Formation in the eastern Texaco Bovie Lake J-72 well indicate a middle to late Givetian age for the top of the Nahanni (Appendix 1 of Meijer-Drees, 1993) near the western limit of the Arrowhead Salient of the Presqu'ile Barrier (Fig. 7). The eastward 'younging' of the upper contact of these strata with the overlying Besa River black shale closely resembles the similar southeastward 'younging' of the upper contact of the Dunedin Formation towards the Keg River, or Presqu'ile Barrier of northeastern British Columbia (Morrow, 1978; Taylor and Mackenzie, 1970). Strata close to the top of the Dunedin Formation near its northern limit in northeastern British Columbia are as old as Emsian (Chatterton, 1978). There is even evidence of intertonguing of Besa River shales with uppermost beds of Nahanni strata in the gas fields, similar to that which occurs in outcrop at the top of the Dunedin Formation in northeastern British Columbia (Morrow and Aulstead, 1995; Morrow, 1978).

The Headless Formation strata in the gas field wells is also somewhat different from Headless strata farther north in the outcrop belt of the Mackenzie Mountains. At the latitude of the southern Mackenzie Mountains, the Headless Formation gradually thickens westward from a feather edge in the Interior Plains to more than 250 metres thick in westernmost sections (Morrow and Cook, 1987). At its eastern limit, the Headless Formation is only a few metres thick and its basal contact is an unconformity that merges with the unconformity represented by the Ebbutt Break and the mid-Chinchaga detrital zone (Fig. 4). Throughout almost the entire Interior Plains east of the disturbed belt the Headless Formation is less than 30 metres, and commonly less than 10 metres, thick (Fig. 40 in Meijer-Drees, 1993). The eastern part of the Headless Formation is dolomitic and contains peritidal features such as finely laminated intervals containing fenestral fabric and lime mudflakes and mudlumps in pockets of green and ochre-coloured pyritic argillaceous material (Morrow and Cook, 1987; Meijer Drees, 1993). The thicker Headless in western sections is a shaly, open marine, completely subtidal limestone sequence quite different from the eastern Headless. The western Headless sequence was deposited on a submarine apron that accumulated in front of the westward-prograding shallow water shelf, or platform, limestones of the Nahanni Formation (Morrow and Cook, 1987; Noble and Ferguson, 1971).

The Headless Formation in the gas fields is about 150 metres thick and is distinctively argillaceous (Fig. 6). In core, however, it does not resemble the open marine fossiliferous shaly lime wackestones of the Headless Formation that is also about 150 metres thick in the southern Mackenzie Mountains. Instead the lithologies of the Headless interval in the gas fields more closely resemble the peritidal deposits of the thin Headless east of the disturbed belt. The gas field Headless interval also is lithologically and sedimentologically similar to the lower part of the Dunedin Formation in northeastern British Columbia. The lower part of the Dunedin, the dolomitic wackestone facies, has a maximum measured thickness of 130 metres and is composed of laminated and thin-bedded dolomitic lime mudstones containing fenestral fabric and dololaminites containing little fauna (Morrow, 1978). It has a log signature similar to the gas field Headless strata (Fig. 7).

These observations reinforce the concept (Morrow and Aulstead, 1995) that the Headless interval in the gas fields is better regarded as a northward continuation of the lower part of the Dunedin, rather than a southward continuation of the Headless Formation. The

TEXT BOUND INTO

THE SPINE

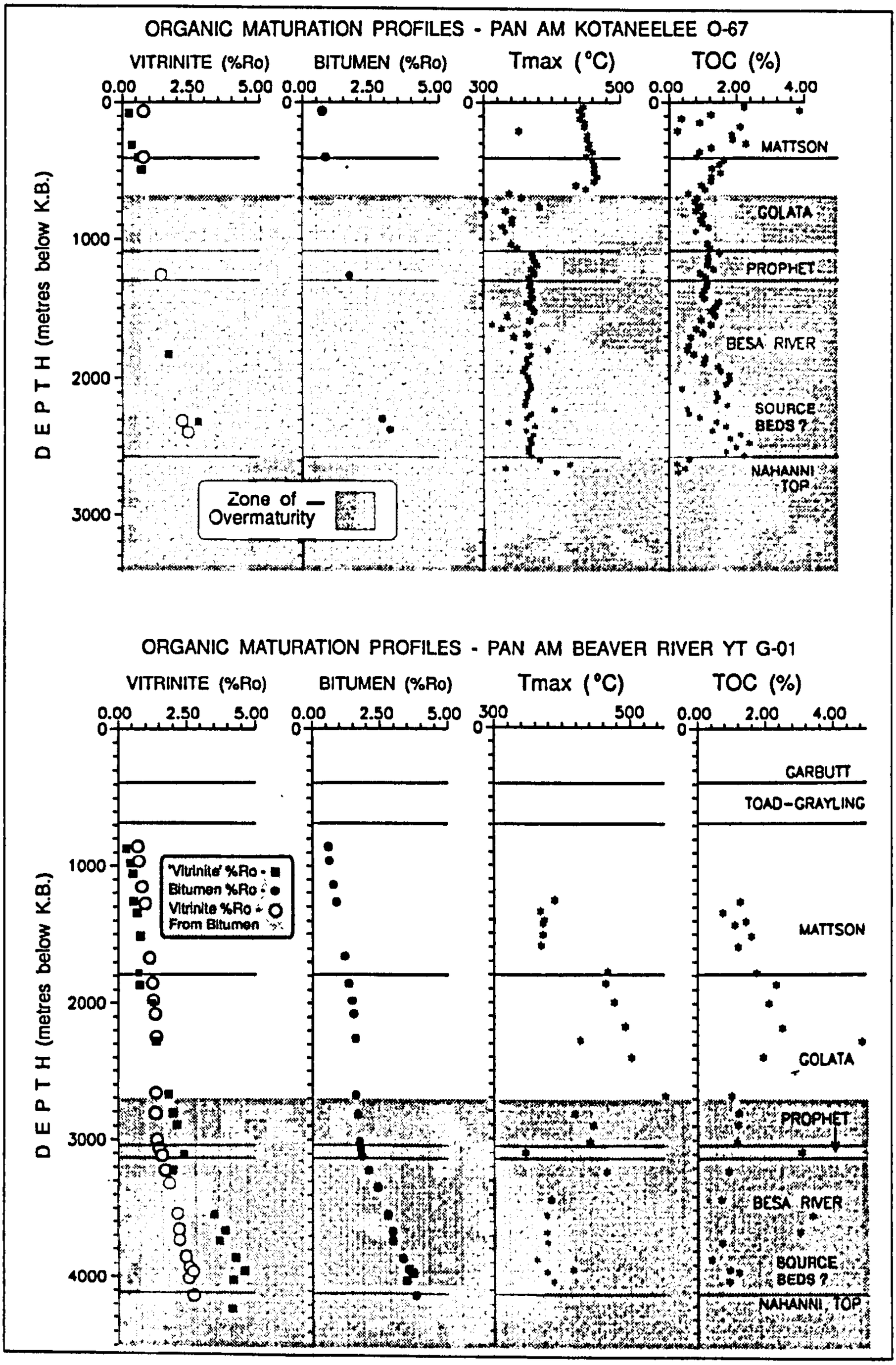

Fig. 5. Profiles of organic maturation from well cuttings in the Pan Am Beaver River YT G-01 and Pan Am Kotaneelee O-67 wells. The open circles represent vitrinite reflectance values calculated from bitumen reflectances (Jacob, 1985). True vitrinites are present only in the Mattson and Golata formations.

southward limit of the upward-shallowing regressive sedimentary package of the Nahanni and Headless formations coincides approximately with the northern edge of the Arrowhead Salient (Fig. 7). South of this limit, Emsian-Eifelian deposition of the Dunedin Formation accompanied, rather than followed, marine transgression onto

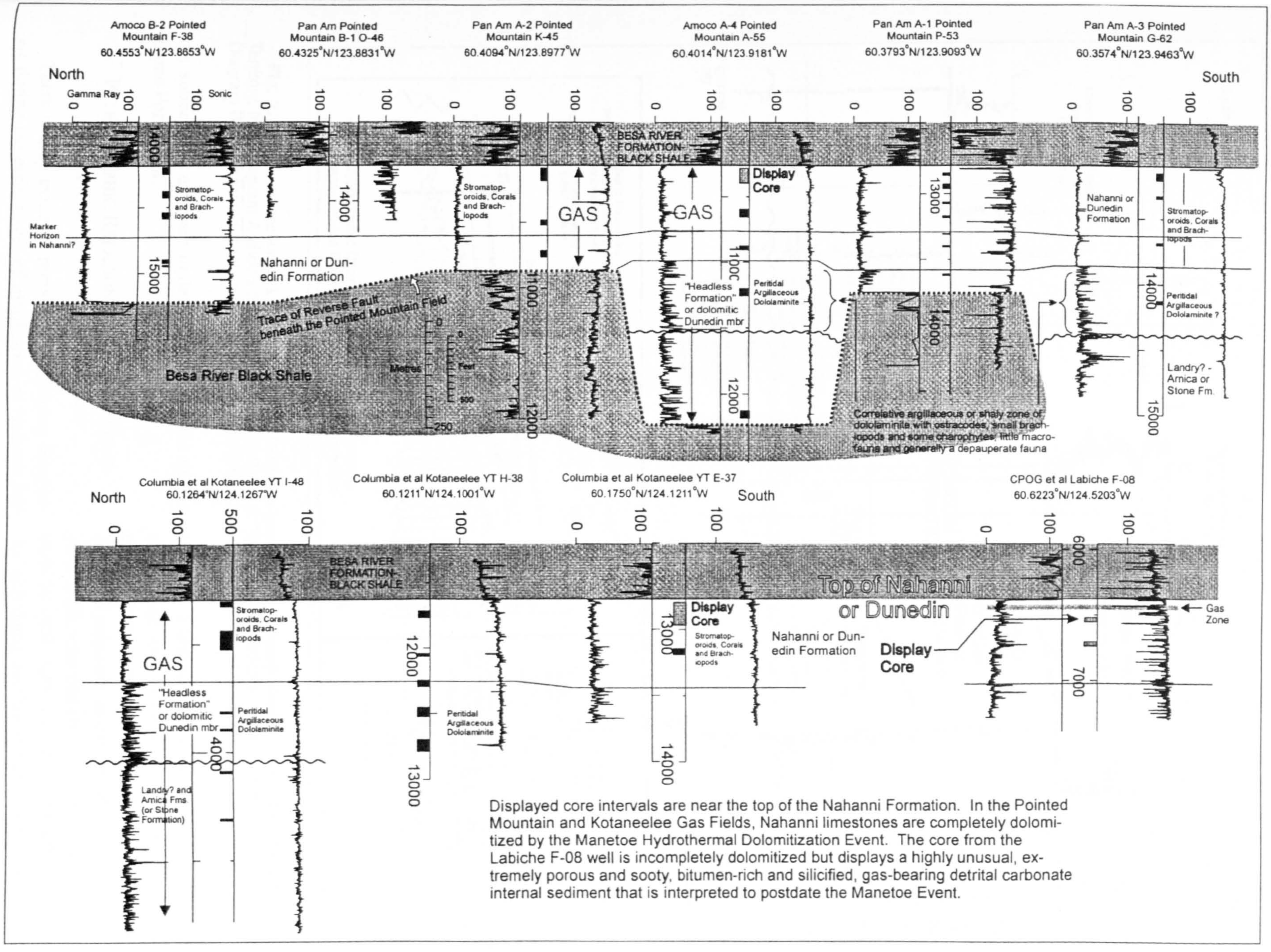

Fig. 6. Stratigraphic cross-sections of wells through the Pointed Mountain and Kotaneelee fields. The CPOG *et al.* La Biche F-08 well represents the La Biche gas field.

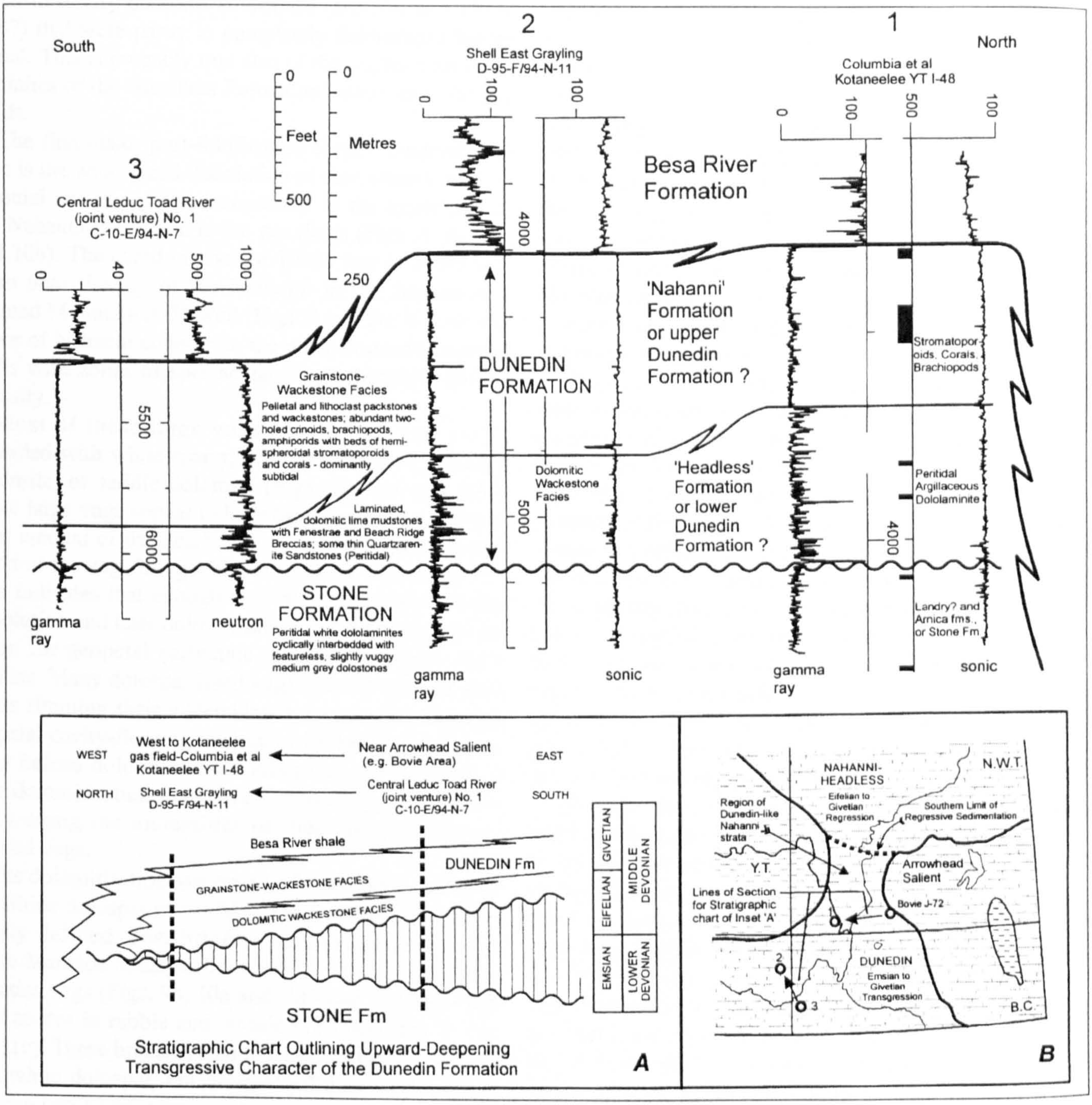

Fig. 7. Well cross-section of Lower and Middle Devonian strata from northeast British Columbia northwards to the Yukon Territory. Inset diagram **A** shows the transgressive character of "Nahanni" deposition in the region of the Liard Basin gas fields. Diagram **B** shows the boundary of regressive versus transgressive sedimentation of Nahanni-equivalent strata.

the subaerially exposed underlying dolostones of the Stone Formation.

Petrographic Relationships - Pore Space Modification and Cementation

There is little evidence remaining concerning diagenesis during the early stages of lithification of Nahanni and Headless limestones and argillaceous limestones or during early diagenesis of Landry limestone. Probably the fine grained lime sediments in these Middle Devonian units were deposited originally as calcite rather than the more soluble polymorph, aragonite (*see* James and Choquette, 1990). The peritidal cyclic light and dark brownish-grey dolostones of the underlying Sombre and Arnica formations are typical

synsedimentary platform dolostones (Morrow and Cook, 1987) that were partly to completely dolomitized before burial. This is probably true also of the argillaceous dololaminites of the 'Headless Formation' intervals in the gas fields.

The first major post-lithification feature observable in core is the widespread dissolution of macrofauna, such as colonial corals and stromatoporoids in the upper part of the Nahanni Formation in the gas fields (Figs. 8, 9b, 10a and 10b). The cored interval of 10296 feet to 10348 feet from near the top of the Nahanni in the Amoco A-4 Pointed Mountain A-55 well (Figs. 8 and 9b) is representative of Nahanni cores from the other Pointed Mountain wells with zones of spectacular vuggy biogenic moldic porosity.

Most of these large vugs are occluded or partly occluded with white sparry, centripetal (*i.e.* vug-lining), dolomite, or saddle dolomite (Figs. 9b, 10a and 10b). Some large vugs appear to have been floored by a significant amount of dark carbonate sediment before precipitation of the vug-filling white dolomite cement (Fig. 9b). This indicates that enough time elapsed between cavity dissolution and later dolomitization and dolomite cementation for geopetal carbonate sediments to floor these cavities. Many dolospar-lined vugs have ill-defined, dark bands rimming their undersides that may also represent geopetal cavity-flooring internal sediments that accumulated before dolomitization. Alternatively, dissolution after dolomitization may have formed cavities preferentially along the undersides of these large dolospar-rimmed vugs.

The dolomitization associated with the white, coarsely crystalline dolospar of the Manetoe Dolomite is the first clearly defined, post-lithification cementation event. White Manetoe dolospar lines and, partly to completely, occludes vugs (Figs. 9b, 10a and 10b) and fills interfragment spaces in rubble and mosaic breccias (Figs. 8, 10b and 11c). These breccias tend to be completely cemented with white dolospar, but unoccluded pore space occurs between some larger fragments (Figs. 10b and 11c). Part of the interfragment space in these breccias is filled with particulate, or detrital, silt- and sand-sized carbonate (Figs. 10b and 11c). Subvertical to oblique, thin, sharp-walled fractures cemented with white dolospar occur within and around breccia masses, particularly where these tend to have an overall vertical orientation (Figs. 9b, 10a and 10b).

Under cathodoluminescence, the coarsely crystalline white dolospar of the Manetoe Dolomite exhibits very low intensity, or dull to very dull luminescence (Fig. 12). This is unlike the bright cathodoluminescence that is commonly observed in dolomites precipitated from anoxic, or from reducing basinal fluids in deep burial diagenetic environments (Machel, 1985). Brightly luminescent burial calcite and dolomite cements generally have manganese contents of at least several mole per cent (*ie.* several thousands of parts per million; Machel, 1985). The near nonluminescence of the Manetoe dolospar cements is consistent with their very low manganese concentrations of only a few tens to a few hundreds of parts per million. White dolospar of the Manetoe Dolomite contains very low concentrations of contaminant elements in general, as may be seen in Appendix 3 of Morrow *et al.* (1990).

The next clearly defined event that definitely postdates at least part of the Manetoe dolomitization event is a dissolution and cavity-filling episode that is particularly well developed in core from the Pointed Mountain gas field (Figs. 8 and 9b) but is also visible in core from the Kotaneelee field (Fig. 10c). Dark, fine grained carbonate sediment infilled small caverns which were clearly excavated within pre-existing Manetoe Dolomite. Small calcite-cemented fractures contained entirely within these cavern-fillings (Fig. 9b) may be shrinkage cracks related to the dewatering and lithification of these internal sediments. These cavern-fillings also contain small millimetre to centimetre-sized fragments of white dolospar which have apparently been reworked from the walls and floors of caverns (Figs. 9b and 10c).

Although there are dark cavern-fillings that postdate Manetoe Dolomite unequivocally, at least in the intervals in which they occur, there are other dark bands that strongly resemble the cavern-fillings that have been fractured or brecciated by the Manetoe Dolomite in core from both Pointed Mountain and from Kotaneelee (Figs. 10c and 10d). This, combined with the previous suggestion of geopetal sediment deposition in vugs which may have predated Manetoe dolomitization, may indicate that this early dissolution, or karst event may have occurred, in part, contemporaneously with Manetoe dolomitization, and, possibly, may have begun before dolomitization. This inference is consistent also with the general aspect of the fauna preserved within cavity-filling sediments which strongly resemble fauna, such as the colonial coral *Alveolites*, amphiporids and crinoids, typical of the Middle to Late Devonian.

Hydrocarbon in the form of solid bitumen, or reservoir bitumen (Lomando, 1992) forms the next petrographically distinct paragenetic phase in cores from the Pointed Mountain and Kotaneelee fields. Ubiquitous, solid black bitumen either coats the interiors of dolospar-lined open vugs (Fig. 9b) or totally infills vug interiors

Table 1. Rock-Eval data for core samples from the Columbia *et al.* Kotaneelee YT E-37 well

Depth (feet)	Wt. (mg)	Tmax	S1	S2	S3	PI	S2/S3	PC	TOC	HI	OI*
12792	100.3	593	0.03	0.19	1.17	0.14	0.16	0.01	4.39	4	26
12792	100.3	594	0.02	0.18	1.20	0.10	0.15	0.01	6.02	2	19
12987	100.1	592	0.10	0.57	0.73	0.15	0.78	0.05	10.56	5	6
12987	99.5	591	0.12	0.59	0.73	0.17	0.80	0.05	5.14	11	14

*-see Peters (1986) for explanation of Rock-Eval parameter abbreviations (*e.g.* OI=Oxygen Index)

(Figs. 10a, 11b and 11d). Thin irregular, subvertical to subhorizontal, bitumen-filled, sharp-walled fractures crosscut fabrics of the Manetoe Dolomite (Fig. 11). These bitumen-filled fractures also crosscut the post-Manetoe cavern-filling internal sediments (Figs. 10c and 10d). In some instances, reservoir bitumen seems to have infilled stylolites or solution seams developed subparallel to bedding (Fig. 11b).

The sparse core coverage available from wells in the Pointed Mountain and Kotaneelee fields largely precludes an assessment of vertical trends in the amounts of reservoir bitumen. In cores from the Pointed Mountain Field there is a definite tendency for the amount of macroscopic bitumen to increase in amount downwards from Nahanni equivalent strata to the deeper Landry and Arnica equivalent strata in wells such as Amoco A-4 Pointed Mountain A-55 which have core from deeper Arnica equivalent strata (Fig. 6). In the Kotaneelee field, cores from the Nahanni and Headless intervals in the structurally high wells of Columbia *et al.* Kotaneelee YT I-48 and H-38 contain small amounts of reservoir bitumen throughout. However, core from the Nahanni interval in the structurally low Columbia *et al.* Kotaneelee YT E-37 well contains anomalously large amounts of black reservoir bitumen infilling vugs (Fig. 10a) and post-Manetoe fractures.

Rock-Eval analyses (Imperial Oil Resources Ltd., pers. comm.) of selected reservoir bitumen samples from the E-37 well are shown in Table 1. These reservoir bitumens from the Manetoe Dolomite have extremely high TOC values but virtually insignificant pyrolyzable carbon (PC) reflecting low S1 and S2 peaks (Table 1). This is consistent with their passage through the oil window to gas generation. Their low HI/OI ratios preclude classification according to original organic material type on van Krevelen-like plots of HI versus OI (*e.g.* Espitalié, 1986). The S2 peaks gave extremely high Tmax values which are beyond even the high maximum Tmax values of about 500°C observed in organic material in the siliciclastic sequence overlying the Manetoe Dolomite (Fig. 5).

A re-evaluation of the petrographic characteristics of organic matter in the Upper Devonian and Lower Carboniferous shales in the Pan Am Beaver G-01 and Pan Am Kotaneelee O-67 wells indicates that organic matter is composed of various populations of indigenous solid bitumens and that true vitrinite is rare (Potter, in prep.). Most of these bitumens were generated in situ as byproducts of maturation of various species of organic materials which initially were a liptinitic, possibly sulphur-rich, kerogen (Potter, in prep.). The observed range of Tmax values is consistent with a downhole increase in maturity of Type II/III kerogen for Mattson-Golata interval in Kotaneelee 0-67.

Tmax profiles through the post-Middle Devonian sequence overlying the Nahanni-Manetoe carbonates (Fig. 5) are also consistent with the very high Tmax temperatures observed in the Kotaneelee E-37 Manetoe bitumens. Tmax temperatures in the nearby Pan Am Kotaneelee and Pan Am Beaver River YT G-01 wells reach maximums of up to and even greater than 500°C in the Golata shale more than 1000 metres above the contact of the Besa River shales with the Nahanni Formation (Fig. 5). Vitrinite reflectances and vitrinite-equivalent reflectances from bitumen at this level are about 1.40% to 1.50% Ro (Fig. 5). This is consistent with the correlation between Tmax and vitrinite reflectances established by Espitalié (1986) for type III coal series organic material in the Paris Basin (Fig. 8 in Espitalié, 1986) and may indicate that there is some admixture of type III organic material within these sediments.

Indigenous bitumens in the post-Devonian, dominantly siliciclastic upper Paleozoic sequence including the organic-rich Besa River shale source rocks overlying the Nahanni in wells close to the gas fields display a progressive increase in reflectivity downsection in a manner parallel to that of vitrinite (Fig. 5; Table 2). Bitumens in the Pan Am Beaver River YT G-01 well display a very consistent downhole increase in reflectivity that parallels the downhole increase in vitrinite reflectances. Vitrinite equivalent reflectances calculated

Table 2: Bitumen Reflectances from post Middle Devonian strata - Pan Am Beaver River YT G-01 and Pan Am Kotaneelee 0-67

Pan Am Beaver River YT G-01			Pan Am Kotaneelee 0-67		
Depth (Feet Kb)	R_{bit}% (measured)	R_{vr}% eq. (Calculated)*	Depth (Feet Kb)	R_{bit}% (measured)	R_{vr}% eq. (Calculated)
2880	0.60	0.77	260	0.71	0.84
3250	0.66	0.81	1320	0.73	0.85
3700	0.71	0.84	4200	1.71	1.46
4135	0.84	0.92	7595	2.91	2.20
5520	1.20	1.14	7800	3.20	2.38
6120	1.40	1.27	Pan Am Beaver River YT G-01		
6540	1.47	1.31	10865	2.41	1.89
6565	1.47	1.31	11635	2.74	2.09
7480	1.52	1.34	12015	2.85	2.16
8766	1.55	1.36	12265	2.90	2.19
9210	1.53	1.35	12665	3.40	2.50
9880	1.72	1.46	12915	3.50	2.56
10129	1.76	1.49	12975	3.70	2.69
10183	1.87	1.56	13185	3.43	2.52
10575	2.02	1.65	13549	3.80	2.75

*- "R_{vr}% eq." is calculated according to the formula R_{vr}% eq. = 0.618(R_{bit}%+0.40), (after Jacob, 1985).

from bitumen reflectances using the relationship of Jacob (1985, R_{vr}% eq. = 0.618(R_{bit}%+0.40) may underestimate vitrinite reflectances by a progressively greater amount downhole (Fig. 5; Table 2). Better fits to vitrinite reflectance data of the G-01 well can be made by linear functions with a steeper slope and lower intercept value (*e.g.* R_{vr}% eq. = 1.05*R_{bit}%+0.20). The degree of misfit between Jacob's (1985) relationship and the G-01 data may be partly explained by the fact that Jacob's (1985) data fitting was limited to vitrinite reflectances of less than 2.0%.

Bitumens in the post-Middle Devonian of the Pan Am Kotaneelee 0-67 well are much more scattered than in the G-01 well although they also show a general downward increase in reflectivity (Fig. 5). The 0-67 bitumens may have originated both as residual in-place bitumen during maturation and as migrated bitumen (*see* Fig. 4 of Morrow *et al.*, 1993).

Drusy quartz infills parts of larger vugs in the Kotaneelee and Pointed Mountain fields. Typically, "dogtooth" or drusy quartz occupies the centres of dolospar-lined vugs (*see* Fig. 10 in Morrow *et al.*, 1990) and also lines abundant open subvertical fractures that crosscut Manetoe Dolomite near the top of the Nahanni in the Columbia *et al.* Kotaneelee YT I-48 well (cored interval 3660 to 3665.7 metres). Some of the dolomitized groundmass in this atypical Manetoe core has been silicified by microcrystalline quartz.

Equant, coarsely crystalline white calcite occurs also as a late-stage, vug-filling cement in dolospar-rimmed and bitumen-lined vugs, particularly in core from the Pointed Mountain Field (Fig. 8). Calcite-filled vugs contained no drusy quartz even in those rare instances where both quartz and calcite-filled vugs were found in the same core, such as in cores 2 and 3 (10,348 to 10,396 ft. and 10,600 to 10,658 ft. K.B.) of the Pointed Mountain A-55 well (Fig. 8). Consequently, there is little petrographic indication of the order of emplacement of calcite versus quartz vug-filling cements. However, the fact that, in these cores, all calcite-filled vugs are totally occluded with calcite cement, whereas quartz-filled vugs are, almost invariably, incompletely filled with drusy quartz and retain unfilled pore space, may indicate that calcite cementation preceded quartz cementation.

In a different mode of occurrence, late-stage equant to bladed white calcite has grown displacively within the bitumen of bitumen-filled vugs (Fig. 10a) or within bitumen-impregnated, cavity-filling internal sediments (Fig. 10c) in core from the Kotaneelee E-37 well. This

COLUMBIA KOTANEELEE YT E-37 CORES 4 AND 5

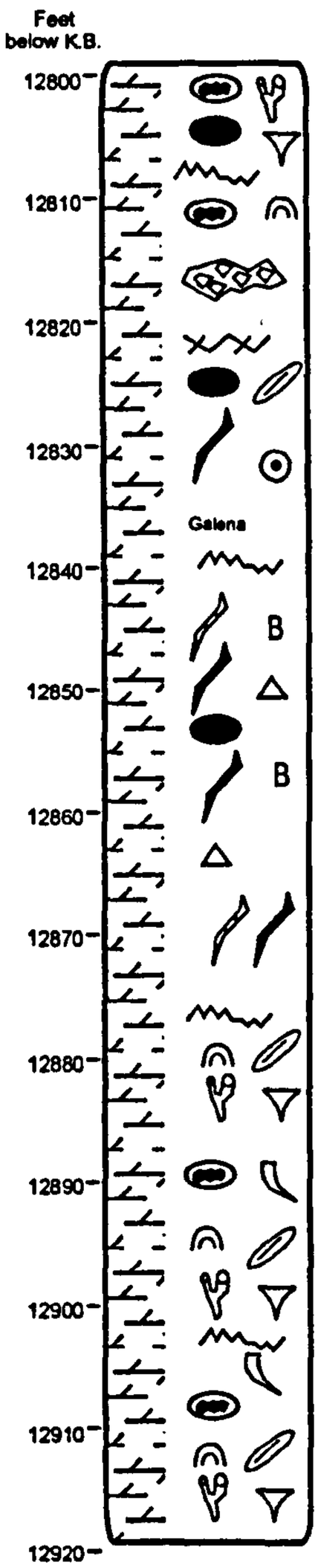

Core 4 (12799 - 12859') Nahanni Formation

Dark gray bituminous and slightly argillaceous finely to medium crystalline dolostone; Mottled and brecciated with 15% to 20% white dolomite cement as vug-lining and collapse breccia cement and as a replacement for fossil material; Black glassy bitumen fills the centres of dolomite-cemented vugs; Bitumen-filled subvertical fracture seams up to 0.75 inches wide intersect dolomite-cemented vug-fillings and breccias; Abundant subhorizontal dolomite-cemented fractures at 12840' cross-cut dolomite-lined vugs; Stylolites are common and cross-cut all fabrics; Many irregular bitumen-filled vugs have thin or incomplete rims of white dolomite cement, slight downhole decrease in white dolomite cement as vug-rimming cements and as fracture-fillings in this core from 15-20% in the upper part to about 10% near the core base; minor quartz crystals in centres of some vugs (postdate bitumen?); Small blebs of galena in vugs at 12831'

Core 5 (12859 - 12919') Nahanni Formation

Dark gray bituminous finely to medium crystalline dolostone
From 12859 to 12865' there is a fine network of white dolomite veining forming 15% of the rock; Minor brecciation; Bitumen in veins and stylolites as in the overlying interval; Minor biogenic material replaced by white dolomite; Cross-cutting stylolites:
From 12865 to 12897' similar to above but more macrofauna (stromatoporoid fragments, corals, brachiopods and amphipora); minor post-white dolomite quartz in vugs; some moldic and fracture porosity; At 12895' a large bitumen-filled vug contains displacive bladed calcite:
From 12897 to 12899' decrease in white dolomite to 5%; minor quartz; minor skeletal debris:
From 12899 to 12909' similar to 12865 to 12897' interval; minor pyrite at 12899 5'; Bitumen-filled vugs at 12907.5' contain displacive calcite:
From 12909 to 12913' similar to 12897 to 12899' interval:
From 12913 to 12919' similar to 12865 to 12897' interval

AMOCO A-4 POINTED MOUNTAIN A-55 CORES 1 AND 2

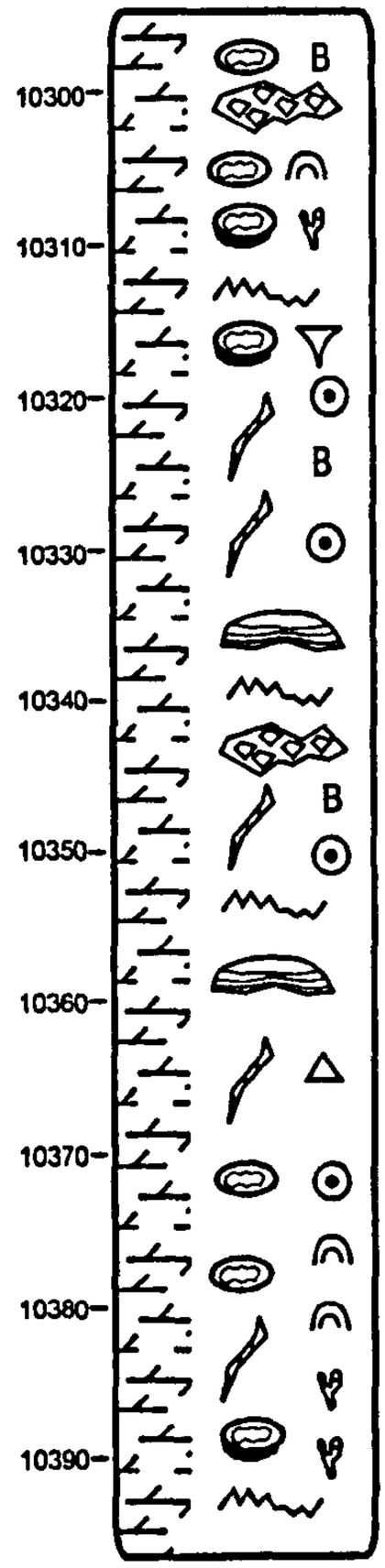

Core 1 (10296 - 10348') Nahanni Formation

Medium gray medium to coarsely crystalline dolostone with a mottled appearance due to crystal size variations; Spectacular vuggy porosity with open vugs up to 8 cm wide lined with white 'Saddle Dolomite'; Larger vugs leached hemispheroidal stromatoporoids; smaller vugs infilled with quartz cement; Crinoids and brachiopods replaced by white dolomite; Irregular, subvertical veins of white dolomite 0.2 to 2 cm wide; White dolomite 15% - 40% of the rock volume; Dolomite cemented mosaic and rubble breccias abundant at 10299 to 10303'; Large whole brachiopods occur in zones; Black bitumen coats distal ends of vug-rimming white dolomite cements in open vugs; Many larger vugs are floored by dark geopetal internal sediments before white dolomite cements were emplaced; Several 10 cm thick dark bands of internal post-dolomitization internal sediment fills that appear to occupy small caverns; Some of these dark bands are brecciated and crosscut by dolospar veins; Stylolites crosscut fabrics

Core 2 (10348 - 10396') Nahanni Formation

Similar to overlying core interval, Black internal sediment band at 10357'; Leached corals and stromatoporoids with white dolospar vug-rimming cements common at 10380 to 10386'; Quartz crystals in many open vugs; Calcite occludes many dolospar-rimmed vugs in this core; Dark geopetal sediments line the bases of leached brachiopods at 10388 to 10390'; Some of this internal sediment appears to predate white dolospar cement; Good vuggy porosity with some open, only partly cemented veins; Common stylolites cross-cut all other fabrics

SYMBOLS

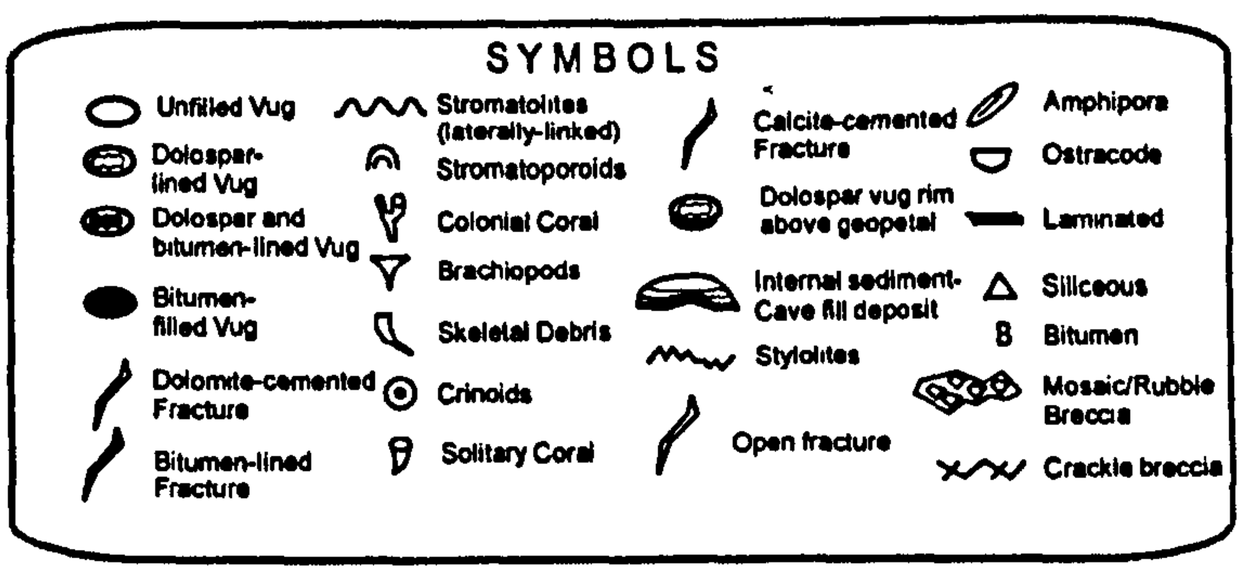

Fig. 8. Graphical logs and descriptions of cores from the Kotaneelee and Pointed Mountain gas fields.

type of calcite appears to be restricted to wells, such as Kotaneelee E-37, which contain relatively large amounts of post-Manetoe bitumen.

Isolated small blebs of coarsely crystalline galena occur as final vug-fillings, and as irregular veinlets crosscutting Manetoe fabrics in the Manetoe Dolomite in the Nahanni equivalent interval as in the Kotaneelee E-37 well (Fig. 8) and in the Kotaneelee H-38 well (Fig. 10a in Morrow *et al.*, 1990). Finely to medium crystalline reddish-brown sphalerite occurs as small veinlets

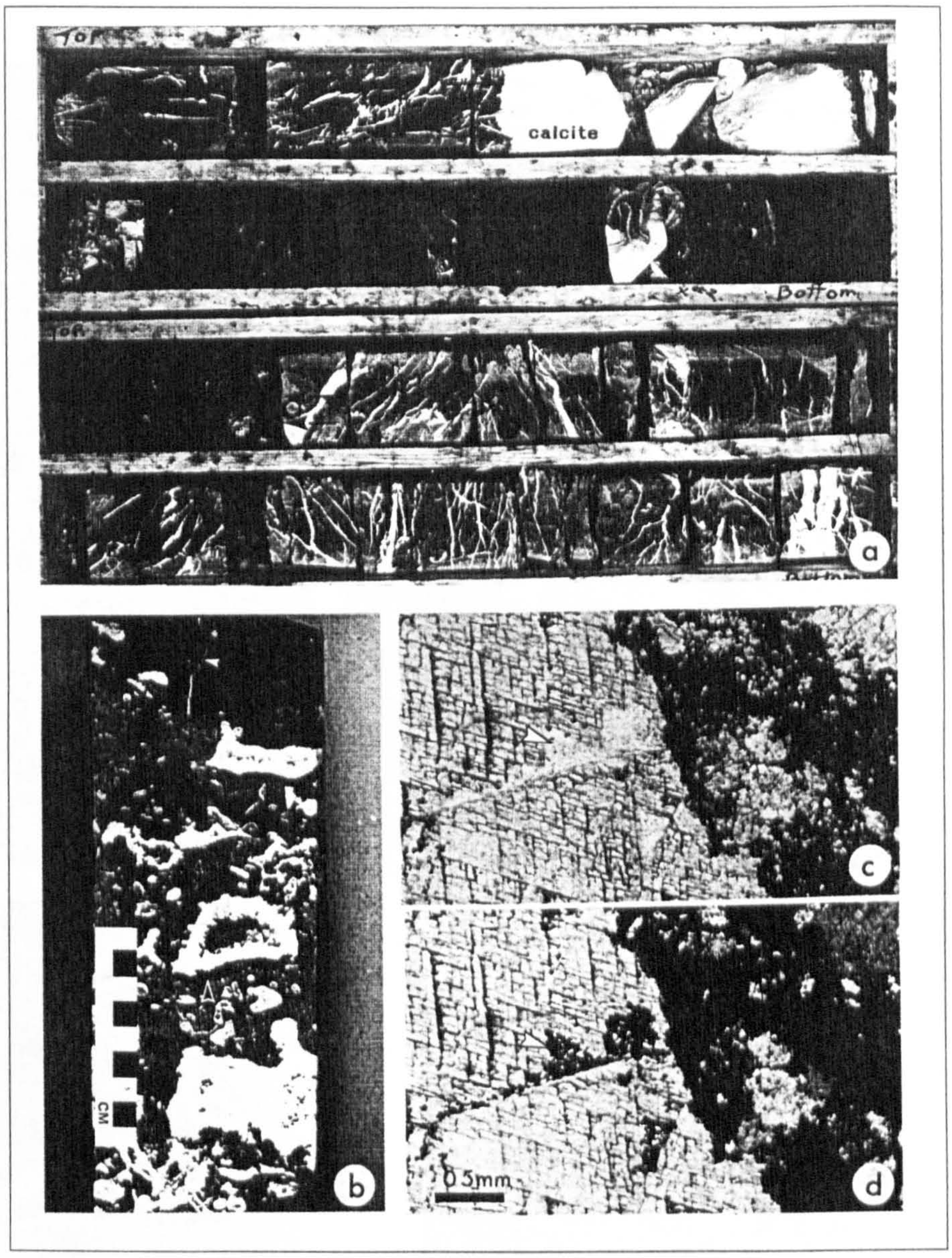

Fig. 9. Core photographs and thin section photomicrographs. Fig. **9a** shows two boxes from core 1 of CPOG *et al*. La Biche F-08. The black arrows mark the base of a sooty, bituminous and silicified cavern-filling at 6527.75 feet (K.B.). Fractured Nahanni limestone overlies and underlies this cavern-fill. Fig. **9b** shows spectacular leached biogenic porosity in Manetoe Dolomite at 10,345 feet (K.B.) in the Amoco A-4 Pointed Mountain A-55 well. Dark, cave-filling deposit occupies upper part of core. Arrow near centre of core points to base of probable internal sediment layer beneath a thick vug lining of white dolospar. Figs. **9c** and **9d** are plain light and crossed nicols thin section views of diagenetic calcite at the base of the white calcite zone at the top of the cavern-filling shown in Fig. 9a. Diagenetic calcite has engulfed the silicified carbonates of the cavern-filling before the introduction of bitumen.

calcite cement zone has a sharp stylolitic contact with the overlying veined Nahanni limestone. The lower contact of the white cement zone with the underlying black sooty cavern-filling is gradational. This lower contact is characterized by an aggregate of poikilotopic white calcite crystals that average about 10 to 20 cms. in size. A thin section view of these calcites shows that the silicified carbonates of the cavern-filling were engulfed by calcite growth before these silicified carbonates were impregnated by sooty reservoir bitumen (Figs. 9c and 9d).

This cavern-filling bears some similarity to a very large, spectacular cavern-filling within the Manetoe Dolomite exposed along the south side of First Canyon in the South Nahanni River (Morrow and Cook, 1987; Aulstead, 1987). This cavern-fill deposit is more than 500 metres broad and tens of metres thick and contains crossbedded carbonate sand and pea gravel (Morrow,

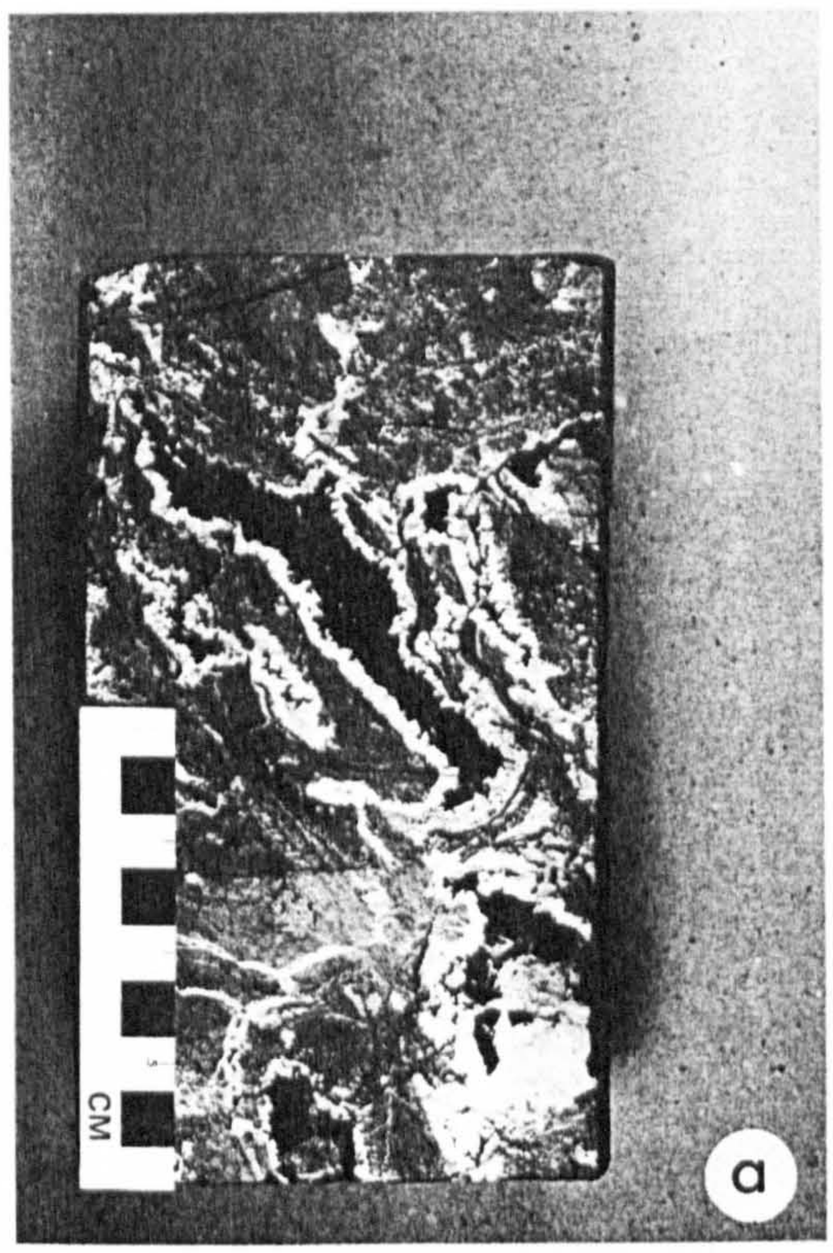

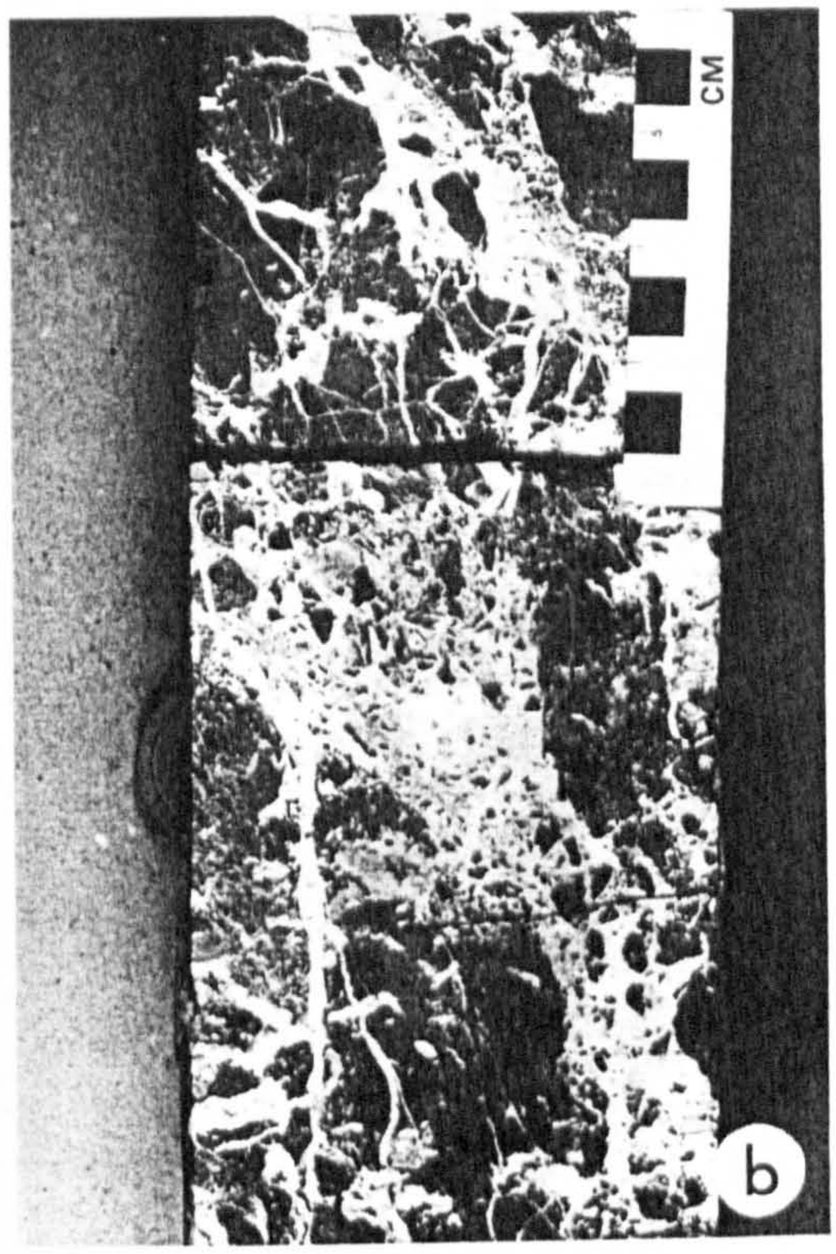

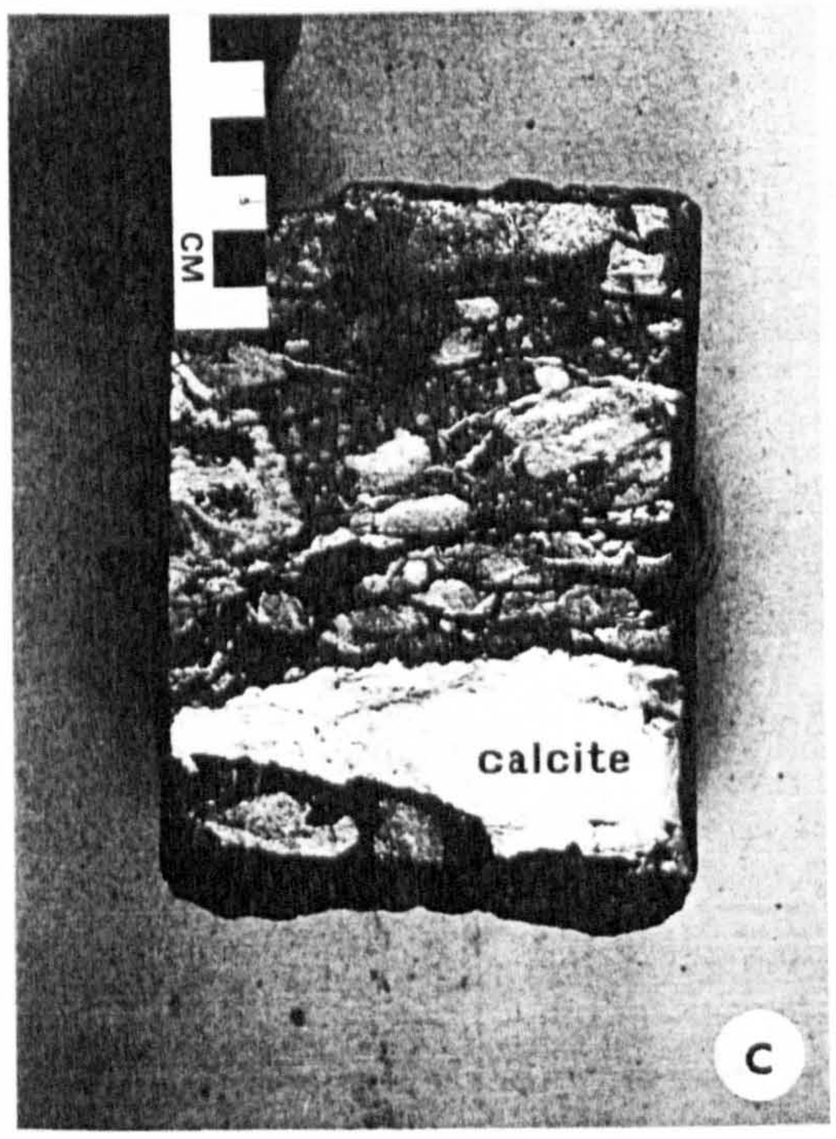

Fig. 10. Photographs of core from the Manetoe Dolomite. Fig. **10a** shows solid reservoir bitumen as large vug-fillings at 12,799.5 feet (K.B.) in the Columbia *et al*. Kotaneelee YT E-37 well. Fig. **10b** shows rubble packbreccia completely cemented by white dolospar at 3661.0 metres (K.B.) in the Pan Am Kotaneelee YT I-48 well. Fig. **10c** shows bitumen-filled fractures and late diagenetic white bladed calcite within a dark bituminous groundmass at 12,926 feet (K.B.). In the Columbia *et al.* Kotaneelee YT E-37 well. Fig. **10d** shows the rounded side of the slabbed core shown in 10c.

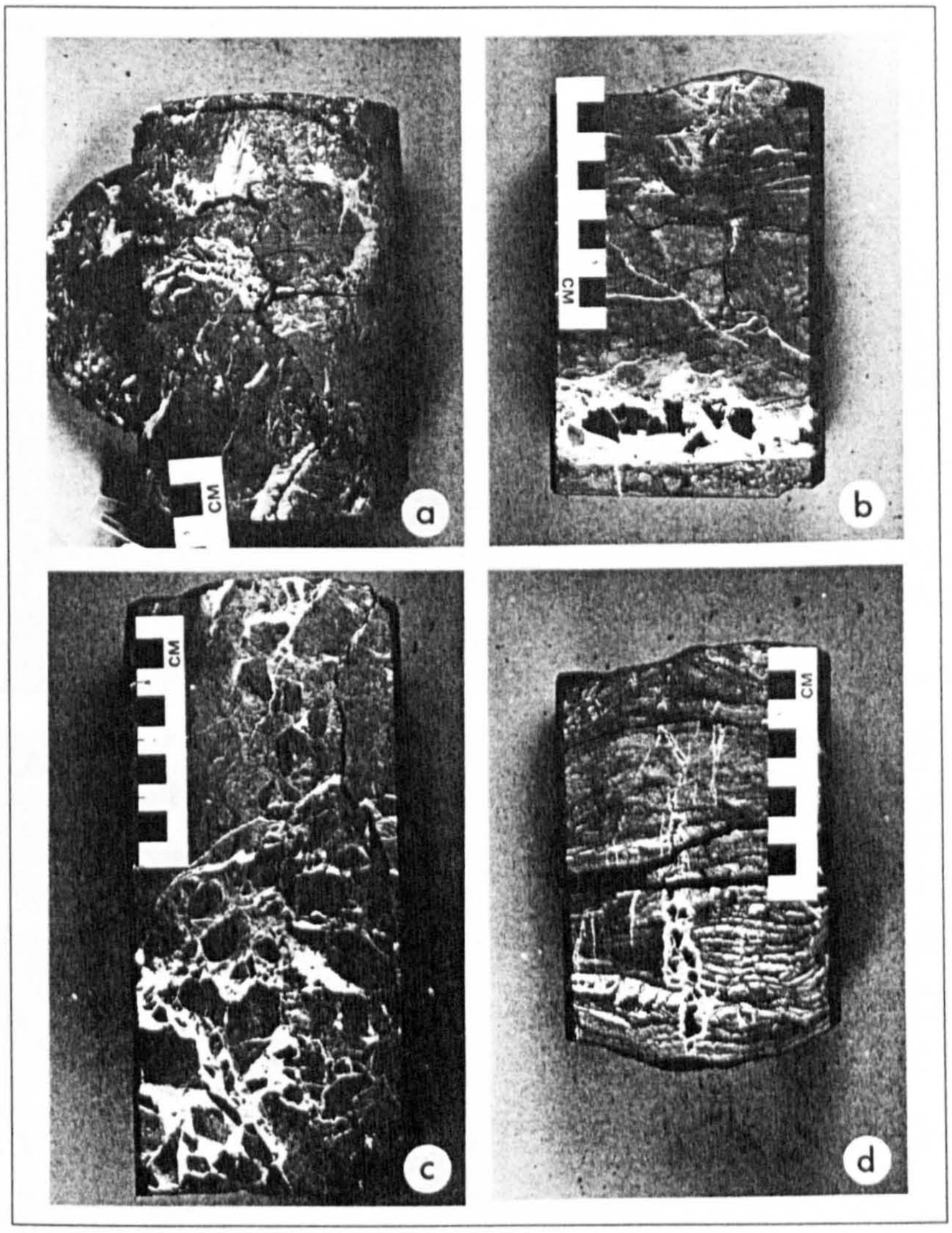

Fig. 11. Photographs of core from the Manetoe Dolomite. Fig **11a** shows bitumen seams crosscutting white dolospar at 13,143 feet (K.B.) in the Columbia *et al.* Kotaneelee YT E-37 well. Fig. **11b** shows black bitumen within white Manetoe dolospar at 11,251 feet (K.B.) in the Amoco A-4 Pointed Mountain A-55 well. Fig. **11c** shows a vertical vein of bitumen crosscutting Manetoe breccia at 12,304 feet (K.B.) In the Columbia *et al.* Kotaneelee YT H-38 well. Fig. **11d** shows a vertical vein of bitumen crosscutting Manetoe laminite at 11,259 feet (K.B.) In the Amoco A-4 Pointed Mountain A-55 well.

1994) that are similar to the crossbedded cavern-filling in the La Biche F-08 core. Spectacular metre-sized and smaller blocks of Manetoe Dolomite occur as dropstones within this cave deposit. This surface cave deposit is not silicified or impregnated with bitumen. It is tentatively assigned a late Tertiary to recent age as a separate, late solution event (Fig. 14) that affected the Manetoe in areas near present day outcrop.

Duplicate Rock-Eval analyses were done on several samples of the bitumen-impregnated sooty cave-fill (samples at 6525 feet and 6526 feet) and of the Nahanni limestone above (sample at 6521.5 feet) and below (sample at 6537 feet) the cave-fill in Core 1 of the La Biche F-08 well (Table 3). TOC for the cave-filling samples ranges from 1.4%-2.24%. The low S1 and S2 peaks, the unreliable and low Tmax, and their very low Hydrogen Indexes (HI), indicate that these bitumens are greatly overmature, which is consistent with their sooty, carbonaceous aspect and with the dry gas produced from Nahanni-equivalent strata slightly above this core (Fig. 6). The Nahanni limestone samples from the La Biche F-08 well contain insignificant amounts of organic material and no measurable S1 or S2 peaks similar to the low TOC contents recorded from the uppermost Nahanni limestones at the Kotaneelee 0-67 well (Fig. 5).

The gas zone of the La Biche field is developed in a 'siltstone'-rich interval (Meding, 1994) just above core 1 of the La Biche F-08 well (Fig. 6). This very porous zone may be largely a cavern-filling similar to the cavern-fill of core 1.

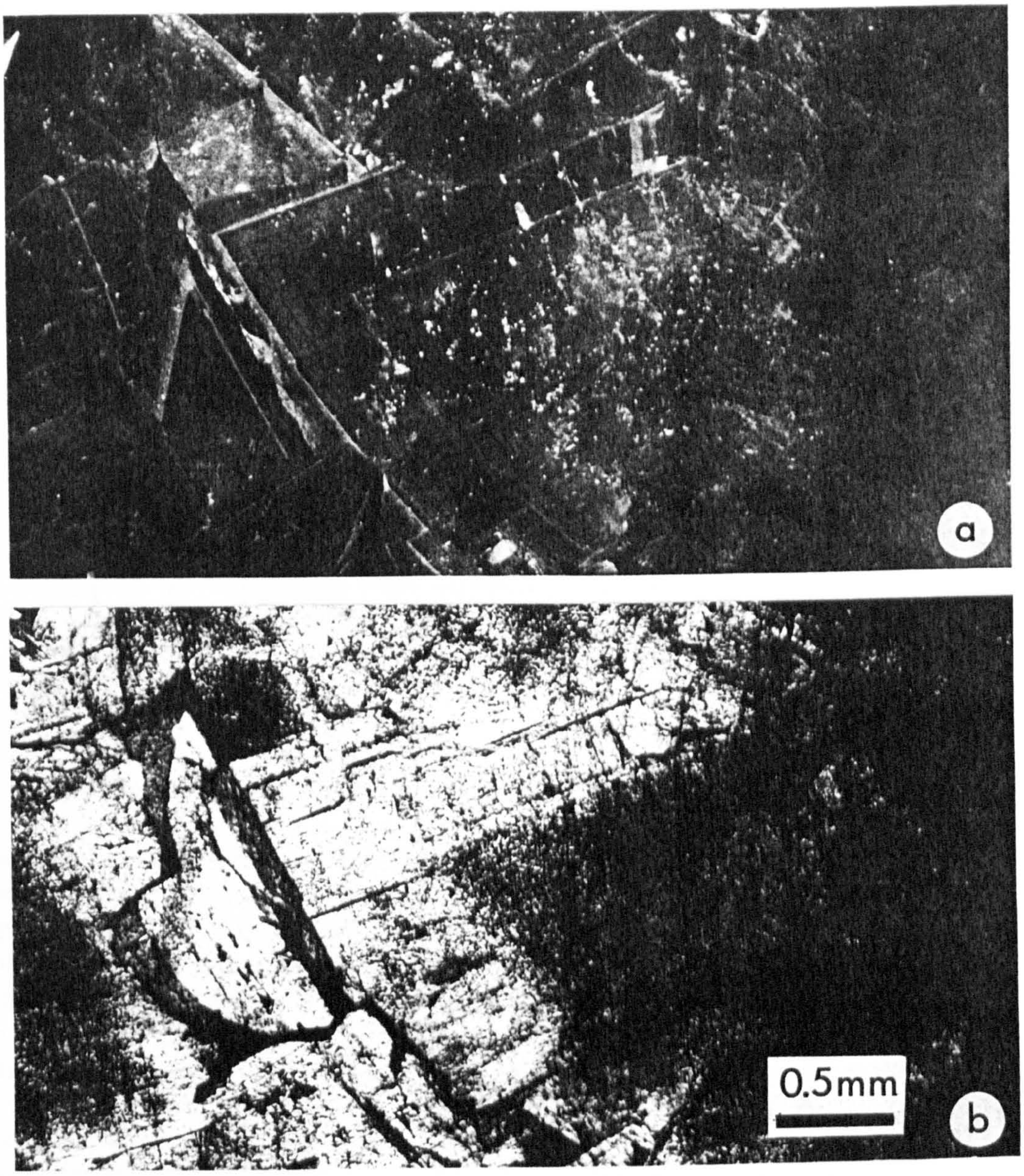

Fig. 12. Thin section photomicrographs of Manetoe vug-filling dolospar in the Columbia *et al.* Kotaneelee YT H-38 well at 12,067 feet (K.B.). Fig. **12a** is a cathodoluminescent view of the dolospar. Luminescence is dull except for thin orange luminescent bands near the distal edges of crystals. Fig. **12b** is a plain light view of cathodoluminescent image in 12a.

Porosity and Permeability

Spectacular vuggy biogenic porosity (Figs. 8 and 9b) occurs in the upper part of the Nahanni Formation in the Pointed Mountain field. Porosity in the completely dolomitized uppermost cores from Nahanni equivalent strata at the Amoco A-4 Pointed Mountain A-55 well ranges from about 1.0% to a high of nearly 10.0% with a weighted average porosity of about 3.6% (Fig. 15). The zones of porosity greater than 4.0% generally correspond to zones with a significant proportion of incompletely occluded macrovugs, most of which are biogenic. But some represent unoccluded interfragment macropores in incompletely cemented collapse breccias. More commonly, however, the interfragment spaces of mosaic and rubble packbreccias in the Manetoe Dolomite tend to be completely cemented with white dolospar (Fig. 11c).

Permeability in the A-55 well tends to be very anisotropic with permeability parallel to bedding typically being several orders of magnitude greater than that

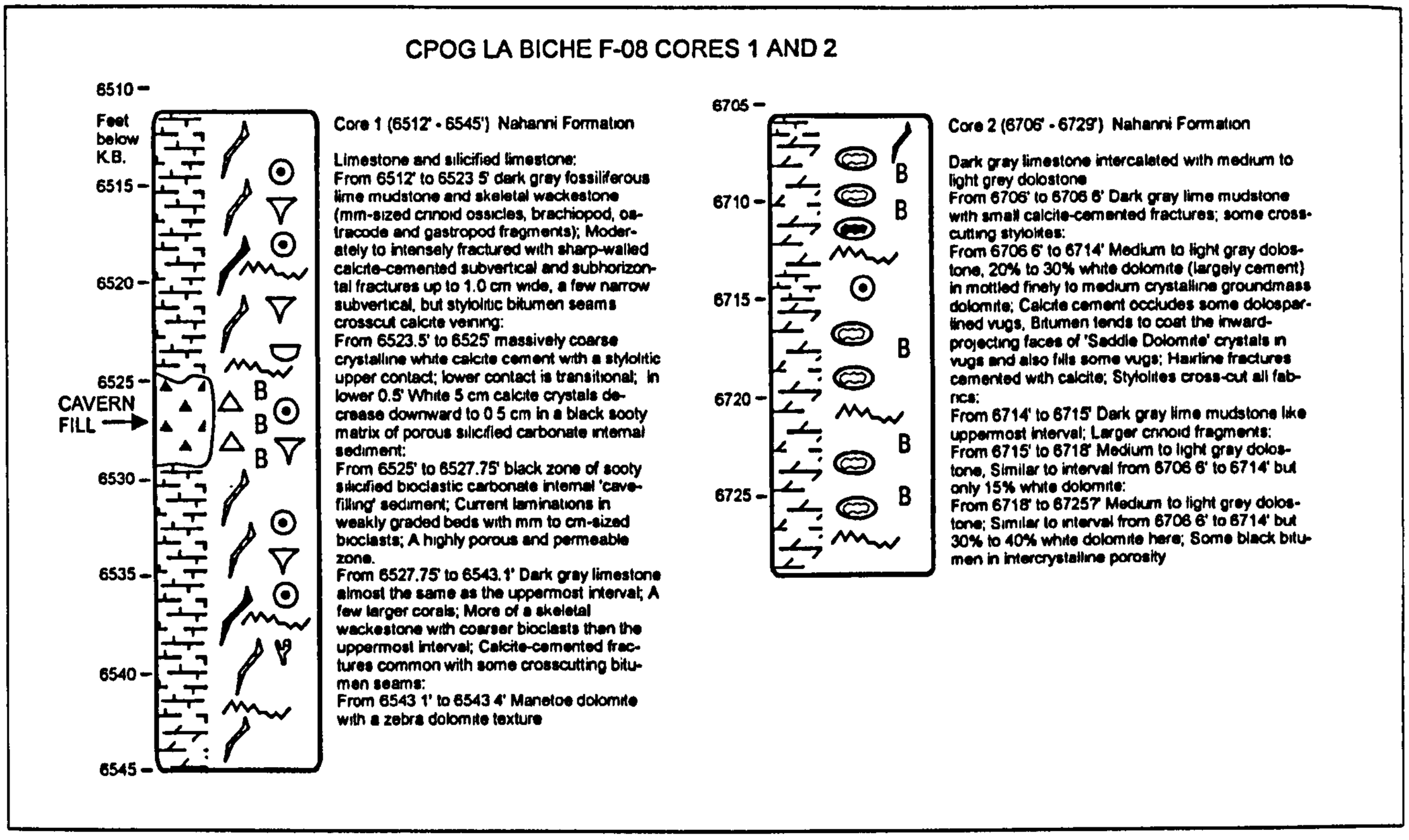

Fig. 13. Graphical logs and descriptions of cores from the CPOG *et al.* La Biche F-08 well. See Figure 8 for legend.

perpendicular to bedding. Many intervals in cores 1 and 2 of the A-55 well have no permeability, or are impermeable, perpendicular to bedding (Fig. 15). Many thin intervals scattered throughout this well exhibit extremely high permeabilities in excess of 30,000 millidarcies parallel to bedding. In general, permeability and porosity in this well appear to exhibit a certain degree of covariance. Zones with high porosity tend to also exhibit relatively high permeabilities both parallel and perpendicular to bedding and vice versa (Fig. 15).

The uppermost cores from the totally dolomitized, Nahanni equivalent strata in the Columbia *et al.* Kotaneelee YT E-37 well, cores 4 and 5, exhibit somewhat lower porosity and permeability than those of the A-55 well. This may be due in large part to the presence of fewer zones with less well developed unoccluded biogenic porosity in the E-37 well than in the A-55 well. Porosity in the E-37 cores ranges from a low of about 2.0% to a high of about 11.0% (Fig. 15). However, porosity is far less variable in the E-37 cores. Porosity throughout these cores tends to fall within limits of between 2.0% and 4.0% porosity, unlike the A-55 core where porosity most commonly ranges from 2.0% - 6.0% (Fig. 15).

Permeability in the E-37 cores is much less anisotropic than in the A-55 cores. This is primarily because permeability perpendicular to bedding is much greater in the E-37 well than in the A-55 well, whereas permeability parallel to bedding in E-37 is considerably less overall than in A-55 (Fig. 15). There is strong covariance between permeabilities parallel and perpendicular to bedding in the E-37 well with generally less than an order of magnitude separation between permeability curves. There is probably even a stronger covariance between porosity and permeabilities in the E-37 cores than in the A-55 cores (Fig. 15).

The much shorter cores 1 and 2 from the CPOG *et al.* La Biche F-08 well are generally much less porous than cores from A-55 and E-37 (Fig. 15) and are only partly dolomitized (Fig. 13). Disregarding the very porous interval representing the silicified bitumen-impregnated cavern-fill (6523.5 to 6525 ft.; Fig. 9a), the average porosity of core 1 at F-08 is only 1.5%. This reflects the very low porosity of the undolomitized, fossiliferous, lime wackestone that forms most of this core (Fig. 13). The cavern-fill interval by contrast is extremely porous, at almost 24% porosity. The subhorizontal to subvertical calcite veining, which is common in the limestone above and below the cavern-fill in core 1 (Fig. 9a), does not appear to contribute significantly to its porosity or

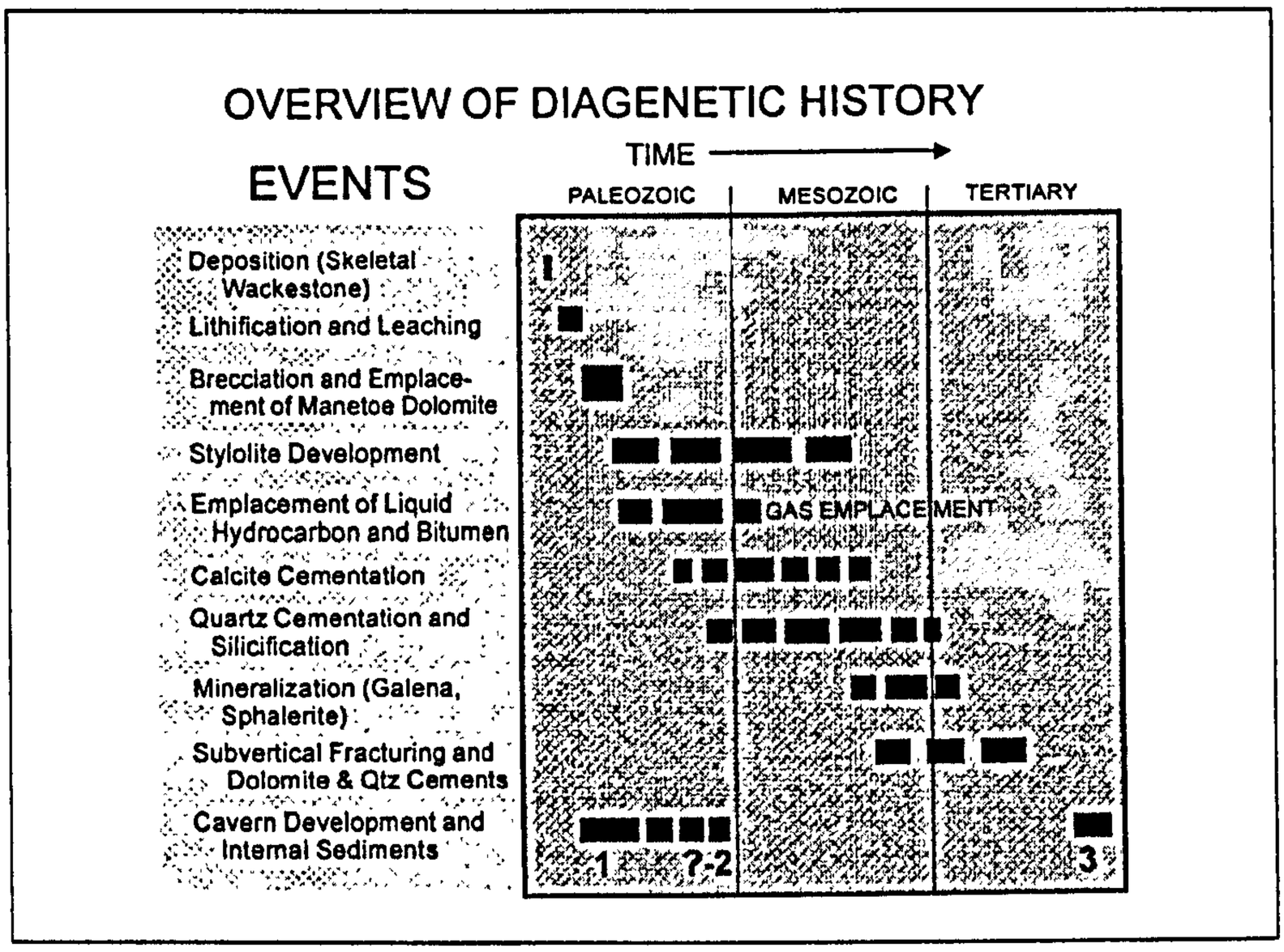

Fig. 14. Diagenetic history of Lower and Middle Devonian carbonate strata that contain the Manetoe Dolomite.

permeability. Average porosity in core 2 is about 2.3%, or slightly greater than that of core 1 if the cavern-fill interval is not included. Porosity values increase slightly downdepth in core 2, possibly reflecting the passage downcore from partial to complete dolomitization. Although there are some intervals with common macropore vugs of biogenic origin in core 2, they tend to be completely occluded with reservoir bitumen and white calcite, and consequently do not contribute to porosity.

Permeability in both the F-08 cores is low, commonly less than 5 millidarcies. In spite of the high porosity of the cavern-fill interval, its permeability is less than 10 millidarcies, but is nearly the same in directions parallel to and perpendicular to bedding. The remainder of core 1 and all of core 2 exhibit the more usual anisotropy with permeability parallel to bedding being greater than that perpendicular to bedding (Fig. 15).

Discussion

The internal stratigraphy of the thick Manetoe Dolomite in the Pointed Mountain and Kotaneelee gas fields may be discerned on geophysical well logs. Correlation of the upper part of the Manetoe in and around the gas fields is more readily made with the Dunedin and Stone formations of northeast British Columbia, rather than with the Nahanni and Headless formations of the southern Mackenzie Mountains. The lithologies and log signatures of the internal subdivisions of the Dunedin Formation strongly resemble the lithologies and log signatures of the upper part of the Manetoe Dolomite in spite of the fact that these are long distance correlations. The available sparse biostratigraphic information indicates that the upper contact of the 'Nahanni' interval within the Manetoe Dolomite is highly diachronous becoming younger eastward towards the Arrowhead Salient. This is similar to the southeastward younging of the upper contact of the Dunedin Formation of British Columbia, which also is Givetian in age, near the junction of the Dunedin with the Presqu'ile, or Keg River Barrier. This intertonguing of Besa River shales and Nahanni carbonates, implied by the eastward 'younging' of the upper contact of Nahanni-equivalent strata around the gas fields, may have provided opportunity for a degree of lateral, as well as downwards, migration of hydrocarbons into Manetoe reservoirs.

The process of dolomitization definitely appears to have enhanced porosity and permeability. This is not likely to have been the consequence of volume loss during dolomitization. The greater porosity and permeability of dolomitized Nahanni versus undolomitized Nahanni limestones in cores from the gas field wells is more likely to have been the result of the preferential preservation of porosity during burial of dolomitized, versus that of undolomitized limestones (Schmoker and Halley, 1982).

A simple calculation, based on extrapolation of depth-dependent porosity functions, shows a considerable

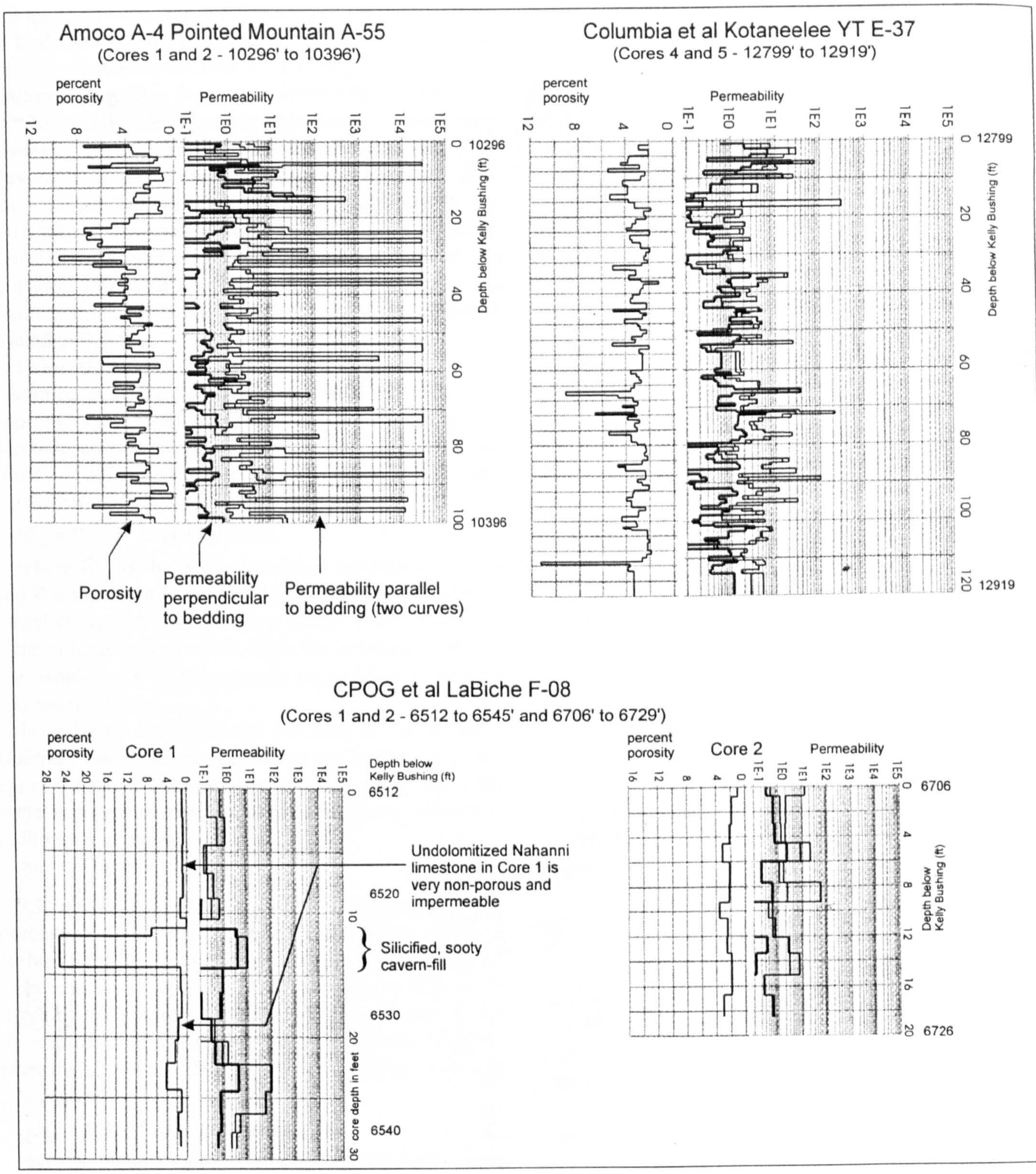

Fig. 15. Porosity and permeability graphs for core from the Pointed Mountain, Kotaneelee and La Biche fields based upon data from Core Laboratories of Canada, Ltd.

difference in the present day expected porosity between dolomitized and undolomitized Nahanni strata. It is clear that dolomitization occurred after lithification and possibly after an episode of karst dissolution, which implies burial to depths of at least tens to hundreds of metres. The absence of evidence for boiling during Manetoe Dolomite precipitation (Aulstead *et al.*, 1988) also indicates a burial depth of several hundred metres, assuming

that the fluid inclusions were entrapped under conditions of hydrostatic equilibrium. On the other hand, the Manetoe dolomite cements were precipitated at depths shallow enough that there is no discernible pressure correction to fluid inclusion homogenization temperatures, assuming that the precipitational solutions were Late Devonian residual connate brines of evaporitic origin and that the dolomites formed in isotopic equilibrium with these connate brines in Late Devonian to Carboniferous time (Aulstead *et al.*, 1988, Morrow and Aulstead, 1995). As a very rough estimate then, we can assert that the Manetoe Dolomite formed at a depth of around 500 metres.

Using this depth estimate for dolomitization, and assuming that the dolomitization process, as a first approximation, conserved rock volume and using the depth-dependent compaction function of Schmoker and Halley (1982) for the decrease in Floridan limestone porosity fraction with depth:

$$\varnothing_{lst} = 0.513^* \exp(-(Z)/1888) \quad (1)$$

where $\varnothing_{lst}$ is the depth-dependent limestone porosity and Z is the depth in metres, we find that at 500 metres a limestone would have 39.4% porosity. If dolomitization were volume conservative, then the resultant dolomite also would have 39.4% porosity as an initial porosity at 500 metres depth.

In order to determine the porosity in the Manetoe Dolomite during deeper burial, we can assume, as a first approximation, that this dependency will follow the same exponential trend as depth-dependent compaction in Floridan dolomites:

$$\varnothing_{dol} = 0.3036^* \exp(-(Z)/4619) \quad (2)$$

(Schmoker and Halley, 1982). The fixed dolomite porosity of 39.4% at 500 metres requires that the initial surface porosity of 30.36% of equation 2 be recalculated to be consistent with the 39.4% porosity at 500 metres depth of the Manetoe Dolomite. This recalculated fictitious initial dolomite surface porosity corresponding to a porosity of 39.4% at 500 metres is 43.9%, so expression 2 becomes:

$$\varnothing_{dol} = 0.439^* \exp(-(Z)/4619) \quad (3)$$

assuming that a simple linear transformation is appropriate.

The resultant dolomite porosity at the 5000 metre maximum depth that the Manetoe Dolomite experienced in Late Cretaceous time (Morrow *et al.*, 1993) following equation 3 is about 14.9%. This figure could be reduced only slightly to 12.7% if dolomitization occurred at depths as deep as 1000 metres, which the fluid inclusion data indicate is unlikely. Limestone porosity at this depth would be only 3.6% according to equation 1. This extreme difference serves to emphasize the perception that at great depths there is a greatly enhanced potential for preservation of porosity in dolomites which formed at much shallower depths.

There is a possibility that the initial average near-surface porosity of the Nahanni skeletal lime wackestones was less than that of the Cenozoic Floridan limestones, which contain a high proportion of wackestones and mudstones (Schmoker and Halley, 1982). Bond and Kominz (1984) found that best fitting average depth-dependent porosities of lime sediments are strongly dependent on initial sediment grain size such that "calcarenites" are much less porous than "micrites" (*i.e.* lime mud) at all burial depths (Fig. 2 in Bond and Kominz, 1984). Lower initial limestone porosities imply correspondingly lower dolomite and limestone porosities at maximum burial. This grain size factor may have contributed to a low initial limestone porosity and might help to explain why the present day porosity of most of the gas field Manetoe Dolomites ranges from about 2.0% to 6.0%, and the limestones have about 1.0% porosity.

The fact that Devonian lime muds, which formed most of the Nahanni were probably calcite rather than aragonite (James and Choquette, 1990), may have also have influenced initial porosity. It seems likely that calcite muds of the Devonian would have had a lower initial porosity than present-day aragonite muds because the more equant calcite crystals are unlikely to exhibit the "jackstraw" style of open packing that characterizes the acicular aragonite crystal masses in the very porous aragonitic seafloor muds of the Bahama Banks (Enos and Sawatsky, 1981). This mineralogical factor may also have contributed to a slightly lower initial limestone porosity for pre-Manetoe Nahanni limestones.

Although the process of dolomitization did not increase porosity at the time of dolomitization, there is some indication that permeability, particularly vertical permeability, was increased by the Manetoe dolomitization event. Undolomitized limestones in the La Biche F-08 core tend to have little or no vertical permeability, whereas dolomitized intervals have measurable vertical permeability. The nearly isotropic permeability of the dolomitized Kotaneelee E-37 cores is also an indication of the enhancement of vertical permeability during dolomitization. This effect is not as evident in the Pointed Mountain A-55 cores, possibly because the circulation of dolomitizing solutions was focussed preferentially parallel to bedding along pre-existing porosity networks of leached biogenic porosity. There may have been a tendency for the rate of

dissolution to be higher relative to the rate of dolomite precipitation because of more rapid solution flow along the more open porosity networks parallel to bedding. If true, this would tend to preferentially enhance permeability parallel to bedding during dolomitization.

There is no indication from the porosity-permeability data, or from visual examination of the cores of this study, that significant vertical fracture permeability exists. Comparison of geophysical logs, such as the neutron and sonic logs, might indicate the existence of open subvertical fracture porosity. Snowdon (1977) and Davidson and Snowdon (1978) suggested that the sporadic nature of gas production from the Manetoe Dolomite at the Beaver River gas field was due to the preferential invasion of water into the pervasive, gas-filled, fracture network which effectively 'sealed in' matrix gas.

The data of this study might be interpreted to indicate another possible cause for sporadic gas production interspersed with water production, particularly for the Pointed Mountain field. Pointed Mountain exhibits an essentially horizontally layered porosity-permeability fabric with weak vertical continuity. Production of gas would tend to quickly deplete the high permeability layers. If these layers intersected fractures open to the pressured aquifer beneath the gas column, water would tend to rise up these fractures and invade the high permeability layers during gas production. Vertical fracturing at Pointed Mountain and Kotaneelee, at a minimum, must be significant near the major faults that segment these fields (Figs. 2 and 3). This interpretation, involving scattered, rather than pervasive, open fractures, represents a variation on the theme of Davidson and Snowdon (1978).

The presence of other mineral cements, such as quartz and particularly calcite, along with reservoir bitumen have a considerable role in porosity reduction. The extent of this reduction has not been studied here, but insoluble residues of core samples from the Kotaneelee E-37 well yielded about 4.0% by weight of insoluble residue after digestion in hydrochloric acid. These insoluble residues were found to be mainly bitumen and quartz (Henderson, 1995). This amount of additional cement and mineral matter would cause a significant further reduction in porosity by at least 4.0% in the low porosity Manetoe Dolomite of this well. Subtraction of these non-carbonate phases from the rock volume would raise dolomite porosity to the range 6.0-10.0%. Henderson (1995) suggested that the release and disaggregation of these acid insoluble phases during secondary acid stimulation of the Kotaneelee field could adversely affect field performance.

Solution seams and stylolites have undoubtedly caused additional porosity loss in the Manetoe Dolomites. It is uncertain, however, whether pressure solution has been any more intense in the Manetoe sequence than in the Floridan carbonate succession examined by Schmoker and Halley (1982). On this basis, we cannot assert that pressure solution in the Manetoe Dolomite is likely to have caused any major departure from the depth-dependent porosity functions of Schmoker and Halley (1982) through porosity destruction.

However, chemical processes, such as pressure-solution, are time-dependent, as well as depth-dependent. Schmoker (1984) has suggested, with some documentation, that porosity in carbonates is best understood as a function of their Time-Temperature Index, or Lopatin TTI:

$$\varnothing_{carbonate} = a*(TTI)^b \quad (4)$$

where TTI is the Time-Temperature Index (*e.g.* Waples, 1980). However, like the variety of depth-porosity functions, there is also considerable variation in the values of constants "a" and "b" in equation 4, with different sets of constants applicable to different carbonate sequences, although there is remarkable internal consistency for each individual sequence. It seems at least possible that part of the difference between the low porosity of the Manetoe Dolomite and Nahanni limestone and the more porous Floridan carbonates may be due to the fact that the TTI values of the Manetoe and associated Nahanni are much higher than in the Floridan carbonates. Therefore, in the absence of direct comparative evidence between the Manetoe Dolomite and the Floridan carbonate sequence, it seems likely, based on equation 4, that there should be considerable porosity destruction in the Manetoe Dolomite sequence beyond that predicted in Floridan Carbonates buried to similar depths, according to the depth-dependent functions of equations 1 and 2. The abundance of well developed stylolites within the Manetoe Dolomite (Figs. 8, 10, 11 and 13) is consistent with this possibility.

Consequently, while there may have been differences between the initial depositional porosities of pre-Manetoe Nahanni limestones and Cenozoic to modern day carbonates, postdepositional processes of mineral cementation, bitumen emplacement and stylolite development are sufficient to adequately explain the lower porosities of the Manetoe Dolomite and Nahanni limestones as compared to porosities predicted from their maximum burial depths according to equations 1 and 2. Dolomitization itself is unlikely to have created porosity. Instead, the low average porosities of the Manetoe Dolomite may

indicate that dolomitization either conserved rock volume or even caused the occlusion of some pre-existing porosity by the precipitation of additional dolomite cement.

Manetoe dolomitization is inferred to have been early in the diagenetic sequence, preceding the generation of hydrocarbons (Fig. 14). The pervasive solid reservoir bitumen coating dolomite crystals lining vugs attests to the post-dolomitization migration of liquid hydrocarbon into these rocks. The presence of subvertical bitumen-filled fractures crosscutting Manetoe Dolomite fabrics implies that there may have been fracturing from gas generation during oil catagenesis. Thermal gas generation in oil pools probably can generate considerable overpressures in the subsurface (Ungerer *et al.*, 1983) which might lead to subsurface fracturing. The extremely low vertical permeability of the overlying Besa River shale and the low permeability of Nahanni limestones adjacent to Manetoe reservoirs would enhance the potential for the generation of overpressures during the thermal cracking of oil to gas in these reservoirs. Viscous, but still mobile bitumen may have been forced into these fractures during gas generation some time following emplacement of the Manetoe Dolomite.

The occurrence of zones with macropore vugs completely occluded by solid bitumen may indicate that much of the bitumen originated not simply as the residual bitumen that remains after the thermal cracking of oil to gas, but rather as deasphalted bitumen (Lomando, 1992), in which the gas-soluble oil fraction has been stripped from the oil by gas passing upwards through the oil column. The relatively massive amounts of bitumen in the Kotaneelee E-37 well may be due to its proximity to a fault which possibly provided a local focus for the upwards flow of gas through the oil column in Mesozoic to Cenozoic time.

The quartz and calcite vug-filling cements clearly postdate bitumen emplacement as do the sphalerite and galena veinlets. It is difficult to be certain of the timing of the cavern-fillings. Those in the Pointed Mountain A-55 core appear almost contemporaneous with the Manetoe dolomitization event, with some evidence that the excavation of macrovug porosity predated dolomitization (Fig. 14).

Silicification of the detrital crossbedded fossiliferous carbonates in the large cavern-filling in the La Biche F-08 well may have been caused by pH changes related to the generation of organic acids during organic maturation. Generation of hydrocarbons in the overlying Besa River shale source beds in Late Paleozoic to Early Mesozoic time would have been accompanied by high solution concentrations of organic acids. These acid solutions on entering the porous cavern-filling may have caused the replacement of carbonates by silica if the pre-existing pore solutions of the cavern-fill were alkaline and enriched in silica (*see* Williams and Crerar, 1985). However, in the absence of definitive age information, it is not possible to be certain concerning the timing of the cavern-filling with respect to liquid oil generation. The sooty bitumen impregnating the cavern-fill could be the later residue of in-place thermal cracking of oil that filled the cavern-fill porosity because the existing porosity of the cavern-filling, at more than 23%, is an order of magnitude greater than the TOC of about 2.0%.

This cavern-filling is shown as a distinct episode of cavern development on Figure 14. However, the "Paleozoic" appearance of the weakly crossbedded and silicified faunas and the probability that cavern excavation occurred before oil migration leaves open the possibility that this cavern-filling formed at the same time as the cavern-fillings in the Pan Am Pointed Mounted A-55 core.

CONCLUSIONS

Examination of cores from selected wells in the Liard Basin, in conjunction with regional geological and geochemical information has led to:

1. Recognition that the Nahanni Formation in the subsurface of Liard Basin more closely resembles the transgressive Dunedin Formation of northeast British Columbia than the regressive Nahanni Formation of the southern Mackenzie Mountains;
2. Identification of one, and possibly two episodes of subsurface cavern excavation and internal sediment infill that postdate Manetoe dolomitization;
3. Recognition that hydrocarbon migration postdated cavern development and emplacement of the Manetoe Dolomite;
4. Recognition that much of the gas field bitumen originated by deasphalting of oil, rather than as a residue of the thermal cracking;
5. Correlation of trends in bitumen reflectance of the upper Paleozoic siliciclastic sequence overlying the Manetoe Dolomite with trends in vitrinite reflectance and in Rock-Eval Tmax;
6. Recognition that the absolute porosities of the Manetoe Dolomite and accompanying Nahanni limestone and their average porosity differences are largely the result of depth-dependent porosity changes during burial, along with additional porosity occlusion by mineral cements and bitumen;
7. Recognition that porosity-permeability tends to be

preferentially developed parallel to bedding and that vertical permeability was enhanced by dolomitization;
8. Recognition that late-stage fracturing, unlike in the Beaver River gas field, did not contribute significantly to porosity or permeability of the Kotaneelee and Pointed Mountain fields.

ACKNOWLEDGMENTS

We wish to thank Dr. J. (Jack) Wendte of GSC-Calgary for informative discussions related to this paper and Drs. Fari Goodarzi and Lloyd Snowdon of GSC-Calgary for assistance and advice concerning analysis and interpretation of organic materials. We thank also Imperial Oil of Canada for its contribution of data. This work was funded under Geological Survey of Canada Project 890064. It is contribution number 1997291 of the Geological Survey of Canada.

REFERENCES

Amoco Canada Petroleum Company Ltd. 1964. Seismic Survey, Pointed Mountain Area. National Energy Board, Open File 060-06-04-47.

Aulstead, K.L. 1987. Origin and Diagenesis of the Manetoe facies, southern Yukon and Northwest Territories, Canada. Unpublished M.Sc. thesis, Department of Geology and geophysics, University of Calgary, Calgary, 143p.

_____, Spencer, R.J. and Krouse, H.R. 1988. Fluid inclusion and isotopic evidence on dolomitization, Devonian of Western Canada. Geochimica et Cosmochimica Acta, v.52, p. 1027-1035.

Bond, G.C. and Kominz, M.A. 1984. Construction of tectonic subsidence curves for the early Paleozoic miogeocline, southern Canadian Rocky Mountains: implications for subsidence mechanisms, age of breakup, and crustal thinning. Geological Society of America Bulletin, v.95, p.155-173.

Chatterton, B.D.E. 1978. Aspects of late Early and Middle Devonian conodont biostratigraphy of western and northwest Canada. *In*: Western and Arctic Biostratigraphy, C.R. Stelck and B.D.E. Chatterton (eds.). Geological Association of Canada, Special Paper no. 18, p. 161-231.

Cecile, M.P., Morrow, D.W. and Williams, G.K. 1997. Early Paleozoic (Cambrian to Early Devonian) tectonic framework, Canadian Cordillera. Bulletin of Canadian Petroleum Geology, vol. 45, p. 54-74.

Columbia Gas Development of Canada Ltd. 1979. Geophysical Report on the Kotaneelee Seismic survey, Yukon Territory. JLJ Exploration Consultants Ltd. (R.P. Jordan), National Energy Board, Open File 556-06-04-007.

Davidson, D.A. and Snowdon, D.M. 1978. Beaver River Middle Devonian carbonate: performance review of a high-relief, fractured gas reservoir with water influx. Journal of Petroleum Technology, v. 30, p. 1673-1678.

Douglas, R.J.W. 1976. Geology of the La Biche River map-area, District of Mackenzie, Geological Survey of Canada Map 1380A, 1:250,000.

_____ and Norris, D.K. 1976. Geology, Sibbeston Lake, District of Mackenzie. Geological Survey of Canada, Map 1377A. (Scale 1:250,000).

Enos, P. And Sawatsky, L.H. 1981. Pore networks in Holocene carbonate sediments. Journal of Sedimentary Petrology, v. 51, p. 961-985.

Espitalié, J., 1986. Use of Tmax as a maturation index for different types of organic matter. Comparison with vitrinite reflectance. *In*: Thermal Modelling in Sedimentary Basins, J. Burrus (ed.), Technip, Paris, p. 475-496.

Gabrielse, H. 1967. Tectonic evolution of the northern Canadian Cordillera. Canadian Journal of Earth Sciences, v.4, p. 271-298.

Henderson, G. 1995. Core Report for Anderson Exploration, March 3, 1995 (Report number NRD-95-125): Nowsco Well Service Ltd., Calgary, Alberta, Canada, 9p.

Imperial Oil Resources Ltd. pers. comm. Unpublished report on two bitumen samples from the Manetoe Dolomite of the Pan Am Kotaneelee YT E-37 well. Rock-Eval and biomarker analyses performed at GSC-Calgary under direction of L.L. Snowdon.

Jacob, H. 1985. Dispersed solid bitumen as an indicator for migration and maturity in prospecting for oil and gas. Erdöl Kohle, v.35, p. 365.

James, N.P. and Choquette, P.W. 1990. Limestones - the sea floor diagenetic environment. *In*: Diagenesis, I.A. McIlreth and D.W. Morrow (eds.). Geoscience Canada, Reprint Series 4, p. 13-34.

Lomando, A.J. 1992. The influence of solid reservoir bitumen on reservoir quality. American Association of Petroleum Geologists Bulletin, v. 76, no. 8, p.1137-1152.

Machel, H.G. 1985. Cathodoluminescence in calcite and dolomite and its chemical interpretation. Geoscience Canada, v. 12, p. 139-148.

Meding, M.G. 1994. Analysis of Selected Northwest Territories Hydrocarbon Pool Data: Geostar Consultants Inc., Report prepared for Department of Energy, Mines and Resources, Government of the Northwest Territories.

Meijer Drees, N.C. 1993. The Devonian Succession in the Subsurface of the Great Slave and Great Bear Plains, Northwest Territories. Geological Survey of Canada, Bulletin 393, 222p.

Morrell, G.R., Fortier, M., Price, P.R. and Polt, R. 1995. Mackenzie valley, southern territories and interior plains. *In*: Petroleum Exploration in Northern Canada - A Guide to Oil and Gas Exploration, G.R. Morrell (ed.), Northern Oil and Gas Directorate, Indian and Northern Affairs Canada, p. 7-22.

Morrow, D.W. 1978. The Dunedin Formation: A Transgressive Shelf Carbonate Sequence. Geological Survey of Canada, Paper 76-12, 35p.

_____ 1994. Manetoe Dolomite Field Trip, Southern Mackenzie Mountains. Unpublished Field Trip Guide Book, 12p.

_____, 1996. The Manetoe Dolomite exploration play in the Liard Basin of the Yukon and Northwest Territories. Abstract In Pools' 96 - Oil and Gas Pools of the Western Canada Sedimentary Basin, Core Conference Abstracts, p. 12.1-12.2.

_____ and Aulstead, K.L. 1995. The Manetoe Dolomite - a Cretaceous-Tertiarty or a Paleozoic event? Fluid inclusion and isotopic evidence: Bulletin of Canadian Petroleum Geology, v. 43, No. 3, p. 267-280.

_____, _____ and Cumming, G.L. 1990. The gas-bearing Devonian Manetoe Facies, Yukon and Northwest Territories. Geological Survey of Canada Bulletin 400.

_____ and Cook, D.G. 1987. The Prairie Creek Embayment and lower Paleozoic stratigraphy of the southern Mackenzie Mountains. Geological Survey of Canada, Memoir 412.

_____, Potter, J., Richards, B. and Goodarzi, F. 1993. Paleozoic burial and organic maturation in the Liard Basin region, northern Canada. Bulletin of Canadian Petroleum Geology, v.41, No.1, p. 17-31.

Noble, J.P.A. and Ferguson, R.D. 1971. Facies and faunal relations at the edge of early mid-Devonian carbonate shelf, Soouth Nahanni River area, N.W.T., Bulletin of Canadian Petroleum Geology, v. 19, p. 570-588.

Peters, K.E. 1986. Guidelines for evaluating source rock using programmed pyrolysis. American Association of Petroleum Geologists Bulletin, v.70, no.3, p. 318-329.

Potter, J. in prep. The Organic Petrology, Thermal Maturity and Hydrocarbon Potential of the Upper Devonian and Lower Carboniferous in the Liard Basin, Northern Canada. Ph.D. Thesis, University of Newcastle-upon-Tyne, U.K.

Price, P.R. 1994. Petroleum Resources of the Liard Plateau Area, Southern Yukon Territory, Canada. Unpublished National Energy Board Report (Draft), 31p.

Snowdon, L.R. 1995. Rock-Eval Tmax suppression: Documentation and amelioration. American Association of Petroleum Geologists, Bulletin, v. 79, p. 1337-1348.

Snowdon, D.M. 1977. Beaver River gas field: a fractured carbonate reservoir. *In*: The Geology of Selected Carbonate Oil, Gas and Lead-Zinc Reservoirs in Western Canada, I.A. McIlreath and R.D. Harrison (eds.), Canadian Society of Petroleum Geologists, 5th Core Conference, p. 1-18.

Schmoker, J.W. 1984. Empirical relation between carbonate porosity and thermal maturity - an approach to regional porosity prediction. American Association of Petroleum Geologists, Bulletin, v. 68, p. 1697-1703.

_____ and Halley, R.B. 1982. Carbonate porosity versus depth - a predictable relation for south Florida. American Association of Petroleum Geologists, Bulletin, v. 66, p. 2561-2570.

Spencer, R.J. 1987. The origin of Ca-Cl brines in Devonian formations, western Canada sedimentary basin. Applied Geochemistry, v.2, p. 373-384.

Taylor, G.C. and Mackenzie, W.S. 1970. Devonian Stratigraphy of northeastern British Columbia. Geological Survey of Canada, Bulletin 186.

Ungerer, P.E., Behar, E., and Discamps, D. 1983. Tentative calculations of the overall volume expansion of organic matter during hydroacarbon genesis from geochemistry data: implications for primary migration. *In*: Advances in Organic Geochemistry: Chichester. John Wiley, p. 129-135.

Ward, G.S. 1994. Hydrodynamic Evaluation of the Devonian to Precambrian Formations - Liard Arch, N.W.T. (59°30'-63° 00'N, 121° 00' - 125° 00'W): Ward Hydrodynamics Ltd., 89p.

Waples, D. 1980. Time and temperature in petroleum formation: Application of Lopatin's method to petroleum exploration. American Association of Petroleum Geologists Bulletin, v.64, p. 916-926.

Williams, G.K. 1981. Subsurface geological maps, southern Northwest Territories. Geological Survey of Canada, Open File 793.

Williams, L.A. and Crerar, D.A. 1985. Silica diagenesis, II. General mechanisms. Journal of Sedimentary Petrology, v. 55, p. 312-321.

International Journal of Coal Geology, 24 (1993) 113–140
Elsevier Science Publishers B.V., Amsterdam

The petrology and origin of coals from the Lower Carboniferous Mattson Formation, southwestern District of Mackenzie, Canada

J. Potter[a,*], B.C. Richards[b] and A.R. Cameron[b]

[a]*Newcastle Research Group for Fossil Fuels and Environmental Geochemistry, University of Newcastle-upon-Tyne, Newcastle-upon-Tyne, NE1 7RU, UK*

[b]*Institute of Sedimentary and Petroleum Geology, Geological Survey of Canada, 3303, 33rd St. N.W., Calgary, Alberta T2L 2A7, Canada*

(Received September 10, 1992; revised version accepted April 14, 1993)

ABSTRACT

Petrographic analyses were carried out on thin coals and coaly sediments from the Lower Carboniferous Mattson Formation at Clausen Creek and Jackfish Gap–Yohin Ridge in the northern part of the Liard Basin, northern Canada. The composition and optical characteristics indicate that the coals are high-volatile bituminous B, predominantly sapropelic (canneloid) and accumulated subaquatically.

The coals are dominantly composed of inertinite-rich and exinite-rich durites with subsidiary inertites and clarodurites; vitrite is minor and liptite is rare. The inertinite-rich microlithotypes are dominated by semifusinite, but micrinite, semimacrinite and ?resino-inertinites are abundant. Sporinite, comprising megaspores, crassispores, tenuispores and miospores, is the dominant liptinite maceral with subsidiary cutinite and minor alginite. Except for pyrite, mineral matter is minimal.

Three populations of telocollinite are observed: a low-reflectance variety (I), commonly associated with micrinite (as vitrinertite), displays weak brown fluorescence and a reflectance some 0.4–0.5% lower than type II; type II is non-fluorescing telocollinite, with intermediate reflectance (0.67–0.74% R_om), it occurs as vitrite and is also associated with micrinite; and a higher-reflectance telocollinite (III), having no fluorescence or association with micrinite, has variable reflectance (0.74–0.8% R_om) implying higher oxidation or gelification levels.

The abundance of semimacrinite, macrinite and ?resino-inertinites in inertites and durites (I) suggests that much of the peat accumulated subaquatically. Furthermore, fluorescing vitrinite and an abundance of micrinite (derived by oxidation or coalification of bituminite), suggest that the coal accumulated under anaerobic conditions. The predominance of semifusinite in humic laminae and micrinite in sapropelic layers suggests extensive surface or near-surface oxidation of the peat. Oxidised sporinites suggest that they were wind-borne.

Depositional environment is interpreted as marginal marine, perhaps in shallow lakes in the middle to upper delta plain. Peat accumulations probably began subaquatically at the oxygen–hydrogen sulphide interface, but periodic subaerial exposure and natural oxidation gave rise to the high inertinite coals. Upper Mattson coals are interbedded with algal laminites and probably accumulated in a lagoonal setting.

*Corresponding author.

INTRODUCTION

Most of the Carboniferous coals found in western Europe are bituminous, humic coals formed in fluvio-deltaic environments. In Canada, Carboniferous coals of bituminous rank occur only in eastern Canada (predominantly in Nova Scotia and New Brunswick but also in Newfoundland), the Yukon Territory (Whitehorse Trough and British Mountains) and District of Mackenzie (Liard Basin). The coals in eastern Canada are of Westphalian age and were deposited in non-marine, fluvial (floodplain) or lacustrine environments (Hacquebard and Donaldson, 1969) in numerous separate fault-

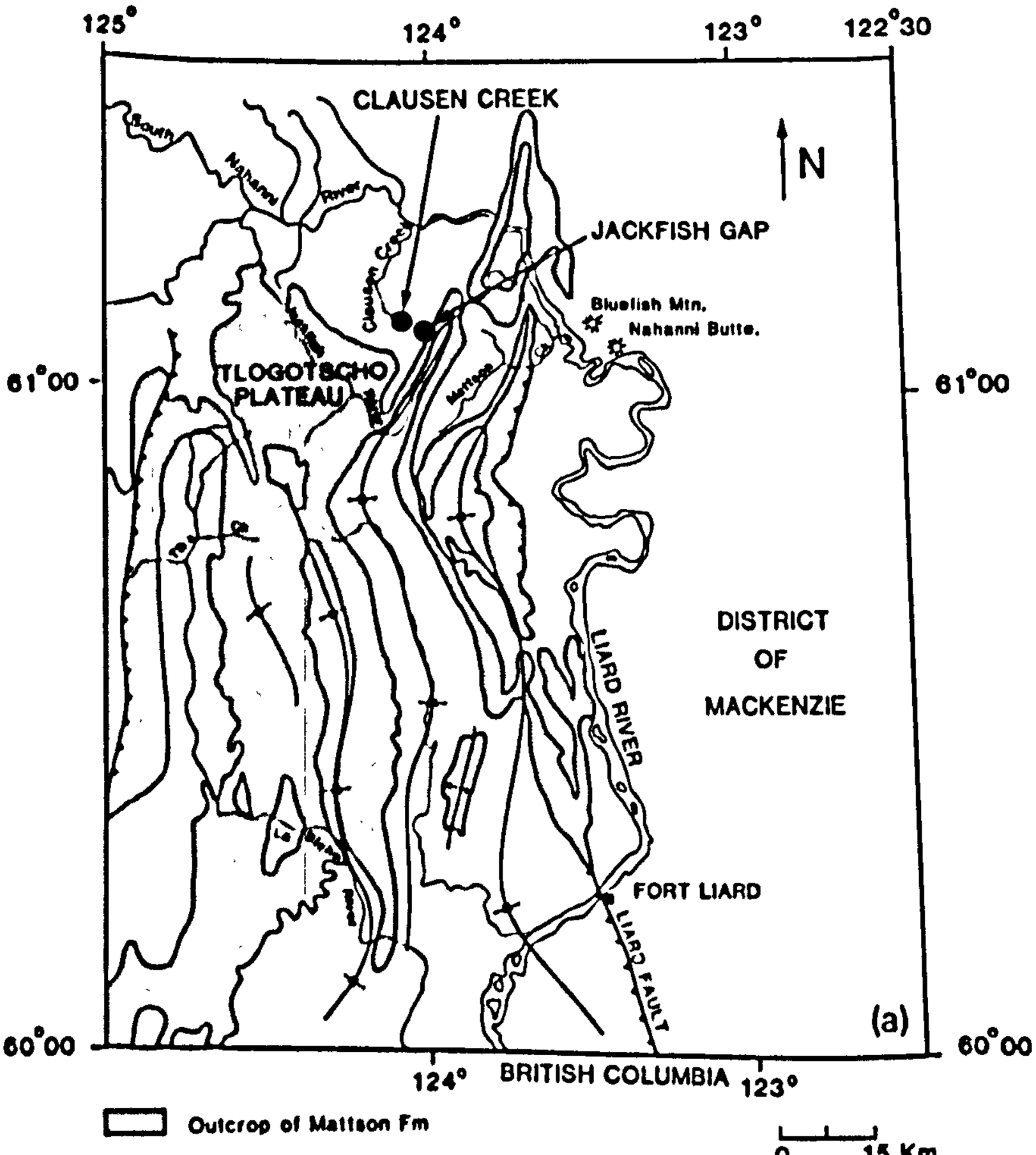

Fig. 1 (a).

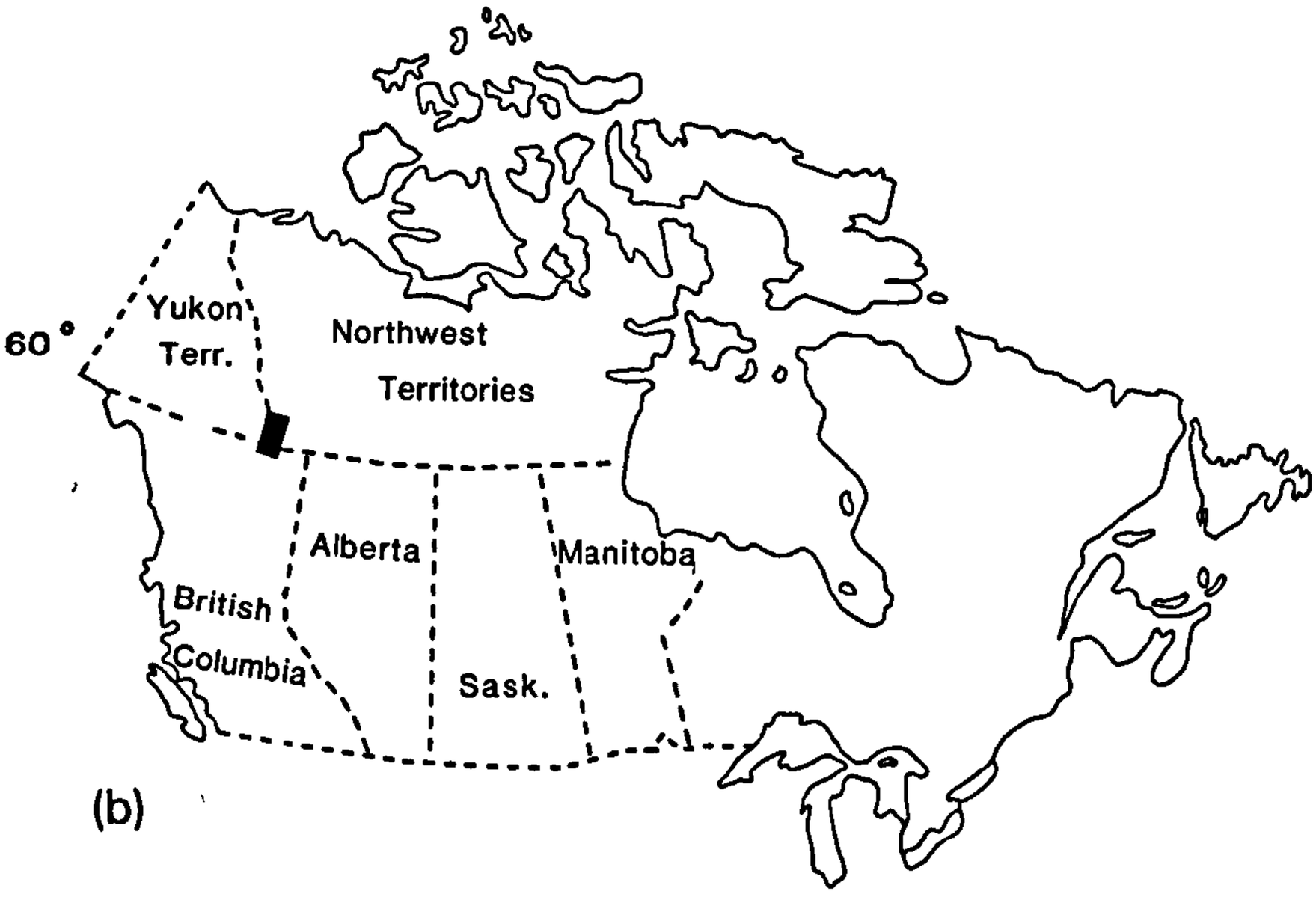

Fig. 1. (a) Outcrop of Mattson Formation in the study area (from Richards, 1989). (b) Location map of NW Canada showing study area.

bounded intermontane subbasins (Smith, 1989). The coals in the Sydney Basin are humic (banded); they are rich in vitrinite (>70%), inertinite (ca. 20%) with subordinate liptinite macerals (<10%) (Hacquebard and Donaldson, 1969). Micro-banded, hypautochthonous and cannel coals associated with lacustrine environments occur in the Pictou Coalfield (Hacquebard and Donaldson, 1969; Kalkreuth and Macauley, 1987). In general, vitrinites constitute less than 50% of the coal, inertinites as much as 40%, liptinites generally less than 10% and mineral matter can be as high as 20% of the coal (ibid.). Unlike the coals in eastern Canada, the coals in the Mattson Formation in the Liard Basin, southwestern District of Mackenzie are thin inertinite- and liptinite-rich coals which suggests a rather different depositional setting.

Numerous thin coal seams and lenses occur within the Lower Carboniferous Mattson Formation, north of 59°30′N, and are widely exposed in the eastern Cordillera, southwestern District of Mackenzie, Northwest Territories (Fig. 1). Coals ranging in thickness from 0.3 to 1.5 m occur mainly within the middle and upper members of the Mattson Formation, as defined by Richards (1989), a deltaic succession comprising sandstone, with subordinate siltstone, shale and carbonates of late Viséan (V3) to early Serphukovian age (Richards, 1989; Bamber et al., 1984).

Petrographic analyses of coal samples and associated shales from two sections of the Mattson Fm. exposed at Jackfish Gap–Yohin Ridge (61°06′N 123°59′W) and Clausen Creek (61°03′55″N 124°07′08″W) (Fig. 1) were

carried out to determine the rank and composition of the coals as part of a regional study of the thermal maturity and oil and gas potential of the Upper Devonian and Carboniferous in the Liard Basin.

GENERAL GEOLOGY

The study area, in the southeastern Yukon Territory and southwestern District of Mackenzie, is located in the Mackenzie Fold Belt and borders on the Interior Platform (Richards, 1989). Upper Devonian and Carboniferous strata in this area consist of a shallowing-upwards succession of basinal to shelf carbonates and terrigenous clastics deposited in the eastern Prophet Trough along the western margin of the ancestral North American Plate (Richards, 1989; Richards et al., 1989). The Mattson Formation outcrops extensively throughout the western and central portions of the study area in a series of north–south striking anticlines and synclines. It is preserved mainly as a down-faulted succession lying west of the northwest-trending Bovie normal fault. It is less than 15 m thick east of the Bovie fault but thickens westwards, attaining over 1410 m in the southern Mackenzie Fold Belt (Richards, 1989). At Jackfish Gap, the type locality, it is 1020 m thick (Fig. 2).

The Mattson Formation was deposited in deltaic and related environments during several delta cycles (Richards, 1989; Richards et al., 1989). Most of the Mattson deltas are classified as fluvially dominated, wave- and tide-influenced deltas of lobate form. Thick Platte-type braided-stream deposits (probably distributary channels) are common within the delta plain facies of the middle and upper members. Coals, shales and sandstones in coarsening-upward sequences of overbank and delta-front origin, are associated with the braided-stream deposits. Toward the southwest (basinward), the delta plain–delta front lithofacies grade into delta-slope deposits of the lower member, which in turn grade basinward into prodelta shales of the Golata and Besa River Formations (Fig. 3).

Patton (1958) formally introduced the name Mattson Formation and described the type section at Jackfish Gap. Douglas and Norris (1959, 1960) and Harker (1961) elaborated on the lithological character and regional occurrence of the Mattson. More recently it has been the subject of detailed lithofacies analysis by B.C. Richards (pers. commun., 1993). Work on the coals from this area is limited to an early report by Hacquebard and Barss (1957), who reported on palynology of coals on the south Nahanni River, and an unpublished GSC internal report on the petrography of the coals at Jackfish Gap by Cameron and Pratt (1982). Palynological studies of the Mattson Formation have also been carried out by Braman and Hills (1977), Bamber et al. (1984) and J. Utting (in Richards, 1983, 1989).

The samples used in this study, which comprise thin coals, coaly clasts from siltstones and interbedded laminites and coals, were collected by Richards

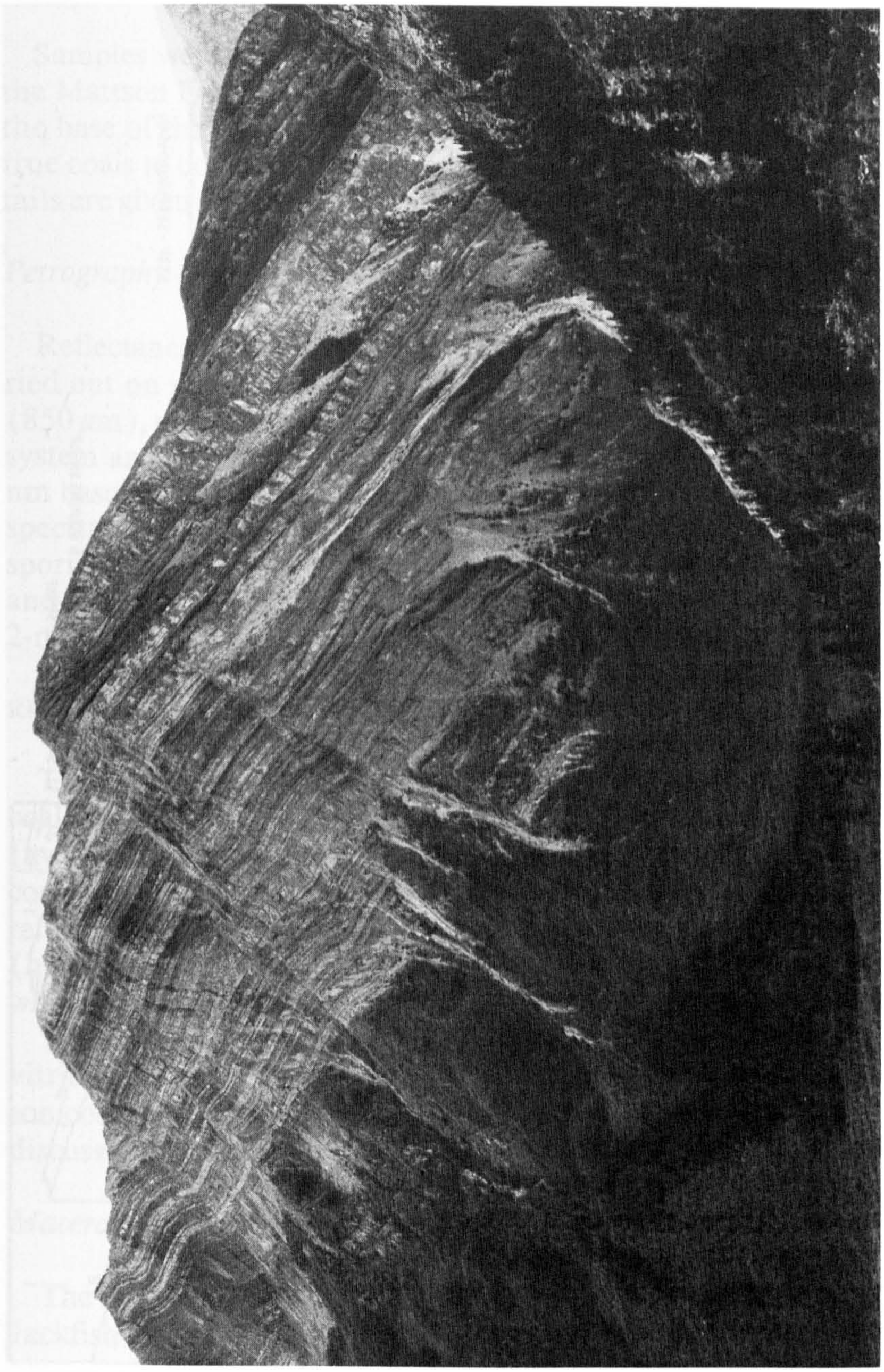

Fig. 2. Photograph showing the lower and middle Mattson succession at the type section at Jackfish Gap where the Mattson attains a thickness of 1020 m. Arrow marks the base of the Mattson.

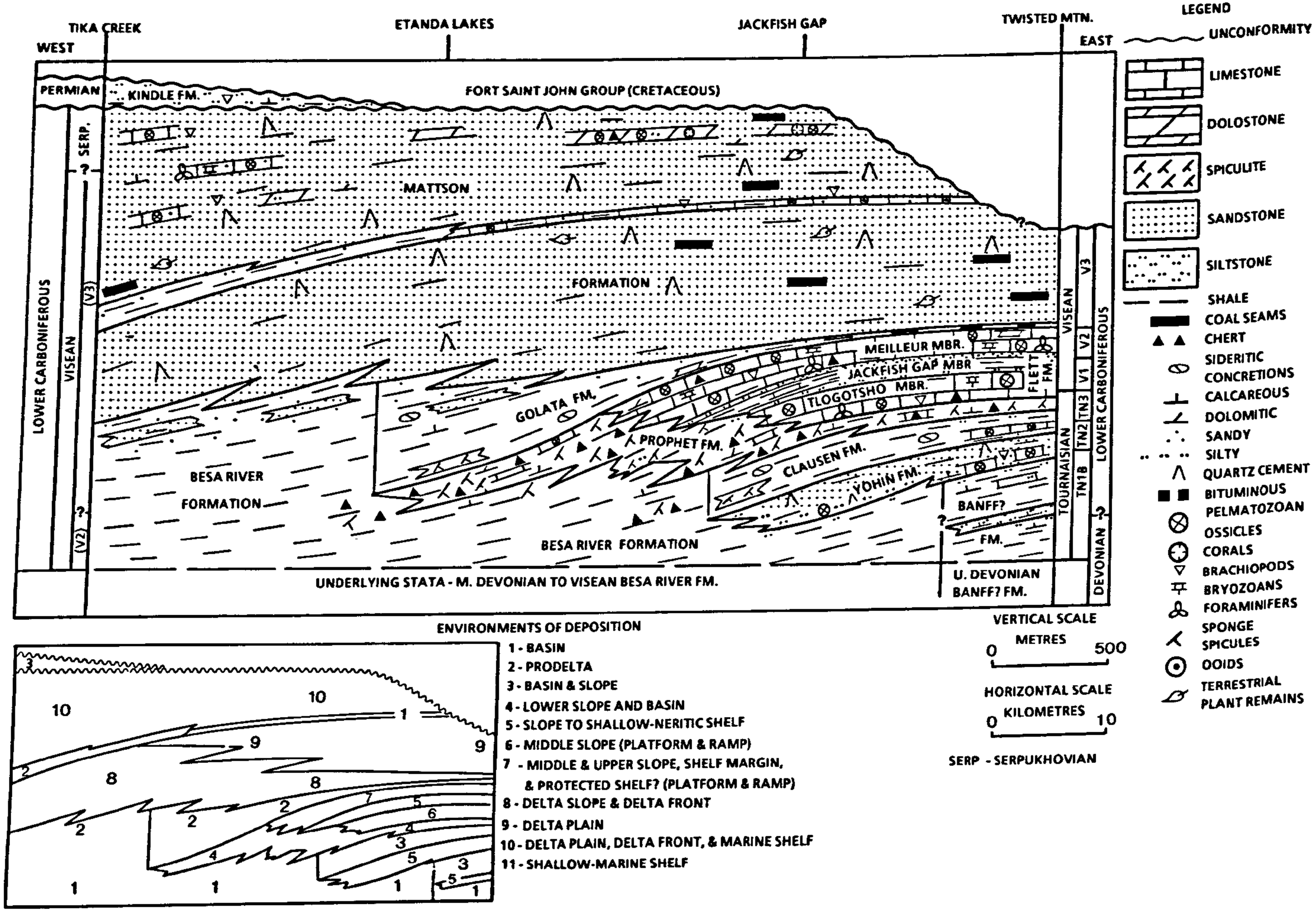

Fig. 3. Upper Devonian and Carboniferous stratigraphy and facies relationships (from Richards, 1989).

during a regional geological and sedimentological study of the Upper Devonian and Lower Carboniferous of the Liard Basin (Richards, 1989).

METHODOLOGY

Sampling intervals

Samples were collected at 266 m, 300 m and 1006.5 m above the base of the Mattson Formation at Jackfish Gap (Figs. 4 and 5) and 1305.5 m above the base of the Mattson section at Clausen Creek. The samples ranged from true coals to coaly inclusions in sandstone/siltstone units to coaly shales; details are given in Table 1.

Petrography

Reflectance photometry and quantitative petrographic analysis were carried out on polished pellet mounts of coal crushed to −20 Tyler mesh size (850 μm), using oil immersion objectives, a Zeiss UMSP II-HP300 computer system and Zeiss Coflex software. Reflectance (R_om) was measured at 546 nm based on 50 measurements on each of three populations of vitrinite. UV spectral fluorescence measurements were made at 365 nm excitation, on sporinites and alginites, using a similar microscope, a Zonax microcomputer and Zeiss Spectral scan software. Five spectral measurements were made at 2-min intervals and averaged to obtain λmax and R/G quotients.

RESULTS

The elemental compositions of two of the Mattson coal samples and the coal/laminite are shown in Table 2. The volatile matter contents of the coals (av. 33%, d.a.f.) and elemental carbon (av. 79%, d.a.f.) values suggest the coals are high-volatile bituminous A in rank. This is inconsistent with the reflectance data (Table 4) which suggests that the coals are of lower rank (high-volatile bituminous B). This suggests that the chemical analysis of the whole coals are affected by the coal composition.

The coals are dominated by inertinite- and liptinite-rich durites, inertite, vitrinertite and clarodurite. Microlamination is quite distinctive in the Mattson coals and, although microlithotypes are clearly divisible, the results and discussion in this paper will concentrate on the maceral compositions.

Maceral groups

The maceral compositions of four coals (Fig. 6) from outcrop sections at Jackfish Gap (Yohin Ridge) and Clausen Creek are shown in Table 3. The

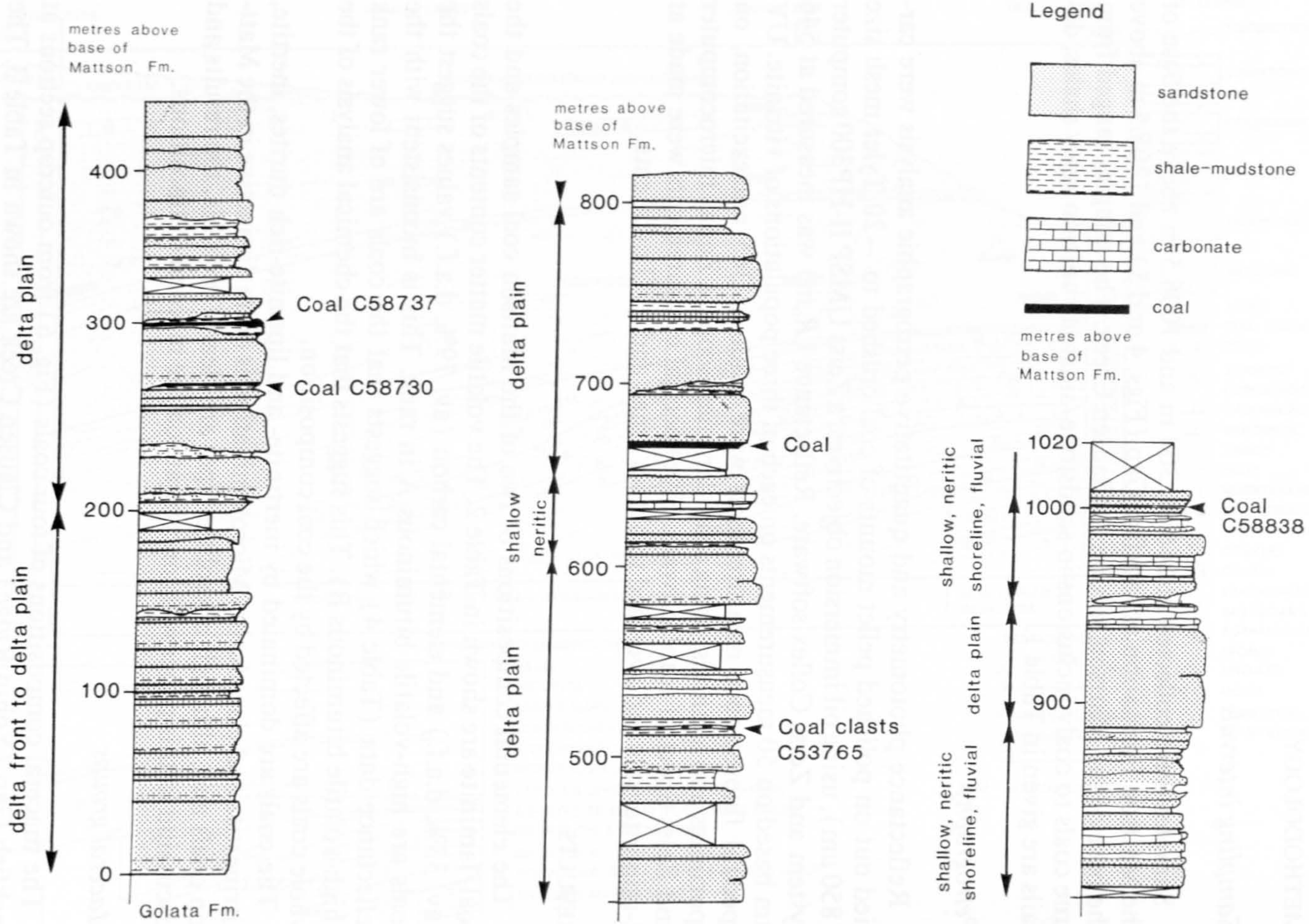

Fig. 4. Diagrammatic representation of Mattson section at Jackfish Gap showing the sampling intervals.

Fig. 5. Photograph of 1.5 m coal seam in the middle Mattson exposed at Jackfish Gap.

TABLE 1

Sampling intervals and localities

Sample No.	Location	Ht. (m) above base of Mattson Fm.	Sample type	Seam thickness (m)
C58730	Jackfish Gap	266	coal	0.3
C58738	Jackfish Gap	300	coal	1.4
C58764	Jackfish Gap	514	coal clasts	–
C58838	Jackfish Gap	1006.5	coal/laminite	–
C73409	Clausen Creek	1305.5	coals	0.5

most significant feature of the Mattson coals is the exceptionally high inertinite content. Inertinites account for 57% to 67% of the coal macerals and are represented by a great variety of macerals. These coals are also rich in liptinite. The coals at Yohin Ridge have a minimum of 20% liptinite, mostly occurring with inertinites as durite and clarodurite, and, to a much lesser extent, as liptite, clarite or duroclarite. The coal at Clausen Creek has a slightly lower liptinite content (17%) than coals at Jackfish Gap. Vitrinites form a rather small proportion of these Mattson coals (15–22%). Most commonly, vitrinites are associated with micrinite as vitrinertite and rarely occur as vitrite,

TABLE 2

Proximate and ultimate analyses of Mattson coals

Locality:	Jackfish Gap		Clausen Creek
Sample No.:	C58730	C58838	C74309
Moisture	3.4	7.8	2.54
Ash	2.4	43.9	4.32
Volatile matter (d.a.f.)	34.5	45.1	32.5
Fixed carbon (d.a.f.)	65.5	54.9	67.5
Total sulphur (d.a.f.)	1.25	0.35	1.64
Carbon	78.4	72.53	79.57
Nitrogen	1.03	0.72	1.11
Sulphur	1.25	0.35	1.64
Hydrogen	4.44	2.98	4.53
Oxygen	14.88	23.42	13.1

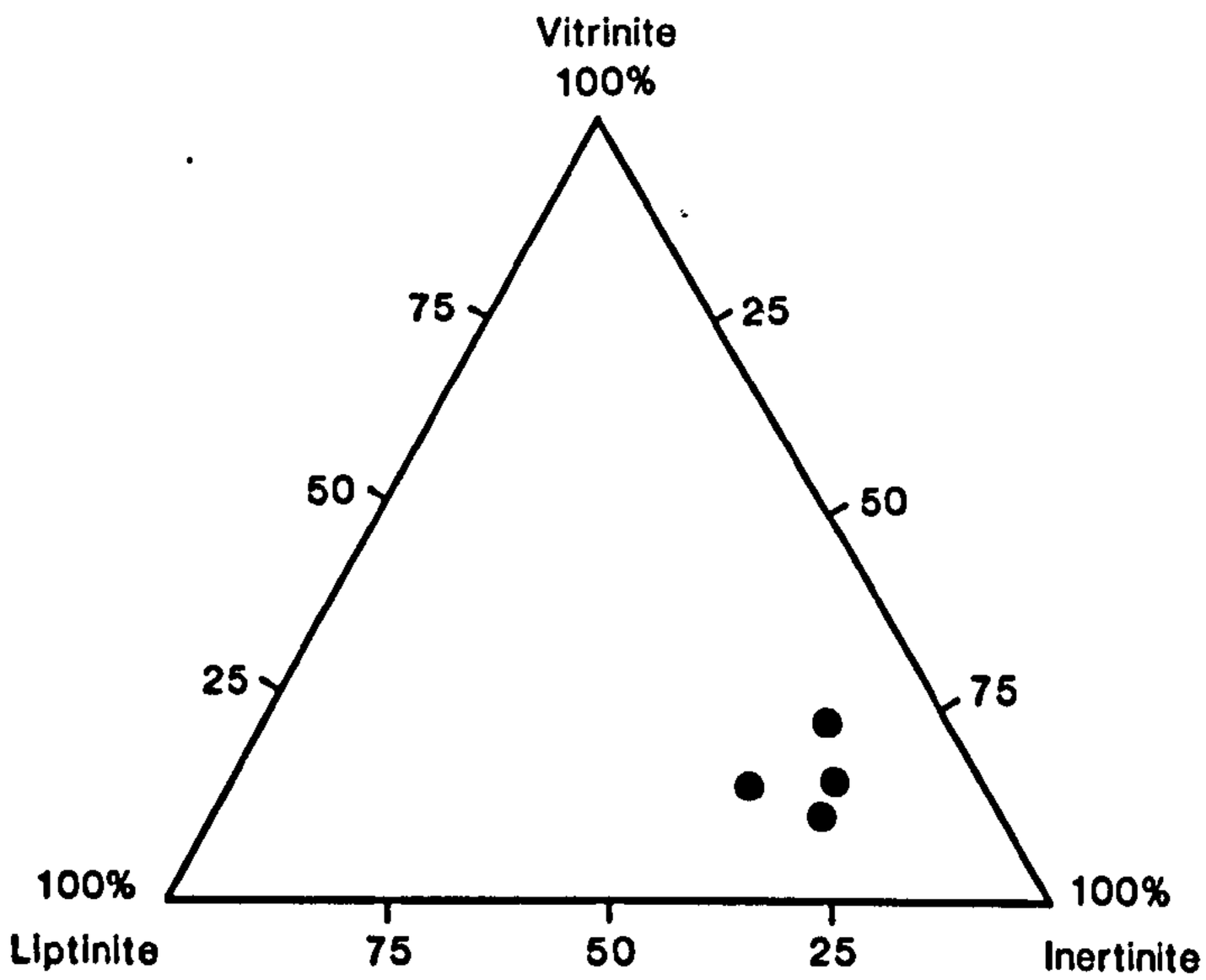

Fig. 6. Maceral composition of the Mattson coal samples.

clarite or trimacerite. The lack of vitrite (telocollinite) was noted by Cameron and Pratt (1982).

Ash (Table 2) and mineral matter contents are very low, amounting to < 1% at Yohin Ridge, and 2% at Clausen Creek (Table 3). Mostly it occurs in the form of pyrite (or oxidation products thereof); there is very little by way of detrital components (e.g. clay) and authigenic minerals.

TABLE 3

Maceral composition of coals from the Mattson Formation

	telocollinite	desmocollinite	gelocollinite	**total vitrinite**	sporinite	cutinite	liptodetrinite	alginite	**total liptinite**	fusinite	semifusinite	macrinite	semimacrinite	micrinite	sclerotinite	inertodetrinite	**total inertinite**	mineral matter
Jackfish Gap																		
C58730	3	12	<1	15	23	2	2	-	27	1	17	3	15	17	1	2	57	<1
C58737	3	10	-	13	18	2	+	+	20	3	28	8	7	19	1	<1	67	<1
C58764	4	18	1	23	19	<1	<1	-	20	1	34	+	7	14	1	1	57	<1
Clausen Creek																		
C74309	7	7	1	15	12	3	2	+	17	1	27	5	6	26	2	1	67	2

Liptinites

The liptinites are dominated by sporinite with subordinate cutinite and rare alginite (*Botryococcus* or *Rheischia*-type) and resinite (exsudatinite). A tremendous variety of sporinite occurs in the Mattson coals ranging from large, thick- and thin-walled, megaspores (Fig. 7) to microspores (crassispores, tenuispores and miospores) many of which are recognisable as far as genus (and occasionally, species) (Fig. 8).

Megaspores

The thick-walled megaspores range from 800 μm to > 1000 μm in diameter (Fig. 7a). They are trilete and characterized by a granular morphology and dense external ornamentation in the form of elongate, processes or appendages, up to 100 μm in length, in the equatorial plane, which have a somewhat resinous appearance. The dimensions and external ornament suggest they may belong to the genus *Setosisporites* or *Radiatisporites* which have been described from Westphalian and upper Viséan strata in Lublin Coal Basin, Poland (Dybova-Jachowicz et al., 1987). Heavily ornamented megaspores are known also from the Upper Devonian coals in the Canadian Arctic region (Goodarzi and Gentzis, 1991).

The thin-walled structures are characteristically granular and approximately 900 μm in diameter/long with 10–15 μm thick wall which is slightly sculptured (Fig. 7b).

The reflectance of the megaspores is 0.39% R_om and they display relatively weak, brownish-yellow fluorescence and a λmax in the order of 690 (R/G>2). Without exception, these spores show signs of oxidation suggesting the possibility of being transported into the peat swamp by wind or oxygenated waters.

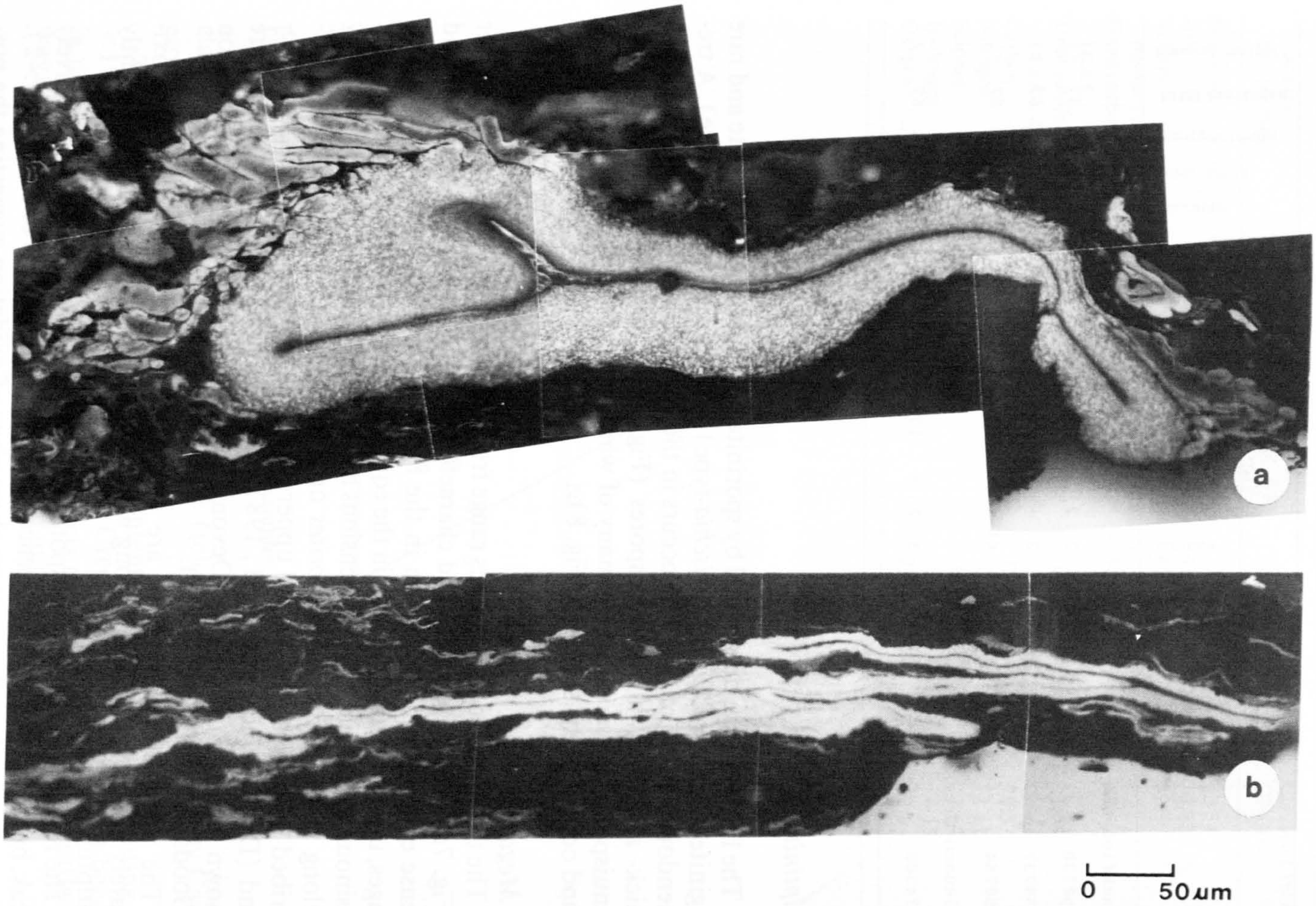

Fig. 7. Composite photomicrographs of megaspores: (a) thick-walled, highly ornamented, cf. *Setosisporites*; (b) thin-walled. Polished sections viewed in reflected blue light under oil immersion.

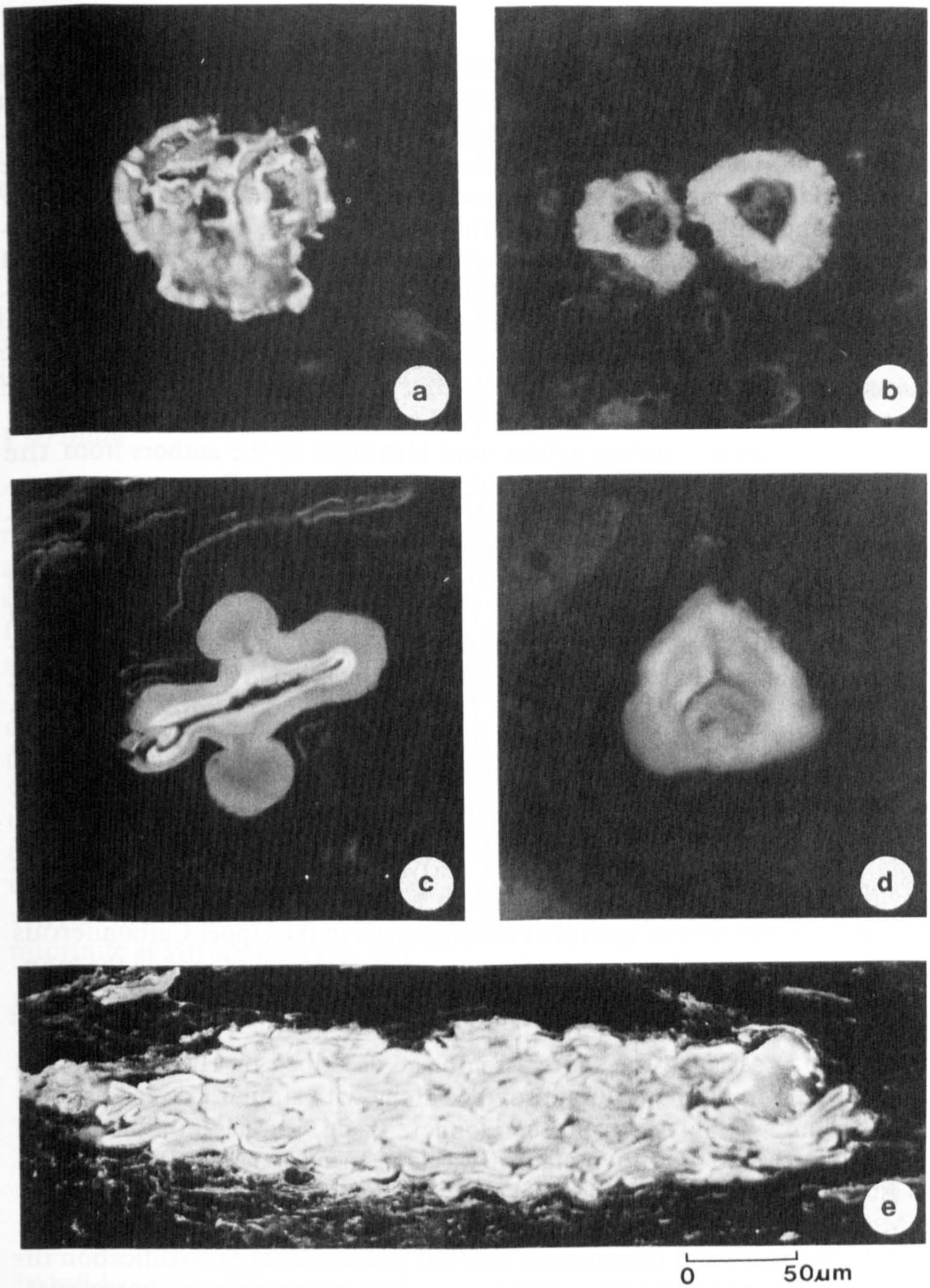

Fig. 8. Photomicrographs of Carboniferous microspores: (a) *Reticulatisporites*; (b) *Densosporites* sp.; (c) *Murospora* sp.; (d) *Murospora aurita*; and (e) microspore sporangium. Magnifications are the same for (a) to (e). Polished sections viewed in reflected blue light under oil immersion.

Microspores

Microspores ranging in size from 25 μm to 100 μm are also very common constituents of the Mattson coals (Figs. 8a–8d). Hacquebard and Barss (1957) recognized three species of *Reticulatisporites* (Fig. 8a) and many species of *Densosporites* (Fig. 8b). As many as 114 species of microspores were identified from coals and associated sediments in the Mattson Formation by Braman and Hills (1977) and J. Utting (in Richards, 1989). Many compressed reticulate and muronate microspores resembling *Baculexinus* and *Stratexinus* from the Baldur Seam, Ruhr Coalfield (Stach, 1968) are moderately common also; the dimensions and ornamentation suggest a strong affiliation with *Reticulatisporites* or *Convolutispora*. Microspore sporangia, similar to those found in the Middle to Upper Devonian of Melville Island, Arctic Canada (Goodarzi and Goodbody, 1990) are also well-preserved (Fig. 8e).

The following microspore genera were identified by the authors from the coals and associated shales: *Reticulatisporites* (Fig. 8a); *Densosporites* (numerous species, unidentified) (Fig. 8b); *Murospora* (Fig. 8c) including *Murospora aurita* (Fig. 8d); *?Labiadensites* and *?Convolutispora*.

All of these were recognised from palynological studies by Hacquebard and Barss (1957) and Braman and Hills (1977). Braman and Hills (1977) dated the Mattson as Visean (Meramician to Chesterian) on the basis of microspore assemblages. In studies of Carboniferous beds of Nova Scotia, J. Utting (in Richards, 1983, 1989) notes that *Densosporites* and *Murospora* are common in the Visean (V2). The spore assemblage in the upper Mattson coal, located 1000.6 m above the base of the Mattson, contains *Murospora aurita*, which Utting considers may be indicative of an early Namurian age. *Murospora* and *Densosporites* are dominant in the coals from the Mattson Formation. These genera are thought to be derived from Lycopods and Pteridophytes. Utting (1987) notes that "some workers (e.g. Habib et al., 1966) consider the presence of species of *Densosporites* in the Upper Carboniferous to indicate a marginal marine environment not unlike that found in the mangrove swamps of the southern Florida Everglades", and that species of this genus "are probably derived from herbaceous lycopods". Furthermore, Sullivan (1965) assigned the spore assemblage described by Hacquebard and Barss to the *Monilospora* floral province along with similar Lower Carboniferous spore assemblages from the Donnetz Basin, Russia and Spitzbergen and deduced that the provincialism was due to palaeoclimatic conditions consistent with palaeolatitudes of 45°N/S of the Equator.

Most of the sporinite (particularly megaspores) is oxidised precluding the use of reflectance and fluorescence spectral measurement as coalification indices. The fluorescence colour of the unoxidised microspores is characteristically a rich "buttercup" yellow and λ_{max} for crassispores is in the order of 650 nm to 670 nm with an R/G of 1.7 to 1.9.

Alginites

Alginite is generally a minor component of these coals. At both the Jackfish Gap and Clausen Creek localities, the coals contain freshwater, colonial alginite of *Botryococcus* or *Rheischia* affinity. In the coal located at Clausen Creek, rare dinoflagellates are present and ?*Tasmanales* alginite is present which shows signs of bacterial attack.

Other liptinites

Small amounts of weakly fluorescing exsudatinite (or bitumen) showing positive alteration are found infilling fusinite in coal sample C58737 from Jackfish Gap. Bitumen (R_om 0.32) with included micrinite and semimacrinite is present in C58764. Thin cutinite is also common.

Vitrinites

Desmocollinite, telocollinite, and oxygen-rich vitrinite (?gelocollinite) are the dominant vitrinites found in the Mattson coals (Table 3); gelocollinite and corpocollinites are minor components. In the coals from Jackfish Gap, desmocollinite is the dominant vitrinite maceral. Typically, it has lower reflectance than telocollinite (Table 4) and shows weak brown fluorescence suggesting it is perhydrous (Teichmüller, 1982a).

Telocollinite occurs in roughly the same proportions as desmocollinite in coal from the Clausen Creek section but it is subordinate to desmocollinite in coals from Jackfish Gap. In one sample it is less than 2%. The reflectance varies from 0.67% to 0.74% R_om, being slightly higher in rank at Jackfish Gap than at Clausen Creek. Using Ting's formula to determine the maximum reflectance, this would equal 0.79% $R_o$max, which agrees with reflectance values obtained by Cameron and Pratt (1982). The telocollinite rarely occurs as vitrite (in the humic coal) and is most commonly intimately associated with micrinite as vitrinertite (Fig. 9a).

There appears to be a considerable spread in the reflectance of the telocollinite (Table 4) and three separate populations are identified on the basis of

TABLE 4

Vitrinite reflectance data (%R_om)

	Jackfish Gap				Clausen Creek
	C58730	C58738	C58764	C58838	C74309
Telocoll. I	0.62	0.63	0.67	0.62	0.55
Telocoll. II	0.70	0.73	0.74	0.68	0.60
Telocoll. III	0.79	0.79	0.79	0.78	0.73
Telocoll. in shale	–	–	–		–

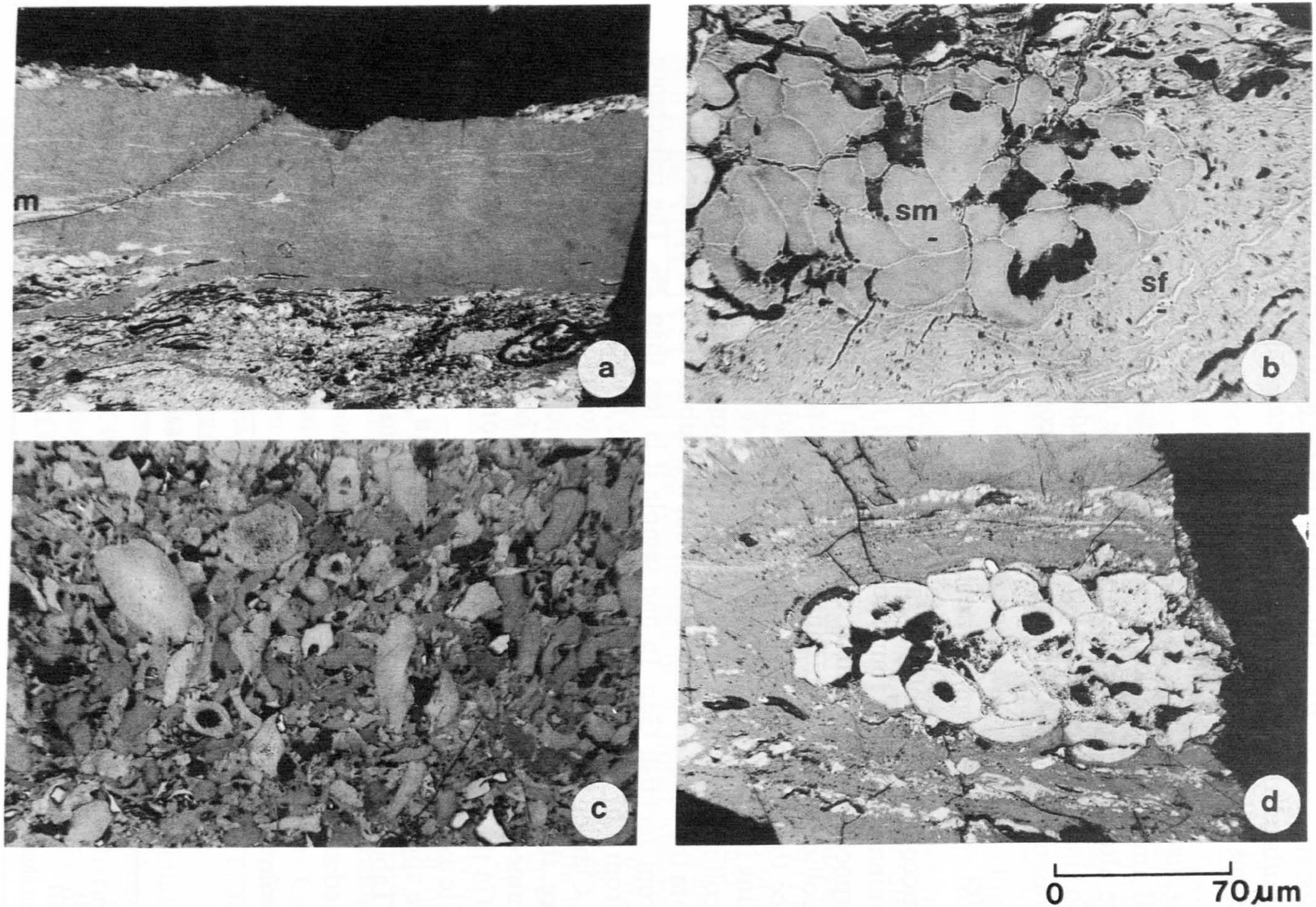

Fig. 9. Photomicrographs showing inertinite macerals and inertinite-dominated microlithotypes: (a) vitrinite in vitrinertite with lenses of micrinite (*m*) threaded throughout; (b) semifusinite (*sf*) derived from highly gelified woody tissue with clusters of semimacrinite bodies (*sm*); (c) clastic or detrital inertinite mostly composed of semimacrinite and macrinites having various morphologies; (d) vesicular macrinites with fusinite reflectance enclosed in vitrinite and micrinite possibly derived from ?cortical tissue. Polished sections viewed in white light under oil immersion.

reflectance. Telocollinite associated with the more humic coal (telocollinite I) has reflectance similar to desmocollinite but lower by ca. 0.4% than other telocollinite in the same sample and displays weak brown fluorescence. Goodarzi et al. (1987) and Robert (1988) indicated that vitrinite suppression was commonly associated with perhydrous vitrinites which also typically show fluorescence. The elemental analyses do not suggest any hydrogen enrichment but, as indicated earlier, the chemical analyses of the whole coals appear to be influenced by the high inertinite content of the coal (Table 3). Numerous authors have reported on the suppression of vitrinite reflectance in coals and associated shales which can be attributed to a variety of factors which are reviewed by Barker (1991). However, Barker (ibid.) also described other causes of vitrinite reflectance suppression which may be more applicable to the Mattson coals given the depositional setting and associated macerals: (1) microbial alteration of vitrinite; and (2) the retention of bitumen in the vitrinite. Given the intimate association of telocollinite with micrinite-rich layers lenses (Figs. 9a, 10a, 10d) observed in these coals, it is suggested that microbial activity is the cause of the vitrinite reflectance suppression expressed by the telocollinite I. This interpretation also fits very well with the interpretation and discussion on the origin of micrinite in these coals in the following sections of this paper. Although exsudatinite was observed in very small amounts in these coals, the generation of hydrocarbons, and therefore bitumens which might be retained within the vitrinite cannot be ruled out since low rank bitumens are found in Mattson strata. Most of the ?telocollinite is non-fluorescing (type II) and it is considered that the reflectance of this variety (0.73% R_o) is representative of the natural coalification attained which would indicate a rank of high-volatile bituminous B. Small amounts of highly reflecting vitrinite (type III) are present which display significantly higher reflectance than the telocollinite II. It is also commonly associated with micrinite in vitrinertite bands, and with macrinite and semimacrinite in durite and clarodurite. Other than reflectance, there is very little morphological difference between this material and the telocollinite II. The telocollinite II is perhaps more oxygen-rich by virtue of its association with micrinite and may be the result of early diagenetic, surface oxidation. Alternatively, the highly reflecting vitrinite telocollinite III may be transitional to gelocollinite, implying oxidative gelification at an early stage in the development of the peat. Small amounts of gelocollinite are present in most of the samples. Goodarzi et al. (1987) found three populations of vitrinite reflectance in coals from the Lower Carboniferous Emma Fiord Formation in the Canadian Arctic Islands and related these to variations in alginite content of the coal. While alginite is a minor component of these coals, other liptinites, such as bituminite/micrinite may have generated hydrocarbons during coalification which resulted in variations in absorption, and subsequently, reflectance of the telocollinite.

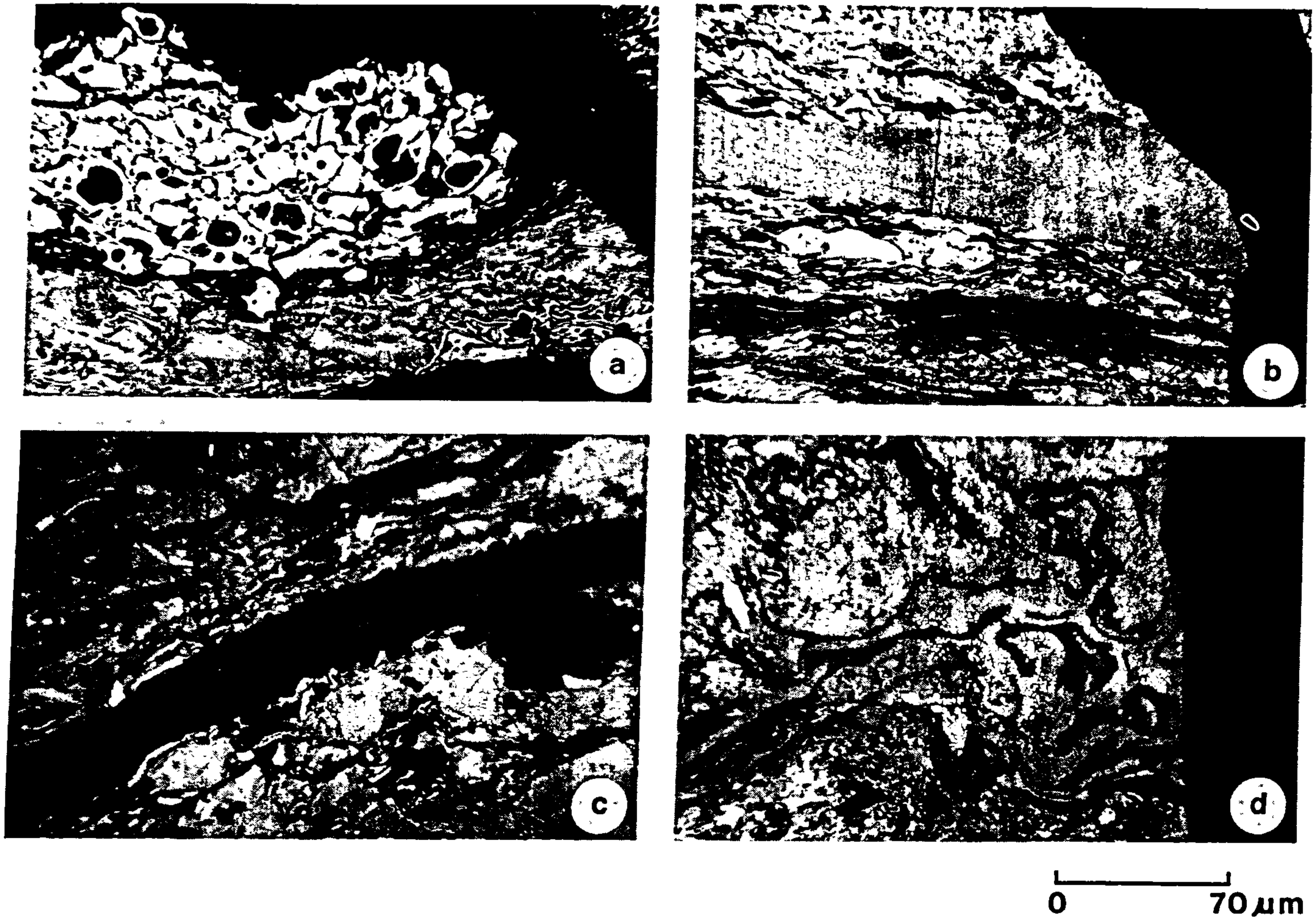

Fig. 10. Photomicrographs showing inertinite macerals and inertinite-rich microlithotypes: (a) ?resino-inertinites from seed fern; (b) micrinite bands in micrinite-rich durite; (c) durite with highly sculptured megaspore and microspores; (d) micrinite and vitrinite intermixed, possibly derived by mixing of humic gels and bituminite at a hydrogen sulphide/oxygen interface. Polished sections viewed in white light under oil immersion.

Inertinites

Without exception, inertinite macerals are the principal components of the Mattson coal samples examined, durites (I), clarodurites and inertite being the dominant microlithotypes. The dominant macerals are semifusinite, micrinite and semimacrinite.

The semifusinites occur in thick bands of inertite (Fig. 9b) as well as with other macerals in bimacerites and trimacerites. The semifusinite rarely shows the open pore structures associated with well-preserved, lignified tissue. Typically, it is highly gelified, exhibiting micropores < 1 μm in diameter or occluded pores. This suggests that the peat either underwent extensive oxidative (bacterial) gelification or oxidation under subaerial conditions during peatification. Much of the semifusinite shows a morphological transition to semimacrinite.

Macrinite is commonly associated with the more abundant semimacrinites. Large concentrations of these macerals occur in inertite and form a groundmass in durites. Such macrinites are typical of South African (Gondwana) coals (Stach, 1968) and the non-marine coals from the Pictou Coalfield in Nova Scotia (i.e. "massive micrinite" of Hacquebard and Donaldson, 1969) which Haquebard and Donaldson interpreted as having formed subaquatically. Teichmüller (1982a) found large concentrations of macrinite as an amorphous groundmass in sub-aquatically accumulated brown coals. Moore (1968) also noted a close association between durites and the colloidal, ulmic groundmass of sapropelic coals. Pyrite (or oxidation products thereof) is locally abundant and intimately mixed with semimacrinite and also inertite composed entirely of individual macrinite bodies giving the durite a distinctly clastic or detrital appearance (Fig. 9c). In sample 74309, the "clastic macrinite" is commonly intermixed with inertodetrinite. Taylor et al. (1989) found similar material in durites in Permian coals from Australia. This suggests that the macrinites accumulated subaquatically, settling out of suspension into a reducing environment. The localized abundances of pyrite infer ample sources of sulphate, perhaps introduced by short-lived, periodic influxes of marine waters. The distribution of pyrite, i.e. impregnation of porosity in fusinite and semifusinite, suggests it may have been emplaced originally as gypsum since it would appear that the original material was introduced from circulating fluids.

There is significant variation in the morphology of components counted as macrinite for want of better definition. Some of the macrinites and semimacrinites resemble the corpohuminites and phlobaphenites of low rank coals (Fig. 9b). Others are solid or have fine vesicles and resemble the sections of resin rodlets, derived from the seed fern *Medullosa,* which has been described in the Pennsylvanian Pomeroy coal of West Virginia (Lyons et al., 1982) and the resino-inertinites of Permian Gondwana coals (Misra et al., 1990). Typ-

ically they are isotropic and vary in shape from rounded to subcircular to oval and sub-triangular bodies, having semifusinitic to fusinitic reflectance. Some are solid (type I of Misra et al., 1990), others are variously vesicular (type II of Misra et al., 1990) and may occur singularly in durite or in clusters of mixed varieties and shapes. Unlike the resin rodlets or resino-inertinites found in Gondwana coals, they do not exhibit fractures and they are found, albeit rarely, in large clusters as cortical material enclosed by vitrinitic material (Fig. 9d). It is suggested that the solid forms were derived from phlobaphenitic materials or tannins formed by early condensation of humic materials derived from aquatic plants. Such colloidal humic substances may have penetrated down through the peat and infilled empty vessels of root structures such as Cohen (1968) observed in mangrove peats from southern Florida. Other "macrinites" bear some similarities to sclerotinites (Stach et al., 1982). However, it is unlikely that, in this case, they are derived from fungal hyphae because of the inconsistent structure, arrangement and affinities with other macerals. Many have large internal cavities with discrete wall structures resembling cenospheres but they are isotropic (rare anisotropic cenospheres are present). Others have irregular vesiculation (Fig. 10a). The latter varieties may have been the product of combustion generated by wildfires (Scott, 1992) in areas marginal to the mires in which the coals at Jackfish Gap and Clausen Creek were deposited.

The other major inertinite component is micrinite. Micrinite accounts for as much as 25% of some of the samples. It occurs in high concentrations, as inertite (micrite) (Fig. 10b) and forms the bulk of the groundmass of the durite and clarodurite (Fig. 10c). It is also commonly intimately associated with vitrinites as lenses and inclusions in vitrinertite (Fig. 10d). It is associated with liptinites and desmocollinite in clarite and clarodurite, with the low-reflectance, weakly fluorescing telocollinite (type I) and with non-fluorescing telocollinite (type II) having intermediate reflectance. In the non-humic coal, the vitrinite and micrinite are "swirled" together implying that they formed by mixing of organic slurries or gels, perhaps representing the results of degradation at a redox interface. The observed relationship between vitrinite and micrinite and the occurrence of micrinite in high concentration (micrite) is strong evidence of a primary or early diagenetic origin for the micrinite in the Mattson coals.

Associated sediments

The coal clasts in the middle Mattson (C58764) have compositions and optical properties identical to the coals in the section. However, the upper Mattson sample (GSC locality C-58838, 1,006.5 m above the base of the Mattson at Jackfish Gap), incorporates thin humic coal laminae composed of clarite, interbedded with algal laminite. The proximate analysis (Table 2)

of this sample shows relatively high ash content (44%) and the volatile matter (45% d.a.f.) is significantly higher than the pure coals, the carbon content is significantly lower (72% elemental; 55% fixed carbon d.a.f.) and the oxygen content significantly higher than in the coals (23.4% versus 14% elemental oxygen). The high volatile matter content may be attributed to a higher hydrocarbon yield from the alginite.

The clarite is dominated by desmocollinite and telocollinite with fusinite, sporinites and rare bituminite. The coaly laminae are vitrinite-rich (79%) and have relatively small amounts of inertinite (13%) and sporinite (8%). The desmocollinite and thin telocollinite bands fluoresce quite strongly suggesting they are perhydrous despite a relatively low hydrogen content (3%). The microspores are similar to those observed in the coals, also showing signs of oxidation probably related to wind or subaerial transport. The reflectance of the telocollinite is 0.68% R_om (Table 4).

The kerogen in the shale laminae is predominantly composed of amorphous matter (bituminous matrix) which fluoresces light yellow to brown under blue light, fluorescing bituminite I (Teichmüller and Ottenjahn, 1977) and alginites (lamalginite and telalginite). In some of the shales in the sequence, colonial alginites of freshwater origin (*Botryococcus* or *Rheischia*-type) and marine (*Tasmanales*-type, ?*Nostocopsis*) occur together indicating a mixing of fresh and marine waters. The reflectance of the vitrinite in the shale is 0.60% R_om. (Numerous other coaly shales occur in the Mattson section which are essentially algal laminites interbedded with humic coal. In these intervals, the vitrinitic bands in the shaley interbeds have higher reflectance than that of the associated coals, and is interpreted as gelocollinite).

Pyrolytic carbon

Pyrolytic carbon occurs in the coals from the middle member of the Mattson Formation. Typically, it is anisotropic and has the appearance of cenospheres produced by hydroliquefaction (Mitchell et al., 1977) or combustion of coal (International Committee for Coal Petrology, 1987). Goodarzi (1985) observed naturally occurring pyrolytic carbon in subbituminous coal and Goodarzi and Gentzis (1990) observed pyrolytic carbon in heat-affected coals from western Canada and concluded it was formed by thermal cracking of volatile matter generated by the burning of carbonaceous matter during forest or peat fires. This suggests that pyrolytic char fragments in the Mattson coals came from fires in nearby peats or forests and were probably blown into the peats during subaerial exposure, early in diagenesis. It is unlikely that the coal-forming peat in the immediate area burned due to the lack of isotropic or anisotropic chars although it is possible that the extensive vesiculation in some of the macrinites (?resino-inertinites) could have resulted from devolatilization due to heating from fires. Furthermore, Scott (1992) has indicated that

large proportions of semifusinites are created as a result of the burning of recent peats.

DISCUSSION

The Mattson coals are dominated by durites and inertites. Spore-rich durites are typical of subaquatic ooze deposits (Hacquebard, 1964) and Smith (1964) regards spore-rich crassidurites containing *Densosporites* as forming in ombrogenous bogs from a Lepidodendrales flora. Furthermore, numerous workers have found micrinite to be a common constituent of durites of sapropelic facies and cannel coals (Teichmüller, 1950; Stach, 1968; Hook and Hower, 1988). Hook and Hower (1988) found 95% of the groundmass of the Linton cannel coal from Ohio to consist of micrinite and very little inherent mineral matter. Such features are very typical of the coals in the middle member of the Mattson Formation in the Liard Basin. Microlayering, which was also observed, was observed by Hacquebard and Donaldson (1969) in hypautochthonous coals in the Pictou Coal Basin of Nova Scotia, and by Goodarzi and Gentzis (1991) in cannel and canneloid shales from the Middle to Upper Devonian of Arctic Canada, which they reported to be "an unusual feature of cannel coals, probably due to deposition in open water in a relatively calm environment". In the Mattson coals, the occurrence of "clastic macrinite" would seem to support this. Despite the low amounts of vitrinite, vitrite bands composed of telocollinite, interbedded with duroclarite and clarite suggest that a transition from sapropelic to more humic peat occurred at some time during its accumulation.

Hook and Hower (1988) also report a very large variety of sporinites (megaspores, microspores, sporangia) which is also typical of the coals of the Mattson Formation. However, many microspores and, without exception, the megaspores are oxidised, suggesting that they may have been aerially transported, prior to deposition in water; they may not therefore be representative of the actual peat-forming flora.

The bulk of the inertinite (macrinite and semimacrinite) is probably derived by oxidative decay of aquatic plants with some contribution from seed ferns. These may have been washed in from areas with better water circulation to form the "inertoclastic" groundmass of the durites very early in diagenesis, or, as Teichmüller (1982a) suggests, the coal may have formed from a dy-gyttjae, i.e. subaquatically, at the oxygen/hydrogen sulphide interface. Under these conditions, tannins or phlobaphinite could have formed from aquatic vegetation, giving rise to macrinite and semimacrinite, while at the same time, humic materials forming under anaerobic conditions would generate bituminite from protein and fats (Teichmüller, 1982a), particularly from bacterial remains. If the micrinite is derived from bacterial remains then this would account not only for the lack of vitrinite in the Mattson coals due to

intense biochemical activity, but also for the intimate association of perhydrous vitrinite and micrinite, the abundance of macrinite and semimacrinite and the mutual occurrence of anaerobically formed components and oxygen-rich macerals. The lack of lignin in aquatic plants would certainly be conducive to rapid breakdown of the cellulose concentrating tannins and phlobaphinitic materials. The occurrence of fluorescing, perhydrous vitrinites is consistent with extensive microbial activity and anaerobic decay of lipid-rich organic matter in the associated sediments (Goodarzi et al., 1993).

The origin of micrinite has been debated on numerous occasions. Spackman and Barghoorn (1966), and Cohen and Spackman (1980) proposed a primary origin for micrinite (cell walls). Stach (1968) proposed a secondary origin for micrinite on the basis of its association with sporinites in coals from the Ruhr region of Germany, inferring that sporinite is a product of the coalification of liptinitic protoplasm. Teichmüller (1944, 1982b) also considers micrinite to be a secondary maceral, arising through coalification/maturation of liptinites during the bituminous coal stage, particularly in sapropelic to semisapropelic facies. Teichmüller and Wolf (1977) linked micrinite formation to maturation of sporinite and formation of petroleum and Teichmüller and Ottenjahn (1977) proposed that micrinite formed by bituminitization of bituminite, a product of biochemical alteration of alginite. Taylor and Liu (1989) have conducted a very thorough review of the theories on the origin of micrinite and conclude, as a result of Transmission Electron Microscope studies of micrinite, that most micrinite comprises finely particulate matter formed during diagenesis of lipid-rich organic matter.

In the Mattson coals, there is an abundance of sporinite, the coal rank is bituminous rank, oxidation has evidently occurred during early diagenesis and subaquatic facies and sapropelic origins have been established. In other words, any of the proposed origins for micrinite could be applicable in this case. However, the micrinite in the Mattson coals is not necessarily associated with the structured liptinites (sporinites, alginites). Furthermore, the author(s) have previously observed micrinite in low rank coals (lignites) almost devoid of sporinite, but in which bituminite was a common constituent. Teichmüller (1950) also considered bituminite to be a precursor of micrinite. Shibaoka (1983) has also observed micrinite in brown coals from Australia and considers it to be a product of the oxidation of porigelinite.

It is suggested that the micrinite found in the Mattson, and other sapropelic coals, is formed by either coalification or oxidation of bituminite, a prominent component of the groundmass originally formed under anaerobic conditions, either from humic degradation products or from the bacterial protein which would be abundant under relatively alkaline conditions. Such a mode of formation would account for the high hydrogen content and reactivity that characterizes micrinite and sets it apart from all other inertinite macerals, and the perhydrous nature of the vitrinite associated with it.

Much of the micrinite in the Mattson coals may be a secondary product of changing redox conditions early in diagenesis. Elevation from the reducing zone to slightly more oxygenated waters during sea level regressions, i.e. above the hydrogen sulphide–oxygen interface, may have transformed the bituminite to micrinite, or it may be a product of coalification (?or even burning) of bituminite. Unlike other liptinites, which have a primary origin, bituminite is a product of anaerobic degradation of organic matter formed at low temperatures and pressures which makes it more susceptible to thermal alteration earlier in the coalification process (Tissot and Welte, 1982).

The abundance of semifusinite, the occurrence of more humic coal and the presence of sclerotinite and pyrolytic carbon in the Mattson coals attest to eventual infilling of the mire, and the subsequent drying and subaerial oxidation of the peats under dry, climatic conditions prior to burial with inclusions of air-borne products from fires, also normally associated with dry conditions. Furthermore, the abundance and predominance of sporinites, which are almost entirely oxidised, suggests that the spores were transported subaerially, by wind. Indeed, in the middle member of the Mattson Formation, sandstones occur which are considered to have an aeolian origin. The changes in the water table and palaeogeography were probably a minor consequence of the repeated emergence and submergence responsible for cyclic delta formation during Mattson time (Richards, 1989). (It may have been during these cycles that the bituminite was altered to micrinite.)

The lithology and sedimentary structures in the Mattson Formation and the petrology of the coals contained within the middle and upper members of the Mattson indicate deposition in a deltaic setting. It is suggested that the peats, from which the middle Mattson coals formed, accumulated in ponds or lakes in the upper delta plain (Fig. 11). Here, inertinite and exinite-rich durites and sapropelic coals formed from aquatic vegetation and wind- or water-transported spores. Early peat accumulations were marked by gyttjae formation under anaerobic bottom conditions and at the interface between oxic and anoxic waters where humic colloids accumulated from subaquatic plants. Emergence and lowering of the water table resulted in periodic subaerial exposure and severe oxidation. Since all the coals in the middle and upper Mattson are of a similar nature, it would appear that water level changes occurred numerous times: this scenario fits with the progradational–aggradational depositional setting for the Mattson Formation postulated by Richards (1989) and Richards et al. (1989) which can be related to minor oscillations in global sea level during the Carboniferous (Ramsbottom, 1973). While subaerial exposure and oxidation of the peats may therefore have been the result of decreases in sea level during Mattson time, the rare occurrence of unicellular marine algal cysts (*Tasmanites*) and concentrations of pyrite (possibly sourced by gypsum) also suggest subsequent incursions of sulphate-rich, marine water implying frequent oscillations in sea level.

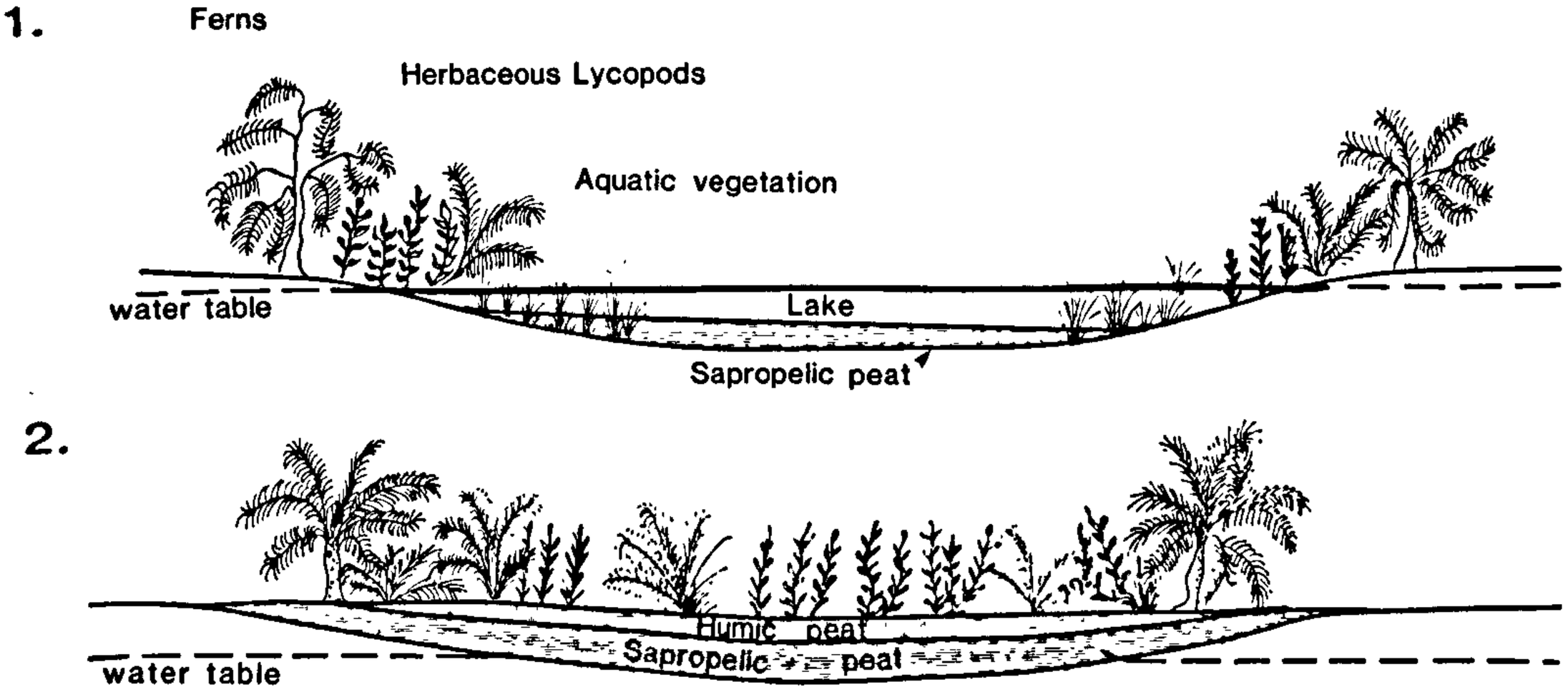

DEPOSITIONAL SETTING OF MATTSON COALS

1. accumulation of sapropelic peat under anaerobic conditions on the lake bottom:

2. accumulation of humic peat as lake infills and water table is lowered due to uplift

Fig. 11. Depositional setting envisioned for the Mattson coals. Stage 1: accumulation of sapropelic peat under anaerobic conditions on the lake bottom. Stage 2: accumulation of humic peat as the lake infills and the water table is lowered.

Coals in the upper member of the Mattson at Jackfish Gap occur above a series of shallow, neritic and shoreline carbonates and sandstones. They are interbedded with algal laminites having mixed, freshwater and marine affinities suggesting that they are probably of lagoonal origin. Evans (1975) reports on the occurrence of the Santo Thomas cannel coals in Texas having a lagoonal origin set in wave-dominated deltas associated with fluvial systems.

CONCLUSIONS

The coals of the Mattson Formation are predominantly sapropelic in origin, forming from aquatic plants, herbaceous lycopods and pteridosperm floras. Significant proportions of macrinite and semimacrinite (?resino-inertinites) are predominantly due to a significant contribution to the coal-forming flora from aquatic plants. Micrinite, a common constituent of these coals, is thought to have formed by oxidation of bituminite which, in turn, formed either by anaerobic decay of the humic groundmass or from bacterial remains. Furthermore the intimate relationship between micrinite and vitrinite suggests that the peat was in a semi-liquid condition consistent with gyttjae-

formation. Sporinites are derived from wind-borne mega- and micro-spores and the presence of pyrolytic carbon suggests that peat fires occurred in the surrounding area; these factors suggest that relatively arid conditions prevailed in the northern part of the Liard Basin during Mattson time. In addition, the high inertinite contents suggest that the coals were probably subjected to long periods of subaerial exposure and oxidation, under dry climatic conditions, prior to burial, possibly as a result of periodic emergence.

While the overall depositional setting of the Mattson Formation is deltaic, the coals/peats in the middle Mattson appear to have accumulated anaerobically in shallow lakes in the middle to upper delta plain. Coals in the upper member are partly algal laminites which accumulated in a lagoonal setting.

REFERENCES

Bamber, E.W., Macqueen, R.W. and Richards, B.C., 1984. Facies relationships at the Mississippian carbonate platform margin, western Canada. In: E.S. Belt and R.W. Macqueen (Editors), Part 3, Sedimentology and Geochemistry, Neuvième Congrès International de Stratigraphie et de Géologie du Carbonifère, 1979, Compt. Rend., 3: 461–47.

Barker, C.E., 1991. An update on the suppression of vitrinite reflectance. Soc. Org. Petrol. Newsl., (Dec.) 8 (4): 8–11.

Braman, D.R. and Hills, L.V., 1977. Palynology and paleontology of the Mattson Formation, Northwest Canada. Bull. Can. Pet. Geol., 25 (3): 582–630.

Cameron, A.R. and Pratt, K., 1982. Report on rank and maceral composition of coals in the Mattson Formation, Mackenzie District, N.W.T. Geol Surv. Can., internal report.

Cohen, A.D., 1968. The petrology of some peats of southern Florida (with special reference to coal). Ph.D. Thesis, Pennsylvania State Univ., 352 pp.

Cohen, A.D. and Spackman, W., 1980. Phytogenic organic sediments and sedimentary environments in the Everglades mangrove complex os Florida, Part III. The alteration of plant material in peats and the origin of coal macerals. Palaeontographica, Abt. B, 162: 125–149.

Douglas, R.J.W. and Norris, D.K., 1959. Fort Liard and La Biche map-areas, Northwest Territories. Geol. Surv. Can. Pap., 59-6.

Douglas, R.J.W. and Norris, D.K., 1960. Virginia Falls and Sibbeston Lake map-areas, Northwest Territories, 95F and 95G. Geol. Surv. Can. Pap., 60-19.

Dybova-Jachowicz, S., Jachowicz, A., Karczewska, J., Lachkar, G., Loboziak, S., Pierart, P., Turnau, E. and Zoldani, Z., 1987. Revision of Carboniferous Megaspores with Gula (Part Three). Prace Instytutu Geologicznego CXXXI, Wydawnictwa Geologiczne, Warsaw.

Evans, T.J., 1975. Cannel coal and stratigraphic setting. In: Uranium, Coal and Gas, Triple Energy Field Trip Guide Book, Duval, Webb and Zapata Counties, Texas. Corpus Christi Geological Society.

Goodarzi, F., 1985. Optically anisotropic fragments in a western Canadian subbituminous coal. Fuel, 64: 1294–1300.

Goodarzi, F. and Gentzis, T., 1990. The lateral and vertical reflectance and petrological variation of a heat-affected bituminous coal seam from southeastern British Columbia, Canada. Int. J. Coal Geol., 15: 317–339.

Goodarzi, F. and Gentzis, T. 1991. Petrology, depositional environment and utilization potential of Devonian cannel coals from Melville Island, Arctic Canada. Bull. Soc. Géol. Fr., 162: 239–253.

Goodarzi, F. and Goodbody, Q., 1990. Nature and depositional environment of Devonian coals from Melville Island, Arctic Canada. Int. J. Coal Geol., 14: 175–196.

Goodarzi, F. Nassichuk, W.W., Snowdon, L.R. and Davies, G.R., 1987. Organic petrology and Rock-Eval analyses of the Carboniferous Emma Fjiord Formation in the Sverdrup Basin, Canadian Arctic Archipelago. Mar. Pet. Geol., 4: 132–145.

Goodarzi, F., Snowdon, L.R. and Pearson, D., 1993. Petrological and chemical characteristics of liptinite-rich coals from Alberta. Mar. Pet. Geol., in press.

Habib, D., Riegel, W. and Spackman, W., 1966. Relationship of spore and pollen assemblages in the Lower Kittaning Coal to overlying faunal facies, J. Paleontol., 40: 756–759.

Hacquebard, P.A., 1964. Die Ablagerungsbedingungen des Flözes Harbour im Sydney-Kohlengebiet von Neuschottland (Kanada). Fortschr. Geol. Rheinl. Westfalen, 12: 331–356.

Hacquebard, P.A. and Barss, M.S., 1957. A Carboniferous spore assemblage, in coal from the South Nahanni River Area, Northwest Territories. Geol. Surv. Can. Bull., 40: 1–63.

Hacquebard, P.A. and Donaldson, J.R., 1969. Carboniferous coal deposition associated with flood-plain and limnic environments in Nova Scotia. In: E.C. Dapples and M.E. Hopkins (Editors), Environments of Coal Deposition. Geol. Soc. Am., Spec. Pap., 114: 143–191.

Harker, P., 1961. Summary of Carboniferous and Permian formations, southwestern District of Mackenzie. Geol. Surv. Can. Pap., 61-1, 9 p.

Hook, R.W. and Hower, J.C., 1988. Petrography and taphonomic significance of the vertebrate-bearing cannel coal of Linton, Ohio (Westphalian D, Upper Carboniferous). J. Sediment. Petrol., 58 (1): 72–80.

International Committee for Coal Petrology, 1987. Minutes of the ICCP Commission III meeting in Beijing, China, September 1977. Proc. ICCP—Combustion Group, App. 3.1.

Kalkreuth , W.D. and Macauley, G., 1987. Organic petrology and geochemical studies on oil shales and coals from the Pictou and Antigonish areas, Nova Scotia. Bull. Can. Pet. Geol., 35: 263–295.

Lyons, P.C., Finkelman, R.B., Thompson, C.L., Brown, F.W. and Hatcher, P.G., 1982. Properties, origin and nomenclature of rodlets of the inertinite maceral group in coals of the Central Appalachian Basin, U.S.A. Int. J. Coal Geol., 1 (4): 313–346.

Misra, B.K., Singh, B.D. and Navale, G.K.B., 1990. Resino-inertinites of Indian Permian coals—their origin, genesis and classification. Int. J. Coal Geol., 14 (4): 277–293.

Mitchell, G., Davis, A. and Spackman, W., 1977. A classification of residues from the hydrogenation of bituminous coals. In: R.T. Ellington (Editor), Liquid Fuels from Coal. Academic Press, New York, pp. 255–270.

Moore, L.R., 1968. Cannels, bogheads and oil shales. In: D.G. Murchison and T.S. Westoll (Editors) Coal and Coal-Bearing Strata. Oliver and Boyd, Edinburgh, pp. 19–29.

Patton, W.J.H., 1958. Mississippian Succession in South Nahanni River area, Northwest Territories. In: A.J. Goodman (Editor), Jurassic and Carboniferous of Western Canada. Am. Assoc. Pet. Geol., Allan Memorial Vol., pp. 309–326.

Ramsbottom, W.H.C., 1973. Transgressions and regressions in the Dinantian: a new synthesis of British Devonian stratigraphy. Proc. Yorks. Geol. Soc., 39: 567–607.

Richards, B.C., 1983. Uppermost Devonian and Lower Carboniferous stratigraphy, sedimentation and diagenesis, southwestern District of Mackenzie and southeastern Yukon Territory. unpubl. Ph.D. Thesis, Univ. of Kansas, 373 pp.

Richards, B.C., 1989. Uppermost Devonian and Lower Carboniferous stratigraphy, sedimentation, and diagenesis, southwestern District of Mackenzie and southeastern Yukon Territory. Geol. Surv. Can. Bull., 390, 135 pp.

Richards, B.C., Bamber, E.W., Higgins, A.C. and Utting, J., 1989. Carboniferous. In: D.F. Stott and J.D. Aitken (Editors), Sedimentary Cover of the North American Craton: Canada. Geol. Surv. Can. Spec. Publ. (Vol. D-1, Decade of North American Geology Series).

Robert, P., 1988. Organic Metamorphism and Geothermal History. Reidel, Dortrecht, 311 pp.

Scott, A.C., 1992. The influence of fire in Carboniferous Ecosystems. Proceedings of a symposium on the Euramerican Coal Province, Geol. Soc. Can. Annu. Meet. (Wolfville, N.S., May 25th–26th), 1992.
Shibaoka, M., 1983. Genesis of micrinite in some Australian coals. Fuel, 62: 639–644.
Smith, A.H.V., 1964. Zur Petrologie und Palynologie der Kohlenflöze des Karbons und ihrer Begleitschichten. Fortschr. Geol. Rheinl. Westfalen, 12: 285–302.
Smith, G.G., 1989. Coal resources of Canada. Geol. Surv. Can. Pap., 84-4, 146 pp.
Spackman, W. and Barghoorn, E.S., 1966. Coalification of woody tissue as deduced from a petrographic study of Brandon Lignite. Coal Sci., Adv. Chem. Ser., 55: 695–705.
Stach, E., 1968. Basic principles of coal petrology: macerals, microlithotypes and some effects of coalification. In: D.G. Murchison and T.S. Westoll (Editors), Coal and Coal-Bearing Strata. Oliver and Boyd, Edinburgh, pp. 3–17.
Stach, E., Mackowsky, M.-Th., Teichmüller, M., Taylor, G.H., Chandra, D. and Teichmüller, R., 1982. Stach's Textbook of Coal Petrology. Borntraeger, Berlin.
Sullivan, H., 1965. Palynological evidence concerning the regional differentiation of Upper Mississippian floras. Pollen Spores, 7: 539–563.
Taylor, G.H. and Liu, S.Y., 1989. Micrinite—its nature, origin and significance. Int. J. Coal Geol., 14: 29–46.
Taylor, G.H., Liu, S.Y. and Diessel, C.F.K., 1989. The cold-climate origin of inertinite-rich Gondwana coals. Int. J. Coal Geol., 11: 1–22.
Teichmüller, M., 1944. Zur Petrographie zweier oberschlesischer Flöze mit ähnlichem Inkohlunsgrad, aber verschiedenen Kokungseigenschaften. Z. Prakt. Geol., 52: 1–6.
Teichmüller, M., 1950. Zum petrographischen Aufbau und Werdegang der Weichbraunkohle (mit Berücksichtigung genetischer Fragen der Steinkohlenpetrographie). Geol. Jahrb., 64: 429–488.
Teichmüller, M., 1982a. Origin of the petrographic constituents of coal. In: E. Stach, M.-Th. Mackowsky, M. Teichmüller, G.H.Taylor, D. Chandra and R. Teichmüller, Stach's Textbook of Coal Petrology. Borntraeger, Berlin, pp. 219–294.
Teichmüller, M., 1982b. Fluorescence-microscopical changes of liptinites and vitrinites during coalification and their relationship to bitumen generation and coking behaviour. Geol Surv. Nordrhein-Westfalen, Krefeld, 1982.
Teichmüller, M. and Ottenjahn, K., 1977. Liptinite und Lipoide Stoffe in einem Erdölmuttergestein. Erdöl Kohle, 30: 387–389.
Teichmüller, M. and Wolf, M., 1977. Application of fluorescence microscopy in coal petrology and oil exploration. J. Microsc., 109: 47–73.
Tissot, B. and Welte, D., 1982. Petroleum Formation and Occurrence: A New Approach to Petroleum Exploration. Elsevier, Amsterdam, 538 pp.
Utting, J., 1987. Palynology of the Lower Carboniferous Winsor Group and Winsor–Cansco Boundary Beds of Nova Scotia, New Brunswick and Newfoundland. Geol. Surv. Can. Bull., 374.
Von Hamberger, K. and Grudzien, G., 1967. Sapropelites of the Upper Silesian Coal Basin. Freib. Forschungsh., C, 242: 57–62.

Reprinted from

PALAEO
GEOGRAPHY
CLIMATOLOGY
ECOLOGY

Palaeogeography, Palaeoclimatology, Palaeoecology, 106 (1994): 135–155
Elsevier Science B.V., Amsterdam

Coal and oil shale of Early Carboniferous age in northern Canada: significance for paleoenvironmental and paleoclimatic interpretations

A.R. Cameron[a], F. Goodarzi[a] and J. Potter[b]

[a]*Geological Survey of Canada, 3303 33 St. N.W., Calgary, Alta. T2L 2A7, Canada*
[b]*Newcastle Research Group in Fossil Fuels and Environmental Geochemistry, University of Newcastle, Newcastle-upon-Tyne, NE1 7RU, UK*

(Received November 23, 1992; revised and accepted March 10, 1993)

ELSEVIER

PALAEO GEOGRAPHY CLIMATOLOGY ECOLOGY

Scope of the journal

Palaeogeography, Palaeoclimatology, Palaeoecology is an international medium for the publication of original studies and comprehensive reviews in the field of palaeo-environmental geology. It is hoped that the journal will contribute to the sound development of this field by bringing together under one cover interesting results in many disciplines involved in palaeo-environment investigations.

General information

Subscription information

Palaeogeography, Palaeoclimatology, Palaeoecology (ISSN 0031–0182). For 1994 volumes six are scheduled for publication. A combined subscription to *Palaeogeography, Palaeoclimatology, Palaeoecology* and *Global and Planetary Change* (Vols. 9–10) at reduced rate is available. Subscription prices are available upon request from the publisher. Subscriptions are accepted on a prepaid basis only and are entered on a calendar year basis. Issues are sent by surface mail except to the following countries where air delivery via SAL is ensured: Argentina, Australia, Brazil, Canada, Hong Kong, India, Israel, Japan, Malaysia, Mexico, New Zealand, Pakistan, PR China, Singapore, South Africa, South Korea, Taiwan, Thailand, USA. For all other countries airmail rates are available upon request. Claims for missing issues must be made within six months of our publication (mailing) date. Please address all your requests regarding orders and subscription queries to: Elsevier Science B.V., Journal Department, P.O. Box 211, 1000 AE Amsterdam, The Netherlands. Tel.: 31-20-5803642, fax: 31-20-5803598.

US mailing notice — *Palaeogeography, Palaeoclimatology, Palaeoecology* (ISSN 0031-0182) is published monthly by Elsevier Science Publishers (Molenwerf 1, Postbus 211, 1000 AE Amsterdam). Annual subscription price in the USA US$ 1186.00 (US$ price valid in North, Central and South America only), including air speed delivery. Second class postage paid at Jamaica, NY 11431.
USA POSTMASTERS: Send address changes to *Palaeogeography, Palaeoclimatology, Palaeoecology* Publications Expediting, Inc., 200 Meacham Avenue, Elmont, NY 11003.
Airfreight and mailing in the USA by Publication Expediting.

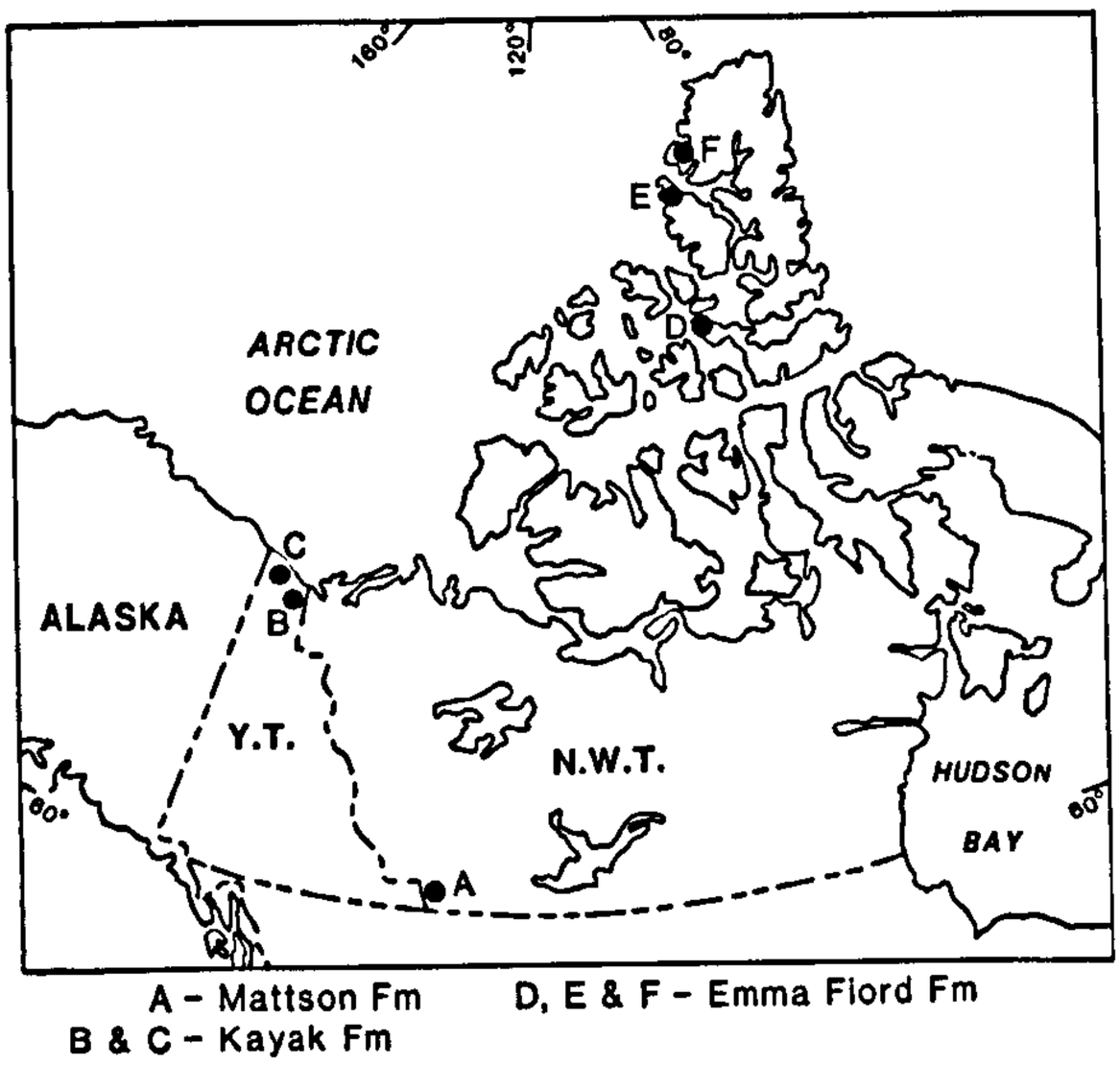

Fig. 1. Location map for coal and oil shale deposits of Early Carboniferous age in northern Canada.

The third Lower Carboniferous unit in northern Canada containing coal, but more importantly thick beds of oil shale, is the Emma Fiord Formation exposed on Devon, Axel Heiberg and Ellesmere Islands (Fig. 1, Sites D, E and F, respectively). The Emma Fiord Formation was first described by Thorsteinsson (1974). More detailed sedimentological and compositional characteristics have been reported on by Goodarzi et al. (1987) and Davies and Nassichuk (1988).

Compositional characteristics of these northern Canadian coals and oil shales will be discussed with reference to paleoenvironmental and paleogeographic interpretations. In the second part of the paper the relationship of these Canadian deposits to Lower Carboniferous coal and oil shale occurrences in other parts of the Northern Hemisphere will be explored.

Geological context of coal-bearing units

The Mattson Formation

The Mattson Formation is composed mainly of cyclical deposits of sandstone combined with lesser amounts of siltstone and shale and minor carbonate. It was deposited in a deltaic-fluvial, marginal marine setting associated with fluctuating sea levels during which several deltaic sequences were formed. During periods of regression progradation was westward into the Prophet Trough. At the end of the Mattson times transgression spread marine strata to the northeast (Richards et al., 1993). The Mattson has a maximum thickness of 1410 m; at the type section (Jackfish Gap) it is 1040 m thick. Coal beds occur at several levels, mainly in the lower and middle parts of the formation. These beds appear to be associated with sedimentary sequences of overbank and delta front genesis and may be sapropelic (Potter et al., 1993).

Hacquebard and Barss (1957) were the first to study the palynology and petrography of the Mattson coals and identified them as Early Carboniferous in age. Later studies by Braman and Hills (1977) and Utting (1991) suggested an age of late Viséan (V3) to Serpukhovian for the Mattson Formation and almost exact correlation with the Hart River Formation in the northern Yukon Territory. Figure 2 is a simplified stratigraphic section showing the relationship of the Mattson Formation to overlying and underlying units.

The Kayak Formation

The Kayak Formation consists of shale and volumetrically subordinate sandstone and carbon-

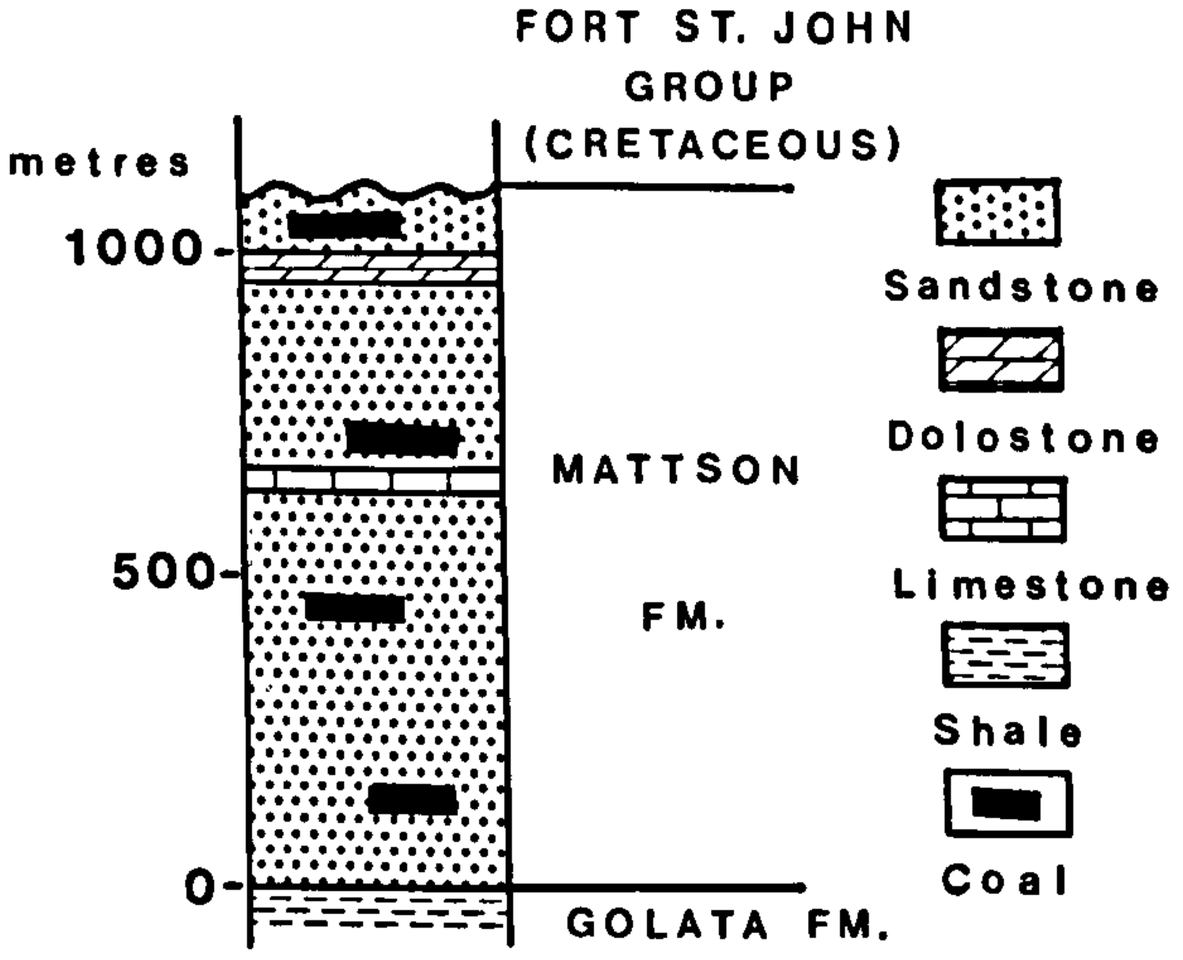

Fig. 2. Summarized stratigraphic column for the Mattson Formation, representative of section near Jackfish Gap, Northwest Territories (modified from Richards, 1989).

ates. It rests gradationally on the conglomerates and sandstones of the Kekiktuk Formation and passes upward into finer-grained clastics and carbonates of shallow marine origin. The latter are indicative of marine transgression to the northeast (Richards et al., in press). These various facies appear to grade laterally and vertically into one another. The coals are associated with the base of the formation and appear to have formed in marginal marine to continental environments. In the British Mountains the Kayak is over 350 m thick. Bamber and Waterhouse (1971) indicated a thickness of 275 m for strata assigned to the Kayak in the Barn Mountains near Hoidahl Dome. The section shown in Fig. 3 is modified from a figure by Richards et al. (1993), and represents the stratigraphic sequence for the Lower Carboniferous in the area of the eastern British Mountains and Barn Range in the northern Yukon Territory (vicinity of Site B, Fig. 1).

Faunal remains in the Kayak suggest an early middle to early late Viséan age (Bamber and Waterhouse, 1971). Palynological observations by Utting (1991) suggests a totally Viséan age for the Kayak, spanning the interval from Vl to early V3. He suggests there is no age overlap with the Mattson which he believes to be younger.

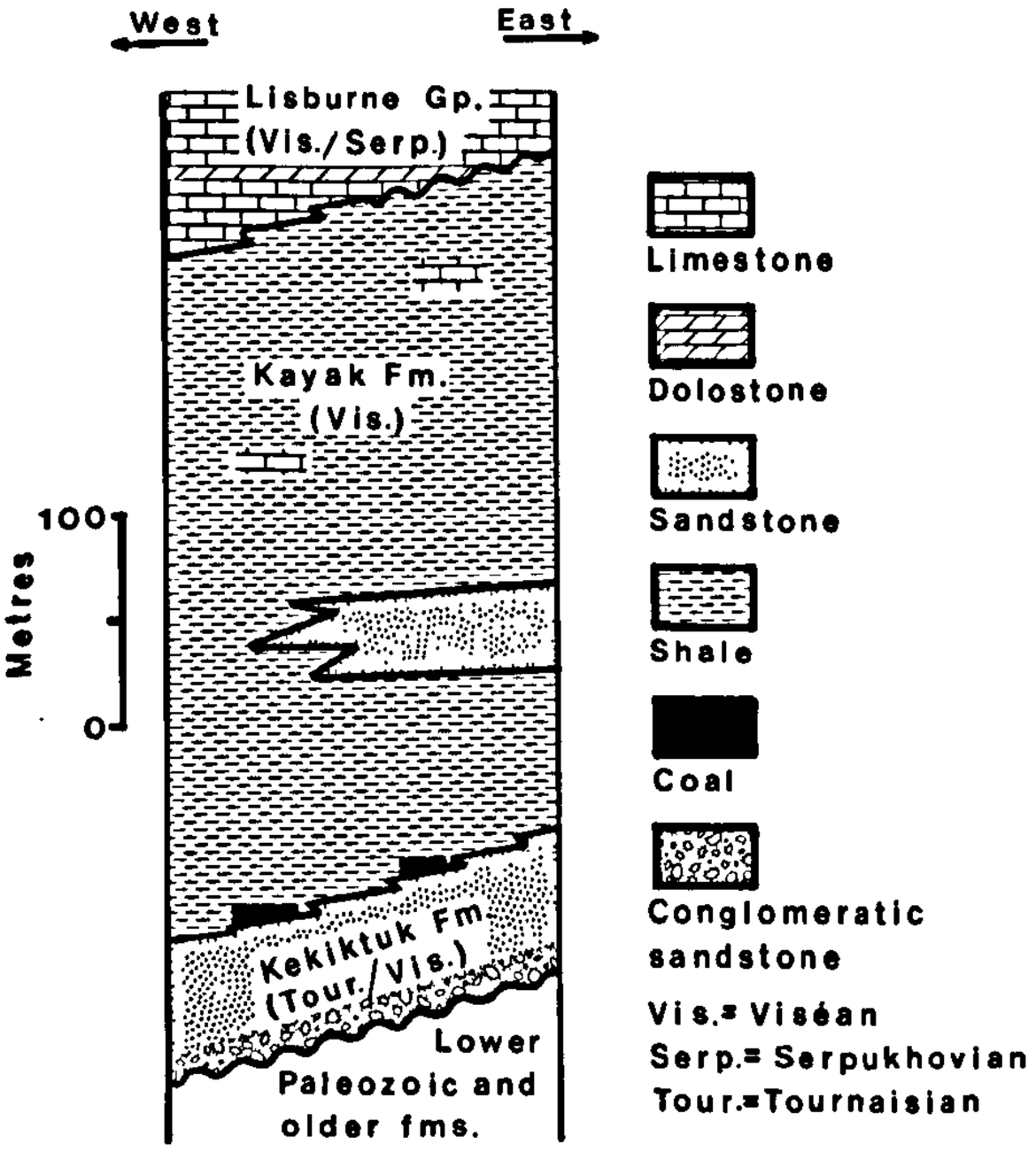

Fig. 3. Stratigraphic section for the Kayak Formation, Hoidahl Dome area, northern Yukon Territory.

The Emma Fiord Formation

The Emma Fiord Formation has been described by Davies and Nassichuk (1988) as consisting of carbonaceous and calcareous shale, siltstone and marlstone with thin coal seams, and minor sandstone, conglomerate and algal limestone. Much of the calcareous shale is sufficiently rich in kerogen of suitable maturity and type to be classed as oil shale. At Grinnell Peninsula (Fig. 1, Site D) on northern Devon Island it is about 135 m thick, whereas on Kleybolte Peninsula (Fig. 1, Site F) on northwestern Ellesmere Island it is nearly 400 m thick (Thorsteinsson, 1974). At location E (Fig. 1), formation thickness has been estimated at 120 m. At each of the three sites thin coal seams (<1 m) have been observed. According to Davies and Nassichuk the Emma Fiord was laid down in a lacustrine environment that may have been thermally and chemically stratified resulting in excellent preservation conditions at the bottom of the basin. Analyses of megaflora and palynomorphs indicate a Viséan age for the Emma Fiord Formation (Playford and Barss, 1963; Thorsteinsson, 1974). Utting (1991) has placed the Emma Fiord entirely in the V3 zone and considers it coeval with part of the Mattson Formation. Figure 4 is a summarized stratigraphic column for the Emma Fiord Formation and adjacent strata on Devon Island.

Sampling history

Sample location data are given in Table 1. All samples were collected from outcrop. The Mattson samples were collected by B.C. Richards of the Geological Survey of Canada (Calgary office). They are channel samples, representative of four seams exposed in two sections (see Table 1). The Kayak Formation coal samples were obtained from four sections in the Hoidahl Dome area and one section in the British Mountains. In addition several samples of carbonaceous shale were col-

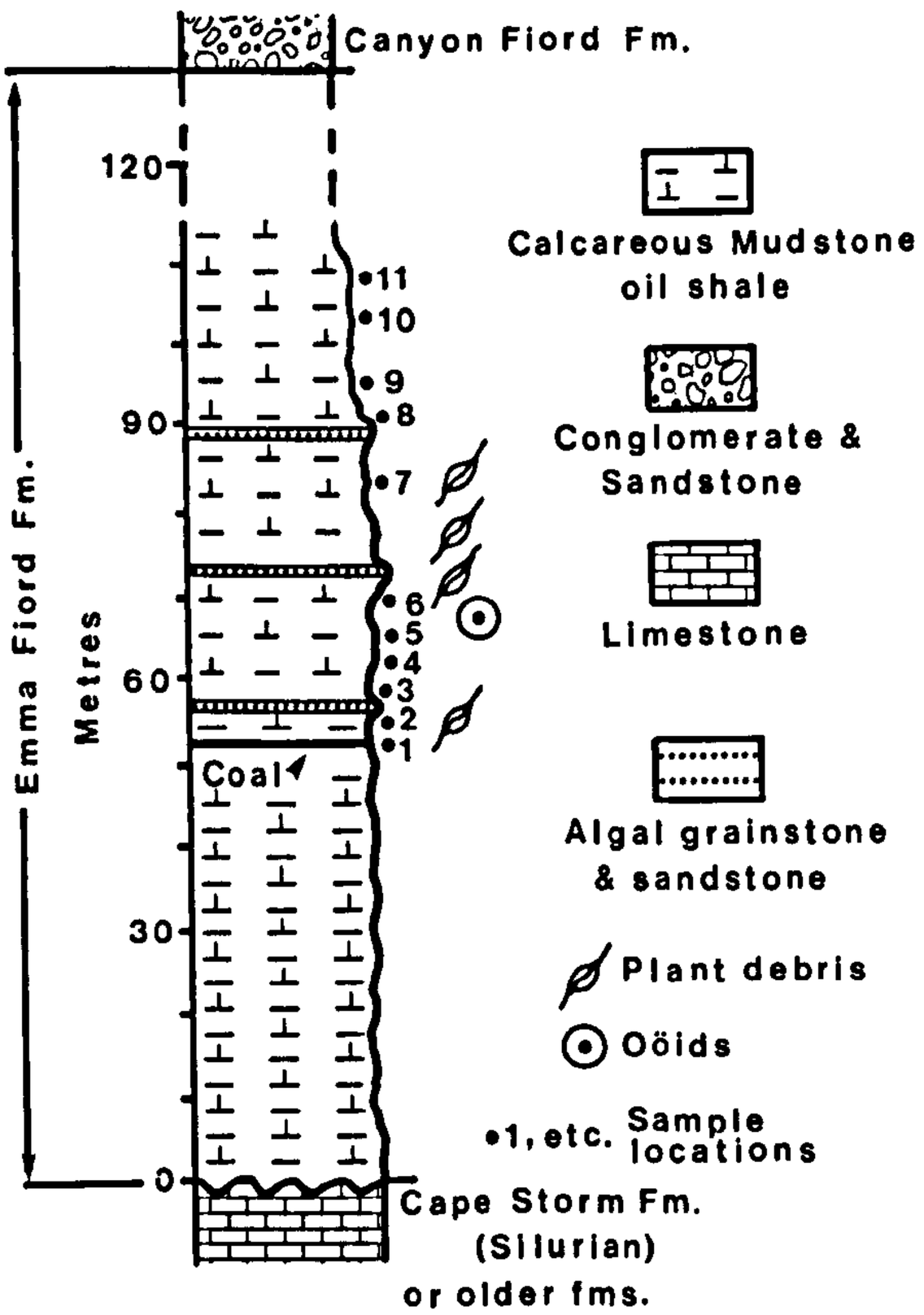

Fig. 4. Summarized stratigraphic section for the Emma Fiord Formation, Grinnell Peninsula, Devon Island, northern Canada (modified from Davies and Nassichuk, 1988).

lected in the British Mountains and analyzed for reflectance values. Most of the Kayak samples were taken at locations first visited by D.K. Norris, now retired from the Geological Survey of Canada. The samples from the Emma Fiord Formation came from two sections. One of these sites is on Grinnell Peninsula on Devon Island (Fig. 1, Site D). From this location ten samples of carbonaceous shale and marlstone and one sample of coal were collected by W.W. Nassichuk, also of GSC, Calgary. These samples cover a stratigraphic interval of about 55 m in the formation. The second set of Emma Fiord samples (also collected by Nassichuk) came from the Kleybolte Peninsula, Ellesmere Island (Fig. 1, Site F). There are six samples in this suite, representing six separate beds, and they occur in a stratigraphic interval of some 250 m in the section.

Sample preparation and analysis procedures

All samples were crushed to minus 20 mesh (840 μm) and a small portion split out for pelletizing and polishing prior to microscopic examination. A second representative split was removed from each sample for chemical analyses. In addition Rock-Eval analyses were carried out on the Emma Fiord samples from Devon Island.

Microscopic analyses consisted of maceral determinations by point count (500 points/sample) and reflectance measurements for rank evaluation. Fifty reflectance measurements on vitrinite were made on the Mattson and Kayak samples. In most instances fewer measurements were made on the Emma Fiord material because of a scarcity of vitrinite fragments suitable for measurement.

Maceral determinations on the coal samples and kerogen typing on the oil shale samples were carried out with both "normal" white light and in the fluorescence mode. Both Leitz and Zeiss equipment was used in the analysis. The Leitz set-up utilized an Orthoplan microscope with MPV II photometric accessories. Observations were carried out at a magnification of X650 under partially polarized light. The Zeiss equipment consisted of a Universal microscope-photometer to which was attached a HP300 computer system with Zeiss Coflex software. With the Zeiss equipment observations were made at a magnification of X640.

Compositional characteristics

Mattson coal samples

Compositional properties of the Mattson coal are discussed in detail elsewhere (Potter et al., 1993) and only a summary will be presented here. Figure 5 is a graphic representation of the petrographic composition of these coal samples. The Mattson coal samples are extraordinarily high in inertinite; 55–67%. Vitrinite contents range from 12 to 23% and liptinite from 17 to 28%. Table 2 lists petrographic data for the samples examined and Table 3 shows values from the chemical analyses of some of them. Ash contents of these coal samples are normally quite low (< 5.0%, dry

TABLE 1

Location data for samples analyzed in this study, see Fig. 1

Area (Fig. 1)	NTS map No.	Easting/Northing Zone	GSC No.	*n*	Field No.
Mattson Formation					
A	95G	E.447500 N.6772000 Zone 10	58730	1	
			58737	1	
			58764	1	
			58838	1	
	95F	E.440000 N.6768000 Zone 10	74309	1	
Kayak Formation					
B	117A	E.383300 N.7578850 Zone 8W	99883	11	HD
		E.381700 N.7578250 Zone 8W	98801	13	CQ660
		E.385150 N.7580350 Zone 8W	98803	4	CQ662
		E.385100 N.7580350 Zone 8W	98805	5	CQ664
		E.385150 N.7579900 Zone 8W	98804	4	CQ663
C	117C	E.511830 N.768950 Zone 7	99889	1	873NC(D)
			99888	1	873NC(C)
Emma Fiord Formation					
D		E.443100 N.8537500 Zone 15	See Table 3	11	
F	560D	E.527400 N.9054900 Zone 15	31170	1	
			31167	1	
			31167	1	
			31151	1	
			31150	1	
			31148	1	
			31146	1	

n = no. of samples.

basis). One of the samples shown on Table 3 is a carbonaceous shale (c-58838).

Within the inertinite maceral group micrinite is an abundant constituent (30–40% of total inertinite). It is often intimately associated with vitrinite, usually as discrete bands or "swirls" (see Plate I, A). Semifusinite and macrinite are also abundant constituents in the Mattson coal. Macrinite includes porous to nonporous bodies resembling the corpohuminites and phlobaphenites of brown coals. Many are vesicular and are similar to the porous inertinitic bodies described by Lyons et al. (1982). Similar bodies were also observed in the Kayak coal. The majority of the liptinite consists of sporinite with subordinate amounts of cutinite and rare alginite (Plate I, B). The overall petrographic aspect of these coals suggests a sapropelic origin, possibly in shallow lakes within a delta plain environment (Potter et al., in press). Reflectances measured on telocollinite in the Mattson samples range from 0.67 to 0.74% R_om. This indicates an ASTM rank range from high volatile C to B bituminous.

Kayak coal

The Kayak coal samples, studied mainly from the Hoidahl Dome area in the northern Yukon, also show a high content of inertinite (18–45%). Two complete sections of a 5 m thick bed, each section collected in 0.5 m thick increments, were

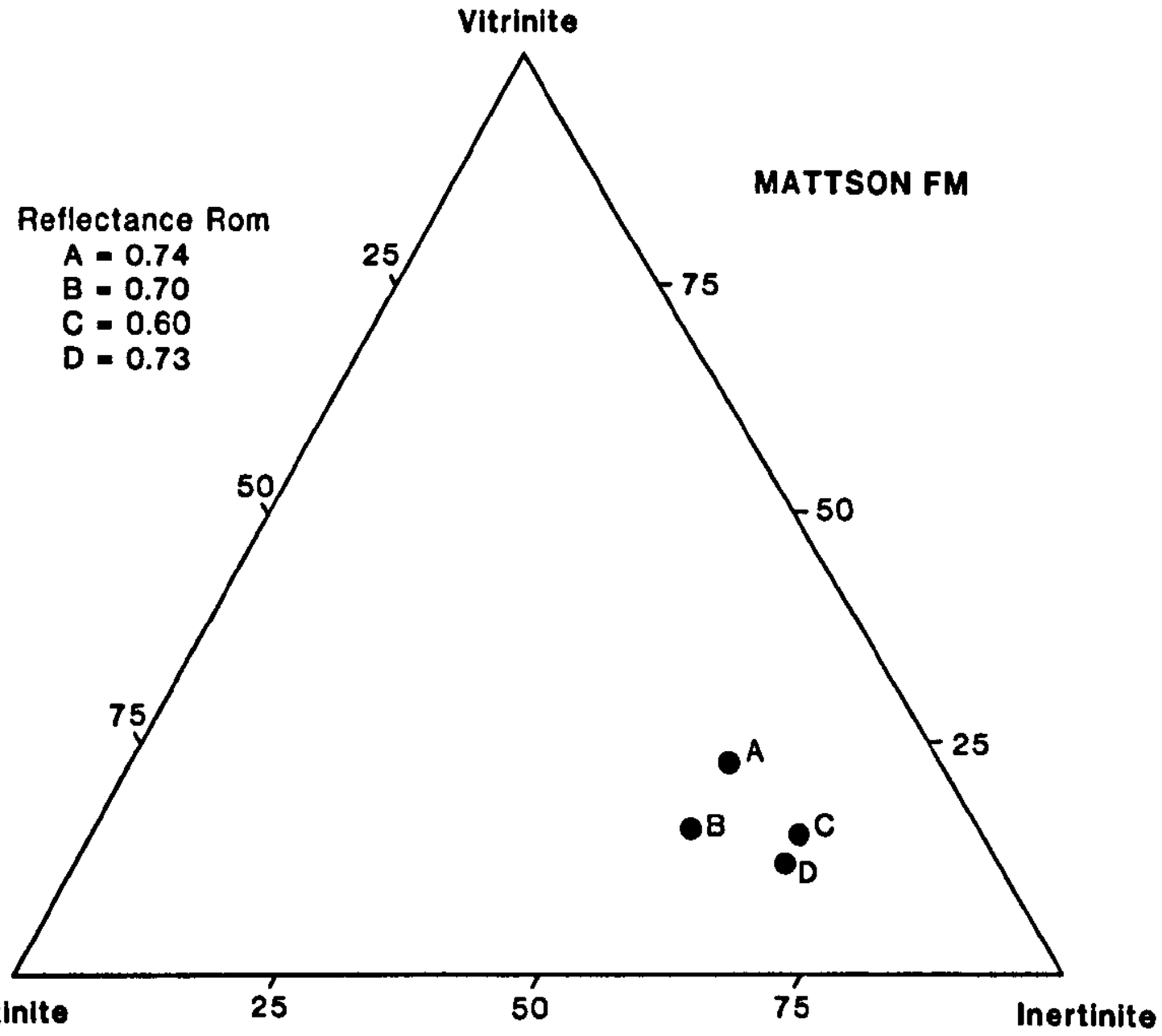

Fig. 5. Ternary diagram showing maceral group distribution (mineral-matter free) in samples of Mattson Formation coal (from Potter et al., 1993). A = sample C-58764; *B* = C-58730; *C* = C-74309; *D* = C-58738 (see Tables 2 and 3).

TABLE 2

Maceral compositions of Mattson coal samples[1] (from Potter et al., 1993)

Samples	Macerals[2] Te.	De.	Gel.	Vit.[3]	Sp.	Cu.	Ld.	Alg.	Lip.[3]	Fus.	Sf.	Mac.	S.Mac.	Mic.	Scl.	Id.	In.[3]	Mins.
Jackfish Gap																		
C58730	3	12	<1	15	23	2	2	–	27	1	17	3	15	17	1	2	57	<1
C58737	3	10	–	13	18	2	+	+	20	3	28	8	7	19	1	<1	67	<1
C58764	4	18	1	23	19	<1	<1	–	20	1	34	+	7	14	1	1	57	<1
Clausen Creek																		
C74309	7	7	1	15	12	3	2	+	17	1	27	5	6	26	2	1	67	2

[1]Data in vol.%.
[2]Te. = telocollinite; De. = desmocollinite; Gel. = gelocollinite; Vit. = vitrinite; Sp. = sporinite; Cu. = cutinite; Ld. = liptodetrinite; Alg. = alginite; Lip. = liptinite; Fus. = fusinite; Sf. = semifusinite; Mac. = macrinite; S. Mac. = semimacrinite; Mic. = micrinite; Scl. = sclerotinite; Id. = inertodetrinite; In. = inertinite; Mins. = mineral matter.
[3]Total.
–: not present; +: present in trace amounts.

studied petrographically and by proximate chemical analysis. Thinner beds exposed at several other sites in the Hoidahl Dome area were also sampled and studied. The geographic locations of these sites and the sampling sequence within the sections are shown in Figs. 6 and 7, respectively. The exact relationship of the beds shown at stations 3, 3A and 4 (Figs. 6 and 7) to the thicker seam at stations 1 and 2 is not known. They may be splits of the major bed, much reduced in thickness, or they may be different beds. Covered intervals between the sections and some evidence of deformation makes correlation between the sections very difficult at present.

TABLE 3

Proximate and ultimate analyses data for Mattson coal[1] (from Potter et al., 1993)

Locality:	Jackfish Gap		Clausen Creek
Sample No.:	C58730	C58838	C74309
Moisture (AR)[2]	3.4	7.8	2.54
Ash (AR)	2.4	43.9	4.32
Volatile matter (daf)[3]	34.5	45.1	32.5
Fixed carbon (daf)	65.5	54.9	67.5
Total sulphur (daf)	1.25	0.35	1.64
Carbon (daf)	78.4	72.53	79.57
Nitrogen (daf)	1.03	0.72	1.11
Sulphur (daf)	1.25	0.35	1.64
Hydrogen (daf)	4.44	2.98	4.53
Oxygen (daf)	14.88	23.42	13.1

[1]Data in vol.%.
[2]AR = as received basis.
[3]daf = dry ash-free basis.

Figure 8 is a ternary plot of the maceral distribution for the Kayak coal samples, whereas Table 4 summarizes petrographic and chemical data. Comparison of individual increments show vitrinite contents ranging from 48 to 71%; average values on a whole seam basis vary from 58 to 67%. Most of the inertinite is semifusinite and fusinite. Micrinite is fairly abundant in some samples, ranging up to 6% and often appears to be filling cell cavities in vitrinite (Plate I, C). A common inertinite component in the Kayak coal samples has the form of spherical porous bodies, similar to those described by Lyons et al. (1982) and believed to be derived from medullosan remains (Plate I, D). Often the cavities within these bodies in the Kayak coal samples are filled with vitrinite suggesting formation of the bodies very early in the depositional history of the coal, possibly in the peat stage with migration of colloidal pre-vitrinitic material into the cavities. Table 4 shows that the thicker bed, represented by sample series HD and CQ 660, is of high quality with ash contents on the whole seam basis averaging 6–7% and most sulphur values below 0.6 per cent. The chemical analyses (Table 4) for the Hoidahl Dome samples all indicate coal of semi-anthracite rank by ASTM standards (ASTM, 1981), though the reflectance data suggest that some of them are anthracite based on reflectance boundaries proposed by Davis (1978). Included in Table 4 are data on two samples collected from the Kayak in the British Mountains (Fig. 1, Site C). These are identified in Table 4 as 873NC (C and D). They are also relatively high in inertinite and higher in ash than the Hoidahl Dome coals. Reflectance values on the British Mountains samples are significantly higher than those at Hoidahl Dome suggesting a westward increase in rank for the carbonaceous matter in the Kayak Formation.

The Emma Fiord Formation

The Emma Fiord material constitutes a sample suite quite different from the other two in that it contains only one coal sample whereas the remainder of the samples are carbonaceous shales and marlstones with kerogen of sufficient quantity and quality to be called oil shales. The compositional characteristics of these samples have been described in detail by Goodarzi et al. (1987), and only a summary will be presented here. The samples from the Devon Island section (Fig. 1, Site D) fall into three groups. One group consists of material with a dominant carbonate matrix in which the associated organic matter is dominantly alginite. In these samples the organic component does not exceed 8%. Another sample group has a clay–carbonate matrix and is much richer in organic matter, particularly matrix bituminite. Matrix bituminite is believed to be formed from the decomposition of algal matter (Creaney, 1980). In addition a population of discrete bodies identifiable as alginite is an important constituent of this sample group. Plate II, A and B show representative photomicrographs of Emma Fiord material. Rock-Eval analysis on the clay–carbonate group confirms that these samples have a very high hydrocarbon potential (Table 5). The third lithology in the Devon Island section is coal, represented by a single sample with a high content of vitrinite (> 85%), associated with about 7% liptinite. Figure 9 is a series of ternary diagrams summarizing kerogen type and/or maceral group distribution in the Devon Island samples.

Six samples from the section on Ellesmere Island (Fig. 1, Site F) were examined microscopically. The only determinations made on them were meas-

PLATE I

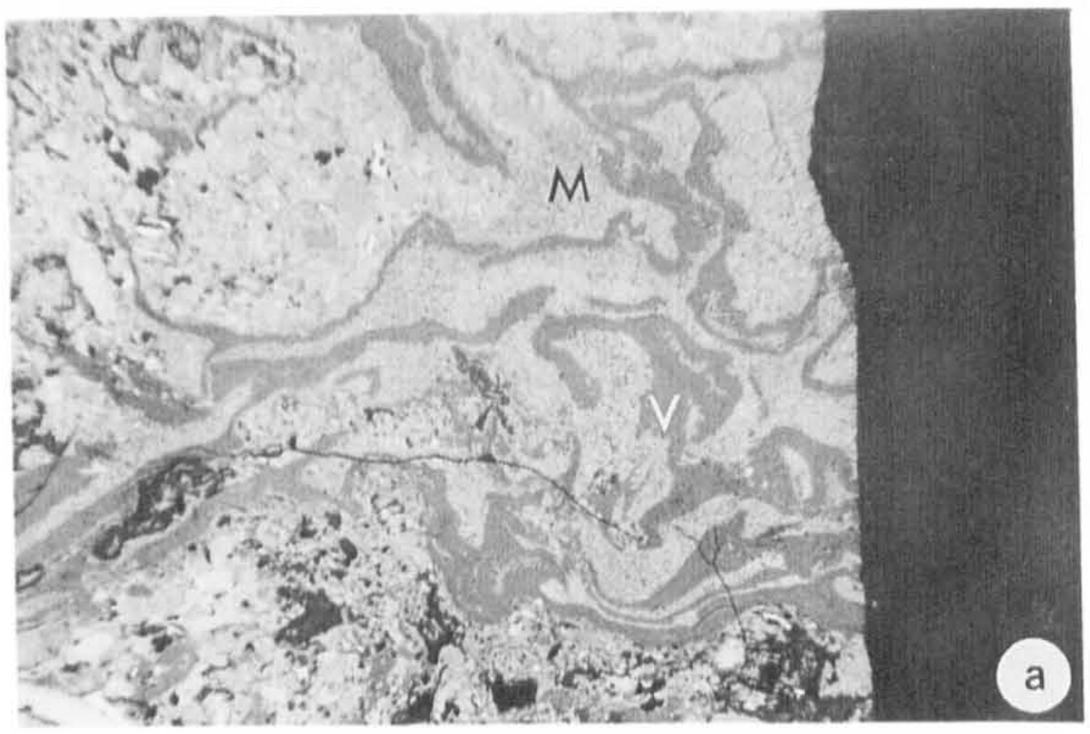

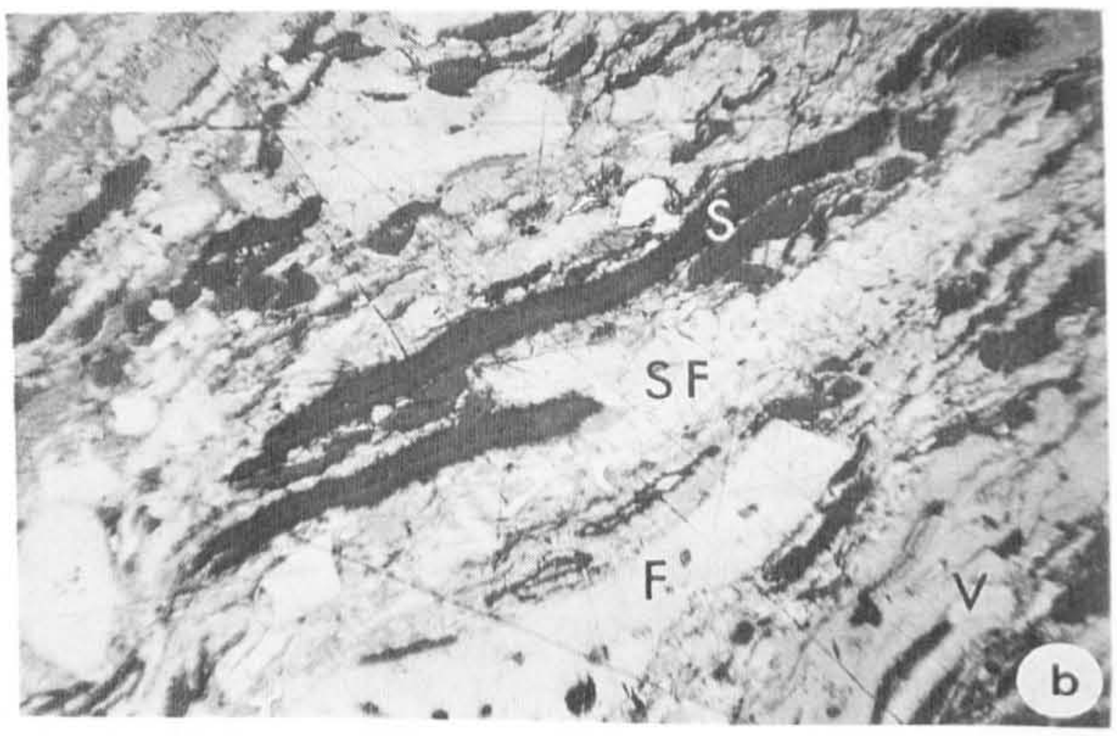

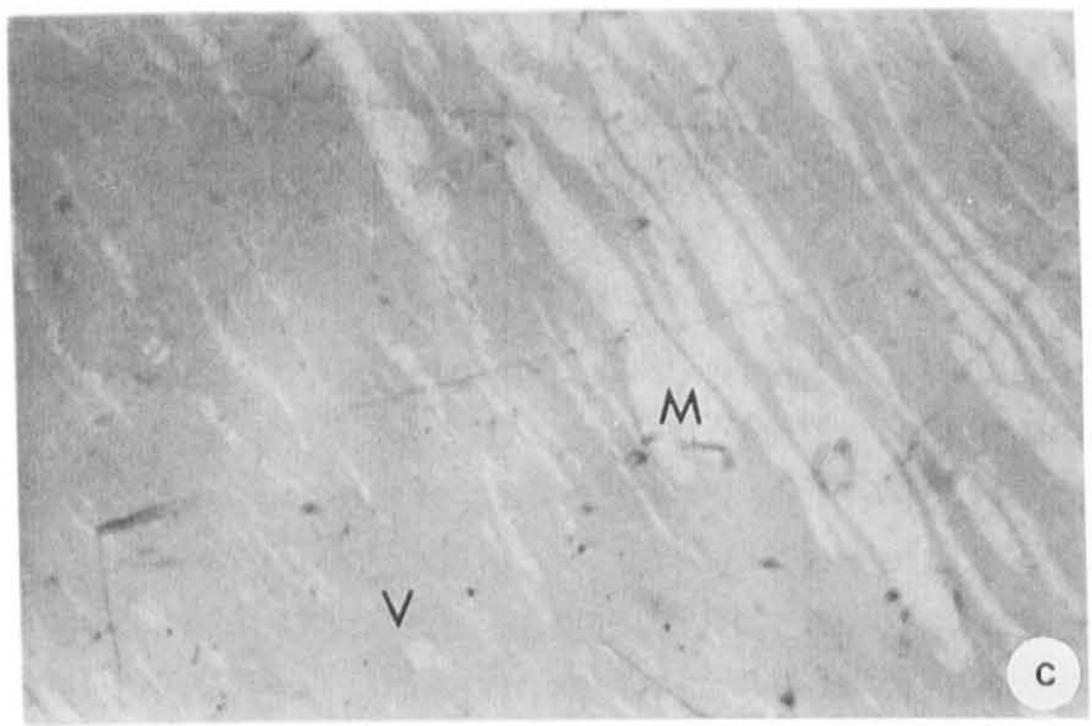

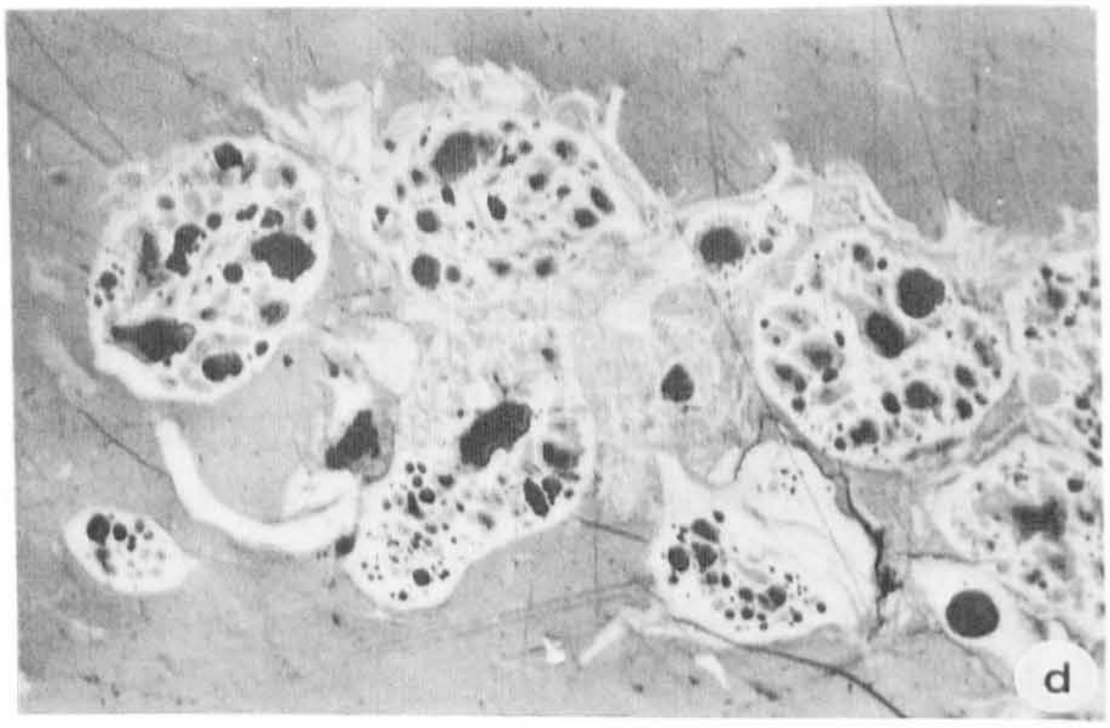

Photomicrographs of Mattson and Kayak coal samples.

A. Micrinite (*M*) intimately associated with thin strands of vitrinite (*V*); Mattson coal, magnification—long axis of photo = 240 μm); ISPG Photo 3709-17.
B. Typical maceral association with high inertinite content in Mattson coal; *SF* = semi-fusinite, *F* = fusinite, *S* = sporinite, *V* = vitrinite, magnification—long axis of photo = 240 μm); ISPG Photo 3602-9.
C. Micrinite (*M*) and vitrinite (*V*) maceral assemblage in Kayak coal; magnification—long axis of photo = 240 μm; ISPG Photo 4004-52.
D. Cluster of subspherical vesiculated bodies (sclerotia or fusinized cell-fillings) in Kayak coal; magnification—long axis of photo = 240 μm; ISPG Photo 4004-20.

urements of reflectance. Because of their rank (meta-anthracite), maceral discrimination was not possible. These Ellesmere samples were all carbonaceous shale.

There is a drastic difference in maturation level between the Devon Island and Ellesmere Island samples. Vitrinite in the former has a reflectance range between 0.26 and 0.50% R_om, whereas the latter show a range of 5.11 to 5.49% $R_o$max. Clearly the Ellesmere Island samples were subjected to a much more severe thermal regime than their Devon Island counterparts. Deeper burial of the Emma Fiord sediments on Ellesmere Island and the influence of igneous activity, both extrusive and intrusive, are believed to have been major factors in the high maturity levels at this location.

Relationship to other Lower Carboniferous coal and oil shale

Contemporaneous with formation of coal and oil shale in northern Canada during the Early

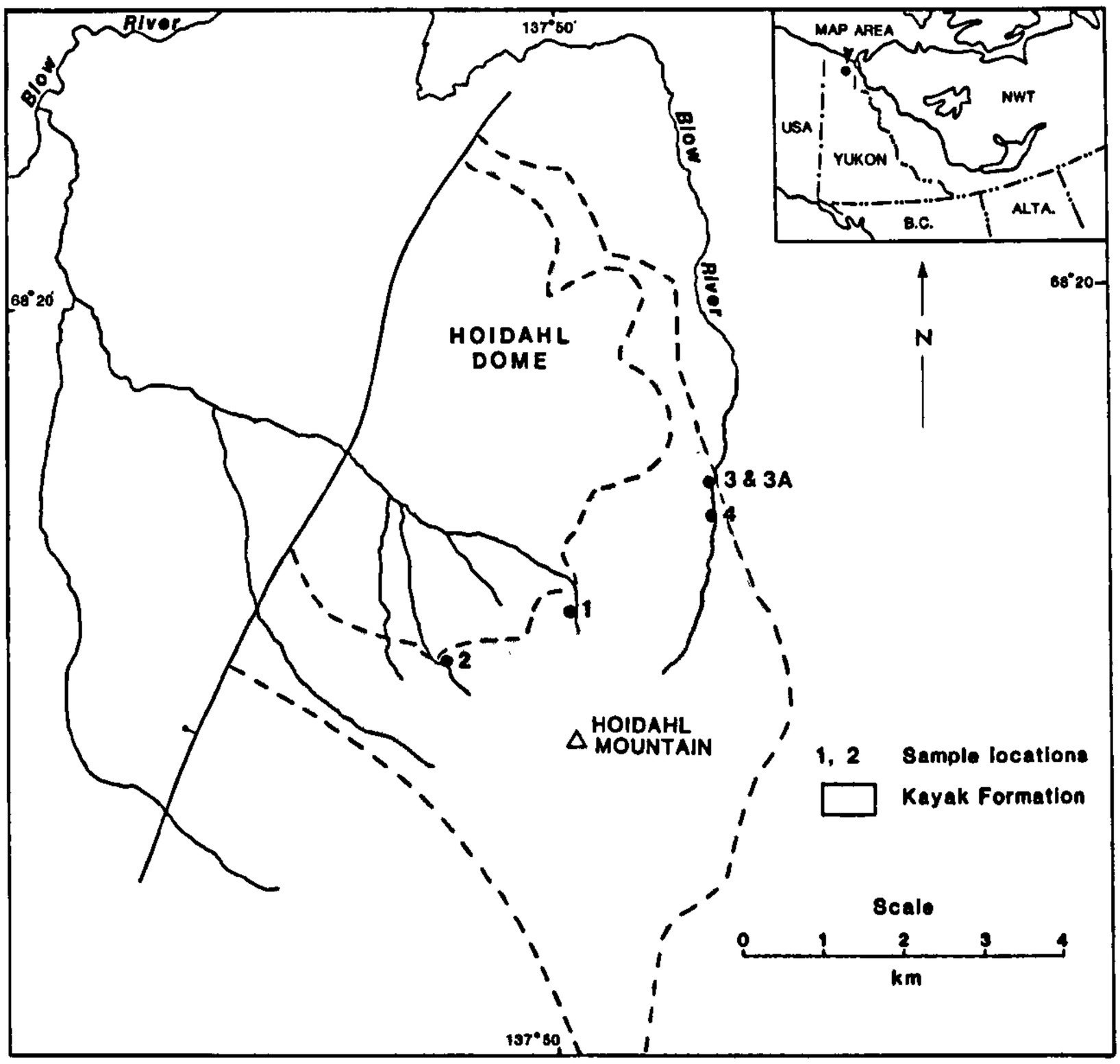

Fig. 6. Map of Hoidahl Dome area, northern Yukon Territory, showing location of sampling sites for Kayak Formation coal beds (from Cameron et al., 1988); sampling locations equivalent to stations on Fig. 7.

Carboniferous was the accumulation of similar deposits in other parts of the world. The map shown in Fig. 10 and the listing in Table 6 is not an exhaustive compilation but does indicate that conditions favourable for the accumulation and preservation of organic material prevailed in a number of areas during the Early Carboniferous. Most of the listed deposits are dated as Viséan, though a few are Tournaisian. As the map and table show, Lower Carboniferous coal occurs in northeast Greenland, east central Greenland, Svalbard (Spitzbergen), Bjørnøya (Bear Island), Scotland and northeast England, Western and Central Europe (France, Germany and Poland), and Russia, both east and west of the Urals. There are also Lower Carboniferous coal beds in China and in the Endicott Group in northern Alaska. In the Appalachian area of the United States there are Mississippian (Lower Carboniferous) coals in various formations located in states from Virginia to Alabama. The most important beds seem to be in Virginia and Tennessee where they were mined at one time (Englund, 1979; Milici et al., 1979).

These Early Carboniferous deposits are more widely separated now than they were at the time of their deposition and occur in present-day climatic regimes as diverse as the Canadian Arctic and the temperate–subtropical environments of Georgia and Alabama. To place the Canadian deposits in a more global context at the time of peat formation, it is worth studying published views concerning the paleogeography and climate during Viséan times, particularly in the continent of Laurussia.

Paleogeography of Laurussia

Laurussia designates the land mass formed by the progressive amalgamation, during Paleozoic time, of North America, Greenland, Scandinavia and the Russian Platform west of the Urals (Ziegler et al., 1977; Rowley et al., 1985). This progressive amalgamation came to a climax in late

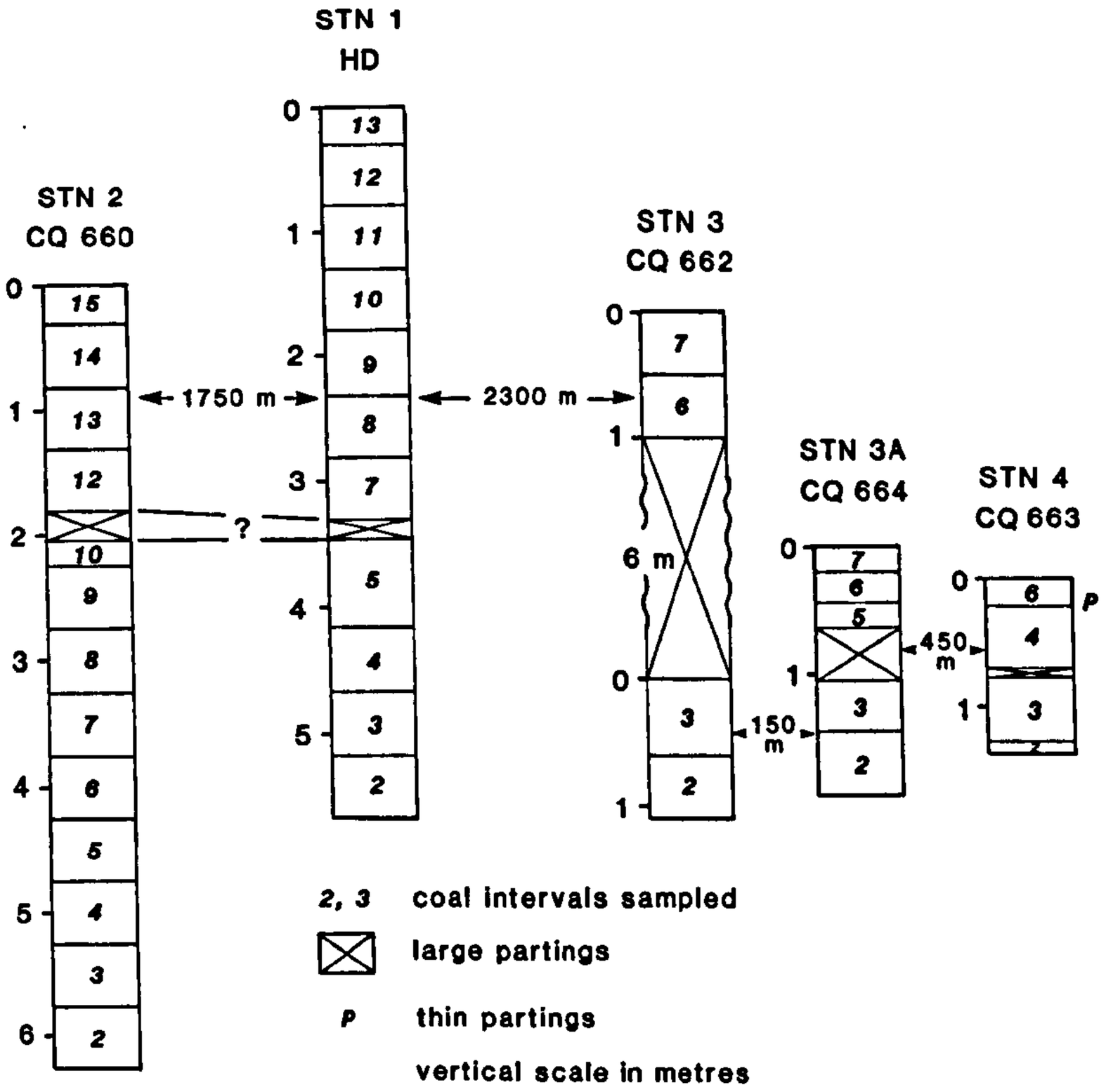

Fig. 7. Schematic seam sections showing sampling sequence for Kayak coal in Hoidahl Dome area. See Fig. 6 for station (sample) locations (from Cameron et al., 1988).

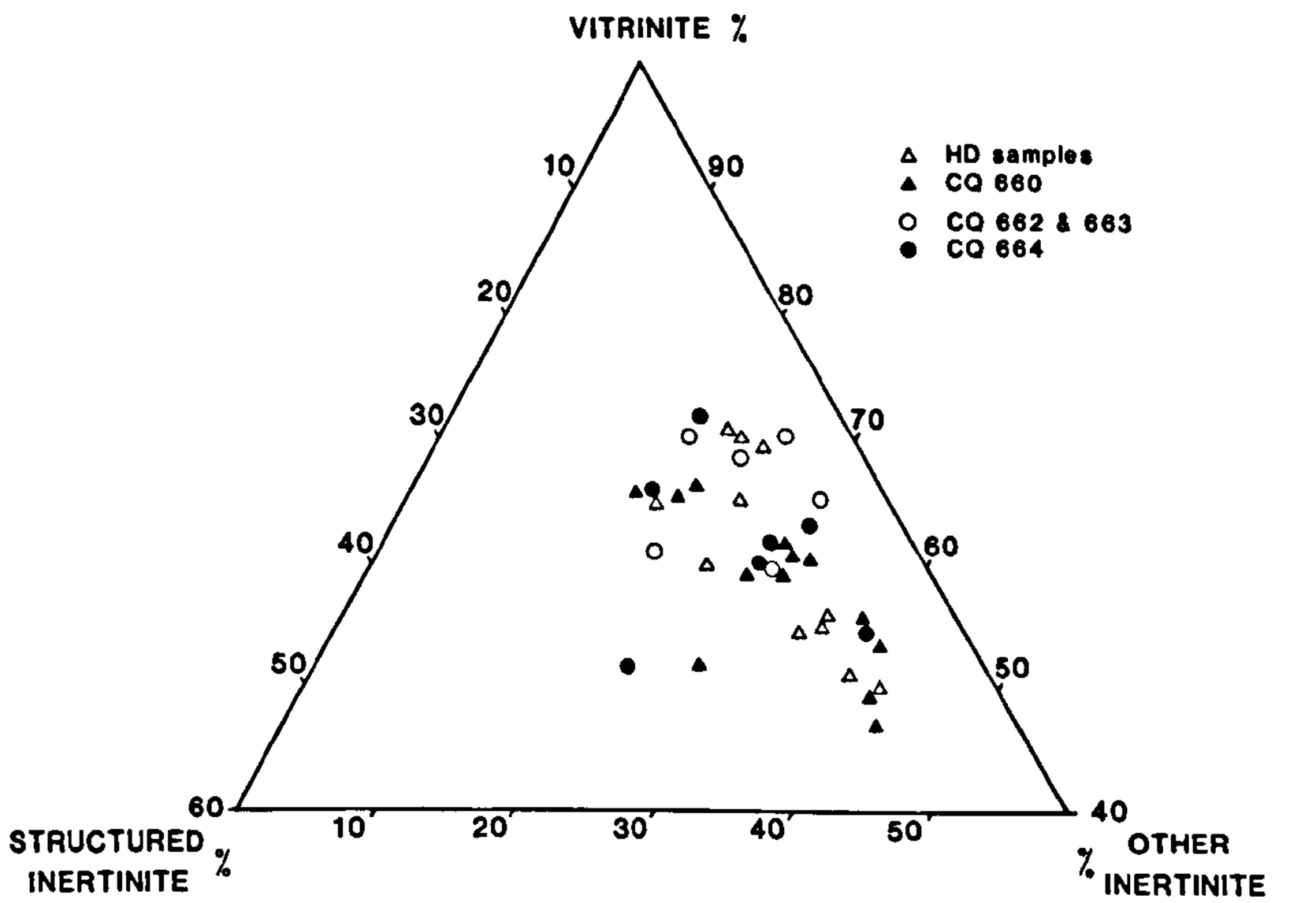

Fig. 8. Ternary diagram showing maceral distribution in samples of Kayak coal from Hoidahl Dome. See Figs. 6 and 7 and Table 4, structured inertinite equals semifusinite and fusinite (from Cameron et al., 1988).

TABLE 4

Summary of petrographical data and some chemical data on Kayak coal samples[1] (from Cameron et al., 1986, 1988)

Sample	Vitrinite	Semifusinite fusinite	Other inertinite	$R_o$max	Ash dry	S dry	VM[2] dmmf
HD	60.6	10.8	28.6	2.95	7.3	0.53	11.9
CQ660	57.7	11.1	31.2	2.89	6.4	0.62	9.3
CQ662	59.4	8.9	31.7	3.27	5.7	0.59	8.5
CQ663	66.9	15.1	18.0	3.21	14.0	1.27	9.4
CQ664	65.1	8.0	26.9	3.19	5.7	0.61	8.2
873NC(D)	57.7	18.2	24.1	4.03	13.8	0.41	
873NC(C)	61.7	10.0	28.3	3.94	41.4	0.26	

[1]Maceral data in vol.%, mineral-matter-free basis; ash and sulphur in wt.%. Data are average values on whole-seam basis.
[2]VM = Volatile matter (dry, mineral-matter free).

Carboniferous and Permian time when Laurussia and Gondwana joined to form the super continent Pangea (Ziegler, 1989). Figure 11 is a reconstruction of Laurussia in Viséan time, taken from P.A. Ziegler's 1989 book *Evolution of Laurussia*. Shown on this figure are the salient geological features that have influenced the distribution of coal and oil shale formed at this time. A large part of the continent is identified as cratonic or anorogenic. The southern part of the continent is bounded by a complex of active and inactive fold belts including, as major components, the Appalachian and Variscan orogens. Associated with these fold belts are several terrains accreted or about to be accreted to the southern boundary of Laurussia. The northern boundary of Laurussia is somewhat similar tectonically and includes as main elements the Innuitian and Lomonosov Fold Belts, both indicated as inactive. To the east during Viséan times the Russian Platform (Moscow Platform of P.A. Ziegler, 1989) was the site of extensive shallow marine deposition including both clastics and carbonates. The central part of the platform, the Moscow coal basin, saw the accumulation of coal seams during early and middle Viséan times (Belskaya et al., 1975). These include the famous Moscow brown coal deposits.

A major tectonic feature shown on Fig. 11 is the North Atlantic Megashear zone extending as a curvilinear feature for hundreds of kilometres from Newfoundland to the eastern end of the Innuitian Fold Belt, north of Greenland. Figure 11 indicates a number of basins containing continental clastics of Viséan age as being associated with splays of this zone. Several of these basins contain coal, including the Wandell Sea Basin of northeastern Greenland, east-central Greenland, Spitzbergen and Bjørnøya (Table 4, Fig. 70). Several eastward-trending splays appear to be related to coal- and oil-shale bearing basins in Scotland (Midland Basin) and northern England (Northumbrian Trough). The Viséan coal beds of France are found in several small basins near the Loire Valley, possibly associated with depositional sites in the Central Armorican Basin. In the eastern United States Lower Carboniferous coal beds are the product of accumulation in the Appalachian Foreland Basin. Although some of these may be Viséan [Osagean–Chesterian according to Englund (1979), Milici et al. (1979) and Thomas and Cramer (1979)], many may also be Namurian (Witzke, 1990).

In northern Canada the Mattson and Kayak coal beds formed in an environment of low tectonic activity (Richards et al., 1993). The Mattson coal was deposited in a temporarily prograding delta setting extending into the Prophet Trough and were later onlapped by marine sediments. The Kayak coal was formed in the northern extension of the Prophet Trough and is part of a gradually transgressive package of strata overlying folded Devonian and older rocks deformed in the Ellesmerian Orogeny. This was the climactic event that produced the Innuitian Fold Belt. This fold belt seems to have been a major provenance area for siliciclastics in the Mattson and Kayak formations. The oil shales of the Emma Fiord Formation occur within

PLATE II

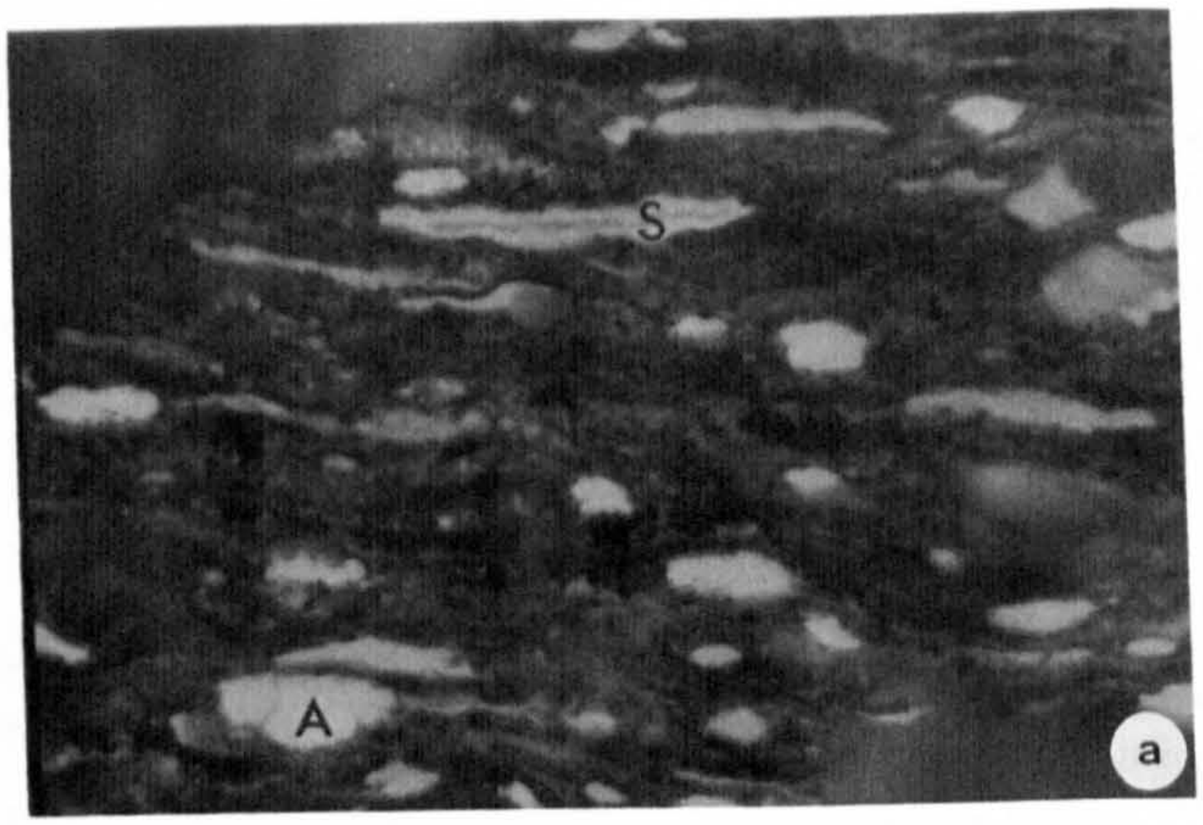

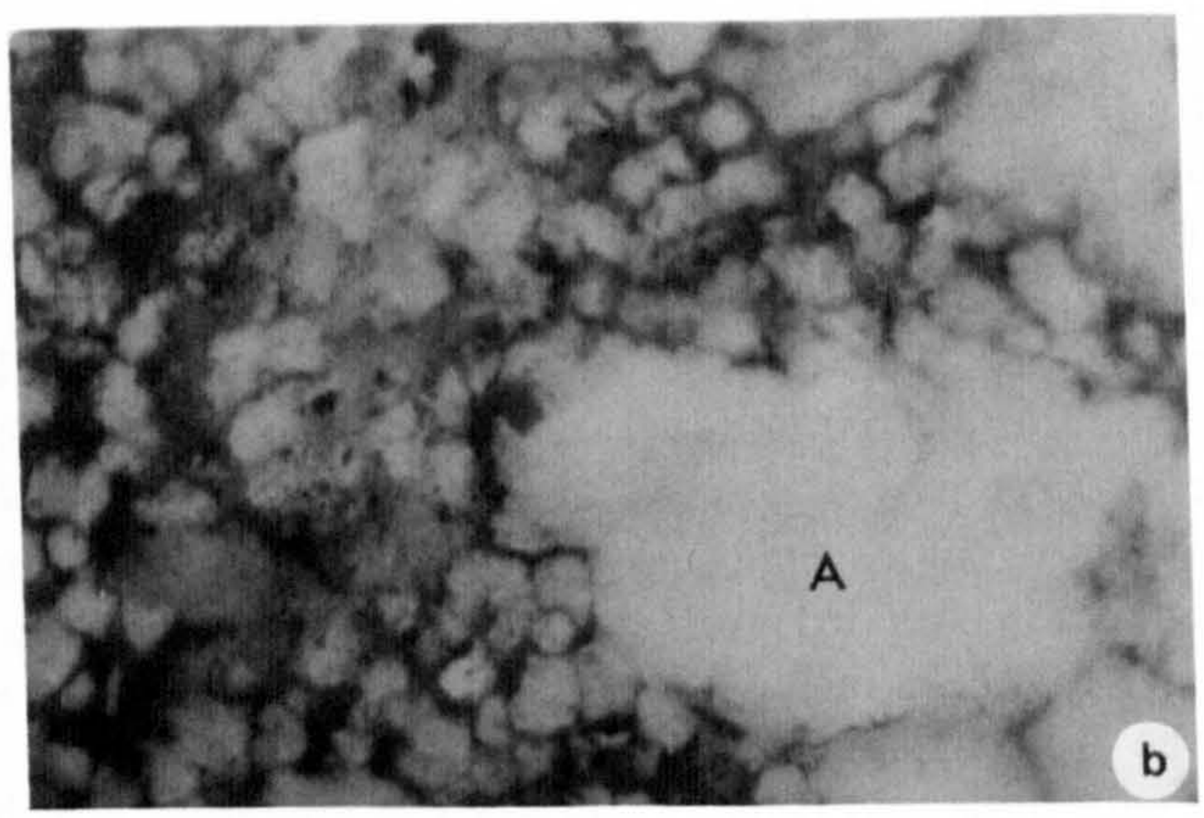

Photomicrographs of Emma Fiord oil shale samples.

A. Sporinite (*S*) and small algal bodies (*A*) in Grinnell Peninsula sample; ground mass is a carbonate/clay mixture; photo taken in the fluorescent mode with blue light irradiation; magnification—long axis of photo = 240 μm.

B. Large algal mass (*A*) with many smaller masses of algal origin in Grinnell Peninsula sample; photo taken in fluorescent mode using blue light irradiation; magnification—long axis of photo = 240 μm.

the Innuitian Fold Belt. Their tectonic genesis appears to have been quite different from that of the Mattson and Kayak deposits. The Emma Fiord beds formed in grabens and half grabens produced by the tensional stresses that initiated subsidence in the Sverdrup Basin (Davies and Nassichuk, 1988). A similar tectonic regime may have prevailed in the Midland Valley of Scotland.

Paleoclimate in the Viséan

Paleogeography during Viséan times was a major factor in determining the climatic conditions of temperature and rainfall. These conditions are of critical importance in determining the ratios of organic productivity to decay that are favourable for the net accumulation and preservation of carbonaceous matter. An important aspect of world climate is the zoned arrangement of low and high atmospheric pressure regimes relative to equator and poles. An equatorial band extending about 15° north and south of the equator is characterized generally by low pressure (Fig. 12). This band is flanked by two high-pressure belts, one in each hemisphere, extending from approximately 15–35° latitude. These in turn are bounded by two zones of low pressure extending to about 60°. The low-

TABLE 5

Rock Eval/TOC pyrolysis of samples from Grinnell Section, Devon Island[1], see Fig. 4 for sample position (from Goodarzi et al., 1987)

Sample no.	GSC no.	T_{max}	S1	S2	S3	TOC	HI	OI
11	32919	433	0.05	5.58	2.45	1.52	367	161
10	32917	434	0.09	6.14	3.18	1.87	328	170
09	32916	431	3.96	243.01	18.67	39.36	617	047
08	32915	435	11.23	376.08	25.15	47.46	792	052
07	32914	434	3.81	224.32	23.81	33.26	674	071
06	32910	431	0.26	15.20	4.20	4.59	331	091
05	32908	433	0.21	15.47	3.75	4.16	371	090
04	32900	436	0.89	89.10	10.81	16.44	541	065
03	32899	433	7.62	258.98	33.89	53.60	483	063
02	32893	434	0.06	3.70	1.88	1.14	324	164
01	32891	421	1.85	47.01	52.78	69.59	067	075

T_{max} = maximum temperature in °C at which max. generation of hydrocarbons occurs and related to S2 curve; S1 = mg free hydrocarbons/g of sample; S2 = mg hydrocarbons/g of sample produced by thermal conversion of kerogen in sample; S3 = mg CO_2/g sample produced by pyrolysis of sample; TOC = percent total organic carbon in sample; HI = hydrogen index = (S2/TOC) × 100; OI = oxygen index = (S3/TOC) × 100. These parameters are defined in Espitalié et al., 1977.

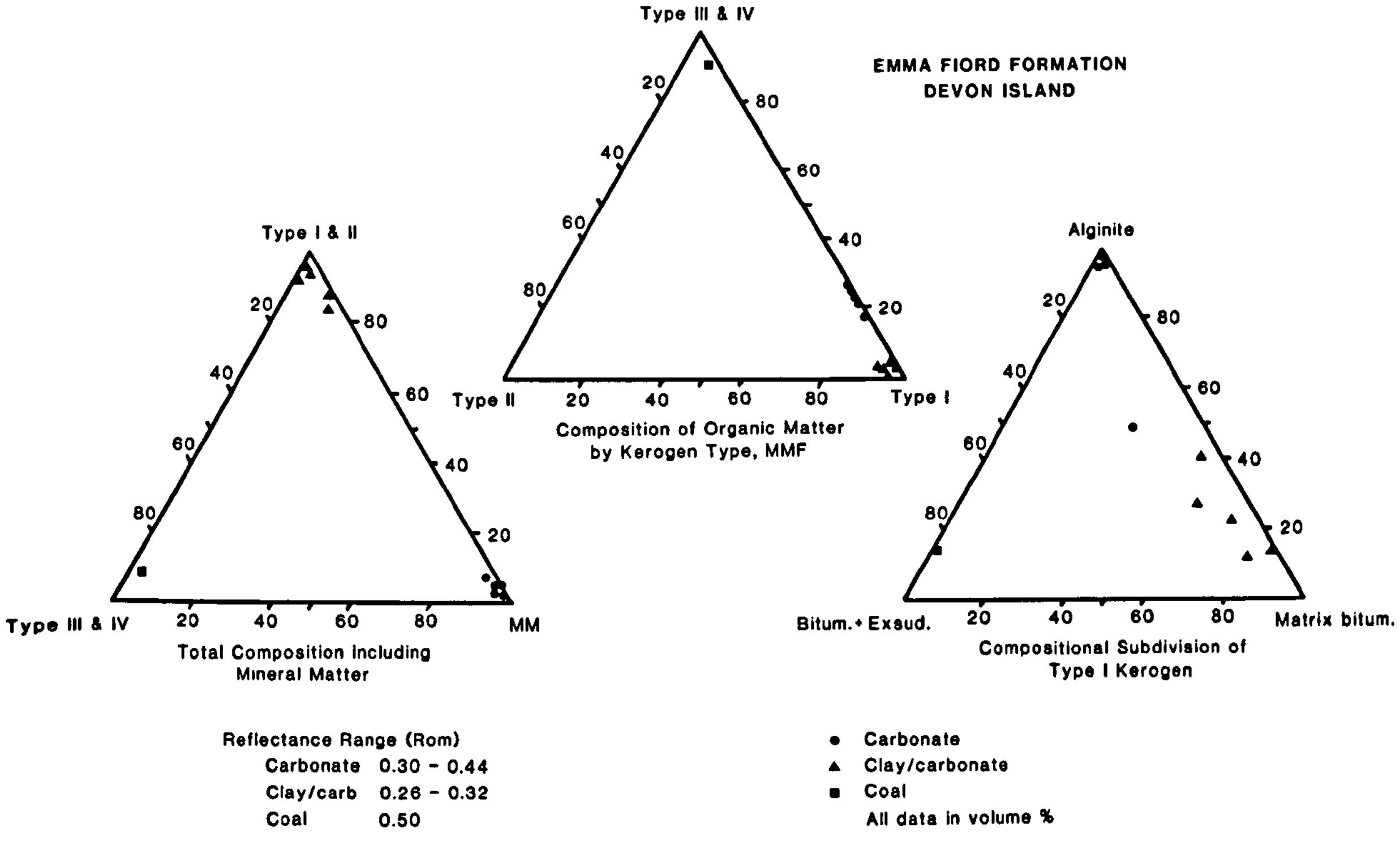

Fig. 9. Ternary diagrams showing petrographic compositional characteristics for Emma Fiord Formation samples collected at Grinnell Peninsula, Devon Island, northern Canada; *bitum.* = bituminite; *exsud.* = exsudatinite (data from Goodarzi et al., 1987).

pressure bands are characterized generally by greater precipitation than the high-pressure zones. This zonal arrangement is somewhat theoretical and would exist in more perfect form if the planet's surface was homogeneous. Uneven distribution of continents and oceans within each hemisphere relative to the equator and the existence of high mountain chains distort the model to a significant degree,

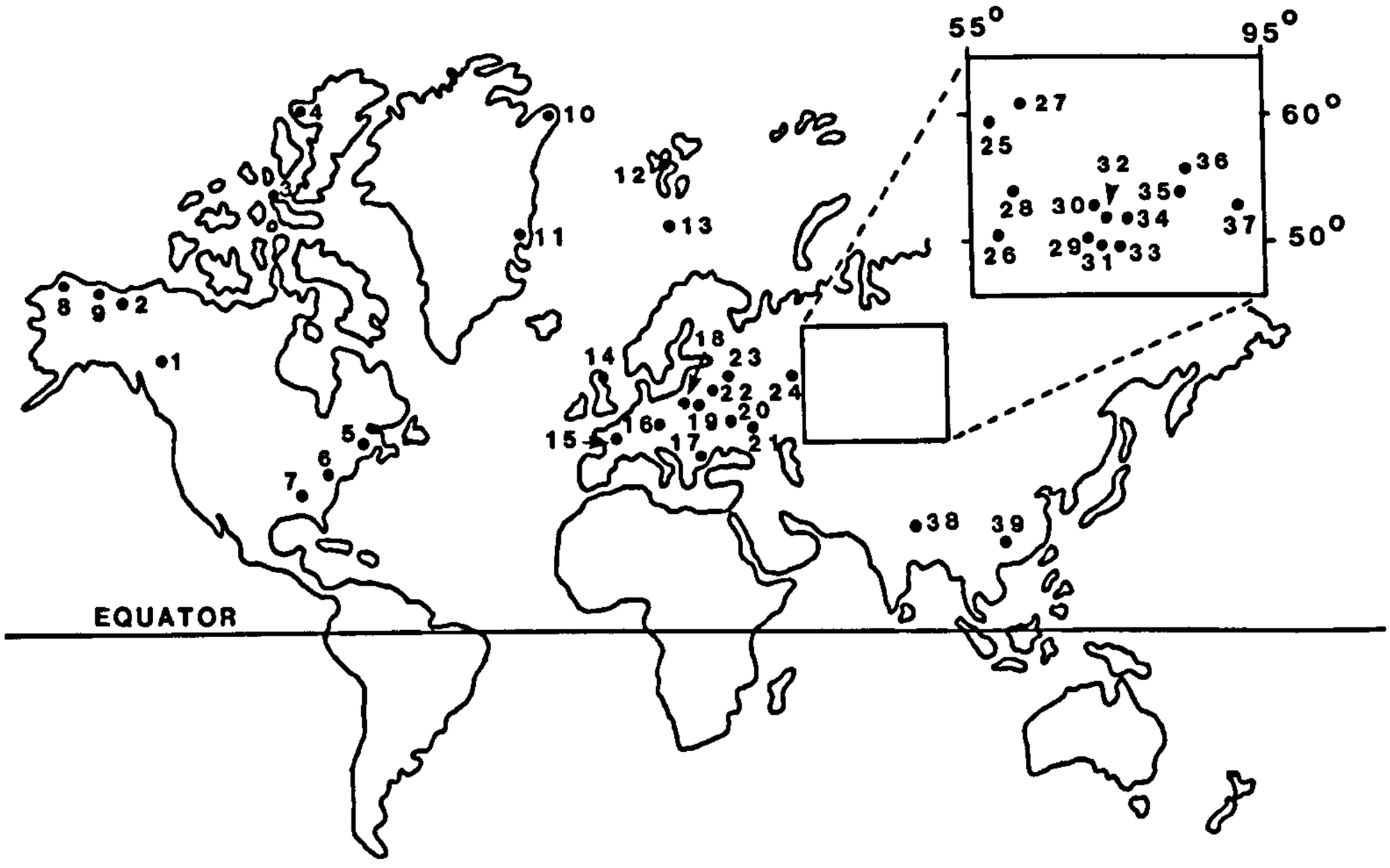

Fig. 10. Global distribution of some Early Carboniferous coal-bearing strata; see Table 6.

though it is thought that the pattern, albeit often modified, has been a persistent feature, at least since Paleozoic times (A.M. Ziegler et al., 1981).

Relative to the formation of Lower Carboniferous coal deposits in Laurussia, it is important to consider two aspects of paleogeography upon which most experts seem to agree. These involve the drift of Gondwana and Laurussia and the closing of the Proto-Atlantic Ocean. Gondwana was drifting north on a collision course with Laurussia, which was also drifting north though apparently at a slower rate. P.A. Ziegler (1989) suggested that in Viséan times the Proto Atlantic Ocean, between western Gondwana and the North American part of Laurussia, had closed to a width of 600–800 km and that large-scale collision had begun in the late Viséan. Scotese et al. (1979) seem to favour slightly later large-scale collision.

These movements must have had a profound effect on the climate of the time because they would have altered wind circulation and ocean current patterns. Of particular importance is the position of Laurussia relative to the equatorial low-pressure zone. P.A. Ziegler's reconstruction (Fig. 11) shows the equator passing through the complex fold belt on the southern border of the continent, that is through the Variscan Orogen, westward through the Maritime provinces of Canada and across the Great Lakes. Figure 13 shows another Viséan paleogeographic reconstruction by Rowley et al. (1985) which displays a somewhat different configuration, particularly with respect to Scandinavia and the rest of the European part of Laurussia. These areas are shown considerably farther south of the position plotted in P.A. Ziegler's figure (compare Figs. 11 and 13). However, the position of the equator and latitude 20° north, relative to North America and Greenland, in Fig. 13 is not greatly different from P.A. Ziegler's reconstruction. In both instances the position of the coal deposits of Greenland and northern Canada seem to be considerably north of the equatorial zone. There are some indications that the positioning of at least the North American part of Laurussia is too far north in these two reconstructions. Keppie (1977) in his reconstruction of Early Carboniferous paleogeography showed that all of the Viséan coal deposits of northwestern Canada, Greenland and Spitzbergen and the oil shales of the Emma Fiord would have been formed between the equator and 20° north.

The occurrence of reefs of this age with diagnostic faunal assemblages in northwestern Canada and the Canadian Arctic Archipelago also indicate geographic positioning nearer the equator (20–30°) than that suggested by Figs. 11 and 13 (Davies et al., 1989; B.C. Richards, pers. commun., 1992).

Yet another reconstruction by Scotese and McKerrow (1990) is in agreement with that of Keppie in that it shows geographical locations for the formation of Viséan coal deposits in Greenland, Spitzbergen, western Europe and Russia west of the Urals as being south of 20° north. However, according to the Scotese–McKerrow model Viséan coal and oil shale formation in northern Canada and Alaska would have occurred between 20° and 30° north. This would put such sites within the belt of high pressure and lowered rainfall (between 15° and 30° north) according to the zonal arrangement shown in Fig. 12. Witzke (1990) using lithic paleoclimate indicators, such as coal, evaporites, etc., developed a "best fit" model that showed the Viséan equator passing through northern Greenland and diagonally across northern Canada, well north of Hudson Bay. By using lithic indicators, Witzke was attempting independent verification of paleogeographic reconstructions from paleomagnetic data for the Paleozoic. He concluded that in most instances reconstructions by the two methods agreed fairly closely. Perhaps unfortunately for the present study, he also indicated that the greatest differences were for Devonian and Early Carboniferous times. A further complicating factor is the likelihood of global warming during Viséan times as indicated by Kelley et al. (1990). If accompanied by significant rainfall, this might result in northward migration of regimes favouring enhanced growth of vegetation and peat mire development.

It is not likely that the occurrence and location of coal deposits in northern Canada can be attributed solely to the global zonal arrangement of climatic belts. A.M. Ziegler et al. (1979) and Rowley et al. (1985) have emphasized strongly the influence of the position of land masses relative to the location of climatic regimes. As the major axis for the distribution of the continents becomes more strongly oriented north–south, a trend that was becoming more evident in the Viséan prior to the formation of Pangea, the more likely is the possibility of climatic asymmetry in an E–W direction. Thus a rainfall distribution for Laurussia proposed by Rowley et al. (1985) shows a SE–NW decrease in precipitation (Fig. 13). A somewhat similar pattern was proposed by Bless et al. (1987). These patterns fall in quite nicely with the occurrences of coals in Greenland and Svalbard, because they would have formed on the eastern side of Laurussia in the wet or humid zones as defined by Rowley et al. (Fig. 13). However, the coal deposits in the Mattson and Kayak formations of northwestern Canada do not fit so easily into the Rowley et al. model because they are located in the "dry" zone of the model.

There is one possible explanation for this apparent anomaly. The paleogeographic reconstruction of Rowley et al. (1985) shows the paleolatitude of the Mattson and Kayak coal deposits to be close to or north of 30° in which case they might be located in the belt of prevailing westerly winds. The coal deposits were formed to the west or southwest of the Yukon–Innuitian Fold Belt and if the fold belt was an area of high elevation, precipitation from the westerly winds might have been higher in the area where the Mattson and Kayak swamps were located. This interpretation has to be balanced against earlier discussion that this area might have been farther south than the model of Rowley et al. shows.

It should be noted also that the high inertinite contents of the Mattson and Kayak coals, particularly the former, suggest there were periods of drought during the formation of these coals. Such periods of drought would increase the possibility of surface oxidation of peat and the occurrence of fires. Potter et al. (1993) compared some varieties of inertinite in the Mattson to "resino inertinites" of the Gondwana coals of India. These appear to have formed in dry climatic conditions (Misra et al., 1990). Richards (pers. commun., 1992) interprets some of the sandstones in the Mattson Formation as aeolian. This is further evidence for dry conditions during deposition of this stratigraphic unit. These indications of reduced rainfall would fit with the climatic interpretation of Rowley et al., but not with that of Van der Zwan et al.

TABLE 6

List of some Lower Carboniferous coal and oil shale deposits

Map ref.[1]	Area or coal basin	Age	No. of beds	Rank[2]	Max/Av. thickness thickest seam (m)	Remarks
Canada						
1	Liard Basin	Viséan/ Serpukhovian	3	Bit.	1.5/	Potter et al., 1993
2	North Yukon	Viséan	1	Anthra.	5.5/	Cameron et al., 1986; may be more than 1 seam
3	Sverdrup Basin	Viséan	1	Subbit.	1/	Goodarzi et al., 1987; at least 1 seam in a 35 m, mainly oil shale, section
4	Sverdrup Basin	Viséan	3	Meta-anthra.	1/	Thorsteinsson, 1974; Goodarzi et al., 1987
5	New Brunswick	Tournaisian		Vitr. refl. 0.33–0.86	60	Macauley et al., 1984; oil shale
USA						
6	Virginia	Osagean	2–5	Bit.	2.40/ 1.50–2.00	IGCP, 1982; Englund, 1979; 2 coal fields
7	Tennessee/ Georgia	Chesterian		Bit.		Milici et al., 1979; Thomas and Cramer, 1979
8	North slope Alaska	late Mississippian	several	Bit. to meta-anthra.		Magoon and Bird, 1988
9	Alaska North slope Endicott Field	Tournaisian/ Viséan	14			Ravn, 1991; Melvin, 1987
Greenland						
10	Holm Land, NE Greenland	Early Carb.	several		0.5/	Schiener, 1976
11	Hudson Land, E. central Greenland	Early Carb.				Frebold, 1932; Schiener, 1976
Norway						
12	Spitzbergen	Tournaisian to Viséan	6	Bit	2.9/	Cutbill et al., 1976
13	Bjornoya (Bear Is.)	Tournaisian	3	Bit	0.7/	Harland et al., 1976; Coal-bearing strata believed to be Devonian underlie the Tournaisian
Scotland						
14	Scottish Basin		3–80	Bl.	0.30–30.0/ 0.20–5.20	IGCP, 1982; 11 separate fields; some contain oil shales
France						
15	Central France	Culm	1–3	Bl.		IGCP, 1982; 2 coal fields

TABLE 6 (*continued*)

Map ref.[1]	Area or coal basin	Age	No. of beds	Rank[2]	Max/Av. thickness thickest seam (m)	Remarks
Germany						
16	Doberlug-Kirchhain + Erzgebirge Depression	Viséan	5–17	Bl.	1.2–3.0	Baumann and Vulpius, 1991; several coal fields
Bulgaria						
17	Dobrudza	Viséan		Bl.		IGCP, 1982
Poland						
18	Lublin	Viséan	1	Bl.	2.00	IGCP, 1982
7						
Ukraine						
19	Lvov-Volyn	Viséan	36	Bl.	1.10/0.70	IGCP, 1982
20	Dnepr-Donets	Viséan/ Serpukhovian	50	Bl.	1.90–2.50/ 0.50–0.60	IGCP, 1982; several coal fields
21	Donets	Viséan/ Serpukhovian	19	Bl.	0.75–1.75/ 0.60–1.25	IGCP, 1982; several coal fields
Byelorussia						
22	Pripyat	Viséan/ Serpukhovian	16	Bl.	1.80–3.80/ 0.60–0.70	IGCP, 1982; several coal fields
Russia						
23	Moscow Basin	Viséan	24	Br./Bl.	0.70–8.00/ 0.30–2.20	IGCP, 1982; Belskaya et al., 1975; 8 separate fields
24	Kizel	Viséan	19–29	Bl.	5.00/1.0–2.0	IGCP, 1982
25	Kama	Viséan	8	Bl./Br.	24.40/15.0	IGCP, 1982
26	Orenburg	Tournaisian	50	Bl.	5.00/2.50	IGCP, 1982
27	Egorshino-Kamenskyi	Viséan	32	Bl.	14.00/	IGCP, 1982
28	Poltava-Bredy	Tournaisian	40	Bl.	10.00/5.50	IGCP, 1982
34	Novosibirsk	Serpukhovian	1	Bl.	0.15/	IGCP, 1982
35	Kuznets	Tournaisian/ Serpukovian	8	Bl.	4.80/	IGCP, 1982
36	Minusinsk	Serpukhovian	17	Bl.	3.40/	IGCP, 1982
Kazakstan						
29	Tselinograd	Viséan	2	Bl.	2.00/0.80	IGCP, 1982
30A	Yablonov	Viséan	2	Bl.	2.20/1.60	IGCP, 1982
30B	Koksengir	Viséan	1	Bl.	3.50	IGCP, 1982
31A	Zavyalov-Skoye	Viséan	23	Bl.	1.70/1.05	IGCP, 1982
31B	Samarskoye	Viséan	15	Bl.	1.10/0.85	IGCP, 1982
32	Karaganda	Viséan	22	Bl.	3.80/3.00	IGCP, 1982
33	Ekibastuz	Viséan	1	Bl.	9.00/	IGCP, 1982
China						
37	Tarim					Yang, 1986
38	South Qilian	Datangian/ Dewvian[3]				Yang, 1986
39	West Sichuan/ North Xizang	Datangian/ Dewvian[3]				Yang, 1986

[1] See Fig. 10.
[2] Bit. = bituminous; Anthra. = anthracite; Meta-anthra. = meta-anthracite; Subbit. = subbituminous; Bl. = black (rank identification according to IGCP, 1982); Br. = brown (rank identification according to IGCP, 1982).
[3] = Viséan/Serpukovian.

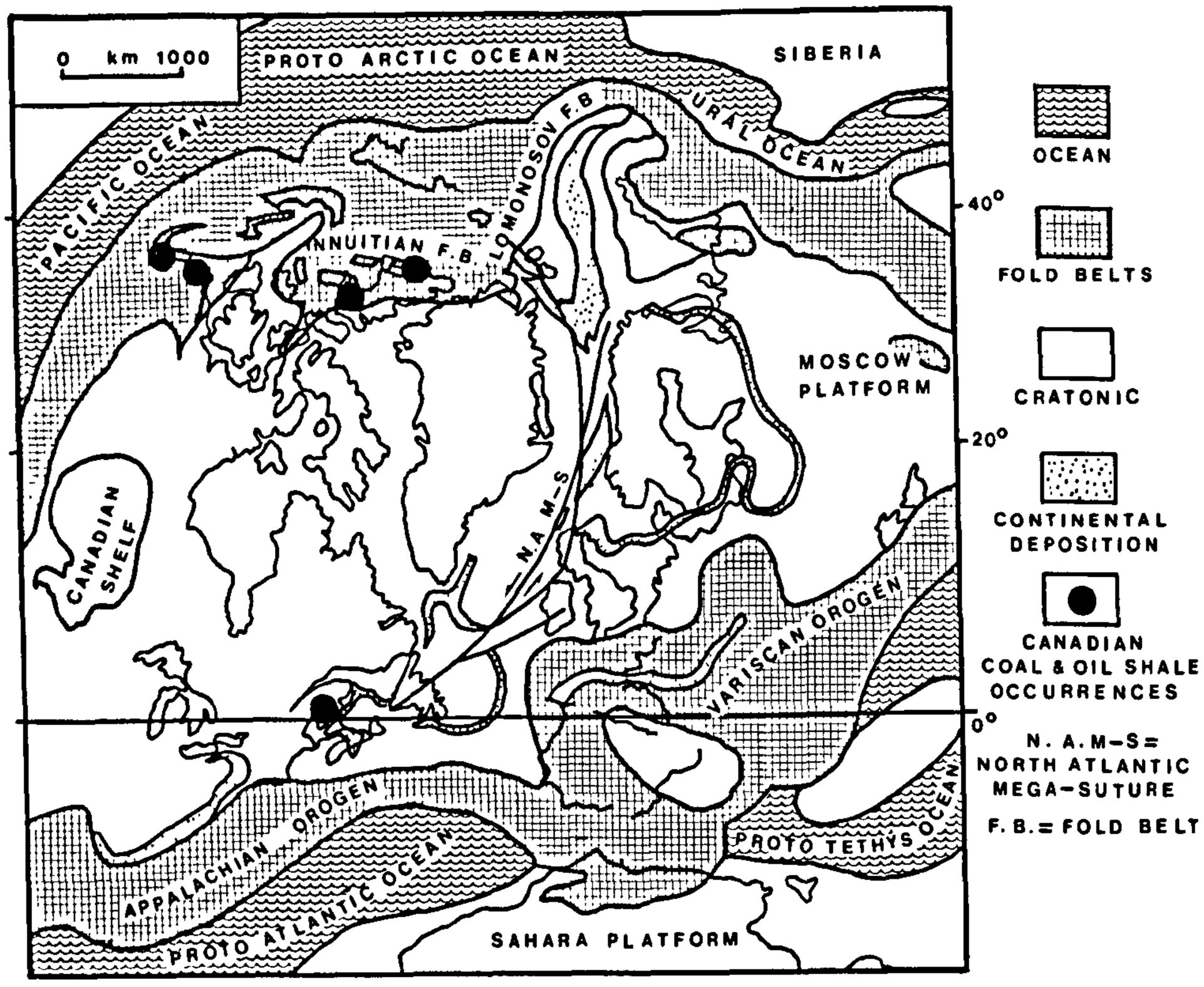

Fig. 11. Paleogeographic reconstruction of Laurussia during Viséan time (modified from P.A. Ziegler, 1989).

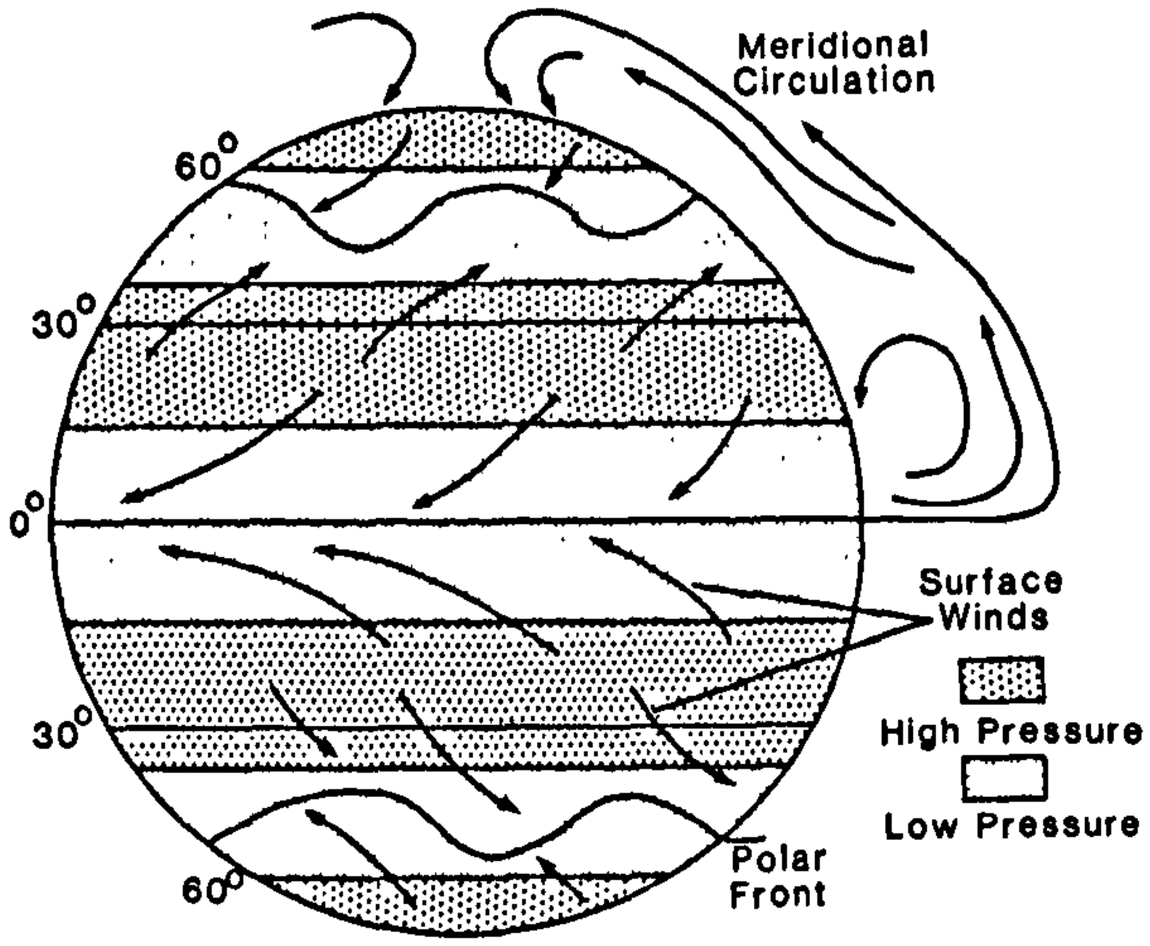

Fig. 12. Idealized global distribution of zones of low and high atmospheric pressure and direction of surface winds (from J.R. Parrish, 1982; copyright American Association of Petroleum Geologists, by permission; also in J.T. Parrish and Barron, 1986).

(1985) who suggested a more humid climate for the Mattson, based on statistical analysis of palynological data.

The "dry" zone of the Rowley et al. (1985) model extends into the area of the Arctic Archipelago where the Emma Fiord sediments were being deposited. This interpretation is somewhat at variance with that of Davies and Nassichuk (1988), who suggested moderate rainfall, though possibly seasonal. Their interpretation was based, at least in part, on a paleogeographic reconstruction by Tarling (1985). This model suggested a location for the Sverdrup basin within 10–15° of the equator during Early Carboniferous times.

There is another view that merits consideration in attempting explanations for anomalies such as discussed above. Because of the northward drift of Laurussia, geographic areas that were in the equatorial zone during early Viséan times may, by late Viséan times, have drifted into a drier climatic zone. The effect of this drift on the distribution of

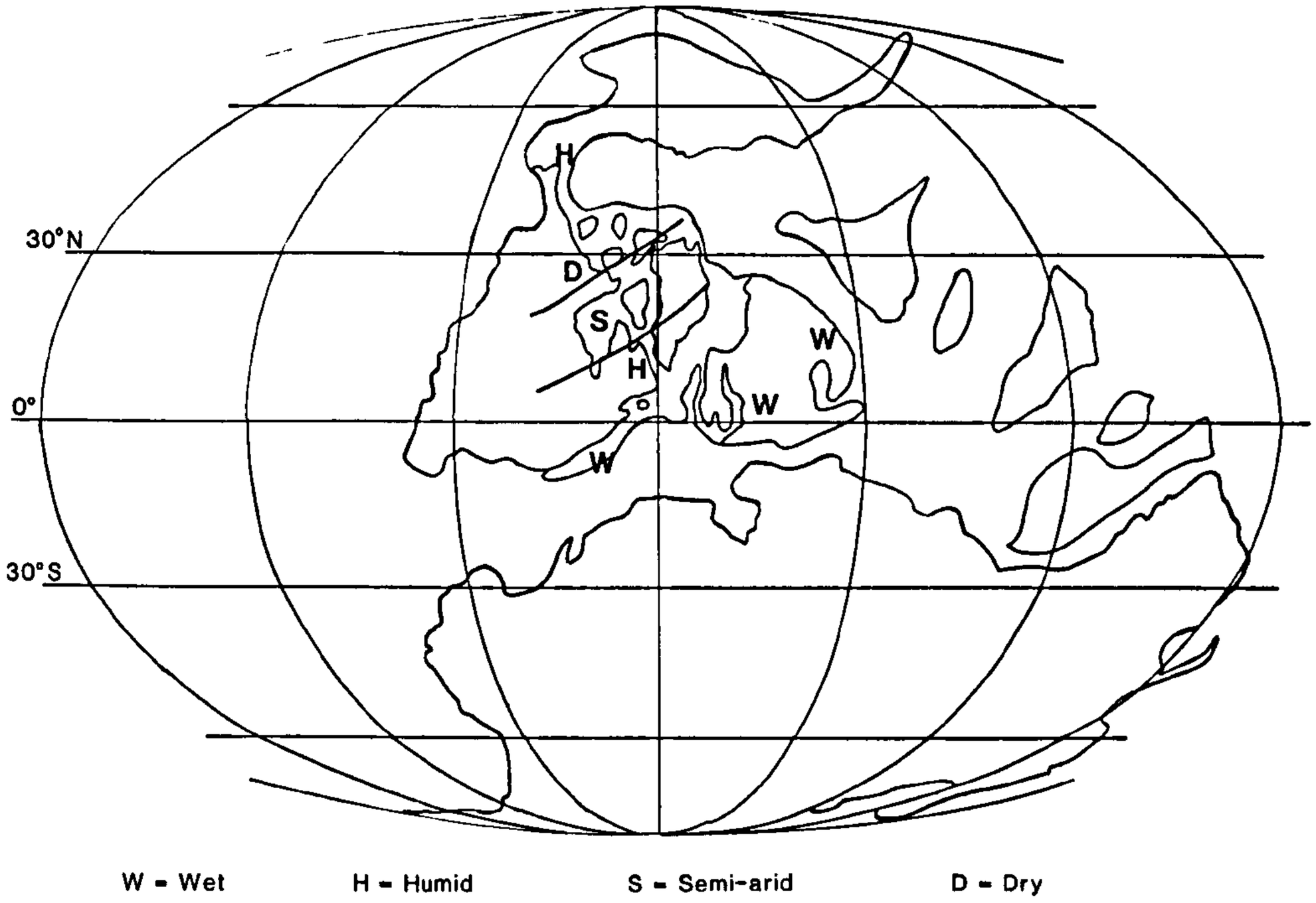

Fig. 13. Paleogeographic reconstruction and rainfall pattern for Viséan times (from Rowley et al., 1985).

fossil fauna and flora has been pointed out by Bless et al. (1987). Cecil (1990) demonstrated that it could be used to explain the distribution of Carboniferous coal beds in the eastern United States. Long-term climate cycles may also have been important as shown by Kelley et al. (1990).

The various reconstruction models involving paleogeography, temperature and rainfall lead to contradictory interpretations regarding the formation of coals and oil shales in northern Canada. Clearly there is some interesting research to be done. It may not always be necessary to have tropically wet climates for the formation of coals. What is more important is that the preservation of organic matter exceed decay (Schopf, 1973). However, a certain minimum amount of moisture is necessary to promote plant growth and, in mires, to preserve this plant material after its death.

Acknowledgement

This is Geological Survey of Canada Contribution no. 44392.

References

American Society for Testing and Materials (ASTM), 1981. Annual Book of ASTM Standards. Part 26. ASTM, Philadelphia, PA.

Bamber, E.W. and Waterhouse, J.B., 1971. Carboniferous and Permian stratigraphy, northern Yukon Territory, Canada. Bull. Can. Pet. Geol., 19(1): 29–250.

Baumann, L. and Vulpins, R., 1991. Die Lagerstätten fester mineralischer Rohstoffe in den neuen Bundesländern. Glückauf Forschungsh., 52: 53–82.

Belskaya, T.N., Ilkhovsky, R.A., Ivanova, E.A., Maklina, M.K., Maslennikov, V.R., Mikailova, E.V., Osipova, A.I., Reitlinger, E.A., Shik, E.M, Shik, S.M. and Yablokov, V.S., 1975. Field excursion guidebook for the Carboniferous sections of the Moscow Basin. Proc. 7th Int. Congr. on Carboniferous Stratigraphy and Geology, pp. 75–120.

Bless, M.J., Bouckaert, J. and Paproth, E., 1987. Fossil assemblages and depositional environments: Limits to stratigraphical correlations, In: J. Miller, A.E. Adams and V.P. Wright (Editors), European Dinantian Environments. Wiley, New York, NY, pp. 61–73.

Braman, D.R. and Hills, L.V., 1977. Palynology and paleoecology of the Mattson Formation, northwest Canada. Bull. Can. Pet. Geol., 245: 582–630.

Cameron, A.R., Norris, D.K. and Pratt, K.C., 1986. Rank and other compositional data on coals and carbonaceous shales of the Kayak Formation, northern Yukon Territory. In:

Current Research, Part B. Geol. Surv. Can. Pap., 86-1B: 665–670.

Cameron, A.R., Boonstra, C. and Pratt, K.C., 1988. Compositional characteristics of anthracitic coals in the Hoidahl Dome area, northern Yukon Territory. In: Current Research, Part D. Geol. Surv. Can., Pap. 88-1D: 67–74.

Cecil, C.B., 1990. Paleoclimate controls on stratigraphic repetition of chemical and siliciclastic rocks. Geology, 18: 533–536.

Creaney, S., 1980. The organic petrology of the Upper Cretaceous Boundary Creek Formation, Beaufort–Mackenzie Basin. Bull Can. Pet. Geol., 28: 112–129.

Cutbill, J.L., Henderson, W.G. and Wright, N.J.R., 1976. The Billefjorden Group (Early Carboniferous) of Central Spitzbergen. Nor. Polarinst. Skr., 164: 67–89.

Davies, G.R. and Nassichuk, W.W., 1988. An Early Carboniferous (Viséan) lacustrine oil shale in Canadian Arctic Archipelago. Bull. Am. Assoc. Pet. Geol., 72(1): 8–20.

Davies, G.R., Richards, B.C., Beauchamp, B. and Nassichuk, W.W., 1989. Carboniferous and Permian reefs in Canada and adjacent areas. In: H.H.J. Geldsetzer, N.P. James and G.E. Tebbutt (Editors). Can. Soc. Pet. Geol. Mem., 13: 565–574.

Davis, A., 1978. The reflectance of coal. In: C. Karr (Editor), Analytical Methods for Coal and Coal Products. Academic Press, New York, NY, 1, pp. 27–81.

Douglas, R.J.W. and Norris, D.K., 1959. Fort Liard and La Biche map-areas, Northwest Territories and Yukon, 95B and 95C. Geol. Surv. Can. Pap., 59-6, 23 pp.

Englund, K.J., 1979. The Mississippian and Pennsylvanian (Carboniferous) systems in the United States—Virginia. U.S. Geol. Surv. Prof. Pap., 1110-C: C1–C21.

Espitalié, J., Laporte, J.L., Madec, M., Marguis, F., Leplat, P., Paulet, J. and Boutefeu, A., 1977. Méthode rapide de charactérisation des roches mères de leur potentiel pétrolier et de leur degré d'évolution. Rev. Inst. Fr. Pét., 32: 23–42.

Frebold, H., 1932. Geologie der JuraKohleu des nördlichen ostgrönland. Medd. Grønl., 84(5), 65 pp.

Goodarzi, F., Nassichuk, W.W., Snowdon, L.R. and Davies, G.R., 1987. Organic petrology and Rock-Eval analysis of the Lower Carboniferous Emma Fiord Formation in the Sverdrup Basin, Canadian Arctic Archipelago. Mar. Pet. Geol., 4: 132–145.

Hacquebard, P.A. and Barss, M.S., 1957. A Carboniferous spore assemblage, in coal from the South Nahanni River area, Northwest Territories. Geol. Surv. Can. Bull., 40, 63 pp.

Harker, P., 1961. Summary account of Carboniferous and Permian formations, southwestern district of Mackenzie. Geol. Surv. Can. Pap., 61-1, 9 pp.

Harland, W.B., Pickton, C.A.G. and Wright, N.J.R., 1976. Some coal-bearing strata in Svalbard. Nor. Polarinst. Skr., 164: 7–28.

IGCP (International Geological Correlation Program), 1982. World Coalfields (IGCP 166). Rijks Geologische Dienst, Haarlem.

Kelley, P.H., Raymond, A. and Lutken, C.B., 1990. Carboniferous brachiopod migration and latitudinal diversity: a new paleoclimatic method. In: W.S. McKerrow and C.R. Scotese (Editors), Palaeozoic Palaeogeography and Biogeography. Geol. Soc. London Mem., 12: 325–332.

Keppie, J.D., 1977. Plate tectonic interpretation of Paleozoic world maps (with emphasis on circum-Atlantic orogens and southern Nova Scotia). N. S. Dep. Mines Pap., 77–3, 45 pp.

Lyons, P.C., Finkelman, R.B. Thompson, C.L., Brown, F.W. and Hatcher, P.G., 1982. Properties, origin and nomenclature of rodlets of the inertinite maceral group in coals of the central Appalachian basin, U.S.A. Int. J. Coal Geol., 1: 313–346.

Macauley, G., Ball, F.D. and Powell, T.G., 1984. A review of the Carboniferous Albert Formation oil shales, New Brunswick. Bull. Can. Pet. Geol., 32(1): 27–37.

Magoon, L.B. and Bird, K.V., 1988. Evaluation of petroleum source rocks in the National Petroleum Reserve in Alaska, using organic-carbon content, hydrocarbon content, visual kerogen and vitrinite reflectance. In: G. Gryc (Editor), Geology and Exploration of the National Petroleum Reserve in Alaska, 1974 to 1982. U.S. Geol. Surv. Prof. Pap., 1399: 381–450.

Melvin, J., 1987. Fluvio-paludal deposits in the Kekiktuk Formation (Mississippian), Endicott Field, northeast Alaska. In: F.G. Ethridge, R.M. Flores and M.D. Harvey (Editors), Recent Developments in Fluvial Sedimentology. Soc. Econ. Paleontol. Mineral. Spec. Publ., 39: 343–352.

Milici, R.C., Briggs, G., Knox, L.M., Sitterly, P.D. and Statler, A.T., 1979. The Mississippian and Pennsylvanian (Carboniferous) systems in the United States—Tennessee. U.S. Geol. Surv. Prof. Pap.., 1110-G: G1–G38.

Misra, B.K., Singh, B.D. and Navale, G.K.B., 1990. Resino-inertinites of Indian Permian coals—their origin, genesis and classification. Int. J. Coal Geol., 14(4): 277–293.

Parrish, J.R., 1982. Upwelling and petroleum source rocks, with reference to Paleozoic. Bull. Am. Assoc. Pet. Geol., 66: 750–774.

Parrish, J.T. and Barron, E.J., 1986. Paleoclimates and economic geology. Soc. Econ. Paleontol. Mineral., Lect. Notes Short Course 18, 162 pp.

Patton, W.J.H., 1958. Mississippian succession in South Nahanni River area, Northwest Territories. In: A.J. Goodman (Editor), Jurassic and Carboniferous of Western Canada (Allan Memorial Vol.). Am. Assoc. Pet. Geol., Washington, pp. 309–326.

Playford, G. and Barss, M.S., 1963. Upper Mississippian microflora from Axel Heiberg Island, District of Franklin. Geol. Surv. Can. Pap., 62-36, 5 pp.

Potter, J., Richards, B.C. and Cameron, A.R., 1993. The petrology and origin of coals from the Lower Carboniferous Mattson Formation, southwestern District of Mackenzie, Canada. Int. J. Coal Geol., 24.

Ravn, R.L., 1991. Miospores of the Kekiktuk Formation (Lower Carboniferous), Endicott Field Area, Alaska North Slope. Am. Assoc. Stratigr. Palynol. Found. Contrib. Ser., 27, 173 pp.

Richards, B.C., 1989. Uppermost Devonian and Lower Carboniferous stratigraphy, sedimentation and diagenesis, southwestern District of Mackenzie and southeastern Yukon Territory, Geol. Surv. Can. Bull., 390, 135 pp.

Richards, B.C., Bamber, E.W., Higgins, A.C. and Utting, J., 1993. Carboniferous. In: D.F. Stott and J.D. Aitken

(Editors), Sedimentary Cover of the Craton in Canada. Geol. Surv. Can., Spec. Publ., 5 (also in: The Geology of North America. Geol. Soc. Am., Vol. D-1), pp. 202–271.

Rowley, D.B., Raymond, A., Parrish, J.T., Lottes, A.L., Scotese, C.R. and Ziegler, A.M., 1985. Carboniferous paleogeographic phytogeographic and paleoclimate reconstructions. Int. J. Coal Geol., 5: 7–42.

Schiener, E.J., 1976. Coal geology. In: A. Escher and W.S. Watt (Editors), Geology of Greenland. Geol. Surv. Greenland, pp. 507–516.

Schopf, J.M., 1973. Coal, climate and global tectonics. In: D.J. Tarling and S.K. Runcorn (Editors), Implications of Continental Drift to the Earth Sciences. Academic Press, London, I, pp. 609–622.

Scotese, C.R., Bambach, K.R., van der Voo, R. and Ziegler, A.M., 1979. Paleozoic basemaps. J. Geol., 87: 217–277.

Scotese, C.R. and McKerrow, W.S., 1990. Revised world maps and introduction. In: W.S. McKerrow and C.R. Scotese (Editors), Palaeozoic Palaeogeography and Biogeography. Geol. Soc. London Mem., 12: 1–21.

Tarling, D.H., 1985. Carboniferous reconstruction based on paleomagnetism. Proc. 10th Int. Congr. on Carboniferous Stratigraphy and Geology, 4: 153–162.

Thomas, W.A. and Cramer, H.R., 1979. The Mississippian and Pennsylvanian (Carboniferous) systems in the United States—Georgia. U.S. Geol. Surv. Prof. Pap., 1110-H: H1–H37.

Thorsteinsson, R., 1974. Carboniferous and Permian stratigraphy of Axel Heiberg Island and western Ellesmere Island, Canadian Arctic Archipelago. Geol. Surv. Can. Bull., 224, 115 pp.

Utting, J., 1991. Lower Carboniferous miospore assemblages from the Hart River Formation, northern Yukon Territory. Contrib. Can. Paleontol. Geol. Surv. Can. Bull., 412: 81–99.

Van der Zwan, C.J., Boulter, M.C. and Hubbard, R.N.L.B., 1985. Climatic change during the Lower Carboniferous in Euramerica, based on multivariate statistical analysis of palynological data. Palaeogeogr., Palaeoclimatol., Palaeoecol., 52: 1–20.

Witzke, B.J., 1990. Palaeoclimatic constraints for Palaeozoic Palaeolatitudes of Laurentia and Euramerica. In: W.S. McKerrow and C.R. Scotese (Editors), Palaeozoic Palaeogeography and Biogeography. Geol. Soc. London Mem., 12: 57–73.

Yang, Z., 1986. The Carboniferous system. In: The Geology of China. Clarendon Press, Oxford, pp. 102–112.

Ziegler, A.M., Bambach, R.K., Parrish, J.T., Barrett, S.F., Gierlowski, E.H., Parker, W.C., Raymond, A. and Sepkoski, J.J., 1981. Paleozoic biogeography and climatology. In: K.J. Niklas (Editor), Paleobotany, Paleoecology and Evolution (Praeger Spec. Stud., 2). Praeger, 2, pp. 230–266.

Ziegler, A.M., Scotese, C.R., McKerrow, W.S., Johnson, M.E. and Bambach, R.K., 1977. Paleozoic biogeography of continents bordering the Iapetus (Pre-Caledonian) and Rheic (Pre-Hercynian) Oceans. In: R.M. West (Editor), Paleontology and Plate Tectonics. Milwaukee Publ. Mus., Spec. Publ. Biol.–Geol., 2: 1–22.

Ziegler, A.M., Scotese, C.R., McKerrow, W.S., Johnson, M.E. and Bambach, R.K., 1979. Paleozoic biogeography. Annu. Rev. Earth Planet. Sci., 7: 473–502.

Ziegler, P.A., 1989. Evolution of Laurussia—a Study of Late Paleozoic Plate Tectonics. Kluwer, Dordrecht, 102 pp.

(continued from inside front cover)

Note to contributors

A detailed *Guide for Authors* is available upon request, and will also be printed in the first issue to appear each year. You are kindly asked to consult this guide. Please pay special attention to the following notes:

Preparation of the text

a) The manuscript should be typewritten with double spacing and wide margins and include at the beginning of the paper an abstract of not more than 500 words. Words to be printed in italics should be underlined. The metric system should be used throughout.
b) The title page should include, the title, the name(s) of the author(s) and their affiliations.

References

a) References in the text start with the name of the author(s), followed by the publication date in brackets.
b) The reference list should be in alphabetical order and on sheets separate from the text.

Tables

Tables should be compiled on separate sheets. A title should be provided for each table and they should be referred to in the text.

Illustrations

a) All illustrations should be numbered consecutively and referred to in the text.
b) Drawings should be completely lettered, the size of the lettering being appropriate to that of the drawings, but taking into account the possible need for reduction in size (preferably not more than 50%). The page format of *Palaeogeography, Palaeoclimatology, Palaeoecology* should be considered in designing the drawings.
c) Photographs must be of good quality, printed on glossy paper.
d) Figure captions should be supplied on a separate sheet.

Proofs

One set of proofs will be sent to the author, to be checked for printer's errors. In case of two or more authors please indicate to whom the proofs should be sent.

Reprints

Fifty reprints of each article published are supplied free of charge. Additional reprints can be ordered on a reprint order form, which will be sent to the first author upon receipt of the accepted article by the publisher.

Submission of manuscripts

Authors are requested to submit, with their manuscripts, the names and addresses of *four* potential referees.
All manuscripts should be sent in triplicate to: Editorial Office *Palaeogeography, Palaeoclimatology, Palaeoecology*, P.O. Box 1930, 1000 BX Amsterdam, The Netherlands. Illustrations should also be submitted in triplicate. One set should be in a form ready for reproduction: the other two may be of lower quality. The FAX number for the Amsterdam office is: 020-5862696.

Submission of electronic text

In order to publish the paper as quickly as possible after acceptance, authors are encouraged to submit the final text also on a 3.5" or 5.25" diskette. Both double density (DD) and high density (HD) diskettes are acceptable. Make sure, however, that the diskettes are formatted according to their capacity (HD or DD) before copying the files onto them. Similar to the requirements for manuscript submission, main text, list of references, tables and figure legends should be stored in separate text files with clearly identifiable file names. The format of these files depends on the word processor used. Texts made with DisplayWrite, MultiMate, Microsoft Word, Samna Word, Sprint, Volkswriter, Wang PC, WordMARC, WordPerfect, Wordstar, or supplied in DCA/RFT, or DEC/DX format can be readily processed. In all other cases the preferred format is DOS text or ASCII. Essential is that the name and version of the wordprocessing program, type of computer on which the text was prepared, and format of the text files are clearly indicated. Authors are encouraged to ensure that **the disk version and the hardcopy must be identical.** Discrepancies can lead to proofs of the wrong version being made.

Submission of an article is understood to imply that the article is original and unpublished and is not being considered for publication elsewhere.
Upon acceptance of an article by the journal, the author(s) resident in the U.S.A. will be asked to transfer the copyright of the article to the publisher. This transfer will ensure the widest possible dissemination of information under the U.S. Copyright Law.

0031-0182/94/$07.00

This issue is printed on acid-free paper.

PRINTED IN THE NETHERLANDS

BULLETIN OF CANADIAN PETROLEUM GEOLOGY
VOL. 41, NO. 1 (MARCH, 1993) P. 17-31

Paleozoic burial and organic maturation in the Liard Basin Region, northern Canada

D.W. MORROW, J. POTTER, B. RICHARDS, AND F. GOODARZI
Institute of Sedimentary and Petroleum Geology
3303 - 33rd Street N.W.
Calgary, Alberta T2L 2A7

ABSTRACT

The vitrinite reflectances (R_o%) of well cuttings from two wells from the Liard Basin increase downsection from low values of about 0.30% at the top of the Carboniferous Mattson Formation up to values of about 4.50% at the top of the Devonian Nahanni Formation. Simulations of these coalification profiles indicate that geothermal gradients and heat flows were probably higher in the Paleozoic than at present and may have been as high as 65° C/km and 135 mW/m^2 respectively. The low level of organic maturity of Paleozoic strata at the top of the well sequences and their outcrop equivalents indicate that little post-Paleozoic burial occurred and that post- Paleozoic geothermal gradients and heat flows could not have been greater than their present day values of 38 °C/km and 85 mW/m^2 respectively.

Maturation and migration of oil and gas probably occurred in the Liard Basin during late Paleozoic to early Mesozoic even if low average Paleozoic geothermal gradients and heat flows are assumed. This indicates that the Manetoe Facies dolomite, which forms the reservoir rock for the Liard Basin gas fields, formed before the Cretaceous.

RÉSUMÉ

La réflectance de la vitrinite (R_o%) dans des débris de forage prélevés pour deux puits dans le bassin Liard augmente avec la profondeur depuis des valeurs d'à peu près 0,30% au sommet de la formation Mattson carbonifère jusqu'à approximativement 4,50% au sommet de la formation Nahanni dévonienne. Des simulations de ces profils de houillification indiquent que les gradients géothermiques et les flux de chaleur étaient probablement plus élevés durant le Paléozoïque qu'à présent, et auraient pu être aussi élevés que 65°C/km et 135 mW/m^2 respectivement. Le faible taux de maturité organique des strates paléozoïques qui recouvrent ces séquences dans les puits et leurs équivalents en affleurement indique que peu d'enfouissement post-paléozoïque eut lieu et que les gradients géothermiques et les flux de chaleur post-paléozoïques n'ont pas pu être plus importants que les valeurs actuelles de 38°C/km et 85 mW/m^2 respectivement.

La maturation et la migration d'huile et de gaz dans le bassin Liard eut probablement lieu durant l'intervalle allant du Paléozoïque supérieur au Mésozoïque inférieur, même si de faibles gradients géothermiques et flux de chaleur moyens sont présumés. Ceci indique que la dolomie du faciès Manetoe, qui est la roche réservoir dans les champs de gaz du bassin Liard, se forma avant le Crétacé.

Traduit par Patrice de Caritat

INTRODUCTION

The Liard Basin (Fig. 1), in southeastern Yukon Territory and northeastern British Columbia, was defined on the basis of its anomalously thick upper Paleozoic sedimentary fill which is widely exposed throughout this region (Gabrielse, 1967). Petroleum exploration in this basin has been focussed on the Middle Devonian carbonate reservoirs that are buried beneath this thick, siliciclastic and organic-rich upper Paleozic sequence.

West of Liard River, in the Liard Basin, are Canada's northernmost producing gas fields: the Beaver River, Kotaneelee and Pointed Mountain fields (Fig. 1). These fields are developed in white, coarsely crystalline dolomite of the Manetoe Facies (Morrow *et al.*, 1986). They were estimated to have potential reserves of several trillion cubic feet in place (de Wit *et al.*, 1973; Snowdon, 1977). The Manetoe Facies has continued to be a target for hydrocarbon exploration in Liard Basin in the extreme southeastern corner of the Yukon Territory and in northeastern British Columbia. There is little available information, however, concerning the source and maturation history of hydrocarbons in these gas fields.

The purpose of the present study is to investigate the thermal and burial histories of the Liard Basin region through the examination of organic constituents from continuous well sections. The level of vitrinite reflectance (R_o%), in particular, indicates the present day level of organic maturity of strata in Liard Basin. Quantitative modelling of vitrinite reflectance can also be used to help unravel the thermal and maturation histories of this area (*e.g.*, Bustin, 1989; Waples, 1980; Sweeney and Burnham, 1990). This can provide an estimate of when generation of oil and gas phase hydrocarbons may have occurred and provide information concerning the most

probable time for migration of hydrocarbons from their source rocks into reservoirs (Waples, 1980).

Data and interpretations concerning organic maturation in the Liard Basin also have a direct bearing on the question of the time of origin of the porous reservoir rock that is the host for these gas fields. The reservoir rock is a white, coarsely crystalline dolomite, termed the Manetoe Facies (Morrow *et al.*, 1986), which has replaced limestones of the Nahanni Formation and other underlying Devonian carbonates (Fig. 3). This dolomite has higher porosity and permeability than the surrounding limestones (Snowdon, 1977). Consequently, the age of the dolomitization event that formed the reservoir rock (*i.e.*, Manetoe Facies) imposes a limitation on the time of entrapment of hydrocarbons based upon the assumption that dolomitization preceded hydrocarbon migration. Cretaceous-Tertiary dolomitization would require a post-Cretaceous time for hydrocarbon migration into Manetoe reservoirs. Conversely, an interpretation of maturation and migration of hydrocarbons in the pre-Cretaceous would imply pre-Cretaceous origin for the Manetoe Facies dolomite.

Aulstead *et al.* (1988), based on fluid inclusion and oxygen isotope determinations, suggested that the Manetoe Facies was formed by precipitation from heated (150° to 200° C) subsurface connate solutions at shallow depths before the end of Devonian time. Spencer (1987) and Aulstead and Spencer (1985) further suggested that these solutions were residual brines derived from the continual evaporation of seawater which occupied the Elk Point Basin in the Devonian (see Bebout and Maiklem, 1973). Spencer (1987) suggested that these dense brines sank to great depths in the subsurface and were recirculated by geothermal heating to very shallow subsurface depths of less than a kilometre and dolomitized Devonian limestones, such as the Nahanni Formation.

Other authors have suggested different scenarios for the origin of coarsely crystalline or saddle dolomites of western Canada. Qing and Mountjoy (1989), in a study of dolomite in the Devonian, Rainbow reefs of northwestern Canada, suggested that the coarsely crystalline saddle dolomites in these reservoirs were probably precipitated from subsurface fluids during the Columbian and Laramide orogenies in the Cretaceous to Tertiary (see also Machel and Mountjoy, 1987). Other origins for the coarsely crystalline white saddle dolomites of western Canada are, of course, possible (Morrow *et al.*, 1986; Machel and Mountjoy, 1987) but the hypotheses of Devonian or Cretaceous-Tertiary dolomitization have been given the most serious consideration.

The maturity of palynomorphs, conodonts and vitrinite from outcrop samples in and around the Liard Basin (Fig. 2) indicate that Carboniferous strata range in maturation level from a vitrinite reflectance equivalent to about 0.50R_o% at the top of the Carboniferous (Mattson Fm.) to about 1.50R_o% near the base of Carboniferous strata (Banff Fm.). The underlying Devonian carbonates (Nahanni and sub-Nahanni) only 1000 to 1500 metres below the Banff Formation display a much higher level of organic maturation of about 3.0R_o% to 4.0R_o% (Fig. 3). Morrow *et al.* (1990) inferred that this abrupt post-Nahanni decrease in the level of organic maturity provided support for

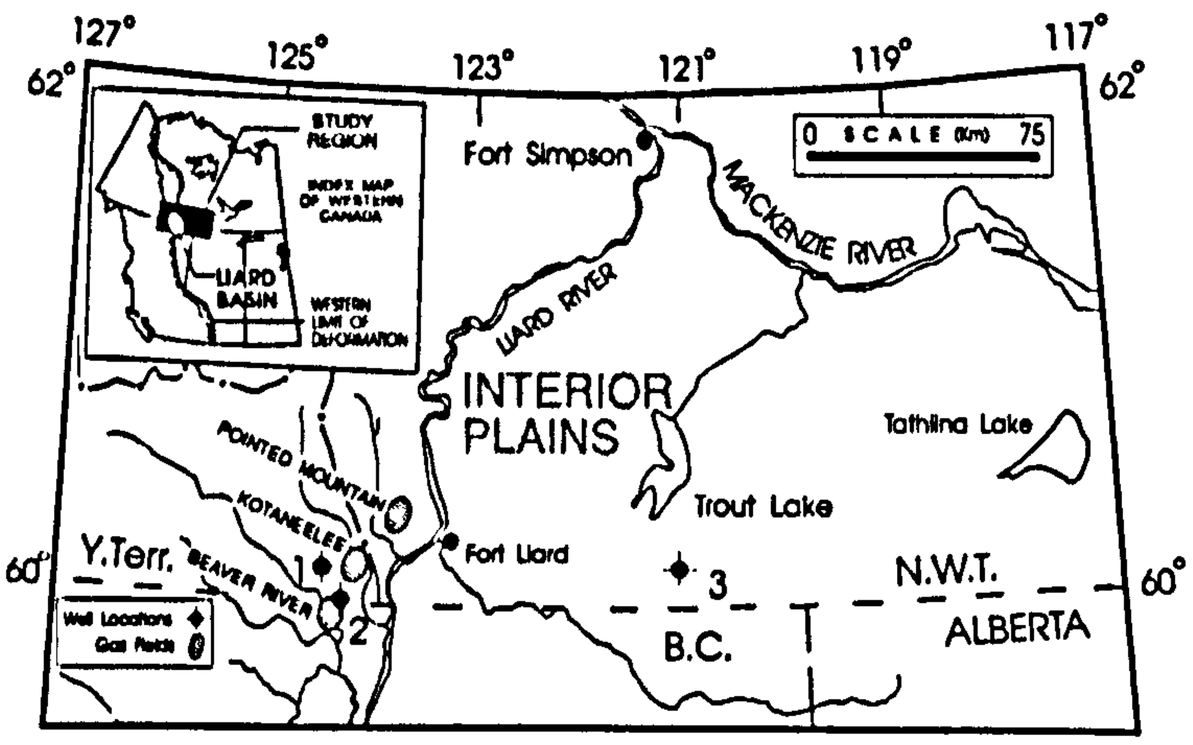

Fig. 1. Locality index map showing Liard Basin in southeastern-part of the Yukon Territory. Two of the wells examined, the Pan Am Kotaneelee O-67 (1-·at 61° 26′ 51″ N/124° 11′ 56″ W) and the Pan Am Beaver River YT G-01 (2- at 60° 00′ 25″ N/124° 15′ 48″ W) wells are in Liard Basin, whereas the third well, the Imperial Island River No. 1 well (3- at 60° 09′ 29″ N/121° 08′ 16″ W), is in the Interior Plains. Also shown are the gasfields of southeastern Yukon Territory including, from south to north, the Beaver River, the Kotaneelee and the Pointed Mountain fields.

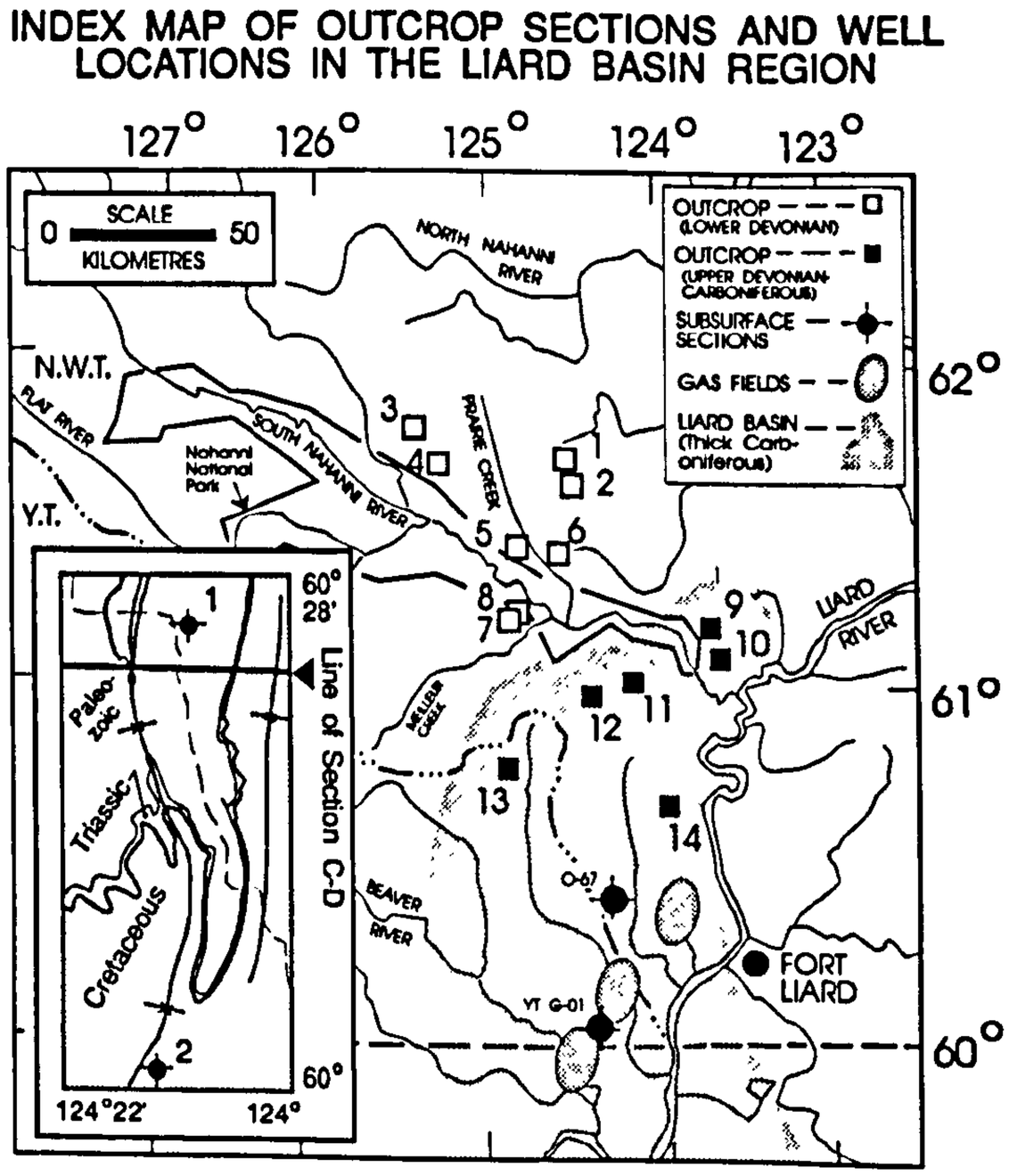

Fig. 2. Index map of outcrop and well sections in Liard Basin.The shaded area represents the present limit of thick(>200 m) Carboniferous strata (Richards, 1989). The northern border of this area is also the preservational limit of Carboniferous strata. The inset diagram in the lower left part of the diagram is a geological map in the vicinity of the Pan Am Kotaneelee O-67 (1) and Pan Am Beaver River YT G-01 (2) wells. The Kotaneelee Syncline in the eastern part of this geologic map contains 700 m of Cretaceous strata along cross-section C-D (Douglas, 1976).

a Late-Devonian episode of anomalous heating of the Middle Devonian in the manner suggested by Spencer (1987).

Quantitative modelling of the level of organic maturation of stratigraphic sequences from this region has the potential to provide an independent means of evaluating hypotheses, such as those of Spencer (1987) and Qing and Mountjoy (1989), for the origin of the Manetoe Facies dolomites, in addition to determining the time of hydrocarbon maturation and migration. Solitary determinations of organic maturity from many disparate outcrop localities (Fig. 2), while provocative, are not adequate for thermal modelling of organic maturity of thick sequences in a restricted area. Sampling of well cuttings provide the only means of acquiring stratigraphically continuous maturation data at individual localities in the Liard Basin region that are suitable for this purpose.

Methods

The optical reflectance of vitrinite in well cuttings from three wells have been analyzed (Table 1). Two of these wells (Pan Am Beaver River YT G-01 and Pan Am Kotaneelee O-67) are in Liard Basin and the third well (Imperial Island River No. 1) is located in the Interior Plains east of the Liard Basin (Fig. 1). This provided a comparison between coalification profiles from the Interior Plains Region where the upper Paleozoic sequence is thin, and those of the thicker upper Paleozoic Liard Basin sequences.

Reflected light intensity measurements of organic materials were performed on a Zeiss MPM II microscope fitted with white (halogen) and blue-violet light sources, using an Epiplan-Neofluor oil immersion objective (N.A. 0.90 × 40), following procedures outlined by Bustin (1989). Samples were prepared for reflectance measurements according to ASTM procedures (1981).

Measurements of vitrinite reflectance were obtained from well cuttings selected from darker, organic-rich shaly and coalbearing intervals. All measurements were made from dispersed vitrinite in well cuttings (Fig. 4). The small sample size afforded by well cuttings precluded the acquisition of a statistically uniform data base and the simple arithmetic means of these data for each sample were used to represent the true mean values without regard for the possible influence of sampling error on mean reflectance values. However, the use of well cuttings is the only practical means available to obtain the continuous profiles of vitrinite reflectance that are necessary for determining thermal histories.

Only some vitrinite-like macerals could be identified unequivocally as vitrinite on the basis of relict cellular morphology or by direct association with inertinite (Fig. 4). However, the consistent relationship between the reflectances of bitumen and of the vitrinite-like macerals (with the reflectance of the vitrinite-like material being slightly greater than bitumen reflectance at any given stratigraphic level in both the Beaver River YT G-01 and Imperial Island River No. 1 wells) supports the inference that the vitrinite-like material is truly vitrinite. Bitumen in these samples is commonly recognizable by its tendency to fill intergranular and intercrystalline pore space in irregular networks parallel to bedding (Fig. 4). Bitumen reflectances were also systematically measured and recorded, but are not reported here, as was reworked vitrinite.

Additional verification of the levels of organic maturation was provided by Rock-Eval analyses of well cutting samples

Table 1. Reflectivity of vitrinite in the Imperial Island River No. 1 and Beaver River YT G-01 Wells.

Imperial Island No. 1				Beaver River YT G-01			
Feet	Metres[1]	Ro%	Range of Values[2]	Feet	Metres[1]	Ro%	Range of Values[2]
1994	608	**0.58**	0.42 - 0.80	2860	872	**0.31**	0.26 - 0.35
2134	651	**0.72**	0.62 - 0.90	3220	982	**0.47**	0.38 - 0.56
2310	704	**0.76**	N/A	3470	1058	**0.55**	0.43 - 0.67
2747	838	**0.64**	0.55 - 0.85	4140	1262	**0.58**	0.49 - 0.63
2760	842	**0.61**	0.59 - 0.63	4400	1342	**0.70**	N/A
3275	999	**0.73**	0.62 - 0.85	4970	1515	**0.82**	N/A
3465	1,056	**0.68**	0.59 - 0.76	5840	1781	**0.76**	N/A
3482	1,062	**0.82**	0.62 - 0.90	6120	1866	**0.80**	0.63 - 0.90
3787	1,155	**0.89**	0.87 - 0.92	6560	2000	**1.27**	N/A
5409	1,649	**1.05**	0.99 - 1.22	8765	2672	**1.85**	1.51 - 2.27
5899	1,799	**1.13**	0.98 - 1.36	9220	2811	**2.00**	1.72 - 2.29
6240	1,902	**1.20**	1.18 - 1.32	9490	2893	**2.15**	1.72 - 250
6400	1,951	**1.28**	1.25 - 1.32	10184	3105	**2.41**	1.90 - 3.00
6814	2,077	**1.53**	1.30 - 1.68	10570	3223	**2.00**	1.72 - 2.29
7313	2,230	**2.00**	N/A	11630	3546	**3.50**	3.30 - 3.56
–	–	–	–	12020	3665	**3.91**	3.12 - 4.92
–	–	–	–	12270	3741	**3.70**	3.15 - 4.10
–	–	–	–	12670	3863	**4.30**	N/A
–	–	–	–	12970	3954	**4.60**	4.46 - 4.86
–	–	–	–	13190	4021	**4.20**	3.60 - 4.80
–	–	–	–	13364	4166	**4.18**	3.40 - 5.30

[1] – Depths below Kelly Bushing
[2] – Between 3 and 50 measurements per sample (average 10)
N/A means only a single measurement

probable time for migration of hydrocarbons from their source rocks into reservoirs (Waples, 1980).

Data and interpretations concerning organic maturation in the Liard Basin also have a direct bearing on the question of the time of origin of the porous reservoir rock that is the host for these gas fields. The reservoir rock is a white, coarsely crystalline dolomite, termed the Manetoe Facies (Morrow *et al.*, 1986), which has replaced limestones of the Nahanni Formation and other underlying Devonian carbonates (Fig. 3). This dolomite has higher porosity and permeability than the surrounding limestones (Snowdon, 1977). Consequently, the age of the dolomitization event that formed the reservoir rock (*i.e.*, Manetoe Facies) imposes a limitation on the time of entrapment of hydrocarbons based upon the assumption that dolomitization preceded hydrocarbon migration. Cretaceous-Tertiary dolomitization would require a post-Cretaceous time for hydrocarbon migration into Manetoe reservoirs. Conversely, an interpretation of maturation and migration of hydrocarbons in the pre-Cretaceous would imply pre-Cretaceous origin for the Manetoe Facies dolomite.

Aulstead *et al.* (1988), based on fluid inclusion and oxygen isotope determinations, suggested that the Manetoe Facies was formed by precipitation from heated (150° to 200° C) subsurface connate solutions at shallow depths before the end of Devonian time. Spencer (1987) and Aulstead and Spencer (1985) further suggested that these solutions were residual brines derived from the continual evaporation of seawater which occupied the Elk Point Basin in the Devonian (see Bebout and Maiklem, 1973). Spencer (1987) suggested that these dense brines sank to great depths in the subsurface and were recirculated by geothermal heating to very shallow subsurface depths of less than a kilometre and dolomitized Devonian limestones, such as the Nahanni Formation.

Other authors have suggested different scenarios for the origin of coarsely crystalline or saddle dolomites of western Canada. Qing and Mountjoy (1989), in a study of dolomite in the Devonian, Rainbow reefs of northwestern Canada, suggested that the coarsely crystalline saddle dolomites in these reservoirs were probably precipitated from subsurface fluids during the Columbian and Laramide orogenies in the Cretaceous to Tertiary (see also Machel and Mountjoy, 1987). Other origins for the coarsely crystalline white saddle dolomites of western Canada are, of course, possible (Morrow *et al.*, 1986; Machel and Mountjoy, 1987) but the hypotheses of Devonian or Cretaceous-Tertiary dolomitization have been given the most serious consideration.

The maturity of palynomorphs, conodonts and vitrinite from outcrop samples in and around the Liard Basin (Fig. 2) indicate that Carboniferous strata range in maturation level from a vitrinite reflectance equivalent to about 0.50R_o% at the top of the Carboniferous (Mattson Fm.) to about 1.50R_o% near the base of Carboniferous strata (Banff Fm.). The underlying Devonian carbonates (Nahanni and sub-Nahanni) only 1000 to 1500 metres below the Banff Formation display a much higher level of organic maturation of about 3.0R_o% to 4.0R_o% (Fig. 3). Morrow *et al.* (1990) inferred that this abrupt post-Nahanni decrease in the level of organic maturity provided support for

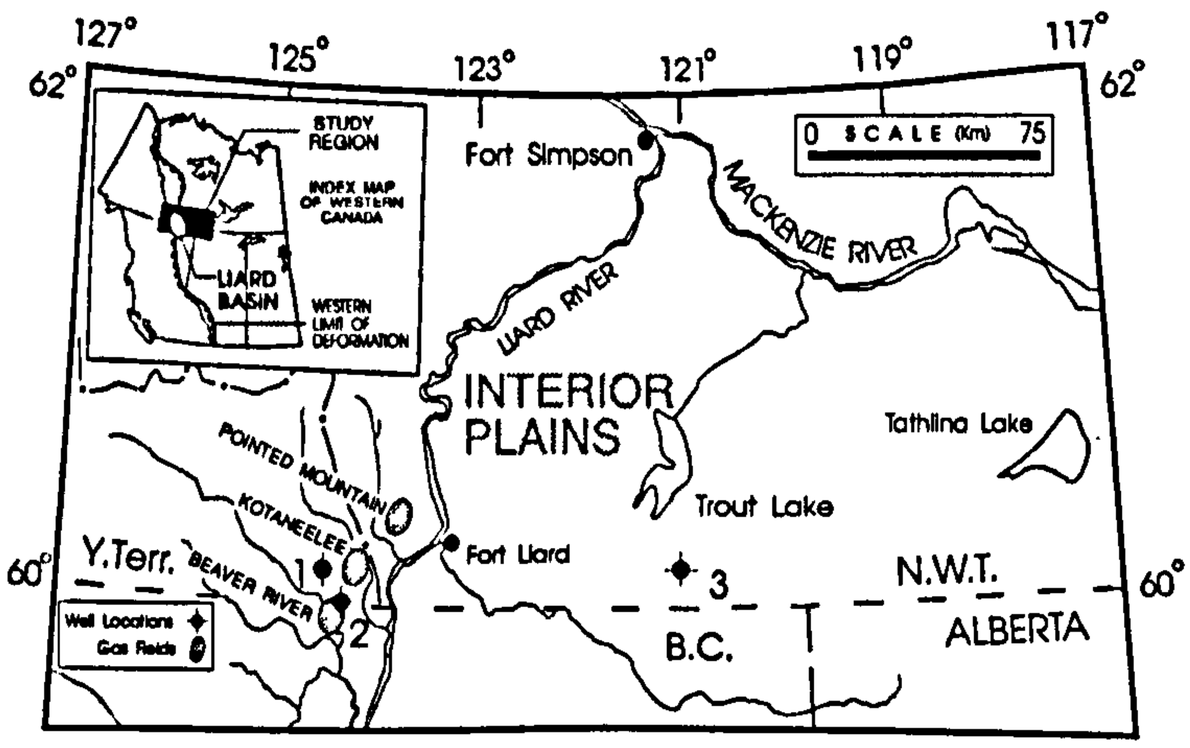

Fig. 1. Locality index map showing Liard Basin in southeastern-part of the Yukon Territory. Two of the wells examined, the Pan Am Kotaneelee O-67 (1-·at 61° 26′ 51″ N/124° 11′ 56″ W) and the Pan Am Beaver River YT G-01 (2- at 60° 00′ 25″ N/124° 15′ 48″ W) wells are in Liard Basin, whereas the third well, the Imperial Island River No. 1 well (3- at 60° 09′ 29″ N/121° 08′ 16″ W), is in the Interior Plains. Also shown are the gasfields of southeastern Yukon Territory including, from south to north, the Beaver River, the Kotaneelee and the Pointed Mountain fields.

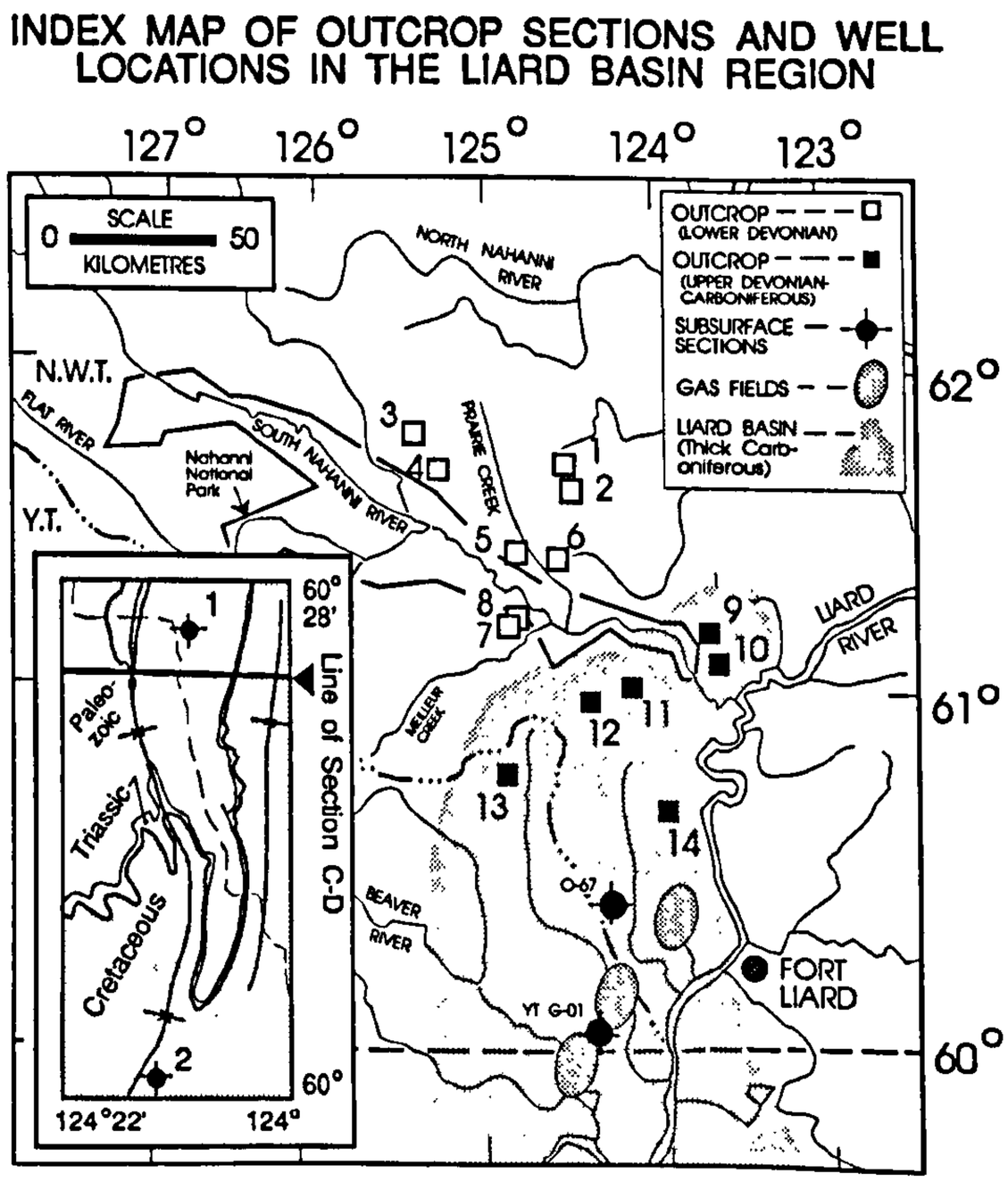

Fig. 2. Index map of outcrop and well sections in Liard Basin.The shaded area represents the present limit of thick(>200 m) Carboniferous strata (Richards, 1989). The northern border of this area is also the preservational limit of Carboniferous strata. The inset diagram in the lower left part of the diagram is a geological map in the vicinity of the Pan Am Kotaneelee O-67 (1) and Pan Am Beaver River YT G-01 (2) wells. The Kotaneelee Syncline in the eastern part of this geologic map contains 700 m of Cretaceous strata along cross-section C-D (Douglas, 1976).

a Late-Devonian episode of anomalous heating of the Middle Devonian in the manner suggested by Spencer (1987).

Quantitative modelling of the level of organic maturation of stratigraphic sequences from this region has the potential to provide an independent means of evaluating hypotheses, such as those of Spencer (1987) and Qing and Mountjoy (1989), for the origin of the Manetoe Facies dolomites, in addition to determining the time of hydrocarbon maturation and migration. Solitary determinations of organic maturity from many disparate outcrop localities (Fig. 2), while provocative, are not adequate for thermal modelling of organic maturity of thick sequences in a restricted area. Sampling of well cuttings provide the only means of acquiring stratigraphically continuous maturation data at individual localities in the Liard Basin region that are suitable for this purpose.

Methods

The optical reflectance of vitrinite in well cuttings from three wells have been analyzed (Table 1). Two of these wells (Pan Am Beaver River YT G-01 and Pan Am Kotaneelee O-67) are in Liard Basin and the third well (Imperial Island River No. 1) is located in the Interior Plains east of the Liard Basin (Fig. 1). This provided a comparison between coalification profiles from the Interior Plains Region where the upper Paleozoic sequence is thin, and those of the thicker upper Paleozoic Liard Basin sequences.

Reflected light intensity measurements of organic materials were performed on a Zeiss MPM II microscope fitted with white (halogen) and blue-violet light sources, using an Epiplan-Neofluor oil immersion objective (N.A. 0.90 × 40), following procedures outlined by Bustin (1989). Samples were prepared for reflectance measurements according to ASTM procedures (1981).

Measurements of vitrinite reflectance were obtained from well cuttings selected from darker, organic-rich shaly and coalbearing intervals. All measurements were made from dispersed vitrinite in well cuttings (Fig. 4). The small sample size afforded by well cuttings precluded the acquisition of a statistically uniform data base and the simple arithmetic means of these data for each sample were used to represent the true mean values without regard for the possible influence of sampling error on mean reflectance values. However, the use of well cuttings is the only practical means available to obtain the continuous profiles of vitrinite reflectance that are necessary for determining thermal histories.

Only some vitrinite-like macerals could be identified unequivocally as vitrinite on the basis of relict cellular morphology or by direct association with inertinite (Fig. 4). However, the consistent relationship between the reflectances of bitumen and of the vitrinite-like macerals (with the reflectance of the vitrinite-like material being slightly greater than bitumen reflectance at any given stratigraphic level in both the Beaver River YT G-01 and Imperial Island River No. 1 wells) supports the inference that the vitrinite-like material is truly vitrinite. Bitumen in these samples is commonly recognizable by its tendency to fill intergranular and intercrystalline pore space in irregular networks parallel to bedding (Fig. 4). Bitumen reflectances were also systematically measured and recorded, but are not reported here, as was reworked vitrinite.

Additional verification of the levels of organic maturation was provided by Rock-Eval analyses of well cutting samples

Table 1. Reflectivity of vitrinite in the Imperial Island River No. 1 and Beaver River YT G-01 Wells.

Imperial Island No. 1				Beaver River YT G-01			
Feet	Metres[1]	Ro%	Range of Values[2]	Feet	Metres[1]	Ro%	Range of Values[2]
1994	608	**0.58**	0.42 - 0.80	2860	872	**0.31**	0.26 - 0.35
2134	651	**0.72**	0.62 - 0.90	3220	982	**0.47**	0.38 - 0.56
2310	704	**0.76**	N/A	3470	1058	**0.55**	0.43 - 0.67
2747	838	**0.64**	0.55 - 0.85	4140	1262	**0.58**	0.49 - 0.63
2760	842	**0.61**	0.59 - 0.63	4400	1342	**0.70**	N/A
3275	999	**0.73**	0.62 - 0.85	4970	1515	**0.82**	N/A
3465	1,056	**0.68**	0.59 - 0.76	5840	1781	**0.76**	N/A
3482	1,062	**0.82**	0.62 - 0.90	6120	1866	**0.80**	0.63 - 0.90
3787	1,155	**0.89**	0.87 - 0.92	6560	2000	**1.27**	N/A
5409	1,649	**1.05**	0.99 - 1.22	8765	2672	**1.85**	1.51 - 2.27
5899	1,799	**1.13**	0.98 - 1.36	9220	2811	**2.00**	1.72 - 2.29
6240	1,902	**1.20**	1.18 - 1.32	9490	2893	**2.15**	1.72 - 250
6400	1,951	**1.28**	1.25 - 1.32	10184	3105	**2.41**	1.90 - 3.00
6814	2,077	**1.53**	1.30 - 1.68	10570	3223	**2.00**	1.72 - 2.29
7313	2,230	**2.00**	N/A	11630	3546	**3.50**	3.30 - 3.56
–	–	–	–	12020	3665	**3.91**	3.12 - 4.92
–	–	–	–	12270	3741	**3.70**	3.15 - 4.10
–	–	–	–	12670	3863	**4.30**	N/A
–	–	–	–	12970	3954	**4.60**	4.46 - 4.86
–	–	–	–	13190	4021	**4.20**	3.60 - 4.80
–	–	–	–	13364	4166	**4.18**	3.40 - 5.30

[1] – Depths below Kelly Bushing
[2] – Between 3 and 50 measurements per sample (average 10)
N/A means only a single measurement

from the three wells of this study using a Rock-Eval analyzer (Espitalié *et al.*, 1985) according to procedures outlined in Snowdon (1989). All Rock-Eval analyses were performed on well cuttings that were washed and dried at room temperature.

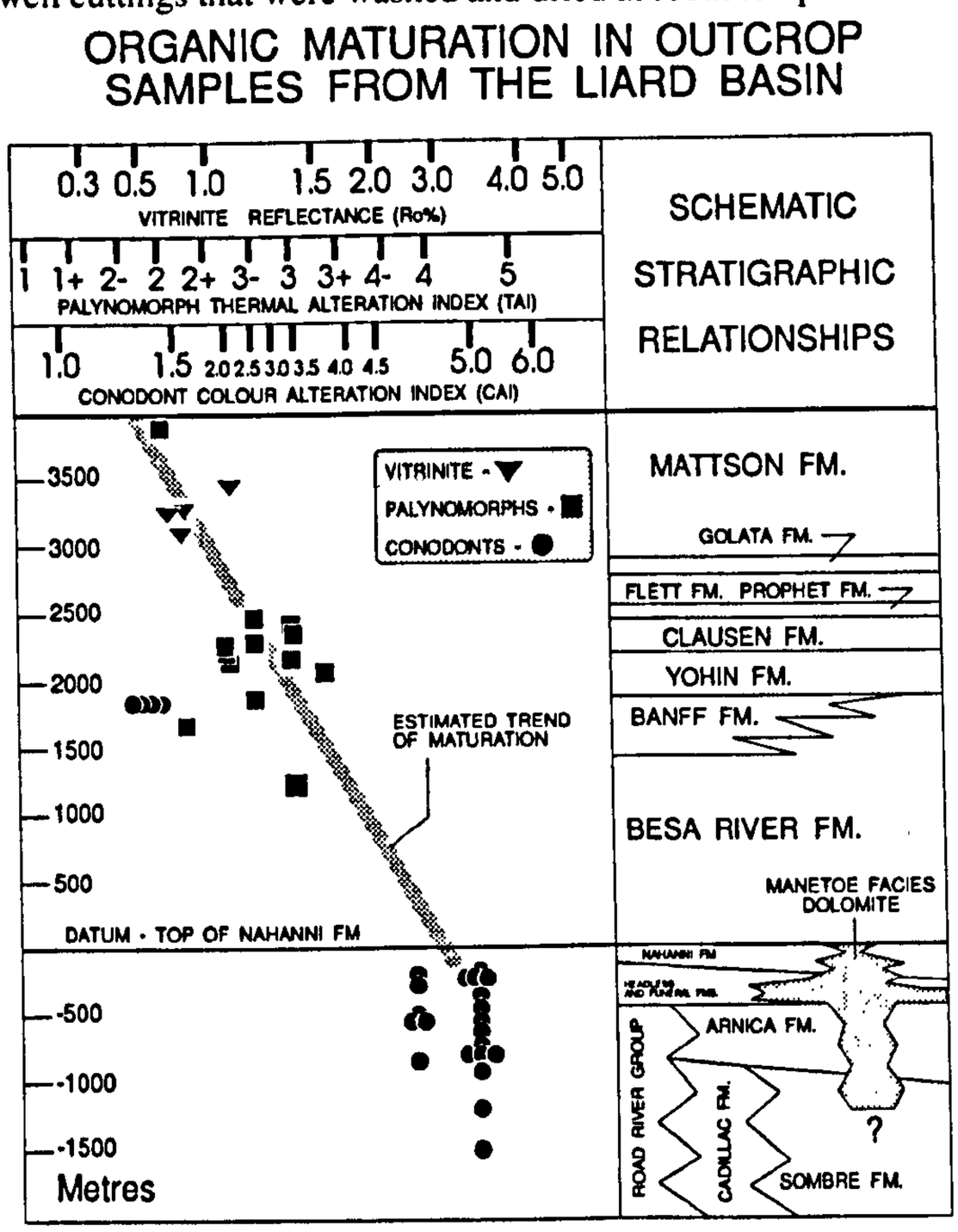

Fig. 3. A stratigraphic plot of maturation data from the outcrop localities shown in Figure 2. Vitrinite reflectances (R_o%), palynomorph thermal alteration indices (TAI) and conodont colour alteration indices (CAI) are plotted with reference to an empirically-based comparative scale (Utting *et al.*, 1989; see also Bustin, 1989). TAI class values appended with + and – symbols indicate values slightly greater and slightly less than integer values. These data, along with conodont determinations, are single values only and often are given as a range between integral values. The vitrinite reflectances from Mattson coal beds are more precise with standard deviations of 0.05% R_o. There is a rapid downsection increase in the level of organic maturity from about 0.5%R_o at the top of the Mattson Formation to about 3.5%R_o at the top of the Nahanni Formation. Also shown is a schematic view of the Paleozoic stratigraphy of Liard Basin and the stratigraphic position of the Manetoe Facies reservoir dolomite at the Beaver River and Kotaneelee Gas Fields.

Maturation Data

Vitrinite reflectance values increase consistently down section in these wells. Reflectances increase from 0.26% at 79 m to 1.76% at 1829 m in the Kotaneelee O-67 well, from 0.31% at 262 m to 4.40% at 3546 m in the Beaver River YT G-01 well and from 0.58% at 608 m to 2.00% at 2230 m in the Imperial Island River No. 1 well (Figs. 5,6). The uniformity of the downsection increase of the degree of reflectance with stratigraphic level down to the top of the Nahanni Formation is much more evident in these well sections than in the plot of maturation indicators of outcrop samples from widely scattered localities (Fig. 2).

The levels of reflectance for the Kotaneelee O-67 well are similar to those of the more numerous data from Beaver River YT G-01 well at equivalent stratigraphic levels. The slightly higher reflectance values recorded at the Kotaneelee O-67 well for a given depth may be attributed to the slightly higher structural position of the Kotaneelee O-67 well with respect to the Beaver River YT G-01 well (Fig. 5).

Vitrinite reflectance values in the Imperial Island River No.1 well east of Liard Basin (Fig. 6) display a lower rate of downward increase with stratigraphic level than in the Liard Basin wells (Figs. 5,6). In general, vitrinite macerals in the Imperial Island River well have lower reflectances than vitrinites at equivalent stratigraphic levels in the Liard Basin wells.

Extensive Rock-Eval pyrolysis data were collected for the Kotaneelee well, but only reconnaissance level Rock-Eval surveys were made of the other wells (Figs. 5,6). The Tmax values of the S_2 peak of the Kotaneelee O-67 well display a consistent pattern with respect to depth or stratigraphic level down to the top of the overmature zone (Fig. 5). In the top 550 m of the well there is a consistent downhole increase of Tmax from 440° C at 61 m to 466° C at 549 m. Below this depth, in the middle of the Golata Formation to the bottom of the hole, Tmax is below 430° C. Rock-Eval pyrolysis chart traces of these samples indicate that a distinct S_2 peak is present down to 549 m but is usually absent below this depth. This downhole disappearance of the S_2 peak is not the consequence of a corresponding downhole decrease in total organic material (TOC), which remains between one and four per cent down to the level of the Nahanni Formation near the bottom of the hole

Fig. 4. Photomicrographs of kerogen:

a) Vitrinitic kerogen (grey, centre left, 0.72% R_o) in the Banff Formation, associated with inertinite (white, top left and centre right); Imperial Island River No. 1 at 837 m (KB).
b) Vitrinite-like kerogen (reflectance: 0.61% R_o) in the Golata Formation, associated with highly reflective pyrite; Pan Am Kotaneelee at 402 m (KB).
c) Vitrinite-like component of the Mattson Formation (0.43% R_o); Pan Am Beaver G-01 at 1058 m (KB).
d) Vitrinite-like kerogen in the Besa River Formation showing cellular morphology and semi-anthracite reflectance (2.05% R_o); Pan Am Beaver G-01 at 3322 m (KB).
e) Low reflectance bitumen (0.47% R_o), in shaley interstices of dolomitic siltstone in the Banff Formation. The bitumens are slightly recessed and exhibit cross-hatched striations indicative of softness; Imperial Island River No. 1 at 837 m (KB).
f) Low-reflecting bitumen (0.38% R_o) in the Exshaw Formation is oriented parallel to bedding and forms a dispersed network throughout the shale matrix; Imperial Island River No. 1 at 1056 m (KB).
g) Bitumen (1.30% R_o) with a vesicular appearance infills matrix porosity in the Besa River Formation; Pan Am Kotaneelee at 2134 m (KB).
h) Highly-reflective, pore-filling bitumen (ca. 3.50% R_o) associated with rhombic dolomite in the Besa River Formation; Pan Am Kotaneelee at 2134 m (KB).


a

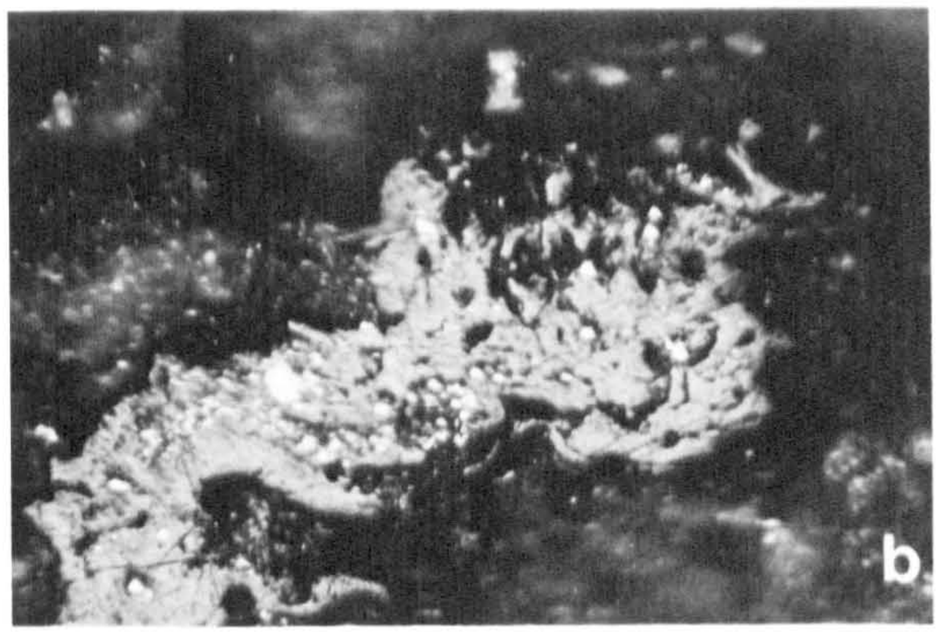
b

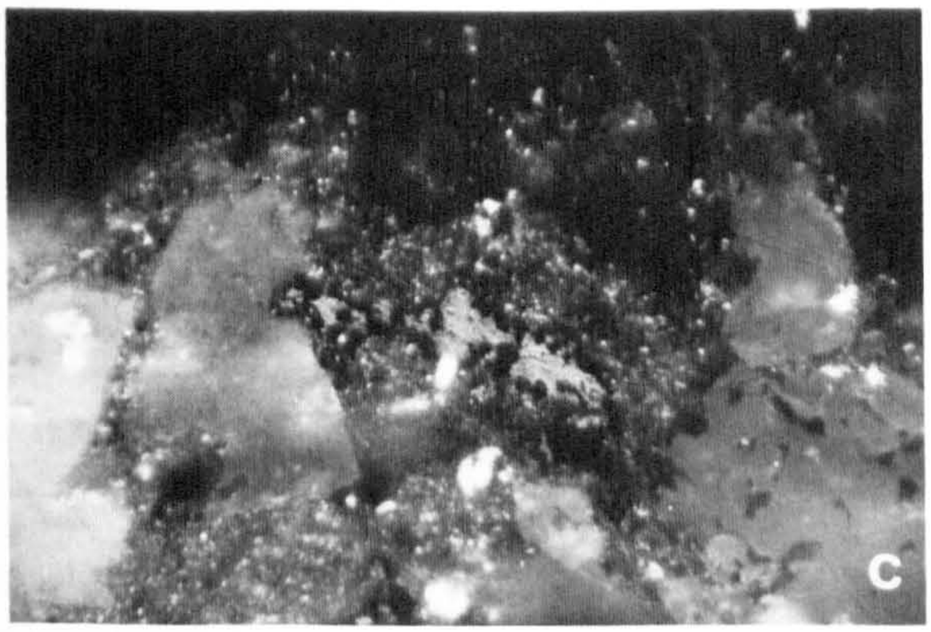
c


d


e


f

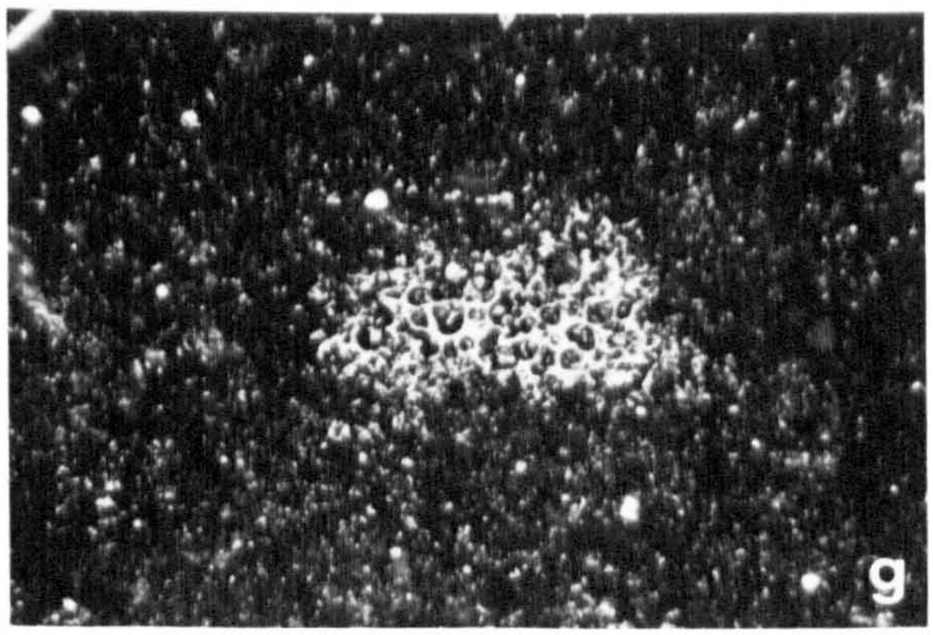
g

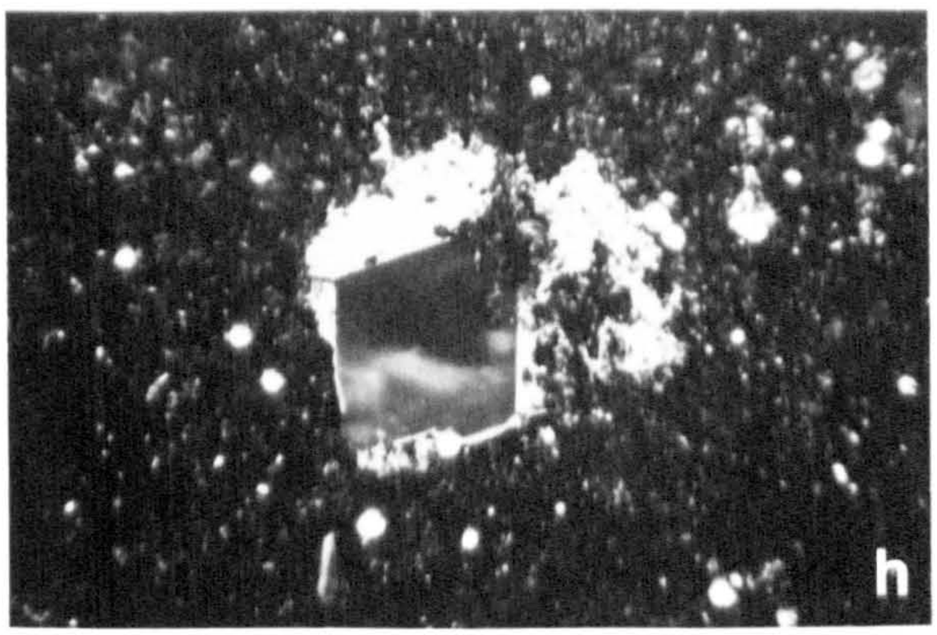
h

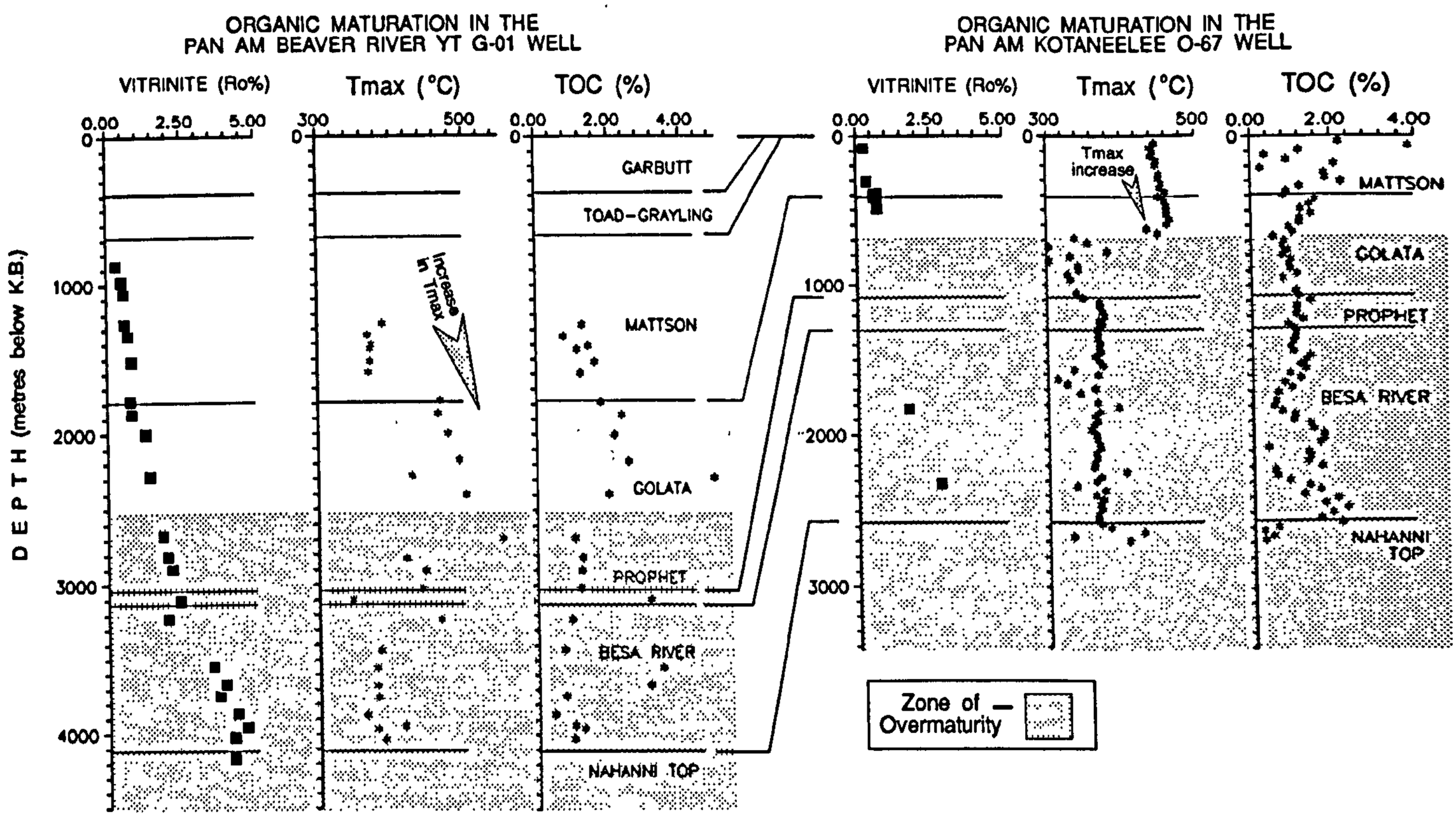

Fig. 5. Vitrinite reflectances (Table 1), Rock-Eval Tmax and total organic carbon (TOC) for the Pan Am Kotaneelee O-67 and Beaver River YT G-01 wells. Total organic carbon averages about 1.0% in the Upper Paleozoic siliciclastics above the Nahanni Formation but is up to 4.0% in the lower part of the Besa River Formation shales. In the Kotaneelee well Tmax increases uniformly downhole from 440° C at 61 m to 466° C at 549 m within the Golata Formation. Below this depth the S_2 peak disappears and Tmax is unreliable. In the Beaver River well, The low Tmax values below 2683 m also indicates the disappearance of the S_2 peak within the Golata Formation.

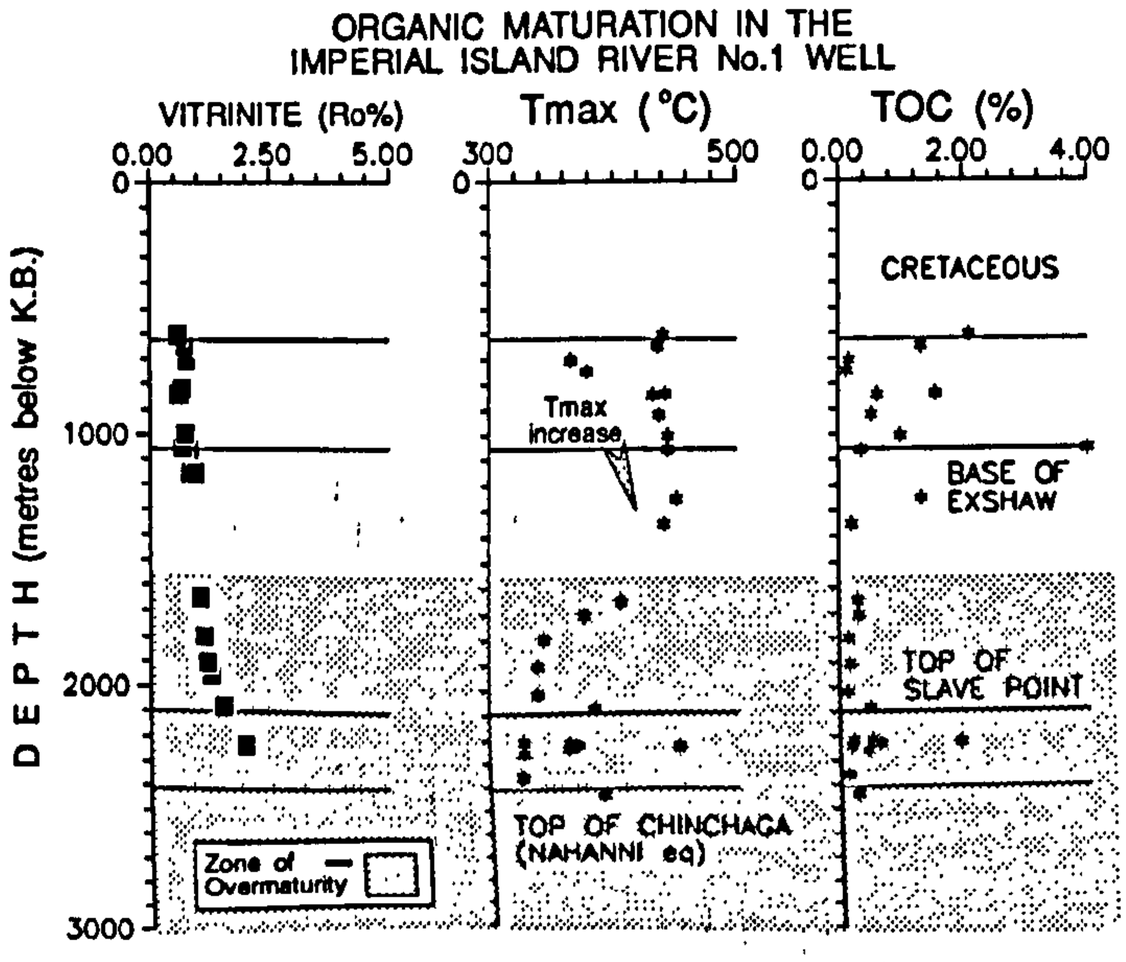

Fig. 6. Vitrinite reflectances (Table 1), Rock-Eval Tmax and total organic carbon (TOC) for the Imperial Island River No. 1 well. The total organic carbon is much lower overall for this well than in the Liard Basin wells and averages about 0.30%. Tmax tends to increase downhole from 432° C at 841 m to 452° C at 1249 m within the Tetcho Formation below the Exshaw Formation. Below this depth Tmax falls below 400° C reflecting the disappearance of the S_2 peak.

(Fig. 5), but instead is caused by maturation of the sequence past the point of oil preservation.

In the Beaver River well (Fig. 5) the low Tmax values below about 2683 m (or below the middle of the Golata Formation) can also be discounted because the S_2/S_3 peak ratio falls to very low values below this depth-indicating the disappearance of the S_2 peak. Above this level, there is a trend of upwardly decreasing Tmax values, from 536° C at 2681 m to 469° C at 1780 m. Above 1780 m to the top of the hole, however, sample Tmax values decrease abruptly to very low values of between 368° C and 392° C without any consistent trend. These low Tmax values in the upper part of the well may reflect contamination by organic additives. The well history report notes that a "hot oil string" was run at 800 m below kelly bushing. Such additives are known to cause contamination of the well cuttings (Peters, 1986).

Rock-Eval data from the Imperial Island River No. 1 well (Fig. 6) indicates that Tmax rises downhole from 432° C at 841 m to 452° C at 1249 m. Below a depth of about 1500 m, the sample Tmax values fall off abruptly indicating the disappearance of the S_2 peak consistent with passage through the oil window (Peters, 1986). In all wells the S_2 peak tends to be diminished or absent at stratigraphic levels below strata characterized by vitrinite reflectances of 1.50% (R_o%) or more. This would seem to indicate the disappearance of oil fraction hydrocarbons during the generation of wet gas from oil, which

is at a peak at a level of thermal maturation equivalent to a vitrinite reflectance of about 1.00% (R_o%) (Dow, 1977) with a consequent diminution in the S_2 peak intensity at progressively greater values of vitrinite reflectance.

In spite of the overmaturity of a large part of the Liard Basin well sequences, dark shales of the Besa River Formation overlying the Nahanni Formation have retained up to 4.0% TOC (Fig. 5) and contain abundant bitumen (Fig. 4). This is an indication that the Besa River Formation was a good potential source rock for hydrocarbons in the Liard Basin gas fields. The bitumen in the Besa River Formation in these wells has high reflectance (Fig. 4) indicative also of a high level of organic maturity (Jacob, 1985).

Rock-Eval data plotted on hydrogen and oxygen index crossplots of pseudo-Van Krevelen diagrams (not shown) indicate that the bulk of the analyzed organic material in these wells is probably a mixture of type II and type III kerogens (Tissot and Welte, 1984) in agreement with the visual identification of kerogens as a mixture of bitumen, vitrinite and exinite (Fig. 4). Type III organic material is typically gas prone (Snowdon, 1989) and, under ideal sampling conditions, the Rock-Eval Tmax of this organic type exhibits a strong positive correlation with vitrinite reflectance (Peters, 1986). However, much of the overmature kerogen in these wells may have been derived from type II organic material and now cannot be discriminated from type III organic material where both of these now have hydrogen and oxygen index values close to zero.

Depth-maturation Relationships

Plots of the logarithm of vitrinite reflectances with respect to depth display the generally log-linear trend (Fig. 7) shown by Dow (1977) to be typical for organic material in basins that underwent continuous subsidence under the influence of time invariant, linear geothermal gradients during their periods of major organic metamorphism. Middleton (1982) found that the empirical relationship of Dow (1977) could be used directly to infer paleogeothermal gradients from depth profiles of vitrinite reflectance. In his extension of Dow's rule for basins with constant geothermal gradients, the paleogeothermal gradient G can be expressed in terms of the slope 'm' of the log (R_o%) *versus* depth curve for depths in kilometres by the relationship:

$$G = 194.8(m)$$

for basins that underwent their major period of organic metamorphism under the influence of an approximately linear, time invariant geothermal gradient.

This slope value for the Beaver River well is 0.334 and for the Imperial Island River well is 0.293 (Fig. 7). These slopes indicate paleogeothermal gradients of 65° C/km and 57° C/km at the time of maturation of organic material. These calculated geothermal gradients are much higher than the present geothermal gradients in the regions around these wells, which were found by Majorowicz *et al.* (1988) to range from only 30° C/km to 40° C/km.

The divergence between these estimated paleogeothermal gradients and present day gradients reflects the fact that the Liard Basin and adjacent Interior Plains region have had a complex subsidence history that has involved several phases of subsidence interrupted several times by episodes of uplift and erosion. Paleogeothermal gradients estimated by the method of Middleton (1982) may approximate the actual geothermal gradients during organic maturation but there is

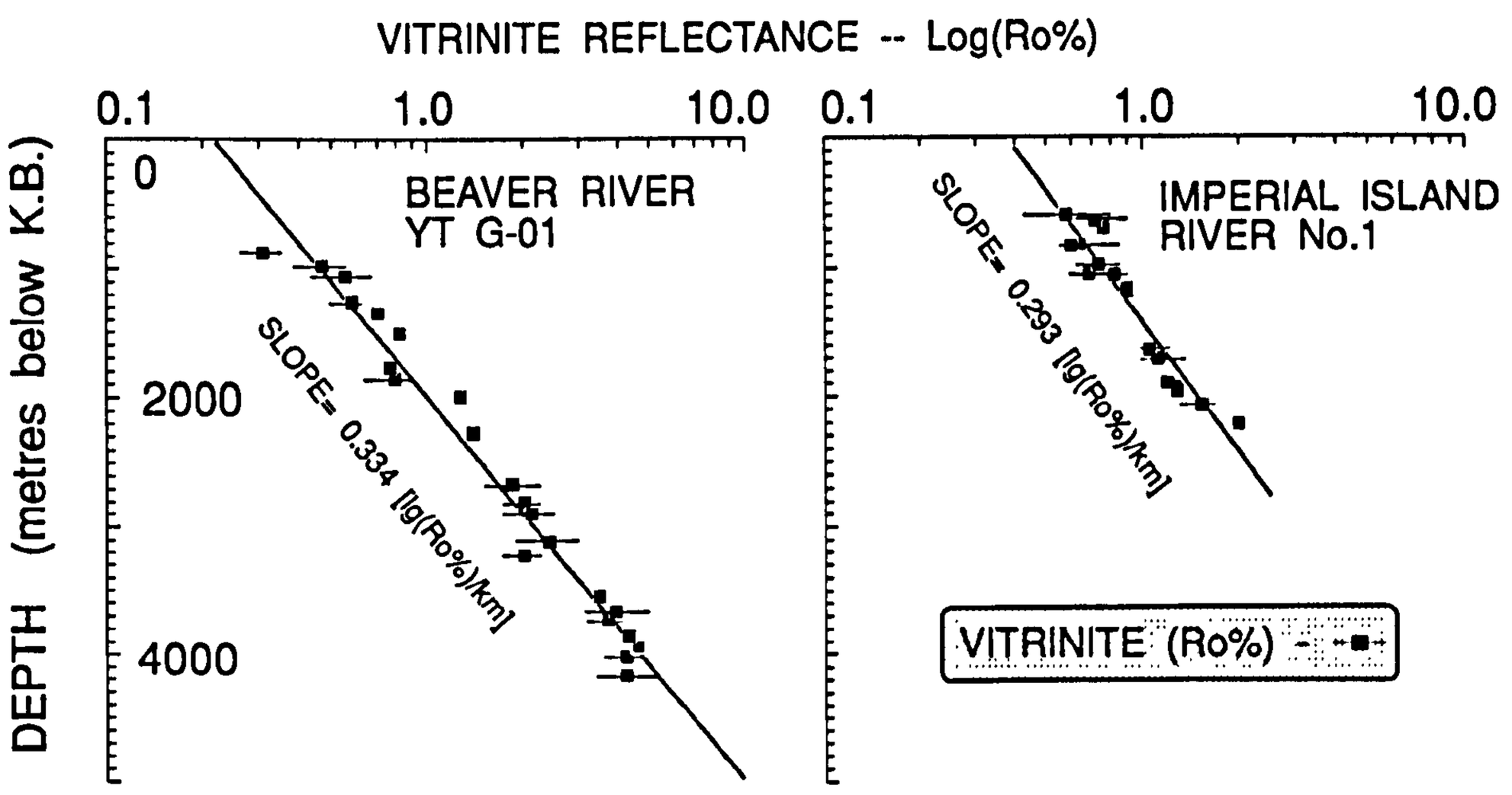

Fig. 7. Plots of the logarithms of vitrinite reflectances (R_o%) *versus* depth from the Beaver River and Imperial Island Riverwells. A best fit line to the Beaver River vitrinite data is: log (R_o%) = 0.334 [Depth (km)] –0.665, with a correlation coefficient of 0.98. A best fit line to the Imperial Island well vitrinite data is: log (R_o%) = 0.293 [Depth(km)] –420, with a correlation coefficient of 0.90. Vitrinite reflectance increases more rapidly down section in the Beaver River well.

little indication as to the time during which this maturation occurred due to the complex geologic history of these areas.

Geohistory and Simulations of Maturation

Construction of geohistory or subsidence plots are a method for the estimation of the cumulative time-temperature history of sedimentary sequences (Waples, 1980). The burial depth of a specific stratigraphic horizon at any time in its burial history may then be used to estimate its paleotemperature. The temperature history of this horizon can then be used to simulate the progressive maturation of vitrinite and predict the increase of vitrinite reflectance with time (*e.g.*, Waples, 1980; Kalkreuth and McMechan, 1984). Arrhenius-based algorithms, such as the EASY%R_o method (Sweeney and Burnham, 1990), provide the means for accurate prediction of vitrinite maturity and reflectance (R_o%) after a temperature history is determined.

Subsidence Histories

Subsidence or geohistory plots were constructed (Fig. 8) to estimate the temperature history of well sequences. The original thicknesses of units eroded at major unconformities were estimated from their thickness in nearby areas where they underwent less erosional truncation. Douglas (1970) and McCrossan and Glaister (1964) were basic sources of information. More specific references pertinent to the Liard Basin and the adjacent Interior Plains east of Liard Basin include Morrow and Cook (1987) for Devonian stratigraphy, Richards (1989) for Devonian to Permian stratigraphy, Harker (1963) for Carboniferous to Permian stratigraphy, Poulton (1989) for Jurassic stratigraphy, Stott (1982) for Cretaceous stratigraphy and Williams (1979) for Permian to Tertiary relationships and stratigraphy. Important stratigraphic information is also contained on several geologic maps: the La Biche River map (Douglas, 1976), the Fort Liard map (Douglas and Norris, 1976) and the Trout River map (Douglas, 1974).

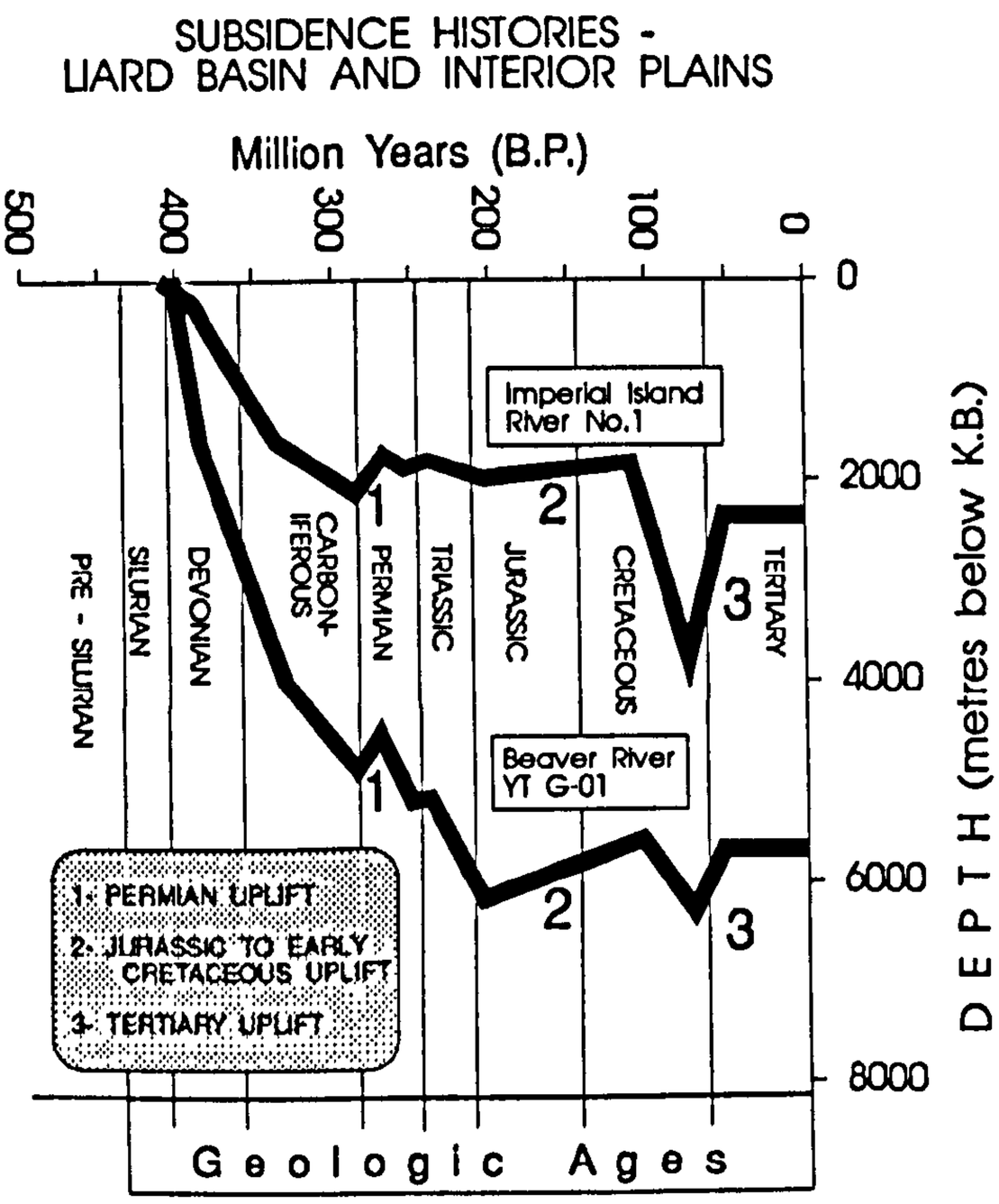

Fig. 8. Subsidence or geohistory plots of the post lurian burial history of the Imperial Island River No. 1 and the Beaver River YT G-01 wells. These estimates of the subsidence histories are based on the stratigraphy preserved in these wells and in regions adjacent to these wells (Table 2). Note the relatively large amount of Late Devonian to Carboniferous subsidence that occurred in the Liard Basin.

Figure 9 is a comparison of the stratigraphic sequences preserved in the Beaver River and Imperial Island River wells. Liard Basin is characterized by the thick Carboniferous basin fill of the upper part of the Besa River Formation and of the Golata and Mattson Formations. The Liard Basin also contains some Permian and Triassic strata preserved between the sub-Cretaceous, subTriassic and sub-Permian unconformities. In contrast, Carboniferous strata are thin in the Imperial Island River well; Permian and Triassic strata are absent and, as well, have been eroded beneath the sub-Cretaceous unconformity. Jurassic strata are absent across the entire study area beneath this unconformity.

Table 2 is a summary of the depositional and erosional history of the post-Silurian succession at the Beaver River well in the Liard Basin *versus* the Imperial Island River well in the Interior Plains. These data served as input for burial-maturation simulations of well sequences using the EASY%R_o algorithm and a burial-decompaction and maturation program (Osadetz and Mottershead, 1992) used to generate burial plots and simulated vitrinite reflectances for these sequences.[1]

The estimates of sub-Permian erosion given in Table 2 are based primarily on the assumption that the Mattson Formation was present, but thinly deposited, in the Interior Plains Region, unlike in Liard Basin where the Mattson is assumed to have been originally much thicker than its present thickness. The assumption of an originally thicker Mattson in Liard Basin is based primarily upon the rather large time interval from the top of the Mattson, estimated to be Early Carboniferous or about 333 Ma. to the base of the unconformably overlying Permian Kindle Formation at about 268 Ma. (see Richards, 1989).

There are uncertainties with regard to amounts of erosional removal associated with each of the unconformities in the Paleozoic and Mesozoic strata of these well sequences. However, only the sub-Cretaceous unconformity displays regional truncation of underlying strata (Williams, 1979). Consequently, about 500 m and 200 m of erosional removal have been estimated to be associated with this unconformity in the Liard Basin and in the Interior Plains Region respectively,

[1]This program has been modified to calculate vitrinite reflectances using the EASY%R_o algorithm.

Table 2. Comparison of the subsidence histories of the Liard Basin and the Interior Plains.

Description of Depositional or Erosional Events	Liard Basin Region	Interior Plains Region
Erosion beneath the sub-Tertiary unconformity	550m removed	900m removed
- Laramide Orogeny	**2150m removed***	**600m to 1500m removed**
Deposition of the Cretaceous sequence	700m deposited	1500m deposited
(Mainly Fort St. John Gp.)	**2300m deposited**	**1200m to 2100m deposited**
Erosion beneath the sub-Cretaceous unconformity	503m removed	195m removed
Deposition of the Triassic sequence	800m deposited	100m deposited
(Toad and Grayling Formations)		
Erosion beneath the sub-Triassic unconformity	11m removed	20m removed
Deposition of the Permian sequence	420m deposited	40m deposited
(Kindle and Fantasque Formations)		
Erosion beneath the the sub-Permian unconformity	255m removed	300m removed
Deposition of the Exshaw to Mattson sequence	2954m deposited	579m deposited
Deposition of post-Nahanni to pre-Exshaw sequence	571m deposited	1314m deposited
Deposition of Nahanni, Chinchaga and	1477m deposited	116m deposited
underlying Devonian strata		

* – Thicknesses in normal type are estimates based on existing geological information. Thicknesses in **bold type** are alternate estimates. Cretaceous and post-Cretaceous thickness values rounded to nearest 50 m.

in contrast to the small amounts of erosion assigned to the sub-Permian and sub-Triassic unconformities (Table 2, Fig. 9).

The 700 m thickness of Cretaceous strata preserved in synclines flanking the Beaver River well site provides a minimum estimate for Cretaceous subsidence (Fig. 2, Table 2; Douglas, 1976). An arbitrary maximum of 2300 m for Cretaceous subsidence for this well site (Table 2) is the approximate maximum thickness of Cretaceous strata in northeast British Columbia. (Stott, 1982). In addition, a recent determination of 1.5 km for Cretaceous subsidence in the Interior Plains west of Pine Point, N.W.T., based on apatite fission track analyses (Arne, 1991), was used as an initial estimate of Late Cretaceous subsidence at the Imperial Island River No. 1 well location (Table 2, Fig. 8). A range of values, from 1200 m to 2100 m, for Cretaceous subsidence were considered for this well site (Table 2).

Organic Maturity of the Mattson Formation

Vitrinite reflectances (R_o%) in the Mattson Formation range from a minimum only about 0.4% at the top of the unit to a maximum of about 0.7% at the base of the Mattson in the Beaver River and Kotaneelee wells (Fig. 10). Vitrinite reflectance data from Mattson coal-bearing outcrop samples from the Jackfish Gap Section in the northern part of Liard Basin (Section 12, Fig. 2; Potter *et al.*, *in press*), are similar to the data reported here, although in the upper part of the formation, there is some divergence (Fig. 10). Reflectance measurements of vitrinite in coal samples from the upper part of the Mattson are slightly elevated because the vitrinite macerals in these coals are perhydrous and gelified, whereas reflectance measurements of the dispersed vitrinite in the shale samples from the lower Mattson are unaltered, more normal vitrinite (Potter *et al.*, *in press*).

Potter *et al.* (*in press*) estimate that the average reflectance for vitrinite at the top of the Mattson Formation in Liard Basin is less than 0.5% (Fig. 10). This is consistent with the vitrinite reflectances of about 0.5%R_o recorded by Leckie *et al.* (1991) in a few samples from basal Cretaceous coal-bearing units exposed in outcrops close to the Liard Basin wells of this study. This low level of maturity of the top of the Mattson places severe constraints on post-Mattson burial depths and post-Mattson geothermal gradients.

Vitrinite reflectance profiles calculated for the Mattson Formation, using the minimum estimate of 700 m for Cretaceous subsidence (Table 2) and average paleogeothermal gradients of 25° C/km, 30° C/km and 35° C/km, all fall within the range of observed values (Fig. 10). These geothermal gradients are lower than the present average geothermal gradient of 40° C/km for Liard Basin (Majorowicz *et al.*, 1988). In contrast, vitrinite reflectances calculated with the same array of low to moderate geothermal gradients (*e.g.*, Klemme, 1975) (but using the greater estimate of 2300 m for Cretaceous burial [Table 2]) greatly exceed observed vitrinite reflectances, particularly in the lower part of the Mattson.

These simulations indicate that Cretaceous burial could not have greatly exceeded the present thickness of 700 m for Cretaceous strata preserved in regional synclines adjacent to the Beaver River and Kotaneelee wells (Fig. 2); and that the average post-Mattson geothermal gradient was probably less than the present average gradient of 40° C/km in Liard Basin. The low level of maturity at the top of the Paleozoic in Liard Basin also limits the potential thickness of strata eroded beneath the sub-Cretaceous unconformity.

Pan Am Beaver River YT G-01

The determination that 700 m is a reasonable estimate for the amount of Cretaceous burial consistent with the level of organic maturity observed at the top of the Mattson Formation lends credence to the subsidence history for the Beaver River well site as shown in Figure 8. Using this as our best estimate for the subsidence history, we can simulate the effect of variations in heat flow (or geothermal gradients) on vitrinite reflectance throughout the entire sequence using a burial-decompaction program (Osadetz and Mottershead, 1992).

An array of time invariant heat flows ranging from 40 to 140 milliwatts per square metre (mW/m^2) brackets the

observed vitrinite reflectances (Fig. 11). Almost all the data are contained between the 60mW/m² and 100mW/m² heat flow simulations. However, the slope of observed vitrinite reflectances diverges from these simulated reflectance profiles. For example, the 100mW/m² heat flow profile matches vitrinite reflectances below the Mattson Formation but overestimates reflectances within the Mattson Formation itself.

This suggests that heat flows and geothermal gradients were not time invariant in Liard Basin. Low Mesozoic and Tertiary heat flows (or geothermal gradients) are required to

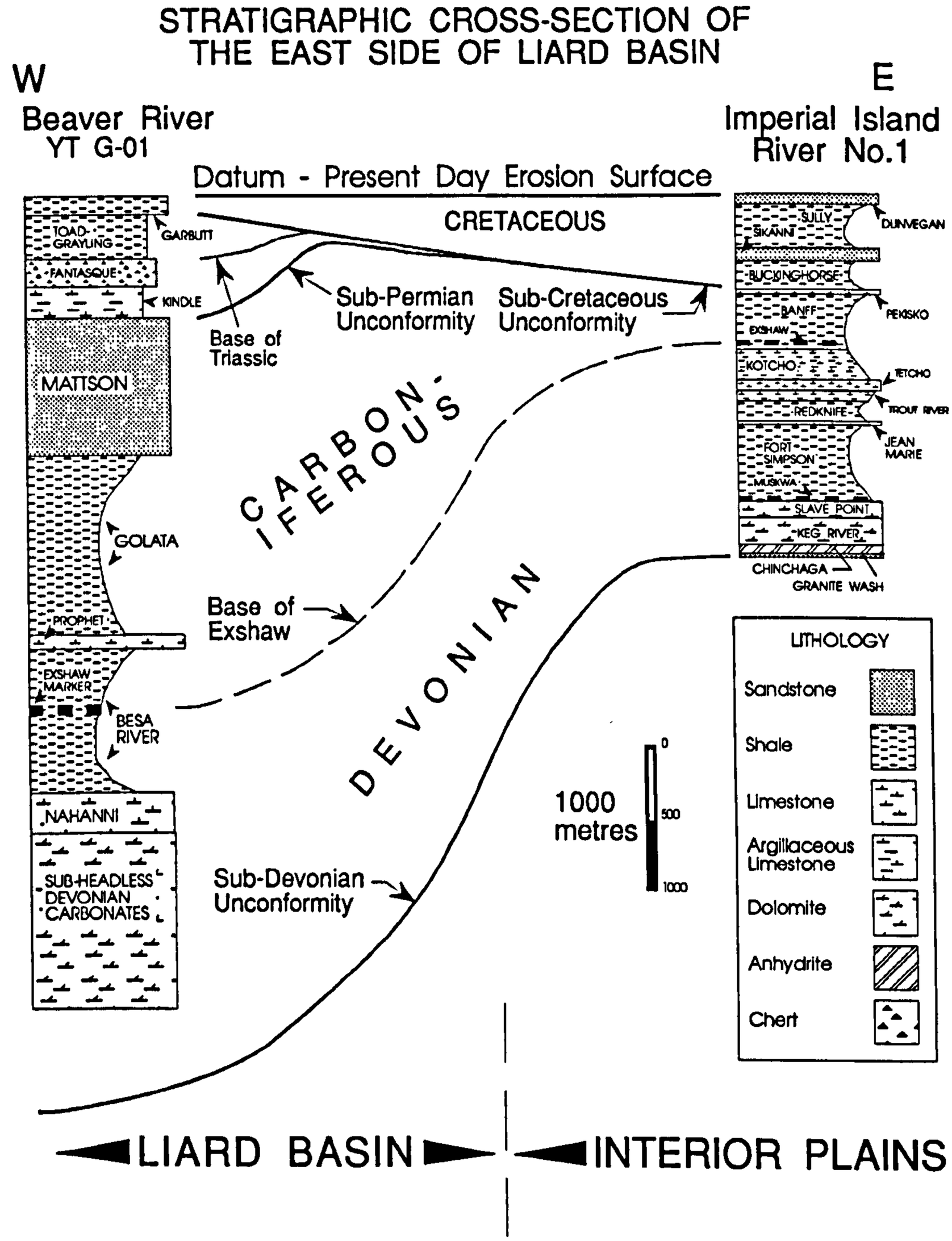

Fig. 9. A comparison of the present day stratigraphic sequences in the Beaver River YT G-01 and Imperial Island River No. 1 wells (Fig. 1). Solid correlation lines are unconformities and the dashed correlation is a marker horizon. All named stratigraphic units are formations except for the "sub-Headless Devonian carbonates" of the Beaver River well which includes equivalents of the Arnica and Landry Formations. The Headless Formation itself is a thin shale unit that separates the Nahanni Formation limestones from the underlying Lower Devonian carbonates. Devonian strata are predominantly Lower Devonian carbonates in the Beaver River well and Upper Devonian siliciclastics in the Imperial Island well. Carboniferous strata are thick in the Liard Basin but thin in the Interior Plains sequence of the Imperial Island River well.

preserve the low maturity level of the Mattson Formation, as previously discussed. But the rapid downward increase of vitrinite reflectance below the Mattson Formation indicates that average heat flow was high during Paleozoic deposition (Fig. 11). A good fit was obtained with a Paleozoic heat flow of 135mW/m^2 – equivalent to a paleogeothermal gradient of about 55° C/km to 60° C/km and lower Mesozoic and Tertiary heat flows of 80mW/m^2 and 60mW/m^2 respectively (Fig. 12).

Scenarios involving low Paleozoic to Mesozoic heat flow followed by high Cretaceous-Tertiary heating generate vitrinite reflectances that greatly overestimate observed reflectances (Fig. 11). Greater estimates for Cretaceous burial in this region would further reduce the likelihood of high Cretaceous-Tertiary heat flow.

Imperial Island River No. 1

The same array of time invariant heat flows used for the Beaver River well (Fig. 11) was applied to the burial history of the Imperial Island River well (Fig. 12). Here, heat flows of 80mW/m^2 to 100mW/m^2 (corresponding to geothermal gradients of 35° C/km to 45° C/km) bracket almost all the observed vitrinite reflectance data using the burial history shown in Figure 8 with a Cretaceous burial of 2100 m. Lesser amounts of Cretaceous burial fit the data less well (Fig. 12). This is a clear indication that the amount of Cretaceous burial at the Imperial Island River well site could not have been much less than 2000 m and corroborates this estimate of Arne (1991) for about 1.5 to 2 km of Cretaceous burial in the Interior Plains Region, immediately east of the Imperial Island River No. 1 well.

A conservative hypothesis would be that heat flow was, in fact, time invariant at this site. However, simulations involving high Paleozoic heat flows of up to 140mW/m^2 (not shown) yield profiles that are almost indistinguishable from those of Figure 12. This is because most of the organic maturation and increase in reflectance of vitrinite was accomplished during the Cretaceous during maximum burial. Pre-Cretaceous history has little effect on maturation profiles at this well site.

History of Hydrocarbon Generation and Discussion

The rapid downsection increase of organic maturity documented from outcrop samples of Paleozoic strata in the Liard Basin (Fig. 3) has been corroborated by profiles of vitrinite reflectance in samples from well sections. The correlation between the reflectance of low reflectance-type bitumen and vitrinite reflectance in all wells may indicate that this bitumen responds to thermal stress in a manner similar to vitrinite (*e.g.*, Jacob, 1985), and corroborates the downward increase of vitrinite reflectance in Liard Basin (Potter *et al.*, *in press*).

Rock-Eval Tmax, as previously noted, is also consistent with the vitrinite reflectance values in the Imperial Island

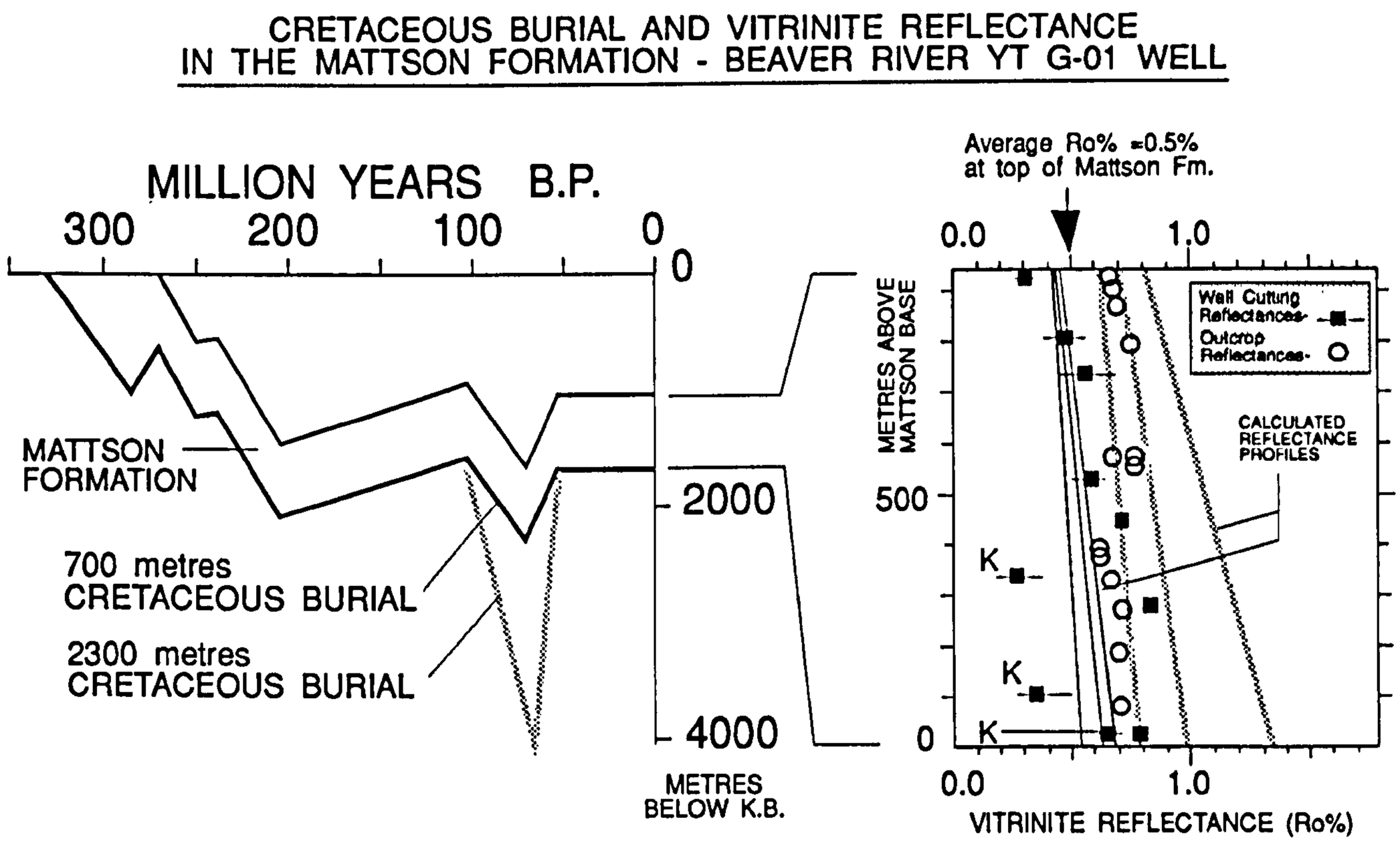

Fig. 10. A subsidence plot of the Mattson Formation at the Beaver River well site is shown on the left. On the right are shown the vitrinite reflectance values recorded from the Mattson Formation in the Beaver River and Kotaneelee wells (K), as well as reflectance values recorded from Mattson outcrop samples by Potter *et al.* (*in press*). The average vitrinite reflectance value (R_o%) of 0.5% for the top of the Mattson Formation in Liard Basin is from Potter *et al.* (*in press*). Vitrinite reflectance profiles for the Mattson were calculated using the EASY%R_o algorithm of Sweeney and Burnham (1990) with three time invariant geothermal gradients of 25° C/km, 30° C/km and 35° C/km. The solid vitrinite profiles were calculated assuming 700 m of Cretaceous subsidence (*i.e.*, equal to the present preserved Cretaceous thickness) versus the patterned profiles that were calculated using 2300 m of Cretaceous subsidence.

River No. 1 well according to the relationship of Peters (1986) for type III organic material. For example, the Tmax of the Imperial Island River well at 1300 m is about 450° C (Fig. 6) which is equivalent to an R_o% value of 0.7% to 1.2% (Fig. 14 *In:* Peters, 1986). The observed R_o% value at this depth is about 1.0 (Table 1).

In both the Beaver River and Kotaneelee wells, the Rock-Eval S_2 peak disappears below the approximate mid-point of the Golata Formation at maximum Tmax values somewhat greater than 450° C (Fig. 5). The maximum Tmax of 466° C in the Kotaneelee well equates to a vitrinite reflectance of about 1.5 (Fig. 14 *In:* Peters, 1986) which is, perhaps, a bit high compared to a value for vitrinite reflectance of about 1.0 that could be reasonably interpolated between the stratigraphically closest vitrinite reflectance values (Table 1; Fig. 5), but there are too few data for rigorous comparisons. In the Beaver River well, vitrinite reflectances of 1.40 to 1.85 appear to correlate with the stratigraphic level at which the S_2 peak disappears.

The higher Tmax values attained in the Beaver River and Kotaneelee wells may indicate that the organic material in these wells is more hydrogen-rich than that in the Imperial Island River well. This is consistent with the slightly higher average hydrogen indices recorded for Rock-Eval analyses of the Beaver River and Kotaneelee wells. The highly reflective and microscopically vesicular bitumen in the Kotaneelee well (Fig. 4g) may indicate rapid maturation of kerogen and generation of hydrocarbons.

Superimposition of the oil window on a burial maturation plot of the Beaver River YT G-01 well indicates that oil generation began in the Besa River shales overlying the Nahanni Formation in the Early Carboniferous about 340 million years ago. Oil generation may have reached its peak in the late Carboniferous even if a relatively low average heat flow of 80 mW/m² is assumed (Fig. 13). By about 300 million years ago the lower part of the Besa River Formation had passed through the oil generation window and had begun to generate gas phase hydrocarbons. By about 230 million years ago, the Besa River Formation had moved entirely through the oil window and was generating dry gas only. Besa River shales, which have up to 4.0% total organic carbon, are the most probable source rock for hydrocarbons in the Liard Basin gas

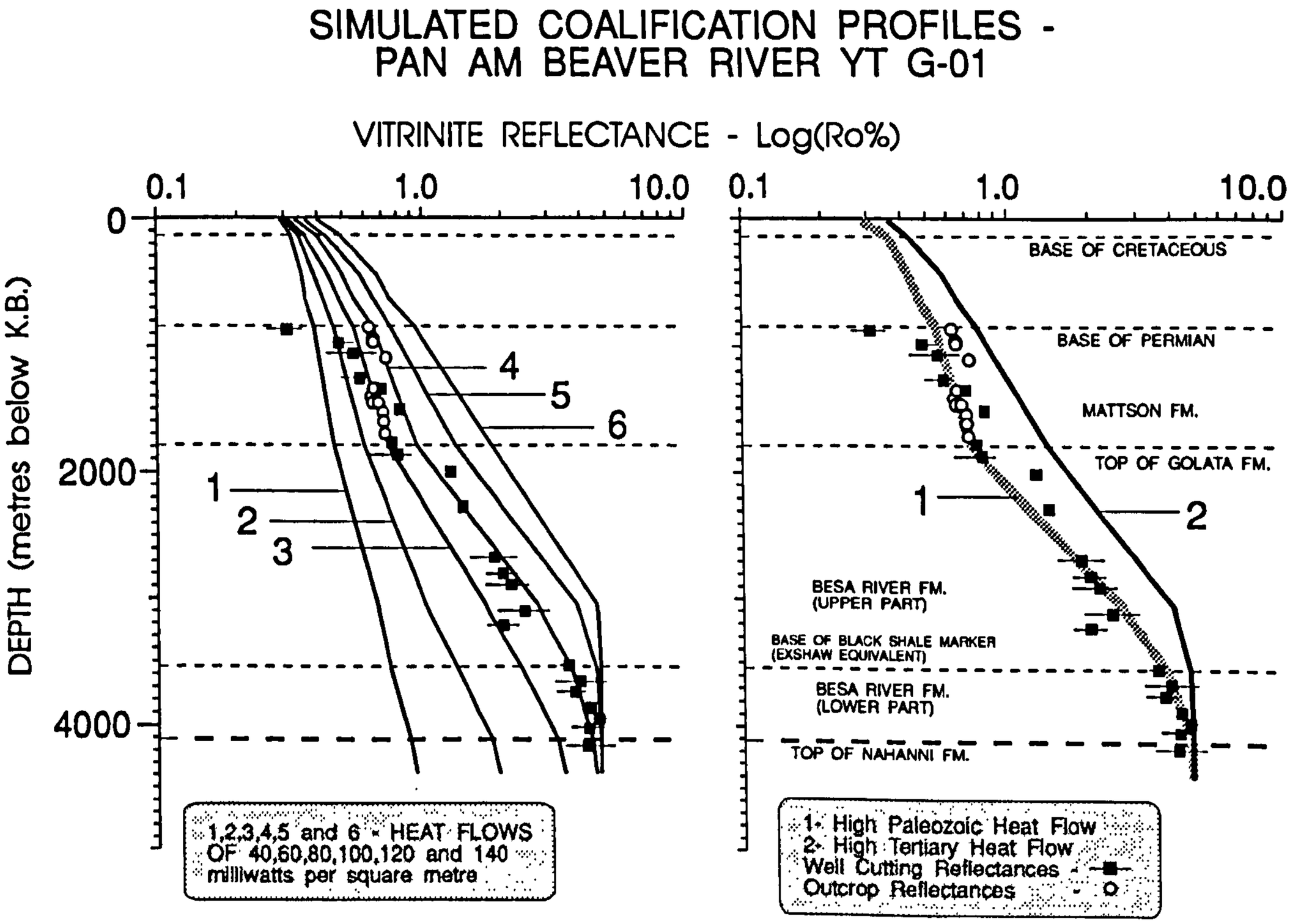

Fig. 11. Calculated vitrinite reflectance profiles for the Beaver River YT G-01 well using the Osadetz and Mottershead (1992) decompaction program and the subsidence history of Figure 9. The means and ranges of observed vitrinite reflectances are shown. Also shown are the reflectance data of Potter *et al.* (*in press*) for the Mattson Formation. The left diagram shows vitrinite reflectances calculated using six time invariant heat flows. None of these match the slope of the data but most observed reflectances fall between the 80 mW/m² and the 100mW/m² calculated profiles. In the plot on the right, a better overall fit to the data is shown in profile 1 in which the Paleozoic heat flow is 135 mW/m² followed by a Mesozoic heat flow of 80 mW/m² and a Tertiary heat flow of 60 mW/m². Profile 2 shows the result of an alternate scenario in which Tertiary heat flow is 135 mW/m² and Paleozoic heat flow is 60 mW/m².

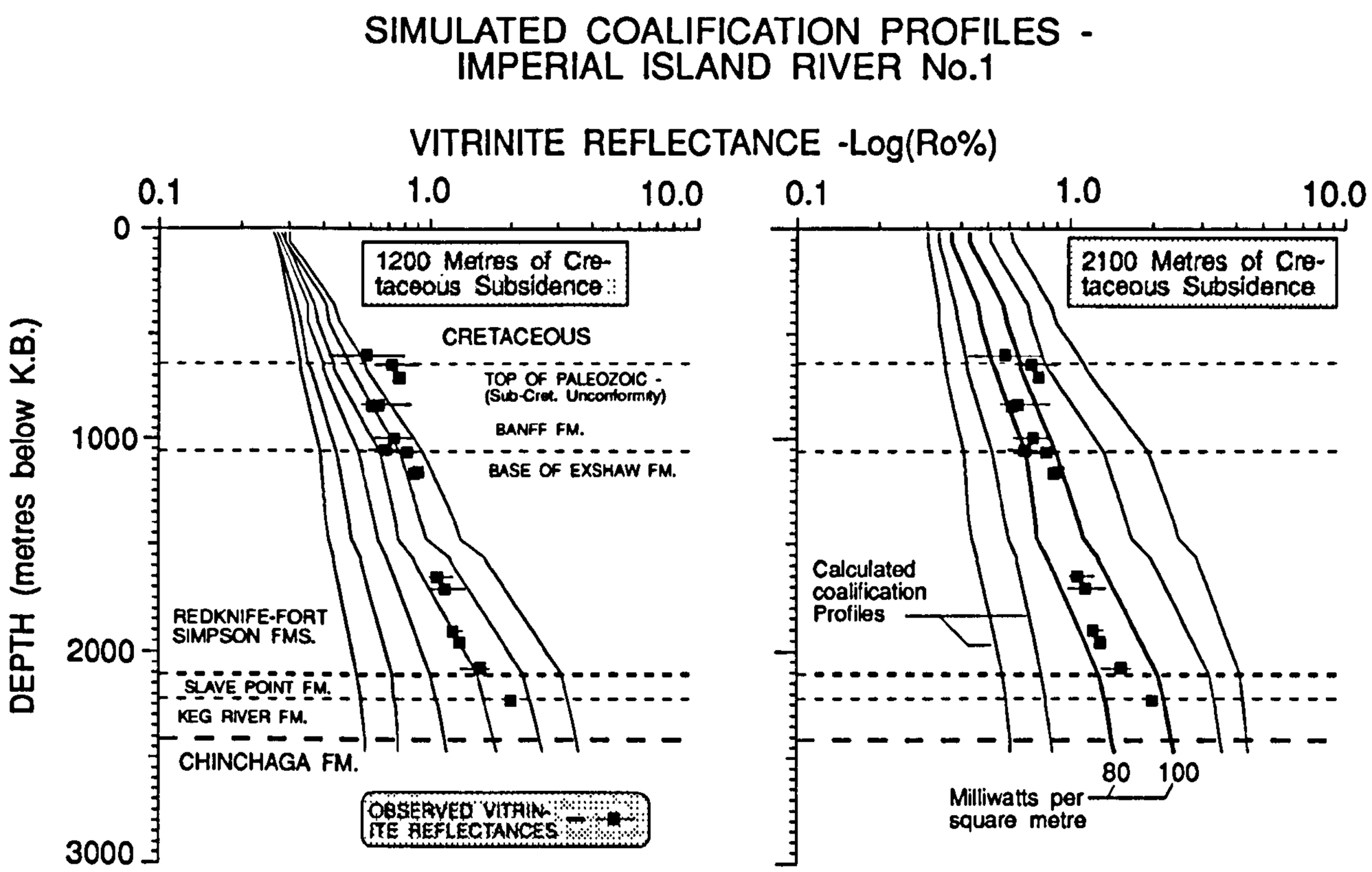

Fig. 12. Calculated vitrinite reflectance profiles for the Imperial Island River No. 1 well using the subsidence history shown in Figure 8 but with two different estimates for Cretaceous subsidence. The same array of constant heat flows that were used in Figure 11 are used in both graphs. The graph on the left, incorporating the smaller amount of Cretaceous subsidence (1200 m - Table 2), does not fit the data very well. On the right, using a larger estimate for Cretaceous subsidence (2100 m - Table 2), almost all the observed vitrinite reflectances fall within the domain between reflectances calculated using the 80 mW/m^2 and 100 mW/m^2 heat flows. This implies that the average paleoheat during deposition was about 90 mW/m^2, or the same as the modern day heat flow (Majorowicz *et al.*, 1988) at this well site.

fields because of the proximity of these shales to the underlying Manetoe Facies gas reservoirs (Fig. 3). Hydrocarbons may have moved downward from these organic-rich shales into Manetoe reservoirs as oil, during the late Carboniferous when sufficient oil had been generated to permit migration as a continuous liquid phase, or later, as gas phase hydrocarbons, in the Permian to Triassic, during the thermal cracking of oil to gas.

The large amounts of bitumen present in the gas fields of the Liard Basin as vug-fillings postdating dolomitization (Morrow *et al.*, 1986; 1990, Snowdon, 1977) may indicate that hydrocarbons migrated into these fields as oil, rather than as gas. This implies that migration of hydrocarbons into these gas fields can have occurred only if dolomitization occurred early, in the Late Devonian to Carboniferous. Alternatively, if migration of hydrocarbons occurred in the gas phase, the most likely period of migration would be the Permian to Triassic, which coincided with the peak of gas generation near the base of the oil window (Dow, 1977). In either case, a Cretaceous or Tertiary origin for the Manetoe Facies dolomite is less likely than a pre-Cretaceous origin.

If the host rock dolomite of the Manetoe reservoirs formed in the Cretaceous or Tertiary, migration of hydrocarbons from the Besa River shales would have occurred as dry gas only and residual bitumen should not be expected in these reservoirs. This is consistent with the conclusions of Aulstead *et al.* (1988) who also suggested, based on fluid inclusion data, that the diagenetic dolomites of the Manetoe Facies were emplaced in the late Devonian, rather than during the Cretaceous-Tertiary. Manetoe dolomitization was probably not coeval with hydrocarbon maturation and migration because hydrocarbons were not identified in any dolomite fluid inclusions (Aulstead *et al.*, 1988).

Small Devonian gas reservoirs are common in wells near the Imperial Island River No. 1 well (Williams, 1981). As in the Liard Basin, generation of oil in the region of the Imperial Island River well began in the late Devonian if even a relatively low heat flow of 80mW/m^2 is assumed. However, the Devonian sequence in this well did not pass through the oil window until the late Cretaceous unless higher average heat flows are assumed. Consequently, because of this more lengthy maturation history, it is uncertain when these smaller gas reservoirs formed in the Interior Plains Region.

Simulations of organic maturation have indicated that Paleozoic geothermal gradients were on average higher than present gradients in the Liard Basin Region primarily because of the very low level of organic maturity of the top of the Paleozoic sequence and the rapid downward increase in maturity. This is consistent with the data and conclusions of Feinstein *et al.* (1991) which suggest that the sub-Cretaceous sequence of the south-central part of the Mackenzie Mountains north of the Liard Basin was subjected to anoma-

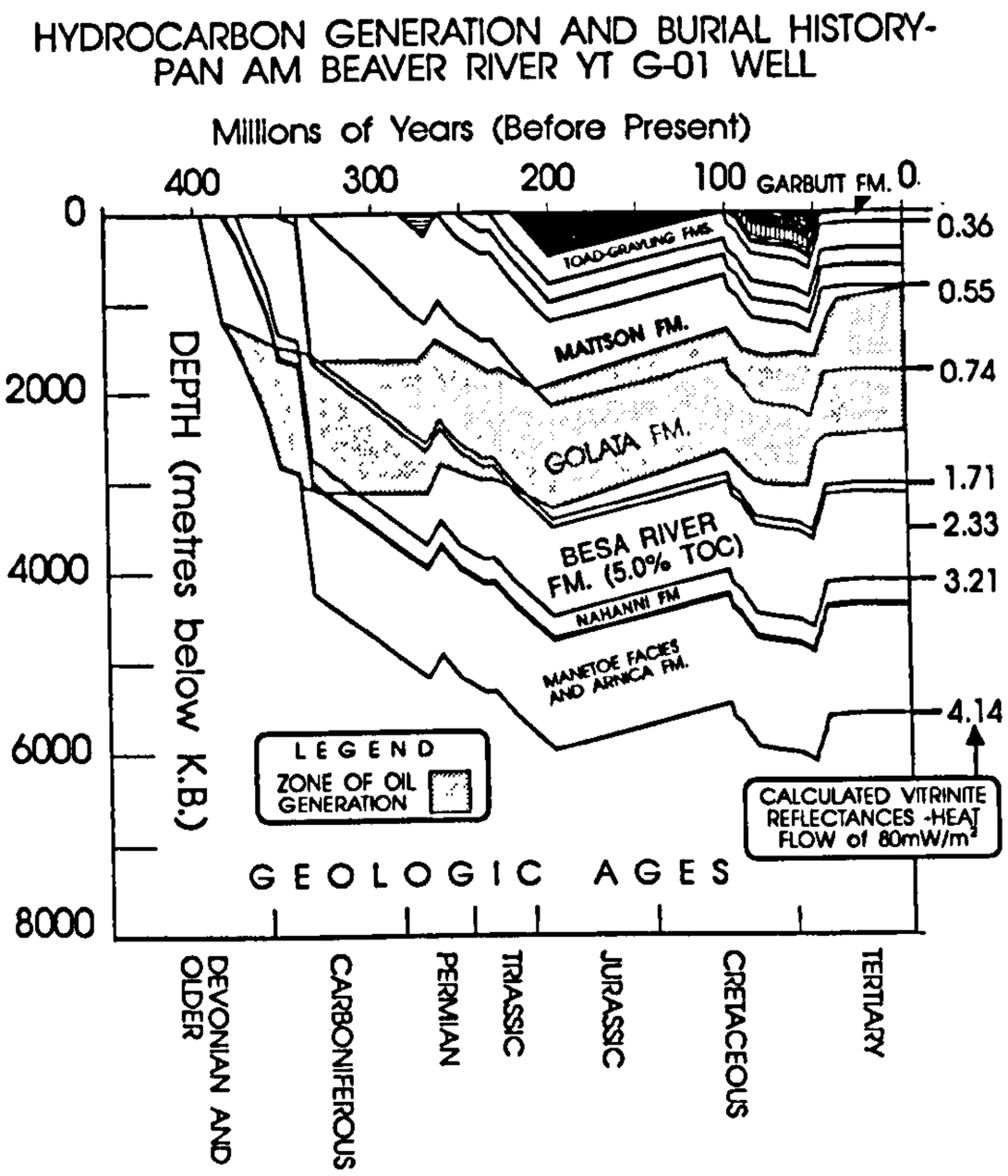

Fig. 13. Burial history and organic maturation plot of the Pan Am Beaver River YT G-01 calculated using the decompaction program of Osadetz and Mottershead (1992) modified to calculate vitrinite reflectances R_o% according to the EASY%R_o algorithm (Sweeney and Burnham, 1990). Eroded intervals are shaded. Organic-rich shales of the Besa River Formation enter the oil window in Carboniferous time, even using a heat flow of 80 mW/m², which underestimates the level of maturity in the lower part of this sequence. Migration of oil downward into underlying Manetoe dolomite may have occurred at that time. This oil may then have then evolved to gas phase hydrocarbons and to abundant residual pyrobitumen that coats vug-filling dolomite crystals in Manetoe reservoirs. Alternatively, gas phase hydrocarbons may have entered Manetoe reservoirs from the overlying Besa River in the late Paleozoic to early Mesozoic during thermal cracking of oil to gas.

lously high pre-Cretaceous geothermal gradients of 50° to 55° C/km.

Simulations of organic maturation in the Interior Plains Region are less well constrained. The model tentatively adopted here of deep late Cretaceous burial coupled with a constant heat flow or geothermal gradient similar to that of the present heat flow and gradient at the Imperial Island River No. 1 well is consistent with the conclusions of Arne (1991) that the Interior Plains Region, between the Imperial Island River No. 1 well and the Pine Point Mine at Great Slave Lake, was subjected to late Cretaceous burial of 1.5 km to 2.0 km, based on analysis of apatite fission track data. Models with lesser amounts of late Cretaceous burial do not fit the trend of observed vitrinite reflectances as well.

Conclusions

The main conclusions of this study are:

1. The low vitrinite reflectances (R_o%), of between about 0.3 and 0.7 within the Mattson Formation of the early Carboniferous, indicates that Cretaceous burial did not greatly exceed the 700 m thickness of locally preserved Cretaceous strata. These low reflectances also indicate that the average post-Paleozoic geothermal gradient was less than the present gradient of 40° C/km in Liard Basin.
2. The rapid increase in vitrinite reflectance downsection below the Mattson Formation indicates that the average Paleozoic heat flow and geothermal gradient was high. Simulations of vitrinite reflectance or coalification profiles of the Beaver River G-01 well in the Liard Basin that involve high Paleozoic geothermal gradients (65°/km) or heat flows (135mW/m²) provide good fits to the observed data predicting low vitrinite reflectances of about 0.5%R_o at the top of the Mattson Formation and high reflectances of about 4.5%R_o at the level of the Nahanni Formation. This is consistent with previous suggestions regarding a late Devonian thermal event (Aulstead *et al.*, 1988) or of high average Paleozoic heat flow (Feinstein *et al.*, 1991).
3. Simulations of the observed vitrinite reflectance profile of the Imperial Island River No. 1 well indicate that late Cretaceous burial was about 2.0 km under the influence of a geothermal gradient and heat flow of about 45°/km and 90mW/m² respectively. Consequently, late Cretaceous burial was probably much greater in the Interior Plains than in the Liard Basin north of 60° N latitude.
4. Oil and gas generation and migration in Liard Basin is inferred to have occurred during the Late Paleozoic to Early Mesozoic. This implies a pre-Cretaceous, rather than a Cretaceous-Tertiary, origin for the dolomitized Manetoe Facies reservoir rock of the Liard Basin gas fields. The time of oil and gas generation in Liard Basin is largely independent of the choice of the heat flow models examined in this study because, even under the assumption of a low average Paleozoic geothermal gradient and heat flow, the hydrocarbon source rocks of the Besa River Formation, including equivalents of the Exshaw Formation, pass through the oil window in the late Paleozoic.

Acknowledgment

We wish to thank CSPG Bulletin reviewers Ian Moffat, Steve Creaney, Hans Wielens, Lloyd Snowdon and an anonymous reviewer for their numerous, constructive and helpful comments. Similarly, we extend our appreciation to Associate Editors, Glen Stockmal and Peter Aukes and, finally, to the former Editor, Ian Hutcheon for his patience and assistance in expediting the review process. This paper was funded by the Geological Survey of Canada Project 850031.

References

American Society for Testing and Materials, 1981. Microscopical determination of the reflectance of the organic components in a polished specimen of coal: Philadelphia. American Society for Testing and Materials, Standard D2798-79, 4p.

Arne, D.C. 1991. Regional thermal history of the Pine Point Area Northwest Territories, Canada from apatite fission track analysis. Economic Geology, v. 86, p. 428-435.

Aulstead, K.L., Spencer, R.J. and Krouse, H.R. 1988. Fluid inclusion and isotopic evidence on dolomitization, Devonian of Western Canada. Geochimica et Cosmochimica Acta, v. 52, p. 1027-1035.

_____ and _____ 1985. Diagenesis of the Keg River Formation, northwestern Alberta: Fluid inclusion evidence. Bulletin of Canadian Petroleum Geology, v. 33, p. 167-183.

Bebout, D.G. and Maiklem, W.R. 1973. Ancient anhydrite facies and environments, Middle Devonian Elk Point Basin, Alberta. Bulletin of Canadian Petroleum Geology, v. 21, p. 287-343.

Bustin, R.M. 1989. Diagenesis of Kerogen. *In:* Short Course in Burial Diagenesis, Short Course Handbook, v. 15, Montreal, May 1989, I.E. Hutcheon (ed.). Mineralogical Association of Canada, p. 1-38.

de Wit, R., Gronberg, E.C., Richards, W.B. and Richmond, W.O. 1973. Tathlina area, District of Mackenzie. *In:* Future Petroleum Provinces of Canada, R.G. McCrossan (ed.). Canadian Society of Petroleum Geologists, Memoir 1, p. 187-212.

Douglas, R.J.W. (ed.). 1970. Geology and Economic Minerals of Canada. Geological Survey of Canada, Economic Geology Report No. 1, 838p.

_____ 1974. Geology of the Trout River map-area, District of Mackenzie. Geological Survey of Canada Map 1371A, 1:500,000.

_____ 1976. Geology of the La Biche River map-area, District of Mackenzie, Geological Survey of Canada Map 1380A, 1:250,000.

_____ and Norris, D.K. 1976. Geology of the Fort Liard map-area, District of Mackenzie, Geological Survey of Canada Map 1379A.

Dow, W.G. 1977. Kerogen studies and geological interpretations. Journal of Geochemical Exploration, v. 7, p. 79-99.

Espitalié, J., Deroo, G. and Marquis, F. 1985. Rock-Eval pyrolysis and its applications. Institut Francais du Petrole preprint #27299, 132p. *In:* Revue de l'Institut Francais du Petrole, v. 40, no. 5, p. 563-580; v. 40, no. 6, p. 755-784; v. 41, no. 1, p. 73-90. Published in French.

Feinstein, S., Williams, G.K., Snowdon, L.R., Goodarzi, F. and Gentzis, T. 1991. Thermal maturation of organic matter in the Middle Devonian to Tertiary section, Fort Norman area (Central Mackenzie Plain). Canadian Journal of Earth Sciences, v. 28, p. 1009-1018.

Gabrielse, H. 1967. Tectonic evolution of the northern Canadian Cordillera. Canadian Journal of Earth Sciences, v. 4, p. 271-298.

Harker, P. 1963. Carboniferous and Permian rocks, southwestern District of Mackenzie. Geological Survey of Canada, Bulletin 95.

Jacob, H. 1985. Dispersed solid bitumen as an indicator for migration and maturity in prospecting for oil and gas. Erdöl Kohle, v. 35, p. 365.

Kalkreuth, W. and McMechan, M.E. 1984. Regional pattern of thermal maturation as determined from coal-rank studies, Rocky Mountain Foothills and Front Ranges north of Grand Cache, Alberta -Implications for petroleum exploration. Bulletin of Canadian Petroleum Geology, v. 32, p. 249-271.

Klemme, H.D. 1975. Geothermal gradients, heat flow and hydrocarbon recovery. *In:* Petroleum and Global Tectonics, A.G. Fischer and S. Judson (eds.). Princeton University Press, 322p.

Leckie, D.A., Potocki, D.J. and Visser, K. 1991. The Lower Cretaceous Chinkeh Formation: A frontier-type play in the Liard Basin of Western Canada. American Association of Petroleum Geologists Bulletin, v. 75, no. 8, p. 1324-1352.

Machel, H.G. and Mountjoy, E.W. 1987. General constraints on extensive pervasive dolomitization -and their application to the Devonian carbonates of western Canada. Bulletin of Canadian Petroleum Geology, v. 35, p. 143-158.

Majorowicz, J.A., Jones, F.W. and Jessop, A.M. 1988. Preliminary geothermics of the sedimentary basins in the Yukon and Northwest Territories (60° N - 70° N) - Estimates from petroleum bottom-hole temperature data. Bulletin of Canadian Petroleum Geology, v. 36, p. 39-51.

McCrossan, R.G. and Glaister, R.P. 1964. Geological History of Western Canada. Published by the Alberta Society of Petroleum Geologists, Calgary, Alberta, Canada, 232p.

McKenzie, D.P. 1981. The variation of temperature with time and hydrocarbon maturation in sedimentary basins formed by extension. Earth and Planetary Science Letters, v. 55, p. 87-98.

Middleton, M.F. 1982. Tectonic History from vitrinite reflectance. Geophysical Journal of the Royal Astronomical Society, v. 62, p. 121-132.

Morrow, D.W. and Cook, D.G. 1987. The Prairie Creek Embayment and lower Paleozoic stratigraphy of the southern Mackenzie Mountains. Geological Survey of Canada, Memoir 412, 195p.

_____, Cumming, G.L. and Koepnich, R.B. 1986. Manetoe Facies- a gas-bearing, megacrystalline, Devonian dolomite, Yukon and Northwest Territories, Canada. American Association of Petroleum Geologists, Bulletin, v. 70, p. 702-720.

_____, Aulstead, K.L. and Cumming, G.L. 1990. The gasbearing Devonian Manetoe Facies, Yukon and Northwest Territories. Geological Survey of Canada, Bulletin 400, 54p.

Osadetz, K.G. and Mottershead, K.E. 1992. *in press.* Burial: A program that calculates and draws the burial history curves and thermal maturity history for a stratigraphic section. Geological Survey of Canada, Paper 19-91.

Peters, K.E. 1986. Guidelines for evaluating source rock using programmed pyrolysis. American Association of Petroleum Geologists, Bulletin, v. 70, no. 3, p. 318-329.

Potter, J., Richards, B.C. and Goodarzi, F. *in press.* Organic Petrology and thermal maturity of Lower Carboniferous and Upper Devonian in the Liard Basin, southwestern District of Mackenzie and southeastern Yukon Territory, Canada: Implications for hydrocarbon exploration. Energy Sources.

Poulton, T.P. 1989. Upper Absaroka to Lower Zuni: The transition to the foreland basin. *In:* Western Canada Sedimentary Basin - A Case History, B.D. Ricketts (ed.). Canadian Society of Petroleum Geologists, p.233-247.

Qing, H. and Mountjoy, E.W. 1989. Multistage dolomitization in Rainbow buildups, Middle Devonian Keg River Formation, Alberta, Canada. Journal of Sedimentary Petrology, v. 59, p.114-126.

Richards, B.C. 1989. Uppermost Devonian and Lower Carboniferous stratigraphy, sedimentation, and diagenesis southwestern District of Mackenzie and southeastern Yukon Territory. Geological Survey of Canada, Bulletin 390, 135p.

Snowdon, D.M. 1977. Beaver River gas field: a fractured carbonate reservoir. *In:* The Geology of Selected Carbonate Oil, Gas and Lead-Zinc Reservoirs in Western Canada, I.A. McIlreath and R.D. Harrison (eds.). Canadian Society of Petroleum Geologists, 5th Core Conference, p. 1-18.

Snowdon, L.R. 1989. Organic matter properties and thermal evolution. *In:* Short Course in Burial Diagenesis, Short Course Handbook, v. 15, Montreal, May 1989, I.E. Hutcheon (ed.). Mineralogical Association of Canada, p. 39-60.

Spencer, R.J. 1987. The origin of Ca-Cl brines in Devonian formations, western Canada sedimentary basin. Applied Geochemistry, v. 2, p.373-384.

Stott, D.F. 1982. Lower cretaceous Fort St. John Group and Upper Cretaceous Dunvegan Formation of the Foothills and Plains of Alberta, British Columbia, District of Mackenzie and Yukon Territory. Geological Survey of Canada, Bulletin 328, 124p.

Sweeney, J.J. and Burnham, A.K. 1990. Evaluation of a simple model of vitrinite reflectance based on chemical kinetics. American Association of Petroleum Geologists, Bulletin, v. 74, p. 1559-1570.

Tissot B.P. and Welte, D.H. 1984. Petroleum Formation and Occurrence. Second revised and enlarged edition, SpringerVerlag, Berlin, 699p.

Utting, J., Goodarzi, F., Dougherty, B.J. and Henderson, C.M. 1989. Thermal maturity of Carboniferous and Permian rocks of the Sverdrup Basin, Canadian Arctic Archipelago. Geological Survey of Canada, Paper 89-19, 20p.

Waples, D. 1980. Time and temperature in petroleum formation: Application of Lopatin's method to petroleum exploration. American Association of Petroleum Geologists, Bulletin, v. 64, p. 916-926.

Williams, G.K. 1979. An update of subsurface information, Cretaceous rocks, Trout Lake area, southern Northwest Territories. *In:* Current Research Geological Survey of Canada, Paper 78-1A, p.545-553.

_____ 1981. Subsurface geological maps, southern Northwest Territories. Geological Survey of Canada, Open File 793.

Manuscript received: January 9, 1992.

Revised manuscript accepted: June 11, 1992.

Energy Sources, Volume 15, pp. 289–314
Printed in the UK.

0090-8312/93 $10.00 +.00

The Organic Petrology and Thermal Maturity of Lower Carboniferous and Upper Devonian Source Rocks in the Liard Basin, at Jackfish Gap-Yohin Ridge and North Beaver River, Northern Canada: Implications for Hydrocarbon Exploration

JUDITH POTTER

Newcastle Research Group in Fossil Fuels and Environmental Geochemistry
The University of Newcastle-upon-Tyne
Newcastle-upon-Tyne, NE1 7RU, U.K.

BARRY C. RICHARDS
FARIBORZ GOODARZI

Institute of Sedimentary and Petroleum Geology
Geological Survey of Canada
Calgary, Alberta, Canada T2L 2A7

Abstract *Organic petrology and geochemical studies (Rock-Eval/TOC) were carried out on shales from the Besa River (Upper Devonian-Lower Carboniferous), Yohin, Clausen, Prophet, Golata, and Mattson Formations (Lower Carboniferous) in exposed sequences at Jackfish Gap-Yohin Ridge and in a subsurface section in the North Beaver River area of the Liard Basin.*

Basinal shales of the Besa River Fm. have TOC values ranging from 1 to 4% and contain abundant type II, dominantly amorphous, kerogen of marine origin. Shales in the Yohin Fm. (slope to neritic shelf), Clausen Fm. (basin and slope deposits), Prophet Fm. (carbonate slope), and Golata Formations are of mixed marine and terrestrial origins and yield TOC values of 1 to 3%. Kerogen in the Golata (prodelta shales) and Yohin Formations are dominated by terrestrial components, while the Clausen and Flett kerogen comprises marine liptinites and bitumens. Kerogen from the deltaic Mattson shales at Jackfish Gap are types II and III, having mixed marine and terrestrial origins consistent with shallow, nearshore, subtidal environments. The coals, which are rich in inertinite and liptinite (up to 30%), are sapropelic and probably lacustrine in origin. Algal laminites associated with coals in the Upper Mattson have >10% TOC values, while non-laminite shales contain between 2 and 5% TOC. Comparable measured and calculated vitrinite reflectance data indicate that kerogen in the Lower Carboniferous at Jackfish Gap is mature (0.5–1.1%). Kerogen in correlative formations in the subsurface at North Beaver River is more marine. Vitrinites are rare and oxidized, but four populations of bitu-

mens are distinguished on the basis of relative reflectivity and morphological or petrophysical associations. Types A and B bitumens are primary and by-products of hydrocarbon generation from type II (algal and amorphous) kerogens. Correlations between depth and reflectance of bitumens A and B are very good (r^2 = 0.97%). Vitrinite reflectance data calculated from bitumen reflectance measurements for the Besa River (1.6–2.1%), Prophet (1.5%), and Golata (1.2%) indicate that they are potential sources of catagenic gas. The Mattson kerogen is mature (0.84–1.0% VR_o), oil and gas-prone.

Keywords Kerogen, sapropelic coals, primary bitumens, reflectance, maturation, catagenic gas

Introduction

Lower Carboniferous and Upper Devonian rocks are exposed over large areas of the Liard Basin in the southeastern Yukon territory and southwestern District of Mackenzie, NWT, Canada, between latitudes N60° and N61° and W122° and W125° (inset, Figure 1). Since gas production from Middle Devonian (fractured dolomite) reservoirs was established in the Beaver River (approx. 124°20′ and 60°04′) and Pointed Mountain areas (123°50′ and 60°30′) in the late 1950s to early 1960s, there has been a hiatus in drilling activity in this area. Although renewed interest in the Liard Basin has led to exploration drilling in northeastern British Columbia, the region north of latitude 60° and west of longitude 124° remains largely unexplored. A detailed examination of the source rock potential and thermal history of the Upper Paleozoic strata of the Liard Basin is therefore highly relevant to the economic potential of this region.

These preliminary studies of the hydrocarbon potential of the Lower Carboniferous and Upper Devonian in the area west of Fort Liard are based on organic petrological studies (kerogen characterization, vitinite and bitumen reflectance measurement) supplemented by estimation of Total Organic Carbon (TOC) and Rock-Eval pyrolysis studies. Two sections were examined: (1) a subsurface section in the Canada Southern et al. N. Beaver River YT 1-27 well at N60°07′ W124°37′ (NTS 95 B/2), where the Lower Carboniferous and Upper Devonian occurs between 1000 and 4000 m depth; and (2) surface exposures of the Upper Devonian and Lower Carboniferous at Jackfish Gap and Yohin Ridge at N61°05′54 W123°59′26″, where Upper Paleozoic strata occur at 2000 to 3000 m elevation and an expanded section of the Mattson Formation attains a thickness of 1030 m. Analyses were carried out predominantly on shales, siltstones, and coals from the Mattson, Golata, Flett, Prophet, Clausen, Yohin (Viséan-Serphukovian), and Besa River (Frasnian-Fammenian) Formations.

The purpose of this article is to present some of the preliminary data on the kerogen type and potential source rocks in the Liard Basin and to demonstrate the use of bitumen reflectance data in thermal maturity studies. The Lower Carboniferous and Upper Devonian sequence in this area is dominated by carbonate rocks that tend to be poor or lacking in vitrinite. Data presented here show that the reflectance of primary bitumens can be used as an alternative to vitrinite reflectance measurement in thermal maturity studies of marine sequences and source rocks.

Geology

The regional geology is shown in Figure 1 (Douglas et al. 1963). Upper Devonian and Carboniferous strata consist of a shallowing-upward succession of basinal to shelf carbonates and terrigenous clastics deposited in the eastern Prophet Trough, a broad,

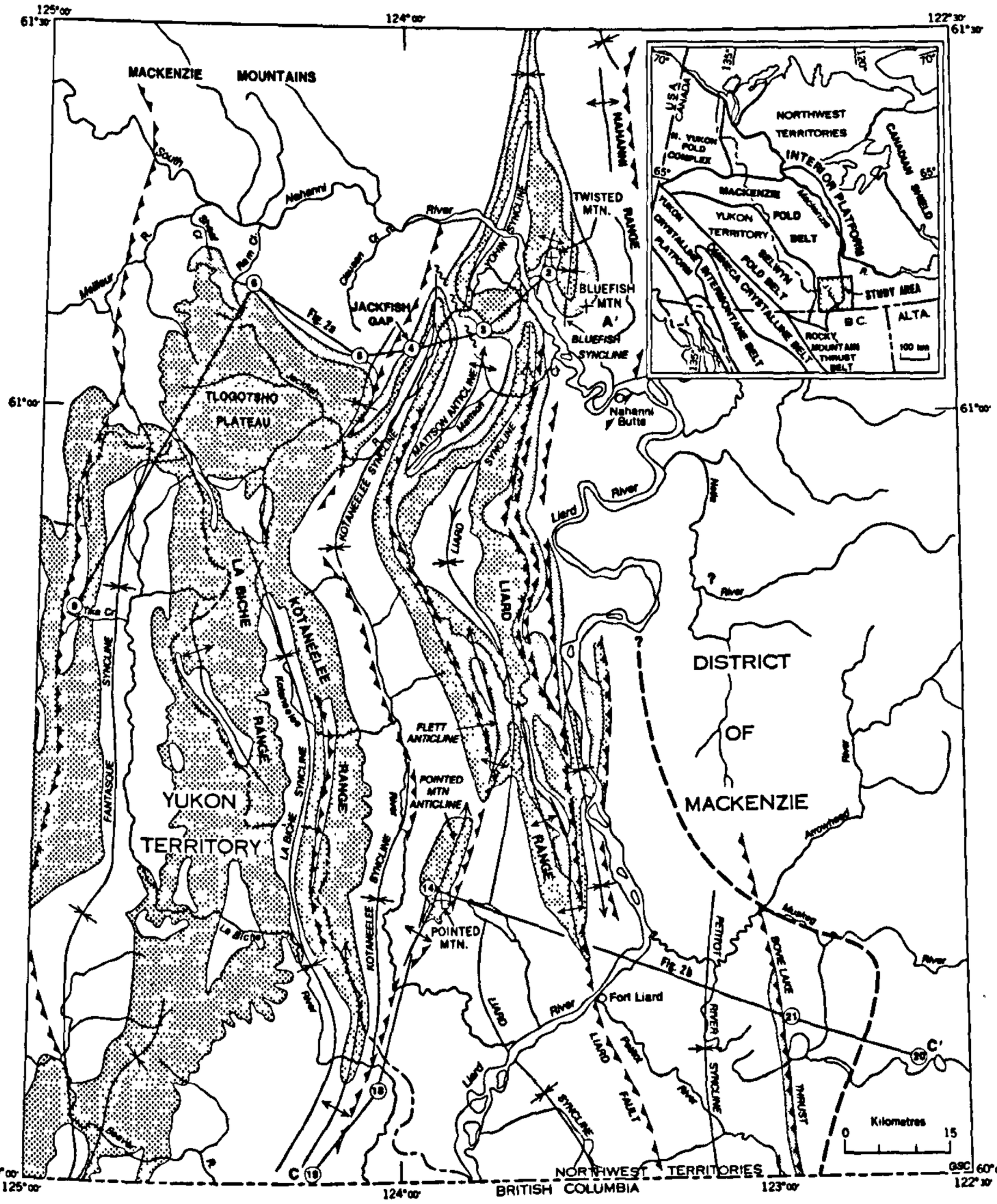

Figure 1. Surface geology of the Liard Basin west of W122° and north of N60°, southeastern Yukon and southwestern District of Mackenzie. Jackfish Gap is shown at location 4 and Canada Southern et al. N. Beaver River at location 18. (Reproduced from Richards 1989).

north northwest–south southeast-trending trough-shaped basin produced by subsidence of the western margin of the ancestral North American Plate (Richards 1989; Richards et al. 1989). The Lower Carboniferous succession in the Liard Basin has been interpreted by Richards (1989) as deltaic and shallow marine shelf, slope, and basinal sediments. Figure 2 shows the stratigraphic correlations between the Lower Carboniferous and Upper Devonian in the Liard Basin in the Southern Yukon, District of Mackenzie, and Northeastern British Columbia. The stratigraphy and depositional environments of the Upper Devonian-Lower Carboniferous at Jackfish Gap-Yohin Ridge succession are described in detail by Richards (1989). At Jackfish Gap-Yohin Ridge, a thick sequence of Lower Carboniferous includes the Besa River, Yohin, Clausen,

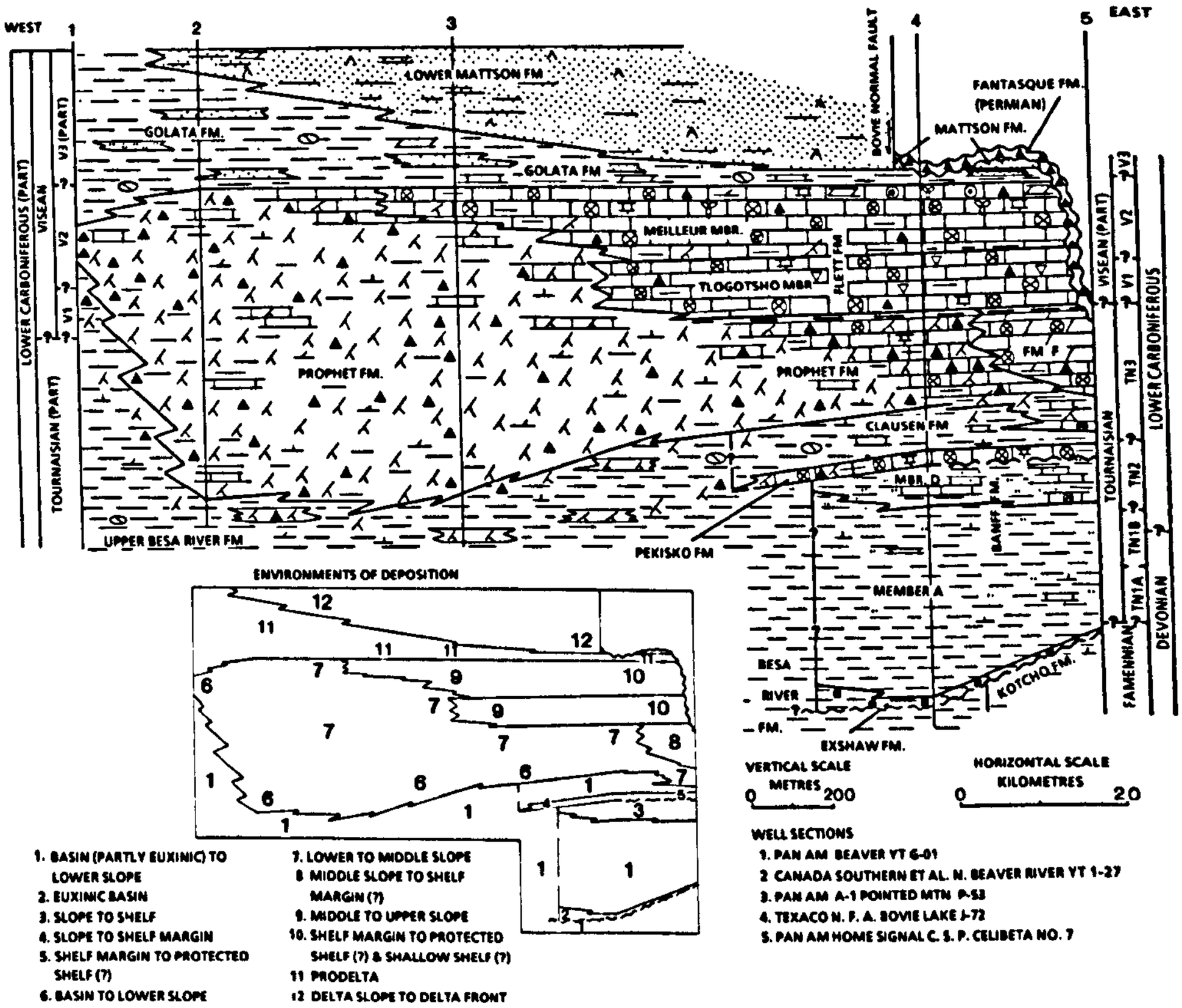

Figure 2. Partially schematic, restored east-west cross section showing stratigraphy and depositional environments of Lower Carboniferous and Upper Devonian strata in the Liard Basin, District of Mackenzie. Section at Canada Southern et al. N. Beaver River is No. 2. (Reproduced from Richards 1989.)

Prophet, Flett, and Golata Formations. The Besa River Formation comprises a thick unit of basinal shales and mudstones of Middle Devonian to late Viséan (V3) age, which conformably underlies the Prophet and is 3060 m thick in the Canada Southern et al. well at N. Beaver River. The upper Besa River thins northward and eastward and is correlative with the Banff, Clausen, and Golata Formations at Jackfish Gap-Yohin Ridge. The sandstone-dominated facies of the Yohin Formation is restricted to the northern section, where it attains a thickness of 160 m. Richards (1989) interpreted the Yohin as slope and shallow neritic shelf deposits. The slope and basinal shales of the Clausen at Jackfish Gap are 150 m thick and grade laterally and southward into the basinal shales of the Besa River Formation. The Prophet is a shale-dominated unit of lower to middle slope and basinal deposits that is 125 m thick at Yohin Ridge but reaches a thickness of 765.4 m in the subsurface at Canada Southern et al. N. Beaver River. The Flett Formation represents carbonate ramp and platform deposits and associated shelf margin and slope facies, of which 350 m are exposed at Yohin Ridge but which pinch out to the south and are absent at N. Beaver River. The shale-dominated Golata Formation represents prodelta facies that is only 12 m thick at Yohin Ridge but attains a thickness of 900 m in the subsurface at N. Beaver River. The Mattson is of

Upper Viséan (V3) to Early Serpukovian age (Patton 1958; Bamber and Mamet 1978; Braman and Hills 1977; Utting 1981) and is thickest (1020 m) at the type section at Jackfish Gap. It is a sandstone-dominated sequence including siltstones, subordinate shales, coals, and carbonates, deposited in deltaic and related environments during several delta cycles (Richards 1989). The lower Mattson at Jackfish Gap represents prograding delta plain facies (Richards, pers. comm.) recording a major regression during late Viséan and subsequently a marine transgression during uppermost Viséan to early Serpukovian. In the Canada Southern et al. well, the lithofacies are interpreted as delta slope to delta front deposits. Aeolian sandstones in the Upper Mattson at Jackfish Gap suggest deposition of the Mattson culminated under relatively dry, emergent conditions (Richards 1991).

Sampling and Analytical Methods

For this study, shales, siltstones, and coals samples were collected from surface exposures of the Besa River, Yohin, Clasen, Prophet, Golata, and Mattson Formations by Richards during a regional study of the Lower Carboniferous and Upper Devonian in this area (Richards 1983, 1989). Drill cuttings were hand-picked from the Besa River, Prophet, Golata, and Mattson Formations in the Canada Southern et al. N. Beaver River well. Sample splits were (a) mounted as epoxy resin pellets and polished for reflected light microscopy, and (b) pulverized for TOC and Rock-Eval pyrolysis.

Qualitative analysis of the kerogen was carried out with a Zeiss USMP-microscope using non-polarized, incident white and fluorescent (400–440 nm) light and oil immersion objectives (×40). The small particle size limited reflectance measurements to random reflectance, which was measured at 546 nm on vitrinite-like components and primary bitumens. Measurements were made predominantly in the plane of the bedding in order to minimize the reflectance variations attributable to anisotropy at elevated thermal maturity levels. The total number of measurements obtained for each organic component and sample varied according to the TOC content and kerogen composition. Rock-Eval pyrolysis was carried out following the method of Espitalié et al. (1985).

Maturation profiles for the two sections are based on both vitrinite and bitumen reflectance. For samples from the Jackfish Gap-Yohin Ridge section, reflectance was measured on vitrinite, which is relatively abundant in both coals and shales throughout the section (excluding the Flett Formation). However, in the subsurface at North Beaver River, vitrinite is rare to absent in most formations. Where vitrinite does occur, it is severely oxidized, probably due in part to extensive dolomitization and in part to prolonged storage, hence reflectance measurements were taken exclusively on indigenous bitumens in this section.

Results and Discussion

Kerogen Composition

The petrographic, geochemical characteristics and organic richness (total organic carbon, TOC) of the kerogens in Lower Carboniferous and Upper Devonian shales and siltstones at Jackfish Gap-Yohin Ridge and Canada Southern et al. well at N. Beaver River are summarized in Tables 1 to 4 and Figure 3. The kerogen compositions are discussed formation by formation.

Table 1
Organic Petrology of Samples from Lower Carboniferous and Upper Devonian Strata, Jackfish Gap-Yohin Ridge (N61°05'54" W123°59'26")

Formation	Kerogen Type	
	Dominant	Subordinate
Mattson (coals)	Inertinites:[a] micrinite semifusinite, resino-intertinite Liptinites: sporinite with minor alginite and liptodetrinite	Vitrinite: perhydrous desmocollinite, gelocollinite, telocollinite Mineral matter (minor)
Mattson (shales)	Structured liptinites: sporinite (megaspores, crassispores, tenuispores) Vitrinite: gelocollinite, perhydrous desmocollinite, reworked telocollinite (upper Mattson) Unstructured liptinites: matrix bituminite, bituminite II Structured liptinite: lamalginite	Unstructured liptinites: matrix bituminite, bituminte II, lamalginite, exsudatinite Structured Liptinites: Tasmanites, ?Reinschia, ?Pila Inertinites: micrinite, semifusinite, fusinite
Golata	Unstructured liptinite: bituminite Structured liptinite: reworked alginite Bitumen: type A (algal)	Liptinite: alginite Vitrinite: telocollinite Inertinite: fusinite
Flett	Liptinite: large colonial alginite Bitumen: type A (algal), type B (amorphous) Unstructured liptinite: bituminite	Liptinites: rare alginite, reworked alginite, liptodetrinite, rare sporinite (reworked)
Prophet	Vitrinite: reworked Bitumen: type A (algal)	Liptinite: alginite (rare)
Clausen	Liptinite: liptodetrinite (?algal) Unstructured liptinite: matrix bituminite	Inertinite: semifusinite, macrinite fusinite; Vitrinite (rare); reworked vitrinite-like
Yohin	Vitrinite: "fresh" and reworked; gelocollinite	Inertinite: semifusinite, macrinite, sclerotinite Liptinite: degraded sporinite, alginite (?Botryococcus), liptodetrinite ?Chitin

[a]In order of abundance.

Table 2
Organic Petrology of Samples from Lower Carboniferous and Upper Devonian Strata, Canada Southern et al. N. Beaver River (N60°07′ W124°04′)

	Kerogen Type	
Formation	Dominant	Subordinate
Mattson	Bitumen: type A (algal); type B (amorphous); Unstructured liptinite: bituminite (algal)	Bitumen: pyrobitumen type D
Golata	Bitumen: type B (amorphous)	Bitumen: type A (algal); pyrobitumen (type D) Unstructured liptinite: bituminite (algal) Inertinite: fusinite
Prophet	Bitumen: type A (algal) Unstructured liptinite: bituminite (algal)	Bitumen: type B (amorphous) pyrobitumen (types C & D)
Besa River	Bitumen: type A (algal)	Bitumen: type B (amorphous), pyrobitumen Unstructured liptinite: algal bituminite; matrix bituminite

Besa River Formation. The Besa River Formation was sampled only in the Canada Southern et al. borehole. Kerogen accounts for between 2 and 6 wt.% of the shale in the Besa River Formation (Table 4). It is dominated by unstructured liptinite comprising a dark bituminite-micrite groundmass derived by maturation of what was previously a rich amorphous bituminous matrix (Figure 4a). Also present are thin lenses of dark brown to black bituminite of the order of 100 μm long, lying parallel to the bedding. The form and distribution suggests that this is either a degradation or a maturation product of algal components such as Leiosphaeridiales. These components are consistent with a marine type II kerogen. Hydrogen indices are low, which may be attributed to elevated maturity.

Indigenous bitumens are present also. Initially these were distinguished on the basis of differences in reflectance, but morphological/petrophysical associations are effectively the predominant distinguishing characteristics. The dominant type in the Besa River is a relatively low-reflecting, isotropic solid (type A), which is somewhat vesicular at 3310.13 m. It is concentrated along the bedding planes and associated with a laminated fabric imposed by the ?algal bituminite. It commonly occurs as a thin (<3 μm) lining on the surface of pores occupied by the bituminite. Medium reflectance bitumens (type B) and highly reflective pyrobitumens (types C and D) are also present in

Table 3
Reflectance, TOC, and Rock-Eval Analyses of Samples from Lower Carboniferous and Upper Devonian Strata, Jackfish Gap-Yohin Ridge (N61°05′54″ W123°59′26″)

Sample No.	Height (m) Above Base of Section	Height (m) Above Base of Form'n	Formation	Percent Reflectance: Alginite	Bitumen A	Bitumen B	Vitrinite Meas.	Vitrinite Calc.[a]	TOC %	Rock-Eval Data: T_{max}	S1	S2	S3	PI	HI	OI
C58505	12.2	7.5	Yohin								0.07	0.25	0.33	0.23	16	21
C52163	35.7	31	Yohin							475	0.12	0.26	0.25	0.31	21	22
C52166	45.9	41.2	Yohin													
C58503	99.9	95.2	Yohin							476	0.04	0.33	0.32	0.21	19	16
C52174	116.5	111.8	Yohin													
C58502	154.6	149.9	Yohin							474	0.06	0.25	0.2	0.2	26	22
C52180	314.9	157.7	Clausen			0.68	0.96	0.82	1.52	458	0.2	0.63	0.23	0.23	40	15
C52181	315.9	158.7	Clausen													
C52064	445.7	95.7	Prophet			0.63		0.79								
C52067	470.7	120.7	Prophet			0.49		0.70	0.5	434	0.07	0.28	0.45			80
C52106	621.5	271.5	Flett	0.29	0.38	0.45		0.68								
C52115	687.9	337.9	Flett	0.30	0.39					437	0.27	0.36	0.19	0.43	131	70
C58522	727.4	377.4	Flett	0.27	0.34	0.45										
C74336	755.9	405.9	Flett			0.56		0.75	0.66	440	0.13	0.57	0.36	0.19	85	55
C74338	762.7	412.7	Flett			0.53		0.73	0.48	438	0.06	0.27	0.35	0.2	56	74
C52152	806.4	456.4	Flett	0.20	0.39					438	0.15	0.46	0.31	0.25	100	68
C52157	824.3	474.3	Flett	0.30	0.38	0.47		0.69	0.28	424	0.18	0.45	0.45	0.46	65	158
C58517	832.3	482.3	Golata	0.22	0.31	0.41		0.65	1.35	437	0.05	0.63	0.22	0.07	46	16

C58711	887	55	Mattson			441	0.07	0.64	0.56	0.1	44	38
C58713	920.5	88.5	Mattson		5.02	434	0.16	6.99	0.02	0.02	138	16
C58719	1017	185	Mattson		2.60	447	0.08	1.43	0.6	0.05	55	26
C58723	1062.5	230.5	Mattson			444	0.32	10.38	1.1	0.03	140	15
C58726	1084	252	Mattson			443	0.15	2.58	0.48	0.05	78	14
C58730	1121	289	Mattson									
C58736	1153	321	Mattson									
C58737	1154	322	Mattson									
C58749	1209	377	Mattson									
C58750	1212	380	Mattson		3.39	442	0.14	4.3	0.44			12
C58753	1220.7	388.7	Mattson		2.20	443	0.08	0.36	0.74	0.19	15	33
C58764	1391	559	Mattson		coal	441			0.53	0.03		
C58765	1391	559	Mattson		4.92	441	0.26	8.14	0.54	0.03	170	12
	1391.5	559.5	Mattson									
C58783	1569	737	Mattson									
C58793	1618	786	Mattson	0.73	1.83	443	0.13	2.14	0.77	0.06	116	42
C58804	1721.5	889.5	Mattson	0.67								
C58806	1730.5	898.5	Mattson	0.66	35.00	448	1.04	17.44	11.65	0.06	50	33
C58838	1880.5	1048	Mattson	0.65	45.14	452	0	0.9	12.43	0	2	27

[a]Calculated from measured reflectance on bitumen B.

Table 4
Reflectance, TOC, and Rock-Eval Analyses of Samples from Lower Carboniferous and Upper Devonian Strata, Canada Southern et al., N. Beaver River (N60°07′ W124°04′)

Sample No.	Depth (ft)	Depth (m)	Formation	Percent Reflectance: Bitumen A	Bitumen B	Bitumen C	Bitumen D	Vitrinite Equivalent[a] A	Vitrinite Equivalent[a] B	Vitrinite Equivalent[a] C	Vitrinite Equivalent[a] D	TOC %	Rock-Eval T_{max}	Rock-Eval S1	Rock-Eval S2	Rock-Eval S3	Rock-Eval PI	Rock-Eval HI	Rock-Eval OI
C186754	3280-3299		Kindle									9.97	446	5.14	23.55	0.85	0.19	260	5
C186754	3540-3559	1082	Mattson	0.71	0.90	1.62	2.32	0.84	0.96	1.40	1.83	4.80	440	3.00	4.68	1.10	0.39	90	25
C186754	4370-4419	1338.1	Mattson	0.84	1.30		2.30	0.92	1.20		1.82	2.12	441	0.88	1.15	0.99	0.43	56	46
C186754	4570-4589	1385.7	Mattson	1.09	1.98	2.51	3.68	1.07	1.62	1.95	2.67	1.29	443	0.57	0.56	0.59	0.44	52	55
C186754	4750-4789	1454.3	Mattson									12.50	446	1.90	10.80	5.34	0.15	72	44
C186754	4880-4889	1489.3	Mattson	1.20	1.40	2.30		1.14	1.27	1.82		18.40	420	2.77	16.93	11.81	0.14	90	63
C186754	5130-5149	1566.8	Mattson	1.05	1.50	2.10		1.05	1.33	1.70		1.25	452	0.27	0.52	0.54	0.34	40	45
C186754	5970-6019	1825.9	Golata	1.30	1.60	2.20	4.16	1.20	1.39	1.76	2.97	2.27	457	0.58	1.15	3.66	0.34	53	33
C186754	6330-6369	1935.7	Golata	1.35	1.75	2.04		1.23	1.48	1.66		1.58	486	0.25	0.47	0.60	0.35	29	45
C186754	6630-6659	2024.4	Golata									1.40	493	0.19	0.38	0.71	0.34	22	30
C186754	7130-7150	2176.5	Prophet	1.60	1.87	2.10		1.39	1.56	1.70		1.06	503	0.19	0.18	0.34	0.54	19	29
C186754	7530-7550	2298.8	Prophet	1.80	2.00		3.60	1.51	1.64		2.62	1.50	395	0.50	0.33	0.41	0.60	22	25
C186754	7850-7860	2396.3	Prophet	1.80	2.10	2.50		1.51	1.70	1.95		3.25	427	0.43	1.49	2.15	0.26	47	64
C186754	8570-8599	2617.4	Prophet	1.83	2.10	2.90		1.53	1.70	2.19		5.15	428	0.59	3.13	3.07	0.16	67	63
C186754	8810-8819	2687.5	Prophet	1.87				1.56				6.20	425	0.66	2.72	3.17	0.20	43	50
C186754	8890-9019	2743.6	Prophet										438	0.50	1.68	1.45	0.23	63	55
C186754	9120	2780.5	Besa River	2.10			4.70	1.70			3.30	1.82	420	0.60	0.17	0.45	0.79	9	23
C186754	9370-9399	2862.5	Besa River	2.18	2.70	3.50	4.60	1.75	2.07	2.56	3.24	1.95	423	0.41	0.47	1.55	0.47	51	35
C186754	9650-9669	2944.8	Besa River	2.14	2.70	3.50		1.72	2.07	2.56		1.34	384	0.54	0.25	0.33	0.69	17	24
C186754	10310-10329	3146	Besa River	2.39	3.00	3.54		1.88	2.25	2.59		3.25		0.56	1.04	1.41	0.36	52	35
C186754	10660-10679	3251.5	Besa River			3.60	4.90				3.32	3.32	465	0.63	0.52	0.86	0.54	16	25
C186754	10869-10879	3315.6	Besa River	2.80	3.35	4.20	4.65	2.13	2.47	3.00	3.27	6.02	380	1.06	0.30	0.28	0.79	7	7
C186754	10930-10949	3335.1	Besa River		3.50	3.40	5.13		2.56	3.12	3.57	4.17	418	1.46	0.61	0.70	0.71	14	16
C186754	12510-12529	3816.8	Nahanni	3.30	3.70	4.25		2.44	2.69	3.03		16.11	418	4.58	17.33	12.51	0.20	107	78

[a]Calculated according to Jacob (1985).

SAMPLE NO.	DEPTH (ft)	DEPTH (m)	FORM-ATION	% REFLECTANCE BITUMEN Low	Med	High	V Hi	*VITRINITE Low	Med	High	V high	% TOC	ROCKEVAL DATA Tmax	S1	S2	S3	PI	HI	OI
C186760	3280-3299		Kindle									9.97	446	5.14	23.55	0.85	0.19	260	5
C186760	3540-3559	1082	Mattson	0.71	0.90	1.62	2.32	0.84	0.96	1.40	1.83	4.80	440	3.00	4.68	1.10	0.39	90	25
C186760	4370-4419	1338.1	Mattson	0.84	1.30		2.30	0.92	1.20		1.82	2.12	441	0.88	1.15	0.99	0.43	56	46
C186760	4570-4589	1385.7	Mattson	1.09	1.98	2.51	3.68	1.07	1.62	1.95	2.67.	1.29	443	0.57	0.56	0.59	0.44	52	55
C186760	4750-4789	1454.3	Mattson									12.50	446	1.90	10.80	5.34	0.15	72	44
C186760	4880-4889	1489.3	Mattson	1.20	1.40	2.30		1.14	1.27	1.82		18.40	420	2.77	16.93	11.81	0.14	90	63
C186760	5130-5149	1566.8	Mattson	1.05	1.50	2.10		1.05	1.33	1.70		1.25	452	0.27	0.52	0.54	0.34	40	45
C186760	5970-6019	1825.9	Golata	1.30	1.60	2.20	4.16	1.20	1.39	1.76	2.97	2.27	457	0.58	1.15	3.66	0.34	53	33
C186760	6330-6369	1935.7	Golata	1.35	1.75	2.04		1.23	1.48	1.66		1.58	486	0.25	0.47	0.60	0.35	29	45
C186760	6630-6659	2024.4	Golata									1.40	493	0.19	0.38	0.71	0.34	22	30
C186760	7130-7150	2176.5	Prophet	1.60	1.87	2.10		1.39	1.56	1.70		1.06	503	0.19	0.18	0.34	0.54	19	29
C186760	7530-7550	2298.8	Prophet	1.80	2.00		3.60	1.51	1.64		2.62	1.50	395	0.50	0.33	0.41	0.60	22	25
C186760	7850-7860	2396.3	Prophet	1.80	2.10	2.50		1.51	1.70	1.95		3.25	427	0.43	1.49	2.15	0.26	47	64
C186760	8570-8599	2617.4	Prophet	1.83	2.10	2.90		1.53	1.70	2.19		5.15	428	0.59	3.13	3.07	0.16	67	63
C186760	8810-8819	2687.5	Prophet	1.87				1.56				6.20	425	0.66	2.72	3.17	0.20	43	50
C186760	8890-9019	2743.6	Prophet									2.60	438	0.50	1.68	1.45	0.23	63	55
C186760	9120	2780.5	Besa River	2.10			4.70	1.70			3.30	1.82	420	0.60	0.17	0.45	0.79	9	23
C186760	9370-9399	2862.5	Besa River	2.18	2.70	3.50	4.60	1.75	2.07	2.56	3.24	1.95	423	0.41	0.47	1.55	0.47	51	35
C186760	9650-9669	2944.8	Besa River	2.14	2.70	3.50		1.72	2.07	2.56		1.34	384	0.54	0.25	0.33	0.69	17	24
C186760	10310-10329	3146	Besa River	2.39	3.00	3.54		1.88	2.25	2.59		3.25		0.56	1.04	1.41	0.36	52	35
C186760	10660-10679	3251.5	Besa River			3.60	4.90			2.62	3.43	3.32	465	0.63	0.52	0.86	0.54	16	25
C186760	10869-10879	3315.6	Besa River	2.80	3.35	4.20	4.65	2.13	2.47	3.00	3.27	6.02	380	1.06	0.30	0.28	0.79	7	7
C186760	10930-10949	3335.1	Besa River		3.50	4.40	5.13		2.56	3.12	3.57	4.17	418	1.46	0.61	0.70	0.71	14	16
C186760	12510-12529	3816.8	Nahanni	3.30	3.70	4.25		2.44	2.69	3.03		16.11	418	4.58	17.33	12.51	0.20	107	78

*calculated according to Jacob (1985)

Table 4

SAMPLE NO.	HEIGHT ABOVE SECTION	(M) ABV BASE OF FORM'N	FORM-ATION	% REFLECTANCE Algin-ite	BITUMEN Low	BITUMEN Med	VITRINITE meas	VITRINITE calc*	% TOC	ROCKEVAL DATA Tmax	S1	S2	S3	PI	HI	OI
C58505	12.2	7.5	Yohin						1.50	483	0.07	0.25	0.33	0.23	16	21
C52163	35.7	31	Yohin				1.06		1.12	475	0.12	0.26	0.25	0.31	21	22
C52166	45.9	41.2	Yohin				0.99									
C58503	99.9	95.2	Yohin				0.98		1.58	476	0.04	0.33	0.32	0.21	19	16
C52174	116.5	111.8	Yohin													
C58502	154.6	149.9	Yohin				0.93		1.00	474	0.06	0.25	0.2	0.2	26	22
C52180	314.9	157.7	Clausen			0.68	0.96	0.82	1.52	458	0.2	0.63	0.23	0.23	40	15
C52181	315.9	158.7	Clausen				0.80									
C52064	445.7	95.7	Prophet			0.63		0.79								
C52067	470.7	120.7	Prophet			0.49		0.70		435					54	80
C52106	621.5	271.5	Flett	0.29	0.38	0.45		0.68								
C52115	687.9	337.9	Flett	0.30	0.39				0.27	437	0.27	0.36	0.19	0.43	131	70
C58522	727.4	377.4	Flett	0.27	0.34	0.45										
C74336	755.9	405.9	Flett			0.56		0.75	0.66	440	0.13	0.57	0.36	0.19	85	55
C74338	762.7	412.7	Flett			0.53		0.73	0.48	438	0.06	0.27	0.35	0.2	56	74
C52152	806.4	456.4	Flett	0.20	0.39				0.46	438	0.15	0.46	0.31	0.25	100	68
C52157	824.3	474.3	Flett	0.30	0.38	0.47		0.69	0.28	424	0.18	0.45	0.45	0.46	65	158
C58517	832.3	482.3	Golata	0.22	0.31	0.41		0.65	1.35	437	0.05	0.63	0.22	0.07	46	16
C58711	887	55	Mattson						1.44	441	0.07	0.64	0.56	0.1	44	38
C58713	920.5	88.5	Mattson				0.72		5.02	434	0.16	6.99	0.02	0.02	138	16
C58719	1017	185	Mattson				0.71		2.60	447	0.08	1.43	0.6	0.05	55	26
C58723	1062.5	230.5	Mattson						7.40	444	0.32	10.38	1.1	0.03	140	15
C58726	1084	252	Mattson						3.30	443	0.15	2.58	0.48	0.05	78	14
C58730	1121	289	Mattson				0.71									
C58736	1153	321	Mattson				0.66									
C58737	1154	322	Mattson				0.70									
C58749	1209	377	Mattson													
C58750	1212	380	Mattson				0.62			442					141	12
C58753	1220.7	388.7	Mattson				0.60		2.20	443	0.08	0.36	0.74	0.19	15	33
C58764	1391	559	Mattson				0.64		coal	441		7.66	0.53	0.03		
C58765	1391	559	Mattson				0.74		4.92	441	0.26	8.14	0.54	0.03	170	12
	1391.5	559.5	Mattson				0.74									
C58783	1569	737	Mattson													
C58793	1618	786	Mattson				0.73		1.83	443	0.13	2.14	0.77	0.06	116	42
C58804	1721.5	889.5	Mattson				0.67									
C58806	1730.5	898.5	Mattson				0.66		35.00	448	1.04	17.44	11.65	0.06	50	33
C58838	1880.5	1048.5	Mattson				0.65		45.14	450	0	0.9	12.43	0	2	27

*calculated from med Ro bitumen, after Jacob (1985)

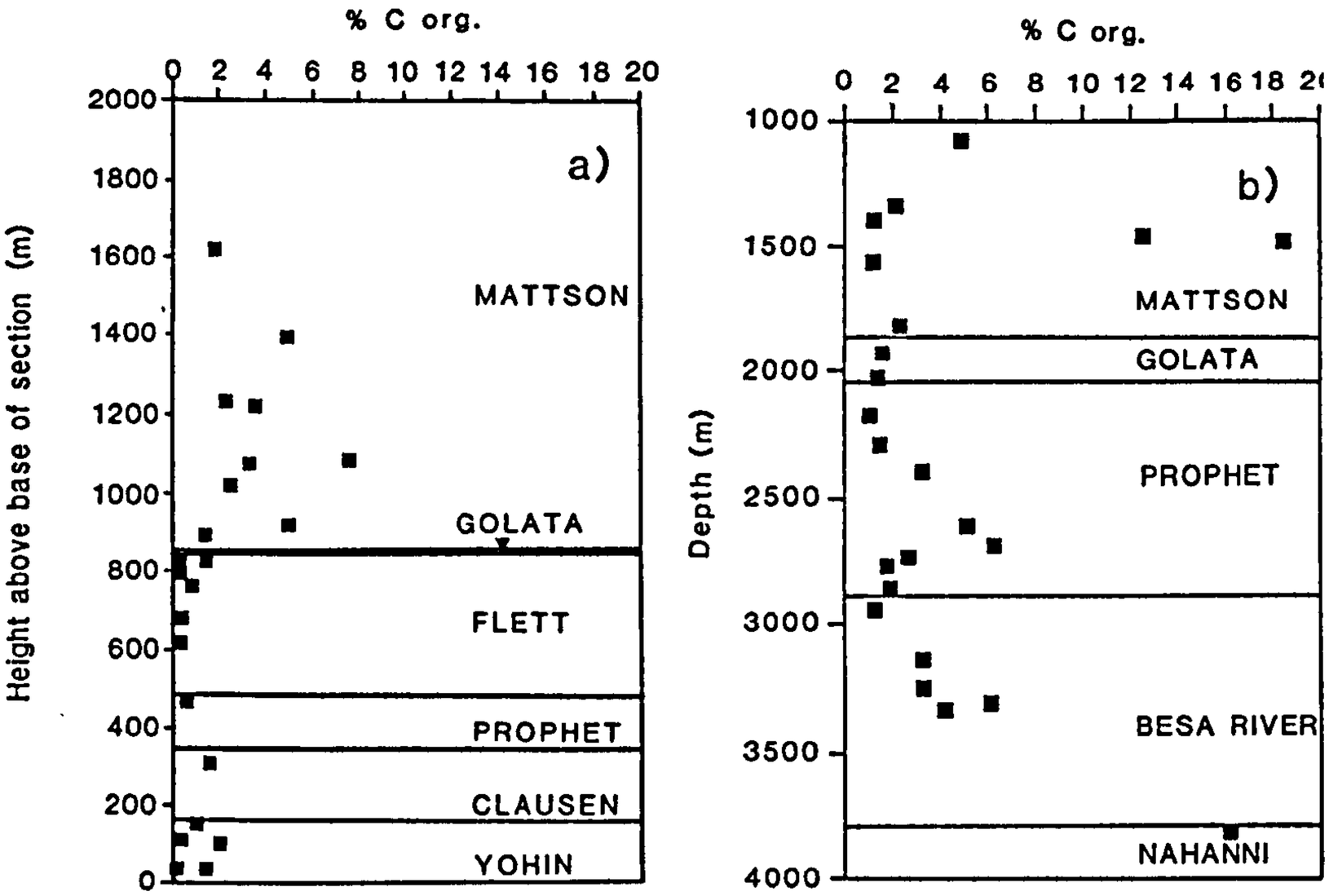

Figure 3. Abundance of organic matter in the Upper Devonian-Lower Carboniferous at (*a*) Jackfish Gap-Yohin Ridge; (*b*) Canada Southern et al., N. Beaver River, YT.

small amounts (Figure 4b). The type B bitumen is normally present in small pores (<30 μm) or lenses parallel to bedding in a fine-grained, clay mineral-rich matrix containing amorphous kerogen. It is also considered as a product of hydrocarbon generation, most likely from the amorphous matrix bituminite. The highly reflecting bitumens (types C and D) are anisotropic and are also pore-filling, but they are typically associated with pores partially filled by dolomite. Type D is more highly reflecting and highly anisotropic.

Yohin Formation. The Yohin Formation is exposed in the Yohin Ridge section only and comprises cherty paper shales with TOC values in the 1–1.6% range (Table 3). The shales contain coaly kerogen, dominated by vitrinite, with subordinate inertinite (semifusinite and semimacrinite). Although the low hydrogen indices are consistent with the dominantly terrestrial organic matter, in this case they may reflect elevated maturity since the oxygen content is also unusually low for terrestrial kerogen and may also reflect elevated maturity (T_{max} 474–488 °C). Both geochemical and petrological data are compatible with the interpretation of a shallow neritic depositional environment presented by Richards (1983). Much of the vitrinite population is reworked, and a significant proportion of the "fresh" vitrinite comprises gelocollinite. Liptodetrinite and chitin are present in minor amounts.

Clausen Formation. Total organic carbon in the platy, slightly cherty black shales exposed at Yohin ridge amounts to only 1.5% (Table 3). The kerogen is characterized by a dark, amorphous bituminous matrix typical of marine shales, and abundant and perva-

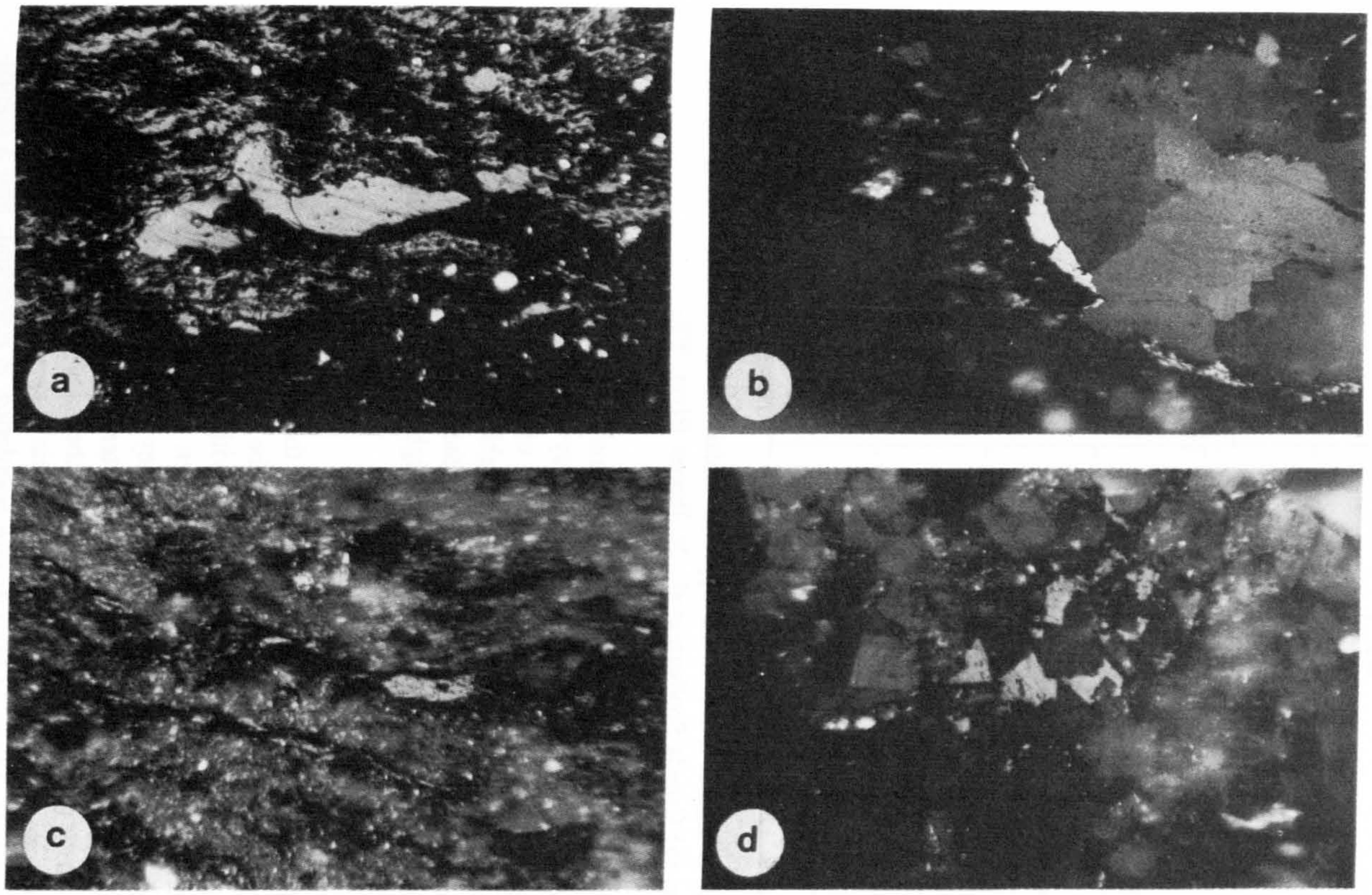

Figure 4. Photomicrographs of petrographic constituents of kerogen in Upper Devonian and Lower Carboniferous shales from the Canada Southern et al. well at N. Beaver River (white, incident light, oil immersion objective). The long axis of each photomicrograph is 240 μm. (*a*) Organic-rich shale in the Besa River Fm. showing granular carbonaceous residue from matured amorphous bituminous matrix and solid medium-reflectance (type B) bitumen (center, R_o 2.9%), at 3315.6 m depth. (b) Medium-reflectance (type B) bitumen in pores associated with xenotopic dolomite in the Besa River at 2980.5 m depth. (c) Low-reflectance (type A) bitumen associated with matured alginite in the Mattson Fm. (d) Pore-filling, medium-reflectance (type B) bitumen associated with dolomite in the Prophet Fm.

sive liptodetrinite (possibly derived from marine algae, <10 μm). Terrestrial components are subordinate, being dominated by inertinites (fusinite, semifusinite, and macrinite; Table 1) and including vitrinite-like material (associated with micrinite as bimacerite). Low hydrogen and oxygen indices may be a reflection of the elevated maturity of the amorphous kerogen (T_{max} 458 °C). The Clausen Formation has been interpreted by Richards (1983) as basin and slope deposits.

Flett Formation. The Flett formation occurrs only in the Yohin Ridge section. Only the marly beds of the Jackfish Gap member were sampled in this carbonate-dominated unit comprising carbonate platform and ramp lithofacies (Richards 1983). Total organic carbon values are characteristically low (<0.7 wt.%). The organic components are distinctively marine and differ significantly from the clastic-dominated units above and below. Large (>1000 μm) colonial alginites (Figure 5a) and amorphous kerogen dominate the organic components with liptodetrinite, lamalginite, and ?algal bituminite subordinate (Table 1). The slightly higher hydrogen indices (100, 131) in some intervals probably reflect contributions from algal components. The marls of the Flett Formation are extensively dolomitized. A weakly fluorescing, low-reflectance bitumen (type A), possibly albertite, is commonly associated with the alginite (Figure 5b), and medium-reflectance bitumen (type B) is a minor component associated with porosity in the dolomitized matrix.

Prophet Formation. Samples were obtained from the Prophet Formation at both localities. At Yohin Ridge, the fissile shales formed on the middle to lower slope (Figure 2) consist of cherty, spiculitic mudstones that contain abundant fossil fragments (bryozoans, corals, and sponge spicules). Total organic carbon values are only 0.5 wt.% (Table 4), but numerous intervals in the Canada Southern et al. well (at 2396.3 m and 2687.5 m) have significantly greater amounts (3.5 and 6.2 wt.%, respectively). Petrographic analysis suggests that kerogen is not abundant in shales of the Prophet Formation and comprises reworked vitrinite and primary (low- and medium-reflectance) bitumens (Figures 4c and 4d). T_{max} values are anomalous (395–503 °C), as are the high TOC values, which may be attributed to cavings from the overlying Mattson Formation.

The low-reflecting bitumen (type A) shows weak brown fluorescence under blue light and is commonly associated with pores occupied also by non-fluorescing bituminite of ?algal origin. The medium-reflectance bitumen (type B) is associated with pores in the matrix partially filled by carbonate.

Golata Formation. Shales of the Golata Formation are present at Yohin Ridge and in the subsurface at N. Beaver River. Total organic carbon varies from 1.35 to 2.27 wt.%. At Yohin Ridge, the prodelta shales of the Golata Formation contain mixed marine and nonmarine kerogen that is dominated by terrestrial inertinite macerals (semifusinite, fusinite, and macrinite) and reworked vitrinitic components (Table 1). In the North Beaver section, low-reflectance bitumen (type A) is associated with alginite predominates, while matrix bituminite, vitrinites, and inertinites are minor components suggesting a greater marine influence.

The hydrogen indices are low in both sections (Tables 3 and 4); in the subsurface at Beaver River this may be due to elevated maturity (T_{max} 457–493 °C), while at Yohin Ridge the kerogen is significantly less mature (T_{max} 437 °C).

Mattson Formation. Shales in the basal section of the Mattson Formation at Jackfish

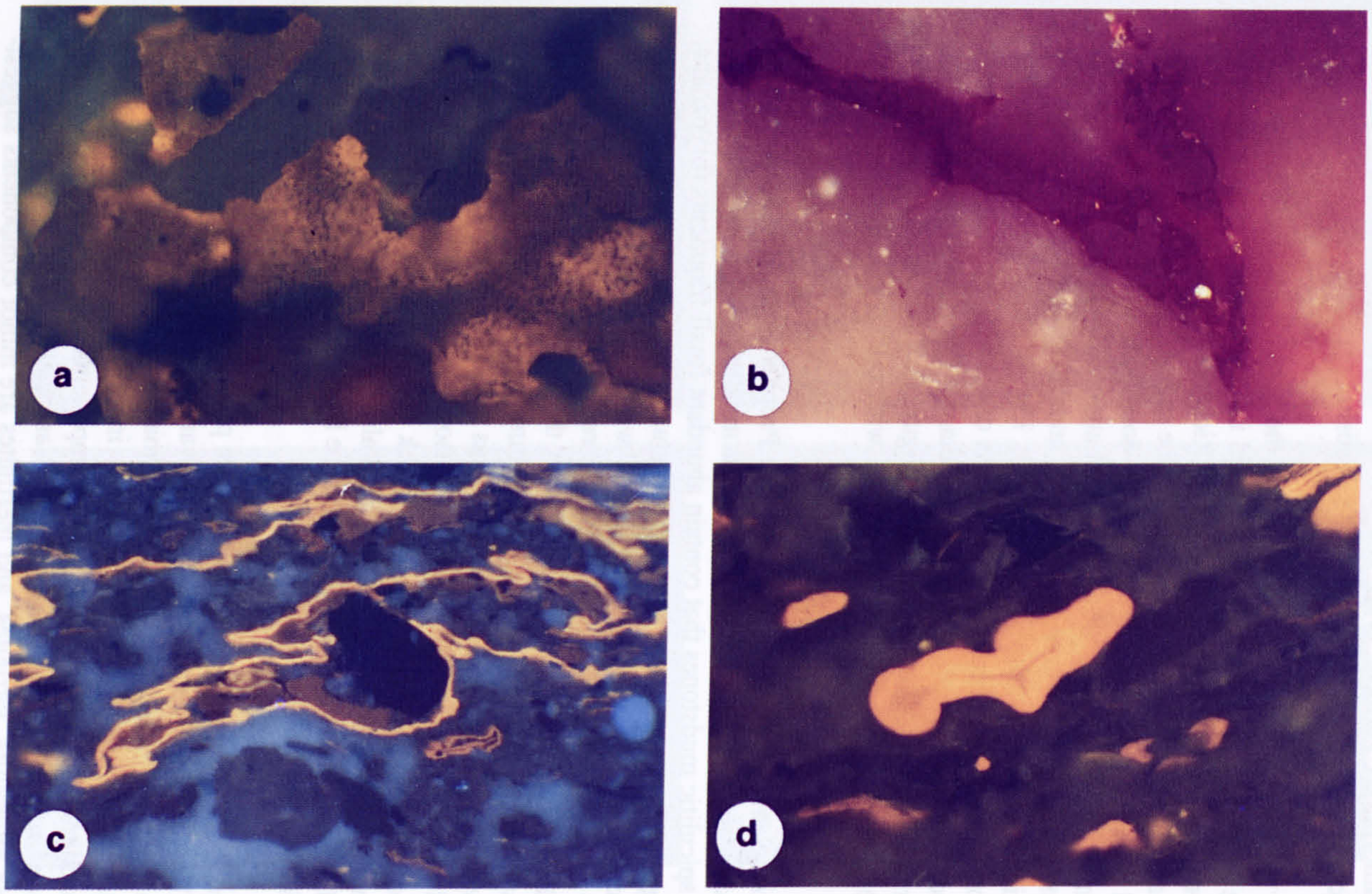

Figure 5. Photomicrographs of petrographic constituents of kerogen in Upper Devonian and Lower Carboniferous shales from the Jackfish Gap-Yohin Ridge section (incident light, oil immersion: (a) and (d) were taken in blue light; (b) in white light; and (c) in ultraviolet light). The long axis of each photomicrograph is 240 μm. (a) Highly structured, colonial alginite is dominant in organic-rich intervals in the Flett, at 271.6 m depth. (b) Fracture-filling, low-reflectance (type A) bitumen associated with alginite in the Flett, at 271.6 m depth. (c) Liptinite (cutinite) in the Mattson Fm. at 920.5 m above the base of the Yohin Fm. (d) Thick-walled, microspores (?Murospora) are very common in coals and shales of the Mattson Fm. (this sample 887 m above the base of the Yohin Fm.).

Gap-Yohin Ridge are black, fissile and paper shales with TOC values ranging from 1.4 to 18.4 wt.% (Table 3). Petrographic analysis of the kerogen suggests mixed marine and terrestrial origins. Typically, amorphous and structured liptinites dominate the kerogen, with sporinites and cutinites (Figure 5c) abundant. Sporinites are derived from highly sculptured megaspores and a large variety of crassispores and tenuispores (Figure 5d) (Potter et al. in progress). The strong lamination reflects an abundance of marine alginite (Leiosphaeridiales type) oriented parallel to bedding. Samples with an abundance of algal components (C58750, C58749, C58765) (Figure 4c) also have hydrogen indices greater than 150 (Table 3). Terrestrial components such as vitrinite, fusinite, and minor inertodetrinite are relatively abundant. Vitrinite occurs in trimacerites and bimacerites. Primary vitrinites exhibit a weak brown fluorescence, indicating that they are perhydrous. Reworked vitrinites are abundant. Marine Tasmanites, which also show evidence of extensive reworking, and freshwater Reinschia- or Pila-type alginites and cutinites are minor components. The maceral assemblage suggests a shallow marginal marine depositional environment with considerable mixing of marine and fresh water.

Thin coals are common in the middle to upper portions of the Mattson Formation (samples C58764, C58838). Samples C58764 and C58838 are sapropelic coals and shales, respectively, with a large proportions (>50%) of inertinite (dominated by micrinite, semifusinite, and resino-inertinites) and liptinite (ca. 30%), dominated by sporinites, with <20% vitrinite (perhydrous vitrinites and gellocollinites) and little or no mineral matter. These are typical of coals accumulated subaquatically, under highly reducing conditions, perhaps in a lacustrine setting (Goodarzi et al. 1987; Potter et al. in progress). The coals also contain weakly fluorescing bitumen (0.32 $\%R_o$) and strongly fluorescing exsudatinite. Argillaceous rocks in the middle Mattson are dominantly siltstones with ca. 1–18 wt.% TOC comprising liptinites (sporinite), vitrinite, and inertinites. The coals in the upper portion of the Mattson Formation are also sapropelic in nature and are commonly interbedded with, or associated with, black shales (3.5 wt.% TOC) comprising algal laminites (sample C58806) dominated by lamalginite and unstructured liptinite (matrix bituminite). This is reflected in a higher hydrogen index (116) than most of the Mattson kerogen.

Sapropelic coals and algal shales in the Mattson have low oxygen contents and slightly higher hydrogen indices. Cross plots of hydrogen versus oxygen indices for the Jackfish Gap-Yohin Ridge (Figure 6a) show that most of the kerogen in the Upper Devonian-Lower Carboniferous strata are predominantly gas-prone and are overmature. Petrographic analysis suggests that kerogen in most formations, including much of the Mattson, are of terrestrial (mixed types III and IV) origin. Only samples from intervals in the Flett and Mattson Formations have hydrogen indices over 100, which probably reflects type I and II components. Hydrogen versus oxygen indices for the subsurface section at North Beaver River (Figure 6b) also indicate that the kerogen in the Upper Devonian and Lower Carboniferous are gas-prone and overmature. However, petrographic analysis of the kerogen suggests that shales in the Besa River, Clausen (mixed terrestrial and marine), Prophet, and Flett Formations probably contain type II kerogens of amorphous and algal origins, while the Golata and Mattson Formations contain predominantly terrestrially sourced organic matter.

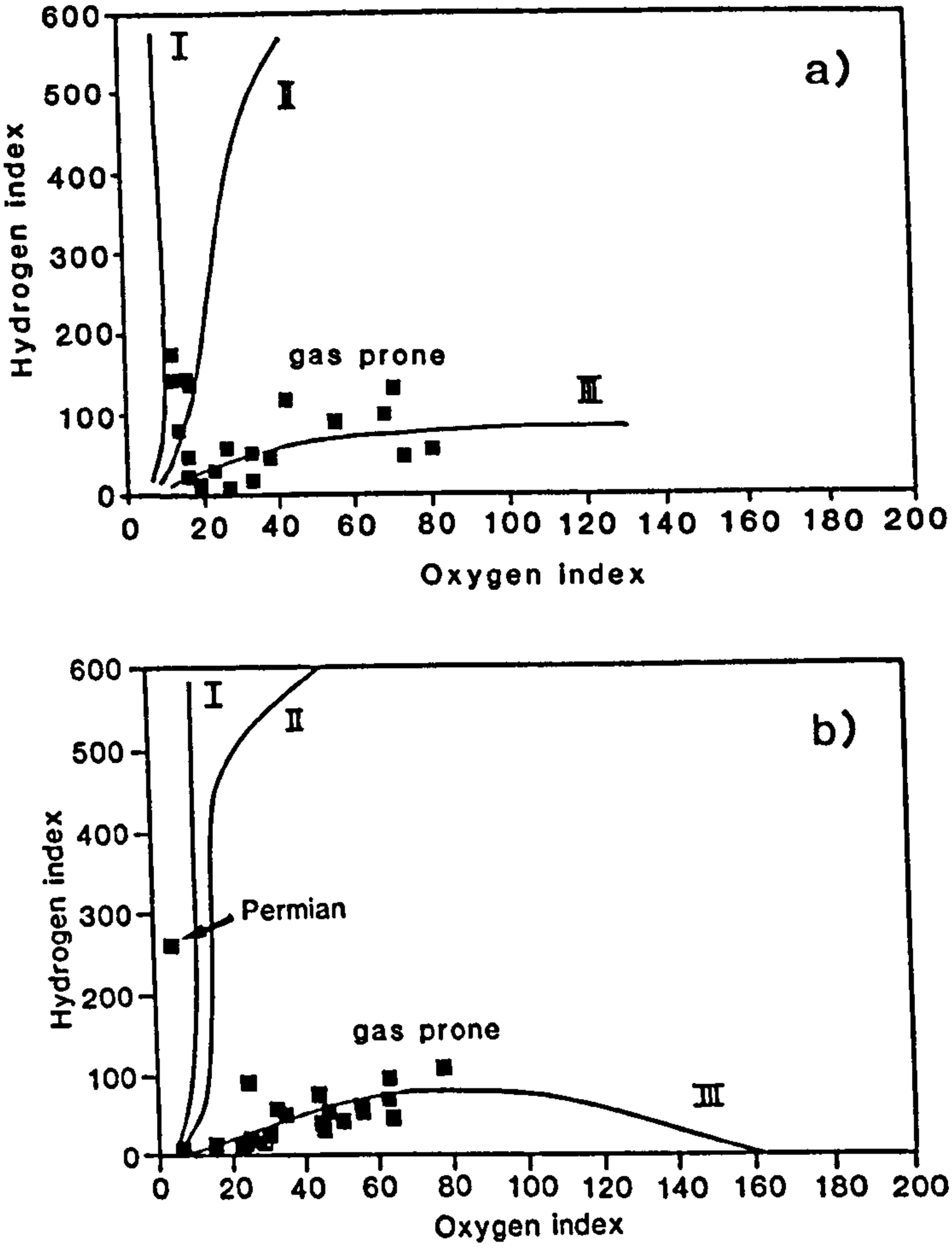

Figure 6. Plot of hydrogen index versus oxygen index for kerogen from shales in Upper Devonian-Lower Carboniferous at (*a*) Jackfish Gap-Yohin Ridge; (*b*) Canada Southern et al. N. Beaver River, YT.

Maturation

T_{max}. In both sections studied, the T_{max} data are generally inconsistent and vary considerably within a given formation. For most of the samples, the S2 peak is less than 1, which suggests that during pyrolysis, hydrocarbon generation did not produce a well-defined peak with a clearly defined T_{max}. The resulting anomalous and wide-ranging T_{max} values are therefore generally unreliable as maturation indices. In a few cases (when S2 exceeds 1.0), the calculated vitrinite reflectance data (Tables 3 and 4) fit within the range of values reported by Espitalié (1986), but none of the data show any good correlation. This may be due, in part, to the fact that the majority of samples are overmature and, in part, to the fact that the organic matter is predominantly in the form of bitumens, i.e., relicts of kerogen maturation and hydrocarbon generation rather than hydrocarbon precursors.

Reflectance. Figure 7 shows the vitrinite reflectance data plotted against height above

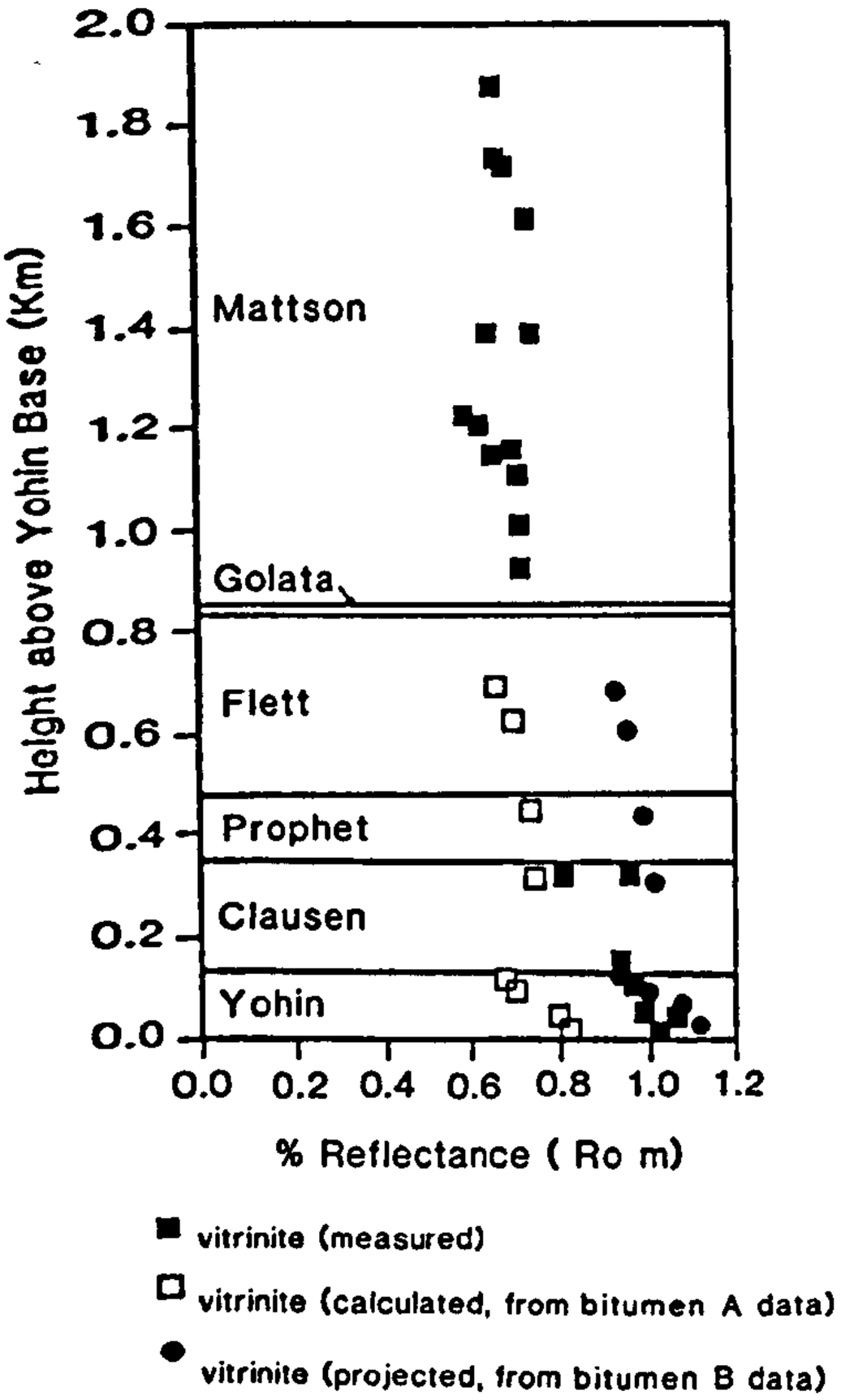

Figure 7. Reflectance of primary bitumens versus depth in Lower Carboniferous strata at Jackfish Gap-Yohin Ridge.

the base of the section at Jackfish Gap-Yohin Ridge (see Table 3). Measured data are limited to the Mattson, Clausen, and Yohin intervals and are derived from vitrinite in coals and shales in the Mattson and from vitrinite in shales in the basal part of the Clausen and in the Yohin Formations. Vitrinite is absent in the Flett Formation and reworked or oxidized and, therefore, unsuitable for measurements in the Golata and Prophet Formations (much of the oxidation is attributed to oxidation by dolomitizing fluids). Reliable vitrinite reflectance data were therefore restricted to samples obtained from the exposures at Jackfish Gap and Yohin Ridge. Furthermore, the latter intervals contain low-reflecting bitumen (type A), which appears to be generated during maturation and/or subsequent migration of hydrocarbons from alginite or algal bituminite (Figure 4c). The correlation between vitrinite reflectance and depth is reasonably good. The data from the lower Mattson fits in with the trend shown by measured and calculated data from the Clausen and Yohin Formations. Data from the upper Mattson are derived predominantly from coals. These coals show a broad range of vitrinite reflectance values consistent with perhydrous and highly gelified vitrinite. In one of the samples collected at 1.39-km elevation (sample C58765), the higher value was measured on vitrinite in coal and the lower on vitrinite in the interbedded shale. Variations in vitrinite reflectance associated with variations in lithology of the enclosing rock are cited in the literature (Jones et al. 1972; Bostick and Foster 1975; Stasiuk 1988; Durand et al. 1986; Goodarzi et al. 1989). The reflectance of numerous populations of primary bitumens correlate well with depth and have been used to model the geothermal history of the region (Morrow et al. in press).

Bitumens as Thermal Indicators. Due to the absence of vitrinite in the subsurface at N. Beaver River, only bitumen reflectance was measured. Following the method of Jacob (1985), the relationship

$$R_{\text{vitrinite}} = 0.618R_{\text{bitumen}} + 0.40\%$$

is used to calculate vitrinite reflectance from the low- (type A) and medium-reflectance (type B) bitumen. Jacob (1985, 1989) established a correlation between the refelctance of vitrinites and primary "migrabitumens" and found that, below a reflectance of 1%, bitumen reflectance is lower than the vitrinite; above 1%, the bitumen reflectance exceeds that of the vitrinite. Goodarzi and Macqueen (1990) found a similar trend in Middle Devonian rocks from Pine Point, NWT.

Durand et al. (1986) pointed out that "dispersed organic particles whose reflectance can be measured are rarely true vitrinite, i.e., material derived from ligno-cellulosic parts of higher plants. In marine and lacustrine sediments they are mostly bituminites from a planktonic source and may often be mistaken for vitrinites. Their physico-chemical properties, hence their response to thermal stresses' are not the same than for true vitrinites." They (ibid.) further point out that work by Buiskool Toxopeus (1983), in which different maturation trends were recognized for a variety of vitrinites in shales, originally interpreted to represent trends for a variety of vitrinite types, may actually represent vitrinites and bituminites. Caution is therefore advised in the use and interpretation of "vitrinite" reflectance data in thermal modeling. There are therefore many advantages to be considered in using bitumen reflectance in thermal studies:

(1) In marine sequences, vitrinite may be rare or absent; bitumens appear to be present even in relatively lean source rocks.
(2) Unlike vitrinite, primary bitumen cannot be reworked or oxidized prior to deposition, thereby eliminating the potential for reflectance variations due to second-cycle vitrinite.
(3) Identification is relatively easy in marine rocks, whereas vitrinite or vitrinite-like components may be faunal or marine in origin.
(4) Use of bitumen reflectance may circumvent problems associated with reflectance suppression in hydrogen-rich vitrinite (Price and Barker 1985; Goodarzi et al. 1987; Feinstein et al. 1991; Raymond and Murchison 1991; Barker 1992).
(5) Bitumen reflectance does not appear to vary with enclosing lithology in clastic rocks.
(6) The presence of primary bitumens is also an indication of maturity of kerogen, generation and subsequent migration of hydrocarbon.

In the present study three, and occasionally four, populations of bitumen are present in most samples (Figure 8). The population with the lowest reflectance (type A) is without exception intimately associated with alginite or algal bituminite (Figures 4c and 5b); the shape and distribution of the bitumen often mirrors the remnant morphology of the precursor. It is normally found as a coating on matured alginite or algal bituminite or on the walls of mutual pores, and is therefore interpreted as a by-product of in-situ maturation, hydrocarbon generation, and subsequent movement of the lighter hydrocarbons from alginites and algal bituminite. Gentzis and Goodarzi (1990) described numerous populations of primary bitumen in Upper Devonian rocks of the Canadian Arctic and observed that the low-reflecting bitumens have a "wispy form and appear to be primary autochthous." The second population of bitumen (type B) is commonly most abundant

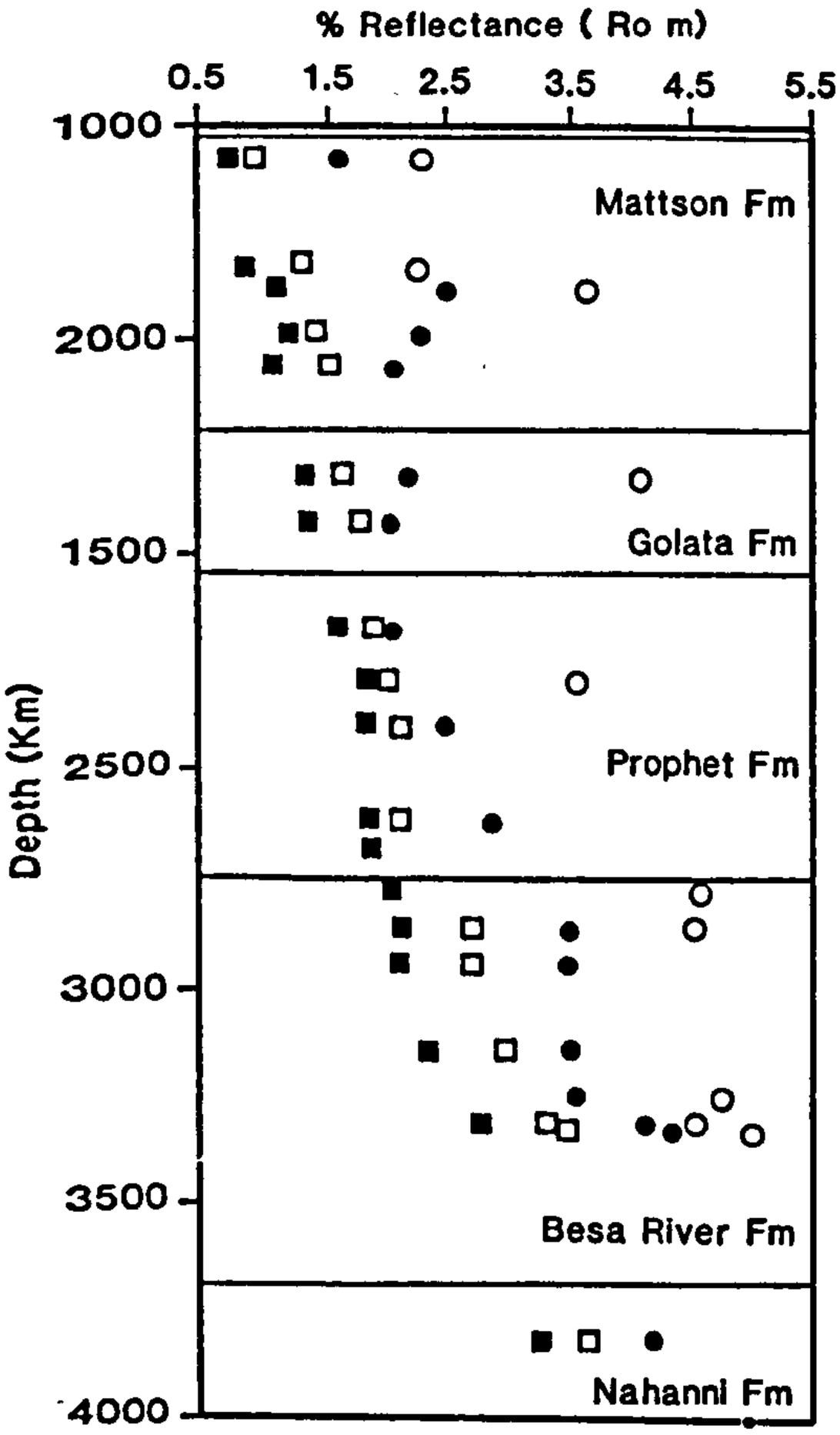

Figure 8. Reflectance versus depth of primary bitumens in Upper Devonian and Lower Carboniferous strata in Canada Southern et al. well at North Beaver River.

throughout the Upper Devonian-Lower Carboniferous succession; it characteristically has a medium reflectance and is usually observed filling pores in the matrix (Figures 4b and 4d). It does not show affinities with any identifiable macerals, but it is normally abundant in samples with matured amorphous liptinite such as matrix bituminite and therefore could conceivably be a maturation by-product also. Its having a greater reflectance than the type A bitumen indicates that the source must be kerogen that matures earlier than structured lipinites (ca. 0.72%; Powell and Snowdon 1983). The source must be therefore be unstructured type II kerogen, since the structured liptinites (type II) and type III kerogen that dominates the clastic succession mature around 0.7%VR_o. Also, the latter are gas- rather than oil-prone and therefore would not be expected to yield bitumen. This explains why the type B bitumen is present in shales in the early stages of maturity. Powell and Snowdon (1983) have suggested that mild thermal events are a viable mechanism for the conversion of NSOs/asphaltenes to insoluble bitumens. Furthermore, our observations and interpretations regarding the timing and genesis of bitumens are consistent with results of hydrous and anhydrous pyrolysis studies of kerogenous shales by Lewan (in press).

Two populations of high-reflecting bitumen (types C and D) are also present. These are, without exception, pore-filling or fracture-filling bitumens. The pore-filling varieties are interpreted as by-products of early oil generation (Robert 1981; Goodarzi et al. 1985) or possibly biodegraded oils (Powell 1984) or migrated oil from an external source. The reflectance of type C shows a large range of values, which can be attributed to development of anisotropy; the range reflects the minimum and maximum reflectance and there is a slight increase with depth (Figure 8). Type D shows an even larger scatter but still increases slightly with depth (Figure 8). Gentzis and Goodarzi (1990) observed a similar relationship in the Devonian of Melville Island, Arctic Canada. By contrast, correlations between the reflectance of the low- (type A) and medium-reflectance (type B) bitumens with depth is very good (r^2 = 0.85 for type A; r^2 = 0.97 for type B), indicating the excellent potential for use as indicators of thermal maturity. Gentzis and Goodarzi (1990) likewise found good correlations between the reflectance of primary bitumens and depth in Paleozoic rocks in Arctic Canada. The rate of increase in reflectance with depth follows similar trends for the types A and B bitumens, but a slight divergence occurs at increased depths (see Figure 10). At a reflectance of 1%, the difference between the two is 0.3%; but at a reflectance of 3.0%, they deviate by 0.6%. The variation with increasing depth may be due, in part, to differences in the rate of increase in anisotropy with depth.

The use of bitumen reflectance as a maturation parameter can be ominous if more than one population of primary bitumen is present in a rock (Robert 1981; Goodarzi et al. 1985). Which data set should be used to calculate equivalent vitrinite reflectance? Gentzis and Goodarzi (1990) suggested using the population with the lowest reflectance (which is closest to that of vitrinite), However, it does not correlate with the low-reflectance (type A) bitumen in this study.

In the ensuing discussion, the bitumen reflectance data sets from both Jackfish Gap-Yohin Ridge and the Canada Southern et al. well at N. Beaver River are used, in conjunction with factors such as T_{max}, kerogen type, fluorescence properties, and associated morphological components/petrophysical features, to determine which data should be used to calculate equivalent vitrinite reflectance values. Figures 7 and 9 show the measured vitrinite and type A bitumen reflectance data from the succession at Jackfish Gap-Yohin Ridge. Only one population of bitumen (type A, low-reflectance bitumen associated with alginite) was present in the carbonate-dominated interval for which vitrinite data were not available. The type A bitumen reflectance best-fit line plots parallel to the best-fit line for reflectance of alginite, from which it is thought to have formed, and parallel to the vitrinite reflectance trend. This is taken as a good indication that the bitumen, alginite, and vitrinite have followed similar thermal maturation patterns (Figure 9). Furthermore, the first appearance of the bitumen, at around 700 m depth (0.42% reflectance) coincides with a vitrinite reflectance of 0.85%, which is considered the peak of hydrocarbon generation from alginite. The vitrinite reflectance equivalent, calculated from the low-reflectance bitumen (type A) data, following Jacob's method (Jacob, 1985), falls below the vitrinite reflectance line. Although there is no medium-reflectance bitumen in the succession at Jackfish Gap-Yohin Ridge, the observed relationship (0.3% difference) between the reflectance of the low- (type A) and medium-reflectance (type B) bitumens in the Canada Southern well (from Figure 10) suggests that the medium bitumen (type B) reflectance values would fall between 0.72 and 0.92%. Using Jacob's formula, the vitrinite reflectance calculated from the medium-reflectance bitumen would therefore increase from 0.86 to 0.99% for the same interval in which type A bitumen occurrs; these values would plot along the measured vitrinite reflectance line shown in

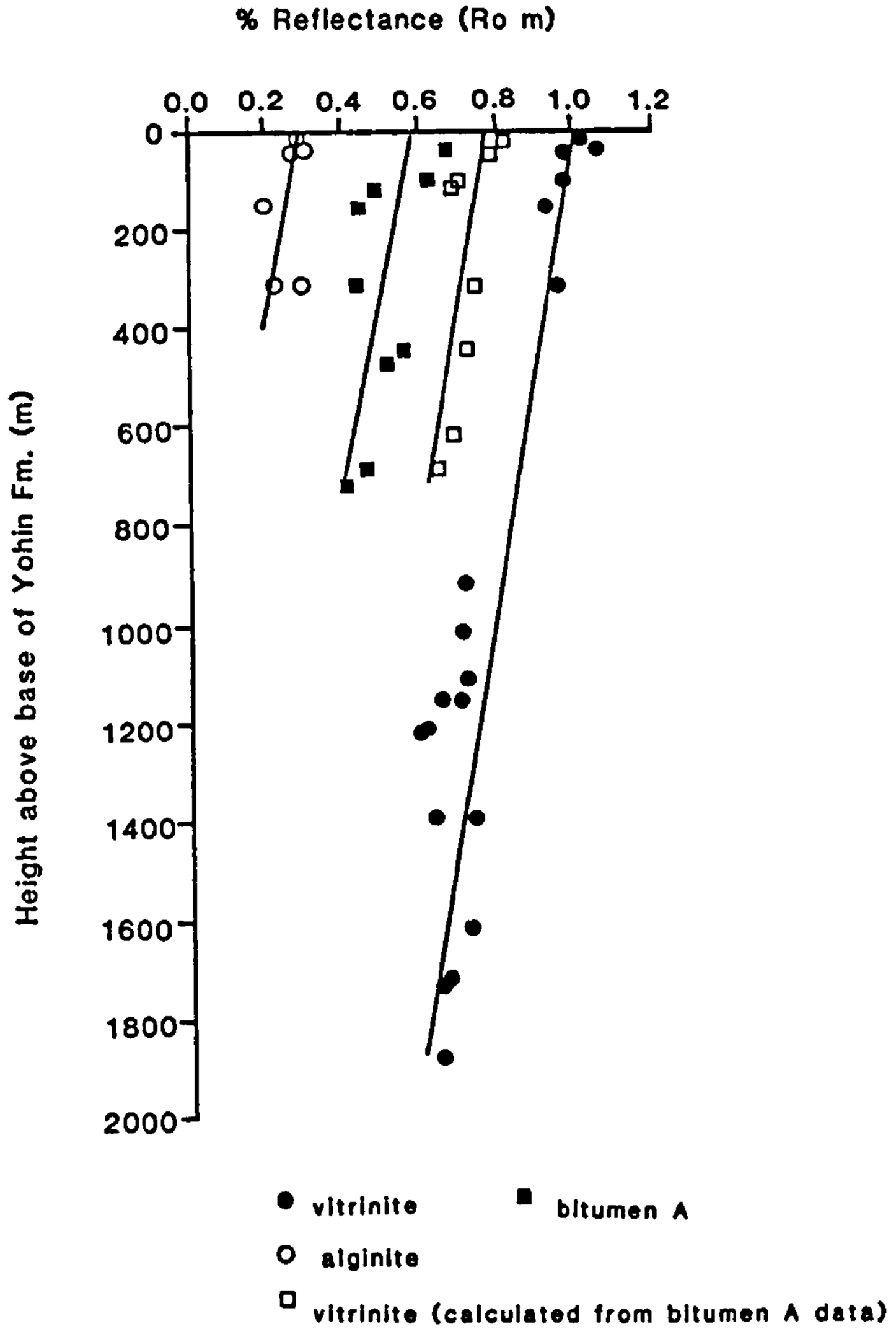

Figure 9. Measured and calculated vitrinite reflectance data for the Upper Devonian-Lower Carboniferous succession at Jackfish Gap-Yohin Ridge (legend as Figure 8).

Figure 9. This suggests that in the Liard Basin, the reflectance of the type B (medium reflectance) bitumen should be used to calculate the vitrinite reflectance.

If this line of reasoning is applied to the subsurface section at N. Beaver River, and medium-reflectance (type B) bitumen is used to calculate vitrinite reflectance equivalent, the upper part of the Mattson Formation would plot in the oil window (Figure 11a) and the rest of the Lower Carboniferous and Devonian succession would plot within the gas window (Dow 1977). If the low-reflectance (type A) bitumen reflectance is used to plot the vitrinite reflectance trend for the same succession (Figure 11b), all of the Mattson and Golata formations would fall in the oil window and the Prophet and Besa River would be in the condensate and wet gas window. However, T_{max} values from samples in which the S2 peak is >1 (Table 4) indicates that the kerogen is overmature in all but the uppermost Mattson Fm. Furthermore, liptinitic kerogen in the Mattson and Golata Formations show no significant fluorescence below 1347 m depth. This further supports the

use of data derived from the medium-reflectance (type B) bitumen to draw the limits of the oil window. Finally, Rock-Eval data and qualitative optical evaluation of the principal kerogen types in the Lower Carboniferous and Upper Devonian sequence show that, except in the Flett Formation where alginite dominates, unstructured or amorphous liptinitic kerogen is the principal source of hydrocarbon and therefore bitumen.

Source Potential. T_{max} and vitrinite reflectance data from the Upper Devonian and Lower Carboniferous at Jackfish Gap-Yohin Ridge (Table 3) indicate that shales in most formations, with the exception of the Mattson, contain overmature kerogen and are therefore gas-prone. Despite the occurrence of more marine kerogens in correlative strata in the subsurface at North Beaver River, low hydrogen indices and correspondingly low oxygen indices indicate that the kerogens are gas-prone.

Kerogen microscopy and vitrinite and bitumen reflectance measurements suggest that the liptinite-rich coals and associated algal-shales and laminites in the Mattson Formation have some hydrocarbon potential. Above the present-day sea level, the kerogen in the Mattson Formation is mature. In the subsurface at Beaver River, the upper Mattson is mature, suggesting that hydrocarbons may have been generated recently while the middle and Lower Mattson kerogen could potentially be a source of condensate and wet gas. However, geothermal studies in the Beaver River area by Morrow et al. (in press) suggest that the Mattson entered the oil window around 230 million years ago. The reflectance variations observed in the vitrinites in coals from the Mattson Formation and work by Potter et al. (in progress) may be considered further evidence of early hydrocarbon generation. Weakly fluorescing vitrinite-like stringers have a reflectance of 0.58%

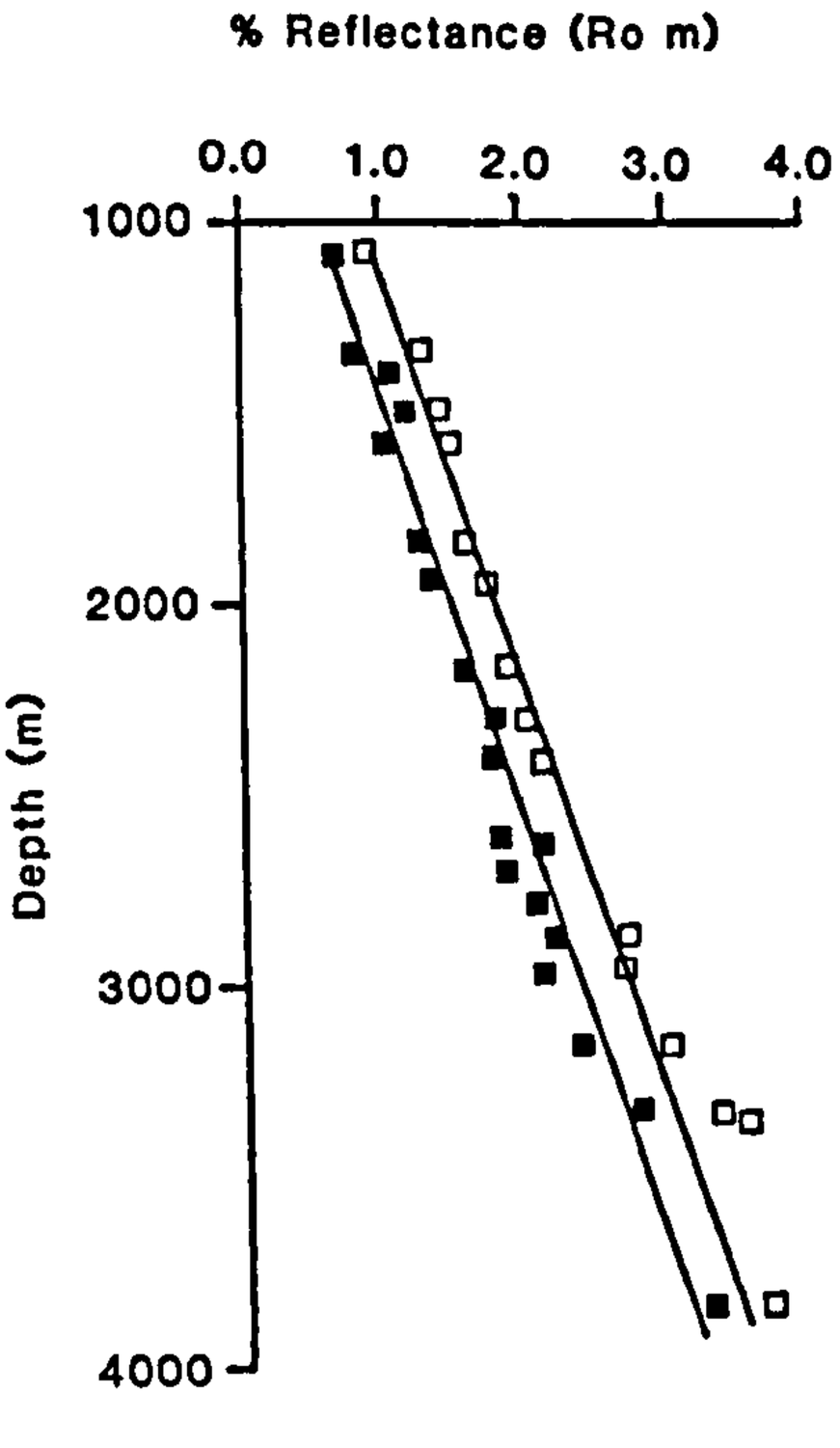

Figure 10. Vitrinite reflectance data for the Upper Devonian-Lower Carboniferous succession at Canada Southern et al. N. Beaver River YT 1-27, calculated from type A and type B bitumens.

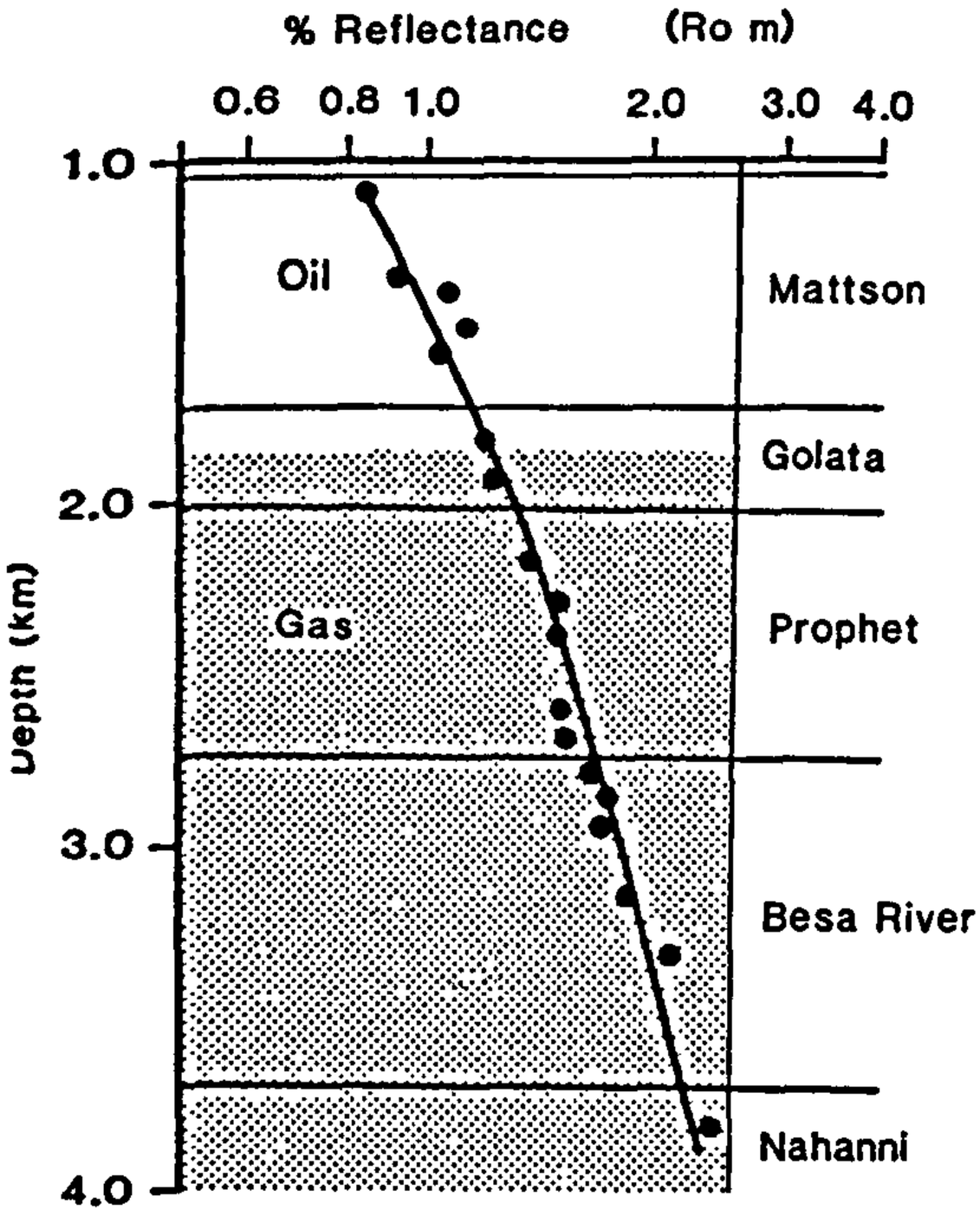

Figure 11. Relationship among maturity, hydrocarbon potential, and vitrinite reflectance (a) calculated from the low-reflectance (type A) bitumen; and (b) the medium-reflectance (type B) bitumen (limits of the oil and gas windows after Dow 1977).

compared to nonfluorescing telocollinite in the same sample having a reflectance of 0.70%. This is typical of perhydrous vitrinite (Teichmüller and Teichmüller 1982; Price and Barker 1985; Goodarzi et al. 1987) which is oil-prone. Furthermore, the occurrence of primary bitumens indicates that hydrocarbons were generated within the shales of the Mattson Formation.

Golata shales contain gas-prone kerogen, and shales in the lower part of the Prophet and Uppermost Besa River have probably generated condensate and wet gas from type II kerogen. Below 3 km depth, the Besa River may well have been a prolific source of catagenic gas, since it entered the gas window approximately 280 million years ago and may have contributed significantly to the gas reserves in the Beaver River Gas fields.

Conclusions

(1) Rock-Eval, TOC, and petrographic data suggest that Upper Devonian and Lower Carboniferous strata, particularly, the Besa River and Mattson Formations, have been significant sources of hydrocarbons, particularly gas, in the North Beaver River area of the Yukon Territory.
(2) Kerogens in the Upper Devonian and Lower Carboniferous succession are mixed types II and III (mixed marine and terrestrial) with rare types I and II (algal) sources.
(3) A lack of unoxidized vitrinite and the predominance of primary bitumens over vitrinite makes bitumens the preferred indicators of thermal maturity.

(4) Correlations between bitumen reflectance and depth are very good.
(5) The sources of the low- (type A) and medium- (type B) reflectance populations of bitumen are alginites, algal bitumens, and amorphous kerogen, respectively.
(6) The reflectance trends, source, and timing of generation of the medium (type B)-reflectance bitumen suggest that it is the preferred index of maturation in the Liard Basin.

Acknowledgments

We gratefully acknowledge support for this research provided by the Geological Survey of Canada and the Saskatchewan Oil and Gas Corporation (SaskOil). Thanks are extended to Lloyd Snowdon and Ron Fanjoy of the GSC for Rock-Eval analyses. The manuscript benefitted from critical reviews by L. D. Stasiuk and T. Gentzis.

References

Bamber, E. W. and B. L. Mamet. 1978. Carboniferous biostratigraphy and correlation, northeastern British Columbia and southwestern District of Mackenzie. *Geol. Surv. Can. Bull.* 266.

Barker, C. E. 1992. An update on the suppression of vitrinite reflectance. *Soc. Organic Petrol. Newsletter* 8(4):8–11.

Bostick, N. H. and Foster, J. N. 1975. Comparison of vitrinite reflectance in coal seams and in kerogens of sandstones, shales and limestones in the same part of a sedimentary section. In B. Alpern (Ed.), *Pétrographie organique et potentiel pétrolier.* Paris: Éditions du Centre de le Recherche Scientifique, pp. 13–25.

Braman, D. R., and L. E. Hills. 1977. Palynology and paleoecology of the Mattson Formation, northwest Canada. *Bull. Can. Petrol. Geol.* 25:582–630.

Buiskool Toxopeus, J. M. A. 1983. Selection criteria for the use of vitrinite reflectance as a maturation tool. In J. Brooks (Ed.), *Petroleum Geochemistry and Exploration of Europe.* London, Blackwell, pp. 295–307.

Douglas, R. J. W., P. Harker, and D. K. Norris. 1963. Geology of the southern Mackenzie Mountains area, Yukon Territory and District of Mackenzie. Geol. Surv. Can. Map 1141A.

Dow, W. G. 1977. Kerogen Studies and Geological Interpretations, *J. Geochem. Explor.* 7:79–99.

Durand, B., B. Alpern, J. L. Pittion, and B. Pradier. 1986. Reflectance of vitrinite as a control of thermal History of Sediments. In *Thermal Modelling in Sedimentary Basins.* Paris: Éditions Technip, pp. 471–474.

Espitalié, J. 1986. Use of T_{max} as a maturation index for different types of organic matter. Comparison with vitrinite reflectance. In *Thermal Modelling in Sedimentary Basins.* Paris: Éditions Technip, pp. 475–498.

Espitalié, B., G. Deroo, and F. Marquis. 1985. Rock Eval pyrolysis and its applications. Inst. Fr. Petrol. preprint 27299.

Feinstein, S., P. W. Brooks, Z. Aizenshtat, and J. Slager. 1991. Petrological and geochemical characterization of hydrogen-rich coaly matter in the Agur 1 drillhole, Negev, Israel. *Energy Sources* 13:389–405.

Gentzis, T., and F. Goodarzi. 1990. A review of the use of bitumen reflectance in hydrocarbon exploration with examples from Melville Island, Arctic Canada. In V. F. Nuccio and C. E. Barker (Eds.), *Applications of Thermal Studies to Energy Exploration*, 23–36. Denver, CO: Rocky Mountain Sec. Soc. Econ. Paleont. Mineral.

Goodarzi, F., P. W. Brooks, and A. F. Embry. 1989. Regional maturity as determined by organic petrography and geochemistry of the Schei Point Group (Triassic) in the Western Sverdrup Basin, Canadian Arctic Archipelago. *Marine Petrol. Geol.* 6:290–302.

Goodarzi, F., G. R. Davis, W. W. Nassichuk, and L. R. Snowdon. 1987. Organic petrology and

RockEval analysis of Lower Carboniferous Emma Fjiord Formation in Sverdrup Basin, Canadian Arctic Archipelago. *Marine Petrol. Geol.* 4:132–145.

Goodarzi, F., P. R. Gunther, W. A. M. Jenkins, and L. R. Snowdon. 1985. Preliminary organic petrography of Palaeozoic rocks from the Grand Banks, Newfoundland. *Marine Petrol. Geol.* 4:254–259.

Goodarzi, F., and R. W. Macqueen, 1990. Optical/compositional character of six bitumen species from Middle Devonian rocks of the Pine Point Pb-Zn property, Northwest Territories. *Current Res. Part C, Geol. Surv. Can.* Pr. 89-1C:197–216.

Jacob, H. 1985. Disperse solid bitumens as an indicator for migration and maturity in prospecting for oil and gas. *Erdöle und Kohle, Ergas and Petrochemie* 38:365.

Jacob, H. 1989. Classification, structure, genesis and practical importance of natural solid oil bitumen ("migrabitumen"). *Int. J. Coal Geol.* 11:65–79.

Jones, J. M., D. G. Murchison, and S. A. Saleh 1972. Variation of vitrinite reflectivity in relation to lithology. In H. R. von Gaertner and H. Wehner (Eds.), *Advances in Organic Geochemistry 1971,* Oxford: Pergamon Press, pp. 601–612.

Lewan, M. D. (in press). *Primary oil migration and expulsion as determined by hydrous pyrolysis.* Proceedings of the World Petroleum Congress, Buenos Aires, 1991.

Morrow, D. A., J. Potter, B. C. Richards, and F. Goodarzi (in press). Thermal organic maturation in the Liard Basin. Bull. Can. Petrol. Geol.

Patton, W. J. H. 1958. Mississippian succession in South Nahanni River area, Northwest Territories. In A. J. Goodman (Ed.), *Jurassic and Carboniferous of Western Canada,* Am. Assoc. Petrol. Geol. Alln Memorial Volume, pp. 309–332.

Potter, J., B. C. Richards, and A. R. Cameron (in progress). *The petrology and origin of coals from the Lower Carboniferous Mattson Formation, southwestern District of Mackenzie, Canada.* Proceedings of the Cameron Symposium, Joint GAC-MAC, Wolfville, Nova Scotia, May 29–31st, 1992. *Int. J. Coal Geology.*

Powell, T. G. 1984. Some aspects of the hydrocarbon geochemistry of a Middle Devonian barrier-reef complex, Western Canada. In J. G. Palacas (ed.), Petroleum Geochemistry and Source Rock Potential of Carbonate Rocks. *Am. Assoc. Petrol. Geol. Studies Geol. Ser.* 18:45–62.

Powell, T. G., and L. R. Snowdon. 1983. A composite hydrocarbon generation model. Implications for evaluation of basins for oil and gas. *Erdöl und Kohle—Erdgas-Petrochemie* 36:163–170.

Price, L., and C. E. Barker. 1985. Suppression of vitrinite reflectance in amorphous rich kerogen. A major unrecognised problem. *J. Petrol. Geol.* 8:59–84.

Raymond, A. C., and D. G. Murchison. 1991. Influence of exinitic macerals on the reflectance of vitrinite in the Carboniferous of the Midland Valley of Scotland. *Fuel* 70:155–161.

Richards, B. C. 1983. Uppermost Devonian and Lower Carboniferous stratigraphy, sedimentation and diagenesis, southwestern District of Mackenzie and southeastern Yukon. Unpublished Ph.D thesis, University of Kansas: Lawrence, Kansas.

Richards, B. C. 1989. Uppermost Devonian and Lower Carboniferous stratigraphy, sedimentation and diagenesis, southwestern District of Mackenzie and southeastern Yukon Territory. *Geol. Surv. Can. Bull.* 390.

Richards, B. C. 1991. *Lithostratigraphy, biostratigraphy and sedimentology of the Mattson Formation, southwestern District of Mackenzie, southeast Yukon and northeast British Columbia.* Unpublished internal report, Geol. Surv. Can.

Richards, B. C., E. W. Bamber, A. C. Higgins, and J. Utting. 1989. Carboniferous. In D. F. Stott and J. D. Aitken, (Eds.), *Sedimentary Cover of the North American Craton,* Geol. Surv. Can. Spec. Publ. Vol. D-1, Decade of North American Geology Series.

Robert, P. 1981. Classification of organic matter by means of flourescence; application to hydrocarbon source rocks. *Int. J. Coal Geology* 1:101–138.

Stasiuk, L. D. 1988. Thermal maturation and organic petrology of Mezozoic strata of southern Saskatchewan. Unpublished M.Sc. thesis, University of Regina, Regina, Saskatchewan.

Teichmüller, M., and Teichmüller, R. 1982. The geological basis of coal formation. In E. Stach, M.-Th. Mackowsky, M. Teichmüller, G. H. Taylor, D. Chandra, and R. Teichmüller (Eds.), *Stach's Textbook of Coal Petrology.* Berlin: Gebrüder Borntraeger.

Utting, J. 1981. *Palynological study of samples from the Mattson Formation (Mississippian) of the Jackfish Gap, S. W. District of Mackenzie.* NTS 95 G4. Geol. Surv. Canada, Internal Reports Nos. 1-1981-JU, 2-1981-JU, Paleontology Subdivision.

INTERNAL STRATIGRAPHY, PETROGRAPHY AND POROSITY DEVELOPMENT OF THE MANETOE DOLOMITE IN THE REGION OF THE POINTED MOUNTAIN AND KOTANEELEE GAS FIELDS

D. W. MORROW AND J. POTTER
Institute of Sedimentary and Petroleum Geology
3303 - 33rd Street N.W.
Calgary, Alberta T2L 2A7

ABSTRACT

Cores of the thick peritidal argillaceous dololaminite shoreface sequence in the Headless equivalent of the subsurface Manetoe Dolomite in Liard Basin display lithologies similar to the thick peritidal dolomitic wackestone facies of the lower part of the Dunedin Formation of northeast British Columbia. This supports the concept that the Nahanni and Headless formations in the subsurface of Liard Basin were a transgressive sedimentary package similar to the Dunedin before dolomitization, unlike the Nahanni-Headless sequence of the Mackenzie Mountains.

Manetoe Dolomite in cores from gas fields in Liard Basin display evidence of at least one, and possibly several, solution excavation events. Cavern-fill deposits postdate, and possibly formed contemporaneous with, emplacement of the Manetoe Dolomite. Movement of hydrocarbons into Manetoe Dolomite reservoirs postdates the episode(s) of cavern excavation. Gas and bitumen in the Labiche Field indicates that cavern-fillings are in contact with source rock. Reservoir bitumens that completely occlude prebitumen porosity of the Manetoe Dolomite may represent deasphalted oil. Bitumens in overlying strata display a consistent downward increase in reflectivity that parallels the downward increase in vitrinite reflectance and in Tmax.

The present day porosities of the Manetoe Dolomite and Nahanni limestone in cores from the gas fields are consistent with depth-dependent burial porosity loss accompanied by occlusion of porosity by mineral cements and bitumen. Additional porosity loss may have occurred from more time-dependent processes such as stylotization. Permeability, particularly vertical permeability, has been enhanced by dolomitization, except possibly in cases where pre-dolomitization porosity and permeability was high. Late stage fracture porosity is not pervasive, and, in most cores, is not present.

INTRODUCTION

The Manetoe Dolomite and its associated gas fields lie in the subsurface of the Liard Basin (Gabrielse, 1967) west of the Liard River, across the border of the Yukon and Northwest Territories (Fig. 1). Large masses of fractured white sparry dolomite form the reservoir rock at depths ranging from 2600 metres to 3400 metres subsea in the Pointed Mountain and Kotaneelee gas fields (Figs. 2 and 3). Other nonproducing fields, such as the Liard and Labiche fields (Price, 1994), developed within the Manetoe Dolomite of this region and occur at shallower depths. The Manetoe Dolomite itself extends north to nearly 63 E N latitude. It is present across an area of more than 30,000 km2 in the south-central Mackenzie Mountains (Morrow *et al.*, 1990). The Manetoe Dolomite is mainly stratiform, or stratabound, and is confined to a thin stratigraphic interval, commonly 10 - 40 metres thick, within the Landry and uppermost Arnica formations and immediately underneath the shaly limestones of the Headless Formation (Fig. 4). However, in some areas, such as at the gas fields, the Manetoe Dolomite extends vertically several hundred metres upwards through the Headless Formation and into the overlying Nahanni Formation (Fig. 4). It is in these areas where dolomitization extends vertically upwards into the Nahanni that the Manetoe is prospective for hydrocarbons.

The Beaver River, Kotaneelee and Pointed Mountain gas fields have an initial combined estimated gas reserve of about 15.5×10^9 m^3, and have had a cumulative gas production of about 10.0×10^9 m^3 (Morrell *et al.*, 1995). Gas in these fields is almost entirely contained within intercrystalline pore space of the matrix dolomite (Snowdon, 1977) and is almost entirely methane (Ward, 1994). Other gases present include CO_2 (<15%) and N_2 (<10%). H_2S constitutes less than a few per cent and He (0.05%) is present in trace amounts (Ward, 1994).

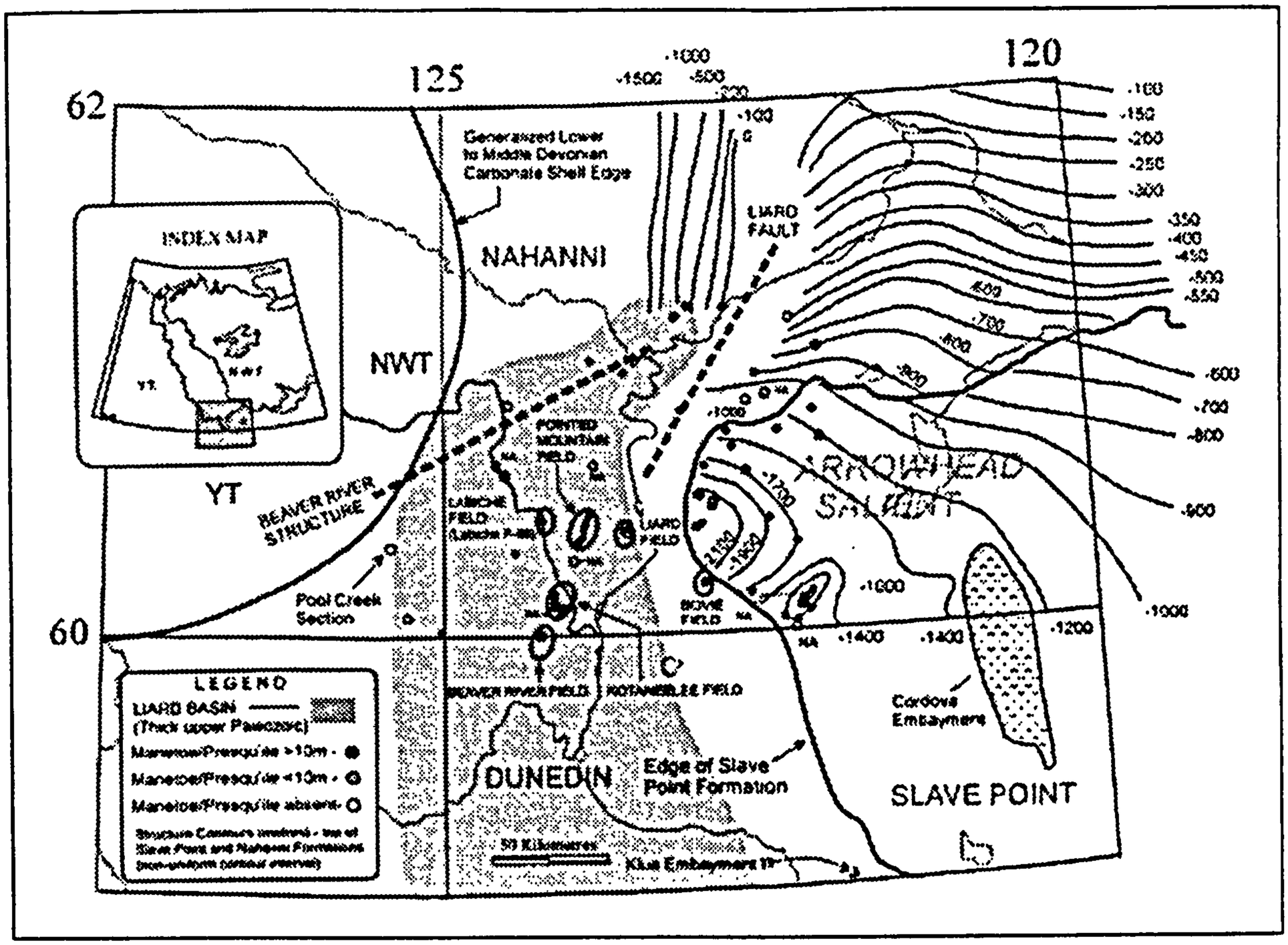

Fig. 1. Index map showing locations of gas fields, Liard Basin, Arrowhead Salient of the Presqu'ile Barrier and trends of major basement structures (Liard Fault and Beaver River Structure).

Gas columns in these fields are in excess of 600 metres and production is aided by an active water drive in addition to gas expansion (Ward, 1994; Meding, 1994). This water drive is provided by a regional aquifer which flows through lower Paleozoic carbonate strata west to east from the Mackenzie and Franklin Mountains and discharges rather saline water into the Liard and Mackenzie Rivers (Ward, 1994). The basal black shales of the Besa River Formation, or Horn River equivalent shales (Fig. 4), act as an upward confining layer to this regional aquifer. These black shales also act as a seal against the upward migration of gas which is entrapped in dolomitized sections of Arnica to Nahanni strata (Fig. 4) in areas of structural closure such as at the Pointed Mountain and Kotaneelee fields (Figs. 2 and 3). These organic-rich shales with up to 5% TOC (total organic material) probably also were the main source beds for hydrocarbon in these fields (Fig. 5; Morrow *et al.*, 1993).

Liquid hydrocarbons were generated from Besa River source beds in late Paleozoic time and initial migration of oil probably occurred before the end of Paleozoic time (Morrow *et al.*, 1993). This was primarily the consequence of rapid and deep Carboniferous burial in the Liard Basin (Fig. 1) under conditions of high heat flow (Morrow *et al.*, 1993). The northern edge of this upper Paleozoic depocentre is close and parallel to the northeast contination of the Beaver River Fault in the La Biche River map area (Douglas, 1976). The Beaver River Fault and its northeast continuation are named here as the "Beaver River Structure" (Fig. 1). The prominent east-west bend in the Nahanni Thrust Fault at Nahanni Butte (at the junction of the South Nahanni and Liard rivers) as mapped on the Sibbeston Lake map area (Douglas and Norris, 1976), marks the eastern traceable limit of this hypothesized Beaver River Structure.

There is a profound difference in structural style north and south of the Beaver River Structure. Thrust faults north of the structure are almost all eastward-verging, with the normal eastward-directed movement on Laramide thrusts. South of the structure, thrust faults are dominantly west-verging. West-verging thrust faults,

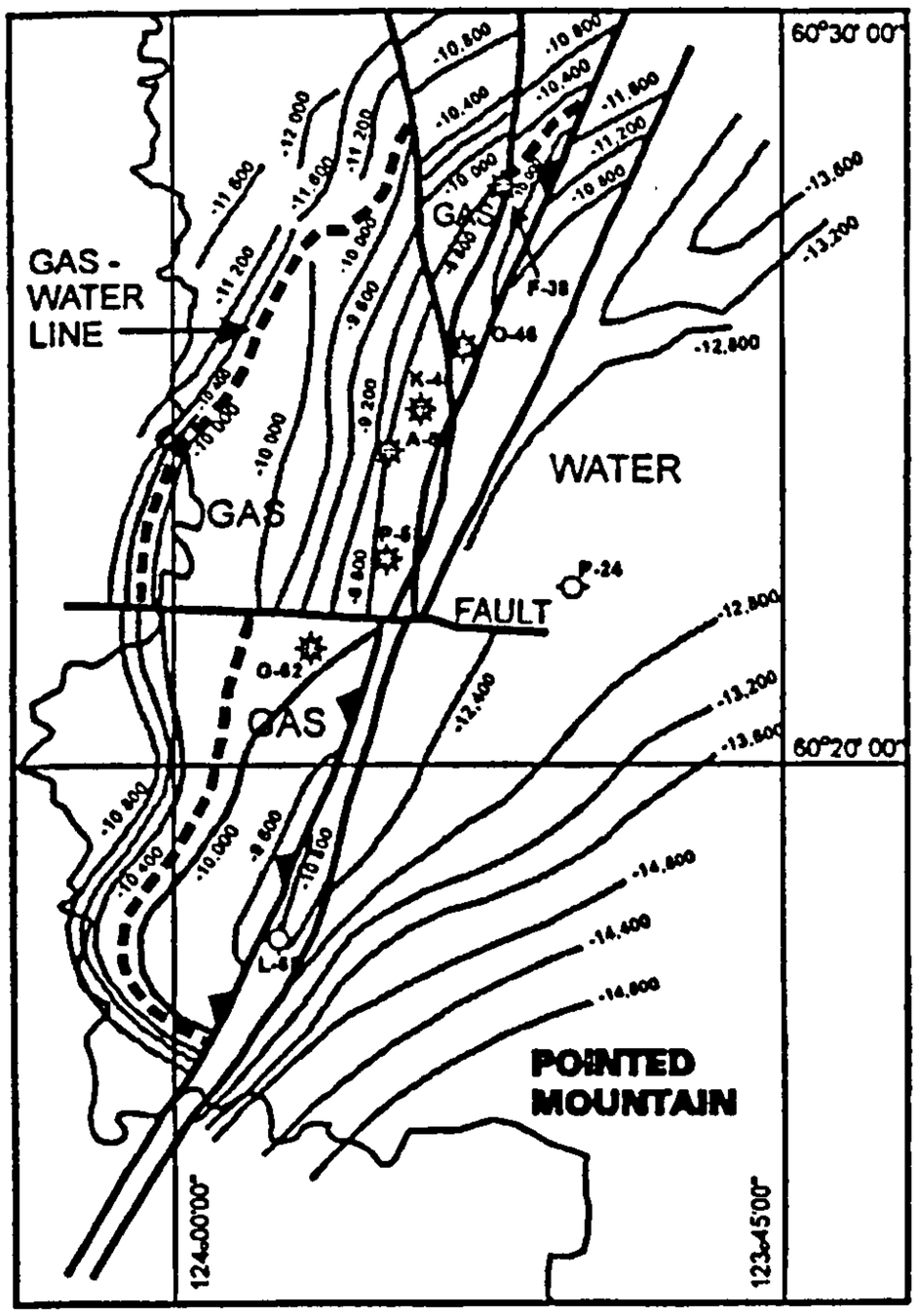

Fig. 2. Seismic depth map of the top of the Manetoe Dolomite (Nahanni equivalent) at the Pointed Mountain gas field, Northwest Territories (Amoco Canada Petroleum Company Ltd., 1964).

such as the Beaver River Thrust, the Larsen Thrust, the LaBiche Fault, the Dendale Thrust, and the Kotaneelee Fault (Douglas and Norris, 1976 and Fig. 3), are the norm, rather than the exception south of the Beaver River Structure. The more "normal", eastward dominant sense of Laramide thrust fault movement reasserts itself only south of the border with British Columbia.

It seems possible that this profound change in structural style is a manifestation of a deep Precambrian crustal fault that was periodically reactivated during times of tectonism, such as the Laramide Orogeny. The Beaver River Structure also may have played an earlier role in forming the northern margin of Liard Basin in late Paleozoic time. Other, similar ancient northeast-southwest oriented Precambrian crustal faults are known to have segmented the miogeocline of western Canada in Paleozoic time (Cecile *et al.*,1997).

In addition to the hypothesized Beaver River Structure, the Liard Fault is another ancient fault that may have been active in late Paleozoic time within the region of the gas fields. The Liard Fault is a NNE-SSW trending structure that has offset the top of the Devonian carbonates (Williams, 1981; Fig. 1). Morrow *et al.* (1990) suggested that the Pointed Mountain, Kotaneelee and Beaver River Fields fall along the southward continuation of this fault. They suggested that post-Devonian movement along this fault may have provided vertical permeability that localized, or focussed the upward flow of brines responsible for Manetoe dolomitization.

This study is an attempt to define more precisely stratigraphic correlations within the intensely dolomitized Manetoe Dolomite of the gas fields, and to document episodes of mineral cementation (*e.g.* dolomite, calcite, quartz) and of bitumen emplacement, or the bitumen-like residual hydrocarbons that are commonly referred to as "reservoir bitumen" (Lomando, 1992). Petrographic relationships between these phases are used to define the sequence of events during burial diagenesis and fluid movements within Liard Basin. The inferred time of oil generation and migration is a key factor in determining the age of the Manetoe dolomitization event (Morrow and Aulstead, 1995). Another objective is to identify and characterize episodes of pore space creation and porosity destruction. The data and interpretations contained here are derived from a core display given at a core conference (Morrow, 1996) which accompanied the 1996 annual meeting of the Canadian Society of Petroleum Geologists (Pools '96).

Stratigraphy of Manetoe Reservoirs - Pointed Mountain Kotaneelee and Labiche Fields

Stratigraphic cross-sections across the Pointed Mountain and Kotaneelee fields are shown in Figure 6 in addition to the "one well field" at Labiche F-08. In all wells of the Pointed Mountain and Kotaneelee fields the lower Devonian carbonates beneath the top of the Nahanni Formation and beneath the Middle to Upper Devonian Besa River shale are completely dolomitized and overprinted by the Manetoe Dolomite. However, the correlative sequence in the CPOG *et al.* Labiche F-08 well is incompletely dolomitized and contains numerous intervals of undolomitized Nahanni fossiliferous lime wackestone. Across most of the southern Mackenzie Mountains and in the subsurface of the Interior Plains east of the Mackenzie Mountains, the Manetoe Dolomite is more stratiform and is confined stratigraphically to a zone of variable thickness commonly less than 30 metres thick and is dominantly, or entirely, developed within the Landry Formation (Morrow *et al.*, 1990).

In spite of the total dolomitization of the Arnica to

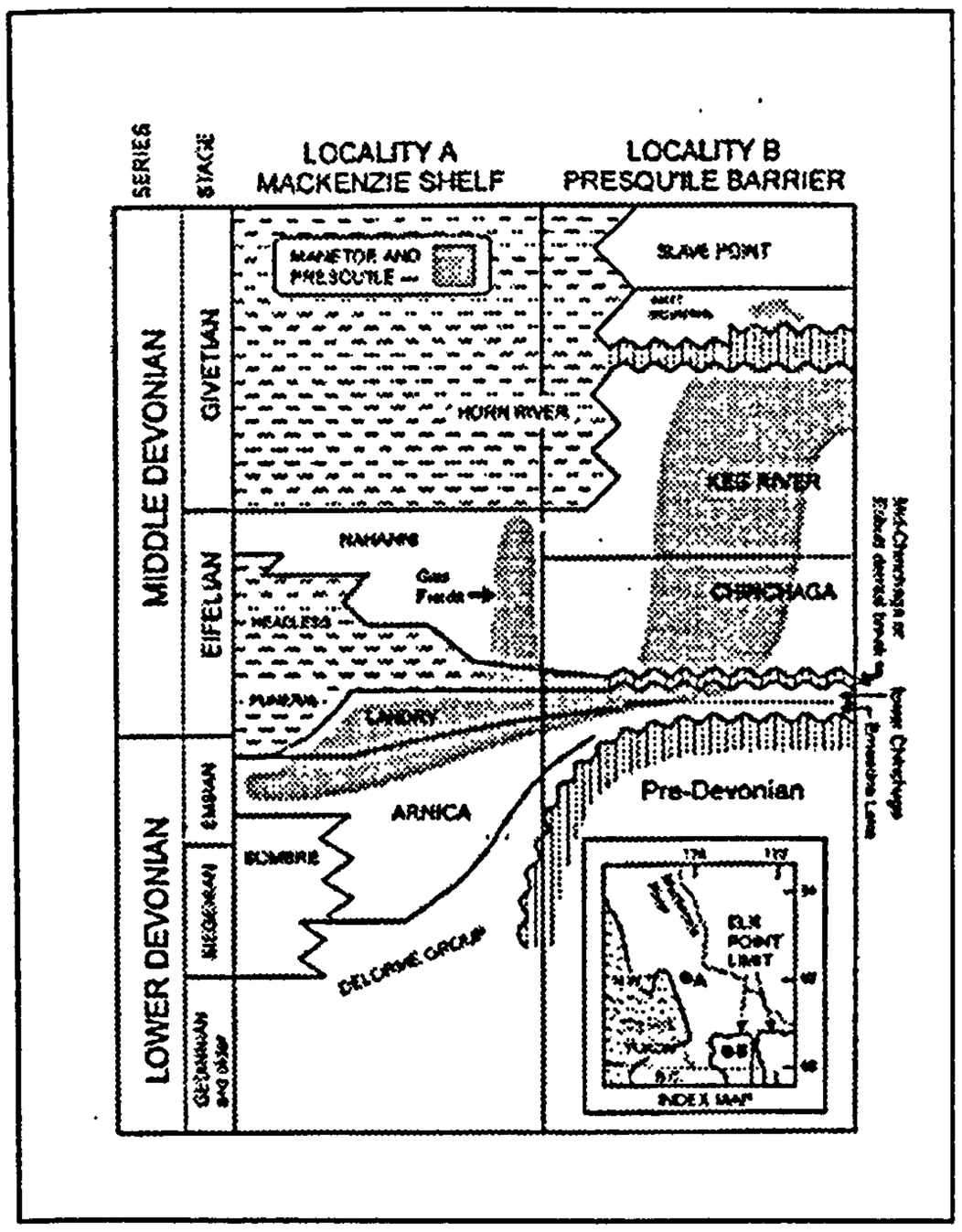

Fig. 4. Schematic stratigraphic chart illustrating the distribution of the Presqu'ile and Manetoe dolomites from the Arrowhead Salient of the Presqu'ile Barrier northwestwards to the Mackenzie Shelf sequence beneath Liard Basin and the southern Mackenzie Mountains.

younger eastward towards the Arrowhead Salient (Morrow and Aulstead, 1995). Conodonts collected from the uppermost beds of the Nahanni Formation in the eastern Texaco Bovie Lake J-72 well indicate a middle to late Givetian age for the top of the Nahanni (Appendix 1 of Meijer-Drees, 1993) near the western limit of the Arrowhead Salient of the Presqu'ile Barrier (Fig. 7). The eastward 'younging' of the upper contact of these strata with the overlying Besa River black shale closely resembles the similar southeastward 'younging' of the upper contact of the Dunedin Formation towards the Keg River, or Presqu'ile Barrier of northeastern British Columbia (Morrow, 1978; Taylor and Mackenzie, 1970). Strata close to the top of the Dunedin Formation near its northern limit in northeastern British Columbia are as old as Emsian (Chatterton, 1978). There is even evidence of intertonguing of Besa River shales with uppermost beds of Nahanni strata in the gas fields similar to that which occurs in outcrop at the top of the Dunedin Formation in northeastern British Columbia (Morrow and Aulstead, 1995; Morrow, 1978).

The "Headless Formation" strata in the gas field wells is also somewhat different from Headless strata farther north in the outcrop belt of the Mackenzie Mountains. At the latitude of the southern Mackenzie Mountains, the Headless Formation gradually thickens westward from a feather edge in the Interior Plains to more than 250 metres thick in westernmost sections (Morrow and Cook, 1987). At its eastern limit, the Headless Formation is only a few metres thick and its basal contact is an unconformity that merges with the unconformity represented by the Ebbutt Break and the mid-Chinchaga detrital zone (Fig. 4). Throughout almost the entire Interior Plains east of the disturbed belt the Headless Formation is less than 30 metres, and commonly less than 10 metres, thick (Fig. 40 in Meijer-Drees, 1993). The eastern part of the Headless Formation is dolomitic and contains peritidal features such as finely laminated intervals containing fenestral fabric and lime mudflakes and mudlumps in pockets of green and ochre-coloured pyritic argillaceous material (Morrow and Cook, 1987; Meijer-Drees, 1993). The thicker Headless in western sections is a shaly, open marine, completely subtidal limestone sequence quite different from the eastern Headless. The western Headless sequence were deposited on a submarine apron that accumulated in front of the westward-prograding shallow water shelf, or platform, limestones of the Nahanni Formation (Morrow and Cook, 1987; Noble and Ferguson, 1971).

The 'Headless Formation' in the gas fields is about 150 metres thick and is distinctively argillaceous (Fig. 6). In core, however, it does not resemble the open marine fossiliferous shaly lime wackestones of Headless Formation that is also about 150 metres thick in the southern Mackenzie Mountains. Instead, the lithologies of the 'Headless' interval in the gas fields more closely resemble the peritidal deposits of the thin Headless east of the disturbed belt. The gas field Headless interval also is lithologically and sedimentologically similar to the lower part of the Dunedin Formation in northeastern British Columbia. The lower part of the Dunedin, the dolomitic wackestone facies, has a maximum measured thickness of 130 metres and is composed of laminated and thin bedded, dolomitic lime mudstones containing fenestral fabric and dololaminites containing little fauna (Morrow, 1978). It has a log signature similar to the gas field 'Headless' strata (Fig. 7).

These observations reinforce the concept (Morrow and Aulstead, 1995) that the 'Headless' interval in the gas fields is better regarded as a northward continuation of the lower part of the Dunedin, rather than a southward

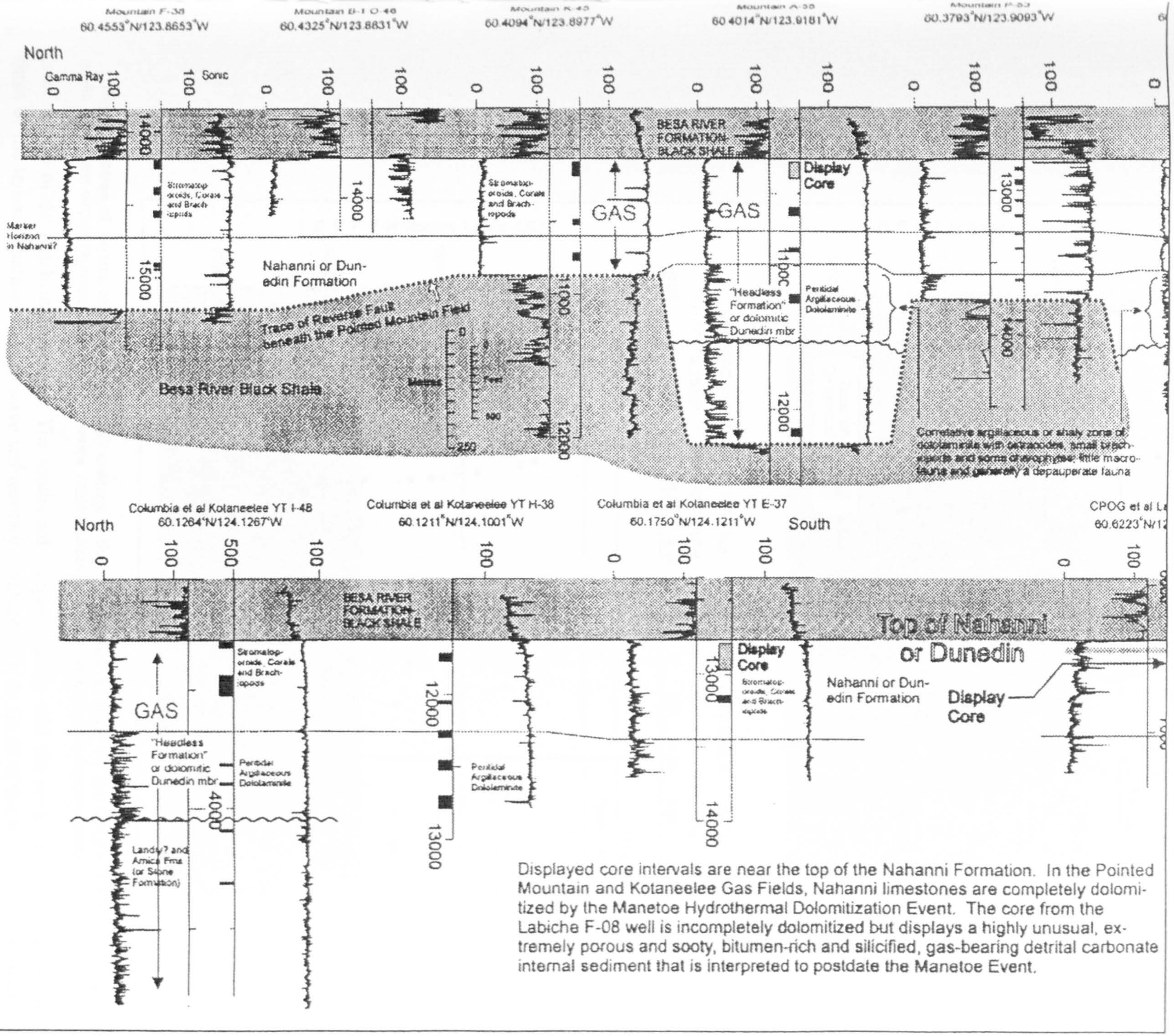

Displayed core intervals are near the top of the Nahanni Formation. In the Pointed Mountain and Kotaneelee Gas Fields, Nahanni limestones are completely dolomitized by the Manetoe Hydrothermal Dolomitization Event. The core from the Labiche F-08 well is incompletely dolomitized but displays a highly unusual, extremely porous and sooty, bitumen-rich and silicified, gas-bearing detrital carbonate internal sediment that is interpreted to postdate the Manetoe Event.

6.6

Stratigraphic cross-sections of wells through the Pointed Mountain and Kotaneelee fields. The CPOG *et al.* LaBiche F-08 well represents the Labiche gas field.

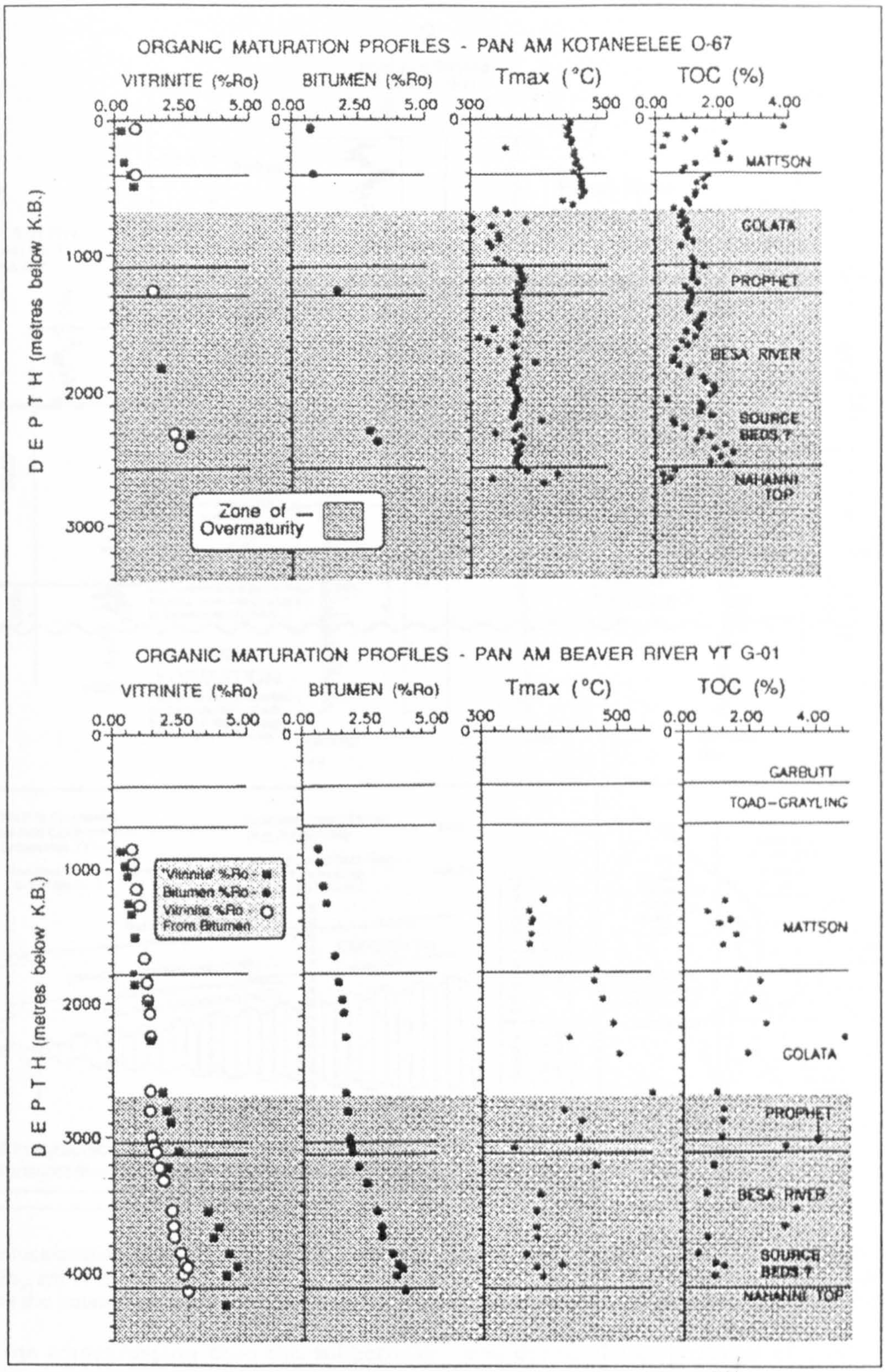

Fig. 5. Profiles of organic maturation from well cuttings in the Pan Am Beaver River YT G-01 and Pan Am Kotaneelee O-67 wells. The open circles represent vitrinite reflectance values calculated from bitumen reflectances (Jacob, 1985).

continuation of the Headless Formation. The southward limit of the upward-shallowing, regressive sedimentary package of the Nahanni and Headless formations coincides approximately with the northern edge of the Arrowhead Salient (Fig. 7). South of this limit, Emsian-Eifelian deposition of the Dunedin Formation accompanied, rather than

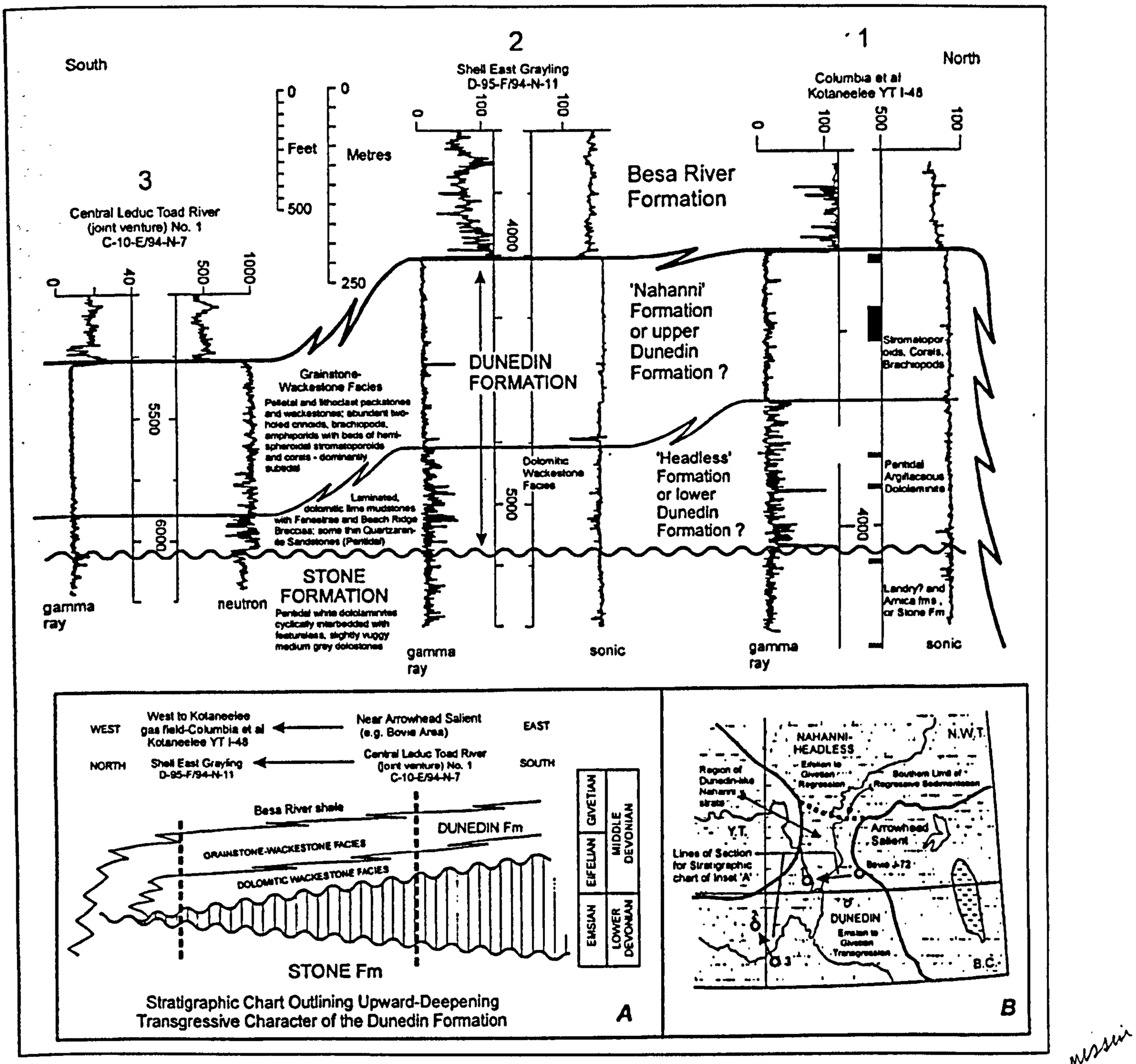

Stratigraphic Chart Outlining Upward-Deepening Transgressive Character of the Dunedin Formation

Fig. 7. Well cross-section of Lower and Middle Devonian strata from northeast British Columbia northwards to the Yukon Territory. Inset diagram **A** shows the transgressive character of "Nahanni" deposition in the region of the Liard Basin gas fields. Diagram **B** shows the boundary of regressive versus transgressive sedimentation of Nahanni-equivalent strata.

followed, marine transgression onto the subaerially exposed underlying dolostones of the Stone Formation.

Petrographic Relationships - Pore Space Modification and Cementation

There is little evidence remaining concerning diagenesis during the early stages of lithification of Nahanni and Headless limestones and argillaceous limestones or during early diagenesis of Landry limestone. Probably the fine grained lime sediments in these Middle Devonian units were deposited originally as calcite rather than the more soluble polymorph, aragonite (*see* James and Choquette, 1990). The peritidal cyclic light

and dark brownish-grey dolostones of the underlying Sombre and Arnica formations are typical synsedimentary platform dolostones (Morrow and Cook, 1987) that were partly to completely dolomitized before burial. This is probably true also of the argillaceous dololaminites of the 'Headless Formation' intervals in the gas fields.

The first major post-lithification feature observable in core is the widespread dissolution of macrofauna, such as colonial corals and stromatoporoids in the upper part of the Nahanni Formation in the gas fields (Figs. 8, 9b, 10a and 10b). The cored interval of 10296 feet to 10348 feet from near the top of the Nahanni in the Amoco A-4 Pointed Mountain A-55 well (Figs. 8 and 9b) representative of Nahanni cores from the other Pointed Mountain wells with zones of spectacular vuggy biogenic moldic porosity.

Most of these large vugs are occluded or partly occluded with white sparry, centripetal (*i.e.* vug-lining), dolomite, or saddle dolomite (Figs. 9b, 10a and 10b). Some large vugs appear to have been floored by a significant amount of dark carbonate sediment before precipitation of the vug-filling white dolomite cement (Fig. 9b). This indicates that enough time elapsed between cavity dissolution and later dolomitization and dolomite cementation for geopetal carbonate sediments to floor these cavities. Many dolospar-lined vugs have ill-defined, dark bands rimming their undersides that may also represent geopetal, cavity-flooring internal sediments that accumulated before dolomitization. Alternatively, dissolution after dolomitization may have formed cavities preferentially along the undersides of these large dolospar-rimmed vugs.

The dolomitization associated with the white, coarsely crystalline dolospar of the Manetoe Dolomite is the first clearly defined, post-lithification cementation event. White Manetoe dolospar lines and, partly to completely, occludes vugs (Figs. 9b, 10a and 10b) and fills interfragment spaces in rubble and mosaic breccias (Figs. 8, 10b and 11c). These breccias tend to be completely cemented with white dolospar, but unoccluded pore space occurs between some larger fragments (Figs. 10b and 11c). Part of the interfragment space in these breccias is filled with particulate, or detrital, silt- and sand-sized carbonate (Figs. 10b and 11c). Subvertical to oblique, thin, sharp-walled fractures cemented with white dolospar occur within and around breccia masses, particularly where these tend to have an overall vertical orientation (Figs. 9b, 10a and 10b).

Under cathodoluminescence, the coarsely crystalline, white dolospar of the Manetoe Dolomite exhibits very low intensity, or dull to very dull luminescence (Fig. 12). This is unlike the bright cathodoluminescence that is commonly observed in dolomites precipitated from anoxic, or from reducing basinal fluids in deep burial diagenetic environments (Machel, 1985). Brightly luminescent burial calcite and dolomite cements generally have manganese contents of at least several mole per cent (ie. several thousands of parts per million; Machel, 1985). The near nonluminescence of the Manetoe dolospar cements is consistent with their very low manganese concentrations of only a few tens to a few hundreds of parts per million. White dolospar of the Manetoe Dolomite contains very low concentrations of contaminant elements in general, as may be seen in Appendix 3 of Morrow *et al.* (1990).

The next clearly defined event that definitely postdates at least part of the Manetoe dolomitization event is a dissolution and cavity-filling episode that is particularly well developed in core from the Pointed Mountain gas field (Figs. 8 and 9b) but is also visible in core from the Kotaneelee field (Fig. 10c). Dark, fine grained carbonate sediment infilled small caverns which were clearly excavated within pre-existing Manetoe Dolomite. Small calcite-cemented fractures contained entirely within these cavern-fillings (Fig. 9b) may be shrinkage cracks related to the dewatering and lithification of these internal sediments. These cavern fillings also contain small millimetre to centimetre-sized fragments of white dolospar which have apparently been reworked from the walls and floors of caverns (Figs. 9b and 10c).

Although there are dark cavern-fillings that postdate Manetoe Dolomite unequivocally, at least in the intervals in which they occur, there are other dark bands that strongly resemble the cavern-fillings that have been fractured or brecciated by the Manetoe Dolomite in core from both Pointed Mountain and from Kotaneelee (Figs. 10c and 10d). This, combined with the previous suggestion of geopetal sediment deposition in vugs which may have predated Manetoe dolomitization, may indicate that this early dissolution, or karst event may have occurred, in part, contemporaneously with Manetoe dolomitization, and, possibly, may have begun before dolomitization. This inference is consistent also with the general spect of the fauna preserved within cavity-filling sediments which strongly resemble fauna, such as the colonial coral *Alveolites* , amphiporids and crinoids typical of the Middle to Late Devonian.

Hydrocarbon in the form of solid bitumen, or reservoir bitumen (Lomando, 1992) forms the next petrographically distinct paragenetic phase in cores from the Pointed Mountain and Kotaneelee fields. Ubiquitous,

Table 1. Rock-Eval data for core samples from the Columbia et al Kotaneelee YT E-37 well

Depth (feet)	Wt. (mg)	Tmax	S1	S2	S3	PI	S2/S3	PC	TOC	HI	OI*
12792	100.3	593	0.03	0.19	1.17	0.14	0.16	0.01	4.39	4	26
12792	100.3	594	0.02	0.18	1.20	0.10	0.15	0.01	6.02	2	19
12987	100.1	592	0.10	0.57	0.73	0.15	0.78	0.05	10.56	5	6
12987	99.5	591	0.12	0.59	0.73	0.17	0.80	0.05	5.14	11	14

*-see Peters (1986) for explanation of Rock-Eval parameter abbreviations (*e.g.* OI=Oxygen Index)

solid black bitumen either coats the interiors of dolospar-lined, open vugs (Fig. 9b) or totally infills vug interiors (Figs. 10a, 11b and 11d). Thin irregular, subvertical to subhorizontal, bitumen-filled, sharp-walled fractures crosscut fabrics of the Manetoe Dolomite (Fig. 11). These bitumen-filled fractures also cross-cut the post-Manetoe cavern-filling internal sediments (Figs. 10c and 10d). In some instances, reservoir bitumen seems to have infilled stylolites or solution seams developed subparallel to bedding (Fig. 11b).

The sparse core coverage available from wells in the Pointed Mountain and Kotaneelee fields largely precludes an assessment of vertical trends in the amounts of reservoir bitumen. In cores from the Pointed Mountain Field there is a definite tendency for the amount of macroscopic bitumen to increase in amount downwards from Nahanni equivalent strata to the deeper Landry and Arnica equivalent strata in wells such as Amoco A-4 Pointed Mountain A-55 which have core from deeper Arnica equivalent strata (Fig. 6). In the Kotaneelee field, cores from the Nahanni and Headless intervals in the structurally high wells of Columbia et al Kotaneelee YT I-48 and H-38 contain small amounts of reservoir bitumen throughout. However, core from the Nahanni interval in the structurally low Columbia et al Kotaneelee YT E-37 well contains anomalously large amounts of black reservoir bitumen infilling vugs (Fig. 10a) and post-Manetoe fractures.

Rock-Eval analyses (Imperial Oil Resources Ltd., pers. comm.) of selected reservoir bitumen samples from the E-37 well are shown in Table 1. These reservoir bitumens from the Manetoe Dolomite have extremely high TOC values but virtually insignificant pyrolyzable carbon (PC) reflecting low S1 and S2 peaks (Table 1). This is consistent with their passage through the oil window to gas generation. Their low HI/OI ratios preclude classification according to original organic material type on Van Krevelen-like plots of HI versus OI (*e.g.* Espitalié, 1986). The S2 peaks gave extremely high Tmax values which are beyond even the high maximum Tmax values of about 500°C observed in organic material in the siliciclastic sequence overlying the Manetoe Dolomite (Fig. 5).

A re-evaluation of the petrographic characteristics of organic matter in the Upper Devonian and Lower Carboniferous shales in the Pan Am Beaver G-01 and Pan Am Kotaneelee O-67 wells indicates that organic matter is composed of various populations of indigenous solid bitumens and that true vitrinite is rare (Potter, in prep.). Most of these bitumens were generated in situ as byproducts of maturation of various species of organic materials which initially were a Type-II, possibly sulphur-rich, kerogen (Potter, in prep.). The high maximum Tmax values of 500°C observed in the dispersed bitumens of the Mattson-Golata interval (Fig. 5) may actually be somewhat lower than they potentially might have been in sulphur-depleted bitumens (Snowdon, 1995).

Tmax profiles through the post-Middle Devonian sequence overlying the Nahanni-Manetoe carbonates (Fig. 5) are also consistent with the very high Tmax temperatures observed in the Kotaneelee E-37 Manetoe bitumens. Tmax temperatures in the nearby Pan Am Kotaneelee and Pan Am Beaver River YT G-01 wells reach maximums of up to and even greater than 500°C in the Golata shale more than 1000 metres above the contact of the Besa River shales with the Nahanni Formation (Fig. 5). Vitrinite reflectances and vitrinite-equivalent reflectances from bitumen at this level are about 1.40% to 1.50% Ro (Fig. 5). This is consistent with the correlation between Tmax and vitrinite reflectances established by Espitalié (1986) for type III coal series organic material in the Paris Basin (Fig. 8 in Espitalié, 1986) and may indicate that there is some admixture of type III organic material within these sediments.

Indigenous bitumens in the post-Devonian, dominantly siliciclastic, upper Paleozoic sequence including the organic-rich Besa River shale source rocks overlying the Nahanni in wells close to the gas fields, display a progressive increase in reflectivity downsection in a manner parallel to that of vitrinite (Fig. 5; Table 2). Bitumens in

Table 2: Bitumen Reflectances from post Middle Devonian strata - Pan Am Beaver River YT G-01 and Pan Am Kotaneelee 0-67

Pan Am Beaver River YT G-01			Pan Am Kotaneelee 0-67		
Depth (Feet Kb)	R_{bit}% (measured)	R_{vr}% eq. (Calculated)*	Depth (Feet Kb)	R_{bit}% (measured)	R_{vr}% eq. (Calculated)
2880	0.60	0.77	260	0.71	0.84
3250	0.66	0.81	1320	0.73	0.85
3700	0.71	0.84	4200	1.71	1.46
4135	0.84	0.92	7595	2.91	2.20
5520	1.20	1.14	7800	3.20	2.38
6120	1.40	1.27	Pan Am Beaver River YT G-01		
6540	1.47	1.31	10865	2.41	1.89
6565	1.47	1.31	11635	2.74	2.09
7480	1.52	1.34	12015	2.85	2.16
8766	1.55	1.36	12265	2.90	2.19
9210	1.53	1.35	12665	3.40	2.50
9880	1.72	1.46	12915	3.50	2.56
101291.76	1.49	12975	3.70	2.69	
10183	1.87	1.56	13185	3.43	2.52
10575	2.02	1.65	13549	3.80	2.75

*- "R_{vr}% eq." is calculated according to the formula R_{vr}% eq. = 0.618(R_{bit}%+0.40 (after Jacob, 1985)

the Pan Am Beaver River YT G-01 well near the display a very consistent downhole increase in reflectivity that parallels the downhole increase in vitrinite reflectances. Vitrinite equivalent reflectances calculated from bitumen reflectances using the relationship of Jacob (1985, R_{vr}% eq. = 0.618(R_{bit}%+0.40) may underestimate vitrinite reflectances by a progressively greater amount downhole (Fig. 5; Table 2). Better fits to vitrinite reflectance data of the G-01 well can be made by linear functions with a steeper slope and lower intercept value (e.g. R_{vr}% eq. = 1.05(R_{bit}%+0.20). The degree of misfit between Jacob's (1985) relationship and the G-01 data may be partly explained by the fact that Jacob's (1985) data fitting was limited to vitrinite reflectances of less than 2.0%.

Bitumens in the post-Middle Devonian of the Pan Am Kotaneelee 0-67 well are much more scattered than in the G-01 well although they also show a general downward increase in reflectivity (Fig. 5). The 0-67 bitumens may have originated both as residual in-place bitumen during maturation and as migrated bitumen (*see* Fig. 4 of Morrow *et al.*, 1993).

Drusy quartz infills parts of larger vugs in the Kotaneelee and Pointed Mountain fields. Typically, "dogtooth" or drusy quartz occupies the centres of dolospar-lined vugs (*see* Fig. 10 in Morrow *et al.*, 1990) and also lines abundant open subvertical fractures that crosscut Manetoe Dolomite near the top of the Nahanni in the Columbia et al. Kotaneelee YT I-48 well (cored interval 3660-3665.7 metres). Some of the dolomitized groundmass in this atypical Manetoe core has been silicified by microcrystalline quartz.

Equant, coarsely crystalline white calcite occurs also as a late stage vug-filling cement in dolospar-rimmed and bitumen-lined vugs, particularly in core from the Pointed Mountain Field (Fig. 8). Calcite-filled vugs contained no drusy quartz even in those rare instances where both quartz and calcite-filled vugs were found in the same core, such as in cores 2 and 3 (10,348 - 10,396 ft. and 10,600 - 10,658 ft. K.B.) of the Pointed Mountain A-55 well (Fig. 8). Consequently, there is little petrographic indication of the order of emplacement of calcite versus quartz vug-filling cements. However, the fact that, in these cores, all calcite-filled vugs are totally occluded with calcite cement, whereas quartz-filled vugs are, almost invariably, incompletely filled with drusy quartz and retain unfilled pore space, may indicate that calcite cementation preceded quartz cementation.

In a different mode of occurrence, late stage equant to bladed white calcite has grown displacively within the bitumen of bitumen-filled vugs (Fig. 10a) or within bitu-

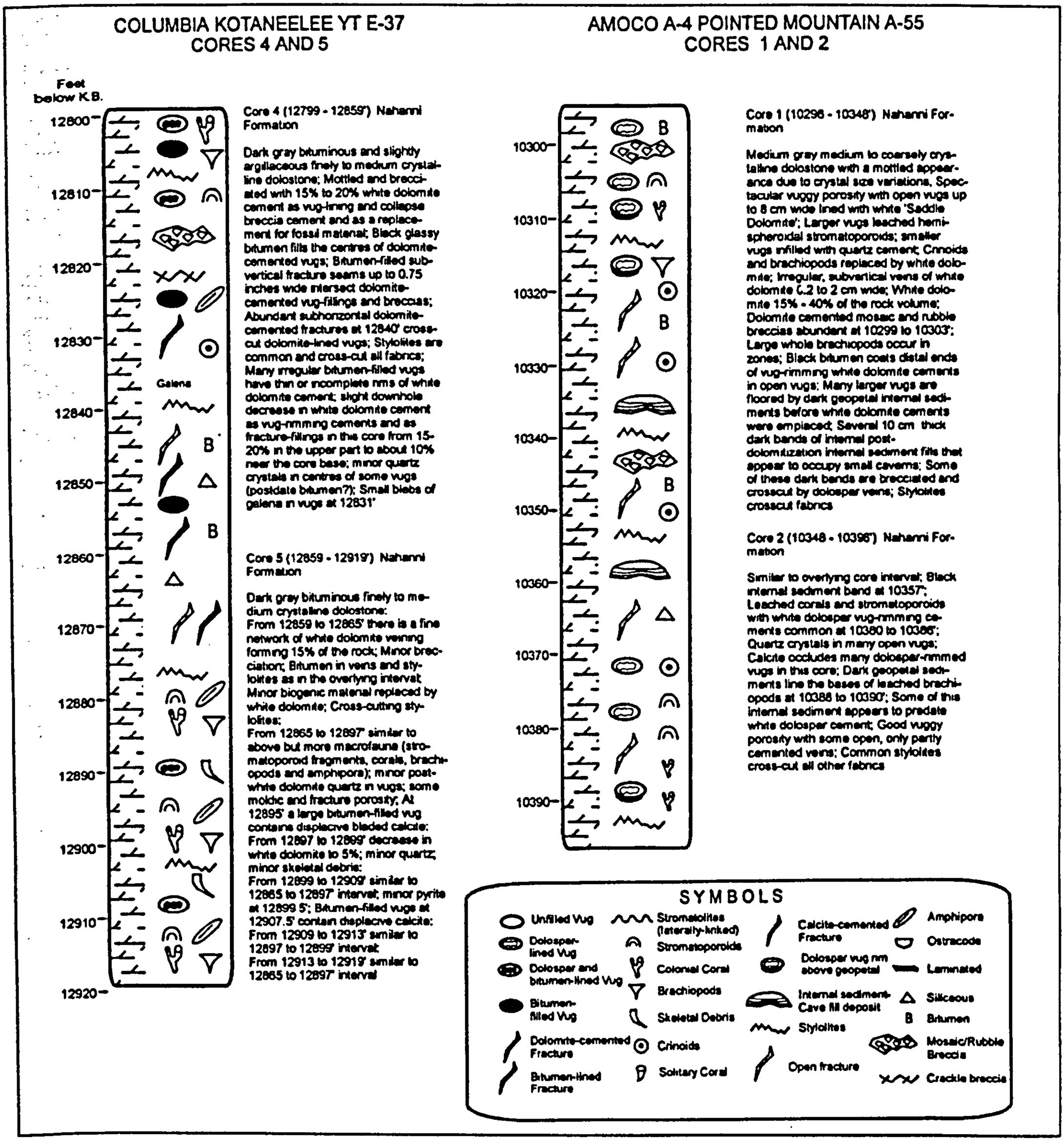

Fig. 8. Graphical logs and descriptions of cores from the Kotaneelee and Pointed Mountain gas fields.

men-impregnated, cavity-filling internal sediments (Fig. 10c) in core from the Kotaneelee E-37 well. This type of calcite appears to be restricted to wells, such as Kotaneelee E-37, which contain relatively large amounts of post-Manetoe bitumen.

Isolated small blebs of coarsely crystalline galena occur as final vug-fillings, and as irregular veinlets crosscutting Manetoe fabrics in the Manetoe Dolomite in the Nahanni equivalent interval as in the Kotaneelee E-37 well (Fig. 8) and in the Kotaneelee H-38 well (Fig.

Table 3. Rock-Eval data for core samples from the CPOG et al LaBiche F-08 well

Depth (feet)	Wt. (mg)	Tmax	S1	S2	S3	PI	S2/S3	PC	TOC	HI	OI*
6525	101.7	303	0.16	0.07	0.16	0.73	0.43	0.01	2.15	3	7
6525	103.0	423	0.16	0.09	0.20	0.67	0.45	0.02	2.24	4	8
6526	102.8	303	0.18	0.03	0.25	0.90	0.12	0.01	1.45	2	17
6526	103.2	393	0.19	0.03	0.22	0.86	0.13	0.01	1.40	2	15
6521.5	100.0	***	0.00	0.00	0.14	***	0.00	0.00	0.41	0	34
6521.5	100.0	***	0.00	0.00	0.13	***	0.00	0.00	0.39	0	33
6537	101.7	***	0.00	0.00	0.06	***	0.00	0.00	0.06	0	100
6537	102.9	***	0.00	0.00	0.07	***	0.00	0.00	0.06	0	116

*-see Peters (1986) for explanation of Rock-Eval parameter abbreviations
(*e.g.* OI=Oxygen Index)

10a in Morrow *et al.*, 1990). Finely to medium crystalline, reddish-brown sphalerite occurs as small veinlets crosscutting Manetoe fabrics and as fine disseminations within cores from Nahanni equivalent strata in most wells. Striking sphalerite mineralization occurs in the uppermost Nahanni-equivalent cores of the Columbia et al Kotaneelee YT I-48 well.

High amplitude, sutured stylolites commonly crosscut the dolomitized fabrics of the Manetoe Dolomite (Fig. 8; see also Fig. 10d in Morrow *et al.*, 1990). Some thin subvertical white dolospar-cemented fractures are cut by stylolites, as in the core interval at 12,144 - 12,204 ft. in the Pointed Mountain A-55 well.

Late-stage large fractures, either open or cemented are not common in the Liard Basin Manetoe gas fields. Where present, they are confined to local horizons, such in the previously mentioned uppermost part of the Manetoe at the Columbia et al. Kotaneelee YT I-48 well where an unusual zone of open, subvertical fractures is developed in the cored interval from 3660 - 3665.7 m. Almost all fractures in the Manetoe Dolomite of the Liard Basin gas fields are completely cemented with white dolospar, tend to be small, and commonly are associated with masses of dolomite-cemented Manetoe rubble breccia. Late tectonic fracturing, particularly with open, incompletely cemented, very large subvertical fractures of the type observed in the Manetoe Dolomite of the Beaver River gas field (Davidson and Snowdon, 1978) 20 kilometres south of the Kotaneelee Field, is almost entirely absent in the Pointed Mountain and Kotaneelee fields.

A very large scale internal sediment, or cavern-filling deposit, may be seen in the uppermost Nahanni cored interval of the CPOG La Biche F-08 well (Figs. 6 and 13). In this core, an extremely porous and permeable, black, sooty interval of silicified carbonate forms an internal sediment filling interval about 2.75 feet (0.84 metres) thick with the base of the interval at about 6,527.67 feet below K.B. (Figs. 13 and 9a). This sooty, cavity-filling deposit rests with a sharp and erosional lower contact on typical, dense fossiliferous lime mudstone of the Nahanni Formation (Fig. 9). The Nahanni limestone above and below this interval contains abundant white calcite-filled fractures that are oriented parallel to, and oblique to bedding. The base of the cavern-filling appears to have erosionally truncated one of these large calcite-filled fractures (Fig. 9a).

The fact that the calcite veining is totally absent from the dark sooty cavern-filling, as well as the truncation of calcite veins by the cavern-fill, indicate clearly that this episode of cavern excavation and filling postdates the time of calcite veining. It is not known with certainty whether this cavern-filling deposit postdates emplacement of the Manetoe Dolomite, some of which occurs at the base of this core, in the undolomitized Nahanni limestone below the cavern-filling (Fig. 13). However, the fact that the cavern-filling postdates calcite veining in the Nahanni may indicate that this episode of cavern solution excavation and filling also postdates emplacement of the Manetoe Dolomite. This is implied, because, elsewhere, calcite veining postdates Manetoe Dolomite (Morrow *et al.*, 1990). However, a pre-Mesozoic, or late Paleozoic age is indicated for the cavern-filling sediments from the appearance of the abundant bioclasts which include probable Paleozoic crinoid and brachiopod fragments.

The top of the cavern-filling is marked by a 1.0 foot (0.3 metre) thick interval of massive, coarsely crystalline, milky white calcite (Fig. 9a). It seems likely that this massive calcite represents an episode of cementation of

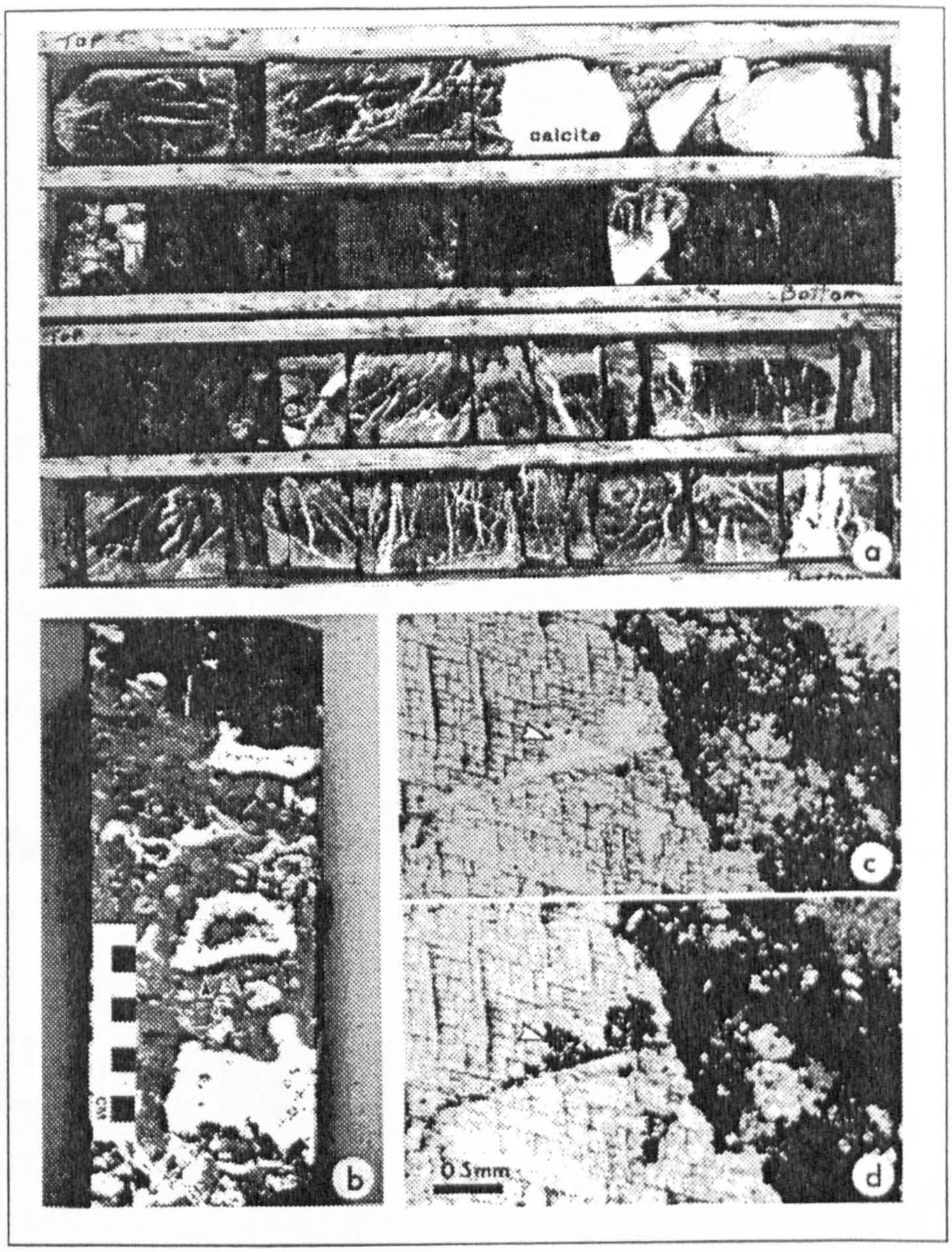

Fig. 9. Core photographs and thin section photomicrographs. Fig. 9a shows two boxes from core 1 of CPOG et al LaBiche F-08. The black arrows mark the base of a sooty, bituminous and silicified cavern-filling at 6527.75 feet (K.B.). Fractured Nahanni limestone overlies and underlies this cavern-fill. Fig. 9b shows spectacular leached biogenic porosity in Manetoe Dolomite at 10,345 feet (K.B.) in the Amoco A-4 Pointed Mountain A-55 well. Dark, cave-filling deposit occupies upper part of core. Arrow near centre of core points to base of probable internal sediment layer beneath a thick vug lining of white dolospar. Figs. 9c and 9d are plain light and crossed nicols thin section views of diagenetic calcite at the base of the white calcite zone at the top of the cavern-filling shown in Fig. 9a. Diagenetic calcite has engulfed the silicified carbonates of the cavern filling before the introduction of bitumen.

former unfilled void space at the top of the ancient cavern-filling. The uppermost part of this calcite cement zone has a sharp stylolitic contact with the overlying veined Nahanni limestone. The lower contact of the white cement zone with the underlying black sooty cavern-filling is gradational. This lower contact is characterized by an aggregate of poikilotopic white calcite crystals that average about 10 to 20 cms. in size. A thin section view of these calcites shows that the silicified carbonates of the cavern-filling were engulfed by calcite growth before these silicified carbonates were impregnated by sooty reservoir bitumen (Figs. 9c and 9d).

This cavern-filling bears some similarity to a very large, spectacular cavern-filling within the Manetoe Dolomite exposed along the south side of First Canyon in the South Nahanni River (Morrow and Cook, 1987; Aulstead, 1987). This cavern-fill deposit is more than 500 metres broad and tens of metres thick and contains

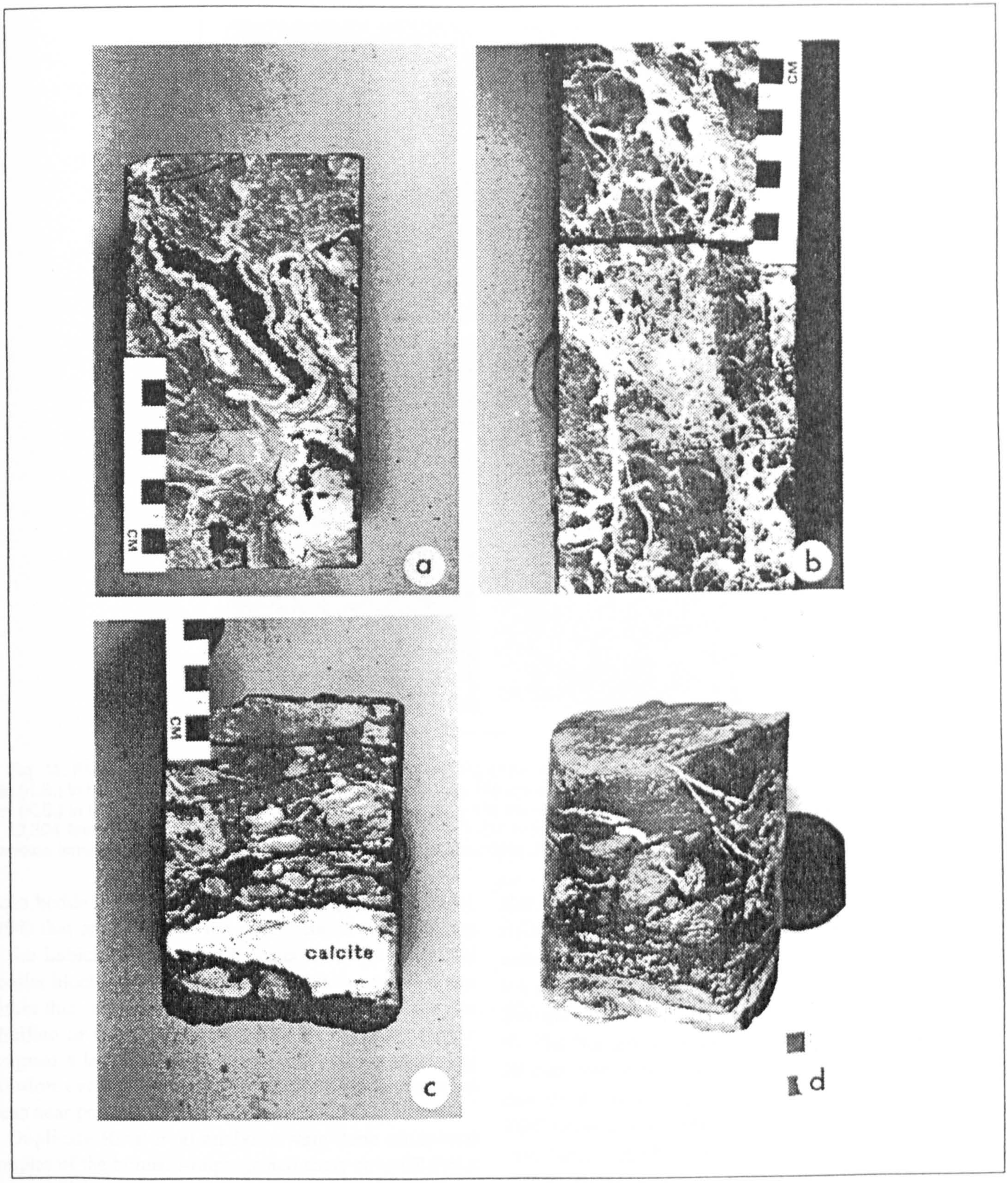

Fig. 10. Photographs of core from the Manetoe Dolomite. Fig. 10a shows solid reservoir bitumen as large vug-fillings at 12,799.5 feet (K.B.) in the Columbia et al Kotaneelee YT E-37 well. Fig. 10b shows rubble packbreccia completely cemented by white dolospar at 3661.0 metres (K.B.) in the Pan Am Kotaneelee YT I-48 well. Fig. 10c shows bitumen-filled fractures and late diagenetic white bladed calcite within a dark bituminous groundmass at 12,926 feet (K.B.). In the Columbia et al Kotaneelee YT E-37 well. Fig. 10d shows the rounded side of the slabbed core shown in 10c.

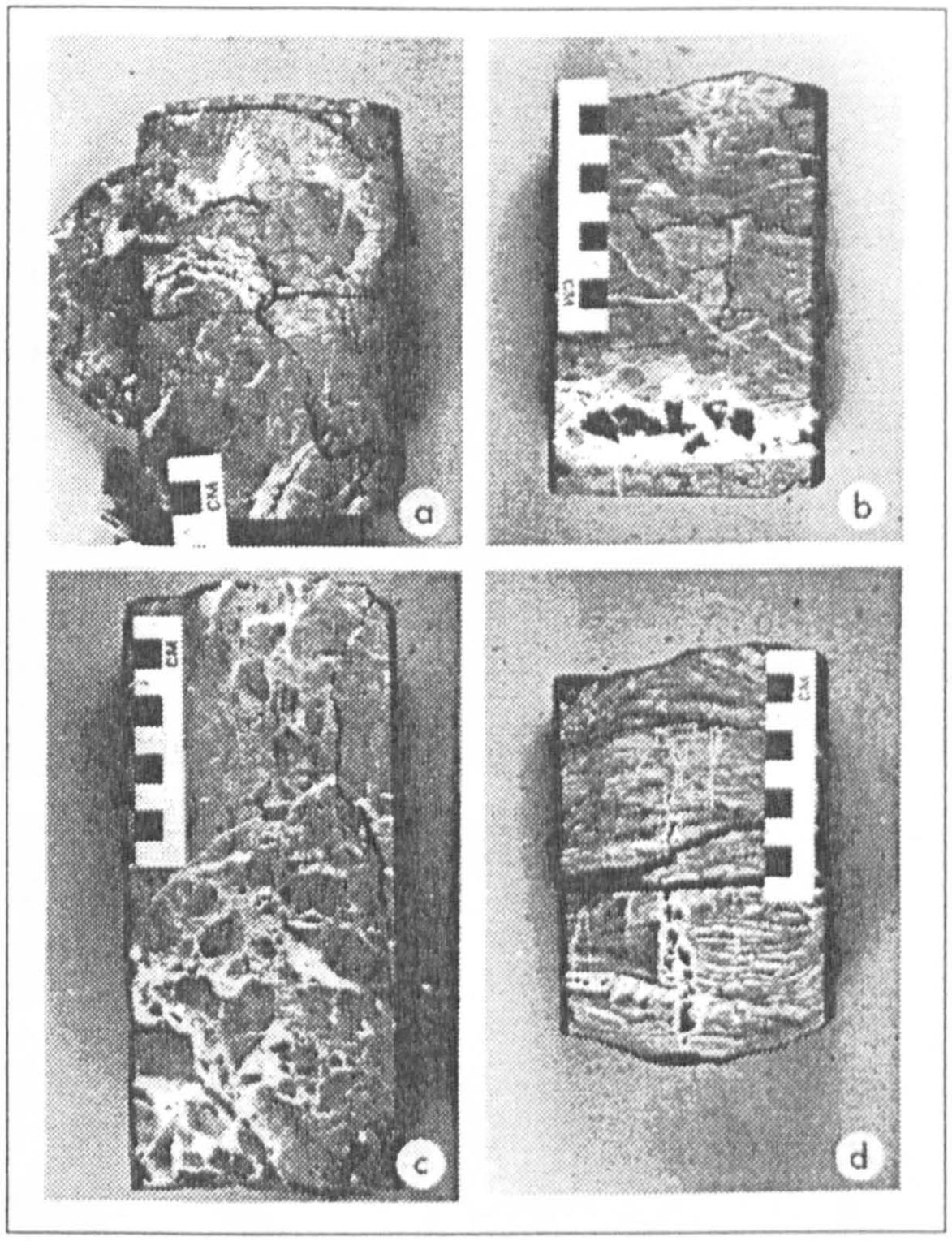

Fig. 11. Photographs of core from the Manetoe Dolomite. Fig 11a shows bitumen seams crosscutting white dolospar at 13,143 feet (K.B.) in the Columbia et al Kotaneelee YT E-37 well. Fig. 11b shows black bitumen within white Manetoe dolospar at 11,251 feet (K.B.) in the Amoco A-4 Pointed Mountain A-55 well. Fig. 11c shows a vertical vein of bitumen crosscutting Manetoe breccia at 12,304 feet (K.B.) In the Columbia et al Kotaneelee YT H-38 well. Fig. 11d shows a vertical vein of bitumen crosscutting Manetoe laminite at 11,259 feet (K.B.) In the Amoco A-4 Pointed Mountain A-55 well.

cross bedded carbonate sand and pea gravel (Morrow, 1994) that are similar to the cross bedded cavern-filling in the Labiche F-08 core. Spectacular metre-sized and smaller blocks of Manetoe Dolomite occur as dropstones within this cave deposit. This surface cave deposit is not silicified or impregnated with bitumen. It is tentatively assigned a late Tertiary to recent age as a separate, late solution event (Fig. 14) that affected the Manetoe in areas near present day outcrop.

Duplicate Rock-Eval analyses were done on several samples of the bitumen-impregnated sooty cave-fill (samples at 6525 feet and 6526 feet) and of the Nahanni limestone above (sample at 6521.5 feet) and below (sample at 6537 feet) the cave-fill in Core 1 of the LaBiche F-08 well (Table 3). TOC for the cave-filling samples ranges from 1.4% - 2.24%. The low S1 and S2 peaks, ~~the unreli~~able and low Tmax, and their very low Hydrogen Indexes (HI), indicate that these bitumens are greatly overmature and were not indigenous, consistent with their sooty, carbonaceous aspect and with the dry gas produced from Nahanni-equivalent strata slightly above this core (Fig. 6). The Nahanni limestone samples from the Labiche F-08 well contain insignificant amounts of organic material and no measurable S1 or S2 peaks similar to the low TOC contents recorded from the uppermost Nahanni limestones at the Kotaneelee 0-67 well (Fig. 5).

The gas zone of the Labiche field is developed in a 'siltstone'-rich interval (Meding, 1994) just above core 1 of the Labiche F-08 well (Fig. 6). This very porous zone may be largely a cavern-filling similar to the cavern-fill of core 1.

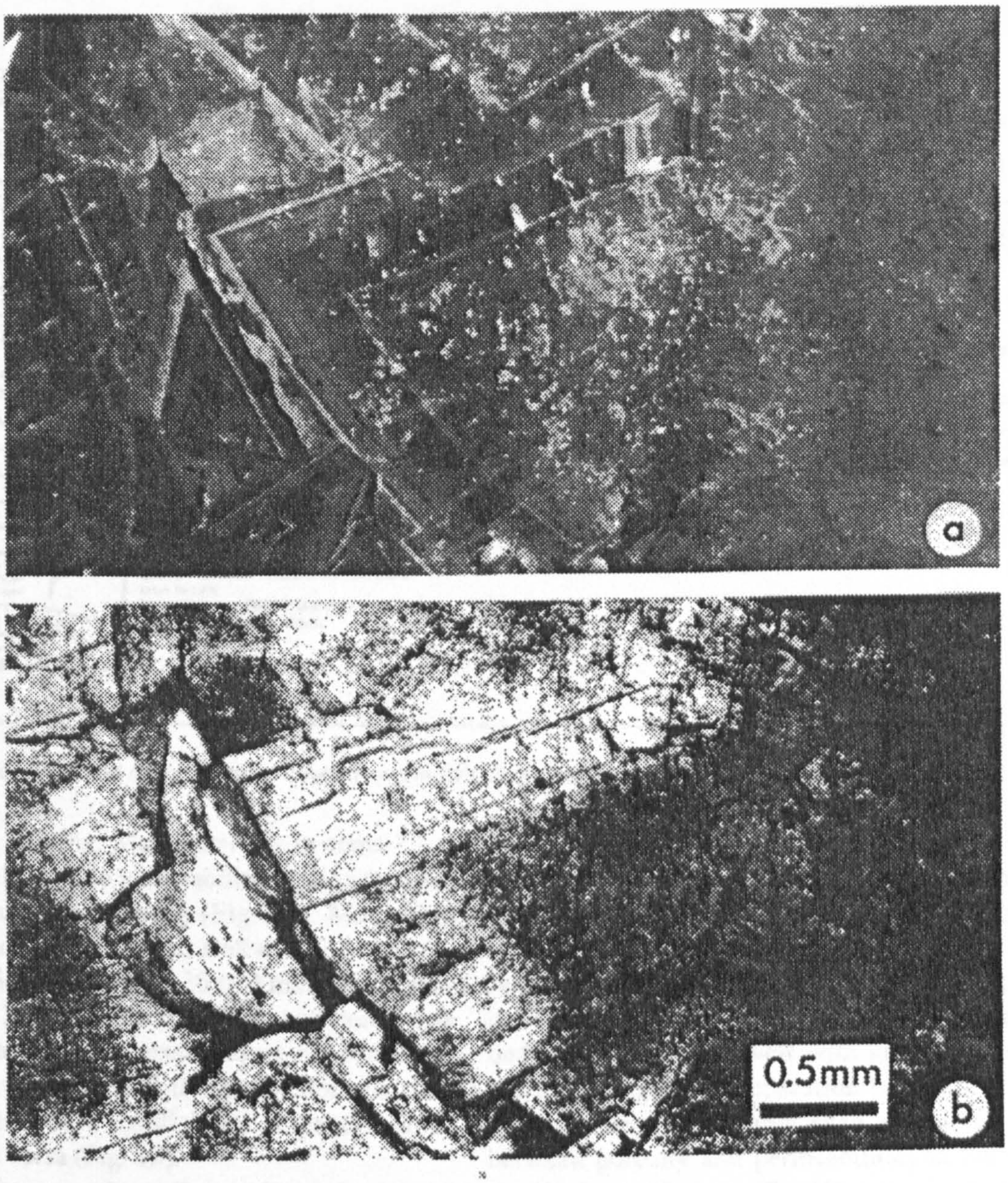

Fig. 12. Thin section photomicrographs of Manetoe vug-filling dolospar in the Columbia et al, Kotaneelee YT H-38 well at 12,067 feet (K.B.). Fig. 12a is a cathodoluminescent view of the dolospar. Luminescence is dull except for thin orange luminescent bands near the distal edges of crystals. Fig. 12b is a plain light view of cathodoluminescent image in 12a.

POROSITY AND PERMEABILITY

Spectacular vuggy biogenic porosity (Figs. 8 and 9b) occurs in the upper part of the Nahanni Formation in the Pointed Mountain Field. Porosity in the completely dolomitized uppermost cores from Nahanni equivalent strata at the Amoco A-4 Pointed Mountain A-55 well ranges from about 1.0% to a high of nearly 10.0% with a weighted average porosity of about 3.6% (Fig. 15). The zones of porosity greater than 4.0% generally correspond to zones with a significant proportion of incompletely occluded macrovugs, most of which are biogenic. But some represent unoccluded interfragment macropores in incompletely cemented collapse breccias. More commonly, however, the interfragment spaces of mosaic and rubble packbreccias in the Manetoe Dolomite tend to be completely cemented with white dolospar (Fig. 11c).

Permeability in the A-55 well tends to be very anisotropic with permeability parallel to bedding typically being several orders of magnitude greater than that

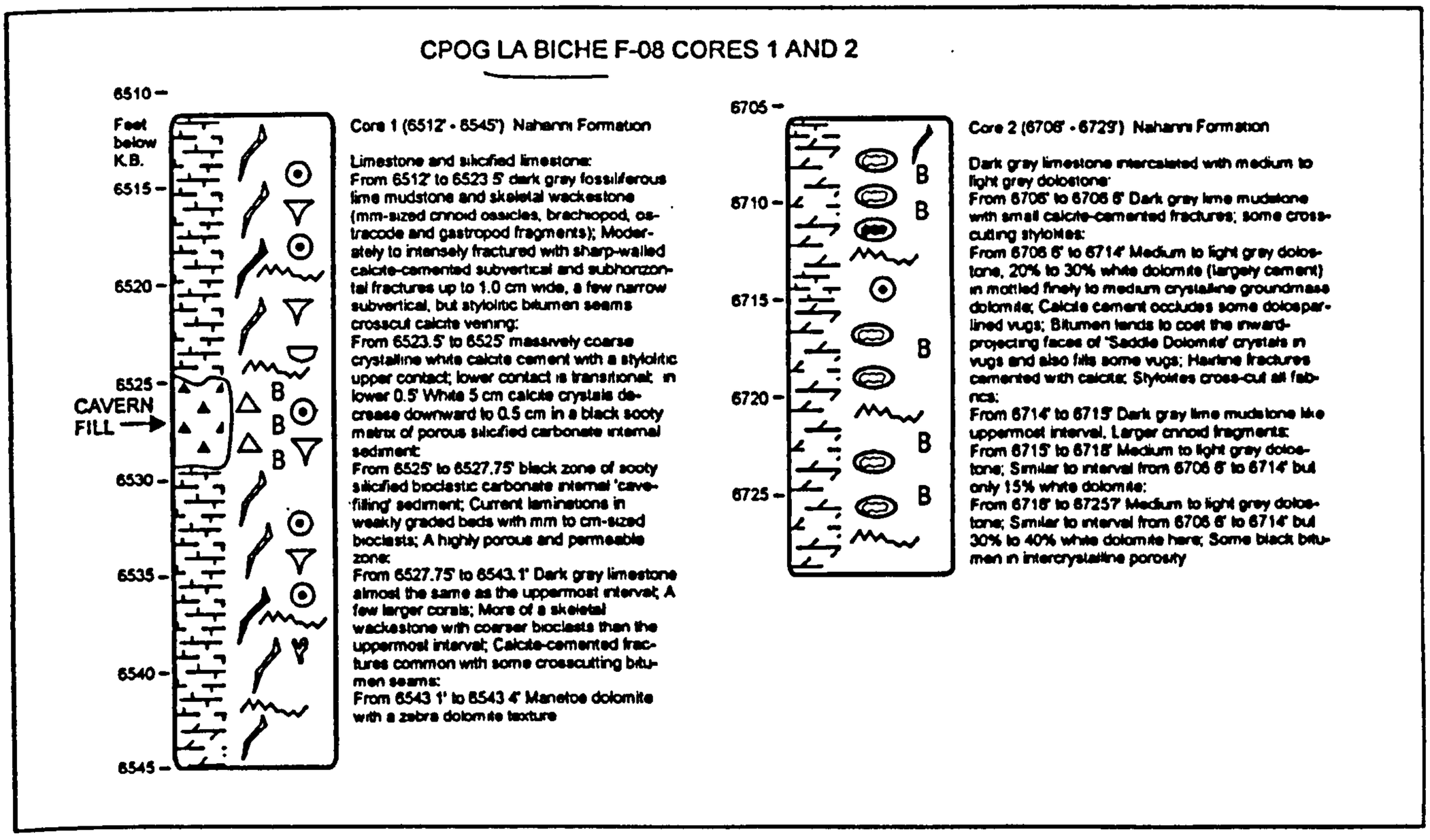

Fig. 13. Graphical logs and descriptions of cores from the CPOG et al. LaBiche F-08 well. See Figure 8 for legend.

perpendicular to bedding. Many intervals in cores 1 and 2 of the A-55 well have no permeability, or are impermeable, perpendicular to bedding (Fig. 15). Many thin intervals scattered throughout this well exhibit extremely high permeabilities in excess of 30,000 millidarcies parallel to bedding. In general, permeability and porosity in this well appear to exhibit a certain degree of covariance. Zones with high porosity tend to also exhibit relatively high permeabilities both parallel and perpendicular to bedding and vice versa (Fig. 15).

The uppermost cores from the totally dolomitized, Nahanni equivalent strata in the Columbia et al. Kotaneelee YT E-37 well, cores 4 and 5, exhibit somewhat lower porosity and permeability than those of the A-55 well. This may be due in large part to the presence of fewer zones with less well developed, unoccluded biogenic porosity in the E-37 well than in the A-55 well. Porosity in the E-37 cores ranges from a low of about 2.0% to a high of about 11.0% (Fig. 15). However, porosity is far less variable in the E-37 cores. Porosity throughout these cores tends to fall within limits of between 2.0% and 4.0% porosity, unlike the A-55 core where porosity most commonly ranges from 2.0% - 6.0% (Fig. 15).

Permeability in the E-37 cores is much less anisotropic than in the A-55 cores. This is primarily because permeability perpendicular to bedding is much greater in the E-37 well than in the A-55 well, whereas permeability parallel to bedding in E-37 is considerably less overall than in A-55 (Fig. 15). There is strong covariance between permeabilities parallel and perpendicular to bedding in the E-37 well with generally less than an order of magnitude separation between permeability curves. There is probably even a stronger covariance between porosity and permeabilities in the E-37 cores than in the A-55 cores (Fig. 15).

The much shorter cores 1 and 2 from the CPOG et al. LaBiche F-08 well are generally much less porous than cores from A-55 and E-37 (Fig. 15) and are only partly dolomitized (Fig. 13). Disregarding the very porous interval representing the silicified bitumen-impregnated cavern-fill (6523.5 - 6525 ft.; Fig. 9a), the average porosity of core 1 at F-08 is only 1.5%. This reflects the very low porosity of the undolomitized, fossiliferous, lime wackestone that forms most of this core (Fig. 13). The cavern-fill interval by contrast is extremely porous, at almost 24% porosity. The subhorizontal to subvertical calcite veining, which is common in the limestone above and below the cavern-fill in core 1 (Fig. 9a), does not appear to contribute significantly to its porosity or per-

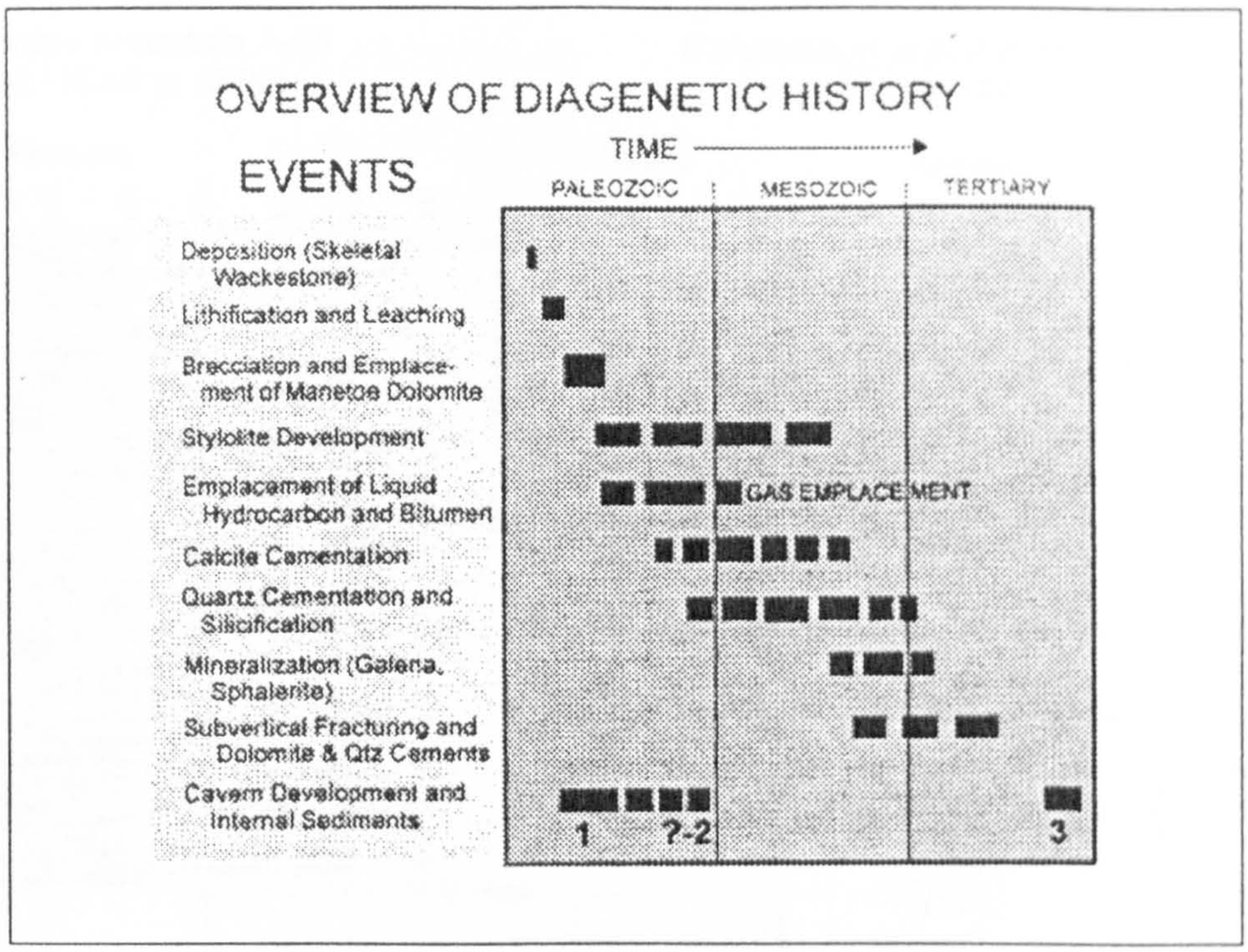

Fig. 14. Diagenetic history of Lower and Middle Devonian carbonate strata that contain the Manetoe Dolomite.

meability. Average porosity in core 2 is about 2.3%, or slightly greater than that of core 1, if the cavern-fill interval is not included. Porosity values increase slightly downdepth in core 2, possibly reflecting the passage downcore from partial to complete dolomitization. Although there are some intervals with common macropore vugs of biogenic origin in core 2, they tend to be completely occluded with reservoir bitumen and white calcite, and consequently do not contribute to porosity.

Permeability in both the F-08 cores is low, commonly less than 5 millidarcies. In spite of the high porosity of the cavern-fill interval, its permeability is less than 10 millidarcies, but is nearly the same in directions parallel to and perpendicular to bedding. The remainder of core 1 and all of core 2 exhibit the more usual anisotropy, with permeability parallel to bedding being greater than that perpendicular to bedding (Fig. 15).

Discussion

The internal stratigraphy of the thick Manetoe Dolomite in the Pointed Mountain and Kotaneelee gas fields may be discerned on geophysical well logs. Correlation of the upper part of the Manetoe in and around the gas fields is more readily made with the Dunedin and Stone formations of northeast British Columbia, rather than with the Nahanni and Headless formations of the southern Mackenzie Mountains. The lithologies and log signatures of the internal subdivisions of the Dunedin Formation strongly resemble the lithologies and log signatures of the upper part of the Manetoe Dolomite in spite of the fact that these are long distance correlations. The available sparse biostratigraphic information indicates that the upper contact of the 'Nahanni' interval within the Manetoe Dolomite is highly diachronous becoming younger eastward towards the Arrowhead Salient. This is similar to the southeastward younging of the upper contact of the Dunedin Formation of British Columbia, which also is Givetian in age, near the junction of the Dunedin with the Presqu'ile, or Keg River Barrier. This intertonguing of Besa River shales and Nahanni carbonates, implied by the eastward 'younging' of the upper contact of Nahanni-equivalent strata around the gas fields, may have provided opportunity for a degree of lateral, as well as downwards, migration of hydrocarbons into Manetoe reservoirs.

The process of dolomitization definitely appears to have enhanced porosity and permeability. This is not likely to have been the consequence of volume loss during dolomitization. The greater porosity and permeability of dolomitized Nahanni versus undolomitized Nahanni limestones in cores from the gas field wells is more likely to have been the result of the preferential preservation of porosity during burial of dolomitized versus that of undolomitized limestones (Schmoker and

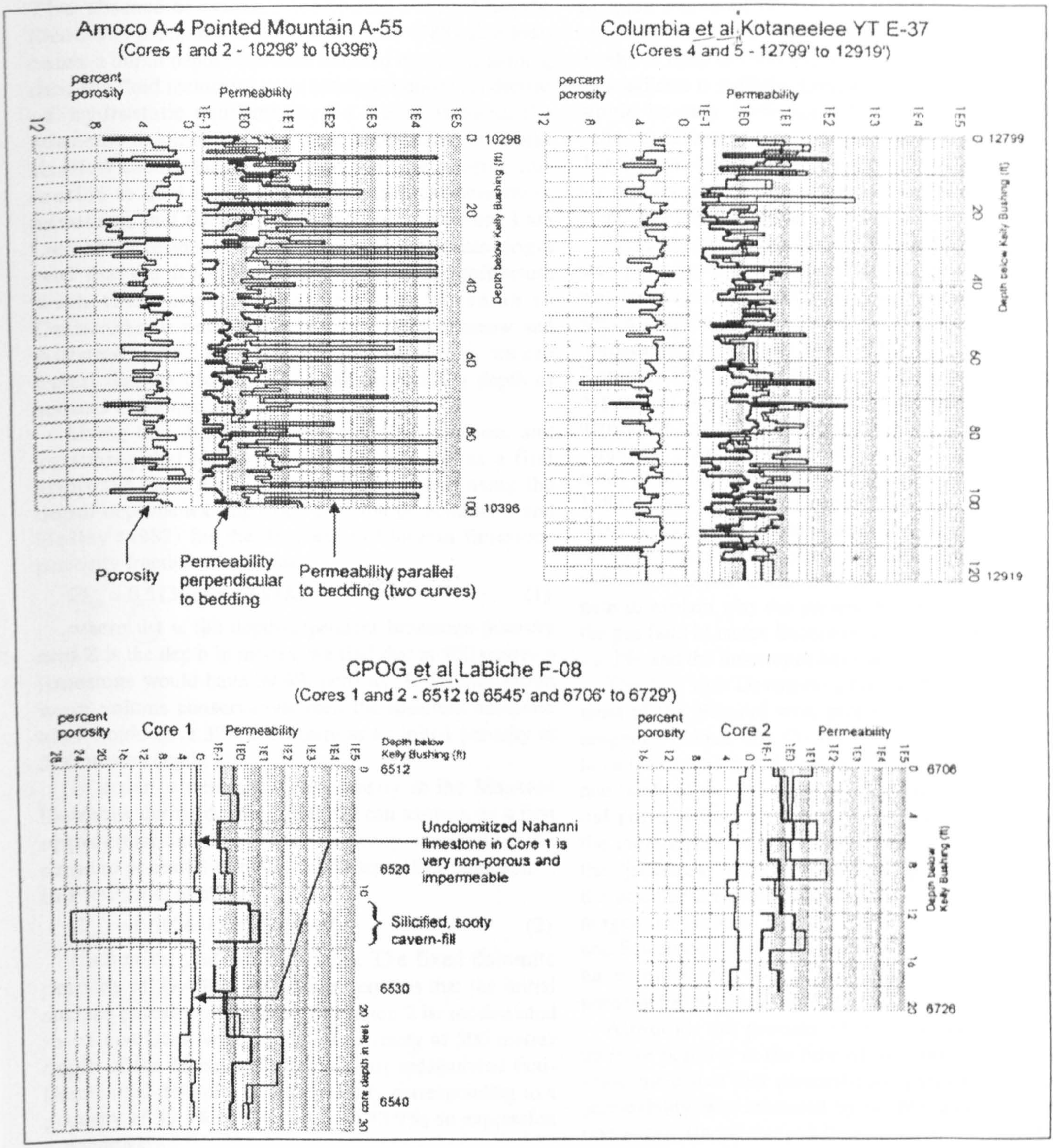

Fig. 15. Porosity and permeability graphs for core from the Pointed Mountain, Kotaneelee and Labiche fields based upon data from Core Laboratories of Canada, Ltd.

Halley, 1982).

A simple calculation, based on extrapolation of depth-dependent porosity functions, shows a considerable difference in the present day expected porosity between dolomitized and undolomitized Nahanni strata. It is clear that dolomitization occurred after lithification and possibly after an episode of karst dissolution, which implies burial to depths of at least tens to hundreds of metres.

The absence of evidence for boiling during Manetoe Dolomite precipitation (Aulstead *et al.*, 1988) also indicates a burial depth of several hundred metres, assuming that the fluid inclusions were entrapped under conditions of hydrostatic equilibrium. On the other hand, the Manetoe dolomite cements were precipitated at depths shallow enough that there is no discernible pressure correction to fluid inclusion homogenization temperatures, assuming that the precipitational solutions were Late Devonian residual connate brines of evaporitic origin and that the dolomites formed in isotopic equilibrium with these connate brines in Late Devonian to Carboniferous time (Aulstead *et al.*, 1988, Morrow and Aulstead, 1995). As a very rough estimate then, we can assert that the Manetoe Dolomite formed at a depth of around 500 metres.

Using this depth estimate for dolomitization, and assuming that the dolomitization process, as a first approximation, conserved rock volume and using the depth-dependent compaction function of Schmoker and Halley (1982) for the decrease in Floridan limestone porosity fraction with depth:

$$\varnothing_{lst} = 0.513(\exp(-(Z)/1888) \quad (1)$$

where ilst is the depth-dependent limestone porosity and Z is the depth in metres, we find that at 500 metres a limestone would have 39.4% porosity. If dolomitization were volume conservative, then the resultant dolomite also would have 39.4% porosity as an initial porosity at 500 metres depth.

In order to determine the porosity in the Manetoe Dolomite during deeper burial, we can assume, as a first approximation, that this dependency will follow the same exponential trend as depth-dependent compaction in Floridan dolomites:

$$\varnothing_{dol} = 0.3036(\exp(-(Z)/4619) \quad (2)$$

(Schmoker and Halley, 1982). The fixed dolomite porosity of 39.4% at 500 metres requires that the initial surface porosity of 30.36% of equation 2 be recalculated to be consistent with the 39.4% porosity at 500 metres depth of the Manetoe Dolomite. This recalculated fictitious initial dolomite surface porosity corresponding to a porosity of 39.4% at 500 metres is 43.9%, so expression 2 becomes:

$$\varnothing_{dol} = 0.439(\exp(-(Z)/4619) \quad (3)$$

assuming that a simple linear transformation is appropriate.

The resultant dolomite porosity at the 5000 metre maximum depth that the Manetoe Dolomite experienced in Late Cretaceous time (Morrow *et al.*, 1993) following equation 3 is about 14.9%. This figure could be reduced only slightly to 12.7% if dolomitization occurred at depths as deep as 1000 metres, which the fluid inclusion data indicate is unlikely. Limestone porosity at this depth would be only 3.6% according to equation 1. This extreme difference serves to emphasize the perception that at great depths there is a greatly enhanced potential for preservation of porosity in dolomites which formed at much shallower depths.

There is a possibility that the initial average near-surface porosity of the Nahanni skeletal lime wackestones was less than that of the Cenozoic Floridan limestones, which contain a high proportion of wackestones and mudstones (Schmoker and Halley, 1982). Bond and Kominz (1984) found that best fitting average depth-dependent porosities of lime sediments are strongly dependent on initial sediment grain size such that "calcarenites" are much less porous than "micrites" (*i.e.* lime mud) at all burial depths (Fig. 2 in Bond and Kominz, 1984). Lower initial limestone porosities imply correspondingly lower dolomite and limestone porosities at maximum burial. This grain size factor may have contributed to a low initial limestone porosity and might help to explain why the present day porosity of most of the gas field Manetoe Dolomites ranges from about 2.0% - 6.0%, and the limestones have about 1.0% porosity.

The fact that Devonian lime muds, which formed most of the Nahanni were probably calcite, rather than aragonite (James and Choquette, 1990) may have also have influenced initial porosity. It seems likely that calcite muds of the Devonian would have had a lower initial porosity than present-day aragonite muds because the more equant calcite crystals are unlikely to exhibit the "jackstraw" style of open packing that characterizes the acicular aragonite crystal masses in the very porous aragonitic seafloor muds of the Bahama Banks (Enos and Sawatsky, 1981). This mineralogical factor may also have contributed to a slightly lower initial limestone porosity for pre-Manetoe Nahanni limestones.

Although the process of dolomitization did not increase porosity at the time of dolomitization, there is some indication that permeability, particularly vertical permeability, was increased by the Manetoe dolomitization event. Undolomitized limestones in the Labiche F-08 core tend to have little or no vertical permeability, whereas dolomitized intervals have measurable vertical permeability. The nearly isotropic permeability of the dolomitized Kotaneelee E-37 cores is also an indication of the enhancement of vertical permeability during dolomitization. This effect is not as evident in the Pointed Mountain A-55 cores, possibly because the

circulation of dolomitizing solutions was focussed preferentially parallel to bedding along pre-existing porosity networks of leached biogenic porosity. There may have been a tendency for the rate of dissolution to be higher relative to the rate of dolomite precipitation because of more rapid solution flow along the more open porosity networks parallel to bedding. If true, this would tend to preferentially enhance permeability parallel to bedding during dolomitization.

There is no indication from the porosity-permeability data, or from visual examination of the cores of this study, that significant vertical fracture permeability exists. Comparison of geophysical logs, such as the neutron and sonic logs, might indicate the existence of open subvertical fracture porosity. Snowdon (1977) and Davidson and Snowdon (1978) suggested that the sporadic nature of gas production from the Manetoe Dolomite at the Beaver River Gas Field was due to the preferential invasion of water into the pervasive, gas-filled, fracture network which effectively 'sealed in' matrix gas.

The data of this study might be interpreted to indicate another possible cause for sporadic gas production interspersed with water production, particularly for the Pointed Mountain Field. Pointed Mountain exhibits an essentially horizontally layered, porosity-permeability fabric with weak vertical continuity. Production of gas would tend to quickly deplete the high permeability layers. If these layers intersected fractures open to the pressured aquifer beneath the gas column, water would tend to rise up these fractures and invade the high permeability layers during gas production. Vertical fracturing at Pointed Mountain and Kotaneelee, at a minimum, must be significant near the major faults that segment these fields (Figs. 2 and 3). This interpretation, involving scattered, rather than pervasive, open fractures, represents a variation on the theme of Davidson and Snowdon (1978).

The presence of other mineral cements, such as quartz and particularly calcite, along with reservoir bitumen have a considerable role in porosity reduction. The extent of this reduction has not been studied here, but insoluble residues of core samples from the Kotaneelee E-37 well yielded about 4.0% by weight of insoluble residue after digestion in hydrochloric acid. These insoluble residues were found to be mainly bitumen and quartz (Henderson, 1995). This amount of additional cement and mineral matter would cause a significant further reduction in porosity by at least 4.0% in the low porosity Manetoe Dolomite of this well. Subtraction of these non-carbonate phases from the rock volume would raise dolomite porosity to the range 6.0 - 10.0%. Henderson (1995) suggested that the release and disaggregation of these acid insoluble phases during secondary acid stimulation of the Kotaneelee field could adversely affect field performance.

Solution seams and stylolites have undoubtedly caused additional porosity loss in the Manetoe Dolomites. It is uncertain, however, whether pressure solution has been any more intense in the Manetoe sequence than in the Floridan carbonate succession examined by Schmoker and Halley (1982). On this basis, we cannot assert that pressure solution in the Manetoe Dolomite is likely to have caused any major departure from the depth-dependent porosity functions of Schmoker and Halley (1982) through porosity destruction.

However, chemical processes, such as pressure-solution, are time-dependent, as well as depth-dependent. Schmoker (1984) has suggested, with some documentation, that porosity in carbonates is best understood as a function of their Time-Temperature Index, or Lopatin TTI:

$$\varnothing_{carbonate} = a*(TTI)^b \qquad (4)$$

where TTI is the Time-Temperature Index (*e.g.*Waples, 1980). However, like the variety of depth-porosity functions, there is also considerable variation in the values of constants "a" and "b" in equation 4, with different sets of constants applicable to different carbonate sequences, although there is remarkable internal consistency for each individual sequence. It seems at least possible that part of the difference between the low porosity of the Manetoe Dolomite and Nahanni limestone and the more porous Floridan carbonates may be due to the fact that the TTI values of the Manetoe and associated Nahanni are much higher than in the Floridan carbonates. Therefore, in the absence of direct comparative evidence between the Manetoe Dolomite and the Floridan carbonate sequence, it seems likely, based on equation 4, that there should be considerable porosity destruction in the Manetoe Dolomite sequence beyond that predicted in Floridan Carbonates buried to similar depths, according to the depth-dependent functions of equations 1 and 2. The abundance of well developed stylolites within the Manetoe Dolomite (Figs. 8 ,10,11 and 13) is consistent with this possibility.

Consequently, while there may have been differences between the initial depositional porosities of pre-Manetoe Nahanni limestones and Cenozoic to modern day carbonates, post-depositional processes of mineral cementation, bitumen emplacement and stylolite development are

sufficient to adequately explain the lower porosities of the Manetoe Dolomite and Nahanni limestones as compared to porosities predicted from their maximum burial depths according to equations 1 and 2. Dolomitization itself is unlikely to have created porosity. Instead, the low average porosities of the Manetoe Dolomite may indicate that dolomitization either conserved rock volume or even caused the occlusion of some pre-existing porosity by the precipitation of additional dolomite cement.

Manetoe dolomitization is inferred to have been early in the diagenetic sequence, preceding the generation of hydrocarbons (Fig. 14). The pervasive solid reservoir bitumen coating dolomite crystals lining vugs attests to the post-dolomitization migration of liquid hydrocarbon into these rocks. The presence of subvertical bitumen-filled fractures crosscutting Manetoe Dolomite fabrics implies that there may have been fracturing from gas generation during oil catagenesis. Thermal gas generation in oil pools probably can generate considerable overpressures in the subsurface (Ungerer *et al.*, 1983) which might lead to subsurface fracturing. The extremely low vertical permeability of the overlying Besa River shale and the low permeability of Nahanni limestones adjacent to Manetoe reservoirs would enhance the potential for the generation of overpressures during the thermal cracking of oil to gas in these reservoirs. Viscous, but still mobile bitumen may have been forced into these fractures during gas generation some time following emplacement of the Manetoe Dolomite.

The occurrence of zones with macropore vugs completely occluded by solid bitumen may indicate that much of the bitumen originated not simply as the residual bitumen that remains after the thermal cracking of oil to gas, but rather as deasphalted bitumen (Lomando, 1992), in which the gas-soluble oil fraction has been stripped from the oil by gas passing upwards through the oil column. The relatively massive amounts of bitumen in the Kotaneelee E-37 well may be due to its proximity to a fault which possibly provided a local focus for the upwards flow of gas through the oil column in Mesozoic to Cenozoic time.

The quartz and calcite vug-filling cements clearly postdate bitumen emplacement as do the sphalerite and galena veinlets. It is difficult to be certain of the timing of the cavern-fillings. Those in the Pointed Mountain A-55 core appear almost contemporaneous with the Manetoe dolomitization event, with some evidence that the excavation of macrovug porosity predated dolomitization (Fig. 14).

Silicification of the detrital, crossbedded, fossiliferous carbonates in the large cavern-filling in the Labiche F-08 well may have been caused by pH changes related to the generation of organic acids during organic maturation. Generation of hydrocarbons in the overlying Besa River shale source beds in Late Paleozoic to Early Mesozoic time would have been accompanied by high solution concentrations of organic acids. These acid solutions, on entering the porous cavern-filling, may have caused the replacement of carbonates by silica if the pre-existing pore solutions of the cavern-fill were alkaline and enriched in silica (*see* Williams and Crerar, 1985). However, in the absence of definitive age information, it is not possible to be certain concerning the timing of the cavern-filling with respect to liquid oil generation. The sooty bitumen impregnating the cavern-fill could be the later residue of in-place thermal cracking of oil that filled the cavern-fill porosity because the existing porosity of the cavern-filling, at more than 23%, is an order of magnitude greater than the TOC of about 2.0%.

This cavern-filling is shown as a distinct episode of cavern development on Figure 14. However, the "Paleozoic" appearance of the weakly crossbedded and silicified faunas and the probability that cavern excavation occurred before oil migration leaves open the possibility that this cavern-filling formed at the same time as the cavern-fillings in the Pan Am Pointed Mounted A-55 core.

CONCLUSIONS

Examination of cores from selected wells in the Liard Basin, in conjunction with regional geological and geochemical information has led to:

- Recognition that the Nahanni Formation in the subsurface of Liard Basin more closely resembles the transgressive Dunedin Formation of northeast British Columbia than the regressive Nahanni Formation of the southern Mackenzie Mountains;
- Identification of one, and possibly two episodes of subsurface cavern excavation and internal sediment infill that postdate Manetoe dolomitization;
- Recognition that hydrocarbon migration postdated cavern development and emplacement of the Manetoe Dolomite;
- Recognition that much of the gas field bitumen originated by deasphalting of oil, rather than as a residue of the thermal cracking;
- Correlation of trends in bitumen reflectance of the upper Paleozoic siliciclastic sequence overlying the Manetoe Dolomite with trends in vitrinite reflectance and in Rock-Eval Tmax ;

- Recognition that the absolute porosities of the Manetoe Dolomite and accompanying Nahanni limestone and their average porosity differences are largely the result of depth-dependent porosity changes during burial, along with additional porosity occlusion by mineral cements and bitumen;
- Recognition that porosity-permeability tends to be preferentially developed parallel to bedding and that vertical permeability was enhanced by dolomitization;
- Recognition that late stage fracturing, unlike in the Beaver River gas field, did not contribute significantly to porosity or permeability of the Kotaneelee and Pointed Mountain fields

ACKNOWLEDGMENTS

We wish to thank Dr. J. (Jack) Wendte of GSC-Calgary for informative discussions related to this paper and Drs. Fari Goodarzi and Lloyd Snowdon of GSC-Calgary for assistance and advice concerning analysis and interpretation of organic materials. We thank also Imperial Oil of Canada for its contribution of data. This work was funded under Geological Survey of Canada Project 890064.

REFERENCES

Amoco Canada Petroleum Company Ltd. 1964. Seismic Survey, Pointed Mountain Area. National Energy Board, Open File 060-06-04-47.

Aulstead, L.L. 1987. Origin and Diagenesis of the Manetoe facies, southern Yukon and Northwest Territories, Canada. Unpublished M.Sc. thesis, Department of Geology and geophysics, University of Calgary, Calgary, 143p.

Aulstead, K.L., Spencer, R.J. and Krouse, H.R. 1988. Fluid inclusion and isotopic evidence on dolomitization, Devonian of Western Canada. Geochimica et Cosmochimica Acta, v.52, p. 1027-1035.

Bond, G.C. and Kominz, M.A. 1984. Construction of tectonic subsidence curves for the early Paleozoic miogeocline, southern Canadian Rocky Mountains: implications for subsidence mechanisms, age of breakup, and crustal thinning. Geological Society of America Bulletin, v.95, p.155-173.

Chatterton, B.D.E. 1978. Aspects of late Early and Middle Devonian conodont biostratigraphy of western and northwest Canada. *In*: Western and Arctic Biostratigraphy, C.R. Stelck and B.D.E. Chatterton (eds.). Geological Association of Canada, Special Paper no. 18, p. 161-231.

Cecile, M.P., Morrow, D.W. and Williams, G.K. 1997. Early Paleozoic (Cambrian to Early Devonian) tectonic framework, Canadian Cordillera. Bulletin of Canadian Petroleum Geology, vol. 45, p. 54-74.

Columbia Gas Development of Canada Ltd. 1979. Geophysical Report on the Kotaneelee Seismic survey, Yukon Territory. JLJ Exploration Consultants Ltd. (R.P. Jordan), National Energy Board, Open File 556-06-04-007.

Davidson, D.A. and Snowdon, D.M. 1978. Beaver River Middle Devonian carbonate: performance review of a high-relief, fractured gas reservoir with water influx. Journal of Petroleum Technology, v. 30, p. 1673-1678.

Douglas, R.J.W. 1976. Geology of the La Biche River map-area, District of Mackenzie, Geological Survey of Canada Map 1380A, 1:250,000.

_____ and Norris, D.K. 1976. Geology, Sibbeston Lake, District of Mackenzie. Geological Survey of Canada, Map 1377A. (Scale 1:250,000).

Enos, P. And Sawatsky, L.H. 1981. Pore networks in Holocene carbonate sediments. Journal of Sedimentary Petrology, v. 51, p. 961-985.

Espitalié, J., 1986. Use of Tmax as a maturation index for different types of organic matter. Comparison with vitrinite reflectance. *In*: Thermal Modelling in Sedimentary Basins, J. Burrus (ed.), Technip, Paris, p. 475-496.

Gabrielse, H. 1967. Tectonic evolution of the northern Canadian Cordillera. Canadian Journal of Earth Sciences, v.4, p. 271-298.

Henderson, G.,1995. Core Report for Anderson Exploration, March 3, 1995 (Report number NRD-95-125): Nowsco Well Service Ltd., Calgary, Alberta, Canada, 9p.

Imperial Oil Resources Ltd. pers. comm. Unpublished report on two bitumen samples from the Manetoe Dolomite of the Pan Am Kotaneelee YT E-37 well. Rock-Eval and biomarker analyses performed at GSC-Calgary under direction of L.L. Snowdon.

Jacob, H. 1985. Dispersed solid bitumen as an indicator for migration and maturity in prospecting for oil and gas. Erdöl Kohle, v.35, p. 365.

James , N.P. and Choquette, P.W. 1990. Limestones - the sea floor diagenetic environment. *In*: Diagenesis, I.A. McIlreth and D.W. Morrow (eds.). Geoscience Canada, Reprint Series 4, p. 13-34.

Lomando, A.J. 1992. The influence of solid reservoir bitumen on reservoir quality. American Association of Petroleum Geologists Bulletin, v. 76, no. 8, p.1137-1152.

Machel, H.G. 1985. Cathodoluminescence in calcite and dolomite and its chemical interpretation. Geoscience Canada, v. 12, p. 139-148.

Meding, M.G. 1994. Analysis of Selected Northwest Territories Hydrocarbon Pool Data: Geostar Consultants Inc., Report prepared for Department of Energy, Mines and Resources, Government of the Northwest Territories.

Meijer-Drees, N.C. 1993. The Devonian Succession in the Subsurface of the Great Slave and Great Bear Plains, Northwest Territories. Geological Survey of Canada, Bulletin 393, 222p.

Morrell, G.R., Fortier, M., Price, P.R. and Polt, R. 1995. Mackenzie valley, southern territories and interior plains. *In*: Petroleum Exploration in Northern Canada - A Guide to Oil and Gas Exploration, G.R. Morrell (ed.), Northern Oil and Gas Directorate, Indian and Northern Affairs Canada, p. 7-22.

Morrow, D.W. 1978. The Dunedin Formation: A Transgressive Shelf Carbonate Sequence. Geological Survey of Canada, Paper 76-12, 35p.

_____ 1994. Manetoe Dolomite Field Trip, Southern Mackenzie Mountains. Unpublished Field Trip Guide Book, 12p.

_____, 1996. The Manetoe Dolomite exploration play in the Liard Basin of the Yukon and Northwest Territories. Abstract In Pools' 96 - Oil and Gas Pools of the Western Canada Sedimentary Basin, Core Conference Abstracts, p. 12.1-12.2.

_____ and Aulstead, K.L. 1995. The Manetoe Dolomite - a Cretaceous-Tertiarty or a Paleozoic event? Fluid inclusion and isotopic evidence: Bulletin of Canadian Petroleum Geology, v. 43, No. 3, p. 267-280.

_____, _____ and Cumming, G.L. 1990. The gas-bearing Devonian Manetoe Facies, Yukon and Northwest Territories. Geological Survey of Canada Bulletin 400.

_____ and Cook, D.G. 1987. The Prairie Creek Embayment and lower Paleozoic stratigraphy of the southern Mackenzie Mountains. Geological Survey of Canada, Memoir 412.

_____, Potter, J., Richards, B. and Goodarzi, F. 1993. Paleozoic burial and organic maturation in the Liard Basin region, northern Canada. Bulletin of Canadian Petroleum Geology, v.41, No.1, p. 17-31.

Noble, J.P.A. and Ferguson, R.D. 1971. Facies and faunal relations at the edge of early mid-Devonian carbonate shelf, Soouth Nahanni River area, N.W.T., Bulletin of Canadian Petroleum Geology, v. 19, p. 570-588.

Peters, K.E. 1986. Guidelines for evaluating source rock using programmed pyrolysis. American Association of Petroleum Geologists Bulletin, v.70, no.3, p. 318-329.

Potter, J. in prep. The Organic Petrology, Thermal Maturity and Hydrocarbon Potential of the Upper Devonian and Lower Carboniferous in the Liard Basin, Northern Canada. Ph.D. Thesis, University of Newcastle-upon-Tyne, U.K.

Price, P.R. 1994. Petroleum Resources of the Liard Plateau Area, Southern Yukon Territory, Canada. Unpublished National Energy Board Report (Draft), 31p.

Snowdon, L.R. 1995. Rock-Eval Tmax suppression: Documentation and amelioration. American Association of Petroleum Geologists, Bulletin, v. 79, p. 1337-1348.

Snowdon, D.M. 1977. Beaver River gas field: a fractured carbonate reservoir. *In*: The Geology of Selected Carbonate Oil, Gas and Lead-Zinc Reservoirs in Western Canada, I.A. McIlreath and R.D. Harrison (eds.), Canadian Society of Petroleum Geologists, 5th Core Conference, p. 1-18.

Schmoker, J.W. 1984. Empirical relation between carbonate porosity and thermal maturity - an approach to regional porosity prediction. American Association of Petroleum Geologists, Bulletin, v. 68, p. 1697-1703.

_____ and Halley, R.B. 1982. Carbonate porosity versus depth - a predictable relation for south Florida. American Association of Petroleum Geologists, Bulletin, v. 66, p. 2561-2570.

Spencer, R.J. 1987. The origin of Ca-Cl brines in Devonian formations, western Canada sedimentary basin. Applied Geochemistry, v.2, p. 373-384.

Taylor, G.C. and Mackenzie, W.S. 1970. Devonian Stratigraphy of northeastern British Columbia. Geological Survey of Canada, Bulletin 186

Ungerer, P.E., Behar, E., and Discamps, D. 1983. Tentative calculations of the overall volume expansion of organic matter during hydrocarbon genesis from geochemistry data: implications for primary migration. *In*: Advances in Organic Geochemistry: Chichester. John Wiley, p. 129-135.

Ward, G.S. 1994. Hydrodynamic Evaluation of the Devonian to Precambrian Formations - Liard Arch, N.W.T. (59E30'-63E 00'N, 121E 00' - 125E 00'W): Ward Hydrodynamics Ltd., 89p.

Waples, D. 1980. Time and temperature in petroleum formation: Application of Lopatin's method to petroleum exploration. American Association of Petroleum Geologists Bulletin, v.64, p. 916-926.

Williams, G.K. 1981. Subsurface geological maps, southern Northwest Territories. Geological Survey of Canada, Open File 793.

Williams, L.A. and Crerar, D.A. 1985. Silica diagenesis, II. General mechanisms. Journal of Sedimentary Petrology, v. 55, p. 312-321.